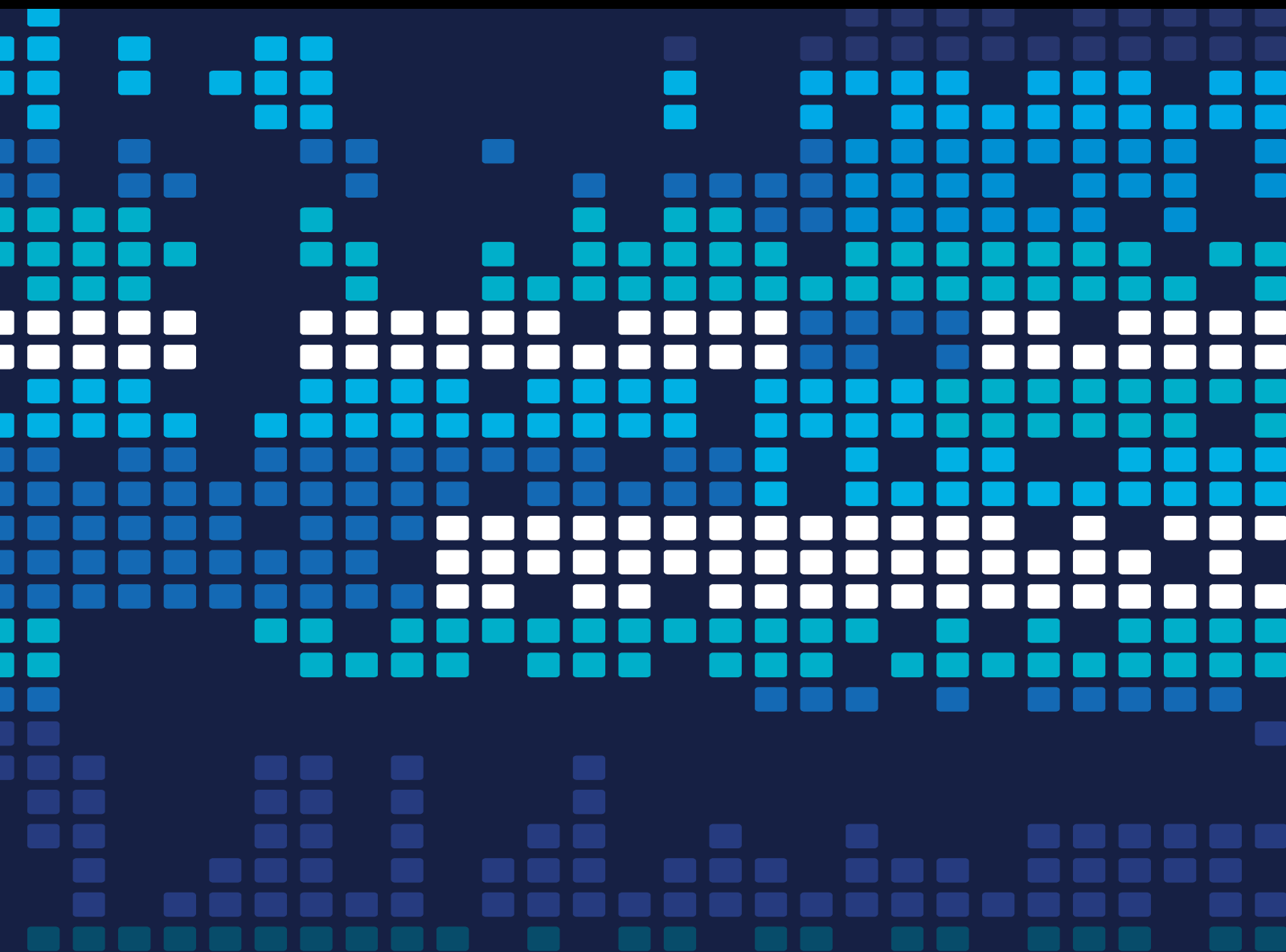


Recent Advances of High-Performance Dimensionality Reduction in Big Data Era

Lead Guest Editor: Hangjun Che

Guest Editors: Zheng Yan, Man Fai Leung, and Wenming Cao





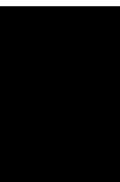
Recent Advances of High-Performance Dimensionality Reduction in Big Data Era

Scientific Programming

Recent Advances of High-Performance Dimensionality Reduction in Big Data Era

Lead Guest Editor: Hangjun Che


Guest Editors: Zheng Yan, Man Fai Leung, and Wenming Cao



Copyright © 2023 Hindawi Limited. All rights reserved.

This is a special issue published in "Scientific Programming." All articles are open access articles distributed under the Creative Commons Attribution License, which permits unrestricted use, distribution, and reproduction in any medium, provided the original work is properly cited.

Chief Editor

Emiliano Tramontana , Italy

Academic Editors

Marco Aldinucci , Italy
Daniela Briola, Italy
Debo Cheng , Australia
Ferruccio Damiani , Italy
Sergio Di Martino , Italy
Sheng Du , China
Basilio B. Fraguera , Spain
Jianping Gou , China
Jiwei Huang , China
Sadiq Hussain , India
Shujuan Jiang , China
Oscar Karnalim, Indonesia
José E. Labra, Spain
Maurizio Leotta , Italy
Zhihan Liu , China
Piotr Luszczek, USA
Tomàs Margalef , Spain
Cristian Mateos , Argentina
Zahid Mehmood , Pakistan
Roberto Natella , Italy
Diego Oliva, Mexico
Antonio J. Peña , Spain
Danilo Pianini , Italy
Jiangbo Qian , China
David Ruano-Ordás , Spain
Željko Stević , Bosnia and Herzegovina
Kangkang Sun , China
Zhiri Tang , Hong Kong
Autilia Vitiello , Italy
Pengwei Wang , China
Jan Weglarz, Poland
Hong Wenxing , China
Dongpo Xu , China
Tolga Zaman, Turkey

Contents

Retracted: Analysis of Key Indicators Related to the Teaching of Floral Art Skills Competition Based on Fuzzy Hierarchical Model

Scientific Programming

Retraction (1 page), Article ID 9872525, Volume 2023 (2023)

Retracted: Dynamic Correlation between Ozone and Volatile Organic Compounds in the Southeastern Coastal Region

Scientific Programming

Retraction (1 page), Article ID 9870193, Volume 2023 (2023)

Retracted: NSGA-II-Based Microchannel Structure Optimization Problem Study

Scientific Programming

Retraction (1 page), Article ID 9794341, Volume 2023 (2023)

Retracted: Influence of Management Efficiency of Sports Equipment in Colleges and Universities Based on the Intelligent Optimization Method

Scientific Programming


Retraction (1 page), Article ID 9769870, Volume 2023 (2023)

Retracted: Analysis and Optimization of Online Music Teaching System Based on Dynamic Model

Scientific Programming


Retraction (1 page), Article ID 9846576, Volume 2023 (2023)

Analysis and Evaluation of Enterprise Performance Appraisal Index Based on Fuzzy AHP Model

Yulin Xia, Xiaoyan Wei , and Jian Tang


Research Article (9 pages), Article ID 6915812, Volume 2022 (2022)

Optimization and Allocation Method of Regional Groundwater Pollution Investigation Based on Analytic Hierarchy Process Model

Feng Zhang 


Research Article (9 pages), Article ID 7321576, Volume 2022 (2022)

Engineering Cost Prediction Model Based on DNN

Bingxin Li , Quanying Xin, and Lixin Zhang


Research Article (8 pages), Article ID 3257856, Volume 2022 (2022)

Voice Anomaly Detection and Music Website Teaching Design for 5G Internet of Things

Jin Chen 

Research Article (13 pages), Article ID 7028473, Volume 2022 (2022)

Research of Consumption Behavior Prediction Based on Improved DNN


Yu Tian, Yuhong Lai, and Chao Yang 

Research Article (9 pages), Article ID 6819525, Volume 2022 (2022)

Evaluation of Ecological Environment Quality in Chongqing Main City Area Based on Principal Component Analysis

Chunyang Chen , Quansheng Ge, Zexing Tao, and Liang Liang
Research Article (10 pages), Article ID 7374034, Volume 2022 (2022)

An Approach to Oral English Assessment Based on Intelligent Computing Model

Caihong Jing, Xiaoling Zhao , Haiyan Ren, Xuexia Chen, and Naren Gaowa
Research Article (8 pages), Article ID 4663574, Volume 2022 (2022)

Multimedia Application and Network Architecture Design Based on Multiterminal Collaboration

Lian Wu  and Lee Jong Han
Research Article (9 pages), Article ID 7997773, Volume 2022 (2022)

Research on Classroom Teaching Quality Evaluation and Feedback System Based on Big Data Analysis

Yuankui Zhang and Jing Gao 
Research Article (13 pages), Article ID 7870113, Volume 2022 (2022)


Research on Recommendation of Big Data for Higher Education Based on Deep Learning

Ang Zhao and Yanhua Ma 
Research Article (8 pages), Article ID 5448442, Volume 2022 (2022)

Prediction of Sports Performance Combined with Deep Learning Model and Analysis of Influencing Factors

H. ZhaoriGetu 
Research Article (13 pages), Article ID 4082906, Volume 2022 (2022)

Animation Expression Control Based on Facial Region Division

Liangjun Zhang 
Research Article (13 pages), Article ID 5800099, Volume 2022 (2022)

Research on Methods of Physical Aided Education Based on Deep Learning

Wei Su and Jian Feng 
Research Article (13 pages), Article ID 6447471, Volume 2022 (2022)

Research on the Sound Quality Evaluation Method Based on Artificial Neural Network

Xiedong Song and Wei Yang 
Research Article (8 pages), Article ID 8686785, Volume 2022 (2022)

Construction of Surface Water Pollution Prediction Model Based on Machine Learning


Yuanhong Che, Zhangdong Wei , and Jing Wen 
Research Article (8 pages), Article ID 7211094, Volume 2022 (2022)

Emotional Analysis and Personalized Recommendation Analysis in Music Performance

Bo Sun 
Research Article (9 pages), Article ID 9548486, Volume 2022 (2022)




Contents

Prediction of Soil Heavy Metal Content Based on Deep Reinforcement Learning

Yongqi Zhao, Zhangdong Wei , and Jing Wen

Research Article (10 pages), Article ID 1476565, Volume 2022 (2022)

A Novel Multiobjective Particle Swarm Optimization Combining Hypercube and Distance

Xiaoli Shu , Yanmin Liu , Qian Zhang, and Meilan Yang 


Research Article (21 pages), Article ID 9448419, Volume 2022 (2022)

Evaluation and Prediction Method of System Security Situational Awareness Index Based on HMM Model

Mengjie Qian 


Research Article (11 pages), Article ID 6800135, Volume 2022 (2022)

Construction of a Coupled Mathematical Model of Oil and Gas Risk Relying on Distributed Computing

Yao Hu , Sha He, Xiaoli Yang, and Chuanping Wang


Research Article (11 pages), Article ID 5327266, Volume 2022 (2022)

[Retracted] NSGA-II-Based Microchannel Structure Optimization Problem Study

Linlin Wang 


Research Article (7 pages), Article ID 6368018, Volume 2022 (2022)

Wireless Sensor Network Security Based on Improved Identity Encryption

Hao Zhou and Haochang Bi 

Research Article (10 pages), Article ID 2308825, Volume 2022 (2022)

A Sentiment Classification Model of E-Commerce User Comments Based on Improved Particle Swarm Optimization Algorithm and Support Vector Machines

Xuehui Jiang 

Research Article (9 pages), Article ID 3330196, Volume 2022 (2022)

Research on Stock Price Time Series Prediction Based on Deep Learning and Autoregressive Integrated Moving Average

Daiyou Xiao  and Jinxia Su


Research Article (12 pages), Article ID 4758698, Volume 2022 (2022)

[Retracted] Analysis of Key Indicators Related to the Teaching of Floral Art Skills Competition Based on Fuzzy Hierarchical Model

Ningling Wu  and Jieliang Zhou


Research Article (8 pages), Article ID 7765024, Volume 2022 (2022)

Rule Analysis of Teaching Evaluation System Based on Data Mining under Web Platform

Jing Wang 


Research Article (12 pages), Article ID 7133380, Volume 2022 (2022)

Research on Simulation Analysis of Physical Training Based on Deep Learning Algorithm

Zhao Hui , Chen Jing, and Wang Taining


Research Article (11 pages), Article ID 8699259, Volume 2022 (2022)

Multiple Musical Instrument Signal Recognition Based on Convolutional Neural Network

Lei Lei 


Research Article (11 pages), Article ID 5117546, Volume 2022 (2022)

Deep Collaborative Online Learning Resource Recommendation Based on Attention Mechanism

Cuiping Hao and Ting Yang 


Research Article (10 pages), Article ID 3199134, Volume 2022 (2022)

Construction and Simulation of the Market Risk Early-Warning Model Based on Deep Learning Methods

Yuchen Lei and Yinghui Li 


Research Article (8 pages), Article ID 4733220, Volume 2022 (2022)

Data Analysis and Prediction Modeling Based on Deep Learning in E-Commerce

Lei Feng 


Research Article (12 pages), Article ID 1041741, Volume 2022 (2022)

Student Performance Prediction in Mathematics Course Based on the Random Forest and Simulated Annealing

Shaohai Huang and Junjie Wei 


Research Article (9 pages), Article ID 9340434, Volume 2022 (2022)

[Retracted] Dynamic Correlation between Ozone and Volatile Organic Compounds in the Southeastern Coastal Region

Hao Li and Xing Nie 


Research Article (9 pages), Article ID 8566454, Volume 2022 (2022)

Analysis of Aerobics Auxiliary Training Based on Deep Learning

Can Li 

Research Article (7 pages), Article ID 9269988, Volume 2022 (2022)

Research on System Economic Operation and Management Based on Deep Learning

Wangtao, Zhenzhu Zheng, Peiyuan Wang, and Xiaobin Liu 

Research Article (10 pages), Article ID 4845014, Volume 2022 (2022)

Analysis of the Coupling and Coordination Relationship between the Evolution of Enterprise Spatial Structure and Economic Development Based on the Deep Learning Model

Lei Wang, Yuan He, and Yao Qi 

Research Article (11 pages), Article ID 6117804, Volume 2022 (2022)


Contents

[Retracted] Analysis and Optimization of Online Music Teaching System Based on Dynamic Model

Miao Miao 

Research Article (9 pages), Article ID 4426555, Volume 2022 (2022)

[Retracted] Influence of Management Efficiency of Sports Equipment in Colleges and Universities Based on the Intelligent Optimization Method

Shuai Wang 


Research Article (8 pages), Article ID 7126743, Volume 2022 (2022)

Construction and Simulation of Market Risk Warning Model Based on Deep Learning

Li Zhao, Yafei Gao , and Dongwei Kang


Research Article (9 pages), Article ID 3863107, Volume 2022 (2022)

The Motor Action Analysis Based on Deep Learning

TianYu Zhang 

Research Article (11 pages), Article ID 9436736, Volume 2022 (2022)

Study on Machine Learning Applications in Ideological and Political Education under the Background of Big Data

Yanjie Li and He Mao 


Research Article (9 pages), Article ID 3317876, Volume 2022 (2022)

E-Commerce Precision Marketing Model Based on Convolutional Neural Network

Xia Liu 


Research Article (11 pages), Article ID 4000171, Volume 2022 (2022)

Agricultural Product Sales Prediction of ICM Neural Network Improvement by Sparse Autoencoder

YingHui Li 


Research Article (11 pages), Article ID 4712351, Volume 2022 (2022)

Research on Aided Judgment of Rural Sports Posture Based on Deep Learning

Hao Guo and Qi Hao 

Research Article (11 pages), Article ID 5916301, Volume 2022 (2022)

Research on Financial Risk Prediction Based on Improved Random Subspace

Yinghui Li 


Research Article (10 pages), Article ID 3406176, Volume 2022 (2022)

Research on Evaluation Model of Music Education Informatization System Based on Machine Learning

Daliang Wang  and Xiaowen Guo

Research Article (12 pages), Article ID 9658735, Volume 2022 (2022)

Implementation of Financial Audited Robot Question and Answer Technology of Feature Processing and Improved Bi-LSTM

Bingru Liu and Qing Zhao 



Research Article (10 pages), Article ID 7213395, Volume 2022 (2022)

The Social Public Issues Analysis Model Based on Deep Learning

Yanqiong Gu  and Jianyong Shi


Research Article (9 pages), Article ID 8676124, Volume 2022 (2022)

Research on 3D Rendering Effect of Marine Bionic Packaging Container Based on Deep Learning and Visualization

Jie Ning , Xiaonan Ren, and Joung Hyung Cho 


Research Article (12 pages), Article ID 7067342, Volume 2022 (2022)

Quality Improvement of College Students' Innovation and Entrepreneurship Education Based on Big Data Analysis under the Background of Cloud Computing

Wenhui Zhang 

Research Article (10 pages), Article ID 8734474, Volume 2022 (2022)

Research on High-Quality Development of Auto Parts Manufacturing Industry Based on Machine Learning Model

Xuchang Yang, Qian Zheng, Yueying Hu, Ronghui Chen , Xuepeng Wang, and Yanan Liu


Research Article (9 pages), Article ID 3659742, Volume 2022 (2022)

Research on Children's Education App Network Transmission Based on 5G Mobile Computing Technology

Mou Tangjuan  and Kim Il-Tae


Research Article (11 pages), Article ID 7781604, Volume 2022 (2022)

Design and Analysis of Chinese-Korean Translation System Based on Deep Transfer Learning

Jun Xu 


Research Article (14 pages), Article ID 8431412, Volume 2022 (2022)

Design and Analysis of Nanchong Sports Public Service Information Platform Based on Multiobjective Optimization

Dujuan Li 


Research Article (13 pages), Article ID 4702493, Volume 2022 (2022)

Automatic Scoring of Spoken Language Based on Basic Deep Learning

Zhong Cheng and Zonghua Wang 

Research Article (14 pages), Article ID 6884637, Volume 2022 (2022)

Analysis of Key Indicators in English Teaching Evaluation Based on Big Data Model

Weili Hou 

Research Article (14 pages), Article ID 1231700, Volume 2022 (2022)


Contents

Research and Implementation of English Grammar Check and Error Correction Based on Deep Learning

Xiuhua Wang and Weixuan Zhong 

Research Article (10 pages), Article ID 4082082, Volume 2022 (2022)

Research on Village Planning and Rural Architectural Design Based on Discrete Dynamic Modeling Technology

Junhang Lin 

Research Article (9 pages), Article ID 9031664, Volume 2022 (2022)

Retraction

Retracted: Analysis of Key Indicators Related to the Teaching of Floral Art Skills Competition Based on Fuzzy Hierarchical Model

Scientific Programming

Received 29 August 2023; Accepted 29 August 2023; Published 30 August 2023

Copyright © 2023 Scientific Programming. This is an open access article distributed under the Creative Commons Attribution License, which permits unrestricted use, distribution, and reproduction in any medium, provided the original work is properly cited.

This article has been retracted by Hindawi following an investigation undertaken by the publisher [1]. This investigation has uncovered evidence of one or more of the following indicators of systematic manipulation of the publication process:

- (1) Discrepancies in scope
- (2) Discrepancies in the description of the research reported
- (3) Discrepancies between the availability of data and the research described
- (4) Inappropriate citations
- (5) Incoherent, meaningless and/or irrelevant content included in the article
- (6) Peer-review manipulation

The presence of these indicators undermines our confidence in the integrity of the article's content and we cannot, therefore, vouch for its reliability. Please note that this notice is intended solely to alert readers that the content of this article is unreliable. We have not investigated whether authors were aware of or involved in the systematic manipulation of the publication process.

Wiley and Hindawi regrets that the usual quality checks did not identify these issues before publication and have since put additional measures in place to safeguard research integrity.

We wish to credit our own Research Integrity and Research Publishing teams and anonymous and named external researchers and research integrity experts for contributing to this investigation.

The corresponding author, as the representative of all authors, has been given the opportunity to register their agreement or disagreement to this retraction. We have kept a record of any response received.

References

- [1] N. Wu and J. Zhou, "Analysis of Key Indicators Related to the Teaching of Floral Art Skills Competition Based on Fuzzy Hierarchical Model," *Scientific Programming*, vol. 2022, Article ID 7765024, 8 pages, 2022.

Retraction

Retracted: Dynamic Correlation between Ozone and Volatile Organic Compounds in the Southeastern Coastal Region

Scientific Programming

Received 29 August 2023; Accepted 29 August 2023; Published 30 August 2023

Copyright © 2023 Scientific Programming. This is an open access article distributed under the Creative Commons Attribution License, which permits unrestricted use, distribution, and reproduction in any medium, provided the original work is properly cited.

This article has been retracted by Hindawi following an investigation undertaken by the publisher [1]. This investigation has uncovered evidence of one or more of the following indicators of systematic manipulation of the publication process:

- (1) Discrepancies in scope
- (2) Discrepancies in the description of the research reported
- (3) Discrepancies between the availability of data and the research described
- (4) Inappropriate citations
- (5) Incoherent, meaningless and/or irrelevant content included in the article
- (6) Peer-review manipulation

The presence of these indicators undermines our confidence in the integrity of the article's content and we cannot, therefore, vouch for its reliability. Please note that this notice is intended solely to alert readers that the content of this article is unreliable. We have not investigated whether authors were aware of or involved in the systematic manipulation of the publication process.

Wiley and Hindawi regrets that the usual quality checks did not identify these issues before publication and have since put additional measures in place to safeguard research integrity.

We wish to credit our own Research Integrity and Research Publishing teams and anonymous and named external researchers and research integrity experts for contributing to this investigation.

The corresponding author, as the representative of all authors, has been given the opportunity to register their agreement or disagreement to this retraction. We have kept a record of any response received.

References

- [1] H. Li and X. Nie, "Dynamic Correlation between Ozone and Volatile Organic Compounds in the Southeastern Coastal Region," *Scientific Programming*, vol. 2022, Article ID 8566454, 9 pages, 2022.

Retraction

Retracted: NSGA-II-Based Microchannel Structure Optimization Problem Study

Scientific Programming

Received 29 August 2023; Accepted 29 August 2023; Published 30 August 2023

Copyright © 2023 Scientific Programming. This is an open access article distributed under the Creative Commons Attribution License, which permits unrestricted use, distribution, and reproduction in any medium, provided the original work is properly cited.

This article has been retracted by Hindawi following an investigation undertaken by the publisher [1]. This investigation has uncovered evidence of one or more of the following indicators of systematic manipulation of the publication process:

- (1) Discrepancies in scope
- (2) Discrepancies in the description of the research reported
- (3) Discrepancies between the availability of data and the research described
- (4) Inappropriate citations
- (5) Incoherent, meaningless and/or irrelevant content included in the article
- (6) Peer-review manipulation

The presence of these indicators undermines our confidence in the integrity of the article's content and we cannot, therefore, vouch for its reliability. Please note that this notice is intended solely to alert readers that the content of this article is unreliable. We have not investigated whether authors were aware of or involved in the systematic manipulation of the publication process.

Wiley and Hindawi regrets that the usual quality checks did not identify these issues before publication and have since put additional measures in place to safeguard research integrity.

We wish to credit our own Research Integrity and Research Publishing teams and anonymous and named external researchers and research integrity experts for contributing to this investigation.

The corresponding author, as the representative of all authors, has been given the opportunity to register their agreement or disagreement to this retraction. We have kept a record of any response received.

References

- [1] L. Wang, "NSGA-II-Based Microchannel Structure Optimization Problem Study," *Scientific Programming*, vol. 2022, Article ID 6368018, 7 pages, 2022.

Retraction

Retracted: Influence of Management Efficiency of Sports Equipment in Colleges and Universities Based on the Intelligent Optimization Method

Scientific Programming

Received 29 August 2023; Accepted 29 August 2023; Published 30 August 2023

Copyright © 2023 Scientific Programming. This is an open access article distributed under the Creative Commons Attribution License, which permits unrestricted use, distribution, and reproduction in any medium, provided the original work is properly cited.

This article has been retracted by Hindawi following an investigation undertaken by the publisher [1]. This investigation has uncovered evidence of one or more of the following indicators of systematic manipulation of the publication process:

- (1) Discrepancies in scope
- (2) Discrepancies in the description of the research reported
- (3) Discrepancies between the availability of data and the research described
- (4) Inappropriate citations
- (5) Incoherent, meaningless and/or irrelevant content included in the article
- (6) Peer-review manipulation

The presence of these indicators undermines our confidence in the integrity of the article's content and we cannot, therefore, vouch for its reliability. Please note that this notice is intended solely to alert readers that the content of this article is unreliable. We have not investigated whether authors were aware of or involved in the systematic manipulation of the publication process.

Wiley and Hindawi regrets that the usual quality checks did not identify these issues before publication and have since put additional measures in place to safeguard research integrity.

We wish to credit our own Research Integrity and Research Publishing teams and anonymous and named external researchers and research integrity experts for contributing to this investigation.

The corresponding author, as the representative of all authors, has been given the opportunity to register their agreement or disagreement to this retraction. We have kept a record of any response received.

References

- [1] S. Wang, "Influence of Management Efficiency of Sports Equipment in Colleges and Universities Based on the Intelligent Optimization Method," *Scientific Programming*, vol. 2022, Article ID 7126743, 8 pages, 2022.

Retraction

Retracted: Analysis and Optimization of Online Music Teaching System Based on Dynamic Model

Scientific Programming

Received 8 August 2023; Accepted 8 August 2023; Published 9 August 2023

Copyright © 2023 Scientific Programming. This is an open access article distributed under the Creative Commons Attribution License, which permits unrestricted use, distribution, and reproduction in any medium, provided the original work is properly cited.

This article has been retracted by Hindawi following an investigation undertaken by the publisher [1]. This investigation has uncovered evidence of one or more of the following indicators of systematic manipulation of the publication process:

- (1) Discrepancies in scope
- (2) Discrepancies in the description of the research reported
- (3) Discrepancies between the availability of data and the research described
- (4) Inappropriate citations
- (5) Incoherent, meaningless and/or irrelevant content included in the article
- (6) Peer-review manipulation

The presence of these indicators undermines our confidence in the integrity of the article's content and we cannot, therefore, vouch for its reliability. Please note that this notice is intended solely to alert readers that the content of this article is unreliable. We have not investigated whether authors were aware of or involved in the systematic manipulation of the publication process.

Wiley and Hindawi regrets that the usual quality checks did not identify these issues before publication and have since put additional measures in place to safeguard research integrity.

We wish to credit our own Research Integrity and Research Publishing teams and anonymous and named external researchers and research integrity experts for contributing to this investigation.

The corresponding author, as the representative of all authors, has been given the opportunity to register their agreement or disagreement to this retraction. We have kept a record of any response received.

References

- [1] M. Miao, "Analysis and Optimization of Online Music Teaching System Based on Dynamic Model," *Scientific Programming*, vol. 2022, Article ID 4426555, 9 pages, 2022.

Research Article

Analysis and Evaluation of Enterprise Performance Appraisal Index Based on Fuzzy AHP Model

Yulin Xia,¹ Xiaoyan Wei ,² and Jian Tang¹

¹The Engineering & Technical College of Chengdu University of Technology, Leshan 614000, China

²School of Economics and Law, University of Science and Technology Liaoning, Anshan 114051, Liaoning, China

Correspondence should be addressed to Xiaoyan Wei; 320083900059@ustl.edu.cn

Received 23 March 2022; Revised 2 June 2022; Accepted 9 June 2022; Published 15 July 2022

Academic Editor: Hangjun Che

Copyright © 2022 Yulin Xia et al. This is an open access article distributed under the Creative Commons Attribution License, which permits unrestricted use, distribution, and reproduction in any medium, provided the original work is properly cited.

The decisive and decision-making challenges of business investment are for the good development of enterprises. In order to have a better market advantage of chemical granules for enterprises, the analytic hierarchy process (AHP) is constructed to analyze the company's performance. Under the environment of state-owned enterprises and foreign enterprises competing for market resources together, building a performance evaluation system suitable for the development stage of the company can adjust the planning strategy and analyze its own disadvantages in time. When analyzing the effective combination of performance appraisal and enterprise development, as well as the effective communication between employees and enterprise managers, feedback information is obtained through the experimental results. Under this analysis condition, this paper describes the feasibility and soundness of the AHP model system for enterprises, and what favorable decision-making methods can be provided for later development. Based on the selection of performance evaluation indicators, AHP analysis can clearly get the weight of each indicator and the correlation between them, in order to improve and build a new system of evaluation indicators. This paper concludes the following: (1) based on the analysis of enterprise performance appraisal indicators, using the AHP model evaluation method to calculate the indicators, the optimized indicators for the performance appraisal of the comprehensive and efficient significantly improved. (2) Comparing the traditional AHP calculation with the optimized model calculation, the results show that under the optimized calculation, the index is more concise and the fluctuation is reduced, which reduces the burden on administrators. (3) In the membership degree of index evaluation grade, the membership degree with an excellent grade is 0.9, which shows that the index plays a very important role in evaluation. (4) According to the development indicators of enterprises in recent years, it is found that the growth rate of resources is growing slowly, the demand for the talent market is still in a stable state as always, and its financial resources have increased by 120% in 2016.

1. Introduction

In today's world, enterprises are undergoing great changes, and various industries are entering the high-end leading market. In the early stage of enterprise development, it is necessary to carry out performance appraisals to meet the requirements of commercial supply and demand, so it is particularly important to choose appropriate and accurate evaluation indicators. Under the experimental research of the analytic hierarchy process, the reasonable and accurate selection of indicators will be the only way for the development of enterprises and security considerations. The economic situation at home and abroad has become

complicated, competition is fierce, and management strengthening, innovation reform, and economic performance are very urgent. Grasping the future development environment of an enterprise is the basic guarantee for the survival of the future market, and a reasonable evaluation of performance from the side is the performance of improving competitiveness. At the present stage of development, who first realizes a complete set of performance system evaluation standards will greatly improve the scientific nature of enterprise operation and management operation. Understand the scientific performance evaluation method, establish a correct, objective, and fair way to judge the economic effect of enterprises, and improve the performance of

enterprises by the AHP classification method, so as to realize the overall economic development. This paper analyzes the relationship between executives and compensation and evaluates whether it is reasonable to evaluate the actual ability of executives by performance appraisal [1]. It discusses the influence of innovative technology on enterprise performance and proves that the improvement of performance will promote the development of innovative enterprises [2]. It puts forward the concept of big data enterprise and discusses it, and studies the relationship between business performance and R&D investment [3]. The capital increment rate of added value is used to measure the performance of enterprises, and the simultaneous equations model is constructed to empirically analyze the effect of compensation incentives and equity incentives for R&D investment managers on high and new technology [4]. It systematically combs the research trends of performance correlation in China and clearly points out three basic characteristics of this research field [5]. Using Poisson fixed-effect model regression method, this paper tests the moderating effect of executives' incentives, innovation investment, and innovation performance, and executives' "dual" capital [6]. It discusses the influence of salary control on R&D activities of state-owned enterprises and reveals the mechanism between them [7]. It is analyzed that motivating employees has a high development effect on the production of enterprises to achieve high performance, and makes financial performance, and operational performance play a full regulatory role [8]. Selecting communication equipment, computer and other electronic equipment manufacturing, pharmaceutical manufacturing, and daily chemical products manufacturing as samples, this paper analyzes the impact of R&D expenditure and advertising expenditure on enterprise economic performance in these three industries [9]. Investment in R & D and personnel incentives will have a good chemical reflection on the innovation performance of enterprises, which is a good development strategy for enterprises [10]. The theoretical model of technological innovation performance is constructed, and regression analysis is used to analyze enterprise resources [11]. Exploring the influence relationship between R&D investment intensity and enterprise value is conducive to promoting enterprises to successfully break through the life cycle limit through R&D strategy [12]. It examines the relationship between executive compensation incentives and enterprise performance and shows that the relationship between them has a significant negative moderating effect [13]. This paper explores the potential mechanism of the impact of venture capital support on enterprise innovation and further analyzes the impact of venture capital support on enterprise innovation investment efficiency [14]. It discusses the mathematical relationship between industry input and output and carries out a linear regression analysis on the relationship between investment and performance of the manufacturing industry in China [15]. In enterprise performance management, usually because of more index systems, in order to correctly evaluate and describe the role of different indicators in enterprise performance management, it is

necessary to carry out a hierarchical analysis of the index system, so as to determine the weight of each index in the different index system. In order to achieve in the enterprise management of some indicators continue to improve the corresponding indicators, and improve the enterprise management system.

2. Fuzzy AHP Model Analysis

2.1. Fuzzy Sets and Membership Functions. It is defined in the region U , and A is a fuzzy subset of the region. For any element in the region, there is a deterministic function, that is,

$$\begin{aligned} f &= UA(x), \\ x &\in [0, 1]. \end{aligned} \quad (1)$$

As a mathematical tool for the analysis of uncertain problems, fuzzy sets usually adopt the method of a comprehensive evaluation to combine quantitative and qualitative analysis.

2.1.1. Analysis of Fuzzy Comprehensive Evaluation Method. In order to combine fuzzy mathematics with realistic evaluation problems and use quantitative methods to evaluate problems, objective index data sets are constructed to determine the membership degree. The specific evaluation steps are as follows:

- (1) The establishment of evaluation object and index set
The index set of evaluation object P is

$$U = \{u_1, u_2, \dots, u_n\}. \quad (2)$$

Where n is the number of evaluation factors and u is the index value.

- (2) Determination of evaluation grade V
Grade function [16] is defined as

$$v = \{v_1, v_2, \dots, v_m\}. \quad (3)$$

M is the number of index grades, and V can select the appropriate evaluation grade, such as

$$V = \{Excellent, Good, Medium, bad\}. \quad (4)$$

- (3) Calculate the weight vector A [17].
Determine the importance of indicators.

$$A = \{a_1, a_2, \dots, a_n\}. \quad (5)$$

A represents indicator weights and satisfies

$$\sum_{i=1}^n a_i = 1. \quad (6)$$

- (4) Establishing fuzzy evaluation matrix R
The evaluation matrix R is obtained by fuzzy evaluation of the evaluation grade V in the U region.

Evaluation matrix [18]:

$$R = \begin{bmatrix} r_{11} & \cdots & r_{1m} \\ \vdots & & \vdots \\ r_{n1} & \cdots & r_{nm} \end{bmatrix}, \quad (7)$$

where R is the evaluation object, which meets the conditions

$$\sum r_{ij} = 1. \quad (8)$$

(5) Comprehensive evaluation index [19]:

The comprehensive result of weight vector A and evaluation matrix R is obtained by fuzzy synthesis algorithm, which is represented by B :

$$B = A \bullet R = \{b_1, b_2, \dots, b_m\}. \quad (9)$$

B is the membership degree under each level, and the comprehensive index is obtained from single-level fuzzy evaluation to multi-level calculation.

(6) The final evaluation result of the experiment.

According to the evaluation score, the final grade is obtained, and the specific steps are as shown in Figure 1.

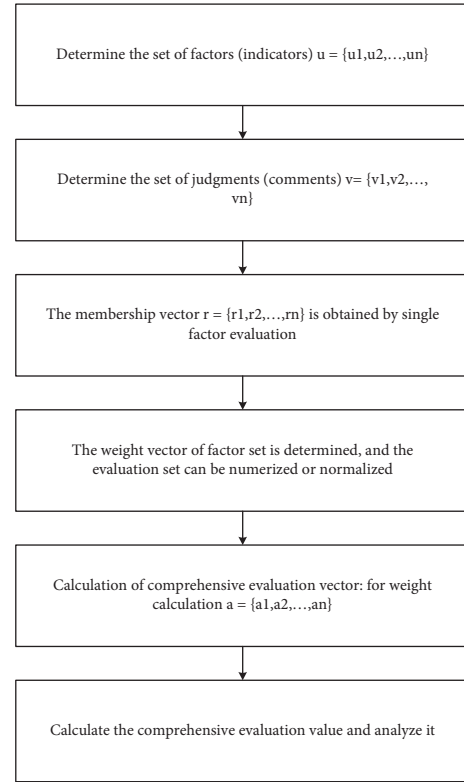


FIGURE 1: Specific steps of fuzzy comprehensive evaluation method.

2.2. An Overview of AHP Theory. Based on quantitative analysis, the model research method of structural decision is constructed. Its main content is the multi-level model construction, through the weight of the proportion of the relationship to achieve comprehensive evaluation. The unique idea of AHP skillfully uses the comprehensive consideration analysis method of modeling, hierarchy, and systematization to realize the evaluation of the total performance weight score of the evaluation object. Test the consistency of evaluation objects and build a judgment matrix, with subjective awareness of identification and judgment, and good evaluation feedback to carry out the next optimization measures.

2.2.1. AHP Construction Steps. AHP (Analytic Hierarchy Process) model is a qualitative and quantitative combination, systematic, hierarchical analysis method. The characteristic of this method is that based on deeply studying the essence, influencing factors, and their internal relations of complex decision-making problems, it makes the thinking process of decision-making mathematized by using less quantitative information, thus providing a simple decision-making method for complex decision-making problems with multiple objectives, multiple criteria or no structural characteristics. It is a model and method for making decisions on complex systems which are difficult to be completely quantified.

Taking the establishment of the company's performance appraisal system as the main purpose, the weight distribution system is obtained by comprehensive consideration and analysis. Therefore, when calculating the weight, AHP

will scientifically realize the weight ranking of the importance of factors at all levels, and effectively obtain the comprehensive specific gravity value under each stage. The basic steps are carried out as shown in Figure 2.

2.2.2. Establish a Hierarchy. Based on the performance evaluation system of the company, the hierarchical index is established, and the decision-making objectives and influencing factors are decomposed into various levels, so as to build the hierarchical structure. The structure diagram of hierarchical analysis according to the development of the enterprise is as follows in Figure 3.

2.2.3. Establishment of Judgment Matrix. In order to establish a complete fuzzy AHP model, a judgment matrix will be further established to judge the importance of index weight, so as to calculate the important score. The judgment matrix is in the following form:

$$B_k = \begin{pmatrix} c_{11} & \cdots & c_{1n} \\ \vdots & \ddots & \vdots \\ c_{m1} & \cdots & c_{mn} \end{pmatrix}. \quad (10)$$

It compares and judges the matrix through the comparison and difference between bid evaluation indicators, and has the following requirements:

The judgment matrix [20] is defined as

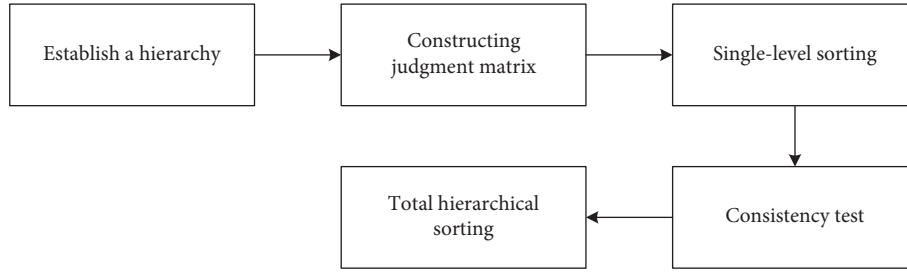


FIGURE 2: Basic construction steps of AHP.

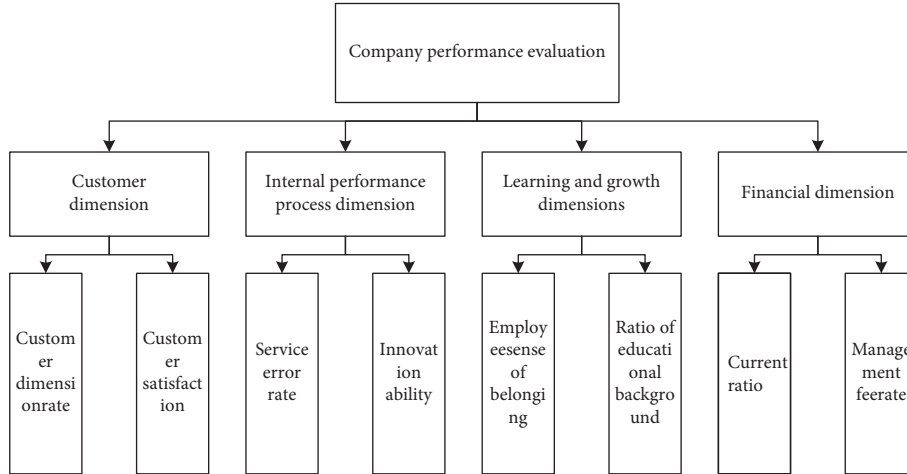


FIGURE 3: Analysis diagram of enterprise hierarchy.

$$\begin{aligned}
 C_{ij} &> 0, \\
 C_{ij} &= \frac{1}{C_{ji}}, \\
 C_{ii} &= 1 \quad (i = 1, 2, \dots, n).
 \end{aligned} \tag{11}$$

The basic theory shows that the greater the value of C_{ij} , the stronger the important correlation between evaluation indexes i and j .

2.2.4. Implementation of Single-Level Sorting

- (1) Calculation of product of influencing elements on each row of the matrix.

$$\bar{W}_i = \left(\prod_{j=1}^n a_{ij} \right)^{1/n} \quad i, j = 1, 2, \dots, n. \tag{12}$$

- (2) Normalization [21]:

$$W_i = \frac{\bar{W}_i}{\sum_{j=1}^n \bar{W}_j}, \quad i, j = 1, 2, \dots, n. \tag{13}$$

$$W^T = [W_1, W_2, \dots, W_n]^T, \tag{14}$$

the eigenvector is obtained.

- (3) Calculate the maximum eigenvalue [22].

$$\lambda_{\max} = \frac{1}{n} \sum_{i=1}^n \frac{\left(\sum_{j=1}^n a_{ij} W_j \right)}{W_i}, \quad i, j = 1, 2, \dots, n, \tag{15}$$

where λ_{\max} is the maximum eigenvalue.

2.2.5. Consistency Test. Calculate the eigenvalue of the matrix [23].

$$\sum_{i=1}^n \lambda_i = n. \tag{16}$$

The condition of the consistency matrix is as follows:

$$\begin{aligned}
 n &= \lambda_{\max}, \\
 \lambda_1 &= \lambda_{\max} > n.
 \end{aligned} \tag{17}$$

When the characteristic roots are 0 and inconsistent, the remaining roots are treated as follows:

Remaining roots [24]:

$$\sum_{i=2}^n \lambda_i = n - \lambda_{\max}. \tag{18}$$

Consistency indicators [25]. That is,

$$CI = \frac{\lambda_{\max} - n}{n - 1}. \quad (19)$$

When $CI=0$, it means that the evaluation indexes are completely consistent, and the smaller it is, the stronger the consistency is

$$CR = \frac{CI}{RI} < 0.1. \quad (20)$$

CR is the ratio of consistency index to RI of the same order, which is called the random consistency ratio.

2.2.6. Total Hierarchical Sorting. The target layer, criterion layer, and index layer will be sorted on the weight, and the final fuzzy index will be formed.

$$W_j = \sum W_i W_j^i. \quad (21)$$

3. Feasibility and Necessity of Enterprise Performance Analysis Based on AHP

3.1. Feasibility Analysis of AHP

3.1.1. Systematicness under the Process. The quantitative analysis of the relationship factors between different levels and the judgment and influence degree of key points is relatively clear. Adhering to the system performance evaluation with multicriteria, multidecision-making, and multiobjective without structural characteristics will make a good start for enterprises in the development process.

3.1.2. The Rapidity and Simplicity of the Method. Analytic Hierarchy Process (AHP) can understand the development of the company under the high depth, optimize the complex company structure in many aspects, and achieve the transformation of dealing with problems and making decisions one by one. It is more convenient and easy for managers to carry out the accurate mathematical calculation and simple solution, and compare the relationships under various influencing factors. Easy to understand the evaluation index so that decision-making managers in the implementation process can quickly and efficiently complete the task so that each employee can understand their own value.

3.1.3. Minimization of Data Information. In order to understand the comprehensive factors that enterprises need to influence employees, facilities, costs, and interests in the decision-making process, an important index analysis is given by adopting hierarchical thinking logic judgment. Considering the actual environment, combined with the cultural literacy of enterprise engineering technology and management concept to enhance the global position of enterprises.

3.2. Necessity Analysis of AHP. Performance evaluation systems and indicators have been used in various fields, including the use of the weighted-average method in calculating the frequency of weights will become more

practical. In order to solve the problem of recursive structure, AHP adopts the qualitative analysis under circumvention to solve the problem of complex structure. Multi-objective and multi-level stage remarkable effect will perfectly improve the defects of the evaluation system and realize the index selection under high dimension. Compared with the traditional performance evaluation methods, the performance evaluation system based on AHP has a substantial promotion effect on the development of enterprises. In the case of evaluating the work efficiency and performance progress among employees, running for excellent employees will select excellent talents as basic equipment for the future development of enterprises. Establish a complete and comprehensive system structure, and the dimension splitting and detailed indicators under the structure are the components of the system.

3.3. Selection Principles of Performance Appraisal Indicators

3.3.1. Objectivity. In the evaluation index selected by enterprises to assess employees, it is necessary to choose according to the company's development concept. There will be special circumstances in the performance appraisal on each node, and the indicators may not be applicable, which cannot achieve the evaluation purpose.

3.3.2. Comprehensiveness. According to the development of each stage and the evaluation of personal emotional factors, the comprehensive index is applied to the assessment to achieve comprehensive evaluation. This is the basic requirement for the fairness and impartiality of performance appraisal. In the face of nonconflicting results, we should make comprehensive and comprehensive selection indicators in everyone's selection. Realize the effectiveness of the evaluation and achieve the purpose of this assessment.

3.3.3. Operability. Therefore, in order to make the indicators convenient for people to carry out, that is, when the operability of indicators is reduced, the performance can be carried out smoothly. For employees, the announcement of assessment results is an incentive to people, and the enthusiasm for the next work will have a great impact.

3.4. Improvement of the Evaluation Method. Under the traditional mode, the assessment methods are mainly subjective and objective. The subjective method is based on the evaluation of the decision-maker's attention to the personnel, while the objective method is based on the assessment method of job performance, difficulty, and weight. Therefore, the reasonable approach is to combine the weight coefficients obtained by different weighting methods and explore the calculation of specific weight values on the effectiveness standard. Considering the objective conditions, considering the correlation between indicators, whether the gap will be difficult to control when the real value is combined with reality, and how to set and improve the methods next.

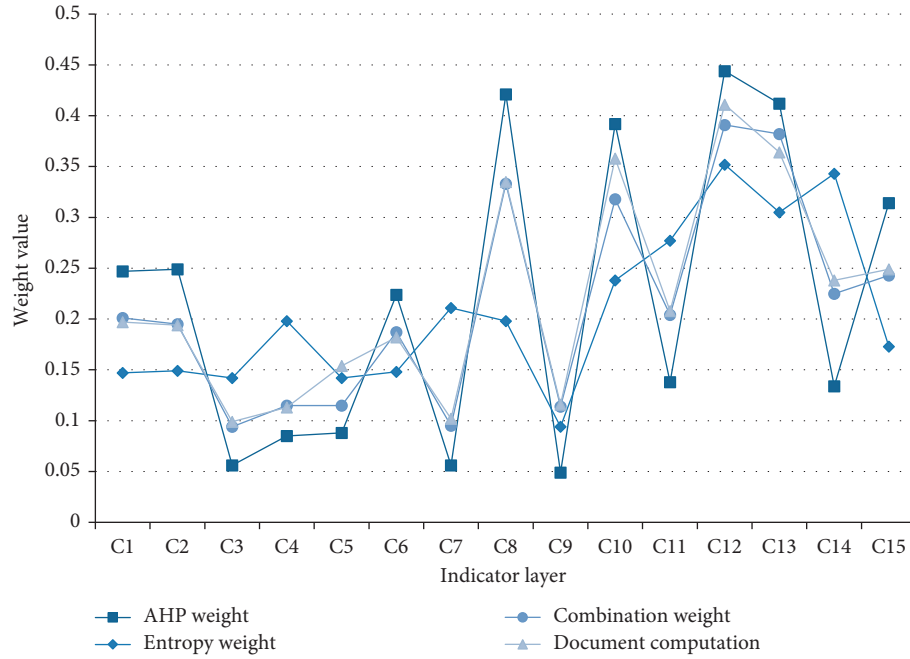


FIGURE 4: Comparison chart underweight calculation results.

3.4.1. Objective Analysis-Entropy Weight Method. Through the early assessment of the problems of enterprises, the AHP model in in-depth analysis and improvement, optimization method will be given according to the importance of the weight of value right. Relevant experts put forward the objective weighting method, which can calculate the weight more accurately, meet the evaluation requirements and ensure the overall utilization rate of index quality. The specific steps are as follows:

- (1) Dimensionless processing of the original matrix.
- (2) Calculate the index weight P_{ij} under the evaluation object:

$$P_{ij} = \frac{x_{ij}}{\sum_{j=1}^n x_{ij}}. \quad (22)$$

- (3) Calculate the entropy of the evaluation index

$$H_i = -k \sum_{j=1}^n p_{ij} \ln p_{ij}. \quad (23)$$

H_i is the index entropy value, k is the constant, and p_{ij} is the weight. When $H_i = 1$, the index will have no effect on this assessment.

- (4) Defining entropy weights

$$u_i = \frac{(1 - H_i)}{[\sum_{i=1}^m (1 - H_i)]}. \quad (24)$$

- (5) The establishment of subjective and objective empowerment.

Combining the judgment matrix and the final weight under the system analysis, subjective and objective weighting

methods under the combination form, will re-establish the weight proportion. The subjective weight of AHP and the objective weight of the entropy weight method are used to calculate the comprehensive weight, and the error is calculated by average distribution.

3.5. Establishment of Evaluation Model. Based on the evaluation system of the company's performance appraisal management, through the comprehensive and operable index standard treatment, and the analytic hierarchy process to calculate the weight of comprehensive indicators. Finally, the fuzzy analytic hierarchy process model is obtained, and its specific evaluation steps are as follows:

- (1) Construct the Enterprise Performance Management Index System based on the principle of selecting the target index by AHP.
- (2) AHP gives subjective weight to the management evaluation index.
- (3) The entropy method is used to weigh the index of management evaluation objectively.
- (4) Subjective and objective weighting to calculate index weights.
- (5) The comprehensive evaluation model is obtained.

4. Guiding Experiment of Fuzzy AHP Model in Enterprise Performance Appraisal

4.1. Calculation Results of Weight Index under Hierarchy. To verify the weight ratio between each level, we get more detailed data sets to build the evaluation index system. The judgment result of index weight is shown in Figure 4.

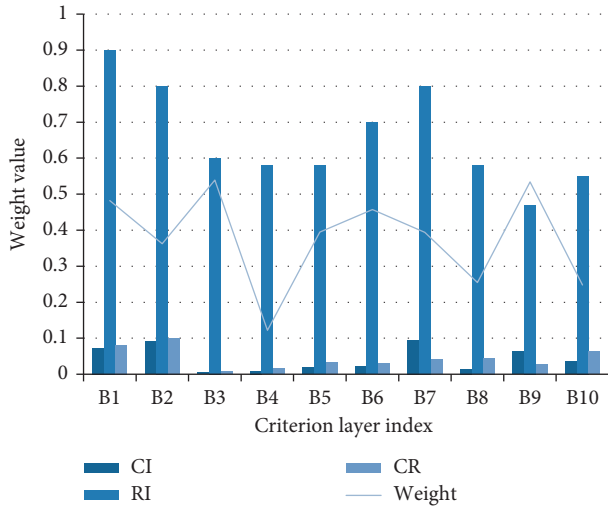


FIGURE 5: Judgment matrix and consistency of development ability.

In Figure 4, the abscissa represents 15 evaluation indexes, and the ordinate represents the weight value of each index. In literature calculation, it is a qualitative analysis method to describe the development trend of the company by using statistical algorithms in mathematical methods to evaluate indexes and forecast methods. According to the weight values under the four calculation results, it is found that the AHP method has an extreme value in weight calculation, and its fluctuation is too strong. Enterprise performance appraisal is mainly a decision-making means for the future development of the company, which is convenient for analysis and optimization. Combination weight and literature calculation are mainly in the central position, which shows that the stability of the two methods in the implementation process is convenient to get the real index weight.

4.2. Judgment Matrix and Consistency Test of Performance Appraisal. According to the current development of enterprises to judge the financial performance at the end of the year, at the same time, build a judgment matrix and carry out consistency test calculation index weight calculation. The resulting diagram is as shown in Figure 5.

It can be seen from the experimental results that when $CR < 0.1$, the development of the enterprise is good. B in the figure represents the criterion layer in the analytic hierarchy process, which is the index of the second layer, aiming at building the consistency test of the judgment matrix.

4.3. Membership Matrix of Performance Evaluation Grade. According to the Membership Matrix of the evaluation grade between each level, it lays a good foundation for the next step to get a fuzzy set, and will combine the practical problems to complete the work perfectly. Its index membership matrix is shown in the following Figure 6.

According to the rating results of membership degree in the figure, the difference in C11 and the excellent membership

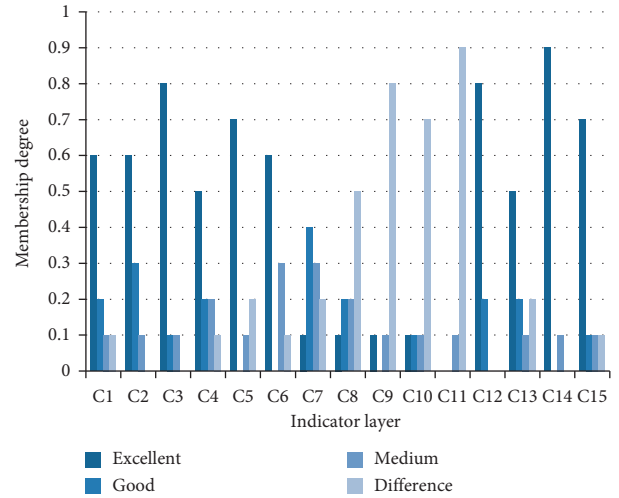


FIGURE 6: Membership matrix of evaluation index.

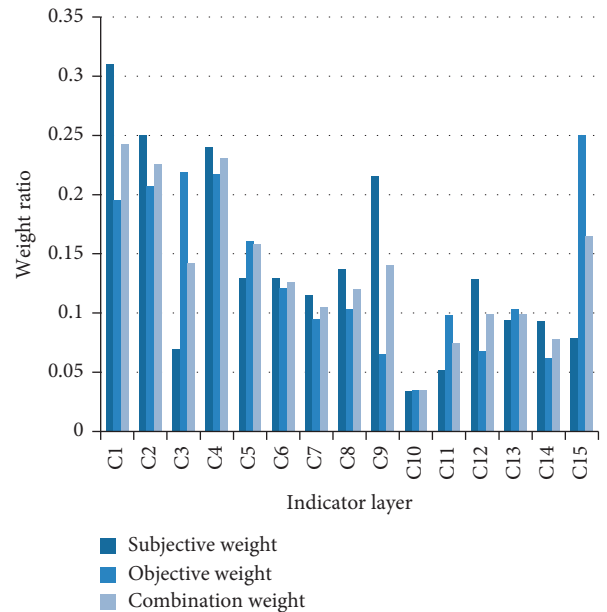


FIGURE 7: Comparison of subjective and objective weights.

degree in C14 are 0.9, which also shows that the index weight under the given level is very high, and the assessment needs to be taken more seriously. When the membership degree of some index layers is 0, it should not be ignored, but should be considered according to the actual situation.

4.4. Fuzzy Comprehensive Index Evaluation. Combined with subjective and objective weight calculation, a fuzzy comprehensive evaluation will reflect the importance of indicators. The analysis results are as shown in Figure 7.

Through the calculation results, we can see that the weight value of subjective weight is obviously higher than that of objective weight, and objective weight cannot reflect part of the weight. The combined weight of this paper is obviously between the two, which can reflect the importance of different indicators.

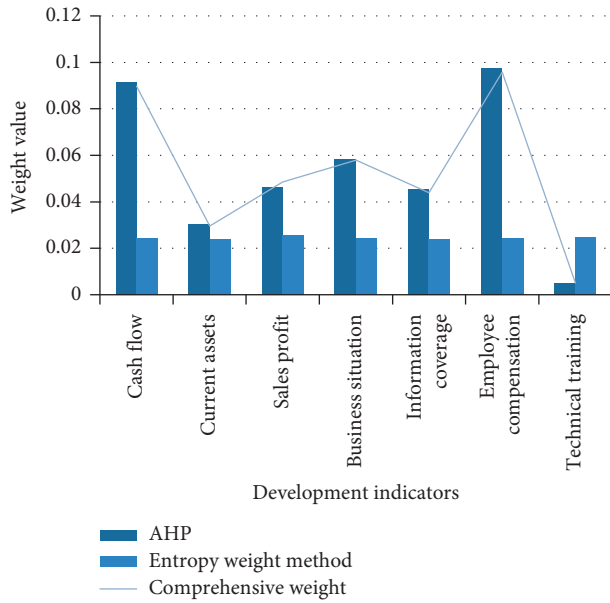


FIGURE 8: Weight result diagram of enterprise development index.

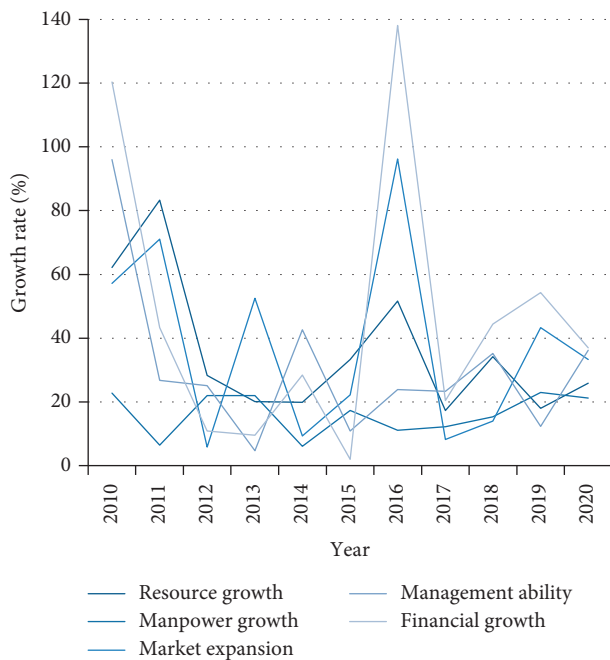


FIGURE 9: AHP calculation of evaluation index growth rate from 2010 to 2020.

4.5. Comprehensive Weight Value of Enterprise Development Index. It is a case study on the transitional stage of an enterprise by taking the actual operation situation, the interests' situation, and the staff training that an enterprise needs to face during its development. The experimental analysis results of income indicators and business indicators are as shown in Figure 8.

At the end of the year and midterm performance, an appraisal is a necessary management means, but the main concern of enterprises is the income situation in that year,

and employees consider salary. That is, in the weight ratio, the employee salary accounts for 0.0976 and the current flow weight ratio of 0.0914. This is also the focus of the company's development and the concept of market survival, which builds a working atmosphere for a good living environment.

4.6. General Analysis of AHP Performance Appraisal. According to the weight calculated by AHP, multiplying the production index of enterprises, we can get the growth of enterprises in various aspects in recent years. The experimental growth rate results are shown in the following figure.

As can be seen from Figure 9. From 2010 to 2020, the resource growth of enterprises is weakening, which is lower than the growth rate of 60%. In 2016, the financial growth increased by 120% compared with 2015, achieving a year of high economic income. There is no obvious fluctuation in the market in terms of personnel training. Based on the level of 15%, recruitment is only carried out according to market demand.

5. Conclusion

In combination with the development of enterprises and the influence of internal and external environmental factors, quantitative and qualitative index analysis of assessment indicators will greatly improve the objectivity and accuracy of indicators. For the imprecision and low performance of some evaluation indexes, the comparison of weights is realized by combining subjective and objective calculation methods (combined weighting method). In the overall evaluation results of the whole enterprise system, calculating the true weight value and getting the total evaluation score will fully explain that new measures will be made in the development stage of the enterprise. The experimental contents are summarized as follows: (1) Under the analysis of the analytic hierarchy process model, the enterprise performance appraisal shows a comprehensive and comprehensive result, and the index combination that is difficult to understand is given a weighting treatment method. (2) Comprehensive weight under the combination of subjective and objective functions, qualitative index analysis is carried out, which greatly improves the accuracy of the analysis. (3) Fuzzy AHP model for the evaluation of enterprise assessment indicators, there is a great gap in the grade, further optimization of the actual use of more convenient. (4) The calculation result of the entropy method is closer to the real weight, which will fully explain that enterprise managers should fully understand the examiners in detail before implementing it.

The deficiency and improvement of the evaluation system are as follows: (1) Fuzzy synthesis method cannot understand the correlation between indicators, which is easy to cause the reuse of information. (2) Judges need to understand the meaning of each index, and choose the index again, so they will reject the index that is not suitable for this assessment. (3) In order to ensure the rational development of efficient information systems, an objective and accurate evaluation must be carried out to achieve a

high-value contribution to system application performance. (4) To improve the accuracy of the weighting method, more in-depth research is needed, including the consideration of emotional factors in the assessment process, which fully reflects the comprehensiveness of evaluation indicators.

Data Availability

The experimental data used to support the findings of this study are available from the corresponding author upon request.

Conflicts of Interest

The authors declared that they have no conflicts of interest regarding this work.

Acknowledgments

This work was sponsored in part by the fund of Sichuan Provincial Department of Education to research and optimize the innovation and entrepreneurship education system (JG2018-930).

References

- [1] L. Wu, J. Fan, and K. Wang, "Private shareholders stationed directors, executive compensation and enterprise performance," *Dong Yue Lun Cong*, vol. 40, no. 01, pp. 143–154, 2019.
- [2] M. Yin, S. Lei, and W. Li, "Executive incentive, innovation investment and corporate performance--an empirical study of different industries from endogenous perspective," *Nankai Management Review*, vol. 21, no. 01, pp. 109–117, 2018.
- [3] T. Zhang and X. Deng, "Research on the relationship between business performance and R&D investment of listed big data enterprises," *Industrial Technology Economics*, vol. 35, no. 09, pp. 77–84, 2016.
- [4] F. Zhou and D. Yang, "Executive incentive, R&D investment and performance of high-tech enterprises: a study based on endogenous perspective," *Journal of Nanjing Audit University*, vol. 16, no. 01, pp. 71–80, 2019.
- [5] W. Zhu and C. Xia, "What is the relationship between R&D investment and enterprise performance Dynamic analysis from domestic research," *Management Modernization*, vol. 37, no. 03, pp. 54–57, 2017.
- [6] H. Sun, X. Sun, D. Huang, L. Wu, and S. Yu, "Cerebral cortex impairment in neuromyelitis optica spectrum disorder: A case report and literature review," *Multiple sclerosis and related disorders*, vol. 32, no. 10, pp. 9–12, 2019.
- [7] J. Shao and J. Diao, "Does salary control inhibit the innovation of state-owned enterprises," *Economic and Management Review*, vol. 36, no. 05, pp. 42–55, 2020.
- [8] X. Qi, W. Wang, and Z. Wu, "Research on the relationship between R&D investment and enterprise performance under the regulation of executive incentives," *Scientific and Technological Progress and Countermeasures*, vol. 33, no. 15, pp. 76–82, 2016.
- [9] Y. Ma, X. Zhang, and Y. Ma, "R&D expenditure, advertising expenditure and enterprise economic performance-an empirical study based on different manufacturing sub-sectors in China," *Journal of Dalian University of Technology*, vol. 36, no. 04, pp. 30–34, 2015.
- [10] W. Ma, Yu Hou, and G. Zhu, "The influence mechanism of R&D investment and personnel incentive on innovation performance-a comparative study based on emerging industries and traditional industries," *Science of Science and Technology Management*, vol. 34, no. 03, pp. 58–68, 2013.
- [11] M. Xing and Li Gu, "The impact of innovation investment on the performance of agricultural enterprises-an empirical test based on A-share agricultural listed companies," *Science and Technology Management Research*, vol. 39, no. 12, pp. 110–116, 2019.
- [12] H. Liu and H. Teng, "Threshold effect of R&D investment on enterprise value based on life cycle," *Scientific Research Management*, vol. 41, no. 01, pp. 193–201, 2020.
- [13] Li Ye and Y. Yan, "Executive compensation incentive, property rights nature and enterprise performance--adjusting effect based on ownership concentration," *Industrial Technology Economics*, vol. 36, no. 09, pp. 85–92, 2017.
- [14] M. Li and T. Yan, "Venture capital, technological innovation and enterprise performance: influencing mechanism and its empirical test," *Scientific research management*, vol. 41, no. 07, pp. 70–78, 2020.
- [15] D. Li, Z. Liao, and H. Cheng, "Research on the nonlinear relationship between industry R&D input and output performance-from the perspective of innovative industry classification," *Industrial Technology Economics*, vol. 32, no. 10, pp. 8–16, 2013.
- [16] Yi Liu, Z. Wang, and L. Yin, "Executive compensation, pay gap and performance of commercial banks," *Journal of Hunan University*, vol. 27, no. 05, pp. 78–83, 2013.
- [17] J. Lv, "Management incentive structure, R&D investment and company value," *Investment Research*, vol. 38, no. 07, pp. 105–118, 2019.
- [18] X. He, "Theoretical research on the relationship among executive incentives, corporate governance and performance," *Science and Technology Management Research*, vol. 33, no. 13, pp. 173–180, 2013.
- [19] W. Jiang and D. Liu, "Research on the relationship between R&D investment, redundant resources and enterprise performance," *Financial Theory and Practice*, vol. 37, no. 05, pp. 57–62, 2016.
- [20] X. Dai and L. Cheng, "Research on threshold effect of R&D investment intensity on enterprise performance," *Science of Science Research*, vol. 31, no. 11, pp. 1708–1716 +1735, 2013.
- [21] J. Shan and K. Wu, "The influence mechanism of enterprise innovation strategy on performance-an empirical analysis based on electronic manufacturing enterprises," *East China Economic Management*, vol. 29, no. 02, pp. 130–135, 2015.
- [22] T. Duan, Xi Zhang, and Yi Hu, "Research on threshold effect between R&D intensity and performance of listed companies in Chinese pharmaceutical manufacturing industry," *Management Review*, vol. 32, no. 09, pp. 142–152, 2020.
- [23] C. Yang and Q. Yi, "The influence of government subsidies on R&D investment and performance of enterprises-an empirical study based on biomedical manufacturing industry," *Research on Science and Technology Management*, vol. 38, no. 01, pp. 40–46, 2018.
- [24] Y. Du, Bo Yan, and J. Chen, "Research on the influence of R&D investment on the business performance of high-tech enterprises," *Scientific and technological progress and countermeasures*, vol. 31, no. 02, pp. 87–92, 2014.
- [25] S. Chen, Z. Zou, and L. Duan, "The impact of technological innovation capability life cycle and R&D investment on enterprise performance," *Scientific and Technological Progress and Countermeasures*, vol. 32, no. 12, pp. 72–78, 2015.

Research Article

Optimization and Allocation Method of Regional Groundwater Pollution Investigation Based on Analytic Hierarchy Process Model

Feng Zhang 

School of Electronic and Information Engineering, Anhui Water Resources and Hydropower Vocational and Technical College, Hefei 231603, China

Correspondence should be addressed to Feng Zhang; zfeng@ahsdx.edu.cn

Received 23 March 2022; Revised 16 May 2022; Accepted 27 May 2022; Published 11 July 2022

Academic Editor: Hangjun Che

Copyright © 2022 Feng Zhang. This is an open access article distributed under the Creative Commons Attribution License, which permits unrestricted use, distribution, and reproduction in any medium, provided the original work is properly cited.

In urban construction, various heavy metals and pollutants have become an important source of urban pollution, and groundwater has become its main pollution object. In order to investigate and analyze the water pollution in the main urban area of HeFei, this article firstly analyzes the whole process through the investigation of groundwater status and characteristics and simulates each step effectively using the analytic hierarchy process (AHP). Then, taking the nine districts of HeFei as the actual investigation site and research object, a systematic and comprehensive investigation and simulation of groundwater pollution in the HeFei area was carried out. The results showed that the weight of chemical pollution is 0.450, environmental factors 0.241, and domestic pollution 0.309 in the target layer of HeFei's main urban area, while the sample distribution weight of each unit was the highest in Baohe District and the lowest in Chaohu City. Finally, the countermeasures for regional water pollution are put forward.

1. Introduction

Groundwater is an indispensable natural water resource for human beings, and it is one of the most important and widely used water resources on Earth. In some rural areas, groundwater is indispensable drinking water for them. However, with the development of industry, the wastewater discharged from industry enters the groundwater, which makes its water quality no longer as good as before. In this case, if people use groundwater again, it will affect their health. Groundwater pollution is becoming more and more serious, which will endanger the ecological environment of nature and, in the long run, the Earth on which human beings depend will be affected, and finally, affect human life. By comparing the number of algae in the water of the Chaohu raw water treatment plant in Hefei in different seasons, it is found that the annual average total number of algae at different sampling points in different seasons at different times is different [1]. The current situation of water

pollution in Dianchi Lake is analyzed, and it is found that there are many reasons for water pollution, including the internal reasons of Dianchi Lake itself and the external man-made reasons. On this basis, suggestions and countermeasures for improving water pollution in Dianchi Lake are put forward, and a series of scientific methods are used to predict the improvement of the water environment by introducing external water and changing the operation mode of the lake [2]. By analyzing the surface subsidence caused by underground coal mining and the serious rupture of bedrock channels [3], it is found that the aquatic ecosystem is polluted by the outflow of heavy metal particles such as iron, manganese, zinc, nickel, strontium, barium, and lithium. Very low dissolved oxygen is usually associated with groundwater upwelling through channel crevices. Aiming at the method of establishing water pollution monitoring stations along the river to control river pollution [4], this article first carefully selects the sampling points, then gives the mathematical expression of the problem and the effective

algorithm to solve the problem, and finally gives the actual data for analysis. Starting from the relationship between the lake and its surrounding land, the most easily polluted aquatic animals of the lake are described [5]. Taking Khazar Lake as an example, the physical and inorganic chemical parameters of water samples from five different depths of nine sampling points are analyzed, and the water quality is determined. According to Karaguzel R' classification, Khazar Lake is identified as Grade I and Grade III water quality. The impact of human factors on the water quality in the Jarvac basin is analyzed. The surface flow and underground flow of the lake were measured, and the main factors affecting the water quality of the Jarvac River Basin were analyzed, which were mainly divided into domestic pollution, industrial pollution, and agricultural pollution [6]. According to the known point source pollution, the sampling points of surface water and groundwater were established for specific analysis. The sampling point method was used to investigate the use of agrochemicals and fertilizers in golf courses. Six drainage samples were taken from three golf courses, and high levels of imipramine and cimipramine were detected, with the highest levels exceeding 8 and 3 g/L, respectively [7]. Through the determination of the content of chromium (Cr) and other metal elements in the soil around an abandoned chromate chemical plant in Hangzhou, it was found that heavy metal particles seriously polluted the groundwater [8]. However, the surface water in the rivers near the abandoned chemical plant is not affected by heavy metal particles, so the concentration of metal particles in different places is different, and the degree of pollution to surface water is also different. Measurements of heavy metal particles in a lake in Nagpur, Maharashtra, India, revealed that the dissolved composition of heavy metal particles was above the range of unpolluted water [9]. Therefore, lead, iron, and zinc are more serious in water pollution. Through the calculation of the water index of each place, the water quality was classified, the heavy metal pollution of soil caused by industrial wastewater was determined, and the water quality model was established to simulate the water quality parameters of Tunggak River. The water quality model was tested using data collected by collecting and analyzing water and soil samples [10]. Using 8 points to investigate the water quality in different areas, it was found that the odor was obvious and the pollution was serious from No. 5 Bridge to No. 15 Bridge of the Yellow River, and the field investigation results were consistent with the micronucleus technology [11]. In total, 48 samples of domestic water sources from 12 communities in the eastern part of Obolo were tested for one year [12], and three pollution indexes, water quality index (WQI), heavy metal evaluation index (HEI), and heavy metal pollution index (HPI), were used to determine the pollution of the water body. The acidification rate of domestic water sources and related factors change with the season. Through the measurement of heavy metal particles in Asa, Agba, Unilorin, and Sobi (Moro) Earth dam water in the central north of Nigeria by atomic absorption spectrophotometry, the trace metal pollution in the surface water of Earth dam was evaluated by metal index (MPI) and metal pollution index. It

is found that the total metal pollution of Pb and Cd is more than 6.0, so the water pollution is more serious by Pb and Cd [13]. Having carried out sampling, bacteriological, physical, and chemical tests on a number of wells in the vicinity of the Behesht-e Zahra cemetery in Tehran, Iran, the results of these tests were then compared with the distance from the bottom of the cemetery to the aquifer, the distance from the cemetery to the water point, the amount of rainfall at the site, the topography and hydrogeology at the site, and the type and structure to analyze the pollution potential of groundwater [14]. This article makes a concrete, effective, and reasonable investigation and analysis of groundwater pollution using the AHP [15]. Groundwater is easy to be polluted. GA, AHP, and FA are used to construct a combination statistical method, and factor analysis is carried out for 32 scenarios. Analytic hierarchy process and genetic algorithm score and weigh all scenes. The results of the study are important for groundwater vulnerability assessment and provide a new reference for groundwater pollution assessment in the future [16].

2. Field Investigation of Regional Groundwater

Regional groundwater field investigation regional groundwater field investigation is an effective way to obtain data and samples, which can more reflect the real situation. If you want to be close to the real situation, you have to carry out the practice, and you have to start to collect the data needed for experiments and research. It mainly includes the following: data preparation, equipment preparation, prior analysis, route determination, and sampling point layout. Preparation in advance is the most basic part of the whole survey, which mainly includes data preparation, equipment preparation, analysis of preparation in advance, determination of route, and layout of sampling points.

2.1. Preparation in Advance. Data preparation: it is mainly for the preparation before field investigation. Good advance data can save manpower cost and time cost. Advance data mainly refer to the investigation background needed in the whole investigation process. Therefore, advance data are the basis of the whole field investigation. Advance data mainly include the following: determination of route, geographical location of unit layer, temperature and rainfall of unit layer, and investigation and research report. The specific data of monographs, papers, and charts are divided into necessary data, unnecessary data, and auxiliary data.

Equipment preparation: the commonly used equipment for water quality detection includes geological compass, steel tape, and altimeter, and the most important equipment is small, fast drilling equipment.

Prior analysis: first of all, read the water quality report and other documents, analyze and judge the distribution characteristics and storage capacity of groundwater in the sampling area, understand and analyze the pollution sources of groundwater, understand and judge the way of groundwater pollution, and divide the groundwater system

TABLE 1: Indicators of groundwater in the affected area.

Target layer	Criterion layer	Index layer	Direction	Unit layer
Unit weight of regional groundwater pollution investigation	Chemical pollution	Contents of mercury, cadmium, lead, arsenic, and other elements	Inverse	Unit layers 1, 2, 3, ..., N
		Organic pesticide content	Inverse	Unit layers 1, 2, 3, ..., N
	Environmental factor	Lithology of main aquifer	Moderate	Unit layers 1, 2, 3, ..., N
		The measure of area	Just	Unit layers 1, 2, 3, ..., N
		Population	Inverse	Unit layers 1, 2, 3, ..., N
	Domestic pollution	Domestic sewage	Inverse	Unit layers 1, 2, 3, ..., N
		Domestic garbage	Inverse	Unit layers 1, 2, 3, ..., N

in the investigation area into several or even more than ten investigation units.

Determine the layout of routes and sampling points. Find the map and other data in advance, determine the sampling route, and determine a route to save cost, time, manpower, and financial resources.

2.2. Using AHP to Determine the Number of Survey Points in the Unit. Three factors should be considered in the distribution of groundwater samples: chemical, industrial, and living factors.

Step 1. Select statistical indicators and establish an index system.

The selection of statistical indicators needs to consider its systematicness, comprehensiveness, and continuity; that is, there must be a certain logical relationship, comprehensiveness, and hierarchy between indicators. This analysis is divided into four levels: target layer, criterion layer, index layer, and unit level.

Target layer: it is the weight of the regional groundwater pollution investigation unit.

Standard layer: it is composed of chemical pollution, environmental factors, and life pollution.

Chemical pollution: chemical pollution will change the pH of the water body, change the living environment of groundwater organisms, and even some chemical pollutants are toxic, which will affect the ecosystem of groundwater, thus affecting the quality of groundwater.

Environmental factors: different environments have different groundwater-specific conditions.

Domestic pollution: if the garbage produced in life is not properly disposed of, it will pollute the quality of groundwater.

Index layer: the content of elements such as mercury, cadmium, lead and arsenic (E), organic pesticide content (G), lithology of main aquifer (H), area (M), population (R), domestic sewage (K), and domestic waste (L). These factors will have different effects on groundwater quality. The higher the content of mercury, cadmium, lead, and arsenic, the higher the content of organic pesticides, the more serious the

pollution of groundwater. Unit layer: it is composed of unit layer 1 and unit layer 2. All layers are listed in Table 1.

“Direction” represents the extent to which pollution can be recovered. Unit layer N is different target requirements under different indicators, which is mainly manifested in the index coefficients of index layers under different first-level indicators and second-level indicators, which can fully reflect the composition of the next-level indicators of the index layer and comprehensively construct the comprehensive evaluation of the index layer.

Step 2. Compare the indicators in pairs and construct the judgment matrix.

When index a is more important than index B , it is assigned to 9; when index a is more important than index B , it is assigned to 7; when indicator a is more important than indicator B , it is assigned to 5. When indicator a is slightly more important than indicator B , it is assigned to 3; when index a is as important as index B , it is assigned to 1; when index a is less important than index B , 1/9 is allocated; when indicator a is stronger and less important than indicator B , allocate 1/7; when index a is less important than index B , it is assigned 1/5; when indicator a is slightly less important than indicator B , 1/3 is allocated.

The index importance assignment is shown in Table 2.

The judgment matrix A is constructed according to the index degree assignment table above.

Step 3. Calculate the weight of each index in the index layer

The row vectors of the judgment matrix are geometrically averaged and then normalized. Finally, the weight of each index and the eigenvector W are obtained. The geometric mean is normalized by multiplying each line of the judgment matrix by the n th power of each element.

Judgment matrix is

$$A = \begin{pmatrix} a_{11} & \cdots & a_{1n} \\ a_{21} & & a_{2n} \\ \vdots & & \vdots \\ a_{n1} & \cdots & a_{nn} \end{pmatrix}. \tag{1}$$

TABLE 2: Index importance assignment.

Importance	Assignment	Importance	Assignment
Extremely important	9	Extremely unimportant	1/9
Strongly important	7	Intensity does not matter	1/7
Important	5	Unimportance	1/5
A little more important	3	It does not matter a bit	1/3
Just as important	1		

We have

$$\prod a_{mn} = \begin{Bmatrix} a_{12} * a_{12} * a_{13} * \dots * a_{1n} \\ a_{22} * a_{22} * a_{23} * \dots * a_{2n} \\ \vdots \\ a_{n2} * a_{n2} * a_{n3} * \dots * a_{nn} \end{Bmatrix} = \begin{Bmatrix} B_1 \\ B_2 \\ \vdots \\ B_n \end{Bmatrix}. \quad (2)$$

Every element to the nth power is

$$\sqrt[n]{B} = \begin{Bmatrix} \sqrt[n]{B_1} \\ \sqrt[n]{B_2} \\ \vdots \\ \sqrt[n]{B_n} \end{Bmatrix} = \bar{w}_i. \quad (3)$$

Moreover, W_i is defined as

$$W_i = \frac{\bar{W}_i}{\sum_{i=1}^n \bar{W}_i},$$

$$w = \begin{Bmatrix} W_1 \\ W_2 \\ \cdot \\ \cdot \\ \cdot \\ W_n \end{Bmatrix}. \quad (4)$$

In formula (4), it is more convenient and more accurate to calculate the correlation adjustment coefficient. It can reflect the application of the weight coefficient more objectively and fairly.

The geometric mean is normalized to get the weight.

Step 4. Conduct the consistency test.

In order to avoid the logical contradiction between indicators, it is necessary to test the consistency of judgment matrix A. The test first calculates the maximum eigenvalue of the judgment matrix λ_{\max} ; then C_i and C_r were calculated.

Matrix A judges the matrix of index w and weight of each index in the index layer:

$$\lambda_{\max} = \frac{1}{n} \sum_{i=1}^n \frac{(AW_i)}{W_i},$$

$$C_i = \frac{(\lambda_{\max} - n)}{(n - 1)}, \quad (5)$$

$$C_r = \frac{C_i}{R_i},$$

where R_i is defined in Table 3.

Generally, when C_r is less than 0.1, the consistency test of the judgment matrix is considered to pass; otherwise, it will not be passed.

Step 5. Unit reselection priority method

According to the relatively important weight of each index, the impact of each index on groundwater pollution can be known, and the distribution weight of each unit can be determined. Combined with the total workload, the number of samples allocated by each unit can be calculated, and the results can be used.

To determine the number of measurement points in the unit, the following measures were taken:

- (1) Regional control takes the groundwater as different samples collected in the upper, middle, and lower reaches. The characteristics of groundwater in different regions are different, and the collected index data are also different. Therefore, the targeted collection is adopted according to the information that can be provided by different regions. The upper reaches are sparsely populated, and two samples of lithology and area are mainly collected; in the areas with strong human activities in the middle and lower reaches, chemical pollution and domestic pollution control are the main control measures, and the samples with E, G, R, K, L, and other indicators are the main ones.
- (2) : Conditional possibilitythe collectability, data contrast, background possibility, pollution index, and importance of water quality should be considered when collecting samples. In the process of collecting data, we should make use of the data prepared before.
- (3) Field investigation: according to the design scheme of the survey, the effective means of transportation, sampling tools, and field topographic map are used to carry out the field survey. Field investigation is to collect the data and other effective information needed in the experiment and research, and then according to this information, it is combined with the specific steps of AHP for specific analysis.

Well flushing is an important part of sampling. There are certain pollutants in the monitoring well. These pollutants will affect the results of groundwater measurement. In order to ensure the authenticity and integrity of the collected information, well flushing will be carried out before sampling.

TABLE 3: Average random consistency index of orders 1–15.

n	1	2	3	4	5	6	7	8	9	10	11	12	13	14	15
R_i	0	0	0.58	0.90	1.12	1.24	1.32	1.41	1.46	1.49	1.52	1.54	1.56	1.58	1.59



FIGURE 1: Geographical location of HeFei’s main urban area.

After completion of well flushing, samples can be taken. The principle of sample integrity should be followed when sampling, and false report, fabrication, and omission of data are not allowed.

3. Application Examples

AHP introduced in this article has been effectively used in the groundwater of HeFei. Now, taking the groundwater of various districts in the main city of HeFei as an example, the specific application of this method is introduced.

3.1. Selection of the Sample Collection Area. The main urban areas of HeFei were Changfeng County, Feidong County, Luyang District, Yaohai District, Shushan District, Baohe District, Feixi County, Chaohu City, and Lujiang County. The survey area is about 11,445 square kilometers. In total, 130 groups of chemical samples are planned to be arranged in this investigation. The structure of the groundwater

distribution model in the main urban area of HeFei is shown in Figure 1.

The distribution structure of groundwater in HeFei’s main city area is shown in Table 4.

The calculation of target level index weight because the target level includes too large a range, leading to the weight of the indicators of this level cannot be quantified, can only be given artificial weight, that is, only qualitative comparison, so the index scale method is used for valuation, and the subsequent process can be carried out after the indicators of the first level are weighted. The relative important weight values of the target layer can be obtained through the index scale are shown in Table 5.

$$W^T \geq \{0.21, 0.13, 0.202, 0.123, 0.101, 0.102, 0.122\}. \quad (6)$$

In Table 5, the weight coefficients of the first-class index and the second-class index are used to see their index relationship.

The judgment matrix of different regions in HeFei is shown in Table 6.

TABLE 4: Distribution structure of groundwater in HeFei’s main city area.

Target level	Allocation weight of urban units in HeFei
Standard level	Chemical pollution, environmental factors, and domestic pollution
Indicator layer	Content of mercury, cadmium, lead, zinc, and other elements and content of organic pesticide, main lithology of aquiclude, area, population, domestic sewage, and domestic garbage
Unit level	Changfeng County, Feidong County, Luyang District, Yaohai District, Shushan District, Baohe District, Feixi County, Chaohu City, and Lujiang Count

TABLE 5: Weight of the target layer and indicator layer.

Target layer	Value	Indicator layer	Value
Chemical pollution	0.350	Chemical element content	0.210
		Organic pesticide content	0.130
Environmental factor	0.202	Aquifer lithology	0.202
		Area	0.123
Domestic pollution	0.448	Population	0.101
		Domestic sewage	0.102
		Domestic garbage	0.122

TABLE 6: The judgment matrix of different regions in HeFei.

Index	Changfeng	Feidong	Luyang	Yaohai	Shushan	Baohe	Feixi	Chaohu	Lujiang
Changfeng	1	3	5	3	1/3	1/7	9	1/9	5
Feidong	1/3	1	7	5	3	1/9	5	7	3
Luyang	1/5	1/7	1	3	1/3	5	3	1/7	9
Yaohai	1/3	1/5	1/3	1	3	7	5	9	3
Shushan	3	1/3	3	1/3	1	9	3	7	5
Baohe	7	9	1/5	1/7	1/9	1	5	3	1
Feixi	1/9	1/5	1/3	1/5	1/3	1/5	1	3	5
Chaohu	9	1/7	7	1/9	1/7	1/3	1/3	1	7
Lujiang	1/5	1/3	1/9	1/3	1/5	1	1/5	1/7	1

TABLE 7: Weight judgment matrix of the criteria layer and element layer.

Index	e (mg/L)	g (mg/L)	h /class	m (km ²)	r (ten thousand)	k (L)	l (kg)
Changfeng	0.23	0.09	0.15	0.07	0.06	0.12	0.09
Feidong	0.101	0.08	0.09	0.07	0.08	0.11	0.10
Luyang	0.08	0.102	0.11	0.09	0.13	0.09	0.15
Yaohai	0.17	0.11	0.08	0.14	0.12	0.08	0.21
Shushan	0.06	0.13	0.11	0.16	0.07	0.07	0.13
Baohe	0.07	0.08	0.12	0.10	0.13	0.14	0.09
Feixi	0.05	0.07	0.09	0.103	0.14	0.12	0.08
Chaohu	0.06	0.14	0.10	0.12	0.09	0.15	0.09
Lujiang	0.18	0.27	0.15	0.147	0.18	0.12	0.06

In Table 6, the pairwise comparison of the importance among the nine districts of HeFei’s main city reflects the importance among different urban areas.

After matrix operation, the maximum characteristic root vector is (0.23, 0.101, 0.08, 0.17, 0.06, 0.07, 0.05, 0.06, 0.18) to find $CR = 0.021$, so the matrix passes the consistency test. Similarly, the characteristic root vector of other indexes can be calculated, and the weight judgment matrix of the criterion layer element layer can be obtained in Table 7.

Finally, the total weights of each region are distributed as a whole, as shown in Figure 2.

The sampling quantity in the main urban area of HeFei is shown in Figure 3.

In Figure 3, the number of samples in the main urban area of HeFei is explained. The sample size is studied in this article, and the number is relatively sufficient. Therefore, the number and range of samples used in this article can fully reflect the application requirements in this article.

The regional density of HeFei sampling is shown in Figure 4.

4. Consequences of Regional Water Pollution

Groundwater pollution will lead to a decrease in soil quality, thus affecting crops, affecting the activity of underground organisms, resulting in changes in the biological system, and

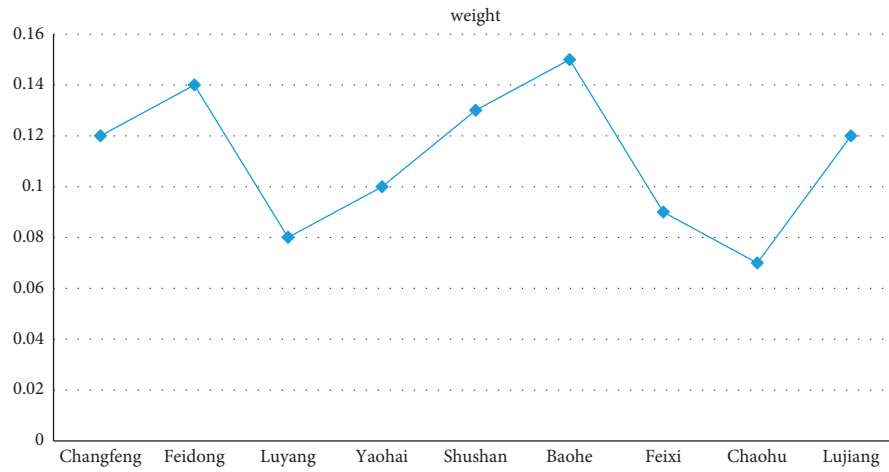


FIGURE 2: Regional total weight distribution.

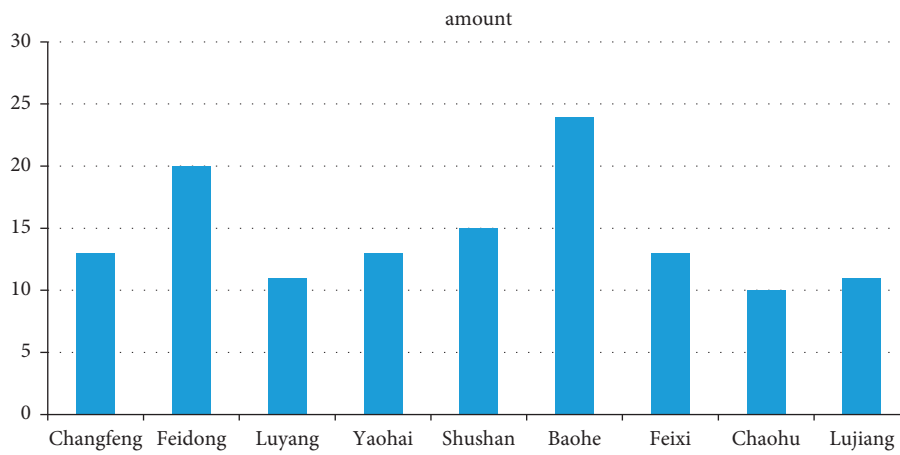


FIGURE 3: Number of regional samples.

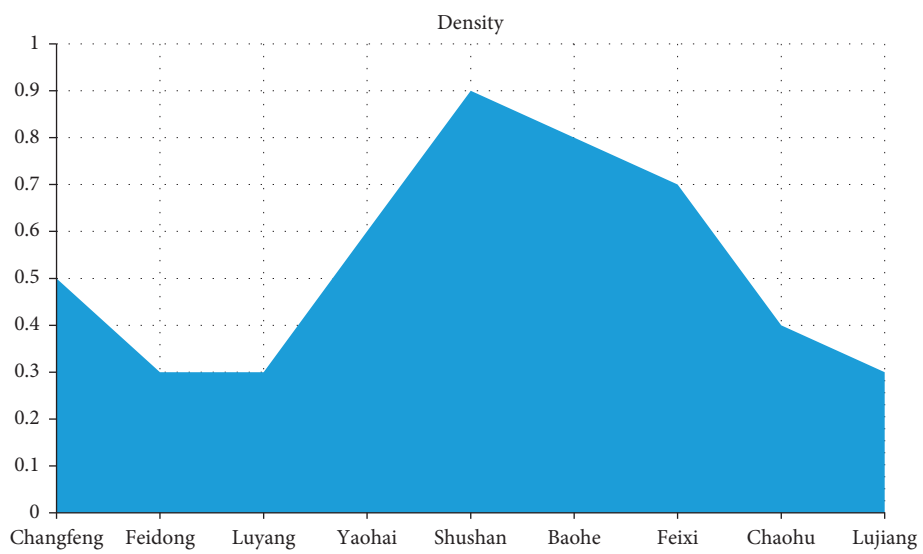


FIGURE 4: Regional density.

most importantly, affecting human health, resulting in a series of diseases. Thus, the quality of the soil is affected. After the groundwater is polluted, the pollutants in the water penetrate the soil and the soil is also polluted, resulting in a significant decrease in grain output. Every year, due to soil pollution, China's grain output decreases by an unlimited number, resulting in heavy losses for the country. The GDP of the country and the governments in various regions decreases to varying degrees, affecting the biological system in groundwater. Long-term pollution of groundwater will cause changes in the pH value of water. As a result, the acidity of water will increase, which will directly affect the living environment of aquatic organisms, affect their activities, and even cause their extinction. At the same time, a large number of bacteria will be produced in the polluted underground water, thus affecting the original biological system. Affected by class, after the groundwater is polluted, there are some carcinogens in the water.

Groundwater pollution will affect human health, so it is very important to control and prevent groundwater pollution. The prevention and control of groundwater should increase the investment in capital and manpower, and continue to carry out relevant research, so as to find more effective treatment methods, and avoid increasing from the source, discovery, protection, and water pollution in other areas.

4.1. Reducing the Generation and Discharge of Pollutants from the Source. Controlling pollutants from the source is the most effective way to prevent groundwater from being polluted. Before enterprises discharge sewage and waste gas, they should be treated to meet the standards before discharging. At present, China attaches great importance to groundwater pollution and other environmental pollution and has actively taken measures to solve this problem.

4.2. Strengthening Underground Water Testing. The pollutant detection equipment mainly includes acid detector, water pollution detector, and dynamic detector, which regularly detects the quality of underground water, analyzes and judges whether each indicator exceeds the standard, and records each detection.

4.3. Strengthening Publicity and Education. Recognize the vital importance of underground water to human life, let the masses supervise each other, reduce the harm of domestic pollution factors to underground water, and minimize the pollution of underground water. Promote the dissemination of knowledge related to the protection of underground water and improve the influence of education policies through the use of big data and information technology.

4.4. Optimization of Water Pollution Prevention and Control Technology. Improve science and technology and optimize filtration and separation technology so that groundwater has the opportunity to play a new role. Filtration and separation technology can be used for membrane filtration, primary filtration, microfiltration, and particle filtration, and

separation operations are carried out according to different pollution levels and different filtration requirements. The polluted groundwater can be effectively purified, and then the polluted groundwater can be reused for the benefit of humankind.

4.5. The Government Has Taken Measures. In the face of serious underground water pollution and serious harm of underground water, governments at all levels should take corresponding measures to control and prevent underground water pollution. They should recognize the seriousness of underground water pollution and take measures in a timely manner so that the underground water pollution will be effectively controlled and will not continue to bring harm to human life.

5. Conclusion

In this article, the present situation of groundwater is analyzed from the degree and area of groundwater pollution and sustainability, and the characteristics of groundwater are analyzed from the aspects of concealment and irreversibility. Then, the relative importance of each index calculated by the AHP, combined with the total amount of work, determines the number of samples that each unit should take, followed by an on-site investigation, and then analyzes the harm of underground water pollution from the aspects of soil properties, human life, and ecosystem. Finally, reasonable suggestions are put forward to solve the underground water pollution, including reducing the generation and discharge of pollutants from the source, strengthening the underground water detection, strengthening publicity and education, optimizing the water pollution prevention and control technology, and taking measures by the government. After further research work, considering more pollution sources in the main urban area of HeFei, an AHP analysis is carried out, and other methods are comprehensively analyzed to compare whether there is a similarity in the results. At present, there are still some difficulties in obtaining the number of pollution sources, and there are many problems in data sampling and analysis. Finally, the collaboration between relevant parts is important to solving data problems together, and data processing and analysis methods should be better adopted for application.

Data Availability

The experimental data used to support the findings of this study are available from the author upon request.

Conflicts of Interest

The author declares that they have no conflicts of interest regarding this work.

Acknowledgments

This work was supported by the Research and Practice of Water Quality Monitoring and Pre-Warning System for

Drinking Water Source of Dongpu and Dafangying Reservoir. This work was sponsored by the Provincial National Science Research Project of Colleges and Universities of Anhui Province (KJ2014A094).

References

- [1] Y. Zhao and Z. Q. Wang, "Investigation on water pollution by algae at locations of water collection in Chaohu lake," *Journal of Environment and Health*, vol. 19, no. 4, pp. 316–318, 2002.
- [2] M. A. Wei, L. I. Jin-Xiu, and X. R. Tian, "Investigation on countermeasures for water environment management and water pollution prevention in Dianchi Lake," *Journal of China Institute of Water Resources and Hydropower Research*, vol. 25, 2007.
- [3] K. Morrison, J. Reynolds, and I. A. Wright, "Underground coal mining and subsidence, channel fracturing and water pollution: a five-year investigation," in *Proceedings of the 9th Australian Stream Management Conference*, Hobart, Australia, August 2018.
- [4] L. J. Alvarez-Vázquez, A. Martínez, M. E. Vázquez-Méndez, and M. Vilar, "Optimal location of sampling points for river pollution control," *Mathematics and Computers in Simulation*, vol. 71, no. 2, pp. 149–160, 2006.
- [5] A. nlü, F. oban, and M. S. Tun, "Investigation of Lake Hazar water quality according to physical and inorganic chemical parameters," *Environmental Earth Sciences*, vol. 23, 2008.
- [6] I. I. Soyaslan and R. Karaguezel, "Investigation of water pollution in the yalvac basn into egirdir lake, Turkey," *Environmental Geology and Water Sciences*, vol. 23, 2008.
- [7] S. Tomimori, Y. Nagaya, and T. Taniyama, "Water pollution caused by agricultural chemicals and fertilizers in the drainage from golf links," *Japanese Journal of Crop Science*, vol. 63, no. 3, pp. 442–451, 1994.
- [8] L. Zou, S. Wang, L. Liu, M. Z. Hashmi, X. Tang, and J. Shi, "Multi-element pollution in soil, ground and surface water from abandoned chromate chemical plants: a case study in Hangzhou, China," *Environmental Earth Sciences*, vol. 74, no. 4, pp. 2861–2870, 2015.
- [9] P. J. Puri, M. Yenkie, S. P. Sangal, and S U. Meshram, "Study regarding lake water pollution with heavy metals in Nagpur city (India)," *International Journal of Chemical, Environmental and Pharmaceutical Research Pharmaceutical Research*, vol. 2, no. 1, pp. 34–39, 2011.
- [10] H. M. Amjed, *Assessment of Industrial Pollution and Water Quality index of Tunggak River at Gebeng Pahang*, Malaysia, 2014.
- [11] P. Liu and L. I. Xue-Ping, "Application of micronucleus technique in monitoring of water pollution in xinli river," *Bulletin of Soil and Water Conservation*, vol. 24, 2014.
- [12] I. A. Igbemi, I. L. Nwaogazie, and O. Akaranta, "Water quality assessment by pollution indices in eastern Obolo coastline communities of Nigeria," *American Journal of Water Resources*, vol. 7, no. 3, pp. 111–120, 2019.
- [13] C. O. Ogunkunle, K. Mustapha, S. Oyedeji, and P. O. Fatoba, "Assessment of metallic pollution status of surface water and aquatic macrophytes of earthen dams in Ilorin, north-central of Nigeria as indicators of environmental health," *Journal of King Saud University Science*, vol. 28, no. 4, pp. 324–331, 2016.
- [14] S. K. Pour and S. M. Khezri, "Assessing the groundwater resources pollution potential by Beheshte Zahra Cemetery," in *Proceedings of the Chemistry and Chemical Engineering (ICCCCE), 2010 International Conference on*, September 2010.
- [15] J. T. Zheng, Y. E. Cheng-Ming, and J. Z. Wang, "Design of inertial sampling pump for investigation on groundwater pollution," *Exploration Engineering*, vol. 30, 2010.
- [16] Y. N. Gharakezloo, M. R. Nikoo, A. Karimi-Jashni, and M. G. Mooselu, "A hybrid statistical decision-making optimization approach for groundwater vulnerability considering uncertainty," *Environmental Science and Pollution Research*, vol. 29, no. 6, pp. 8597–8612, 2021.

Research Article

Engineering Cost Prediction Model Based on DNN

Bingxin Li , Quanying Xin, and Lixin Zhang

College of Urban Construction, Hebei Normal University of Science & Technology, Qin Huangdao 066004, China

Correspondence should be addressed to Bingxin Li; lbx2237@hevttc.edu.cn

Received 11 March 2022; Revised 13 May 2022; Accepted 30 May 2022; Published 6 July 2022

Academic Editor: Man Fai Leung

Copyright © 2022 Bingxin Li et al. This is an open access article distributed under the Creative Commons Attribution License, which permits unrestricted use, distribution, and reproduction in any medium, provided the original work is properly cited.

A DNN-based cost prediction method is proposed for the difficult problem of cost calculation in engineering cost accounting, combined with deep neural networks. Firstly, we introduce the basic information of artificial neural network and select the DNN structure to calculate the engineering cost price according to the characteristics of the data related to engineering cost price. Secondly, the DNN-based engineering cost price prediction model is constructed, and the two types of index systems, engineering characteristics and list item characteristics, are used as model inputs. In addition, the total quotation and each subitem engineering quotation and tax are used as model outputs by analyzing previous relevant studies. Based on this, simulation experiments are conducted on the DNN-based engineering cost price prediction model, and it is concluded from the training model that the DNN model has a better prediction effect. Among them, the relative error of total price forecast by DNN is 4.203%, and the relative error of integrated unit prices V1 and V2 is 2.98% and 4.52%, respectively, with small relative error. Finally, by reasonably adjusting the integrated unit price, the cost price of the integrated unit price and the cost price of the total offer can be calculated.

1. Introduction

In recent years, with the continuous improvement of China's economic level and comprehensive national power, construction projects have been developing, and more and more construction enterprises have been born. The surge of construction enterprises brings great pressure and challenges to the construction engineering market, and it is increasingly difficult for construction engineering to gain a foothold in the market and continue to grow and develop. With the slowdown of economic development, construction enterprises should enhance their competitiveness and base themselves on domestic and international markets. The primary task is to reduce the project cost scientifically. The cost of the enterprise is controlled within a reasonable plan to maximize the profit of the enterprise. Therefore, cost forecasting for construction enterprises is an inevitable trend in the current construction industry and is an extremely important task. However, most of the engineering cost forecasting methods on the market at present have problems such as unscientific methods and uncritical processes, which cannot effectively improve the competitiveness of enterprises and are not conducive to the long-

term development of construction enterprises [1–7]. In this regard, Xu et al. proposed to use BP neural network to predict the project cost of substation and introduced sparrow search algorithm (SSA) to optimize the parameters of traditional BP algorithm. The results show that this method has high prediction accuracy. Sharqi and Bhattarai compared several machine learning algorithms such as ELM and PLS and used them to predict the cost of field channels. The results show that the SC model has great potential. Xiaodong et al. used SIMCA-P algorithm to predict the cost of dynamic real estate projects. The results show that the average error of prediction is 0.006582346, showing high accuracy. However, the above methods mainly use the traditional machine learning algorithm.

Based on this research, a DNN-based engineering cost price prediction model is constructed by combining the widely used deep learning and giving full play to its learning and classification characteristics. Through this model, the accurate prediction and classification of construction project cost are realized. It provides a scientific and effective cost prediction method for the construction industry, which has a certain practical significance. The deep learning algorithm

to predict the project cost is also an innovation of this paper, giving full play to the characteristics of deep learning and improving the accuracy of prediction.

2. DNN

Compared with other neural network structures, the main feature of DNN is its excellent nonlinear processing capability. Thanks to the compact and efficient nonlinear mapping structure, DNN can handle mathematical and physical problems with larger datasets and more complex features. In addition, DNN can take full advantage of its own multiple hidden layer structure to train a large amount of data, and generally the accuracy of the results used for prediction will be higher. More layers indicate a more complex model, which has better nonlinear characteristics and can learn richer features. Theoretically, the links between the layers of the network structure are fully linked and the neurons of each layer can also be connected to each other [8–11]. Therefore, combined with experience, DNN is selected. The neural network structure of DNN is shown in Figure 1, which contains multiple hidden layers, an input layer, and an output layer.

As can be seen from the above figure, the DNN structure mainly consists of an input layer, a hidden layer, and an output layer. The network is characterized by the inclusion of multiple implicit layers. The input layer is represented as $X = [x_1, x_2, x_n]$, which is an n -dimensional column vector. The input data can be wind power, wind speed, wind direction, temperature, etc. In the input layer, the activation function is the standard constant function, and the input quantity needs to be transformed by the standard constant function and then output to the first layer. (w_n, b_n) denotes the weight parameter w_n for the n implied layers and the threshold parameter b_n . The data in the hidden layer are derived from the input of the upper layer. After nonlinear processing of the input variables using the activation function of this layer, the output of the processed data is then passed to the lower layer, and the final output combined with y is obtained, which is the value of wind power to be predicted.

The DNN can be expressed as follows [12–15].

The output value after the data into the classification water processing is transferred to the hidden layer using the input layer, and the first relationship of hidden layer input and output is obtained and expressed as

$$R_1 = f(w_1 \cdot X + b_1), \quad (1)$$

where R_1 denotes the output matrix of the first hidden layer and w_i and b_i denote the weight parameter and threshold parameter between the input layer and the first hidden layer, respectively.

If the first hidden layer variable is denoted as $r_{1,p}$, i.e., the p th variable, $w_{1,p,i}$ denotes the i th cause in the p th row of the weight matrix between the input layer and the first hidden layer, $b_{1,p}$ denotes the p th variable value in the threshold vector between the input layer and the first hidden layer, and then each output value in R_1 is the value obtained from the original column vector x transformed by the activation function f as follows:

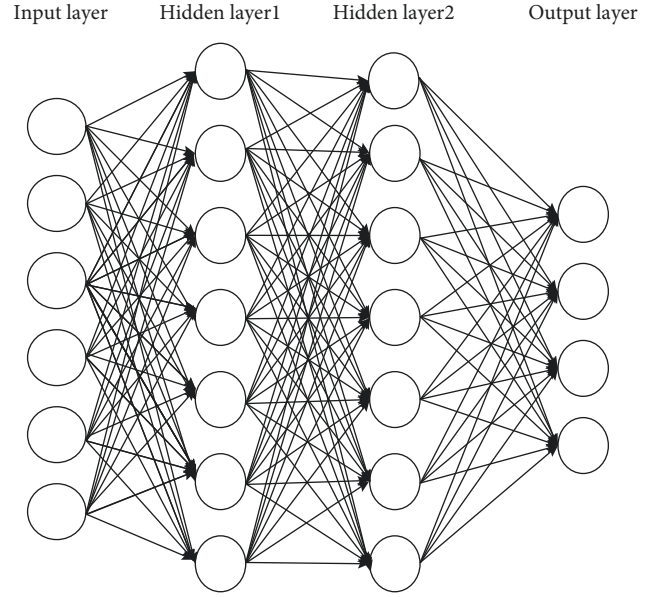


FIGURE 1: DNN with 2 hidden layers.

$$r_{1,p} = F \left(\sum_{i=1}^n w_{1,p,i} \cdot X_i + b_{1,p} \right). \quad (2)$$

According to the principle of DNN, the output of the previous hidden layer is the input of the next hidden layer, and then the output R_m expression of the m th hidden layer of the DNN model is

$$R_m = f(w_m \cdot R_{m-1} + b_m). \quad (3)$$

The input quantity X is processed by the input layer and transmitted to the hidden layer, and after performing the hidden layer processing, it is transmitted to the output layer, which can be expressed as

$$y = g(w_{n+1} \cdot R_n + b_{n+1}), \quad (4)$$

where w_{n+1} and b_{n+1} denote the weight parameter and the threshold parameter between the last hidden layer and the output layer, respectively, g denotes the activation function of output layer in DNN.

The activation function is a tool for nonlinear processing of the output quantity of each layer, which can enhance the data processing and optimization ability of neural networks. The common activation function sigmoid can be expressed as [16–19]

$$\text{sigmoid}(x) = \frac{1}{1 + e^{-x}}, \quad (5)$$

where x indicates the input variable and e indicates the constant, which takes the value of 2.7183.

3. Cost Prediction Model Construction Based on DNN

Combining the good nonlinear mapping ability and strong generalization ability of DNN, this paper uses the DNN model to predict engineering cost.

3.1. Inputs to the DNN Model. There are many factors affecting the cost price of construction projects, and these factors influence and relate to each other. In order to analyze the project cost comprehensively, this paper refers to the research results of some scholars and divides these influencing factors into engineering characteristics and list item characteristics.

3.1.1. Engineering Characteristics. For the engineering characteristics, the indicators are divided as shown in Table 1.

3.1.2. List Item Characteristics. The list items are usually coded with 12 bits, and the first 9 bits of the code are set according to the different categories. Based on this, conversions are made between the inventory codes and the model. The last 3 bits of the code are coded in order from 001 according to the specific conditions of the construction drawings, and the item code cannot be repeated.

The list item characteristics are the same as the engineering characteristics, which need to be classified and given the corresponding values according to the description of the item characteristics, and if there is no subitem in the list, it will be given 0. Due to the large amount of inventory item data, quantification of the entire engineering characteristics has great complexity, so this paper takes the two subprojects of solid brick walls and beamed slabs as examples for quantification, as shown in Table 2.

3.2. Outputs of the DNN Model. When judging the project cost, we usually use methods such as checking and comparing to reasonably judge the total quotation and each subitem project quotation and tax, among which the total quotation and subitem project quotation are the main judging contents. For this feature, it is used as the output of the DNN model to reasonably predict the price, and thus a reference is provided for the expert's evaluation. In summary, the inputs and outputs of the DNN model are shown specifically in Table 3.

3.3. DNN Structure Design

3.3.1. Network Parameter Selection

(1) Activation Functions. In order to make the DNN model more expressive, a nonlinear function needs to be introduced as the activation function. The commonly used activation functions include sigmoid function, ReLU function, and tanh function. Since the DNN model is prone to gradient disappearance or explosion when reverse transfer is performed, the ReLU function can solve this problem, and the convergence speed of the ReLU function is faster, so the ReLU function is used as the activation function in this paper. Its function image is shown in Figure 2.

(2) Loss Functions. The loss function is used to represent the difference between the true value Y and the predicted value $f(x)$ of the model. If the loss function is smaller, the model

TABLE 1: Engineering characteristic indicators and categories.

	Building height X_1
	Total building area X_2
	Standard floor building area X_3
	Standard floor height X_4
	Number of floors above ground X_5
	Basement floor height X_6
	Number of basement floors X_7
Engineering characteristic influencing factor	Basement floor area X_8
	Floor area X_9
	Construction period X_{10}
	Building type X_{11}
	Structure type X_{12}
	Foundation form X_{13}
	Foundation soil type X_{14}
	Type of door and window X_{15}
	Site condition X_{16}

TABLE 2: Quantification of solid brick wall and beam slab project.

Project code	Project name	Project characteristics
0103022001	Solid brick wall	Quantity of work U10
		Brick variety U11
		Wall type U12
		Mortar strength U13
106062001	Beam slab	Quantity of work U20
		Concrete type U21
		Strength grade U22

has stronger fitting ability and higher precision. In general, the loss function is denoted by $L(Y, f(x))$, and its standard form is [20]

$$L(Y, f(x)) = \sum (Y - f(x))^2. \quad (6)$$

(3) Weight Initialization. Before the model is trained, the weights need to be initialized. The current weight initialization methods include two main types: one is to initialize the weights to very small values, and the other is to set the weights to +1 and -1 with equal numbers. Considering that the second method is too subjective, in order to reach better effect of the model training, the first method is used in this paper to initialize the weights with random numbers in the range of $[-1, 1]$ that fit the normal distribution.

(4) Network Structure. The network structure mainly includes network nodes and hidden layer, which directly affect the performance of DNN. Generally, only one hidden layer is considered, and under this hidden layer, the optimal hidden node is found. Figure 3 shows the error of different nodes under a hidden layer after 500 calculations. According to the results of Table 4, when the hidden node is 23, the error is the smallest, but it is still difficult to meet the requirements.

Generally speaking, the more the hidden layers, the higher the accuracy of the model, so a DNN model with 2 hidden layers is used. After determining the number of hidden layers, the number of hidden layer nodes is

TABLE 3: Input and output parameters of the DNN model.

Input	Output	
Building height X_1	Total quotation Y	
Total building area X_2		
Standard floor building area X_3		
Standard floor height X_4		
Number of floors above ground X_5		
Basement floor height X_6		
Number of basement floors X_7		
Basement floor area X_8	Integrated unit price $V1$	
Floor area X_9		
Construction period X_{10}		
Building type X_{11}		
Structure type X_{12}		
Foundation form X_{13}		
Foundation soil type X_{14}		
Type of door and window X_{15}		
Site condition X_{16}		
0103022001 (solid brick wall)	Quantity of work U_{10} Brick variety U_{11} Wall type U_{12} Mortar strength U_{13} Quantity of work U_{20} Concrete type U_{21} Strength grade U_{22}	Integrated unit price $V2$
106062001 (with beam slab)		

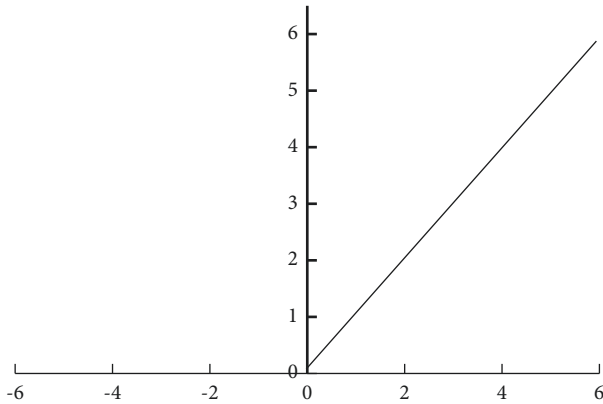


FIGURE 2: ReLU function image.

determined. Generally speaking, if the number of nodes in the hidden layer is insufficient, it will cause poor learning ability of the model, thus increasing the error; if it is too large, it will cause overfitting phenomenon and reduce the generalization ability of the model. By analyzing the previous experience, the optimal ratio of the number of nodes in first hidden layer to that in second hidden layer is 3 : 1. Therefore, when the number of nodes in the two layers is set to 15 and 5, respectively, the final DNN structure is shown in Figure 3 [21–24].

4. Simulation Experiments

4.1. DNN Model Training

4.1.1. Model Training Samples and Environment. The sample data of this model come from an engineering cost website, in which nearly 20 sets of engineering cost data from a certain

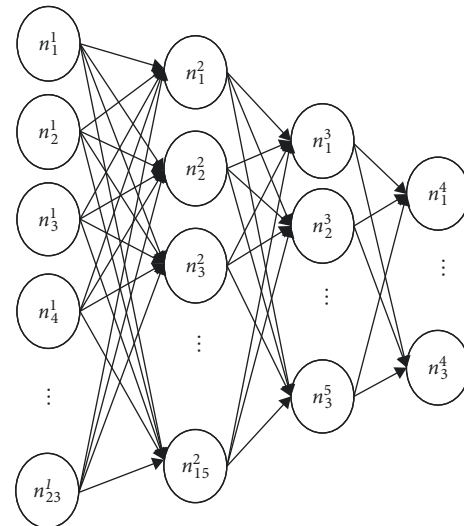


FIGURE 3: Schematic diagram of DNN structure.

region are selected as samples, including 15 sets of training samples and 5 set of testing samples. The model writing procedure uses the Spyder software in Python environment, and the model is trained using an improved BP algorithm that introduces a momentum term, which allows the error surface to avoid falling into local minimum and thus obtains a more optimal solution. Let the learning rate η be 0.001, momentum coefficient α be 0.8, iterations be 5000, and the error range ε be less than 0.001.

4.1.2. Model Training and Results. Before conducting the model training, the sample data need to be normalized to control the data output and input within the interval, and the

TABLE 4: Relationship curve between node and error under single hidden layer.

Number of hidden layer nodes	Error (%)
10	0.83
11	0.52
12	0.67
13	0.48
14	0.49
15	0.55
16	0.8
17	0.7
18	0.45
19	0.53
20	0.3
21	0.27
22	0.38
23	0.3
24	0.32
25	0.54
26	0.39
27	0.46
28	0.34
29	0.36
30	0.42

error value is about 0.00289 after 5000 iterations of this model calculation, as shown in Figure 4. The fitted curves of the total quotation and the integrated unit price of the branch subitem project are shown in Figure 5, from which it can be seen that the curve fitting effect of the sample value and the actual value is consistent.

In order to compare the prediction effect of DNN, BP neural network is introduced while DNN prediction is carried out. The comparison results show that the prediction of DNN is closer to the real price, while the error between BP neural network and the real value is large. It is concluded that the prediction effect of DNN is better.

In order to verify the effectiveness of the DNN model in practical applications, the trained DNN model is used to test the test sample, i.e., by analyzing the test sample error, if it is within the error range, it means the DNN model has validity. In this paper, a set of test samples is randomly selected for testing, and the output values are shown in Table 5.

As can be seen from the above table, the relative errors between the output values of DNN model and the true values are all below 5%, which indicates that the DNN model can predict the engineering cost well.

4.2. Determination of Cost. The project cost has been predicted above, but the prediction result is not the cost price because (1) the model sample is random and does not consider factors such as individual enterprise management ability, so the predicted value of the model only belongs to the social average and (2) when the model is trained, its output value is the settlement price, including the enterprise profit, while the cost price should be the difference between the settlement price and the profit. Therefore, the model predictions need to be adjusted in order to obtain the cost price.

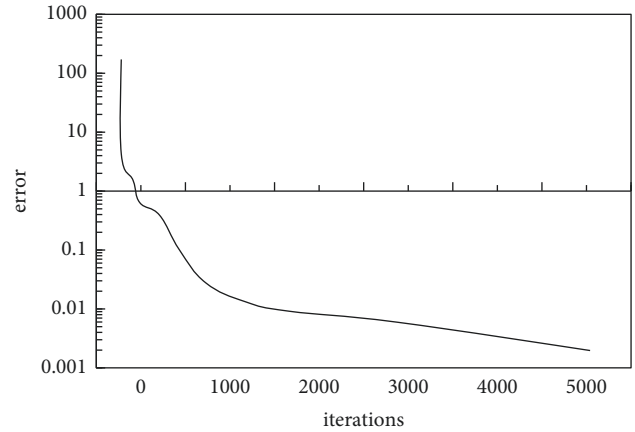


FIGURE 4: Model training error convergence.

4.2.1. Cost Price of Branch Subitem Project. Considering the characteristics of the branch subitem project cost and the proportion of the integrated unit price, this paper adopts the weighted average algorithm to multiply the integrated unit price by the adjustment factor to obtain the cost price, and the adjustment method is shown in Table 6. Assuming that P denotes the cost price and V denotes the model output value, the adjustment equations are shown in equations (7) and (8) [25–29].

$$\text{Adjustment coefficient } \phi = \sum_{i=1}^5 \alpha_i \beta_i, \tag{7}$$

$$\text{cost price } P = V \phi. \tag{8}$$

Because of the different proportions of the various costs of the integrated unit price, statistics on the percentage of the integrated unit price costs α are required. According to the first 9 digits of the code, the computer finds the matching list items, and using Table 6 as an example for proportional calculation, we can get the percentage of labor cost α_1 as follows:

$$\alpha_1 = 0.207. \tag{9}$$

In the same way, $\alpha_2 = 0.657$, $\alpha_3 = 0.008$, $\alpha_4 = 0.025$, and $\alpha_5 = 0.103$. Then, the cost coefficients of the integrated unit price are calculated. According to the relevant research, the labor costs, material costs, construction tool usage costs, and enterprise management costs are generally not lower than the average social components of 90%, 98%, 70%, and 70%, respectively, while some enterprises can make use of zero profit to expand the market, so the profit can be ignored. In this regard, the integrated unit cost factors are shown in Table 7.

Substituting the above table data into formula (7), the integrated unit price adjustment factor of solid brick wall can be calculated as 0.85. Since the integrated unit price output of the solid brick wall is \$468, the cost price is

$$P_1 = V_1 \phi_1 = 468 \times 0.85 = 397.8 \text{ yuan}. \tag{10}$$

According to the above method, each integrated unit price can be adjusted to obtain the corresponding cost price.

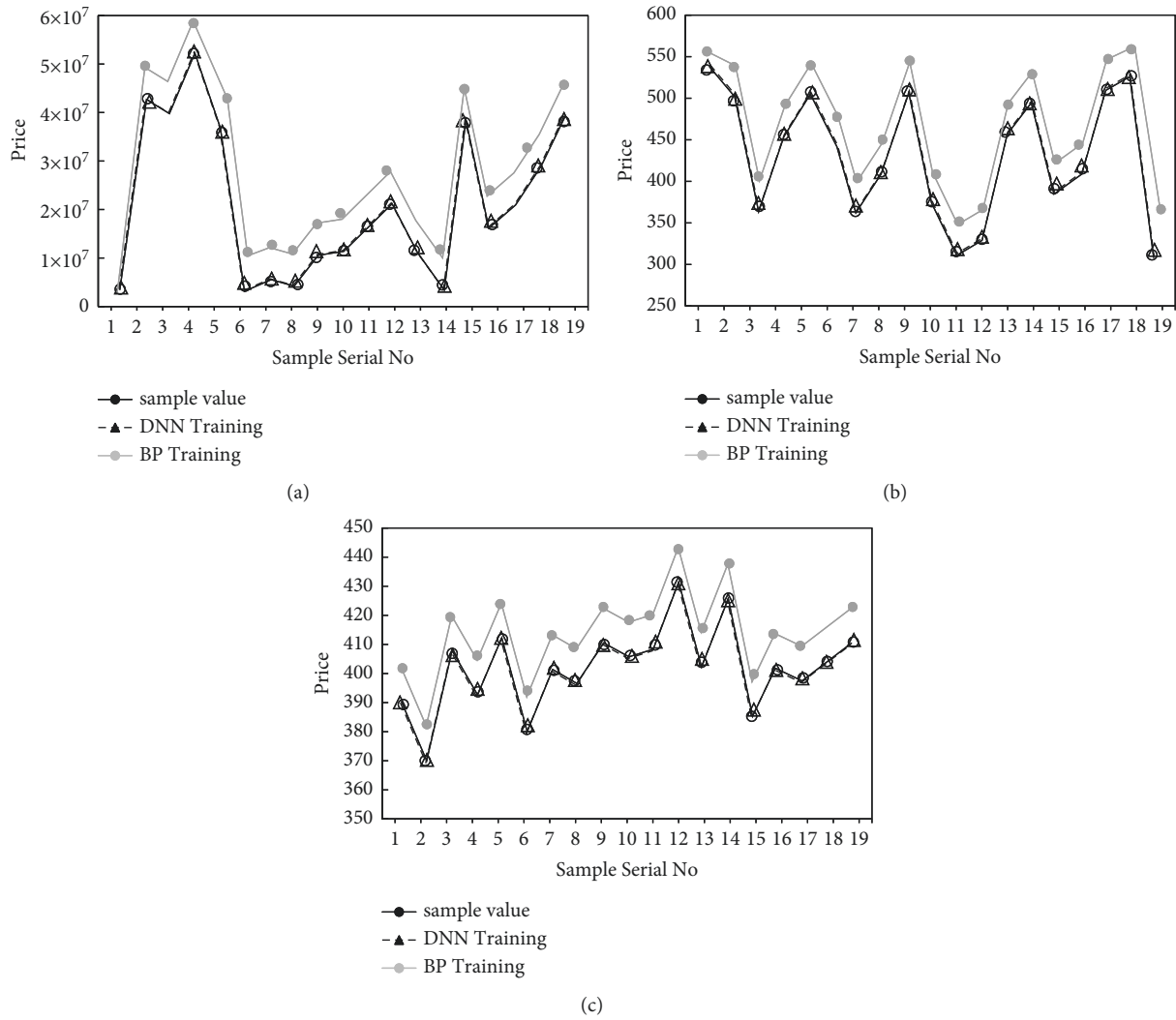


FIGURE 5: DNN model curve fitting effect. (a) Total quotation fitting. (b) Integrated unit price V1 fitting. (c) Integrated unit price V2 fitting.

TABLE 5: Model validation result.

Output variable	Output value	True value	Difference value	Relative error
Total quotation Y	40 423 575	42 197 507	1773932	4.203%
Integrated unit price V_1	488	503	15	2.98%
Integrated unit price V_2	359	376	17	4.52%

TABLE 6: Integrated unit price adjustment method.

Cost components	Labor costs	Material costs	Machinery costs	Management costs	Profit
Cost proportion	α_1	α_2	α_3	α_4	α_5
Cost coefficient	β_1	β_2	β_3	β_4	β_5

TABLE 7: Coefficient adjustment calculation.

Cost components	Labor costs	Material costs	Machinery costs	Management costs	Profit
Cost proportion	0.207	0.657	0.008	0.025	0.103
Cost coefficient	0.85	0.98	0.70	0.70	0

The total cost price of the total quotation can be obtained by aggregating the adjusted cost prices.

5. Conclusion

In summary, the key to solving the cost pricing problem lies in the accurate calculation of the project cost price. Based on previous research, this paper constructs a DNN engineering cost price prediction model, divides the engineering index system into two categories: engineering characteristics and project characteristics, and then randomly selects 20 sets of sample data to train and predict the model. The results show that the DNN prediction model has less error and can effectively predict the engineering cost. Since the engineering cost prediction is random in nature and the result output is the settlement price, the DNN prediction result is reasonably adjusted. Specifically, the weighted average algorithm is used to calculate the cost price of the integrated unit price of each subitem project and the cost of the total quotation, and finally the cost price of the whole project is obtained. Also, the study provides new ideas for the information budget of engineering cost.

Data Availability

The experimental data used to support the findings of this study are available from the corresponding author upon request.

Conflicts of Interest

The authors declare that they have no conflicts of interest.

References

- [1] P. Pandey, N. D. Gundi, P. Basu et al., "Challenges and Opportunities in Near-threshold DNN accelerators around Timing errors," *Journal of Low Power Electronics and Applications*, vol. 10, no. 4, p. 33, 2020.
- [2] C. Tang, N. Luktarhan, and Y. Zhao, "SAAE-DNN: deep learning method on Intrusion Detection," *Symmetry*, vol. 12, no. 10, p. 1695, 2020.
- [3] W. Zhou and Z. Zhu, "A novel BNMF-DNN based speech reconstruction method for speech quality evaluation under complex environments," *International Journal of Machine Learning and Cybernetics*, vol. 12, no. 4, pp. 959–972, 2020.
- [4] D. Rethage, J. Pons, and X. Serra, "A wavenet for speech denoising," in *Proceedings of the 2018 IEEE international conference on acoustics speech signal processing*, pp. 1927–1930, IEEE, Calgary, AB, Canada, April 2018.
- [5] Y. Shanshan, L. Jian, and C. Lin, "Low-thrust spacecraft trajectory optimization via a DNN-based method[J]," *Advances in Space Research*, vol. 66, no. 7, pp. 1635–1646, 2020.
- [6] G. Yue and O. Takashi, "Co-design of Binary processing in Memory ReRAM Array and DNN model optimization algorithm:Regular Section[J]," *IEICE - Transactions on Electronics*, vol. E103.C, no. 11, pp. 685–692, 2020.
- [7] M. C. Pravin, M. Mukilan, G. Vishnu Prakash, P. Nithish, B. Monish Kanna, and E. Logesh, "Predicting the Emissive characteristics of an IC engine using DNN," *IOP Conference Series: Materials Science and Engineering*, vol. 995, no. 1, Article ID 012010, 2020.
- [8] X. Xu, L. Peng, Z. Ji, S. Zheng, Z. Tian, and S. Geng, "Research on substation project cost prediction based on sparrow search algorithm optimized BP neural network," *Sustainability*, vol. 13, no. 24, Article ID 13746, 2021.
- [9] S. S. Sharqi and A. Bhattarai, "Evaluation of several machine learning models for field canal improvement project cost prediction [J]," *Complexity*, vol. 2021, Article ID 8324272, 2021.
- [10] T. Xiaodong, X. Tang, and X. Zhang, "Dynamic real estate project cost prediction based on SIMCA-P[J]," *IOP Conference Series: Earth and Environmental Science*, vol. 526, no. 1, Article ID 012178, 2020.
- [11] A. Yousefi, H. Guo, M. Birouk, B. Liko, and S. Lafrance, "Effect of post-injection strategy on greenhouse gas emissions of natural gas/diesel dual-fuel engine at high load conditions [J]," *Fuel*, vol. 32, p. 290, 2021.
- [12] K. Li, X. Chen, R. Zhang, and E. Pickwell-MacPherson, "Classification for Glucose and Lactose Terahertz Spectrums based on SVM and DNN methods," *IEEE TRANSACTIONS ON TERAHERTZ SCIENCE AND TECHNOLOGY*, vol. 10, no. 6, pp. 617–623, 2020.
- [13] H. Han, L. Xu, X. Cui, and Y. Fan, "Novel Chiller fault Diagnosis using deep neural network (DNN) with simulated Annealing (SA)[J]," *International Journal of Refrigeration*, vol. 121, pp. 269–278, 2020.
- [14] C. Xiao, X. Wang, Q. Chen, F. Bin, Y. Wang, and W. Wei, "Strength Investigation of the Silt-based Cemented Paste Backfill using Lab experiments and deep neural network[J]," *Advances in Materials Science and Engineering*, vol. 2020, Article ID 6695539, 2020.
- [15] R.-E. Mihaescu, M. Chindea, C. Paleologu, S. Carata, and M. Ghenescu, "Person Re-Identification across data distributions based on general Purpose DNN Object Detector," *Algorithms*, vol. 13, no. 12, p. 343, 2020.
- [16] Y. Ibrahim, H. Wang, J. Liu et al., "Soft errors in DNN accelerators: a comprehensive review," *Microelectronics Reliability*, vol. 115, Article ID 113969, 2020.
- [17] A. Makuvaza, D. S. Jat, and A. M. Gamundani, "Deep neural network (DNN) Solution for real-time Detection of distributed Denial of Service (DDoS) Attacks in software Defined networks (SDNs)[J]," *SN Computer Science*, vol. 2, no. 2, 2021.
- [18] J. Chen, H. Zheng, H. Xiong et al., "FineFool: a novel DNN Object Contour Attack on image recognition based on the Attention Perturbation Adversarial Technique[J]," *Computers & Security*, vol. 104, Article ID 102220, 2021.
- [19] K. Inoue, S. Hara, M. Abe, N. Hojo, and Y. Ijima, "Model architectures to extrapolate emotional expressions in DNN-based text-to-speech," *Speech Communication*, vol. 126, pp. 35–43, 2021.
- [20] A. K. Mishra and V. Ponnusamy, "DNN-based distributed sequential uplink processing in cell-free massive MIMO based on radio stripes[J]," *IET Networks*, vol. 10, no. 3, 2021.
- [21] A. Yazid, C. Benoit, and Z. Wei-Ping, "DNN-based Calibrated-Filter models for speech Enhancement[J]," *Circuits, Systems, and Signal Processing*, vol. 40, pp. 1–24, 2021.
- [22] H. Deng and C. T. Albert, "A Parametric level set method for Topology optimization based on deep neural network[J]," *Journal of Mechanical Design*, vol. 143, no. 9, 2021.
- [23] S. Li, J. Hou, A. Yang, and J. Li, "DNN-based distributed Voltage Stability online Monitoring method for large-Scale power Grids[J]," *Frontiers in Energy Research*, vol. 9, 2021.
- [24] D. Ding, L. Wang, Z. Yang, K. Hu, and H. He, "ACIMS: Analog CIM simulator for DNN Resilience," *Electronics*, vol. 10, no. 6, p. 686, 2021.

- [25] T. Yao, F. Gao, Q. Zhang, and Y. Ma, "Multi-feature gait recognition with DNN based on sEMG signals," *Mathematical Biosciences and Engineering: MBE*, vol. 18, no. 4, pp. 3521–3542, 2021.
- [26] Z. Yonggang, X. Yuanlun, Z. Yan, Q. Junbo, and W. Sunxin, "The adoption of deep neural network (DNN) to the prediction of soil liquefaction based on shear wave velocity[J]," *Bulletin of Engineering Geology and the Environment*, vol. 80, pp. 5053–5060, 2021.
- [27] W. M. Zhang, L. Zhang, Z. Zhang, and M. Sun, "IBD1: the metrics and evaluation method for DNN processor benchmark while doing Inference task[J]," *Journal of Intelligent and Fuzzy Systems*, vol. 40, no. 5, pp. 1–13, 2021.
- [28] S. Jung, J. H. Bong, S.-J. Kim, and S. Park, "DNN-based FES control for gait Rehabilitation of Hemiplegic Patients[J]," *Applied Sciences*, vol. 11, no. 7, p. 3163, 2021.
- [29] D. Preethi and N. Khare, "An Intelligent network Intrusion Detection system using Particle Swarm optimization (PSO) and deep network networks (DNN)[J]," *International Journal of Swarm Intelligence Research*, vol. 12, no. 2, pp. 57–73, 2021.

Research Article

Voice Anomaly Detection and Music Website Teaching Design for 5G Internet of Things

Jin Chen 

Hengyang Normal University, Hengyang 421001, China

Correspondence should be addressed to Jin Chen; ttdzy0705@hynu.edu.cn

Received 11 February 2022; Revised 11 May 2022; Accepted 24 May 2022; Published 28 June 2022

Academic Editor: Hangjun Che

Copyright © 2022 Jin Chen. This is an open access article distributed under the Creative Commons Attribution License, which permits unrestricted use, distribution, and reproduction in any medium, provided the original work is properly cited.

Information technology has brought tremendous changes to many industries. 5G and Internet of Things technology have also driven the development of the music industry. Network communication has replaced the traditional method and has become a brand-new method of music communication. An online music instructional teaching website based on Internet of Things is designed, the basic functions of the website are introduced, and a voice anomaly detection system was designed from the landing test, search function test, song display, administrator maintenance, and management of songs. The basic functions of the website were tested in four aspects. According to the needs of music websites, a voice anomaly detection system is designed. The system includes two aspects, namely, an abnormal sound classification system and a microphone array abnormal sound detection system; two music rhythm algorithms are proposed, based on international music detection. The music data of the wrong retrieval platform was tested on two different music algorithms, and it was found that the two different detection methods have different results for different types of music, and the Bossa-Brazil music type has the highest error rate. In order to detect the accuracy of the detection of the abnormal voice system, a comparison experiment of three different voice detection systems was set up under the condition of no noise and noise, to test their experimental accuracy. The music teaching system designed in this paper has the highest accuracy, which can meet most of the requirements and improve the efficiency of music detection. In the design of music teaching, because the music website has rich functions and various products, it improves the effect of online teaching and the efficiency of teaching design. Instructional design is applied to online learning to improve the dissemination of music and art, and high-quality pronunciation is also one of the important contents.

1. Introduction

With the development of the Internet, people cannot leave the Internet for a long time, and there are more and more young people who love music. They enjoy sharing their favorite music with others and sharing their feelings and thoughts about music. Now, if most music websites want to use a complete cloud service, they need to download the client, and due to copyright competition, more manufacturers spend money to buy copyright and ignore some cloud services, as well as updating the front-end layout, and traditional pages have almost similar application functions. The single-page application function of VUE is inherently weak, which leads to many unfavorable factors such as inconvenient use, cumbersome operation, and long loading time for

many online music websites. In order to avoid this problem, the online music system came into being.

Based on the above background, the article proposes a national music website construction plan, which has played a certain role in accelerating the development of informationized music business. There are diversified forms of websites, one of which is through software development, through which we can develop very interesting websites. The music anomaly detection method proposed in [1] can quickly identify music anomaly signals. Literature [2] established Beatme online music communication media to connect relevant music-related devices to the cloud system. It realizes the hierarchical management of users and has new significance for the development of personalized music online network. Literature [3] introduces the design and

implementation of music website. The online music sharing website is a functional website that can meet many of our requirements and provide us with basic listening services. Literature [4] introduces the development of ASP programming technology to establish and maintain a back-end database. Literature [5] designed and developed an online music website system based on PHP + MySQL programming language. The system has not only basic functions such as online listening and music downloading, but also functions such as message delivery, music on demand, and other functions, which can meet the needs of most people. Literature [6] explains how to use PHP and MySQL programming to create a music group website. Generally, there will be multiple pages, each with different functions. This article assignment explains the detailed website development steps. Literature [7] discusses the method of playing WMA music files online based on ASP technology and Access database and analyzes the key technologies in detail. Literature [8] proposed a grade analysis method to detect abnormal signals in music. Literature [9] proposed a new hybrid method to determine abnormal data based on GARCH, K-means, neural network, and other anomaly detection methods. Literature [10] proposed a hierarchical framework to automate the task of emotion detection in original music data. The emotions expressed by each music signal are different, and everyone has a different understanding of music. The layered framework proposed in the article can extract music intensity, timbre, and rhythm, which can help us better understand music signals. Literature [11] describes an audio-based video indexing method that can detect music and voice independently. Literature [12] focuses on the artist or source detection component, and we show that it can correctly classify 91% of the small song collection and 70% of the artist space in the larger song collection. The pitch and scale information of music is very important for music classification and retrieval, but we have done very little work on the key detection of music. Literature [13] proposed a method of extracting pitch contour features from audio signals. More than 80 music works were tested in the experiment, and the test success rate was as high as 90%. Literature [14] proposed a system and method to use music features extracted from music to detect music emotions within the framework of hierarchical emotion detection. Literature [15] proposed a method for detecting music in a speech signal with multiple frames. This method can effectively distinguish whether the sound signal is noise or music. The method is to extract frames from the music signal and then define a parameter of the noise signal, and then you can distinguish the type of music.

Under the influence of today's music trend, the music industry has gradually begun to climax, because music has always been inseparable from people, and if you want more people to see interesting music works, an online music website is essential. The Internet of Things is an efficient information platform from which people can find a lot of value, which makes it easier for more and more people to appreciate music online and at the same time improves the sharing of resources on the Internet [16]. We are in an intelligent information system [17]. The convenience of the

network has brought a lot of convenience to our lives [18]. Using the network to share resources is fast and efficient, and it can also shorten the distance between people. How to use the convenience of the Internet to design an online music sharing website is a question we have to think about. The article uses Internet technology to design a network sharing music website, which has many convenient functions, and designs a music anomaly detection system based on the website, which can effectively detect abnormal signals in music at a high speed. The Internet of Things technology realizes the intelligent collection, processing, and analysis of music signals through the real-time transmission of information between wired/wireless networks, which has the advantages of comprehensive perception, reliable transmission, convenience, and rapidity. A music feature recognition model based on the Internet of Things (IOT) technology is designed to realize the perception, transmission, and recognition of music signals. In that physical perception layout of the system, sound sensors are arranged at different positions to collect original music signals, and a TMS320VC5402 digital signal processor is adopted to carry out music signal analysis and process. And the music feature analysis module in the application layer acquires the maximum similarity between the test template and the reference template by adopting a dynamic time warping algorithm, realizes music signal feature identification, and identifies music feature content corresponding to a music form and a music emotion according to an identification result. The experimental results show that the model runs stably and can collect high-quality music information.

2. Technical Descriptions

2.1. Website Functional Design. We must first take into account the aesthetic views of the general public and pay attention to color matching on the front page to highlight the style and characteristics of our website. The front-end web page design is mainly oriented to ordinary users. You can use this web page to realize online music playback, download songs, and inquire about music, and users can register and leave their personal information and views on the web page. And the website has the function of listening to the name of the song. When some users do not remember the name of the song, they can search for the lyrics in the song or play it. The website has an intelligent recognition function. The website also has a message board function, where users can leave messages and comments on favorite songs; they can also make relevant suggestions to the website.

The website manager enters his account and password to log in successfully, and then he can enter the background management page. You can change the track page by changing any of the words such as "song name" to change the track information; in the deleted song page, you only need to enter the track number to remove any messages about this song. On the homepage of a music website, people can view various functions available on the website, such as searching for music tracks, querying artist information, querying music albums, leaving messages for music of interest, and even querying popular song charts. The

administrator can check netizens' messages, delete some bad comments, and accumulate their opinions.

2.2. Abnormal Sound Detection System. The purpose of the system is to accurately detect the type of abnormal sound. The algorithm mainly extracts the sound signal and then builds a model of the sound signal. The model can not only detect whether there is abnormal sound but also determine what kind of abnormal sound. But the model also requires a lot of sound to model. Because the sound signal characteristics are different, the classification method of the model is also different. According to the sound characteristics, it can be divided into frames and wholes. Frame classification is to detect whether there is abnormal sound in each audio. The flowchart of the algorithm is shown in Figure 1.

In Figure 1, according to "model matching," the sound is classified mainly according to the characteristics of the sound signal, and if the characteristics of the sound are met, the classification method is performed. If the match is not successful, it indicates that there is an abnormal sound, further processing the abnormal sound.

Generally, the matching algorithm is statistical method, clustering method, and anomaly detection method.

The microphone array uses multiple microphones. The advantage is that it can locate the sound position and then

judge whether the localized sound is an abnormal sound based on the air pressure information such as the video. The flowchart of the algorithm is shown in Figure 2.

In Figure 2, the abnormal sound is determined, and the detection is performed based on "abnormal sound" to determine whether or not the sound is abnormal. If not, it may be the pressure information such as video.

3. Method Description

3.1. Music Style Recognition

3.1.1. Separation Algorithm. Music signals usually consist of harmonic sound components and impact sound components, which have different characteristics [19]. According to the difference between the impact sound and the harmonic sound in the frequency spectrum, we can separate the original spectrum W_{fj} into the impact spectrum P_{fj} and the harmonic spectrum, defined as follows:

$$W_{fj} = P_{fj} + H_{fj}. \quad (1)$$

$P_{fj} > 0, H_{fj} > 0$. Formula (2) can realize the separation of impact sound and harmonic sound [20]:

$$Q(H^t, P^t, U^t, V^t) = \frac{1}{\sigma_H^2} \sum_{fj} \left\{ (H_{f,t-1}^t - U_{f,t}^t)^2 - (H_{f,t}^t - U_{f,t}^t)^2 \right\} + \frac{1}{\sigma_P^2} \sum_{fj} \left\{ (P_{f,t-1}^t - V_{f,t}^t)^2 - (P_{f,t}^t - V_{f,t}^t)^2 \right\}. \quad (2)$$

Find the minimum value and update the formula to get

$$\begin{aligned} H_{f,j}^{t+1} &= H_{f,j}^t + \Delta^t, \\ P_{f,j}^{t+1} &= P_{f,j}^t + \Delta^t, \end{aligned} \quad (3)$$

where

$$\begin{aligned} \Delta^t &= \frac{\alpha}{4} (H_{f,j-1}^t - 2H_{f,t+1}^t + H_{f,t+1}^t) \\ &\quad - \frac{1-\alpha}{4} (P_{f,j-1}^t - 2P_{f,t+1}^t + P_{f,t+1}^t), \end{aligned} \quad (4)$$

$$\alpha = \frac{\sigma_y^2}{\sigma_H^2 + \sigma_y^2}.$$

3.1.2. Network Structure. Classification and recognition through functions: the activation function used is

$$X_l^q = \max \left\{ 0, \sum_{X^p \in M_q} X_{l-1}^p \otimes k_l^{pq} + b_l^q \right\}. \quad (5)$$

The formula of the pooling layer is

$$X_l^q = \text{down}(X_{l-1}^p). \quad (6)$$

In backpropagation, the gradient of the convolutional layer is calculated as follows:

$$\begin{cases} y_l = \omega_l x_l + b_l, \\ x_l = f(y_{l-1}), \\ \Delta y_l = f'(y_l) \Delta x_{l+1}. \end{cases} \quad (7)$$

The update rule for ω_l is derived from the following:

$$\begin{cases} \mu_l^{t+1} = \alpha \cdot \mu_l^t - \lambda \cdot \eta \cdot \omega_l^t - \eta \cdot \left\langle \frac{\partial L}{\partial \omega} | \omega \right\rangle_{ly}, \\ \omega_l^{t+1} = \omega_l^t + \mu_l^{t+1}. \end{cases} \quad (8)$$

The regression formula is as follows:

$$p_l = \frac{\exp(X_8^j)}{\sum_{i=1}^m \exp(X_8^i)}. \quad (9)$$

The loss function is defined as

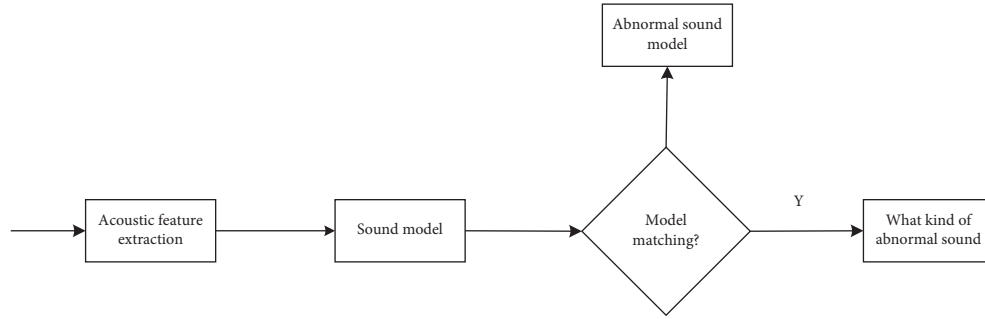


FIGURE 1: Abnormal sound detection model.

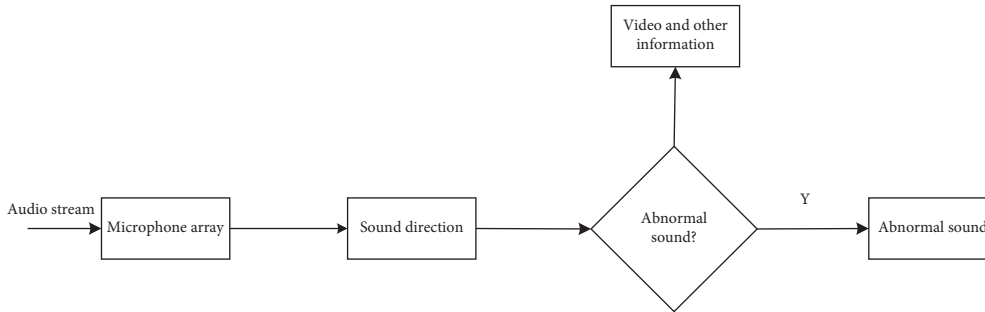


FIGURE 2: Flowchart of abnormal sound detection of microphone array.

$$L = - \sum_{j=1}^m h_j \log p_j. \quad (10)$$

$$f_k = \frac{2\pi}{N} * k * \frac{\text{samplefrep}}{2\pi} = \frac{\text{samplefrep}}{N} * k = \Delta f * k,$$

$$k = \frac{f_k}{\Delta f}.$$

(14)

3.2. Implementation of Abnormal Sound Detection Algorithm

3.2.1. MFCC (Mel-Scale Frequency Cepstral Coefficients) Sound Extraction. The sound extraction flowchart is shown in Figure 3.

The extracted sound signal is transformed into a digital signal, and the flow of the high frequency part of the sound is increased by preemphasis [21]; the expression is

$$w[n] = \begin{cases} 0.54 - 0.46 \cos\left(\frac{2\pi n}{L}\right), & 0 \leq n \leq L-1, \\ 0, & \text{other.} \end{cases} \quad (11)$$

Analyze the signal to get the frequency spectrum, according to the relationship:

$$\text{mel}(f) = 1127 \ln\left(1 + \frac{f}{700}\right). \quad (12)$$

Convert it to

$$\Delta \text{mel} = \frac{\text{mel}(fb_w) - \text{mel}(fb_w)}{\text{filterNum} + 1}. \quad (13)$$

The center frequency can be calculated; then,

The corresponding frequency can be calculated, and the energy of the response frequency is

$$\text{Emel}(i) = \sum_{k_{i-1}}^{k_{i+1}} (a_k * X[K])^2. \quad (15)$$

a_k changes according to the change of the slope, namely,

$$\begin{aligned} \text{for } f_{i-1} \text{ to } f_{i+1}, a_k &= \frac{k - k_i}{k_{i+1} - k_i} \\ \text{for } f_{i-1} \text{ to } f_i, a_k &= \frac{k - k_{i-1}}{k_i - k_{i-1}}, \\ \text{for } f_i \text{ times, } a_k &= 1, \end{aligned} \quad (16)$$

$$\text{for } f_{i-1} \text{ to } f_{i+1}, a_k = \frac{k - k_i}{k_{i+1} - k_i}.$$

The output logarithmic energy is changed by discrete cosine to obtain the MFCC coefficient [22]:

$$C(n) = \sum_{m=0}^{N-1} s(m) \cos\left(\frac{\pi n(m-0.5)}{M}\right) \quad n = 1, 2, \dots, L, \quad (17)$$

$$d(t) = \frac{c(t+1) - c(t-1)}{2}.$$

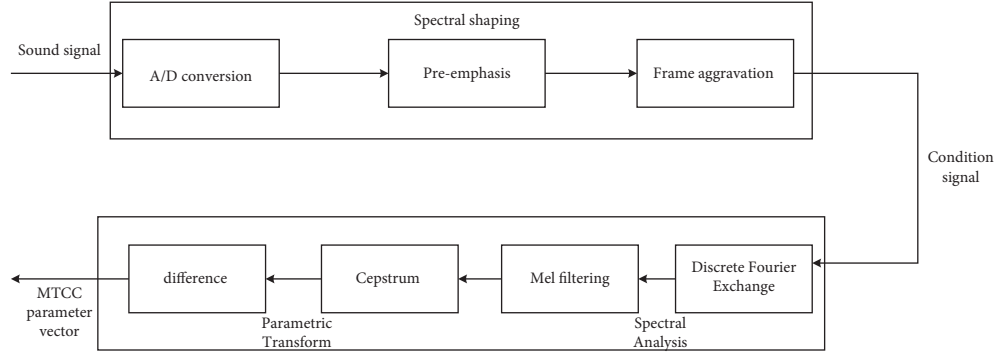


FIGURE 3: Sound extraction flowchart.

3.2.2. *Algorithm Implementation.* The general flowchart of sound detection is shown in Figure 4.

The abnormal sound model is trained by extracting the abnormal sound MFCC feature vector [23]; the sound is a continuous signal, which is a multidimensional distribution function:

$$\hat{b}_j(v) \sum_{k=1}^m \bar{c}_{jk} \left(\frac{1}{(2\pi)^{L/2} |\sum_{JK}|^{1/2}} \right) \cdot \exp\left(-\frac{1}{2}(v - \bar{\mu}_{jk})^t \sum_{JK}^{-1} (v - \bar{\mu}_{jk})\right). \quad (18)$$

Initialize first

$$\alpha_1(j) = \alpha_0 b_j(o_1) 1 \leq j \leq N. \quad (19)$$

Recursion is as follows:

$$\alpha_t(j) = \sum_{i=1}^N \alpha_{t-1}(i) \alpha_{ij} b_j(o_t) 1 \leq j \leq N, 1 \leq t \leq T. \quad (20)$$

Termination is as follows:

$$p(0|0|\lambda) = \alpha_T(q_F) = \sum_{i=1}^N \alpha_T(i) \alpha_{iF}, \quad (21)$$

where

$$p(0|\lambda) = \alpha_T(N) = \beta_T(1) = \sum_{j=1}^N \alpha_T(j) \beta_t(j). \quad (22)$$

Through this algorithm, the parameters of the abnormal sound can be calculated [24].

3.2.3. *Music Classification and Detection Model under Noisy Environment.* When the music sound contains noise, the change curve of the music signal will change to a certain extent. The music signal in the complex noise is

$$y(n) = s(n) - at(n). \quad (23)$$

Noise will cause a certain change in the curve of the music, and the system cannot accurately identify the music signal, so the influence of noise on the music signal should be eliminated. In this paper, the soft threshold wavelet

transform is selected to remove the music signal noise [25]; suppose a music signal with noise before and after the removal curve is shown in Figure 5.

Music Classification and Detection Feature Extraction. When music information changes, there are many features of music classification and detection [26]; the specific calculation formula is as follows:

$$sp = \frac{\sum_{i=1}^N (f_i - \bar{f}_i)^2 P(f_i)}{\sum_{n=1}^N P(f_i)}. \quad (24)$$

The formula for calculating the short-term energy spectrum characteristics of music is as follows:

$$ff = \frac{\sum_{i=1}^N (f_i - \bar{f}_i)^2 P(f_i)}{sp^3 \sum_{n=1}^N P(f_i)}. \quad (25)$$

(2) *BP Neural Network Algorithm.* The number of music short-term energy spectrum features is the number of nodes in the input layer of the BP neural network. The input and output of the neural network are, respectively [27],

$$S_j = \sum_{i=1}^m w_{ij} x(i) - \theta_j, \quad (26)$$

$$b_j = \frac{1}{(1 + \exp(\sum_{i=1}^m w_{ij} x_i - \theta_j))}, \quad j = 1, 2, \dots, p.$$

According to the same principle, the input and output formulas of the output layer can be obtained [28]:

$$L = \sum_{j=1}^n w_{jk} b_j - \theta_k, x_{i+1} = \frac{1}{(1 + \exp(\sum_{k=1}^p w_{kj} b_j - \theta_k))}. \quad (27)$$

4. Website Function Design

We can search for songs based on the album name and song name, leave a message to favorite singers, communicate with netizens, and view the song pop charts of the month, which are the specific functions of the website.

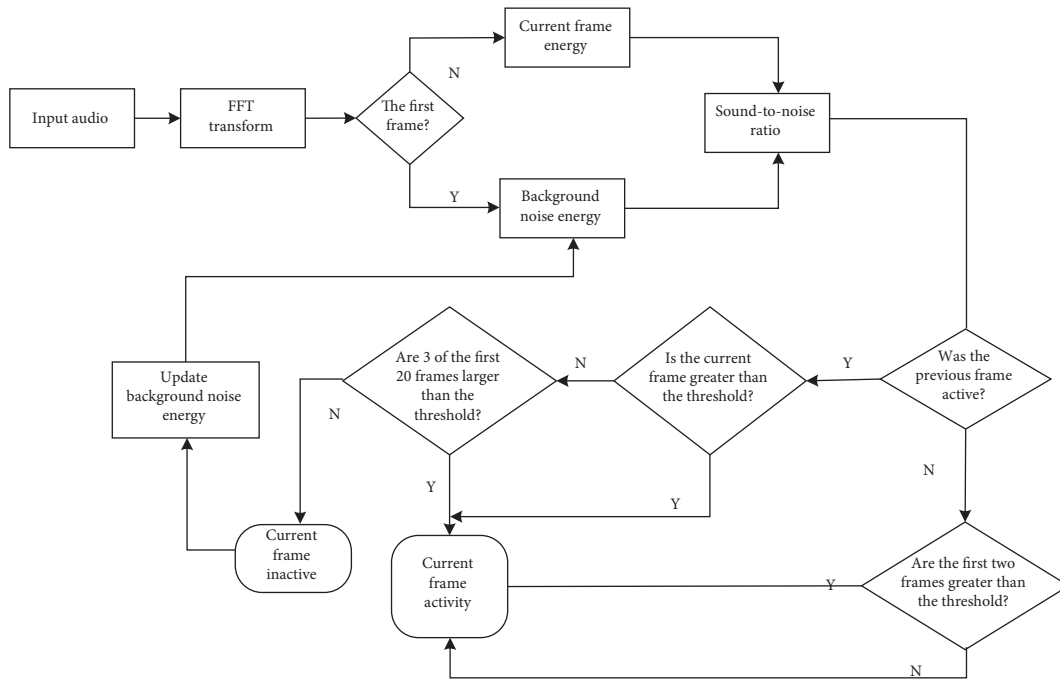


FIGURE 4: Sound detection flowchart.

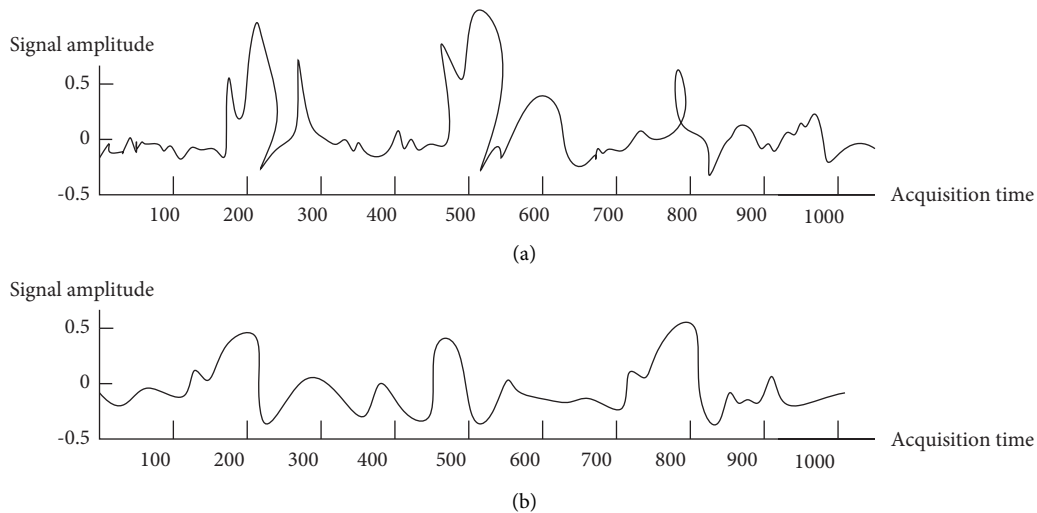


FIGURE 5: Noise effect removal test. (a) Music signal with noise. (b) Music signal to remove noise.

4.1. Website Testing

4.1.1. Login Test. We tested the login function of the website, and the specific conditions are shown in Table 1.

4.1.2. Search Function. We conducted a search function test on the website, and the specific conditions are shown in Table 2.

4.1.3. Song Display. We tested the management function of the website, and the test results are shown in Table 3 [25].

4.1.4. The Administrator Maintains and Manages Songs.

The management function of the website was tested, as shown in Table 4.

4.2. Research on Music Rhythm Detection Algorithm. It mainly introduces a music rhythm algorithm: error concealment. Error concealment can slow down the degradation of audio quality in the compression process. The traditional method includes the function of noise suppression, but the traditional method detaches the smooth music signal to work. In order to solve this problem, we use template matching algorithm to detect music rhythm. The

TABLE 1: Login and registration test cases.

Serial number	Test input	Execution precondition	Expected output
1	Enter the administrator account and password in the login area, and click login.	The user has opened the homepage of the website; the account and password are entered correctly.	The page jumps to the background maintenance and management page.
2	Enter the normal user account and password in the login area, and click to log in.	The user has opened the homepage of the website. The account and password are entered correctly.	The page jumps to the front page and shows that the user has logged in.
3	Enter the wrong user account and password in the login area, click to log in.	The user has opened the homepage of the site. The account and password are entered incorrectly.	The page jumps to the front page and prompts “incorrect account and password.”
4	Click the register button.	The user has opened the homepage of the site.	The page jumps to the registration page.
5	Fill in the user ID on the registration page.	User has entered the registration homepage.	The page prompts “does the user name already exist?”
6	Fill in the user e-mail of the registration page.	Fill in the user ID.	The page prompts “is the e-mail format correct?”
7	Fill in the password of the registration page.	User has entered the registration homepage.	The page prompts “the two passwords are not the same.”
8	Click add.	Fill in e-mail.	The page prompts “added successfully.”

TABLE 2: Search function test case.

Serial number	Test input	Execution precondition	Expected output
1	Enter the full name of the song in the search area.	The user has opened the homepage of the website. Tick the search type as the song title. The song exists on the site.	Jump to the search page and display song information.
2	Enter part of the song name in the search area.	The user has opened the homepage of the website. Tick the search type as the song title. The song exists on the site.	Jump to the search page and display song information.
3	Enter the artist’s full name in the search area.	The user has opened the homepage of the website. Check the search type as singer. The song exists on the site.	Jump to the search page and display the corresponding song information of the singer.
4	Enter part of the singer’s name in the search area.	The user has opened the homepage of the website. Check the search type as singer. The song exists on the site.	Jump to the search page and display the corresponding song information of the singer.
5	Enter the full name of the album in the search area.	The user has opened the homepage of the website. Check the search type as album. The song exists on the site.	Jump to the search page and display the corresponding song information of the album.
6	Enter part of the album name in the search area.	The user has opened the homepage of the website. Check the search type as album. The song exists on the site.	Jump to the search page and display the corresponding song information of the album.
7	Enter songs, artists, and albums that do not exist in the search area.	The user has opened the homepage of the website. Check the search type as album. The song or artist does not exist on the website.	Jump to the search page, and display “no related files found.”

TABLE 3: Song display test case.

Serial number	Test input	Execution precondition	Expected output
1	Click on the music charts.	The user has opened the homepage of the site.	Display music ranking information, sorted in descending order of total visits.
2	Click on the singer rankings.	The user has opened the homepage of the site.	Show singer ranking information, sorted in descending order of total visits.
3	Click on the album chart.	The user has opened the homepage of the site.	Display album ranking information, sorted in descending order of total visits.
4	Click on the song name of the music chart.	The user has opened the homepage of the site.	Jump to the song play page and play this song.
5	Click the music chart song download button.	The user has opened the homepage of the site.	Pop up the download prompt box.
6	Click on my favorites.	The user has opened the homepage of the site. User logged in.	Show the user's favorite songs.
7	Click on my favorites.	The user has opened the homepage of the site. User is not logged in.	"You have not logged in yet. Please log in first!"

TABLE 4: Test cases for administrator maintenance and management functions.

Serial number	Test input	Execution precondition	Expected output
1	Click music to add.	The administrator has logged in the website back-end.	Jump to the music adding page.
2	Click the browse button on the music add page.	The administrator has logged in the website back-end. The administrator has entered the music adding page.	Choose to add a file. Box pops up.
3	Click the add button on the music add page.	The administrator has logged in the website back-end. The administrator has entered the music adding page. There is missed or incorrectly filled in information.	The prompt is displayed on the page, and the prompt is correct.
4	Click music edit.	The administrator has logged in the website back-end.	Jump to the music modification page.
5	Click the delete button on the music modification page.	The administrator has logged in the website back-end. The administrator has entered the music modification page.	A prompt box "whether to delete the record" pops up, click OK, and return to the front page. The song will be deleted from the music list.
6	Click the edit button for music edit.	The administrator has logged in the website back-end. The administrator has entered the music modification page.	Jump to the music modification page. The song information displayed on the page is correct.
7	Click artist to edit.	The administrator has logged in the website back-end.	Jump to the page modified by the singer.
8	Click the edit button modified by the singer.	The administrator has logged in the website back-end. The administrator has entered the artist modification page.	Jump to the artist modification page. The artist information displayed on the page is correct.
9	Click to log out.	The administrator has logged in the website back-end.	Exit the background management and return to the homepage of the website.

TABLE 5: Experimental result table.

Estimation method	Number of songs	Strong accuracy (%)	Weak accuracy (%)	Error rate (%)
Error concealment	427	59.95	84.07	15.93
Template matching	463	55.29	77.53	22.46

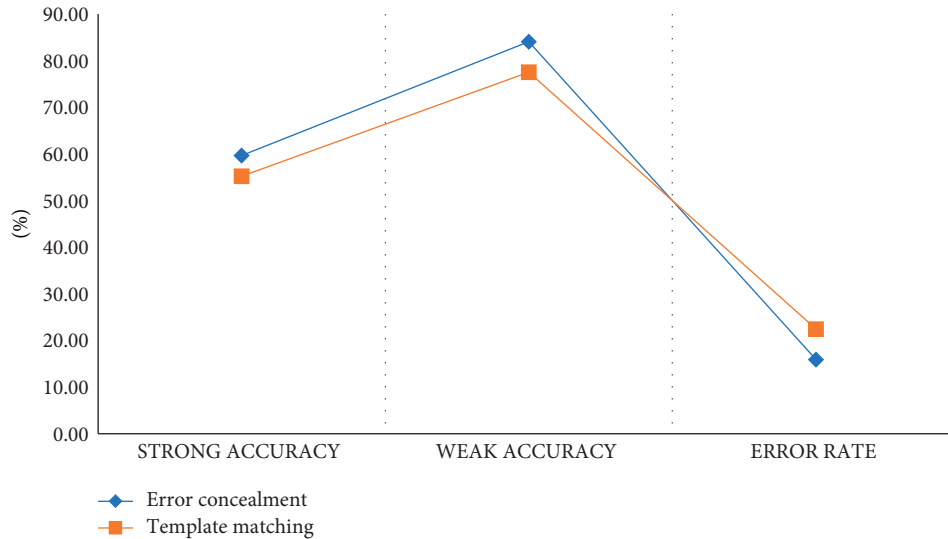


FIGURE 6: Result trend graph.

TABLE 6: Experimental results of error concealment method.

Number of songs	Song type	Strong accuracy (%)	Weak accuracy (%)	Error rate (%)
186	Pop	63.98	88.17	11.83
120	Rock	70.00	90.84	9.16
28	Jazz	46.42	74.99	25.00
35	Bossa-Brazil	25.71	62.85	37.14
43	Soul	55.48	74.41	25.58
15	Funky	53.33	73.34	26.66

TABLE 7: Template matching method experiment results.

Number of songs	Song type	Strong accuracy (%)	Weak accuracy (%)	Error rate (%)
198	Pop	60.10	82.83	17.17
137	Rock	61.31	79.57	20.43
31	Jazz	41.93	67.75	32.25
37	Bossa-Brazil	24.31	40.56	59.44
43	Soul	53.48	74.42	25.58
17	Funky	47.05	64.71	35.29

experiment involves a variety of music forms such as rock, jazz, and pop music. We analyze the two estimation methods of error concealment method and template matching method, and the experimental results are shown in Table 5 and Figure 6.

We conducted experiments on the training data of the International Music Retrieval and Evaluation Competition. The experimental results are shown in Tables 6 and 7.

From Figures 7 and 8, we can see that the two different detection methods have different results for different types of music, and the Bossa-Brazil music type has the highest error rate.

4.3. Test Model Performance Comparison

4.3.1. Test Platform. In order to detect the effect of voice abnormality detection under normal and noisy conditions, on the same test platform, the music detection model

without noise removal neural network and the KNN music detection model with noise removal were selected, and the corresponding algorithms are proposed. The performances of the voice anomaly detection model are compared and analyzed. The selected test platform settings are shown in Table 8.

4.3.2. Analysis of Detection Accuracy. The experiment selected 5 different music type numbers and divided them into two categories with noise and without noise, as shown in Table 9.

We used the voice anomaly detection model, neural network music detection model, and KNN music detection model designed in the article to detect the music data in the table. The experimental results are shown in Figures 9 and 10.

According to the results in Figures 9 and 10, the detection accuracy of the KNN model and the neural network model is low, and there are many requirements

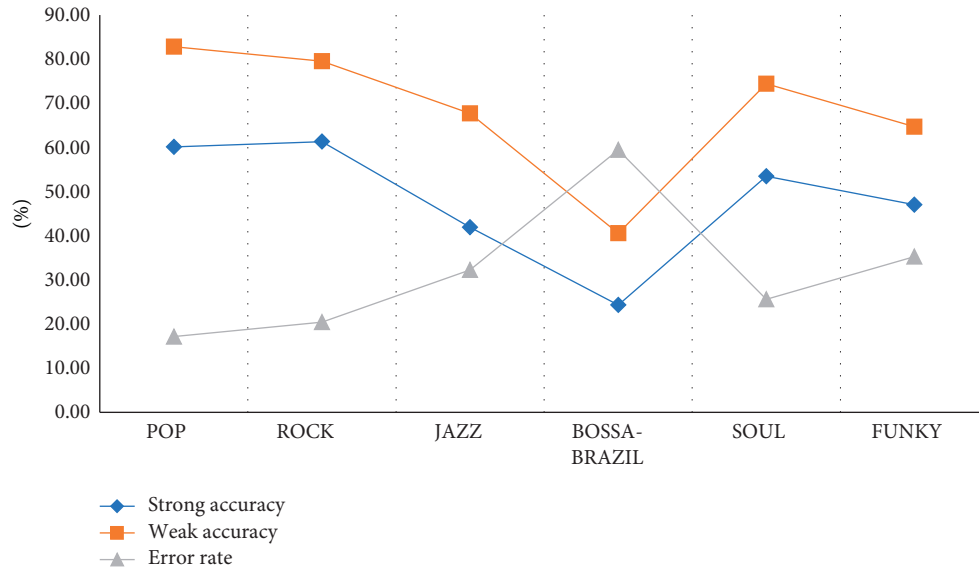


FIGURE 7: Trend of error concealment method.

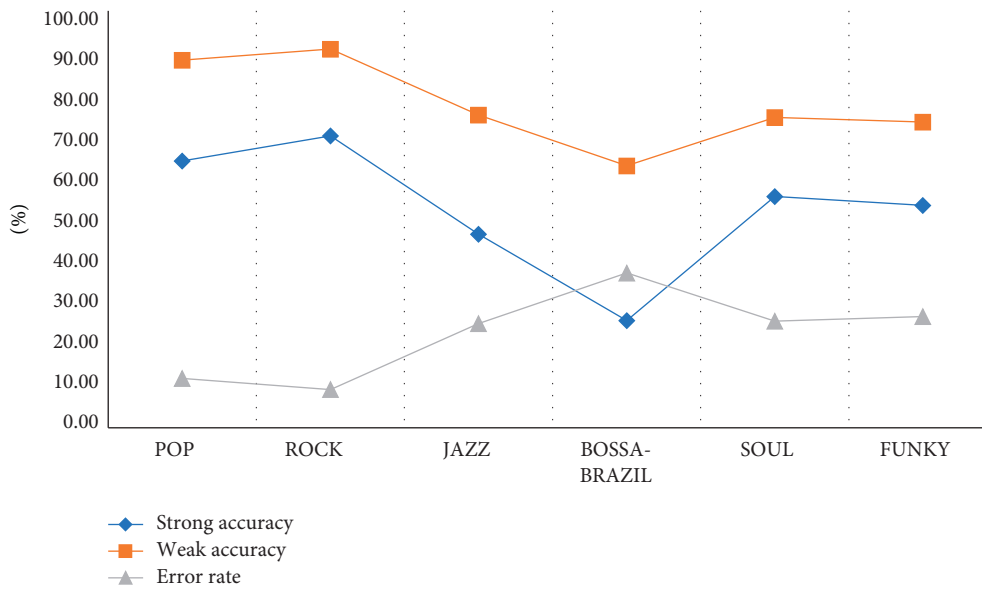


FIGURE 8: Trend chart of template matching method.

TABLE 8: Testing platform design.

Platform parameters	Parameter
CPU type	Intel
CPU frequency	2.86 GHz
Memory type and size	DDR 3400 16 GB
Hard disk type and size	Solid state, 320 GB
Programming tools	VC++6.0

TABLE 9: Music classification and detection object table.

Music type number	Noise	No noise
1	10	30
2	10	30
3	20	40
4	10	40
5	20	50

for the types of music signals. In the case of no noise, the detection accuracy of the KNN model can only reach 86%. In the case of noise, the detection accuracy will show a lower situation, and the detection accuracy of the neural network model under the condition of noise is higher,

which can explain the certain noise recognition function of the neural network system. The detection accuracy of the model proposed in this article can be maintained above 90% in the absence of noise and can reach above 85% in the presence of noise, which is the one with the highest detection accuracy among the three different

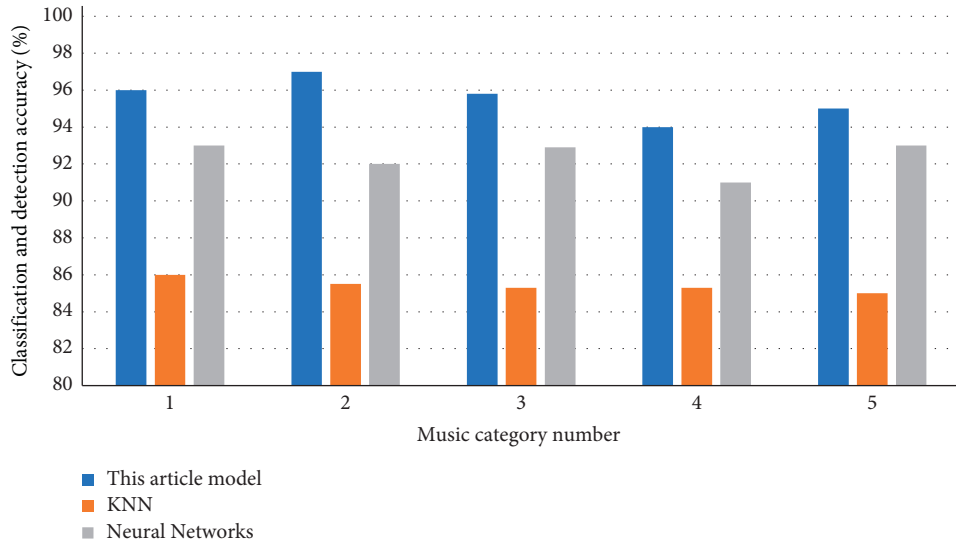


FIGURE 9: Comparison of boring music classification and detection accuracy.

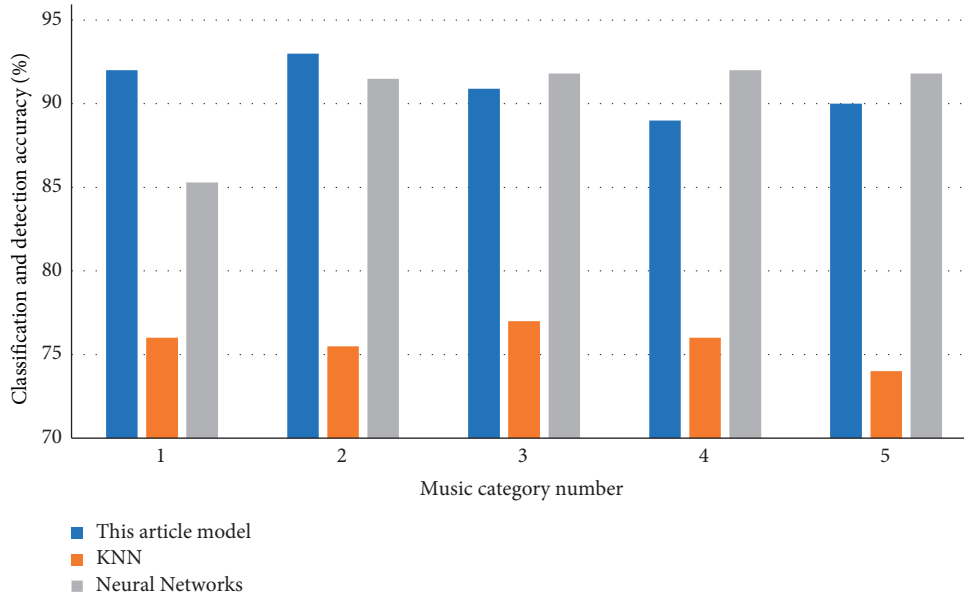


FIGURE 10: Comparison of dry music classification and detection accuracy.

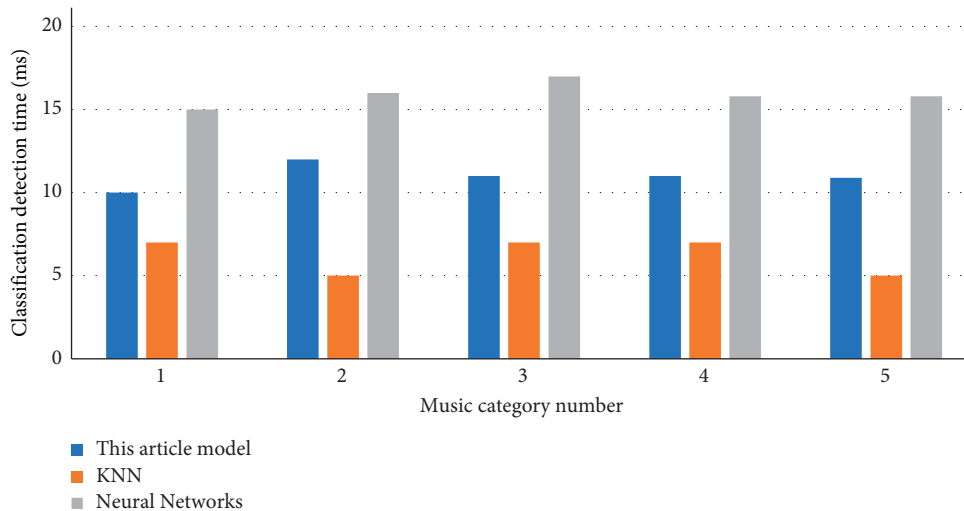


FIGURE 11: Music detection time comparison.

systems, the types of music detected are relatively more, and the efficiency of music detection is improved.

4.3.3. Analysis of Detection Efficiency. For music in a complex music environment, we have counted the music detection time of three models, and the experimental results are shown in Figure 11.

From Figure 11, we can see that although the KNN music detection model takes the shortest time to check, the KNN music detection model has a low detection accuracy rate and cannot meet the requirements of the system. The detection world of the model designed in this article is lower than that of the neural network detection model. It also shows that the influence of noise on the music signal is detected to a certain extent, and the efficiency of music detection is improved.

5. Conclusion

Based on 5G and Internet of Things technology, this paper also drives the development of music industry. Network communication has replaced the traditional way of communication and become a brand-new way of music communication. The main content of this paper is to design an online music website based on the Internet of Things, introduce the basic functions of the website, and design a voice anomaly detection system from login test, search function test, song display, administrator maintenance, and song management. In order to detect the accuracy of abnormal speech system, the experiment was to set up three different speech detection systems in the condition of noise and noise contrast experiment and test their experimental accuracy. The system designed in this paper has the highest accuracy, which can meet most requirements and improve the efficiency of music detection. The future work will further study the multi-intelligent recommendation algorithm of music websites, use real-time big data technology to analyze the similarity of multiple customers at the same time, and recommend that the customer attributes in different time periods are similar, so as to perform the group calculation of different users.

Data Availability

The experimental data used to support the findings of this study are available from the corresponding author upon request.

Conflicts of Interest

The authors declare that they have no conflicts of interest regarding this work.

Acknowledgments

This work was supported by Find a Funder: Department of Education of Hunan Province, Hunan Provincial Higher Education Reform Research Project (no. 666, 2019), and

Research on the Development of “Incorporating Educational Technology into Subject Knowledge” (TPACK) for Preservice Music Teachers.

References

- [1] L. He, Q. Xie, and U. Xian, “The design and development of music website[J],” *Electronics Test*, vol. 6, pp. 22–56, 2014.
- [2] A. S. D. Martha, A. I. Wuryandari, and Y. Priyana, “Design and interaction music search by humming on beatme online,” in *Proceedings of the 2014 IEEE 4th International Conference on System Engineering and Technology (ICSET)*, pp. 1–6, Bandung, Indonesia, October 2014.
- [3] L. Jin and L. Zhan, “Design and implementation of music website based on struts[J],” *Digital Technology and Application*, vol. 22, pp. 08–11, 2016.
- [4] X. J. Liu, S. W. Luo, and J. Wan, “Application and design about aesthetics of interface and format in on-line music website[J],” *Computer Knowledge and Technology (Academic Exchange)*, vol. 52, pp. 85–119, 2007.
- [5] J. Chen and C. B. Huang, “Design and development of online music website[J],” *Modern Computer*, vol. 23, pp. 85–119, 2012.
- [6] A. Rifaldi, “Design and development of savinof music group website using PHP,” *MYSQL[J]*, vol. 23, pp. 117–121, 2011.
- [7] Y. F. Zou, “Design and implementation of on-line music website[J],” *Computer Era*, vol. 23, pp. 77–100, 2011.
- [8] S. Batthalla, M. Swarnkar, N. Hubballi, and M. Natu, “VoIP profiler: profiling voice over IP user communication behavior,” in *Proceedings of the international conference on availability*, no. 20, pp. 85–106, IEEE, Salzburg, Austria, 02 September 2016.
- [9] N. Deo, V. Gupta, A. Acu, and P. Agrawal, Eds., in *Proceedings of the Mathematical Analysis II: Optimisation, Differential Equations and Graph Theory*, New Delhi, India, October 23–25 2018.
- [10] L. Dan, L. Lu, and H. J. Zhang, “Automatic Mood Detection from Acoustic Music Data,” in *Proceedings of the 4th International Conference on Music Information Retrieval*, pp. 81–87, Baltimore, Maryland, USA, October 27–30, 2003.
- [11] K. Minami, A. Akutsu, and H. Y. Hamada, “Video handling with music and speech detection,” *IEEE Multimedia*, vol. 5, no. 3, pp. 17–25, 1998.
- [12] B. Whitman, G. Flake, and S. Lawrence, “Artist detection in music with minnowmatch,” in *Proceedings of the neural networks for signal processing XI: proceedings of the 2001 IEEE signal processing society workshop (IEEE cat. No.01TH8584)*, no. 85, pp. 110–150, IEEE, North Falmouth, MA, USA, 12–12 September 2001.
- [13] Y. Zhu, M. S. K. ankanhalli, and S. Gao, “Music key detection for musical audio,” in *Proceedings of the 11 th International Multimedia Modelling Conference*, pp. 30–37, Melbourne, VIC, Australia, June 2005.
- [14] L. Dan, L. Lu, and H. J. Zhang, “Automatic mood detection from acoustic music data,” in *Proceedings of the 4th International Conference on Music Information Retrieval*, Baltimore, Maryland, USA, October 27–30, 2003.
- [15] Z. Tang, J. Wang, J. Wang, and J. Song, “A low-complexity detection algorithm for uplink NOMA system based on Gaussian approximation,” in *Proceedings of the 2017 IEEE Wireless Communications and Networking Conference (WCNC)*, pp. 1–6, San Francisco, CA, USA, October 2017.
- [16] D. M. Lofaro, Oh P, Oh], and al. et, “Interactive musical participation with humanoid robots through the use of novel

- musical tempo and beat tracking techniques in the absence of auditory cues,” in *Proceedings of the IEEE- RAS International Conference on Humanoid Robots*, July 2010.
- [17] X. Ning, K. Gong, W. Li, L. Zhang, X. Bai, and S. Tian, “Feature refinement and filter network for person re-identification,” *IEEE Transactions on Circuits and Systems for Video Technology*, vol. 31, no. 9, pp. 3391–3402, 2021.
- [18] S. Qi, X. Ning, G. Yang et al., “Review of multi-view 3D Object recognition methods based on deep learning,” *Displays*, vol. 69, Article ID 102053, 2021.
- [19] X. Ning, F. Nan, S. Xu, L. Yu, and L. Zhang, “Multi-view frontal face image generation: a survey,” *Concurrency and Computation: Practice and Experience*, vol. 1, Article ID e6147, 2020.
- [20] D. A. Reynolds and R. C. Rose, “Robust text-independent speaker identification using Gaussian mixture speaker models,” *IEEE Transactions on Speech and Audio Processing*, vol. 3, no. 1, pp. 72–83, Jan.1995.
- [21] D. A. Reynolds, “Comparison of background normalization methods for text-independent speaker verification,” in *Proceedings of the Fifth European Conference on Speech Communication and Technology*, DBLP, Rhodes, Greece, September 22-25, 1997.
- [22] D. A. Reynolds, T. F. Quatieri, and R. B. Dunn, “Speaker verification using adapted Gaussian mixture models,” *Digital Signal Processing*, vol. 10, no. 1-3, pp. 19–41, 2000.
- [23] M. Kawamoto, F. Asano, K. Kurumatani, and Y. Hua, “A system for detecting unusual sounds from sound environment observed by microphone arrays,” in *Proceedings of the 2009 Fifth International Conference on Information Assurance and Security*, pp. 729–732, Xi’an, China, January 2009.
- [24] N. Sawhney and C. Schmandt, “Nomadic radio,” *ACM Transactions on Computer-Human Interaction*, vol. 7, no. 3, pp. 353–383, 2000.
- [25] O. I. Pavlov and F. F. Dubrovka, “Evaluation of potential efficiency of speech coding using different parameters of linear prediction,” *Radioelectronics and Communications Systems*, vol. 63, no. 9, pp. 449–464, 2020.
- [26] S. Pini, G. Borghi, and R. Vezzani, “A systematic comparison of depth map representations for face recognition[J],” *Sensors*, vol. 21, no. 3, p. 944, 2021.
- [27] D. Battaglia, T. Boudou, E. C. A. Hansen et al., “Dynamic Functional Connectivity between order and randomness and its evolution across the human adult lifespan,” *NeuroImage*, vol. 222, Article ID 117156, 2020.
- [28] N. P. M. Todd, “The auditory “Primal Sketch”: a multiscale model of rhythmic grouping,” *Journal of New Music Research*, vol. 23, no. 1, pp. 25–70, 1994.

Research Article

Research of Consumption Behavior Prediction Based on Improved DNN

Yu Tian,¹ Yuhong Lai,¹ and Chao Yang ^{2,3}

¹Management Engineering Department, Sichuan Water Conservancy Vocational College, Chengdu 610000, China

²Bioengineering Department, Sichuan Water Conservancy Vocational College, Sichuan 610000, China

³College of Veterinary Medicine, Sichuan Agricultural University, Sichuan 611130, China

Correspondence should be addressed to Chao Yang; 2020403180@stu.sicau.edu.cn

Received 22 February 2022; Revised 15 March 2022; Accepted 1 June 2022; Published 25 June 2022

Academic Editor: Hangjun Che

Copyright © 2022 Yu Tian et al. This is an open access article distributed under the Creative Commons Attribution License, which permits unrestricted use, distribution, and reproduction in any medium, provided the original work is properly cited.

In terms of the low accuracy and unsatisfactory effect of traditional prediction models for consumption behavior, in the study of deep learning DNN model, a consumption behavior prediction model based on rDNN model is proposed. By choosing the appropriate function as the activation function of the model, the random sampling method is used to select negative samples of consumer behavior data to determine the N/P ratio, which improves the DNN model. Based on the improved DNN model, a consumer behavior prediction model based on the rDNN model is constructed. The results show that when the tanh function is used as the activation function and the ratio of N/P is 3, the rDNN model has the best prediction effect on consumption behavior, with AUC value of 0.8422 and the fastest operation efficiency of 434.36 s. Compared with traditional prediction models, DNN, and KmDNN deep learning models, the proposed model has more reliable prediction results and can be used to predict actual consumption behavior.

1. Related Work

Consumption behavior reflects the characteristics of consumers' consumption, individual preference, and inherent law. By analyzing consumption behavior, it is good for businesses to know more about consumers' real demand and market demand, so as to realize accurate recommendation of commodities and increase purchase rate. There are many factors affecting consumer behavior, including consumer's economy, consumer groups, and commodity value. How to screen out effective information from these massive data to predict consumer behavior is the main problem that needs to be solved at present. The analysis and prediction of consumption behavior has crossed the stage of qualitative analysis, and the machine learning model has been used for data studying, which effectively improves the prediction efficiency of consumption behavior. For example, Guo et al. proposed to analyze and predict consumer behavior by using a regression model. In this research method, the most crucial thing is to use individual consumption interests and habits

as the basic data for the whole prediction model. The results indicated that the regression model is feasible [1]. Zhao et al. mainly analyzed the characteristics of consumer behavior, which provided reference for the feature input of machine learning [2]. Xiao and Tong proposed to improve the efficiency of clustering by clustering the data before performing regression prediction; the results showed that the prediction accuracy of the method was over 98% [3]. Chung et al. analyzed data from 252 real EV charging users and then applied ensemble learning and machine learning for behavior prediction, which resulted in improved accuracy of charging behavior prediction [4]. In addition to behavioral prediction, some machine learning algorithms are also used for prediction in other fields, such as Parhizkar et al. [5] and Shapi Mel Keytingan et al. [6]. The principal component analysis method is applied to the prediction of energy consumption. Ren et al. and Yang et al. applied machine learning algorithms to the prediction of environmental energy consumption and glider energy consumption, and these provide more references for the application of machine

learning. However, with the development of e-commerce, the above methods can no longer meet the actual demand of consumer behavior [7, 8]. In order to better predict the consumption behavior, this paper intends to learn the consumption behavior from different perspectives and realize the prediction of consumption behavior through deep learning. Considering the large amount of consumption behavior data and in order to better explore the deep features of the data, the deep neural network (DNN) model is used as the basic model, and the rDNN model is constructed to predict consumption behavior by selecting the appropriate proportion of positive and negative samples and activation function.

2. Basic Method

2.1. Introduction of the DNN. The DNN is essentially a feedforward neural network with multiple hidden layers. With increasing the number of hidden layers in the neural layer, the feature learned by the model is richer, and the prediction effect of the model is improved. Compared with shallow neural network, the DNN has stronger learning ability, and its structure is shown in Figure 1 [9].

The DNN model training includes forward propagation and backward propagation. Assuming that the DNN model contains two hidden layers and the activation function is tanh function, the input layer is $g(x)$, $g(x) \in R^{n_k \times 1}$. In this expression, n represents the word vector dimension, and k represents data categories, which means the first hidden layer of forward propagation contains n_1 neurons. The input and output of this layer can be expressed by expressions (1) and (2) [10, 11]:

$$z_i^{(1)} = H_1 g(x) + b_1, \quad (1)$$

$$z_o^{(1)} = \tanh(z_i^{(1)}). \quad (2)$$

The second hidden layer contains n_2 neurons, and the input and output of this layer can be expressed by expressions (3) and (4):

$$z_i^{(2)} = H_2 z_o^{(1)} + b_2, \quad (3)$$

$$z_o^{(2)} = \tanh(z_i^{(2)}). \quad (4)$$

The output layer of the model is [12]

$$y = U \tanh(z_o^{(2)}) + b_3. \quad (5)$$

In expressions (1)–(5), H_1, H_2, U represent the weight matrix of hidden layer 1, hidden layer 2, and output layer, respectively, and b_1, b_2, b_3 represent the threshold matrix of hidden layer 1, hidden layer 2, and output layer, respectively.

Using θ to express all the parameters in the DNN, it will be

$$\theta = (H_1, H_2, U, b_1, b_2, b_3). \quad (6)$$

Use $y \in R^{n_3 \times 1}$ to show the function of θ , and y_i is the log probability of sample i of output layer; after normalization, it can be expressed as [13]

$$p(f_i|x, \theta) = \frac{e^{y_i}}{\sum_{j=1}^{N_3} e^{y_j}}. \quad (7)$$

In this expression, $f^{(i)}$ indicates the category of training sample i .

Backward propagation means that the labeled sample $(x^{(i)}, f^{(i)})$, $i \in N$, is used as the number of training samples, and $x^{(i)}$ represents the training sample i . Finding the parameter θ to maximize the log-likelihood probability of $R(\theta)$ with regular term, the likelihood function will be like the following expression [14]:

$$L(\theta) = \sum_{i=1}^N \log p(f^{(i)}|x^{(i)}, \theta) + R(\theta). \quad (8)$$

The random gradient ascending method is used to learn θ , and the backward propagation algorithm is used to iterate and update the parameters until the preset accuracy is reached. The iteration formula is shown in the following expression:

$$\theta \leftarrow \theta + \eta \frac{\partial \log p(f|x, \theta)}{\partial \theta}. \quad (9)$$

In this expression, η means learning rate.

The DNN model has good feature learning ability, but it is easy to have the problem of slow training speed because of its many parameters [15, 16]. To solve this problem, the DNN model is improved in this paper. According to the above analysis, the parameter quantity is closely related to the selection of activation function in the DNN model, so the model parameter quantity is reduced by selecting suitable activation function. In addition, the imbalance between positive and negative samples of data has some influence to the performance of the model. In order to further improve the performance of the model, the DNN model is improved by choosing the appropriate ratio of negative and positive samples, which is recorded as the N/P ratio.

2.2. Improvement of the DNN Model

2.2.1. Selection of Activation Function. The most frequently used activation functions are sigmoid, tanh, and relu. The mathematical expression of sigmoid function is shown in expression (10) [17]. The mathematical expression of tanh function is shown in expression (11). After simplifying calculation, tanh function is shown in expression (12) [18]. The mathematical expression of relu function is shown in expression (13). Compared with sigmoid function and tanh function, Relu has advantages in solving the problem of gradient disappearance. Therefore, the Relu function is chosen as the activation function.

$$\sigma_s = \frac{1}{1 + e^{-s}}, \quad (10)$$

$$\tanh = \frac{e^x - e^{-x}}{e^x + e^{-x}}, \quad (11)$$

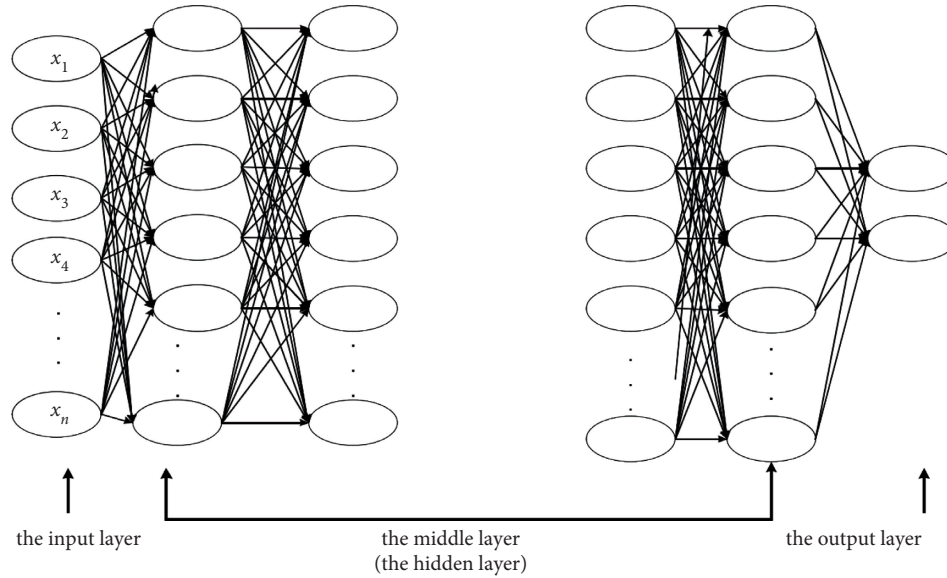


FIGURE 1: The DNN model's structure.

$$\tanh(x) = \frac{2}{1 + e^{-2x}} - 1, \quad (12)$$

$$\text{Relu} = \max(0, x). \quad (13)$$

2.2.2. *N/P Ratio Selection.* An appropriate N/P ratio can avoid the problem of data feature's singularity and improve the generalization ability of the model. Before selecting the N/P ratio, balancing the positive and negative samples of data should be done first. Referring to the literature [19, 20], random sampling of negative samples is used in this paper to balance the sample data. Subsamples with a certain proportion with positive samples are randomly selected from negative samples to balance them with positive samples, as shown in Figure 2. In this figure, white represents positive samples and black represents negative samples.

Based on the above improvements, this paper constructs an improved DNN model, which is called rDNN model, and this model is used to predict the consumption behavior. The structure of the rDNN model is shown in Figure 3.

3. Prediction Method of Consumption Behavior Based on the rDNN Model

3.1. *Feature Selection of Consumer Behavior.* Feature selection is the basis of constructing the prediction model of consumption behavior, and the most suitable data feature for consumption behavior is conducive to improving the prediction accuracy and efficiency of the model. Combining the literature [21] and the characteristics of consumption behavior data, this paper selects the characteristics of consumption behavior data from six dimensions in Table 1.

Considering that the dimensions and units of the features mentioned above are not united, in order to avoid their influence on the prediction of the model, min-max

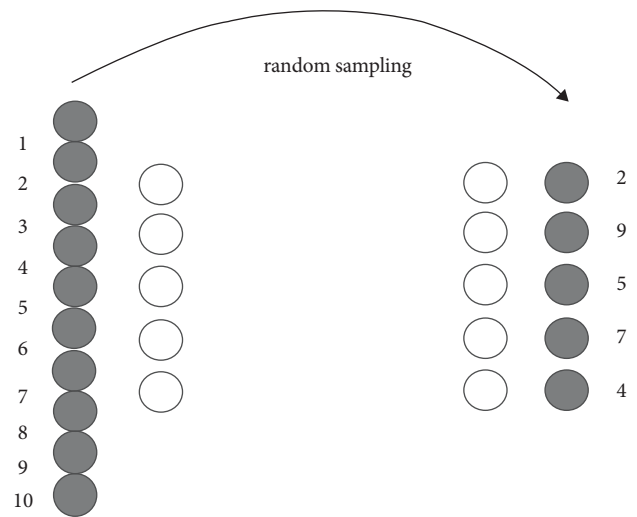


FIGURE 2: Diagram with N/P ratio of 1.

standardization is carried out on them, which is shown in expression (14) [22]. The missing values of the features are filled with 0 to obtain a large-scale sparse matrix of features.

$$X^* = \frac{X - X_{\min}}{X_{\max} - X_{\min}}. \quad (14)$$

3.2. *Construction of the rDNN Model.* The way of constructing the rDNN model is by reducing the redundancy of model training data, improving the efficiency of model training, and realizing more accurate analysis and prediction of consumption behavior. The specific construction process of the rDNN model is as follows:

- (1) Collect and pretreat consumption behavior data and divide them into training set and verification set in time sequence.

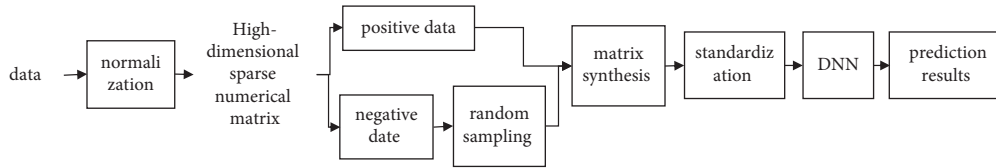


FIGURE 3: Diagram of the rDNN model structure.

TABLE 1: Choice of consumer behavior characteristics.

Users	Each count of the users' every behavior on the 1st, 2nd, and 5th day before the inspection date Total count of the users' every behavior on the 1st, 2nd, and 5th day before the inspection date User purchase conversion rate (purchase count/behaviors' total count)
Commodity	Commodity's total number of users on the 1st, 2nd, and 5th day before the inspection date Commodity's total number of every behavior on the 1st, 2nd, and 5th day before the inspection date Commodity's each count of every behavior on the 1st, 2nd, and 5th day before the inspection date Commodity purchase conversion rate (purchase count/behaviors' total count)
Commodity category	Category's total number of users on the 1st, 2nd, and 5th day before the inspection date Category's total number of behaviors on the 1st, 2nd, and 5th day before the inspection date Category's each count of every behavior on the 1st, 2nd, and 5th day before the inspection date Category purchase conversion rate (purchase count/behaviors' total count)
User-commodity	User-commodity's count of behaviors on the 1st, 2nd, and 5th day before the inspection date User-commodity rank behaviors of user's interaction commodities
User-commodity category	User-commodity category's total number of behaviors on the 1st, 2nd, and 5th day before the inspection date User-commodity category's each count of every behavior on the 1st, 2nd, and 5th day before the inspection date User-commodity category rank behaviors of user's all commodities
Commodity-commodity category	Commodity's rank of total number of behaviors in commodity category Commodity's rank of the number of users in commodity category

- (2) Divide the training set into positive and negative samples with certain rules and balance the data categories with randomly getting negative samples.
- (3) Construct the DNN model, initialize model parameters, and train the model using the training set.
- (4) Use backward propagation to adjust the model parameters until the model has the best prediction of consumption behavior data, and then the model is used as the best model to predict the consumption behavior data.
- (5) Input the preprocessed data into the optimal rDNN model, and the output result is the prediction result.

In the above process, the rDNN model building process can be illustrated in Figure 4.

4. Simulation Experiment

4.1. Construction of Experimental Environment. This experiment runs on Windows 7, i5 processor, and 8G + 4G memory and is programmed with Python 2.7.

4.2. Data Source and Processing

4.2.1. Data Sources. In this experiment, the real data of consumer behavior in "Tianchi Big Data Competition" were selected as the experimental dataset. The dataset includes two

parts: user-commodity behavior dataset and commodity subset. The specific data formats are shown in Tables 2 and 3 [23].

4.2.2. Data Preprocessing. Through statistical analysis of experimental dataset, it can be seen that there is a problem of missing features in the data, and the processing effect of hash coding is not good, so this experiment deletes it. In addition, the study finds that consumer behavior has certain periodicity in all data except the "Double 12" day. Therefore, it is divided into four groups according to the characteristics, which are shown in Table 4. Group 3 contains data of the "Double 12" day, and the data explosion can easily affect the prediction effect of the model, so it was deleted in this experiment, and take group 1 as the training set, group 2 as the verification set, and group 4 as the test set.

Type 1 is defined as positive samples, and other types are samples from statistics of behavior category data. The data distribution is shown in Figure 5. It can be seen that the category data of consumer behavior are seriously unbalanced, with 325,797,507 positive samples and 23,058,448 negative samples, and the ratio is close to 1 : 99. To solve the problem of unsatisfactory model prediction results caused by unbalanced data categories, in this experiment, millions of negative samples are selected according to the characteristics of the selected dataset. Negative samples were obtained by random sampling technique. It reduces the large proportion of positive and negative samples and achieves the balance of data categories.

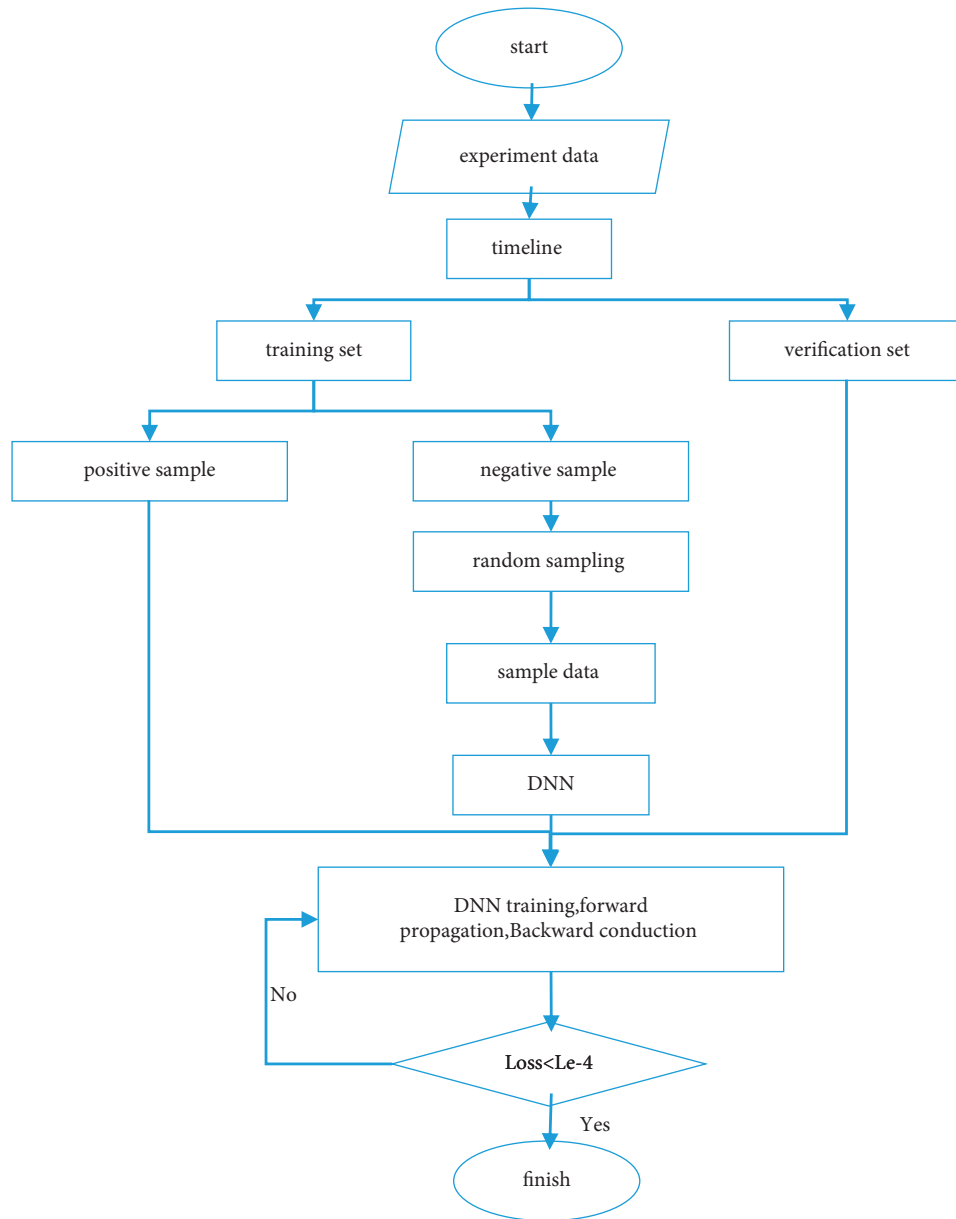


FIGURE 4: rDNN model building process.

TABLE 2: User-commodity behavior dataset form.

Field	Field description	Extraction description
user_id	User number	Sample and field mask
item_id	Item number	Field mask
behavior_type	User behavior type	1 means browse, 2 means collect, 3 means add commodity into shopping cart, and 4 means purchase
user_geoliash	User space location	After latitude and longitude encryption processing
item_category	Commodity category	Field mask
Tune	User behavior time	Accurate calculation to the hour

TABLE 3: Data format of commodity subset.

Field	Field description	Extraction description
item_id	Item number	Field mask
item_geoliash	Commodity space location identification	After longitude and latitude encryption
item_categoiy	Commodity category	Field mask

TABLE 4: Data partition.

Number	Date
Group 1	11.22~11.28
Group 2	11.29~12.5
Group 3	12.6~12.12
Group 4	12.13~12.18

TABLE 5: Basic parameter settings of rDNN model.

Parameters	Parameter setting
Model structure	128-64-64-30-2
Objective function	binary_crossentropy
The maximum number of training iterations	200
Activation function	Relu

TABLE 6: K-means parameter setting.

Parameters	Parameter setting
The maximum number of iterations	200
Cluster number	1000
The number of sampling subsets	200

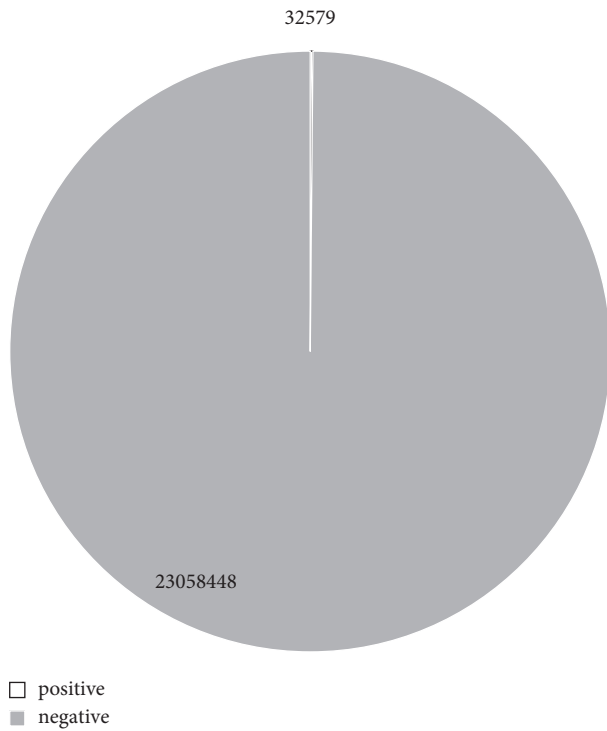


FIGURE 5: Distribution of consumer behavior category data.

4.3. Evaluation Indicators. In this experiment, AUC value is selected as the performance index of the evaluation model, and it is calculated by the following expression [24–26]:

$$= \frac{TP + TN}{TP + TN + FP + FN}, \quad (15)$$

where TP represents true positive, FN represents false negative, FP represents false positive, and TN represents true negative.

4.4. Parameter Settings. The basic parameters of the rDNN model and the DNN model in this experiment are shown in Table 5. The parameters of K-means in the KmDNN model are shown in Table 6.

4.5. Experimental Results

4.5.1. Model Verification. To verify the availability of the proposed model, this paper compared the effects of different N/P ratios and activation functions on the prediction [27, 28].

(1) *Different N/P Ratios.* Set the N/P ratios to 1, 2, 3, 4, and 5, respectively, and test the influence of the change of N/P ratio in a small range on the prediction effect of the model. The results are shown in Figure 6. It can be seen that when the N/P ratio is adjusted in a small range, the AUC value is around 0.8. When the N/P ratio is expanded and set to 10, 20, 30, 40, and 50 to study the prediction effect of the model in a wide range, the results are shown in Figure 7. It can be seen that with the increase of N/P ratio, the AUC value fluctuates greatly, and the maximum AUC value is 0.8214, with the N/P ratio of 10. Therefore, the experiment controls the range in (0,10) and studies the prediction effect of the model to ensure the best N/P ratio. Set the N/P ratios of 6, 7, 8, and 9 for the experiment, and the AUC value is shown in Figure 8. The figure further proves that when the N/P ratio is adjusted in a small range, the N/P ratio has little influence on the prediction effect of the model. Comparing Figure 6 with Figure 8, it can be seen that when the ratio of N/P is 3, the AUC value is the biggest, which is 0.8359, indicating that the model has the best prediction effect at this time, so this study set the ratio of N/P to 3.

(2) *Different Activation Functions.* The prediction performance of the rDNN model constructed by different activation functions is shown in Figure 9. It can be seen that when the sigmoid function is used as activation function, the AUC value of the rDNN model is the biggest with the number of hidden layers of 2. As the number of hidden layers increases, the AUC value of the model gradually

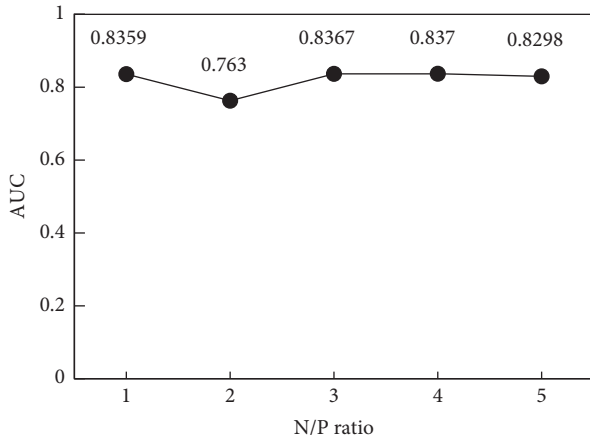


FIGURE 6: Prediction effect of different N/P ratio models in a small range.

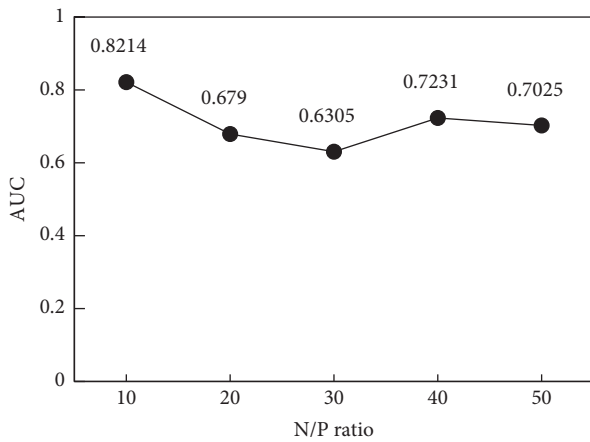


FIGURE 7: Prediction effect of different N/P ratio models in a wide range.

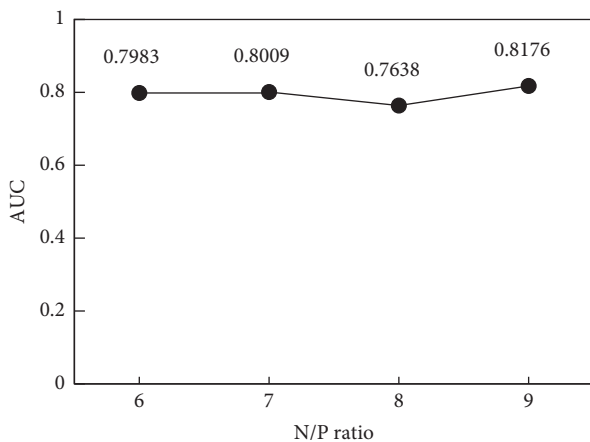


FIGURE 8: Comparison of prediction effects of different N/P ratio models.

decreases, indicating that when sigmoid function is used as the activation function, the optimal number of hidden layers of the rDNN model is 2. When relu function is used as

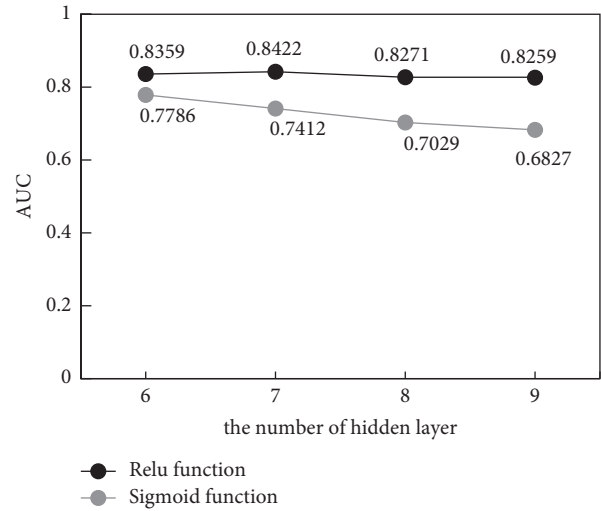


FIGURE 9: Influence of adjusting the number of hidden layers on model performance with different activation functions.

activation function, the largest AUC value corresponds to 3 hidden layers, which means that when relu function is the activation function, the optimal number of hidden layers of the rDNN model is 3. Comparing sigmoid function with relu function, when relu function is used as activation function, the AUC value of relu function is bigger, and the difference of AUC value is small. When sigmoid function is used as the activation function, the AUC value of the rDNN model is greatly reduced, which indicates that the number of hidden layers has little influence on the prediction effect of the rDNN-rule model but greatly affects the prediction effect of the rDNN-sigmoid model. This proves that relu function is in favour of improving the stability of the rDNN model.

In terms of training time, the time of the rDNN-sigmoid model is 714.76 s, while the time of the rDNN-rule model is 434.36 s, which is obviously better than rDNN-sigmoid model. To sum up, relu function is more suitable as the activation function of the rDNN model than sigmoid function. Therefore, this paper chooses relu function as the activation function of the rDNN model.

4.5.2. Model Comparison. In order to verify the superiority of the proposed model, the prediction results of different deep learning models are compared. To avoid accidental errors, the experiment was repeated 50 times with different depth learning models, and the average value was taken as the final experimental result, which is shown in Table 7. It can be seen that compared with the DNN model, the AUC value of the rDNN model proposed in this study is bigger, which indicates that choosing an appropriate N/P ratio to reduce the gap between positive and negative samples is conducive to improving the performance of the model. Compared with the KmDNN model with K-means algorithm, the AUC value of the proposed rDNN model is bigger, and the prediction effect is better. The reason is that the K-means algorithm needs to set the number of cluster in advance when clustering negative samples [29–31]. It leads

TABLE 7: Comparison of prediction effects of different deep learning models.

Deep learning model	Average AUC
DNN	0.7907
rDNN	0.8297
KmDNN	0.8103

TABLE 8: Effect comparison of different models.

	Model	AUC
Traditional prediction model	Logistics model	0.7203
	Neural network	0.7208
	Random forest	0.7498
Deep learning model	DNN	0.7907
	rDNN	0.8297
	KmDNN	0.8103

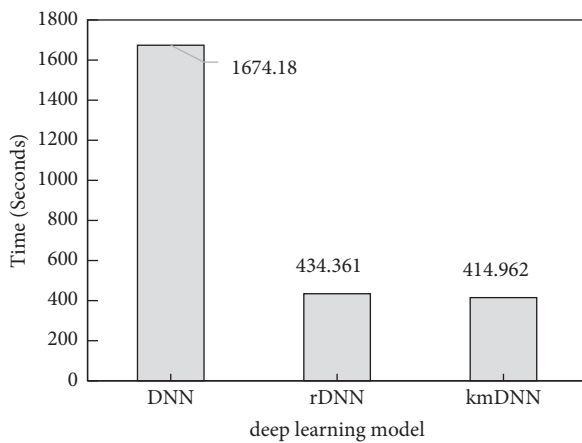


FIGURE 10: Comparison of running time.

to the inability to extract samples of different clusters with equal probability and affects the clustering accuracy, making the prediction result of the KmDNN model not optimal. To sum up, the proposed rDNN model is better than the standard DNN model and the KmDNN model with K-means algorithm.

To further verify the superiority of the proposed model, this paper compares the performance of the proposed model with the traditional prediction model, and the results are shown in Table 8. It shows that the prediction effect of the deep learning model is better than the traditional prediction model. Among the deep learning models, the rDNN model has the best prediction effect. The reason is that during training, the rDNN model reduces numerous negative samples of unbalanced data with redundant information and greatly decreases the scale of model training data, exerting good performance of positive samples of balanced data [32–34]. This improves the prediction effect of the model.

(1) *Comparison of Operation Efficiency.* To verify the effectiveness of the proposed rDNN model, the training time of this model is compared with that of standard DNN model and KmDNN model, and the results are shown in Figure 10.

The figure indicates that the training time of DNN model is the longest because the dataset trained by DNN model is the original dataset, which has a large amount of data and an unbalanced proportion of positive and negative samples categories. The KmDNN model and the rDNN model have little difference in training time because the KmDNN model and rDNN model randomly sample the original data, which greatly reduces the amount of training data. But the rDNN model has a wider application range and is more suitable for applications in the background of big data. Therefore, with comprehensive analysis, the rDNN model proposed in this study has better performance, and it is more suitable for recommendation systems in big data environment, which can meet the requirements of high timeliness and precision.

5. Conclusion

To sum up, the deep learning model based on the rDNN model proposed in this paper improves the DNN model by selecting the appropriate activation function and N/P ratio. When the model chooses tanh function as the activation function, the number of hidden layers is 3, and the N/P ratio is 3, and the model can predict the consumption behavior more accurately. Compared with the traditional prediction models, such as random forest, neural network, logistics model, DNN, and KmDNN models, the proposed one has a more efficient and accurate prediction effect, and the AUC value is increased from 0.7893 (the AUC value predicted by the DNN model) to 0.8422, and the training time of the model is only 434.36 s, which is effective and can be used for actual consumption behavior prediction. Due to the limited experimental conditions, there are some shortcomings in this study. For example, when using random sampling method to reduce the amount of negative samples, the number of negative samples to be processed in practical application is often more than that in the experiment, so how to reduce the amount of negative samples should be further explored.

Data Availability

The experimental data used to support the findings of this study are available from the corresponding author upon request.

Conflicts of Interest

The authors declare that they have no conflicts of interest.

References

- [1] L. Guo, B. Zhang, and X. Zhao, “A Consumer Behavior Prediction Model Based on Multivariate Real-Time Sequence Analysis,” *Mathematical Problems in Engineering*, vol. 2021, Article ID 6688750, 5 pages, 2021.
- [2] B. Zhao, “Analysis of household green food consumption behavior based on machine learning prediction,” *Journal of Ambient Intelligence and Humanized Computing*, pp. 1–13, 2021.

- [3] S. Xiao and W. Tong, "Prediction of user consumption behavior data based on the combined model of TF-IDF and logistic regression," *Journal of Physics: Conference Series*, vol. 1757, no. 1, Article ID 012089, 2021.
- [4] Y. Chung, B. Khaki, T. Li, C. Chu, and R. Gadh, "Ensemble machine learning-based algorithm for electric vehicle user behavior prediction," *Applied Energy*, vol. 254, no. C, Article ID 113732, 2019.
- [5] T. Parhizkar, E. Rafeipour, and A. Parhizkar, "Evaluation and improvement of energy consumption prediction models using principal component analysis based feature reduction," *Journal of Cleaner Production*, vol. 279, 2021.
- [6] M. Shapi Mel Keytingan, R. N. Azuana, and J. Awalil Lilik, "Energy consumption prediction by using machine learning for smart building: case study in Malaysia," *Developments in the Built Environment*, vol. 5, 2021.
- [7] L. Ren, W. Zhonghang, C. Haihong, and Y. Jie, "Research on energy consumption prediction based on machine learning," *IOP Conference Series: Earth and Environmental Science*, vol. 791, no. 1, 2021.
- [8] S. Yang, X. Xudong, W. Yanhui, Y. Shaoqiong, M. Wei, and W. Peng, "Energy consumption prediction method based on LSSVM-PSO model for autonomous underwater gliders," *Ocean Engineering*, vol. 230, 2021.
- [9] M. Wang, T. Sun, K. Song, L. Shuang, J. Jing, and S. Linjun, "An efficient sparse pruning method for human pose estimation," *Connection Science*, vol. 34, pp. 1–15, 2021.
- [10] L. Sun, Q. Yu, D. Peng, S. Subramani, and X. Wang, "Fogmed: a fog-based framework for disease prognosis based medical sensor data streams," *Computers, Materials & Continua*, vol. 66, no. 1, pp. 603–619, 2021.
- [11] I. Giancarlo, L. B Lucia, and P. Gaetano, "Personal Protection Equipment detection system for embedded devices based on DNN and Fuzzy Logic," *Expert Systems with Applications*, vol. 184, 2021.
- [12] Z. Li, V. Chang, H. Hu, M. Fu, J. Ge, and F. Piccialli, "Optimizing makespan and resource utilization for multi-DNN training in GPU cluster," *Future Generation Computer Systems*, vol. 125, pp. 206–220, 2021.
- [13] L. Sun, Y. Wang, Z. Qu, and N. N. Xiong, "BeatClass: a sustainable ECG classification system in IoT-based eHealth," *IEEE Internet of Things Journal*, vol. 9, no. 10, pp. 7178–7195, 2022.
- [14] A. Rehman, S. Saleem, U. G. Khan, S. Jabeen, and M. O. Shafiq, "Scene recognition by joint learning of DNN from bag of visual words and convolutional DCT features," *Applied Artificial Intelligence*, vol. 35, no. 9, pp. 623–641, 2021.
- [15] S. Ismail, N. A. Bou, N. Nawel, E. Ashraf, A. Adi, and P. Kemal, "Novel hybrid DNN approaches for speaker verification in emotional and stressful talking environments," *Neural Computing and Applications*, vol. 33, pp. 1–23, 2021.
- [16] T. Upadhaya, H. Minea, L. Floriane et al., "Radiomics based deep fully connected neural network (R-DNN) for prognostication of lung cancer," *Journal of Nuclear Medicine*, vol. 59, 2018.
- [17] S. Lee, S. Cho, S.-H. Kim et al., "Deep neural network approach for prediction of heating energy consumption in old houses," *Energies*, vol. 14, no. 1, p. 122, 2020.
- [18] C. Yan, G. Pang, X. Bai et al., "Beyond triplet loss: person re-identification with finegrained difference-aware pairwise loss," *IEEE Trans. Multimedia*, 2021.
- [19] X. Ning, P. Duan, W. Li, and S. Zhang, "Real-time 3D face alignment using an encoder-decoder network with an efficient deconvolution layer," *IEEE Signal Processing Letters*, vol. 27, pp. 1944–1948, 2020.
- [20] L. C. Sing, M. Zhenyao, W. Ting, Y. Haoliang, N. Wing, and L. L. Lei, "Load forecasting based on deep neural network and historical data augmentation," *IET Generation, Transmission and Distribution*, vol. 14, no. 24, pp. 5927–5934, 2020.
- [21] M. RoxanaElena, C. M. C. Mihai, P. Constantin et al., "Person Re-identification across data distributions based on general purpose DNN object detector," *Algorithms*, vol. 13, no. 12, p. 343, 2020.
- [22] Y. Zhang and L.-S. Young, "DNN-assisted statistical analysis of a model of local cortical circuits," *Scientific Reports*, vol. 10, no. 1, Article ID 20139, 2020.
- [23] C. Wang, J. Zhou, B. Xiao et al., "Uncertainty estimation for stereo matching based on evidential deep learning," *Pattern Recognition*, vol. 124, 2021.
- [24] N. Rahaman, B. Aristide, A. Devansh et al., "On the spectral bias of deep neural networks," 2018, <http://arxiv.org/abs/1806.08734>.
- [25] L. Young, "Towards a mathematical model of the brain," *Journal of Statistical Physics*, vol. 180, pp. 612–629, 2020.
- [26] L. Chariker, R. Shapley, and L.-S. Young, "Rhythm and synchrony in a cortical network model," *Journal of Neuroscience*, vol. 38, no. 40, pp. 8621–8634, 2018.
- [27] C. Tan, "Digital confucius? exploring the implications of artificial intelligence in spiritual education," *Connection Science*, vol. 32, no. 3, pp. 280–291, 2020.
- [28] Z. Liu, F. Han, and Q.-H. Ling, "A novel particle swarm optimisation with mutation breeding," *Connection Science*, vol. 32, no. 4, pp. 333–361, 2020.
- [29] K. Junya, T. Shinnosuke, M. Masanori, S. Hiroshi, and S. Shigeki, "DNN-based full-band speech synthesis using GMM approximation of spectral envelope:regular section," *IEICE-Transactions on Info and Systems*, vol. 103, no. 12, pp. 2673–2681, 2020.
- [30] C. L. Betty and P. G. Fernando, "Adam and the ants: on the influence of the optimization algorithm on the detectability of DNN watermarks," *Entropy*, vol. 22, no. 12, 2020.
- [31] S. Qi, X. Ning, G. Yang et al., "Review of multi-view 3D object recognition methods based on deep learning," *Displays*, vol. 69, no. 1, 2021.
- [32] W. Cai, D. Liu, X. Ning, W. Chen, and X. Guojie, "Voxel-based three-view hybrid parallel network for 3D object classification," *Displays*, vol. 69, no. 1, 2021.
- [33] X. Bai, X. Wang, X. Liu et al., "Explainable deep learning for efficient and robust pattern recognition: a survey of recent developments," *Pattern Recognition*, vol. 120, Article ID 108102, 2021.
- [34] X. Wang, C. Wang, B. Liu et al., "Multi-view Stereo in the Deep Learning Era: A Comprehensive Review," *Displays*, vol. 70, 2021.

Research Article

Evaluation of Ecological Environment Quality in Chongqing Main City Area Based on Principal Component Analysis

Chunyang Chen ¹, Quansheng Ge,¹ Zexing Tao,¹ and Liang Liang²

¹Institute of Geographic Sciences and Natural Resources Research, CAS, Beijing 100101, China

²School of Geography, Geomatics and Planning, Jiangsu Normal University, Xuzhou 221116, China

Correspondence should be addressed to Chunyang Chen; chency.10s@igsrr.ac.cn

Received 23 March 2022; Revised 12 May 2022; Accepted 26 May 2022; Published 15 June 2022

Academic Editor: Hangjun Che

Copyright © 2022 Chunyang Chen et al. This is an open access article distributed under the Creative Commons Attribution License, which permits unrestricted use, distribution, and reproduction in any medium, provided the original work is properly cited.

With the rapid development of social productive forces in China, the process of urbanization has been accelerating, resulting in the deterioration of urban environmental quality and the destruction of ecosystems, such as debris flow, drought, water bloom, large-scale haze weather, and other ecological and environmental problems. The quality of the urban ecological environment is not only related to the stability of urban ecological function but also affects the sustainable development of the city. Many scholars have studied the problem of ecoenvironmental quality assessment, but there are still some shortcomings in the evaluation process, such as the construction of the index system and the application of related methods. Taking Chongqing as the research object, after referring to the representative evaluation index system in China, the evaluation index system of ecological environment quality in Chongqing was constructed from three aspects of nature, economy, and society. In this article, the principal component analysis (PCA) method is used to construct the ecoenvironmental quality evaluation system of Chongqing, and the economic development, pollutant control, natural protection and pollution reduction investment, urban and rural cooperation, land area, and other aspects are comprehensively evaluated. The relationship between simulated variables and the regression equation was also assessed. Through the comparative analysis of the two evaluation methods, it can be seen that the evaluation results of the PCA method and the fuzzy comprehensive evaluation method are basically the same in the longitudinal trend, which shows that the application of this method in the field of ecological environment quality evaluation has certain scientific rationality.

1. Introduction

Ecological harmony and sustainable development play an increasingly important role in the history of human development. As the gathering point of human development, the quality of the ecological environment is related to the stability of the ecological system and the long-term development of cities. However, due to the emergence of new cities and the continuous expansion of old cities, there have been a series of ecological and environmental problems such as explosive growth of urban population, traffic congestion, urban overload, shortage of water resources, and overall fragility of the urban ecosystem. Under the cross-influence of the contradiction between environmental protection and economic development, the importance of sustainable development has become increasingly prominent. The

construction and protection of the ecological environment and corresponding academic research are the basis of making urban environmental planning and urban economic and social development planning. The construction and protection of the ecological environment have important guiding significance.

Some scholars have studied the ecological evaluation system and discussed the ecological environment level of Chongqing and concluded that there is a strong correlation between the fluctuation of urban ecological environment quality and the investment level of ecological level [1]. Some researchers use time series analysis (PCA) to evaluate the environmental quality of Chongqing. It can be seen that the rural subsystem and the urban subsystem are opposite, and there is a negative evolution problem [2]. Some researchers have analyzed the evolution law and driving factors of

urbanization quality in Chongqing by entropy method, factor contribution rate, and contribution elasticity analysis and found that ecological environment and urban-rural coordinated development quality are the “main engines” for improvement [3]. Using quantitative methods of landscape ecology and RS-GIS techniques [4], some researchers explored the contradictions among human activities, urban enrollment expansion, and natural ecological landscape development in Chongqing. Some researchers combined GIS and AHP methods, combined with the regional environmental characteristics of western Chongqing, constructed the ecological environment evaluation index system in western Chongqing, and studied the correlation between ecological environment and social, economic, and environmental pollution factors [5]. Some researchers use RS and GIS technology to evaluate the ecological environment quality of the Three Gorges Reservoir [6]. It is concluded that the horizontal distribution of ecological environment quality is closely related to the vertical difference of slope and the regional difference in reservoir area. Some researchers have studied the environmental problems in the Qianjiang area of Chongqing and given corresponding schemes and measures, which are beneficial to the sustainable development of the Qianjiang area [7]. Some scholars have constructed the hierarchical structure of ecological data indicators and the dynamic monitoring and early warning system of ecological quality in Chongqing [8], which provides theoretical support for improving the efficiency of the urban ecological environment and the early warning level of ecological security in Chongqing. Based on the coordination degree model, some researchers discussed the urbanization level and regional differences in the Chengdu-Chongqing area [9] and concluded that economy, population, and infrastructure levels are the main driving factors affecting the spatial differences in urbanization quality in the Chengdu-Chongqing area. Some researchers investigated the factors of water stress and the effectiveness of water management measures in Chongqing. The research shows that the improvement of the water resources system is mainly due to the increase in forest coverage rate and the continuous investment in the ecological management of the Three Gorges Reservoir [10]. Some researchers have completed the calculation and analysis of ecological footprint in Chongqing from 2000 to 2013, and the results reflect the stress trend of ecological environment sustainable development ability and ecological capacity in the study area. According to the ecological security situation of land resources in Chongqing [11], some researchers put forward some suggestions on coordinating land resources, strengthening land management, and ecological environment protection [12]. Based on the theory of regional division of labor, some researchers have analyzed the driving mechanism of urbanization in Chongqing and put forward the strategic policy of sustainable urbanization [13]. Among some researchers, after investigating the Nan’an District of Chongqing, it is concluded that the increase in the proportion of the nonagricultural population and economic development are important factors affecting the ecological environment index [14]. Overexploitation of land and other factors have a negative impact on natural

ecology. Some researchers have studied the dynamic changes in land use and landscape pattern in the Chongqing metropolitan area in the past 20 years and concluded that the management and decision-making departments should formulate scientific and reasonable land use planning and urban development planning and strengthen ecological environment protection while developing economy [15]. In the introduction to describe the relevant literature, in the current study, it can be seen that different regions, using different methods have different effects. According to different regions and different time periods in Chongqing, the method is analyzed and applied, and it has been widely used. In different applications, due to the differences in methods, the analysis results are also different. The PCA model can be used to analyze the correlation degree of different index parameters in depth.

Section 2 of the article explains some concepts and concepts of ecological environment quality assessment in the main urban area of Chongqing. Section 3 establishes the evaluation index system of ecological environment quality in Chongqing. Section 4 demonstrates the ecological environment quality evaluation by PCA in Chongqing.

2. Related Theories of Ecological Environment Quality Evaluation in the Main Urban Area of Chongqing

2.1. Urban Ecosystems. A city is the product of coordinated survival and development of human beings, which has the characteristics of sufficient population, and the trinity of culture, economy and science, and technology. The urban ecosystem refers to the combination of the urban environment and organic life within the city, which is mainly formed by the human transformation of the natural ecosystem. The urban ecological environment includes natural ecological environment, social environment, economic environment, and artificial ecological environment. Various environmental components interact and restrict each other through material exchange, energy circulation, information circulation, and other functions, forming an organic unity. Through the evaluation of nature, culture, and economy, we can quantitatively understand the ecological environment quality of the evaluated city and further explore the concrete planning of urban sustainable development and understand the specific situation of specific urban areas.

At present, most of the mainstream views focus on long-term development, and scholars also use this view to evaluate the quality of the ecological environment. For example, the Environmental Sustainable Development Index (ESI) jointly constructed by Yale University, Columbia University, and the World Economic Forum in 2000 is predictable abroad and is an important reference for evaluating the environmentally sustainable development of all countries in the world. Similarly, the Human Development Index proposed by the United Nations Development Programme and the developmental financial dividend model created by the Canadian Institute for Sustainable Development. In the 1980s, China’s ecological environment just

began to appear. In 2000, Ye and Liu [16] established an ecological environment evaluation system based on the current situation and causes of the ecological environment. In 2002, Yongming [17] established an ecological environment evaluation index system in Mizhi County, Shaanxi Province, based on the restrictive factors of ecological environment quality. At the same time, the task of quantitative evaluation and analysis of ecological environment quality in the whole county was completed.

2.2. Regional Overview of the Main Urban Area of Chongqing. The main urban area of Chongqing, also known as the urban developed economic circle, is located in the central and western part of Chongqing, and its geographical area, resident population, and rural area are similar to those of the provincial capital city of a medium-sized province. The main urban area of Chongqing includes nine administrative districts, including Yuzhong District, Dadukou District, Jiangbei District, Shapingba District, Jiulongpo District, Nan'an District, Beixian County, Yubei District, and Banan District, covering an area of 5,473 square kilometers. At the end of 2011, the total population was about 6,228,500, and the resident population was 7,723,100, forming 21 large-scale settlements.

The main urban area of Chongqing is the political, economic, cultural, financial, and industrial center of the whole city, belonging to the core area of the "one-hour economic circle" and the key development zone of the main functional area. In the area accounting for 7% of the whole city, 24.7% of the population of the whole city lives, creating about 43.6% of the GDP of the whole city.

3. Establishment of Ecological Environment Quality Evaluation Index System in Chongqing

3.1. Selection and Composition of Index System. This article takes the natural environment quality and ecological quality as the main evaluation objects and considers the close relationship between urban natural environment quality and economy, humanities, and society, so as to improve the level of urban development, pollution control, and resource utilization, including 12 evaluation indicators, 9 ecological quality evaluation indicators and 8 urban development level, pollution control, and resource utilization level indicators, totaling 37 evaluation indicators. Among them, according to the special physical and geographical characteristics of the main urban area of Chongqing and the development characteristics of cluster urbanization, the indicators such as water surface coverage, water network density, heat island intensity, landscape diversity index, landscape fragmentation index, biological abundance index, and vegetation coverage index are selected in Table 1.

3.2. Evaluation Method and Calculation Model. Many methods can be used to evaluate the quality of the ecological environment, but due to the influence of guiding ideology and objective conditions, the choice of specific schemes

varies from person to person. In this article, from the perspective of eliminating the restriction of subjective factors to the maximum extent, On the basis of the subjective scoring method of experts, combined with advanced technologies such as geographic information system and remote sensing to obtain relevant geospatial data information, AHP analytic hierarchy process is adopted to calculate the weight of the set indicators, and reasonable evaluation standard values are set to comprehensively evaluate and analyze the ecological environment quality of the study area.

AHP is a qualitative and quantitative decision analysis method by American operational research scientist T.L. Carl in the 1970s. It is often used in multiobjective, multi-standard, multifactor, multilevel unstructured, and complex decision-making problems. The analysis of elements and their internal relations is thorough. At the same time, AHP decision analysis has some subjectivity. In the actual analysis, in order to eliminate the inaccurate factors caused by subjectivity, this article has conducted a large number of consultations with experts in this field and synthesized the different opinions of various experts so that the index weight obtained is objective and fair to the maximum.

3.3. Determination of Evaluation Weight.

- (1) When determining the weight of each index, the first step is to construct a judgment matrix B for each index of the same level (see Table 2).

In the matrix, B_n is the destination layer of A_k , and b_{ij} represents the mathematical degree of mutual importance among elements B_i , B_j , and A_k . B_{ij} uses five scales 1, 3, 5, 7, and 9 in the matrix; namely, 1 means that B_i and B_j are at the same level; 3 means that B_i is a little more important than B_j ; 5 means that B_i is much more important than B_j ; 7 means B_i is more important than B_j ; 9 indicates that B_i is extremely important than B_j . In practical application, 2, 4, 6, and 8 can be selected to characterize the relative importance of B_i and B_j .

Obviously, for any judgment matrix, it should satisfy the following:

$$b_{ij} = \frac{1}{b_{ji}} \quad (i, j = 1, 2, \dots, n), \quad (1)$$

n in the above formula belongs to N .

- (2) Hierarchical single sorting: single sorting can be used to obtain the weight ratio of importance between adjacent elements. It is the basis for ordering the importance of all elements in this layer to the previous layer. The task of hierarchical single ranking can be reduced to the problem of calculating the eigenvalues and eigenvectors of the judgment matrix, that is, for the judgment matrix B , calculate the eigenvalues and eigenvectors of the following formula:

$$BW = \lambda_{\max} W. \quad (2)$$

TABLE 1: Index composition of evaluation system.

Criterion layer	Indicator layer
City size	Built-up area, specific population density, per capita construction land, economic density, expansion intensity of built-up area, greening of built-up area, population density, per capita road area, specific coverage rate of water area, etc.
Natural environment quality	Water surface coverage rate, water network density, per capita water area, excellent air quality ratio, acid rain frequency, heat island intensity, water quality comprehensive pollution index, water nutrition status index, water quality compliance rate in water functional areas, water quality compliance rate in centralized drinking water sources, regional environmental noise, and traffic trunk noise
Ecological quality factors	Ecological land use ratio, landscape diversity index, landscape fragmentation index, land degradation index, soil environmental quality comprehensive index, endangered species index, biological invasion risk, biological abundance index, and vegetation coverage index
Pollution control and energy coordination capabilities	Safe disposal rate of hazardous waste, harmless treatment rate of garbage, comprehensive disposal utilization rate of industrial solid waste, clean energy utilization rate, water resources carrying capacity, water consumption per unit GDP, urban sewage treatment rate, and added value of energy consumption per unit above designated size

TABLE 2: Hierarchical judgment matrix.

A_k	B_1	B_2	...	B_n
B_1	b_{11}	b_{12}	...	b_{1n}
B_2	b_{21}		...	
\vdots	\vdots	\vdots	...	\vdots
B_n	b_{n1}	b_{n2}	...	b_{nm}

In the above formula, λ_{\max} is the largest eigenroot of B , W is the normalized eigenvector corresponding to λ_{\max} , and the component W_i of W is the weight value of single-order corresponding elements.

When there is $b_{ij} = b_{ik}/b_{jk}$ ($i, j, k = 1, 2, \dots, n$) in the judgment matrix B , then the judgment matrix B is completely consistent, $\lambda_{\max} = n$. However, it is impossible under normal circumstances. Therefore, it is necessary to calculate the consistency of the matrix:

$$CI = \frac{\lambda_{\max} - n}{n - 1}. \quad (3)$$

In the formula, when $CI = 0$ and n belongs to \mathbb{N} , the judgment matrix is completely consistent; on the contrary, the larger the CI , the worse the consistency of the judgment matrix.

In order to test whether the judgment matrix has satisfactory consistency, it is necessary to compare CI with the average random consistency index RI (see Table 3).

Generally speaking, the first-order or second-order judgment matrix is always the same. For judgment matrices above grade 2, the ratio of consistency index CI to equivalent average random consistency index RI is called the random consistency ratio of judgment matrix, which is recorded as CR . Generally speaking, when $CR < 0.10$, we think that the judgment matrix has satisfactory consistency; that is, the relative importance of the assigned indicators is desirable.

The calculation method of CR is shown in the following formula:

$$CR = \frac{CI}{RI}. \quad (4)$$

- (3) Hierarchical total sorting: using a single sorting result of all levels in the same level, you can calculate the weight value of all elements in that level to the previous level, which is called total level sorting. Hierarchical total sorting needs to be done hierarchically from top to bottom. For the highest level, its hierarchical single sorting is its total sorting.

If the total hierarchical ordering of all elements A_1, A_2, \dots, A_m in the previous hierarchy has been completed, the obtained weight values are A_1, A_2, \dots , respectively, and the hierarchical single ordering result of the current hierarchical elements B_1, B_2, \dots, B_n corresponding to A_j is $[b_1^j, b_2^j, \dots, b_n^j]$ (here, when B_i is irrelevant, $A_i, b_1^j = 0$). See Table 4 for the overall ranking of levels.

Obviously,

$$\sum_{i=1}^n \sum_{j=1}^m a_j b_n^j = 1. \quad (5)$$

That is, the total ranking of levels is normalized normal vectors. n in the above formula belongs to \mathbb{N} .

- (4) Consistency test: after the ranking list is sorted, it is necessary to count CI, RI, CR , etc. and complete the consistency check of the calculation results of the total ranking.

$$\begin{aligned} CI &= \sum_{j=1}^m a_j CI_j, \\ RI &= \sum_{j=1}^m a_j RI_j, \\ CR &= \frac{CI}{RI}. \end{aligned} \quad (6)$$

Among the above three types, CI is the consistency index of the total ranking; CI_j is the consistency index

TABLE 3: Average random consistency index.

Order	1	2	3	4	5	6	7	8	9	10	11	12	13	14	15
RI	0	0	0.58	0.90	0.12	1.24	1.32	1.41	1.45	1.49	1.52	1.54	1.56	1.58	1.59

TABLE 4: Hierarchical total sorting table.

Hierarchy B	A_1	A_2	\dots	A_m	B-level total sorting
	a_1	a_2	\dots	a_m	
B_1	b_1^1	b_1^2	\dots	b_1^m	$\sum_{j=1}^m a_j b_j^i$
B_2	b_2^1	b_2^2	\dots	b_2^m	
\vdots	\vdots	\vdots	\vdots	\vdots	
B_n	b_n^1	b_n^2	\dots	b_n^m	

of the B -level judgment matrix corresponding to aj ; RI is the random consistency index of total ranking; RI_j is the random consistency index of B -level judgment matrix corresponding to aj ; CR is the random consistency ratio of the total ranking of hierarchies.

Similarly, when CR is 0.10, it is considered that the calculation results of the hierarchical total ranking are relatively consistent, and the relative importance judgment matrix can be accepted; otherwise, the judgment matrix needs to be adjusted to make the overall hierarchy more consistent.

- (5) Calculation of data: according to the constructed judgment matrix, the following calculations are made:

Step 1: Judge the product of matrix elements:

$$M_i = \prod_{j=1}^n b_{ij} \lim_{x \rightarrow \infty} \quad (i = 1, 2, \dots, n), \quad (7)$$

n in the above formula belongs to N .

Step 2: Calculate M_i to the n th power:

$$\overline{W}_i = \sqrt[n]{M_i} \quad (i = 1, 2, \dots, n). \quad (8)$$

Step 3: Normalization of eigenvectors:

$$W_i = \frac{\overline{W}_i}{\sum_{i=1}^n W_i} \quad (i = 1, 2, \dots, n). \quad (9)$$

Step 4: Maximum characteristic root:

$$\lambda_{\max} = \sum_{i=1}^n \frac{(BW)_i}{nW_i}. \quad (10)$$

In the above formula, $(BW)_i$ represents the i -th component of the vector BW .

Through the above-mentioned four-step calculation, a random consistency test can be carried out to know whether the constructed judgment matrix is satisfactory or not.

4. Evaluation of Ecological Environment Quality by Principal Component Analysis in Chongqing

4.1. Construct Principal Component Evaluation Model.

Step 1: The original data are processed in the same direction and standardized.

Step 2: Check the applicability of the original data and determine the correlation between the index data.

Step 3: Calculate the correlation coefficient matrix R :

$$R = (\rho_{ij})_{p \times p} = \begin{bmatrix} \rho_{11} & \rho_{12} & \dots & \rho_{1p} \\ \rho_{21} & \rho_{22} & \dots & \rho_{2p} \\ \vdots & \vdots & \ddots & \vdots \\ \rho_{p1} & \rho_{p2} & \dots & \rho_{pp} \end{bmatrix}, \quad (11)$$

ρ_{ij} is the correlation coefficient between variables x_i and x_j , $\rho_{ij} = \rho_{ji}$ ($i, j = 1, 2, 3, \dots, p$), which can be calculated as follows:

$$\rho_{ij} = \frac{1}{n} \times \frac{\sum_{k=1}^n (x_{ij} - \overline{x}_i)(x_{kj} - \overline{x}_j)}{S_i S_j}. \quad (12)$$

Step 4: Calculate the eigenvalue λ_i of the correlation coefficient matrix R and the corresponding unit eigenvector \overline{a}_i and determine the principal component:

$$N_i = a_{i1}z_1 + a_{i2}z_2 + \dots + a_{ip}z_p, \quad i = 1, 2, 3, \dots, p. \quad (13)$$

The relationship between the factor load coefficient u_{ij} and the eigenvalue λ_i is used to obtain the eigenvector \overline{a}_i , and then the principal component is obtained:

$$a_{ij} = \frac{u_{ij}}{\sqrt{\lambda_i}} \quad (i = 1, 2, 3, \dots, m; j = 1, 2, 3, \dots, p). \quad (14)$$

Step 5: Calculate the variance contribution rate and cumulative contribution rate and determine the principal component score.

Calculation formula of variance contribution rate:

$$F_1 = \frac{\lambda_i}{\sum_{i=1}^p \lambda_i}. \quad (15)$$

Calculation formula of cumulative contribution rate:

$$F_2 = \sum_{i=1}^m \left(\frac{\lambda_i}{\sum_{i=1}^p \lambda_i} \right). \quad (16)$$

In the usual definition, when the cumulative contribution rate is greater than 85%, it can be considered that the selected new principal component can complete the replacement of the original variable and can also summarize most of the information of the original variable. Here, we take m principal components that satisfy the conditions.

4.2. Indicator Data Preprocessing. Before the PCA, we need to normalize the original index data so as to compare and

analyze the indexes in the same evaluation index system. The evaluation index attributes involved in this article are divided into two categories: positive index, that is, the higher the index value, the better the ecological environment quality; negative index, that is, the lower the index value, the better the ecological environment quality. Before normalizing the dimension, it is necessary to convert the negative index into the positive index, and the usual method is to take the reciprocal of the original value. At present, the most commonly used dimension normalization method is the standard deviation normalization method, which is calculated according to the following formula:

$$zx_{ij} = \frac{x_{ij} - \bar{x}_j}{S_j}, \tag{17}$$

where $\bar{x}_j = 1/n \sum_{i=1}^n x_{ij}$; x_{ij} is the original value of j index; \bar{x}_j and S_j are the sample mean and standard deviation of j index, respectively; N is the number of samples.

According to the above steps, combined with the software SPSS19.0, the data of Chongqing ecological environment quality evaluation index are normalized in dimensions, and the results are shown in Table 5 and Figure 1.

4.3. Calculation of Ecological Environment Index.

(1) Applicability test of component analysis

It can be seen from Table 6 that the KMO value is 0.748, which is greater than 0.5, indicating that this set of index data can be used for PCA. The adjoint probability of the Bartlett ball test is 0.000, which is less than the significance level of 0.05. The original

hypothesis of Bartlett’s sphericity test is rejected, so it is considered to be suitable for PCA.

- (2) The correlation degree between indexes is preliminarily determined by the correlation coefficient matrix R . The results are shown in Table 7.
- (3) Calculate the eigenvalue input, variance contribution rate, and cumulative contribution rate of correlation coefficient matrix R , and determine the number of principal components.

It can be seen from Table 8 that the cumulative contribution rate of the first principal component $N1$, the second principal component $N2$, and the third principal component $N3$ is 88.400%, which is more than 85%, indicating that these three principal components can reflect the natural ecological environment indicators. Most of the information provided. Therefore, the first principal component $N1$, the second principal component $N2$, and the third principal component $N3$ are used to evaluate the natural ecological environment quality of Chongqing.

- (4) Calculate the feature vector corresponding to the selected principal component and write out the principal component expression in Table 9.

The principal component load represents the correlation coefficient between each index and a principal component. Feature vectors represent the weights of each index in different principal components. The principal component expression is as follows:

$$\begin{aligned} N_1 &= \left(\frac{0.114Z_{x1} - 0.983Z_{x2} + 0.896Z_{x3} + 0.871Z_{x4} + 0.860Z_{x5} + 0.699Z_{x6} + 0.571Z_{x7} + 0.866Z_{x8} + 0.931Z_{x9}}{\sqrt{5.711}} \right), \\ N_2 &= \left(\frac{0.759Z_{x1} + 0.021Z_{x2} - 0.304Z_{x3} - 0.380Z_{x4} + 0.252Z_{x5} + 0.498Z_{x6} + 0.318Z_{x7} - 0.143Z_{x8} - 0.091Z_{x9}}{\sqrt{1.255}} \right), \\ N_3 &= \left(\frac{0.470Z_{x1} + 0.010Z_{x2} - 0.010Z_{x3} - 0.026Z_{x4} - 0.130Z_{x5} - 0.054Z_{x6} - 0.728Z_{x7} + 0.418Z_{x8} - 0.206Z_{x9}}{\sqrt{0.990}} \right). \end{aligned} \tag{18}$$

4.4. Trend Chart of Evaluation Results. In order to reflect the change trend of the ecological environment in Chongqing more intuitively, the change trend chart of the ecological environment index and the change trend chart of principal components of the ecological environment system in Chongqing from 2009 to 2019 were obtained, as shown in Figures 2 and 3.

4.5. Analysis of Trend Chart Results. According to the principal component model, the comprehensive scores of each grade are positive and negative. In fact, the values here do not represent the true meaning of each index. It shows the relative position of the ecological environment quality in a certain year in all years, that is, the positional relationship

between the ecological environment quality in a certain year and the average level in recent years. Taking the average level of ecological environment quality in Chongqing as the zero point, the farther away it is from the zero point, the better the corresponding ecological environment quality is; the farther the negative value is from zero, the worse the corresponding ecological environment quality is.

It can be seen from Figure 1 that if only the natural environment index is considered, the ecological environment index in 2018 is less than 0, lower than the average level, and its index value is greater than that in 2018, indicating that in terms of ecological environment quality, 2018 is better than 2019. On this basis, considering economic and social factors comprehensively, the index value obtained by analysis is lower than that in 2019, and its absolute value is

TABLE 5: Standardization of raw data.

Year	zx1	zx2	zx3	zx4	zx5	zx6	zx7	zx8	zx9
2009	-0.339	1.407	-0.771	-0.865	-2.579	-1.028	-1.17	-0.645	-1.143
2010	-0.962	1.407	-0.816	-0.663	-0.832	-2.592	-2.084	-1.385	-1.382
2011	-0.861	0.749	-0.732	-0.793	-0.333	0.184	-0.696	-1.196	-0.545
2012	2.434	0.419	-0.642	-0.728	0.083	0.151	0.646	-0.803	-0.874
2013	-0.993	0.09	-0.612	-0.727	0.067	0.712	0.726	-0.677	-0.844
2014	0.653	0.09	-0.411	-0.397	0.271	0.164	0.228	-0.299	0.143
2015	0.515	-0.24	-0.313	-0.335	0.279	0.066	-0.632	0.85	0.203
2016	0.399	-0.24	-0.002	0.054	0.598	1.011	-0.757	1.023	1.025
2017	-0.647	-0.569	0.777	1.087	0.679	0.516	0.776	1.023	1.13
2018	-0.201	-1.557	1.352	1.72	0.851	0.457	0.786	1.023	1.13
2019	0.004	-1.557	2.172	1.647	0.916	0.36	0.786	1.086	1.16

Data changes after standardization

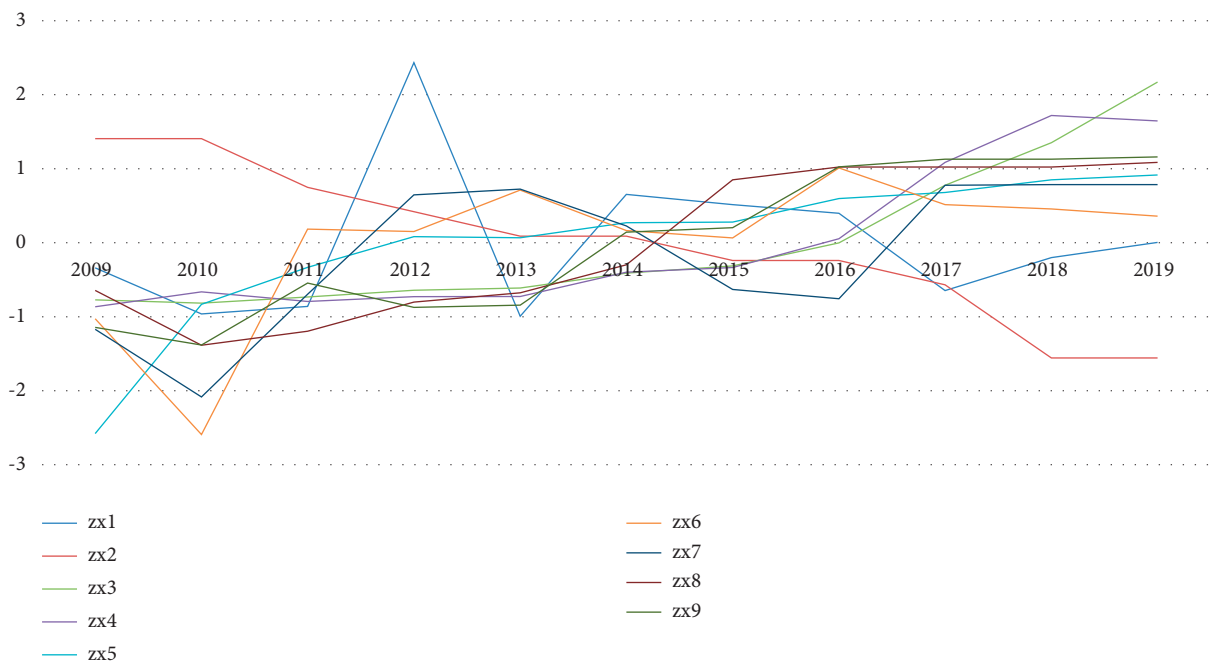


FIGURE 1: Standardized data change chart.

TABLE 6: Test results of KMO and Bartlett.

Kaiser-Meyer-Olkin measure	0.748	
Bartlett sphericity test	Approximate chi-square	87.767
	Df	36.00
	Sig	0.00

TABLE 7: Correlation coefficient matrix of natural ecological environment index.

Indicators	X1	X2	X3	X4	X5	X6	X7	X8	X9
X1	1	-0.103	-0.016	-0.072	0.205	0.247	0.031	0.109	0.055
X2	-0.103	1	-0.89	-0.869	-0.833	-0.664	-0.563	-0.849	-0.889
X3	-0.016	-0.89	1	0.984	0.642	0.401	0.459	0.761	0.795
X4	-0.072	-0.869	0.984	1	0.636	0.307	0.436	0.739	0.779
X5	0.205	-0.833	0.642	0.636	1	0.654	0.624	0.643	0.765
X6	0.247	-0.664	0.401	0.307	0.654	1	0.536	0.586	0.652
X7	0.031	-0.563	0.459	0.436	0.624	0.536	1	0.132	0.338
X8	0.109	-0.849	0.761	0.739	0.643	0.586	0.132	1	0.933
X9	0.055	-0.889	0.795	0.779	0.765	0.652	0.338	0.933	1

TABLE 8: Eigenvalue and contribution rate table of ecological environment indicators.

Composition	Eigenvalue	Contribution rate of variance	Cumulative contribution rate
N1	5.711	63.459	63.459
N2	1.255	13.945	77.404
N3	0.99	10.996	88.4
N4	0.631	7.017	95.417
N5	0.257	2.852	98.269
N6	0.075	0.832	99.102
N7	0.053	0.593	99.694
N8	0.021	0.228	99.922
N9	0.007	0.078	100

TABLE 9: Principal component index table of ecological environment.

Indicators	Principal component		
	N1	N2	N3
X1	0.114	0.759	0.47
X2	-0.983	0.021	0.01
X3	0.896	-0.304	-0.01
X4	0.871	-0.38	-0.026
X5	0.86	0.252	-0.13
X6	0.699	0.498	-0.054
X7	0.571	0.318	-0.728
X8	0.866	-0.143	0.418
X9	0.931	-0.091	0.206

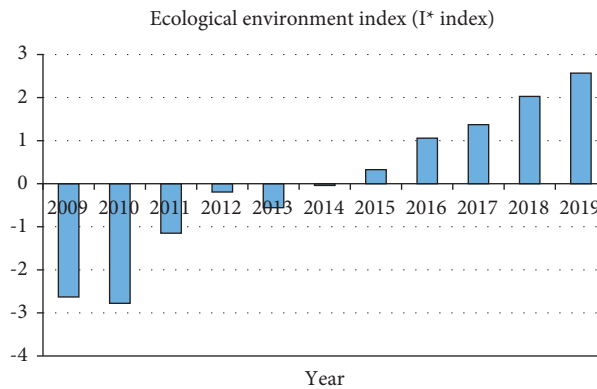


FIGURE 2: Change trend chart of ecological environment index in Chongqing.

higher than that when only considering natural environment indicators. In other years, after considering economic and social factors, the same situation exists. It can be seen from Figure 2 that the change of the first principal component generally shows an upward trend from 2009 to 2019, which is basically consistent with the change range and trend of the ecological environment index of the natural subsystem, indicating that there is a good correlation between them. Land resource utilization, pollution emission intensity, pollution control, and urban greening construction are the main influencing factors of the natural subsystem. In the initial stage of ecocity construction, the value of the first principal component is less than 0, and there are some problems such as high pollution emission intensity, insufficient pollution control, and imperfect urban greening construction. This shows that economic and social factors

have a significant impact on the ecological environment. If only the natural environment indicators are considered, the evaluation results cannot fully reflect the actual ecological environment in the evaluation area. In recent years, Chongqing's GDP, environmental protection investment, and public awareness of environmental protection have been improved. Only by paying equal attention to the environment, economy, and society can the sustainable development of the urban ecological environment be better realized.

In this article, the PCA method is used to analyze the ecological environment quality evaluation of the main urban area of Chongqing, and the correlation of indicators is practical in theory, so it is of great guiding significance to study different environmental indicators in the main urban area of Chongqing. In the third and fourth parts of the article, PCA method is used to evaluate the ecological

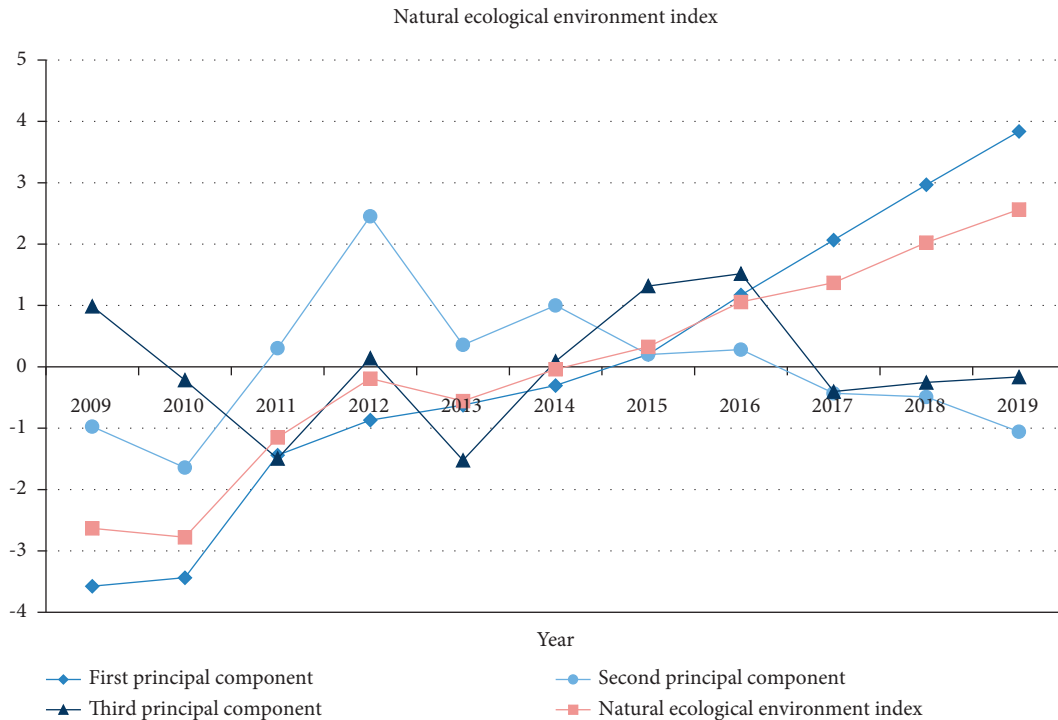


FIGURE 3: Change trend chart of principal components of ecological environment system in Chongqing.

environment of Chongqing, the data credibility is high, and the example process is rich. Therefore, the research methods in this article have important research significance.

5. Conclusion

When constructing the evaluation index system, if we only consider the selection of natural environment indicators and weaken the economic and social information, it will not fully reflect the quality of the urban ecological environment. According to the understanding of the meaning of urban ecological environment quality in this article, a relatively complete evaluation index system of urban ecological environment quality is constructed from three aspects of nature, economy, and society so as to obtain relatively reasonable evaluation results.

Compared with the fuzzy comprehensive evaluation method and ecological environment index method, the results obtained by the PCA method are basically consistent with them in terms of longitudinal change trend, which shows that the application of this method in urban ecological environment quality evaluation is feasible and the evaluation results are credible. By constructing the ecological environment quality evaluation system and evaluating and analyzing the main urban area of Chongqing in 2019, the results show that the overall score of ecological environment quality evaluation in the main urban area of Chongqing is 82.939 points, ranging from 70 to 85 points, and the ecological environment quality evaluation result is good.

The evaluation results show that from 2009 to 2019, the ecological environment quality of Chongqing is generally on the rise, and it is in a benign development state. The development process can be roughly divided into two stages:

2009~2014 is the initial stage of Chongqing ecocity construction. The index value rises rapidly, but the urban ecological environment quality is generally lower than the average level and is not ideal; from 2009 to 2019, it is the development stage of ecological city construction in Chongqing. The index value keeps increasing continuously, and the ecological environment quality is higher than the average level, developing well. In the future ecological environment construction and protection in Chongqing, we should pay attention to the pollution degree of economic development to the environment, the influence of environmental protection investment on pollution control, and the pressure of population factors on cultivated land resources, further improve environmental protection investment, and improve environmental protection investment construction; adjust the land use structure and relieve the pressure of cultivated land resources; optimize the industrial structure and improve the economic environment.

Data Availability

The experimental data used to support the findings of this study are available from the corresponding author upon request.

Conflicts of Interest

The authors declare that they have no conflicts of interest regarding this work.

Acknowledgments

This work was supported by the National Natural Science Foundation of China (Grant no. 41901014).

References

- [1] L. Yang, "Assessment of city environmental quality in western China based on matter element extension—a case study of chongqing," *Energy Procedia*, vol. 5, no. 1, pp. 619–623, 2011.
- [2] G. B. Luo and H. E. Bing-Hui, "Evaluation research on eco-environment system of chongqing city based on the background of balancing rural and urban development," *Journal of Chongqing Normal University(Natural Science)*, vol. 28, no. 1, pp. 27–30, 2011.
- [3] L. R. Jia, T. U. Jian-Jun, R. Hou, Y. A. N. G. Quan-wu, and Z. H. O. U. Xue-rong, "Urbanization quality evaluation and its driving factors analysis in chongqing city China," *Journal of South China Normal University (Social Science Edition)*, vol. 40, no. 6, pp. 68–73, 2015.
- [4] X. Xiaosong Lin and Y. Hua Yang, "Ecological security in downtown area of Chongqing City," in *Proceedings of the 2011 International Conference on Remote Sensing, Environment and Transportation Engineering*, pp. 2111–2114, Nanjing, China, June 2011.
- [5] J. Wang, H. E. Zhengwei, and Y. U. Huan, "Combination of GIS and AHP comprehensive assessment evaluation of the ecological environment: A case study in Western of Chongqing," *Ecology and Environmental Sciences*, vol. 20, no. Z2, pp. 1268–1272, 2011.
- [6] J. Meng, W. Shen, and X. Wu, "Integrated landscape ecology evaluation based on RS/GIS of three-gorge area," *Acta Scientiarum Naturalium Universitatis Pekinensis*, vol. 5, no. 2, pp. 295–302, 2005.
- [7] Y. Zhang, Z. Zhang, and Y. Luo, "Existing problems and solutions to ecological environment in Qianjiang district, chongqing," *Environment and Ecology in the Three Gorges*, vol. 35, no. 3, pp. 59–62, 2013.
- [8] F. Sun, J. M. Zhao, and F. H. Zhang, "Construction of ecological quality monitoring, evaluation, and ecological security early warning system for chongqing city," *Journal of Southwest University(Natural Science Edition)*, vol. 34, no. 12, pp. 81–86, 2012.
- [9] X. Zhang, Z. Yin, and Y. Yao, "Measure and spatial differences analysis of urbanization quality in chengdu-chongqing area," *Areal Research and Development*, vol. 36, no. 3, pp. 66–70, 2017.
- [10] J.-Y. Zhang and L.-C. Wang, "Assessment of water resource security in Chongqing City of China: what has been done and what remains to be done?" *Natural Hazards*, vol. 75, no. 3, pp. 2751–2772, 2015.
- [11] L. Yuan, H. L. Shang, and K. University, "The ecological environment development capacity evaluation of Chongqing based on the ecological footprint model," *Journal of Foshan University (Social Science Edition)*, vol. 35, no. 02, pp. 61–65, 2017.
- [12] R. Q. Shu, H. E. Tai-Rong, and R. B. Ban, "Evaluation of the land resources ecologic security in chongqing city," *Journal of Chongqing Normal University*, vol. 30, no. 5, pp. 44–49, 2013.
- [13] Z. M. Liang, W. B. Feng, and C. Chen, "Strategy choice and comprehensive evaluation of urbanization level of three Gorges reservoir area of chongqing," *World Regional Studies*, vol. 20, no. 3, pp. 95–102, 2011.
- [14] X. Zou, W. Zhao, P. U. Haixia, and J. Zhou, "Study on urban boundary expansion and ecological environment effect in Nan'an district of chongqing city," *Research of Soil and Water Conservation*, vol. 26, no. 4, pp. 252–258+264, 2019.
- [15] J. T. Jia, H. Yang, X. Zeng, and Y. J. Zhang, "Analysis on landscape pattern of land use in a mountain city: A case study from metropolitan area in chongqing," *Journal of Chongqing Normal University(Natural Science)*, vol. 30, no. 4, pp. 35–40+171, 2013.
- [16] Y. Ye and L. Liu, "Study on the evaluation index system of ecological environment quality in China," *Environmental Science Research*, vol. 24, no. 3, pp. 33–36, 2000.
- [17] Y. Ni, "Theory and Method of County Ecological Environment Quality Assessment—A Case Study of Mizhi County, Shaanxi Province," *Northwest University*, vol. 20, 2002.

Research Article

An Approach to Oral English Assessment Based on Intelligent Computing Model

Caihong Jing,¹ Xiaoling Zhao ,¹ Haiyan Ren,¹ Xuexia Chen,¹ and Naren Gaowa²

¹Nursing College, Inner Mongolia Medical University, Hohhot 010010, China

²Law and Business Department, Inner Mongolia Chifeng College, Chifeng 010010, China

Correspondence should be addressed to Xiaoling Zhao; jingch@immu.edu.cn

Received 9 February 2022; Revised 28 April 2022; Accepted 3 May 2022; Published 8 June 2022

Academic Editor: Wenming Cao

Copyright © 2022 Caihong Jing et al. This is an open access article distributed under the Creative Commons Attribution License, which permits unrestricted use, distribution, and reproduction in any medium, provided the original work is properly cited.

“English craze” has become a key topic of concern to the majority of the people. Apart from setting English as a compulsory course like Chinese and Mathematics in schools, various English training institutions outside the school are also emerging one after another. Due to the English teaching mode in class, dumb English appears. In recent years, with the popularity of virtual electronic devices, more and more researchers try to use virtual reality (VR) to create an immersive English learning environment. Oral English teaching is an important part of the whole English teaching. In the traditional English classroom teaching practice, teachers’ pronunciation is not standard, and students are difficult to learn the correct pronunciation standard, which makes oral English very passive. The most important problem in oral English teaching is to improve students’ interest in oral English, make students willing to speak and realize English communication. Oral English teaching is an important link in both primary and secondary schools and universities. Teachers are afraid of nonstandard pronunciation in limited classrooms, and they are afraid to speak and unwilling to speak, which leads to passive oral English teaching. Therefore, this paper will set up an intelligent computing model to evaluate and analyze spoken English in a standard and accurate way. Artificial intelligence speech synthesis and imitation of voice change are typical applications of decoupling representation learning in speech, the oral evaluation is based on the proposition that speech is a dynamic and complex process. With the help of the rapidly developed computer speech synthesis and imitation technology, an oral evaluation path based on speech synthesis and imitation is proposed, that is, oral evaluation is carried out by using the network parameters and output of deep learning of computer speech imitation.

1. Introduction

With the gradual internationalization of society, English is one of the common languages in the world, and the use of spoken English has become the most basic way of communication in various social behaviors such as tourism, foreign trade, and learning. However, many English studies are too limited to the study on paper, while ignoring the oral English study which can be really used in practice. Xiao [1] mainly describes the formative systematic assessment of oral English in middle school classrooms, while Li et al. [2] make a dynamic assessment study of information-based oral English classrooms. Zhuang [3] studies the identification of nonlinear systems based on intelligent computing model, which can also be used for oral English evaluation. Li [4]

expounds the value of intelligent computing in modeling. Based on the fuzzy logic theory in reference [5], an evaluation model of oral English is established. Wan [6] expands the application of oral English in international teaching. Based on the background of artificial intelligence in literature [7], APP is used for students’ oral learning mode. Based on the literature [8], the evaluation research of learning theory in oral English teaching class of higher vocational colleges is constructed. Through the artificial intelligence in literature [9], the artificial spoken pronunciation is recognized, and whether the pronunciation emits standard spoken language is judged. The results can be measured more conveniently by using the automatic speech recognition instrument in reference [10]. A study of oral English learning and assessment in SELL-Corpus and VR

environment was conducted in [11]. Chen and Li [12] describe the present situation and development trend of oral English learning. Liu and Zhanji [13] make a dynamic assessment of the oral quality of current English learners. Finally, Xian [14] and Zhong [15] talk about the effective measures and methods of teaching oral English in universities and primary and secondary schools.

2. The Development Status of Oral Evaluation

2.1. Development of Oral English Assessment Abroad. In recent years, with the rapid development of computer technology and the development of intelligent speech recognition technology, using intelligent computing model to evaluate the standardization of spoken language has become a research hotspot. However, foreign countries have developed rapidly in oral evaluation, and they have designed a language learning system VILTS for speech interaction to evaluate the speech spoken by users. The system scores intelligently from four different aspects of phonetic research: similarity, phonetic accuracy, phonetic emotion, and speech speed. There are many big differences between computer automatic evaluation and artificial evaluation, and people constantly improve the evaluation methods in constant exploration. Gina-Anne levow lists the difficulties faced by simulators in modeling artificial scores from two aspects: process and result, and points out that it is impossible to model the evaluation process comprehensively in the field of speech features and speech recognition at present. In addition, the recognizer adopts a wide range of grammatical forms, which enables it to accept different grammatical and semantic changes based on the target language. In the nonacoustic field, machine learning technology is applied to gather human recognition related features. At the same time, the network-based oral English learning is also developing rapidly, which is to solidify the ready-made speech evaluation technology into oral evaluator, which greatly facilitates oral practitioners. To sum up, foreign countries have carried out in-depth research and analysis on oral English assessment, and have involved a wider field of oral English features. Some systems have been recognized by some professional language experts for assessing spoken English pronunciation from different levels such as sentences, words, or phonemes.

2.2. Development of Oral English Assessment in China. The research on oral English assessment has just started in China, and only some research institutes in Taiwan have carried out some related research. The evaluation of speech is divided into three parts: the content of the uttered speech piece, the pronunciation standard, and the oral evaluation of the speech database. The first part is obtained by calculating the HMM probability of the given speech normalization. In the second part, the Viterbi decoded syllables are identified by GMM-based tone recognition. The third part is realized by the greedy search algorithm. It is not necessary to apply the whole process of speech recognition to speech evaluation, but only to build a linear grid of text-based speech

model. Then, Viterbi decoding is used to align the mesh model that users said and built. Based on speech recognition and accent adaptation technology based on implicit Markov model, oral evaluation in mainland China studies the accuracy and fluency information of phoneme pronunciation, gives phoneme-level pronunciation quality scores, and further obtains the scoring results of the whole sentence. This method has gained most recognition from some specialized experts.

3. Oral Fuzzy Logic Combined with Neural Network Learning

3.1. The Concept of Fuzzy Relations. The fuzzy set on the direct product $U \times N$ is defined, with U and N as computational domains, and R is defined as the fuzzy relation of U on N ; $R(x, y)$ expresses the degree of connection between x and y for (y) and $u(x)$. If R is a classical set on the direct product $U \times N$, then the relation R is U and N is a general relation, so the fuzzy relation is the extension of the classical relation, and the classical relation is a special fuzzy relation. Suppose U is a finite computational domain composed of m elements and N is a finite universe composed of n elements. The fuzzy relation R from U to N can be expressed by a matrix of $m \times n$, namely,

$$\begin{bmatrix} r_{11} & \cdots & r_{1n} \\ \vdots & \ddots & \vdots \\ r_{m1} & \cdots & r_{mn} \end{bmatrix}. \quad (1)$$

It can also be expressed as $R = (r_{ij})_{m \times n}$. It is not difficult to find that there is a certain mapping relationship between fuzzy matrix and fuzzy relation. Definition (fuzzy relation has composition): let U, N, W be the universe, R be a fuzzy relation from U to N , and Q be a fuzzy relation from N to W , then the composition T from R to Q is also a fuzzy relation.

$$u_{RO}(X, Z) = N_{y \in V} (u_R(x, y) \wedge u_Q(y, z)) (x \in U, z \in W). \quad (2)$$

Let $R = (r_{ij})_{m \times n}$, $Q = (q_{jk})_{n \times i}$ be two matrices with fuzzy relations, and their composite $R \times Q$ is a fuzzy matrix S with n rows and one column, and the elements of row i and column k of S are

$$S_{ik} = N_{j=1}^n (r_{ij} \wedge q_{jk}). \quad (3)$$

3.2. Fuzzy Logical Reasoning Method

3.2.1. Zadeh Reasoning Method. Let F be a fuzzy set on U , G be a fuzzy set on N , and the fuzzy implication relation "if F then G " is expressed by $F \longrightarrow G$. Zadeh defined it as a fuzzy relation on $U \times N$, namely,

$$R = F \longrightarrow G (F \times G) (F^c \times N). \quad (4)$$

It belongs to the function:

$$R(x, y) = [F(x) \wedge G(y)] \vee [1 - A(x)]. \quad (5)$$

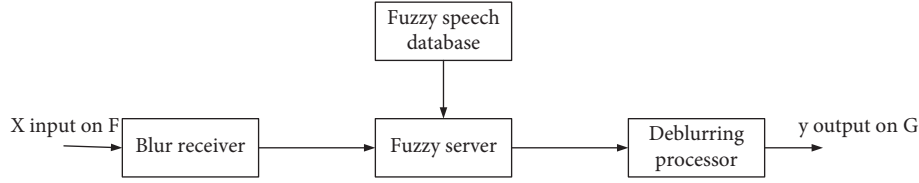


FIGURE 1: Fuzzy system structure.

When a fuzzy relation R is set, a fuzzy relation transformation is determined. Using the synthesis of fuzzy relations, there are the following reasoning rules:

Given the fuzzy relation R of the fuzzy implication relation $F \longrightarrow G$, for a given $F' \in U$, we can infer G' , $G' \in N$, $G' = F' \times R$. That is, when W is a finite universe:

$$G'(y) = W\{F'(X) \wedge [F(x) \wedge G(y) \vee (1 - F(x))]\}. \quad (6)$$

3.2.2. Mamdani Reasoning Method. In Mamdani's reasoning method, the fuzzy implication relation $F \longrightarrow G$ is expressed by the direct product of F and G , that is, $R = F \longrightarrow G = F \times G$, which can also be written as

$$R(x, y) = F(x) \times G(y). \quad (7)$$

3.2.3. Most of Them Are Input Fuzzy Reasoning Methods. It is known that the major preconditions of reasoning are "if A and B then C ," $A \in F(x)$, $B \in F(y)$, $C \in F(z)$, and the fuzzy implication relation is "if A and B then C ":

$$\begin{aligned} R &= A \times B \times C = (A \times B) \longrightarrow C, \\ R(x, y, z) &= A(x) \wedge B(y) \wedge C(z). \end{aligned} \quad (8)$$

3.3. Establishment Process of Fuzzy System

- (1) Composition of fuzzy system: the fuzzy system refers to those systems associated with fuzzy essentials and fuzzy logic. It consists of four parts: fuzzy receiver, fuzzy speech library, fuzzy server, and defuzzy processor, as shown in Figure 1:
- (2) Fuzzy speech: assuming that a variable has a value of "X", F is called X fuzzification if "X" is replaced by a set of functions. Commonly used fuzzification methods include single-factor fuzzification, Gaussian function fuzzification, and trigonometric function fuzzification. The blur receiver completes the blur operation.
- (3) Establishing fuzzy speech database: fuzzy speech library is composed of a series of "if-then" fuzzy conditional sentences, in which the prelude is input and state, and the postlude is control variable. There are two common methods to establish fuzzy rule base, one is from the experience of experts, which is summarized into a group of rules according to the experience of experts. The other is through self-

learning methods, such as neural network or genetic algorithm.

- (4) Fuzzy reasoning of speech: fuzzy reasoning is to transform the fuzzy "if-then" of fuzzy speech database into some kind of mapping according to fuzzy logic rules. Fuzzy reasoning generally includes three parts: aggregation, that is, the calculation of IF part of rules, composition, calculation of THEN part of rules.
- (5) Defuzzification: after the fuzzy reasoning, the results are still expressed by data speech. We must convert linguistic variables to a certain value, that is, map a fuzzy set to a certain point. This stage is called defuzzification. The relationship between linguistic values and corresponding values is given by the definition of membership function. The general method of defuzzification includes two stages: first, calculate the linguistic value of each linguistic variable to get a "typical value," and the method of calculating each linguistic typical value is to find the maximum value of each membership function; then, the best compromise value of fuzzy logic reasoning is calculated.

3.4. Learning Methods of Neural Networks

- (1) A learning algorithm for correcting computational errors. It continuously adjusts the neurons according to the increasing intensity of voice data and output error data.

Let $y_k(n)$ be equal to the actual output of neuron k at time n when the target input $x(n)$, k is assumed, and $d_k(n)$ is the known output given by the training sample, then the output error can be expressed as

$$e_k(n) = d_k(n) - y_k(n). \quad (9)$$

The learning algorithm for correcting computational errors is to minimize the objective function value based on $e_k(n)$, so that the actual output of each output neuron in the network is close to the output in a certain statistical sense. This problem is also the problem of transforming to find the minimum value. The most commonly used error objective function is the mean of the sum of squares of errors, which is

$$E_n = \frac{1}{2} \sum_k e_k^2(n). \quad (10)$$

If the relation weight of neurons i to j is w_{ij} , the adjustment amount of weight is

$$\Delta w_{ij} = \eta \delta_j v_i. \quad (11)$$

In the formula, η is the learning rate, δ_j is the partial derivative of the error function to the input of neuron j , and v_i is the output of the i -th neuron.

- (2) Hebb learning algorithm: according to the mechanism of conditioned reflex in biology, it belongs to unsupervised learning by psychologist in 1949. This rule means that if two neurons are activated synchronously, the strength of the connection increases, and vice versa are described mathematically as follows:

$$\Delta w_{kj} = f(x_j n, y_k(n)), \quad (12)$$

where $x_j n$ and $y_k(n)$ are the states of neurons connected to w_{kj} , respectively, and the most commonly used f function is as follows:

$$\Delta w_{kj} = \eta x_j n \times y_k(n). \quad (13)$$

- (3) Random learning algorithm: the error learning algorithm usually adopts gradient descent method, but the problem of this algorithm is that it may lead to local optimum. The stochastic learning algorithm achieves global optimum by introducing unstable factors.
- (4) Competitive learning algorithm: it means that the outputs of neural network compete with each other, and the strongest will be activated. The rules of competitive learning are

$$\Delta w_{ij} = \begin{cases} \eta(x_i - w_{ij}), & \text{if neuron } j \text{ wins the competition,} \\ 0, & \text{if neuron } j \text{ fails to compete.} \end{cases} \quad (14)$$

3.4.1. BP Neural Network Algorithm. The specific implementation steps of BP standard algorithm are as follows:

- (1) Network initialization.
- (2) Take any p -th input sample and its corresponding expected output

$$d(p) = (d_1(p), d_2(p), \dots, d_n(p)). \quad (15)$$

- (3) Calculate the hidden layer input and output. The formula is as follows:

$$h_i(p) = \sum_{i=1}^n x_i(p) - b_j, \quad j = 1, 2, 3, \dots, n, \quad (16)$$

$$h_o_j = f(h_i, p), \quad j = 1, 2, 3, \dots, n.$$

- (4) Calculate the input and output of the output layer.

$$y_{ik} p = \sum_{i=1}^n w_{ik} x_i(p) - b_k, \quad k = 1, 2, \dots, m. \quad (17)$$

- (5) The partial derivative of the error function to each neuron in the output layer is calculated:

$$\delta_k(p) = (d_k(p) - y_{ok}(p))(1 - y_{ok}(p)), \quad k = 1, 2, \dots, m. \quad (18)$$

- (6) Using error correction algorithm, the partial derivatives of neurons in the hidden layer are obtained:

$$\delta_j(p) = \left(\sum_{k=1}^m \beta_k(p) w_{jk} \right) (h_o_j(p)(1 - h_o_j(p))), \quad j = 1, 2, \dots, n. \quad (19)$$

- (7) Adjust the connection weight between the hidden layer and the output layer.

$$w_{jk}^{N+1}(p) = w_{jk}^N(p) + \eta \delta_j(p) x_i(p), \quad (20)$$

$$b_k^{N+1}(p) = b_k^N(p) + \eta \delta_k p.$$

- (8) Adjust the connection weight between the input layer and the hidden layer.

$$v_{ij}^{N+1}(p) = v_{ij}^N(p) + \eta \delta_j(p) x_i(p), \quad (21)$$

$$b_j^{N+1}(p) = b_j^N(p) + \eta \delta_j p.$$

- (9) Find the error E of the whole calculation process, and the calculation formula is as follows:

$$E = \frac{1}{2m} \sum_{p=1}^l \sum_{k=1}^m (d_k(p) - y_{ok}(p))^2. \quad (22)$$

- (10) Judge whether to continue training: when $E < \varepsilon$ or the number of learning times is greater than the set maximum number of times M , the training ends. Otherwise, randomly select another learning sample, return to step 3, and carry out circular training. The BP neural network algorithm is enough for the daily use of oral evaluation, and the improved BP algorithm can be superior to BP algorithm in complex environment.

4. Experiment

4.1. Sample Selection. In artificial neural network and adaptive fuzzy neural system, samples are the object of network training, and the difference degree of sample selection directly affects the evaluation results of the model, so the selection of samples must be representative. The samples used in this study were 5 men and 5 women of the same age and with the same oral literacy from different regions for oral evaluation. Because this experiment is to evaluate spoken English, the representative samples must first be people who can speak English but do not have spoken English in local dialects so that they can evaluate spoken English correctly. The relevant collection sources have been explained in the experiment. The speech information in this paper is processed data, and the main work of this paper is the research of spoken language recognition. At present, there are many speech processing tools, such as prefiltering,

TABLE 1: Hierarchical cross error of fuzzy logic combined with neural network.

Classify samples correctly (%)	Error classification sample (%)	Kappa	Average absolute error	Root mean square error	Relative absolute error (%)	Relative square root error (%)
86.16	12.31	0.72	0.0092	0.212	23.1	43.21

TABLE 2: Accuracy rate of fuzzy logic combined with neural network.

Correct rate	Error rate	Precision rate	Feedback rate	ROC area	Category
0.882	0.024	0.843	0.882	0.992	Good
0.877	0.021	0.844	0.877	0.868	Excellent
0.912	0.012	0.793	0.912	0.911	Excellent
0.932	0.013	0.792	0.932	0.893	Good
0.878	0.022	0.851	0.878	0.994	Excellent

TABLE 3: Stratified cross error of the ANFIS model.

Classify samples correctly (%)	Error classification sample (%)	Kappa	Average absolute error	Root mean square error	Relative absolute error (%)	Relative square root error (%)
78.16	15.31	0.82	0.0098	0.202	33.1	63.21

TABLE 4: Accuracy of ANFIS model.

Correct rate	Error rate	Precision rate	Feedback rate	ROC area	Category
0.782	0.047	0.743	0.882	0.992	Good
0.677	0.081	0.644	0.877	0.868	General
0.812	0.022	0.893	0.912	0.911	Excellent
0.732	0.043	0.792	0.932	0.893	Good
0.678	0.092	0.751	0.878	0.994	General

TABLE 5: Hierarchical cross error of bp neural network.

Classify samples correctly (%)	Error classification sample (%)	Kappa	Average absolute error	Root mean square error	Relative absolute error (%)	Relative square root error (%)
68.16	20.31	0.83	0.0138	0.302	43.1	83.21

A/D conversion, pre-emphasis, framing, windowing, end-point detection, and so on.

4.2. *Experimental Testing.* Based on fuzzy logic combined with neural network intelligent computing model, people from different regions are found for the oral evaluation test, and the relevant data we get are as follows:

Hierarchical cross-validation errors are shown in Table 1.

People from five different regions were found to take the oral evaluation test, and the accuracy rate is as shown in Table 2:

Based on the ANFIS model, we found the same batch of people for oral evaluation test, and the relevant data we got are as follows:

Hierarchical cross-validation errors are shown in Table 3.

The accuracy of the ANFIS model is shown in Table 4.

Based on the bp neural network, we found the same batch of people for oral evaluation test, and the relevant data we got are as follows:

Hierarchical cross-validation errors are shown in Table 5.

The accuracy of the bp neural network is shown in Table 6.

4.2.1. *Model Comparison.* We compare the fuzzy logic with the neural network intelligent computing model, ANFIS network model, and bp neural network model to evaluate the accuracy of spoken English as shown in Figure 2.

This work makes statistics on the error and accuracy of hierarchical cross-validation of models so that readers can intuitively know the error rate and accuracy of each model.

4.3. *Experimental Analysis.* Spoken language evaluation based on the fuzzy logic combined with the neural network intelligent computing model. In order to test the reliability of the model more concretely, we decided to add speech emotion index to test the comprehensive evaluation results of pronunciation quality. We found the same sample to evaluate oral English in four states: happiness, sadness,

TABLE 6: Accuracy of bp neural network.

Correct rate	Error rate	Precision rate	Feedback rate	ROC area	Category
0.782	0.047	0.743	0.882	0.992	Good
0.677	0.081	0.644	0.877	0.868	General
0.812	0.022	0.893	0.912	0.911	Excellent
0.732	0.043	0.792	0.932	0.893	Good
0.678	0.092	0.751	0.878	0.994	General

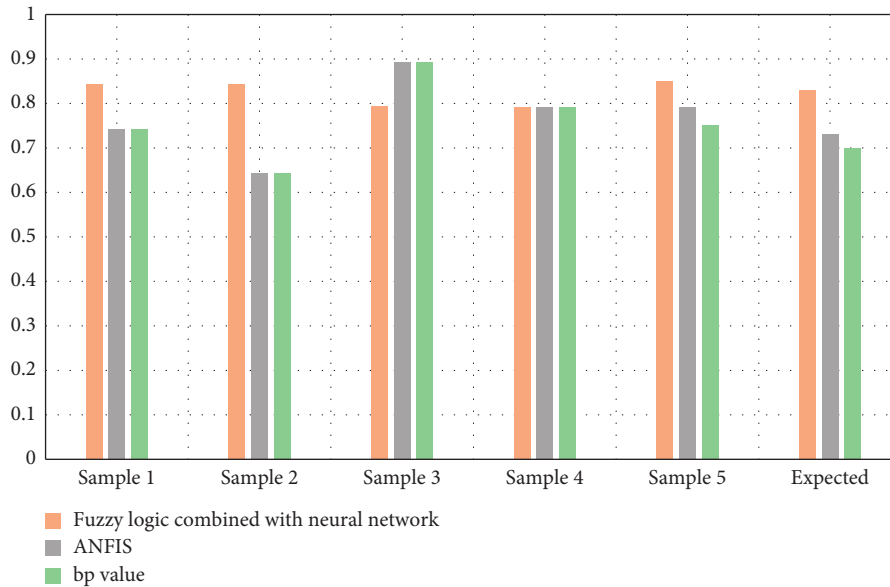


FIGURE 2: Model comparison diagram.

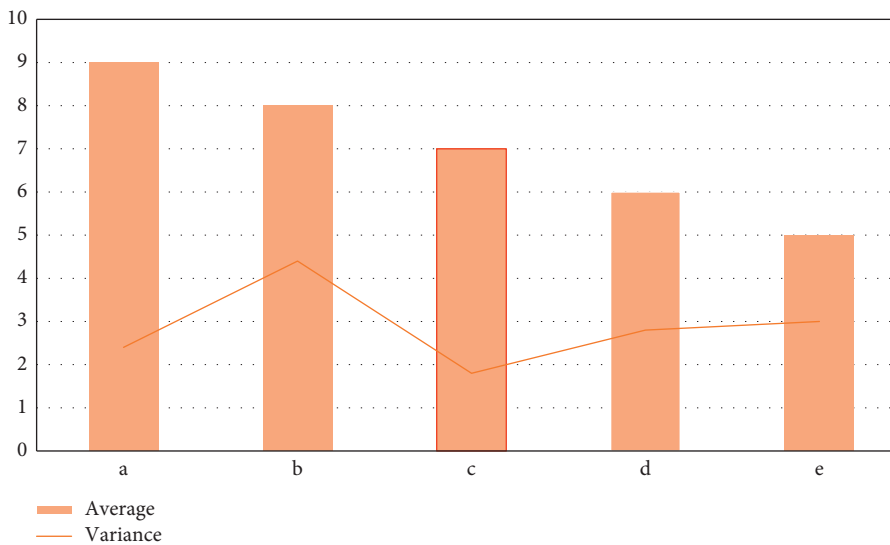


FIGURE 3: Evaluation results when happy.

anger, and surprise, and showed the mean and variance of speech emotion evaluation results in different manual ratings, as shown in Figures 3–6.

Through the oral evaluation charts of four different emotional states, we can see that the variance of the evaluation results is the smallest and the most stable in the surprised state. In sad mood, the variance is the largest, and the oral evaluation results are the most fluctuating.

4.4. Contrast Test. According to the experimental test in this paper, the fuzzy logic combined with the neural network intelligent computing model has achieved the most accurate accuracy for oral English evaluation. We are now conducting a comparative experiment between artificial evaluation and this model, as shown in Table 7.

Table 7 lists the average number of spoken language evaluation results of four kinds of speech emotion under

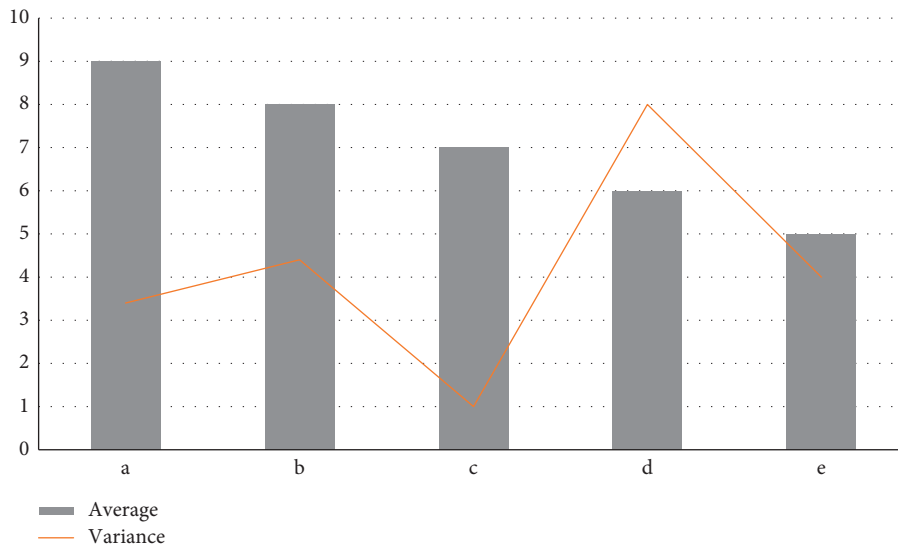


FIGURE 4: Evaluation results when you are sad.

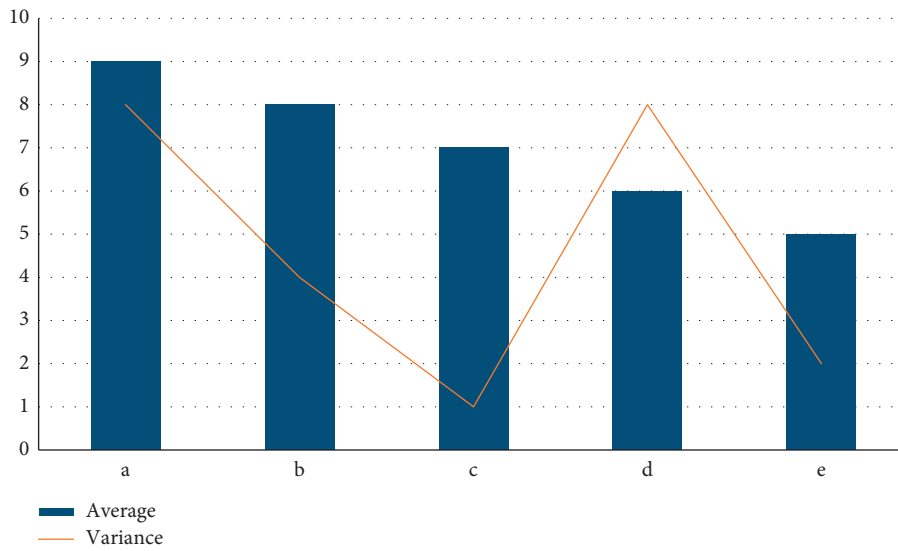


FIGURE 5: Evaluation results when angry.

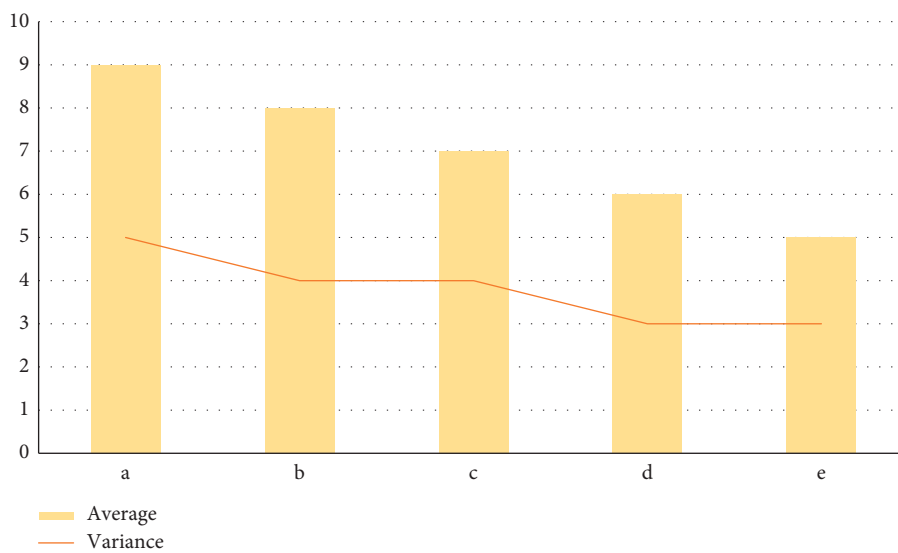


FIGURE 6: Evaluation results when surprised.

TABLE 7: Comparative experiment.

Artificial evaluation	Intelligent computing model of fuzzy logic combined with neural network			
	Happy	Sad	Anger	Surprise
A	0.35	0.34	0.37	0.47
B	0.32	0.45	0.41	0.45
C	0.28	0.61	0.43	0.46
D	0.29	0.33	0.73	0.45
Univariate variance E	6.6	5.0	6.8	7.0
F of one-way variance	0	0	0	0

different manual ratings, which shows that different ratings can be distinguished. However, whether the mean difference of different manual ratings is essential or random, this paper uses one-way ANOVA to test. By observing the p values in the data results table, we can see that the p values under the four emotions are all less than 0.05, which shows that the differences between different emotional pronunciation quality levels have statistical significance.

5. Conclusion

With the gradual internationalization of society, we cannot avoid oral English communication with foreign compatriots not only at home but also abroad. Also, designing a standardized model for testing spoken English has become a concrete problem that we need to solve now. Based on the intelligent computing model, this paper analyzes the standardized methods of export language evaluation more accurately. The research results are as follows:

- (1) By comparing the fuzzy logic combined with the neural network intelligent calculation model, the BP neural network calculation model and ANFIS network model, it is known that the accuracy rate of fuzzy logic combined with neural network intelligent calculation model is as high as 80%, and the error rate is less than 2%.
- (2) This paper combines the fuzzy logic algorithm and BP neural network algorithm to form a computational method that can measure spoken language standardization.
- (3) The analysis of the experiment is always through the further specific test of the speech in four different emotional States. The accuracy and error rates in the four emotional states are inconsistent. The variance of people's oral evaluation in the state of surprise is the smallest and the most stable.
- (4) In the comparative experiment, the intelligent computing model of fuzzy logic combined with neural network is compared with manual evaluation under four emotional states, and the intelligent computing model far exceeds the standardization of manual evaluation.

Data Availability

The experimental data used to support the findings of this study are available from the corresponding author upon request.

Conflicts of Interest

The authors declared that they have no conflicts of interest regarding this work.

References

- [1] L. Xiao, "Formative assessment of oral English teaching for middle school students," *Overseas English*, vol. 23, pp. 135-136, 2020.
- [2] Y. Li, Q. Li, Y. Huang, X. Tian, and Q. He, "Research on dynamic evaluation of information technology embedded in college oral English classroom," *China Education Informatization*, vol. 12, pp. 93-96, 2020.
- [3] L. Zhuang, "Hybrid intelligent computing method and its application analysis," *Modern Industrial Economy and Informatization*, vol. 5, no. 15, pp. 85-86, 2015.
- [4] Z. Li, "Value analysis of intelligent computing in mathematical modeling," *Electric Drive*, vol. 50, no. 02, p. 134, 2020.
- [5] J. Zhang, "Progress of educational information processing in colleges and universities based on intelligent computing," *Journal of Yibin University*, vol. 10, no. 12, pp. 88-90, 2010.
- [6] Z. Wan, "Application of intercultural communication strategies in oral English teaching," *Shanxi Youth*, vol. 07, pp. 112-113, 2021.
- [7] N. Zhang, W. Ruixing, and Blair, "Research on oral English learning mode of college students based on app under the background of artificial intelligence," *Digital World*, vol. 07, pp. 71-82, 2020.
- [8] Li Sang, L. Tong, and M. Luo, "Research on the evaluation of oral English teaching in higher vocational colleges based on constructivist learning theory," *Modern Vocational Education*, vol. 5, no. 36, pp. 12-13, 2019.
- [9] Z. Liu, "Discussion on oral English evaluation path of artificial intelligence speech recognition," *Information Record Materials*, vol. 20, no. 11, pp. 92-95, 2019.
- [10] T. Teng, "Design of automatic evaluation system for oral English pronunciation quality," *Automation and Instrumentation*, vol. 06, pp. 175-179, 2019.
- [11] H. Jing, N. Zhao, and H. Lan, "Research and design of data analysis method based on intelligent computing," *Railway Computer Application*, vol. 18, no. 06, pp. 7-9, 2009.
- [12] G. Chen and S. Li, "Network on chip for enterprise information management and integration in intelligent physical systems," *Enterprise Information Systems*, vol. 15, no. 7, pp. 935-950, 2021.
- [13] L. Liu and F. Zhanji, "Backwash effect of dynamic assessment of oral production ability on oral teaching for English majors," *Chinese Journal (Foreign Language Education and Teaching)*, vol. 8, no. 10, pp. 124-126, 2016.
- [14] C. Xian, "On the effective countermeasures of oral English teaching in colleges and universities," *Shanxi Youth*, vol. 14, p. 146, 2016.
- [15] R. Zhong, "Effective ways of oral English teaching in primary schools," *Scientific Chinese*, vol. 36, p. 175, 2015.

Research Article

Multimedia Application and Network Architecture Design Based on Multiterminal Collaboration

Lian Wu ¹ and Lee Jong Han²

¹*School of Digital Arts, Suzhou Art&Design Technology Institute, Suzhou 215009, China*

²*General Graduate Schools, Hoseo University, Asan 31499, Republic of Korea*

Correspondence should be addressed to Lian Wu; wulian@sgmart.edu.cn

Received 1 March 2022; Revised 20 April 2022; Accepted 27 April 2022; Published 2 June 2022

Academic Editor: Hangjun Che

Copyright © 2022 Lian Wu and Lee Jong Han. This is an open access article distributed under the Creative Commons Attribution License, which permits unrestricted use, distribution, and reproduction in any medium, provided the original work is properly cited.

In the rapid development of network technology, most users can simultaneously or alternately use multiple communication terminals. At this time, how to build a control platform of integrated network to help users manage multiple terminals has become the focus of mobile network technology research and development. On the basis of understanding the design content of the network control platform and according to the three types of network selection algorithm, this paper analyzes how to build the architecture of the multiterminal collaborative network control platform based on the open source Mobicents design and conducts test research on its system implementation.

1. Introduction

In the development of the information era, both the Internet and the telecommunications industry are in a state of competitive innovation, especially under the background of the extensive promotion of optical communication technology, digital technology, and other content, all kinds of wireless networks blend with each other and gradually break through a business development mode built by a single network. From the practical point of view, the ultimate purpose of the integrated development of Guangzhou Power Grid, computer network, and telecommunications network is to meet the continuously rising business needs of users and rationally use various business resources to improve the development level of China's information industry. This research topic proposal has attracted the attention of relevant scientific research scholars at home and abroad. At this stage, two terminal collaborative architecture designs have been built for this content, one refers to overlay, and the other refers to the business agent model. Meanwhile, Shaoyong Guo, Lanlan Rui, Xuesong Qiu, and others [1] in the business-based multiterminal dynamic collaborative framework mechanism research concluded that, combined

with the heuristic multiterminal cooperative construction mechanism, in simulation analysis, the built system can not only support differential business, but also reduce business restart. Thus, it proves that this mechanism has application advantages; Hui Tian, Zheng Hu, and Ping Zhang [2] found when studying the business flow control content based on multiterminal collaboration that the future network will be a network with integrated operation and terminals providing users with cross-heterogeneous communication services, it must be deeply explored based on multiterminal collaborative applications and related technologies, and it not only provides new options for the business, but can also provide a basic guarantee for the coordinated application of the business environment; for example, Niemegeers and Groot S [3, 4] proposed to design networking Fednets in the research and development exploration, and based on the construction of personal networks, different types of personal networks share the terminal facilities and services of users. Zhang, Chen, Li [5], and others studied the personal mobility of the application layer combined with the SIP protocol and thus concluded that the SIP protocol has the basic guarantee for personal mobility in the application layer, which can effectively solve the problems caused by mobility by the

underlying mobile protocol and provide a supplement to the actual missing environment. Therefore, it can be seen that when the future mobile communication network innovates towards the direction of diversified and digital development, the most important thing is to rationally use all the network resources to provide high-quality services for users. Therefore, it is crucial to strengthen the multimedia application and network architecture design and analysis based on the multiterminal pedigree.

2. Architecture and Algorithm Design

2.1. Design and Analysis of the Network Control Platform. Combination of the following is shown in Figure 1; architecture diagram analysis shows that the converged network control platform must be able to meet the requirements of various network resource transmission interfaces, service control-oriented service interfaces, and support the requirements of multi-service coordinated trigger control, resource scheduling management, mobility management, etc. Only in this way can the end users in the system be guaranteed to experience the same service no matter what network or application they are in [6, 7].

From the perspective of hierarchy analysis, the network control platform is mainly divided into three aspects: first, the business layer, which is mainly used to control business and design business logic; second, the control layer, which is mainly responsible for optimal connection management, with network control environment; third, the bearer layer and the terminal layer, which include the ubiquitous network and all kinds of terminals and refer to the bearer of the network and the actual receiver and initiator of the application [7, 8]. As shown in Figure 2, the network architecture is mainly composed of terminal application and server network architecture. Terminal application refers to mobile intelligent terminal, which can be used on intelligent terminals of Android and iOS systems and computers. The server network architecture mainly includes the operation system, the core application, the operation and maintenance system, the network architecture components, and the basic parts. The network architecture is a mobile multimedia intelligent terminal to achieve enterprise communication. The integration experience of cloud office network architecture effectively improves the efficiency of information sharing and use between multimedia, and reduces the communication cost within the enterprise. The problem of internal management coordination has been effectively solved, and the precise connection between enterprises and external resources multimedia applications has been realized, which lays a foundation for the healthy and stable development of enterprises. The network architecture supports a variety of forms of information transmission, mainly including text, voice, pictures, and files. Enterprise multimedia can be the most convenient to choose their own needs. The most intuitive way to communicate with each other is to create groups for discussion.

In this paper, a data processing center network architecture is designed, which includes four subnets including input, operation, output, and monitoring, and the first

three subnets have a redundant structure, as shown in Figure 3.

2.2. Network Selection Algorithm. Combined with the analysis of multiterminal and multinet network collaboration scheme, the network selection algorithm is mainly divided into the following categories.

First is the network selection algorithm based on multiple attribute decision making (MADM). Generally, the factors that influence network selection are divided into four categories, which relate to network performance, terminal performance, business requirements, and user preferences. In order to reduce the dimensional effect of each factor, normalization treatment must be implemented because of the large gap between different influencing factors. By integrating all factors into a study, and weighting each decision factor, the absolute importance contained in it was clarified by representation, and then the specific weight value was studied by combining the analytic hierarchy process (AHP). Taking simple weighting method (SAW) and exponential weight multiplication method (MEW) as examples, the former requires linear weighting calculation using various attributes in order to obtain the best network decision. The latter is to use exponential multiplication to access the best network, and the specific formula is as follows:

$$G_{\text{SAW}} = \sum_{j=1}^M (w_j * v_{i,j}), \quad (1)$$

$$G_{\text{MEW}} = \prod_{j=1}^M v_{i,j}^{w_j}.$$

In formula (1), w_j represents the weight value of the j attribute and $v_{i,j}$ represents the normalized value of the j attribute of the i network. The MEW algorithm is more computationally difficult than the SAW algorithm, but the final simulation is not much different.

The distance method needs to be closer as the best evaluation scheme when calculating and analyzing the relative distance between all the evaluation schemes and the positive and negative ideal schemes. The specific formula is shown as follows:

$$G_{\text{TOPSIS}} = \frac{D_{w,j}}{D_{b,j} + D_{w,j}}, \quad (2)$$

$$D_{w,j/b,j} = \sqrt{\sum_{j=1}^M w_j^2 (v_{i,j} - r_{w,j/b,j})}.$$

In the above formula, $D_{w,j}$ represents the distance difference between a candidate network and the reference optimal (worst) network, w_j represents the weight value of the property j , and $r_{w,j/b,j}$ represents the worst value and the optimal value of the property j . This algorithm is more scientific than the previous two, but it is extremely sensitive to handling user preference weights.

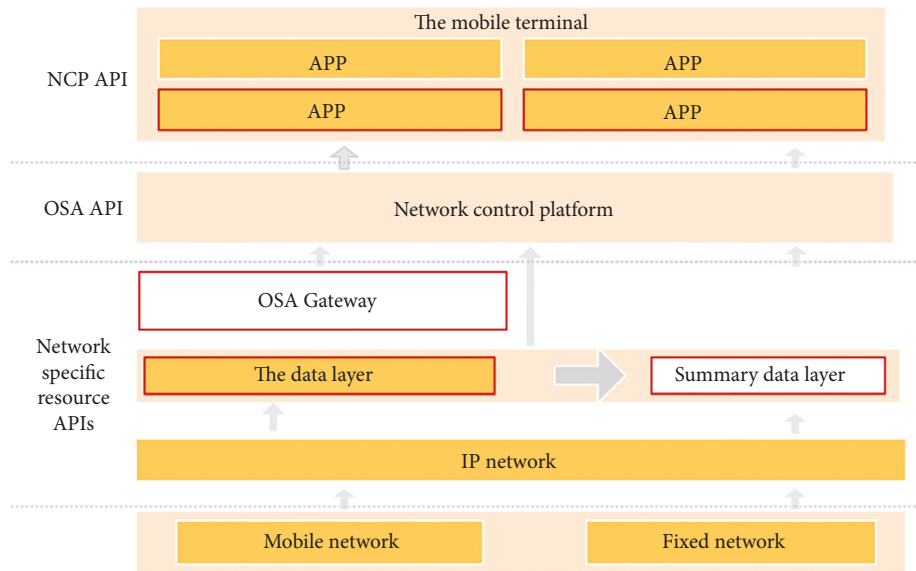


FIGURE 1: Structure diagram of network control platform design.

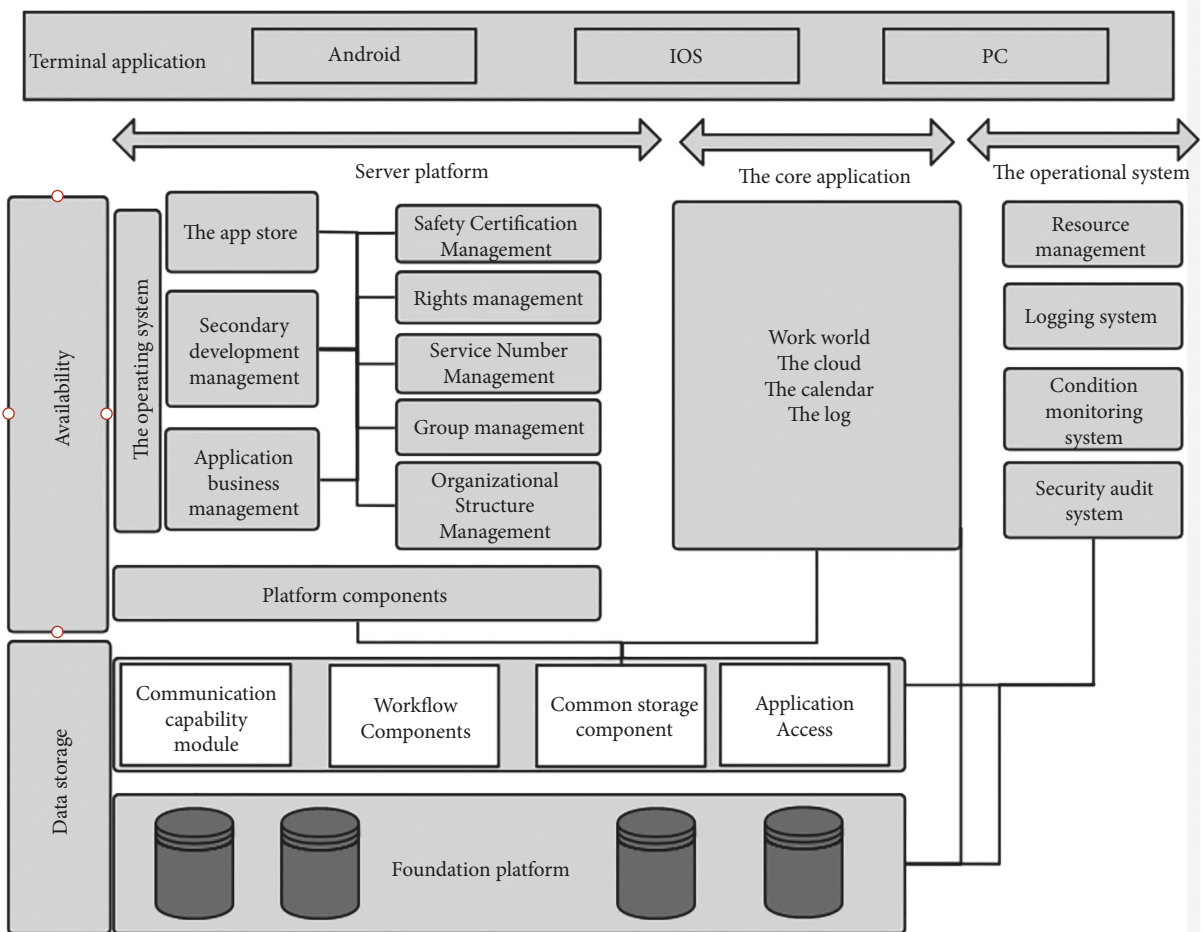


FIGURE 2: A schematic diagram of the overall network architecture for multimedia applications.

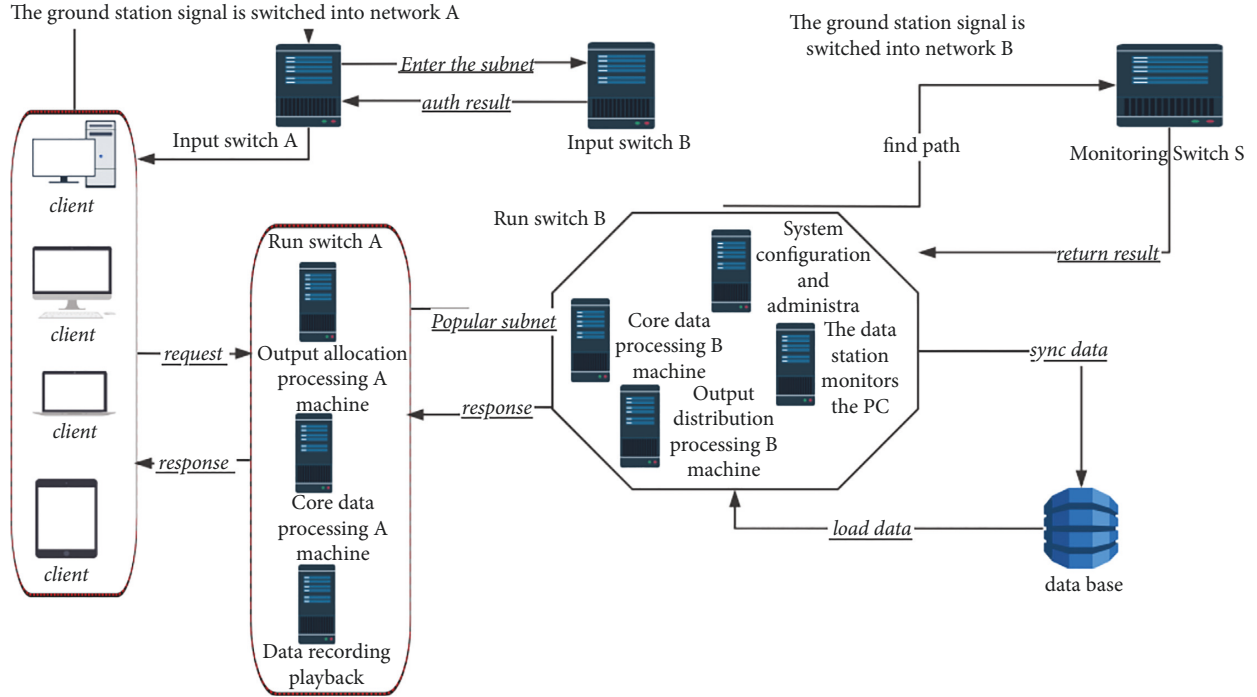


FIGURE 3: Multimedia application network infrastructure.

Using the grey relation analysis (GRA) method to the network selection algorithm, a grey relation coefficient (GRC) is generally defined to show the proximity of each candidate network and the ideal reference network, which needs to be obtained by the best value of a certain property. The specific formula is as follows:

$$G_{\text{GRA}} = \frac{1}{\sum_{j=1}^M w_j |v_{i,j} - R_j| + 1}. \quad (3)$$

In the above formula, R_j represents the best value of the j attribute.

The network selection algorithm is based on user preferences. From a practical point of view, this algorithm is mainly divided into two aspects. On the one hand, it refers to the calculation of the index weight value, and on the other hand, the network preference weight value.

According to the above picture analysis, the network selection process is mainly divided into three steps: First step is collection of data. This work is mainly used to obtain business demand, network status, service price, and other information indicators, which are mainly the main factors affecting the network selection decision, but also the core object of data processing; second is processing the data. Level through to build network selection model, the paper puts forward the AHP judgment matrix and the network parameter matrix and then uses the AHP method to calculate the subjective weight of the clear network parameters, the application position method to get the objective weights of network parameters, and then according to the needs of the business and scientific adjustment of the correlation coefficient between the two user preferences, and synthesis weights of the network parameters. At the same time, the distance analysis method should be used to clarify the

objective weight data of network preferences, and the subjective and objective weight data of network preferences should be used to clarify the comprehensive weight data of network preferences, and finally, the comprehensive effect data of candidate networks should be determined through planning and processing. Finally comes the decision part. According to the comprehensive effect value of the candidate network, the target access network is defined, and the executive network is connected.

In this study, network bandwidth is a benefit parameter, while time-continuance muscle jitter and service price are cost parameters. Normalization is carried out for these parameters, and the specific formula is as follows:

$$x'_{ij} = 1 - \frac{|x_{ij} - x_{j_max}|}{x_{j_max} - x_{j_min}}, \quad (4)$$

$$x'_{ij} = 1 - \frac{|x_{ij} - x_{j_min}|}{x_{j_max} - x_{j_min}}.$$

In the above formula, X_{ij} represents the current value of the j parameter of the i network; the numerical size is directly related to the specific parameters of the current network; X'_{ij} represents the current value of the j parameter of the i network; X_{j_max} represents the maximum value of the j parameter in each candidate network; and X_{j_min} represents the minimum value of the j parameter in each candidate network.

When calculating the network parameter weight, a hierarchical analysis model is constructed to clearly judge that the matrix is $C_x = (c_{ij})_{3 \times 3}$ ($x = B, D, J, L, C, i, j = n1, n2, n3$).

And the product of each row of elements of the corresponding matrix is as follows:

$$V_i = \prod_{j=1}^n a_{ij} \quad (i = 1, 2, \dots, n). \quad (5)$$

The n secondary root of the V_i is

$$\sqrt[n]{V_i} = \sqrt[n]{\prod_{j=1}^n a_{ij}}. \quad (6)$$

After normalization treatment is

$$u_i = \frac{\sqrt[n]{V_i}}{\sum_{i=1}^n \sqrt[n]{V_i}}. \quad (7)$$

Therefore, the evaluation parameter weight of the criterion layer is

$$\{u_B, u_D, u_J, u_L, u_C\}. \quad (8)$$

In order to avoid inconsistency, consistency detection is generally performed on the constructed judgment matrix, and the specific process is as follows.

The indicator CI for consistency is defined as follows:

$$CI = \frac{\lambda_{\max} - n}{n - 1}. \quad (9)$$

In the above formula, λ_{\max} represents the maximum eigenvalue of the judgment matrix and n represents the order of the judgment matrix.

Secondly, the need is to find the corresponding average random consistency index RI where $n = 1, 2, \dots, 9$, and the specific values of RI are shown in Table 1.

Finally, the proportional CR , formula for the analysis consistency, is as follows:

$$CR = \frac{CI}{RI}. \quad (10)$$

When CR is less than 0.10, the consistency of the judgment matrix is considered acceptable; otherwise, appropriate adjustments are needed.

In the process of calculating the objective weight value, the information entropy of network parameters should be studied first. The specific formula is as follows:

$$X(j) = -k \sum_{i=1}^n a_{ij} \ln a_{ij}. \quad (11)$$

In the above formula, a_{ij} represents the normalized value of j parameter of i network, n represents the number of candidate networks, and k represents specific elaboration. Generally, it can be regarded as 1 after simplification.

Then calculate the analysis difference degree, and the specific formula is as follows:

$$Y(j) = 1 - X(j). \quad (12)$$

Finally, calculate the analysis weight vector, and the specific formula is

$$u'_j = \frac{Y(j)}{\sum_j Y(j)}. \quad (13)$$

TABLE 1: Numerical analysis of the RI .

n	1	2	3	4	5	6	7	8	9
RI	0	0	0.58	0.90	1.12	1.24	1.32	1.41	1.45

It makes it clear that the weights of the network parameters are

$$\{u'_B, u'_D, u'_J, u'_L, u'_C\}. \quad (14)$$

The comprehensive weight calculation formula of the network parameters is

$$w_i = \alpha * u_i + (1 - \alpha) * u'_i \quad (i = B, D, J, L, C). \quad (15)$$

In the above formula, α represents the adjustment coefficient and conforms to the condition of $0 < \alpha < 1$, which directly proves the user's subjective preference and the difference of decision value in the decision indicator and makes clear the user's preference demand for service QoS. Generally speaking, $\alpha = 0.5$.

Assume that the number of evaluation parameters is i and the network preference weight is j , then the subjective weight UI can be used to clarify the subjective preference weight of all users for each candidate network. The specific formula is

$$p_k = \sum_i C_i(k) * u_i \quad (i = B, D, J, L, C, k = n1, n2, n3). \quad (16)$$

The corresponding consistency ratio $RI(j)$ calculation formula is

$$CR = \frac{\sum_j CI(j) * u_j}{\sum_j RI(j) * u_j}. \quad (17)$$

Under $CR < 0.10$, the acquired preference weights meet the consistency requirements.

Using objective weight to be preference, the information network parameter matrix is assumed to be X' , and x represents the j parameter value of the i network, then it can be obtained after standardized processing

$$X' = (x'_{ij})_{3 \times 5}. \quad (18)$$

The ideal values X^+ and negative ideal values X^- are calculated:

$$\begin{aligned} X^+ &= (x'^+_B, x'^+_D, x'^+_J, x'^+_L, x'^+_C) \\ X^- &= (x'^-_B, x'^-_D, x'^-_J, x'^-_L, x'^-_C). \end{aligned} \quad (19)$$

In the above formula, the following conditions are met:

$$\begin{aligned} x'^+_l &= \max(x'^-_{1l}, x'^-_{2l}, x'^-_{3l}), x'^-_{1l} \\ &= \min(x'^-_{1l}, x'^-_{2l}, x'^-_{3l}), l = B, D, J, L, C. \end{aligned} \quad (20)$$

The European distance between the two is

$$D_k^+ = \sqrt{\sum_{l=1}^5 (x_{kl} - x_l^+)^2}$$

$$D_k^- = \sqrt{\sum_{l=1}^5 (x_{kl} - x_l^-)^2}. \quad (21)$$

The relative proximity between the network and the ideal network is

$$C_k = \frac{D_k^-}{(D_k^+ + D_k^-)}. \quad (22)$$

The normalization treatment of the above formula is obtained as follows:

$$p_k' = \frac{C_k}{\sum_{k=1}^3 C_k}, k = 1, 2, 3. \quad (23)$$

In the above formula, $p_k'p_k'$ represents objective preference weight values for the weight of each candidate network obtained.

The corresponding comprehensive weight formula is

$$W_k = \beta * p_k + (1 - \beta) * p_k' (k = n1, n2, n3). \quad (24)$$

In the above formula, β represents the coefficients of the user policy, which represents a linear weighted proportion of the user's network subjective and objective preferences and meets the conditions of $0 < \beta < 1$.

It can be seen that the optimal access network selection formula is

$$U(i) = \left[\sum_j (x_{ij}' * w_j) \right] * W_i (i = n1, n2, n3; j = B, D, J, L, C). \quad (25)$$

3. Result Analysis

3.1. Algorithm Implementation. According to the existing multiterminal collaborative selection mechanism, the corresponding selection algorithm is analyzed and designed, and the terminal and the connected network are regarded as a virtual terminal unit (VTU), and the algorithm of the terminal and network collaborative selection (NCS) algorithm is clarified. The experiment explores the selection process of the cooperative terminal set (CTS). There are three cases of subjective weights as follows: First, Case 1 means that all parameters are consistent; Case 2 means that the parameters available bandwidth (AB) and packet loss rate (L) together occupy 70% of the weight, and other parameters occupy 30% of the weight, in other words, that is, for the environment of data services; Case 3 means that parameters AB, time delay (DE) jitter (L), etc., occupy 70% of the total, while other parameters account for 30%, in other words, for the environment of voice services.

Combined with the parameter design conditions shown in Table 2, the corresponding network access options are shown in Figure 4. Starting from this, comparing and analyzing the throughput of different algorithms, it can be seen

that under the condition that the number of cooperative working terminals continues to increase, the business throughput will also increase. When in Case 1, the number of terminals is less than or equal to 2, and the SAW is greater than or equal to MEW. When the number of terminals is 3, 4, and 5, the throughputs of the two are the same; when in the sum, the number of terminals is less than or equal to 2, and the throughput of the two algorithms is the same. But when the number of terminals reaches 3, the MEW is larger than the SAW, and when the number exceeds 3, the throughput of the two is the same. The details are shown in Figure 5.

3.2. Verification Analysis of Environmental Testing. Test as a system development the key link; only through the test, we can accurately detect a system function integrity and accuracy, and we can control the business environment which involves the function of the terminal group registration, terminal status updates, more terminal voice calls, media flow guide control function, the short message function business logic control, etc. So, the actual test starts with the above content.

First, the terminal needs to register. This functional test requires registration in conjunction with the web page. The web page is configured in the Apache server, and it can be verified whether it meets the expected functional requirements by entering the full information of the terminal registered by the user through the web page. After filling out the information, click Submit to complete the registration. After successful registration, the newly registered terminal group information can be queried in the data system.

Second is terminal status updates. At this stage, the dynamic innovation of SIP terminals has been completed. In other words, SIP terminals can be automatically acquired and updated in offline SCE. After the successful registration of the terminal, the default ONLINE status of the SIP terminal is Offline, and the default status of the mobile phone is Online. After the SIP terminal goes online, the Proxy Server will use the SIP register packet that can be intercepted, and the relevant Register information will be first sent to the SIP Proxy component in the SCE. These components will send the SIP number, message, and other information in the message to the Terminal Group Management component. It is then forwarded to the SIP server. At this point, if we check the terminal state in the SCE database again, we can find that it has changed from Offline to Online, which proves that the dynamic innovation of terminal state has been successful [9, 10].

Third is multiterminal voice calls. There are multiple terminals in the user terminal group. If you want to select the optimal terminal, you need to follow the following rules for analysis and processing. If the SIP terminal is assumed to be online, call the SIP terminal. Assuming that there are multiple SIP terminals online, it is necessary to select the SIP terminal with the latest online time. If the SIP terminal is not online, it is necessary to return the newly registered mobile terminal number again. If there is no mobile terminal number at this time, it is an error that has returned [11].

TABLE 2: Parameter design based on network selection.

	$AB(\text{Mbit/s})$	$TB(\text{Mbit/s})$	$SS(\%)$	$u(\%)$	$DE(\text{ms})$	$J(\text{ms})$	$L(/10)$	$C(\%)$
AN1	1	2	100	20	50	10	50	60
AN2	1.2	2	100	25	50	10	20	80
AN3	6	11	100	40	150	20	30	10
AN4	30	54	90	60	150	20	80	12
AN5	20	60	90	80	90	10	40	70
AN6	40	60	90	30	100	10	30	100

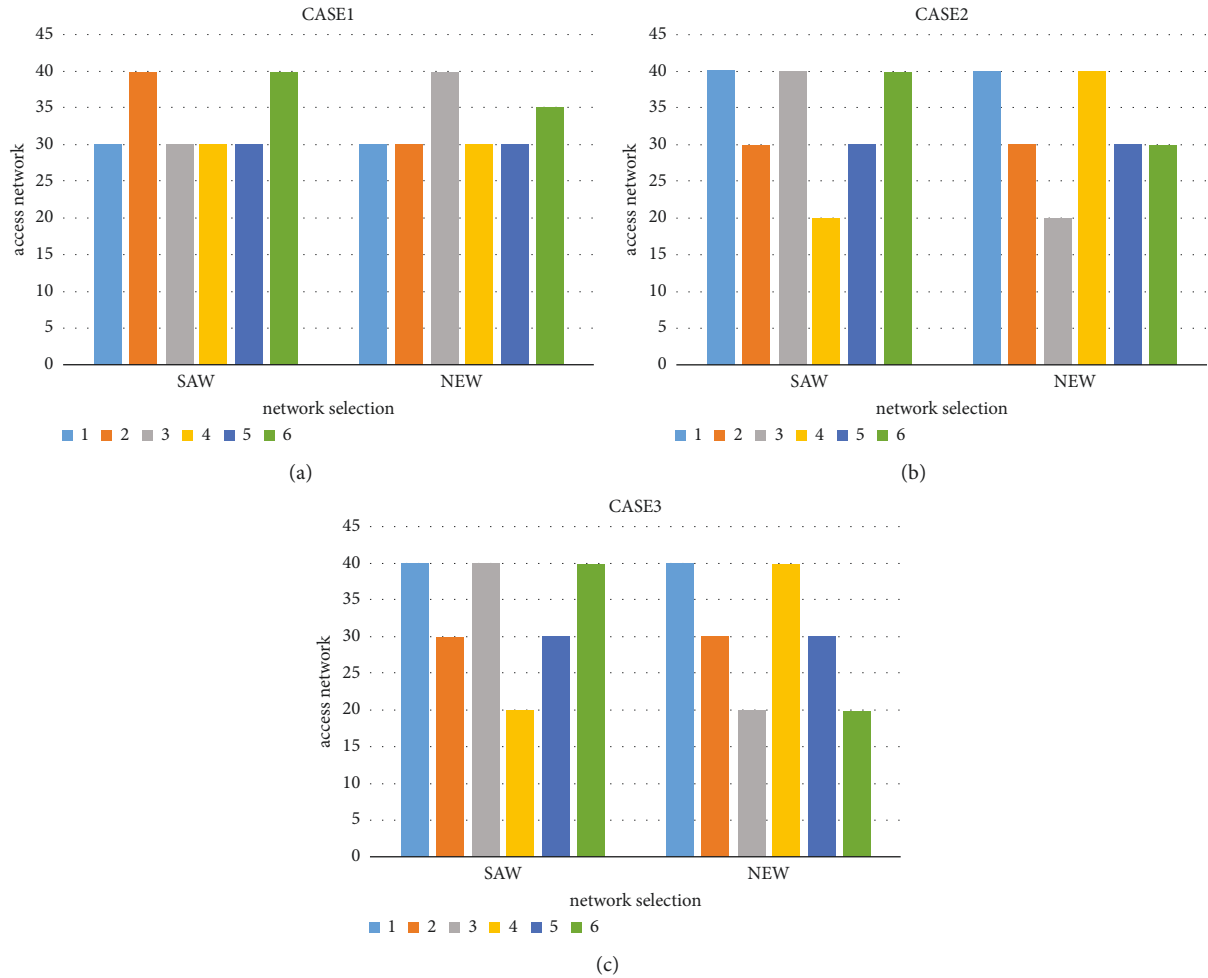


FIGURE 4: Network selection results.

Fourth is media stream guidance and control. This function is demonstrated in the remote control program developed by the platform. First, click the update button at the terminal to obtain the corresponding terminal group information. The message returned by the SCE will be displayed in the Debugging Information section below. At this time, it can be clear how many terminals have been returned, and the specific IP address will also be displayed directly. Combined with the status information bar of terminal equipment, the above presentation terminal can be studied to determine whether it is available or not. Secondly, select the desired terminal and click the Play button. Then, you can see that the lower right corner of the first terminal icon in the interface will mark the playback

symbol, which proves that the current terminal is in the playback state. Finally, the video is played on the selected terminal [12].

Fifth is short message function business logic control. This functional test mainly verifies the business logic function of short message sending. The actual interface design contains three contents: first is the mandatory parameters, which involve the number of the sender, the number of the receiver, and the message content; next is optional parameters, which involve the text message need to copy well and logo and other content; finally, there is the service endpoint information, which refers to the information data on the server side, such as the user name and password. The key parameter is the mandatory parameters.

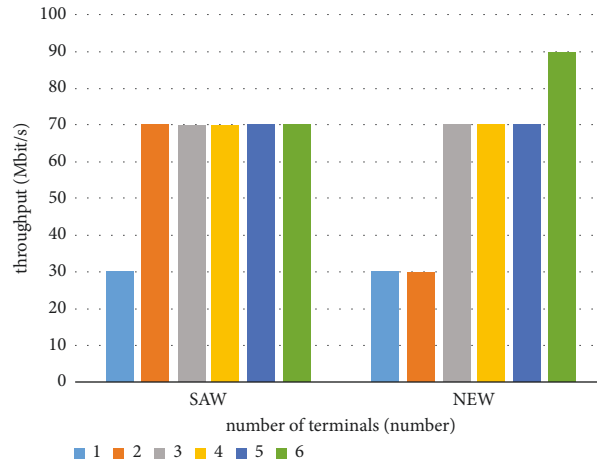


FIGURE 5: Comparison results of the algorithm throughput.

After completing information filling, click “Submit” below, and then the network platform can obtain the web page to submit the application. The specific code is as follows [13].

```

("deliveryInfoNotification":{"senderAddress":"tel:+1890000991","message":"Message
from SCE.,"deliveryInfo":{"deliveryStatus":"DeliveredToTerminal","address":"tel
:+13500000991"},"deliveryStatus":"DeliveredToTerminal","address":"tel:+1350000099
2"},"deliveryStatus":"DeliveredToTerminal","address":"tel:+13500000993"},"delive
ryStatus":"DeliveredToTerminal","address":"tel:+13500000994"},"deliveredStatus":"
DeliveredToTerminal","address":"tel:+13500000995"}}}
18:05:22,195 INFO [CPEHttpResourceAdaptor] POST /oneapiserver /snsdeliverynotftca
tton HTTP/1.1

```

This component then converts the message form into a pattern recognized by the SMS Gateway and passes it to and through the SMS Gateway [14].

Combined with the content analysis of multiterminal collaborative multimedia application and network architecture design outlined above, it can be seen that the overall system design applies the idea of layering, including the business control layer, the network control layer, and the bearing layer from top to bottom, and the interface is needed to communicate with each other. From the perspective of business control environment, it is necessary to use the componentized design idea to divide larger functions into multiple components, so that the components can complete the task in cooperative operation and facilitate subsequent business expansion and development. In the design of terminal group business logic, the ultimate purpose of business environment control is to control the terminal group business logic, such as how to store and update the terminal group information and how to make full use of all terminal business capabilities to provide users with quality

services. Combined with the analysis of the network control environment, in order to build a flexible and modifiable system software platform, it is necessary to select an appropriate network selection algorithm and implement differentiated queue control rules according to different business requirements.

4. Conclusion

To sum up, in the comprehensive promotion of information network technology, most users can skillfully use or alternately use multiple communication terminals, and these terminals can be connected to different or heterogeneous networks. At this time, in order to guarantee the quality and safety of system operation, it is necessary to build a control platform of fusion network based on practical development requirements, which can not only help users comprehensively control multiple terminals, but also make reasonable use of the business capabilities of each terminal. Combined with the research and analysis of the design form of network

control platform and network selection algorithm in this paper, the overall design is mainly divided into three layers, and the selected algorithm mainly has three kinds, including FAHP-GRA algorithm, based on the AHP and entropy method, and based on AHP and TOPSIS algorithm. According to the overall system design form, the comparison and analysis of the three alternative algorithms show that the application performance of the algorithm based on AHP and TOPSIS is better, showing a strong application advantage in both unnecessary conversion rate and user satisfaction. And test validation analysis was carried out on the overall system design, which mainly includes the function of the terminal groups registered, terminal status updates, more terminal voice calls, media flow guide control function, the short message function business logic control, and other functions, and through the test and analysis, we found that various functions can be fully present in the development of practice [15–17].

Data Availability

The experimental data used to support the findings of this study are available from the corresponding author upon request.

Conflicts of Interest


The authors declare that they have no conflicts of interest regarding this work.

References

- [1] S. Guo, L. Rui, X. Qiu, and L. M. Meng, “Business-oriented mechanism,” *Journal of Electronics and Information*, vol. 34, no. 7, pp. 1703–1708, 2012.
- [2] P. Zhang, J. Miao, Z. Hu, and T. Hui, “A review of general network research,” *Journal of Beijing University of Posts and Telecommunications*, vol. 033, no. 005, pp. 1–6, 2010.
- [3] C. Zhang, M. Chen, and B. Li, “Analysis of application layer personal mobility under SIP protocol,” *Computer Technology and Development*, vol. 020, no. 007, pp. 109–113, 2010.
- [4] I. G. Niemegeers and S. M. H. De Groot, “FEDNETS: context-aware ad-hoc network federations,” *Wireless Personal Communications*, vol. 33, no. 3-4, pp. 305–318, 2005.
- [5] H. Tian, Z. Hu, and P. Zhang, “Business flow control based on multi-terminal collaborative,” *ZTE Technology*, vol. 18, no. 3, pp. 16–19, 2012.
- [6] S. Yang, B. Yang, H. S. Wong, and K. Zhongfeng, *Cooperative Traffic Signal Control Using Multi-step Return and Off-Policy Asynchronous Advantage Actor-Critic Graph algorithm*, Knowledge-Based Systems, College Station, TX, USA, 2019.
- [7] A. I. Delis, I. K. Nikolos, and M. Papageorgiou, “Macroscopic traffic flow modeling with adaptive cruise control: development and numerical solution,” *Computers & Mathematics with Applications*, vol. 70, no. 8, pp. 1921–1947, 2015.
- [8] R. Chandrasekaran and K. P. K. Y. P. S. N. Nair, “Multi-terminal multipath flows: synthesis,” *Discrete Applied Mathematics*, vol. 143, no. 1-3, pp. 182–193, 2004.
- [9] Z. Li, Y. Liu, S. Xu, and Y. Qian, “Analytical studies on an optimized adaptive cruise control model of traffic flow based on self-stabilizing strategy,” *International Journal of Modern Physics C*, vol. 31, no. 4, 2020.
- [10] Y. Zhang, Y. Yang, W. Zhou, and O. Xiaocao, *Multi-city Traffic Flow Forecasting via Multi-Task learning*, pp. 1–19, Applied Intelligence, Surrey, LN, UK, 2021.
- [11] Y. Liu, R. J. Cheng, Y. Q. Ma, and H.X Ge, “The control method for the multi-phase traffic model,” *International Journal of Modern Physics C*, vol. 27, no. 10, Article ID 1650111, 2016.
- [12] S. I. Roumeliotis and I. M. Rekleitis, “Propagation of uncertainty in cooperative multirobot localization: analysis and experimental results,” *Autonomous Robots*, vol. 17, no. 1, pp. 41–54, 2004.
- [13] S. Erhart and S. Hirche, “Internal force analysis and load distribution for cooperative multi-robot manipulation,” *IEEE Transactions on Robotics*, vol. 31, no. 5, pp. 1238–1243, 2015.
- [14] Z. Zhen, D. Zhao, J. Gao, D. Wang, and Y. Dai, “FMRQ-A multiagent reinforcement learning algorithm for fully cooperative tasks[[]],” *IEEE Transactions on Cybernetics*, vol. 47, no. 6, pp. 1367–1379, 2016.
- [15] I. F. Akyildiz, J. Liebeherr, and I. Nikolaidis, “Multi-level rate-based flow control for ABR traffic,” *Performance Evaluation*, vol. 31, no. 1-2, pp. 107–131, 1997.
- [16] S. Lakshmanan and R. Sivakumar, “Proteus: multiflow diversity routing for wireless networks with cooperative transmissions,” *IEEE Transactions on Mobile Computing*, vol. 12, no. 6, pp. 1146–1159, 2013.
- [17] A. Torreño, E. Onaindia, and A. Komenda, “Cooperative multi-agent planning: a survey[[]],” *ACM Computing Surveys*, vol. 50, no. 6, pp. 1–32, 2017.

Research Article

Research on Classroom Teaching Quality Evaluation and Feedback System Based on Big Data Analysis

Yuankui Zhang¹ and Jing Gao ²

¹Education and Teaching Department, Zhengzhou Preschool Education College, Zhengzhou 450099, China

²School of Business, Guangxi University, Nanning 530004, China

Correspondence should be addressed to Jing Gao; 2102402004@st.gxu.edu.cn

Received 24 March 2022; Revised 20 April 2022; Accepted 28 April 2022; Published 1 June 2022

Academic Editor: Hangjun Che

Copyright © 2022 Yuankui Zhang and Jing Gao. This is an open access article distributed under the Creative Commons Attribution License, which permits unrestricted use, distribution, and reproduction in any medium, provided the original work is properly cited.

With the development of information technology, the era of big data has gradually entered classroom teaching, and the evaluation of students' learning quality and classroom teaching efficiency has been widely concerned. In order to further improve the quality of classroom teaching in colleges and universities, this paper analyzes the classroom teaching quality evaluation and feedback system based on the big data. Principal component analysis is used to analyze the evaluation index of classroom teaching quality and feedback information to apartment. Through the study of education quality estimate and feedback system under big data, the feedback mechanism of classroom teaching quality evaluation is improved to achieve high-quality and efficient teaching.

1. Introduction

The classroom teaching quality estimate and feedback system refers to the comprehensive analysis of the information in the teaching process and the determination of improvement plans based on the feedback results [1–3]. In recent years, with the deepening of networked information in the era of big data, networked data analysis has been applied to every field of life and become an indispensable part of teaching activities in the new field [4]. Compared with the conventional classroom teaching quality evaluation model, teachers as the main body, through students, peers, leaders, and supervisors to improve the teaching work of teachers, using big data to analyze teaching quality can suggest to improve the reasonable appraise system, leading to the results being not ideal. In the big data, how to use big data for analysis technique to analyze the current of the evaluation of teaching is very significant [5, 6].

At present, big data teaching analysis is mainly a quality evaluation and feedback system. The quality of teaching is based on big data analysis. Literature [7] conducts big data

on teaching quality data, finds out the factors affecting teaching quality, and makes correlation analysis. Literature [8] collects all kinds of data related to teaching quality and stores, analyzes, and displays the data based on the deficiencies existing in current evaluation of teaching quality in colleges. Using big data technology can achieve objective evaluation of teaching quality, with timely monitoring, warning, and improvement. In [9], weights are assigned to each evaluation item through network hierarchy analysis, a teaching quality index system is constructed, and teaching evaluation feedback is given through multiple evaluation subjects. Literature [10] has established a multievaluation system and conducted in-depth analysis on the existence of problems in the multievaluation system. On this basis, the application of big data in the comprised system of colleges is proposed.

For big data analysis methods, Gong [11] uses k-means clustering analysis to conduct feature classification management for different teacher evaluations, in order to improve the accuracy of evaluating teaching quality in colleges. Literature [12] proposed to optimize and improve the teaching evaluation system by using the marginal

computing path, so as to improve and ensure the accuracy of the appraisal and the efficiency of the evaluation. In the literary world [13], the computer system is used to regress the classroom quality of colleges and universities for data collection and statistics, and the most advanced teaching feedback mode is established based on large amounts of data. In the literary world [14], Cite Space measurement visualization analysis software is used to conduct evaluation and analysis of teaching, and the evaluation system is quantitatively processed to improve the deficiencies existing in the system. Literature [15] uses cluster analysis to analyze online teaching quality evaluation, which has achieved the purpose of improving teaching quality. Based on information data analysis, literature [16] establishes a perfect network evaluation system and carries out multi-directional and angle data mining, aiming at improving teaching quality.

The above literature uses big data to analyze the problems existing in the classroom teaching quality evaluation and feedback system and uses data analysis technology to establish and improve the teaching quality evaluation index system, so as to improve the accuracy of teaching quality evaluation. Using different data analysis methods to analyze the feedback results of classroom teaching quality evaluation, the improvement can promote the quality of classroom teaching in colleges and universities. Based on the above, this paper mainly uses principal component analysis to analyze the evaluation indicators of classroom teaching quality and analyzes and optimizes the problems existing in the analysis of the principal components. Finally, the teacher rating of a school is taken as an example to verify and analyze the representativeness of the original method and the improved method, so that the classroom teaching quality evaluation feedback system can be improved and the quality of classroom teaching in colleges and universities can be improved.

2. Data Analysis Classroom Teaching Quality Evaluation and Feedback System

2.1. Big Data Analysis

- (1) In big data analysis, data is usually acquired, integrated, analyzed, and displayed. The foundation of big data analysis is data collection and the data source of teaching quality evaluation feedback system model. Data integration mainly includes data extraction, cleaning, and loading. Data analysis is the key step of big data analysis and data processing. Data presentation is the visualization of data, the original data, and analysis results for visual processing. The big data analysis process is shown in Figure 1.
- (2) This study analyzes the feedback system of classroom teaching quality evaluation based on big data and divides the evaluation system into three levels, namely, input layer, kernel layer, and output layer. By analyzing the evaluation index system, an analysis

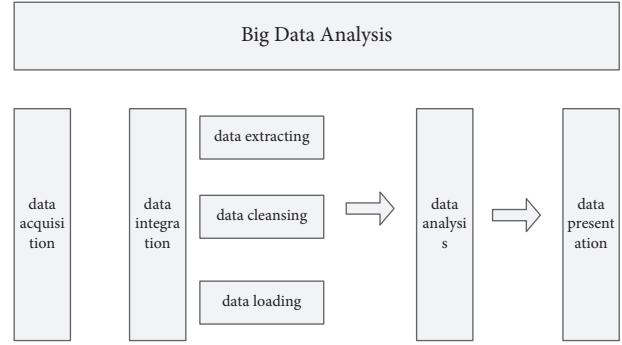


FIGURE 1: Big data analysis process.

algorithm is determined to optimize the evaluation index system and then improve the quality of classroom teaching, as shown in Figure 2.

2.2. Classroom Teaching Quality Evaluation and Feedback System Model. Classroom teaching quality and feedback system is the monitoring and evaluation of teachers' classroom teaching quality. The traditional teaching quality evaluation and feedback system model is primarily composed of school leadership, teaching management, teachers, students, administrative departments, and units that select and employ individuals, such as outside experts, as the main body. Teachers need to manage and monitor the teaching process and evaluate the teaching objectives. Then, the evaluation results are evaluated after feedback analysis, as shown in Figures 3 and 4.

2.3. Analysis Principles and Methods. Data analysis classroom teaching quality evaluation is an effective teaching means, in the classroom, which can effectively increase students' enthusiasm for learning and teachers' level of classroom teaching quality. The investigation of classroom teaching quality assessment and feedback system based on data analysis can make a deep analysis of the evaluation results, find the problems in the evaluation results more deeply, provide a good basis for the assessment of teachers' teaching abilities, and provide long-term guidance for teachers' self-improvement of teaching level.

2.3.1. Principal Component Analysis. (1) *Principle of principal component analysis.* Principal component analysis is a statistical analysis technique that reduces a large number of indicators to a small number of indicators [17]. Principal component analysis can shed light on the large number of elements in the original data by using fewer unrelated variables.

(2) *Principal component analysis algorithm flow.* For principal component analysis, there are m index variables: x_1, x_2, \dots, x_m are a total of n comprised objects. The JTH index of the I evaluation object is x_{ij} , and all indexes x_{ij} are transformed into standardized indexes \tilde{x}_{ij} .

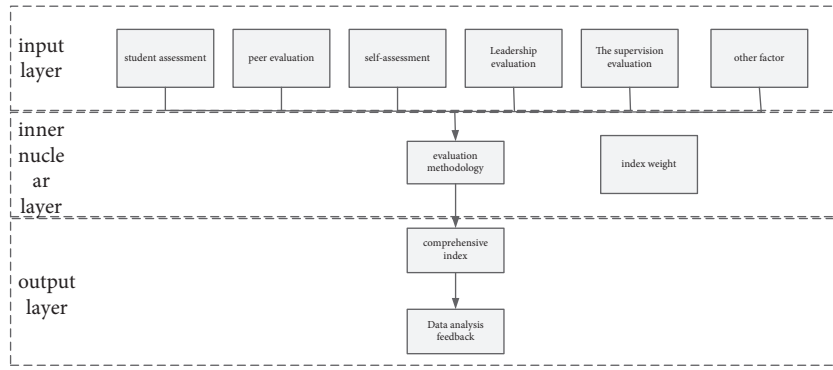


FIGURE 2: Big data analysis model framework.

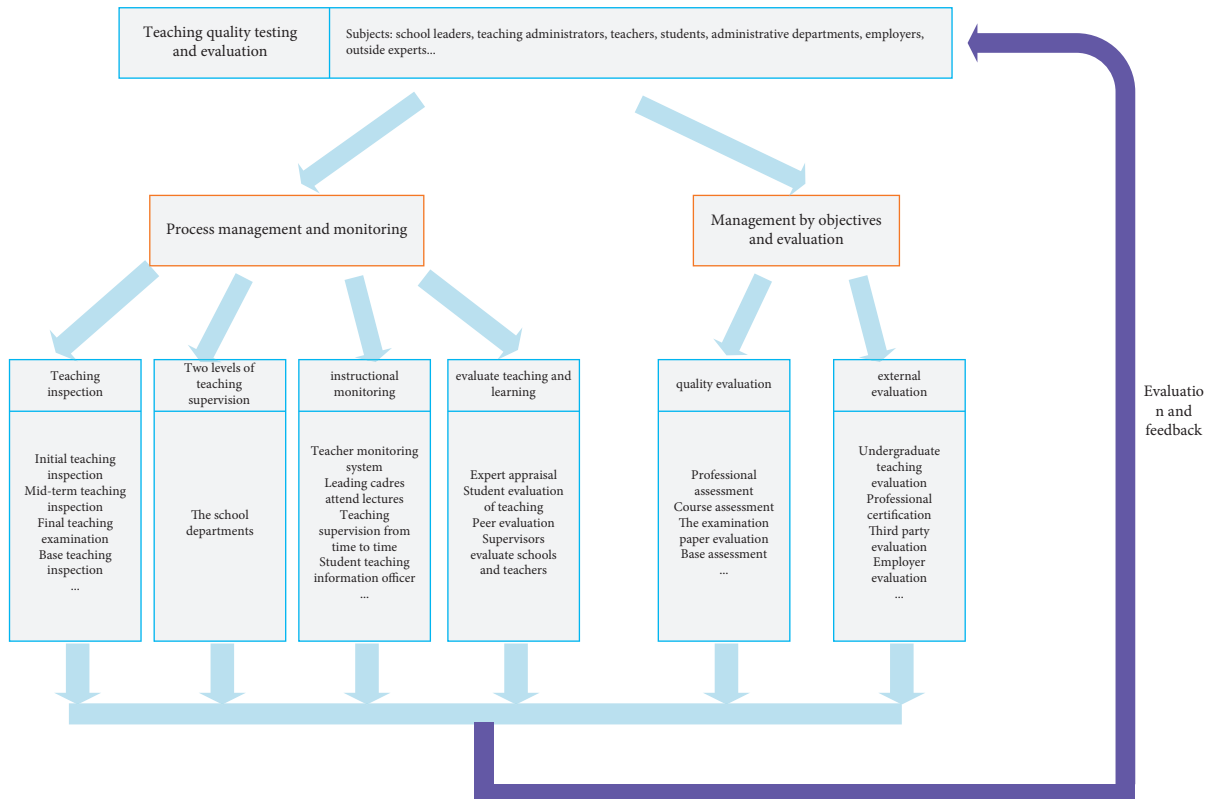


FIGURE 3: Traditional teaching quality evaluation feedback system.

$$\tilde{x}_{ij} = \frac{x_{ij} - \tilde{x}_{ij}}{s_j} \quad (i = 1, 2, \dots, n, j = 1, 2, \dots, m). \quad (1)$$

$$\tilde{x}_i = \frac{x_i - \tilde{x}_i}{s_i} \quad (i = 1, 2, \dots, m). \quad (4)$$

$$\tilde{x}_j = \frac{1}{n} \sum_{i=1}^n x_{ij}. \quad (2)$$

It is standardized index variable.
Matrix of correlation coefficients

$$R = (r_{ij})_{m \times m}. \quad (5)$$

$$s_j = \sqrt{\frac{1}{n-1} \sum_{i=1}^n (x_{ij} - \tilde{x}_j)^2} \quad (j = 1, 2, \dots, m). \quad (3)$$

$$r_{ij} = \frac{\sum_{k=1}^n \tilde{x}_{kj} \tilde{x}_{ki}}{n-1}, \quad (6)$$

And \tilde{x}_j, s_j are the sample mean and standard deviation of the i th indicator, which are called according to them

where $r_{ii} = 1, r_{ij} = r_{ji}, r_{ij}$ is the correlation coefficient between the i th and j th indices.

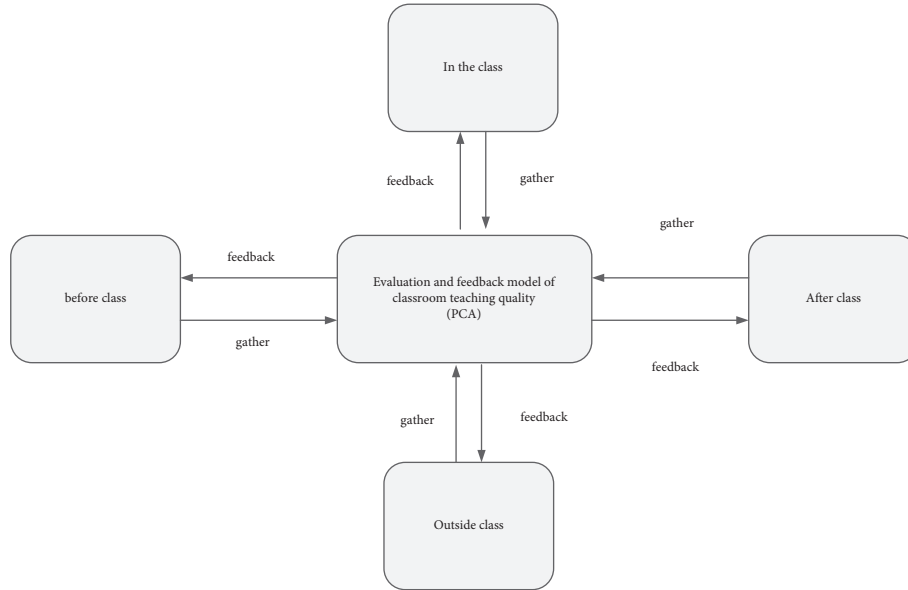


FIGURE 4: Evaluation feedback model.

Determine the eigenvalues [18] and eigenvectors.

The eigenvalues are sorted from largest to smallest.

Determine the correlation coefficient's eigenvalue matrix $\lambda_1 \geq \lambda_2 \geq \lambda_3 \dots \geq \lambda_m \geq 0$, and corresponding characteristic vectors $\mu_1, \mu_2, \dots, \mu_m$, where

$\mu_j = (\mu_{1j}, \mu_{2j}, \dots, \mu_{nj})^T$ feature vectors are used to create new index variables.

$$\begin{cases} y_1 = \mu_{11}\tilde{x}_1 + \mu_{21}\tilde{x}_2 + \dots + \mu_{n1}\tilde{x}_n \\ y_2 = \mu_{12}\tilde{x}_1 + \mu_{22}\tilde{x}_2 + \dots + \mu_{n2}\tilde{x}_n, \\ \dots \end{cases} \quad (7)$$

where y_1 is the first principal component in the formula, y_2 is the second principal component, and y_m is the MTH principal component.

$P (P \leq M)$ principal components were selected to calculate the comprehensive evaluation value.

I calculate the eigenvalue $\lambda_j (j = 1, 2, \dots, M)$ rate of information contribution and accumulation contribution rate, according to

$$b_j = \frac{\lambda_j}{\sum_{k=1}^m \lambda_k}, j = 1, 2, \dots, m. \quad (8)$$

The main component's information contribution rate y_j :

$$\alpha_p = \frac{\sum_{k=1}^p \lambda_k}{\sum_{k=1}^m \lambda_k}. \quad (9)$$

Main components are Y_1, Y_2, \dots . When α_P is close to 1 ($\alpha_P = 0.85, 0.90, 0.05$), the first P index variables y_1, y_2, \dots, y_p as P principal components are used instead of the original M index variables, allowing for a more comprehensive analysis of p principal components.

Ii calculate the overall score

$$Z = \sum_{j=1}^P b_j y_j, \quad (10)$$

where b_j is the information contribution rate of the JTH principal component as measured by the comprehensive score value.

(3) Process of principal component analysis method: it is shown in Figure 5.

(a) Selection principle of evaluation indexes for analysis of the principal components: in the evaluation of classroom teaching quality, the selection of evaluation indicators is very important. To some extent, evaluation quality has nothing to do with the number of evaluation indicators but is primarily related to the role of evaluation indicators in the evaluation process. The main indicators are the indicators which thus play a decisive role in the evaluation process. The level of evaluation quality has nothing to do with the evaluation quality and the number of evaluation indexes, but only with the proportion of evaluation indexes in the evaluation system. Therefore, the principle of evaluation indicators is particularly important. The common selection methods of evaluation indicators are as follows.

(4) Least variance method: N objects to be evaluated are usually selected in the evaluation process: Y_1, Y_2, \dots, Y_n , where each object has m evaluation indexes represented by $X_{ij} (i = 1, 2, \dots, n \text{ and } j = 1, 2, \dots, M)$; assuming that the evaluation index values all fluctuate within a certain range, when the impact of an evaluation index on the evaluation result is small enough, we can exclude these evaluation indexes and optimize and screen the index system through the principle of least variance [19]:

$$Y_j = \left(\frac{1}{n} \sum_{i=1}^n (X_{ij} - \bar{X}_j)^2 \right)^{1/2} \quad j = 1, 2, \dots, m. \quad (11)$$

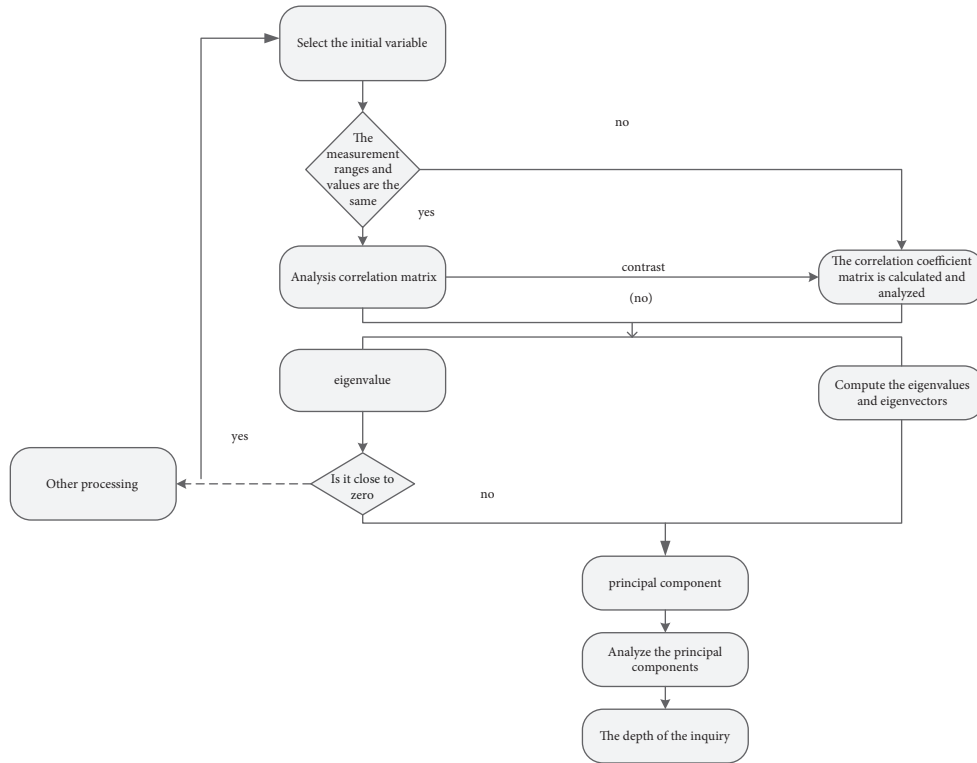


FIGURE 5: Flowchart of principal component analysis.

It is the sample mean square error of n evaluation objects:

$$\bar{X}_j = \frac{1}{n} \sum_{i=1}^m X_{ij} \quad j = 1, 2, \dots, m. \quad (12)$$

It is the sample mean obtained at the end. Suppose there is l_0 ($1 \leq l_0 \leq m$), such that

$$Y_{l_0} = \min_{1 \leq j \leq m} \{Y_j\}. \quad (13)$$

When $Y_{l_0} \approx 0$, the corresponding $X_{(l_0)}$ of $Y_{(l_0)}$ can be deleted.

(5) Minimax deviation method: for evaluation objects, the maximum distance X_j of evaluation index S_j is solved one by one:

$$S_j = \max_{1 \leq j, l \leq n} \{|X_{ij} - x_{lj}|\}. \quad (14)$$

Find the minimum value of S_j and S_0 :

$$S_0 = \min_{1 \leq j \leq n} \{S_j\}, \quad (15)$$

and when $S_0 \rightarrow 0$, the corresponding evaluation index of S_0 can be deleted [20].

(b) Problems of analysis of the principal components: the original principal components data cannot truthfully reflect the actual problems. In the comprehensive evaluation of various influencing factors, information overlap often exists and the main characteristics cannot be determined. The

contribution rate of the first principal component is often not prominent, leading to the lack of comparability and objective correlation among the selected indicators. Therefore, it is difficult for principal component analysis to obtain correct evaluation results.

3. Improve Lecture Quality Evaluation and Feedback System Based on Data Analysis

3.1. Improvement of Analysis Methods. By using principal component analysis (PCA) to assess classroom teaching quality, the original data is first processed using the original PCA model. When the difference of index information of original data is small and the distinction is not obvious, the effect of dimension reduction in analysis is not obvious. Therefore, we improved the principal component analysis method, transformed the original index into an optimized index, and carried out mean processing at the same time, so as to achieve the effect of will. Index optimization was carried out through cosquare difference matrix [21].

3.1.1. Processing of Original Data. According to the original data model of principal component analysis, there are known m evaluation indexes and N evaluation objects.

Among them,

$$\bar{x} = \frac{1}{m} \sum_{k=1}^m x_i. \quad (16)$$

It is the mean value of the original index:

$$V = \frac{1}{m-1} \sum_{k=1}^m (x_i - \bar{x}_i)(x_j - \bar{x}_j). \quad (17)$$

It is the covariance of the original index:

$$\omega_{ij} = \lambda_{ij} \frac{y_{ij}}{\sum_{i=1}^m v_i} + (1 - t\lambda_{ij}) \frac{g_i}{\sum_{i=1}^m g_i}, \quad (i=1,2,\dots,n; j=1,2,\dots,m). \quad (18)$$

It is the inertia coefficient corresponding to the original index.

$\omega_1 x_1, \omega_2 x_2, \dots, \omega_m x_m$ is the first-level optimization index, where

$$x = 1mk = 1m\omega_k x_k, \quad (19)$$

$$\bar{x} = \frac{1}{m} \sum_{k=1}^m \omega_k x_k.$$

It is the first-order optimized mean value.

$$\bar{V} = \frac{1}{m-1} \sum_{k=1}^m (\omega_{ki} x_i - \bar{x}_i)(\omega_{kj} x_j - \bar{x}_j). \quad (20)$$

It is the first-order optimization covariance.

y_1, y_2, \dots, y_m is the second-level optimization index, where

$$\tilde{V} = \frac{1}{m-1} \sum_{k=1}^m (y_{ki} - \bar{y}_i)(y_{kj} - \bar{y}_j) = \frac{1}{\bar{x}_i \bar{x}_j} \bar{V}. \quad (21)$$

It is the second-level optimization index covariance [22].

3.1.2. Data Analysis. The covariance matrix of the evaluation index matrix is obtained

$$\tilde{V} = \frac{1}{m-1} \sum_{k=1}^m (y_{li} - \bar{y}_i)(y_{lj} - \bar{y}_j). \quad (22)$$

The principal component expression $Z = UY$ is obtained, and the corresponding eigenvector matrix is

$$U = \begin{bmatrix} u'_1 \\ \dots \\ u'_m \end{bmatrix} = \begin{bmatrix} u_{11} & \dots & u_{1m} \\ \dots & \dots & \dots \\ u_{m1} & \dots & u_{mm} \end{bmatrix}. \quad (23)$$

The variance contribution α and cumulative variance contribution β were calculated

$$\alpha = \frac{\lambda_i}{\sum_{i=1}^m \lambda_i}. \quad (24)$$

$$\beta = \frac{\sum_{i=1}^p \lambda_i}{\sum_{i=1}^m \lambda_i} \quad p < m. \quad (25)$$

The number of principal components P was selected according to the principle of $\beta \geq 85\%$ [23].

Calculate the principal component factor load matrix.

$$\begin{cases} z_1 = \mu_{11}\tilde{x}_1 + \mu_{21}\tilde{x}_2 + \dots + \mu_{m1}\tilde{x}_m \\ z_2 = \mu_{12}\tilde{x}_1 + \mu_{22}\tilde{x}_2 + \dots + \mu_{m2}\tilde{x}_m \\ \dots \end{cases} \quad (26)$$

Construct comprehensive evaluation function

$$F = \alpha Z = \alpha_1 z_1 + \alpha_2 z_2 + \dots + \alpha_p z_p. \quad (27)$$

Principal component analysis method was improved, which can solve the problem of the first principal component contribution rate that is not up to standard, increasing the contribution of the very first primary component. The feature extraction (pca) was improved, and the cumulative contribution of the index of the first component is more outstanding, reduces the dimension of evaluation index, and improves the efficiency of the principal component analysis method.

3.2. Improved Teaching Quality Evaluation Feedback System. It is shown in Figure 6.

4. Practical Application of Principal Component Analysis

4.1. Evaluation Index System of Classroom Teaching Quality. It is shown in Table 1.

4.2. Data Collection. The teaching quality evaluation adopts the method of online teaching evaluation. After the teacher completes the teaching plan, the educational affairs department issues the teaching performance assessment form to each student's educational administration system, and the student logs in the teaching system to evaluate teaching. The evaluation index is divided into four grades: excellent, good, pass, and fail (9.5 for excellent, 7.5 for good, 6.0 for pass, and 4.0 for fail). The average score is calculated according to the score assigned by the students. In order to improve the rationality of the score, all votes filled in with the same score are invalid. For teachers t01-T02, the party's indicators are summarized in Table 2.

4.3. Evaluation and Analysis of Classroom Teaching Quality Indicators. The original principal component analysis method was used to extract the characteristics of the indicators to find out the main factors affecting the evaluation indicators. The cluster analysis method was being used. This experiment processed the indicator data obtained in Table 2 and calculated the eigenvalues, the evaluation indicators' variability contribution rate, and combined contribution rate. The data obtained are shown in Table 3.

The characteristics of indicators were harvested using mean - mean principal component analysis (PCA). In this experiment, the principal component analysis (PCA) method was used to process the index data obtained in Table 1 and calculate the feature vector, variance

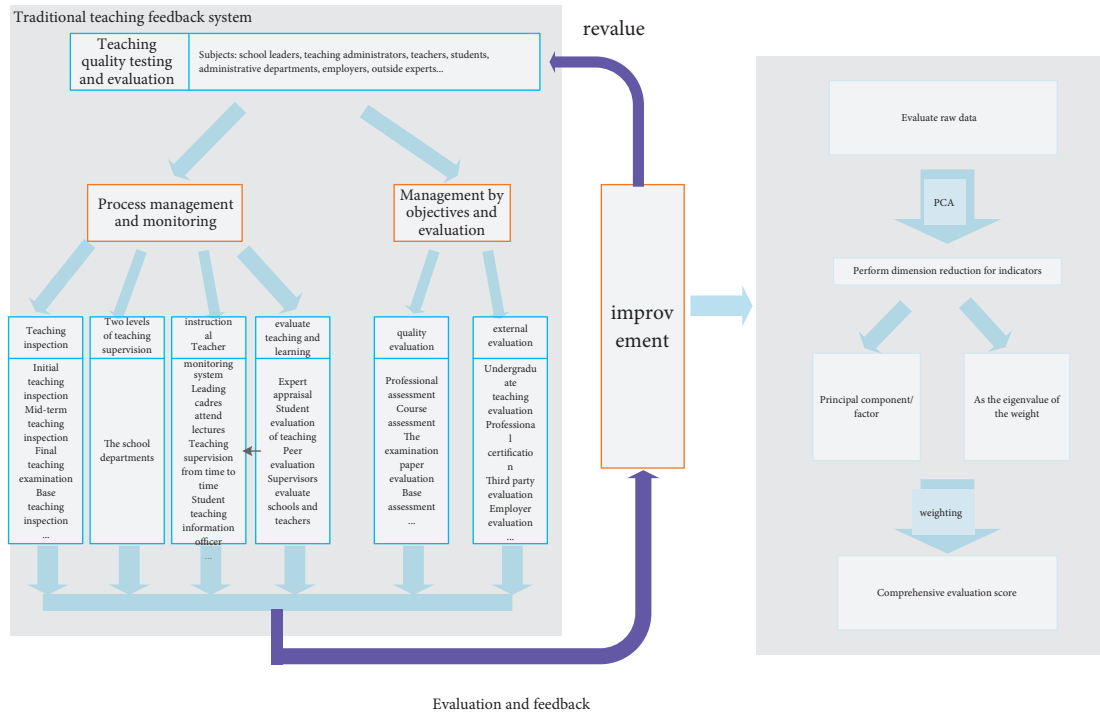


FIGURE 6: The improved classroom teaching quality evaluation system.

TABLE 1: Evaluation index system of classroom teaching quality.

General objective	Level indicators	The secondary indicators
Improve teaching quality	Teaching attitude	Rigorous teaching attitude, as a model, compliance with discipline and punctuality, care for and strict requirements of students, listening to students' suggestions and opinions modestly. A1
		Teaching enthusiasm, teaching earnest, devotion, demonstration guidance standard, tour guidance patient, and meticulous. A2
		Sufficient preparation before practice can ensure that the experimental equipment and instruments are in good condition, the equipment and components are fully prepared, the practice teaching site is clean, and there are no factors affecting the teaching in the room. A3
	Teaching content and organization	Rich knowledge, concrete and substantial practice content, reasonable personnel allocation. A4
		Be able to combine theory with practice and integrate with advanced technology and technology. A5
	Teaching method	Attach importance to classroom discipline, students experiment, and practice operation in order, without experimental accidents. A6
Standard blackboard writing, clear; the language is fluent, concise, clear, and vivid. A7		
Emphasize operation essentials, operation rules, and precautions before operation and demonstrate correct and skilled operation. A8		
Teaching efficiency	Teaching and practice time allocation is reasonable and can timely troubleshoot and answer questions accurately. A9	
	Teaching method is reasonable, enlightening, and inducing, step by step, teaching according to their aptitude can fully mobilize the initiative of students, pay attention to the training of students' operational ability, and encourage creative practice. A10	
		Students can master the contents of lectures and the operation methods and actions of practical projects
		Technical specifications and requirements can be completed independently. A11
		The students showed great interest in the course and learned a lot from the teacher
		The professional knowledge, operation skills, and many truths of life, teachers, and students harmonious relationship. A12

TABLE 2: Teacher classroom teaching quality subindex data table.

Index items	T01	T02	T03	T04	T05	T06	T07	T08	T09	T10	T11	T12	T13	T14	T15
Index1	8.85	8.45	7.1	8.15	8.95	7.75	8.18	9.2	8.4	8.2	6.98	9.25	9.05	8.1	8.65
Index2	8.82	8.4	7.05	8.2	9.05	7.85	8.15	9.2	8.3	8.25	7.1	9.2	9.1	8.08	8.65
Index3	8.6	8.3	6.96	8.03	8.6	6.9	8.85	9.5	8.25	7.2	7.06	8.5	8.07	8.3	8.6
Index4	9.1	8.5	7.45	7.71	8.6	6.75	8.5	8.7	8.8	7.5	7.77	8.5	7.95	7.7	8.05
Index5	8.6	9	7.25	7.55	8.3	6.88	7.83	7.95	8.1	7.35	7.41	9.1	7.93	8.1	8.3
Index6	9	8.7	6.85	7.95	8.1	7.25	8.83	9.5	8.25	7.1	6.71	8.1	8.5	7.7	8.7
Index7	9.05	7.65	7.16	7.61	8.8	6.65	8.5	8.3	8.2	7.5	7.29	8.3	8.66	8.1	8.43
index8	9.1	8.6	6.95	8.03	8.5	7.5	7.83	8.54	8.08	7.33	7.17	8.26	8.6	7.7	8.57
Index9	9.2	8.3	6.89	7.61	8.5	6.68	9.17	9.5	8.79	7	6.82	8.5	8.68	8.3	8.43
Index10	9.25	8.4	7	8.34	9.1	6.88	8.17	9.5	8.5	7.6	7.65	8.45	8.95	8.5	8.45
Index11	8.9	8.7	6.75	7.82	8.4	7.15	9.17	8.7	8.35	7.05	6.71	8.3	7.98	8.3	8.58
Index12	8.8	8.65	6.9	7.9	8.25	7.06	9.08	8.78	8.2	6.98	6.89	8.35	7.9	7.65	8.6

TABLE 3: Original principal component analysis.

Principal component number	Characteristic value	Contribution rate (%)	Cumulative contribution rate (%)
1	9.7663	81.3854	81.3854
2	0.8029	6.691	88.0765
3	0.4977	4.1474	92.2239
4	0.3906	3.2548	95.4787
5	0.2254	1.878	97.4787
6	0.189	1.5747	98.9314
7	0.053	0.4419	99.3733
8	0.0425	0.3538	99.7271
9	0.0228	0.1901	99.9172
10	0.0077	0.0641	99.9813
11	0.0014	0.0114	99.9926
12	0.0009	0.0074	100

TABLE 4: Averaging principal component analysis method.

Principal component number	Characteristic value	Contribution rate (%)	Cumulative contribution rate (%)
1	8.4675	79.3932	82.7765
2	0.7638	7.4178	90.1943
3	0.3795	4.2844	94.4787
4	0.3602	2.0042	96.4829
5	0.1883	1.4203	97.9032
6	0.0945	1.2859	99.1891
7	0.024	0.3698	99.5589
8	0.0278	0.2986	99.8575
9	0.0119	0.0875	99.945
10	0.0039	0.0398	99.9848
11	0.0013	0.0113	99.9961
12	0.0005	0.0039	100

TABLE 5: Principal component analysis has now been improved.

Principal component number	Characteristic value	Contribution rate (%)	Cumulative contribution rate (%)
1	7.1398	78.9847	83.1915
2	0.6894	8.1453	91.3366
3	0.5894	3.5098	94.8486
4	0.2947	2.1298	96.9762
5	0.1148	1.3639	98.3401
6	0.0381	1.0371	99.3772
7	0.0251	0.2987	99.6759
8	0.0198	0.1984	99.8743
9	0.0101	0.0839	99.9582
10	0.0029	0.0289	99.9871
1	7.1398	78.9847	83.1915
2	0.6894	8.1453	91.3366

TABLE 6: Comparison of three principal component analysis results.

	Original principal component analysis			Mean value principal component analysis			Improved principal component analysis		
	Characteristic value	Contribution rate (%)	Cumulative contribution (%)	Characteristic value	Contribution rate (%)	Cumulative contribution (%)	Characteristic value	Contribution rate (%)	Cumulative contribution (%)
1	9.7663	81.3854	81.3854	8.4675	79.3932	82.7765	7.1398	78.9847	83.1915
2	0.8029	6.691	88.0765	0.7638	7.4178	90.1943	0.6894	8.1453	91.3366
3	0.4977	4.1474	92.2239	0.3795	4.2844	94.4787	0.5894	3.5098	94.8486
4	0.3906	3.2548	95.4787	0.3602	2.0042	96.4829	0.2947	2.1298	96.9762
5	0.2254	1.878	97.4787	0.1883	1.4203	97.9032	0.1148	1.3639	98.3401
6	0.189	1.5747	98.9314	0.0945	1.2859	99.1891	0.0381	1.0371	99.3772
7	0.053	0.4419	99.3733	0.024	0.3698	99.5589	0.0251	0.2987	99.6759
8	0.0425	0.3538	99.7271	0.0278	0.2986	99.8575	0.0198	0.1984	99.8743
9	0.0228	0.1901	99.9172	0.0119	0.0875	99.945	0.0101	0.0839	99.9582
10	0.0077	0.0641	99.9813	0.0039	0.0398	99.9848	0.0029	0.0289	99.9871
11	0.0014	0.0114	99.9926	0.0013	0.0113	99.9961	0.0009	0.0108	99.9979
12	0.0009	0.0074	100	0.0005	0.0039	100	0.0002	0.0021	100

contribution rate, and cumulative value of the evaluation index. The calculated data are shown in Table 4.

For improvements based on principal component analysis method, to calculate the main factors affecting the evaluation index and the dimension of principal component analysis (PCA) in Table 2 and for standardizing, first calculate the correlation coefficient matrix, and then calculate the characteristic value of evaluation indexes, the variance contribution rate, and cumulative contribution rate, and calculate the obtained data shown in Table 5.

Three kinds of analysis of the principal components were carried out to compare the evaluation index system, and the analysis results were obtained, as shown in Table 6.

As shown in Table 5, there are three kinds in the data analysis of classroom teaching quality evaluation index. From the improved cluster analysis, we can clearly see that the average value of the improved cluster analysis method is compared with that of the principal component analysis method. Using the improved principal component analysis method, the contribution rate of the first component has been improved to a certain extent, which shows that the greater the role of the first component evaluation index, the more accurate the evaluation results. Using the improved principal component analysis method can make the cumulative contribution rate of the first component index more prominent, reduce the dimension of evaluation index, and improve the efficiency of principal component analysis method. As shown in Figure 7 and 8, the statistical charts obtained by the three principal component analysis methods show that the improved component analysis has obvious construction effect.

Variance contribution rate is an indicator to measure the relative importance of each factor. In statistics, it is generally believed that as long as the cumulative contribution rate of principal component analysis reaches over 85%, a small number of principal components can be used to replace the vast majority of information of multiple indicators. As can be seen from Table 6 above, no matter using the original principal component analysis method, averaging principal component analysis method, or the improved principal component analysis method, the accumulative contribution rate of the first two principal components of the improved principal component analysis method reaches more than 85%, and the cumulative total payment of the improved cluster analysis method's first two important components was 91.3366 percent. It clearly shows that the improved correlation-based method is representative and remarkable.

Figure 9 represents the cumulative contribution rate of the original cluster analysis method's first two principal components. The cumulative contribution rate of the first two principal components of the meaning-based cluster analysis method is represented by B, and the cumulative contribution rate of the first two principal components of the improved cluster analysis method is represented by C. It is not difficult to see that the accumulative contribution rate of the first two terms has increased significantly after the original principal component analysis is improved by means.

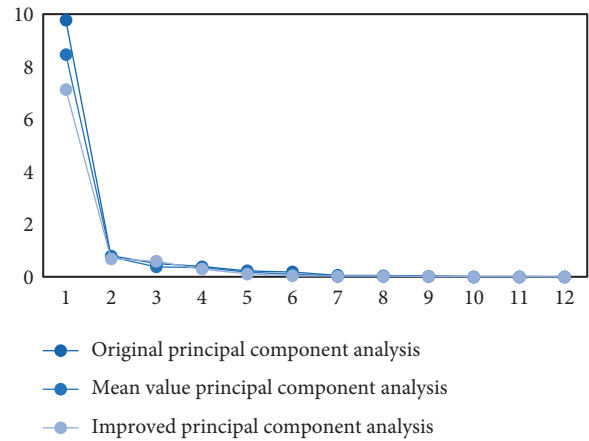


FIGURE 7: Statistical chart of three principal component analysis methods.

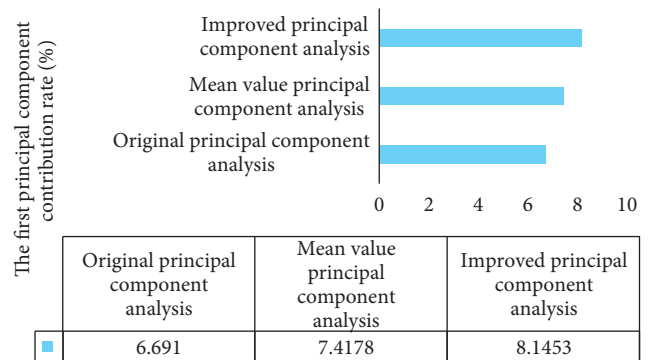


FIGURE 8: The first principal component contribution ratio comparison.

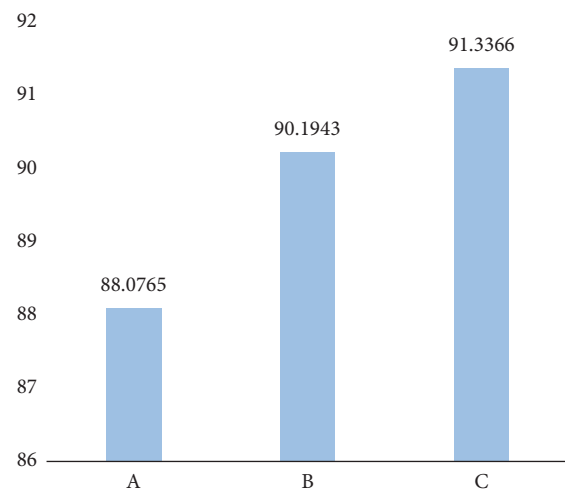


FIGURE 9: The cumulative contribution rates of the two principal components.

The load matrix calculation of each principal component is shown in Table 7 below. The first principal component is all positive load, indicating that the changes of each index of the first principal component have similar influence on the score. In the second principal component, only indicators

TABLE 7: Table of principal component load matrix.

	F1	F2	F3	F4	F5	F6	F7	F8	F9	F10	F11	F12
IndexA1	0.2828	0.4577	-0.2464	-0.005	0.1547	0.2424	-0.0522	-0.0522	0.0765	0.1134	-0.4096	-0.5644
IndexA2	0.2752	0.5062	-0.2788	-0.0587	0.144	0.1976	0.1452	0.1136	-0.1482	0.0297	0.2937	0.6197
IndexA3	0.2988	-0.2164	-0.1901	-0.215	-0.133	0.431	-0.3422	0.3384	0.3314	-0.4591	0.1209	-0.1063
IndexA4	0.2765	-0.2664	0.516	-0.2089	-0.1734	0.3189	0.6187	0.0906	-0.0549	0.0684	-0.0569	0.0948
IndexA5	0.2567	0.27	0.5547	0.5715	-0.0334	0.2213	-0.3502	-0.1307	0.1147	0.0521	0.1425	-0.0302
IndexA6	0.2949	-0.2688	-0.3456	0.1228	-0.2613	-0.0638	0.0945	-0.3126	0.4394	0.507	0.2775	-0.0302
IndexA7	0.2846	0.0627	0.2997	-0.3653	0.5387	-0.4533	-0.0732	0.1421	0.3907	0.0926	0.0942	-0.0226
IndexA8	0.2921	0.215	-0.0117	0.1648	-0.4899	-0.5646	0.2188	0.0542	0.0922	-0.461	-0.099	0.0288
IndexA9	0.3074	-0.1912	-0.0327	-0.1321	0.2399	0.0327	-0.0747	-0.7653	-0.2928	-0.3755	-0.0938	0.0979
IndexA10	0.2963	0.1086	0.0855	-0.4421	-0.3971	-0.1112	-0.4274	0.0204	-0.4621	0.3426	-0.0286	-0.1129
IndexA11	0.2974	-0.2717	-0.1369	0.3152	0.2647	-0.1416	0.1366	0.255	-0.4829	0.3426	0.4302	-0.3542
IndexA12	0.2977	-0.3148	-0.1224	0.3035	0.1507	-0.0636	-0.167	0.2694	-0.0638	0.1717	-0.646	0.3564

TABLE 8: Teacher scores and rankings.

Teacher's number	First principal component (F1)	Ranking	Second principal component (F2)	Ranking
T1	4.0297	1	-0.2026	8
T2	1.703	6	-0.2868	10
T3	-5.3995	15	-0.6224	13
T4	-1.0543	11	-0.025	7
T5	2.3628	3	0.7413	4
T6	-4.985	14	0.4939	5
T7	1.8302	5	-2.1412	15
T8	3.963	2	-0.4327	11
T9	1.0903	9	-0.6553	14
T10	-3.4549	12	1.0028	3
T11	-4.8487	13	-0.5002	12
T12	2.2021	4	1.2428	2
T13	1.6667	7	1.6505	1
T14	-0.7647	10	-0.2497	9
T15	1.6593	8	0.0393	6

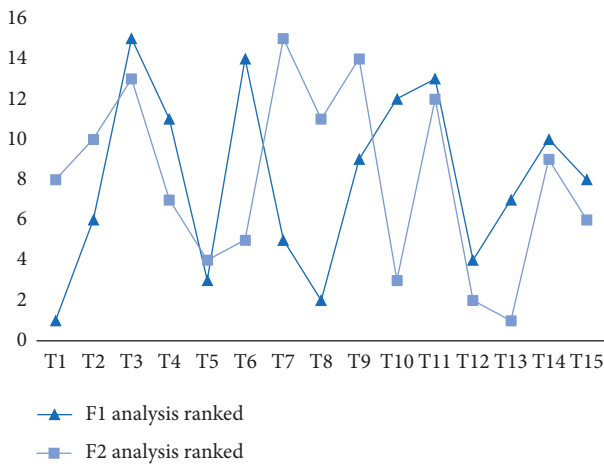


FIGURE 10: Comparison of F1 and F2 rankings.

A1 and A2 have a large contribution rate, while other indicators have a small contribution rate, indicating that other components have a small impact on the score and can be ignored. According to the formula, the principal components and score rankings are calculated as shown in Table 8.

For the above analysis, the score ranking of F1 and F2 has a great influence, so the improved principal

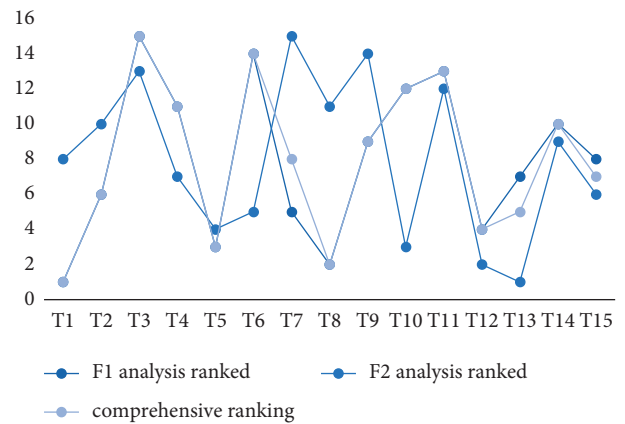


FIGURE 11: Comprehensive analysis of teacher rankings.

component analysis method is used for analysis, as shown in Figure 10.

The improved principal component analysis method was used for comprehensive analysis to calculate the score ranking, as shown in Figure 11 and Table 9 below.

Using the improved principal component analysis to evaluate the teaching quality of teachers, the evaluation results are more correct.

TABLE 9: A comprehensive analysis calculates rankings.

Comprehensive ranking	Ranking
3.266	1
1.3668	6
-4.436	15
-0.8597	11
1.9726	3
-4.0277	14
1.3462	8
3.1964	2
0.8435	9
-2.7447	12
-3.9796	13
1.8753	4
1.4669	5
-0.6391	10
1.3531	7

5. Conclusion

In the world of big data, improving school teaching quality is a long-term and difficult task that necessitates the collaboration of teachers and students. Based on big data technology, this paper analyzes the classroom teaching quality evaluation and feedback system and analyzes the teaching quality index using the principal component analysis method, discovering that there are corresponding problems in the correlation-based method. From the above experiments, it can be seen that the use of improved principal component analysis (PCA) can effectively improve the cumulative total of the first principal component contribution rate, thereby improving the accuracy of the evaluation results. The improved principal component analysis (PCA) is used to carry out factor analysis of comprehensive evaluation index on the data, so as to obtain an effective feedback system of classroom teaching quality evaluation.

Data Availability

The experimental data used to support the findings of this study are available from the corresponding author upon request.

Conflicts of Interest

The authors declare that they have no conflicts of interest regarding this work.

References

- [1] Y. Han, Ni Jiang, H. Gu et al., *Chinese journal of medical education*, vol. 34, no. 2, pp. 295–298, 2014.
- [2] A. Li and Y. Zhao, “Evaluation system of classroom teaching quality for PCA-based ideology and politics in colleges and universities,” *Bio-Technology: An Indian Journal*, vol. 10, no. 23, p. 1, 2014.
- [3] C. Xiao, “Design of a hybrid classroom teaching quality evaluation system based on information technology,” *Journal of Physics: Conference Series*, vol. 1852, no. 3, p. 1, 2021.
- [4] X. Chen, “Big data under the background of higher vocational computer education network management,” *Journal of policy analysis and application of digital technology*, vol. 42, no. 5, pp. 220–222, 2020.
- [5] Z. Jiang, “Research on data analysis literacy cultivation and implementation in Classroom Teaching based on problem solving,” *Chinese Journal of Mathematics*, vol. 60, no. 4, pp. 38–42, 201.
- [6] Li Li and Qi Wang, *Training the Concept of Data Analysis in Solving Practical Problems -- Teaching Record and Comment on “Data Collection and Collation (I)”*, Primary Mathematics Education, no. Z1, , pp. 110–112, 2017.
- [7] Q. Zheng, “Application of teaching big data analysis technology to improve classroom teaching quality,” *China University Teaching*, vol. 2, pp. 15–18+39, 2017.
- [8] S. Li and X. Wang, “Research on the application of big data analysis in teaching quality evaluation of higher vocational colleges,” *Education Information Technology*, no. 4, pp. 59–61, 2017.
- [9] Y. Sun, H. Cao, and X. Yuan, “Science and engineering course education teaching evaluation index system of building research,” *Journal of Jiangsu University*, vol. 23, no. 6, pp. 77–88, 2021.
- [10] D. Jin, “Research and analysis of big data in teaching quality evaluation system of higher vocational colleges,” *China New Communications*, vol. 23, no. 18, pp. 107–108, 201.
- [11] Y. Gong, “Analysis and research on university governance and education based on campus big data Platform,” *Software*, vol. 42, no. 12, pp. 134–136, 201.
- [12] G. Luo, Z. Chen, X. Yuan, and M. Elhoseny, “Adaptive entropy theory polymerization method for path optimization in edge computing educational systems,” *Journal of Intelligent and Fuzzy Systems*, vol. 40, no. 2, p. 1, 2021.
- [13] J. Jian, “Ideological and political education in colleges and universities based on large data analysis,” *International Journal of Educational Technology*, vol. 2, no. 1, pp. 18–22, 201.
- [14] S. H. Liu, B. Yan, and P. P. Wang, “A comparative study on domestic teaching evaluation from 2000 to 2019 -- quantitative visualization analysis based on CNKI data,” *Forest Teaching*, vol. 42, no. 9, pp. 33–35, 2020.
- [15] F. Zhuang, *Chinese and Foreign Enterprise Culture*, vol. 23, no. 6, pp. 153–154, 2020.
- [16] J. Zhang, Bo Yang, and Y. Hu, “Online teaching Evaluation model of classroom teaching quality based on Data Analysis: a case study of Yuxi Normal University,” *Software Tribune (education technology)*, vol. 19, no. 6, pp. 22–27, 2019.
- [17] R. Abdalhamid, I. Syed, and S. Ahmed, “Sparse principal component analysis using bootstrap method,” *Chemical Engineering Science*, vol. 2021246, no. 1, pp. 390–397.
- [18] R. Wang and X. Liao, “Eigenvalue and eigenvector and its application cases,” *Journal of education modernization*, vol. 5, no. 27, pp. 258–261, 2018.
- [19] L. Lei Xu and Yuille, “Robust principal component analysis by self-organizing rules based on statistical physics approach,” *IEEE Transactions on Neural Networks*, vol. 6, no. 1, pp. 131–143, 1995.
- [20] B. Schölkopf, A. Smola, and K.-R. Müller, “Nonlinear component analysis as a kernel eigenvalue problem,” *Neural Computation*, vol. 10, no. 5, pp. 1299–1319, 1998.

- [21] Q. Liu, X. Chen, X. Hou, J. Chen, and J. Wang, *Science and Technology Innovation and Application*, vol. 11, no. 32, pp. 97–100+104, 201.
- [22] A. Voronina and A. Letun Sergey, “Extra-linguistic information and its explanatory potential in teaching the Korean language,” *Society. Communication. Education*, vol. 12, no. None, p. 1, 2021.
- [23] Helen, “Mathematical modeling of the principal component analysis (pca),” *Journal of horizon of science and technology*, vol. 15, pp. 223-224, 2014.

Research Article

Research on Recommendation of Big Data for Higher Education Based on Deep Learning

Ang Zhao¹ and Yanhua Ma² 

¹Dean's Office, Nanjing University of Economics and Finance, Nanjing 210023, China

²School of Mechano-Electronic Engineering, Hebei Normal University of Science & Technology, Qinhuangdao 066600, China

Correspondence should be addressed to Yanhua Ma; mayanhua3557@hevttc.edu.cn

Received 18 January 2022; Accepted 14 March 2022; Published 19 May 2022

Academic Editor: Man Fai Leung

Copyright © 2022 Ang Zhao and Yanhua Ma. This is an open access article distributed under the Creative Commons Attribution License, which permits unrestricted use, distribution, and reproduction in any medium, provided the original work is properly cited.

To improve the recommendation accuracy of educational resources, an intelligent recommendation method based on autoencoder has been proposed by combining intelligent recommendation algorithm and autoencoder. The method uses the dimension reduction advantage of autoencoder to obtain the required feature vector. Then, the prediction score is utilized to recommend educational resources. Finally, it is verified from the algorithmic and system perspective. The results show that this recommendation method is the most efficient method. The efficiency on the dataset is 0.90, respectively. Furthermore, it can score different recommended articles, and the recommendation of different educational resources is realized.

1. Introduction

For the improvement of users' attention, most e-commerce platforms such as Taobao and JD have developed intelligent recommendation systems based on big data technology, which has attracted a large number of users for them. An intelligent recommendation system is designed to attract customer traffic. However, with the blessing of front-end technologies such as Internet of things, mobile Internet, and so on, the intelligent recommendation system shows a broader application space, thus attracting the attention of many scholars. One of the research hotspots is to introduce big data recommendation system in the field of higher education. According to students' big data in the educational scene, specific education information, education resources, and others can be pushed to specific students, which can improve the utilization rate of educational resources and students' learning efficiency. Regarding the study of recommendation algorithms, Duan created the collaborative filter recommendation algorithm, which takes both the direct impact of expert users on prediction scores and the indirect influence of trustees on prediction scores into account [1]. Thus, it shows better application performance. Ya-Zhi et al. created an adaptive learning service

recommendation algorithm based on big data, which has excellent performance in coverage, accuracy, recall rates, and others. In addition, the algorithm is especially useful for learning service recommendation practices [2]. Han et al. improved the traditional collaborative filtering algorithm and proposed a time-weighted collaborative filtering algorithm based on the clustering of mini batch K means. Compared with the traditional algorithm, the accuracy of rating prediction has been significantly improved. Also, the application space of the collaborative filtering algorithm has been further expanded [3]. In addition, Huang et al. created diversified recommendation algorithms for specific application scenarios. The autoencoder based on the deep learning algorithm can achieve feature learning, data dimension reduction, and other functions [4]. Introducing autoencoder into the recommendation system can obtain more ideal application effects. For example, Simpson et al. introduced a stacked noise reduction autoencoder in the recommendation system and supplemented by project information and user information, and thus the quality of its recommendation has been greatly improved [5]. Wu et al. also proposed the big data recommendation method for educational resources and verified the effect of recommendation methods, respectively [6–10]. Therefore, based

on the above research, a recommendation method of big data for higher education resources is proposed, and the feasibility of this method is verified. However, due to the huge number of higher education data resources, the film viewing data of middle school students on campus network are taken as the entry point to explore the recommendation of higher education big data resources.

2. Convolutional Denoising Autoencoder

Autoencoder is essentially a kind of unsupervised network, which can be divided into three different parts, namely, encoder, decoder, and hidden layer. The functions of each part are different. The encoder and decoder are mainly used to realize the conversion of data between different dimensions. The specific structure is shown in Figure 1 [11, 12].

In this network, the relationship between the hidden layer and the input layer can be expressed as follows:

$$y = S(W_1x + b_1). \quad (1)$$

It can be seen from the above formula that x and y represent the data of input and hidden layer, respectively. b_1 and W_1 represent the bias and weight of adjacent nodes, respectively. $s(x)$ represents the corresponding activation function. This formula actually corresponds to the encoding process, while the decoding is expressed as follows:

$$z = S(W_2y + b_2), \quad (2)$$

where z represents the data of output layer; $\frac{2}{b}$ and W_2 represent the bias and weight of adjacent nodes, respectively; and $s(y)$ represents the corresponding activation function.

Based on AE and adding some noise, the denoising autoencoder can be obtained. The advantage is that it can get the characteristics of high robustness. The specific structure is shown in Figure 2 [13].

In this structure, $L(\bar{x}, z)$ represents the loss function, which generally needs to be placed at a lower level to maintain a high consistency between the features obtained by the hidden layer and the original data. The basic form of the function is as follows:

$$L(\bar{x}, z) = - \sum_{n=1}^d [x_n 1gz_n + (1 - \bar{x}_n) 1g(1 - z_n)]. \quad (3)$$

The above analysis shows that the process of adding noise actually is to process the data of two neurons (1, 3). The reconstructed data \bar{x} can be obtained after setting to 0; then, the difference value between the input and output data can be calculated, so as to realize the update of offset vector and weighting matrix, which ensures that the model can be trained continuously.

3. Collaborative Filtering Recommendation of Hybrid Self-Coding Network Model

Based on the previous analysis, the basic definition of self-coding model is defined, and on this basis, the recommendation algorithm is studied and designed. The algorithm

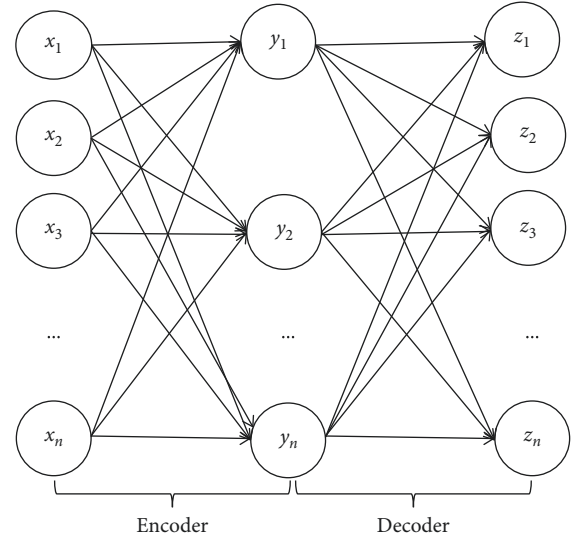


FIGURE 1: The network structure of autoencoder.

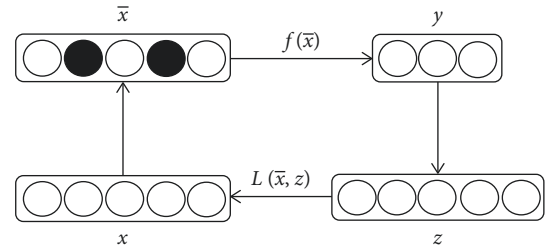


FIGURE 2: The network structure of denoising autoencoder.

is mainly divided into two steps, and the first is the process of obtaining feature vectors. In this stage, the denoising autoencoder is used to obtain the required feature vectors [14]. The second is to predict the score, which needs to make use of the feature vectors obtained in the previous step to learn the interactive network model, and then the scoring results can be obtained. The basic structure of the network is shown in Figure 3.

The score depends on the students' interest level in the article, and the overall score ranges from 1 to 5. The highest and the lowest interest scores are 5 points and 1 point, respectively, which means that with the increase of the score, the interest degree gradually increases.

The number of articles and users is n and m , respectively, and the set of the two is represented as $I = \{I_1, I_2, \dots, I_n\}$ and $U = \{U_1, U_2, \dots, U_m\}$ in turn. It can be seen that the corresponding interaction scoring matrix is $R_{m \times n}$. Assuming that there are user u and article i , the score that u gives i is expressed as $R_{u,i}$. If it is equal to zero, it does not mean that the user does not like the article but may not have read the article and therefore did not score it.

In practice, there may be multiple users scoring the same article or one user scoring multiple articles. Among them, the vector obtained after different users scoring the same article i is $(R_{1i}, R_{2i}, \dots, R_{ni}) \in R_m$. Also, the vector formed after a user scoring each article is $(R_{1i}, R_{2i}, \dots, R_{ni}) \in R_m$.

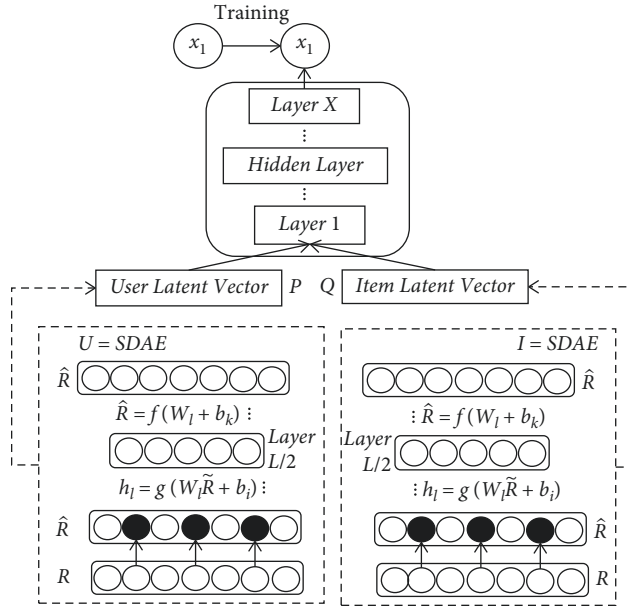


FIGURE 3: The network model diagram of hybrid autoencoder.

3.1. User-Item Latent Vector Construction. As shown in Figure 4, the left and right sides are the feature vectors of learning users and learning articles, which are represented as U -SDAE and I -SDAE, respectively. They are basically consistent in the structure [15, 16].

The latter is taken as an example for analysis in this study, and the specific contents are shown below.

In the research process, the stack autoencoder structure is adopted. There are some differences between the network and the traditional autoencoder, and the number of the hidden layers is more. The input data are mainly $R = \{r_1, r_2, \dots, r_n\}$, $r(u) = (R_{u1}, R_{u2}, \dots, R_{un})$.

First of all, the damage score matrix $\tilde{R} = (\tilde{r}_1, \tilde{r}_2, \tilde{r}_3, \dots, \tilde{r}_n)$ is obtained, that is, random noise is added to the original data. Then, the matrix is connected to the autoencoder network, where the low-dimensional feature vector Q can be obtained through coding, and then R_i can be obtained through decoding.

The basic form of each hidden layer is as follows [17]:

$$h_l = g(W_l \tilde{R} + b_l). \quad (4)$$

The output layer L is expressed as

$$\tilde{R} = f(W_l + b_R). \quad (5)$$

The target loss function is shown as follows:

$$\min \|\tilde{R} - R\|. \quad (6)$$

Among them, f and g represent the encoding and decoding functions in turn, and the encoding and decoding parts are the front and back $L/2$ layers in the network, respectively. In addition, the activation function adopted in the training is sigmoid function, and the objective function is used to reduce the reconstruction error and keep it within the appropriate range.

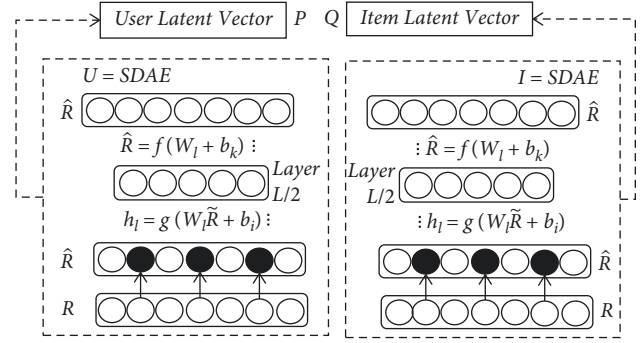


FIGURE 4: The network model diagram of constructing latent feature vector.

After training, the corresponding latent feature vectors, including article and user vectors, can be obtained. At the same time, compared with the input data, the two dimensions are significantly reduced, which is mainly related to the application of autoencoder [18, 19]. It can be seen that it avoids the occurrence of sparsity. Then, add the obtained latent feature vectors to the interaction model and continue to perform the subsequent processing.

3.2. Learning User-Item Interaction Networks. By establishing the user-item interaction network, the deep information between the item and the user can be obtained and applied to the subsequent prediction. Based on the above process, the project and user feature vector matrix can be obtained. Q and P are used as the embedding layers of the network.

The predicted result can be obtained after passing multiple hidden layers. Each hidden layer here actually belongs to a deep semantic relationship. Also, the predicted result y can be obtained in the process of reducing their dimension. Significantly, the data that are not scored should be eliminated in the training, that is, the scored data must be used.

The deviation between the target value and the predicted value should be controlled at a low level in the process of training, and the objective function should be determined according to this principle. As can be seen from the above analysis, the basic form of the interactive network is obtained as follows [20]:

$$\tilde{y}_{ui} = f(P^k, Q^k | P, Q, \theta_f). \quad (7)$$

Here, $f(\beta)$ represents the interaction function, θ_f represents the corresponding model parameters, θ_f and $P \in R_{m \times k}$ represent the potential feature vector matrices of users and items, respectively, and the basic form of loss function is shown as follows [21–23]:

$$L_{sqr} = \sum_{(u,i) \in Z} (y_{ui} + \tilde{y}_{ui})^2. \quad (8)$$

The above formula shows that Z represents the scored data, which needs to be used in the training. However, there may be missing values, which need to be processed by certain methods. Otherwise, the accuracy of prediction results will

be inevitably reduced. Some scholars have proposed different processing methods, and the commonly used method is to calculate the average score. Although missing values can be processed, there is still shortcoming, which is that different users adopt different scoring methods. So, the scored data are directly used in the training process. In the training, the algorithm is optimized based on the stochastic gradient descent method, and the prediction score is obtained. The specific form is as follows [24]:

$$\bar{R}_{ui} = f(P^u, Q^i | P, Q, \theta_f), \quad (9)$$

where Q^i and P^u correspond to the latent feature vectors of i and u , respectively, and the predicted results can be obtained after processing based on interactive network.

The implementation of the collaborative filtering recommendation algorithm based on hybrid autoencoder has been described in detail. Also, this algorithm is systematically referenced in this paper. First of all, it is necessary to preprocess the collected 201028 user scoring data. The collected data include the article data filtering out the rating behavior less than 20 times and the user data filtering out the interaction behavior less than 20 times. Thus, 186532 user scoring data are obtained, which are included in the experimental training set. The training parameters of the network are as follows: the noise rate of the stack noise reduction autoencoder is 0.2. The activation function is the sigmoid function, and the dimension of implicit feature vector is $k \in 10, 40, 80, 200, 400$. The number of network layer neurons in U-SDAE module is 128-64-32-64-128 in turn. In addition, the learning rate is 0.005, and the dropout is 0.15. The number of network layer neurons in I-SDAE module is 128-64-32-64-128 in turn. The learning rate is 0.005, and dropout is 0.15. Furthermore, the learning rate of deep interactive neural network is 0.001. The activation function is sigmoid function, and dropout is 0.10. Here, stitching project and user's hidden semantic vectors are used to construct the embedding layer of interactive neural network. The number of network layer neurons is 64-32-8 in order.

After completing the parameter setting, the prediction score of the user u for the article i can be obtained through the algorithm operation, which helps the article to be sorted. Also, the Top-N article is selected to be included in the user recommendation list.

Use the content-based recommendation algorithm to determine the Top-N recommendation list of courses and articles and use the collaborative filtering recommendation algorithm to determine the Top-N recommendation list of another article. Thus, a total of one course Top-N recommendation list and two article Top-N recommendation lists are obtained. Also, the two article Top-N recommendation lists are re-sorted in accordance with the established rules, so as to obtain the unique version of the article Top-N recommendation list. The calculation process is as follows.

The article Top-N lists determined by content-based recommendation algorithms and based on collaborative filtering recommendation algorithms are B and F , respectively,

and the final version of article Top-N list is R . The equation is as follows [25]:

$$R = B \cap F + \alpha B + \beta F. \quad (10)$$

The weight $\alpha = 0.6$ and $\beta = 0.4$ are obtained through experimental training, and the final version of the article Top-N recommendation list is determined to achieve the recommendation service.

4. Verification of Recommendation Algorithm

4.1. Verification of Algorithm Effect. The interactive behavior data between the item and the user are analyzed and applied to the designed recommendation algorithm; meanwhile, the use of the latent factor mode is helpful to solve the sparse problem. Then, it is necessary to test and analyze the application effect of the model, and appropriate datasets must be selected. In this design, taking the video data that students browse on the campus network of some colleges and universities, dataset A analyzing learning video that can be used for big data analysis is constructed, and then the big data recommendation method constructed in this study is utilized to make recommendations.

The basic information for the dataset is shown in Table 1.

The data should be uniformly divided into two parts: training set for the training process and test set for the test process. Also, the number of the two should be reasonably set. The ratio of the two is set as 9:1. Appropriate indicators are used to evaluate and analyze the application effect of the recommendation algorithm, and RMSE is a root sign based on MAE, which can better describe the error of data. Therefore, RMSE is selected in this paper.

In addition, the denoising autoencoder adopts sigmoid function, where the noise rate is 0.3, and the latent feature vector dimension is $k \in 20, 40, 80, 200, 400, 500$. The basic parameters of each module are set. Here, the number of neurons in module U -SDAE is 943-700-400-700-943, and the number of neurons in module I -SDAE is 1682-900-400-900-1682. The learning rate of the two modules is consistent with that of dropout, which are 0.004 and 0.15, respectively. For the interaction network part, dropout and learning rate are 0.15 and 0.001, respectively. Selecting the sigmoid function, the corresponding number of neurons is 800-400-32.

Comparing and analyzing the application effect of the algorithm and using the quantitative indicators to evaluate, the difference in application effect between the algorithm and other models is analyzed. For UserAverage and ItemAverage, they both use the mean scores of items and users. For SVD algorithm, it is necessary to analyze whether there are missing data first. If there is a need to be filled, the mean score is adopted in this process. The K dimension after decomposed should meet certain requirements, namely, sum of the squares of the first k singular values needs to achieve 90% of the total singular value, and then the similarity of different users should be calculated. On this basis, the final score can be obtained. For autoencoder, the number of neurons is 943-500-943, and the unobserved data, hidden layer dimension, and regular coefficient are 3, 500, and 0.001,

TABLE 1: Training dataset.

Number of users	Number of items	Number of interaction records	Sparsity
6040	3706	More than 1 million	2.57%

respectively. For PMF, stochastic gradient descent and exponential decay methods are used in the process of model training and learning rate setting, respectively, so as to realize the improvement of the model.

According to the obtained feature matrix, the score prediction results can be obtained. The efficiency information of each model is shown in Table 2.

4.2. Practical Application Verification of the Algorithm

4.2.1. System Architecture Design. The platform for learning career development is researched and designed, and the intelligent recommendation algorithm is integrated in the whole system, which is convenient to combine users' needs and preferences to recommend interested information, including book information, course information, and so on. The core part of the system is the collaborative filtering algorithm, which combines with the actual teaching requirements to design the system function modules, so as to meet the personalized needs of students in learning. Combined with the basic requirements of the whole platform to design the system architecture scheme, the specific implementation route is shown in Figure 5 [26].

As can be seen from the figure, the whole system is generally divided into three layers, namely, data layer, application layer, and recommendation layer. Each layer is connected, which realizes the overall function based on data sharing and interaction mode. The basic introduction of each part is as follows.

(1) Data Layer. The data layer is the basic part of the whole platform. It mainly realizes the storage and management of basic data and responds to data requests from other parts. After completing the operation, the relevant data information can be returned. In addition to the management of basic business data, the generated recommendation result data are also involved. The common data management mode is relational database, which needs to design the standardized data tables for management. Considering the basic requirements of system performance, in addition to using the traditional relational database, the non-relational database is used in this design, which helps to achieve higher response speed. The crawler tool can efficiently obtain the educational information from the network and then save it in the database, which can be used for the subsequent queries and processing operations.

(2) Application Layer. This layer belongs to the core part of the whole platform, which needs to realize the basic logical business and complete the implementation of each functional module based on the user's needs. Considering the needs of system expansion and upgrade, the whole is divided into two parts, namely, front-end and back-end. The former

TABLE 2: Efficiency information of each model.

Model	Dataset of students watching a video recording
UserAverage	0.76
ItemAverage	0.83
SVD	0.85
PMF	0.86
Autoencoder	0.87
Ours	0.90

is mainly related to interface display and layout. The latter mainly realizes the specific logical functions and data transmission, and based on the coordination of the two, it can present the required pages and data for the users. This part is divided into several modules, such as online communication and course reservation, and so on. It needs to call the relevant interface of WeChat server to complete the authorization operation and obtain the user's profile picture, nickname information, and other information. After the authorization is successful, other functions can be used.

(3) Recommendation Layer. This part realizes the recommendation function, and it combines the collected basic data for unified processing and analysis, including business system data and user behavior data. In addition, this module will form personalized recommendation for different users' needs and interests, so as to meet different users' requirements. In this part, the Spark framework is used to improve the processing efficiency with the help of the distributed processing platform. Meanwhile, the user interest model needs to be updated regularly, and the collected log data are utilized to improve the service quality.

4.2.2. Implementation of the Recommendation Service Based on Spark. The previous analyses show that the basic principle of recommendation service has been clarified. This part will design the basic structure and process of the whole recommendation framework, which is specifically divided into multiple processes, such as data source, data processing, and so on. The basic implementation route is shown in Figure 6 [27].

In the above framework design, considering the amount of higher education resources and the scalability of the system, the Spark framework is adopted to construct the system, and HDFS is utilized to store massive higher education resource data, so as to better lay the foundation for subsequent big data analysis.

4.2.3. System Development Environment. According to the configuration of the basic environment of system development and combined with the previous analysis, it can be seen that the system is generally divided into two parts,

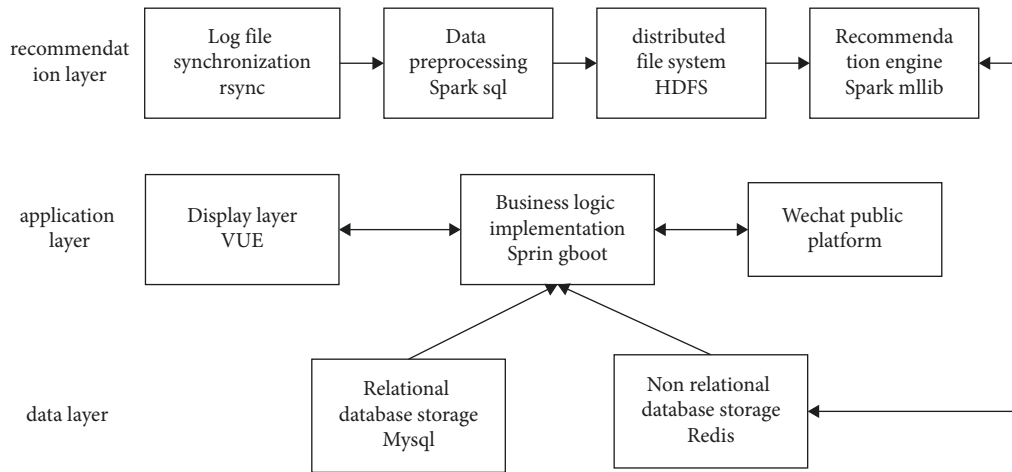


FIGURE 5: Implementation route of the system architecture scheme.

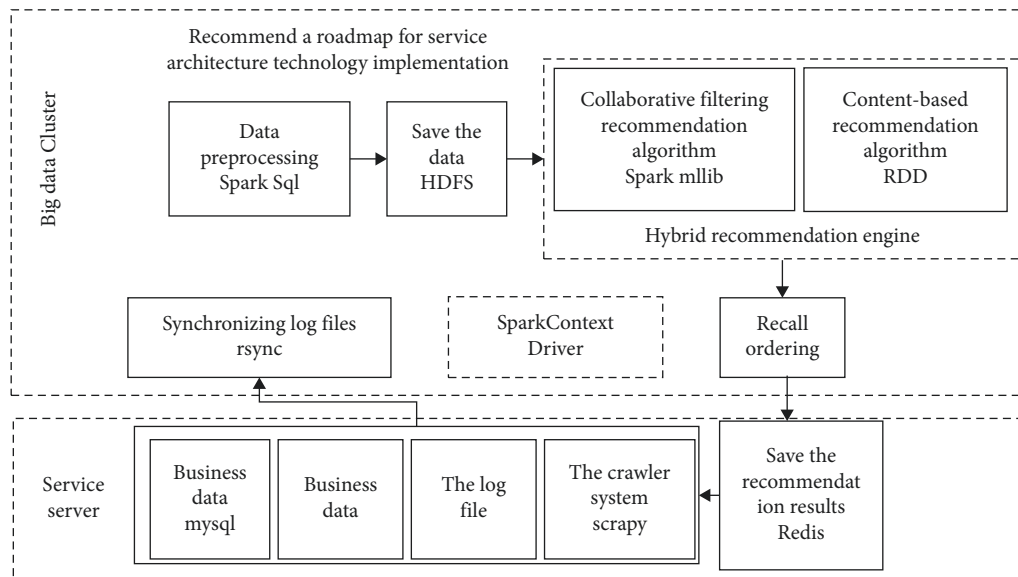


FIGURE 6: Implementation route of the recommendation service architecture scheme.

TABLE 3: Big data cluster configuration information.

The serial number	Hardware and software information	Configuration information
1	CPU	8 cores and 16 threads
2	Memory	16 G
3	The operating system	CentOS 6.8
4	Scala version	2.12.0
5	Hadoop version	2.7.3
5	Spark version	2.1.0
6	Maven version	3.3.9

among which the front-end part adopts WebStorm and Vue. The background uses MySQL, IntelliJ IDEA, and Spring Boot. In addition to the above parts, the mature distributed frameworks including Spark and others are used in big data processing.

Three servers are used to configure the Spark cluster. The specific parameters are given in Table 3.

The installation process is divided into several steps, which is shown as follows.

- (1) Download the Spark and JDK installation packages from the network.
- (2) Install and configure JDK.
- (3) Configure SSH to deploy the cluster.

TABLE 4: Big data cluster machine parameter.

Serial number	Machine name	IP address
1	Hadoop001	58.1 19.1 12.15
2	Hadoop002	58.1 19.112.16
3	Hadoop003	58.1 19.112.17

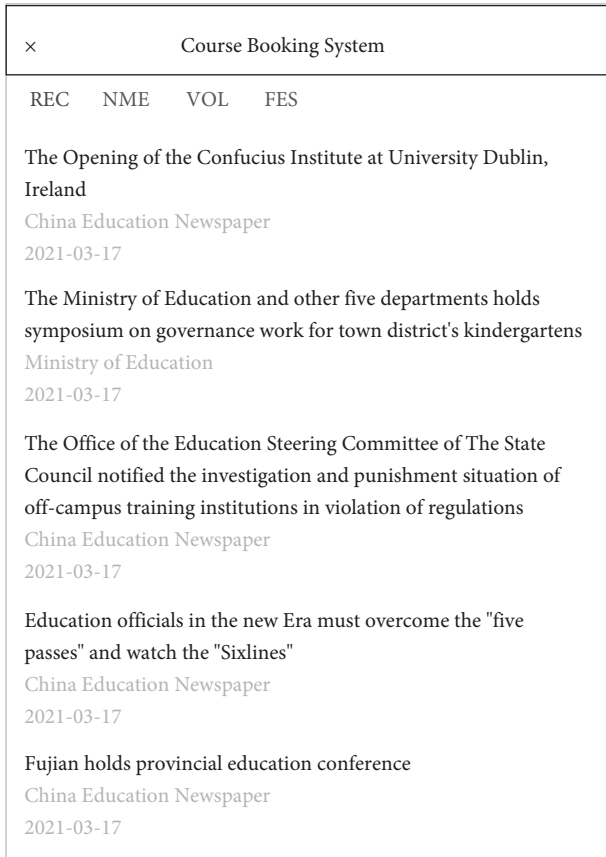


FIGURE 7: Recommendation result interface.

- (4) After the above steps, install and configure Hadoop and set the information in the configuration file.
- (5) Install and configure Spark by referring to Step (4). The basic parameters are given in Table 4.

The Jenkins scheme is adopted in this design, which can automatically and efficiently complete packaging, deployment, and other operations. Users can execute Maven operation after submitting push operation, which helps the jar packaging operation to be realized. In consideration of the possible errors in the above process, an effective notification mechanism is designed, that is, the relevant information is timely transmitted to the developer through e-mail, which ensures the accuracy and reliability of the deployment process.

4.2.4. *Recommendation Results.* The core part of the recommendation system is the collaborative filtering recommendation algorithm, which needs to calculate the item and user feature vectors first. Here, the RDD operation is mainly

utilized, and the recommendation results can be obtained after the calculation of interactive similarity. Spark MLlib is used in the algorithm implementation, but the neural network class needs to be designed by oneself. After the algorithm design is completed, inputting data can get the recommendation result, and then save the final result in Redis. The recommendation result interface is shown in Figure 7.

5. Conclusion

The recommendation system in this paper effectively overcomes the sparsity problem of the recommendation algorithm. It performs well in precision, coverage, and other aspects, which can meet the personalized recommendation needs of educational resources. The recommendation system improves the traditional feature processing method, and neural network is used to extract feature vector, which greatly improves the recommendation accuracy.

Data Availability

The experimental data used to support the findings of this study are available from the corresponding author upon request.

Conflicts of Interest

The authors declare that they have no conflicts of interest.

References

- [1] Z. Duan, W. Xu, Y. Chen, and L. Ding, "ETBRec: a novel recommendation algorithm combining the double influence of trust relationship and expert users," *Applied Intelligence*, vol. 52, pp. 1-13, 2021.
- [2] Ya-zhi Yang, Y. Zhong, and M. Woźniak, "Improvement of adaptive learning service recommendation algorithm based on big data," *Mobile Networks and Applications*, vol. 26, pp. 1-12, 2021.
- [3] X. Han, Z. Wang, and X. Hui Jun, "Time-weighted collaborative filtering algorithm based on improved mini batch K-means clustering," *Materials, Computer Engineering and Education Technology*, vol. 6258, pp. 309-317, 2021.
- [4] Z. Huang, H. Ma, S. Wang, and Y. Shen, "Accurate item recommendation algorithm of ItemRank based on tag and context information," *Computer Communications*, vol. 176, 2021.
- [5] T. Simpson, D. Nikolaos, and C. Eleni, "Machine learning approach to model order reduction of nonlinear systems via autoencoder and LSTM networks," *Journal of Engineering Mechanics*, vol. 147, no. 10, 2021.
- [6] L. Wu, Q. Liu, W. Zhou, G. Mao, J. Huang, and H. Huang, "A semantic web-based recommendation framework of educational resources in E-learning," *Technology, Knowledge and Learning*, vol. 25, pp. 1-23, 2018.
- [7] G. Sun, T. Cui, G. Beydoun et al., "Towards massive data and sparse data in adaptive micro open educational resource recommendation: a study on semantic knowledge base construction and cold start problem," *Sustainability*, vol. 9, no. 6, 898 pages, 2017.

- [8] A. Morales, J. Gonzalez, K. Alquerque, J. Reyes, and S. Sanchez, "Recommendation system with graph-oriented databases for repository of open educational resources," *IOP Conference Series: Materials Science and Engineering*, vol. 1154, no. 1, 2021.
- [9] B. Gan and C. Zhang, "Design of personalized recommendation system for online learning resources based on improved collaborative filtering algorithm," *E3S Web of Conferences*, vol. 214, Article ID 01051, 2020.
- [10] E. Peterfreund, O. Lindenbaum, F. Dietrich et al., "Local conformal autoencoder for standardized data coordinates," *Proceedings of the National Academy of Sciences*, vol. 117, no. 49, pp. 30918–30927, 2020.
- [11] L. Wang, J. Li, S. Zhang et al., "Multi-task autoencoder based classification-regression model for patient-specific VMAT QA," *Physics in Medicine and Biology*, vol. 65, no. 23, 235023 pages, 2020.
- [12] W. Pan, J. Li, and X. Li, "Portfolio learning based on deep learning," *Future Internet*, vol. 12, no. 11, 202 pages, 2020.
- [13] S. Chen and M. Wu, "Attention collaborative autoencoder for explicit recommender systems," *Electronics*, vol. 9, no. 10, 1716 pages, 2020.
- [14] H. Sewani and R. Kashef, "An autoencoder-based deep learning classifier for efficient diagnosis of autism," *Children*, vol. 7, no. 10, 182 pages, 2020.
- [15] A. B. Dincer, J. D. Janizek, and S.-I. Lee, "Adversarial deconfounding autoencoder for learning robust gene expression embeddings," *Bioinformatics*, vol. 36, no. Supplement_2, pp. i573–i582, 2020.
- [16] X. Ning, Y. Qiang, Z. Zhao, J. Zhao, and J. Lian, "Tumour growth prediction of follow-up lung cancer via conditional recurrent variational autoencoder," *IET Image Processing*, vol. 14, no. 15, pp. 3975–3981, 2020.
- [17] Z. Jiang, "SDAE-based feature selection method for biological Omics data," *Journal of Physics: Conference Series*, no. 1, p. 1848, 2021.
- [18] N. Lu, C. Chen, W. Shi, J. Zhang, and J. Ma, "Weakly supervised change detection based on edge mapping and SDAE network in high-resolution remote sensing images," *Remote Sensing*, vol. 12, no. 23, 3907 pages, 2020.
- [19] C. Li and Y. Liu, "Online dynamic security assessment of wind integrated power system using SDAE with SVM ensemble boosting learner," *International Journal of Electrical Power & Energy Systems*, vol. 125, p. 106429, 2021.
- [20] Y. Liu, L. Duan, Z. Yuan, N. Wang, and J. Zhao, "An intelligent fault diagnosis method for reciprocating compressors based on LMD and SDAE," *Sensors*, vol. 19, no. 5, 1041 pages, 2019.
- [21] Y. Ding, R. Dong, T. Lan et al., "Multi-modal brain tumor image segmentation based on SDAE," *International Journal of Imaging Systems and Technology*, vol. 28, no. 1, pp. 38–47, 2018.
- [22] H. Yu, "Apriori algorithm optimization based on Spark platform under big data," *Microprocessors and Microsystems*, vol. 80, p. 103528, 2021.
- [23] H. Mohamed, M. Tantawy Mohsen, and M. S. El Soudani Magdy, "Implementing a deep learning model for intrusion detection on Apache Spark platform," *IEEE Access*, vol. 8, Article ID 163660, 2020.
- [24] K. Wang, M. M. H. Khan, N. Nguyen, and S. Gokhale, "Design and implementation of an analytical framework for interference aware job scheduling on Apache Spark platform," *Cluster Computing*, vol. 22, no. 1, pp. 2223–2237, 2019.
- [25] M. Meoni, V. Kuznetsov, L. Menichetti, J. Rumševičius, T. Boccali, and D. Bonacorsi, "Exploiting Apache Spark platform for CMS computing analytics," *Journal of Physics: Conference Series*, vol. 1085, no. 3, 032055 pages, 2018.
- [26] Y. Yang, J. Yu, M. Yang, P. Ren, Z. Yang, and G. Wang, "Probabilistic modeling of renewable energy source based on Spark platform with large-scale sample data," *International Transactions on Electrical Energy Systems*, vol. 29, no. 3, p. n/a, 2019.
- [27] C. Fang, N. Wang, B. Yu, Y. Qin, and L. Wang, "A strategy of parallel seed-based image segmentation algorithms for handling massive image tiles over the Spark platform," *Remote Sensing*, vol. 13, no. 10, 1969 pages, 2021.

Research Article

Prediction of Sports Performance Combined with Deep Learning Model and Analysis of Influencing Factors

H. ZhaoriGetu 

Physical Education Department, Inner Mongolia University of Technology, Hohhot 010051, China

Correspondence should be addressed to H. ZhaoriGetu; zhaorigetu@imut.edu.cn

Received 21 January 2022; Revised 21 February 2022; Accepted 22 April 2022; Published 19 May 2022

Academic Editor: Hangjun Che

Copyright © 2022 H. ZhaoriGetu. This is an open access article distributed under the Creative Commons Attribution License, which permits unrestricted use, distribution, and reproduction in any medium, provided the original work is properly cited.

Physical education class helps students develop whole-body and fine motor skills and improve their strength, balance, and cardiovascular health. Sports also provide students with numerous social, psychological, and emotional benefits, which in turn improve their learning status and academic achievements. Nowadays, sports achievements are becoming more and more important, and many schools pay more and more attention to the development of sports. In order to improve sports achievements and predict sports achievements, we can combine them with relevant deep learning models to analyze sports achievements from multiple angles and factors, so as to improve sports achievements and predict sports achievements according to relevant influencing factors. Combined with the experimental part in this paper, the gradient compression algorithms under the deep learning model are compared. According to the data, the compression ratio of the AdaComp algorithm model is 1%, the training time is 5839 s, the average accuracy rate is about 90.9%, and the average loss value is 0.324. The compression ratio of the ProbComm-LPAC algorithm model is 1%, the training time is 5505 s, the average accuracy rate is about 91.8%, and the average loss value is 0.271. The compression ratio of the LAQ algorithm model is approximately 1%, the training time is 5467 s, the average accuracy rate is about 90.8%, and the average loss value is 0.554. When the number of training rounds increases from 20 to 5000, the accuracy of the three algorithm models is on the rise, but the accuracy of ProbComp-LPAC model is higher among the three models. When the number of training rounds increases, the data set loss rate of the three models is declining, indicating that the more the training times, the higher the correct rate, the smaller the loss value, and the higher the efficiency. Through four dimensions related to the influence of sports achievements-interest in seeking knowledge, ability pursuit, altruistic orientation, and reputation acquisition, this paper studies the influencing factors of sports achievements. According to the research data, most people think that the interest in seeking knowledge accounts for a large proportion of the factors affecting sports performance, with an average of 38.6709, accounting for 32% in the four dimensions. Through the study of students' gender and origin, this paper explores the analysis of the four dimensions of sports performance. It is believed that interest in knowledge is the most important factor. The average values of the four dimensions are 48.98, 52.37, 48.12, and 51.34, respectively. In order to accurately predict sports achievements, the characteristics of sports achievements prediction are sorted, among which the maximum number of action exercises is 0.24, the average score of sports action tests is 0.16, the video viewing time is 0.13, the sign-in rate is 0.09, and the minimum homework completion rate is 0.03. Predicting sports achievements through these characteristics can improve the accuracy of prediction. When the number of features in sports performance prediction gradually increases, the accuracy of sports performance prediction is also increasing. When the number of features is 8 and 9, the prediction accuracy is about 0.64.

1. Introduction

In order to better improve sports achievements, this paper studies and analyzes the prediction process and model of sports achievements and then analyzes the influencing factors of sports achievements through experiments,

combined with the gradient compression model algorithm of deep learning to improve sports achievements. Through four dimensions to analyze the influencing factors of sports performance, it can use the analysis of sports characteristics to predict sports performance and improve the prediction accuracy.

In the paper [1], the structure and function of protein are understood in detail by deep learning. This method makes a great breakthrough in protein research, and this method is greatly superior to the existing methods. Combined with the latest CASP, it can obtain the highest *F1* score of the free modeling target, so that it can better study protein. In literature [2], the deep hidden neurons in physiological features are extracted separately, so as to construct a set of deep classifiers. Experiments show that the proposed method improves the classification rate by 5.26% compared with the previous method, and its performance superiority has been proved. Literature [3] combining deep learning model with breast cancer can further improve the automatic classification of breast cancer by pathological images under computer and further distinguish breast cancer categories. It provides a better method for the classification of breast cancer in clinical environment. Literature [4] in order to solve the problem of facial attraction prediction, we will discuss it with the method of deep learning. Literature [5] uses the kinect model to provide data to identify human physical activities. Nowadays, human activity recognition is an active field. Kinect model and CAD-60 database are used to identify human activity, which reduces the time of preprocessing and data collection and improves the efficiency. At the same time, this method also has a high accuracy, which proves that this method is very effective in recognizing human activities. In literature [6], in order to extract useful features for fault detection, we combine standard fault detection with the FDC model. However, through research, it is found that this method will have some defects such as information loss and loud interference. Therefore, we build the FDC model through SdA to reduce noise interference. In literature [7], the AdaMix model is used to improve the convergence degree of deep learning to reconstruct the error. The convergence of deep learning under different learning strategies is verified by combining autoencoder with MNIST database, so as to minimize the reconstruction error. Experiments show that this method can significantly improve the convergence of deep learning model. Literature [8] proves the effectiveness of the forecast through various forecasts, such as environment, stock price and weather. At the same time, through three prompts and league samples, we can find that the method of random prediction is slightly lower than that of prompts. Through further testing, only one of the three prompts successfully utilized the relevant results and other unspecified information, which was better than a single prompt. In literature [9], we propose a whole learning algorithm to classify attributes and study their performance through the prediction model and data collection model. Through the simulation experiment on Hadoop platform, the rainfall forecast model is developed, which improves the accuracy and efficiency of rainfall forecast." Literature [10] predicts the anxiety state of domestic shooters by SMMU. We compare SMMU with SAS, SAI, and TAI scores for better results. Through the research and results comparison, we know that SMMU is better in predicting anxiety degree of domestic shooters. In literature [11], accurate prediction of business and sports performance is an essential part. Through research, we know that the

accuracy of FIFA World Cup prediction is better than that of world ranking prediction by comparing the accuracy of FIFA World Cup prediction with that of ranking prediction. Literature [12] shows that dynamic characteristics have a positive effect on our sports endurance. Lactic acid is produced for high-intensity exercise, which reduces the efficiency of exercise. Literature [13] studies chronobiology for repetitive testing of athletic performance. Most of the components of motor performance, such as physical flexibility and muscle strength, change in a sinusoidal way every day and peak in the evening. Through 24-hour continuous monitoring, it is verified whether the motion control task changes with time during the day. Literature [14] tested whether the average correlation between self-efficacy and athletic performance was 0.38 by meta-analysis. The results show that variable control, univariate, and multivariate adjustment analyses are needed to improve efficiency and performance indicators in order to carry out more accurate test. Literature [15] developed and verified the exercise anxiety scale in order to show that anxiety in the exercise performance environment is mostly a measurement. In order to make the exercise focus scale can also be reflected in children, alternative items of level 4 or below have been prepared. The anxiety table can alleviate the anxiety of children and parents.

2. Prediction and Influencing Factors of Sports Achievements under Deep Learning

2.1. Neural Network. Neural network DNN model is also called perceptron, which is composed of many parts. The general input layer is in the first layer, the middle layer is the hidden layer, and the last layer is the output layer [16]. However, with the increase of the number of network layers, the more the network parameters, the more time it takes as shown in Figure 1.

2.2. Influence of Sports Performance. The influence of learning motivation on academic performance is analyzed concretely. From the image analysis, we can see that the combination of learning motivation and learning effect when learning motivation is too low or too high will have a small impact on the learning behavior effect. Appropriate motivation will promote the increase of learning effect. Therefore, too low or too high motivation level in physical education learning will not have a great impact on sports achievements, while medium motivation level has a better effect on sports achievements [17] as shown in Figure 2.

2.3. Sports Achievement Prediction. The neural network prediction model diagram of sports performance is shown as follows. First, select the indicators that need to be predicted, input the relevant network parameters, and then input the data of sampling samples after the input, in which the sample data is a new sample [18]. After the sample input is completed, the data are preprocessed, which includes network prediction and output prediction results [19]. Carrying out network self-learning mode after pretreatment, judging

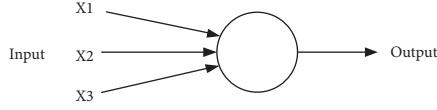


FIGURE 1: Perceptron.

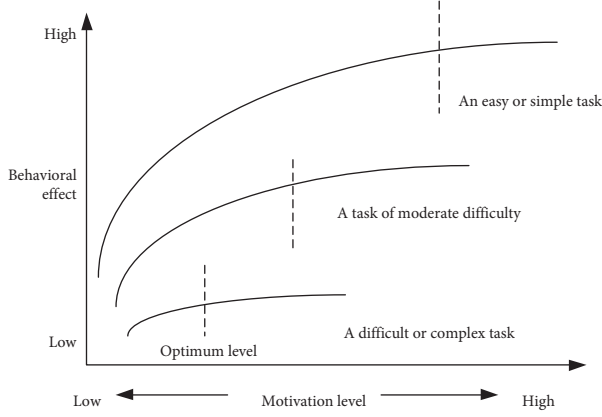


FIGURE 2: Motivation and behavior effect.

whether the learning efficiency of the network is satisfied after self-learning is completed, if not, returning to the step of inputting network parameters, and then carrying out circulation again. If the efficiency of network learning is met, save the results and exit as shown in Figure 3.

The accuracy of sports performance prediction is compared, and the data are normalized by the mean smoothing method [20]. Then, the sports test action is decomposed, and the sample data of the decomposed action are divided into two types: training set and test set. Train the training set data by W-LSTM model, judge whether the target standard rate is reached after training, updating relevant training parameters if the standard rate is not reached, and then retrain by the W-LSTM model. If the accuracy rate is reached, enter the test set type, use convergent neural network to test, then output the relevant test results, and compare the results and finally draw a conclusion. W-LSTM can usually achieve excellent results for predicting time data, and now, it has become one of the most popular algorithms to deal with this kind of problems. An efficient time series analysis method based on wavelet decomposition is presented. By separating the signals of different frequency bands from the data, the multiangle observation of the data can be realized as shown in Figure 4.

3. Correlation Formula

3.1. Deep Learning Model

3.1.1. CNN Neural Network Model. In formula (1), S is the output of $N \times N$ convolution kernel, w_{ij} is the weight in convolution kernel, b is the offset, x_{ij} is the pixel in the input image, and f is the nonlinear activation function.

Convolution layer formula:

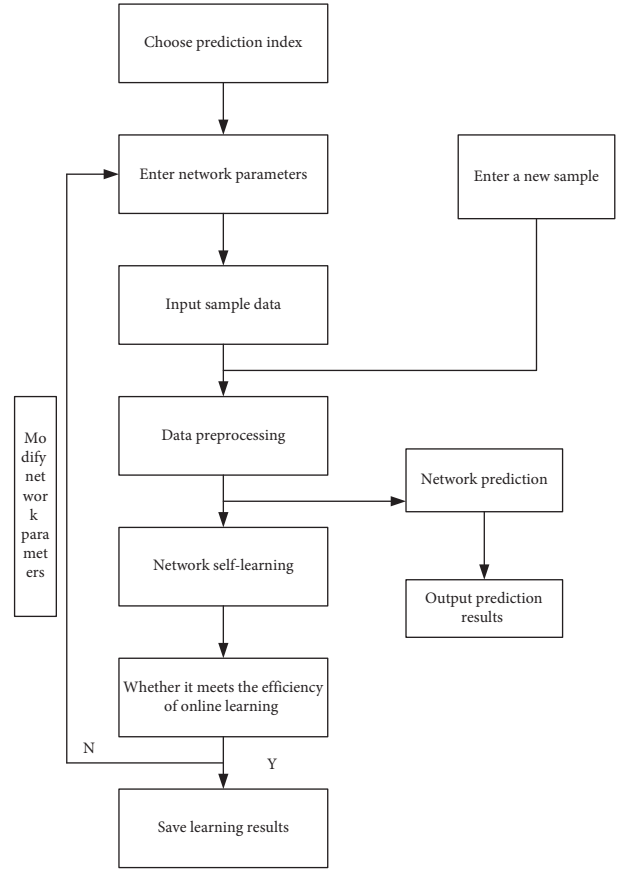


FIGURE 3: Performance prediction process.

$$S = f \left(\sum_{i,j} w_{i,j} x_{i,j} + b \right). \quad (1)$$

Activation function:

$$\text{ELU}(x) = \begin{cases} x, & x > 0 \\ \alpha(e^x - 1), & x \leq 0 \end{cases}, \quad (2)$$

$$\text{sigmoid}(x) = \frac{1}{1 + e^{-x}}, \quad (2)$$

$$\text{tanh}(x) = \frac{e^x - e^{-x}}{e^x + e^{-x}}.$$

3.1.2. RNN Cyclic Neural Network Model

$$\begin{aligned} O_i &= g(W_2 H_i), \\ H_i &= f(W_0 I_i + W_1 H_{i-1}). \end{aligned} \quad (3)$$

In order to solve the gradient disappearance and gradient explosion problems in the neural network, the formula is improved [21].

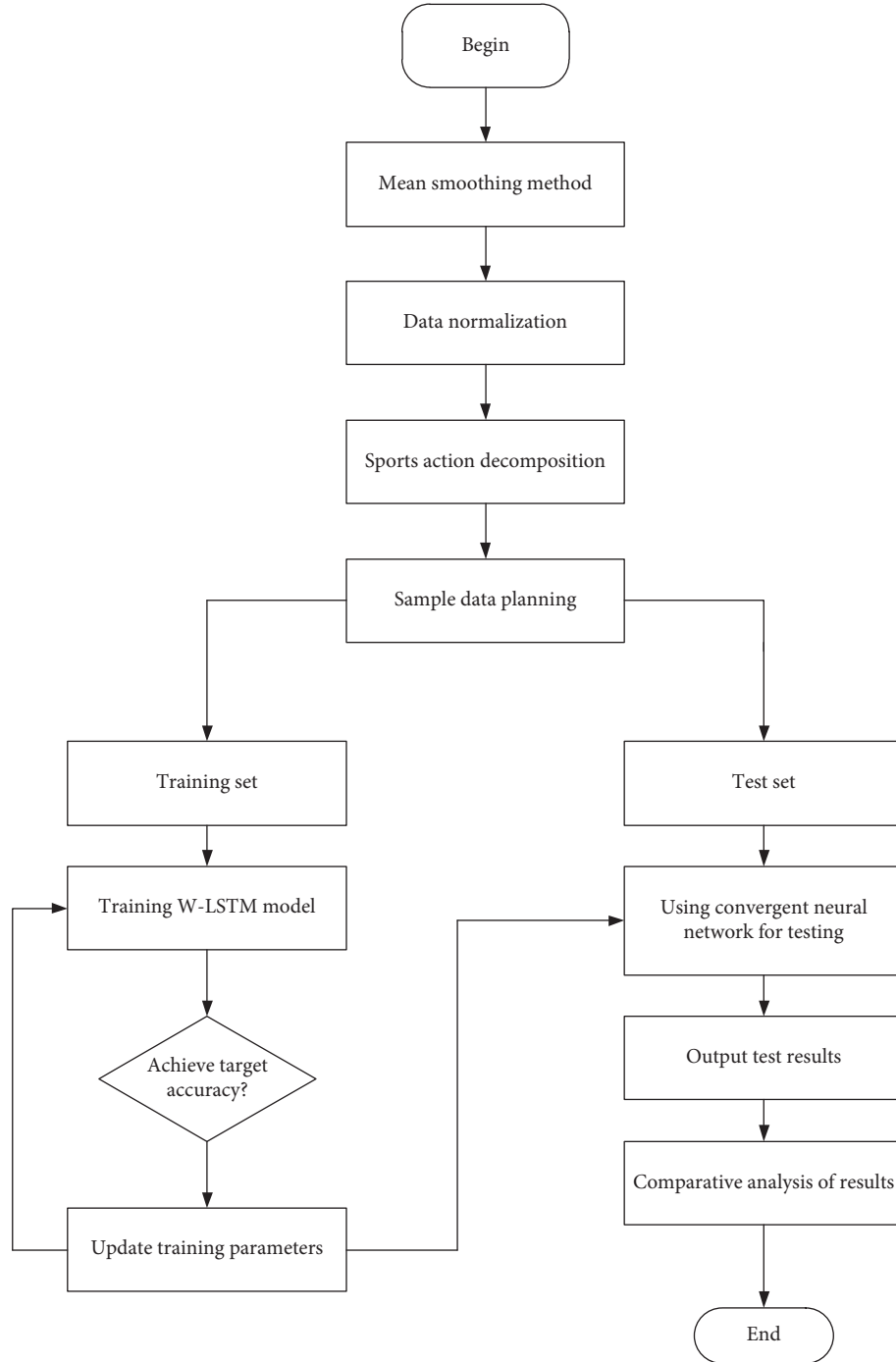


FIGURE 4: Comparison of performance predictions.

$$\begin{aligned}
 \text{input}_t &= \text{Sigmoid}(W_{ix}x_t + W_{ih}h_{t-1} + b), \\
 \text{forget}_t &= \text{Sigmoid}(W_{fx}x_t + W_{fh}h_{t-1} + b_f), \\
 c_t &= \text{forget}_t * c_{t-1} + \text{input}_t \\
 &\quad * \tanh(W_{cx}x_t + W_{ch}h_{t-1} + b_c), \\
 \text{output}_t &= \text{Sigmoid}(W_{ox}x_t + W_{oh}h_{t-1} + b_o), \\
 h_t &= \text{output}_t * \tanh(c_t).
 \end{aligned} \tag{4}$$

3.1.3. GRU Cyclic Neural Network Model

$$\begin{aligned}
 r_t &= \text{Sigmoid}(W_r x_t + U_r h_{t-1}), \\
 z_t &= \text{Sigmoid}(W_z x_t + U_z h_{t-1}), \\
 h'_t &= \tanh(W_h x_t + r_t U_h h_{t-1}), \\
 h_t &= \tanh(W_h x_t + r_t U_h h_{t-1}).
 \end{aligned} \tag{5}$$

3.2. Sports Achievement Prediction

3.2.1. *Time Series Model Method.* Proportional change practice:

$$C_{t+1}^{\wedge} = C_t \left(1 + \frac{C_t - C_{t-1}}{C_{t-1}} \right). \quad (6)$$

Moving average model:

$$C_{t+1}^{\wedge} = \frac{C_t + C_{t-1} + \dots + C_{t-n+1}}{N} \quad t \geq N. \quad (7)$$

Weighted moving average model:

$$C_{t+1}^{\wedge} = \frac{a_0 C_t + a_1 C_{t-1} + \dots + a_{N-1} C_{t-n+1}}{N} \quad t \geq N, \quad (8)$$

where a_0 , a_1 , and a_{N-1} are weighting factors [22].

Exponential smoothing model:

$$C_{t+1}^{\wedge} = a C_t + (1 - a) C_t^{\wedge}. \quad (9)$$

3.2.2. *Evaluation of Prediction Methods of Sports Achievements.* Evaluation criteria:

$$MAPE = \frac{\sum_{i=1}^N |(x_i - y_i)| / y_i}{n} \times 100\%, \quad (10)$$

$$R = \frac{\sum_{i=1}^n (x_i \times y_i)}{\sum_{i=1}^n (x_i)^2 \times \sum_{i=1}^n (y_i)^2}$$

where x_i represents the model analog input value and y_i is the actual value [23].

3.2.3. *Metaregression Model.* The logarithm of the effect quantity index of each study is established as the dependent variable to carry out regression analysis on sports activities [24].

$$Y_i = \beta_0 + \sum_{k=1}^n \beta_k X_{ki} + \varepsilon_i. \quad (11)$$

3.2.4. *Improved BP Neural Network Algorithm Based on MATLAB*

$$\Delta X(k+1) = mc \times \Delta X(k) + lr \times \frac{\partial E}{\partial X} \quad 0 < lr < 1. \quad \partial. \quad (12)$$

K is the training times, mc is the momentum factor, lr learning rate, and e is the error function [5].

$$\Delta X = lr \times \frac{\partial E}{\partial X}, \quad (13)$$

$$\Delta X(k+1) = mc \times \Delta X(k) + lr \times mc \times \frac{\partial E}{\partial X}.$$

After formula optimization,

$$lr(k+1) = \begin{cases} 1.05lr(k)mse(k+1) < mse(k), \\ 0.7lr(k)mse(k+1) > 1.04mse(k), \\ lr(k), & \text{others.} \end{cases} \quad (14)$$

4. Prediction and Analysis of Sports Achievements under Deep Learning

4.1. Analysis of Deep Learning Model

4.1.1. *Comparison of Performance Prediction of Frequency Division Multiple Access Deep Learning Model.* Compared with the traditional model, the FDPN model has higher accuracy, precision, recall, $F1$, AUC, and other performance. Compared with other algorithms, the ProbComm-LPAC gradient compression algorithm has higher average accuracy, lower average loss, and higher efficiency. Through the analysis of the factors affecting sports achievements, we can have a deep understanding of the composition of sports achievements, so as to improve sports achievements. The accuracy, precision, recall, $F1$, AUC, and other performances of FDPN model are compared under different neuron numbers. Through the observation of relevant experimental data, it is known that when the number of neurons is 256, its performance is the best, and the accuracy is 0.8668 (accuracy: 0.8680; recall rate: 0.9499; $F1$: 0.9071; AUC: 0.8179). When the number of neurons in the hidden layer is 32, 64, 128, 256, 512, and 102, the FDPN prediction model analyzes its accuracy, precision, recall, $F1$, and AUC data. It is found that when the number of neurons in the hidden layer is 256, the research values reach the highest, and its FDPN prediction performance is the best.

According to Table 1 and Figure 5, each performance data reaches the peak when the number of neurons is 256, which shows that the FDPN model has the best prediction performance when the number of neurons is 256. FDPN model includes three parts: FM, DNN, and PNN, which is a model for predicting grades. The prediction effect of the model is related to the activation function setting of hidden layer neurons. When the activation function is ReLU, the prediction accuracy, recall rate, $F1$, and AUC of FDPN model are improved by about 2%, and the prediction effect is better.

4.1.2. *Comparison of Gradient Compression Algorithms for Deep Learning Models.* In order to solve the problem of gradient disappearance in deep learning function, we compare gradient compression algorithms through AdaComp, ProbComm-LPAC, and LAQ models. The compression ratio of the three models is approximately 1%, and the longest training time of AdaComp model is 5839s, the shortest training time of ProbComm-LPAC model is 5505s, and the shortest training time of LAQ model is 5467s. The average accuracy of the AdaComp model and ProbComm-LPAC model is similar, which is 90.9% and 90.8%, respectively, and the average accuracy of ProbComm-LAPC model is 91.8%. In terms of average loss value, the lowest average loss value of ProbComm-LPAC model is 0.271, and the average loss value of AdaComp model is 0.324, while the highest average loss value of LAQ model is 0.554. Therefore, from the comprehensive analysis of compression ratio, training time, average accuracy, and average loss value, it is concluded that the average accuracy rate of ProbCom-LPAC

TABLE 1: Performance comparison of FDPN models.

Hidden layer neuron number	Accuracy	Precision	Recall rate	F1	AUC
32	0.8532	0.8593	0.9395	0.8976	0.8025
64	0.8590	0.8621	0.9453	0.9018	0.8082
128	0.8619	0.8634	0.9483	0.9039	0.8111
256	0.8668	0.8680	0.9499	0.9071	0.8179
512	0.8607	0.8656	0.9431	0.9027	0.8124
1024	0.8578	0.8647	0.9395	0.9005	0.8099

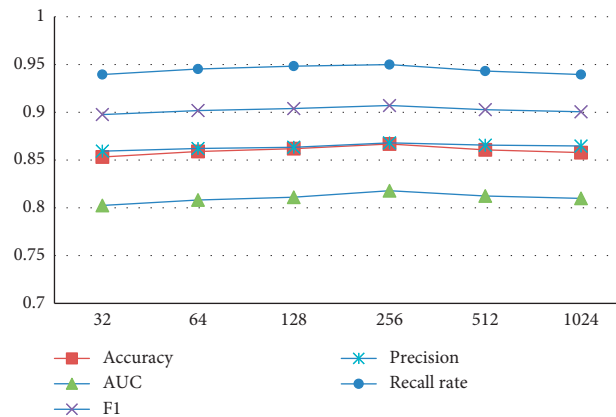


FIGURE 5: Performance comparison of the FDPN model.

model is higher and the average loss value is lower, which shows that the ProbComm-LPAC model has more advantages in comparison, and the gradient compression algorithm for deep learning model is more efficient, so it should be preferred when selecting the deep learning model.

According to the Table 2, when the number of training rounds is 1000, 2000, 3000, 4000, and 5000, when the number of training rounds is less than 1000, the accuracy of data sets of the three deep learning models is approximately 0. When the number of training rounds is 1000, the accuracy of ProbComm-LPAC model is higher than 0.87, followed by AdaComp model with 0.72 and LAQ model with 0.72. When the number of training rounds is 2000, the accuracy of the data set is 0.89, 0.80, and 0.75 in turn, and the corresponding models are ProbComp-LPAC, AdaComp, and LAQ models; when the number of training rounds is 3000, 4000, and 5000, the accuracy of ProbCom-LPAC model is 0.9, 0.91, and 0.95 respectively. The accuracy of the LAQ model was 0.77, 0.8, and 0.83 when the number of training rounds was 3000, 4000, and 5000. However, from the overall data of the accuracy of the three models, with the increase of the number of experimental rounds, the accuracy of the data sets of the three models is on the rise, which shows that the more the experiments, the high the accuracy.

From the Figures 6 and 7, when the number of training rounds is close to 0, the data set loss values of the three models are all high, the data set loss values of LAQ model are 4.2, AdaComp model are about 4, and ProbComp-LPAC model are 3.7, which are relatively low. When the number of training rounds is 1000, 2000, 3000, 4000, and 5000, the loss value of ProbComp model is 0.5, 0.44, 0.4, 0.37, and 0.27, respectively. Through the observation of the whole data, with

the increase of the number of training rounds, the loss values of the three models all decreased, but the ProbComp-LPAC model decreased the most.

4.2. Analysis of Sports Achievements

4.2.1. Analysis on the Proportion of Sports Achievements.

The boys' sports test items are 1000-meter running, standing long jump, 50-meter running, pull-ups, and throwing solid balls. Girls' sports test items are 800-meter running, standing long jump, 50-meter running, sit-ups, and throwing solid balls. According to the proportion of total scores of each project, the total scores of students' related sports are calculated. According to the data, 1000/800-meter running accounts for 30% of the total sports achievements, standing long jump and solid ball account for 15% of the total sports achievements, and 50-meter running and sit-ups/pull-ups account for 20% of the total sports achievements. According to the proportion analysis, we know that, to make sports achievements, we should mainly improve the achievements of 1000/800 meters running because the achievements of 1000/800 meters account for a large proportion in the total sports achievements as shown in Tables 3 and 4.

From Figure 8, it can be seen that the scores of 1000/800 meters running are relatively large in sports test items, followed by solid ball and sit-ups/pull-ups, and finally standing long jump and solid ball items.

4.2.2. Analysis on the Influence Factors of Sports Achievements.

In order to analyze the influencing factors of sports achievements, the influencing factors are analyzed

TABLE 2: Gradient compression algorithm.

Gradient compression algorithm	Compression ratio	Training time (s)	Average accuracy (%)	Average loss value
AdaComp	1%	5839	90.9	0.324
ProbComm-LPAC	1%	5505	91.8	0.271
LAQ	Approximately 1%	5467	90.8	0.554

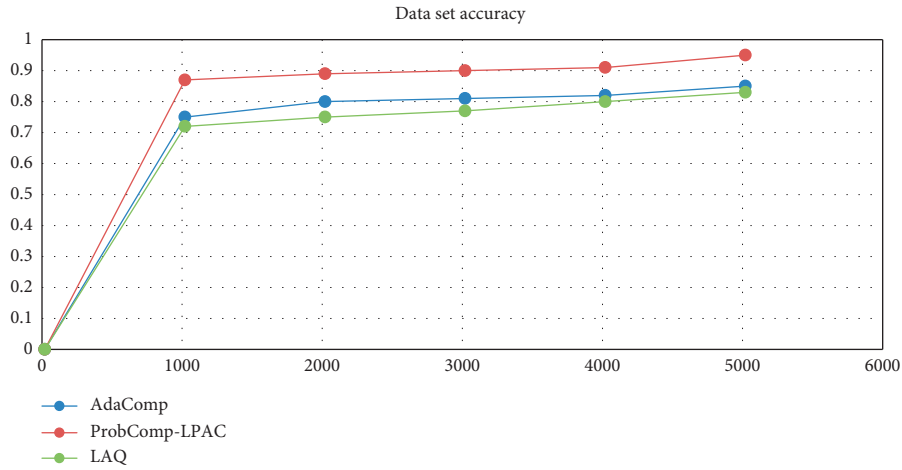


FIGURE 6: Accuracy of the four-dimensional data set.

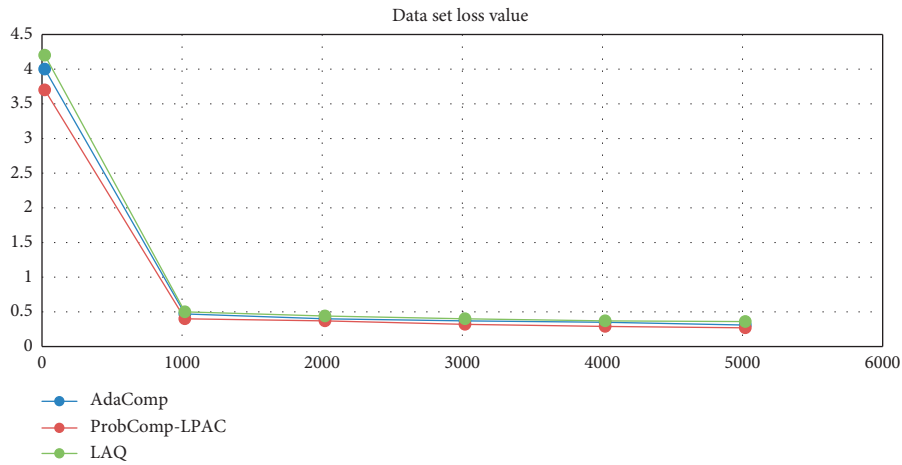


FIGURE 7: Loss value of the four-dimensional data set.

TABLE 3: Distribution of sports achievements (male).

Item score	1000 meters running (minutes and seconds)	Standing long jump (CM)	Run 50 meters (seconds)	Pull-up (times)	Throw solid ball forward (m)
100	3'40"	250	7.3	15	9.6
90	3'50"	240	7.5	13	9
80	4'05"	225	7.7	11	8.4
70	4'30"	205	8.7	9	6.9
60	4'55"	185	9.7	6	5.4
50	5'15"	180	9.9	5	5.1

from four dimensions: interest in seeking knowledge, ability pursuit, altruistic orientation, and reputation acquisition. As can be seen from Table 5, in the following four dimensions,

the average value of choosing interest in seeking knowledge is 38.6709, and its standard deviation is 9.0268. The average value of selection ability pursuit is 30.6582, and the standard

TABLE 4: Distribution of sports achievements (female).

Item score	800 meters running (minutes and seconds)	Standing long jump (CM)	Run 50 meters (seconds)	Sit-ups	Throw solid ball forward (m)
100	3'10"	1.97	8.1	50	6.70
90	3'20"	1.89	8.3	46	6.30
80	3'30"	1.81	8.5	42	5.90
70	3'40"	1.73	8.7	38	5.50
60	3'50"	1.65	8.9	34	5.10
50	4'00"	1.57	9.1	30	4.70

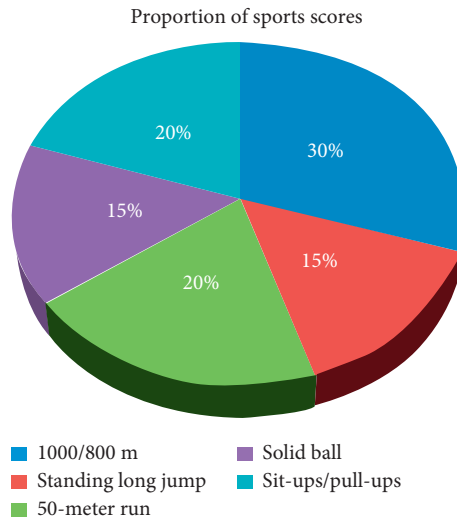


FIGURE 8: Proportion of sports scores.

TABLE 5: Influencing factors of four dimensions of sports achievements.

Dimension name	Number of items	Mean value	Standard deviation
Summary of influencing factors	34	123.9367	9.0268
Interest in seeking knowledge	12	38.6709	5.1058
Ability pursuit	9	30.6582	3.3673
Altruistic orientation	8	30.0759	3.1813
Reputation acquisition	7	21.2152	4.4712

deviation is 3.3673. The mean value of altruistic orientation is 30.0759, and the standard deviation is 3.1813. The average value of reputation acquisition is 21.2152, and the standard deviation is 4.4712. According to the data, the most important factor affecting sports performance is interest in knowledge, and the influence of reputation acquisition on sports performance is less. This shows that most students affect their sports achievements because of their love for sports. Among them, the number of people who think that ability pursuit and altruistic orientation are also more, and their average value is about 30.

It can be seen from Figure 9 that the interest in seeking knowledge accounts for a large proportion of sports achievements, and the reputation acquisition accounts for the smallest proportion, with 18%. The research shows that interest is an important factor to achieve higher grades in a subject.

From Table 6, we can see that, through different genders, we can explore the specific situation of the influence of these four dimensions on sports achievements. Through the

random investigation of 75 male masses and 26 female masses, it can be seen that the female masses choose to think that the interest in seeking knowledge has a great influence on sports achievements, with an average value of 52.37 and a standard deviation of 3.670. Female people think that reputation acquisition has a relatively small impact on sports performance, with an average of 32.66 and a standard deviation of 4.778. Male people think that the interest in seeking knowledge has the greatest impact on sports performance, accounting for 48.98, and the standard deviation is 5.235. Male people think that reputation acquisition has little influence on sports performance, with an average of 32.54 and a standard deviation of 4.454. It can be seen that male and female people think that interest in seeking knowledge is the relative main factor affecting sports achievements. *T* value is the value obtained by testing independent samples, and *P* value represents significant difference. When *P* is less than or equal to 0.05, there is significant difference.

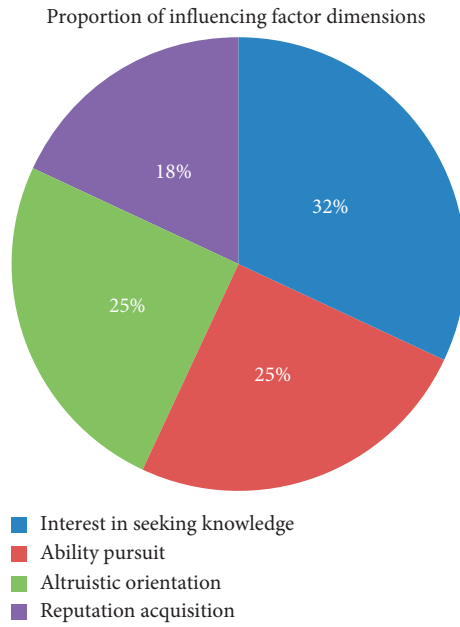


FIGURE 9: Proportion of four-dimensional influencing factors.

TABLE 6: Analysis of influencing factors by different genders.

Dimension name	Gender	Sample size	Mean value	Standard deviation	T value	P value
Total factor score	Male	75	123.67	9.186	-2.825	0.026
	Female	26	129.70	7.954		
Interest in seeking knowledge	Male	75	48.98	5.235	-2.963	0.006
	Female	26	52.37	3.670		
Ability pursuit	Male	75	41.56	3.358	-1.263	0.231
	Female	26	42.76	2.976		
Altruistic orientation	Male	75	40.99	3.103	-0.872	0.235
	Female	26	41.57	3.879		
Reputation acquisition	Male	75	32.54	4.454	-0.067	0.996
	Female	26	32.66	4.778		

It can be clearly seen from the curve trend in the Figure 10 that the highest proportion of factors affecting sports achievements is interest in seeking knowledge, followed by ability pursuit and altruistic orientation, and finally reputation acquisition.

By dividing the types of students into rural areas and cities, this paper analyzes these four influencing factors. From the data in Table 7, it can be seen that students from rural areas think that the dimension of interest in seeking knowledge has the greatest impact on sports achievements, with an average value of 51.34 and a standard deviation of 1.141; the influence of reputation acquisition on sports achievement is 31.21, and its standard deviation is 4.447. Students from cities think that interest in knowledge is the biggest influence factor on sports achievement, with an average of 48.12, and its standard deviation is 5.532.

It can be seen from the Figure 11 that the average value of choosing interest in seeking knowledge as a major factor affecting sports achievements is larger, while the proportion of those who think that reputation acquisition has a greater impact on sports achievements is relatively small.

It can be seen from the data in Table 8 that there is a big gap between boys and girls in theoretical subjects and special subjects. The average score of women in theoretical subjects is 87.264, while that of boys is 81.936. Girls' scores in theoretical subjects are higher than those of boys, which shows that girls have better scores in a series of subjects that need to calm down, such as thinking and recitation, while boys are more active and easily influenced by external factors, so their scores are lower than those of women as can be seen from Table 8.

Combined with the analysis of tables and Figure 12, it can be seen that boys are more susceptible to external factors than girls, so girls' scores in theoretical subjects are relatively higher.

4.3. Prediction and Analysis of Sports Achievements. As can be seen from Figure 13, the prediction of sports achievements is analyzed from several aspects, such as homework completion rate, classroom interaction amount, sign-in rate, video viewing time, average score of sports action test, and

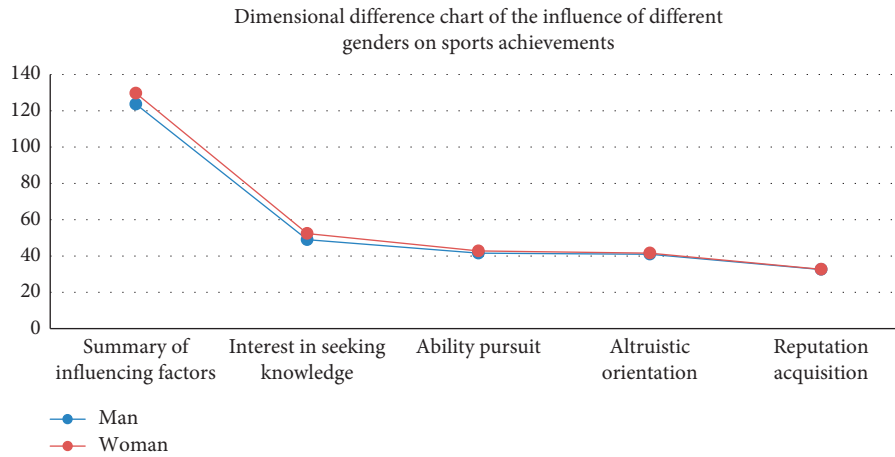


FIGURE 10: Influence of different genders on sports performance.

TABLE 7: Analysis of influencing factors of different places of origin.

Dimension name	Type of students	Sample size	Mean value	Standard deviation	T value	P value
Total factor score	City	52	134.15	10.876	-7.95	0.425
	Rural	49	135.79	6.0571		
Interest in seeking knowledge	City	52	48.12	5.532	-2.914	0.004
	Rural	49	51.34	1.141		
Ability pursuit	City	52	41.61	3.767	-1.313	0.986
	Rural	49	41.76	3.012		
Altruistic orientation	City	52	41.13	3.115	0.132	0.875
	Rural	49	41.03	3.487		
Reputation acquisition	City	52	33.15	4.403	1.944	0.056
	Rural	49	31.21	4.447		

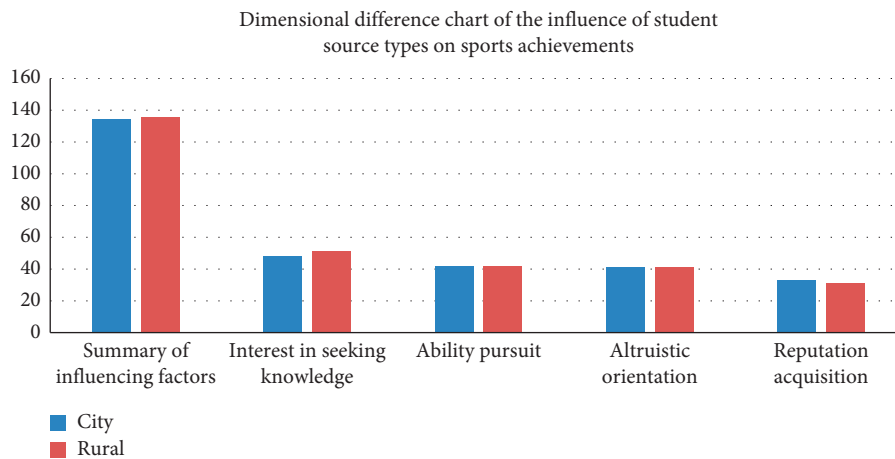


FIGURE 11: Influence of different places of origin on sports achievements.

number of action contact times. Among them, the number of movement exercises ranks first, which shows that the number of movement exercises is of great importance to the prediction of sports achievements.

With the number of features gradually increasing from 1 to 9, the accuracy of sports performance

prediction is slightly improved. When the number of features is 9, the highest accuracy of sports performance prediction is 0.635. From the experimental data, it can be seen that the correct rate of sports performance prediction is related to the number of reference features as shown in Figure 14.

TABLE 8: Analysis of gender achievements.

Name of academic achievement	Gender	Sample size	Mean value	Standard deviation	T value	P value
Achievements in theoretical subjects	Male	75	81.936	6.065	-3.287	0.002
	Female	26	87.264	2.979		
Scores of special subjects	Male	75	89.908	6.065	-1.105	0.323
	Female	26	90.926	2.711		

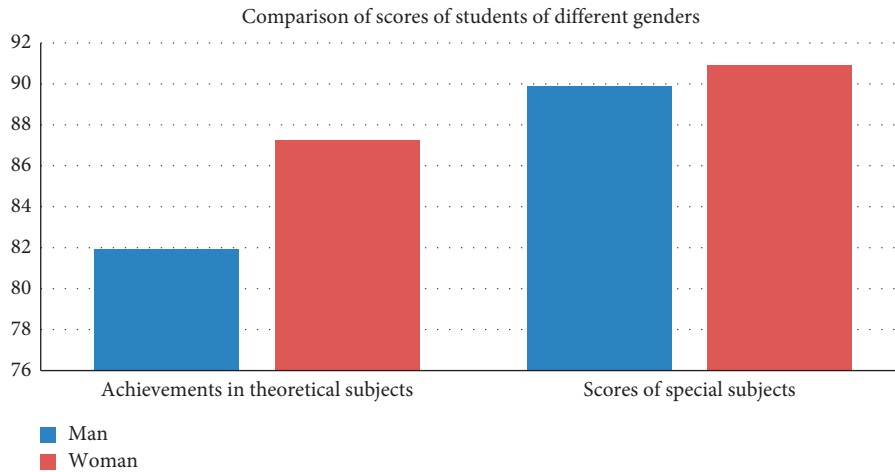


FIGURE 12: Comparison of gender achievements.

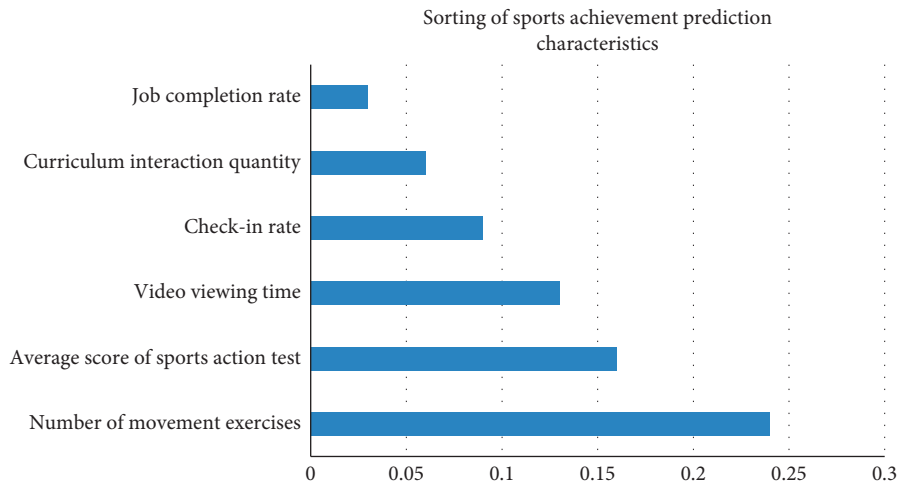


FIGURE 13: Ranking of sports performance prediction characteristics.

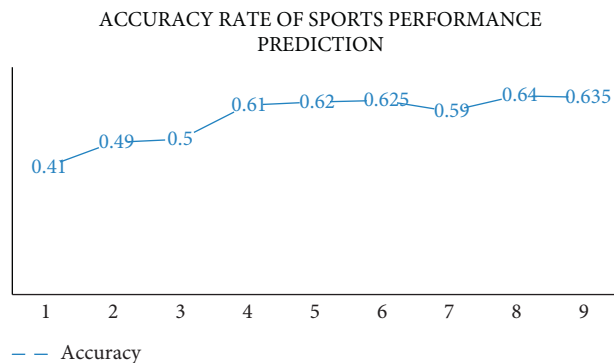


FIGURE 14: Accuracy rate of sports performance prediction.

5. Conclusion

In order to solve the gradient disappearance problem of the deep learning DNN model, we compare gradient compression algorithms through three models. Through experimental data, it can be seen that ProbComm-LPAC model has higher average accuracy, lower average loss rate, and the best performance. And, through the number of hidden layer neurons to FDPN model accuracy, precision, recall, $F1$, AUC experimental analysis, according to the experimental data, when the number of hidden layer neurons is 256, FDPN model prediction performance is the best. According to the sports test items and the proportion of project scores, this paper analyzes the students' sports scores, and the analysis results show that the proportion of 1000/800 meters in sports test is larger than other items. Through four dimensions to analyze the influencing factors of sports performance and improve the correct rate of sports performance prediction according to sports characteristics, we analyze the influencing factors of sports performance and predict sports scores to better improve sports performance. In order to improve the accuracy of sports performance prediction, we should analyze the performance of relevant prediction models and experiment from various factors, so as to achieve the highest performance value. At the same time, we should also strengthen physical exercise in peacetime and enhance our interest in sports, so as to improve sports performance.

Data Availability

The experimental data used to support the findings of this study are available from the corresponding author upon request.

Conflicts of Interest

The author declares no conflicts of interest regarding this work.

References

- [1] W. Sheng, S. Sun, and L. Zhen, "Accurate de novo prediction of protein contact map by ultra-deep learning model," *PLoS Computational Biology*, vol. 13, no. 1, Article ID e1005324, 2017.
- [2] Z. Yin, M. Zhao, Y. Wang, J. Yang, and J. Zhang, "Recognition of emotions using multimodal physiological signals and an ensemble deep learning model," *Computer Methods and Programs in Biomedicine*, vol. 140, pp. 93–110, 2017.
- [3] Z. Han, B. Wei, Y. Zheng, Y. Yin, K. Li, and S. Li, "Breast cancer multi-classification from histopathological images with structured deep learning model," *Scientific Reports*, vol. 7, no. 1, p. 4172, 2017.
- [4] J. Xu, L. Jin, and L. Liang, "A new humanlike facial attractiveness predictor with cascaded fine-tuning deep learning model," *Computer Science*, vol. 70, no. 1, pp. 45–79, 2015.
- [5] M. J. Barnes, "Alcohol: impact on sports performance and recovery in male athletes," *Sports Medicine*, vol. 44, no. 7, pp. 909–919, 2014.
- [6] H. Lee, Y. Kim, and C. O. Kim, "A deep learning model for robust wafer fault monitoring with sensor measurement noise," *IEEE Transactions on Semiconductor Manufacturing*, vol. 301 page, 2016.
- [7] Y. Y. He and B. Q. Li, "A combinatory form learning rate scheduling for deep learning model," *Acta Automatica Sinica*, vol. 7, pp. 23–42, 2016.
- [8] D. Forrest and R. Simmons, "Forecasting sport: the behaviour and performance of football tipsters," *International Journal of Forecasting*, vol. 16, no. 8, pp. 24–37, 2000.
- [9] W. Zhu, W. Ma, Y. Su et al., "Low-dose real-time X-ray imaging with nontoxic double perovskite scintillators," *Light: Science & Applications*, vol. 9, no. 1, pp. 112–123, 2020.
- [10] N. Hu, C. Chen, and Y. Jin, "Shooters' anxiety prediction and the relationship with sports performance," *China Journal of Health Psychology*, vol. 5, no. 2, pp. 12–31, 2010.
- [11] S. Luckner, J. Schröder, and C. Slamka, "On the forecast accuracy of sports prediction markets," *Negotiation, Auctions, And Market Engineering*, vol. 7, no. 8, pp. 56–81, 2006.
- [12] M. Burnley and A. M. Jones, "Oxygen uptake kinetics as a determinant of sports performance," *European Journal of Sport Science*, vol. 7, no. 2, pp. 63–79, 2007.
- [13] G. Atkinson and T. Reilly, "Circadian variation in sports performance," *Sports Medicine*, vol. 21, no. 4, pp. 292–312, 1996.
- [14] G. Chen, L. Wang, and M. M. Kamruzzaman, "Spectral classification of ecological spatial polarization SAR image based on target decomposition algorithm and machine learning," *Neural Computing & Applications*, vol. 32, no. 10, pp. 5449–5460, 2020.
- [15] R. E. Smith, F. L. Smoll, S. P. Cumming, and J. R. Grossbard, "Measurement of multidimensional sport performance anxiety in children and adults: the sport anxiety scale-2," *Journal of Sport & Exercise Psychology*, vol. 28, no. 4, pp. 479–501, 2006.
- [16] M. A. Fredericksen, Y. Zhang, M. L. Hazen et al., "Three-dimensional visualization and a deep-learning model reveal complex fungal parasite networks in behaviorally manipulated ants," *Proceedings of the National Academy of Sciences*, vol. 114, no. 47, pp. 12590–12595, 2017.
- [17] Z. Yin and J. Zhang, "Cross-session classification of mental workload levels using EEG and an adaptive deep learning model," *Biomedical Signal Processing and Control*, vol. 33, pp. 30–47, 2017.
- [18] Y. X. He, S. T. Sun, and F. F. Niu, "A deep learning model enhanced with emotion semantics for microblog sentiment analysis," *Chinese Journal of Computers*, vol. 26, no. 3, pp. 31–58, 2017.
- [19] B. Chen, Y. U. Qiuting, and T. Chen, "On deep-learning-model-based sensor activity recognition," *Journal of Zhejiang University of Technology*, vol. 31, no. 2, pp. 112–131, 2018.
- [20] X. Ning, K. Gong, W. Li, and L. Zhang, "JWSAA: joint weak saliency and attention aware for person re-identification," *Neurocomputing*, vol. 453, pp. 801–811, 2021.
- [21] F. Pappenberger, K. Bogner, F. Wetterhall, Y. He, H. L. Cloke, and J. Thielen, "Forecast convergence score: a forecaster's

- approach to analysing hydro-meteorological forecast systems,” *Advances in Geosciences*, vol. 29, pp. 27–32, 2011.
- [22] C. M. Bailey, R. J. Echemendia, and P. A. Arnett, “The impact of motivation on neuropsychological performance in sports-related mild traumatic brain injury,” *Journal of the International Neuropsychological Society*, vol. 12, no. 4, pp. 475–484, 2006.
- [23] A. J. Braakhuis and W. G. Hopkins, “Impact of dietary antioxidants on sport performance: a review,” *Sports Medicine*, vol. 45, no. 7, pp. 939–955, 2015.
- [24] S. J. Haake, “The impact of technology on sporting performance in Olympic sports,” *Journal of Sports Sciences*, vol. 27, no. 13, pp. 1421–1431, 2009.

Research Article

Animation Expression Control Based on Facial Region Division

Liangjun Zhang 

College of Art and Design of Shanghai Jian Qiao University, Shanghai 201306, China

Correspondence should be addressed to Liangjun Zhang; 20083@gench.edu.cn

Received 21 January 2022; Revised 21 February 2022; Accepted 18 April 2022; Published 12 May 2022

Academic Editor: Hangjun Che

Copyright © 2022 Liangjun Zhang. This is an open access article distributed under the Creative Commons Attribution License, which permits unrestricted use, distribution, and reproduction in any medium, provided the original work is properly cited.

Science and technology are developing rapidly in the twenty-first century. With the development of information technology, computers play a great role in people's life. At present, with people's increasing love for animation, exquisite and realistic animation has become people's pursuit goal. Generally speaking, the most impressive thing in animation is the animation character expression. Nowadays, with the rapid development of science, it is necessary to develop a computer technology that can be used in animation expression control technology. The facial division is just met by computer technology. It is very important for the animation to create an animation expression consistent with the character's face. The character face has diversity and uniqueness, which plays an important role in animation expression control. There are many factors in the character's face area that affect animation expression control. The coordinated movement of multiple facial organs shows various emotional states through the changes in muscle movements in various areas of the face, such as eye muscles, facial muscles, and oral muscles. It has strong integrity and particularity and has relatively high technical requirements. Generally, the expression control technology can transform and deform a specific area of the face. Based on the division of the face area, the computer technology is used to calculate the different expression features of the face for recognition, showing a more exquisite and realistic animation expression. Under this background, this paper divides the facial region and introduces the physiological structure of the face and the relationship and influence between facial expression and animation expression control. Several algorithms used in facial structure feature point extraction are compared experimentally. After experimental comparison, it is found that the improved algorithm is much more efficient than the original algorithm in the process of extracting facial feature points, can remove redundancy, greatly reduce the amount of operation data, and lay a good foundation for the follow-up animation expression control technology.

1. Introduction

In recent years, people have higher and higher requirements for the quality of life, especially for entertainment. In this social context, the development space of the animation industry is becoming larger and larger. Its forms are diverse, and its development is changing day by day. It occupies an irreplaceable important position in people's life. While promoting social needs, the animation industry is a global industry that promotes exchanges between different cultures. As a new technology in animation production, animation expression control technology [1] gets rid of the traditional dull and complex animation production mode [2] and can be produced simply and quickly through computer technology [3]. The animation expression control technology realized by computer technology can control and

adjust the facial expression of animation characters [4]. This technology provides a new idea for animation expression production [5]. In order to provide a better visual experience for the audience and make the expression of the animated characters more vivid, the facial expression is combined with the animated scene. This technology can greatly improve the efficiency of animation creation and reduce the large number of repeated drawing work in the creation process.

Animation expression [6], as an important branch of computer animation research, is an insurmountable problem to make animation expression as realistic and vivid as a human face. Facial expression [7] plays a very important role in people's daily communication. People have similar structures and the same feature set [8]. Facial region segmentation [9] has an important impact on animation expression control. When the nose and mouth on the face

change, the two eyes will also change; The change from one face to another, especially the expression of emotion and words, is different [7] When expressing emotions again, the coordinated movement of multiple facial organs has its own characteristics [10]. When expressing feelings [11], we must pay attention to the priority [12] of facial features [13]. Eyes, mouth, eyebrows, and eyelids have higher priority, but chin, nose, tongue, ears, and hair have lower priority. In addition, although the range of head movement is very small, it is also an important feature of distinctive expression. In the research of expression animation, the generation of several representative expressions is mainly considered [14]. In order to convert the whole face or specific area of the face image [15], experimental research shows that very good results can be achieved by using the inherent space method [16] to calculate the features of various expressions [17]. Based on the method of facial feature points [18], the facial features are classified and processed. By adjusting the deformation factor [19], time parameter curve of relevant expression units, the animation process of facial expression is effectively controlled, so as to realize the facial expression control of animated characters. The animation expression produced by the method of animation expression control through facial region division [20] is vivid and realistic, which can achieve an ideal animation effect.

2. The Meaning of Facial Segmentation and the Principle of Animation Expression Control

2.1. Influence of Facial Segmentation on Animation Expression Control. Character facial expression animation is the most complex of all the structures to realize animation, which involves not only simple animation methods. In order to achieve a more vivid effect, the design of characters' facial expressions involves research in many fields. Because the facial expressions of the characters are very rich, they are roughly divided into joy, anger, sadness, and joy, but the degree of expression is different, and each has its own expression method. The human facial structure is mainly composed of the skull and facial muscles. The skull mainly determines the structure and shape of the whole face, while the control of facial muscles determines the deformation of the whole face. The changes in our facial expressions such as joy, anger, sadness, and joy are produced by the movement of facial muscles. Therefore, according to the local characteristics of facial expression caused by facial muscle movement, the facial region is generally divided into seven regions. In fact, when facial expressions occur, they are not evenly expressed on the whole face. A large number of observations show that they are mainly expressed in the areas of the mouth, nose, eyes, and eyebrows.

Psychological research shows that the expression of different emotions has different facial regions. For example, the surprise is mainly reflected in the movement of mouth muscles and eye muscles, as well as the changes of eye muscles and corner radian; For example, fear is mainly manifested in the closure of the mouth and eyes, the wrinkle of the whole facial contour, and so on. Therefore, when studying the change of animation expression, it is necessary

to correctly identify the facial region related to this expression and correctly remove the regions not related to this expression, so as to achieve the ideal effect of animation. According to the research, the face is generally divided into blocks according to its physiological characteristics to simplify a complex and irregular surface, which provides the basis for animation expression control technology.

A complete face recognition system includes three main modules. Firstly, input the image sequence to be detected, detect the face image through the face car inspection module, extract the expression feature, recognize it, and enter the final classification as shown in Figure 1.

2.1.1. Animation Expression Control Principle. When designing different animation characters' expressions, the regional changes of each character are very different every time they express their emotions; there are also different emotional characteristics between characters. The most important parts of the face to express emotion are eyes, eyebrows, nose, and mouth. These parts are driven by the data of the expression-driving unit to achieve the combination of different expressions. The facial animation expression is divided into three driving modules: feature location, expression driving, and expression animation; then, the expression animation studied is mainly divided into three parts: eye blinking, eyebrow movement, and mouth opening and closing. As shown in Figure 2, the expression system of face animation is briefly described.

Then, according to this design idea, the system principle of face animation is proposed. Firstly, the face image is input in the face feature location module, and the input image is simplified by using the commonly used image processing method of the computer. Then, the face is located by using the method of the active shape model to find the feature points. This module prepares for the next module processing; next, the facial animation expression module is processed: module 1 is automatically matched from ASM to the new model; finally, face animation is processed as shown in Figure 3.

In the schematic diagram of the face animation system, the animation system is divided into three modules. In the specific implementation process, the most important modules are modules 1 and 2. Firstly, input the image data in module 1, find the facial feature part, and use ASM to model to match the expression data unit to module 2. The face model is established in module 2. The face model forms the face animation through the movement of the three most basic areas, namely eyebrow blinking, eye blinking, and mouth movement. Finally, the animation is generated.

2.2. Application of Animation Expression Control Technology

2.2.1. Animation Deformation Control Technology Based on MPEG-4. As early as the twentieth century, character animation based on MPEG-4 began to appear. Taking character animation parameters as the driving standard, we found the feature points on the character animation face model and made a new modification to the position information

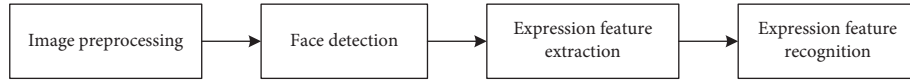


FIGURE 1: Flow chart of the facial expression recognition system.

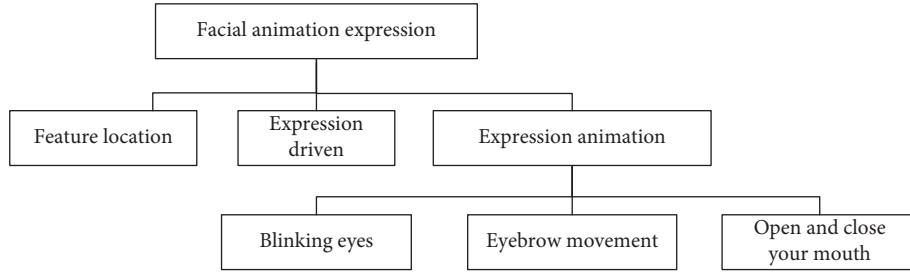


FIGURE 2: Block diagram of facial animation expression system.

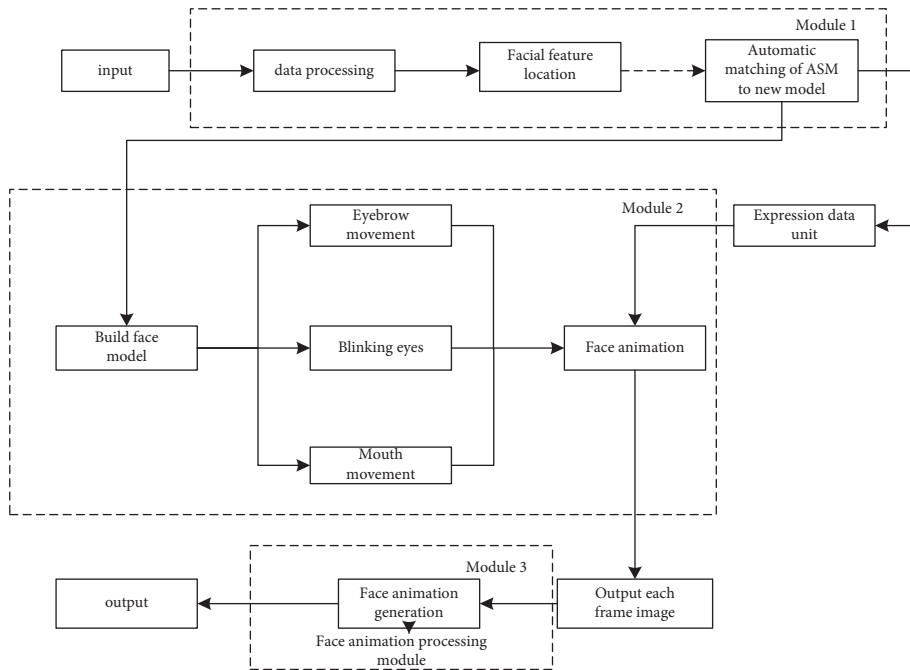


FIGURE 3: Schematic diagram of the face animation system.

through calculation, so as to form the latest facial animation expression. Use f to represent the corresponding feature point displacement data and use d , u , and D to represent the corresponding offset as follows:

$$f = \frac{D}{U} * d. \quad (1)$$

2.2.2. Animation Deformation Control Technology Based on PCA. The principal component analysis is mainly used to reduce the dimension of features. If the number of data features is very large, we can think that only some of them are really interesting and meaningful, while other features are either noise or redundant with other features.

PCA technology is a diversified statistical analysis method. It puts the original high-dimensional space into the low-dimensional vector space through a special vector

matrix, which has relative independence. Finally, the most reasonable feature points are extracted; F is taken as the statistical vector of various emotion parameters; and F_{av} represents the average value of the vector:

$$F = F_{av} + \vec{k}E, \quad (2)$$

$$F = G(E_m) = F_{av} + g(E_m)E.$$

Based on the above two formulas, the following equation is established:

$$\vec{k}_r = (F_r - F_{av})E_R^{-1}, \quad (3)$$

where generalized inverse matrix (right inverse) is defined as follows:

$$E_R^{-1} = E^T E E^T^{-1}. \quad (4)$$

The new position coordinates of the feature point can also be transformed through the new feature point f as follows:

$$P = P_0 + f * U * d, \quad (5)$$

where P_0 is the coordinate of the feature point under ordinary neutral expression, u is the FAPU related to the feature point, and d is the unit vector.

By recording nine emotions including fear, surprise, and happiness, the information of the horizontal direction of the marker point is obtained, and the eigenvalue, contribution rate, and cumulative contribution rate of each main component are obtained, as shown in Table 1.

According to the expression method of the above feature quantity, the facial animation expression is controlled to make the animation expression more vivid.

3. Facial Features and Facial Region Division

3.1. Facial Features. There are about 7.8 billion people in the world. Everyone's face looks different from others and has their own unique facial features. It is precise because people can distinguish different faces by relying on different facial features. Although each face is different and has its own characteristics, there are many kinds of the same movement rules in the face. For example, the expression of the face is the same, and the movement rules of each area of the face and internal muscle groups are the same; For example, the positional relationship of facial regions or organs will not change. According to the basic features of the face, the aforementioned "three courtyards and five eyes" are shown in Figure 4.

3.2. Facial Region Segmentation. In the research of facial region segmentation, the initial researchers only regard the face as an overall structure to establish an animated character model, not specific to a certain region of the face. If you want to realize the expression change of a certain part or an organ or deal with the eyes, nose, or mouth separately, you will find that this implementation is very difficult. Staff requires advanced and complex technical requirements. Therefore, at first, the application of this model has certain limitations, and it cannot achieve the ideal effect. Later, in order to solve this problem, researchers proposed a 3D face machine model based on face segmentation. The biggest feature of this model is that it no longer treats the face as a whole but divides the whole face into multiple block structures according to a certain law. Each block structure is modeled and processed separately. Each block structure is independent, interdependent, and inseparable, so as to realize the structural mode of low cohesion and high coupling. Finally, these individually processed block structures can be combined again to form complete and different facial expressions. Although, on the surface, facial expressions look different, the face has many of the same properties, such as the basic proportional relationship of the three courtyards and five eyes of the face and the positional structure relationship of the face nose, eyes, and mouth, which will not

change due to the difference of the face or the change of expression. Therefore, the researchers found that this provides the possibility for facial region segmentation or can be used as the basis of segmentation. The advantage of this model is that the face segmentation will not destroy the integrity of the face and the relative position and proportion relationship between various parts or organs and will not change due to the segmentation. In the process of modifying from a general face geometric model to a specific face geometric model, the face surface will not be seriously deformed. The animation provides great convenience for the production of facial expressions.

At the same time, the researchers have shown in the experiment that the face is an elastomer. If the model is not adapted at the beginning and if a point on the model is moved arbitrarily during the interactive modification of the ordinary facial geometric model, it is necessary to calculate the position change of the vertices of the whole facial model. The amount of calculation required by this method is huge and complex, and in practical application, it wastes humans, materials, and resources. If the facial expression is divided into several small blocks, it is stipulated at the beginning that the motion of each point only affects other points in the block where the point is located, not the points of other blocks. In this way, it will simplify the complex and huge amount of calculation, significantly reduce the amount of calculation, and improve the accuracy and efficiency of calculation. Therefore, it is very necessary and effective to divide the face into regions.

After the face is divided into blocks, in order to operate and process the geometric model of the face, it is necessary to design a good data structure for this geometric model. This data structure needs to meet the following requirements: there is a separate data block; this data block can be stored separately for the segmented organs or regions of the face or the regions that need to be stored separately so that it can be simply and quickly separated from the whole in the process of processing, and the topological relationship between them remains unchanged. This model needs to be able to clearly mark which points are feature points. In the process of access, it can quickly locate and access any vertex in the model anytime and anywhere. It can quickly find the edges associated with vertices.

3.3. Face Segmentation Method. Simply block the face, then train the corresponding CNN module for each block, and extract the feature cascade of the full connection layer, which can improve the accuracy and efficiency of face recognition. The bone block of the face is used as a scaffold, which is a framework to support facial muscles and skin. When the expression occurs, each bone block moves, regardless of the thickness of the bone block, and the bone block will not undergo elastic deformation. When the movement occurs, there is only geometric deformation. At the same time, considering the convenience of controlling the face model, it is assumed that the topological structure of facial bone blocks is also consistent. As an important part of facial movement, muscle is a layer of soft tissue with a certain thickness attached to the bone frame. Skin is used as an

TABLE 1: Eigenvalue, contribution rate, and cumulative contribution rate of main components.

	λ_1	λ_2	λ_3	...	λ_{18}
Characteristic value	9.6205	5.0245	1.5894	...	-0.0000
Contribution rate	0.5364	0.2548	0.0598	...	-0.0000
Cumulative contribution rate	0.5354	0.8944	0.9546	...	1

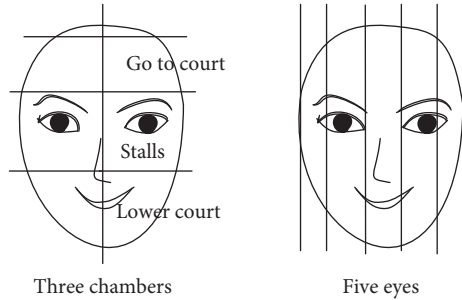


FIGURE 4: Overview of facial features.

elastic mold to wrap stock price and muscle, and its thickness is different everywhere; And there are many fascia connecting facial structures between skeleton, muscle, and skin, which also have a certain impact, and the thickness is also different.

For the face model, in order to facilitate research and control, the whole face is divided into blocks according to the distribution of organs and muscles of the face. It is divided into forehead, left and right parts of eyebrows, left and right parts of eyes, left and right parts of temples, and left and right parts of cheeks, followed by nose, mouth, and chin, as well as other transition parts. According to this distribution, a 3D face geometric model based on facial structure division is formed.

3.4. Global Feature Extraction of Facial Expression. The extraction of facial expression features plays an important role in the follow-up animation expression control. In the whole animation expression control, the extraction effect of facial expression features is the primary character. Firstly, the facial expression is holistic, and various parts and organs cooperate to complete the corresponding expression, although the degree of participation of some organs is less than that of other organs. However, when expression occurs, each region is more or less involved. Secondly, when expressing emotions, each different person is affected by different environment, culture, personality, and personal experience. Therefore, when expressing emotions, their forms of expression are diverse and different. In the production process, in addition to the predictable results in a specific environment, it can also be carried out in some cases, such as when the environment changes and becomes complex, so it also has a certain anti-interference ability. Finally, the extraction process should also achieve due speed and efficiency.

Everyone is an independent individual, and the cultures of each country and region are very different. For example, the Chinese people are delicate and introverted in expressing their emotions, while the European and American people are

open and exaggerated in expressing their emotions. Therefore, it is difficult to recognize the facial organ characteristics of each expression in the extraction process. Through experiments, researchers found that the universality of expression forms limited the expression to seven modes, reducing the difficulty of expression recognition.

In the selection of feature points, if only all regions contained in the whole face are selected, such as nose, eyes, eyebrows, and other regions, the dimension of feature extraction will be increased, and the corresponding operation time will be increased, which cannot achieve the ideal effect. And some extracted feature points cannot express the motion characteristics and laws of the region they represent. Often these feature points will be useless in postproduction and become huge redundant data. This has an impact on identification production.

Therefore, in order to change this disadvantage, researchers extract feature points through the global features of the face, in order to quickly distinguish the types with large differences in each expression. The most intuitive influence of the expression made by the face in expressing emotion is the changes in eyes, eyebrows, nose, and mouth. In these organs, the mouth area, eye area, and eyebrow area are more obvious, especially the mouth. Therefore, these parts play an important role in facial expression. In the extraction of feature points, we should focus on these parts, the most representative key points of these parts.

3.5. Extraction of Facial Feature Vector. Due to the great difference in human face, only relying on simple feature point extraction cannot meet more accurate calculation.

Therefore, it is necessary to extract the feature vector in the calibrated feature region. In the whole facial expression, the mouth and eyebrow regions are more recognizable than other regions. Different weights are set for these different regions to lay a foundation for improving the recognition accuracy in the future.

Gabor is a linear filter applied to edge extraction. Its filtering and direction expression are closer to the human visual system and the sensory system. It can provide good characteristics of direction selection and scale selection and is not sensitive to illumination changes. Therefore, it is widely used in the field of computer vision, so it can be applied to an expression.

Gabor filter can be expressed as follows:

$$J_j(x) = \int I(x)\psi_j(x - x^2)dx, \quad (6)$$

where $J(x)$ is the feature vector obtained by Gabor transformation of pixels $x = (x, y)$ in facial expression image $I(x)$ as a filter.

$\psi_j(x)$ is a Gabor kernel function used for feature extraction as follows:

$$Y_j(x) = \frac{k_j^2}{s^2} \exp\left(-\frac{k_j^2 x^2}{2s^2}\right) \left[\exp(ik_j x) - \exp\left(-\frac{s^2}{2}\right) \right], \quad (7)$$

where k_j is the wave vector parameter, including k_{jx} and k_{jy} two components.

$$k_j = \begin{pmatrix} k_{jx} \\ k_{jy} \end{pmatrix} = \begin{pmatrix} k_v \cos \phi_u \\ k_v \sin \phi_u \end{pmatrix}, \quad (8)$$

where k_v is the sampling frequency of the filter; ν is the frequency coefficient, representing the wavelet transform scale; and ϕ_u is the direction coefficient, representing the direction of wavelet transform, and wavelet transforms the image in all directions and scales:

$$k_\nu = 2^{\nu+2/2} \pi (\nu = 0, 1, 2, 3, 4), \quad (9)$$

$$\phi_u = u \frac{\pi}{8} (u = 0, 1, 2, 3, 4, 5, 6, 7).$$

The extraction range of feature vector should include mouth region, eye and eyebrow region, nose, and stria region. In order to facilitate the subsequent process, the corresponding weight is set for each region feature vector because each region changes differently when the expression occurs. Set all the extracted pixel points as p ; set each part with dotted pixel points as p_e, p_m, p_n ; and set their respective weights as w_e, w_m, w_n .

$$w_{e0} = 1, \quad (10)$$

$$w_{m0} = w_{n0} = 0.$$

The feature vector of the image is extracted through the dimension of $5 * 8$ and then multiplied by the weight coefficient to reach the initial threshold setting. At this time, the weight value is w_{et}, w_{mt}, w_{nt} as follows:

$$w_e = \frac{w_{et}}{w_{et} p_e + w_{mt} p_m + w_{nt} p_n}. \quad (11)$$

Then, roughly locate the feature points of the whole face image, carry out convenient operations globally, and search the feature points of each region:

$$S(J, J') = \frac{\sum_{n=1}^N a_n'}{\sqrt{\sum_{n=1}^N a_n^2 \sum_{n=1}^N (a_n')^2}}. \quad (12)$$

\vec{d} is the position deviation between J, J', ϕ_n, ϕ_n' , which indicates the phase response of the n the Eigenvector.

In order to make the face matching recognition process more efficient and accurate, two algorithms are improved based on the original algorithm. One of the algorithms is called improved algorithm 1. Firstly, the face model is defined, and the feature points are marked. Roughly locate several basic parts on the image face and then calculate the feature points of each area to find out the law and determine the best position. Using the weighted feature vector, the image degree of the basic expression is calculated. The

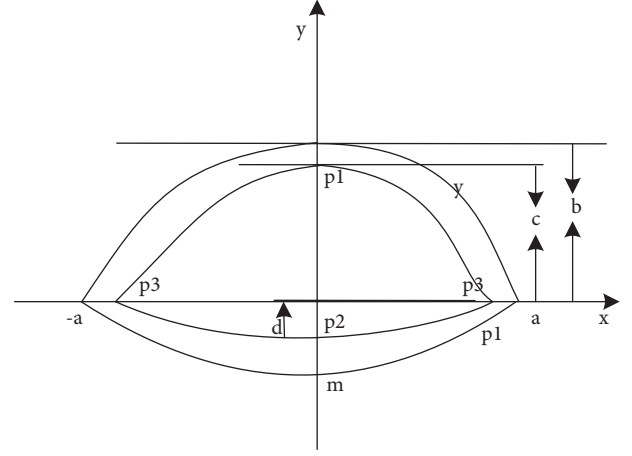


FIGURE 5: Eye limits and coordinate system.

algorithm directly searches the segmented area, eliminates the search in the face range of the original algorithm, and reduces the search difficulty and time. In addition to this algorithm, there is another algorithm called improved algorithm 2. The previous steps are basically the same, but after rough positioning, the Euclidean distance between each feature point and the positioning face template will be calculated:

$$S(J, J') = \sum_{n=1}^N \sqrt{(x - x')^2 + (y - y')^2}. \quad (13)$$

More strictly match the eyes, eyebrows, and mouth areas. After the best position is found, the weight of the feature vector is used.

Calculate the acquaintance degree between the basic expression and the positioning template as follows:

$$S(J, J') = \frac{\langle J, J' \rangle}{|J||J'|}, \quad (14)$$

where $\langle J, J' \rangle$ means to find the inner product and $|J||J'|$ is to operate the two ball binomials.

Compared with the original algorithm, the two algorithms are simpler and have less computation.

3.6. Facial Eye Movement. Eye limits and coordinate system are shown in Figure 5.

Firstly, the displacement component of the upper eyelid is considered. Let the displacement component of any point of the upper eyelid displacement be U and V variables. According to the displacement variational method of elastic deformation, the formula is

$$U(x, y) = u_0(x, y) + \sum_m A_m u_m(x, y), \quad (15)$$

$$V(x, y) = v_0(x, y) + \sum_m B_m v_m(x, y),$$

where $u_m(x, y)$ and $v_m(x, y)$ are undetermined coefficients and $u_0(x, y)$ and $v_0(x, y)$ are displacement functions at the boundary satisfying eye boundary conditions, in which A_m

and B_m are also undetermined coefficients and independent of each other.

According to the principle of elasticity, the displacement function of a certain point of upper eyelid displacement is as follows:

$$U(x, y) = \frac{35cxy}{42b + 20a} \left(1 - \frac{x^2}{a^2}\right) \left(1 - \frac{y}{b}\right), \quad (16)$$

$$U(x, y) = \left[\left(1 - \frac{x^2}{a^2}\right) \left(1 - \frac{y}{b}\right) \right] \left(c + \frac{5cby}{16a^2 + 2b^2} \right).$$

The movement process of the eye moves along the horizontal and vertical directions, so the new coordinate of each vertex after deformation is

$$(x', y', z')^T = (x, y, z)^T + (u, v, 0). \quad (17)$$

The movement of our entire upper eyelid and lower eyelid is not infinitely extended, and there are certain restrictions on the movement radian, so we should also meet certain agreed conditions. In addition, the eyelid never leaves the eye surface during the whole movement process, so this movement process should also meet the spherical equation:

$$(x - x_0)^2 + (y - y_0)^2 + (z - z_0)^2 = r^2. \quad (18)$$

The coordinates of the eye center (x_0, y_0, z_0) are the eye radius.

By changing the c value to change the coordinate change, we can get the formula of the upper eyelid motion law: similarly, the motion principle of the lower eyelid is similar to that of the upper eyelid, but the lower eyelid is much smaller than that of the upper eyelid.

$$u_0(x, y) = 0, v_0(x, y) = -d \left(1 - \frac{x^2}{a^2}\right). \quad (19)$$

Therefore, the solution and calculation method of the lower eyelid is the same as that of the eyelid, that is, the motion displacement equation of the lower eyelid is:

$$U(x, y) = \frac{35axy}{42e + 20a} \frac{xy}{ae} \left(1 - \frac{x^2}{a^2}\right) \left(1 - \frac{y}{b}\right),$$

$$U(x, y) = -d \left(1 - \frac{x^2}{a^2}\right) - \frac{5dey}{16a^2 + 2e^2} \left(1 - \frac{x^2}{a^2}\right) \left(1 - \frac{y}{b}\right). \quad (20)$$

Similarly, the motion coordinates of the lower eyelid can be realized by changing the d value.

3.7. Closure of the Mouth of the Face. Similarly, the movement mode of the mouth is the same as that of the eyes. The mouth is regarded as an ellipse, which is reflected in the two-dimensional rectangular coordinate system. The closing of the mouth is in equilibrium, and the yawning is the maximum opening of the mouth. The movement of the mouth is regarded as the movement of an elastomer as shown in Figure 6.

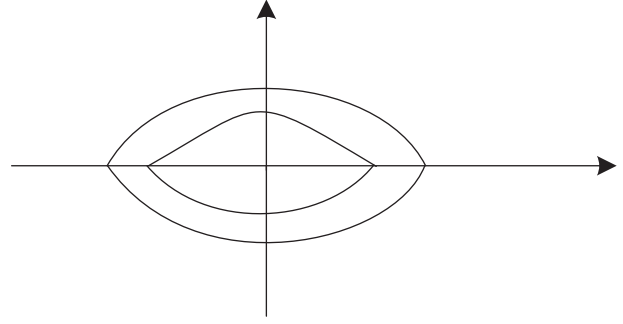


FIGURE 6: Mouth boundary and coordinate system diagram.

4. Experimental Comparison and Analysis

The improved algorithms of the above four methods are compared by experiments. Experiments verify the operability and effectiveness of the algorithm. This experiment mainly uses the Jaffe database and the Cohn-Kanade database.

There are 213 images in the Jaffe data set. They were divided into 7 expression types, namely, anger, disgust, fear, happiness, sadness, surprise, and neutrality. Each expression is different in degree as shown in Figure 7.

The Cohn-Kanade database includes 593 expression sequences of the faces of 123 male and female individuals with different skin colors and different ages. Some individuals have 7 expression sequences, and the rest have 6 expression sequences other than disgusting expressions. The expression sequence is from calm to peak expression. FACS was used to encode the expression peak as shown in Figure 8.

In the experiment, 213 images were selected from the Jaffe library, and 97 individuals were selected from the Cohn-Kanade library, including 692 images. The so-called k -fold cross-validation means that in each experiment, the samples are evenly divided into k parts, and the training samples and the samples to be tested are evenly divided according to a certain proportion, which is usually distributed according to the proportion of $k-1:1$. After K experiments are repeated, the results of each experiment are averaged to obtain the final results of the experiment. In the experiment done in this paper, the 50% cross-validation is selected, but because the number of database samples cannot meet the absolute bisection, the sample data is approximately divided into 5 bisections: 3 are training samples and 2 are test samples. In the experiment, all pictures were changed in the size of $90 * 100$, and the $15 * 4$ area of the eye eyebrow area and the $8 * 6$ area of the mouth area were selected for feature extraction. The total eye eyebrow area was given a weight value of 0.46; the mouth area was given a weight value of 0.36; and the last 0.18 was given to the nose area. In the experiment, for the sake of fairness, the positioning face data used are not selected from the experimental data.

4.1. Comparison of Experimental Results. The recognition results of the original algorithm and the improved algorithm in the Cohn-Kanade library are shown in the Figure 9. The recognition results are obtained from the Jaffe library. The abscissa is the parameter of the Gabor transform, and the



FIGURE 7: Schematic diagram of Jaffe database sample.



FIGURE 8: Schematic diagram of Cohn-Kanade database sample.

ordinate is the average recognition rate. When the feature extraction dimension is too small, the feature is not enough to express more complete information. Therefore, the

experiment is carried out when the Gabor scale parameters, and direction parameters are greater than half of the full extraction (8 * 5) as shown in Figures 9 and 10.

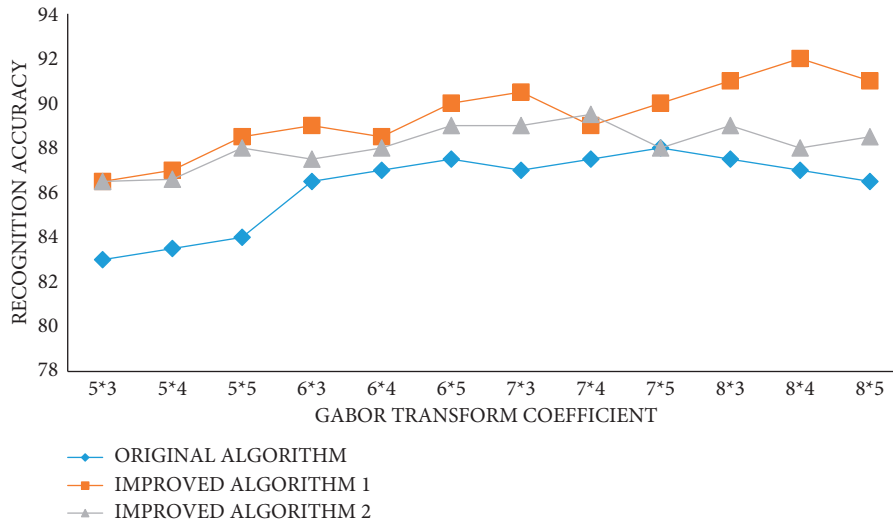


FIGURE 9: Comparison of recognition results of three algorithms in the CK database.

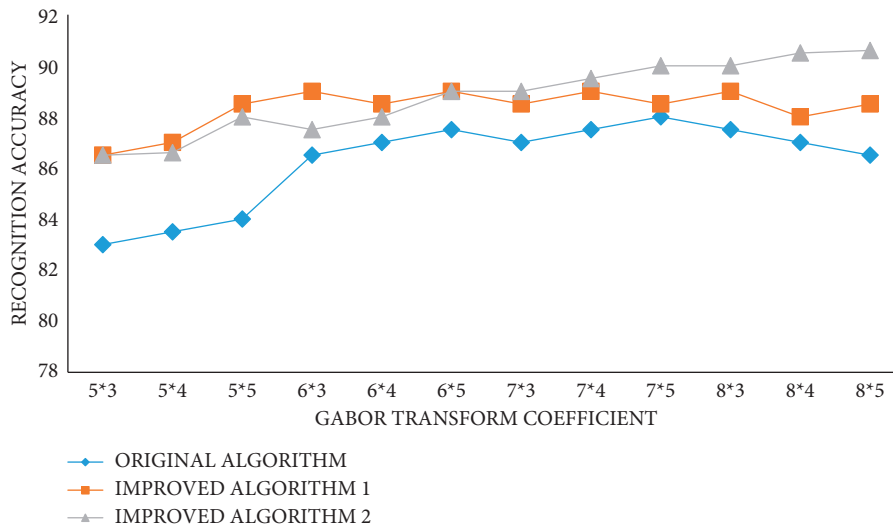


FIGURE 10: Comparison of recognition results of three algorithms in the Jaffe Library.

From the experimental results and the recognition rate, the improved algorithms 1 and 2 are much better than the original algorithm. The expressions in the Cohn-Kanade library are the facial expressions of European and American characters, and their expressions are put out. The expression of Japanese female characters in the Jaffe library is more implicit than that of Europeans and Americans. Therefore, the expression recognition difficulty in the Cohn-Kanade library is slightly less than that in the Jaffe library, and the recognition rate will be slightly higher than that in the Jaffe library.

Average one face image processed by the three algorithms, in milliseconds, as shown in Figure 11.

Through comparative research, it is found that as shown in Figure 11, the efficiency of the improved two algorithms is significantly higher than that of the original algorithm. Therefore, it is necessary to study the algorithm. Especially in algorithm 2, the operation time is significantly reduced.

In order to accurately identify each expression type, separate data statistics are mainly carried out for algorithm 2. The recognition rate of happy and surprised expressions in the Cohn-Kanade database is the highest, reaching more than 95%; the recognition rate of anger, disgust, sadness, and neutrality is close, reaching more than 85%; and the recognition rate of fear is the lowest, only 83.7%. On the other hand, the confusion probability of anger, disgust, and fear is the highest. These three expressions are also relatively difficult to identify. They all have a high probability of being misjudged as the other two expressions, and the probability of fear being misjudged as a surprise is the highest, up to 8.2%. In the Jaffe library, the highest recognition rate is still happy and surprised, which are more than 93%, and the lowest is the recognition accuracy of neutral expressions, which is less than 80%, and the recognition rates of other types are more than 80%. In the Jaffe library, the confusion probability between expressions is higher than that in the

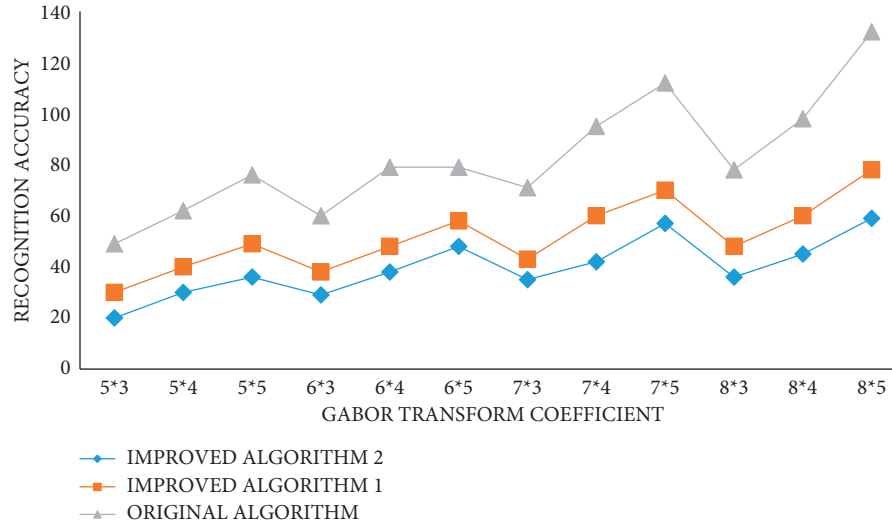


FIGURE 11: Comparison of average processing time of one image by three algorithms.

TABLE 2: Confusion matrix of algorithm 3 in the CK database.

	Anger	Hate	Fear	Happy	Sad	Surprised	Neutral
Anger	85.6	5.7	3.8	0.0	4.9	0.0	0.0
Hate	1.3	91.3	1.7	0.0	0.5	4.3	0.9
Fear	3.8	3.4	83.7	0.5	0.3	8.2	0.1
Happy	0.2	0.0	0.7	97.8	0.4	0.9	0.0
Sad	1.9	2.7	2.2	0.5	86.8	0.8	5.1
Surprised	0.1	0.7	0.5	3.3	0.1	95.3	0.0
Neutral	3.6	1.4	2.9	0.5	3.1	1.8	86.7

TABLE 3: Confusion matrix of algorithm 3 in the Jaffe Library.

	Anger	Hate	Fear	Happy	Sad	Surprised	Neutral
Anger	83.1	8.0	2.7	0.0	2.3	0.0	3.9
Hate	4.2	85.8	5.5	0.2	1.7	0.0	2.6
Fear	2.0	7.9	81.1	2.4	0.5	3.3	2.8
Happy	0.5	0.0	1.0	96.1	0.3	2.1	0.0
Sad	1.8	0.9	3.2	0.1	90.4	0.0	3.6
Surprised	0.5	1.7	0.4	2.9	0.0	93.7	0.8
Neutral	5.9	8.5	0.8	2.7	0.8	3.4	77.9

Cohn-Kanade library, especially the errors misjudged as disgusting and neutral are the most common. The confusion probability among anger, disgust, and neutral is the most obvious. Anger, neutral, and fear all have a probability of nearly 8% to be wrongly identified as disgust. The confusion matrix in the Cohn-Kanade library and the Jaffe library is shown in Tables 2 and 3.

By comprehensively comparing the above two figures, it is not difficult to find that the recognition rate of happiness and surprise is the highest in the two databases because the changes in these two kinds of expressions are the most obvious, while the recognition rate of fear expressions does not exceed 85% on both sides, which may be misjudged as surprise and disgust. In essence, the pupils of surprise are enlarged; the mouth is open; and the frown of disgust. The

changes in facial organs such as open mouth coincide with the changes of fear expression, so it has a high probability of misjudgment. In particular, the recognition rate of neutral expression on Jaffe database is lower than 80%. The reason is that the expression on the Jaffe database is more implicit, the change of facial features is relatively not obvious, and it is difficult to locate and extract feature points. Therefore, it has a high probability of mutual misjudgment with another disgusting expression with little change of facial features.

In order to compare the methods used in this paper with other similar methods, this paper counts the relevant global feature recognition effects and applies the methods of FACS algorithm, PCA algorithm, and feature vector + texture information because, in some papers, only six kinds of expression recognition except neutral expression are used. In

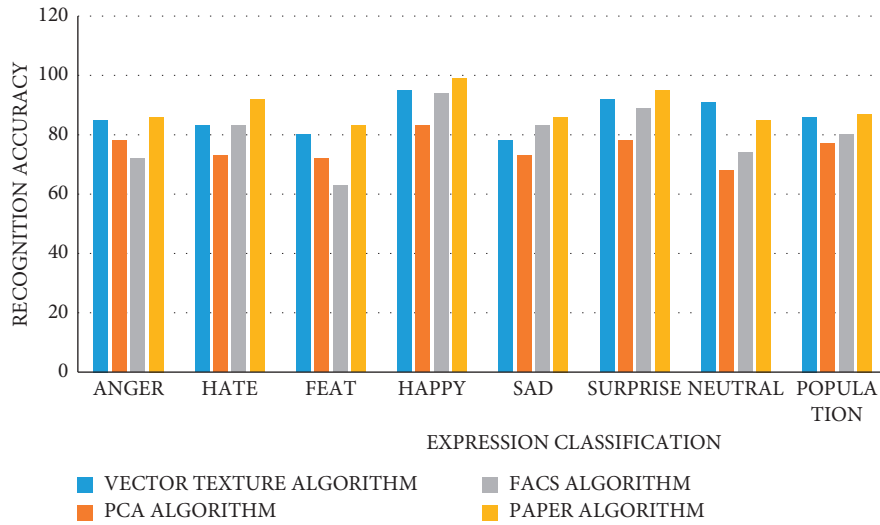


FIGURE 12: Comparison of recognition rate of global feature database.

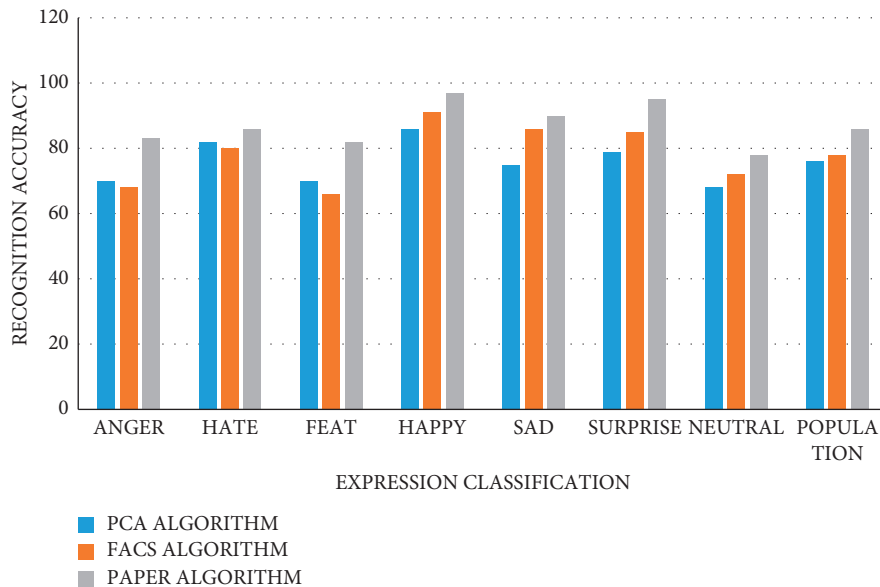


FIGURE 13: Comparison of recognition rate of global feature Jaffe library.

addition, some of the methods used are not tested in the same database and are not comparable. What this paper does is the recognition of seven expressions. Therefore, some open-source algorithms are tested, and the other algorithms are counted according to the experimental data of relevant papers. Comparing the recognition rate in the Cohn-Kanade library, this method refers to algorithm 2, which performs feature extraction under the condition of $6 * 3$. Jaffe database is the same as shown in Figures 12 and 13.

In the Cohn-Kanade library, the overall recognition rate of this method is improved compared with the relevant global feature methods, and the recognition rate of some types, such as happy and surprised, is improved, but the recognition method of neutral and angry expressions is slightly inferior. The reason is that these kinds of expressions, especially neutral expressions, pay more attention to the distinction between details. Neutral expressions and

expressions with little change in other facial organs, such as disgust and anger, are less distinguished from each other, so it is difficult to distinguish them as a whole. Compared with the vector texture algorithm, the feature point topology of facial organs focuses more on the overall characteristics of the whole world. Therefore, the recognition results of neutral and angry classes are not as good as the texture method.

The comparison of the recognition rate on the Jaffe database shows that the overall recognition rate of this method on the Jaffe database is improved compared with the relevant global feature methods, but the judgment of some expressions, such as disgusting expressions, needs to be improved. The reason is to improve the speed of recognition, so as to reduce the feature points that contribute less to recognition, but at the same time, their role is completely reduced. Therefore, for some expression types that need more feature points to be accurately defined, the results

obtained are not as good as those using more feature points, and the definition of aversion class is also more difficult. Therefore, the recognition rate of this kind is reduced.

After the whole experiment, through the experimental data, it can be seen that the extraction method of the facial feature vector in face division is very important for animation expression control. This extraction method can reduce the amount of data calculation, improve efficiency, and remove redundancy.

4.2. Experimental Summary. Through the comparison of several algorithms in the above experiments, it is not difficult to see that the improved algorithm is obviously superior to the original algorithm in terms of computational efficiency and accuracy. This algorithm can achieve better results under the Cohn-Kanade library and the Jaffe library. Therefore, in the division of facial features and facial regions, it is very important to extract facial feature vectors. This extraction method can reduce the amount of data calculation, improve efficiency, and remove redundancy. It can lay a good foundation for subsequent animation expression control.

5. Conclusion

Nowadays, various animation production technologies continue to emerge. These animation technologies have a super exquisite and realistic appearance and bring a strong visual impact to the audience. Animation expression control technology is an essential branch of animation technology. Technicians are required to be able to produce an animated expression similar to the structural image of facial expression, which requires technicians to understand its internal structure and be very familiar with it. This is not only related to the mastery of animation technology but also related to psychology, anatomy, and other aspects. The division of facial expression structure divides the complex expression structure of the face and simplifies the complex problem, so as to solve the difficult problem of animation control technology. Therefore, the division of facial modules is essential for animation expression control technology. With the gradual globalization of the animation industry, it has penetrated people's lives and becomes an indispensable part of life. Relevant technicians should strengthen their research. For animation production, character animation plays a leading role, and the research of character face control technology is very important for animation production. It may become the main research and development direction of technicians in the future. Only by constantly pushing through the old and bringing forth the new and constantly innovating facial expression control technology can we promote the development of the animation industry.

Data Availability

The experimental data used to support the findings of this study are available from the corresponding author upon request.

Conflicts of Interest

The author declares that there are no conflicts of interest regarding this work.

References

- [1] L. Juan, "Facial expression animation technology and its applications in film and television animation," *Journal of Qinghai University (Nature ence)*, vol. 29, 2011.
- [2] X. Ning, W. Li, X. Dong, and S. Xu, "Continuous learning of face attribute synthesis," in *Proceedings of the 25th International Conference on Pattern Recognition (ICPR)*, pp. 4282–4289, Milan, Italy, 2021.
- [3] G. Chen, J. Qi, and C. Tang, "Analysis and research of key genes in gene expression network based on complex network," *Complexity*, vol. 2020, Article ID 8816633, 12 pages, 2020.
- [4] T. Fukuda, M. Nakashima, and F. Arai, "Generalized facial expression of character face based on deformation model for human-robot communication," in *Proceedings of the International Workshop on Robot & Human Interactive Communication*, IEEE, Berlin, Germany, September 2002.
- [5] N. Sheng and J. F. Gu, "Silent genes provide new ideas for microbial pharmaceutical research," *Chinese Journal of New Drugs*, vol. 23, no. 18, pp. 2165–2168, 2014.
- [6] Z. Yu, E. C. Prakash, and E. Sung, "A new physical model with multilayer architecture for facial expression animation using dynamic adaptive mesh," *IEEE Transactions on Visualization and Computer Graphics*, vol. 10, no. 3, pp. 339–352, 2004.
- [7] T. K. Pitcairn, "The perception of facial expression," *Ethology and Sociobiology*, vol. 10, no. 5, p. 397, 1989.
- [8] N. Nacer, B. Mahmoud, and M. H. Bedoui, "VLIW processor architecture exploration for facial-feature and component extraction," *International Journal of Scientific Engineering and Technology*, vol. 3, no. 7, 2014.
- [9] B. Menser and M. Wien, "Segmentation and tracking of facial regions in color image sequences," *Proceedings of SPIE - The International Society for Optical Engineering*, vol. 4067, no. 4067, pp. 731–740, 2000.
- [10] J. D. Subtelny, "A longitudinal study of soft tissue facial structures and their profile characteristics, defined in relation to underlying skeletal structures," *American Journal of Orthodontics*, vol. 45, no. 7, pp. 481–507, 1959.
- [11] S. Bell, "Consumers Express Mixed Feelings on Differential Pricing," 2010.
- [12] B. Robert, B. Ruth, H. Richard et al., "Priority actions for the non-communicable disease crisis," *The Lancet*, vol. 377, no. 9775, 2011.
- [13] T. E. Herman, A. Chines, W. H. Mcalister, G. S. Gottesman, M. C. Eddy, and M. P. Whyte, "Metachondromatosis: report of a family with facial features mildly resembling trichorhinophalangeal syndrome," *Pediatric Radiology*, vol. 27, 1997.
- [14] S. Bin and G. Sun, "Optimal energy resources allocation method of wireless sensor networks for intelligent railway systems," *Sensors*, vol. 20, no. 2, p. 482, 2020.
- [15] A. J. Hudson, "Misidentification syndromes related to face specific area in the fusiform gyrus," *Journal of Neurology, Neurosurgery & Psychiatry*, vol. 69, no. 5, pp. 645–648, 2000.
- [16] S. Takeuchi, M. Yoshii, and M. Yamamoto, "New ellipsometric approach to critical dimension metrology utilizing form birefringence inherent in a submicron line-and-space

- pattern,” *Japanese Journal of Applied Physics*, vol. 36, no. 2, p. 181, 1997.
- [17] Y. Dwivedi, J. S. Rao, H. S. Rizavi et al., “Abnormal expression and functional characteristics of cyclic adenosine monophosphate response element binding protein in post-mortem brain of suicide subjects,” *Archives of General Psychiatry*, vol. 60, no. 3, pp. 273–282, 2003.
- [18] H. Duan, Y. Cheng, and Y. Wang, “Tracking facial feature points using kanade-lucas-tomasi approach,” *Journal of Computer Aided Design and Computer Graphics*, vol. 16, no. 3, pp. 279–283, 2004.
- [19] G. Chen, L. Wang, and M. M. Alam, “Intelligent group prediction algorithm of GPS trajectory based on vehicle communication,” *IEEE Transactions on Intelligent Transportation Systems*, vol. 22, no. 7, pp. 3987–3996, 2020.
- [20] W. Yao and L. Song, “Segmentation and description of human facial features region,” *Advances in Intelligent Systems and Computing*, vol. 298, pp. 499–507, 2014.

Research Article

Research on Methods of Physical Aided Education Based on Deep Learning

Wei Su¹ and Jian Feng² 

¹Basic Education Department, Shanghai Communications Polytechnic, Shanghai 200431, China

²Department of Physical Education of Tongji University, Shanghai 200092, China

Correspondence should be addressed to Jian Feng; 91786@tongji.edu.cn

Received 15 December 2021; Revised 11 February 2022; Accepted 25 March 2022; Published 9 May 2022

Academic Editor: Hangjun Che

Copyright © 2022 Wei Su and Jian Feng. This is an open access article distributed under the Creative Commons Attribution License, which permits unrestricted use, distribution, and reproduction in any medium, provided the original work is properly cited.

In order to better meet the training needs of sports and improve the standardization of sports training, an openpose-based sports posture estimation method and assisted training system are proposed, combining the basic structure and principle of openpose network. Firstly, the human posture estimation algorithm is constructed by combining with the openpose network; secondly, the overall framework, specific operation process, image acquisition, posture estimation, and other modules of the sports assistance system are designed in detail; finally, the openpose posture estimation method constructed above is validated. The results show that the value of the loss function obtained by the algorithm gradually stabilizes after 250 iterations. By using the COCO dataset as the training base and comparing it with the standard posture, it is found that the algorithm can correctly identify different badminton action postures, and the recognition rate can reach up to 94%. This shows that the algorithm is feasible and can be used for posture estimation and training of badminton sports movements.

1. Related Work

With the development of people's livelihood, ordinary people pay more and more attention to personal health, and the discussion about physical health and sports in the society is becoming more and more heated. However, most people do not master the standard motion posture, so that the best motion effect cannot be obtained, and even suffer unnecessary injuries during exercise. Therefore, it is necessary to process human movement recognition. In the past, people rely on assistant equipment to recognize human posture, so as to judge whether human movement is standard. With the mature of the machine learning algorithm and deep learning algorithm, researchers proposed diversified human movement recognition algorithms, including SVM classifiers, image processing, and deep neural networks. Furthermore, in human motion recognition technology, researchers also pioneered human body posture estimation technology, human motion recognition technology, and so on.

Human posture estimation has always been a popular research topic in academic research. For example, Amir

Nadeem created the A-HPE method. There are four benchmark data sets, namely, significant profile detection, entropy Markov model, multidimensional cues from whole body profile, and robust body part model, used to detect human body parts. Its detection accuracy is significantly higher than that of traditional algorithms [1]. In addition, it can provide technical support for human-computer interaction. Poojitha Sing obtained data of various components of each parts of the human body by measuring the point cloud data of human posture in RGB images, which avoids the ambiguity of features and thus shows better detection performance [2]. Xinwei Li estimated the human joint moment by analyzing the dynamic human-computer interaction between the human elbow torque and the exoskeleton output [3]. Wei Quan et al. created an unsupervised learning algorithm based on a forward kinematics model of human skeleton, but the algorithm has not been tested. After the establishment of the human posture estimation algorithm, it is also necessary to introduce the integrated particle swarm optimization (PSO) for optimization. The advantage of the optimized algorithm is that

no pretraining data is required, and the posture estimation of the human body is more concise [4]. After that, this method is tested by a series of experiments. Many scholars have studied human motion recognition. For example, Xiaojun Zhang created a human motion recognition technology based on deep learning. The LSTM algorithm is used to optimize deep learning algorithms, which requires advanced smart wearables devices [5]. Bi Zhuo created a multimodal deep neural network model based on the joint cost function, which used MSR Action3D data sets to identify human motion processes. And, the overall application performance is excellent [6]. Liu Shuqin proposed a human posture estimation method based on discrete point 3D reconstruction algorithm. In this method, the data features are extracted using principal component analysis, and then the estimation of human posture is achieved by means of two-dimensional posture prediction [7]. Jalal Ahmad et al. proposed a 3D Cartesian approach to feature extraction, by which the features are made to contain rich feature information [8]. Licciardo Gian Domenico and others then proposed a posture estimation method of FCN, and the results showed that the method obtained an average accuracy of 96.77% for 17 posture recognition [9]. Combined with the above research, the purpose of this study is to build an auxiliary system that can be used for badminton training and try to realize the estimation of posture through the matching of key bone points of human body, so as to better assist the movement training of badminton lovers. The contribution of this study lies in the extraction of sports posture through in-depth learning, and then through similarity comparison, the standardization standard of sports action is constructed, which provides more accurate information reference for sports training.

2. Estimation of Human Key Bone Points Based on the Openpose Model

2.1. Basic Structure. Openpose model uses the multistage convolutional neural network for training and testing. The first 10 layers of VGGNet-19 are used to initialize the human body image and then fine-tune the initialized human body image. Finally, to input, a set of human body characteristics map F can be achieved. The predicted values for subsequent stages are related to their corresponding image features. Using the three consecutive 3×3 kernels to replace the 7×7 convolution kernel in the earlier output PAFs, which can not only ensure the receiving fields but also greatly reduce the amount of computation, so as to effectively improve the work efficiency of the network model. By referring to the DenseNet method, each output in the three convolution kernels is cascaded together. The network model can synchronously save high-level features and low-level features.

The network structure of the openpose model is shown in Figure 1.

In the first stage, the convolutional neural network generates a set of partial affinity field. In the subsequent stages, the prediction results of the previous stage are cascaded with the original graph feature F . So, more accurate prediction can be made [10]. \mathcal{O}^t represents the convolutional

neural network at stage $t \leq T_p$, and T_p represents the total PAF prediction stage.

After T_p iterations, take the latest PAF prediction stage as the first stage and repeat this process to predict the confidence map [11]. Here, ρ^t represents the convolutional neural network at stage T_p and $T_p + T_C$, and T_C represents the total prediction stage of the confidence map.

2.2. Estimation of Human Key Bone Points Based on Optimization Model Structure. The openpose model is created to recognize and estimate multihuman postures. Its innovation is reflected in three aspects: firstly, the human body vector inclined field PAFs is established to estimate the confidence map of human limb features, which is among the constrained bone points in the human pose model. The constraint relationship is strengthened by combining the human key points hot spot map. And, the classification of multihuman posture key points is simplified. Secondly, six stage layers are created. The next stage layer will re-estimate the human key point hot spot map and the confidence map of human limb features, which output from the previous stage layer. And, the estimation accuracy can be further improved. Thirdly, during the training process, the loss function of each stage is monitored to ensure that the overall loss is minimized. According to the test results, the openpose model has the advantages of high estimation accuracy, but also has the disadvantages of long estimation time.

For badminton, athletes' postures change quickly. The action frequency is higher than that of human body under normal circumstances. In order to track the change process of motion posture in real time, it is necessary to ensure the efficient operation of the estimation module and evaluation module in the human body posture evaluation system. Consider that the openpose model evaluates the head region according to the five bone points in the head, which have little impact on the body posture of badminton players. And, the estimated time is indirectly extended [12]. Therefore, taking the modified human posture model as reference, this paper created a new deep neural network model to estimate the two-dimensional coordinates of human skeleton points of badminton players in a single frame image. Its architecture is shown in Figure 2 [13].

Firstly, the VGG neural network is introduced into the improved human posture evaluation model, and then the evaluation of human posture is realized through two-stage processing of openpose. The basis of the VGG neural network in Figure 2 is the CNN. Convolutional neural network is used to extract image features. CNN network includes convolutional layer, pooling layer, full connected layer, and output layer.

The convolution operation is

$$x_j^l = f \left(\sum_{i \in M_j} x_j^{l-1} * k_{ij}^l + b_j^l \right), \quad (1)$$

where k represents the convolution kernel; l represents the number of layers; M_j represents the j th feature graph; and b represents the bias term.

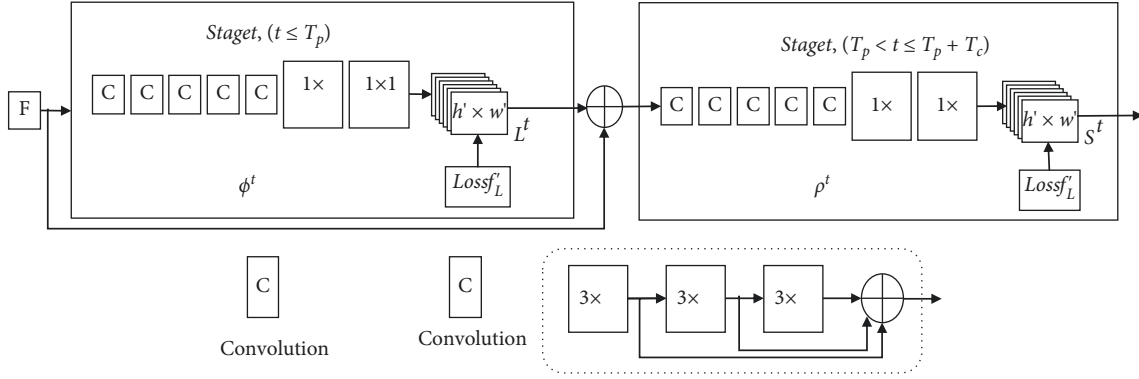


FIGURE 1: The network structure of the openpose model.

The calculation of the pooling layer is

$$x_j^l = f(\beta_j^l \text{down}(x_j^{l-1}) + b_j^l), \quad (2)$$

where down represents the lower sampling function and β and b represent the feature graph corresponding to each output, respectively.

The training process of CNN includes forward propagation and back propagation.

Among them, forward propagation can calculate corresponding actual output results after layer by layer transformation by inputting data (X_p, Y_p) to CNN, and the calculation formula of this process is as follows:

$$O_p = F_n(\dots(F_2(F_1(X_p W_1) W_2)) \dots W_n). \quad (3)$$

Back propagation is the calculation of the error between the actual output O_p and the target output Y_p , and then the error is back-propagated according to the principle of error minimization, and its weight is constantly adjusted.

The training process of CNN is as follows:

2.2.1. Back-Propagation Algorithm. In the process of forward propagation, the squared error cost function is used to measure the error. If the category is class c and the number of training samples is N , then E^N can be expressed as

$$E^N = \frac{1}{2} \sum_{n=1}^N \sum_{k=1}^c (t_k^n - y_k^n)^2. \quad (4)$$

In formula (4), t_k^n and y_k^n represent the target output of n th sample and the k -dimension of actual output, respectively.

In the process of back propagation, the sensitivity of base is used to represent the error of back propagation, which represents the change rate of error to the base b , and the expression is as follows:

$$\frac{\partial E}{\partial b} = \frac{\partial E}{\partial u} \frac{\partial u}{\partial b} = \delta. \quad (5)$$

In formula (5), since $\partial u / \partial b = 1$, $\partial E / \partial b = \partial E / \partial u = \delta$, which means that the sensitivity of a neuron's base b is equal to the derivative $\partial E / \partial u$ of error E with its all input u .

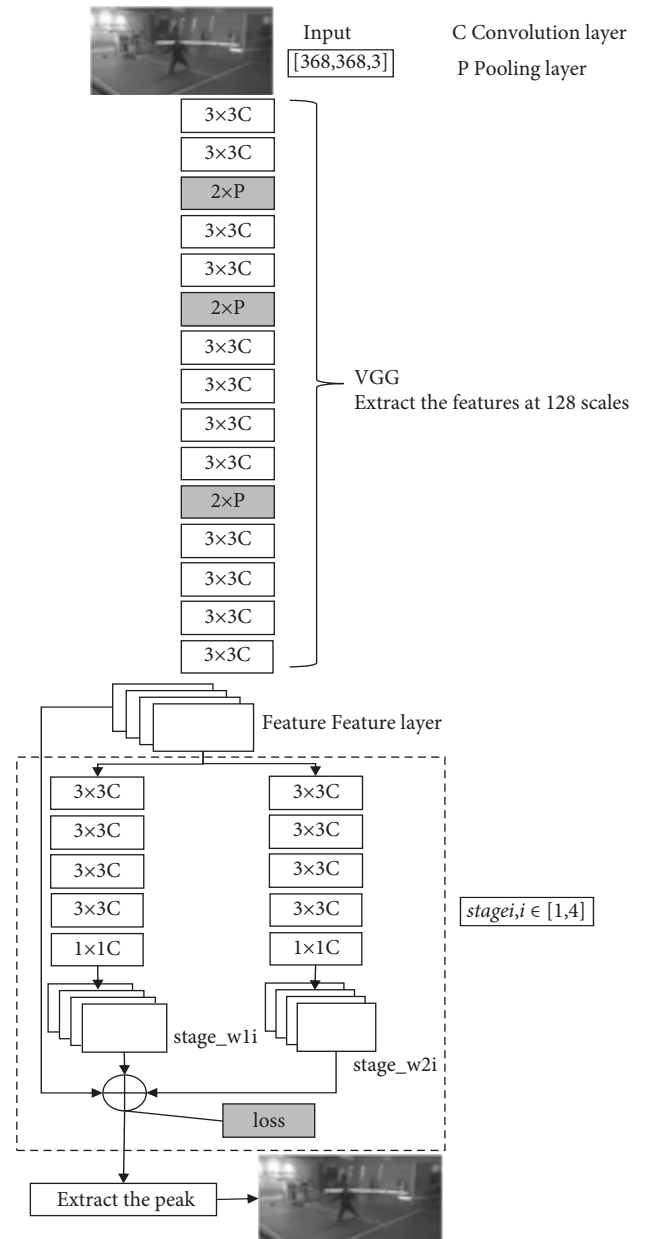


FIGURE 2: Estimation model structure.

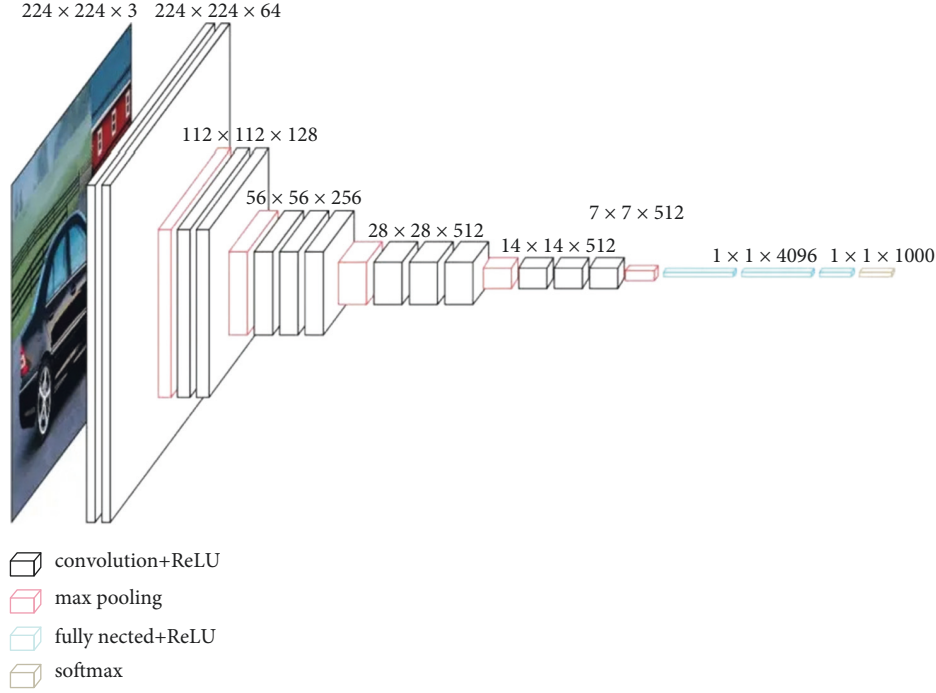


FIGURE 3: VGG model.

2.2.2. Weight Update. Weight update process of the convolutional layer: the calculation formula of weight update of this layer is the same as the calculation formula (1) of the convolution layer. The feature graph is input into a trainable convolution kernel for convolution operation, and a bias term is added. Finally, the output feature graph can be obtained through an activation function.

M_j represents the combination of input feature graphs. The corresponding convolution kernels of each output feature graph are different. Even though both output feature graph map_{*j*} and output feature graph map_{*k*} are obtained by convolution from input feature graph map_{*i*}, their corresponding convolution kernels are still different.

If there is a downsampling layer $l + 1$ under each convolutional layer l , a pixel of the output feature map of the convolutional layer corresponds to the sensitivity D corresponding to one pixel in the downsampling layer. In order to effectively calculate the sensitivity of the convolutional layer l , the sensitivity map corresponding to the upsampling in downsampling will be used to upsample, so that the size of map is the same as the feature map size of the convolutional layer l . In addition, the sensitivity δ^l of the convolutional layer l can be obtained by multiplying the sensitivity by the parameter β . The calculation formula is

$$\delta_j^l = \beta_j^{l+1} (f'(u_j^l) \circ up(\delta_j^{l+1})). \quad (6)$$

Here, up represents the upsampling operation, and \circ represents the multiplication of each element. If the sampling factor during downsampling is n , upsampling is to replicate each pixel in horizontal and vertical directions, respectively, so as to achieve the upsampling size recovery goal. Upsampling can be realized by Kronecker product:



FIGURE 4: Input coordinate system distribution.

$$up(x) = x \otimes \mathbf{1}_{n \times n}. \quad (7)$$

On this basis, its sensitivity map can be obtained according to a given feature graph on the convolution layer. Firstly, the gradient of base b is calculated, that is, the sensitivity of all elements in the sensitivity map is summed, and the formula is

$$\frac{\partial E}{\partial b_j} = \sum_{u,v} (\delta_j^l)_{uv}. \quad (8)$$

According to the weight sharing feature, the gradient solution is carried out for the point through all the connections associated with the weight, and then the gradient is obtained and summed. The expression is

$$\frac{\partial E}{\partial k_{ij}^l} = \sum_{u,v} (\delta_j^l)_{uv} (p_i^{l-1})_{uv}. \quad (9)$$

Here, $(p_i^{l-1})_{uv}$ represents the block in x_i^{l-1} convolved with k_{ij}^l , namely, a unit input of convolution layer l .

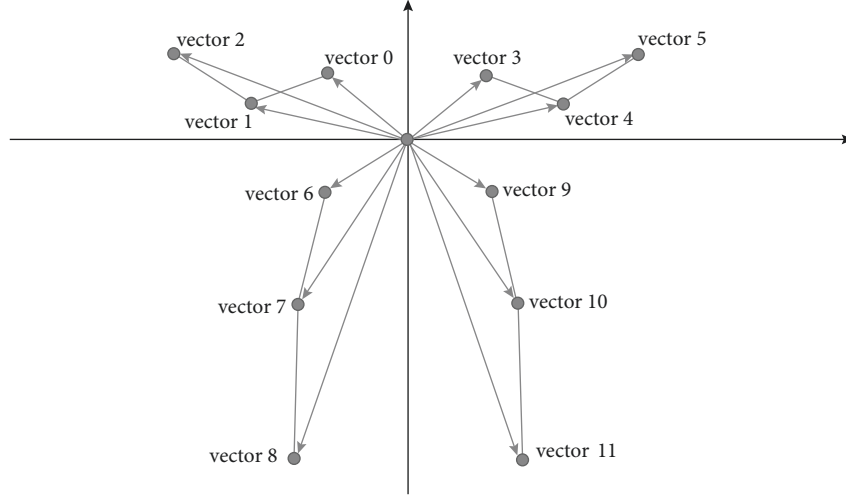


FIGURE 5: Converting the coordinates of the estimated bone points into vectors.

Formula (9) can be calculated by using the convolution function in MATLAB, and the following formula can be obtained:

$$\frac{\partial E}{\partial k_{ij}^l} = \text{rot180}(\text{conv2}(x_i^{l-1}, \text{rot180}(\delta_j^l), 'valid')). \quad (10)$$

Here, $\text{rot180}(\delta_j^l)$ means to rotate it. After rotation, cross-correlation calculation can be carried out, and then the input is reversed.

Weight updating process of the downsampling layer: the weight updating process of downsampling layer is the same as the calculation formula (2) of the pooling layer. If the sensitivity map of the down sampling layer needs to be calculated, the updated values of parameters β and b can be calculated by using formula (8).

If the current downsampling layer is fully connected with the subsequent convolutional layer, the sensitivity map of the downsampling layer can be calculated by the BP algorithm, and the sensitivity can be calculated by back-propagation:

$$\delta_j^l = f'(u_j^l) \circ \text{conv2}(\delta_j^{l+1}, \text{rot180}(k_j^{l+1}), 'full'). \quad (11)$$

Here, δ_j^{l+1} represents the sensitivity reversely propagated to it by the next convolution layer of current downsampling layer, and $\text{rot180}(k_j^{l+1})$ represents the rotated convolution kernel.

Then, the gradient of bias β and b is computed. The gradient calculation method of bias b is to add all elements in sensitivity map, and the calculation formula is the same as calculation formula (8) of the convolutional layer.

For the gradient calculation of bias β , the downsampled map in the forward propagation process should be obtained, and the expression of downsampled map is

$$d_j^l = \text{down}(x_j^{l-1}). \quad (12)$$

Thus, the gradient of β can be calculated as

$$\frac{\partial E}{\partial \beta_j} = \sum_{u,v} (\delta_j^l \circ d_j^l)_{uv}. \quad (13)$$

Through the above construction, the VGg model network structure of this study is obtained in Figure 3.

Through the above image processing and then combined with the two-stage pose estimation in Figure 2, the pose of human motion is obtained.

3. Human Posture Evaluation

3.1. Similarity Calculation. The above improvement is about how to estimate human posture and ensure the real-time and accuracy of estimation. After estimating a group of reliable skeletal points which can be referenced to the modified human pose model, how to identify human body posture according to human posture skeletal points has become the key of the human posture evaluation system. Considering that badminton belongs to the upper limb movement, the standard posture in various badminton sports is concentrated in the upper limb area. Therefore, on the basis of human skeletal point estimation, similarity is used to evaluate the similarity between the posture of badminton lovers and the standard badminton action library, so as to realize the objective evaluation of badminton action.

The human posture evaluation process consists of three steps: (1) convert the coordinates of the input bone points; (2) match with the standard posture library; (3) process and output the matching results.

A set of human bone point coordinates of a single frame image in the camera coordinate system is input into the human posture evaluation system, and the modified human posture model is used as the reference. In the human posture coordinate set index_T , each coordinate group has 13 points, as shown in Figure 4.

In the evaluation stage, the input coordinate system (image pixel coordinate system) should be transformed first, so as to prepare for the subsequent posture evaluation. In the coordinate conversion process, the camera's internal parameter matrix and external parameter matrix will be involved. Here, the former is fixed, and the latter depends on the location and angle of the camera lens. Therefore, in this regard, the camera's external matrix needs to be precalibrated

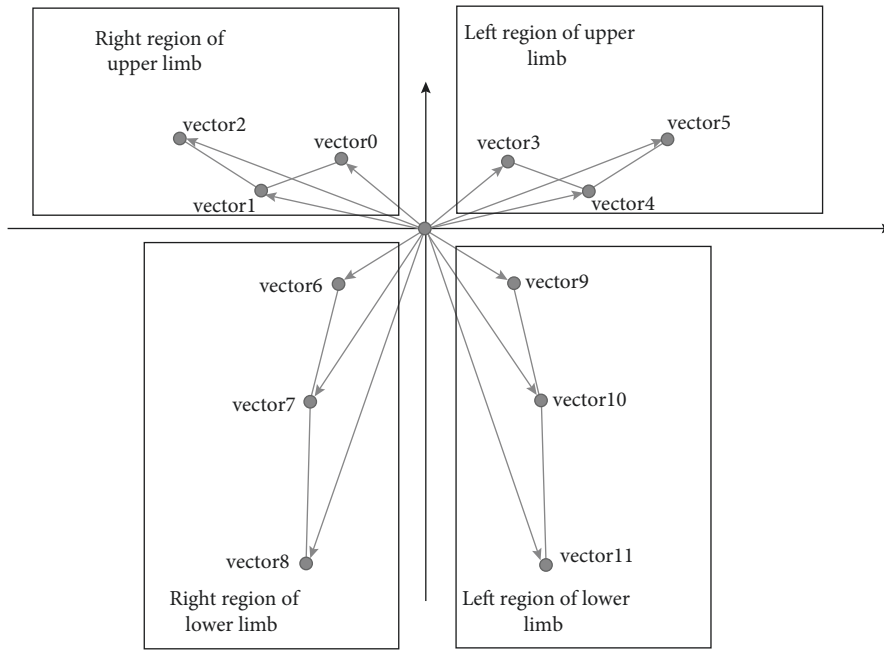


FIGURE 6: Human limbs partition diagram.

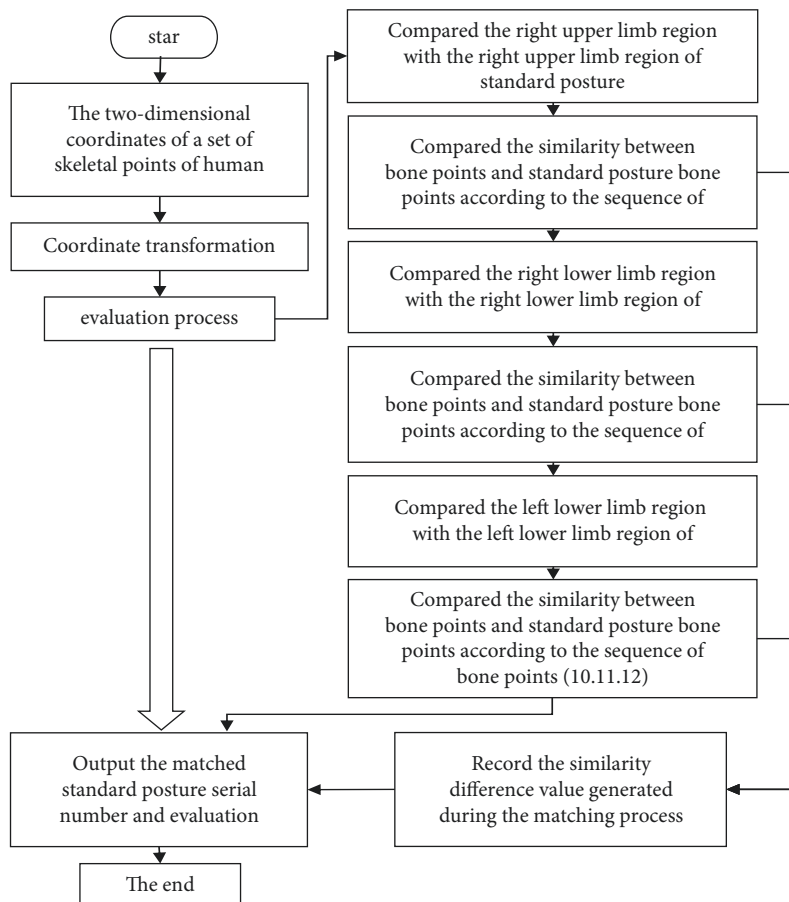


FIGURE 7: Human posture evaluation algorithm process.

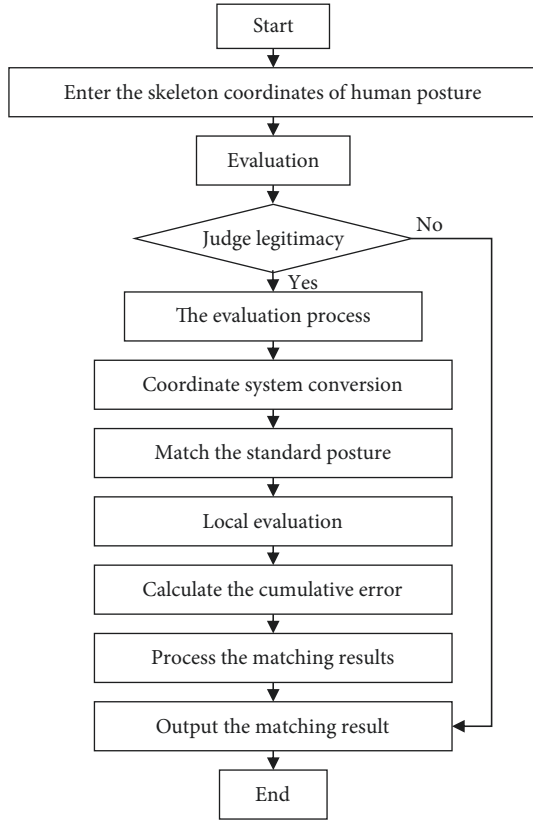


FIGURE 8: Human posture evaluation algorithm process.

to ensure the validity of the external matrix. Although the above process is feasible, it is difficult to operate in practice. So, a new coordinate transformation method is proposed in this paper, that is, (a) convert from an image pixel coordinate system to a rectangular coordinate system with the neck point as the origin in the human bone point; (b) transform from the rectangular coordinate system with the neck point as the origin to the polar coordinate system with the neck point as the origin and determine the angle between the other 12 points in the polar coordinate system and the positive x axis.

The coordinate transformation step (a) solves the matching problem of human posture and standard posture caused by different positions, and step (b) solves the uncertainty of human posture evaluation caused by individual body size difference.

After the coordinate transformation is completed, 12 included angle values of the positive X -axis and the vector $[0, 11]$ are obtained, respectively, as shown in Figure 5 [14].

The calculation process of coordinate transformation is as follows:

- (i) Input the human bone point coordinate $\{a_0, a_1, \dots, a_{12}\}$ in the image pixel coordinate system and establish the rectangular coordinate system with a_0 as the origin
- (ii) The vector set $\{t_0, t_1, \dots, t_{11}\}$ is established after the coordinates $\{a_1, \dots, a_{12}\}$ of the remaining 12 human bone points subtracts a_0

TABLE 1: Structural parameters of the optimization model.

Training data set	Human images in the COCO data set and acquiring the badminton player images
Input number of images	10
Maximum iteration	200000
Basic learning rate	5×10^{-5}
Initial value of weight value	5×10^{-4}
Initial value of weight correction	0.01
The optimizer	Stochastic gradient descent $loss = \sum_{i=1}^4 k_i \cdot (stage_w1_i - pafmap)^2 + (stage_w2_i - heatmap)^2 / batch_size \times 2$
Loss function	Pafmap human bone point grayscale of the preset image Heatmap human bone point grayscale of the preset image

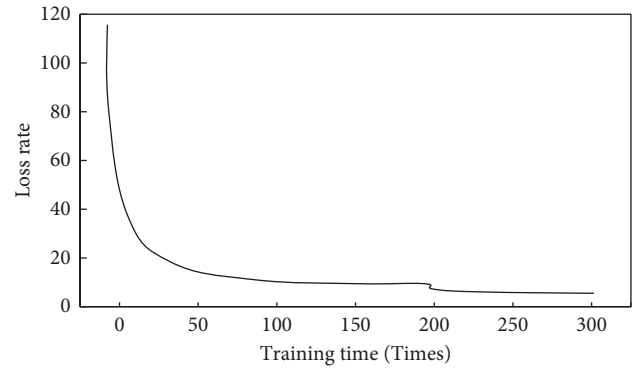


FIGURE 9: Loss curve of retraining optimization model.

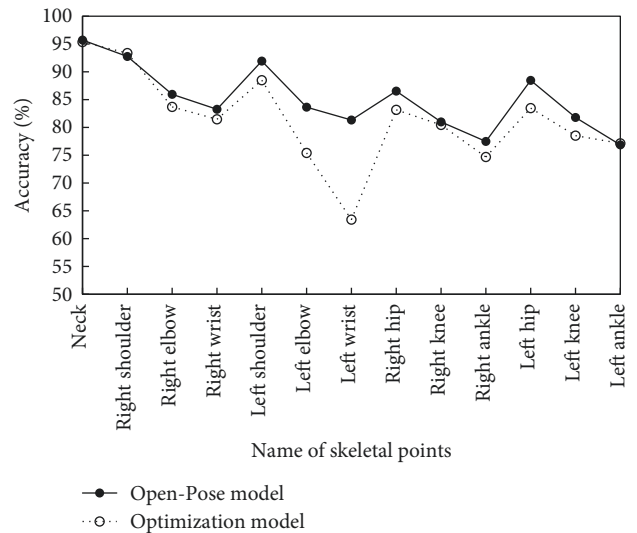


FIGURE 10: Model estimation accuracy of each bone point in the modified human posture model.

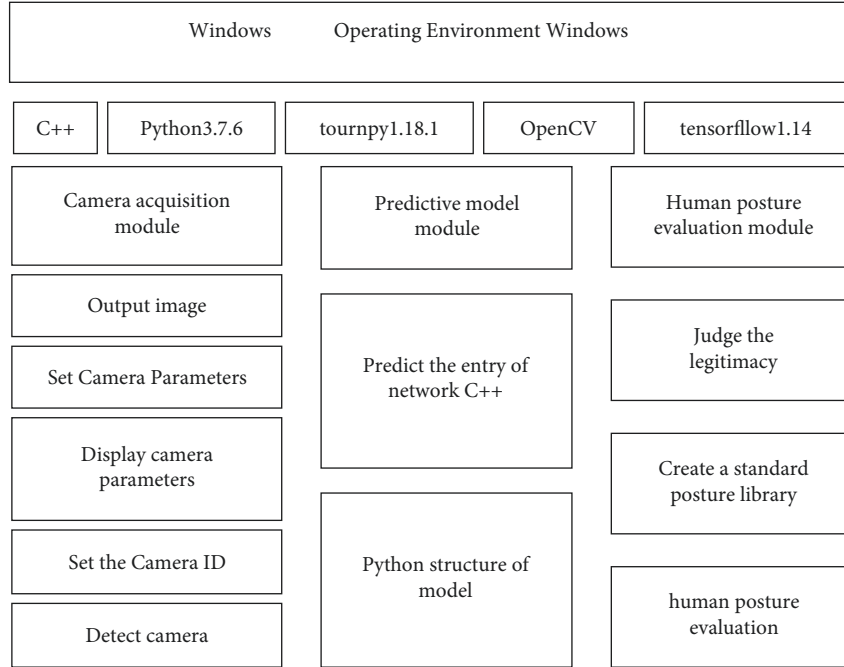


FIGURE 11: Software architecture of the human posture evaluation system.

- (iii) Apply formula (14) to solve the included angle value between each vector in the vector set and the positive X -axis and establish the included angle set $\{\theta_0, \theta_1, \dots, \theta_{11}\}$ [15]:

$$\theta_i \begin{cases} \cos^{-1} \left(\frac{\vec{t}_i \cdot \vec{y}}{\|\vec{t}_i\| \cdot \|\vec{y}\|} \right) t_{iy} \geq 0 \\ \cos^{-1} \left(\frac{\vec{t}_i \cdot \vec{y}}{\|\vec{t}_i\| \cdot \|\vec{y}\|} \right) + 180 t_{iy} < 0 \end{cases}, \quad (14)$$

where θ represents the cosine angle.

3.1.1. Matching with the Standard Posture. The human posture evaluation algorithm divides the human body into four regions, as shown in Figure 6 [16].

Coordinate transformation is performed for the other points in the human posture model relative to the neck points to adjust the corresponding serial number. The right region of the upper limb is composed of the right elbow, right shoulder, and right wrist. The coordinate serial number after adjustment is 0, 1, and 2. The left region of the upper limb is composed of left elbow, left shoulder, and left wrist. The coordinate serial number after adjustment is 3, 4, and 5. The right region of lower limbs is composed of right knee, right hip, and right ankle, and the coordinate serial number after adjustment is 6, 7, and 8. The left region of the lower limbs is composed of the left knee, left hip, and left ankle. The coordinates after adjustment are 9, 10, and 11.

The posture evaluation of each small area in all the regions is to compare the posture to be evaluated with the candidate standard posture of the previous stage. And, the accumulative error is calculated. If the accumulative error does not exceed the allowable error of the stage, the standard posture is included in the candidate standard posture set.

3.2. Human Posture Assessment Process. Combined with the above analysis, the evaluation of human posture is mainly divided into the following steps:

For the right upper limb area (including the right shoulder, the right elbow, and the right wrist), the three vectors between bones and neck, as well as the angle of the positive x axis can be solved, respectively. So, the right upper limb regional similarity sets can be established. Then, the absolute values of similarity degree with corresponding standard attitude are solved, respectively. Finally, the similar standard postures are filtered with the predetermined error values.

For the right lower limb region (including right hip, right knee, and right ankle), the three vectors between the skeleton and the neck, as well as the angle of the positive X axis, are solved, respectively, to establish the regional similarity set of the right lower limb. Then, the absolute values of similarity degree with corresponding standard attitude are solved, respectively. Combining with the predetermined error value, the similar standard postures can be filtered.

For the left upper limb area (including the left shoulder, the left elbow, and the right wrist), the three vectors between bones and neck as well as the angle of the positive x axis can be solved, respectively, so as to set up the similarity sets of the left lower limb region. Then, the absolute values of the similarity degree with the corresponding standard attitude

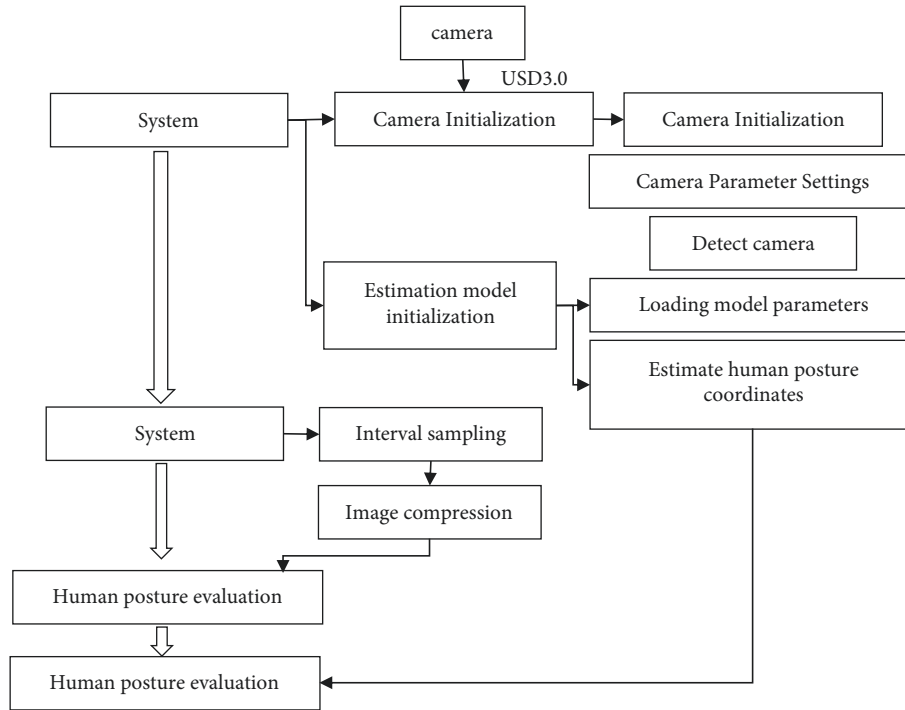


FIGURE 12: System running process.

TABLE 2: Camera hardware parameters.

The parameter name	Recommended parameter
Interface	USB 3.0
Pixel	More than 8 million pixels
Frame rate	More than 60 frames
The focal length	Below 3.1 mm

are solved, respectively. Finally, the similar standard postures are filtered with the predetermined error values.

After the above screening process is completed, the human obtained standard posture is the evaluation result. And, in this process, the cumulatively determined similarity is the evaluation value.

The above process is shown in Figure 7 [17, 18].

To determine the similarity difference in the above matching process, it can be weighted according to the influence degree of different regions on human posture. But this may lead to coupling problem, which means that two different representative values of human posture tend to be consistent after the completion of weighting. Therefore, this paper finally decided to directly output the bone point, evaluation value, and matching standard posture serial number at the end of the matching [19].

Considering that when badminton players hold the racquet with their right hand, their left hand is mainly used for coordination to maintain balance. Therefore, the algorithm in this paper cancels the matching of the left upper limb region. Meanwhile, the weight of the other three regions is optimized. Specifically, the weight of the right upper limb region is the largest, the right lower limb and the left lower limb region are second.

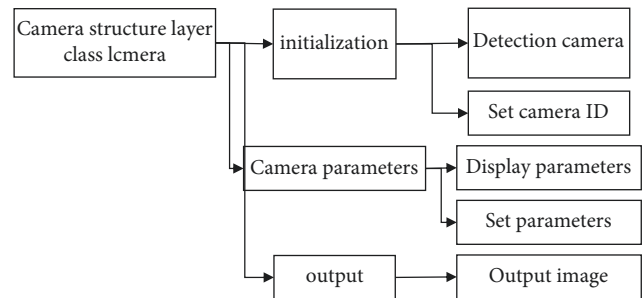


FIGURE 13: Software interface layer of the camera capture module.

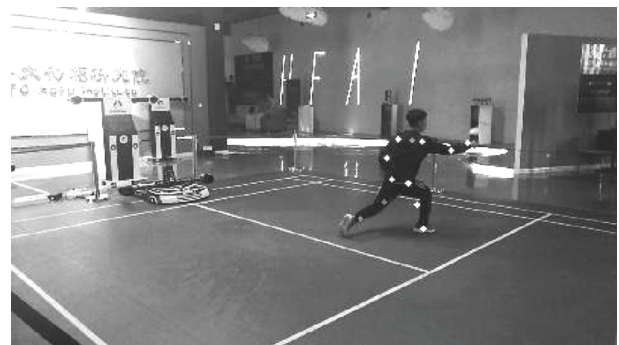


FIGURE 14: Output of stage 4. (a) Confidence map of human limb features. (b) Bone point heat map.

4. Human Posture Evaluator and Evaluation

Figure 8 shows the design idea of human posture evaluation algorithm [20].



FIGURE 15: Evaluation effect display.

- (1) Convert the human bone point coordinate system into the rectangular coordinate system. The vector of each human bone point coordinates to the origin and the angle between the included vector, and the positive x axis is solved.
- (2) Determine the priority of each bone point. According to the size of priority, the margin calculation is made between the selected bone points one by one and the corresponding bone point difference of all posture model in the candidate posture set. Finally, output the cumulative difference value, and after inputting all bone points, step (3) can start.
- (3) Solve the accumulative error. The posture model with the minimum accumulated error is found from the candidate posture set. The output results include the posture model serial number and the accumulative error.

4.1. Matching Result Processing. Through the human posture evaluation, the matched standard human posture serial number and the similarity with the matched standard human posture can be obtained.

The processing procedure of matching results is as follows:

If the output is “-1”, “0,” and “1”, it means that the left area of upper limb “fails to match,” which is the key area of badminton player’s posture matching. Therefore, it can be judged that the athlete’s posture in this frame image does not conform to any posture in the standard library, which means that the athlete’s posture in this frame image is not standard.

If other information is output, the matching result is obtained, and the higher output standard human posture serial number is, the better the matching result is.

5. Method and System Verification

To verify the above method and system, this study attempts to build a badminton posture evaluation system to verify the above methods.

5.1. Method Verification

5.1.1. Data Sources and Training. To verify the above method and system, part of the video image data is selected as the basic data set for verification. Image data are obtained from badminton video, and images collected by camera and human images in COCO data set are used as training data set. The settings of training parameters are listed in Table 1.

Images in the COCO data set are equipped with human limb grayscale images and human bone point grayscale images. The image collected by the camera can become a suitable training data set only after a series of processing. The process is as follows:

- (1) Normalize the collected image to ensure that the pixel value of the image is in the range of $[-0.5, 0.5]$
- (2) Mark the pixel value of each human limbs as 0.5 and save it as the human limbs grayscale
- (3) Mark the pixel value of each human bone point as 0.5 and save it as the human bone point grayscale

In the first training, the model is trained with COCO data set, which ensured that the optimized model can accurately estimate the general human posture. In the subsequent training process, there is no need to use the initial weight, only need to read the weight parameters of the first training. And, the collected images are adopted to carry out training, so as to further improve the evaluation accuracy.

Only reasonably setting the basic learning rate can effectively prevent the problem of excessive learning rate.



FIGURE 16: Frames 138 and 139 (from left to right and top to bottom).

Therefore, the basic learning rate set in this paper is equal to $5e-5$.

5.1.2. Loss Function Curve. After the first training based on COCO data set is completed, the collected images are used for subsequent training. The loss situation after training is shown in Figure 9.

It can be seen that, in the course of multiple training, the loss keeps decreasing trend as a whole. And, the gradient descent tends to be gentle, which finally approaches the optimal solution.

5.1.3. Accuracy and Timeliness of Skeletal Keypoint Estimation. The estimation accuracy of traditional openpose model and structure-optimized openpose model for

each skeletal point is statistically analyzed, and the specific data are shown in Figure 10.

It can be seen from the figure that the estimation accuracy of optimization model is slightly lower than that of the openpose model, and the estimation accuracy of each skeletal point in the left limb is lower than that in the right limb.

5.2. Application Verification. To further verify the feasibility of the above algorithm, an experimental system is set up for verification.

5.2.1. Overall Architecture. The human posture evaluation system consists of camera acquisition module, human posture evaluation module, and prediction model module.

TABLE 3: Records of the frames to be measured and the measured frames.

Video name	Frames to be measured (frame)	Measured frames (frame)	Detection rate
Video 1mmc1	35	23	0.66
Video 2mmc2	34	32	0.94
Video 3mmc3	192	124	0.65
Video 4mmc4	54	33	0.61
Video 5mmc5	23	17	0.74
Video 6mmc6	49	37	0.76

The output result of the system is the matching result and matching loss of human posture and standard posture library in the current frame image. The matching result refers to the highest standard posture with the human posture matching degree in the current frame image, and the matching loss indicates the similarity between the human posture and the standard posture. The overall framework of the human posture evaluation system is shown in Figure 11 [21].

5.2.2. System Operation Process. The operation mechanism of human posture evaluation system is shown in Figure 12 [22].

5.2.3. Camera Acquisition Module. Camera acquisition module includes two parts, namely, hardware parameter and software interface. Among them, the key of hardware parameters is to correctly set the placement angle of the camera and reasonably determine the camera parameters. Combined with the above analysis results, the camera should be placed on the left side of the badminton net and on the right side of the badminton player. In addition, the best height is 1.2 m. The relevant parameters of the camera are listed in Table 2.

The key of the software interface is to make use of the camera interface layer to make the driver compatible, as shown in Figure 13 [23, 24].

ICmera, the base class of this module, stores one worker function and four detection functions.

Above all, the number and ID of cameras used in the human posture assessment system are determined, and the initial deployment is completed. Then, according to the site environment and the requirements for the evaluation, the camera resolution, frame rate, and other parameters are debugged. Therefore, the module sets up two function interfaces, namely, showParam and setParam. Finally, the function work is used to eliminate invalid information in the image information collected, such as resolution, width, height, and so on. The collected image is converted into a unified cv: Mat format.

The base class ICmera is used for compatibility of driver modules of other cameras, and the subsequent evaluation process adopts the form of ICmera. It can be seen that the human posture evaluation system is not sensitive to the camera model. The camera parameters must meet the setting requirements so that the driver can be set by inheriting the base class. If the evaluation is not effective, the function of ICmera can be called to debug the current camera parameters.

5.2.4. Effect Display. Bone point hot spot map: the bone point hot spot map output is shown in Figure 14.

The evaluation effect achieved by the human posture evaluation system in the test stage is shown in Figure 15.

Effect display: the human posture evaluation algorithm proposed in this paper is used to match successive single frame images. The frames 138 to 139 are successfully matched to the standard posture. The evaluation effect of these 8 frames is shown in Figure 16.

The analysis of Figure 15 shows that first, "Frame i: matching failure," which means that the image in frame I failed to match the standard posture. Second, "Frame i: ending stage A, matching standard posture serial number B, matching loss X," which indicates that the serial number of bone point at the exit of frame i matching is A. It successfully matched with standard posture serial number B, and the loss value of the two is X.

5.2.5. Detection Rate. The human posture evaluation system is used to evaluate the posture of 6 videos. The number of the frames to be tested and the measured frames in each video are shown in Table 3.

6. Conclusion

To sum up, through the above design, the application of the openpose neural network in the actual sports is realized, so as to provide a new reference method for the accurate training of sports. The innovation of this paper is the accuracy improvement of attitude estimation. At the same time, through the collection of badminton movements, the real-time estimation of badminton posture movements is realized, which provides a reference way for the application of this method.

Data Availability

The experimental data used to support the findings of this study are available from the corresponding author upon request.

Conflicts of Interest

The authors declare that they have no conflicts of interest regarding this work.


References

- [1] A. Nadeem, J. Ahmad, and K. Kim, "Automatic Human Posture Estimation for Sport Activity Recognition with

- Robust Body Parts Detection and Entropy Markov model,” *Multimedia Tools and Applications*, vol. 80, no. 14, pp. 1–34, 2021.
- [2] P. Sing, R. Lakshmi, and R. Raajan, “Point cloud human posture estimation using single RGB image,” *Materials Today Proceedings*, vol. 33, pp. 3907–3911, 2020.
- [3] X. Li, S. Liu, Y. Chang, S. Li, Y. Fan, and H. Yu, “A human joint torque estimation method for elbow exoskeleton control,” *International Journal of Humanoid Robotics*, vol. 17, no. 3, p. 17, 2020.
- [4] W. Quan, J. Woo, Y. Toda, and N. Kubota, “Human posture recognition for estimation of human body condition,” *Journal of Advanced Computational Intelligence and Intelligent Informatics*, vol. 23, no. 3, pp. 519–527, 2019.
- [5] X. Zhang, “Application of human motion recognition utilizing deep learning and smart wearable device in sports,” *International Journal of System Assurance Engineering and Management*, vol. 12, pp. 1–9, 2021.
- [6] Bi. Zhuo and W. Huang, “Human action identification by a quality-guided fusion of multi-model feature,” *Future Generation Computer Systems*, vol. 116, pp. 13–21, 2021.
- [7] S. Liu, “Discrete pointv3 3D reconstruction algorithm based human pose estimation,” *Microprocessors and Microsystems*, vol. 82, Article ID 103806, 2021.
- [8] J. Ahmad, A. Israr, and K. Kim, “Human posture estimation and sustainable events classification via pseudo-2D stick model and K-ary tree hashing,” *Sustainability*, vol. 12, no. 23, 9814 pages, 2020.
- [9] L. Gian, A. Russo, A. Naddeo, and N. Cappetti, “A resource constrained neural network for the design of embedded human posture recognition systems[J],” *Applied Sciences*, vol. 11, no. 11, p. 4752, 2021.
- [10] W. Kim, J. Sung, D. Saakes, C. Huang, and S. Xiong, “Ergonomic postural assessment using a new open-source human pose estimation technology (OpenPose),” *International Journal of Industrial Ergonomics*, vol. 84, Article ID 103164, 2021.
- [11] K. Fujiwara and K. Yokomitsu, “Video-based tracking approach for nonverbal synchrony: a comparison of Motion Energy Analysis and OpenPose,” *Behavior Research Methods*, vol. 53, no. 6, pp. 2700–2711, 2021.
- [12] L. Needham, M. Evans, D. Cosker, and S. Colyer, “Can markerless pose estimation algorithms estimate 3D mass centre positions and velocities during linear sprinting activities?” *Sensors*, vol. 21, no. 8, p. 2889, 2021.
- [13] P. Trettenbrein and E. Zaccarella, “Controlling video stimuli in sign language and gesture research: the OpenPoseR package for analyzing OpenPose motion-tracking data in R,” *Frontiers in Psychology*, vol. 12, 2021.
- [14] E. Jensen, V. Lugade, J. Crenshaw, E. Miller, and K. Kaufman, “A principal component analysis approach to correcting the knee flexion axis during gait,” *Journal of Biomechanics*, vol. 49, no. 9, pp. 1698–1704, 2016.
- [15] M. Elhoseny, A. Tharwat, A. Hassanien, and H. Aboul, “Bezier curve based path planning in a dynamic field using modified genetic algorithm,” *Journal of Computational Science*, vol. 25, pp. 339–350, 2018.
- [16] N. Alluri, S. Selvarajan, A. Chandrasekhar, B. Saravanakumar, J. Jeong, and S. Kim, “Piezoelectric BaTiO₃/alginate spherical composite beads for energy harvesting and self-powered wearable flexion sensor,” *Composites Science and Technology*, vol. 142, pp. 65–78, 2017.
- [17] I. Takeda, A. Yamada, and H. Onodera, “Artificial Intelligence-Assisted motion capture for medical applications: a comparative study between markerless and passive marker motion capture,” *Computer Methods in Biomechanics and Biomedical Engineering*, vol. 24, no. 8, pp. 864–873, 2020.
- [18] Y. Tsai, L. Hsu, Y. Hsieh, and S. Lin, “The real-time depth estimation for an occluded person based on a single image and OpenPose method,” *Mathematics*, vol. 8, no. 8, p. 1333, 2020.
- [19] J. Yang, T. Ishikawa, T. Tokoro, T. Nakamura, I. Kijiya, and T. Okayasu, “Effect evaluation of drainage condition and water content on cyclic plastic deformation of aged ballast and its estimation models,” *Transportation Geotechnics*, vol. 30, Article ID 100606, 2021.
- [20] N. Wang, J. Ma, D. Jin, and B. Yu, “A special golden curve in human upper limbs’ length proportion: a functional partition which is different from anatomy,” *BioMed Research International*, vol. 2017, pp. 1–6, 2017.
- [21] U. Kristianto, B. Michae, G. Gurme, and S. Manu, “Using probabilistic fault tree analysis and Monte Carlo simulation to examine the likelihood of risks associated with ballasted railway drainage failure,” *Transportation Research Record*, vol. 2675, no. 6, pp. 70–89, 2021.
- [22] N. Nakano, T. Sakura, K. Ueda et al., “Evaluation of 3D markerless motion capture accuracy using OpenPose with multiple video cameras,” *Frontiers in Sports and Active Living*, vol. 2, p. 50, 2020.
- [23] N. Cappetti and M. Di, “Study of the relationships between articular moments, comfort and human posture on a chair,” *Work*, vol. 68, no. s1, pp. S59–S68, 2021.
- [24] T. Ito, K. Ayusawa, E. Yoshida, and H. Kobayashi, “Evaluation of active wearable assistive devices with human posture reproduction using a humanoid robot,” *Advanced Robotics*, vol. 32, no. 12, pp. 635–645, 2018.

Research Article

Research on the Sound Quality Evaluation Method Based on Artificial Neural Network

Xiedong Song^{1,2,3} and Wei Yang⁴ 

¹College of Technology, Yantai Nanshan University, Yantai 265713, China

²Technology Department, Xiaoxing (Shandong) Internet Technology Co.Ltd, Yantai 264000, China

³College of Computing and Information Technology, National University, Manila 0900, Philippines

⁴School of Digital Creativity and Animation, Shenzhen Polytechnic, Shenzhen 518000, China

Correspondence should be addressed to Wei Yang; yangwei@szpt.edu.cn

Received 8 December 2021; Revised 14 February 2022; Accepted 28 March 2022; Published 5 May 2022

Academic Editor: Man Fai Leung

Copyright © 2022 Xiedong Song and Wei Yang. This is an open access article distributed under the Creative Commons Attribution License, which permits unrestricted use, distribution, and reproduction in any medium, provided the original work is properly cited.

For the improvement of the traditional evaluation effect of the automobile sound quality, an evaluation model of automobile sound quality is constructed based on BP neural network. The first is to introduce the basic principle of the BP neural network in detail. The second is to use the MGC parameters to establish the vehicle interior sound conversion model. The converted sound characteristic parameters are taken into the WORLD model to synthesize the new sound signals. Furthermore, the wavelet decomposition method is used to remove noise from the synthesized sound signals. Finally, a sound evaluation model based on BP neural network is established. The sound quality of automobiles can be better evaluated by carrying out the ABX test and MOS test in the field of sound conversion. For the newly synthesized sound signal and the target sound signal, it can be seen that the newly synthesized sound signal is more inclined to the target sound signal, and the sound quality is better. In addition, the sound quality is tested through loudness, roughness, sharpness, and level A in the field of sound quality evaluation. The final results show that the quality of newly synthesized sound is better, and the average errors of sound signals meet the sound standard. Therefore, the constructed sound conversion model and the sound evaluation model are feasible and effective.

1. Related Work

As science and technology continuously develop, people pay more and more attention to the performance of automobiles, so the noise problem has become one of the important indicators of automobile purchase. The noise of automobiles seriously affects the comfort of the person when riding in the vehicle, also interferes with the communication between people, and even seriously damages the auditory characteristics of human ears. At the same time, vibration and noise are also very different in the automobile sound. Therefore, how to better distinguish vibration and noise, and evaluate the automobile noise, has become the focus of current research. In practice, companies such as Nissan, FEV of Germany, and AVL of Austria are all studying the interior sound quality of electric vehicles. The most influential noise sources and special frequencies have been found. Furthermore, some active or

passive technologies are used to eliminate noise and compensate for frequency, which achieves good results.

In the academic field, Xie et al. proposed an adaptive neural network sound evaluation method. The characteristics of the proposed method are simple and fast. At the same time, they introduced a mainstream neural network algorithm [1]. Yin et al. calculated the dither noise of automobile side windows by using the large eddy simulation method. As can be seen that the variation rules of loudness, sharpness, roughness, and undulation with wind speed and window opening are obtained [2]. Yang et al. adopted binaural transfer path analysis (BTPA) to measure the vibration and noise transmission paths of automobiles under transient and steady-state conditions. Then, the characteristics and differences of the internal noise of automobiles under different operating conditions are studied, where the loudness, sharpness, roughness, and A-weighted sound

pressure level are adopted [3]. Park and Kang established a sound quality index model, which reflects the reviewers' different styles. Also, the model is constructed by utilizing K-means clustering, factor analysis, and multiple linear regression. This study provides an additional reference for the evaluation of sound quality [4]. Zhao et al. proposed a DBN based on linear regression (LR-DBN). There are 6 psychoacoustic indicators and 26 Mel frequency cepstrum coefficients being taken as input characteristics. At the same time, the ordinary DBN, multiple linear regression (MLR), and backpropagation neural network (BPNN) are used to verify the performance of LR-DBN. What can be seen is that compared with other methods, the correlation coefficient of LR-DBN is higher, and the prediction error is lower. Furthermore, LR-DBN is more stable. So, this method is a reliable method for evaluating EEV sound [5]. Wang et al. proposed an objective evaluation method of interior noise, which is based on the displacement of the human basal membrane [6]. Firstly, noise samples of different seats are collected under different running conditions. Secondly, the comparison method of adaptive grouping pairs is used to obtain the subjective evaluation value of noise samples. Thirdly, the total parameter model of the human ear is adopted to calculate the average value for the basal membrane displacement response (SMVBMDR). So, the characteristic matrix based on SMVBMDR is established. Finally, there are two BP neural network models constructed to evaluate the interior noise sound quality respectively. Also, they took the traditional psychoacoustic indicators and extracted the feature matrix as the input. The SMVBMDR is very correlated with SEV. Moreover, the sound quality prediction accuracy of the model based on SMVBMDR is higher.

It can be seen from the above research that the qualitative and quantitative methods are used for the present sound quality evaluation. Also, machine learning algorithms, deep learning algorithms, and other algorithms are introduced. However, the above sound evaluation rarely involves the preprocessing of noise data. In this paper, it is proposed that on the basis of parameter extraction of automobile sound feature extraction, BP is used to synthesize automobile sound, and then evaluate sound according to sound quality evaluation parameters so as to provide a new reference for automobile sound quality evaluation.

2. BP Neural Network

2.1. Introduction. BP neural network is a multilayer feed-forward neural network. It is trained by error back-propagation. In addition, the characteristics of the BP neural network are that the model is clear and the structure is simple. The basic ideas for training the BP neural network model are as follows [7]:

Herein, training sample is defined as $(x_1, y_1), (x_2, y_2), \dots, (x_n, y_n)$, where x represents the input vector, y represents the output vector, and n represents the number of training samples. Supposing that layer $l-1$ and layer l contain m and k nodes, respectively, the output a_j^l of the j th node of layer l can be expressed as formula (1), and the vector

a_j^l composed of the output of layer l can be expressed as formula (2).

$$a_j^l = f(z_j^l) = f \sum_{i=1}^m w_{ji}^l a_i^{l-1} + b_j^l, \quad (1)$$

$$a^l = f(z^l) = f(W^l a^{l-1} + b^l). \quad (2)$$

Among them, w_{ji}^l and b_j^l are the weight and bias of node j from $l-1$ to l layer, respectively; $f(z)$ is the activation function; w^l represents $k \times m$ matrix composed of the l th layer weight; b^l represents $k \times 1$ vector composed of the bias outputs of the l layer.

As can be seen from the above formula that the output vector of each layer in the network can be calculated. Then, the loss function is used to find the appropriate weight matrix and bias vector corresponding to all hidden layers and output layers. The gradient descent method is adopted to continuously update the weight matrix and bias vector. Thus, the best weight matrix and bias vector are obtained. Finally, the optimal weight matrix and bias vector are utilized to predict the predicted value which is closest to the actual value. According to Pan et al. [8], the mean square error function is selected as the loss function. The expressions are as follows:

$$\begin{aligned} \text{MSE} &= \left(\frac{\sum_{i=1}^N (d_i - o_i)^2}{N} \right)^{1/2}, \\ R &= \left(1 - \frac{\sum_{i=1}^N (d_i - o_i)^2}{\sum_{i=1}^N o_i^2} \right)^{1/2}, \end{aligned} \quad (3)$$

where d_i and o_i are the target output and actual output vector of the network respectively, and N is the number of test samples.

The structure of the BP neural network is shown in Figure 1 [9–11]. It includes the input layer, the hidden layer, and the output layer. Neurons at all levels of the network are connected by the way of a full connection layer. The hidden layer is in the middle. It includes multiple layers, but there is no connection relationship between neurons at the same level.

2.2. BP Neural Network Structure. In BP neural network, the number of neurons per layer is associated with the actual number of input and output data. In the hidden layer, too large or too small neurons may prolong the training time. It cannot be fitted well. Therefore, continuous search and testing are required to determine the optimal neurons, and available formulas are expressed as

$$\begin{aligned} m &= \sqrt{n+1} + a, \\ m &= \sqrt{nl}, \\ m &= \log_z n, \end{aligned} \quad (4)$$

Here, m , n , and l are the neurons in the hidden layer, input layer, and output layer, respectively; a is a constant, which ranges from 1 to 10.

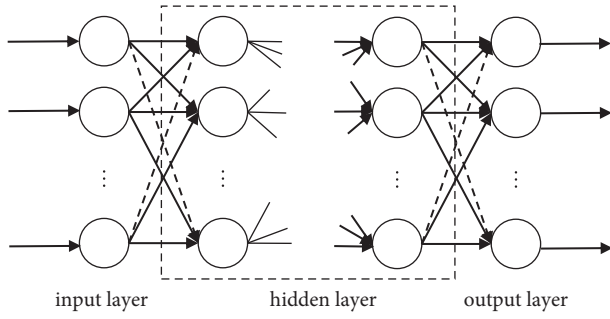


FIGURE 1: Structure of BP neural network.

The input vector and output vector in the BP neural network should be normalized to the range $-1.0\sim 1.0$ so as to effectively avoid the overfitting of output vectors [12–14]. The calculation formulas are as follows:

$$x_{\text{mid}} = \frac{x_{\text{max}} + x_{\text{min}}}{2}, \quad (5)$$

$$\bar{x}_i = \frac{x_i - x_{\text{mid}}}{2(x_{\text{max}} - x_{\text{min}})},$$

The abovementioned formulas show that x_i is the data to be normalized; x_{min} is the minimum value; x_{max} is the maximum value; x_{mid} represents the average value; and \bar{x}_i is the normalized data.

3. Construction of Sound Conversion Model Based on BP Neural Network

3.1. BP Neural Network Sound Conversion Model Based on MGC Parameters. On the basis of the BP neural network, sound characteristic parameters are extracted from the original sound signal through the world sound analysis synthesis system, including one-dimension $lf0$, 60-dimensional MGC parameters, and 5-dimensional bap parameters. Considering that the above three parameters are obtained through the world sound synthesis system and $lf0$ is consistent with the numerical changes of bap parameters, only the 60-dimensional spectrum envelope MGC parameters are performed in modeling training. The BP neural network sound conversion model based on MGC parameters is constructed in this paper, as shown in Figure 2. The neuron number of input and output is 60, the hidden layers are 2, and the neurons of hidden layers is 59 [15–18]. Parameters select the target sound signal value and then place the generated parameters into the WORLD system to synthesize a new sound signal.

Among them, a set of sound signals has 60-dimensional MGC parameters, and one dimension has 117 data, which is represented as $60 * 117$. Here, 45 groups of portable and artificial head data are selected for training, and 5 groups of data are randomly selected as test sets. As the large amount of training data, the parameters are divided into input vector and output vector. For the input vector, there are 45 $60 * 117$ MGC parameters collected by the portable. For output vector, there are 45 $60 * 117$ MGC parameters collected by the artificial head, and the amount of data is large.

Therefore, all of the neurons are 60. In addition, the learning rate of the model algorithm is 0.01; the number of maximum errors is 10; the number of maximum training is 10000, and the accuracy of learning and training is 0.001.

After the transformation model is established, new MGC parameters can be obtained for synthesizing new sounds so as to provide sound parameters for the establishment of subsequent sound evaluation model.

3.2. Sound Signal Denoising Based on Wavelet Decomposition.

In the extraction and synthesis of sound features, the algorithm calculation leads to the sound spectrum decline, frequency offset, resulting in a large amount of noise. These noises will seriously interfere with the quality and evaluation effect of sound signals. Therefore, it is necessary to denoise the transformed and synthesized sound. In this paper, the most widely used wavelet denoising method is adopted. The flow of this method is as follows:

- (1) Decompose the original sound signal $s(n)$ by wavelet. So, the real target sound signal $a(n)$ and noise signal $d(n)$ can be separated;
- (2) Calculate the wavelet coefficients of real sound signals, and remove the wavelet coefficients of noise signals;
- (3) Adopt the inverse transformation method to obtain the new sound signal after wavelet transform so as to complete the denoising of the sound signal.

The formula of an original sound signal with noise signal is

$$s(n) = a(n) + d(n). \quad (6)$$

The formula (6) shows that $s(n)$ is the original sound signal with noise; $a(n)$ is the normal target sound signal; $d(n)$ is the unwanted noise signal. Furthermore, $d(n)$ is subjected to $N(0, \sigma^2)$ distribution, while $a(n)$ is the non-stationary signal subjected to non-Gaussian distribution.

4. Experimental Results and Analysis

After the sound conversion and synthesis, the sound evaluation model based on the field of sound conversion and the automobile sound quality will be established so as to evaluate the new synthetic sound signal better. Then, the subjective evaluation was performed for the field of sound conversion, and the objective parameters of the field of automotive sound quality were used to evaluate the synthetic sound signal.

4.1. Evaluation in the Field of Sound Conversion

4.1.1. Experimental Environment and Data. To achieve better experimental results, this paper selects a meeting room with a strong sound insulation effect in a university for testing, with an indoor temperature of 22°C and the humidity of 45%. Also, the better sound signal can be obtained by using a high-fidelity headphone for sound playback Sennheiser HD650.

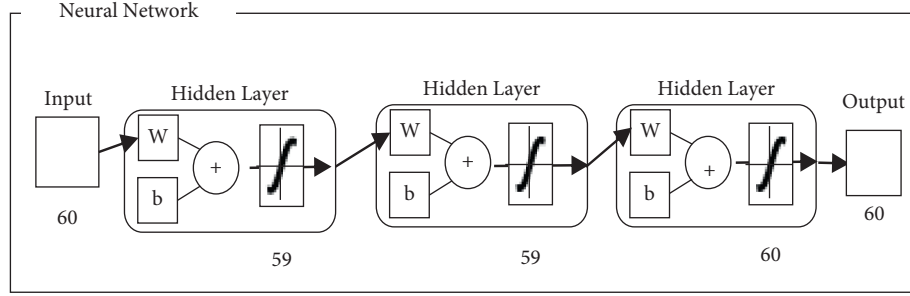


FIGURE 2: The structure of the BP neural network sound conversion model based on the MGC parameters.

The experimental data were derived from 5 healthy and normal hearing postgraduates in a university, including 3 boys and 2 girls.

4.1.2. Test Method. The ABX test and MOS test are adopted to evaluate synthetic sound signals so as to ensure the accuracy of subjective evaluation in the field of sound conversion.

The ABX test is a common method for subjective evaluation of sound conversion. A and B represent the original and target sound signals, respectively, and X represents the converted sound signal. The testing process is to distinguish the similarity between the converted sound signal with the original or target sound signal by different people's subjective auditory feelings. Finally, the probability statistics are used to obtain the ABX score of the system so as to evaluate the conversion performance effect of the system.

ABX calculation process is expressed as [19–21]:

$$ABX = \frac{\sum_{m=1}^M p_m}{M} \times 100\%, \quad (7)$$

where M represents the number of testers and p_m represents the test result. When p_m value is 0, it indicates that the converted sound signal is more similar to the original sound signal. When the p_m value is 1, it indicates that the converted sound signal is more similar to the target sound signal.

The MOS test is also known as average opinion score test. Its main function is to evaluate the tester's overall satisfaction with the converted sound signal. If the MOS test score is high, it indicates that the converted sound signal is up to the standard, and its naturalness and intelligibility are better. The expression is as follows:

$$MOS = \frac{1}{M} \sum_{n=1}^M \text{score}_{n,m}. \quad (8)$$

Here, M represents the total participants in evaluation, N represents the sound signals in the test, and $\text{score}_{n,m}$ represents the evaluation score of the m -th individual on the n th sound signal.

When conducting subjective evaluation experiments, it is necessary to be in a room with a better environment. The temperature of the selected automobile is 22°C, and the humidity is about 45%. In addition, the sound playback selects high-fidelity headphones to obtain a better sound

signal. The sound signals evaluated by the test are mainly four sets of signals obtained through the world sound synthesis system, and the four sets of sound signals correspond to the operating speed of an automobile at 60 km/h, 100 km/h, 30 km/h, and 80 km/h. The four groups correspond to the numbers 1 to 4 in Tables 1 and 2.

The specific evaluation effect is as follows:

(1) ABX test

The results of ABX are shown in Table 1.

According to the above table above, the highest ABX score of the fourth group, reaching 85%, indicates the best effect of this experiment, the lowest ABX score, only 63%; the main reason may be due to too little experimental data. Therefore, the next step is to further expand the amount of data properly. However, comprehensive analysis found that the ABX test score averaged 74%, reaching the experimental standards, with preliminary proof that the newly synthesized sound signal meets the experimental requirements.

(2) MOS test

MOS test results are shown in Table 2.

According to the table, of the four sound signals, the first MOS test score was 4.2, indicating that the experiment was good; the first MOS test score compared with the other three, the lowest score reached only 3, the main reason may be still that the number of data sets is relatively small. The comprehensive analysis shows that the MOS test score was averaged into 3.65, which met the experimental requirements, and preliminarily proved that the newly synthesized sound signal met the experimental requirements. The scoring standards of the MOS test are shown in Table 3.

4.2. Evaluation in the Field of Automobile Sound Quality. First of all, the synthetic sound signal is evaluated by using the objective parameters such as SPL, roughness, loudness, and sharpness [22–24].

Furthermore, the error evaluation is performed between the five groups of synthetic sound signals with the corresponding five groups of portable and five groups of artificial head sound signals. Also, the objective parameters are calculated by LMS Test.Lab.

TABLE 1: ABX test scores.

No.	1	2	3	4
1	0	1	1	1
2	1	0	0	1
3	0	1	1	1
...
30	1	0	1	1
Total	63%	74%	79%	85%

TABLE 2: MOS test scores.

No	1	2	3	4
1	2	3	2	3
2	4	3	4	5
3	1	2	5	4
...
30	5	4	3	5
Total	3	3.4	3.8	4.4

TABLE 3: Scoring standards of MOS test.

Score	Quality evaluation	Distortion degree
5	Excellent	Basically impossible to detect distortion
4	Good	Slightly detect distortion without discomfort
3	Medium	Possible to detect distortion with discomfort
2	Poor	Obnoxious but tolerable
1	Inferior	Obnoxious and intolerable

4.2.1. Roughness. Roughness is a parameter that shows the modulation degree of the sound signal. The unit of roughness value is asper. When the roughness is 1 asper, the sound signal is a sinusoidal pure tone signal with a SPL of 60 dB. Also, beyond that, the frequency is 1 kHz, the modulation amplitude is 1, and the modulation frequency is 70 Hz. It can be seen that the roughness calculation formula is [25]

$$R = 0.3 f_{\text{mod}} \int_0^{24\text{bank}} \Delta L_E(z) dz \text{asper.} \quad (9)$$

Formula (9) shows that f_{mod} represents the modulation frequency, and the unit is kHz. Here, G represents the change value of the excitation stage of a sound signal, expressed as

$$\Delta L_E = 20 \log_{10} \left(\frac{N_{\text{max}}(z)}{N_{\text{min}}(z)} \right), \quad (10)$$

where z represents the critical band Bark number and N_{max} and N_{min} represent the maximum and minimum values of the specified loudness in the feature frequency band for a sound signal, respectively.

As can be seen from the above Figure 3, B, R, and X represent portable, artificial head, and newly synthesized sound signals, respectively. Here, the newly synthesized sound signals were close to the artificial head signals. Using

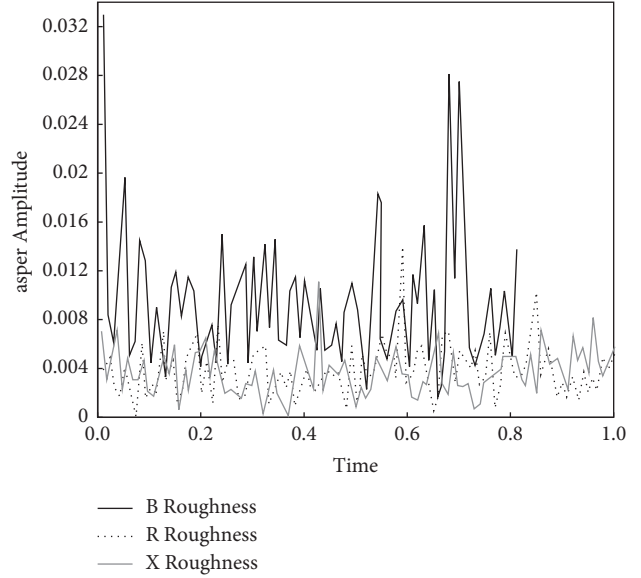


FIGURE 3: Roughness comparison.

LMS Test.Lab to calculate the RMS value, which is found that the portable, artificial head and newly synthesized RMS values are 0.00995 asper, 0.00530 asper, and 0.00494 asper, respectively. The difference between portable and artificial head is 87.74%, while the difference between new synthesized and artificial head is 6.79%. Therefore, the roughness of the newly synthesized sound signal is obviously improved and meets the experimental requirements.

4.2.2. Loudness. Loudness is a parameter proposed to show how the human ear feels about the strength of the sound signal. The magnitude of loudness is determined by the size of the original sound amplitude, which is also associated with the frequency size. The unit of loudness value is expressed as sone (sone). When the loudness value of the sound signal is 1 sone, which means it is a pure sound signal with a SPL of 40 dB, and the frequency size is 1 kHz.

The Zwicker algorithm is commonly used to calculate the loudness, which is expressed as

$$N = 0.08 \left(\frac{E_{TQ}}{E_O} \right) \left[\left(0.5 + 0.5 \frac{E}{E_{TQ}} \right)^{0.23} \right] - 1. \quad (11)$$

Formula (13) shows that E_{TQ} represents the excitation generated by the listening valve when it is relatively quiet, E_O represents the corresponding excitation under the reference sound intensity $I_0 = 10^{-12} \text{ W/m}^2$, and E represents the corresponding excitation of the sound signal calculated by test. At the characteristic frequency band Bark from 0 to 24, performing the integral operation for the feature loudness to obtain the value of the total loudness, and the expression is as follows:

$$N = \int_0^{24\text{bank}} N'(z) dz. \quad (12)$$

Here, N is the total loudness, namely the calculation model of steady-state sound signal loudness.

As can be seen from Figure 4, B, R, and X represent portable, artificial head, and newly synthesized sound signals, respectively. Here, the newly synthesized sound signals are between the portable signals and the artificial head signals. Also, using LMS Test.Lab to calculate the RMS value finds that the portable, artificial head and newly synthesized RMS values are 0.63 sone, 1.24 sone, and 0.95 sone, respectively. In addition, the error of portable and artificial head is 49.19%, and the error of new synthesized and the artificial head is 23.39%, indicating that the loudness of the new synthesized sound signal is significantly improved and reaches the experimental standard.

4.2.3. Sound Pressure Level (SPL). The sound pressure level is one of the important methods to express subjective feelings of loudness. In ANSI S1.8 (1989) and ANSI S1.13 (1995), the sound pressure level is calculated as

$$\text{SPL} = 20 \log_{10} \left(\frac{p_e}{p_{\text{ref}}} \right) \text{dB}. \quad (13)$$

The formula (13) shows that in SPL, p_e represents the effective sound pressure value for testing sound signals, and p_{ref} represents the sound pressure size, that can be heard by human ears in a stable condition, whose sound signal is 1 KHZ. In addition, this sound pressure value is also the audible threshold value. The reference sound pressure refers to the minimum root mean square sound pressure. In other words, at standard atmospheric pressure, and when $p_{\text{ref}} = 2 \times 10^{-5}$ pa, the subjective perception of sound intensity by human ear is not very closely related to the sound pressure level itself. If the loudness increases, the sound pressure level will increase in a logarithmic speed. The expression of Stevens extracting the power relation of both is

$$L = kI^{0.3}, \quad (14)$$

where L represents the perceived loudness of the ear, k represents the coefficient of each subject, and I represents sound intensity.

As can be seen from the comparison diagram, B, R, and X also represent portable, artificial head, and newly synthesized sound signals, respectively. It can be found from Figure 5 that the new synthesis is between the portable signals and the artificial head signals. The RMS values of the three are 47.86 Pa, 45.32 Pa, and 44.98 Pa, respectively. The error of portable and artificial head is 5.60%, and the error of new synthesis and human foreman is 0.75%. It indicates that the A sound level of the newly synthesized sound signal is further improved to meet the requirements.

4.2.4. Sharpness. Sharpness is an objective parameter. It emphasizes the sharpness of sound signal and mainly shows the proportion of high-frequency signal in the total sound spectrum. In a sound signal, the larger the proportion of high-frequency components, the greater the loudness value, and the greater the sharpness of this sound signal.

The unit of sharpness value is acum, and the sound signals with a sharpness of 1 acum are a narrow band noise signal with

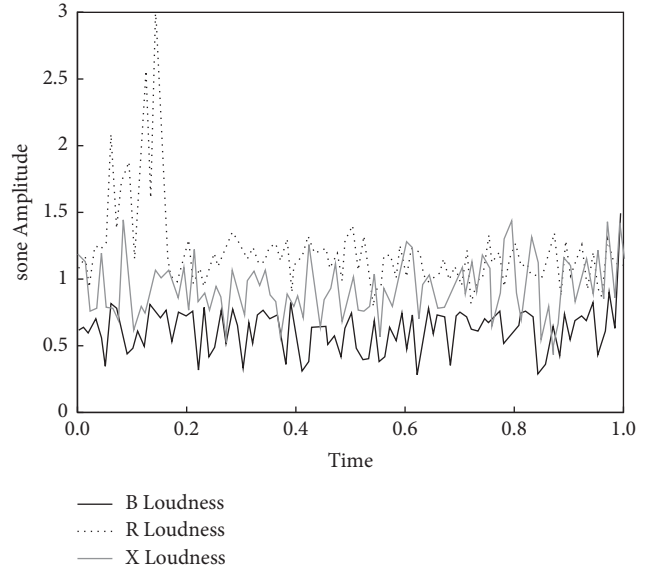


FIGURE 4: Loudness comparison.

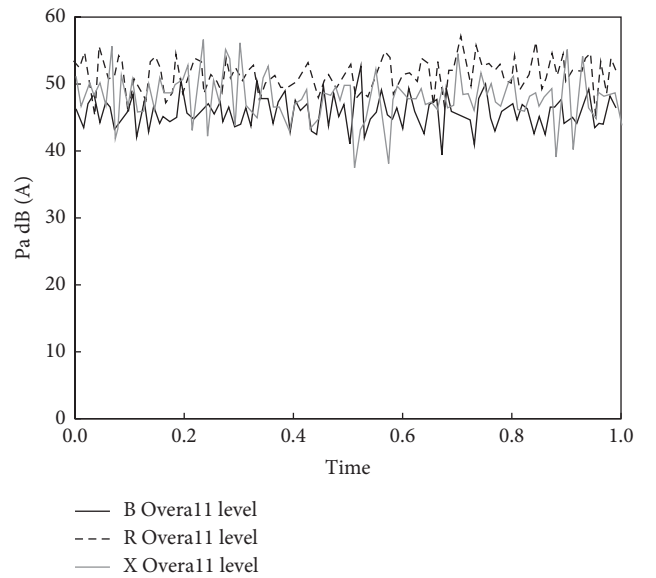


FIGURE 5: Sound pressure level comparison.

a sound pressure level 60 dB. The center frequency size is 1 kHz, and the bandwidth size is 160 Hz. The solution method of sharpness is to conduct the weighted integral calculation for the total loudness and the spectrum response of the critical frequency band, and the expression formula is

$$S = 0.11 \frac{\int_0^{24\text{bark}} N'(Z) \cdot Z \cdot g(Z) dZ}{\int_0^{24\text{bark}} N'(z) dz} \text{acum}, \quad (15)$$

$$g(z) = \begin{cases} 1, & z \leq 16, \\ 0.06e^{0.17z}, & 16 < z \leq 24. \end{cases}$$

Among them, z represents the critical frequency bands number; $N'(z)$ represents the characteristic loudness

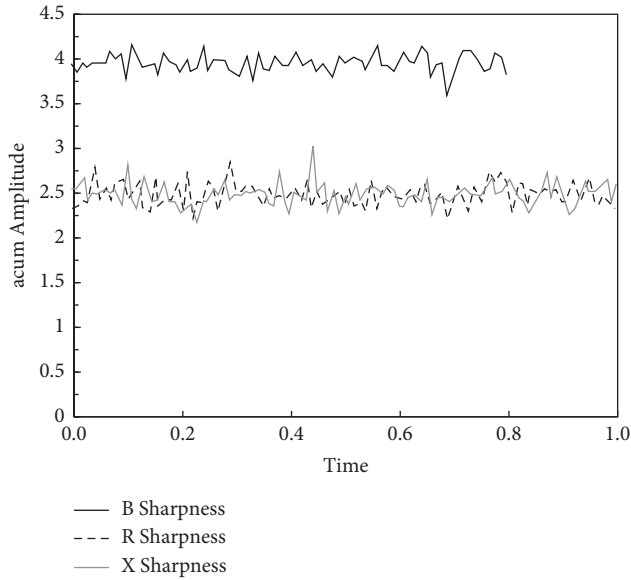


FIGURE 6: Sharpness comparison.

TABLE 4: Grade 10 evaluation scale.

Adjective	Review score
Remarkable	10
Great	9
Very good	8
Satisfied	7
Acceptable	6
Need to improve	5
Offensive	4
Very disgusting	3
Disturbing	2
Intolerable	1

function and $g(z)$ represents the weighting function when the critical frequency band of sound is high. Its numerical change is mainly affected by the critical frequency band.

As can be seen from the sharpness comparison in Figure 6, the newly synthesized sound signal is adjacent to the artificial head signal, and the RMS value can be calculated by LMS Test.Lab. The portable, artificial head and newly synthesized RMS values are 6.54 acum, 2.47 acum, and 2.47 acum, respectively. The error of portable and artificial head is 43.32%, while the error of new synthesized and artificial head is 0.00%, indicating that the sharpness of the new synthesized sound signal is further improved and reaches the experimental standard.

The above evaluation is based on a single index to evaluate the sound inside the automobile, which is obviously not objective enough. On the basis of single index evaluation, a comprehensive evaluation method is proposed to evaluate the new synthetic automobile sound. As the units of above indicators are different and belong to different levels, the following ideas are adopted in the comprehensive evaluation: Firstly, 32 different evaluators are invited to evaluate the new synthetic interior sound signals according to the grade standards in Table 4 and scored them one by one so as to obtain the overall evaluation of new synthetic sound.

TABLE 5: Evaluation results of synthetic sound.

Evaluating indicator	Average score
Roughness	7
Loudness	8
Sound pressure level	9
Sharpness	8
Overall average score	8

At the same time, the test is conducted in a closed environment to avoid interference from the external environment. The number of tests is 10, and the final results are averaged. Based on the abovementioned tests, the obtained results are shown in Table 5.

As can be seen from the above scores, the overall average score of the four indicators is 8, which belongs to the great level. It shows that the synthesized sound can be accepted by the evaluator and get a better evaluation.

5. Conclusion

To sum up, the sound quality evaluation model based on BP neural network constructed in this paper is feasible. The model can effectively evaluate the sound signals of new synthetic, portable, and artificial heads. Also, after testing through subjective evaluation and objective parameters, it is found that the newly synthesized sound signal is very close to the target sound signal, with an average error of less than 10%. As can be seen that in the field of sound quality evaluation, the newly synthesized sound is up to the design standards of this paper. However, due to the limitation of conditions, there are still some shortcomings. The main reason is that there are too few data sets elected in the conversion model, which results in that the final test data may have a low monitoring score. It provides a more comprehensive evaluation method for the research and synthesis of automobile sound.

Data Availability

The experimental data are available from the corresponding author.

Conflicts of Interest

The authors declare that they have no conflicts of interest regarding this work.

References

- [1] X. Xie, Z. Ma, J. Ye, F. Zeng, W. Fan, and B. Chen, "Research and development of sound quality in portable testing and evaluation system based on self-adaptive neural network," *Applied Acoustics*, vol. 154, pp. 138–147, 2019.
- [2] S. Yin, Z. Gu, Y. Zong, L. Zheng, Z. Yang, and T. Huang, "Sound quality evaluation of automobile side-window buffeting noise based on large-eddy simulation," *Journal of Low Frequency Noise, Vibration and Active Control*, vol. 38, no. 2, pp. 207–223, 2019.
- [3] Z. Yang, H. Feng, and S. Lu, "Sound quality evaluation of automobile interior noise under transient and steady-state

- running conditions,” *Journal of the Acoustical Society of America*, vol. 145, no. 3, p. 1882, 2019.
- [4] J. H. Park and Y. J. Kang, “Evaluation index for sporty engine sound reflecting evaluators’ tastes, developed using K-means cluster Analysis,” *International Journal of Automotive Technology*, vol. 21, no. 6, pp. 1379–1389, 2020.
- [5] B. Zhao and C. J. Wu, “Sound quality evaluation of electronic expansion valve using Gaussian restricted Boltzmann machines based DBN,” *Applied Acoustics*, vol. 170, Article ID 107493, 2020.
- [6] Z. Wang, P. Li, H. Liu, J. Yang, S. Liu, and L. Xue, “Objective sound quality evaluation for the vehicle interior noise based on responses of the basilar membrane in the human ear,” *Applied Acoustics*, vol. 172, Article ID 107619, 2021.
- [7] S. D. Loreto, F. Serpilli, V. Lori, and S. Squartini, “Sound quality evaluation of kitchen hoods,” *Applied Acoustics*, vol. 168, Article ID 107415, 2020.
- [8] J. Pan, X. Cao, D. Wang, and J. Chen, “Vehicle interior sound quality evaluation index selection scheme based on grey relational analysis,” *Fluctuation and Noise Letters*, vol. 19, no. 3, Article ID 2050031, 2020.
- [9] T. Feng, Y. Sun, Y. Wang, P. Zhou, H. Guo, and N. Liu, “Sound feature space effects on the performance of annoyance evaluation model based on support vector machine,” *Applied Acoustics*, vol. 154, pp. 99–113, 2019.
- [10] Y. Lu, Y. Zuo, H. Wang, and C. Wu, “Sound quality prediction for power coupling mechanism of HEV based on CEEMD-HT and RVM,” *Neural Computing & Applications*, vol. 33, no. prepublish, pp. 1–16, 2020.
- [11] S. Xu, Z. Lin, G. Zhang, T. Liu, and X. Yang, “A fast yet reliable noise level estimation algorithm using shallow CNN-based noise separator and BP network,” *Signal, Image and Video Processing*, vol. 14, no. prepublish, pp. 1–8, 2019.
- [12] M. Chen, B. Peng, S. Huang, and P. K. L. Chan, “Understanding the meniscus-guided coating parameters in organic field-effect-transistor fabrications,” *Advanced Functional Materials*, vol. 30, no. 1, 2020.
- [13] Image and Video Processing, “New findings in image and video processing described from School of Information Engineering (A fast yet reliable noise level estimation algorithm using shallow CNN-based noise separator and BP network),” *Journal of Technology*, vol. 14, 2020.
- [14] S. Xiaojun and L. Yalin, “Research on financial early warning of mining listed companies based on BP neural network model,” *Resources Policy*, vol. 73, Article ID 102223, 2021.
- [15] Y. Jiang, Y. Liu, D. Yu, and F. Li, “Defect signal detection of station process pipelines based on the BP neural network,” *IOP Conference Series: Earth and Environmental Science*, vol. 804, no. 4, 2021.
- [16] Y. X. Xie, Y. J. Yan, X. Li, T. S. Ding, and C. Ma, “Fault diagnosis method for scintillation detector based on BP neural network,” *Journal of Instrumentation*, vol. 16, no. 07, 2021.
- [17] S. Skoda, A. Fiebig, F. B. Schulte, and J. B. Schweitzer, “How does the focus of attention influence the sound quality evaluation of a complex auditory scene?” *INTER - NOISE and NOISE - CON Congress and Conference Proceedings*, vol. 255, no. 2, p. 5457, 2017.
- [18] C. Ma, C. Chen, Q. Liu et al., “Sound quality evaluation of the interior noise of pure electric vehicle based on neural network model,” *IEEE Transactions on Industrial Electronics*, vol. 64, no. 12, pp. 9442–9450, 2017.
- [19] M. Moravec, G. Ižariková, P. Liptai, M. Badida, and A. Badidová, “Development of psychoacoustic model based on the correlation of the subjective and objective sound quality assessment of automatic washing machines,” *Applied Acoustics*, vol. 140, pp. 178–182, 2018.
- [20] T. Masayuki, K. Iida, T. Shoki, and S. I. Iwamiya, “Sound quality evaluation of noise emitted from brush cutters,” *INTER - NOISE and NOISE - CON Congress and Conference Proceedings*, vol. 258, no. 6, pp. 1238–1248, 2004.
- [21] J. Zhang, S. Xia, S. Ye et al., “Sound quality evaluation and prediction for the emitted noise of axial piston pumps,” *Applied Acoustics*, vol. 145, pp. 27–40, 2019.
- [22] Y. Date, N. Yamagiwa, Y. Morimoto, N. Tanimoto, and S. Ishimitsu, “A study on sound quality evaluation method for vehicle using vital information,” in *Proceedings of the INTER-NOISE and NOISE-CON Congress and Conference Proceedings*, pp. 3369–3378, Madrid, Spain, September 2019.
- [23] W. Sung, P. B. Davies, and J. Stuart, “Sound quality evaluation of residential HVAC&R equipment,” *INTER - NOISE and NOISE - CON Congress and Conference Proceedings*, vol. 258, no. 6, pp. 1066–1074, 2018.
- [24] A. Pereda, Y. Miguel, and E. Stumpf, “Parametric aircraft configuration optimization according to ICAO annex 16 certification standards and sound quality evaluation within conceptual aircraft design,” *INTER - NOISE and NOISE-CON Congress and Conference Proceedings*, vol. 258, no. 7, pp. 307–316, 2018.
- [25] H. B. Huang, R. X. Li, M. L. Yang, T. C. Lim, and W. P. Ding, “Evaluation of vehicle interior sound quality using a continuous restricted Boltzmann machine-based DBN,” *Mechanical Systems and Signal Processing*, vol. 84, pp. 245–267, 2017.

Research Article

Construction of Surface Water Pollution Prediction Model Based on Machine Learning

Yuanhong Che,¹ Zhangdong Wei ¹ and Jing Wen ²

¹Miami College of Henan University, Kaifeng 475002, Henan, China

²Hunan Career Technical College Nonferrous Metal, Zhuzhou, Hunan 412006, China

Correspondence should be addressed to Zhangdong Wei; 10380012@vip.henu.edu.cn and Jing Wen; wenjing@cumt.edu.cn

Received 4 March 2022; Revised 24 March 2022; Accepted 7 April 2022; Published 28 April 2022

Academic Editor: Hangjun Che

Copyright © 2022 Yuanhong Che et al. This is an open access article distributed under the Creative Commons Attribution License, which permits unrestricted use, distribution, and reproduction in any medium, provided the original work is properly cited.

Existing prediction models have low prediction accuracy for surface water pollution with many influencing factors. Taking algal bloom prediction as the entry point of surface water pollution research, LASSO-LARS algorithm is adopted to select the main factors affecting algal bloom variables. At the same time, combined with BP neural network in machine learning, a surface water pollution prediction model based on machine learning is proposed. The results show that the proposed method can accurately predict the algal blooms by using the BP neural network algal bloom prediction model, where the LASSO-LARS algorithm is used to select the variables, such as water temperature, pH, transparency, conductivity, dissolved oxygen, ammonia nitrogen, and chlorophyll a, as model inputs, and the relative error of prediction is less than 5.2%. Thus, the proposed method has certain validity and practical application value.

1. Related Work

Surface water is an important water resource. However, with the acceleration of urbanization, the problem of water pollution is becoming more and more serious, which seriously affects the safety of human domestic water. In recent years, the problem of water quality safety has received attention from all walks of life. In order to continuously improve water quality and strengthen the safety of domestic water, various water treatment technologies and water management methods have emerged. Zhao et al. proposed an in situ loading method for the preparation of nanofiber composite aerogel by using aromatic nanofibers (ANFs) and prepared a high-performance 3D ANF/MnO₂ composite aerogel that can contain more than 90% Pb²⁺ in water, which provides a promising insight for the treatment of Pb²⁺ in water pollution [1]. Ma et al. combined chitosan base modified polymer (MCS) with Fe₃O₄ and SiO₂ by silane coupling agent and successfully prepared a new type of recyclable covalently bonded magnetic flocculant (FS-MC), which can effectively remove emulsified oil in water [2]. Huang et al. used polydimethylsiloxane (PDMS) as the

dispersing phase and glutaraldehyde as the crosslinking agent, and Pickering emulsion stabilized by chitin nanofiber (ChNF) was adopted to prepare hydrophobic aerogel. Nonaqueous phase HOCs are selectively removed from water. It has broad application prospect in water treatment related to HOCs [3]. Saima prepared nitrogen-doped graphene oxide (NGO) nanocomposites (NGO/BQDS-TiO₂) and bismuth oxide quantum dot (BQD)-doped TiO₂ composite photocatalyst, which are used to degrade 2, 4-dichlorophenol (2, 4-DCP) and other organic pollutants and stable dyes [4]. Sun et al. prepared a new type of surface molecularly imprinted polymer (SMIP), which can achieve selective separation and recovery of metal complex dyes in wastewater, providing a theoretical basis for the treatment of metal complex dyes in wastewater [5]. Saravanan et al. [6] discussed the treatment methods of various pollution sources such as heavy metals, dyes, pathogens, and organic matter in water pollution from physical, chemical, and biological aspects and believed that membrane separation and adsorption methods were more suitable for water pollution control. Doyle and Wu et al. prepared polyvinylidene fluoride (PVDF) composite ultrafiltration membrane (PGA

membrane) by blending modification of GO and adsorption and filtration of silver carbonate (Ag_2CO_3) on the membrane surface, which can improve the anti-fouling performance and permeability of PVDF ultrafiltration membrane and effectively treat the slightly polluted surface water [7, 8]. As can be seen, the current research on water pollution is mainly focused on water pollution treatment, and there are fewer studies on prediction. Putri et al. used the Stella model to predict the pollution of the river, and the results show that this method can accurately predict the pollution of each section [9]. Wang et al. proposed a water pollution prediction method based on grey correlation, in which the main influencing factors of water pollution are found out through the grey correlation algorithm, and the water pollution is predicted by white differential equation. The results show that the prediction accuracy of this method is high and the error is small [10]. Wang et al. applied SVM algorithm to water pollution prediction. The results show that this method has good accuracy for small samples and nonlinear data [11]. In addition, the research on water pollution prediction is the key to water pollution treatment. Therefore, in order to better deal with water pollution, LASSO algorithm and BP neural network are adopted to propose a surface water pollution prediction model based on machine learning.

2. Basic Methods

2.1. LASSO Algorithm. LASSO algorithm is a variable selection method. Using the absolute value function of model coefficients as punishment, the regression coefficient is reduced. Moreover, variable selection and parameter estimation are achieved [12]. The main basis of LASSO's algorithm is the accuracy, interpretability, stability, and complexity of variable predictions to the model, and the coefficient of variables is punished. Assume that there are data (x^i, y_i) , $i = 1, 2, \dots, N$, $X^i = (x_{i1}, \dots, x_{ip})^T$ and y_i is the independent variable and response variable corresponding to the observed value i . The linear regression model can be expressed as follows:

$$y_i = a_i + \sum_{j=1}^p \beta_j x_{ij} + \varepsilon_i, \quad \varepsilon_i \in N(0, \sigma^2). \quad (1)$$

Generally, in regression structures, conditions of y_i and x^i are independent [13]. Therefore, x_{ij} is assumed to be standardized; then, there are

$$\begin{aligned} \frac{1}{N} \sum_j x_{ij} &= 0, \\ \frac{1}{N} \sum_j x_{ij}^2 &= 0. \end{aligned} \quad (2)$$

When $t \geq 1$, LASSO's estimate is

$$(\hat{\alpha}, \hat{\beta}) = \arg \begin{cases} \min_{\beta} \sum_i \left(y_i - a_i - \sum_i \beta_j x_{ij} \right)^2, \\ \text{s.t.} \quad \sum_j |\beta_j| \leq t. \end{cases} \quad (3)$$

Although LASSO algorithm has some advantages in theory compared with traditional variable selection methods such as partial least squares method and principal component analysis method, it has the problem of large computation [14]. To solve this problem, Efron reselects variables on each regression residual to reduce the residual, and LARS algorithm is proposed to reduce the computation of LASSO algorithm [15]. Therefore, the LASSO-LARS algorithm is used to select influencing factor variables of surface water pollution.

2.2. BP Network. BP neural network is a typical neural network, which carries out network training through error backpropagation. Its basic structure is shown in Figure 1, consisting of three layers: input layer, output layer, and hidden layer [16, 17].

Assume that the input vector is $x_i = (x_1, x_2, \dots, x_M)^T$, the output vector is $O_j = (y_1, y_2, \dots, y_J)^T$, and the connection weights between input layer and hidden layer and between hidden layer and output layer are ω_{mi} ($i = 1, 2, \dots, I$) and ω_{ij} ($j = 1, 2, \dots, J$), respectively. Therefore, for hidden layer, there are

$$y_i = f(\text{net}_i), \quad i = 1, 2, \dots, I, \quad (4)$$

$$\text{net}_i = \sum_{l=1}^M x_l \omega_{li}, \quad i = 1, 2, \dots, I. \quad (5)$$

For output layer, there are

$$o_k = f(\text{net}_k), \quad k = 1, 2, \dots, J, \quad (6)$$

$$\text{net}_k = \sum_{i=1}^I y_i \omega_{ik}, \quad k = 1, 2, \dots, J. \quad (7)$$

In formulas (4) and (6), $f(x)$ is the transfer function, which usually is sigmoid function and expressed as [18]

$$f(x) = \frac{1}{1 + e^{-x}}. \quad (8)$$

The derivative function is

$$f'(x) = f(x)(1 - f(x)). \quad (9)$$

BP neural network adopts the gradient descent method to adjust weights, and the adjustment formula is [19]

$$\begin{cases} \Delta \omega_{ik} = \eta \delta_{ik}^{\omega} y_i, \\ \Delta \omega_{li} = \eta \delta_{li}^{\omega} x_l. \end{cases} \quad (10)$$

Based on the above analysis, it can be seen that the LASSO-LARS algorithm can ideally select the factor variables affecting surface water pollution, which determines the main influencing factors for accurate prediction of surface water pollution. However, the BP neural network has the characteristics of fast search speed and strong local optimization ability [20]. Therefore, variables selected by LASSO-LARS algorithm are taken as the input of prediction model, and a surface

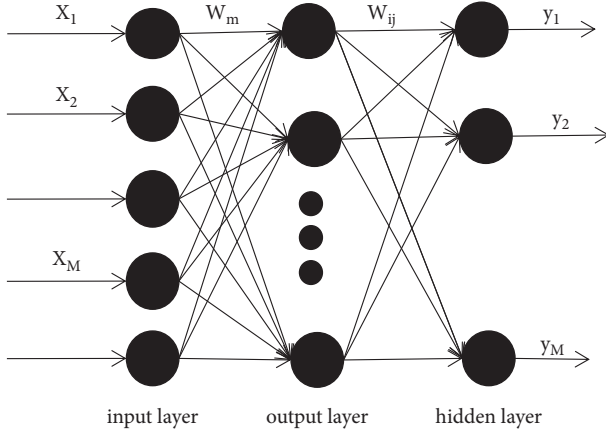


FIGURE 1: Basic structure of BP neural network.

water pollution prediction model based on BP neural network is constructed.

3. Surface Water Pollution Prediction Model Based on Machine Learning

3.1. Selection of Influencing Factor Variables of Surface Water Pollution Based on LASSO-LARS. Algal bloom is one of the main causes of surface water pollution. Algal bloom pollution is taken as a representative to explore surface water pollution prediction based on machine learning. There are many factors affecting algae blooms, including 234 indexes such as water temperature, dissolved oxygen, and metal ions [21]. Among them, 16 indexes such as water temperature, transparency, and chlorophyll a, as shown in Table 1, are the main factors affecting algae blooms [22].

As can be seen, the above 16 indicators are selected as available variables, and logarithmic processing is performed on them, which are represented as $\ln Y, \ln X_1, \ln X_2, \dots, \ln X_{16}$. Moreover, the established linear model is shown as follows:

$$\ln Y = a_0 + a_1 \ln X_1 + a_2 \ln X_2 + \dots + a_{16} \ln X_{16} + \varepsilon, \quad (11)$$

where a_0 is the constant term; a_1, \dots, a_{16} represent the variable coefficient; and ε is the random disturbance term.

LASSO-LARS algorithm is used to calculate the above influencing factors. According to the Akaike information criterion, the smaller the statistical value is, the easier the optimal solution is [23]. Figure 2 shows the values of the variables for which the current model is optimal. $X_1, X_3, X_5, X_7, X_9, X_{12}$, and X_{14} have a great influence on algae blooms, namely, water temperature, pH, transparency, conductivity, dissolved oxygen, ammonia nitrogen, and chlorophyll a. Therefore, the above 7 variables are selected as the main factor variables of algae blooms in surface water.

3.2. Surface Water Pollution Prediction Model Based on BP. Based on the above factors and BP network selected by LASSO-LARS, the construction process of algal outbreak prediction model is designed as follows.

TABLE 1: Selection and definition of influencing factor variables of algae blooms.

Variable name	Variable definition
X1	T (°C)
X2	Fe (mg/L)
X3	pH
X4	Mn (mg/L)
X5	SD (m)
X6	Cu (mg/L)
X7	Sp Cond ($\mu\text{s}/\text{cm}$)
X8	Zn (mg/L)
X9	DO (mg/L)
X10	TN (mg/L)
X11	TP (mg/L)
X12	NH_4^+ (mg/L)
X13	Cd (mg/L)
X14	Chlorophyll a (mg/L)
X15	Pb (mg/L)
X16	Hg (mg/L)

3.2.1. Determination of Sample. The collected surface water quality data can be divided into training sample set and test sample set according to certain rules. Among them, the training sample set is used for BP neural network learning and training, so as to obtain an optimal BP neural network prediction model. The test sample set is used to verify whether the prediction model constructed by the test can achieve the ideal prediction effect for unfamiliar data.

3.2.2. Determination of Network Structure. In general, the standard three-layer BP neural network can achieve relatively accurate prediction [24]. Therefore, three-layer network structure is adopted to construct the prediction model. According to the 7 factors influencing algae blooms selected by LASSO-LARS, the number of neurons in the input layer of BP neural network prediction model can be determined to be 7. Since the algal Q index is the main indicator to measure the extent of algal blooms, the algal Q index is used as the model output [25], and the number of neurons in the output layer is 1. The number of neurons n in the hidden layer can be determined by formula (12). After repeated training, it can be seen that $n=3$.

$$n = \sqrt{P + Q} + \alpha, \quad (12)$$

where n is the number of neurons in the hidden layer, P and Q represent the number of neurons in the input and output layer, and $\alpha \in [1, 10]$.

3.2.3. Data Preprocessing. Due to the different dimensions of different data types in the sample dataset, the input requirements of BP neural network prediction model are not met, and there are problems such as missing values, which affect the final prediction effect of the model. Therefore, before the sample is input into the model, the data need to be preprocessed by normalization, standardization, missing value filling, and so on.

TABLE 2: Variable selection based on LASSO-LARS.

Coefficient	1	2	3	4	5	6	7	8	9	10
α_1	0	0.311	0.317	0.319	0.682	0.557	0.56	0.542	0.542	0.53
α_2	0	0	0	0	0	0.11	0	0	0	0
α_3	0	0	0	0	0	0	0.14	0.126	0.128	0.116
α_4	0	0	0	0	0	0	0	0.026	0	0
α_5	0	0	0	0	0	0	0	0.006	0.004	0.002
α_6	0	0	0	0	0	0	0	0	0	0
α_7	0	0	0	0	0	0	0	0.008	0.009	0.005
α_8	0	0	0	0	0	0	0	0	0	0
α_9	0	0	0	0	0	0.132	0.137	0.159	0.177	0.196
α_{10}	0	0	0	0	0	0	0.121	0	0	0
α_{11}	0	0	0	0	0.04	0	0	0	0	0
α_{12}	0	0	0	0	0	0	0	0.195	0.185	0.116
α_{13}	0	0	0	0	0	0.014	0	0	0	0
α_{14}	0	0.206	0.329	0.322	0.287	0.297	0.18	0.196	0.208	0.291
α_{15}	0	0	0	0.102	0	0	0	0	0	0
α_{16}	0	0	0	0	0	0	0.003	0	0	0
AIC	2.581	3.476	0.964	0.074	0.056	0.034	0.031	0.026	0.022	0.012

3.2.4. *Model Construction and Prediction.* The BP neural network prediction model can be constructed by calling Newff function in MATLAB software, and then the best prediction model retained through repeated training can be used to predict algal blooms. The specific prediction steps are as follows. According to the 7 main factors affecting the algae outbreak, the prediction variables are established by using the obtained data, and then the prediction variables are input into prediction model to obtain the output of variables, namely, the prediction result.

4. Simulation Experiment

4.1. *Experimental Environment.* MATLAB Newff function is called to construct the surface water pollution prediction model, which is run on Windows 7 operating system, and Premnmx function is called to normalize the input data.

4.2. *Data Sources and Preprocessing.* The experimental dataset is collected from the average array of weekly water quality data of a certain water sample from March to November in Daqing city, Heilongjiang Province, from 2003 to 2020 (a total of 648 groups), and the specific collection work is divided into two parts: on-site monitoring and laboratory testing analysis. Water temperature must be measured in the field, and chlorophyll a must be taken back to the laboratory for testing. In order to make the input data meet the input requirements of model, centralization is performed on the input model data by using formulas (13)–(17); the input model data are normalized by using formula (16); and the output model data are reversely normalized by using formula (17) [26–28].

$$\sum_{i=1}^n y_i = 0, \quad (13)$$

$$\sum_{i=1}^n x_{ij} = 0, \quad (14)$$

$$\sum_{i=1}^n x_{ij}^2 = 1, \quad (15)$$

$$\bar{x}_i = \frac{x_i - x_{\min}}{x_{\max} - x_{\min}}, \quad i = 1, 2, \dots, n, \quad (16)$$

$$x_i = \bar{x}_i (x_{\max} - x_{\min}) + x_{\min}. \quad (17)$$

In formulas (16) and (17), x_i represents the input or output data and x_{\min} and x_{\max} are the minimum and maximum values.

576 groups of preprocessed experimental data from 2003 to 2018 are selected as training datasets, and the remaining 72 groups of data are selected as test datasets.

4.3. *Evaluation Indicators.* Relative error δ is selected as an indicator to evaluate the prediction performance of model, and its calculation method is shown in the following formula:

$$\delta = \frac{\Delta}{L * 100\%}, \quad (18)$$

where Δ is the absolute error, which can be calculated by formula (19), and L is the real value.

$$\Delta = X - L, \quad (19)$$

where X is the measured value and L is the real value.

4.4. Experimental Results

4.4.1. *Variable Selection Result.* To verify the effect of LASSO-LARS algorithm on variable selection, nine groups of water quality data in the first week of each month from March to November 2020 are used to illustrate.

(1) *Water Temperature.* Figure 2 shows the distribution characteristics of water temperature in the first week of each

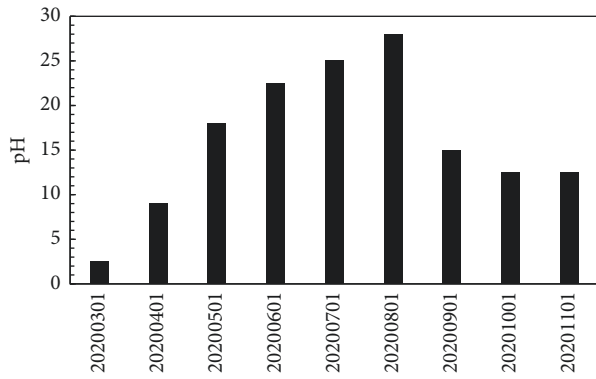


FIGURE 2: Distribution characteristics of water temperature.

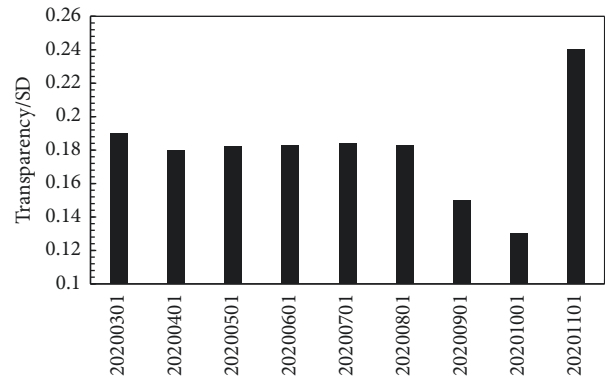


FIGURE 4: Distribution characteristics of transparency.

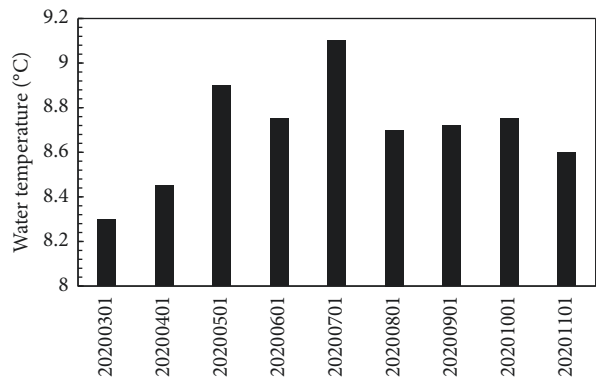


FIGURE 3: Distribution characteristics of pH.

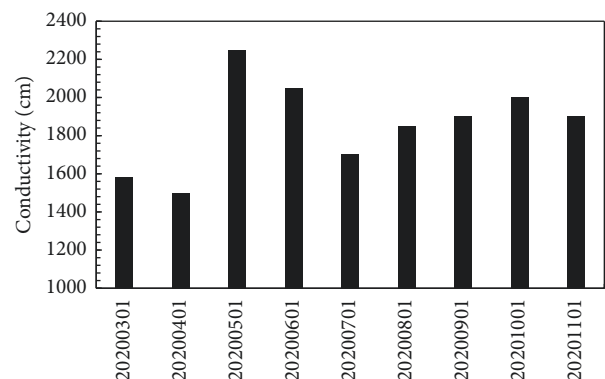


FIGURE 5: Distribution characteristics of conductivity.

month from March to November 2020. As can be seen, the water temperature changes significantly with the seasons. In 2020, the water temperature in this region is below 10°C in March, April, and November and above 10°C from May to September, with an average temperature of 15.42°C. According to the literature, cyanobacteria have certain growth advantages in water temperature of 40°C; Chlorophyta has certain growth advantages in water temperature of 30°C; and diatoms have certain growth advantages in water temperature of 20°C. Overall, the species and quantity of algae are closely related to the water temperature, and the water temperature varies significantly with the season, leading to the seasonal variation of algae species. Thus, there is a strong correlation between water temperature and algal blooms.

(2) *pH*. Figure 3 shows the pH distribution characteristics of water body in the first week of each month from March to November 2020. As can be seen, the pH of the water varies between 8.30 and 9.18, and it is slightly alkaline on the whole.

(3) *Transparency*. Figure 4 shows the transparency distribution characteristics of water body in the first week of each month from March to November 2020. As can be seen, the transparency of this water body is mostly concentrated at 0.18 m, which is generally low. The lowest water transparency is 0.13 m in October, and the highest is 0.24 m in November.

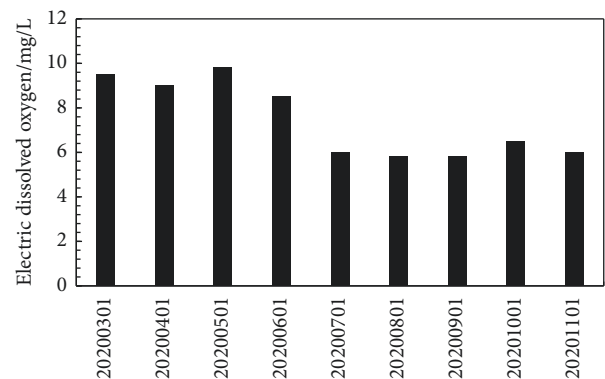


FIGURE 6: Distribution characteristics of dissolved oxygen.

(4) *Conductivity*. Figure 5 shows the conductivity of water body during the study period. In this water environment, the conductivity is generally high, reaching more than 1600 $\mu\text{s/cm}$. The reason is that the selected water is close to the sewage inlet and contains a large amount of industrial wastewater and domestic sewage.

(5) *Dissolved Oxygen*. Dissolved oxygen is an important index of self-clean capacity of the water body, and its concentration reflects the growth of algae. Figure 6 shows the dissolved oxygen concentration of water body in the study area in different periods. As can be seen, the dissolved oxygen concentration of water body presents a wavy

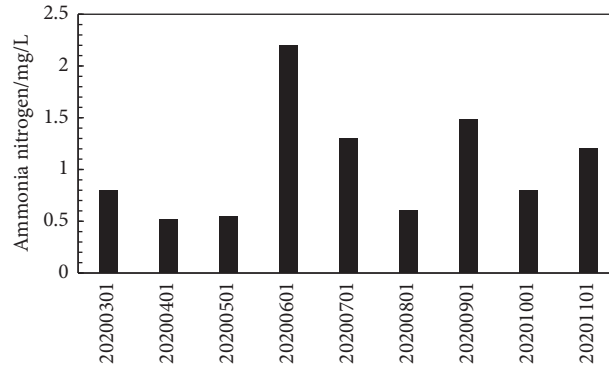


FIGURE 7: Distribution characteristics of ammonia nitrogen.

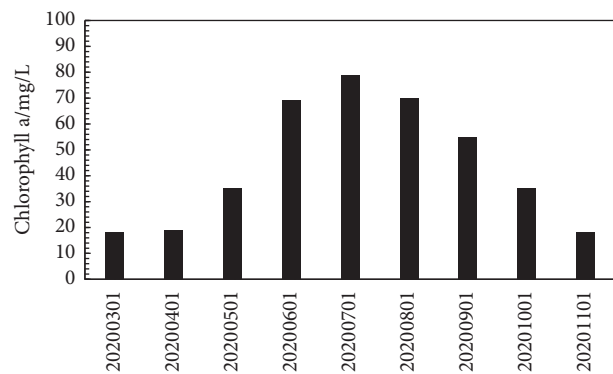


FIGURE 8: Distribution characteristics of chlorophyll a.

TABLE 3: Real values of test sample data.

Time	Water temperature (°C)	pH	Transparency (cm)	Conductivity (μs/cm)	Dissolved oxygen (mg/L)	Ammonia nitrogen (mg/L)	Chlorophyll a (mg/L)	Algal Q index
20200301	2.21	8.31	19	1571	9.51	0.74	17.25	2.54
20200401	9.05	8.47	18	1482	8.92	0.59	18.04	1.34
20200501	17.19	8.87	18.2	2260	9.78	0.63	35.91	1.31
20200601	21.15	8.76	18.35	2055	8.47	2.04	68.58	0.71
20200701	25.23	9.15	18.51	1706	6.02	1.21	78.31	0.57
20200801	27.72	8.71	18.42	1831	5.47	0.59	69.83	0.60
20200901	15.11	8.73	15.24	1936	5.52	1.47	55.05	0.48
20201001	12.46	8.74	13.12	2005	6.32	0.79	34.84	1.85
20201101	8.30	8.61	24.33	1948	5.91	1.12	15.21	2.80

TABLE 4: Comparison between predicted value and real value of the model.

Time	Real value (mg/L)	Predicted value (mg/L)	Absolute error (mg/L)	Absolute error (%)
20200301	2.54	2.64	0.10	4.18
20170401	1.34	1.28	-0.06	4.92
20200501	1.31	1.37	0.06	4.81
20200601	0.71	0.73	0.02	3.68
20200701	0.57	0.54	-0.03	4.73
20200801	0.60	0.63	0.03	4.85
20200901	0.48	0.50	0.02	4.42
20201001	1.85	1.93	0.08	4.71
20201101	2.80	2.65	-0.15	5.19

distribution with seasonal changes, with a variation range of [5.47, 9.78] (unit: mg/L). According to the analysis, when the water surface is wide and agitated, the concentration of dissolved oxygen is high; when the water surface is small and without fluctuation, the concentration of dissolved oxygen is low, and too low dissolved oxygen will lead to the death of a large number of algae and deteriorate the water quality.

(6) *Ammonia Nitrogen*. Figure 7 shows the ammonia nitrogen concentration in water body during the study. As can be seen, ammonia nitrogen concentration in this water body reaches its lowest and highest values in April and June, with obvious seasonal variations.

(7) *Chlorophyll a*. Chlorophyll a concentration is positively correlated with water pollution degree. Figure 8 shows the concentration of chlorophyll a in water body during the study period. It can be seen from the figure that during the study period, the pollution level in the water is high and algae growth is active.

In conclusion, the 7 influencing factor variables selected by LASSO-LARS algorithm are closely related to algae blooms, which indicates that LASSO-LARS algorithm is effective.

4.4.2. Prediction Results of the Model. There are 576 sets of data from the training set adopted to train BP surface water pollution prediction model, and the best prediction model with the minimum error is saved. 72 groups of test data are input into the best prediction model and compared with the real value, and thus the prediction effect of model can be obtained. Due to the large amount of data, only data of the first week of each month from March to November 2020 are presented, as shown in Table 3, and the evaluation indicator values predicted by the model are shown in Table 4. As can be seen from Table 3, the water environment from March to May in 2020 is generally good, with mild pollution and certain tolerance. From June to October, the water quality changed from moderate pollution to severe pollution and eventually returned to moderate pollution. Water body is slightly polluted in November.

As can be seen from Table 4, there is a certain error between predicted value and real value. The absolute error is more than 0.1 in all months except March and November 2020. The relative error is between 3.6% and 5.2%, which is within the allowable error range. Therefore, the proposed prediction model can predict surface water pollution well with high prediction accuracy and good universality.

5. Conclusion

To sum up, the proposed surface water pollution prediction model based on machine learning can accurately predict the algae blooms. Here the BP prediction model is established, and the LASSO-LARS algorithm is utilized to select water temperature, pH, transparency, conductivity, dissolved oxygen, ammonia nitrogen, and chlorophyll a variables as the model input. Furthermore, the relative prediction error

is less than 5.2%, which means that the prediction accuracy is higher. All in all, it provides a theoretical basis for the prediction of surface water pollution. However, due to the limitations of conditions, there are still some problems to be improved. When using BP neural network to construct the surface water pollution prediction model, there are many methods to improve the accuracy of BP network model, for example, optimizing the network parameters by genetic algorithm can improve the prediction accuracy of model to a certain extent. Therefore, to better realize surface water pollution prediction, the next research is to use the above algorithm to improve BP neural network or explore a new prediction model.

Data Availability

The experimental data used to support the findings of this study are available from the corresponding author upon request.

Conflicts of Interest

The authors declare that they have no conflicts of interest.

Acknowledgments

This study was sponsored in part by the Science and Education Joint Project of Hunan Natural Science Foundation (2020JJ7058).

References

- [1] G. Zhao, H. Zhao, L. Shi, B. Cheng, X. Xu, and X. Zhuang, "In situ loading MnO₂ onto 3D Aramid nanofiber aerogel as High-Performance lead adsorbent," *Journal of Colloid and Interface Science*, vol. 600, pp. 403–411, 2021.
- [2] J. Ma, X. Fu, W. Xia et al., "Removal of emulsified oil from water by using recyclable chitosan based covalently bonded composite magnetic flocculant: performance and mechanism," *Journal of Hazardous Materials*, vol. 419, pp. 126529–126539, 2021.
- [3] Y. Huang, H. Sun, and H. Liu, "Fabrication of chitin nanofiber-PDMS composite aerogels from Pickering emulsion templates with potential application in hydrophobic organic contaminant removal," *Journal of Hazardous Materials*, vol. 419, pp. 126475–126485, 2021.
- [4] N. Saima, "Competitive role of nitrogen functionalities of N doped GO and sensitizing effect of Bi₂O₃ QDs on TiO₂ for water remediation," *Journal of Environmental Sciences*, vol. 108, pp. 107–119, 2021.
- [5] Y. Sun, Y. Gu, and Q. Zha, "A novel surface imprinted resin for the selective removal of metal-complexed dyes from aqueous solution in batch experiments: ACB GGN as a representative contaminant," *Chemosphere*, vol. 280, pp. 130611–130617, 2021.
- [6] A. Saravanan, P. Senthil Kumar, S. Jeevanantham et al., "Effective water/wastewater treatment methodologies for toxic pollutants removal: processes and applications towards sustainable development," *Chemosphere*, vol. 280, pp. 130595–130598, 2021.
- [7] S. Doyle, E. Meade, J. Gao et al., "A rapid antimicrobial photodynamic water treatment strategy utilizing a xanthene

- dye with subsequent removal by Goethite Nanoparticles,” *Chemosphere*, vol. 280, pp. 130764–130768, 2021.
- [8] L. Wu, Y. Liu, J. Hu, X. Feng, C. Ma, and C. Wen, “Preparation of polyvinylidene fluoride composite ultrafiltration membrane for micro-polluted surface water treatment,” *Chemosphere*, vol. 284, pp. 131294–131297, 2021.
- [9] F. A. Putri and N. Karnaningroem, “Prediction of water pollution in Kali Surabaya river segment Karangpilang-Ngagel using stella model,” *IOP Conference Series: Earth and Environmental Science*, vol. 259, no. 1, Article ID 012010, 2019.
- [10] R. Wang, F. X. Yang, and G. M. Qu, “Prediction model of agricultural non-point source water pollution based on grey correlation method,” *Nature Environment and Pollution Technology*, vol. 20, no. 2, pp. 633–641, 2021.
- [11] Y. Wang, S. Xue, and J. Ding, “Research on water pollution prediction of township enterprises based on support vector regression machine,” *E3S Web of Conferences*, vol. 228, Article ID 02014, 2021.
- [12] P. Kittisuwan, “Analytical and simple form of shrinkage functions for non-convex penalty functions in fused lasso algorithm,” *The International Journal on Artificial Intelligence Tools*, vol. 29, no. 6, pp. 15–18, 2020.
- [13] J. Lv and M. Pawlak, “Additive modeling and prediction of transient stability boundary in large-scale power systems using the Group Lasso algorithm,” *International Journal of Electrical Power & Energy Systems*, vol. 113, no. C, pp. 963–970, 2019.
- [14] S. Datta, V. A. Dev, and M. R. Eden, “Using correlation based adaptive LASSO algorithm to develop QSPR of antitumour agents for DNA–drug binding prediction,” *Computers & Chemical Engineering*, vol. 122, pp. 28–264, 2019.
- [15] V. Bochkarev, V. Tyurin, A. Savinkov, and B. Gizatullin, “Application of the LASSO algorithm for fitting the multi-exponential data of the NMR relaxometry,” *Journal of Physics: Conference Series*, vol. 1141, no. 1, pp. 012148–012158, 2018.
- [16] B. Ke, H. Nguyen, X.-N. Bui, H.-B. Bui, and T. Nguyen-Thoi, “Prediction of the sorption efficiency of heavy metal onto biochar using a robust combination of fuzzy C-means clustering and back-propagation neural network,” *Journal of Environmental Management*, vol. 293, pp. 112808–112818, 2021.
- [17] S. Jegan, T. B. Pushpa, and R. Gokulan, “Artificial neural network modelling for biodecolorization of Basic Violet 03 from aqueous solution by biochar derived from agro-bio waste of groundnut hull: kinetics and thermodynamics,” *Chemosphere*, vol. 276, pp. 130191–130196, 2021.
- [18] H. Wang, Q. M. J. Wu, D. Wang, J. Xin, Y. Yang, and K. Yu, “Echo state network with a global reversible autoencoder for time series classification,” *Information Sciences*, vol. 570, pp. 744–768, 2021.
- [19] M. Horvat, K. Pastor, and P. Kristian, “Multivariate analysis of water quality parameters in Lake Palic, Serbia,” *Environmental Monitoring and Assessment*, vol. 193, no. 7, pp. 410–414, 2021.
- [20] M. Mario and P. Daniela, “Multivariate analysis of water quality data for drinking water supply systems,” *Water*, vol. 13, no. 13, p. 1766, 2021.
- [21] Z. S. Peng, H. C. Ji, W. C. Pei, B. Y. Liu, and G. Song, “Constitutive relationship of TC4 titanium alloy based on back propagating (BP) neural network (NN),” *Metalurgija*, vol. 60, no. 3-4, pp. 277–280, 2021.
- [22] H. Cui, Q. Zhang, J. Zhang, Z. Wu, and W. Wu, “Classification of grain storage inventory modes based on temperature contour map of grain bulk using back propagation neural network,” *Agriculture*, vol. 11, no. 5, pp. 451–457, 2021.
- [23] Y. Jin, S. Yu, D. H. Kim, E. J. Yun, and K. H. Kim, “Characterization of neogargarooligosaccharide hydrolase BpGH117 from a human gut bacterium *Bacteroides plebeius*,” *Marine Drugs*, vol. 19, no. 5, pp. 271–275, 2021.
- [24] F. Ruan, X. Ding, H. Li, Y. Wang, K. Ye, and H. Kan, “Back propagation neural network model for medical expenses in patients with breast cancer,” *Mathematical Biosciences and Engineering*, vol. 18, no. 4, pp. 3690–3698, 2021.
- [25] H. He, “Learnability and robustness of shallow neural networks learned by a performance-driven BP and a variant of PSO for edge decision-making,” *Neural Computing & Applications*, vol. 33, no. 20, pp. 1–22, 2021.
- [26] H. Liu, J. Liu, Y. Wang, Y. Xia, and Z. Guo, “Identification of grouting compactness in bridge bellows based on the BP neural network,” *Structures*, vol. 32, pp. 817–826, 2021.
- [27] F. Chun, N. Zhao, G. Yin et al., “Artificial neural networks combined multi-wavelength transmission spectrum feature extraction for sensitive identification of waterborne bacteria,” *Spectrochimica Acta Part A: Molecular and Biomolecular Spectroscopy*, vol. 251, pp. 119423–119433, 2021.
- [28] F. Yu, “An active construction dynamic schedule management model: using the fuzzy earned value management and BP neural network,” *KSCE Journal of Civil Engineering*, vol. 68, pp. 1–15, 2021.

Research Article

Emotional Analysis and Personalized Recommendation Analysis in Music Performance

Bo Sun 

*Bo Sun*Hunan City University, Yiyang, Hunan 413000, China

Correspondence should be addressed to Bo Sun; sunbo@hncu.edu.cn

Received 1 March 2022; Revised 18 March 2022; Accepted 28 March 2022; Published 23 April 2022

Academic Editor: Hangjun Che

Copyright © 2022 Bo Sun. This is an open access article distributed under the Creative Commons Attribution License, which permits unrestricted use, distribution, and reproduction in any medium, provided the original work is properly cited.

Music performance belongs to music recreation activities, is through singing, musical instrument performance, and vocal conductor, including a variety of artistic means, to convey music to the audience with real sound effects that can be felt, and can play its social function. Emotional state is a part of the whole attitude, which is consistent with introverted feelings and intentions in attitude, and is a complex and stable physiological evaluation and experience of attitude in physiology. This paper first introduces the concepts of music performance from the perspective of music appreciation and music ability. Then based on the emotional feature learning of matrix factorization constrained nonnegative matrix factorization and model optimization algorithm are used to analyze the emotional aspects of music. Finally, through the experimental comparison of the difficulty of emotion in various artistic creations, a conclusion is drawn. The research involves matrix decomposition, mathematical modeling, model optimization, digital audio technology application, and other fields. In the third part of this paper, the constrained nonnegative matrix factorization, the constrained nonnegative matrix factorization with external information, and the model optimization algorithm are used to study the mathematical modeling.

1. Introduction

In order to study the neural basis of spontaneous musical performance, we found the characteristics of improvisation by using two paradigms with great differences in musical complexity: extensive inactivation of dorsolateral prefrontal cortex and lateral orbital region, local activation of medial prefrontal cortex. This pattern may reflect the combination of psychological processes required for spontaneous improvisation, in which the change of prefrontal lobe activity is accompanied by extensive activation of neocortical sensorimotor area and inactivation of marginal structure [1]. This paper describes an expressive timing method that maps the pianist's musical thoughts to sound performance. In Experiment 1, the three modes of chord asynchronous, Rubato mode, and overlapping are all strong in the performance of experienced pianists, and each mode is weakened when pianists try to play nonmusic. In Experiment 2, the marked melody shows the most consistent amount of overlap between adjacent events [2]. Biofeedback-assisted regulation of cortical electrical activity has been shown to have intrinsic

clinical benefits and has been shown to improve cognitive ability in healthy people. Related investigations have studied the music performance of students in Conservatory of Music under stress conditions [3]. The model of the performance principle of Rule K system is to choose the use rules and the amount of rules and then model the semantic description such as emotional expression. This paper discusses the communicative purpose and limitations of such rules at present and the future improvement [4]. In this paper, a new concept of speech synthesizer is proposed by constructing devices and methods capable of real-time operation. The further development of this concept may lead to the improvement of conversational ability of people with “verbal communicators” [5]. This paper analyzes the emotional state of movies based on emotional information and user experience and proposes movie browsing based on emotional information [6]. Social media has become a convenient platform for expressing opinions by posting messages, from texting to uploading media files or any combination of messages. Existing research on affective computing mainly focuses on a single media, whether it is text subtitles or visual

content. In this paper, we discuss the learning of highly nonlinear relationships between low-level features under different modes of emotion prediction [7]. At present, MTV has become widely loved by people. Emotional analysis can extract emotional states included in MTV, which provides a potential and promising solution for efficient and intelligent access to MTV [8]. In this paper, information features are extracted from heterogeneous inputs to represent human emotions, and a hierarchical multimodal structure based on attention is proposed, which proves the visualization of this model and explains the attention to patterns [9]. Patients' emotional/emotional state is closely related to the rehabilitation process and their health. This paper presents the design and implementation of an emotion analysis module integrated in the existing telemedicine platform. The technical details of the implementation of the scheme are discussed, and the preliminary results of the accuracy and error of the scheme in actual operation are given [10]. With current position in film production, the distance from the camera to the subject greatly affects the narrative power of the lens. This paper investigates the use of shot distance in famous movie scenes, and the results show that the key factor to induce audience's emotional response is the pattern of shot type [11]. This paper describes a convenient method of editing and reproducing music performance data. Music performance data divided into a plurality of parts is edited, and an icon [12] is displayed at the original divided position in order to facilitate positioning the divided position of the block before changing the length. This paper mainly discusses the cognitive modeling of games and animation. Personalization represents a better way of communicating and doing business. Personalization is an opportunity that must be identified and designed to be useful and useable. Personalization has no single answer or solution, because it needs to be reviewed on a case-by-case basis [13]. In order to provide a more robust personalized context, we want to extract a continuum of users' general interests into specific interests, called the User Interest Hierarchy (UIH). A hierarchical clustering (DHC) algorithm is proposed, which does not need user participation, only needs to learn UIHS implicitly, and uses words and phrases to improve the quality of UIHS [14]. This paper introduces the key technologies related to personalization and studies the key technologies of personalization in detail by comparing with the existing prototype system. In addition, three representative personalization systems are analyzed [15].

2. Musical Performance

2.1. Music. Music, as an independent art category, is the most familiar and favorite artistic expression form in people's daily life. However, if specific concepts are mentioned, there will be various discussions. One is the art of expressing people's thoughts and feelings and reflecting real life with organized music. Another expression is that music is an art created by human beings, which exists by means of sound wave vibration, is displayed in time, and causes various emotional reactions and emotional experiences through human auditory organs. Compared with the definitions of the above three

entries, Modern Chinese Dictionary gives a more general explanation, only emphasizing "organized music". If this part is replaced by the expression of art, this definition can also become a general formula to express another kind of art.

2.2. Music Appreciation. Music appreciation, as an independent process of music creation, is an important field that music aesthetics and music psychology have been paying attention to. Music appreciation refers to a kind of aesthetic activity that takes specific music works as the object and understands the true meaning of music by listening and other auxiliary means, such as reading and analyzing music scores and related background materials, so as to get spiritual pleasure.

2.3. Capabilities. The definition of "ability" in Modern Chinese Dictionary is "the ability, strength, or condition to be competent for a certain job or do a good job." According to the functional classification of ability, it can be divided into three types: cognitive ability, operational ability, and social ability. Cognitive ability includes learning, research, understanding, general situation, and analysis ability; operational ability includes the ability to manipulate, make, and move; social ability is the language expression ability in social communication activities. By comprehensive comparison, the first definition is more convincing.

2.4. Music Appreciation Ability. Music appreciation ability can be understood as the level of music skills and music understanding achieved when individuals participate in music appreciation activities, and appreciation mainly includes auditory ability and music reading ability. By studying six basic concepts: music performance specialty, music, music appreciation, ability, music ability, and music appreciation ability, music appreciation in the curriculum system of music performance specialty, we have a clearer theoretical understanding of music and music education from four aspects: art category, discipline and specialty, music creation, and music ability. These concepts are the theoretical support and principle foundation for engaging in music practice activities and also lay an important foundation for the next research on the framework of music appreciation ability.

3. Emotional Feature Learning Based on Matrix Factorization

3.1. Constrained Nonnegative Matrix Factorization. Nonnegative matrix factorization appears to deal with the problem that the dimension of input data is too high in the real world. After the original data is represented as a matrix, we can find two nonnegative matrices by NMF technology, and their products can approximate the original matrix well, thus mapping the features of the two dimensions to a hidden space at the same time. Based on the emotional representation in music field, NMF technology is explained in detail. The main issues in this section are translated into constructing a song list-song matrix, using NMF to map songs and songs to emotional space at the same time, and obtaining the

representation or distribution of song list and songs in emotional space. The corresponding data expression form is as follows: song list-song representation: the cooccurrence information of song list and song is represented as a two-dimensional matrix, in which each row represents a song list and each column represents a song. The value in the matrix is 0 or 1, which indicates whether the corresponding song appears in the song list (1 appears, 0 does not appear). Because of the huge number of songs in the song list, in the data calculation, there will be some problems, such as excessive resource consumption and long time consumption, and the excessive frequency of some songs will interfere with the decomposition effect. Therefore, it is necessary to preprocess the original song list data, select some songs as the features of the song list, and then obtain the original matrix X through matrix representation. Suppose that the size of matrix X is M rows and N columns, M represents the singular number of songs, and N represents the number of songs. The form of matrix X is

$$\begin{pmatrix} a_{11} & \cdots & a_{1n} \\ \vdots & & \\ a_{m1} & \cdots & a_{mn} \end{pmatrix}. \quad (1)$$

Matrix factorization objective: NMF aims to find the nonnegative factorization matrix of two original matrices X to replace U and V and make X close to the factorized result UV^T , that is, minimize the following objective function, and obtain formula

$$\begin{aligned} o &= \|X - UV^T\|_F^2 \\ s.t. & U \geq 0, V \geq 0. \end{aligned} \quad (2)$$

Among them, $\|\cdot\|_F^2$ represents the Frobenius norm of the matrix, and the constraint condition is that the weight distribution value of the decomposed U and V matrices in the emotional dimension is greater than or equal to 0; that is, negative values cannot appear.

Under the problem of emotional representation of music, the original song list matrix is decomposed into song list-emotion matrix U and song emotion matrix V by NMF. Because there is no orthogonal restriction, the final result is the distribution representation of song list and song in emotional space.

3.2. Constrained Nonnegative Matrix Factorization with External Information

3.2.1. Emotional Tag Information. In the context of emotional representation of music, expert labeled song list or emotional label information at song level is introduced as external information to be included in matrix decomposition. The following takes the song label information V_0 marked by the annotator expert as an example to discuss the relevant formulas. The annotator of U_0 is similar to V_0 ; just replace the corresponding V with U .

Let the song emotion label matrix marked by some experts be V_0 , each row corresponds to the song list of the original matrix X , and each column corresponds to emotion.

The value in the matrix is 0 or 1. If the song list has an emotion label, the corresponding value is 1; otherwise it is 0. On the basis of the original matrix decomposition objective, the error between the decomposed matrix V and the prior information matrix V_0 should be as small as possible; that is, the objective function is minimized as formula

$$\|G_V(V - V_0)_0\|_F^2, \quad (3)$$

where G_V is the diagonal indication matrix representing the song level, $G_V(i, i) = 1$ indicates that the i -th song contains emotional indication, and $G_V(i, i) = 0$ does not.

If the emotion representation learned by matrix factorization is inconsistent with the emotion indication contained in the data, this loss function will generate penalty, thus optimizing the direction of the next decomposition in matrix factorization.

3.2.2. B Networks. This kind of external information reflects the correlation between nodes. Similar songs or song lists are more likely to contain similar emotions, and the relationship between nodes is represented by constructing a graph network. In a graph, each node represents a data point, and the edges between nodes represent the correlation between data points. The adjacency matrix of a graph can be defined as formula

$$W^u(i, j) = \begin{cases} 1, & \text{if } u_i \in N(u_j) \text{ or } u_j \in N(u_i), \\ 0, & \text{otherwise.} \end{cases} \quad (4)$$

Among them, u_i is a song in the song list, and $N(u_j)$ represents K nearest residences of song J . Neighbors here can be obtained by many metrics, and the adjacency matrix is further constructed. The loss function of the song list relationship network can be defined as formula

$$R_u = \frac{1}{2} \sum_{i=1}^m \sum_{j=1}^m \|U(i, *) - U(j, *)\|_2^2 W_u(i, j). \quad (5)$$

It can be reduced to formula

$$R_u = Tr(U^T L^u U), \quad (6)$$

where $Tr(\cdot)$ is the trace of a matrix, which is a Laplace matrix, D^u is a diagonal matrix, and $D^u(i, i) = \sum_{j=1}^m W^u(i, j)$. R represents the loss function of the song list relationship network. If two songs are close in the graph but have different emotional labels, this loss function will produce penalty; that is, in the process of matrix factorization training, this loss function will tend to give similar emotional labels to songs close in the graph. The definition of the relationship network of song dimension is similar to that of song list; only the corresponding U needs to be replaced with V .

In the real world environment, there are many kinds of data that can be used to measure the distance relationship between song lists. This paper mainly constructs the relationship network from the perspective of song lists, including two kinds of external information: cooccurrence based on text label features and cooccurrence based on songs in song lists. These two kinds of external information and their respective validity will be explained in detail in the following steps.

Based on the feature similarity of text tags, each song list is mapped to the text feature space formed by tags as feature words and represented in the form of vectors. The neighbors of each song list are determined by calculating the similarity between vectors. The higher the similarity, the closer the two songs. The calculation process is as shown in formula

$$\text{sim}(i, j) = \frac{v_i \cdot v_j}{\|v_i\| \|v_j\|}, \quad (7)$$

$\text{sim}(i, j)$ represents the similarity between song list i and song list j , and v_i and v_j represent the vectorial representation of song list i and song list j in feature space, respectively.

Based on song cooccurrence: One song list contains multiple songs at the same time, and the same song may also be included in multiple songs.

Finally, the objective function incorporating external information can be expressed as formula

$$\begin{cases} \min & J = \|X - UV^T\|_F^2 + \lambda_I^u \|G^u(U - U_0)\|_F^2 + \lambda_I^v \|G^v(V - V_0)\|_F^2 + \lambda_c^u \text{Tr}(U^T L^u U) + \lambda_c^v \text{Tr}(V^T L^v V), \\ \text{s.t.} & U \geq 0, V \geq 0. \end{cases} \quad (8)$$

$\lambda_I^u, \lambda_I^v, \lambda_c^u, \lambda_c^v$ are the coefficient in front of the song list-emotion label information item, the song emotion label information item, the song list relationship network item, and the song relationship network item. It represents the weight of each item in the objective function. The greater the weight, the higher the proportion of corresponding items, and the training direction will tilt towards the direction of fitting the item, that is, the greater the weight of discourse power, the higher the proportion of corresponding items, and the training direction will tilt towards the direction of fitting the item, that is, the "discourse power" is greater. Because of the practical significance of the data, there cannot be negative numbers in matrices U and V .

From the data point of view, the original matrix decomposition revolves around the representation of songs in song lists or song lists on songs and incorporates the matrix decomposition of external information. On the basis of the original information, the information such as the correlation between songs and songs, the correlation between song lists and song lists is supplemented, which makes up for the defect of insufficient original data.

3.3. Model Optimization Algorithm

3.3.1. *A Calculation of Matrix U.* The problem of calculating Matrix U is equivalent to solving the following optimization problem, such as formula

$$\begin{cases} \min & J = \|X - UV^T\|_F^2 + \lambda_I^u \|G^u(U - U_0)\|_F^2 \\ & + \lambda_c^u \text{Tr}(U^T L^u U), \\ \text{s.t.} & U \geq 0. \end{cases} \quad (9)$$

Let Λ_U represent the Lagrange multiplier corresponding to the constraint condition $U \geq 0$; then the Lagrange equation can be defined as formula

$$L(U) = \|X - UV^T\|_F^2 + \lambda_I^u \|G^u(U - U_0)\|_F^2 + \lambda_c^u \text{Tr}(U^T L^u U) - \text{Tr}(\Lambda_U U^T). \quad (10)$$

Let $\nabla_U L(U) = 0$ give formula

$$\begin{aligned} \Lambda_U = & -2XV + 2UV^T V + 2\lambda_I^u G^u(U - U_0) \\ & + 2\lambda_c^u (D^u - W^u)U. \end{aligned} \quad (11)$$

According to the KKT complete condition, formula (12) can be obtained:

$$\Lambda_U(i, j)U(i, j) = 0. \quad (12)$$

KKT complete condition is a method used to solve optimization problems.

Thus, formula (13) can be obtained:

$$\begin{aligned} & [-(XV + \lambda_I^u G^u U_0 + \lambda_c^u W^u U + (UV^T V + \lambda_I^u G^u U + \lambda_c^u D^u U)) \\ & \cdot (i, j)U(i, j) = 0. \end{aligned} \quad (13)$$

The iterative rule of Matrix U is formula

$$U(i, j) \leftarrow U(i, j) \sqrt{\frac{[XV + \lambda_I^u G^u U_0 + \lambda_c^u W^u U](i, j)}{[UV^T V + \lambda_I^u G^u U + \lambda_c^u D^u U](i, j)}}. \quad (14)$$

3.3.2. *B Calculation of Matrix V.* The problem of calculating Matrix V is equivalent to solving the following optimization problem, such as formula

$$\begin{aligned} \min J = & \|X - UV^T\|_F^2 + \lambda_I^v \|G^v(V - V_0)\|_F^2 \\ & + \lambda_c^v \text{Tr}(V^T L^v V) - \text{Tr}(\Lambda_V V^T). \end{aligned} \quad (15)$$

Let Λ_V represent the Lagrange multiplier corresponding to the constraint condition $V \geq 0$; then the Lagrange equation is defined as formula

$$\begin{aligned} L(V) = & \|X - UV^T\|_F^2 + \lambda_I^v \|G^v(V - V_0)\|_F^2 + \lambda_c^v \text{Tr}(V^T L^v V) \\ & - \text{Tr}(\Lambda_V V^T). \end{aligned} \quad (16)$$

Let $\nabla_V L(V) = 0$ give formula (11):

$$\Lambda_U = -2X^T U + 2VU^T U + 2\lambda_l^v G^v (V - V_0) + 2\lambda_c^v (D^v - W^v)V. \quad (17)$$

According to the KKT complete condition, formula (18) can be obtained:

$$\Lambda_V(i, j)U(i, j) = 0. \quad (18)$$

Thus, formula (19) can be obtained:

$$\begin{aligned} & [-(X^T U + \lambda_l^v G^v V_0 + \lambda_c^v W^v V) + (VU^T U + \lambda_l^v G^v V + \lambda_c^v D^v V)] \\ & (i, j)V(i, j) = 0. \end{aligned} \quad (19)$$

The iterative rule of Matrix V is formula

$$V(i, j) \leftarrow V(i, j) \sqrt{\frac{[X^T U + \lambda_l^v G^v V_0 + \lambda_c^v W^v V](i, j)}{[VU^T U + \lambda_l^v G^v V + \lambda_c^v D^v V](i, j)}}. \quad (20)$$

3.4. Music Emotional Representation Learning. The essence of music emotion recognition is the representation of music or songs in emotion space. By using the nonnegative matrix factorization algorithm which fuses external information, we can get song list-emotion matrix U and song emotion matrix V. Matrix V is the representation or distribution of each song in emotion space. In order to obtain more practical results, each row of matrix V is normalized, and each row corresponds to the probability distribution of a song in emotional space. Let the emotional distribution of the first song I be V_i ; then the song I is expressed as formula (21) in k-dimensional emotional space:

$$V_i = (V_{i1}, V_{i2}, \dots, V_{ik}). \quad (21)$$

By normalizing V_i corresponding to the first song I, the emotional probability distribution s_i^* corresponding to the song I can be obtained, and the calculation is as formula

$$s_i^* = \left(\frac{V_{ij}}{\sum_{j=1}^k V_{ij}} \right). \quad (22)$$

K represents the emotional space dimension.

For each song, the emotion class with the highest corresponding value is taken as the emotion class to which the song belongs, and the calculation is as formula

$$e_i^* \leftarrow \arg \max(s_i^*). \quad (23)$$

Therefore, the purpose of song emotion recognition is achieved.

The above algorithm is the complete process of music emotion recognition algorithm based on matrix decomposition. Based on the matrix decomposition method, we can achieve the purpose of emotional representation of songs in the song list. After obtaining the representation of songs in emotional space, we can carry out the work of emotional recognition for users.

4. Analysis of Important Indexes in Music Performance Major

4.1. Analysis of Teaching Results. We evaluate the teaching achievements through three directions: skill assessment, ability growth assessment, and objective analysis of digital audio technology. In order to better understand the situation of students' training and skills mastery, all students' training audio records will be collected every week as a reference for ability evaluation. Audio recordings of live performances will be used as data sources for digital audio technology analysis.

The assessment steps are as follows:

- Students are assessed for on-site skills display in groups, and the assessment place is the Concert Hall of the College. Seven music performance teachers are invited to score the students' on-site skills assessment one by one.
- The assessment place is the digital audio training room, where teachers score students' growth ability according to the staged training audio stored before. On-site skill display score and growth ability score are calculated according to the perfect score of 100.
- The examination place is the digital audio training room, where teachers open the audio files of students' examinations and, through the visual analysis of digital audio technology, count the error rates of students' important and difficult points (there are 15 important and difficult points in total).
- The scores of the numeric group are compared horizontally with those of the traditional group, and then the scores are compared vertically within the numeric group and the traditional group.

4.2. Analysis of Data Results. Through the data analysis in Table 1, it can be found that the overall scores of students in the three sections remain stable, and the grades of "excellent", "good," and "poor" have not changed. It shows that the application of digital audio technology in teaching and practice in a short period of time has not significantly improved the teaching achievements. Although students with good foundation have not been assisted by digital audio technology, they can still achieve good results through traditional teaching mode and their own efforts, so that their professional level can be stably maintained at a certain level. However, through the comparison between the digital group and the traditional group, it is found that the scores of the digital group are slightly higher than those of the traditional group in the same level, and the average score of the digital group is 1.9 points higher than that of the traditional group. The average score of the digital group is 7.2 points higher than that of the traditional group. The average score of the number three group is 5.4 points higher than that of the traditional three groups. The data show that the number group in the skill display assessment has achieved certain advantages compared with the traditional group, and its final scores are slightly higher than each other.

TABLE 1: Statistical table of on-site skill display and assessment of music performance major.

Group	Number of people	Error rate	Rank
Number 1 group	10	92.5	1
Number 2 group	10	88.7	3
Number 3 group	10	75.2	5
Traditional 1 groups	10	90.6	2
Traditional 2 groups	10	91.6	4
Traditional 3 groups	10	92.6	6

TABLE 2: Statistical table of operational ability examination of music performance specialty.

Group	Number of people	Average score	Rank
Number 1 group	10	83.6	2
Number 2 group	10	91.4	1
Number 3 group	10	81.7	3
Traditional 1 groups	10	80.4	4
Traditional 2 groups	10	79.3	5
Traditional 3 groups	10	75.5	6

Through the data analysis in Table 2, we can find that the ranking of growth ability breaks the original balance, and the digital group is higher than the traditional group in terms of ability growth. Compared with the traditional one, the average score of the number one group is 3.2 points higher; compared with the traditional two groups, the average score of digital two groups is 12.1 points higher; compared with the traditional three groups, the average score of digital three groups is 6.2 points higher. It can be seen that, through the application of digital audio technology, the professional and technical level of students in the digital group has grown to a certain extent, and the degree of improvement in business ability is higher than that in the traditional group. Through the comparison within the group, it is found that the number two group gets the highest score of 91.4, which shows that the students with medium professional scores have the greatest ability improvement under the application of digital audio technology. Through the comparison of the growth ability value, it is found that the digital sound forehead technology has achieved certain results in the practical training and self-improvement in the teaching process.

Through Table 3, the ranking of the error rate of important and difficult points evaluated objectively is found to be completely consistent with the ranking in Table 1, which shows that students with good foundation have good performance under the traditional teaching mode. Compared with the students in the traditional group, the level of control error rate in the digital group is slightly higher. The error rate in Table 3 refers to the error frequency of the students surveyed in the performance assessment of music performance major. Compared with the traditional group, the error rate of the digital group is 3% lower; compared with the traditional two groups, the error rate of the digital two groups is 8% lower; compared with the traditional three groups, the error rate of the digital three groups is 5% lower. It can be seen that, through the application of digital audio technology, the professional and technical level of students

TABLE 3: Statistical table of error rate of important and difficult points in performance examination of music performance major.

Group	Number of people	Error rate	Rank
Number 1 group	10	9	1
Number 2 group	10	13	3
Number 3 group	10	27	5
Traditional 1 groups	10	12	2
Traditional 2 groups	10	21	4
Traditional 3 groups	10	32	6

in the digital group has grown to a certain extent, and the degree of improvement in business ability is higher than that in the traditional group. On the other hand, the number group has a slightly better control over the details of the performance. There is a big difference between performing in the sound field of the concert hall and the usual training environment. Students who create analog sound field training through digital audio technology are familiar with the sound feedback of the sound field of the concert hall, so the students in the digital group play more stably and well in the same environment. It can be seen that the practical training of digital audio technology application is helpful for students to improve the accumulation of performance experience and grasp the performance details.

Integrate the data of the three score tables, and get the comparison diagram of the assessment results of instructional design as shown in Figure 1.

By analyzing Figure 1, it is found that the students who apply digital audio technology in teaching have significantly improved their skills, learning accuracy, and error rate control in a short time. Under the traditional teaching mode, students' skills, learning accuracy, and error rate control have also been improved, but compared with the number group, they are slightly inferior.

In order to better analyze the influence of the teaching mode on the teaching results, the teacher also scores the training situation of the target tracks recorded by the students at each stage after each professional class according to the technical level displayed by the students in the training and selects the final assessment score for the fourth time. After the scores are integrated by groups, the average value is calculated, and the data analysis is carried out to obtain the staged evaluation comparison chart as shown in Figure 2.

In Figure 2, the staged evaluation and comparison data of each group show that the application of digital audio technology has advantages and disadvantages, but its disadvantage is that it cannot improve the error rate. According to the analysis of Figure 2, with the teaching progress and the increase of teaching time using digital audio technology, the students' achievements in skill display have increased correspondingly and exceeded the teaching achievements obtained under the traditional mode. It shows that the application of digital audio technology can prove the promotion of students' skills. The ordinate in Figure 2 represents the average value of the scores obtained after the students' technical level is uniformly scored according to the group.

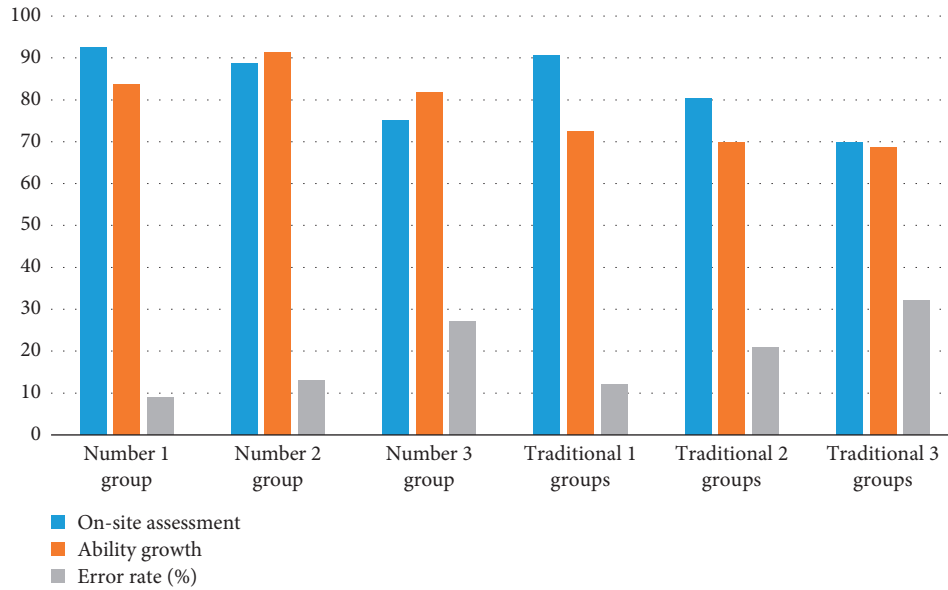


FIGURE 1: Comparison of assessment results.

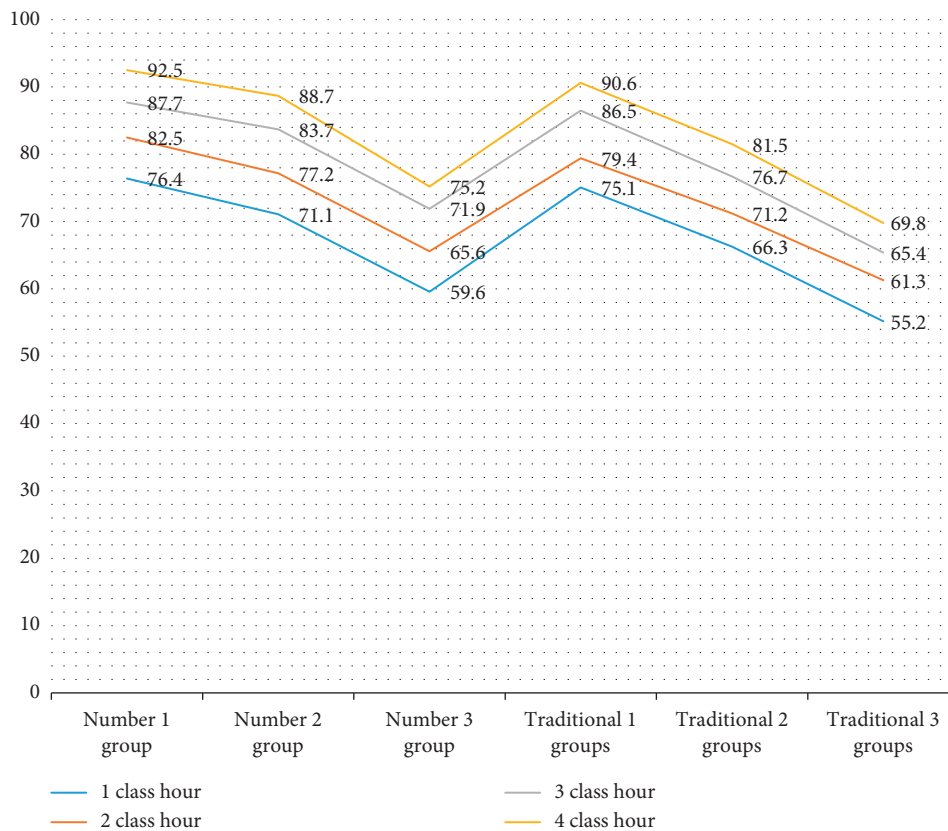


FIGURE 2: Comparison chart of staged evaluation.

4.3. Comparison of Emotional Experience in Music Performance

4.3.1. *There Are Two Kinds of Human Emotions.* One is called self-emotion, which is the emotional experience felt from life; the second is the emotional experience felt from

art, which is also called the second self-emotion. Of course, the emotion in artistic creation refers to the second emotion, that is, aesthetic emotion. The above two kinds of emotions are dynamic psychological factors. The joys and sorrows we often say are not emotions in psychology, but a product between subject and object.

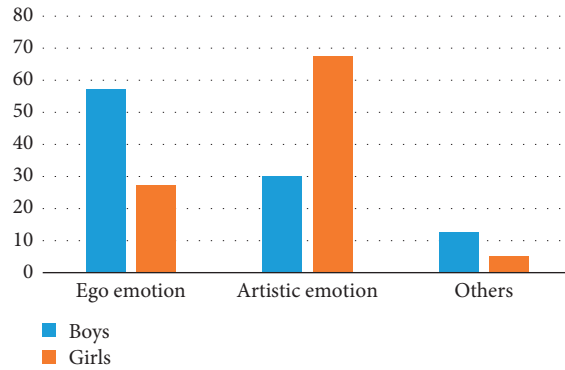


FIGURE 3: Comparison of the proportion of boys and girls who have emotions in music performances.

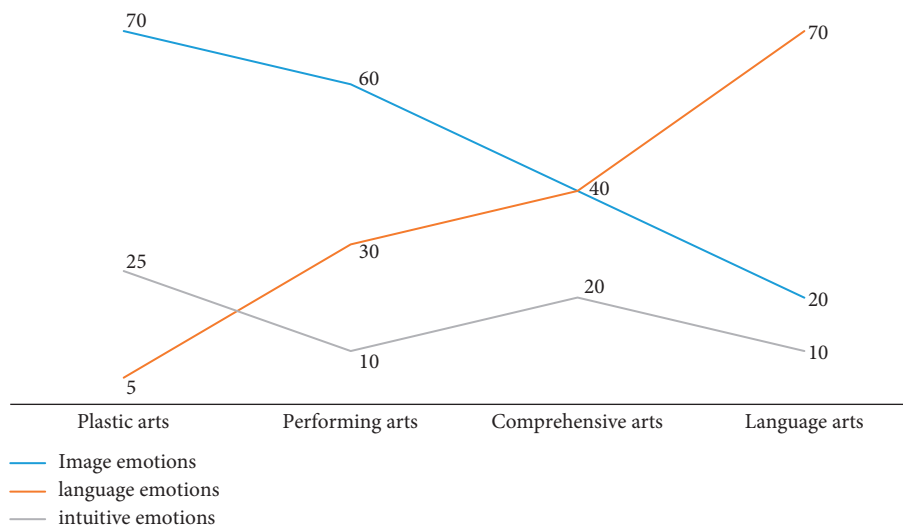


FIGURE 4: Difficulty of producing three emotions in various artistic creations (%).

According to the analysis of Figure 3, girls are more artistic than boys in music performance, and they are more likely to produce artistic emotion.

4.3.2. *In the Process of Creating Art, There Are Usually Three Emotions.* The first is the emotion that can be expressed by image, the second is the emotion that can be expressed by language, and the third is the intuitive emotion, which cannot be expressed by language or vision. When singers face creators' works, if they do not rely on their own emotions, they cannot understand the emotions in their works, and if they do not understand them, they will not resonate naturally.

By analyzing Figure 4, sound can effectively stimulate people's emotional fluctuations, which has a great stimulating effect on people. Music shows life through sound, and music reflects people's psychology through thoughts and feelings, which is also the difference between music and other arts. According to the analysis of Figure 4, art can be divided into four categories: plastic arts, performing arts, comprehensive arts, and language arts. In the process of artistic creation, plastic arts are most likely to produce image

emotion, while language arts are most likely to produce language emotion. Performing arts and comprehensive arts are quite difficult.

5. Conclusion

By comparing the matrix algorithm with the experiment, it is an important content to study the emotional state in the process of music performance, because music performance is a comprehensive and challenging art form, which has a great relationship with the emotional state of singers, so the premise of successful music performance is to have good psychological quality and singing emotion. If you want to have good psychology, you should strengthen psychological training, accumulate performance experience constantly, cultivate your own psychological mobilization ability, and master psychological connotation deeply. Only by doing our best to improve ourselves can we better grasp the psychological state during performance. In the era of information explosion, personalized recommendation greatly solves the problem of information overload. By designing corresponding algorithms to capture users' personalized preferences and recommend items that users may like, it greatly

reduces the difficulty of users' choice and increases the income of service providers. Personalized recommendation is one of the most practical and academic fields in the era of artificial intelligence. In recent years, especially in the last three years, we have witnessed the development of recommendation system, especially with the rise of machine learning and deep learning, the development of recommendation system is more rapid, and now it has expanded many subdivisions. The two models proposed in this paper mainly focus on KG and then combine graph representation learning technology to realize personalized recommendation. Through reading a large amount of latest research, this paper designs a novel graph representation learning algorithm to learn the feature representation of users and items. Experiments show that the model proposed in this paper has achieved good results, but there are still many areas to be improved, and there are still many challenges and research gaps in the future.

Data Availability

The experimental data used to support the findings of this study are available from the corresponding author upon request.

Conflicts of Interest

The authors declare that they have no conflicts of interest regarding this work.

References

- [1] C. J. Limb and A. R. Braun, "Neural substrates of spontaneous musical performance: an fMRI study of jazz improvisation," *Plos One*, vol. 3, no. 2, pp. e16–79, 2008.
- [2] C. Palmer, "Mapping musical thought to musical performance," *Journal of Experimental Psychology: Human Perception and Performance*, vol. 15, no. 2, pp. 331–346, 1989.
- [3] T. Egner and J. H. Gruzelier, "Ecological validity of neurofeedback: modulation of slow wave EEG enhances musical performance," *NeuroReport*, vol. 14, no. 9, pp. 1221–1224, 2003.
- [4] F. Anders, B. Roberto, and S. Johan, "Overview of the KTH rule system for musical performance[J]," *Advances in Cognitive Psychology*, vol. 2, no. 2, pp. 145–161, 2006.
- [5] A. Hunt and R. Kirk, "Mapping strategies for musical performance," *Interpretation and Space*, vol. 12, no. 10, pp. 34–67, 2000.
- [6] A. Subramanian, P. Tamayo, V. K. Mootha et al., "Gene set enrichment analysis: a knowledge-based approach for interpreting genome-wide expression profiles," *Proceedings of the National Academy of Sciences*, vol. 102, no. 43, pp. 15545–15550, 2005.
- [7] L. Pang, S. Zhu, and C.-W. Ngo, "Deep multimodal learning for affective analysis and retrieval," *IEEE Transactions on Multimedia*, vol. 17, no. 11, pp. 2008–2020, 2015.
- [8] R. Lozano, M. Naghavi, and K. Foreman, "Global and regional mortality from 235 causes of death for 20 age groups in 1990 and 2010: a systematic analysis for the Global Burden of Disease Study 2010," *Lancet*, vol. 380, no. 9859, pp. 2095–2128, 2016.
- [9] Y. Gu, K. Yang, S. Fu, S. Chen, X. Li, and I. Marsic, "Multimodal affective analysis using hierarchical attention strategy with word-level alignment," vol. 23, no. 4, pp. 132–156, 2018.
- [10] A. Kallipolitis, M. Galliakis, A. Menychtas, and I. Maglogiannis, "Affective analysis of patients in homecare video-assisted telemedicine using computational intelligence," *Neural Computing & Applications*, vol. 32, no. 23, pp. 17125–17136, 2020.
- [11] D. Moher, A. Liberati, and J. Tetzlaff, "Methods of systematic reviews and meta-analysis preferred reporting items for systematic reviews and meta-analyses: the PRISMA statement," *PLoS Medicine*, vol. 8, no. 7, pp. 336–341, 2009.
- [12] K. Wolf and R. Fiebrink, "Personalised interactive sonification of musical performance data," *Journal on Multimodal User Interfaces*, vol. 13, no. 3, pp. 245–265, 2019.
- [13] D. Riecken, "Introduction: personalized views of personalization," *Communications of the ACM*, vol. 43, no. 8, pp. 26–28, 2000.
- [14] H.-R. Kim and P. K. Chan, "Learning implicit user interest hierarchy for context in personalization," *Applied Intelligence*, vol. 28, no. 2, pp. 153–166, 2008.
- [15] C. Zeng, C. X. Xing, and L. Z. Zhou, "Survey of personalization technology," *Journal of Software*, vol. 13, no. 10, pp. 1952–1961, 2002.

Research Article

Prediction of Soil Heavy Metal Content Based on Deep Reinforcement Learning

Yongqi Zhao,¹ Zhangdong Wei ,¹ and Jing Wen²

¹Miami College of Henan University, Kaifeng 475002, Henan, China

²Hunan Career Technical College Nonferrous Metal, Zhuzhou, Hunan 412006, China

Correspondence should be addressed to Zhangdong Wei; 10380012@vip.henu.edu.cn

Received 4 March 2022; Revised 24 March 2022; Accepted 24 March 2022; Published 15 April 2022

Academic Editor: Hangjun Che

Copyright © 2022 Yongqi Zhao et al. This is an open access article distributed under the Creative Commons Attribution License, which permits unrestricted use, distribution, and reproduction in any medium, provided the original work is properly cited.

Since the prediction accuracy of heavy metal content in soil by common spatial prediction algorithms is not ideal, a prediction model based on the improved deep Q network is proposed. The state value reuse is used to accelerate the learning speed of training samples for agents in deep Q network, and the convergence speed of model is improved. At the same time, adaptive fuzzy membership factor is introduced to change the sensitivity of agent to environmental feedback value in different training periods and improve the stability of the model after convergence. Finally, an adaptive inverse distance interpolation method is adopted to predict observed values of interpolation points, which improves the prediction accuracy of the model. The simulation results show that, compared with random forest regression model (RFR) and inverse distance weighted prediction model (IDW), the prediction accuracy of soil heavy metal content of proposed model is higher by 13.03% and 7.47%, respectively.

1. Introduction

Soil is an important resource for human survival and development, as well as the lifeline of the whole ecosystem. However, with the improvement of production level and the rapid development of economics, the problem of soil pollution has become more and more serious. And heavy metal pollution is one of the most difficult pollutants among all soil pollution sources, which is difficult to be degraded by microorganisms. It not only affects the growth of crops and leads to the decline of crop yield, but also may enter the human body through eating and other ways, so as to threaten human life and health. Liu Xingmei et al. believed that there were both noncarcinogenic and carcinogenic potential risks to human health by eating vegetables contaminated by heavy metals. Therefore, it is necessary to study heavy metals in soil. In recent years, with people's attention to soil heavy metal pollution, more and more relevant researches are carried out, which are more and more in-depth [1]. Lan et al. used pinealone-biochar to stably passivate Pb, Cu, Zn, Cr, and As in soil. As can be seen, the addition of pinealone-biochar and the coexistence of indigenous microorganisms

can effectively reduce biological activity of heavy metals and accelerate passivation of heavy metals [2]. Khan Imran and Yang Dong et al. found that silicon in soil has a certain detoxification mechanism for heavy metals, which provides a certain theoretical basis for reducing toxicity of heavy metals in soil [3, 4]. Guo Xujing and Liu Xingmei et al. used spectroscopy combined with parallel factor analysis and two-dimensional correlation spectra to study the complexing characteristics of heavy metals Cr (III) and Cu (II) in soil with biochar source WEOM [1, 5]. Using corn cobs as raw materials, biochar-derived water extractable organic matter can be obtained under low temperature (300°C) pyrolysis conditions, which can be used for soil heavy metal remediation. Rana Anuj and Zhang Jiachun et al. studied the biological activities of heavy metals (Cd and Cr) in crops and believed that heavy metal pollution in soil could be dealt with by reducing the biological activities of heavy metals [6, 7]. The above research results show that the current research on heavy metals in soil mainly focuses on the treatment, and there are few researches on the prediction of contents, while the content prediction of soil heavy metals is the prerequisite for treating heavy metals in soil [8]. Thus a

prediction model based on deep reinforcement learning is proposed.

2. Basic Methods

2.1. Deep Q Networks. Deep Q network is a representative algorithm of deep reinforcement learning. Combining the perception ability of deep learning with the decision-making ability of reinforcement learning, the spatial coverage problem of state-action in Q table can be solved [9]. The calculation of target value of deep Q network can be solved by state value function, which is shown in formula (1) [10]:

$$y = V^s(s; \theta') = r + \gamma \max_{a'} Q^s(s', a'; \theta'), \quad (1)$$

where θ is online value network; θ' is target value network; S is current state; a is action in s state; r is reward of agent for a ; s' means the next state reached by agent in s state when action a is taken.

Figure 1 shows the operation process of deep Q network.

There is the problem of overestimation existing in the combination of deep Q network with neural network and reinforcement learning, which leads to the estimation error of prediction output value of the model and cannot truly reflect the actual value [11]. In addition, the convergence speed of deep Q network is slow, and the stability after model convergence is poor [12]. Therefore, to solve these problems, state value reuse and fuzzy membership factor are utilized to improve deep Q network. At the same time, adaptive inverse distance weighted method is used to adjust the hyperparameters to improve the prediction accuracy.

2.2. Improvement of Deep Q Network

2.2.1. State Value Reuse. State value reuse is to combine the partial output of value function with the obtained reward value to form total reward value, which can replace the original environment reward value to train the agent, and make the total reward value participate in the weight update of Q network. After each round of training, the network error is calculated, and the weight is updated. As can be seen, the calculation method of reward value in the deep Q network model of state value reuse is shown in formula (2) [13]:

$$R(s, a, p) = r(s, a, p) + \lambda V(s; \theta, \beta), \quad (2)$$

where s is current state; d is the action performed in s state. P is state probability after the execution of a , and $r(s, a, p)$ is reward value of environment to action. $V(s; \theta, \beta)$ represents partial output value; λ is regulating factor, which is responsible for determining the dominant position of reward value returned by environment in the total reward value, so as to avoid the influence of the size of reward value returned by environment on the model convergence.

2.2.2. Dynamic Fuzzy Membership Factor. As can be seen the deep Q network can be optimized by state value reuse. The environmental feedback reward value and state value of

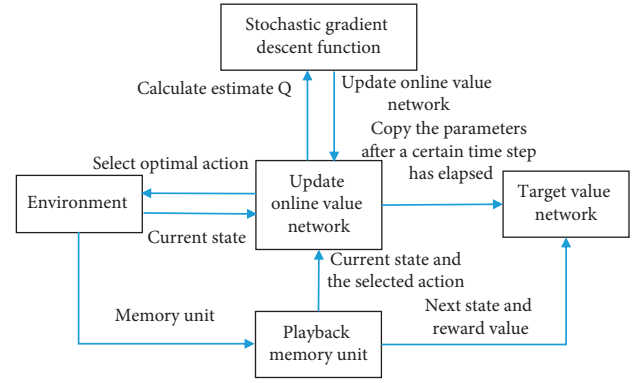


FIGURE 1: Operation process of deep Q network.

Q network are combined in a certain proportion. Moreover, the combination mode remains unchanged in the whole network model training. In practical application, Q network is not sensitive to environmental feedback reward at the initial stage of training, so it cannot accurately judge the advantages and disadvantages of current environment. Therefore, it is necessary to reduce the proportion of state value to improve agent's sensory ability to environment. In the middle of training, parameters of Q network move to the optimal solution, and the network performance is getting higher and higher. The regulatory factor should be appropriately increased to enhance the reward or punishment of environment to agent performing actions. At the later stage of training, parameters of Q network basically remain stable, and the maximum value of regulatory factor should be basically maintained to improve the model convergence rate [14, 15]. Thus in the training process of Q network, the proportion of state value and environmental feedback reward value in total reward value should change dynamically. In addition, dynamic fuzzy membership factor δ is introduced in this paper, which is shown in formula (3) [16]:

$$\delta = \frac{1}{2} - \frac{1}{2} \cos\left(\left(\frac{\pi}{n_{\text{total}}}\right) * n\right), \quad (3)$$

where n is the number of current training steps; n_{total} is the total number of predicted training steps. δ changes with the change of n . When n is small, δ tends to 0. When n is large, δ increases gradually. When $n = n_{\text{total}}$, δ approaches 1.

To sum up, the total reward value calculation method of the improved deep Q network model is as follows [17]:

$$R(s, a, p) = r(s, a, p) + \delta V(s; \theta, \beta), \quad (4)$$

where s is current state; a is the action performed in s state. P is probability of environment transferring to next state, and $r(s, a, p)$ is the reward value of environment to action. $V(s; \theta, \beta)$ represents partial output value of value function in Q network; δ is regulatory factor.

2.3. Adaptive Inverse Distance Weighted Method. Deep Q network model determines the reward value of training environment by the observing interpolation points, which is shown in formula (5). However, the observed value of

interpolation point is an unknown value, which is usually predicted by inverse distance weighted method. According to [18], the inverse distance weighted method has poor interpolation effect because it cannot adapt to complex terrain structure. To solve this problem, an adaptive inverse distance weighted method is proposed.

$$r(s, a) = \sum_{i=1}^m w(i) \left\{ \left[\gamma^{\#}(s, h_i) - \gamma^*(h_i) \right]^2 - \left[\gamma^{\#}(s', h_i) - \gamma^*(h_i) \right]^2 \right\}, \quad (5)$$

where s is current state of agent; a is action performed in s state; s' is the entered next state where agent performs action a in s state; $\gamma^{\#}(s, h_i)$ is fitting value of h_i on mutation function curve corresponding to s ; $\gamma^{\#}(s', h_i)$ is the fitting values of h_i corresponding to s' ; $\gamma^*(h_i)$ is discrete points of mutation function of h_i ; r is reward value with environment to agent carrying out action a in s state.

In the adaptive inverse distance weighted method, hyperparameters of each known point in the model are learned, and the nearest adjacent statistics of each point are calculated. Furthermore, the multidimensional spatial discrete points are formed, and spatial modeling is done by Kriging interpolation method [19, 20]. Finally, the corresponding coordinates of interpolation points to be predicted are input into the spatial model, so as to obtain the corresponding hyperparameters of interpolation points. Thus the final predicted values can be obtained by using this hyperparameter to inversely weight the interpolation point. The adjacent distance is calculated as follows [21]:

$$d_{\text{avg}} = \frac{1}{2(N/A)^{0.5}}, \quad (6)$$

where N is the total number of sample points in research area; A is the area of study area.

The nearest adjacent statistic can be calculated by formula (7) [22]:

$$M = \frac{d_n}{d_{\text{avg}}}, \quad (7)$$

where d_n is the nearest expected distance of prediction point; d_{avg} is the expected nearest distance of study area.

3. Prediction of Soil Heavy Metal Content Based on Improved Deep Q Network

The prediction process of soil heavy metal content is designed as follows:

- (1) Preprocess and divide the collected and sorted original soil heavy metal content into sample point data set and interpolation point data set. The sample point data is the sample data set with known observation value, and the interpolation point data set is the sample data set with unknown observation value.
- (2) Use adaptive deep Q network to train the sample point data set and record the inverse distance weighted optimal hyperparameter of each point.

- (3) Compose all optimal hyperparameters into a new data set, and calculate spatial discrete points of mutation function of the data set to obtain the mutation function model, which is shown in formula (8) [23].

$$\gamma(\vec{h}) = \frac{1}{V} \iiint_V [Z(s + \vec{h}) - Z(s)]^2 dV, \quad (8)$$

where s is a point in support set V in random field z , and \vec{h} is any two-point vector in V . When mutation function is in a second-order stable process, the above equation can be rewritten as

$$\begin{aligned} \gamma(s_1, s_2) &= \text{var}[Z(s_2) - Z(s_1)] \\ &= E[Z(s_2) - Z(s_1) + \mu(s_2) - \mu(s_1)]^2, \end{aligned} \quad (9)$$

where E and var are mathematical expectation and variance operations, and μ is the mathematical expectation of specific point in random field. Since the covariance is related to \vec{h} , formula (9) can be expressed as

$$\begin{aligned} \gamma(s_1, s_2) &= E[Z(s_2) - Z(s_1)]^2, \\ \vec{h} &= s_1 - s_2. \end{aligned} \quad (10)$$

Considering that the covariance is related to Euclidean distance of the two spatial points and has nothing to do with the direction, formula (10) can be expressed as

$$\gamma(s_1, s_2) = \gamma_s(|\vec{h}|). \quad (11)$$

- (4) Use the weight coefficient, as shown in formula (13), establish the fitting standard, as shown in formula (14), and estimate the parameters of mutation function model to obtain the optimal mutation function model and its optimal parameters:

$$w(i) = \frac{N(h_i)}{\sum_{j=1}^m N(h_j)}, \quad (12)$$

$$C_w = \min \left\{ \sum_{i=1}^m w(i) \left[\gamma^{\#}(h_i) - \gamma^*(h_i) \right]^2 \right\}, \quad (13)$$

where $\gamma^{\#}(h_i)$ is fitting value of point h_i on the mutation function curve, $\gamma^*(h_i)$ is discrete point of mutation function of h_i , and C_w is the objective function of model parameter optimization.

- (5) Adopt Kriging method to model the new data set to obtain the hyperparameter distribution model.
- (6) Input the data of interpolation points into hyperparameter distribution model, and introduce the obtained hyperparameters and corresponding interpolation point data into the inverse distance weighted algorithm, so as to obtain the final predicted value of soil heavy metal content.

The above process can be illustrated in Figure 2.

4. Simulation Experiment

4.1. Data Sources and Preprocessing. The soil heavy metal content data set of suburban farmland of Changsha is selected as the experimental data set. Considering that there are geographic data including latitude and longitude in the data set, it is not suitable for direct input into the model. Therefore, the geographic data including latitude and longitude are converted into data in Cartesian coordinate system before the experiment. Meanwhile, to reduce magnitude of geographical data, the converted data coordinates are shifted to the origin as a whole. In addition, considering the existence of missing values in the data set and the different ranges of data values corresponding to different features, mean interpolation or deletion is carried out for the data, and z -score is standardized and preprocessed, which are shown as follows:

$$y_i = \frac{x_i - \bar{x}}{s},$$

$$\bar{x} = \frac{1}{n} \sum_{i=1}^n x_i, \quad (14)$$

$$s = \sqrt{\frac{1}{n-1} \sum_{i=1}^n (x_i - \bar{x})^2}.$$

4.2. Evaluation Indicators. The mean square error (MSE), root mean square error (RMSE), mean absolute percentage error (MAPE), and mean absolute error (MAE) are selected as evaluation indicators in this experiment, and the calculation methods are as follows [24]:

$$\text{MSE} = \frac{\sum_{i=1}^n (X_i - x_i)^2}{N},$$

$$\text{RMSE} = \sqrt{\frac{\sum_{i=1}^n (X_i - x_i)^2}{N}}, \quad (15)$$

$$\text{MAPE} = \frac{100\%}{n} \sum_{i=1}^n \left| \frac{\hat{y}_i - y_i}{y_i} \right|,$$

$$\text{MAE}(X, h) = \frac{1}{m} \sum_{i=1}^m |h(x_i) - y_i|.$$

4.3. Parameter Setting. The initial parameters of all models are set the same, and the specific settings are as follows: The maximum number of training rounds is 5000; the number of training samples in each round is 64; the random seed is 1; the maximum memory size is 500; the initial state of agent is [2, 14]; the difference of training rounds between weight updates of Q network is 200; the learning rate of

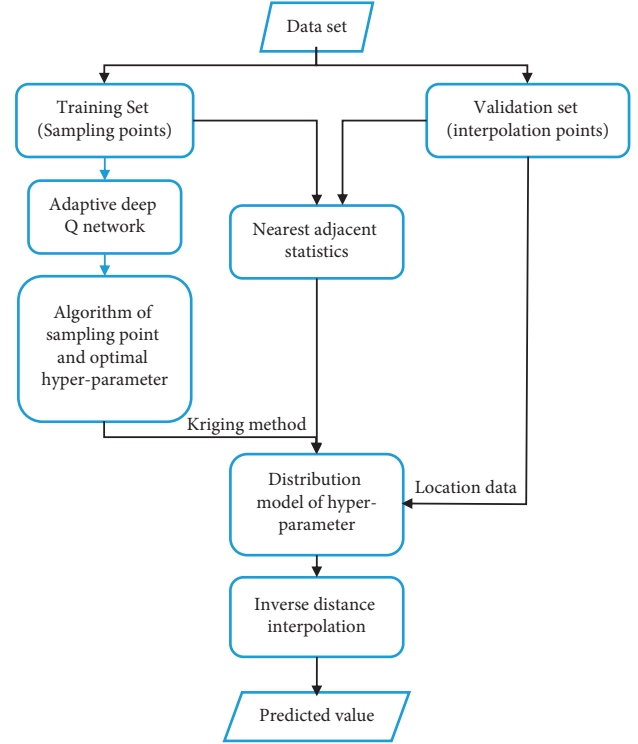


FIGURE 2: Model prediction process.

convolutional neural network is 0.001; the probability factor of e-greedy algorithm is 0.9.

4.4. Experiment Results

4.4.1. Estimation of Model Parameters. To verify the effectiveness of proposed model, the proposed model, deep Q network model, double deep Q network model, and competing deep Q network model are used to learn and train the parameter estimation of inverse distance weighted algorithm, and the training of different models on the data set is recorded. The results are shown in following figures.

As can be seen, the abscissa is the number of training rounds, and the ordinate is the error between predicted value and observed value (mg/kg). To reflect change trend of prediction error more clearly, smoothing processing is carried out on the basis of original graph. Here the initial points of different models are different. The reason is that the agent performs several random decisions before the model training, resulting in different agent states, and then the initial state and initial points of the models are different. However, different initial states of agents do not affect the model performance. For example, on the Ni data set, the initial states of deep Q network and competing Q network model are slightly lower than the proposed model. The convergence speed of proposed model is higher than deep Q network and competing Q network model, which indicates that the initial states of agents do not affect the model performance.

Figure 3 and Figure 4 show that the prediction error of model is not monotone decreasing when all models are

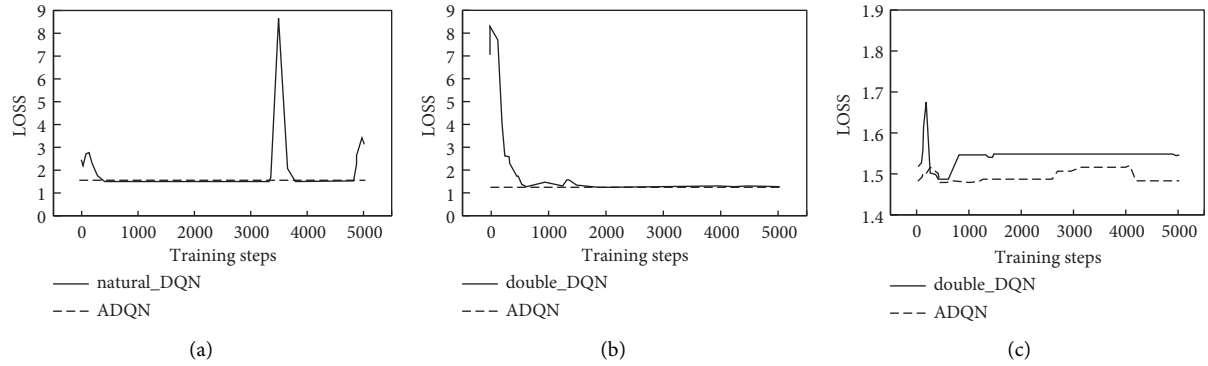


FIGURE 3: Training of different models on Cd data set.

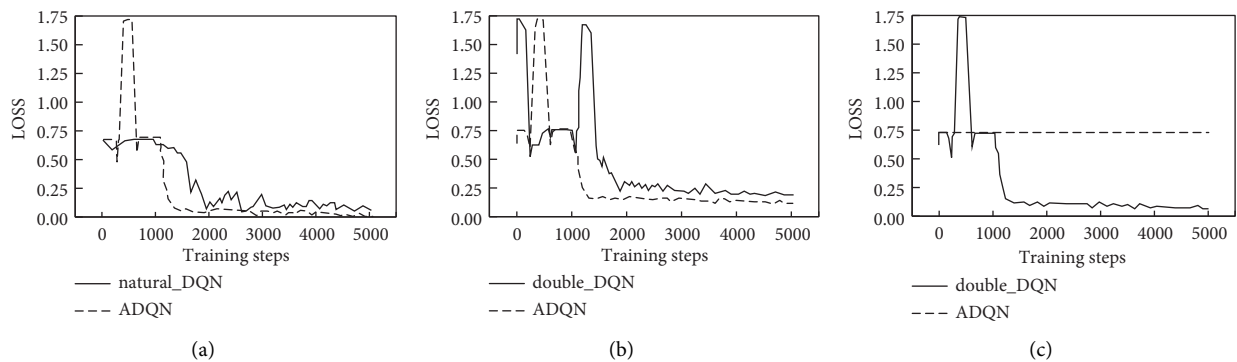


FIGURE 4: Training of different models on Cr data set.

trained, but there is a situation where the minimum error is reached and then moves towards a larger error, and the reason is that the model has reached local optimal state in this learning stage. However, the proposed model can jump out of the local optimal state through adaptive dynamic fuzzy membership factor and converge to the global optimal value; thus the proposed model has certain superiority. Figures 3–5 show that after agent reaches optimal state, it will return to poor state. The reason is that when agent adopts ϵ -greedy strategy to make action decision, there are some unnecessary actions performed, so as to reduce the convergence rate of model and make model return to poor state after reaching optimal state. Figures 3–6 show that, compared with contrast models, the proposed model has faster convergence speed and more stable performance, and it can avoid falling into local optimum.

The convergence time of different models when performing parameter estimation on different soil heavy metal data sets is shown in Table 1. As can be seen, min is minimum convergence time of model repeating 10 times experiment; mean is the average convergence time of model repeating 10 times experiment; >> represents that the model still does not converge after reaching the maximum number of training rounds. According to the table, the convergence time of the same model on different data sets is different, and the convergence time of different models on the same data set is also different. The difference between minimum convergence time and average convergence time of all

models is small, which indicates that each model is stable and the experiment results are reliable. The competing deep Q network model does not converge after reaching the maximum number of training rounds on Cr and Ni data sets. In addition, minimum convergence time and average convergence time of the proposed adaptive deep Q network model on each data set are smaller than those of contrast models; thus the proposed model has better performance and certain advantages. In summary, the convergence speed of proposed model is better than that of contrast models, the performance is better, and the expected effect can be achieved.

4.4.2. Prediction Results of the Model. To verify the prediction effect of proposed model on soil heavy metal content, the prediction effect between proposed and random forest regression model (RFR) and inverse distance weighted model (IDW) is compared. The results are shown in Figures 7~10, and the comparison between predicted value and actual value on test set is shown in Figure 11. In Figures 7~10, the abscissa and ordinate are sampling point and predicted value (mg/kg), respectively. In Figure 11, *a* is the verification result on Cd data set; *b* is the verification result on Cr data set; *c* is the verification result on Ni data set; and *d* is the verification result on Pb data set.

As can be seen from Figures 7(a) and 7(c), for IDW model, the error between predicted value and actual value is

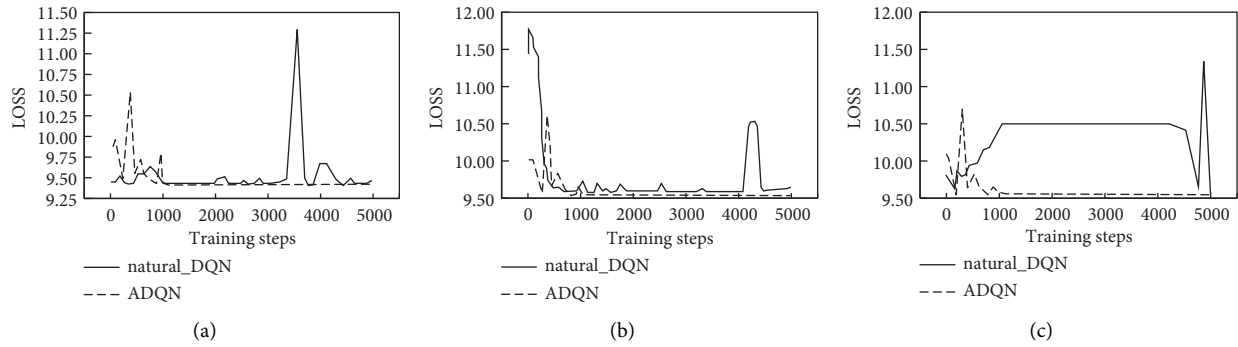


FIGURE 5: Training of different models on Ni data set.

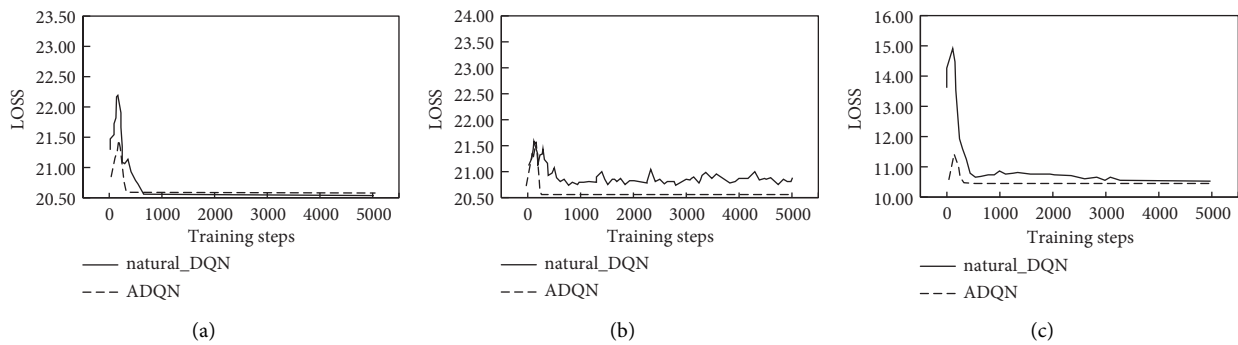


FIGURE 6: Training of different models on Pb data set.

TABLE 1: Convergence time of different models on different data sets (s).

Model —	Cd		Cr		Ni		Pb	
	Min	Mean	Min	Mean	Min	Mean	Min	Mean
DQN	435	4.68	19.50	20.97	6.60	7.10	6.77	7.28
DDQN	4.42	4.76	17.79	19.13	6.39	6.88	9.33	10.04
DuDQN	5.57	5.99	>>	>>	>>	>>	7.45	8.02
ADQN	3.56	3.83	15.22	1637	3.67	3.95	4.59	4.94

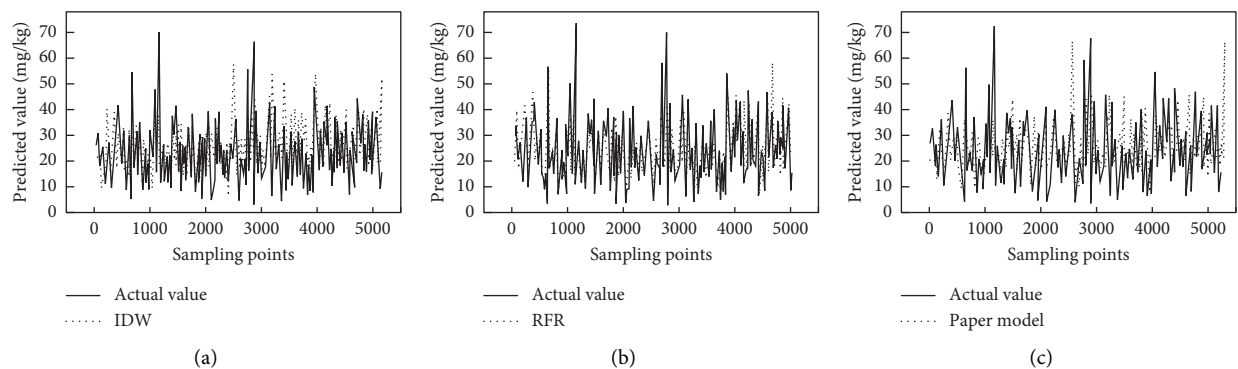


FIGURE 7: Predicted value of different models on Cd data set.

obvious. The proposed model has a large error between predicted value and actual value, and the predicted values of most sampling points basically coincide with the actual

values, thus the hyperparameters of model are adaptively adjusted, and the prediction accuracy of model to spatial data is improved. Moreover, Figures 7(b), 8(b), 9(b), and

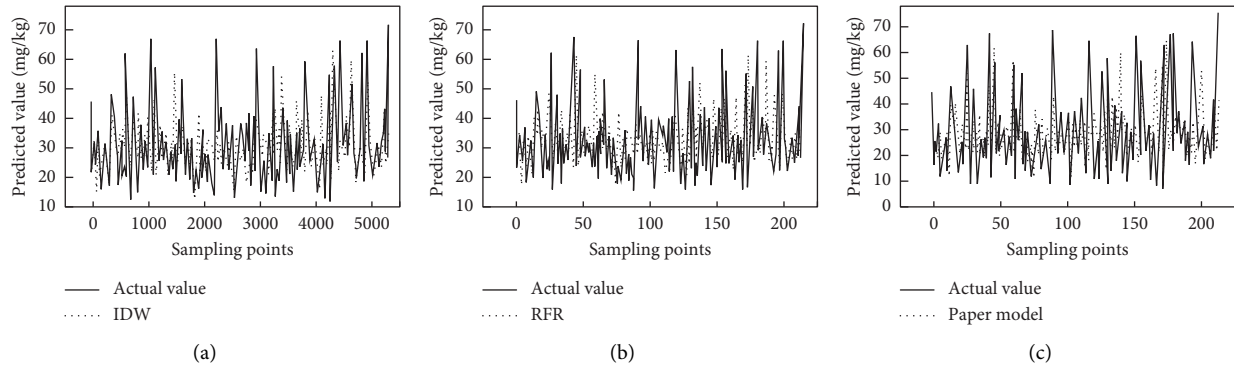


FIGURE 8: Predicted value of different models on Cr data set.

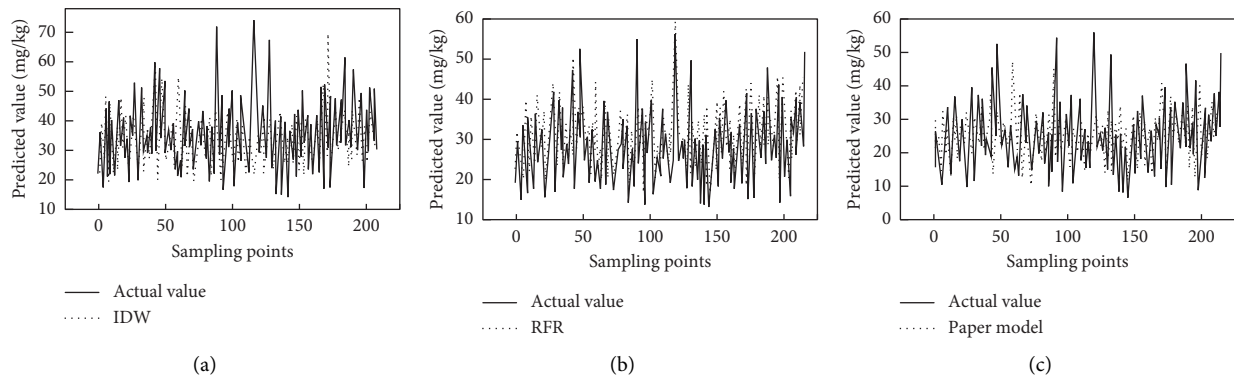


FIGURE 9: Predicted value of different models on Ni data set.

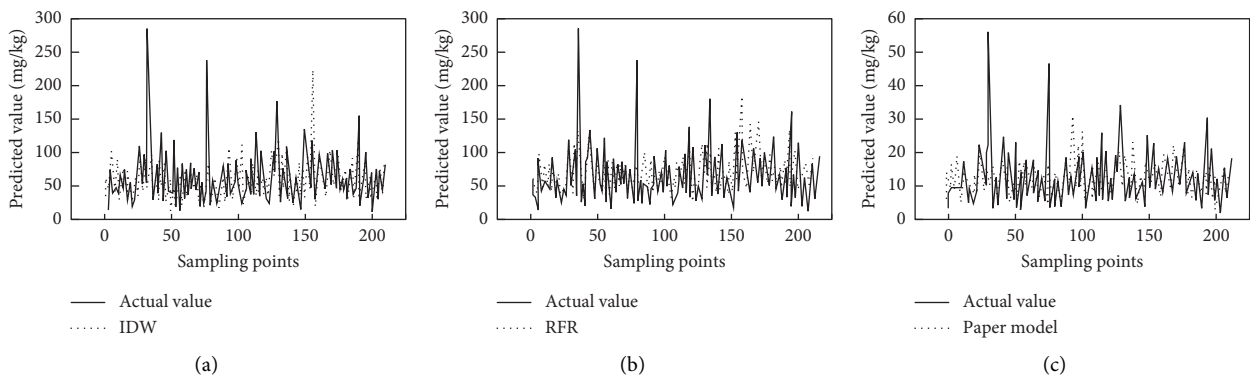


FIGURE 10: Predicted value of different models on Pb data set.

10(b) show that the error between predicted value and actual value of RFR model on training set is the smallest, and the prediction effect is the best. The reason is that RFR model has high feature extraction ability for nonlinear data, and it can adapt to high-dimensional data. Figures 7–10 show that RFR model has the best spatial prediction performance on the training data set. The prediction performance of proposed model and IDW model is poor at a few sampling points, but the error is within the acceptable range.

Figure 11 shows the predicted effect of different models on test data set, and the overall trend is basically the same. For RFR model, the error between predicted

value in test set and actual value is large, which is significantly higher than IDW model and proposed model. The reason may be that there is overfitting in RFR model during training process. What is more, the meaningless features are learned, so as to lead to poor prediction performance. Compared with IDW model, the predicted value of proposed model is closer to the actual value, and there is no abnormal predicted value, which indicates that the proposed model has more stable spatial prediction performance. In conclusion, the prediction performance of proposed model is superior to RFR model and IDW model.

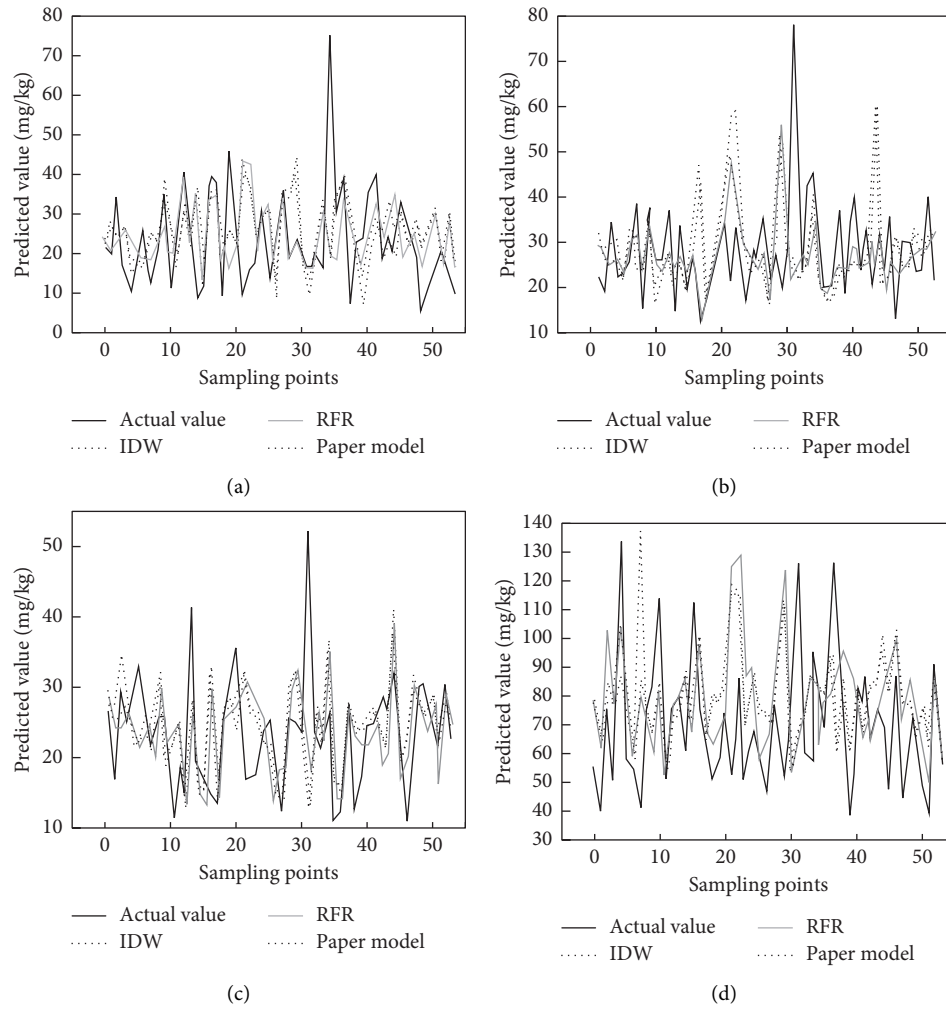


FIGURE 11: Prediction result of different models on different test sets.

TABLE 2: Prediction error of different models on different data sets

Models	Training				Validation				
	MSE	MAE	RMSE	MAPE (%)	MSE	MAE	RMSE	MAPE (%)	
<i>Cd</i>	SAIDW	138.67	8.46	11.77	63.68	203.55	10.11	14.27	84.96
	IDW	174.07	10.22	13.19	7634	225.69	10.84	15.02	89.67
	RFR	57.54	4.55	7.58	31.27	217.05	11.91	14.76	101.04
<i>Cr</i>	SAIDW	97.41	7.11	9.87	28.19	144.41	8.20	12.02	35.25
	IDW	119.63	8.40	10.93	33.22	158.79	8.49	12.60	36.46
	RFR	48.17	3.89	6.94	15.24	168.83	8.91	12.99	38.12
<i>Ni</i>	SAIDW	53.57	5.17	7.31	27.41	69.52	5.52	8.34	27.48
	IDW	76.06	6.59	8.72	33.60	73.63	5.77	8.58	28.04
	RFR	31.61	3.04	5.62	14.40	76.71	6.23	8.76	32.12
<i>Pb</i>	SAIDW	1037.1	18.91	18.91	27.89	690.88	20.63	26.28	34.03
	IDW	1279.24	22.52	35.76	33.87	712.62	21.02	26.69	34.44
	RFR	456.46	10.34	21.36	14.89	886.51	22.03	29.77	39.06

To quantitatively analyze the performance of each model, the evaluation indicators of each model are compared, and the results are shown in Table 2. As can be seen, in training data set, the indicator values of RFR model are lower than those of proposed model and IDW model. However, in

the test set, the indicator values of RFR model are greater than those of proposed model, which indicates that RFR overfits on the training set. To avoid such a situation, the parameters of RFR model need to be adjusted, which will consume a lot of time cost. Compared with IDW and RFR

models, the MSE, RMSE, MAPE, and MAE values of proposed model on the test set are lower. The reason is that the adaptive deep Q network can adaptively allocate the corresponding hyperparameters of each prediction point, which makes model more suitable for the interpolation spatial characteristics of prediction points. Here the prediction results are more accurate and consistent with the above conclusion, which shows that proposed model has the best performance in all indicators. Compared with RFR model and IDW model, the prediction accuracy of proposed model increases by 13.03% and 7.47%, respectively, and the prediction performance of soil heavy metal content is the best.

5. Conclusion

In conclusion, the proposed prediction method of soil heavy metal content based on deep reinforcement learning uses deep Q network as basic model, and it utilizes state value reuse to promote agent to learn the training samples quickly; thus the convergence rate of model is improved. At the same time, adaptive fuzzy membership factor is introduced to change the sensitivity of agent to environmental feedback value in different training periods, which improves the stability of model after convergence. Moreover, adaptive inverse distance interpolation method is adopted to predict the observed values of interpolation points; thus the prediction accuracy of model is improved. Compared with RFR model and IDW model, the proposed model performs better in MSE, RMSE, MAPE, and MAE. The prediction accuracy of soil heavy metal content is higher, which increases by 13.03% and 7.47%, respectively. Although certain research results have been achieved, there are still some shortcomings. Due to the high interpolation accuracy, the proposed prediction model takes a lot of time to complete a training, which has certain disadvantages for the actual prediction of soil heavy metal content. Therefore, a more suitable method needs to be found to train the model, so as to shorten the training time.

Data Availability

The experimental data used to support the findings of this study are available from the corresponding author upon request.

Conflicts of Interest

The authors declare that they have no conflicts of interest regarding this work.

Acknowledgments

This work was sponsored in part by science and education joint project of Hunan Natural Science Foundation (2020JJ7058).

References

- [1] X. Liu, S. Gu, S. Yang, J. Deng, and J. Xu, "Heavy metals in soil-vegetable system around E-waste site and the health risk assessment," *The Science of the Total Environment*, vol. 779, pp. 146438–146448, 2021.
- [2] J. Lan, S. Zhang, Y. Dong et al., "Stabilization and passivation of multiple heavy metals in soil facilitating by pinecone-based biochar: mechanisms and microbial community evolution," *Journal of Hazardous Materials*, vol. 420, pp. 126588–126598, 2021.
- [3] I. Khan, S. A. Awan, M. Rizwan et al., "Effects of silicon on heavy metal uptake at the soil-plant interphase: a review," *Ecotoxicology and Environmental Safety*, vol. 222, pp. 112510–112516, 2021.
- [4] D. Yang, S. Yang, H. Yuan et al., "Co-benefits of biochar-supported nanoscale zero-valent iron in simultaneously stabilizing soil heavy metals and reducing their bioaccessibility," *Journal of Hazardous Materials*, vol. 418, pp. 126292–126296, 2021.
- [5] X. Guo, Y. Wu, N. Li, Y. Tian, Y. Peng, and D. Yuan, "Effects on the complexation of heavy metals onto biochar-derived WEOM extracted from low-temperature pyrolysis," *Ecotoxicology and Environmental Safety*, vol. 221, pp. 112456–112460, 2021.
- [6] A. Rana, M. Sindhu, A. Kumar et al., "Restoration of heavy metal-contaminated soil and water through biosorbents: a review of current understanding and future challenges," *Physiologia Plantarum*, vol. 173, no. 1, pp. 394–417, 2021.
- [7] J. Zhang, G. Mu, Z. Zhang, X. Huang, and H. Fang, "Speciation variation and bio-activation of soil heavy metals (Cd and Cr) in rice-rape rotation lands in karst regions," *International Journal of Environmental Research and Public Health*, vol. 18, no. 3, pp. 1364–1368, 2021.
- [8] Y. P. López, F. A. da Fonseca Breda, E. S. A. Lima, C. da Costa Barros de Souza, J. M. F. González, and N. M. B. do Amaral Sobrinho, "Variability factors of heavy metals in soils and transfer to pasture plants of Mayabeque in Cuba," *Environmental Monitoring and Assessment*, vol. 193, no. 5, pp. 245–247, 2021.
- [9] S. Shao, B. Hu, Y. Tao, Q. You, and Z. Shi, "Comprehensive source identification and apportionment analysis of five heavy metals in soils in Wenzhou City, China," *Environmental Geochemistry and Health*, vol. 38, pp. 1–24, 2021.
- [10] S. Mandal, S. Pu, S. Adhikari et al., "Progress and future prospects in biochar composites: application and reflection in the soil environment," *Critical Reviews in Environmental Science and Technology*, vol. 51, no. 3, pp. 219–271, 2021.
- [11] R. Ramlan, M. B. Cyio, M. Napitupulu et al., "Pollution and contamination level of Cu, Cd, and Hg heavy metals in soil and food crop," *International journal of Environmental Science and Technology*, vol. 25, pp. 1–12, 2021.
- [12] M. Xiang, Y. Li, J. Yang et al., "Heavy metal contamination risk assessment and correlation analysis of heavy metal contents in soil and crops," *Environmental Pollution*, vol. 278, pp. 116911–116917, 2021.
- [13] J. Moon, M. Yang, and J. Jeong, "A novel approach to the job shop scheduling problem based on the deep Q-network in a cooperative multi-access edge computing ecosystem," *Sensors*, vol. 21, no. 13, p. 4553, 2021.
- [14] B. Peng, Q. Sun, S. E. Li, D. Kum, and T. Gu, "End-to-End autonomous driving through dueling double deep Q-network," *Automotive Innovation*, vol. 45, pp. 1–12, 2021.
- [15] T. H. Ho, J. W. Kim, S. H. Son, H. Kim, K. Lee, and J. M. Lee, "Automatic control of simulated moving bed process with deep Q-network," *Journal of Chromatography A*, vol. 1647, pp. 462073–462078, 2021.

- [16] S.-H. Kim, Y.-R. Yoon, J.-W. Kim, and H.-J. Moon, "Novel integrated and optimal control of indoor environmental devices for thermal comfort using double deep Q-network," *Atmosphere*, vol. 12, no. 5, pp. 629–632, 2021.
- [17] Y. Wang, X. Li, P. Wan, L. Chang, and X. Deng, "Dueling deep Q-networks for social awareness-aided spectrum sharing," *Complex & Intelligent Systems*, vol. 23, pp. 1–12, 2021.
- [18] Y. Dai, K. Lee, and S. G. Lee, "A real-time HIL control system on rotary inverted pendulum hardware platform based on double deep Q-network," *Measurement and Control*, vol. 54, no. 3-4, pp. 417–428, 2021.
- [19] D. Kim, S. Y. Kwon, J. Woo, W. M. Kang, and J. H. Lee, "On-chip trainable hardware-based deep Q-networks approximating a backpropagation algorithm," *Neural Computing & Applications*, vol. 46, pp. 1–12, 2021.
- [20] L. Chen, Y. Zhao, H. Zhao, and B. Zheng, "Non-communication decentralized multi-robot collision avoidance in grid map workspace with double deep Q-network," *Sensors*, vol. 21, no. 3, pp. 841–845, 2021.
- [21] Y. Xue, R. Wu, J. Liu, and X. Tang, "Crowd evacuation guidance based on combined action reinforcement learning," *Algorithms*, vol. 14, no. 1, p. 26, 2021.
- [22] A. Skrynnik, A. Staroverov, E. Aitygulov, K. Aksenov, and A. Panov, "Hierarchical deep Q-network from imperfect demonstrations in minecraft," *Cognitive Systems Research*, vol. 65, no. prepublish, pp. 74–78, 2021.
- [23] Z. He, K. P. Tran, S. Thomassey, X. Y. Zeng, J. Xu, and C. H. Yi, "A deep reinforcement learning based multi-criteria decision support system for optimizing textile chemical process," *Computers in Industry*, vol. 56, pp. 103373–103376, 2020.
- [24] S. Shivanshu, B. Chen, C. Chen, H. Wang, and M. Dai, "Deep Q-network learning based downlink resource allocation for hybrid RF/VLC systems," *IEEE ACCESS*, vol. 8, pp. 149412–149434, 2020.

Research Article

A Novel Multiobjective Particle Swarm Optimization Combining Hypercube and Distance

Xiaoli Shu ¹, Yanmin Liu ², Qian Zhang³ and Meilan Yang ³

¹School of Data Science and Information Engineering, Guizhou Minzu University, Guiyang Guizhou 550025, China

²School of Mathematics, Zunyi Normal College, Zunyi Guizhou 563002, China

³School of Mathematics and Statistics, Guizhou University, Guiyang Guizhou 550025, China

Correspondence should be addressed to Yanmin Liu; yanmin7813@163.com

Received 21 December 2021; Revised 13 February 2022; Accepted 15 February 2022; Published 14 April 2022

Academic Editor: Hangjun Che

Copyright © 2022 Xiaoli Shu et al. This is an open access article distributed under the Creative Commons Attribution License, which permits unrestricted use, distribution, and reproduction in any medium, provided the original work is properly cited.

The multiobjective optimization problems are a common problem in various fields in the real society. Therefore, solving the multiobjective optimization problems are one of the important problems studied by many researchers in recent years. From the research in recent years, it can be seen that there is still a lot of room for development of particle swarm optimization in solving multiobjective optimization problems. This paper proposes a novel multiobjective particle swarm optimization combining hypercube and distance, called HDMOPSO. The particle velocity update part in this paper uses a combination of hypercube and distance. In order to prevent the algorithm from falling into the local optimum, the part also uses the nonlinear decreasing opposite mutation strategy, which enables the particles to explore a more area. Finally, a control strategy is used for external archive to improve the convergence and diversity of the algorithm. The algorithm has been simulated in 22 test problems and compared with multiobjective particle swarm optimization algorithms (MOPSOs) and multiobjective evolutionary algorithms (MOEAs). The results show that the HDMOPSO can effectively improve the convergence and diversity, so it is an effective improvement.

1. Introduction

In real life, many problems are composed of multiobjective that conflict and influence each other. When an objective is found to be the best solution, it cannot guarantee that other objectives are also the best solution at the same time, but may lead to degradation. Scientists usually try to make these objectives reach the best state in an enclosed area, which is multiobjective optimization problems (MOPs).

In recent years, it has become one of the important methods to integrate biological information into meta-heuristic algorithms to solve multiobjective optimization problems in evolutionary algorithms. Typical multiobjective evolutionary algorithms (MOEAs) are genetic algorithm [1], multiobjective particle swarm optimization [2], multiobjective bee colony algorithm [3], multiobjective ant colony algorithm [4], and multiobjective differential algorithm [5] and so on. The particle swarm optimization (PSO) is similar

to the genetic algorithm. It is also an algorithm invented based on the behavior of the population in nature. Because of its simple principle, high search efficiency, fast convergence and so on, it is widely used in various fields of industrial production.

When using PSO to deal with MOPs, we should not only consider the common difficulties in the process of traditional multiobjective optimization, but also consider the problems targeted by PSO when applied to MOPs. There are four main problems: (1) The optimal particle selection strategy (i.e., how to select the “leader” particle to lead the entire population to quickly approach the Pareto front while retaining some individual information); (2) Mechanisms for maintaining diversity (i.e., how to guide particles out of the local optimal solution); (3) Convergence improvement means (i.e., how to improve the search efficiency while maintaining the diversity of the population when the external archive set increases sharply, and strengthen the advantage of the

algorithm in terms of convergence velocity); and (4) The balance method of diversity and convergence (i.e., how to dynamically coordinate the relationship between development and local search at different stages of the optimization process to obtain the best optimization results).

In order to solve the above four problems, scientists have proposed various solutions. Among them, how to choose the “leader” particles? Qingling Zhu et al. [6] proposed to select a leader from an external archive set and decompose the multiobjective optimization problems into a single optimization problem. This method greatly reduces the computational complexity of the algorithm and also improves the convergence velocity of the algorithm. The fast convergence speed and high convergence accuracy of the algorithm often lead to poor diversity performance. Dividing the population into multiple subgroups [7] and various maintenance strategies for external archive [8] can effectively improve the diversity of the algorithm. For the method of balancing diversity and convergence, a combination of multiple strategies [9] was required. Generally, combining the selection of the “leader” with the update strategy of the external archive can effectively balance the convergence and diversity of the algorithm. Because a good “leader” selection strategy can more efficiently guide the population to converge to the Pareto front, and a good external archive control strategy can better maintain the diversity of the population. However, Xingyi Zhang et al. [10] proposed a multiobjective particle swarm optimization with a competitive mechanism. This method was different from most multiobjective particle swarm optimization algorithms (MOPSOs) because it does not use external archive. It was more competitive in balancing diversity and convergence compared with most MOPSOs. Means for improving convergence, although the strategy of choosing a good “leader” can effectively improve the convergence of the algorithm, as the dimensionality increases, the convergence of the algorithm will be affected. Since the inertia weight can effectively affect the convergence of the algorithm in the scientific field, some assumptions about the inertia weight can effectively improve the convergence of the algorithm. For example, Peng Guang et al. [11] proposed a dynamic learning factor. Of course, it is not only the above methods that solve the multiobjective optimization problem, but also more extensive exploration in the scientific field. Therefore, the main contributions of this paper are as follows:

- (1) A control strategy for external archive is proposed. In the continuous iterative update of the algorithm, the nondominant solutions produced will gradually increase, which not only increases the complexity of the algorithm, but also affects the convergence and diversity of the algorithm. Therefore, when the total number of nondominant solutions and newly generated nondominant solutions in the external archive exceed the preset threshold, the hypercube technology is used in the external archive to control the nondominant solutions within the preset threshold. First, the hypercube is created in an external archive. Then, a hypercube is created in the densest

hypercube. Finally, a nondominant solution is randomly deleted from it. This cycle continues until the sum of the number of nondominant solutions and the number of newly generated nondominant solutions in the external archive is within the preset threshold. This method can effectively maintain the diversity of solutions and improve the convergence of algorithm.

- (2) A nonlinear decreasing opposite mutation is proposed. This strategy performs nonlinear decreasing opposite mutation on the particles of the nondominant solution generated after each iteration update, which can effectively prevent the algorithm from falling into the local optimal solution. Using the method of nonlinear declining can well balance the global exploration and local exploration capabilities of the algorithm, and is an effective method to balance diversity and convergence.
- (3) The combination of hypercube and distance method is proposed to set the particle velocity to update the social part. First, the hypercube established based on the objective function value of the nondominant solution in the external archive. Second, calculating the average value of the nondominant solutions set in each hypercube obtained. We call this value the “generalized position”. This value is the learning position of the social part of the group. Finally, the Euclidean distance method allows each particle to learn from the generalized position closest to itself. This strategy is an effective means to improve the diversity and convergence of algorithms.

The rest of this paper is organized as follows: In Section 2, the relevant background knowledge of this paper is briefly introduced. Section 3 gives the details of the HDMOPSO. Section 4 verifies the performance of HDMOPSO by comparing with existing MOPSOs and MOEAs. Finally, Section 5 introduces the conclusions and future work of this paper.

2. Background

2.1. MOPs. MOP is an optimization problem composed of n -dimensional decision variables, m objective functions, and $P + Q$ constraints. MOPs can generally be transformed into a minimum problem, so the mathematical form of MOPs is expressed as follows:

$$\begin{aligned}
 \text{Min } y &= F(x) \\
 &= [f_1(x), f_2(x), \dots, f_m(x)], \\
 g_p(x) &\leq 0, \quad p = 1, 2, \dots, P, \\
 h_q(x) &= 0, \quad q = 1, 2, \dots, Q, \\
 L_i &\leq x_i \leq U_i, \quad i = 1, 2, \dots, n,
 \end{aligned} \tag{1}$$

where $x = (x_1, x_2, \dots, x_n)^T \in X \in R^n$ is the n -dimensional decision variable; $y = (y_1, y_2, \dots, y_m)^T \in Y \in R^m$ is the m -dimensional objective variable; P is the number of inequality

constraints; Q is the number of equality constraints; and $[L_i, U_i]$ is the boundary of the i -th dimension of the particle.

In MOPs, the definitions of Pareto dominance, Pareto optimal solution, and Pareto optimal solution set are as follows.

$$\{\forall i \in \{1, 2, \dots, n\}, f_i(x_v) \leq f_i(x_u)\} \wedge \{\exists j \in \{1, 2, \dots, n\}, f_j(x_v) < f_j(x_u)\}. \quad (2)$$

Definition 2 (Pareto optimal solution [12]). $x^* \in X$ is the Pareto optimal solution on X , if and only if

$$\exists x \in X, x \prec x^*. \quad (3)$$

Definition 3 (Pareto optimal solution set [12]). The set of all Pareto optimal solutions becomes Pareto optimal set (P^*). The mathematical definition is as follows:

$$P^* = \{x \in X | \exists x' \in X, f_j(x') \leq f_j(x), (j = 1, 2, \dots, m)\}. \quad (4)$$

Definition 4. (Pareto front (PF) [12]). All objective functions corresponding to nondominant solutions constitute the nondominant optimal objective domain, also known as Pareto front (PF). The mathematical definition is as follows:

$$PF = \{F(x^*) = (f_1(x^*), f_2(x^*), \dots, f_m(x^*)) | x^* \in P^*\}. \quad (5)$$

Definition 1 (Pareto dominance [12]). For two decision vectors $x_u, x_v \in X$, x_v dominates x_u which is expressed as $x_v \prec x_u$, if and only if

2.2. PSO. PSO was first proposed by Eberhart and Kennedy [13] in 1995, and its concept originated from the study of bird flock foraging behavior. Ven den Bergh [14] analyzed and proved the stability and convergence of PSO from a theoretical perspective. In 2002, coello et al. [15] applied the PSO to solve MOPs, called multiobjective particle swarm optimization (MOPSO). Imagine a scene where a group of birds randomly search for food in an enclosed area. There is a lot of food in this area, but all the birds do not know where the food is. They only know how far the food is from the current location. Therefore, the simplest and effective strategy is needed to find the food quickly and efficiently. PSO uses a massless particle to simulate birds in a flock of birds. Particles have only two attributes, velocity and position. Velocity represents the speed of the particle's movement, and position represents the direction of the particle's movement. The particle uses the following equation to update its velocity and position:

$$v_i(t+1) = wv_i(t) + c_1r_1(pb_{best}_i(t) - x_i(t)) + c_2r_2(g_{best}_i(t) - x_i(t)). \quad (6)$$

$$x_i(t+1) = x_i(t) + v_i(t+1). \quad (7)$$

The right side of equation (6) consists of three parts. The first part is the inheritance of the particle to the previous velocity, which represents the particle's trust in its own motion state, and is the inertial motion of the particle's previous velocity. Among them, w is called the inertia weight, and its value is non-negative. When the value is large, the global optimization ability is strong, and the local optimization ability is weak. When the value is small, the global optimization ability is weak, and the local optimization ability is strong. The second part is the self-cognition part of the particle, which means that the particle's thinking about itself is derived from the summary of the past experience so as to implement the next behavior decision. Here pb_{best}_i represents the optimal solution found by the i -th particle in the historical experience, which is called "individual extreme value". The third part is the social part, which represents the process of information sharing and mutual cooperation between particles. Particles can make appropriate adjustments to their flight directions by perceiving their experienced companions. In the standard PSO, g_{best}_i represents the optimal solution found so far by the entire group (i.e., the global optimal). In addition, in equation (6)

and (7), v_i represents the velocity of the i -th particle; r_1, r_2 are random numbers between (0, 1). x_i represents the current position of the i -th particle; c_1, c_2 represent acceleration factors.

2.3. The Existing MOPSOs. Since PSO was proposed to solve MOPs in 2002, many scholars have become more and more interested in it. In the past twenty years, there have been many MOPSOs. Below, we'll take a closer look at some of the existing MOPSOs.

Coello et al. [15] first proposed using PSO to solve MOPs. Pareto front was proposed in this algorithm to select the nondominant solution in the current solution and save it in the archive. The global optimal particle was then determined from the archive. Although compared with traditional non-dominated sorting genetic algorithm II (NSGAI) [16], this algorithm has certain advantages. But the diversity of solutions and convergence performance can be further improved. Nebro et al. [17] proposed a velocity constrained multiobjective particle swarm optimization. In this algorithm, the velocity contraction program was used to prevent

the group explosive in the process of particle movement. Literature [7, 8] proposed different methods for the selection of global optimal particles on the basis of [12]. In reference [7], the optimal solution was selected according to the way of using crowding distance in the nondominant solution in the external archive. In reference [8], the selection of the global optimal solution was based on the grid technology in the archive, and the optimal solution was selected according to the grid distance. Experimental results show that literature [7, 8] was superior to the algorithm proposed in literature [12] in both diversity and convergence.

Zapotecas Martinez S et al. [18] proposed a method that relied entirely on decomposition (dMOPSO). The decomposition method was similar to the algorithm proposed by Qingfu Zhang et al. [19], which was to decompose multi-objective optimization problems into several single-objective optimization problems. It can also be combined with other decomposition methods in dMOPSO. In the literature [18], a set of global optimal solutions can give the set value of the best value of all the sub-problems to update the position of the particle. Of course, the algorithm also has some limitations because this algorithm mainly solves continuous and unconstrained multiobjective optimization problems.

Researchers have also proposed other methods to improve the convergence and diversity of the algorithm. The biggest difference between the algorithm proposed by Xingyi Zhang et al. [10] and other MOPSOs was that it does not use external archives. A competition mechanism was used in the algorithm, which was composed of three parts: nondominant solution selection, pair competition and particle learning. Experimental results showed that this algorithm was more competitive than the existing MOPSO algorithm.

The above algorithms in the paper were almost aimed at some continuous, discontinuous, concave, and convex properties of MOPs. MOPs are more than that. Ying Hu et al. [20] proposed a feature selection problem to solve fuzzy costs, in which fuzzy advantage relations were used instead of traditional Pareto dominance and fuzzy crowded distances were used to update files. A set of nondominant solutions can be calculated by using defined fuzzy concepts applied to an algorithm. This was a highly competitive approach to the problem of feature selection. The algorithm proposed by Zhang Yong et al. [21] was a powerful tool for optimizing building energy preferences. A perturbation strategy was proposed and control parameters such as inertia weight and acceleration were deleted compared with the traditional MOPSOs. The traditional MOPSOs were more sensitive to control parameters.

2.4. Opposite Direction. In 2005, Hamid R. Tizhoosh [22] proposed the concept of the opposite direction. Some researchers used the opposite direction strategy for initialization, two sets of positions were generated when the position was initialized. One set was randomly generated, and the other set was generated in the opposite direction based on the existing position. Literature [23] used the opposite direction for learning strategies. The reason for the

opposite direction is because in a given environment, our search direction may be opposite to the direction of the optimal solution. If we continue to search in the wrong direction, the algorithm will not get better results. So we can observe all directions in the search process. Sometimes it may be advantageous to look in the opposite direction. If the opposite direction is advantageous, then the first step in finding the opposite direction is as follows:

Definition 5 (opposite direction [22]). x is a real number defined in a certain interval, $x \in [L, U]$, if \bar{x} is the opposite value of x , the definition of \bar{x} is as follows:

$$\bar{x} = L + U - x. \quad (8)$$

Similarly, the opposite number can also be defined in the case of multiple dimensions.

Corollary 1 (see [22]). *There is $x = (x_1, x_2, \dots, x_n)$, where $x_1, x_2, \dots, x_n \in R$ and $x_i \in [L_i, U_i]$, then the opposite of \bar{x} is defined by x_1, x_2, \dots, x_n , which is defined as follows:*

$$\bar{x}_i = L_i + U_i - x_i \quad (i = 1, 2, \dots, n). \quad (9)$$

3. HDMOPSO

Research has shown that the choice of “leader” particles in PSO is crucial in recent years. The “leader” particle can choose the best solution the particle has found so far in single-objective optimization, but MOPs is not the same as single-objective optimization because multiobjective optimization is restricted by multiobjective and generates more than one nondominant solution each time. Therefore, a good “leader” selection strategy can effectively improve the convergence and diversity of the algorithm. In addition, Because PSO has a fast convergence speed, it may make the algorithm fall into local optimal in MOPs. The nondominant solution particles after each iteration are used to nonlinearly reduce the opposite mutation so that the particles can explore more area in this paper. Finally, this paper also uses an external archive control strategy to improve the convergence and diversity of the algorithm. The details are introduced as follows.

3.1. Control Strategy for External Archive. The external archive is used to store the nondominant solutions after each iteration, and it is the candidate solutions, also called the solutions. When the external archive is empty, the solutions will directly enter the external archive. Because a new set of solutions is generated after each update population, this new set of solutions is compared to the historical solution in the external archive. Such behavior is called “elitism”. It has three situations. (1) If the new solutions dominate the historical solutions in the external archive, the historical solutions will be deleted in the external archive. (2) If the new solution is dominated by the historical solutions in the external archive, the dominated new solutions will also be automatically discarded. (3) If the historical solutions in the external archive and the new solutions do not dominate each other,

the solutions in the external archive and the newly generated solutions remain unchanged. After judging the above three situations, the final solutions will be placed in an external archive. However, as the number of iterations increases, the nondominant solutions in the external archive gradually increase, which will increase the subsequent calculation work and also easily cause the algorithm to fall into a local optimal situation. Therefore, an external archive control strategy is needed to control the nondominant solutions within a certain threshold. The convergence and diversity of the algorithm are improved at the same time.

This paper uses hypercube technology to control external archive within a certain threshold. The main problem of external archive control is that the particles in the external archive are all nondominant solutions and do not dominate each other. There may be very small nondominant solutions that prevent the algorithm from maintaining diversity. Therefore, this paper mainly builds hypercube based on the value of the objective function value of the nondominant solutions, from which the densest hypercube is selected to create a hypercube, and then one is randomly deleted. The cycle continues until all new solutions after elitism are put into the external archive. Figure 1 shows the control strategy of the external archive when the objective number is two. Begin to establish fixed hypercube according to the objective function value of the current nondominant solutions, and then select a hypercube with high density each time to establish an adaptive hypercube again, and randomly delete one from the hypercube with high density. The above method can effectively delete the denser nondominant solutions in the external archive and increase the diversity of the algorithm. In addition, each time fixed hypercube is established based on the objective function value of the current nondominant solutions, and then an adaptive hypercube is established in the densest hypercube, which greatly reduces the computational complexity of the algorithm.

3.2. Nonlinear Decreasing opposite Mutation Strategy. At present, mutation strategy is often used to improve the performance of the algorithm, but the mutation used in this paper is a combination of exploration and convergence. It differs from most of the mutations proposed by the researchers, because most of the current mutation is to increase the particle's exploration ability and the ability to jump out of the local optimal solution. For example, the mixed mutation and jump mutation proposed in the literature [24]. However, the opposite mutation of nonlinear decreasing in this paper is that the current nondominant solution is not guided by better particles in the social part, so opposite search is carried out to prevent the algorithm from falling into the local optimal solution. In addition, the global search tends to local search in nonlinear decreasing way, which is beneficial to the convergence of the algorithm. So the mutation also has the ability to converge.

In the multiobjective particle swarm optimization, as the iteration increases, the algorithm converges quickly.

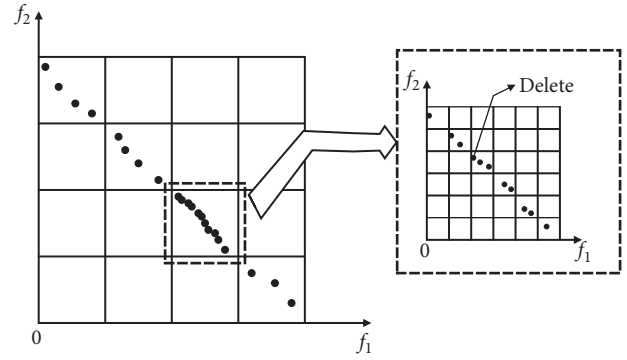


FIGURE 1: Control strategy for external archive.

According to the characteristics of the PSO, all particles are generally searched based on the particles of the nondominant solutions that have been generated. As a result, the particles currently in the nondominant solutions can only judge the next search direction based on the inheritance of the previous velocity and their own experience. If these particles have no particle leadership, the search may deviate from the right direction. If it continues to search in this way, it will not only affect the convergence velocity of the algorithm, but also affect the convergence of the algorithm. Therefore, this paper proposes a nonlinear decreasing opposite mutation strategy. If the particle loses the direction guided by the social part, it may be beneficial to search in the opposite direction. But it is definitely impossible for all particles to search in the opposite direction. Because all the particles search in the opposite direction, the population will gradually move away from the better solution and it is always part of the search process, which makes the algorithm unable to converge well. So, this paper adopts the opposite mutation of the particles that get new nondominant solutions after each iteration. Figure 2 shows mutation simulation that there are 15 particles in a certain area, and after a certain iteration, three nondominant particles are produced. As can be seen from the left image in Figure 2, there are some areas in this area that can be further explored. Therefore, we use the strategy of opposite mutation of nondominant solutions particles so that the particles can explore more areas, the same as 1, 2, and 3 in Figure 2. However, it is impossible to explore farther places all the time, which will hinder the convergence of the algorithm and may also deteriorate the performance of the algorithm. So we used nonlinear decreasing opposite mutation. In the early stage of the algorithm, the particles of the new nondominant solutions undergoing farther opposite mutation can better perform global exploration. With the increase of iterations, the algorithm also enters the final stage, because the algorithm is best to converge to the Pareto front, so it needs to be locally explored to the current nondominant solutions in the later stage. Therefore, a small range of opposite mutation is carried out at the end of the algorithm, and local exploration is carried out, so that the algorithm can gradually converge to the Pareto front. The pseudocode of the nonlinear decreasing opposite mutation search strategy is shown in Figure 3.

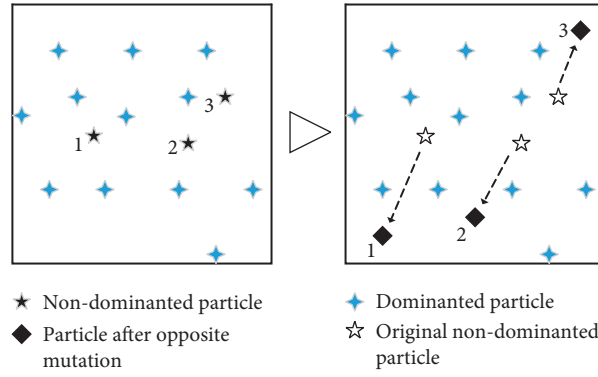


FIGURE 2: Mutation simulation.

```

% position=particle position
% gencount=current iteration
% maxgen=total number of iterations
% a=nonlinear decreasing factor
% rank(i)=1, i is the non-dominated solution at this time
function Opposition-Mutation-Operator(position, gencount, U, L, rank, maxgen)
    a=(1-gencount/maxgen);
    for i=1 to n
        if rank(i)=1
            Position(i,:)=U(i,:)+L(i,:)-a*position(i,:);
        else
            position(i,:)=position(i,:);
        end if
    end for
end function

```

FIGURE 3: Pseudocode of nonlinear decreasing opposite mutation.

3.3. Setting the Social Part Based on the Method of Combining Hypercube and Distance. Figure 4 shows the flying direction of the particle in PSO. The symbols in the figure indicate the reference equation (6). It can be seen from Figure 4 that the particle i finally determines the next flight direction according to three parts. Since the social part of the guidance represents the optimal position that the group finds, the position has more resources, so $gbest_i$ is the key factor for the next flight direction of particle i . From the above analysis, we can know that actually refers to $gbest_i$ position. Since in the single-objective particle swarm optimization algorithm, there is only one optimal solution of the population after each iteration, so the effect of the particle learning of the population following the optimal solution in the population in the social part may be the best. However, there is more than one optimal solution in the multiobjective particle swarm optimization. If one optimal solution is used blindly to lead the particles to fly, it may cause the particles to converge in one direction and lose the diversity of the

algorithm. At present, the most used strategy in this part is roulette-wheel, which uses a certain probability to make each particle choose a leader to lead itself, but this method is more random.

This paper avoids this randomness and proposes a method based on the combination of hypercube and distance to set the social part of the particle velocity update equation under external archive. According to the establishment of hypercube in the external archive, the candidate solutions in the external archive are divided into a certain number of hypercube according to the objective function value. Take the nondominant solutions set in each hypercube to find its average value. In this process, the nondominant solutions in the same hypercube can effectively exchange information. Figure 5 shows the hypercube created by the candidate solutions in the external archive when the problem is two objectives. For any hypercube, if the space has k nondominant solutions, the average of different dimensions is calculated. As shown in (10), where j represents the j -th hypercube, u represents the number of hypercube with nondominant solutions, k represents that the space has k nondominant solutions, and i represents decision variable dimension. It can be seen from Figure 5 that there is more than one such hypercube, so this paper also uses the shortest distance method to make each particle autonomously choose its own average value. As shown in (11), the particles are compared with the average value in each hypercube until the \bar{X}_j corresponding to the minimum d_{\min} is selected. At this time, the velocity update equation of the particle swarm algorithm is shown in (12). In equation (12), \bar{X}_j is the direction guide of the i particle in the social part in t iterations. \bar{X}_j is determined by equation (11). The rest of the parameter analysis is consistent with equation (6).

$$\bar{X}_{j_i} = \frac{x_{j_{i1}} + x_{j_{i2}} + \dots + x_{j_{ik}}}{k}, \quad (i = 1, 2, 3, \dots, n; j = 1, 2, \dots, u), \quad (10)$$

$$d_{\min} = \left(\sum_{j=1}^u \bar{X}_j - x \right)^{1/2}, \quad (11)$$

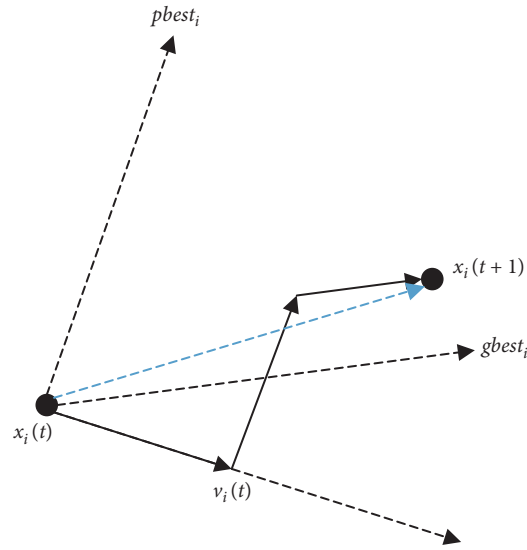


FIGURE 4: Display of the flying direction of particle i .

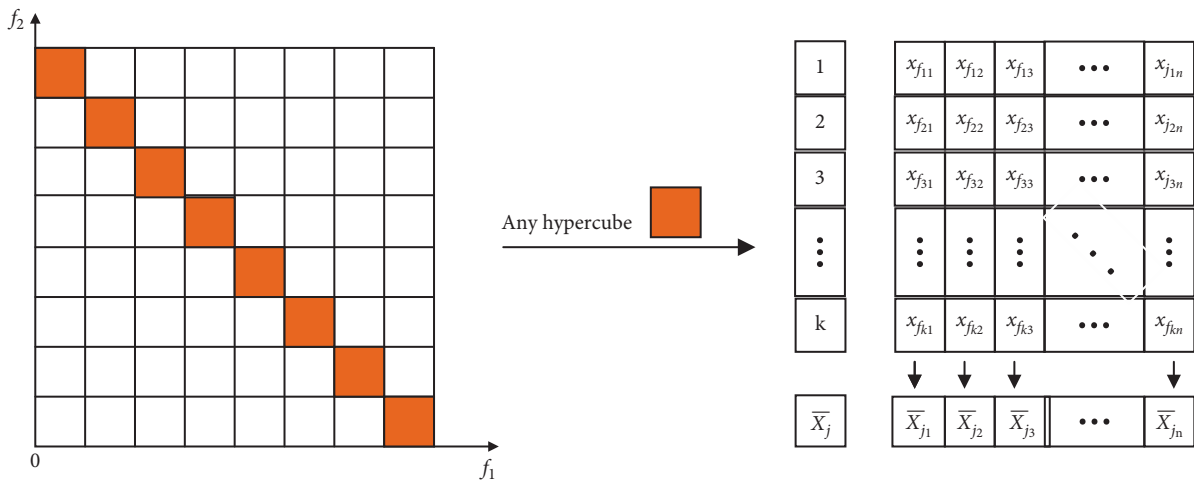


FIGURE 5: The setting of the social part is based on hypercube.

$$v_i(t+1) = wv_i(t) + c_1r_1(pbest_i(t) - x_i(t)) + c_2r_2(\bar{X}_j(t) - x_i(t)). \quad (12)$$

3.4. Steps of HDMOPSO. The steps of HDMOPSO are as follows:

Step 1 (initialize). First, set related parameters, such as population size N , inertia weight w , and learning factors c_1 , c_2 , etc. Secondly, randomly initialize the positions of N particles and set the velocity $v=0$. Finally, the individual extreme value is determined.

Step 2. The dimension of particles is disturbed, similar to literature [12]. However, in this paper, random selection of reference dimensions, random selection of particles and dimensions requiring variation are used to increase the diversity of the algorithm.

Step 3. Calculate the target value for each particle.

Step 4. The Pareto dominant sorting method is used to sort each particle (reference [12]), and the nondominant sorting is selected to be released into the external archive.

Step 5. Update the external archive as described in Section 3.1.

Step 6. The opposite mutation of the method particles is nonlinear decreasing according to Section 3.2.

Step 7. The individual extreme values are updated based on the sorting values of Step 4. If the particle ranks higher, the individual extremum is updated. If there is no promotion, there is no update. If the rank is the same, the choice is made randomly with a probability of 0.5.

Step 8. Set up the social section as described in Section 3.3.

Step 9. The particle velocity and position are updated using equation (12) and (7).

Step 10. If the maximum number of iterations is reached, the algorithm ends; otherwise, return to Step 2.

4. Experimental Study

4.1. Test Problems. In order to better test the performance of HDMOPSO, this paper uses the test problems of ZDT1-4 and ZDT6 [25], which are concave and convex in geometrical problems, and the test problems have two objectives. In order to show the performance of this algorithm as much as possible, this paper also uses DTLZ1-7 [26], the test problems are geometrically linear, convex, and scalable. Finally, this paper also uses the more complex and difficult to converge to the Pareto front UF1-10 [27] test problems to test the performance of the algorithm in this paper.

4.2. Performance Indicators. Inverse generation distance (IGD) [28] and hypervolume (HV) [29], standard deviation (Std.), statistical boxplot, convergence trajectory comparison, and Pareto front simulation are used to compare the performance of each algorithm. The reason for choosing these test indicators is because they are used in most of the literature to compare the performance of various multi-objective optimization algorithms. Both IGD and HV are comprehensive indicators used to evaluate the convergence and diversity of algorithms. But the two are different. IGD is the average of the minimum distance between the set of points on Pareto front surface and the population. HV does not need Pareto front, only a reference point, and the comprehensive performance of the algorithm is evaluated according to the hypervolume obtained from the solution to the reference point. Among them, the smaller the IGD value, the better the convergence and diversity of the algorithm. The larger the value of HV, the better the quality of the solution set. Std. is used to evaluate the stability of the algorithm, and use statistical boxplots to further illustrate the stability of the algorithm. The trajectory compares the convergence velocity of each algorithm.

4.3. Experimental Settings. In this section, we will compare HDMOPSO with seven MOPSOs (MOPSO [15], MOPSOCD [30], dMOPSO [18], SMPSO [17], NMPSO [31], MPSOD [32], CMOPSO [10]) and seven MOEAs (AGEII [33], ANSGAIII [34], DGEA [35], NSGAIII [36], MOEAD [19], ARMOEA [37], and AGEMOEA [38]) to verify its performance (the full name of the acronyms here is shown in Table 1). The settings in the test problems are as follows: ZDT1-4 and ZDT6 are two objective problems, the population size is 200, the number of decision variables of ZDT1-3 is 30 dimensions, and the number of decision variables of ZDT4 and ZDT6 is 10 dimensions; The DTLZ settings are all three objective problems, the population size is 100, and the

number of decision variables is 12 dimensions; UF1-7 is set to two objective problems, while UF8-10 is set to three objective problems, the population size is all 200, and the number of decision variables is all 30 dimensions. Each algorithm is evaluated 10,000 times and each algorithm is independently run 30 times. In order to ensure the fairness of algorithm comparison, other parameters of the comparison algorithm are set with reference to the original text. The parameters data is shown in Table 2. In Table 2, p_c and p_m represent crossover probability and mutation probability respectively. η_c and η_m are the distribution indices of simulating binary crossover (SBX) and polynomial-based mutation (PM) respectively. div is the number of divisions of the coordinate axes. w , c_1 , c_2 , c_3 is a parameter in the speed update in PSO. F and CR are differential evolution parameters set in MPSOD. r is the number of selected elite particles in CMOPSO. R is the number of direction vectors in DGEA. All experimental results are obtained in MATLAB R2020b version in a computer with a PC of 3.60 GHz and 16 GB of storage. The original codes of all comparison algorithms are provided by PlatEMO [39].

4.4. Comparison with MOPSOs. Table 3 shows the average and standard deviation of the IGD obtained from 30 independent runs of the HDMOPSO and MOPSOs on 22 test problems. The following is a data analysis of Table 3 (The best average for each test instance in Table 3 is highlighted in bold. The meaning of bold highlights in Tables 4-6 is the same as in Table 3). It can be seen from Table 3 that the test problems of the HDMOPSO in ZDT have a good IGD value. Especially the effect on ZDT4 is particularly obvious, which shows that the algorithm performs better on convex sets. However, it can be seen from the data of ZDT3 that the HDMOPSO has a significant deterioration compared to other seven algorithms, indicating that the algorithm has a poor effect on discontinuous test problems. UF test problems are obviously better, and 80% of the IGD values of the other seven algorithms show a clear advantage. Especially UF7 and UF10 are an order of magnitude better than the other seven algorithms. However, the experimental result cannot converge to the Pareto front obviously on the UF test problems, and it can be further improved in future research. It can be seen from the test problems of DTLZ that the algorithm is seriously degraded. SMPSO and MPSOD performed well in the test functions of DTLZ, but only two problems well. It is worth noting that the HDMOPSO has achieved better results on DTLZ6. From the overall effect analysis, it can be found that among the 22 test problems given above, the performance of the HDMOPSO is the best.

Table 4 shows the average and standard deviation of HV obtained from 30 independent runs of the HDMOPSO and MOPSOs on 22 test problems. It can be seen from Table 4 that ZDT test problems are obviously better, because 80% of ZDT test problems are better than the other seven algorithms. The test problems of UF have some changes, but there are also 80% test problems that are better. There is still a significant deterioration in the test problems of DTZL. It can be seen from Table 4 that the HDMOPSO and MOPSOs still have strong competitiveness.

TABLE 1: List of acronyms.

Acronyms	The full name of an acronym
MOPSO	MOPSO: a Proposal for multiple objective particle swarm optimization
MOPSOCD	An effective use of crowding distance in multiobjective particle swarm optimization
dMOPSO	A multiobjective particle swarm optimizer based on decomposition
SMPSO	SMPSO a New PSO-based metaheuristic for multiobjective optimization
NMPSO	particle swarm optimization with a balanceable fitness estimation for many-objective optimization problems
MPSOD	A new multiobjective particle swarm optimization algorithm based on decomposition
CMOPSO	A competitive mechanism based multiobjective particle swarm optimizer with fast convergence
AGEII	A fast approximation-guided evolutionary multiobjective algorithm
NSGAIII	An evolutionary many-objective optimization algorithm using reference – point-based non-dominated sorting approach, part I: Solving problems with box constraints
MOEAD	MOEA/D:a multiobjective evolutionary algorithm based on decomposition
ARMOEA	An indicator based multiobjective evolutionary algorithm with reference point adaptation for better versatility
AGEMOEA	An adaptive evolutionary algorithm based on non-Euclidean geometry for many-objective optimization

TABLE 2: Parameter settings of all the compared algorithms.

	Algorithms	Parameters settings
1	MOPSO	$w \in [0.1, 0.5]$, $c_1, c_2 \in [1.5, 2.5]$, $\text{div} = 10$
2	MOPSOCD	$w \in [0.1, 0.5]$, $c_1, c_2 \in [1.5, 2.5]$
3	dMOPSO	$w \in [0.1, 0.5]$, $c_1, c_2 \in [1.5, 2.5]$
4	SMPSO	$w \in [0.1, 0.5]$, $c_1, c_2 \in [1.5, 2.5]$, $p_m = 1/n$
5	NMPSO	$w \in [0.1, 0.5], c_1, c_2, c_3 \in [1.5, 2.5]$, $p_m = 1/n$, $\eta_m = 20$
6	MPSOD	$w \in [0.1, 0.5]$, $c_1, c_2, c_3 \in [1.5, 2.5]$, $p_c = 0.9$, $F = 0.5$, $CR = 0.5$, $p_m = 1/n$, $\eta_m = 20$, $\eta_c = 20$
7	CMOPSO	$r = 10$
8	AGEII	$p_m = 1/n$, $p_c = 0.9$, $\eta_m = 20$, $\eta_c = 20$
9	ANSGAIII	$p_m = 1/n$, $p_c = 1.0$, $\eta_m = 20$, $\eta_c = 20$
10	DGEA	$R = 10$
11	NSGAIII	$p_m = 1/n$, $p_c = 1.0$, $\eta_m = 20$, $\eta_c = 20$
12	MOEAD	$p_m = 1/n$, $p_c = 1.0$, $\eta_m = 20$, $\eta_c = 20$
13	ARMOEA	$p_m = 1/n$, $p_c = 1.0$, $\eta_m = 20$, $\eta_c = 20$
14	AGEMOEA	$p_m = 1/n$, $p_c = 1.0$, $\eta_m = 20$, $\eta_c = 20$
15	HDMOPSO	$w = 0.4$, $c_1 = c_2 = 2$, $\text{div} = 50$

In order to more intuitively see the stability of the algorithm in this paper when compare with MOPSOs, we use a statistical boxplot of the IGD values obtained from 30 independent runs of each algorithm. Figure 6 shows the 12 test problems in Table 3 that perform well. It can be seen from Figure 6 that it is consistent with the results obtained in Table 3. Not only is the optimization result better, but it also shows a better advantage in terms of stability. Although not significant compared with other algorithms in ZDT6, they all performed better than MOPSO, MOPSOCD and MPSOD. The comparison between HDMOPSO, NMPSO and dMOPSO on DTLZ6 is not obvious, but it has obvious advantages over the other five algorithms. For the other 10 test problems, they all showed good advantages, especially UF5, UF7, UF9, and UF10 showed obvious advantages.

Another important performance of HDMOPSO is the speed of convergence. Figure 7 shows the IGD convergence trajectory obtained by HDMOPSO and MOPSOs running 10000 times in ZDT6, UF4, and DTLZ6. Although HDMOPSO is not obvious compared with NMPSO on ZDT6 and DTLZ6, the convergence speed of HDMOPSO on UF4 is significantly better than that of optimal NMPSO. A closer look at the convergence trajectories of ZDT6 and DTLZ6 will reveal that HDMOPSO converges faster than

NMPSO in the early stage of the evaluation. In the data in Table 3, the IGD value of NMPSO on the two test problems of ZDT6 and DTLZ6 is better than that of NMPSO. The above shows that HDMOPSO still has some advantages over NMPSO in terms of convergence speed.

Finally, Figure 8 shows the Pareto front simulation of each algorithm on ZDT4. It can be seen from the figure that HDMOPSO almost all converge to the Pareto front, and the distribution is good. Other algorithms have no convergent Pareto front.

Through the above analysis of the comparison of HDMOPSO and MOPSOs, it can be concluded. Among the 22 test functions of HDMOPSO, 12 test problems performed better on the IGD indicator, and it can be seen from Figure 6 that the stability is also better. On the HV indicator, 13 test problems performed well. Figures 7 and 8 also briefly temporarily show the convergence of HDMOPSO. In particular, it can be concluded from the data in Tables 3 and 4 that HDMOPSO is more competitive than the other seven algorithms in the above ZDT and UF test problems. It also shows that the operator proposed in this paper has good performance in convergence and diversity, which confirms the relevant statement in Section 3 of this paper.

TABLE 3: IGD values of HDMOPSO and MOPSOs on 22 test problems.

Problems	MOPSO	MOPSOCD	dMOPSO	SMPSO	NMPSO	MPSOD	CMOPSO	HDMOPSO
ZDT1	7.5088e-1 (2.92e-1)	3.9812e-3 (5.25e-3)	4.8573e-2 (1.60e-2)	9.5769e-2 (9.47e-2)	3.8449e-2 (2.19e-2)	1.0348e-1 (4.21e-2)	3.1875e-3 (4.35e-4)	3.1535e-3 (1.27e-4)
ZDT2	1.3707e+0 (3.04e-1)	1.1354e-1 (2.14e-1)	3.8831e-2 (1.16e-2)	9.2544e-2 (1.65e-1)	7.5055e-2 (1.16e-1)	1.4178e-1 (7.53e-2)	2.9214e-3 (4.96e-4)	3.3724e-3 (1.66e-4)
ZDT3	7.6697e-1 (2.06e-1)	6.0399e-2 (5.76e-2)	3.6479e-2 (7.25e-3)	2.1381e-1 (9.78e-2)	9.1792e-2 (1.05e-2)	2.2252e-1 (6.02e-2)	3.8754e-3 (8.05e-4)	1.9279e-1 (8.24e-4)
ZDT4	1.4121e+1 (4.52e+0)	1.8729e+1 (5.99e+0)	3.0691e+0 (4.33e+0)	9.3197e+0 (4.44e+0)	1.6335e+1 (6.71e+0)	3.6865e+1 (4.99e+0)	2.0777e+1 (5.99e+0)	3.2676e-3 (1.66e-4)
ZDT6	1.2262e-1 (5.57e-1)	3.8317e-3 (1.75e-3)	5.5255e-3 (5.36e-3)	1.9286e-3 (9.20e-5)	2.2633e-3 (1.88e-4)	1.7753e-2 (9.12e-3)	1.5817e-3 (3.73e-5)	1.4406e-3 (1.40e-4)
UF1	5.4509e-1 (9.68e-2)	7.0292e-1 (1.37e-1)	6.4403e-1 (9.29e-2)	3.8697e-1 (9.73e-2)	1.2881e-1 (2.06e-2)	2.5801e-1 (3.95e-2)	8.9465e-2 (1.16e-2)	1.0285e-1 (3.90e-3)
UF2	1.0642e-1 (1.52e-2)	1.3831e-1 (1.41e-2)	9.5994e-2 (7.11e-3)	1.0196e-1 (9.90e-3)	8.3881e-2 (7.73e-3)	1.1263e-1 (7.82e-3)	6.2882e-2 (7.46e-3)	4.2773e-2 (4.68e-3)
UF3	5.1345e-1 (2.66e-2)	3.7654e-1 (5.93e-2)	3.3278e-1 (8.05e-3)	4.5443e-1 (5.30e-2)	3.4509e-1 (4.01e-2)	5.0080e-1 (1.39e-2)	3.7938e-1 (4.19e-2)	2.2609e-1 (3.25e-2)
UF4	1.1332e-1 (1.32e-2)	7.6570e-2 (8.53e-3)	1.3842e-1 (3.90e-3)	1.1399e-1 (5.74e-3)	6.0533e-2 (7.40e-3)	9.9699e-2 (3.70e-3)	1.1406e-1 (9.14e-3)	5.6199e-2 (3.62e-3)
UF5	3.1549e+0 (4.02e-1)	3.9278e+0 (4.15e-1)	3.2280e+0 (2.91e-1)	2.9766e+0 (5.34e-1)	1.6894e+0 (4.72e-1)	2.8148e+0 (2.29e-1)	8.6853e-1 (2.37e-1)	4.7202e-1 (6.69e-2)
UF6	2.3228e+0 (5.49e-1)	2.6922e+0 (7.84e-1)	2.5325e+0 (6.61e-1)	1.2647e+0 (4.51e-1)	6.2828e-1 (7.21e-2)	1.3585e+0 (2.17e-1)	3.9239e-1 (5.48e-2)	5.7701e-1 (1.12e-1)
UF7	6.1070e-1 (1.01e-1)	6.4461e-1 (1.08e-1)	3.9902e-1 (8.50e-2)	3.8701e-1 (1.41e-1)	1.8045e-1 (1.40e-1)	2.3004e-1 (5.59e-2)	1.5988e-1 (1.35e-1)	5.4736e-2 (4.64e-3)
UF8	4.0988e-1 (4.08e-2)	7.9818e-1 (1.73e-1)	3.4771e-1 (2.78e-2)	3.9381e-1 (5.03e-2)	4.8985e-1 (1.02e-1)	5.5254e-1 (4.72e-2)	6.3473e-1 (9.14e-2)	2.9892e-1 (8.93e-2)
UF9	5.5595e-1 (3.53e-2)	8.6183e-1 (1.14e-1)	5.8222e-1 (3.31e-2)	5.5428e-1 (3.84e-2)	4.5999e-1 (7.11e-2)	6.5550e-1 (4.06e-2)	9.1997e-1 (1.16e-1)	1.3840e-1 (2.20e-2)
UF10	2.2568e+0 (2.69e-1)	4.9302e+0 (7.78e-1)	9.4535e-1 (1.42e-3)	2.8317e+0 (4.19e-1)	1.5045e+0 (2.82e-1)	4.1995e+0 (3.64e-1)	4.3317e+0 (4.34e-1)	5.1341e-1 (9.72e-2)
DTLZ1	6.5415e+1 (2.14e+1)	4.3410e+1 (1.15e+1)	1.1274e+1 (9.86e+0)	1.3471e+1 (1.55e+1)	3.1643e+1 (6.32e+0)	4.0410e+1 (5.50e+0)	6.0047e+1 (1.90e+1)	4.4077e+1 (1.40e+1)
DTLZ2	1.0105e-1 (1.17e-2)	1.0093e-1 (7.88e-3)	1.4135e-1 (1.21e-2)	8.9297e-2 (7.51e-3)	8.0083e-2 (2.41e-3)	5.6798e-2 (8.22e-4)	6.1246e-2 (1.20e-3)	1.0454e-1 (7.54e-3)
DTLZ3	1.5740e+2 (5.27e+1)	1.1338e+2 (3.54e+1)	5.4112e+1 (5.58e+1)	2.9074e+1 (3.08e+1)	9.0109e+1 (1.87e+1)	1.1838e+2 (1.59e+1)	1.3237e+2 (3.85e+1)	1.2671e+2 (3.40e+1)
DTLZ4	4.0345e-1 (1.71e-1)	2.9034e-1 (4.99e-2)	3.1557e-1 (3.37e-2)	4.4687e-1 (1.86e-1)	1.2632e-1 (1.41e-1)	6.2524e-2 (5.04e-3)	1.5281e-1 (2.69e-1)	1.1168e-1 (3.22e-2)
DTLZ5	1.5467e-2 (6.41e-3)	2.1884e-2 (7.37e-3)	4.1222e-2 (5.96e-3)	5.7212e-3 (3.92e-4)	1.2661e-2 (2.12e-3)	5.4102e-2 (5.42e-3)	7.7990e-3 (6.03e-4)	2.2555e-2 (2.85e-3)
DTLZ6	3.1831e+0 (7.91e-1)	1.0237e-2 (1.62e-2)	3.2892e-2 (3.09e-4)	1.1052e+0 (9.46e-1)	1.5140e-2 (2.31e-3)	2.5577e-1 (2.58e-1)	2.3427e-1 (4.95e-1)	7.5019e-3 (1.07e-3)
DTLZ7	1.6046e+0 (7.71e-1)	8.9805e-2 (7.76e-3)	1.3944e-1 (5.84e-3)	2.0575e-1 (1.52e-1)	7.5483e-2 (3.57e-3)	1.6499e-1 (1.57e-2)	1.7726e-1 (2.33e-1)	9.8273e-2 (1.16e-2)
Best/All	0/22	0/22	1/22	2/22	1/22	2/22	4/22	12/22

The best average on each test instance is highlighted in bold.

4.5. *Comparison with MOEAs.* Table 5 shows the average IGD of HDMOPSO and MOEAs for 30 independent runs on 22 test problems. It can be seen from Table 5 that HDMOPSO is significantly better than the other four algorithms in the ZDT test problems. Of course, the performance of the ZDT3 test problem here is not very obvious, which also shows that HDMOPSO is not outstanding in the non-continuous set. For other concave and convex sets, HDMOPSO has obvious advantages over the rest of MOEAs, because ZDT1, ZDT2, and ZDT6 are all an order of magnitude lower than the best value of the other seven algorithms, and it is in the ZDT4 test problem. It is two orders of magnitude lower than the best one of the other

MOEAs algorithms. In addition, the UF test problems also show a clear advantage, because 90% of the 10 UF test problems are better than the other four algorithms. Although the single UF optimization effect is not very obvious, the overall effect is good. In the DTLZ test problem, you can see the algorithm obvious deterioration, and none of the algorithms given can show obvious advantages in the DTLZ test problems, and the better one is AGEMOEA. Because 3 of the 7 DTLZ test problems are better than other test problems. Only one or two of the remaining algorithms performed well on the DTLZ test problems. Such a result may be that each test problem of DTLZ is quite different and contains many local optimal values, which makes it more

TABLE 4: HV values of HDMOPSO and MOPSOs on 22 test problems.

Problems	MOPSO	MOPSOCD	dMOPSO	SMPSO	NMPSO	MPSOD	CMOPSO	HDMOPSO
ZDT1	8.7931e-2 (9.03e-2)	7.1927e-1 (7.63e-3)	6.6243e-1 (1.85e-2)	6.0408e-1 (1.14e-1)	6.7972e-1 (2.38e-2)	5.7261e-1 (5.43e-2)	7.1985e-1 (6.73e-4)	7.2106e-1 (1.67e-4)
ZDT2	0.0000e+0 (0.00e+0)	3.6202e-1 (1.38e-1)	3.8608e-1 (1.89e-2)	3.6414e-1 (1.23e-1)	3.8523e-1 (9.41e-2)	2.7324e-1 (7.70e-2)	4.4470e-1 (8.96e-4)	4.4479e-1 (3.14e-4)
ZDT3	1.1302e-1 (9.47e-2)	5.6641e-1 (4.00e-2)	6.0143e-1 (1.46e-2)	5.1021e-1 (7.81e-2)	5.7190e-1 (5.59e-3)	4.5070e-1 (4.78e-2)	5.9962e-1 (1.34e-3)	6.5930e-1 (5.18e-4)
ZDT4	0.0000e+0 (0.00e+0)	0.0000e+0 (0.00e+0)	6.2941e-2 (7.98e-2)	0.0000e+0 (0.00e+0)	0.0000e+0 (0.00e+0)	0.0000e+0 (0.00e+0)	0.0000e+0 (0.00e+0)	7.2109e-1 (1.94e-4)
ZDT6	3.6205e-1 (8.57e-2)	3.8818e-1 (1.85e-3)	3.8626e-1 (5.94e-3)	3.9003e-1 (9.26e-5)	3.8979e-1 (1.63e-4)	3.7439e-1 (9.32e-3)	3.9034e-1 (4.35e-5)	3.8917e-1 (1.28e-4)
UF1	1.3865e-1 (6.26e-2)	4.8415e-2 (4.52e-2)	6.5077e-2 (5.42e-2)	2.6626e-1 (8.05e-2)	5.2452e-1 (3.33e-2)	3.6635e-1 (4.49e-2)	5.8159e-1 (1.25e-2)	5.8358e-1 (5.07e-3)
UF2	6.0344e-1 (9.56e-3)	5.4564e-1 (1.92e-2)	6.1588e-1 (6.00e-3)	6.0714e-1 (8.34e-3)	6.1881e-1 (8.74e-3)	5.7945e-1 (9.61e-3)	6.4476e-1 (7.24e-3)	6.7344e-1 (5.90e-3)
UF3	1.5813e-1 (1.85e-2)	2.5471e-1 (4.65e-2)	3.0604e-1 (1.01e-2)	2.0705e-1 (4.80e-2)	2.9285e-1 (3.54e-2)	1.7439e-1 (1.29e-2)	2.7643e-1 (3.07e-2)	4.4309e-1 (4.02e-2)
UF4	2.9015e-1 (1.65e-2)	3.3601e-1 (1.17e-2)	2.5150e-1 (4.74e-3)	2.9022e-1 (6.68e-3)	3.6468e-1 (9.76e-3)	3.0708e-1 (4.93e-3)	2.8639e-1 (1.07e-2)	3.6976e-1 (4.36e-3)
UF5	0.0000e+0 (0.00e+0)	0.0000e+0 (0.00e+0)	0.0000e+0 (0.00e+0)	0.0000e+0 (0.00e+0)	0.0000e+0 (0.00e+0)	0.0000e+0 (0.00e+0)	1.4949e-2 (2.77e-2)	1.9772e-2 (2.21e-2)
UF6	0.0000e+0 (0.00e+0)	0.0000e+0 (0.00e+0)	0.0000e+0 (0.00e+0)	1.8676e-3 (7.67e-3)	3.3322e-2 (3.38e-2)	0.0000e+0 (0.00e+0)	1.4986e-1 (7.13e-2)	1.3127e-2 (1.39e-2)
UF7	5.1589e-2 (4.38e-2)	2.0540e-2 (2.93e-2)	1.6202e-1 (6.16e-2)	1.7451e-1 (1.02e-1)	3.8134e-1 (1.10e-1)	2.7511e-1 (6.12e-2)	4.1920e-1 (9.58e-2)	5.0640e-1 (6.73e-3)
UF8	1.7316e-1 (3.13e-2)	8.5853e-3 (1.78e-2)	2.7047e-1 (1.87e-2)	1.6701e-1 (3.92e-2)	2.8249e-1 (6.24e-2)	5.2054e-2 (1.89e-2)	9.4227e-3 (1.56e-2)	3.5290e-1 (1.67e-2)
UF9	2.1069e-1 (3.67e-2)	2.6834e-2 (3.09e-2)	2.2614e-1 (1.75e-2)	2.1584e-1 (3.84e-2)	3.1904e-1 (5.62e-2)	1.1375e-1 (2.83e-2)	1.2671e-2 (1.52e-2)	6.3437e-1 (2.37e-2)
UF10	0.0000e+0 (0.00e+0)	0.0000e+0 (0.00e+0)	9.0885e-2 (4.33e-5)	0.0000e+0 (0.00e+0)	0.0000e+0 (0.00e+0)	0.0000e+0 (0.00e+0)	0.0000e+0 (0.00e+0)	3.1914e-1 (4.40e-2)
DTLZ1	3.0031e-5 (1.64e-4)	0.0000e+0 (0.00e+0)	6.0507e-3 (3.06e-2)	7.7696e-2 (1.78e-1)	0.0000e+0 (0.00e+0)	0.0000e+0 (0.00e+0)	0.0000e+0 (0.00e+0)	0.0000e+0 (0.00e+0)
DTLZ2	4.4743e-1 (2.05e-2)	4.5905e-1 (1.68e-2)	3.6806e-1 (2.25e-2)	4.5953e-1 (1.65e-2)	5.5708e-1 (1.26e-3)	5.4695e-1 (2.35e-3)	5.3735e-1 (3.01e-3)	4.7654e-1 (1.15e-2)
DTLZ3	0.0000e+0 (0.00e+0)	0.0000e+0 (0.00e+0)	0.0000e+0 (0.00e+0)	4.3486e-2 (7.73e-2)	0.0000e+0 (0.00e+0)	0.0000e+0 (0.00e+0)	0.0000e+0 (0.00e+0)	0.0000e+0 (0.00e+0)
DTLZ4	2.5413e-1 (9.14e-2)	3.2113e-1 (6.45e-2)	3.0697e-1 (4.79e-2)	2.9025e-1 (1.12e-1)	5.3648e-1 (6.52e-2)	5.3767e-1 (9.08e-3)	4.8396e-1 (1.33e-1)	5.1071e-1 (1.03e-2)
DTLZ5	1.8647e-1 (5.26e-3)	1.8447e-1 (6.82e-3)	1.5607e-1 (1.02e-2)	1.9841e-1 (3.22e-4)	1.9596e-1 (7.26e-4)	1.4596e-1 (6.89e-3)	1.9642e-1 (5.33e-4)	1.8259e-1 (3.45e-3)
DTLZ6	0.0000e+0 (0.00e+0)	1.9703e-1 (9.32e-3)	1.8259e-1 (2.20e-4)	6.4336e-2 (8.99e-2)	1.9555e-1 (1.02e-3)	1.0561e-1 (5.88e-2)	1.5968e-1 (8.12e-2)	1.9487e-1 (4.19e-3)
DTLZ7	5.2658e-2 (5.50e-2)	2.6585e-1 (2.37e-3)	2.4595e-1 (3.67e-3)	2.3873e-1 (2.32e-2)	2.7377e-1 (1.57e-3)	2.1759e-1 (1.05e-2)	2.6121e-1 (2.34e-2)	2.6668e-1 (3.33e-3)
Best/All	0/22	1/22	0/22	3/22	2/22	1/22	2/22	13/22

difficult to optimize the algorithm. HDMOPSO and MOEAs in a total of 22 test problems, HDMOPSO performs better than the other seven algorithms with 15 and showed obvious advantages in the test problems of ZDT and UF. HDMOPSO is more competitive compared with the other seven algorithms.

In order to further prove the results obtained above, the HV average and standard deviation of each algorithm independently run 30 times are also used. The results are shown in Table 6. It can be seen from the HV indicator that HDMOPSO has a clear advantage over the other algorithms in the ZDT test problems, reaching 100% excellence. UF also show a better advantage than other algorithms, because 80%

of the UF test problems performed better than the other seven MOEAs algorithms. Although the data optimization is not very obvious, the overall data can still see obvious advantages. HDMOPSO deteriorated significantly in the DTLZ test problems. The best performer in DTLZ is AGEMOEA, because 3 out of 7 DTLZ problems are better. Compared to the results in Tables 5 and 6, although there are some differences in the conclusions drawn from the data, it can also be clearly concluded that HDMOPSO is more competitive than other MOEAs in ZDT and UF test problems.

In order to show more clearly that HDMOPSO not only performs excellent numerically, but also performs well in terms of stability. Figure 9 shows the statistical boxplot of the

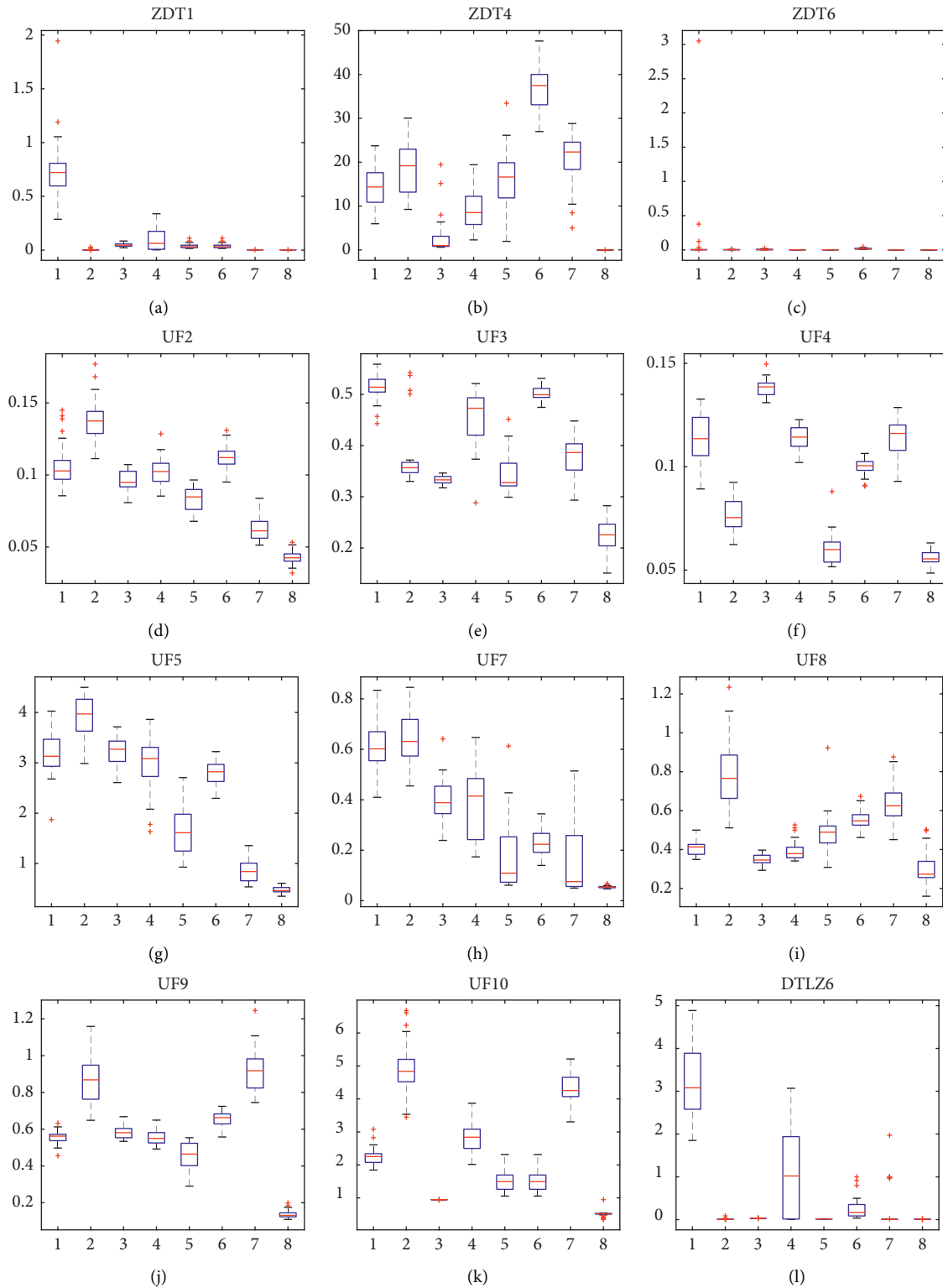


FIGURE 6: IGD values statistical boxplot of HDMOPSO and MOPSOs on ZDT1, ZDT4, ZDT6, UF2-5, UF7-10, and DTLZ6 problems. (1, 2, 3, 4, 5, 6, 7, and 8 in each statistical boxplot represent MOPSO, MOPSOCD, dMOPSO, SMPSO, NMPSO, MPSOD, CMOPSO, and HDMOPSO, respectively).

15 test problems in Table 5 that perform well. It can be seen from Figure 9 that HDMOPSO performs better on ZDT1-2, ZDT4 and ZDT6, and its stability is better than other

MOEAs. HDMOPSO has shown obvious advantages in UF test problems except for UF6, and the stability is better than other algorithms. In the DTLZ test problem, although it is

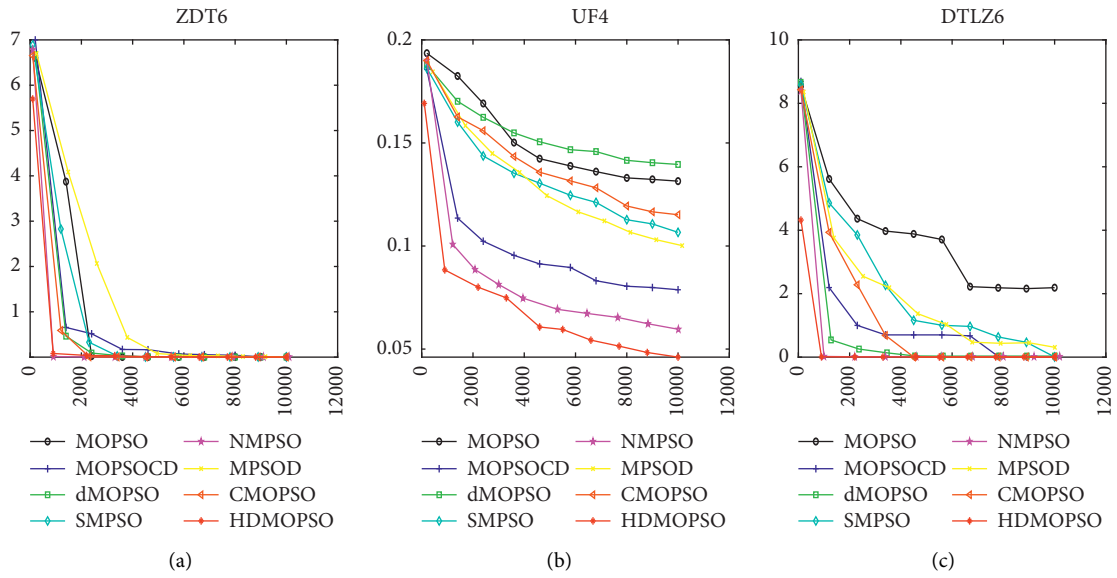


FIGURE 7: IGD values convergence trajectory of HDMOPSO and MOPSOs comparison on ZDT6, UF4, and DTLZ6 problems.

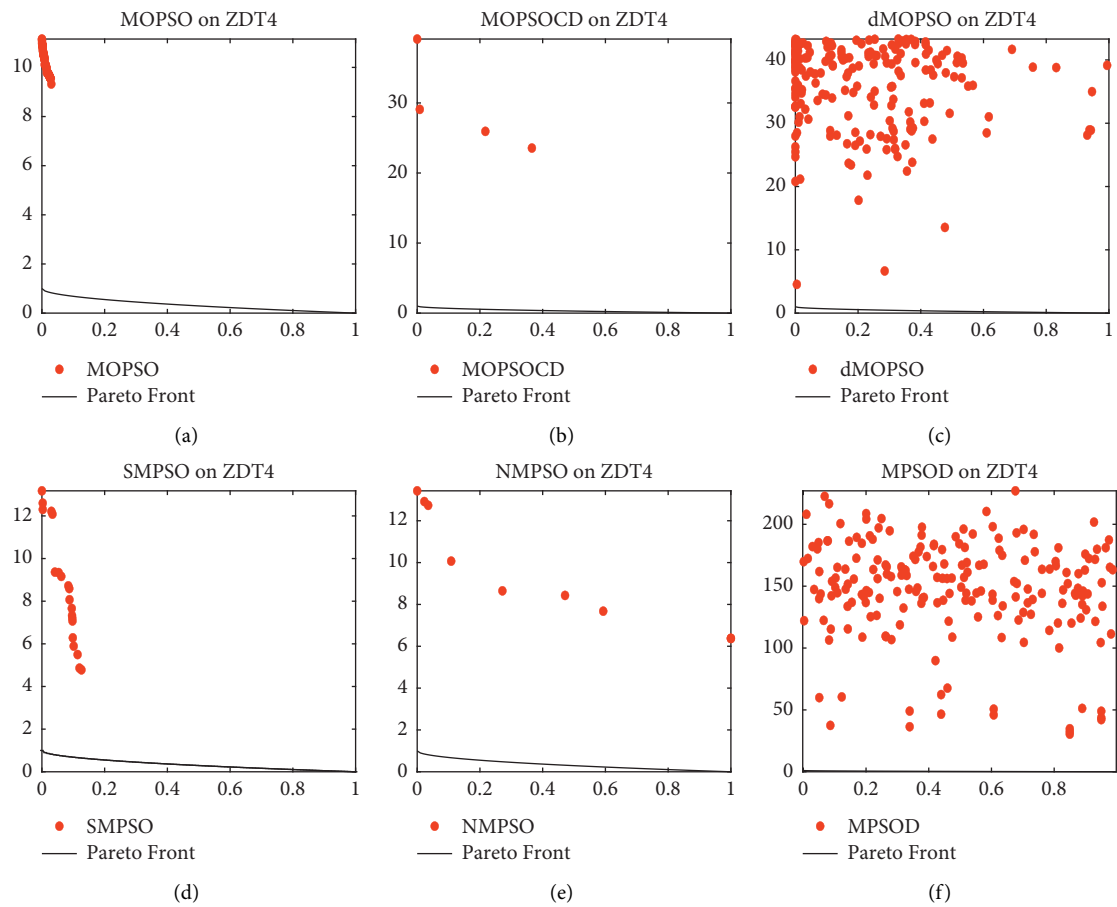


FIGURE 8: Continued.

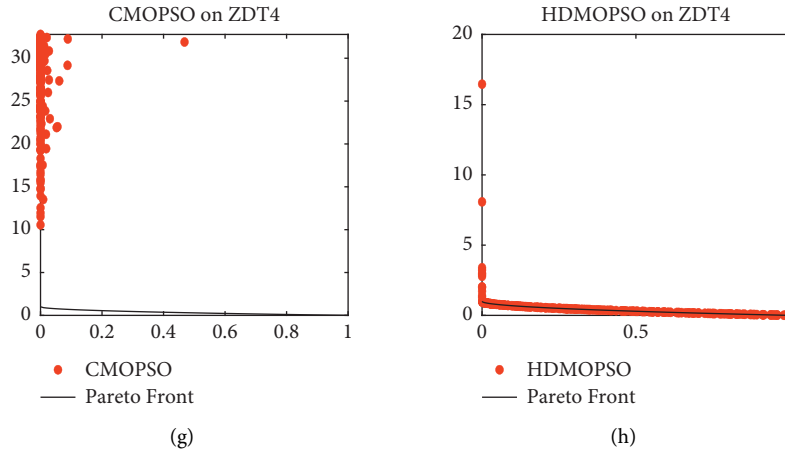


FIGURE 8: The Pareto front simulation of HDMOPSO and MOPSOs on ZDT4 problem.

TABLE 5: IGD values of HDMOPSO and MOEAs on 22 test Problems.

Problems	AGEII	ANSGAIII	DGEA	NSGAIII	MOEAD	ARMOEA	AGEMOEa	HDMOPSO
ZDT1	8.5782e-2 (2.08e-2)	1.0467e-1 (1.70e-2)	1.2053e+0 (2.29e-1)	1.0429e-1 (1.49e-2)	1.9889e-1 (9.18e-2)	7.6736e-2 (3.69e-2)	3.6880e-2 (6.45e-3)	3.1535e-3 (1.27e-4)
ZDT2	1.8054e-1 (8.01e-2)	2.0715e-1 (5.94e-2)	9.0498e-1 (3.82e-1)	1.9997e-1 (3.51e-2)	5.8069e-1 (6.00e-2)	6.7290e-1 (5.31e-2)	7.7285e-2 (1.92e-2)	3.3724e-3 (1.66e-4)
ZDT3	8.9131e-2 (2.48e-2)	9.4678e-2 (1.55e-2)	1.0018e+0 (2.14e-1)	9.3148e-2 (1.44e-2)	1.8357e-1 (6.61e-2)	5.5582e-2 (3.07e-2)	3.2164e-2 (1.03e-2)	1.9279e-1 (8.24e-4)
ZDT4	5.5026e-1 (3.48e-1)	2.5973e+0 (7.71e-1)	8.8328e+0 (6.15e+0)	2.7783e+0 (7.38e-1)	5.5262e-1 (1.82e-1)	1.6582e+0 (7.07e-1)	9.0188e-1 (3.21e-1)	3.2676e-3 (1.66e-4)
ZDT6	2.4504e-1 (1.14e-1)	1.5490e+0 (1.97e-1)	1.2914e-1 (6.77e-1)	1.4790e+0 (2.24e-1)	8.3351e-2 (3.09e-2)	9.1101e-1 (2.46e-1)	3.9277e-1 (1.22e-1)	1.4406e-3 (1.40e-4)
UF1	1.5388e-1 (5.14e-2)	1.3636e-1 (2.85e-2)	6.2298e-1 (1.34e-1)	1.5270e-1 (4.12e-2)	3.0044e-1 (8.04e-2)	1.1692e-1 (2.29e-2)	1.1202e-1 (2.27e-2)	1.0285e-1 (3.90e-3)
UF2	9.2897e-2 (1.19e-2)	8.1301e-2 (7.06e-3)	1.7032e-1 (2.16e-2)	8.2564e-2 (5.03e-3)	2.3152e-1 (5.81e-2)	7.8838e-2 (1.20e-2)	7.0535e-2 (7.08e-3)	4.2773e-2 (4.68e-3)
UF3	4.9379e-1 (3.06e-2)	4.7702e-1 (8.89e-3)	5.7403e-1 (4.99e-2)	4.8138e-1 (7.78e-3)	3.3739e-1 (2.31e-2)	4.3339e-1 (2.91e-2)	4.2878e-1 (2.67e-2)	2.2609e-1 (3.25e-2)
UF4	1.0075e-1 (4.48e-3)	9.4497e-2 (3.05e-3)	1.2237e-1 (8.65e-3)	9.5983e-2 (3.42e-3)	1.1437e-1 (5.47e-3)	8.1805e-2 (2.63e-3)	8.1923e-2 (3.13e-3)	5.6199e-2 (3.62e-3)
UF5	9.9788e-1 (2.90e-1)	1.4897e+0 (3.01e-1)	2.9718e+0 (6.70e-1)	1.4989e+0 (3.52e-1)	1.4515e+0 (2.29e-1)	6.7696e-1 (1.71e-1)	7.2508e-1 (1.92e-1)	4.7202e-1 (6.69e-2)
UF6	6.7744e-1 (2.48e-1)	7.3813e-1 (1.39e-1)	2.5695e+0 (7.97e-1)	7.5191e-1 (1.41e-1)	5.3913e-1 (1.32e-1)	5.0980e-1 (6.57e-2)	5.2598e-1 (7.62e-2)	5.7701e-1 (1.12e-1)
UF7	2.7369e-1 (1.10e-1)	2.0424e-1 (7.04e-2)	7.3512e-1 (1.32e-1)	1.9615e-1 (7.53e-2)	4.5705e-1 (1.11e-1)	2.1657e-1 (1.05e-1)	1.6563e-1 (9.49e-2)	5.4736e-2 (4.64e-3)
UF8	3.6710e-1 (3.96e-2)	3.5163e-1 (3.51e-2)	7.4397e-1 (1.22e-1)	3.4069e-1 (3.59e-2)	5.7647e-1 (2.54e-1)	3.4331e-1 (5.95e-2)	3.5650e-1 (4.59e-2)	2.9892e-1 (8.93e-2)
UF9	5.0642e-1 (9.51e-2)	4.9393e-1 (5.80e-2)	7.6655e-1 (1.05e-1)	4.8937e-1 (4.30e-2)	5.1151e-1 (9.53e-2)	4.5574e-1 (5.93e-2)	4.8648e-1 (7.66e-2)	1.3840e-1 (2.20e-2)
UF10	2.2698e+0 (8.82e-1)	2.2711e+0 (3.91e-1)	4.6292e+0 (8.83e-1)	2.3699e+0 (4.58e-1)	7.2339e-1 (9.63e-2)	1.0200e+0 (2.54e-1)	1.1947e+0 (4.26e-1)	5.1341e-1 (9.72e-2)
DTLZ1	5.1405e+0 (2.27e+0)	4.1193e+0 (1.44e+0)	3.4648e+1 (2.14e+1)	3.9783e+0 (1.45e+0)	3.9079e+0 (2.46e+0)	2.8103e+0 (1.69e+0)	2.3748e+0 (1.02e+0)	4.4077e+1 (1.40e+1)
DTLZ2	9.8293e-2 (3.67e-3)	5.8990e-2 (1.55e-3)	1.0238e-1 (1.29e-2)	5.4934e-2 (1.70e-4)	5.4947e-2 (2.57e-4)	5.5105e-2 (2.49e-4)	5.6639e-2 (6.03e-4)	1.0454e-1 (7.54e-3)
DTLZ3	2.0041e+1 (8.37e+0)	1.0668e+1 (5.22e+0)	9.7820e+1 (5.91e+1)	1.1436e+1 (5.42e+0)	1.7152e+1 (8.56e+0)	7.5904e+0 (4.27e+0)	7.7873e+0 (4.32e+0)	1.2671e+2 (3.40e+1)
DTLZ4	1.7246e-1 (2.01e-1)	1.5477e-1 (1.97e-1)	2.2674e-1 (1.22e-1)	1.9844e-1 (2.52e-1)	5.3593e-1 (3.20e-1)	2.6570e-1 (2.45e-1)	1.2354e-1 (1.74e-1)	1.1168e-1 (3.22e-2)

TABLE 5: Continued.

Problems	AGEII	ANSGAIII	DGEA	NSGAIII	MOEAD	ARMOEA	AGEMOEA	HDMOPSO
DTLZ5	4.3520e-2 (4.17e-4)	1.1211e-2 (1.32e-3)	5.7895e-2 (1.07e-2)	1.2431e-2 (1.53e-3)	3.2469e-2 (7.07e-4)	5.7577e-3 (1.51e-4)	5.7118e-3 (1.72e-4)	2.2555e-2 (2.85e-3)
DTLZ6	9.0139e-2 (1.57e-1)	2.3606e-2 (4.81e-2)	1.3535e+0 (1.06e+0)	2.0972e-2 (5.03e-3)	1.0585e-1 (2.37e-1)	5.1735e-3 (5.18e-4)	5.1700e-3 (1.03e-4)	7.5019e-3 (1.07e-3)
DTLZ7	1.3022e-1 (5.00e-2)	1.1682e-1 (1.06e-1)	4.6400e-1 (3.09e-1)	9.8316e-2 (7.55e-2)	2.3783e-1 (2.25e-1)	3.0406e-1 (2.62e-1)	2.4587e-1 (2.55e-1)	9.8273e-2 (1.16e-2)
Best/All	0/22	0/22	0/22	1/22	0/22	2/22	4/22	15/22

TABLE 6: HV values of HDMOPSO and MOEAs on 22 test problems.

Problems	AGEII	ANSGAIII	DGEA	NSGAIII	MOEAD	ARMOEA	AGEMOEA	HDMOPSO
ZDT1	6.0606e-1 (2.62e-2)	5.8450e-1 (2.08e-2)	4.4826e-3 (2.09e-2)	5.8438e-1 (1.89e-2)	5.1233e-1 (7.39e-2)	6.3314e-1 (2.92e-2)	6.7352e-1 (8.65e-3)	7.2106e-1 (1.67e-4)
ZDT2	2.2885e-1 (6.09e-2)	2.0517e-1 (4.47e-2)	3.0196e-2 (8.64e-2)	2.1195e-1 (2.79e-2)	8.7068e-2 (2.21e-2)	3.8852e-3 (9.36e-3)	3.4325e-1 (2.39e-2)	4.4479e-1 (3.14e-4)
ZDT3	5.4307e-1 (2.30e-2)	5.4222e-1 (1.73e-2)	3.1248e-2 (4.54e-2)	5.3874e-1 (1.11e-2)	5.8582e-1 (5.62e-2)	5.8511e-1 (5.30e-2)	5.8154e-1 (1.81e-2)	6.5930e-1 (5.18e-4)
ZDT4	2.1891e-1 (1.74e-1)	0.0000e+0 (0.00e+0)	0.0000e+0 (0.00e+0)	0.0000e+0 (0.00e+0)	1.6314e-1 (1.11e-1)	8.3158e-3 (2.36e-2)	5.6042e-2 (9.66e-2)	7.2109e-1 (1.94e-4)
ZDT6	1.4324e-1 (7.39e-2)	0.0000e+0 (0.00e+0)	3.7415e-1 (7.16e-2)	0.0000e+0 (0.00e+0)	2.7816e-1 (3.84e-2)	2.6587e-3 (7.76e-3)	6.8723e-2 (4.98e-2)	3.8917e-1 (1.28e-4)
UF1	4.9545e-1 (7.03e-2)	5.1256e-1 (3.37e-2)	9.6182e-2 (7.52e-2)	4.9318e-1 (5.06e-2)	4.2186e-1 (4.74e-2)	5.5831e-1 (2.44e-2)	5.5828e-1 (3.20e-2)	5.8358e-1 (5.07e-3)
UF2	6.0395e-1 (1.02e-2)	6.1498e-1 (7.79e-3)	5.1072e-1 (2.83e-2)	6.1363e-1 (6.45e-3)	5.5211e-1 (2.50e-2)	6.3112e-1 (6.46e-3)	6.3627e-1 (6.09e-3)	6.7344e-1 (5.90e-3)
UF3	1.7440e-1 (2.58e-2)	1.8893e-1 (8.50e-3)	1.1804e-1 (2.74e-2)	1.8488e-1 (7.68e-3)	3.0498e-1 (3.55e-2)	2.0647e-1 (2.47e-2)	2.1327e-1 (1.86e-2)	4.4309e-1 (4.02e-2)
UF4	2.9950e-1 (6.87e-3)	3.1424e-1 (3.80e-3)	2.7710e-1 (1.02e-2)	3.1270e-1 (4.40e-3)	2.8594e-1 (6.95e-3)	3.3215e-1 (3.56e-3)	3.3372e-1 (3.93e-3)	3.6976e-1 (4.36e-3)
UF5	6.5633e-3 (1.76e-2)	0.0000e+0 (0.00e+0)	0.0000e+0 (0.00e+0)	3.4451e-4 (1.53e-3)	0.0000e+0 (0.00e+0)	3.0366e-2 (4.49e-2)	2.5807e-2 (4.27e-2)	1.9772e-2 (2.21e-2)
UF6	3.0354e-2 (4.03e-2)	1.0728e-2 (1.60e-2)	0.0000e+0 (0.00e+0)	9.3560e-3 (1.44e-2)	9.3876e-2 (6.38e-2)	4.8097e-2 (3.11e-2)	3.7781e-2 (3.16e-2)	1.3127e-2 (1.40e-2)
UF7	2.8984e-1 (8.79e-2)	3.2586e-1 (6.92e-2)	1.8432e-2 (2.96e-2)	3.2919e-1 (6.85e-2)	2.2900e-1 (6.15e-2)	3.6263e-1 (7.07e-2)	3.8745e-1 (8.00e-2)	5.0640e-1 (6.73e-3)
UF8	1.7267e-1 (5.81e-2)	2.2906e-1 (3.97e-2)	2.1604e-2 (2.25e-2)	2.2585e-1 (3.84e-2)	1.5686e-1 (6.22e-2)	3.0044e-1 (2.17e-2)	2.9239e-1 (3.78e-2)	3.5290e-1 (1.67e-2)
UF9	2.2393e-1 (7.64e-2)	2.5375e-1 (5.14e-2)	6.5632e-2 (5.11e-2)	2.5881e-1 (4.10e-2)	2.9108e-1 (5.77e-2)	3.1461e-1 (4.40e-2)	2.9501e-1 (5.19e-2)	6.3437e-1 (2.37e-2)
UF10	0.0000e+0 (0.00e+0)	0.0000e+0 (0.00e+0)	0.0000e+0 (0.00e+0)	0.0000e+0 (0.00e+0)	3.4782e-2 (2.76e-2)	3.0422e-5 (1.16e-4)	0.0000e+0 (0.00e+0)	3.1914e-1 (4.40e-2)
DTLZ1	0.0000e+0 (0.00e+0)	0.0000e+0 (0.00e+0)	0.0000e+0 (0.00e+0)	0.0000e+0 (0.00e+0)	0.0000e+0 (0.00e+0)	0.0000e+0 (0.00e+0)	0.0000e+0 (0.00e+0)	0.0000e+0 (0.00e+0)
DTLZ2	5.4387e-1 (2.34e-3)	5.4919e-1 (2.81e-3)	4.4879e-1 (2.60e-2)	5.5562e-1 (6.43e-4)	5.5533e-1 (6.50e-4)	5.5668e-1 (7.25e-4)	5.5633e-1 (7.20e-4)	4.7654e-1 (1.15e-2)
DTLZ3	0.0000e+0 (0.00e+0)	0.0000e+0 (0.00e+0)	0.0000e+0 (0.00e+0)	0.0000e+0 (0.00e+0)	0.0000e+0 (0.00e+0)	0.0000e+0 (0.00e+0)	0.0000e+0 (0.00e+0)	0.0000e+0 (0.00e+0)
DTLZ4	5.0701e-1 (1.04e-1)	5.0866e-1 (8.65e-2)	3.9182e-1 (8.39e-2)	4.8909e-1 (1.19e-1)	3.2464e-1 (1.68e-1)	4.6540e-1 (1.06e-1)	5.2232e-1 (8.82e-2)	5.1071e-1 (1.03e-2)
DTLZ5	1.7846e-1 (1.15e-3)	1.9462e-1 (8.57e-4)	1.6149e-1 (8.23e-3)	1.9336e-1 (1.04e-3)	1.8245e-1 (5.75e-4)	1.9839e-1 (2.37e-4)	1.9854e-1 (1.87e-4)	1.8259e-1 (3.45e-3)
DTLZ6	1.6313e-1 (3.65e-2)	1.8686e-1 (3.31e-2)	4.4790e-2 (7.18e-2)	1.8986e-1 (2.64e-3)	1.6070e-1 (5.38e-2)	1.9938e-1 (2.48e-4)	1.9957e-1 (7.46e-5)	1.9487e-1 (4.19e-3)
DTLZ7	2.3918e-1 (6.10e-3)	2.6170e-1 (1.22e-2)	1.5277e-1 (6.87e-2)	2.6464e-1 (9.25e-3)	2.4079e-1 (1.66e-2)	2.4795e-1 (2.58e-2)	2.5682e-1 (2.65e-2)	2.6668e-1 (3.33e-3)
Best/All	0/22	0/22	0/22	0/22	1/22	2/22	3/22	14/22

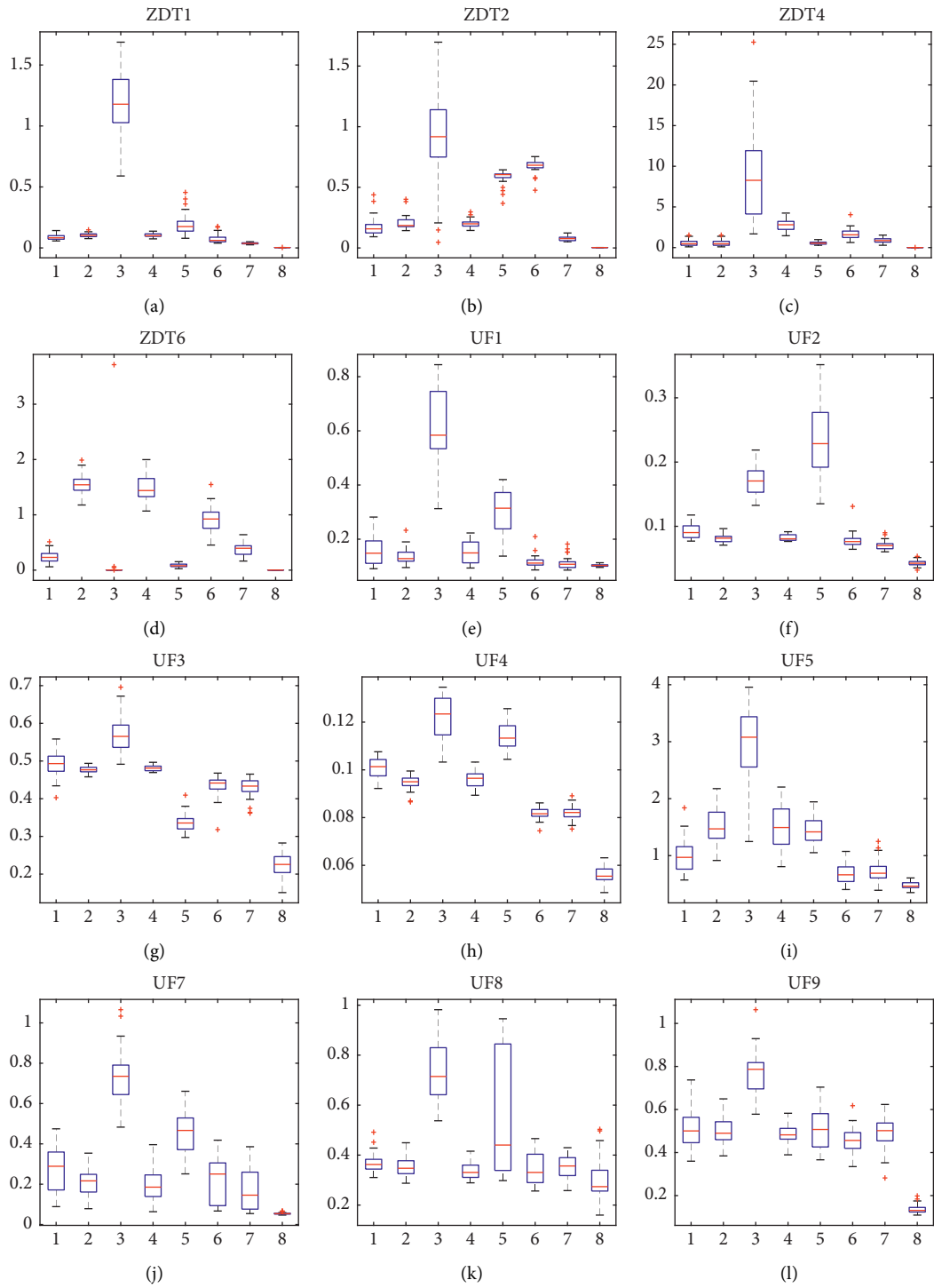


FIGURE 9: Continued.

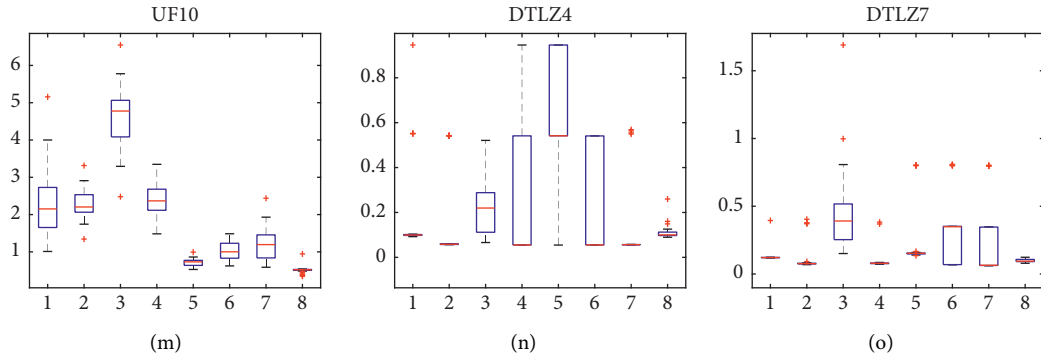


FIGURE 9: IGD value Statistical boxplot of HDMOPSO and MOEAs on ZDT1, ZDT2, ZDT4, ZDT6, UF1-5, UF7-10, DTLZ4, and DTLZ7 problems. (1, 2, 3, 4, 5, 6, 7, and 8 in each Statistical boxplot represent AGEII, ANSGAIII, DGEA, NSGAIII, MOEAD, ARMOEA, AGEMOEA, and HDMOPSO, respectively).

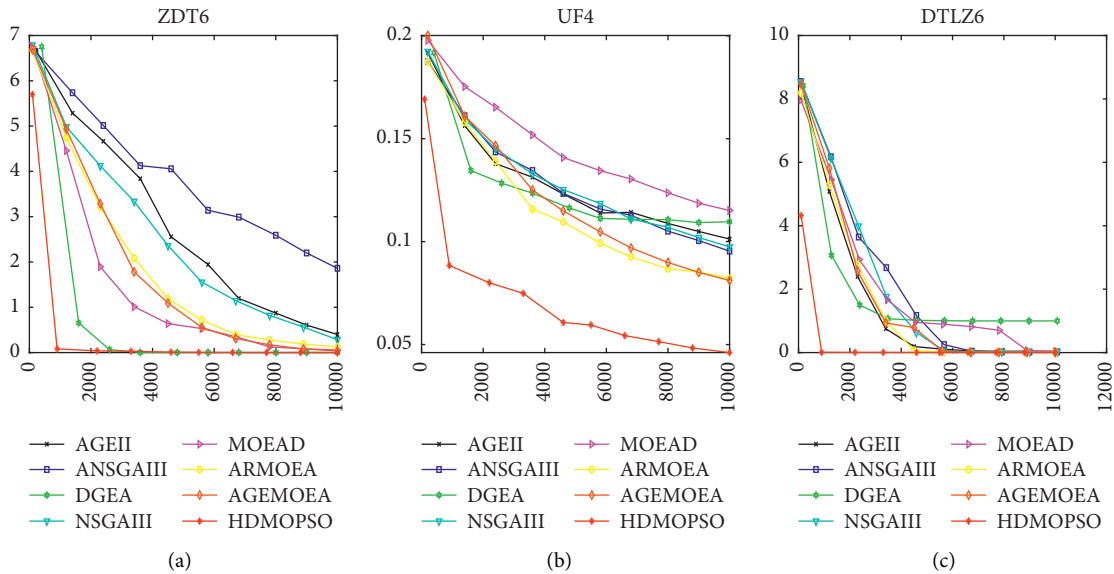


FIGURE 10: IGD values convergence trajectory of HDMOPSO and MOEAs comparison on ZDT6, UF4, and DTLZ6 problems.

obtained from Table 5 that DTLZ4 has obvious advantages over other algorithms compared to DTLZ7, it can be seen from Figure 7 that it is not obvious compared to the ANSGAIII and AGEMOEA on DTLZ4. Nothing is more stable than the ANSGAIII and AGEMOEA and the average value is no better than it except for outliers. Although there are no outliers in DTLZ7, there is still a little difference compared with the ANSGAIII and NSGAIII.

Figure 10 shows the IGD convergence trajectory obtained by HDMOPSO and MOEAs running 10000 times in ZDT6, UF4, and DTLZ6. HDMOPSO is compared with the MOEAs, it not only has an absolute advantage in the convergence speed, but also shows an obvious advantage in the convergence value, which also reflects the fast convergence speed of the particle algorithm.

Finally, Figure 11 shows the Pareto front simulation of HDMOPSO and MOEAs on ZDT4. It can be seen from the figure that the algorithms in this paper almost all converge to

the Pareto front, and the distribution is good. No other algorithm has a convergent Pareto front.

Through the above analysis of the comparison of HDMOPSO and MOEAs, HDMOPSO performs better in 22 test problems and 15 test problems with IGD values. Figure 9 also shows good stability. 14 of HV performed better. From Figures 10 and 11, it can be seen briefly that HDMOPSO has obvious advantages in terms of convergence speed and convergence. Especially, it shows obvious advantages compared with MOEAs in the ZDT and UF test problems. Therefore, HDMOPSO is more competitive than MOEAs.

4.6. *Computational Complexity of HDMOPSO.* The complexity of HDMOPSO algorithm mainly depends on the complexity of the three parts in Section 3 of this article. The following will be analyzed one by one according to the three parts. First, in the maintenance of the external archive, the

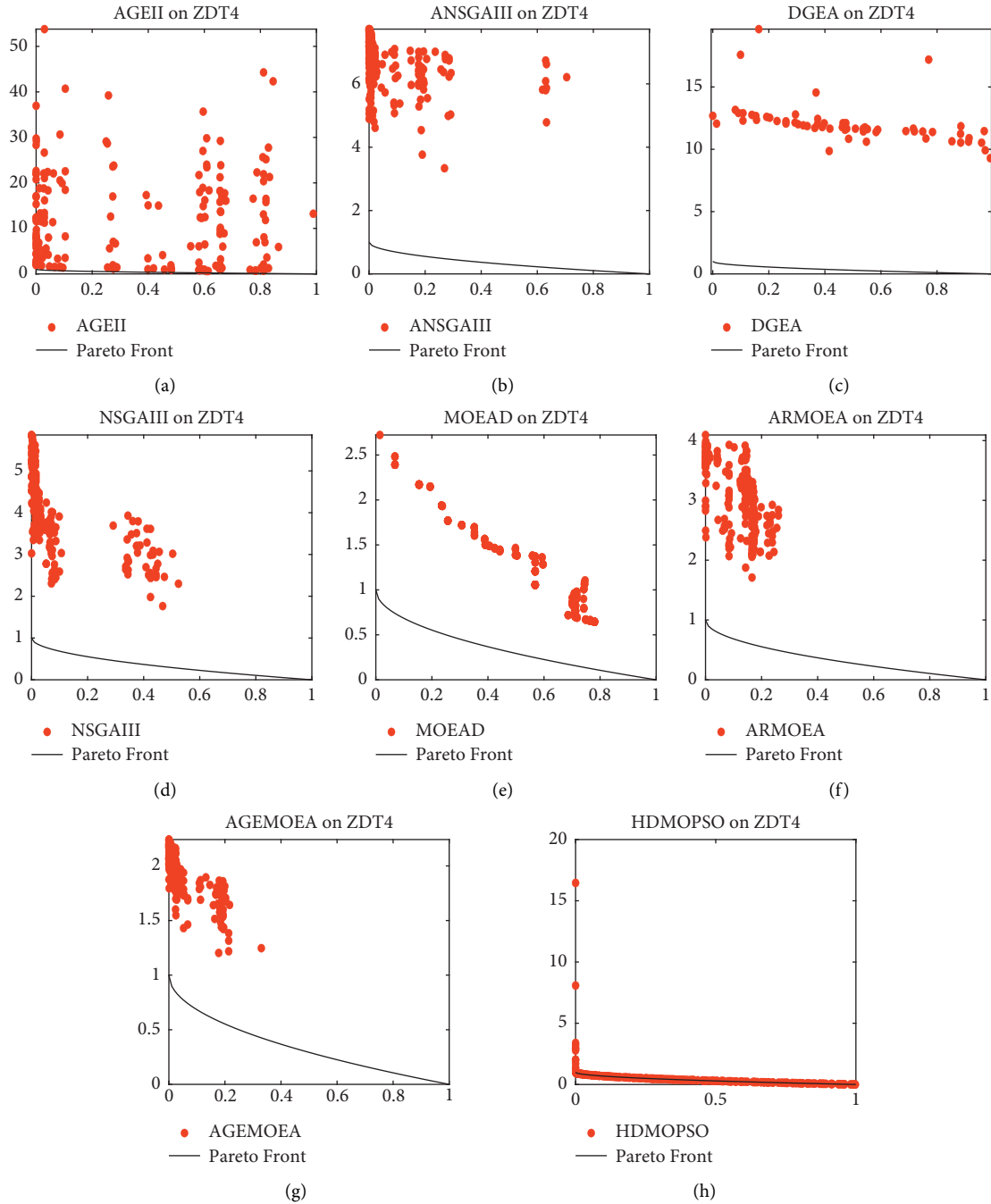


FIGURE 11: The Pareto front simulation of HDMOPSO and MOEAs on ZDT4 problem.

strategy of rebuilding the hypercube is used and there is only one operator. So complexity is $O(m \times div)$ (m is the target number, div is the number of divisions of the coordinate axes). Second, the complexity of the opposite mutation with nonlinear decreasing is $O(N)$ (N is the number of particles) according to the pseudocode in Figure 3. Thirdly, the setting of the social part based on the method of combining hyperspace and distance mainly consists of three parts. First, the hypercube are selected one by one and the optimal positions of each hypercube are averaged. Second, each particle finds its nearest average position. Finally, the particle

determines the flight of the social part according to the shortest average position it finds. So the complexity of the third part is $O(A \times a) + O(N \times A \times m) + O(N)$ (A is the number of optimal solutions to store in the external archive, a is the number of optimal solutions in the hypercube). According to the operation rules of the symbol O , the complexity above can be simplified as $O(A(N \times M + a) + m \times div)$.

In addition, tic and toc codes in MATLAB software are also used to calculate the running time of each algorithm when evaluating (FEs) 10,000 times (unit: *second*) It can be

TABLE 7: Running times of HDMOPSO and MOPSOs on 22 test problems.

Problems	FES	MOPSO	MOPSOCD	dMOPSO	SMPSO	NMPSO	MPSOD	CMOPSO	HDMOPSO
ZDT1	10000	1.8954e-01	2.1995e-01	3.0756e-01	1.5614e-01	5.9784e+00	9.8553e-01	9.6836e-01	6.2169e+00
ZDT2	10000	9.6836e-01	1.8677e-01	3.0587e-01	1.5278e-01	5.7637e+00	8.5288e-01	9.3910e-01	6.3731e+00
ZDT3	10000	1.6025e-01	1.3933e-01	3.1736e-01	1.5136e-01	3.7805e+00	8.8155e-01	3.6910e-01	5.2505e+00
ZDT4	10000	1.4136e-01	1.1535e-01	3.3401e-01	1.2446e-01	1.2178e+00	4.0052e-01	4.4006e-01	4.1853e+00
ZDT6	10000	1.6083e-01	3.0051e-01	3.0535e-01	1.4522e-01	6.9666e+00	6.0061e-01	1.9409e+00	1.1422e+01
UF1	10000	1.5675e-01	1.3745e-01	3.4933e-01	1.5089e-01	5.5508e-01	1.1290e+00	2.4897e-01	3.5535e+00
UF2	10000	1.8101e-01	1.4694e-01	4.0179e-01	1.6999e-01	9.5793e-01	1.1746e+00	2.8913e-01	9.6000e+00
UF3	10000	1.8831e-01	2.4739e-01	3.6602e-01	1.7367e-01	1.0686e+00	1.1528e+00	2.8029e-01	1.4856e+00
UF4	10000	1.6966e-01	1.5075e-01	3.8537e-01	1.6703e-01	2.6208e+00	1.2591e+00	2.9030e-01	9.8464e+00
UF5	10000	1.6004e-01	1.5048e-01	3.8623e-01	1.5731e-01	5.4259e-01	1.0700e+00	2.9916e-01	1.3402e+01
UF6	10000	1.7337e-01	1.5025e-01	3.9267e-01	1.6589e-01	5.3052e-01	1.1377e+00	2.9791e-01	2.6452e+00
UF7	10000	1.6423e-01	1.4502e-01	3.4968e-01	1.6433e-01	7.6412e-01	1.1829e+00	3.1794e-01	8.6314e+00
UF8	10000	2.2966e-01	1.7421e-01	3.9023e-01	2.1134e-01	1.5602e+00	9.6623e-01	5.5715e-01	4.8477e+00
UF9	10000	2.2266e-01	1.7022e-01	3.8962e-01	2.0454e-01	1.3716e+00	1.0086e+00	5.3158e-01	8.8649e+00
UF10	10000	1.9929e-01	1.7375e-01	3.7649e-01	1.9299e-01	6.3617e-01	9.8017e-01	4.5164e-01	1.4856e+00
DTLZ1	10000	1.9451e-01	1.7336e-01	4.2895e-01	1.7963e-01	1.9483e+00	1.4728e+00	3.4286e-01	4.4390e+00
DTLZ2	10000	2.5668e-01	2.1649e-01	4.0326e-01	1.9691e-01	2.8527e+00	1.4684e+00	1.4363e+00	3.8444e+00
DTLZ3	10000	3.6626e-01	1.8473e-01	4.4459e-01	1.9127e-01	1.0501e+00	1.0501e+00	3.6626e-01	1.9394e+00
DTLZ4	10000	2.4343e-01	1.7660e-01	4.4017e-01	1.9800e-01	2.8646e+00	1.2343e+00	1.2343e+00	9.8830e-01
DTLZ5	10000	2.5944e-01	1.9055e-01	4.4258e-01	2.0864e-01	2.2953e+00	9.3072e-01	9.1520e-01	2.3477e+00
DTLZ6	10000	2.4352e-01	3.2588e-01	4.4845e-01	2.1578e-01	3.6248e+00	1.3673e+00	8.9641e-01	5.3365e+00
DTLZ7	10000	2.3549e-01	3.5500e-01	3.5500e-01	2.0576e-01	2.9453e+00	6.8225e-01	9.0226e-01	1.0615e+01

TABLE 8: Running times of HDMOPSO and MOEAs on 22 test problems.

Problems	FES	AGEII	ANSGAIII	DGEA	NSGAIII	MOEAD	ARMOEA	AGEMOEAs	HDMOPSO
ZDT1	10000	1.6906e+01	4.7437e-01	4.2843e-01	2.9046e-01	1.7671e+00	6.4435e-01	2.5825e-01	6.2169e+00
ZDT2	10000	1.3348e+01	4.4615e-01	4.2499e-01	2.9139e-01	1.7384e+00	3.3364e-01	2.4050e-01	6.3731e+00
ZDT3	10000	1.4356e+01	4.5518e-01	4.0627e-01	2.8519e-01	1.7178e+00	8.8620e-01	2.6861e-01	5.2505e+00
ZDT4	10000	8.1142e+00	3.9137e-01	3.3979e-01	2.7679e-01	1.6371e+00	2.7897e-01	2.4642e-01	4.1853e+00
ZDT6	10000	8.1726e+00	4.0665e-01	3.8004e-01	2.7077e-01	1.6758e+00	2.7440e-01	2.1910e-01	1.1422e+01
UF1	10000	2.1910e-01	4.8534e-01	4.2519e-01	2.8050e-01	1.8027e+00	3.9434e-01	2.3187e-01	3.5535e+00
UF2	10000	3.0681e+01	4.8148e-01	4.5153e-01	2.9503e-01	2.0535e+00	9.2059e-01	3.0219e-01	9.6000e+00
UF3	10000	1.5124e+01	4.8845e-01	4.4217e-01	3.0029e-01	2.0223e+00	4.1813e-01	2.5723e-01	4.0495e+00
UF4	10000	6.6710e+01	4.8374e-01	4.5074e-01	3.1567e-01	1.9588e+00	1.0578e+00	2.9759e-01	9.8464e+00
UF5	10000	5.5514e+00	4.6839e-01	4.1768e-01	2.9088e-01	1.9183e+00	3.2421e-01	2.3231e-01	1.3402e+01
UF6	10000	7.9447e+00	4.6724e-01	4.2344e-01	2.9147e-01	1.9433e+00	3.3038e-01	2.3917e-01	2.6452e+00
UF7	10000	2.2273e+01	4.5917e-01	4.2218e-01	2.8460e-01	2.0121e+00	4.4279e-01	2.5829e-01	8.6314e+00
UF8	10000	1.0657e+01	5.7163e-01	4.1730e-01	3.2666e-01	2.1912e+00	2.0018e+00	4.8602e-01	4.8477e+00
UF9	10000	1.0713e+01	5.5393e-01	4.1814e-01	3.1820e-01	2.5255e+00	1.4048e+00	3.9560e-01	8.8649e+00
UF10	10000	8.5054e+00	5.5813e-01	4.1871e-01	3.2024e-01	2.5230e+00	1.0070e+00	2.7937e-01	1.4856e+00
DTLZ1	10000	5.0505e+00	5.7524e-01	4.2878e-01	3.2626e-01	2.4902e+00	9.6535e-01	3.6443e-01	4.4390e+00
DTLZ2	10000	8.7972e+01	5.2632e-01	4.6034e-01	3.6273e-01	2.4898e+00	4.6962e+00	7.8888e-01	3.8444e+00
DTLZ3	10000	1.0630e+02	5.2184e-01	3.9689e-01	3.8554e-01	2.4625e+00	4.2094e+00	7.3357e-01	1.9394e+00
DTLZ4	10000	1.0630e+02	5.2184e-01	3.9689e-01	3.8554e-01	2.4625e+00	4.2094e+00	7.3357e-01	9.8830e-01
DTLZ5	10000	1.8164e+02	6.6040e-01	3.8343e-01	4.0999e-01	2.5314e+00	4.1013e+00	6.1905e-01	2.3477e+00
DTLZ6	10000	1.8625e+01	6.8678e-01	4.2519e-01	4.1715e-01	2.5983e+00	3.8306e+00	7.1626e-01	5.3365e+00
DTLZ7	10000	2.0237e+01	5.7245e-01	3.7660e-01	3.7607e-01	2.4422e+00	4.0381e+00	6.4493e-01	1.0615e+01

seen from Tables 7 and 8 that HDMOPSO is almost in the same order of magnitude as MOPSOs and MOEAs in most of the test problems, but HDMOPSO algorithm is still a little slower than other algorithms. However, statistics after operation depend on computer hardware, software and other environmental factors. Therefore, the data at this time is for reference only.

5. Conclusions and Future Work

In this paper, a multiobjective particle swarm optimization combining hypercube and distance is proposed. Establish a combination of hypercube and distance in the external archive to set the social part of the particle speed update, and improve the optimization ability of the algorithm. In

addition, a nonlinear decreasing opposite mutation strategy is also used. It not only increases the exploration ability, but also prevents the algorithm from premature convergence. Finally, the hypercube technology is used to control the external archive, which improves the computing power of the algorithm while also increasing the diversity of the algorithm. HDMOPSO is compared with MOPSOs and MOEAs. The results show that HDMOPSO has good performance, especially the ZDT and UF test problems have strong competitiveness compared with MOPSOs and MOEAs. Therefore, the strategy of this paper is an effective improvement of particle swarm optimization in solving multiobjective optimization problems.

In the future research work, on the one hand, the optimization of the algorithm is studied. It can be seen from the data in this paper that the optimization effect of the algorithm is poor in complex problems, so more effective strategies are needed to solve most of MOPs. On the other hand, the main reason proposed by the algorithm is that it can effectively solve practical problems in reality, so it is one of the key points of further research to solve practical problems in reality.

Data Availability

No data were used to support this study.

Conflicts of Interest

The authors declare that there are no conflicts of interest regarding the publication of this paper.

Acknowledgments

This work was supported in part by the National Natural Science Foundation of China (Grant nos.71461027) and Innovative talent team in Guizhou Province (Qian Ke HE Pingtai Rencai[2016]5619).

References

- [1] Y. Tian, H. Wang, X. Zhang, and Y. Jin, "Effectiveness and efficiency of non-dominated sorting for evolutionary multi- and many-objective optimization," *Complex & Intelligent Systems*, vol. 3, no. 4, pp. 247–263, 2017.
- [2] B. Qu, C. Li, J. Liang, L. Yan, K. Yu, and Y. Zhu, "A self-organized speciation based multi-objective particle swarm optimizer for multimodal multi-objective problems," *Applied Soft Computing*, vol. 86, Article ID 105886, 2020.
- [3] Y. Zhang, S. Cheng, Y. Shi, D.-w. Gong, and X. Zhao, "Cost-sensitive feature selection using two-archive multi-objective artificial bee colony algorithm," *Expert Systems with Applications*, vol. 137, pp. 46–58, 2019.
- [4] N. Shahabi Sani, M. Manthouri, and F. Farivar, "A multi-objective ant colony optimization algorithm for community detection in complex networks," *Journal of Ambient Intelligence and Humanized Computing*, vol. 11, no. 1, pp. 5–21, 2020.
- [5] Q. Lin, Y. Ma, J. Chen et al., "An adaptive immune – inspired multi-objective algorithm with multiple differential evolution strategies," *Information Sciences*, vol. 430–431, pp. 46–64, 2018.
- [6] Q. Zhu, Q. Lin, W. Chen et al., "An external archive – guided multiobjective particle swarm optimization algorithm," *IEEE Transactions on Cybernetics*, vol. 47, no. 9, pp. 2794–2808, 2017.
- [7] Y. Yang, T. Zhang, W. Yi et al., "Deployment of multistatic radar system using multi-objective particle swarm optimization," *IET Radar, Sonar & Navigation*, vol. 12, no. 5, pp. 485–493, 2018.
- [8] R. Leng, A. Ouyang, Y. Liu, L. Yuan, and Z. Wu, "A multi-objective particle swarm optimization based on grid distance," *International Journal of Pattern Recognition and Artificial Intelligence*, vol. 34, no. 3, Article ID 2059008, 2020.
- [9] Q. Feng, Q. Li, P. Chen et al., "Multi-objective particle swarm optimization algorithm based on adaptive angle division," *IEEE Access*, vol. 7, pp. 916–930, 2019.
- [10] X. Zhang, X. Zheng, R. Cheng, J. Qiu, and Y. Jin, "A competitive mechanism based multi-objective particle swarm optimizer with fast convergence," *Information Sciences*, vol. 427, pp. 63–76, 2018.
- [11] G. Peng, Y.-W. Fang, W.-S. Peng, D. Chai, and Y. Xu, "Multi-objective particle optimization algorithm based on sharing-learning and dynamic crowding distance," *Optik*, vol. 127, no. 12, pp. 5013–5020, 2016.
- [12] C. A. C. Coello, G. T. Pulido, and M. S. Lechuga, "Handling multiple objectives with particle swarm optimization," *IEEE Transactions on Evolutionary Computation*, vol. 8, no. 3, pp. 256–279, 2004.
- [13] J. Kennedy and R. Eberhart, "Particle swarm optimization," in *Proceedings of the ICNN'95-international conference on neural networks*, vol. 4, pp. 1942–1948, Perth, Australia, November 1995.
- [14] F. Van Den Bergh, *An Analysis of Particle Swarm Optimizers (PSO)*, pp. 78–85, University of Pretoria, Pretoria, 2001.
- [15] C. C. Coello and M. S. Lechuga, "MOPSO: a proposal for multiple objective particle swarm optimization," *Proceedings of the 2002 Congress on Evolutionary Computation. CEC'02 (Cat. No. 02TH8600)*, vol. 2, pp. 1051–1056, 2002.
- [16] K. Deb, A. Pratap, S. Agarwal, and T. Meyarivan, "A fast and elitist multiobjective genetic algorithm: nsga," *IEEE Transactions on Evolutionary Computation*, vol. 6, no. 2, pp. 182–197, 2002.
- [17] A. J. Nebro, J. J. Durillo, J. Garcia-Nieto, C. C. Coello, F. Luna, and E. Alba, "SMPSO: a new PSO-based metaheuristic for multi-objective optimization," *IEEE Symposium on computational intelligence in multi criteria decision-making (MCDM)*, vol. 1, pp. 66–73, 2009.
- [18] S. Zapotecas Martinez and C. A. Coello Coello, "A multi-objective particle swarm optimizer based on decomposition," in *Proceedings of the 13th Annual Conference on Genetic and Evolutionary Computation*, pp. 69–76, Dublin, Ireland, July 2011.
- [19] Q. Hui Li and H. Li, "MOEA/D: a multiobjective evolutionary algorithm based on decomposition," *IEEE Transactions on Evolutionary Computation*, vol. 11, no. 6, pp. 712–731, 2007.
- [20] Y. Hu, Y. Zhang, and D. Gong, "Multi-objective particle swarm optimization for feature selection with fuzzy cost," *IEEE Transactions on Cybernetics*, vol. 51, no. 2, pp. 874–888, 2020.
- [21] Z. Yong, Y. Li-Juan, Z. Qian, and S. Xiao-Yan, "Multi-objective optimization of building energy performance using a particle swarm optimizer with less control parameters,"

- Journal of Building Engineering*, vol. 32, Article ID 101505, 2020.
- [22] H. R. Tizhoosh, "Opposition-based learning: a new scheme for machine intelligence," in *Proceedings of the International conference on computational intelligence for modelling, control and automation and international conference on intelligent agents, web technologies and internet commerce (CIMCA-IAWTIC'06)*, vol. 1, pp. 695–701, Vienna, Austria, November 2005.
- [23] L. Kang, R.-S. Chen, W. Cao, and Y.-C. Chen, "Non-inertial opposition-based particle swarm optimization and its theoretical analysis for deep learning applications," *Applied Soft Computing*, vol. 88, Article ID 106038, 2020.
- [24] Y. Zhang, D.-W. Gong, and J. Cheng, "Multi-objective particle swarm optimization approach for cost-based feature selection in classification," *IEEE/ACM Transactions on Computational Biology and Bioinformatics*, vol. 14, no. 1, pp. 64–75, 2015.
- [25] E. Zitzler, K. Deb, and L. Thiele, "Comparison of multi-objective evolutionary algorithms: empirical results," *Evolutionary Computation*, vol. 8, no. 2, pp. 173–195, 2000.
- [26] K. Deb, L. Thiele, M. Laumanns, and E. Zitzler, "Scalable test problems for evolutionary multi-objective optimization," *Evolutionary multi-objective optimization*, vol. 7, no. 2, pp. 105–145, 2005.
- [27] Q. Zhang, A. Zhou, S. Zhao, P. N. Suganthan, W. Liu, and S. Tiwari, "Multi-objective optimization test instances for the CEC 2009 special session and competition," vol. 264 Technical Report CES 487, pp. 1–30, University of Essex, Colchester, UK and Nanyang technological University, Singapore, 2008.
- [28] C. A. C. Coello and N. C. Cortes, "Solving multiobjective optimization problems using an artificial immune system," *Genetic Programming and Evolvable Machines*, vol. 6, no. 2, pp. 163–190, 2005.
- [29] E. Zitzler and L. Thiele, "Multiobjective evolutionary algorithms: a comparative case study and the strength Pareto approach," *IEEE Transactions on Evolutionary Computation*, vol. 3, no. 4, pp. 257–271, 1999.
- [30] C. R. Raquel and P. C. Naval, "An effective use of crowding distance in multi-objective particle swarm optimization," in *Proceedings of the 7th Annual Conference on Genetic and Evolutionary Computation*, pp. 257–264, Washington DC USA, June 2005.
- [31] Q. Lin, S. Liu, Q. Zhu et al., "Particle swarm optimization with a balanceable fitness estimation for many-objective optimization problems," *IEEE Transactions on Evolutionary Computation*, vol. 22, no. 1, pp. 32–46, 2016.
- [32] C. Dai, Y. Wang, and M. Ye, "A new multi-objective particle swarm optimization algorithm based on decomposition," *Information Sciences*, vol. 325, pp. 541–557, 2015.
- [33] M. Wagner and F. Neumann, "A fast approximation-guided evolutionary multi-objective algorithm," in *Proceedings of the 15th Annual Conference on Genetic and Evolutionary Computation*, pp. 687–694, Amsterdam, The Netherlands, July 2013.
- [34] H. Jain and K. Deb, "An evolutionary many-objective optimization algorithm using reference – point based non-dominated sorting approach, part II: handling constraints and extending to an adaptive approach," *IEEE Transactions on Evolutionary Computation*, vol. 18, no. 4, pp. 602–622, 2013.
- [35] C. He, R. Cheng, and D. Yazdani, "Adaptive offspring generation for evolutionary large – scale multi-objective optimization," *IEEE Transactions on Systems, Man, and Cybernetics: Systems*, vol. 52, 2020.
- [36] K. Deb and H. Jain, "An evolutionary many-objective optimization algorithm using reference – point-based non-dominated sorting approach, part i: solving problems with box constraints," *IEEE Transactions on Evolutionary Computation*, vol. 18, no. 4, pp. 577–601, 2013.
- [37] Y. Tian, R. Cheng, X. Zhang, F. Cheng, and Y. Jin, "An indicator-based multiobjective evolutionary algorithm with reference point Adaptation for better versatility," *IEEE Transactions on Evolutionary Computation*, vol. 22, no. 4, pp. 609–622, 2018.
- [38] A. Panichella, "An adaptive evolutionary algorithm based on non-euclidean geometry for many-objective optimization," in *Proceedings of the Genetic and Evolutionary Computation Conference*, pp. 595–603, Prague, Czech Republic, July 2019.
- [39] Y. Tian, R. Cheng, X. Zhang, and Y. Jin, "PlatEMO: a MATLAB platform for evolutionary multi-objective optimization [educational forum]," *IEEE Computational Intelligence Magazine*, vol. 12, no. 4, pp. 73–87, 2017.

Research Article

Evaluation and Prediction Method of System Security Situational Awareness Index Based on HMM Model

Mengjie Qian 

Information Engineering Department, Hebei Vocational University of Technology and Engineering, Xingtai 054000, China

Correspondence should be addressed to Mengjie Qian; polaris119@hdu.edu.cn

Received 7 February 2022; Revised 2 March 2022; Accepted 4 March 2022; Published 12 April 2022

Academic Editor: Hangjun Che

Copyright © 2022 Mengjie Qian. This is an open access article distributed under the Creative Commons Attribution License, which permits unrestricted use, distribution, and reproduction in any medium, provided the original work is properly cited.

In recent years, with the continuous development and progress of information technology and science and technology, big data has entered all walks of life, integrated into the lives of the public, and has become a necessity for social operation; the gradual development of artificial intelligence has also made life in modern times. People in society are more and more convenient. However, the development of science and technology is also accompanied by corresponding problems, and the war in information has gradually started. This paper simulates the possible information security through the hidden Markov model and then verifies the feasibility and effectiveness of the situation assessment method and the situation prediction method, in order to effectively evaluate the relevant information security level and effectively predict the accuracy of the situation value. The experimental results show that the fluctuation of the situation value corresponds to the different attack behaviors carried out by the attacker, accurately describes the information security status of the system, and verifies the effectiveness and accuracy of the situational awareness method proposed in this paper, while the situation prediction method based on ARIMA predictable short-term changes in situational values can be used for short-term forecasts that require high accuracy.

1. Introduction

In recent years, with the continuous improvement of people's economic income, mobile phones and computers have become the necessities of every family. Cybersecurity cases often occur in our lives, our cyberspace security is facing severe challenges, and many enterprises or organizations will also face cyberattacks, such as the once-famous "Aurora Attack," which attacked Google's mail server attacked. Some foreign hacker organizations hope to steal our country's military secrets and understand our country's political and economic situation by attacking our country's software. In China, some criminals use the Internet to attack some websites to steal the internal data of the websites and defraud some elderly people through the Internet. These situations affect the social atmosphere and reduce the happiness of residents' lives. As these problems become increasingly prominent, it should be put on the agenda to improve system security protection capabilities, pay attention to network security, and monitor and predict possible events. When

defending, improve your defense methods and fully understand the network security dynamics; you need to find potential threats as soon as possible, find out possible malicious behaviors, determine the source of the attack, provide important information for eliminating security threats and update network data in a timely manner, and actively fight against security risks.

With the continuous development and progress of information technology and technology, issues related to big data, artificial intelligence, and security posture have entered people's lives, and everyone has gradually become familiar with these once unfamiliar words. Company executives make decisions through big data [1]; the DBES problem [2]; the use of wireless mesh networks [3]; the deployment of intelligent transportation systems [4]; the rise of big data in cloud computing [5]; evaluation research on bank performance [6]; emergence of behavior-oriented artificial intelligence [7]; predicting lake level fluctuations [8]; birth of AIDR [9]; artificial intelligence applications [10]; birth of ADS system [11]; prediction of security situation [11];

security aggregation and configuration related data [12]; analysis of sources and identification methods of information risks [13]; application of artificial intelligence in music education [14]; performance improvement of water pollution monitoring and rapid decision-making systems [15]; network security situation prediction [16]; the combination of artificial intelligence algorithms and physical modeling [17]; and so on.

2. Theoretical Basis

2.1. Situational Awareness

2.1.1. Related Situational Awareness Profiles. Situational awareness was first proposed by Endsley et al. in 1988. It is defined as “the extraction and understanding of the surrounding environmental factors within a certain time and space, and the prediction of the future development trend.” Situational awareness originated from the military field and was soon applied to other fields. The application of situational awareness in network security is even more extensive and far-reaching; in enterprise information security management, the defense-discovery-repair approach is adopted [18].

2.1.2. Situational Awareness Model. The three-layer situational awareness model visually represented in Figure 1 is a widely accepted general theoretical model given by Endsley. The model is composed of situational element extraction, situational understanding, and situational prediction and plays an important role in the subsequent research on network security situational awareness systems.

2.1.3. Security Situation Forecast. Security situation prediction is the highest level technology in the whole situational awareness model [19]. The prediction of network security situation plays an important role in the defense of network security. The definition of situation prediction is to make a preestimation of the events or scenarios that will occur in the future to determine the probability of its occurrence, which usually requires rigorous investigation and observation, and artificial intelligence algorithms such as machine learning and deep learning can discover and identify potential patterns in input data and output of the required prediction information. They have achieved great success in computer vision, natural language processing, and other fields and are widely used in artificial intelligence algorithms. They have also been used in network security situation prediction and achieved initial results. Therefore, according to certain scientific basis, through the analysis and study of relevant factors, a specific prediction model as shown in Figure 2 is established.

2.1.4. Cybersecurity Situational Awareness. The network situation is a network state and changing trend, which is affected by factors such as different types of network operating conditions, network behaviors, and user behaviors. These behaviors are combined together to form a network

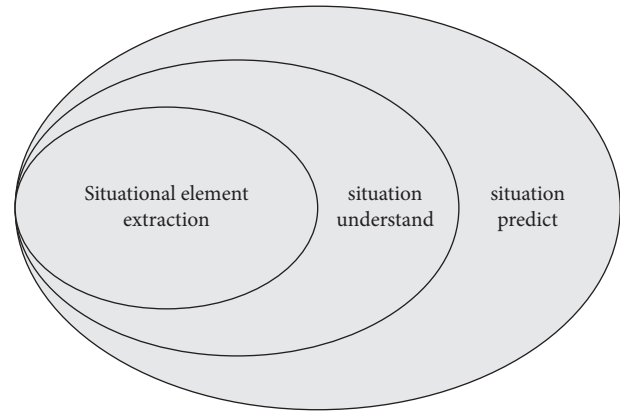


FIGURE 1: 3-layer situational awareness model.

situation. In a large-scale network environment, we can select those security elements for analysis, fully understand the changes in the network situation, and use big data technology to process different types of information. The perception platform integrates user terminals, through different types of perception data sources, fully explores technologies, understands intelligent algorithms, and improves the sensitivity of the network security situational awareness platform.

Situational awareness describes the network system and requires a full understanding of its microstate, which is reflected by various connection parameters. After in-depth mining of parameters, determine the correlation and development trend of information, and use related tools (algorithms or measures) to detect and perceive, and associate the data and information from detection and perception in some way to form knowledge. This completes a basic process of situational awareness as shown in Figure 3.

We know that the biggest feature of network situational awareness [20] is the need to measure the physical network. The following abilities serve as support:

- (1) Big data processing capability: the Internet is huge, and a large amount of concurrent data traffic is transmitted through each node. In this kind of data reanalysis, Network maintenance personnel cannot meet the requirements of the end-of-network activity and the characteristics of the network situation rate. Therefore, the sampling method to detect abnormal network activities cannot meet the requirements. Network situational awareness must have the ability of very good processing power for massive data.
- (2) Fine analysis capability: the detection of data packets must meet fine-grained requirements, and various data streams and parameters must be efficiently retrieved and matched. To achieve a good perception of the network microstate, in addition to the traditional key physical parameters (source and destination addresses, ports, and protocol types), situational awareness technology must also have the ability to identify multiple logical parameters.

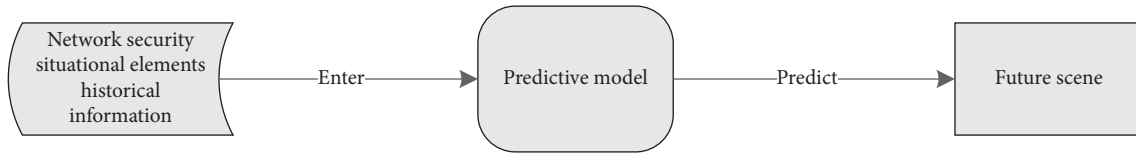


FIGURE 2: Security situation prediction model.

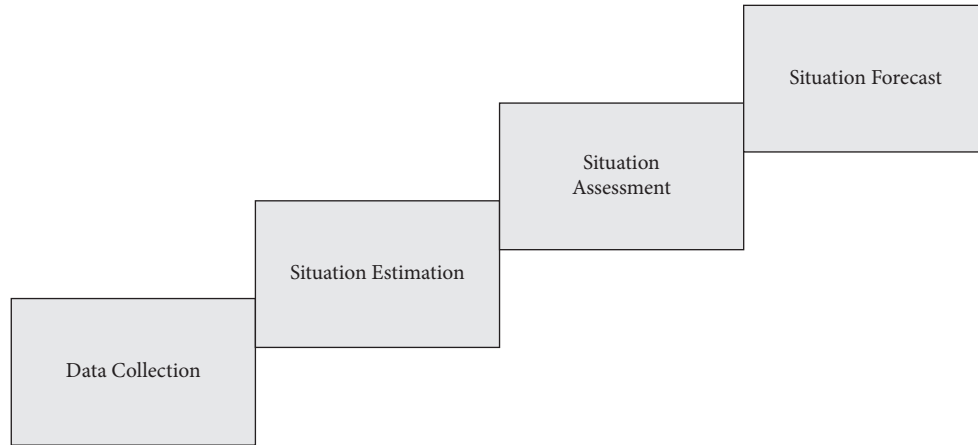


FIGURE 3: Conceptual model of network security situational awareness.

- (3) Protocol identification capability: as an important parameter, the protocol type is very important to accurately identify it. In the process of implementing situational awareness, in addition to identifying widely used Internet standard protocols (such as TCP/IP protocol suite, etc.), other nonstandard and private protocols should also be captured as much as possible. Security poses a threat. For the identified protocol features (fingerprints), a fingerprint database shall be formed, which shall be continuously updated and maintained to support the effective matching retrieval function.
- (4) Reliable operation capability: situational awareness technology equipment needs to have reliable operation capability to ensure long-term normal operation. Any interruption of the operation process may cause inaccurate perception information.
- (5) Business diversion capability: after all kinds of information are accurately identified, they should be redirected in a certain way; that is, after classifying the information, the next step is processed in a targeted manner. This can not only make the data information more accurate, but also greatly reduce the background processing load, improve operating efficiency, and save memory capacity.

3. Hidden Markov Model

Hidden Markov model is a commonly used probability model in statistics. In this section, the concept of hidden Markov model is introduced from the classic stock market problem, and then three types of problems and solutions of hidden Markov model are introduced. The observation

sequence problem extends the one-dimensional hidden Markov model to a multidimensional hidden Markov model.

3.1. Overview of Hidden Markov Models (HMM). Hidden Markov model (HMM) is a powerful probabilistic modeling tool for characterizing implicit stochastic processes with observable sequences. HMM have been used in areas such as signal processing, pattern recognition, and machine learning. At the beginning of the twentieth century, Andrei Markov proposed the mathematical theory of Markov Process. Until 1960, Baum and his colleagues proposed and developed the hidden Markov theory model.

Figure 4 depicts a simple example of a Markov process used to describe changes in the stock market. This stochastic process divides the daily changes of the stock market into three states: A city, B city, and a volatile market, which correspond to three observations of a stock's stock price rising, falling, and remaining unchanged. The transition between states is a Markov process with limited time discrete state space, also known as a Markov chain.

Assuming that the probability that the stock is in city A on the first day is 0.7, if it is observed that the stock is rising-falling-falling for three consecutive days, then it can be inferred that the changing state of the stock for three consecutive days is city A-city B-city B, and we can calculate the probability of this happening as

$$p = 0.7 \times 0.2 \times 0.5. \tag{1}$$

If each state is allowed to correspond to multiple observations, for example, when the stock is in market A, not only is there an increase in one observation, but also a

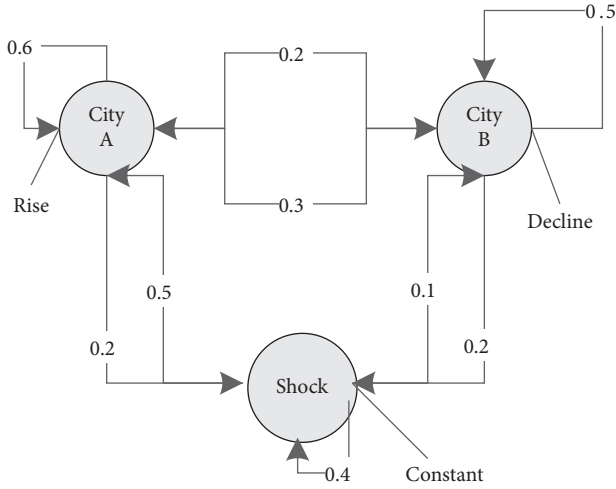


FIGURE 4: Markov process example.

decrease or shock may be observed, and the Markov chain can be extended to a hidden Markov model. This change can make the model more expressive. In Figure 5, the stock may also fluctuate or decline slightly in the state of city A. If the stock is observed to rise-fall-fall for three consecutive days, it cannot be said that the stock must be in the B market, so the stock state is “hidden” and can exist in any state sequence with a certain probability.

The mathematical definition of hidden Markov model can be given as follows:

$$\lambda = (A, B, \pi). \quad (2)$$

S is the set of hidden states and V is the set of observable states:

$$\begin{aligned} S &= (s_1, s_2, \dots, s_N), \\ V &= (v_1, v_2, \dots, v_M). \end{aligned} \quad (3)$$

Then define the hidden state sequence Q of length T and the corresponding observation sequence O :

$$\begin{aligned} Q &= q_1, q_2, \dots, q_T, \\ O &= o_1, o_2, \dots, o_T. \end{aligned} \quad (4)$$

A is the implicit state transition matrix. The element a_{ij} of the matrix represents the probability of transitioning from state i to state j . Note that the state transition probability is independent of time:

$$A = [a_{ij}], a_{ij} = P(q_t = S_j | q_{t-1} = S_i). \quad (5)$$

B is the observation matrix, and the element $b_i(k)$ of the matrix represents the probability of observing v_k in the hidden state i of the system. This probability is also independent of time:

$$B = [b_i(k)], b_i(k) = P(x_t = v_k | q_t = S_i). \quad (6)$$

π is the initial probability distribution matrix, and the elements represent the probability that the system is in each hidden state at the initial moment:

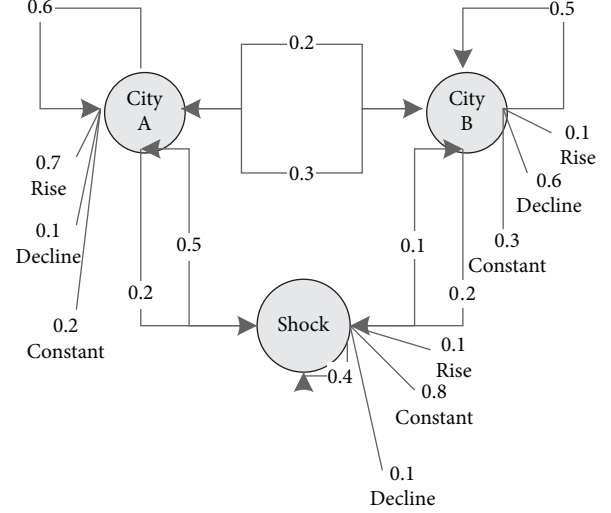


FIGURE 5: Hidden Markov model example.

$$\pi = [\pi_i], \pi_i = P(q_1 = S_i). \quad (7)$$

The HMM makes two assumptions. The first one is called the Markov assumption, which considers that the current state of the system only depends on the state of the system at the previous moment, which is expressed as

$$P(q_t | q_1^{t-1}) = P(q_t | q_{t-1}). \quad (8)$$

The second assumption is called the independence assumption, which considers that the observed state of the system only depends on the implicit state of the system at the current moment, which is expressed as

$$P(o_t | o_1^{t-1}, q_1^t) = P(o_t | q_t). \quad (9)$$

3.2. Hidden Markov Three Kinds of Problems. For HMM to be useful in practical applications, three problems related to them must be solved, which are estimation problem, decoding problem, and learning problem.

3.2.1. Estimation Problem. Given an HMM model λ , calculate the probability $P(O|\lambda)$ of occurrence of observation sequence O . This problem can be viewed as evaluating the ability of a known model to predict a given sequence of observations, and by comparing $P(O|\lambda)$ the most appropriate model can be selected. Given a sequence of hidden states Q , the probability of observing sequence O is

$$P(O|Q, \lambda) = \prod_{t=1}^T P(o_t | q_t, \lambda) = b_{q_1}(o_1) b_{q_2}(o_2) \cdots b_{q_T}(o_T). \quad (10)$$

The probability of occurrence of the hidden state sequence Q is

$$P(Q|\lambda) = \pi_{q_1} a_{q_1 q_2} a_{q_2 q_3} \cdots a_{q_{T-1} q_T}. \quad (11)$$

Given a model, the observation probability can be calculated:

$$\begin{aligned} P(O|\lambda) &= \sum_Q P(O|Q, \lambda)P(Q|\lambda) \\ &= \sum_{q_1 \dots q_T} \pi_{q_1} b_{q_1}(o_1) a_{q_1 q_2} b_{q_2} \\ &\quad \cdot (o_2) a_{q_2 q_3} \dots a_{q_{T-1} q_T} b_{q_T}(o_T). \end{aligned} \quad (12)$$

From this, the probability of occurrence of observation sequence O for a given model can be calculated, but its time complexity is in the exponential form with respect to time T (to be precise, it requires $2T \cdot N^T$ calculations). There are a large number of identical operations in the abovementioned calculation process, and these redundant operations can be reduced by means of cache calculation, so as to achieve the purpose of reducing the time complexity. The meshed grid is used to cache the operations that need to be repeated in the calculation process, and the grid can be moved forward until time T to obtain the result. This method is called the forward algorithm. To this end, an intermediate variable α needs to be introduced, which represents the probability that the implicit state is s_i and the observation sequence o_1, o_2, \dots, o_t is at time t :

$$\alpha_t(i) = P(o_1 o_2 \dots o_t, q_t = s_i | \lambda). \quad (13)$$

The specific algorithm is as follows:

(1) Initialization:

$$\alpha_1(i) = \pi_i b_i(o_1), 1 \leq i \leq N. \quad (14)$$

(2) Recursion:

$$\alpha_{t+1}(j) = \left[\sum_{i=1}^N \alpha_t(i) a_{ij} \right] b_j(o_{t+1}), 1 \leq t \leq T-1, 1 \leq j \leq N. \quad (15)$$

(3) Termination:

$$P(O|\lambda) = \sum_{i=1}^N \alpha_T(i). \quad (16)$$

Strictly speaking, the forward algorithm can solve the evaluation problem, but in order to solve the learning problem, a backward algorithm must be introduced, which can also solve the evaluation problem. Similar to the forward algorithm, define an intermediate variable β , given the state s_i at time t , the probability of observing the sequence from o_{t+1} to o_T :

$$\beta_1(i) = P(o_{t+1} o_{t+2} \dots o_T | q_t = s_i, \lambda). \quad (17)$$

Unlike the forward algorithm, the backward algorithm recurses from the back to the front. The specific algorithm is as follows:

(1) Initialization:

$$\beta_T(i) = 1, 1 \leq i \leq N. \quad (18)$$

(2) Recursion:

$$\left\{ \beta_t(i) = \sum_{j=1}^N a_{ij} b_j(o_{t+1}) \beta_{t+1}(j), t = T-1, T-2, \dots, 1, 1 \leq i \leq N \right\}. \quad (19)$$

(3) Termination:

$$P(O|\lambda) = \sum_{i=1}^N \pi_i b_i(o_1) \beta_1(i). \quad (20)$$

3.2.2. Decoding Problem. The purpose of decoding is to find the hidden state sequence that is most likely to produce a given observation sequence, that is, the known model λ , and to find the hidden state sequence Q that makes the observation sequence O most likely to appear. The best solution to the decoding problem is to use the Viterbi algorithm, which is another grid algorithm, similar to the forward algorithm, except that the probability at each moment is maximized instead of summing. We can define

$$\delta_t(i) = \max_{q_1, q_2, \dots, q_{t-1}} P(q_1 q_2 \dots q_t = s_i o_1, o_2, \dots, o_t | \lambda), \quad (21)$$

which is the probability of the most likely hidden state path that makes the observation sequence appear up to time t . The Viterbi algorithm is as follows:

(1) Initialization:

$$\delta_t(i) = \pi_i b_i(o_1), 1 \leq i \leq N, \Psi_1(i) = 0. \quad (22)$$

(2) Recursion:

$$\begin{aligned} \delta_t(j) &= \max_{1 \leq i \leq N} [\delta_t(i) a_{ij}] b_j(o_t), 2 \leq t \leq T, 1 \leq j \leq N, \\ \Psi_1(j) &= \arg \max_{1 \leq i \leq N} [\delta_t(i) a_{ij}], 2 \leq t \leq T, 1 \leq j \leq N. \end{aligned} \quad (23)$$

(3) Termination:

$$\begin{aligned} P^* &= \max_{1 \leq i \leq N} [\delta_r(i)], \\ q_r^* &= \arg \max_{1 \leq i \leq N} [\delta_r(i)]. \end{aligned} \quad (24)$$

(4) Backtracking of the optimal state sequence:

$$q_t^* = \Psi_{t+1}(q_{t+1}^*), t = T-1, T-2, \dots, 1. \quad (25)$$

The main difference between the Viterbi algorithm and the forward algorithm is that the Viterbi algorithm maximizes the probability in the recursive process, rather than summing it up, and stores the state when the probability is the largest, so as to end the used backtracking.

Backtracking allows finding the optimal sequence of states from the states stored in the recursive steps, and there is no easy way to find a suboptimal sequence of states.

3.2.3. *Learning Problems.* Learning problems are divided into two categories: supervised and unsupervised, corresponding to two standard solutions. Learning problems are divided into two categories: supervised and unsupervised, corresponding to two standard solutions. If the training data set used to solve the learning problem is supervised, that is, when the observation sequence is given, the corresponding hidden state sequence is also specified, and a supervised learning algorithm is used. If the training data set is unsupervised, that is, only the observation sequence is given, the unsupervised learning algorithm, also known as the B-W algorithm, can be used.

The B-W algorithm, jointly proposed by Baum and his colleagues, is a very classic algorithm for solving model parameter selection problems.

In order to describe the estimation process of HMM parameters, the B-W algorithm first defines an intermediate variable to represent the probability of state s_i at time t and state s_{i+1} at time $t+1$ under the premise of given model parameters and observation sequence:

$$\xi_t(i, j) = P(q_t = s_i, q_{t+1} = s_j | O, \lambda). \quad (26)$$

The B-W algorithm uses the forward algorithm at time t and the backward algorithm at time $t+1$, which cleverly combines the forward algorithm and the backward algorithm, also known as the forward-backward algorithm, and $\xi_t(i, j)$ is also called the forward algorithm Backward variable.

According to the Bayesian formula, the forward-backward variable announcement can be written as:

$$\xi_t(i, j) = \frac{\alpha_t(i) a_{ij} b_j(O_{t+1}) \beta_{t+1}(j)}{P(O|\lambda)}, \quad (27)$$

$$\xi_t(i, j) = \frac{\alpha_t(i) a_{ij} b_j(O_{t+1}) \beta_{t+1}(j)}{\sum_{i=1}^N \sum_{j=1}^N \alpha_t(i) a_{ij} b_j(O_{t+1}) \beta_{t+1}(j)},$$

In the formula, the numerator term is $P(q_t = s_i, q_{t+1} = s_j, O|\lambda)$, and the denominator term is $P(O|\lambda)$, which is obtained by the full probability formula.

Define $\gamma_t(i)$ as the probability that the model is in state s_i at time t , and establish the relationship between $\gamma_t(i)$ and $\xi_t(i, j)$ as follows:

$$\gamma_t(i) = \sum_{j=1}^N \xi_t(i, j). \quad (28)$$

The value obtained by the summation of $\gamma_t(i)$ at time t can be used to represent the expectation of the number of visits to state s_i , that is, the expectation of the number of transitions from state s_i . Likewise, the result of summing $\xi_t(i, j)$ over time can be used to express the expectation of the number of transfers from s_i to s_j .

The idea of the B-W algorithm is to iteratively obtain the new model parameter $\bar{\lambda}$. Once $P(O|\bar{\lambda}) > P(O|\lambda)$ is found, $\bar{\lambda}$ is assigned to λ and iteratively calculates until $P(O|\lambda)$ no longer changes significantly. Therefore, unfortunately, this

algorithm can only obtain the local optimum. In order to calculate $\bar{\lambda}$ efficiently, a helper function for $\bar{\lambda}$ is introduced:

$$L(\lambda, \bar{\lambda}) = \sum_Q \log[P(O, Q|\lambda)]P(O, Q|\bar{\lambda}). \quad (29)$$

The expectation of the joint distribution $P(O, Q|\lambda)$ is based on the conditional probability $P(O, Q|\bar{\lambda})$.

The log-likelihood function $f(\lambda) = \log[P(O, Q|\lambda)]$ is a concave function, according to Jensen's inequality:

$$f[E(\lambda)] = f[E(\bar{\lambda})] \geq E[f(\lambda)]. \quad (30)$$

Both sides of the above equation can be written as

$$E[f(\lambda)] = \sum_Q \log[P(O, Q|\lambda)]P(O, Q|\bar{\lambda}) = L(\lambda, \bar{\lambda}),$$

$$f[E(\bar{\lambda})] = \sum_Q \log[P(O, Q|\lambda)]P(O, Q|\bar{\lambda}) = \log P(O|\bar{\lambda}),$$

$$\log P(O|\bar{\lambda}) \geq L(\lambda, \bar{\lambda}).$$

(31)

No matter how $\bar{\lambda}$ changes, as long as $L(\lambda, \bar{\lambda})$ is increased, the infimum of $P(O|\lambda)$ can be increased, and then maximizing $L(\lambda, \bar{\lambda})$ can increase the probability of $P(O|\lambda)$, namely,

$$\max_{\bar{\lambda}} [L(\lambda, \bar{\lambda})] \Rightarrow P(O|\bar{\lambda}) \geq P(O|\lambda). \quad (32)$$

Therefore, iterative calculation can make $P(O|\lambda)$ converge to the maximum point.

$$P(O, Q|\lambda) = \pi_{q_1} b_{q_1}(o_1) a_{q_1 q_2} b_{q_2}(o_2) a_{q_2 q_3} \cdots b_{q_r}(o_r) a_{q_r - 1 q_r}. \quad (33)$$

$L(\lambda, \bar{\lambda})$ can be split into three items:

$$L(\lambda, \bar{\lambda}) = \sum_Q \log[P(O, Q|\lambda)]P(O, Q|\bar{\lambda}),$$

$$L(\lambda, \bar{\lambda}) = \sum_Q \log \pi_{q_1} P(O, Q|\bar{\lambda})$$

$$+ \sum_Q \sum_{t=1}^{T-1} \log a_{q_r q_{r+1}} P(O, Q|\bar{\lambda}) \quad (34)$$

$$+ \sum_Q \sum_{t=1}^T \log b_{q_r}(o_t) P(O, Q|\bar{\lambda}).$$

For solving the above problems, there are three natural constraints:

$$\begin{cases} \sum_{i=1}^N \bar{\pi}_i = 1, \\ \sum_{j=1}^N \bar{a}_{ij} = 1, 1 \leq i \leq N, \\ \sum_{k=1}^M \bar{b}_j(k) = 1, 1 \leq j \leq N. \end{cases} \quad (35)$$

According to the Lagrange multiplier method, combined with the above constraints, the extreme value of each component of $L(\lambda, \bar{\lambda})$ can be obtained, and the one-step optimal estimation of the HMM parameters can be obtained:

$$\begin{aligned}\bar{\pi}_i &= \gamma_t(i), \\ \bar{a}_{ij} &= \frac{\sum_{t=1}^{T-1} \xi_t(i, j)}{\sum_{t=1}^{T-1} \gamma_t(i)}, \\ \bar{b}_j(k) &= \frac{\sum_{t=1, o_t=v_k}^{T-1} \gamma_t(i)}{\sum_{t=1}^{T-1} \gamma_t(i)}.\end{aligned}\quad (36)$$

The new model parameter λ is obtained iteratively from the above. Once $P(O|\bar{\lambda}) \geq P(O|\lambda)$ is found, $\bar{\lambda}$ is assigned to λ , and the iterative calculation is performed until $P(O|\lambda)$ no longer changes significantly, and the final value is used as the parameter estimation result of HMM.

The B-W algorithm cleverly uses the idea of maximum likelihood estimation to obtain the model parameter λ that maximizes $P(O|\lambda)$.

3.3. A Brief Introduction to Multidimensional Hidden Markov Models. For the n -dimensional mutually coupled observation sequence $\{O^{(1)}, O^{(2)}, \dots, O^{(n)}\}$, it can be modeled as $\{\lambda^{(1)}, \lambda^{(2)}, \dots, \lambda^{(n)}\}$, respectively:

$$P^{(1)}(O^{(1)}, O^{(2)}, \dots, O^{(n)}) = P(O^{(1)}) \prod_{m=1, m \neq l}^n P(O^{(m)}|Q^{(l)}), \quad (37)$$

where $l, m = 1, 2, \dots, n$.

The n -dimensional HMM learning algorithm is

$$Q^{(l)} = \text{argmax}_{Q^{(l)}} P(O^{(l)}, Q^{(l)}) \prod_{m=1, m \neq l}^n P(O^{(m)}|Q^{(l)}). \quad (38)$$

4. Experimental Results and Analysis

By selecting the gateway computer that is easy to be attacked, the system is connected to the signal and the ATS intranet at the same time, as the attack object of the experiment. Select DDoS as the main attack method, conduct vulnerability scanning, MS17-010 vulnerability attack, and DDoS attack. Based on the above data, relevant experimental analysis was carried out.

4.1. Situation Assessment Experiment Results and Analysis. By collecting the situational factor index data of gateway computer, CI, and ZC when the system is running normally, the maximum likelihood estimation method is used to fit the probability distribution of the data, and the K-S test is used to determine the distribution and parameters of the data. Then, according to the distribution of the data, the Lloyd–Max method is used to divide the data into states, and the state division interval with the minimum quantization error is obtained.

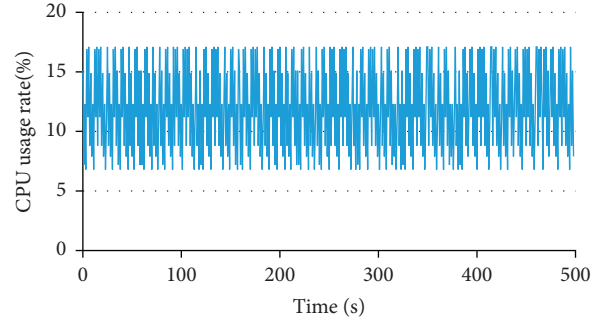


FIGURE 6: Change of CPU usage in the gateway computer.

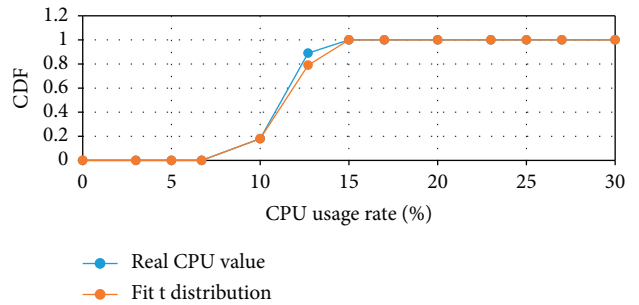


FIGURE 7: Comparison of data of gateway computer and CDF of fitting t distribution.

Taking the gateway computer as an example, the change and distribution of CPU usage within 1 hour are shown in Figures 6 and 7. The real data and the CDF curve of the fitted t distribution basically coincide, and the K-S test result is passed; it can be considered that the gateway computer CPU usage follows a t distribution with parameters $u = 10.6727$, $\sigma = 0.5594$, and $\nu = 4.3870$.

The change and distribution of RAM usage within 1 hour are shown in Figures 8 and 9. The real data and the CDF curve fitting the Gaussian distribution basically coincide, and the K-S test result is passed; it can be considered that the RAM usage of the gateway computer obeys the Gaussian distribution. The parameters are $u = 29.4752$ and $\sigma = 0.3447$.

Figures 10 and 11 show the change and distribution of the network sending rate within 1 hour. The real data basically coincides with the CDF curve fitting the t distribution, and has passed the K-S test. It can be considered that the gateway computer network sending rate obeys the t distribution. The parameters are $u = 16.1603$, $\sigma = 0.3524$, and $\nu = 3.7766$.

Figures 12 and 13 show the change and distribution of the network reception rate within 1 hour. The real data basically coincides with the CDF curve fitting the t distribution and has passed the K-S test. It can be considered that the gateway computer network reception rate obeys the t distribution. The parameters are $u = 21.5830$, $\sigma = 1.0182$, and $\nu = 4.3939$.

The distribution and distribution parameters of each index data of the gateway computer are summarized as shown in Table 1. The table lists the distribution and parameters of the gateway computer's CPU usage, RAM usage,

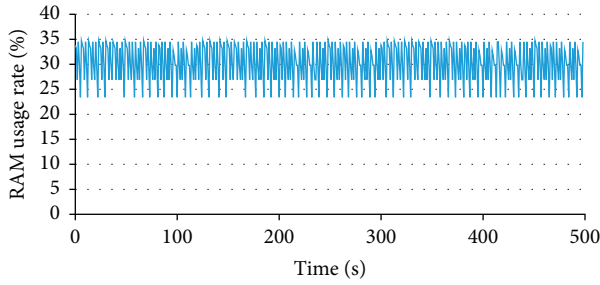


FIGURE 8: Change of RAM usage in the gateway computer.

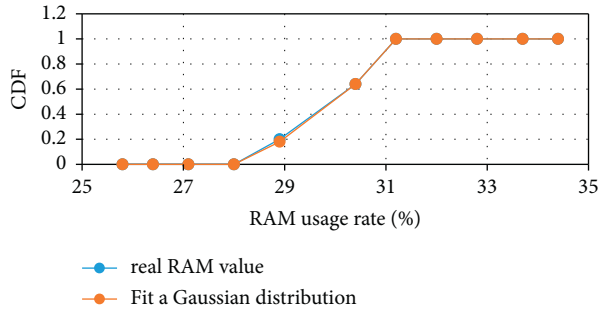


FIGURE 9: Comparison of RAM data of gateway computer and CDF of fitting Gaussian distribution.

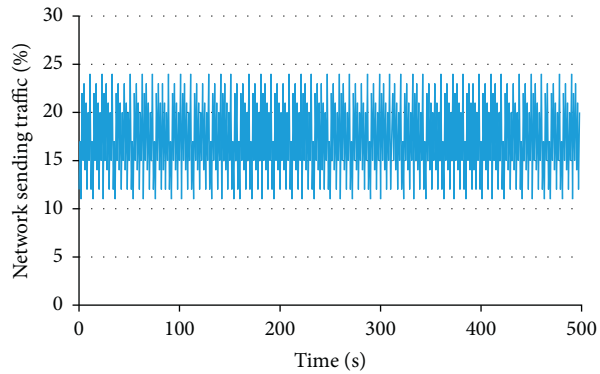


FIGURE 10: Change of transmission rate of the gateway computer network.

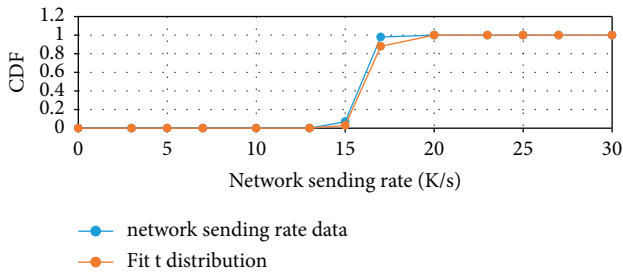


FIGURE 11: Comparison of network transmission rate of gateway computer and CDF of fitting Gaussian distribution.

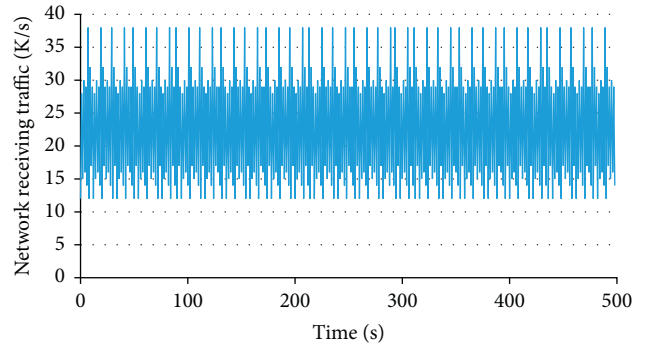


FIGURE 12: Change of receiving rate of the gateway computer network.

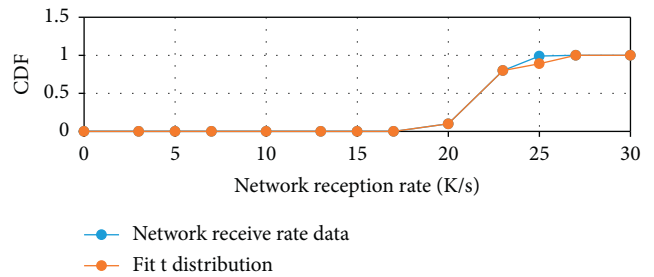


FIGURE 13: Comparison of receiving rate of gateway computer network and fitting t distribution.

network sending rate, and network receiving rate. Since the gateway computer is running, there is basically no data interaction with the disk, and the read rate and write rate of the disk are usually 0, so we will not do much research on it here.

After obtaining the distribution of each indicator data, the Lloyd–Max algorithm can be used to quantify the data. The quantification interval of each indicator is shown in Table 2.

In the same steps, the distribution and distribution parameters of each index of CI are obtained, as shown in Table 3. Since CI performs a large number of logical operations during the running process, it consumes a lot of CPU, and the average CPU usage rate reaches about 61%. However, the memory space occupied by the CI application software when running is smaller than that of the gateway application software, so the average RAM usage of the CI is slightly lower than that of the gateway computer.

The Lloyd–Max algorithm is used to quantify the data of each index of the CI, and the combined index is shown in Table 4.

Table 5 shows the distribution and distribution parameters of ZC index data. ZC simulation software does not have great hardware requirements, so the average of its CPU usage and RAM usage is at a low level.

The Lloyd–Max algorithm is used to quantify the data of various indicators of ZC, and the quantification interval of each indicator is shown in Table 6.

TABLE 1: Distribution and parameters of indicators of gateway computer.

Index	Obeys the distribution	Parameter
CPU usage	t distribution	$u = 10.6727, \sigma = 0.5594, \nu = 4.3870$
RAM usage	Gaussian distribution	$u = 29.4752, \sigma = 0.3447$
Network sending rate	t distribution	$u = 16.1603, \sigma = 0.3524, \nu = 3.7766$
Network reception rate	t distribution	$u = 21.5830, \sigma = 1.0182, \nu = 4.3939$

TABLE 2: Quantitative interval of indicators of gateway computer.

Index	Quantization interval
CPU usage	0 10.2095 11.1813 12.8721 100.0000
RAM usage	0 27.1261 29.1398 32.0861 100.0000
Network sending rate	0 14.6692 15.9972 16.8667 30.0000
Network reception rate	0 19.4237 21.3072 22.9721 40.0000

TABLE 3: Distribution and parameters of indicators of CI.

Index	Obeys the distribution	Parameter
CPU usage	t distribution	$u = 61.2727, \sigma = 0.7584, \nu = 5.0870$
RAM usage	Gaussian distribution	$u = 19.5752, \sigma = 0.5047$
Network sending rate	t distribution	$u = 8.3603, \sigma = 0.3124, \nu = 0.7766$
Network reception rate	t distribution	$u = 21.0120, \sigma = 0.7182, \nu = 0.8939$

TABLE 4: Quantitative interval of indicators of CI.

Index	Quantization interval
CPU usage	0 59.2095 59.1813 61.8721 100.0000
RAM usage	0 16.9261 19.1398 22.0861 100.0000
Network sending rate	0 6.66920 10.9972 17.8667 30.0000
Network reception rate	0 13.4237 19.3072 25.9721 40.0000

TABLE 5: Distribution and parameters of indicators of ZC.

Index	Obeys the distribution	Parameter
CPU usage	t distribution	$u = 15.9727, \sigma = 0.2584$
RAM usage	Gaussian distribution	$u = 21.5752, \sigma = 0.1047$
Network sending rate	t distribution	$u = 9.3603, \sigma = 0.3124, \nu = 0.7726$
Network reception rate	t distribution	$u = 19.0120, \sigma = 1.3182, \nu = 0.9339$

TABLE 6: Quantitative interval of indicators of ZC.

Index	Quantization interval
CPU usage	0 14.2095 16.1813 19.8721 100.0000
RAM usage	0 18.9261 21.1398 24.8861 100.0000
Network sending rate	0 7.66920 12.9872 18.8667 30.0000
Network reception rate	0 13.4937 19.9072 25.9891 40.0000

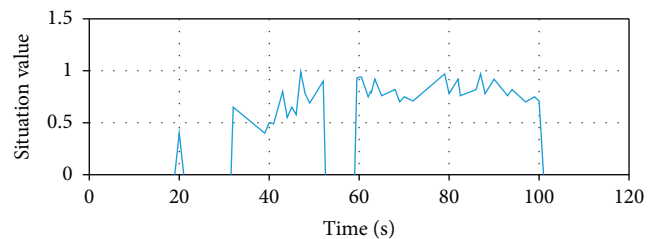


FIGURE 14: Change trend of situation value.

Figure 14 shows the change trend of the basic operation situation value of the system obtained by simulation. It can be seen from the figure that the change of situation value can be divided into three stages according to time. Around 20s, the situational value suddenly increased from 0 to 0.4, which is consistent with the vulnerability scanning event conducted by the attacker at this time. The posture value then returned to 0, indicating that the attacker had been scanning

for vulnerabilities for a short period of time and had no other activity for a period of time. During the period of 34s to 54s, the situation value fluctuated between 0.4 and 0.9, and there was an obvious upward trend. During this period, the attacker used the MS-17010 vulnerability to attack the system and obtained the administrators of the devices in the system

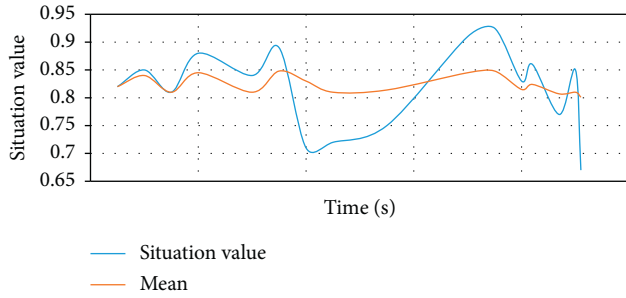


FIGURE 15: The training sample set.

(permission), implanted the DDoS virus on the device, and then stopped activities for a period of time, and the situation value also returned to 0. During the period of 60s to 100s, the situation value fluctuates around 0.8, which is consistent with the event that the attackers control the devices of the system to launch DDoS attacks on the gateway computer. The attacker then ceased activity, and the situational value returned to 0.

The experimental results show that the fluctuation of the situation value corresponds to the different attack behaviors carried out by the attacker, which accurately describes the information security status of the system and verifies the effectiveness and accuracy of the situation awareness method proposed in this paper. And the time node of the change of the situation value is synchronized with the time node of the attacker's attack, which also verifies the real-time performance of the situation assessment method.

4.2. Situation Forecasting Experiment Results and Analysis.

This section selects the trend of situation change from 60s to 70s and uses the first 20 data points as training samples and the last 10 data points as comparison samples to verify the situation prediction method. The selected data is shown in Figure 15. Using ADF to check that the situation sequence is not a stationary sequence, the sequence needs to be stationary.

The selected situation sequence is differentiated once, and the obtained difference sequence passes the ADF stationarity test. Therefore, the sequence difference is stopped, and the subsequent steps of ARIMA can be used to predict the situation sequence. The difference result is shown in Figure 16.

The training samples are fitted by the ARIMA method [22]. Determine the model parameters of ARIMA as $p=3$, $d=1$, $q=4$. The parameters in the formula are obtained by using the maximum likelihood estimation method: the constant term $\mu = -0.026513$; the three autoregressive coefficients are $\phi_1 = -0.20651$, $\phi_2 = -0.33681$, and $\phi_3 = -0.4685$; the four moving average coefficients are $\theta_1 = -0.54385$, $\theta_2 = 0.24325$, $\theta_3 = -0.78119$, and $\theta_4 = 0.081789$. Figure 17 shows the situation prediction result using this estimation model. It can be seen from the figure that the predicted value is basically consistent with the trend of the actual value. This shows that the ARIMA model has a

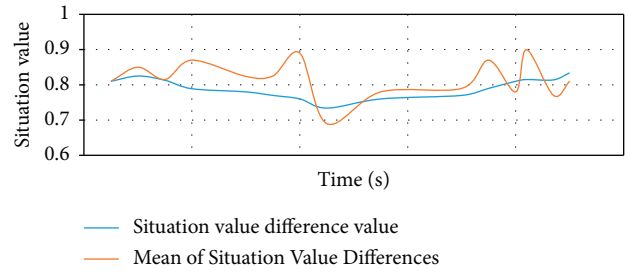


FIGURE 16: The result of 1 difference of situation values.

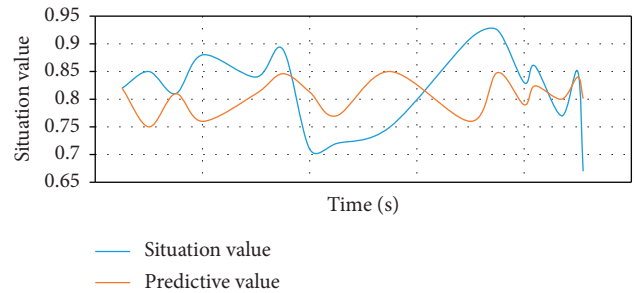


FIGURE 17: The result of the situation value prediction.

high prediction accuracy for the information security situation value of the train control system.

The experimental results show that the situation prediction method based on ARIMA can effectively predict the short-term changes of the situation value, but because the ARIMA method produces the characteristic that the sequence tends to be stable, the predicted value will converge near the mean value of the real value, which cannot reflect the fluctuation of the situation value. It is suitable for short-term forecasts with high accuracy requirements.

5. Conclusion

Information security is an issue that every country should pay attention to. The article is short and mainly explains the use of the hidden Markov model. After simulating the information security experiment, the feasibility and effectiveness of the situation assessment method and the situation prediction method are carried out. After a brief verification, the results also show that the situation assessment method based on the hidden Markov model can effectively assess the level of information security. However, with the passage of time, this method will gradually converge to the mean value of the situation value sequence, so it cannot reflect the fluctuation of the situation. Therefore, the long-term prediction of the situation value can become a follow-up research direction. This article only provides a superficial understanding of security situational awareness and ignores some details in the analysis process. It is hoped that the article can provide ideas for future situational awareness research in the future.

Data Availability

The experimental data used to support the findings of this study are available from the corresponding author upon request.

Conflicts of Interest

The authors declare that they have no conflicts of interest regarding this work.

References

- [1] A. McAfee and E. Brynjolfsson, "Big data: the management revolution," *Harvard Business Review*, vol. 90, no. 10, pp. 60–128, 2012.
- [2] N. Cao, C. Wang, M. Li, K. Ren, and W. Lou, "Privacy-preserving multi-keyword ranked search over encrypted cloud data," *IEEE Transactions on Parallel and Distributed Systems*, vol. 25, no. 1, pp. 222–233, 2014.
- [3] A. R. Palin and I. J. Jacob, "Review on fog based spectrum sensing for artificial intelligence," *International Journal of Scientific Research in Computer Science, Engineering and Information Technology*, vol. 3, pp. 66–70, 2018.
- [4] Y. Lv, Y. Duan, W. Kang, Z. X. Li, and F. Y. Wang, "Traffic flow prediction with big data: a deep learning approach," *IEEE Transactions on Intelligent Transportation Systems*, vol. 16, no. 2, pp. 865–873, 2015.
- [5] A. Ibrahim, T. Hashem, I. Yaqoob, Nor, and B. Anuar, "The rise of "big data" on cloud computing: review and open research issues," *Information Systems*, vol. 47, pp. 98–115, 2015.
- [6] M. D. Fethi and F. Pasiouras, "Assessing bank efficiency and performance with operational research and artificial intelligence techniques: a survey," *European Journal of Operational Research*, vol. 204, no. 2, pp. 189–198, 2010.
- [7] L. Steels, "The artificial life roots of artificial intelligence," *Artificial Life*, vol. 1, no. 1_2, pp. 75–110, 2010.
- [8] O. Kisi, J. Shiri, and B. Nikoofar, "Forecasting daily lake levels using artificial intelligence approaches," *Computers & Geosciences*, vol. 41, pp. 169–180, 2012.
- [9] F. Ofli, P. Meier, M. Imran et al., "Combining human computing and machine learning to make sense of big (aerial) data for disaster response," *Big Data*, vol. 4, no. 1, pp. 47–59, 2016.
- [10] A. Vega-Muoz, "Toward an integrated disaster management approach: how artificial intelligence can boost disaster management," *Sustainability*, vol. 13, 2021.
- [11] Z. Gu, R. Wang, and S. Wang, "Research ON real-time forecast OF security posture OF information system based ON improved grey-Markov chain," *Computer Applications and Software*, vol. 34, no. 8, pp. 1–8, 2017.
- [12] D. Waltermire and D. Harrington, "Endpoint security posture assessment: enterprise use cases," *University of Twente Nikos*, vol. 51, no. 02, pp. 83–102, 2015.
- [13] Y. J. Liu and H. U. Rong, "Research on the information security situational awareness system based on big data and artificial intelligence technology," *Management & Technology of SME*, vol. 10, no. 8, pp. 1–8, 2019.
- [14] X. Zhang and D. Yang, "Research on music assisted teaching system based on artificial intelligence technology," *Journal of Physics: Conference Series*, vol. 1852, no. 2, Article ID 022032, 2021.
- [15] Z. Zhang and L. I. Fang, "Research ON the water pollution monitoring and rapid decision-making system based ON artificial intelligence agent," *Journal of Environmental Protection and Ecology*, vol. 20, no. 3, pp. 1565–1573, 2019.
- [16] Y. Wang, W. Li, and Y. Liu, "A forecast method for network security situation based on fuzzy Markov chain," *Lecture Notes in Electrical Engineering*, vol. 260, pp. 953–962, 2014.
- [17] G. Chen and S. Li, "Network on chip for enterprise information management and integration in intelligent physical systems," *Enterprise Information Systems*, vol. 15, no. 7, pp. 935–950, 2021.
- [18] H. Xiong, "Application of artificial intelligence in computer network technology in the era of big data," *Information and Computer (Theoretical Edition)*, vol. 31, no. 21, pp. 128-129+132, 2019.
- [19] X. Xiao, L. Chun, K. Peng et al., "Research review of security situation prediction technology based on artificial intelligence," *Information Security Research*, vol. 6, no. 06, pp. 506–513, 2020.
- [20] Y. Duan, R. Lin, X. Liu, Z. Xue, and Y. Shi, "Research on the modeling of financial information security indicators based on threat intelligence," *Information & Technology*, vol. 25, no. 06, pp. 1–6, 2018.
- [21] J. Xiong, S. Wu, C. Peng, and Y. Tian, Eds., *Mobile Multimedia Communications. MobiMedia 2021*, Springer, vol. 394, Cham, 2021.
- [22] M. Bhanu, J. Mendes-Moreira, and J. Chandra, "Embedding traffic network characteristics using tensor for improved traffic prediction," *IEEE Transactions on Intelligent Transportation Systems*, vol. 22, no. 99, pp. 1–13, 2020.

Research Article

Construction of a Coupled Mathematical Model of Oil and Gas Risk Relying on Distributed Computing

Yao Hu ¹, Sha He,¹ Xiaoli Yang,² and Chuanping Wang²

¹College of Economics and Management, Southwest Petroleum University, Chengdu 610000, Sichuan, China

²Gas Production Plant of Xinjiang Oilfield Company, China National Petroleum, Kelayayi 834000, Xinjiang, China

Correspondence should be addressed to Yao Hu; 201711000067@stu.swpu.edu.cn

Received 27 January 2022; Revised 21 February 2022; Accepted 9 March 2022; Published 11 April 2022

Academic Editor: Hangjun Che

Copyright © 2022 Yao Hu et al. This is an open access article distributed under the Creative Commons Attribution License, which permits unrestricted use, distribution, and reproduction in any medium, provided the original work is properly cited.

With the rapid economic development in recent years, the development of oil and gas has become more and more rapid. Oil and gas are essential energy sources, but oil and gas risks hinder the development of the oil and gas industry. *Purpose.* This article mainly introduces the relevant theoretical knowledge of distributed computing and the coupled mathematical model of oil and gas risk and relies on the distributed calculation to analyze the oil and gas risk, thereby constructing the mathematical model of coupled oil and gas risk. The coupled mathematical model is based on the theories of rock mechanics, seepage mechanics, and heat transfer to study the interaction between fluid seepage and rock mass deformation under nonisothermal conditions in the reservoir and to establish the mathematical equations of the three fields (seepage field, temperature field and stress field) and their coupling action. *Methodology.* It mainly relies on distributed computing, analyzes oil and gas risks through distributed computing, builds a mathematical model for oil and gas risk coupling, and also inputs oil and gas risks into the network through neural network calculations to achieve the purpose of risk assessment. Finally, through the experiment and analysis of the questionnaire, the whole article is completed. *Research Findings.* The experiment in this article mentioned that the demand for oil and gas has been increasing in recent years, from 350 million tons in 2011 to 10.3 tons in 2016, an increase of 680 million tons, an increase of 48%, but the amount of oil and gas extracted is far below the demand for oil and gas. In 2011, the amount of oil and gas extracted was only 210 million tons, and in 2016, it was only 570 million tons, so the extraction of oil and gas needs to be accelerated. However, there are many risks in oil and gas exploitation. Therefore, how to build a mathematical model of oil and gas risk coupling based on distributed computing is the most important problem to be solved at present. *Research Implications.* Based on previous research results, this paper systematically studies the related issues of oil and gas exploration risk assessment. The thesis first summarizes the current research status of oil and gas exploration risk assessment. The risk of oil and gas exploration is a hot topic in the current research field of oil and gas exploration and development. Its research focuses on the adverse effects of the uncertainty of geology, technology, engineering, ecological environment, etc., on the entire exploration investment project, finds out their gaps and problems through comparison, and clarifies the direction of the next oil and gas exploration risk assessment. *Practical Implications.* This paper uses evidence theory to effectively realize the basic probability distribution of attributes while solving the difficult problems of most qualitative indicators in risk assessment. The two effective combinations provide new ideas for risk assessment and scientific decision-making.

1. Introduction

With the economic development in recent years, the oil and gas industry is also making continuous progress. Oil and gas exploration projects are also facing high risks and high investment. If it succeeds, it can bring relatively rich returns; but if it fails, it will bring no small losses. Therefore, for

exploration projects, scientific risk assessment is needed to make better project decisions. Overseas oil and gas companies are located in different countries or regions. With the continuous innovation and development of Internet technology, relying on the Internet for risk management will bring great convenience and will surely become the trend of future development.

Oil and natural gas exploration is a very complex and large-scale system engineering, and exploration and development are accompanied by many uncertain factors. It has the characteristics of huge investment, long cycles, complex technical requirements, and high risk. Therefore, risk analysis needs to be placed in an important position. The risk assessment of oil and gas exploration is to evaluate the results of various risk events to determine the order of their severity. Distributed computing has a flexible architecture and a distributed management and control mechanism. Based on distributed computing, corresponding countermeasures can be proposed. Research on risk assessment issues is very important for oil and gas projects.

With the rapid development of the oil and gas industry in recent years, oil and gas risks have also followed. Xinhong discovered that submarine pipelines are the main mode of transportation for subsea oil and gas production. Due to the combined effect of internal and external factors, the probability of failure of submarine pipelines is increasing, which is likely to cause oil and gas leakage accidents. Effective risk analysis is essential to prevent and mitigate such potential accidents. He proposed a risk-based accident model and constructed an object-oriented Bayesian network with a smaller and clearer structure by modularizing the primary Bayesian network [1]. Savas *E Y* studies and analyzes whether the hedging activities of oil and gas companies have a significant impact on company performance. He built a panel regression model to estimate the company's value and the coefficient of derivative use. Savas *E Y* stipulates that the speculative use of derivatives is eliminated in the model, and the result provides key information about asymmetric information and signal effects. Since the derivative use coefficient is negative, it illustrates the importance of disclosure for financial health. If the company releases a high level of hedging activity, it may be a warning to investors to avoid investing in the company. He also sought the explanation behind the corporate hedging decision, which was one of the first studies with a wide range of areas and data [2]. Tian *D* mainly proposed a new method to establish a risk matrix to assess the safety risks of the oil and gas industry. The frequency and consequences of risks are two ideal criteria in the process of building a risk matrix. Therefore, a multistandard and multiexpert information integration model is constructed. The method of determining expert weights is introduced, combining objective weights and subjective weights to evaluate scores by experts [3]. Khalilzadeh *M* discovered that oil and gas projects incorporate a large amount of uncertainty due to their unique characteristics, complexity, and uncertain environment. His purpose is to identify and evaluate the main risks of such projects under uncertain conditions. Then, a hybrid fuzzy technique is used to determine the correlation between risk and its importance weight. The final result shows that the problem of underinvestment in oil and gas is mainly due to the failure to attract foreign investors and the lack of regional infrastructure [4]. Cheng *C* found that international oil and gas projects are characterized by high capital intensity, high risk, and diversified contracts. Therefore, in order to help decision-makers make more reasonable decisions under

uncertain circumstances, it is necessary to measure the risks of international oil and gas projects. To this end, he built a probability model based on the traditional economic evaluation model, introduced a valuable risk measurement tool in finance, and used it to measure royalties contracts, production sharing contracts, and services for an international oil and gas project contract. In addition, he also used the simulation results to compare the impact of different risk factors on the project's net present value. The results show that (1) Risk has a great influence on the project's net present value; therefore, if the risk is ignored, the decision may be wrong; (2) The simulation method is used to simulate the random distribution of risk factors in the probability model, so the probability is related to the project's net present value [5]. Trofimov *V T* found that onshore oil and gas production is often accompanied by accidents of varying severity and negative consequences. Operations in the surrounding seas and ocean regions of the world have seriously worsened the situation and pushed most of the emergencies related to hydrocarbon production to the regional and global levels. The application of new technology in the production of shale hydrocarbons has added a new problem, that is, the probability that a large amount of geological environment will be completely polluted by highly toxic chemicals. The discovery of a new and promising fossil energy natural gas hydrate makes it possible to outline only the possible related hazards and indicates that environmental risks may increase many times. In order to resist the threat of emergencies related to the growth of oil and gas production, it is recommended to establish a special control and rapid response agency nationwide. If necessary, such structures can be opened up for international cooperation [6]. Yu *X* found that onshore oil and gas pipeline maintenance process risk assessment research has attracted more and more academic attention. Due to uncertainty, it is difficult to accurately or robustly assess risk spread. Therefore, he considered that decision-makers prefer risk information informed by uncertainty rather than unreliable accurate risk values, and he provided new insights for dealing with the risk assessment of the onshore pipeline maintenance process under uncertainty. The risk assessment model is based on a quantitative risk assessment framework based on the analytic hierarchy process and expert knowledge. At the same time, in order to express and quantify the uncertainty, interval analysis is used to extend the entire model to an interval environment. Therefore, he established an interval quantitative risk assessment model for the onshore pipeline maintenance process. Studies have shown that interval analysis can effectively internalize, represent, quantify, and spread the uncertainty in the risk assessment model [7]. Epelle *E I* found that even under unfavorable technical and environmental conditions, the ever-increasing global energy demand has driven the oil industry to develop more innovative and advanced methods to improve oil recovery. The severity of many operational problems affecting the drilling and production of oil and gas wells has been exacerbated by the inconvenience of transportation, so the overall situation must be remedied. In addition, the pressure loss of the toroidal geometry, as well as the reduced penetration rate due to the accumulation of downhole drill

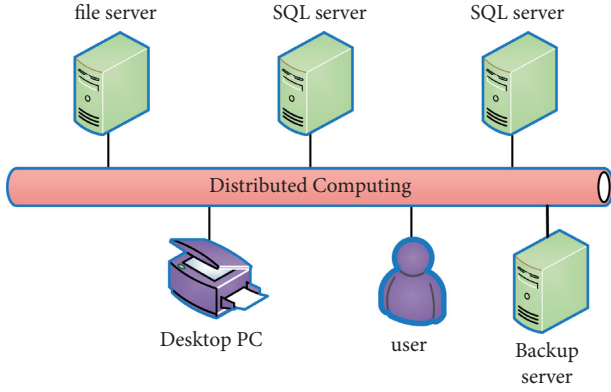


FIGURE 1: Distributed computing project diagram.

cuttings, constitutes an important part of the total energy to be provided. Therefore, if appropriate and economical drilling program design is required, the application of complex modeling techniques and the reliable clarification of phase distribution (solid, liquid and gas) and popular flow patterns become essential [8]. Through the experimental research of scholars, we can know that there are more and more risks in the oil and gas industry, and the traditional model can no longer satisfy the analysis of oil and gas risks. Therefore, how to rely on distributed computing to establish a mathematical model of oil and gas risk coupling so as to reduce oil and gas risks is what needs to be solved most.

The innovations of this paper are as follows: (1) The experiment based on distributed calculation has completed the construction of the oil and gas risk coupling mathematical model and found the oil and gas risk assessment method, which makes the development of the oil and gas industry more effective. (2) Using distributed parallel computing and risk assessment methods to solve risk factors. As a result, the risk of oil and gas is reduced, and the construction of the coupled mathematical model is more complete.

2. Distributed Calculation Method and Neural Network Method

2.1. Distributed Parallel Computing. Distributed computing is a computer science, and the main research object is distributed systems. A distributed system is a software and hardware system composed of several computers interconnected by a network. At present, the most common distributed computing project is the use of global volunteer computers for computing. Volunteer computers transmit idle computing power through the Internet to send data so that they are logically connected as a whole to carry out some scientific research projects that require large-scale calculations [9], as shown in Figure 1.

As shown in Figure 1, compared with other algorithms, distributed computing has the following advantages:

- (1) Rare resources can be shared.
- (2) Through distributed computing, the computing load can be balanced on multiple computers.

- (3) The computing power of cheap computers can be integrated to reach or exceed the performance of some supercomputers in order to complete some projects that require high computing capacity and high performance [10]. Its disadvantage is that if one or more computers fail, or one or more network links fail, it will cause problems in the distributed system.

The distributed SNESIM (single normal equation) design ideas in this article are as follows.

Discretize the training image U , as in the following formula:

$$U = \begin{bmatrix} u_{1,1}, u_{1,2}, u_{1,n} \\ u_{2,1}, u_{2,2}, u_{2,n} \\ \dots \\ u_{m,1}, u_{m,2}, u_{m,n} \end{bmatrix}. \quad (1)$$

Among them, $u_{m,n}$ represents the state value of each grid in the training image, and $m \times n$ is the size of the training image.

The core of the distributed strategy is to use the principle of hierarchical parallelism. Each node in the cluster (except the main node) only has a part of the search tree set, and each part is independent of each other, and the number of events in each subset is also mutually exclusive. Independent, each record only represents a state and corresponding frequency [11]. The data management strategy of SparkRDD (Spark Resilient Distributed Datasets) is shown in Figure 2.

As shown in Figure 2, because the characteristics of RDD cannot ensure the order of data in RDD, it is necessary to make the data independent of each other to fully ensure its computational efficiency [12]. For the grid to be simulated, given a data event on the grid to be simulated, the label of the event can be used to judge whether the data event of the corresponding training image node matches. If it matches, the corresponding event in the global search tree is incremented by one count according to the value of the discrete variable of the point on the training image; conversely, edge probability is used instead of conditional probability, the probability of one event happening has nothing to do with other events. This is the marginal probability. Taking the variables x and y , in their joint distribution, in the joint probability, the events that are not needed in the final result are merged into the full probability of their events and disappear [13].

All these training patterns are stored in the search tree structure, and the following data can be easily retrieved: W is the total number of categories. The ratio of N to K represents the ratio of training modes, and training mode (n_k/n) defines the value of the center position $P(t'_1)$, as in the following formula:

$$P(t'_1) = W|D_n| \\ = \frac{n_k}{n}, k = 0, 1, 2, \dots, k-1. \quad (2)$$

K -type estimation with local data set $n(v)$ as the probability condition, as in the following formula:

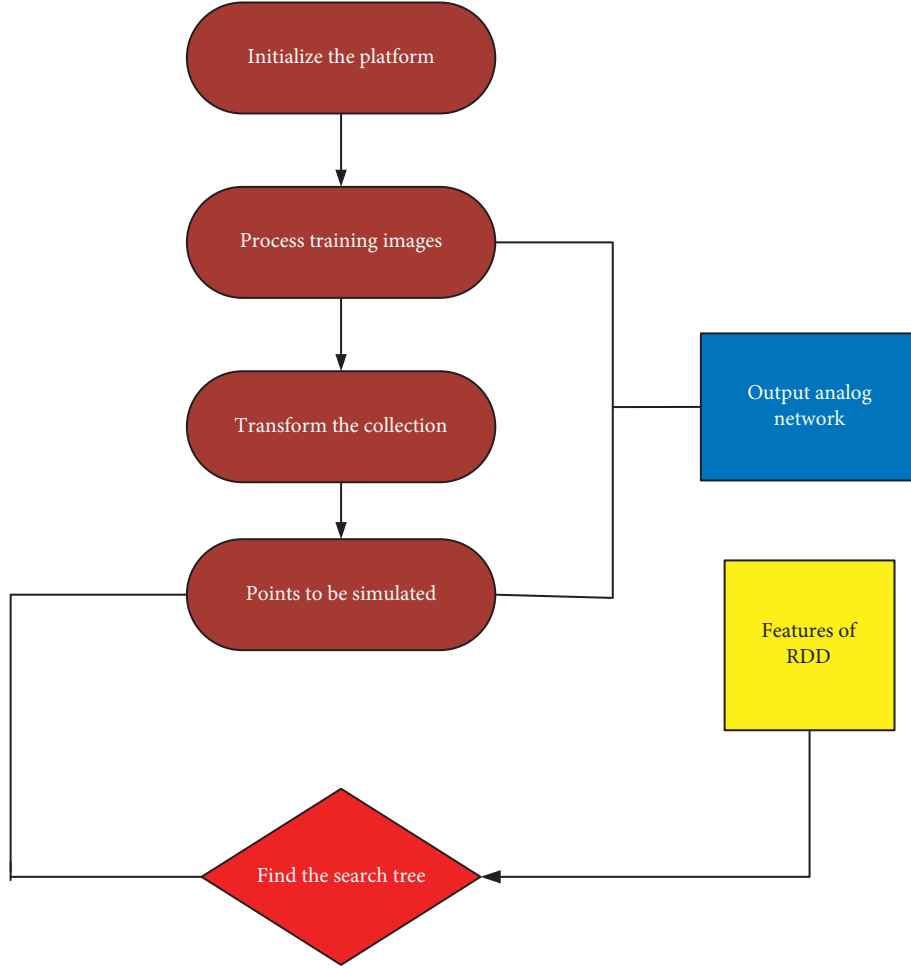


FIGURE 2: Data management strategy diagram of SparkRDD.

$$\text{prob}\{v \in k | n(v)\} \in [0, 1]. \quad (3)$$

The indication of a class can be simulated in each simulation node V , where the indicator refers to the class or type indicator to which the continuous Z value belongs, as in the following formula:

$$\text{prob}\{Z(v) \leq Z_k | n(v)\} \in [0, 1]. \quad (4)$$

Random function $Z(v)$ again uses the same geometry of “simulated” data $Z_{cs}^I(v)$. This process is as follows:

$$Z_{cs}^I(v) = Z_K^*(v) + [Z_{cs}^I(v) - Z_{K_s}^{*(i)}(v)]. \quad (5)$$

For the data value $Z_{cs}(v)$ at the data position v of each random function, ensure that it can satisfy the variance formula of $R(v)$, as shown in the following formula:

$$\text{Var}\{Z_{cs}(v)\} = \text{Var}\{Z_K^*\} + \text{Var}\{R(v)\}. \quad (6)$$

In general, any unsampled value $z(v)$ can be expressed as the sum of its estimated value $z(v)$ and its corresponding error $r(v)$, as in (6):

$$z(v) = z^*(v) + r(v). \quad (7)$$

Therefore, it can be seen that distributed computing is widely used in practice based on covariance simulation algorithms; covariance, as a quantity describing the degree of correlation between X and Y , has a certain effect under the same physical dimension, but the same two quantities adopt different dimensions to make their covariance show great differences in value. Its essence originates from two categories: the first type is a multivariate Gaussian random function model fixed on attributes; the second type is based on the interpretation of an indicator’s expected value as a conditional probability [14].

2.2. Neural Network Algorithm Based on Distributed Computing. A neural network is a kind of computing model which is composed of a large number of nodes (or neurons) connected to each other. Each node represents a specific output function, called the excitation function. Now, neural networks have made great progress. This is a learning algorithm that is often used in the fields of pattern recognition, signal processing, and data mining [15]. Neural network classification algorithms usually use multilayer neural networks [16]. An artificial neural network is imitating the information processing mechanism of the human brain.

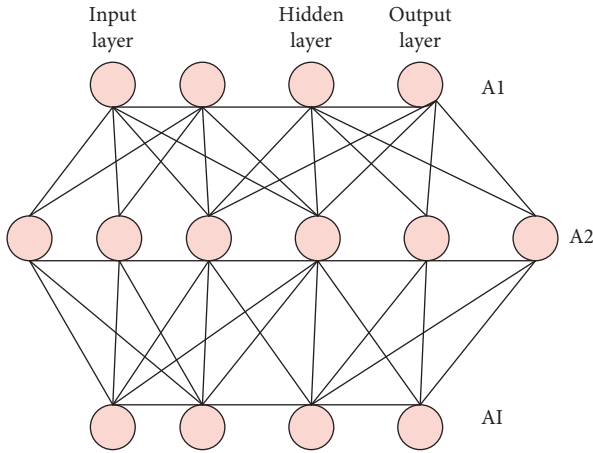


FIGURE 3: Multilayer feedforward neural network.

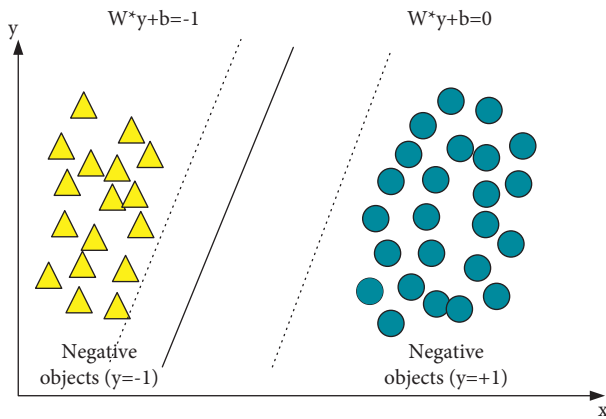


FIGURE 4: Example diagram of dimensionality separability.

Through the abstraction, simplification, and simulation of the brain mechanism, specific functions such as learning, memory, reasoning, and recognition are realized. That is, mathematical models are used to simulate the process of human brain thinking and information processing [17], as shown in Figure 3.

As shown in Figure 3, it consists of an input layer, several hidden layers, and an output layer. In the input mode, the input corresponds to the measured attributes of each training sample [18].

In the field of machine learning, the goal of classification is to gather objects with similar characteristics. A linear classifier makes classification decisions through linear combinations of features to achieve this goal. The data point is represented by n , and the category is represented by y . The learning goal of the linear classifier is to find the classification hyperplane in the n -dimensional data space [19]. The equation can be expressed by (7):

$$\omega^T y + b = 0. \quad (8)$$

In a 2-dimensional plane, there are star-shaped points and circular points. The solid line in the middle separates these two points. This solid line is a classification hyperplane,

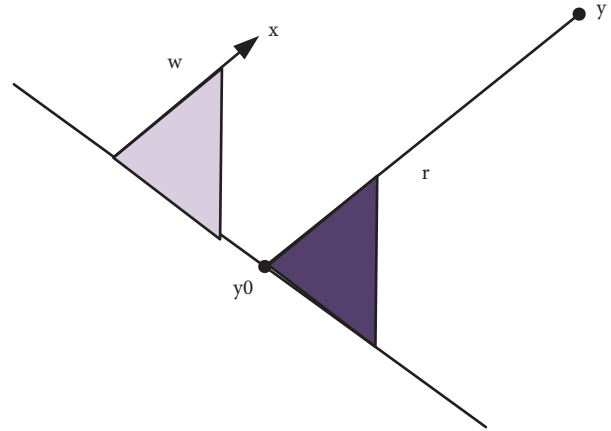


FIGURE 5: “Geometric distance” from Y to the classification hyperplane.

and the point on one side of the hyperplane is $x = -1$, the point $x = 1$ on the other side, as shown in Figure 4.

As shown in Figure 4, the hyperplane in the figure is close to the point of the hyperplane so that the distance can be extended [20]. Finding the maximum distance as follows:

$$f(y) = \omega^T y + b. \quad (9)$$

The distance from the “geometric interval” to the hyperplane is as follows:

$$\begin{aligned} \gamma &= x \frac{\omega^T y + b}{\|\omega\|} \\ &= x \frac{f(y)}{\|\omega\|}. \end{aligned} \quad (10)$$

The “geometric distance” from Y to the classification hyperplane is shown in Figure 5.

As shown in Figure 5, the geometric distance γ is as follows:

$$\begin{aligned} &\max \frac{1}{\|\omega\|}, \\ &\text{s.t. } x_i (\omega^T x_i + b) \geq 1, \quad i = 1, 2, \dots, n. \end{aligned} \quad (11)$$

The above problem can be equivalently transformed into the following formula:

$$\begin{aligned} &\max \frac{1}{2} \|\omega\|^2, \\ &\text{s.t. } x_i (\omega^T x_i + b) \geq 1, \quad i = 1, 2, \dots, n. \end{aligned} \quad (12)$$

By importing the Lagrangian multiplier and combining its constraints into the objective function, the following formula is obtained:

$$L(\omega, a, b) = \frac{1}{2} \|\omega\|^2 - \sum_i^n \alpha_i (\omega^T y + b). \quad (13)$$

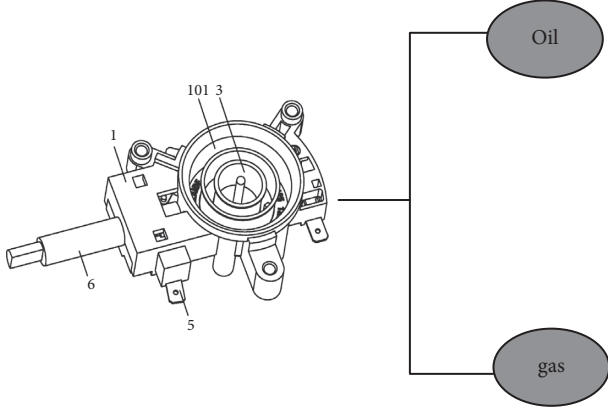


FIGURE 6: Oil and gas risk coupling model.

2.3. The Establishment and Algorithm of the Coupling Model.

The coupling model is a collection of unit bodies, and each unit body is composed of some basic information, such as nodes, material names, and node coordinates. The grid can be generated in the form of a command stream [21]. The coupled model grid is formed by corresponding materials and some parameters, such as initial conditions and boundary conditions. Macroscopically, it is also a collection of unit bodies. The entire model is mainly composed of information such as the direction of the connection between adjacent centers and the area of adjacent surfaces [22].

As shown in Figure 6, the steps to establish a calculation model are as follows: First, split the finite difference grid. Then, select the appropriate composition model and material parameters. Finally, the initial conditions and boundary conditions of the model are set [23].

Regarding the two-phase flow of oil and gas in unsaturated soils, first, assume that the existing pores are filled with gas and oil. The equation for the flow of gas and liquid is shown in (11):

$$\frac{\partial [\varphi W_{\beta} \rho_{\beta}]}{\partial t} + \text{div} (V_{\beta} \rho_{\beta}) = 0. \quad (14)$$

In the formula, β represents oil, φ represents porosity, W_{β} represents saturation of β , and ρ_{β} represents the density of β . Therefore, the fluid phase velocity is as follows:

$$u_{\beta} = -k \frac{k_{rb}(S_1)}{\mu_{\beta}} (\Delta \rho_{\beta} - \rho_{\beta} g). \quad (15)$$

The permeability is as follows:

$$Y_Y = Y \left(1 + \frac{K_b}{\rho} \right). \quad (16)$$

Putting the flow velocity expressed by formula (16) in the mass balance equation of formula (15) can obtain the following formula:

$$\frac{\partial (\varphi s_{\beta} \rho_{\beta})}{\partial u} = \text{div} \left(\rho_{\beta} k \frac{k_{r\beta}}{\mu_{\beta}} \right). \quad (17)$$

With abundant oil and gas resources, oil and gas exploitation has become a top priority. At present, the total oil

TABLE 1: Heavy oil classification table.

Classification	First indicator	Second indicator	Second indicator
Classification	Viscosity	Density	Severe
Heavy oil	200–10000	900–1200	10–23
Heavy oil	300–20000	700–1100	11–22

and gas resources are estimated to be approximately 21 billion tons. Depending on the nature of the high viscosity oil mixture, steam injection is generally used in heat recovery. A few years ago, this technology was applied to the development of heavy oil storage layers and achieved amazing results [24].

Under oil layer conditions, crude oil with a viscosity of more than 50 mpas and a relative density of not less than 0.9 is called heavy oil. The classification of heavy oil is shown in Table 1.

As shown in Table 1, the heat resistance of the first heavy oil reached 200–10000, and the second reached 300–20000. It can be known that the heat resistance of heavy oil is very high, and the viscosity of crude oil will drop drastically when the temperature rises. The higher the viscosity of crude oil, the greater the decrease. The relationship between them is as follows:

$$\mu = \partial e^{(b/t)}. \quad (18)$$

In the case of hot oil recovery, the volume expansion of water, oil, and the storage layer can provide electricity to discharge the oil. The expression of the oil thermal expansion coefficient is (15):

$$C_O = \frac{du_0}{u_0 t} = -\frac{d\rho_0}{\rho_0 dt}. \quad (19)$$

Under certain temperature conditions, the components of oil and gas are decomposed to produce light components such as coke, gas phase, and oil. If there are light ingredients, the oil displacement effect will be greatly improved. When the formation is above the bubble point temperature, the heavy components in the oil exist in the form of liquid, and the light components separate the liquid from the gas. In the presence of steam, the amount of separation of light components will greatly increase. It can burn heavy oil to transfer heat, increase the temperature of the oil layer, and improve the oil replacement effect.

$$-V^0 = 1.21(H) - 0.19(O + N) + 0.34(C) + 0.15(S). \quad (20)$$

Among them, H represents the content of hydrogen elements. O represents the content of the oxygen element. N stands for nitrogen content. C stands for carbon element content. S stands for sulfur content.

At present, in important topics such as energy development, radioactive waste treatment, and foundation engineering, the combination of temperature field,

TABLE 2: Survey of oil and gas consumption.

Year	Consumption	Percentage increase (%)
2011	3.5	12.7
2012	5.4	13.5
2013	6.7	13.8
2014	7.6	14.1
2015	9.7	14.6
2016	10.3	15.1

permeability field, and deformation field plays an important role. In the research process, the uncoupled model developed into a coupled model. The uncoupled model ignores the analysis of the interaction between energy propagation, fluid penetration, and deformation of porous media. The oil-gas coupling model is mainly used to study the interaction between the seepage field and the deformation field. On the contrary, the coupled model can more accurately study the risk of oil and gas, but in this coupled model theory, the change of the temperature field is not considered. In terms of actual coupling issues, the temperature of heavy oil storage and geothermal utilization systems in the oil and gas industry will continue to change.

3. Experiment and Analysis of the Questionnaire Survey

3.1. Overview of Oil and Gas Risks. The decision-making process of oil and gas exploration projects is a dynamic process. From the establishment of the project to the final completion of the detailed evaluation, a process is required. The established risk assessment model should have the ability to adapt to environmental changes, that is, adaptability. The principle of adaptability requires that the evaluation index system be dynamic.

Looking at the last century, the country's oil and gas industry was basically self-sufficient, with no external dependence, so there was no strategic reserve. However, with the development of the national economy, the consumption of oil and gas has increased, and the contradiction between supply and demand has gradually deepened. The country began to import oil and gas, and its dependence on foreign oil and gas has further increased.

3.2. Investigation and Analysis of Oil and Gas Demand and Supply. This article uses questionnaire survey method to investigate the oil and gas consumption in recent years, as shown in Table 2.

As shown in Table 2, the consumption of oil and gas has increased in recent years, from 350 million tons in 2011 to 1.03 billion tons in 2016, an increase of 680 million tons, and the percentage increase is 15.1%. It can be seen that the demand for oil and gas continues to expand, and the demand for oil and gas continues to rise. However, with the development of the national economy, the consumption of oil and gas has increased, and the contradiction between supply and demand has gradually deepened. The country began to

import oil and gas, and its dependence on foreign oil and gas has further increased.

This article then investigates the amount of oil and gas imports from 2011 to 2016, as shown in Table 3.

As shown in Table 3, the demand for oil and gas is much higher than the output of oil and gas, resulting in only oil and gas imports. The degree of dependence on foreign oil and gas has increased from 13.1% in 2011 to 30% in 2016. This means that beyond the current warning line, national oil and gas companies need to pay more attention to the country's energy security tasks, and "increasing income and reducing expenditure" has become a common understanding. Therefore, national oil and gas companies need to strengthen the "going out" strategy and strengthen open source work.

This paper investigates the trend of oil production in the two years from 2015 to 2016, as shown in Figure 7.

As shown in Figure 7, it can be seen that the lowest oil and gas output in 2015 was about 400 million tons, and the highest was 2 billion tons; in 2016, oil and gas production was at a minimum of about 1 billion tons and a maximum of 2.1 billion tons, and the overall increase. It can be seen that the output of oil and gas is increasing year by year. At present, the risk assessment of overseas exploration projects by oil and gas companies is in primitive qualitative and simple subjective phases. Therefore, it is necessary to study how to conduct risk assessment more scientifically and rationally to provide a basis for a better understanding of overseas oil and gas exploration risks, avoiding important risks in advance and project decision-making. In order to provide comprehensive and scientific decision-making for overseas exploration projects, it is necessary to use scientific methods. Taking risk assessment as the starting point, using scientific and mathematical methods to evaluate overseas exploration projects provides the accuracy of risk information, and reduce project risks.

This paper investigates the trend of oil and gas demand from 2015 to 2016, as shown in Figure 8.

As shown in Figure 8, it can be seen that the minimum demand for oil and gas in 2015 was 1 billion tons and the highest was 4.3 billion tons; the minimum demand for oil and gas in 2016 was 1.9 billion tons, and the highest was 4.3 billion tons, which is generally increasing. It can be seen that the demand for oil and gas is increasing year by year. And it is much higher than the output of oil and gas, which leads to the shortage of oil and gas.

3.3. Investigation and Analysis of Oil and Gas Risk Types. Although the existing methods that are suitable for carrying out oil and gas risk assessment can accurately assess the level of potential risks in the current oil and gas status, they are too professional. However, because overseas oil and gas pipeline companies are located in poor and backward countries and regions, the local employees recruited by overseas pipeline companies have limited education and lack professional technical support personnel. This leads to the fact that it is difficult for most of the employees on the enterprise site to participate in the actual risk assessment,

TABLE 3: Survey of oil and gas imports from 2011 to 2016.

Year	Consumption	Import volume	Percentage increase (%)	External dependence (%)
2011	3.5	1.1	12.7	13.1
2012	5.4	1.4	13.5	13.6
2013	6.7	2.6	13.8	21.1
2014	7.6	5.4	14.1	23.3
2015	9.7	4.3	14.6	24.2
2016	10.3	6.3	15.1	30.0

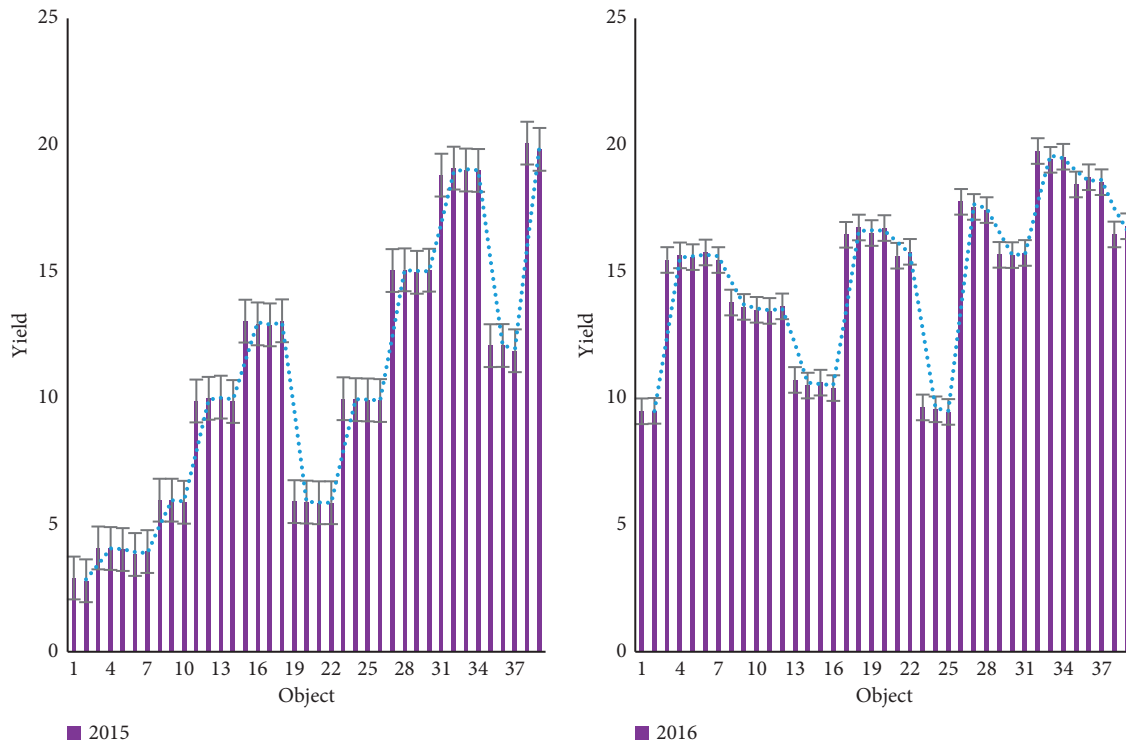


FIGURE 7: Comparison chart of oil production trends from 2015 to 2016.

and most of them require professional and technical personnel to assist or execute.

This paper investigates the consumption of oil and gas from 2013 to 2014 and 2018 to 2019, as shown in Figure 9.

As shown in Figure 9, the consumption of oil and gas is on the rise every year. Driven by the rapid social and economic growth in 2013, the annual apparent consumption of oil and gas was 550 million tons, an increase of 13.3% over 2014. From 2017 to 2018, oil and gas consumption increased rapidly, with the lowest growth rate of 6% and the highest rate of 20%.

Therefore, to a certain extent, the “going out” strategy of oil and gas companies is an important direction for the country to use foreign resources and realize the country’s sustainable development, and it is the internal demand for the country’s sustainable development. Therefore, for the country’s sustainable development, the country urgently needs the “going out” strategy of energy resources, encouraging national oil and gas companies to go abroad and develop international markets. National oil and gas companies must formulate corresponding internationalization

strategies, make full use of foreign oil and gas resources, optimize the allocation of corporate resources, and strive to improve their competitive position in the world. Extracting more oil and gas is currently the most important thing to do. However, there are many risks in the exploitation of oil and gas.

This article takes oil and natural gas exploration risk assessment as an example and adopts a new exploration risk assessment model to conduct a more comprehensive risk assessment of the project. Exploration risk mainly refers to geological risk assessment. This article focuses on geological risk assessment, combining economic risk, reserve risk, financial risk, technical risk, management risk, and geological risk to evaluate projects in this field. The basic attributes of oil and gas exploration risk assessment projects that determine the attributes of the comprehensive index as shown in Table 4.

As shown in Table 4, it can be seen that there is a lot of uncertain information in the process of risk assessment. Due to high information asymmetry, no objective data, and different risk preferences, traditional assessment methods

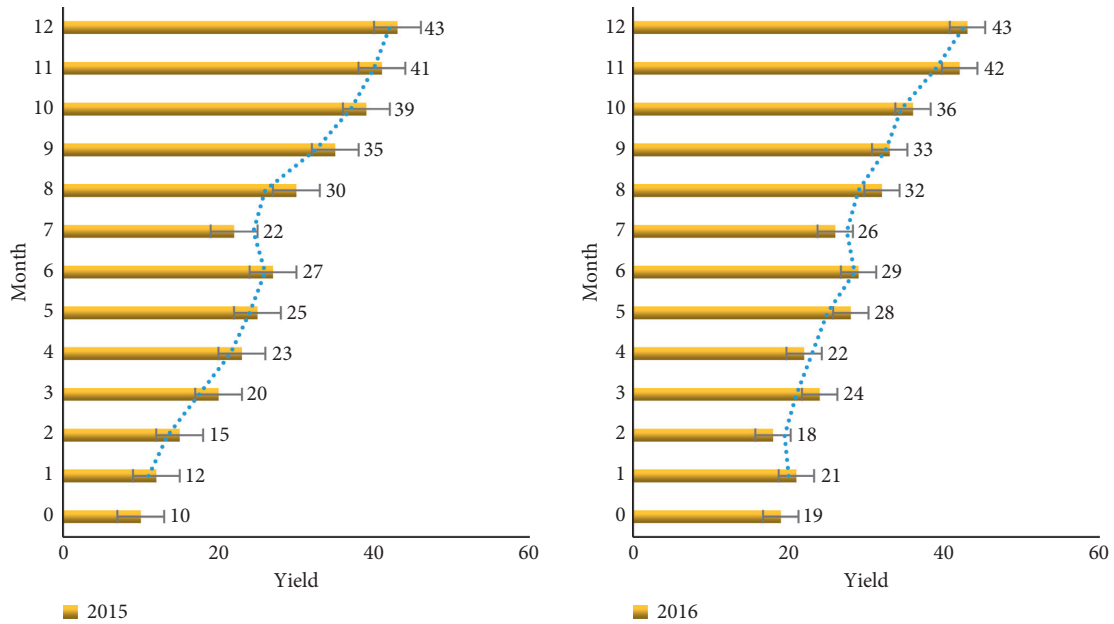


FIGURE 8: Comparison of trends in oil and gas demand for the two years from 2015 to 2016.

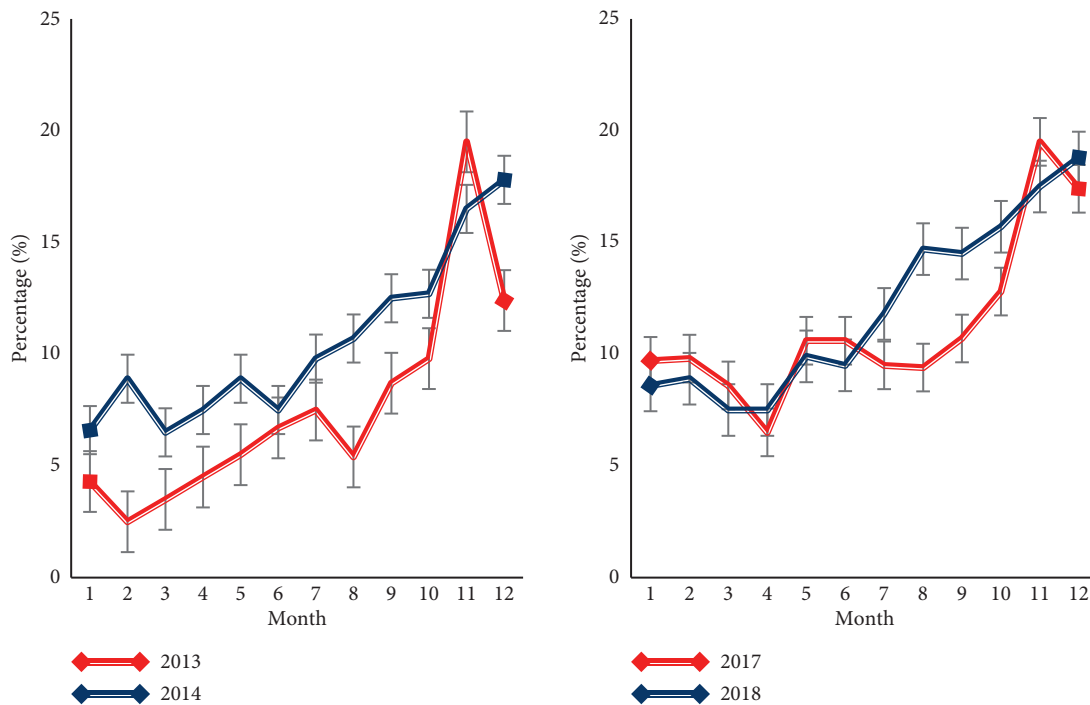


FIGURE 9: Consumption comparison chart between 2013-2014 and 2018-2019.

TABLE 4: Comprehensive index attribute oil and gas exploration risk evaluation table.

Plan	1 (%)	2	3	4 (%)	5 (%)	6 (%)	7 (%)
Reserve risk	16	10%	21%	12	9	12	5
Economic risk	23	26%	21%	19	18	11	16
Financial risk	23	16%	27%	31	32	29	25
Technology risk	6	8%	3%	10	5	9	7
Manage risk	2	4%	7%	5	2	3	5

are no longer suitable for today's complex oil and gas risk assessment. Therefore, when conducting risk assessment, we must adhere to the principle of combining subjectivity and objectiveness. The understanding of any complex system includes subjective and objective knowledge and comprehensively integrates subjective and objective knowledge. In the construction of the model, it not only uses the subjective knowledge of experts and scholars on risk issues to establish a subjective model but also integrates the characteristics of

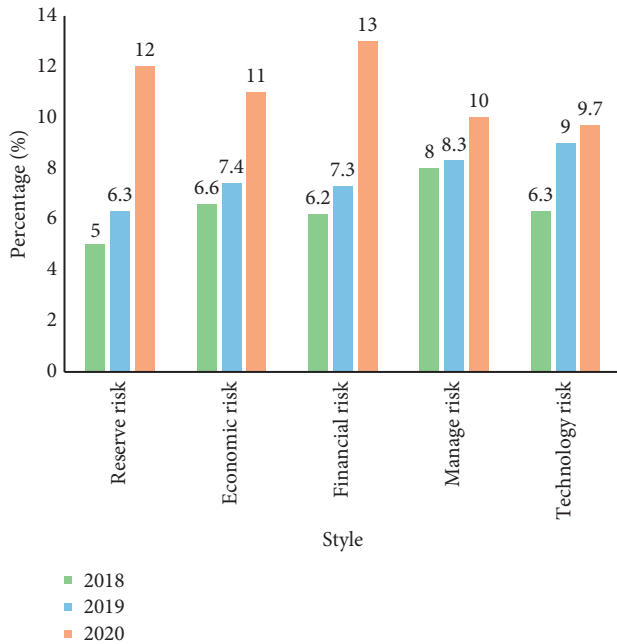


FIGURE 10: Diagram of the proportion of each risk from 2018 to 2020.

the thing itself to find a reasonable objective evaluation model, which is conducive to better evaluation of the research problem.

This paper investigates the proportion of each risk from 2018 to 2020, as shown in Figure 10.

As shown in Figure 10, the proportion of technological risks in each year from 2018 to 2020 is the highest, reaching 12% in 2018, so technological risks are the most important problem to be solved. This requires professionals to improve their professional knowledge and exercise their technical capabilities so as to achieve the purpose of reducing technical risks. Through professional knowledge and technical training for professionals, technical risks can also be reduced. Therefore, based on the analysis and summary of traditional risk assessment methods, the risk assessment model is applied to oil and natural gas exploration risk assessment and use powerful functions to reduce attributes, effectively solve the subjective problems of other optimization models, and use evidence theory to effectively realize the basic probability of attributes, and solve the difficult problems of most qualitative indicators in risk assessment. These two effective combinations will enrich and complete the model theory system of risk assessment and provide new ideas for risk assessment and scientific decision-making.

4. Discussion

This article explains the basic principles of distributed computing algorithms and introduces distributed computing algorithms in detail. At the same time, it also introduces the theoretical basis of neural networks and provides some commonly used methods. This paper draws lessons from the deficiencies and theoretically proves the convergence of the algorithm.

This article analyzed the research progress of oil and gas risks and coupled mathematical models, expounded the related concepts of oil and gas risks and coupled mathematical models, studied the related theories of oil and gas risk based on distributed computing and coupled mathematical models, explored methods based on distributed computing algorithms, and through the analysis of the questionnaire survey to discuss the importance of distributed computing algorithms to the construction of oil and gas risks and coupled mathematical models, and finally took the integration of distributed computing into the construction of coupled mathematical models as an example to explore the correlation between the two.

This article also makes reasonable use of distributed computing algorithms. With the increasing application scope of distributed computing algorithms and their importance gradually becoming more prominent, many scholars have begun to match certain specific fusion theories with real-life application scenarios and propose feasible algorithms. According to the algorithm, the analysis of oil and gas risks based on distributed computing is an essential part of constructing a mathematical model of oil and gas risk coupling.

5. Conclusions

This article mainly starts from distributed computing and oil and gas risk, discusses the relationship between the two, and how to integrate distributed computing into the construction of a mathematical model for oil and gas risk coupling. Based on distributed computing, we can know the importance of distributed computing in the construction of the oil and gas risk coupling mathematical model. Distributed computing is indispensable for the construction of an oil and gas risk coupling mathematical model. Do not blindly imitate and copy, based on distributed computing in the construction of oil and gas risk coupling mathematical model application research has always been a problem studied by many scholars. There is no good solution yet. Therefore, the author may still have many problems and shortcomings in the construction of the mathematical model of oil and gas risk coupling based on distributed computing in this article. However, the author has tried his best, and the author will continue to make progress through continuous learning.

Data Availability

The experimental data used to support the findings of this study are available from the corresponding author upon request.

Conflicts of Interest

The authors declare that they have no conflicts of interest regarding this work.

Acknowledgments

This work was supported by the Study on Energy Development Strategy of Sichuan Province.

References

- [1] L. Xinhong, G. Chen, and H. Zhu, "Quantitative risk analysis on leakage failure of submarine oil and gas pipelines using Bayesian network - ScienceDirect," *Process Safety and Environmental Protection*, vol. 103, pp. 163–173, 2016.
- [2] E. Yildiz Savas and A. Kapusuzoglu, "Risk management activities for oil and gas producers and the impact on firm value," *Environmental Science and Pollution Research*, vol. 27, no. 7, pp. 7087–7095, 2020.
- [3] D. Tian, B. Yang, J. Chen, and Y. Zhao, "A multi-experts and multi-criteria risk assessment model for safety risks in oil and gas industry integrating risk attitudes," *Knowledge-Based Systems*, vol. 156, pp. 62–73, 2018.
- [4] M. Khalilzadeh, H. Shakeri, and S. Zohrehvandi, "Risk identification and assessment with the fuzzy DEMATEL-ANP method in oil and gas projects under uncertainty," *Procedia Computer Science*, vol. 181, no. 3, pp. 277–284, 2021.
- [5] C. Cheng, Z. Wang, M.-M. Liu, and X.-H. Ren, "Risk measurement of international oil and gas projects based on the Value at Risk method," *Petroleum Science*, vol. 16, no. 1, pp. 199–216, 2019.
- [6] V. T. Trofimov, A. V. Nikolaev, A. D. Zhigalin, T. A. Baraboshkina, M. A. Khar'kina, and E. V. Arkhipova, "Expansion of oil and gas production and increase of environmental risk," *Moscow University Geology Bulletin*, vol. 72, no. 4, pp. 235–244, 2017.
- [7] X. Yu, W. Liang, L. Zhang, G. Reniers, and L. Lu, "Risk assessment of the maintenance process for onshore oil and gas transmission pipelines under uncertainty," *Reliability Engineering & System Safety*, vol. 177, pp. 50–67, 2018.
- [8] E. I. Epelle and D. I. Gerogiorgis, "A multiparametric CFD analysis of multiphase annular flows for oil and gas drilling applications," *Computers & Chemical Engineering*, vol. 106, pp. 645–661, 2017.
- [9] A. G. Frank, N. Dalle Molle, W. Gerstlberger, J. A. B. Bernardi, and D. C. Pedrini, "An integrative environmental performance index for benchmarking in oil and gas industry," *Journal of Cleaner Production*, vol. 133, pp. 1190–1203, 2016.
- [10] W. Chaiyapa, M. Esteban, and Y. Kameyama, "Sectoral approaches establishment for climate change mitigation in Thailand upstream oil and gas industry," *Energy Policy*, vol. 94, no. jul, pp. 204–213, 2016.
- [11] M. Y. Aalsalem, W. Z. Khan, W. Gharibi, M. K. Khan, and Q. Arshad, "Wireless Sensor Networks in oil and gas industry: recent advances, taxonomy, requirements, and open challenges," *Journal of Network and Computer Applications*, vol. 113, no. JUL, pp. 87–97, 2018.
- [12] S. A. Kvalheim and Ø. Dahl, "Safety compliance and safety climate: a repeated cross-sectional study in the oil and gas industry," *Journal of Safety Research*, vol. 59, pp. 33–41, 2016.
- [13] I. A. Frigaard, K. G. Paso, and P. R. de Souza Mendes, "Bingham's model in the oil and gas industry," *Rheologica Acta*, vol. 56, no. 3, pp. 259–282, 2017.
- [14] Ø. Dahl and T. Kongsvik, "Safety climate and mindful safety practices in the oil and gas industry," *Journal of Safety Research*, vol. 64, pp. 29–36, 2018.
- [15] B. Anifowose, D. M. Lawler, D. van der Horst, and L. Chapman, "A systematic quality assessment of Environmental Impact Statements in the oil and gas industry," *The Science of the Total Environment*, vol. 572, pp. 570–585, 2016.
- [16] M. Khalil, B. M. Jan, C. W. Tong, and M. A. Berawi, "Advanced nanomaterials in oil and gas industry: design, application and challenges," *Applied Energy*, vol. 191, no. APR.1, pp. 287–310, 2017.
- [17] Y. Redutskiy, "Optimization of safety instrumented system design and maintenance frequency for oil and gas industry processes," *Management and Production Engineering Review*, vol. 8, no. 1, pp. 46–59, 2017.
- [18] W. N. K. Wan Ahmad, M. P. de Brito, and L. A. Tavasszy, "Sustainable supply chain management in the oil and gas industry," *Benchmarking: An International Journal*, vol. 23, no. 6, pp. 1423–1444, 2016.
- [19] N. Wan, J. Rezaei, L. A. Tavasszy, and M. P. de Brito, "Commitment to and preparedness for sustainable supply chain management in the oil and gas industry," *Journal of Environmental Management*, vol. 180, pp. 202–213, 2016.
- [20] C. Bongseok and K. S. Tae, "Price volatility and risk management of oil and gas companies: evidence from oil and gas project finance deals," *Energy Economics*, vol. 76, pp. 594–605, 2018.
- [21] B. T. Ewing, G. Alper, and S. Ugur, "Risk transmission from oil and natural gas futures to emerging market mutual funds," *Emerging Markets Finance and Trade*, vol. 54, no. 7-9, pp. 1827–1836, 2018.
- [22] M. A. Kassem, M. A. Khoiry, and N. Hamzah, "Using probability impact matrix (PIM) in analyzing risk factors affecting the success of oil and gas construction projects in Yemen," *International Journal of Energy Sector Management*, vol. 14, no. 3, pp. 527–546, 2019.
- [23] A. Ey and B. Ms, "The changing role of diesel oil-gasoil-LPG and hydrogen based fuels in human health risk: a numerical investigation in ferry ship operations," *International Journal of Hydrogen Energy*, vol. 45, no. 5, pp. 3660–3669, 2020.
- [24] A. Mannocci, S. Pignalosa, V. Nicosia, R. Saulle, S. Sernia, and G. La Torre, "Cardiovascular Diseases Risk Factors in oil and gas workers: a ten years observational retrospective cohort," *Annali di Igiene: Medicina Preventiva e di Comunita*, vol. 28, no. 2, pp. 122–132, 2016.

Retraction

Retracted: NSGA-II-Based Microchannel Structure Optimization Problem Study

Scientific Programming

Received 29 August 2023; Accepted 29 August 2023; Published 30 August 2023

Copyright © 2023 Scientific Programming. This is an open access article distributed under the Creative Commons Attribution License, which permits unrestricted use, distribution, and reproduction in any medium, provided the original work is properly cited.

This article has been retracted by Hindawi following an investigation undertaken by the publisher [1]. This investigation has uncovered evidence of one or more of the following indicators of systematic manipulation of the publication process:

- (1) Discrepancies in scope
- (2) Discrepancies in the description of the research reported
- (3) Discrepancies between the availability of data and the research described
- (4) Inappropriate citations
- (5) Incoherent, meaningless and/or irrelevant content included in the article
- (6) Peer-review manipulation

The presence of these indicators undermines our confidence in the integrity of the article's content and we cannot, therefore, vouch for its reliability. Please note that this notice is intended solely to alert readers that the content of this article is unreliable. We have not investigated whether authors were aware of or involved in the systematic manipulation of the publication process.

Wiley and Hindawi regrets that the usual quality checks did not identify these issues before publication and have since put additional measures in place to safeguard research integrity.

We wish to credit our own Research Integrity and Research Publishing teams and anonymous and named external researchers and research integrity experts for contributing to this investigation.

The corresponding author, as the representative of all authors, has been given the opportunity to register their agreement or disagreement to this retraction. We have kept a record of any response received.

References

- [1] L. Wang, "NSGA-II-Based Microchannel Structure Optimization Problem Study," *Scientific Programming*, vol. 2022, Article ID 6368018, 7 pages, 2022.

Research Article

NSGA-II-Based Microchannel Structure Optimization Problem Study

Linlin Wang 

School of Information Engineering, Xi'an University of Arts and Science, Xi'an 710065, China

Correspondence should be addressed to Linlin Wang; linlinwang@xawl.edu.cn

Received 29 January 2022; Accepted 14 March 2022; Published 7 April 2022

Academic Editor: Hangjun Che

Copyright © 2022 Linlin Wang. This is an open access article distributed under the Creative Commons Attribution License, which permits unrestricted use, distribution, and reproduction in any medium, provided the original work is properly cited.

A multiobjective genetic algorithm is used to optimize the structure of circular concave cavities and microchannels. The objective functions of thermal resistance and pumping power are constructed by the response plane approximation method according to the simulation results, and then a mathematical model of multiobjective genetic optimization with the structural parameters of microchannels as variables is established. The Pareto optimized solution sets of thermal resistance and pumping power are calculated by the nondominated ranking genetic algorithm NSGA-II, and the comprehensive heat transfer performance is evaluated by the enhanced heat transfer factor. The results show that the multivariate statistical coefficients R^2 of the thermal resistance and pumping power objective functions are 0.932 9 and 0.996 6, respectively, indicating the high accuracy of the fitted functions. The optimized channel structure ($e_1 = 0.036.8$ mm, $e_2 = 0.019.3$ mm) was used to achieve a more uniform temperature field distribution and better integrated heat transfer performance (enhanced heat transfer factor $\eta = 1.23$). When the thermal resistance is larger or the pump work is larger, the comprehensive heat transfer effect is not as good as the working condition when the thermal resistance and pump work are more uniform.

1. Introduction

With the development of microfabrication technology, one of the effective methods of using microchannel high power intensive microelectronic devices with high surface-to-body ratio is widely used in advanced engineering fields such as microelectronics, energy, military nuclear energy, and biochemical industry [1–4]. According to microchannel convective heat transfer theory, the heat transfer performance of microchannel heat sink can be improved by increasing the heat transfer surface area of the channel or improving the heat transfer performance of the fluid, or use boiling heat transfer, such as nanofluids [5–9].

It has been shown [10–12] that the heat transfer performance of complex structured microchannel heat sinks is excellent because the continuous variation of the channel cross section can interrupt the thermal boundary layer development and keep the flow and heat transfer in an underdeveloped state, which serves to enhance the heat

transfer; moreover, the setting of rough elements inside the channel enhances the internal disturbance, which in turn has an important impact on the flow and heat transfer characteristics [13, 14].

In [15], the structures of microchannel heat sink with fan-shaped cavities and microchannel heat sink with triangular-shaped cavities were simulated and optimized, and it was concluded that the cavity action can destroy the microchannel flow and heat transfer boundary layer, thus enhancing the microchannel heat transfer. In [16], the effects of rib spacing ratio to pipe diameter (p/d), rib height ratio to pipe diameter (e/d), and Reynolds number on the flow and heat transfer in circular tubes with microchannels were experimentally studied, and the Nusselt (Nu) number and friction coefficient correlation equations with the three parameters of p/d , e/d , and Reynolds number as variables were proposed to guide engineering applications. Yang and Cao [17] analyzed in detail the effect of sinusoidal structured rough elements on the flow and heat transfer in microchannels and

analyzed that their enhanced heat transfer is due to the change in flow direction and the increase in area. In [18], a complex structured microchannel heat sink with a combination of fan-shaped cavities and inner ribs was proposed, and its single-phase flow and heat transfer were investigated by experimental and simulation methods, and the results showed that its integrated heat transfer performance was significantly better than that of an equal-section microchannel at Reynolds numbers greater than 300. Therefore, complex structured microchannels have obvious advantages in heat transfer.

A reasonable channel structure design can also improve the heat transfer effect. Therefore, heat transfer efficiency and pressure drop are two important parameters to measure the comprehensive heat transfer performance of microchannels. The engineering design generally involves multi-parameter optimization, called multiobjective parameter optimization [19]. Hemmat Esfe et al. [13] used a non-dominated ranking genetic algorithm (NSGA-II) with Nusselt number and friction coefficient as optimization objectives for structural optimization of ribbed and cavity channels with rib height, cavity diameter, height and location as variables.

In [15], the flow and heat transfer in variable cross section and microchannel heat sink with rough elements were investigated, and two objective functions of thermal resistance and pumping power were optimized using a multiobjective genetic algorithm to obtain the Pareto optimization solution set. In [6], the multiobjective genetic algorithm was used to optimize the heat transfer coefficient and pressure drop for microchannels with concave structure using channel height, cavity spacing, and height as variables. Theoretically, the genetic algorithm is able to find the optimal solution of the objective function probabilistically and randomly, which is more adaptable than the conventional optimization algorithm.

To overcome the limitations of straight tube microchannels, researchers have conducted extensive studies for split-recombination (SAR) microchannels. The upstream flow in a SAR microchannel is split into two equal streams, which then hit each other within the mixing element. A series of microchannel units with the same structure interconnect and further enhance the material process. Benefiting from the combination of multiple microchannel units, the synthesis rate in SAR microchannels is significantly greater than that of straight microchannels with only a single microchannel unit [11, 12].

The most common problem with current microchannel structures is the inhomogeneous mixing of reactants caused by insufficient turbulence. The key to promote the mixing effect within microchannels is to further enhance the split-recombination effect of microchannels. At the same time, the SAR microchannel structure still has great potential to further optimize and enhance the passive mixing process. However, insufficient grid accuracy and inaccurate phase interface capture techniques result in the current numerical simulation methods in microchannels to remain imperfect. Therefore, based on the CLSVOF multiphase flow model and the SST $k-\omega$ turbulence model, this

study investigates a series of microchannels with complex structures.

Therefore, based on the CLSVOF multiphase flow model and SST $k-\omega$ turbulence model, this study simulates a series of microreactors with complex structures by using the CLSVOF multiphase flow model for two-dimensional numerical simulation of gas-liquid two-phase flow and carries out multivariate optimization of the throat size and baffle length by the proxy modeling method to predict and analyze the optimal structure of the microreactors.

2. Numerical Simulation Methods

2.1. CLSVOF Multiphase Flow Model. For two incompatible fluids, it is very difficult to capture the free phase interface during dynamic motion [13]. Therefore, Sussman and Puckett proposed the CLSVOF method [14]. The principle of this method is to use the convection equation of the VOF function to achieve mass conservation and the level-set function to calculate the curvature and normal vectors to capture the phase interface smoothly. In the CLSVOF method, the phase interface is reconstructed by a segmented linear scheme [15, 16], and the initialization of the distance function of the level-set equation is achieved based on the reconstructed phase interface. For the level-set model, the mass of the transport equation is not conserved and the normal vector of the curvature calculation in the VOF model is not accurate enough [15, 17, 18]. The CLSVOF model remedies the computational defects of the mass nonconservation and the inaccuracy of the curvature calculation in the level-set and VOF models and combines its computational advantages to capture the phase interface more accurately. Hadad et al. [19] simulated the underwater bomb shock wave by CLSVOF multiphase flow model. The CLSVOF model is able to capture the phase interface more accurately under strong interaction conditions.

In the level-set model, the phase interface is defined as an equivalence surface belonging to an implicit functional equation $\phi(x, t)$, and the value of $\phi(x, t)$ at any moment can be determined by solving the controlling equation to obtain the zero equivalence surface, i.e., the location of the phase interface. $\phi(x, t)$ function is defined as follows:

$$\phi = \begin{cases} d(x, \Gamma(t)) < 0, \\ 0, \\ d(x, \Gamma(t)) > 0. \end{cases} \quad (1)$$

The position of the phase interface at time t is represented by (t) , and $d(x, \Gamma(t))$ is the distance function from the center of the grid to the phase interface $\Gamma(t)$. In the VOF model, different fluids are incompatible with each other. The volume function of fluid within each cell in the VOF model is defined as follows:

$$c = \frac{\text{fluid volume in cell}}{\text{unit volume}}. \quad (2)$$

If $C = 1$, the fluid of the grid is in continuous phase, $C = 0$ is in discrete phase, and $0 < C < 1$ means that the grid is at the phase interface. Therefore, the position and shape of the

phase interface in space can be determined by solving for the volume function C .

In an incompressible fluid, there are

$$\begin{aligned} \frac{DC}{Dt} &= \frac{\partial C}{\partial t} + (\vec{V} \cdot \nabla) \cdot C = 0, \\ \frac{\rho \partial \vec{V}}{\partial t} + \rho \vec{V} \cdot \nabla \vec{V} &= -\nabla P + \nabla \cdot \vec{V} \left[\nabla \vec{V} + (\nabla \vec{V})^T \right] + \rho g + F_{sv}. \end{aligned} \quad (3)$$

The above equation is the convective transport equation for the volume function c as well as the momentum conservation equation. F_{sv} is the surface tension term of the momentum equation.

The CLSVOF model compensates the deficiencies of mass conservation and phase interface parameters of the level-set model and VOF model and combines the advantages of the two models. The CLSVOF model can combine the advantages of both models to capture the phase interface more accurately.

3. NSGA-II-Based Scheme Solution Steps

3.1. NSGA-II Optimization Process. NSGA-II is a multi-objective genetic algorithm using fast sorting and elite mechanism, which has the characteristics of fast operation speed and good convergence [16, 17] and can effectively solve the multiobjective optimization problem in this paper. The Pareto solution set can be obtained by NSGA-II, and the solution steps are as follows.

- (1) Input the parameters of the distribution system and generate the derivative matrix.
- (2) Initialize the algorithm parameters, population number p_0 , crossover parameter f_{ga} , variation parameter C_{ga} , and maximum number of iterations N .
- (3) Randomly create the initial population p_0 and calculate the objective function value for each individual.
- (4) Sort the populations according to nondominance and calculate the crowding factor, and each solution is assigned a fitness value equal to its own nondominance rank.
- (5) Use a binary tournament mechanism to select $p_0/2$ individuals as the parent population and perform genetic inheritance, crossover, and mutation to produce $p_0/2$ offspring populations.
- (6) Invoke the trend calculation program to calculate the objective function values of the offspring populations.
- (7) Merge the resulting offspring populations with the original parent populations, rank the nondominated cases, and calculate the crowding coefficients.
- (8) Select p_0 dominant individuals as the next generation population based on hierarchical analysis, rank nondominance, and calculate crowding coefficients.
- (9) Determine whether the maximum number of iterations N is reached; if yes, output the Pareto solution set; otherwise, proceed to (4) loop.

3.2. Selection of the Multiobjective Optimal Solution. The final optimization result of NSGA-II is a set of Pareto solution sets from which the decision maker needs to select the optimal solution based on the preference information, which is essentially a multiattribute decision problem. In this paper, we adopt the approximate ideal solution ranking method (TOPSIS) to perform the optimal solution selection.

The approximate ideal solution ranking method (TOPSIS) [18], in essence, is a decision-making method by calculating the distance between the alternative solution and the ideal solution and the negative ideal solution, so that the selected solution has the minimum distance from the ideal solution and the maximum distance from the negative ideal solution. Firstly, all the noninferior solutions in the Pareto solution set are obtained to form N alternative solutions $x_1, x_2, x_3, \dots, x_N$, and the number of attributes of the solution is n , i.e., the number of objective functions; then, the m th attribute value of solution x_i is $f_m(x_i)$. First, the attribute values of all solutions are converted to dimensionless attributes, and the m th attribute value of the processed solution x_i is

$$f'_m(x_i) = \frac{f_m(x_i)}{\sqrt{\sum_{m=1}^N f_m^2(x_i)}} \setminus \text{MERGEFORMAT}. \quad (4)$$

The relative distance $d(x_i)$ for scenario x_i is calculated as follows:

$$\begin{aligned} d(x_i) &= \frac{d_+(x_i)}{d_+(x_i) + d_-(x_i)} \setminus \text{MERGEFORMAT}, \\ d_+(x_i) &= \sqrt{\sum_{m=1}^n (\lambda_m f'_m(x_i) - \lambda_m f'_{m+})^2} \setminus \text{MERGEFORMAT}, \\ d_-(x_i) &= \sqrt{\sum_{m=1}^n (\lambda_m f'_m(x_i) - \lambda_m f'_{m-})^2} \setminus \text{MERGEFORMAT}, \end{aligned} \quad (5)$$

where $d_+(x_i)$, $d_-(x_i)$ represent the distance from solution x_i to the ideal solution and the negative ideal solution; λ_m is the weight of attribute f'_m , which is taken as equal weight in this paper; and f'_{m-} , f'_{m+} represent the optimal and inferior values of all solutions after normalization of attributes. The solution with the smallest relative distance among all solutions is the optimal solution in the multiobjective optimization.

4. Microstructure Model

For nonlinear objective functions, the ability of the proxy model to fit is particularly impressive and has great potential for application in various research areas [7].

After obtaining the sample dataset (s, y_s) , the kriging model will perform a linear weighted interpolation for the sample function response values, i.e.,

$$\hat{y}(x) = \sum_{i=1}^n \lambda^{(i)} y^{(i)}. \quad (6)$$

λ is the weighting factor, which is the most critical influence parameter in the agent model building process. The

optimal weighting factor in the kriging model should satisfy the mean squared error:

$$\text{MSE}[\hat{y}(x)] = E\left[\left(\lambda^T Y_S - Y(x)\right)^2\right]. \quad (7)$$

Minimum, x and y the mathematical expectation relation should satisfy

$$E\left[\sum_{i=1}^n \lambda^{(i)} Y(x^{(i)})\right] = E[Y(x)]. \quad (8)$$

Y function is defined as

$$Y = \beta_0 + Z(x), \quad (9)$$

where β_0 is the mathematical expectation of $Y(x)$ and $Z(x)$ is the static random process with mean 0 and variance $\sigma^2 = \sigma^2(x)$.

The weighting factor λ is obtained and substituted into the $\hat{y}(x)$ function to predict the value of the function at any x , thus greatly reducing the computational effort of numerical optimization.

Figure 1 shows the schematic diagram of the three microchannel cells of the microreactor, which is also the flow region of the multiphase fluid. The microchannel size and baffle size are 2.4 mm, the inlet and outlet widths are 5 mm and 3 mm, respectively, and each cell is connected by a narrow throat with a grid number of 120,000 after irrelevance verification. The geometrical dimensions of the throat width and baffle length are the research objectives to be further optimized.

In order to quantitatively compare the effects of different geometries on the gas-liquid mixing effect and then find the optimal microchannel structure, the boundary coefficients are defined here:

$$\sigma_s = \frac{A_\sigma}{S} \times 100\%. \quad (10)$$

A_σ is the area of the region between 0.1 and 0.9 for the volume fraction of the gas phase, and the larger the area of this part, the more adequate the intersection of gas and liquid phases. s is the total area of the three microchannel cells. The magnitude of the boundary coefficient is the ratio of the gas-liquid phase interface area to the total area when the fluid is flowing inside the microreactor, which can measure the mixing effect of the gas-liquid phases in the microchannels.

5. Microstructure Model Optimization Effect

Figure 2 shows the gas-liquid phase distribution when calculating different widths and lengths at the same time, and the boundary coefficients are extracted using post-processing software to compare their gas-liquid phase mixing effects.

By changing the throat size and baffle length, the geometry is optimized for the throat area and the channel area by changing the ratio of the area in front of the throat and the channel area.

The improvement of these two structures is achieved by proxy model optimization. The structure of the proxy model

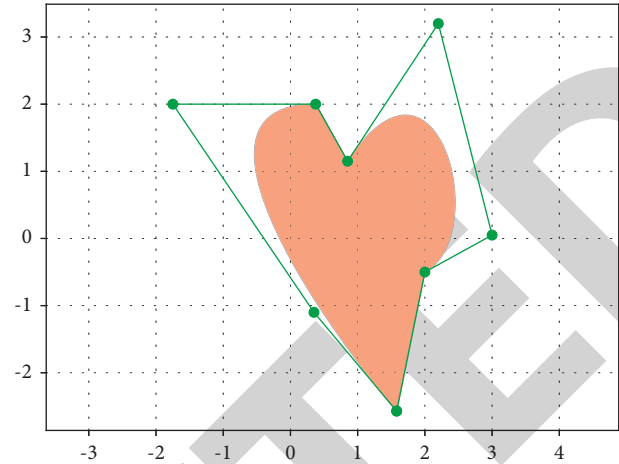


FIGURE 1: Schematic diagram of geometric structure.

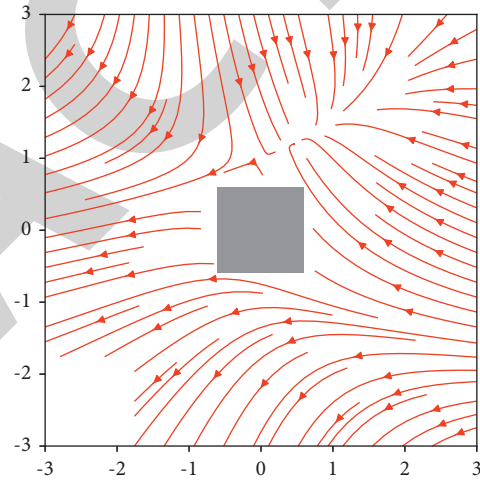


FIGURE 2: Gas-liquid phase distribution for different throat widths and baffle lengths at $t = 150$ ms.

for this problem can be summarized as follows: the maximum value of the relationship between the design variables throat size x_1 , baffle length x_2 and the objective function of the function y boundary coefficient is solved. The objective function of the design variables x_1 and x_2 with respect to the boundary coefficients is refined by collecting a certain number of simulation data points, and the optimal throat size and baffle length geometry is accurately predicted by this objective function.

Figure 3 shows the sensitivity analysis results of the two independent variables of throat size and baffle length. The blue part shows the results of the sensitivity analysis of the throat size, and the yellow part shows the percentage of sensitivity of the baffle length. The left side shows the global sensitivity analysis, i.e., in addition to these two independent variables, the effects of all the remaining unknown independent variables are also considered. In this analysis, the throat size and baffle length are the most important influencing factors of the boundary coefficient, which together account for 82% of the influencing factors, while the remaining variables account for only 18%. The reason for

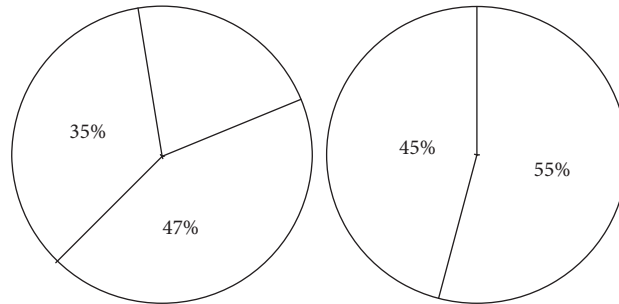


FIGURE 3: Sensitivity analysis results.

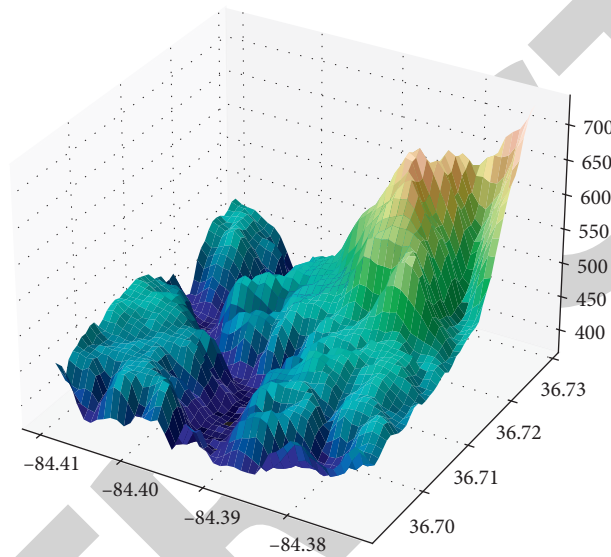


FIGURE 4: Three-dimensional kriging interpolation.

this result is that the throat size affects the flow of gas-phase fluid into the mixing enhancement domain through the throat area, while the baffle length affects the percentage of the channel area in the overall microreactor structure, with the baffle size remaining constant. As it was pointed out in the previous paper, a smaller throat area and a smaller channel area will be more favorable for the increase of the boundary coefficient, and these two variables are the main influencing variables for the throat area and the channel area, which will have a greater impact on the boundary coefficient than the other related variables.

The image on the right shows the comparison between the effect of throat size and baffle length only. The sensitivity of the throat size is 45%, and the sensitivity of the baffle length is 55%. It can be seen that the baffle angle has a greater influence on the boundary coefficient. This is also reflected in the data; as the baffle angle changes, the boundary coefficient will have a more obvious trend. The reason for this result is that the length of the baffle is the most direct variable affecting the area share of the access area, and the area share of the access area and the length of the baffle basically show a linear positive correlation growth relationship. The size of the throat has more influence on the flow of the gas phase from the throat into the mixing domain than the geometry,

and its change does not produce significant geometrical changes on the area share of the throat and mixing domain.

Figure 4 shows the 3D kriging interpolation results for the three variables. The highest boundary coefficient point extracted is (1.4, 8), i.e., the throat size is 1.4 mm and the baffle length is 8 mm. This point is the boundary point of the two design variables, and it can be seen from the three-dimensional coordinate diagram that the throat size and baffle length show a negative linear relationship within the value range, and the boundary coefficient at the lower limit of the two obtains the highest value. There are two main reasons for this conclusion [21].

- (1) The narrow throat size makes it easier for the gas flowing through the throat to separate from a larger bubble cluster into a group of small bubble clusters, which in turn forms a better gas-liquid mixing effect at the front of the baffle and increases the value of the boundary coefficient.
- (2) The length of the baffle plate most directly reduces the area share of the channel area. The boundary coefficient in the channel zone is lower than that in the baffle front and corner zone, and the baffle length is the most direct factor affecting the area of the

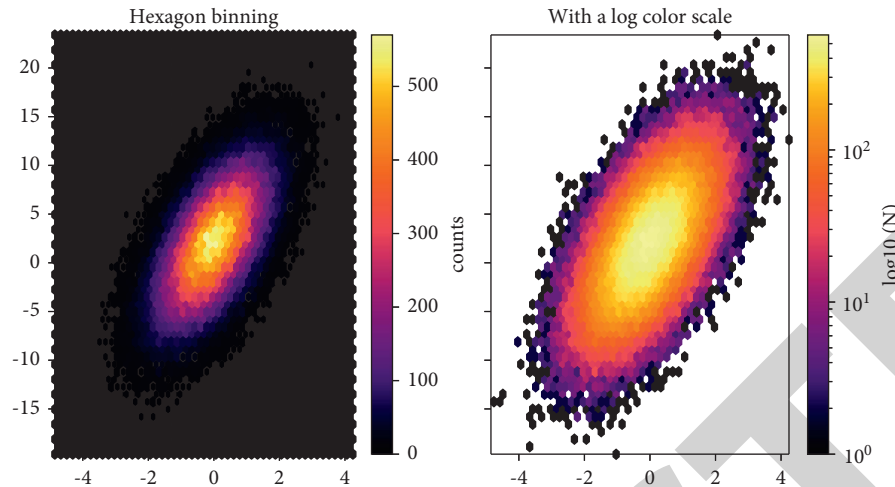


FIGURE 5: Experimental results and simulation results. (a) Experimental results. (b) Microchannel gas-liquid phase distribution diagram.

channel zone; therefore, the reduction of the baffle length will increase the boundary coefficient inside the microreactor very significantly.

The throat and baffle front have an important role in enhancing the gas-liquid phase mixing effect. Figure 5 shows the results of numerical simulations and high-speed camera images. From Figure 5, it can be seen that the inside of the throat and the front of the baffle are the high-pressure areas of the microchannel unit, and the highest pressure is about 8000 Pa, which can greatly increase the mixing effect of the two phases. The gas phase will collide with the baffle wall after flowing through the throat, and the gas momentum direction will change after colliding with the baffle wall, and the large bubbles will be broken into smaller ones. The other part of the bubbles collides with the wall and rejoins with the new influx of fluid at the throat. This is the most important reason why the gas-liquid junction area in this region is significantly higher than the rest of the region.

6. Conclusions

In this paper, a full linear regression of the SAR microchannel is performed using a proxy model. A series of numerical simulations using the CLSVOF multiphase flow model and the SST $k-\omega$ shear pressure transport turbulence model demonstrate outstanding computational accuracy in calculating the gas-liquid two-phase distribution and phase interface capture. The advantages and disadvantages of the level-set model, VOF model, and CLSVOF model are investigated and analyzed for the different multiphase flow models, i.e., the level-set model, the VOF model, and the CLSVOF model. Both of them have different degrees of computational drawbacks when applied individually. Therefore, the CLSVOF model, which combines the two computational models, has a greater computational advantage over the above two models for the study in this paper, which focuses on phase interface capture.

Data Availability

The experimental data used to support the findings of this study are available from the corresponding author upon request.

Conflicts of Interest

The author declares that there are no conflicts of interest regarding this work.

References

- [1] M. Bogdan, T. Vasile, and O. Raluca, "Optimal shape design of microchannel H-cell," in *Proceedings of the 2019 19th International Symposium on Electromagnetic Fields in Mechatronics, Electrical and Electronic Engineering (ISEF)*, pp. 1-2, IEEE, Nancy, France, 29-31 Aug. 2019.
- [2] R. D. Gupta, P. Gupta, and R. Khanna, "Parametric optimization of USM parameters by Taguchi and NSGA-II for the development of μ -channels on pure titanium," *Grey Systems: Theory and Application*, vol. 10, no. 2, pp. 173-192, 2020.
- [3] H.-l. Liu, H.-b. Shi, H. Shen, and G. Xie, "The performance management of a Li-ion battery by using tree-like mini-channel heat sinks: experimental and numerical optimization," *Energy*, vol. 189, Article ID 116150, 2019.
- [4] A. Datta, V. Sharma, D. Sanyal, and P. Das, "A conjugate heat transfer analysis of performance for rectangular microchannel with trapezoidal cavities and ribs," *International Journal of Thermal Sciences*, vol. 138, pp. 425-446, 2019.
- [5] H.-l. Liu, C.-c. Fan, Y.-l. He, and D. S. Nobes, "Heat transfer and flow characteristics in a rectangular channel with combined delta winglet inserts," *International Journal of Heat and Mass Transfer*, vol. 134, pp. 149-165, 2019.
- [6] G. V. Kewalramani, A. Agrawal, and S. K. Saha, "Modeling of microchannel heat sinks for electronic cooling applications using volume averaging approach," *International Journal of Heat and Mass Transfer*, vol. 115, pp. 395-409, 2017.
- [7] P. Sikdar, A. Datta, N. Biswas, and D. Sanyal, "Identifying improved microchannel configuration with triangular cavities and different rib structures through evaluation of thermal performance and entropy generation number," *Physics of Fluids*, vol. 32, no. 3, p. 033601, 2020.

Research Article

Wireless Sensor Network Security Based on Improved Identity Encryption

Hao Zhou¹ and Haochang Bi² 

¹Computer Department, Anhui Post and Telecommunication College, Hefei 230031, China

²Anhui Vocational College of Electronics & Information Technology, Anhui, Bengbu 233030, China

Correspondence should be addressed to Haochang Bi; 2000100018@ahdy.edu.cn

Received 24 January 2022; Revised 18 February 2022; Accepted 12 March 2022; Published 1 April 2022

Academic Editor: Hangjun Che

Copyright © 2022 Hao Zhou and Haochang Bi. This is an open access article distributed under the Creative Commons Attribution License, which permits unrestricted use, distribution, and reproduction in any medium, provided the original work is properly cited.

In order to protect network information security and improve the security of wireless sensor networks, based on chaotic systems, we propose a wireless sensor algorithm based on improved identity encryption. First, the basic principle of chaotic system mapping is specifically analyzed; the two chaotic mapping systems are rectified to obtain the hybrid chaotic mapping system according to the demand of wireless sensing network. After that, an encryption framework and key are designed and the hybrid mapping system is applied to the encryption framework to encrypt the data. In this way, the length of the encryption algorithm is lengthened and the defensibility of the encrypted content is improved. Finally, the performance of the proposed encryption algorithm is tested in terms of information entropy, statistical methods, and ciphertext randomness. The test results show that compared with other encryption algorithms, the running speed of the encryption algorithm proposed in this paper is only 18.51 ms, which is faster than that of other encryption algorithms, and the memory consumption is only 27%, which is much lower than that of other algorithms. It can be seen that the proposed encryption algorithm has strong encryption effect and superior algorithm performance for data encryption in wireless sensor networks.

1. Introduction

With the continuous improvement of Internet technology, computers, cell phones, and many other computer devices are widely used and have become essential products for daily life, enhancing information exchange and enriching people's entertainment. However, the widespread popularity and application of devices such as wireless sensors in computers have also brought about information security problems, and the security of people's information on the network has been seriously threatened. Therefore, encryption technology was born. The current market research on wireless sensor network security mainly includes encryption algorithms and authentication schemes, which serve to guarantee data security and legitimacy. However, the complex node resources and small memory of wireless sensor networks lead to the low computational accuracy and poor results of the existing encryption algorithms for wireless sensor networks. Among

them, chaotic system has the characteristics of sensitivity to initial value, ergodicity, pseudo-randomness, etc., which meets the characteristics of diffusion and obfuscation in encryption algorithms and achieves preliminary application results in information security. For network information encryption, scholars and experts have conducted in-depth research. Maram et al. proposed a dynamic S-box approach to process Unicode text data [1]. Ahmad et al. proposed to use the Diffie–Hellman technique to exchange the encryption key generated by TTI algorithm with another party as a way to improve the security of sensitive information transmission [2]. Liang et al. proposed a dynamic key encryption-decryption neural network chaotic algorithm, and the results showed that the encryption-decryption speed and anti-decryption ability of the method had a great improvement [3]. Chaotic encryption algorithm was widely used, for example, Deng and Xiao applied the chaotic algorithm to the encrypted transmission of RFID, and the

results showed that the algorithm can meet the security requirements of object RFID [4]. Zhang et al. applied chaos algorithm to video transmission encryption to encrypt the differential components of motion vectors in horizontal and vertical directions as well as DC transform coefficients, respectively, and achieved good results [5]. Ge et al. proposed an encryption method for images based on cross-diffusion of logistic mapping and Chebyshev mapping by combining chaos algorithm. The results indicated that the encryption algorithm had high security [6]. Wu et al. proposed a chaotic compressed sensing algorithm for OFDM-PON networks, with results showing that the method can save bandwidth and improve the security of OFDM-PON networks [7]. The above studies show that chaotic algorithm is widely used in the field of data transmission [8–17]. Therefore, this study proposes an improved chaos-based encryption algorithm for wireless networks based on the characteristics of chaos algorithm and verifies the feasibility of the proposed algorithm.

2. Basic Methods

In the field of network information security, chaotic systems possess sensitivity, ergodicity, and unpredictability that have led to smaller applications in information security. Chaotic mappings are mainly divided into logistic mappings and cubic mappings.

Logistic mapping is in one-dimensional form in chaotic systems and can be expressed as

$$x_{n+1} = \mu x_n (1 - x_n), \mu \in (0, 4), x_n \in [0, 1], \quad (1)$$

where μ is a parameter and when $\mu \in (3.57, 4)$, the logistic mapping exhibits chaotic properties.

The cubic mapping is calculated as

$$x_{n+1} = ax_n^3 - bx_n, x_n \in [-1, 1], \quad (2)$$

where both a and b are parameters, the output range of Cubic mapping is shown in Figure 1, and the mapping range becomes progressively smaller with increasing parameter a .

As shown in Figure 2, a bifurcation point will occur when the parameter b is higher than 2.3, and the chaotic system is in a chaotic state at this time. To obtain better pseudo-randomness, a is set to 4 and b is set to 3. The cubic mapping expression is obtained as follows:

$$x_{n+1} = 4x_n^3 - 3x_n, x_n \in [-1, 1]. \quad (3)$$

In wireless sensor networks, chaotic systems cannot perform complex calculations on the network due to the problems of small network memory and poor computational power. To apply chaotic systems to wireless sensor network encryption, the chaotic system needs to be rectified.

The logistic mapping can also be expressed as

$$x_{n+1} = 1 - \lambda x_n^2, \lambda \in [0, 2], x_n \in [-1, 1], \quad (4)$$

where λ is a parameter. The logistic mapping integerization in chaotic systems consists of three main steps, as follows:

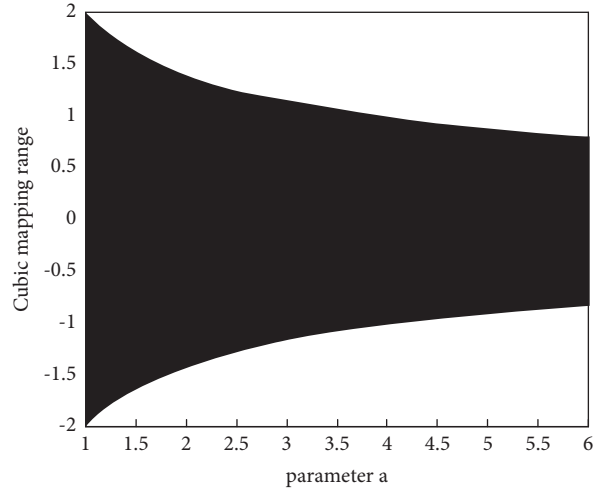


FIGURE 1: Trend of the range of cubic mapping with parameter a .

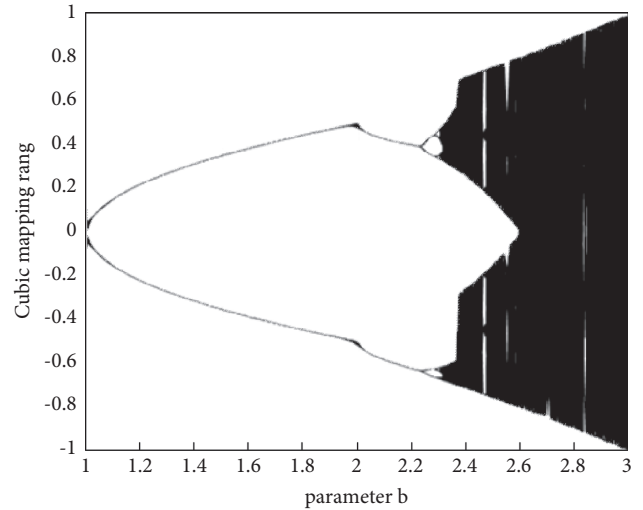


FIGURE 2: Trend of the range of cubic mapping with parameter b .

- (1) Multiply both sides of equation (4) by $m^2 = (m \neq 0)$ at the same time and obtain the following equation

$$m^2 x_{n+1} = m^2 - \lambda (m x_n)^2. \quad (5)$$

- (2) Construct an equation:

$$z_n = m x_n + m. \quad (6)$$

After a simple treatment of equation (6), equation (7) is calculated as follows:

$$\begin{cases} x_n = \frac{z_n}{m} - 1 \\ x_{n+1} = \frac{z_{n+1}}{m} - 1 \end{cases}. \quad (7)$$

- (3) Substitute equation (7) into equation (5) and set the parameter λ to 2. The final integer logistic mapping equation is obtained as

$$z_{n+1} = 4z_n - \frac{2}{m}z_n^2. \quad (8)$$

In equation (6), x_n interval is $[-1, 1]$; z_n interval is $[0, 2m]$; if z_n are integers, then $m = 2^{L-1}$, thus obtaining the z_n interval as $[0, 2^L]$.

Equation (8) contains two zeros, $z_n = 0$ and $z_n = 2m$. If the initial iteration value is 0 or $2m$, the value of all subsequent iterations will be 0. To prevent the above situation, equation (8) will be optimized:

$$\begin{cases} z_{n+1} = 4z_n - \frac{2}{m}z_n^2 - 1, z_n = 0 \text{ or } 2m \\ z_{n+1} = 4z_n - \frac{2}{m}z_n^2 - 1, \text{others} \end{cases}. \quad (9)$$

There are no zeros in equation (9) so that all iteration values will not be 0.

According to the cubic mapping of equation (3), it is integerized as follows:

(1) Construct the following equation:

$$\begin{cases} x_n = \frac{y_n}{c} - 1 \\ x_{n+1} = \frac{y_{n+1}}{c} - 1 \end{cases}. \quad (10)$$

(2) Substitute equation (10) into equation (3) to obtain the following equation:

$$y_{n+1} = \frac{4}{c^2}y_n^3 - \frac{12}{c}y_n^2 + 9y_n. \quad (11)$$

In equation (10), the x_n interval is $[-1,1]$, and the y_n interval is obtained as $[0, 2c]$. If the y_n values are all integers, then $c = 2^{L-1}$, and the y_n interval is $[0, 2^L]$.

Equation (11) contains several zeros, $y_n = 0$, $y_n = 1.5c$, and $y_n = c$. If the initial iteration value is 0, $1.5c$, or c , then all subsequent iterations have a value of 0. Thus, equation (11) is optimized to obtain the following equation:

$$y_{n+1} = \begin{cases} \frac{4}{c^2}y_n^3 - \frac{12}{c}y_n^2 + 9y_n + 1, y_n = 0 \text{ or } \frac{3}{2}c \\ \frac{4}{c^2}y_n^3 - \frac{12}{c}y_n^2 + 9y_n, \text{others} \end{cases}. \quad (12)$$

There are no zeros in equation (12), and the iterative value of 0 does not occur when iterating.

3. Improved Identity Encryption Algorithm

3.1. Cryptographic Framework. The chaotic algorithm after integer is computed by Feistel cryptographic framework as shown in Figure 3, and the encryption process is as follows:

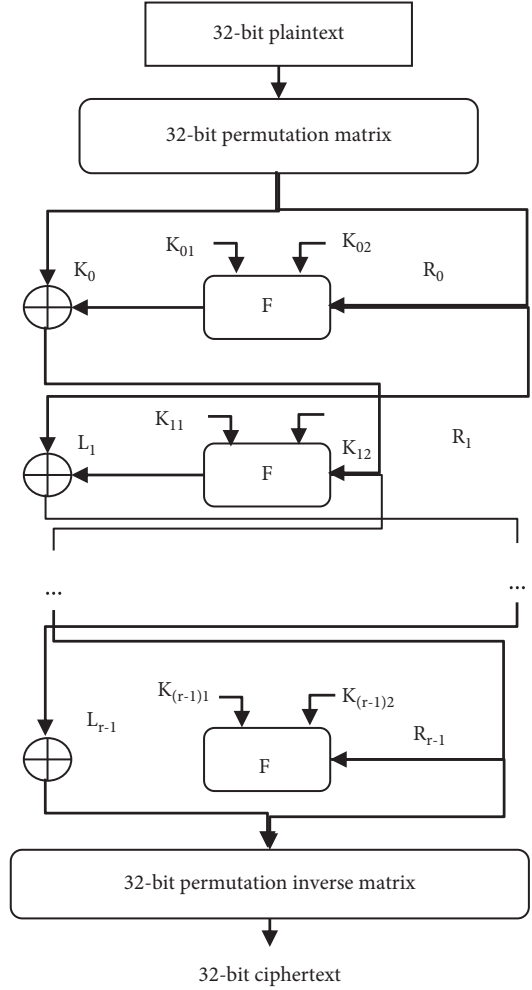


FIGURE 3: Cryptographic framework.

$$\begin{cases} R_{i+1}L_i \oplus F(K_i, R_i) \\ L_{i+1} = R_i \end{cases}. \quad (13)$$

The Feistel structure belongs to a symmetric cryptographic framework in which the round function F has an important impact on the performance of the algorithm. The main details of the round function F are shown in Figure 4.

In Figure 4, \oplus is the XOR operation. The round function encryption process is divided into three main steps, as follows.

- (1) First a 32-bit plaintext is divided into two parts of equal length, each side of length 16; then, a part is divided into two parts of equal length, of length 8.
- (2) The two 8-bit plaintexts are followed by the number "0" to bring their length to 16 bits.
- (3) The round key will be XOR operated on the 16-bit plaintext separately, followed by the logistic and cubic mappings, and then the XOR operation will be performed. Finally, the XOR value is passed through a 16-bit permutation matrix to obtain the output.

The algorithm encrypts a total of 4 rounds, i.e., $r = 4$.

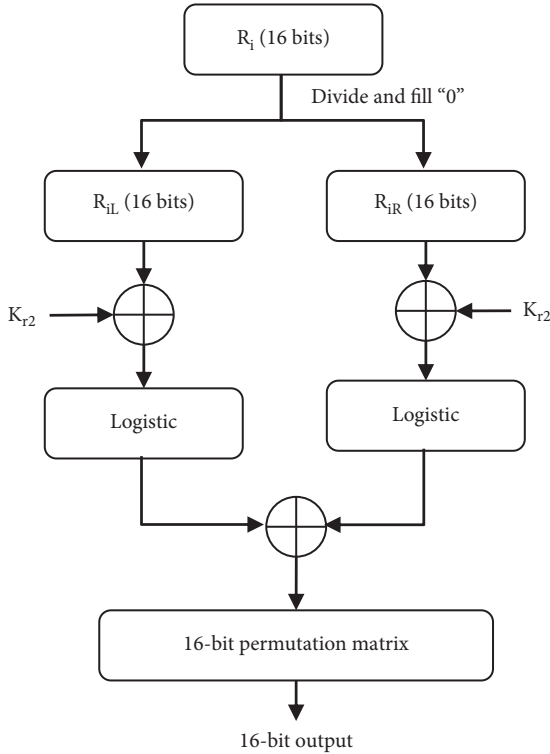


FIGURE 4: Round function F .

3.2. *Generation of Round Key.* In the above, the performance of the two chaotic systems degrades gradually after the integerization, which leads to the reduction of their sequence randomness. Therefore, to solve the above problem, the two chaotic systems are mapped together to obtain one hybrid chaotic system.

Also, this part generates the initial values of the hybrid chaotic system by a linear congruential generator. The linear congruential generator expression is given by [18, 19]

$$y(n+1) = (16807 \times y(n) \bmod (2^{31} - 1)). \quad (14)$$

With the addition of a linear congruential generator to the hybrid chaotic system, the period of the sequence generated by the hybrid chaotic system is extended to $2^{31} - 1$. The specific flow of generating chaotic sequences is shown in Figure 5.

The autocorrelation of integer logistic mapping and integer cubic mapping in a 16-bit processor is shown in Figures 6 and 7.

From Figures 6 and 7, it can be seen that the autocorrelation of logistic and cubic chaotic mappings is poor, which affects their encryption effect. Therefore, the study will use the quantization operation method to enhance the autocorrelation of the two chaotic systems. The autocorrelation of the sequences generated by the quantized hybrid chaotic system is shown in Figure 8, from which it can be found that the autocorrelation image is mainly in the form of impulse function, which indicates that the sequences generated by the quantized hybrid chaotic system have better autocorrelation and can achieve better encryption effect.

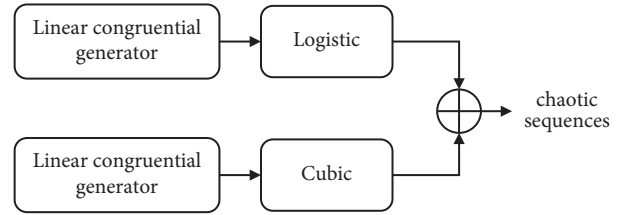


FIGURE 5: Generation of chaotic sequences.

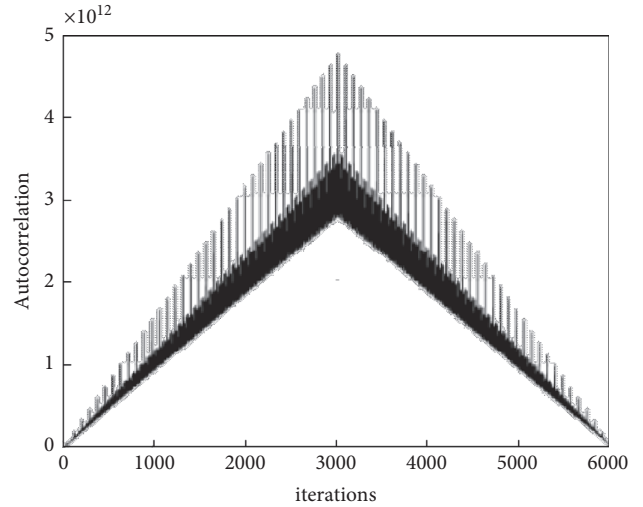


FIGURE 6: Integer logistic mapping.

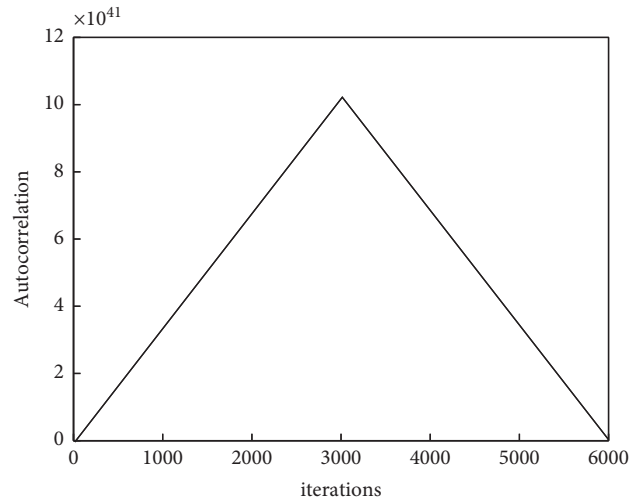


FIGURE 7: Integer cubic mapping autocorrelation.

An arbitrary 32-bit sequence is selected from the sequence generated by the hybrid chaotic system and divided into two parts of equal length, labeled k_1 and k_2 , respectively [20, 21].

As shown in Figure 9, k_1 and k_2 are used as the initial values for generating the round key, the process of which is divided into three main steps, as follows.

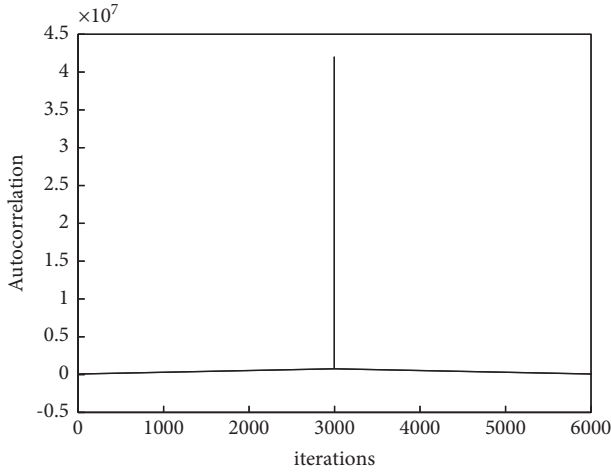


FIGURE 8: Autocorrelation of chaotic sequences.

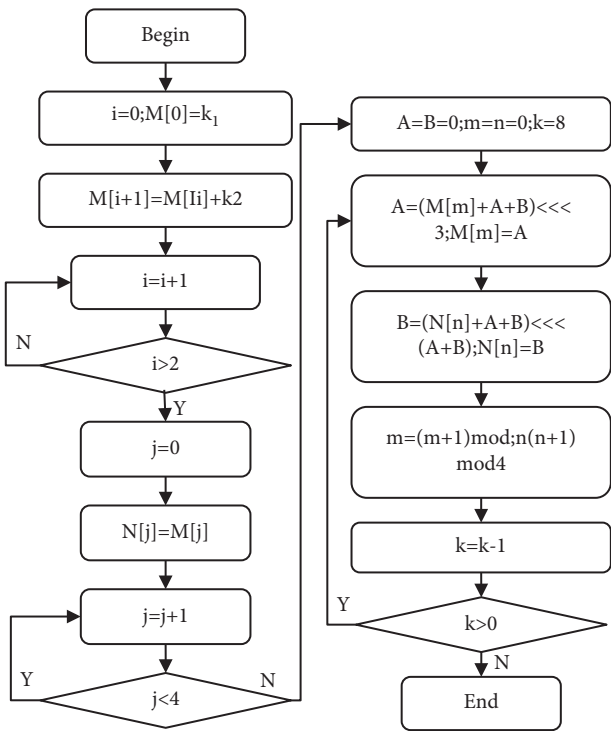


FIGURE 9: The generation of round key.

- (1) The initialization matrix M is generated by k_1 and k_2 .
- (2) Loop the value of matrix M twice and assign all of them to matrix N afterwards.
- (3) Eight shift operations are performed on the matrix and the values in the matrix to obtain the eight round keys needed for encryption.

3.3. *Permutation Matrix.* In cryptography, the permutation operation is a typical practice whose main function is to complicate the relationship between plaintext and ciphertext. In the chaotic encryption algorithm, the study will be represented by a permutation matrix P :

$$P = \begin{bmatrix} 10 & 7 & 12 & 9 \\ 11 & 5 & 1 & 15 \\ 26 & 23 & 28 & 25 \\ 27 & 21 & 17 & 31 \\ 16 & 13 & 3 & 14 \\ 4 & 6 & 8 & 2 \\ 32 & 29 & 19 & 30 \\ 20 & 22 & 24 & 18 \end{bmatrix}. \quad (15)$$

In the matrix, each parameter is the position of the input sequence. The parameter “10” means that when the input sequence passes through the permutation matrix, the parameter at the tenth position becomes the parameter at the first position of the output sequence. This can be expressed as follows:

$$\begin{bmatrix} 1 & 1 & 1 & 0 & 0 & 0 & 0 & 1 \\ 0 & 0 & 1 & 1 & 0 & 1 & 1 & 0 \end{bmatrix} \xrightarrow{P} \begin{bmatrix} 0 & 0 & 1 & 0 & 0 & 0 & 1 & 1 \\ 1 & 0 & 1 & 1 & 0 & 0 & 1 & 1 \end{bmatrix}. \quad (16)$$

3.4. *Decryption.* From the above cryptographic framework, it is clear that the Feistel structure is a symmetric state and the decryption and encryption steps are roughly the same. The difference lies in the order of using the round keys, such as the order in encryption K_1, K_2, K_3, K_4 ; conversely, the decryption round key is the reverse of the encryption round key K_4, K_3, K_2, K_1 . The decryption is calculated as in equation (15) [22–24]:

$$\begin{cases} L_i = R_{i+1} \oplus F(K_i, R_i), \\ R_i = L_{i+1}. \end{cases} \quad (17)$$

Meanwhile, the substitution inverse matrix P^{-1} can be expressed as

$$P^{-1} = \begin{bmatrix} 11 & 16 & 7 & 13 & 10 & 14 & 2 & 15 \\ 4 & 1 & 9 & 3 & 6 & 8 & 12 & 5 \\ 37 & 32 & 23 & 29 & 26 & 30 & 18 & 31 \\ 20 & 17 & 25 & 19 & 22 & 24 & 28 & 21 \end{bmatrix}. \quad (18)$$

From P^{-1} matrix, we can see that the element in the first position of the input sequence becomes the element in the eleventh position of the output sequence after permutation; if we want to restore the element in the eleventh position of the output sequence to the first position of the input sequence again through the permutation inverse matrix, we need to set the first value of the permutation inverse matrix to 11, and so on, to obtain the permutation inverse matrix.

4. Experimental Results and Analysis

4.1. *Experimental Environment.* To verify the effectiveness of the proposed algorithm performance, this experiment will be implemented using C program and the algorithm will be applied to the ZigBee platform, which contains 128 KB of ROM, 4 KB of RAM, and a CC2530 microprocessor.

4.2. Algorithm Evaluation Index

4.2.1. Information Entropy. In order to test the performance of hybrid chaotic systems, i.e., to test the system complexity and security, the experiment will use information entropy to verify the performance of chaotic systems. The higher the value of information entropy, the stronger the complexity of the system. That is, the information entropy can effectively measure the system. If the length of the ciphertext is 8 bits, the information entropy is taken to be about 8 for better encryption. The expression of information entropy is as follows [25]:

$$H(x) = \sum_x P(x) \log_2 \frac{1}{p(x)}. \quad (19)$$

The entropy of various ciphertext information of different lengths is shown in Table 1.

From Table 1, we can visually see that the ciphertext length is extended from 16000 to 800000, and its information entropy is increased from 7.9642 to 7.9999, which is very close to the standard value of 8. This shows that the ciphertext has strong randomness and also proves that the system has better performance, complexity, and security and can effectively avoid external attacks on network information.

4.2.2. Confusion and Diffusion. In encryption algorithms, confusion and diffusion are the two basic principles that must be followed. Confusion serves to complicate the relationship between the plaintext and the ciphertext, and diffusion, i.e., the maximum impact on the ciphertext through the plaintext, further enhances the security of the ciphertext.

In order to verify the confusion and diffusion effect of the encryption algorithm and to evaluate and assess the performance of the encryption algorithm more objectively, the degree of completeness, degree of avalanche, and degree of strict avalanche are used as evaluation indexes in this experiment.

If an encryption algorithm encrypts a plaintext of n bits into a ciphertext of m bits, the performance of the encryption algorithm is measured using the above three criteria. Completeness represents the existence of correlation between each bit of the plaintext and all bits of the ciphertext species, and the completeness expression is as follows:

$$d_c = -1 \frac{1}{nm} \# \{ (i, j) | a_{ij} = 0 \}. \quad (20)$$

The avalanche degree represents that each change of one bit in the plaintext will change at least nearly half of the bits of all ciphertexts, and the avalanche degree expression is as in equation (18):

$$d_a = 1 - \frac{2}{\#X * nm} \sum_{i=1}^n \left| \sum_{j=1}^m j b_{ij} - \frac{m}{2} \#X \right|. \quad (21)$$

TABLE 1: Ciphertext information entropy.

Ciphertext length (bytes)	Information entropy
160.000	7.9642
320.000	7.9765
480.000	7.9835
640.000	7.9926
800.000	7.9999

The strict avalanche degree is the probability that for each bit changed in the plaintext, each bit in the ciphertext is changed at least 50%, which is expressed as follows [26–28]:

$$d_{sa} = 1 - \frac{2}{\#X * nm} \sum_{i=1}^n \sum_{j=1}^m \left| a_{ij} - \frac{1}{2} \#X \right|. \quad (22)$$

In the above equation, a_{ij} denotes the i -th row and j -th column element inside the dependency matrix a containing $n * m$ elements, i takes values in the range $(1, n)$, and j takes values in the range $(1, m)$. If the i -th element of the plaintext is changed, the j -th element of the ciphertext changes; then $a_{ij} = 1$; otherwise $a_{ij} = 0$. b_{ij} denotes the i -th row and $j + 1$ -th column element inside the distance matrix B containing $n * (m + 1)$ elements, i takes values in the range $(0, n)$, and j takes values in the range $(0, m)$. If the i -th element of the plaintext is changed, the plaintext is changed by j bits, and then $b_{ij} = 1$. The symbol X represents the total number of bits in the plaintext; $\#$ indicates the summation symbol.

If the values of d_c , d_a , and d_{sa} meet the criteria of equation (20), it means that the proposed algorithm possesses good results in confusion and diffusion.

$$d_c = 1, d_a \approx 1, d_{sa} \approx 1. \quad (23)$$

The trends of the above three evaluation indexes under different encryption rounds are shown in Figures 10–12.

The change curves of d_c , d_a , and d_{sa} indicators from Figures 10–12 show that when the number of encryption rounds is 4, d_a and d_{sa} show stable trends with no significant change. The optimal number of encryption rounds can be determined to be 4, thus minimizing the resource loss of wireless sensors and ensuring the security of encrypted information.

To further verify the superiority of the proposed encryption algorithm based on hybrid chaotic system, this experiment compares the designed algorithm with the traditional two encryption algorithms of RC5 and RC6 for wireless sensor network for confusion and diffusion, and the comparison results obtained are shown in Table 2.

From the above table, the d_c values of all three algorithms are 1, which indicates that the completeness of all three algorithms is good. d_a and d_{sa} of the proposed algorithm are 0.998 and 0.999, respectively, which are both higher than those of the other two algorithms, by (0.005, 0.12) and (0.007, 0.009), respectively, compared to the RC5 and RC6 encryption algorithms. This shows that the proposed algorithm is more effective in confusion and diffusion, and the algorithm performs better than the traditional encryption algorithm.

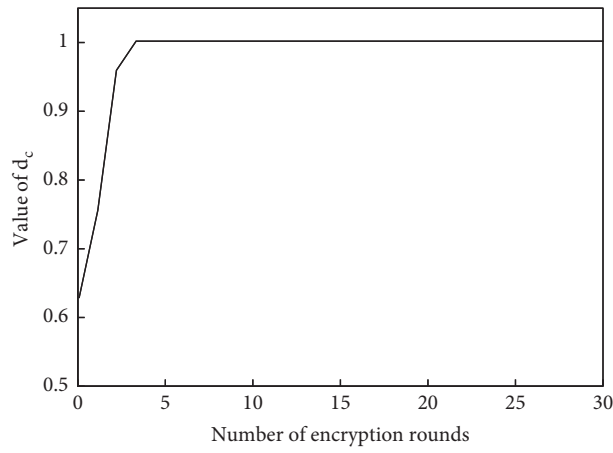
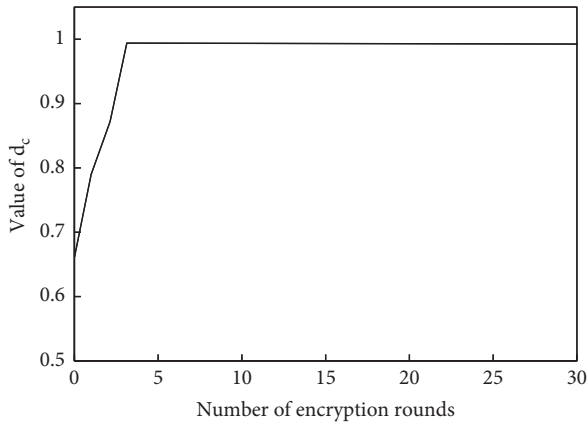
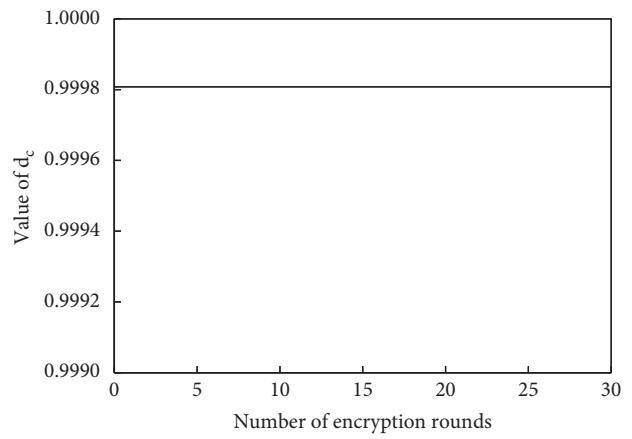


FIGURE 10: Value of d_c for different number of encryption rounds.

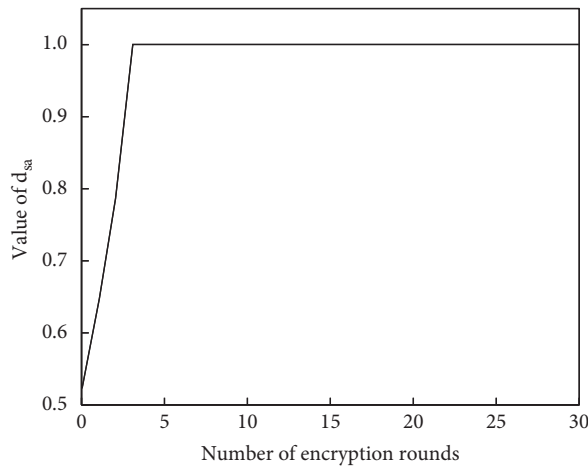


(a)

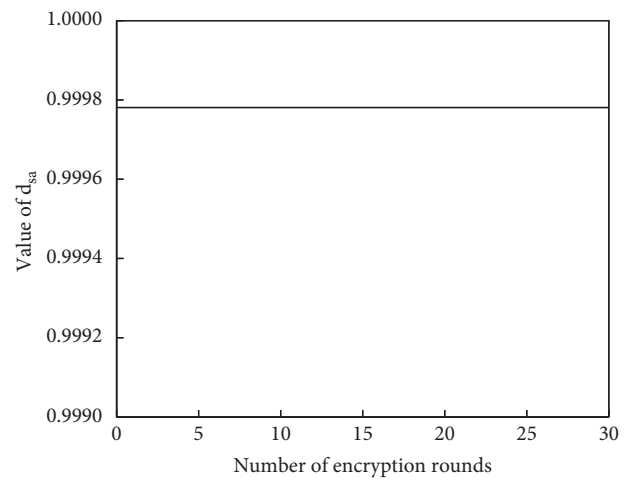


(b)

FIGURE 11: Value of d_a . (a) Encryption from round 1 to round 30. (b) Encryption from round 4 to round 30.



(a)



(b)

FIGURE 12: Value of d_{sa} . (a) Encryption from round 1 to round 30. (b) Encryption from round 4 to round 30.

TABLE 2: Performance comparison of the proposed encryption algorithm and traditional encryption algorithm.

Algorithm	d_c	d_a	d_{sa}
RC5 [29]	1.000000	0.999786	0.999770
RC6 [29]	1.000000	0.999779	0.999799
The algorithm designed in this paper	1.000000	0.999812	0.999772

TABLE 3: Statistical analysis of “0” and “1.”

Length of ciphertext n	Number of “0” k_1	Number of “1” k_2	k_1/n	k_2/n
1,280,000 bits	631,923	648,077	49.369%	50.631%
2,560,000 bits	1,282,425	1,277,575	50.095%	49.905%
3,840,000 bits	1,924,163	1,915,837	50.108%	49.892%
5,120,000 bits	2,557,439	2,562,561	49.950%	50.050%
6,400,000 bits	3,199,671	3,200,329	49.995%	50.005%

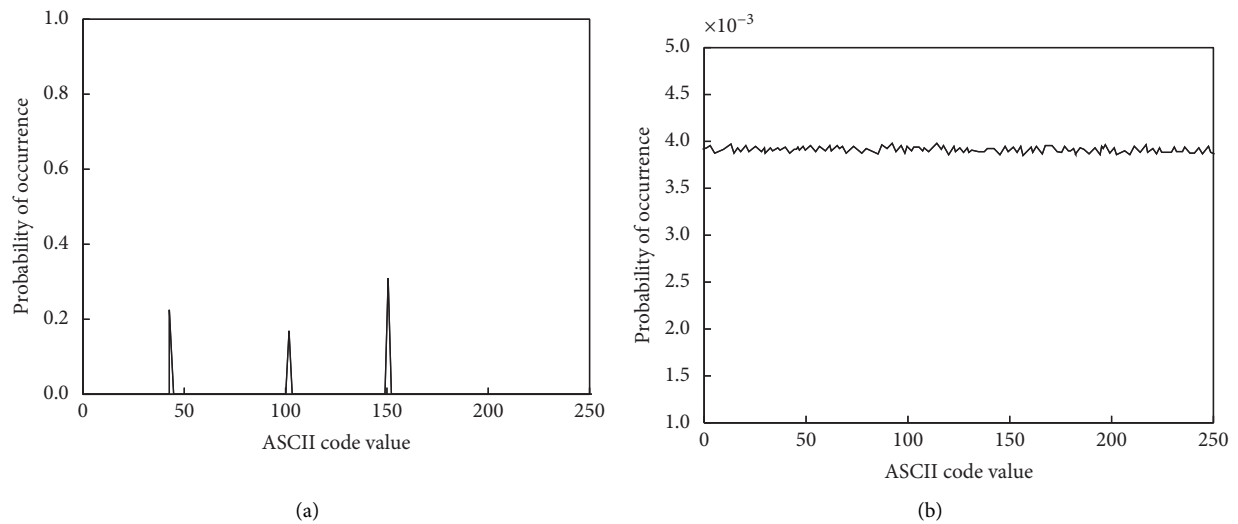


FIGURE 13: ASCII distributions. (a) Plaintext. (b) Ciphertext.

4.3. Statistical Analysis. In order to verify the randomness of the ciphertext after performing the encryption algorithm, this experiment will perform a statistical analysis of the length of the ciphertext, with 0 and 1 as the criteria, and the number of ciphertexts is 0 or 1, indicating that they are roughly the same. The statistical analysis table is shown in Table 3.

From the above table, it can be seen that after encryption by encryption algorithm, ciphertext of different lengths can be obtained. The number of “0” and “1” in the ciphertext is very close to each other and gets closer after increasing the length continuously, indicating that the ciphertext data achieve the 0-1 balance objective.

In the plaintext, the ASCII distribution is uneven. After encryption, the ASCII distribution gradually tends to be homogeneous, which means that the encryption algorithm can effectively defend against probabilistic attacks. The ASCII distributions of both are shown in Figure 13.

As can be seen from the above graph, the plaintext ASCII distribution shows a large undulating peak at 50, 100, and 150, indicating a higher probability of aggressiveness and a

lower defensibility in the plaintext, which makes it vulnerable to external intrusion and threats. After encrypting the plaintext, the ASCII code values shown in Figure 13(b) are obtained. It can be seen that the probability of ASCII code values is all around 40%, which indicates that they are very evenly distributed and further proves that the encrypted ciphertext is more defensive and less likely to be attacked.

4.4. SP 800-22 Test. In order to test whether the ciphertext sequence is secure after using the encryption algorithm, this experiment is conducted to test 15 information security items of SP800-22. There are 1 million bytes in this ciphertext, and it is divided into 400 copies equally. The test results of this information are as follows. If all the P values in the table are more than 0.01, it indicates that the ciphertext sequence information meets the criteria.

As can be seen from Table 4, the P values of the ciphertext sequences are all above 0.01, with the lowest being 0.012351 and the highest being 0.943113. The experimental results show that all the above sequences meet the standard

TABLE 4: SP 800-22 test.

Statistical test	<i>P</i> value	Result
Frequency	0.403216	PASS
Block frequency	0.943113	PASS
Cumulative sums (forward)	0.409276	PASS
Cumulative sums (reverse)	0.545923	PASS
Runs	0.635289	PASS
Longest run	0.246932	PASS
Rank	0.513486	PASS
FFT	0.160782	PASS
Nonoverlapping template	0.172193	PASS
Overlapping template	0.194653	PASS
Universal	0.775869	PASS
Approximate entropy	0.764231	PASS
Random excursions	0.812351	PASS
Random excursions variant	0.797955	PASS
Serial (<i>P</i> value1)	0.667959	PASS
Serial (<i>P</i> value2)	0.791328	PASS
Linear complexity	0.401947	PASS

TABLE 5: Comparison results of running speed and memory consumption of the three algorithms.

Encryption algorithm	Speed (byte/ms)	Memory (bytes) consumption
RC5 [29]	12.82	268
CWSN [30]	16.58	160
The algorithm designed in this paper	18.51	96

and satisfy the requirements of wireless sensor information security protection.

4.5. Running Speed and Memory Consumption. In order to test the suitability of the designed encryption algorithm in wireless sensor networks, the experiment will test the algorithm in terms of its running time and memory consumption and compare the algorithm with the traditional encryption algorithms RC5, SKIPJACK, and CWSN to obtain the following results.

It is obvious from Table 5 that the designed algorithm runs at 18.51byte/ms, which is 5.7, 7.28, and 1.93 higher than that of the other three algorithms, respectively, indicating that the algorithm runs faster; the memory consumption of the proposed algorithm is 96, and that of the other three algorithms is 268, 356, and 160, which exceeds that of the algorithm proposed in the study by 172, 260, and 64. After comprehensive analysis, it is shown that the proposed algorithm runs the fastest and takes up the least memory in wireless sensor networks and is very suitable for the operation of wireless sensor network.

5. Conclusion

In summary, the proposed identity encryption algorithm for hybrid chaotic systems can be applied to wireless sensor network security protection, which can solve the problems of complex node resources and small memory of wireless sensor networks, and the algorithm can further enhance the defense capability of ciphertext and reduce the attack probability. The experimental results suggest that with different ciphertext lengths, the ciphertext information

entropy is close to 8 after using the improved encryption algorithm, the ciphertext randomness is significantly improved, and the performance of the hybrid chaotic system is enhanced. With the number of ciphertext encryption rounds close to 4, the resource loss of the wireless sensor network is minimized, thus simplifying the network nodes, reducing the computational cost, and improving the network security. Finally, after comparing the proposed algorithm with the traditional encryption algorithm, it is found that the improved algorithm has better confusion and diffusion effects than the traditional algorithm, and the algorithm has better performance. The operation speed is faster than that of other algorithms, and the memory consumption is smaller. Comprehensively, it can be seen that the proposed algorithm can be applied and promoted in wireless sensing networks. However, due to the experimental conditions and insufficient research experience, this experiment only encrypted text information, and the proposed algorithm cannot encrypt images and other types of information well, and thus there are certain limitations, and in the future, we will start from this aspect and apply the algorithm to information such as images and videos to improve the performance and applicability of the algorithm.

Data Availability

The experimental data used to support the findings of this study are available from the corresponding author upon request.

Conflicts of Interest

The authors declare that they have no conflicts of interest.

References

- [1] B. Maram, J. M. Gnanasekar, G. Manogaran, and M. Balaanand, "Intelligent security algorithm for UNICODE data privacy and security in IOT," *Service Oriented Computing and Applications*, vol. 13, no. 1, pp. 3–15, 2019.
- [2] A. Ahmad, N. A. Muhammad, M. Zeyad, and A. Bareeq, "A hybrid network security algorithm based on Diffie Hellman and Text-to-Image Encryption algorithm," *Journal of Discrete Mathematical Sciences and Cryptography*, vol. 22, no. 1, pp. 65–81, 2019.
- [3] C. Liang, Q. Zhang, J. Ma, and K. Li, "Research on neural network chaotic encryption algorithm in wireless network security communication," *EURASIP Journal on Wireless Communications and Networking*, vol. 2019, no. 1, pp. 1–10, 2019.
- [4] A. P. Deng and B. Xiao, "Application of chaotic encryption algorithm in RFID secure mechanism," *Advanced Materials Research*, vol. 532-533, no. 532-533, pp. 1695–1699, 2012.
- [5] X. Zhang, S. Yu, P. Chen, J. Lü, J. He, and Z. Lin, "Design and ARM-embedded implementation of a chaotic secure communication scheme based on H.264 selective encryption," *Nonlinear Dynamics*, vol. 89, no. 3, pp. 1949–1965, 2017.
- [6] J. Ge, Z. Sheng, L. Lang, and Z. Yi, "Hybrid chaotic encryption algorithm for securing DICOM systems," *International Journal of Performability Engineering*, vol. 15, no. 5, pp. 1436–1444, 2019.
- [7] T. Wu, C. Zhang, Y. Chen et al., "Compressive sensing chaotic encryption algorithms for OFDM-PON data transmission," *Optics express*, vol. 29, no. 3, pp. 3669–3684, 2021.
- [8] Z. Zhang and S. Yu, "On the security of a Latin-bit cube-based image chaotic encryption algorithm," *Entropy*, vol. 21, no. 9, p. 888, 2019.
- [9] M. Noor, K. Majid, J. S. Sajjad, and M. H. Mohammad, "Cryptanalysis of hybrid secure image encryption based on Julia set fractals and three-dimensional Lorenz chaotic map," *Mathematics and Computers in Simulation*, vol. 190, pp. 826–836, 2021.
- [10] G. Qiu, C. Wang, S. Luo, and W. Xu, "A dual dynamic key chaotic encryption system for industrial cyber-physical systems:LETTER," *IEICE Electronics Express*, vol. 17, no. 24, p. 20200389, 2020.
- [11] Q.-y. Zhang, Y.-z. Li, and Y. jie Hu, "A retrieval algorithm for encrypted speech based on convolutional neural network and deep hashing," *Multimedia Tools and Applications*, vol. 80, no. 1, pp. 1201–1221, 2020.
- [12] F. Wang, B. Zhu, K. Wang, M. Zhao, L. Zhao, and J. Yu, "Physical layer encryption in DMT based on digital multi-scroll chaotic system," *IEEE Photonics Technology Letters*, vol. 32, no. 20, pp. 1303–1306, 2020.
- [13] L. Yin and N. Hassan, "Multi-level encryption algorithm for user-related information across social networks," *Open Physics*, vol. 16, no. 1, pp. 989–999, 2018.
- [14] X. Wang and S. Chen, "Chaotic image encryption algorithm based on dynamic spiral scrambling transform and deoxy-ribonucleic acid encoding operation," *IEEE ACCESS*, vol. 8, pp. 160897–160914, 2020.
- [15] M. Wang, X. Wang, Y. Zhang, and Z. Gao, "A novel chaotic encryption scheme based on image segmentation and multiple diffusion models," *Optics & Laser Technology*, vol. 108, pp. 558–573, 2018.
- [16] Yi Kang, L. Zhang, and D. Zhang, "Study of an encryption system based on compressive temporal ghost imaging with a chaotic laser," *Optics Communications*, vol. 426, pp. 535–540, 2018.
- [17] Y. Xiao, J. Cao, Z. Wang, and C. Long, "Polar coded optical OFDM system with chaotic encryption for physical-layer security," *Optics Communications*, vol. 433, pp. 231–235, 2018.
- [18] L. Kraveva, V. Rijmen, and N. L. Manev, "Correlation Distribution Analysis of a Two-Round Key-Alternating Block Cipher," *Tatra Mountains Mathematical Publications*, vol. 73, no. 1, pp. 109–130, 2019.
- [19] C.-S. Chen, X. Yu, Y. X. Xiang, X. Li, and T. Li, "An improved DPA attack on DES with forth and back random round algorithm," *International Journal on Network Security*, vol. 19, no. 2, pp. 285–294, 2017.
- [20] J. Wang, H. Xu, and M. Yao, "Improvement of the round key generation of AES," *International Journal of Communications, Network and System Sciences*, vol. 05, no. 12, pp. 850–853, 2012.
- [21] Y. Luo, D. Zhang, and J. Liu, "A chaotic block cryptographic system resistant to power analysis attack," *International Journal of Bifurcation and Chaos*, vol. 29, no. 8, p. 13, 2019.
- [22] H. Mai, E. E. Rabaie, M. E. Ibrahim, and F. E. Samie, "3-D image encryption based on rubik's cube and RC6 algorithm," *3D Research*, vol. 8, no. 4, 2017.
- [23] E. B. Villanueva, B. G. Gerardo, and R. P. Medina, "Implementation and performance assessment of the enhanced RC5 (ERC5) algorithm based on addition-then-append key expansion technique[J]," *IOP Conference Series: Materials Science and Engineering*, vol. 482, no. 1, 2019.
- [24] A. Abidi, C. Guyeux, and M. Machhout, "Statistical analysis and security evaluation of chaotic RC5-CBC symmetric key block cipher algorithm," *International Journal of Advanced Computer Science and Applications*, vol. 10, no. 10, 2019.
- [25] S. Kumar, K. Patidar, R. Kushwah, and S. Chouhan, "Text data partitioning and image based RC5 encryption with block based key generation," *International Journal of Advanced Technology and Engineering Exploration (IJATEE)*, vol. 4, no. 31, 2017.
- [26] V. Manikandan and R. Amirtharajan, "On Dual Encryption with RC6 and Combined Logistic Tent Map for Grayscale and DICOM," *Multimedia Tools and Applications*, vol. 80, pp. 1–30, 2021.
- [27] A. I. Sallam, E.-S. M. El-Rabaie, and O. S. Faragallah, "CABAC-based selective encryption for HEVC using RC6 in different operation modes," *Multimedia Tools and Applications*, vol. 77, no. 21, pp. 28395–28416, 2018.
- [28] R. Rajoriya, K. Patidar, and S. Chouhan, "An efficient image encryption algorithm based on RK-RC6," *ACCENTS Transactions on Information Security (TIS)*, vol. 3, no. 9, 2018.
- [29] Y. Chen, S. Su, H. Yin et al., "Optimized non-cooperative spectrum sensing algorithm in cognitive wireless sensor networks," *Sensors (Basel, Switzerland)*, vol. 19, no. 9, p. 2174, 2019.
- [30] P. S. Chatterjee and M. Roy, "Maximum match filtering algorithm to defend spectrum-sensing data falsification attack in CWSN," *International Journal of Wireless and Mobile Computing*, vol. 15, no. 2, pp. 113–122, 2018.

Research Article

A Sentiment Classification Model of E-Commerce User Comments Based on Improved Particle Swarm Optimization Algorithm and Support Vector Machines

Xuehui Jiang 

College of Information Engineering, Zhengzhou University of Industrial Technology, Xinzheng 451150, China

Correspondence should be addressed to Xuehui Jiang; 002664@zzgyxy.edu.cn

Received 17 November 2021; Revised 21 January 2022; Accepted 25 January 2022; Published 1 April 2022

Academic Editor: Hangjun Che

Copyright © 2022 Xuehui Jiang. This is an open access article distributed under the Creative Commons Attribution License, which permits unrestricted use, distribution, and reproduction in any medium, provided the original work is properly cited.

With the rapid increase of the number of Internet users and the amount of online comment data, a large number of referable information samples are provided for data mining technology. As a technical application of data mining, text sentiment classification can be widely used in public opinion management, marketing, and other fields. In this study, a combination approach to SVM (support vector machine) and IPSO (improved particle swarm optimization) is proposed to classify sentiment by using text data. First, the text data of 30,000 goods reviews and corresponding ratings are collected through the web crawler. Then, TFIDF (term frequency-inverse document frequency) and Word2vec are used to vectorize the goods review text data. Next, the proposed classification model is trained by the SVM, and the initial parameters of the SVM are optimized by the IPSO. Finally, we applied the trained SVM-IPSO model to the test set and evaluated the performance by several measures. Our experiment results indicate that the proposed model performed the best for text data sentiment classification. Additionally, the traditional machine learning model SVM becomes very effective after parameter optimization, which demonstrates that the parameters' optimization by IPSO has successfully improved the classification accuracy. Furthermore, our proposed model SVM-IPSO significantly outperforms other benchmark models, indicating that it could be applied to improve the accuracy and efficiency for text data sentiment classification.

1. Introduction

Natural language processing (NLP) refers to the technology of processing human's unique natural language with computer as a tool, which is an important content in the field of artificial intelligence and computer science [1]. Emotional analysis is one of the directions of natural language processing, also known as emotional extraction or opinion mining, and it is a hot topic in text mining [2]. Text information mining can be applied to many aspects, such as user feedback, comment information, advertising recommendation after intelligent analysis, public opinion detection of government departments, and processing of uncivilized and untrue information.

Dave et al. designed the earliest emotion analysis tool [3]. Go et al. used the training set data designed by Hashtag to classify multiple topic-based clusters [4]. Joshi et al. designed

a set of emotional analysis systems, which divided microblog comments into positive and negative emotions based on certain characteristics of the microblog, such as emoticons [5]. Gamon et al. used the function of clustering to obtain users' opinions and analyzed the tendency and intensity of emotional evaluation on cars [6]. Li et al. completed the emotional analysis by feature selection and extraction using SVM, Bayesian classification, and N-element language methods [7]. Li Guwei et al. constructed an unsupervised thematic emotion model to achieve emotion classification [8]. Jasson et al. applied CNN to text and made accurate predictions with the help of one-dimensional structure (word order) of text data [9]. Yoom Kim uses convolution to achieve a sentence-level classification model for English text. Xue et al. proposed a classification model based on convolutional neural network and gating mechanism [10]. Parupalli et al. constructed a corpus with systematic

annotation [11], which supports the use of word-level annotation to enhance emotion analysis tasks. Angelidis et al. proposed an attention-based polarity scoring method for positive and negative text fragments [12]. Gui et al. proposed to extract text emotional reasons through further modeling of context information on the basis of emotion classification [13]. Yuan et al. used a global decoder feedforward network to realize the recognition of multilanguage text, laying a foundation for complex text analysis [14]. Bordoloi et al. designed an effective emotional analysis model, which carried out an advanced analysis on mobile phone comments collected by e-commerce sites based on the graph keyword extraction method [15]. Convolutional neural network (CNN) has been widely applied in many fields such as image recognition and NLP (for example, convolutional neural network [16] has been used to classify texts in social networks emotionally based on graph convolutional neural network [17]. Some scholars have used deep neural network for emotion classification and natural language processing [18]. Other studies have classified text emotions through attentional neural network [19]), and other fields [20]. However, CNNs contain multiple convolutional layers and pooling layers, which require more parameters and require a large cost of parameter optimization and adjustment. At the same time, the problem of gradient disappearance or gradient explosion exists in the CNNs, which limits the accuracy of text classification.

The classification of positive and negative emotions using support vector machine has a good execution efficiency, but the parameters of the support vector machine model are the key factor to determine the prediction accuracy. Therefore, the researchers introduce a particle swarm optimization algorithm (PSO) to optimize the parameters to obtain high accuracy. PSO is an important branch of intelligent optimization algorithm [21] and is proposed in 1995 [22]. The standard PSO algorithm has good performance in solving a variety of nonlinear optimization problems. It controls the entire iterative process with the help of individual optimization and group optimization and has fast convergence speed and high execution efficiency. However, in the late iteration, the diversity of individual particles in the population is small. If the position of the global optimal and local optimal is equal to that of particle, after a certain number of iterations, the algorithm may fall into local optimal, resulting in poor global performance. To improve the performance of PSO, the inertial weight introduced by Shi et al. in 1988 played a key role in improving the performance of PSO [23]. In this study, the adaptive decreasing inertia strategy and crossover operator are combined to improve the searching quality of particle swarm optimization algorithm, and the parameters of the SVM model are optimized with the improved algorithm to further improve the prediction accuracy. Compared with other emotion analysis models, the training speed of this model is faster and the prediction accuracy is better.

The main contribution about this study is (1) the text data of 30,000 goods reviews and corresponding ratings are collected through the web crawler and (2) TFIDF and Word2vec are used to vectorize the goods review text data.

The research results demonstrate that the SVM-IPSO makes up for the deficiency of traditional emotional dictionary which is affected by word order and different contexts and solves the problem of local optimization. Our research avoids the problem of gradient disappearance or dispersion when using convolution, reduces the cost of parameter optimization and adjustment, has higher operation efficiency and accuracy, and can predict text emotion well. The main implication of our study is that the text sentiment classification model proposed by us can be widely used in public opinion management, marketing, and other fields. Help practitioners to provide detailed analysis and portraits of customer reviews.

2. Data Preparation

Before classification, data preparation including data acquisition and preprocessing is necessary.

2.1. Comment on Data Acquisition. Data acquisition can be divided into URL queue acquisition, related web page parsing, data crawling, data cleaning, and data storage.

First, the goods comments' data are extracted from Taobao e-commerce platform. Taobao e-commerce goods comments are a five-star rating mechanism, with one star to five stars: very poor, poor, ok, recommendation, and strong recommendation; in this experiment, one-star and two-star comments were regarded as negative comments, while four-star and five-star comments were regarded as positive comments. Then, based on Scrapy framework to achieve data capture, we generate the corresponding positive and negative emotional comments' csv file. Finally, through further screening, 21000 positive comments and negative comments were obtained 9000, of which 2/3 were used as the training set and 1/3 as the test set. The distribution of experimental data is listed in Table 1.

To obtain the datasets of sufficient scale, it is necessary to realize the simulated login in the crawling process and break through the limitation of web crawler. At the same time, a comment may be incomplete in the current page. Scrapy has a default de-duplication mechanism, which will determine that the second time is repeated crawling, so the problem of URL duplication needs to be solved.

2.2. Text preprocessing. Text preprocessing is to further process the original data to make the data into the next operable object. Word preprocessing consists of word repetition, noise, word segmentation, and word stopping.

- (1) Text weight: there are not only repeated words in the preprocessed text, resulting in storage redundancy, but also an increased amount of calculation, so it is necessary to traverse in duplicate.
- (2) Text denoising: some disturbing words or garbled characters appear in the text, which need to be denoised and improve the accuracy of analysis.
- (3) Word segmentation: the words in the text are segmented and given corresponding parts of speech in

TABLE 1: Data distribution of experimental corpus.

	Number of comments	Positive comments	Negative comments
Training data	20000	14000	6000
Test data	10000	7000	3000

combination with the dictionary. In English, each word is separated by a space, so it is easy to process, while Chinese word segmentation has high requirements on the comprehensive accuracy of the dictionary, so this paper adopts jieba word segmentation in Python language environment.

- (4) Remove stop words: stop words refer to modal particles, adverbs, prepositions, conjunctions, etc., which are not helpful to the experimental results and can be summarized into the stop words list and removed.

2.3. Word Vectorization. Text is unstructured or semi-structured data, which cannot be recognized by SVM classifier. Therefore, the text needs to be transformed into vector form for further analysis and processing. Lexicographical quantization refers to the expression of words in the vector form; at the same time, it is necessary to ensure the correlation of the processed vectors in semantic similarity and relative similarity. Word vectorization can map words or phrases into real number vectors and reduce the features of higher dimensional vector space to lower dimensional space. There are many models to transform words into a real number vectors, such as implicit Dirichlet location (LDA) and implicit semantic analysis (LSA). However, the calculation amount of the above model will increase sharply with the increase of the total amount of data, and word2vec solves this problem well and improves the efficiency.

Word2vec is a deep learning multilayer neural network structure opened by Google in 2013, which can be trained to simplify the processing of text content with K-dimensional vector operations. Its main structure consists of the following component: input layer, several hidden layers, and an output layer. It transforms all feature words into vector values after matching, to give a deeper feature representation of text data. Based on this, this study uses word2vec to realize word vectorization. Assume that the preprocessed text comment are composed of N words, as shown in Table 1, $d_N = w_1, w_2, \dots, w_N$. First, Sogou news corpus is trained by the Skip_gram model in Word2vec; next, the word2vec vector of each word in d_N is calculated by the trained model; because word2vec ignored the importance of words in text comments, the TFIDF model was trained according to the goods review data to obtain the TFIDF weight of each word in the goods review and multiply it by the corresponding word2vec vector. Finally, the support vector machine can recognize the input, and the final vector of each goods review is D :

$$D = \frac{\left(\sum_{i=1}^N \text{word 2 vec}(w_i) \times \text{tfidf}_{w_i}\right)}{N} \quad (1)$$

3. Methods

3.1. The SVM Classification. Supporting vector machine can construct a hyperplane to maximize the distance between positive and negative poles in the decision surface. The main idea is shown in Figure 1.

In Figure 1, four-pointed stars and circles, respectively, represent two types of samples, and SVM maximizes the straight-line distance of these two types of samples. Supposing $x_1 = \{x_i, i \in I_1\}$ and $x_2 = \{x_i, i \in I_2\}$ two training sets, the label of X_1 is +1 and the label of X_2 is -1:

$$\begin{aligned} m &= |I_1|, \\ k &= |I_2|, \\ l &= m + k, \\ X &= X_1 \cup X_2. \end{aligned} \quad (2)$$

When X_1 and X_2 are linearly separable, SVM separates these two types of sample points without error by constructing a linear classification hyperplane, and the classification hyperplane is

$$\begin{aligned} H: \langle \omega \cdot x \rangle &= \lambda, \\ X_2 &= \{x_i, i \in I_2\}. \end{aligned} \quad (3)$$

SVM proposes an optimal plane classification under the condition of linear separability, requiring the model not only to distinguish data without error but also to maximize the classification gap. Linear discriminant functions in multidimensional space are generally expressed as

$$g(x) = wx + b. \quad (4)$$

The equation of the classification surface is ab , and the discriminant function is normalized so that the distance between the two kinds of sample books and the optimal plane is greater than or equal to one.

At this point, the sample closest to the classification plane satisfies $|g(x)| = 1$ so that the sample of equation (5) is the support vector:

$$y_i(w \cdot x_i + b) \geq 1, i = 1, 2, 3, \dots, n. \quad (5)$$

Classification interval is $2/w$, and the minimum of $w^2/2$ is equivalent to the maximum interval, which satisfies $\phi(w) = w^2/2$; at the same time, the classification surface satisfying equation (5) is the optimal classification surface. However, the samples are not linearly separable, that is, SVM algorithm cannot run a solvable scheme. To this end, the set of slack variables is $\xi = (\xi_1, \xi_2, \dots, \xi_n)$:

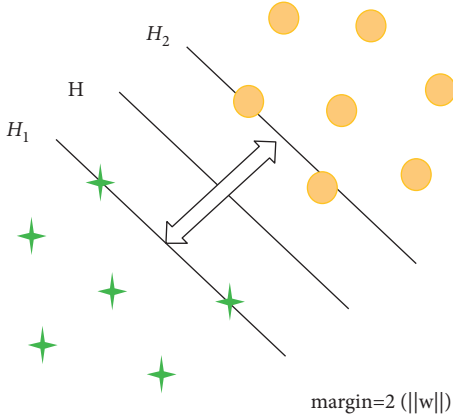


FIGURE 1: SVM classification model.

$$\xi_i^* = \begin{cases} 0, & |f(x) - y_i| < \varepsilon, \\ |f(x) - y_i| - \varepsilon, & |f(x) - y_i| > \varepsilon. \end{cases} \quad (6)$$

Nonlinear problems can be transformed into linear problems by the use of the loss function ε , penalty parameter C , and slack variable ξ , to minimizing the error rate while realizing the sample separation, and the specific formula is as follows:

$$\begin{aligned} \min_{\omega, b, \xi} \phi &= \frac{1}{2} \omega^T \cdot \omega + C \sum_{i=1}^n (\xi_i + \xi_i^*) \text{ s.t. } (w \cdot x_i + b) - y_i \leq \varepsilon + \xi_i, \\ y_i - (w \cdot x_i + b) &\leq \varepsilon + \xi_i^*. \end{aligned} \quad (7)$$

The Lagrange factors a_i and a_i^* are obtained by solving the duality problem. The coefficients of the regression equation are

$$w = \sum_{i=1}^l (a_i - a_i^*) x_i. \quad (8)$$

Using the Gaussian RBF,

$$k(x_i, x) = N(x_i - x; 0, \sigma^2 I), \quad (9)$$

where $N(x; \mu; \Sigma)$ is the standard normal distribution. The point product is replaced by kernel estimation, and the expression of the discriminant function is

$$f(x) = \sum_{i=1}^l (a_i - a_i^*) K(x_i, x) + b. \quad (10)$$

Loss function ε , penalty parameter C , and kernel function parameter σ determine the performance of support vector machines. The loss function ε is the error expectation of the estimation function, which affects the number of support vectors to a certain extent; if the penalty parameter C is too small, it will lead to underlearning, and if it is too large, it will lead to overlearning; σ is a parameter of the kernel function, which reflects the characteristics of the training set and determines the complexity of

understanding. Therefore, the selection of parameters selection plays a very important role in classification efficiency and accuracy; in this research, the improved PSO algorithm is used to achieve parameter optimization.

3.2. Improved PSO. PSO algorithm is derived from the research on the foraging behavior of birds [24], and this algorithm firstly randomly initializes a group of particles, each particle is a feasible solution to the optimization problem, and the fitness is determined according to the objective function. The particle moves in the direction of the current optimal particle; the optimal solution is obtained through generation by generation search. There are two extreme values in each generation population, the optimal solution p_{best} is found by the particle itself, and the optimal solution of g_{best} is found by the whole population. According to these two extreme values, each particle keeps updating and generates a new generation of population. Once these two extremes are found, the particle's position and velocity are updated as follows:

$$\begin{aligned} v_{id}' &= \omega v_{id} + c_1 \text{rand}() (P_{id} - X_{id}) + c_2 \text{rand}() (P_{gd} - X_{id}), \\ X_{id}' &= X_{id} + v_{id}', \end{aligned} \quad (11)$$

where ω is the inertial weight, nonnegative, c_1 and c_2 are nonnegative constants, and v_{id} represents the velocity of the i th particle in the D th dimension. Studies show that the acceleration coefficient should satisfy $c_1 + c_2 < 4(1 + \omega)$ [25]. Martniez et al. proposed that $c_1 = c_2$ can maximize the second-order stability region [26]. In addition, equal acceleration coefficients can give the same weight to all optimal values (global and local) to avoid the algorithm falling into local optimization at the beginning. P_{id} and P_{gd} are the individual and global optimal values of the corresponding dimensions. $\text{rand}()$ generates random numbers between $(0, 1)$.

3.2.1. Improvement of Inertia Weight. The adjustment of inertia weight can be divided into four categories: constant [23], random number [27], time-varying, and adaptive inertia weights. In the initial stage, the step size is large and large inertial weights ω are required. The middle and later stages require strong local development ability, requiring smaller ω . To improve the optimization efficiency and avoid falling into local optimal, this study constructs an inertia decreasing strategy, which gradually reduces the value of ω in the iterative process, introduces the vector h with K elements (K is a constant), and obtains the following algorithm, where k is the modulus of the current iteration number t with respect to K ; $\omega(t)$, ω_{start} , and ω_{end} are the current, start, and stop inertial weights. When the particles' optimal positions are close to each other, $\omega(t)$ increases the reverse trend, preventing premature convergence, and the particles explore more. With each iteration K times, the weight will gradually decrease, thus enhancing the local

optimization ability of the particle and finally effectively improving the optimization ability:

$$\begin{aligned} h(k) &= \max_{1 \leq j \leq D} \{ \text{std}(P_{gd}(t) - X_{id}(t)) \}, 1 \leq k \leq K, \\ \omega(t) &= \omega_{\text{start}} - \omega_{\text{end}} \frac{h(k)}{\max_{1 \leq k \leq K} \{h(k)\}}. \end{aligned} \quad (12)$$

3.2.2. Introducing Crossover Operator. To avoid the possibility of proposed algorithm falling into local optimum at the end of iteration, a crossover operator is introduced to enhance the information exchange between particles. The search process is controlled by individual optimization, population optimization, and individual genetic operation, so as to make up for the defect that it is easy to fall into local optimization so that the proposed method can jump out of local optimization and get the global optimal solution.

3.2.3. Simulation. To evaluate the effectiveness of PSO-W-GA algorithm, four benchmark functions of Sphere, Schewefel, Rastrigin, and Rosenbrock in CEC2014 were selected to evaluate the algorithm's performance. The comparison between the proposed method and the improved method is as follows: (1) standard PSO, (2) APSO, where $\omega = 1/1 + 1.5\exp(-2.6f) \in [0.4, 0.5]$, f is the evolutionary factor calculated by the distance between particles, and (3) AIWPSO, where $\omega = S(t)/N \in [0, 1]$, N is the population size and $S(t)$ is the best position of the population at t time.

According to experience, the value range of ω is $[0.4, 0.9]$ [28]. In this study, $\omega_{\text{start}} = 0.9$, $\omega_{\text{end}} = 0.4$, $c_1 = c_2 = 1.5$, population size is 30, and maximum iteration number is 1000, K is 100, and particle dimension is 30. To evaluate the results of the algorithm, the maximum number of calculation function values is set as FE_S [29]:

$$FE_S = N \times T = N \times 10000 \times \frac{D}{N}. \quad (13)$$

We added the traditional RNN model and CNN model in the simulation experiment for full comparison and experiment; Table 2 shows the experiments results for all listed algorithm.

In Table 2, f_1, f_2, f_3 , and f_4 are the test functions Sphere, Schewefel, Rastrigin, and Rosenbrock in Table 2, respectively. Mean and SD, respectively, represent the mean and standard deviation obtained after running the function. According to Table 2 and Figures 2–5, it can be found that the improved algorithm can converges quickly in the above four test functions and outperforms others in the optimal value of convergence.

Figures 2–5 indicates that, under the four evaluation functions, W-GA-PSO algorithm proposed in this study has the fastest convergence speed, the smallest error, and the highest performance, followed by APSO algorithm, which is slightly inferior to the model proposed by us. Then, AIPSO algorithm ranked third, and PSO algorithm had the worst performance, with poor performance in all evaluation indicators. The experiment proved that the model proposed by us could quickly and accurately help the emotion

classification model to optimize parameters and achieve good classification results.

4. Proposed Model

This study combines the characteristics of PSO global optimization and SVM fast classification and proposes the SVM model optimized by improved PSO to achieve emotion classification. The specific implementation steps are as follows.

- (1) Crawl the comment information from the web page and preprocess the text
- (2) The comments' data were divided into training and test sets with corresponding positive and negative labels.
- (3) Sogou news corpus is trained by the Skip_gram model in Word2vec; next, the word2vec vector of each word in d_N is calculated by the trained model.
- (4) Train the TFIDF model according to the goods review data of this experiment, and obtain the TFIDF weight tfidf_{ω_i} of each word in the goods review.
- (5) The word vector of each goods review is obtained through equation (1), which is used as the input of the support vector machine.
- (6) Initialize the loss function ε , penalty parameter C , and kernel function parameter s of the support vector machine, regard the vector (ε, c, σ) as a particle, define $c_1 = c_2 = 2$ according to the experience, and use formulas (10) and (12) to generate r_1, r_2 , and ω .
- (7) Define fitness function:

$$F_{\text{fitness}} = \frac{1}{m} \sum_{i=1}^m (f_i - y_i)^2, \quad (14)$$

where f_i, y_i , and m represent the prediction value, actual value, and the number of samples, respectively.

- (8) The fitness value of each particle is calculated according to the fitness function, and if the current fitness value is less than the previous fitness value, the original P_{best} is replaced; otherwise, it remains unchanged.
- (9) Take the smallest p_{best} and compare it with g_{best} ; if $P_{\text{best}} < g_{\text{best}}$, replace g_{best} with P_{best} ; otherwise, retain g_{best} .
- (10) The OX crossover operator of GA algorithm is used to generate new particles, and the adaptive values are calculated, and steps (8) and (9) are repeated to update g_{best} and p_{best} .
- (11) Judging whether the number of iterations is arrived maximum; if so, proceed to the next step; otherwise, increase the number of iterations by one and skip to step (6).

TABLE 2: Running results of each algorithm ($D = 30$).

f	Indicators	PSO	AIWPSO	APSO	PSO-W-GA	RNN	CNN
f_1	Mean	1.3×10^{-1}	8.7×10^{-2}	2.4×10^{-2}	1.8×10^{-2}	2.6×10^{-2}	2.8×10^{-2}
	SD	9.1×10^{-2}	1.7×10^{-3}	3.2×10^{-3}	1.5×10^{-3}	3.1×10^{-3}	2.4×10^{-3}
f_2	Mean	9.4×10^{-2}	3.7×10^{-2}	2.8×10^{-2}	2.3×10^{-2}	2.4×10^{-2}	2.6×10^{-2}
	SD	6.3×10^{-2}	4.7×10^{-3}	4.4×10^{-3}	1.4×10^{-3}	4.2×10^{-3}	3.2×10^{-3}
f_3	Mean	7.5	3.8	6.7×10^{-1}	2.4×10^{-1}	3.5×10^{-2}	3.8×10^{-2}
	SD	4.7×10^{-1}	1.5×10^{-1}	4.3×10^{-2}	7.8×10^{-2}	4.5×10^{-3}	4.1×10^{-3}
f_4	Mean	7.3	6.8	4.4	3.1	4.2×10^{-2}	3.9×10^{-2}
	SD	4.9×10^{-1}	3.4×10^{-1}	2.3×10^{-1}	6.5×10^{-2}	5.1×10^{-3}	5.4×10^{-3}

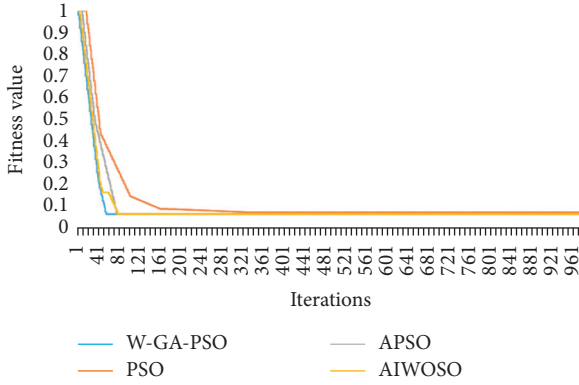


FIGURE 2: Test results for single peak function: sphere.

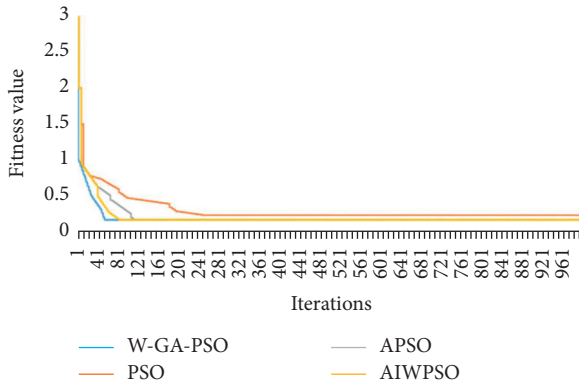


FIGURE 3: Test results for single peak function: Schewefel.

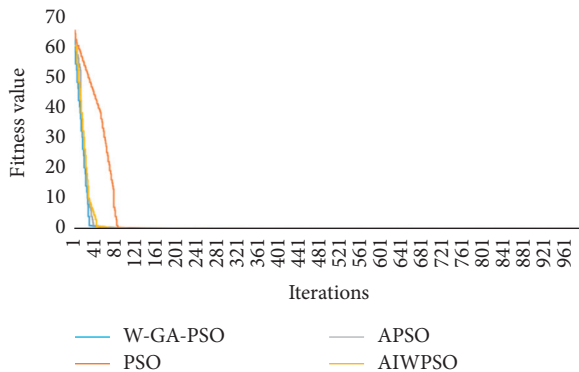


FIGURE 4: Test results for multimodal function: Rastrigin.

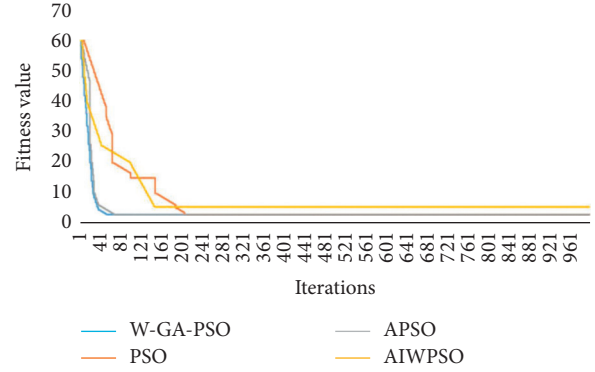


FIGURE 5: Test results for multimodal function: Rosenborck.

- (12) The SVM model was constructed according to the optimized parameters, and the feature vectors processed by weighted word2vec were classified, and the classification results were output.

In this study, the whole experiment process is shown in Figure 6.

5. Experiment Results

Prediction results can be divided into 4 categories: (1) TP, which refers to the number of positive predictions, (2) FN, the positive prediction is the negative quantity, (3) FP, which predicts the negative as the positive quantity, and (4) TN, the negative direction is predicted as the number of negative directions.

The accuracy of positive class is $P_{\text{pos}} = TP / (TP + EP)$; the positive recall rate is $R_{\text{pos}} = TP / (TP + EP)$. The positive class F_1 value is

$$F_1 = \frac{2 \times P_{\text{pos}} \times R_{\text{pos}}}{P_{\text{pos}} + R_{\text{pos}}}. \quad (15)$$

The accuracy rate and F_1 value were used as evaluation criteria. In our study, a total of 7000 positive comments and 3000 negative comments were selected for ROC curve drawing, and AUC was also used as the standard to evaluate the classification effect. The AUC values of SVM-IPSO are introduced Figures 6 in 7.

Finally, the classification effects under different models are compared in Table 3. The research results show that the

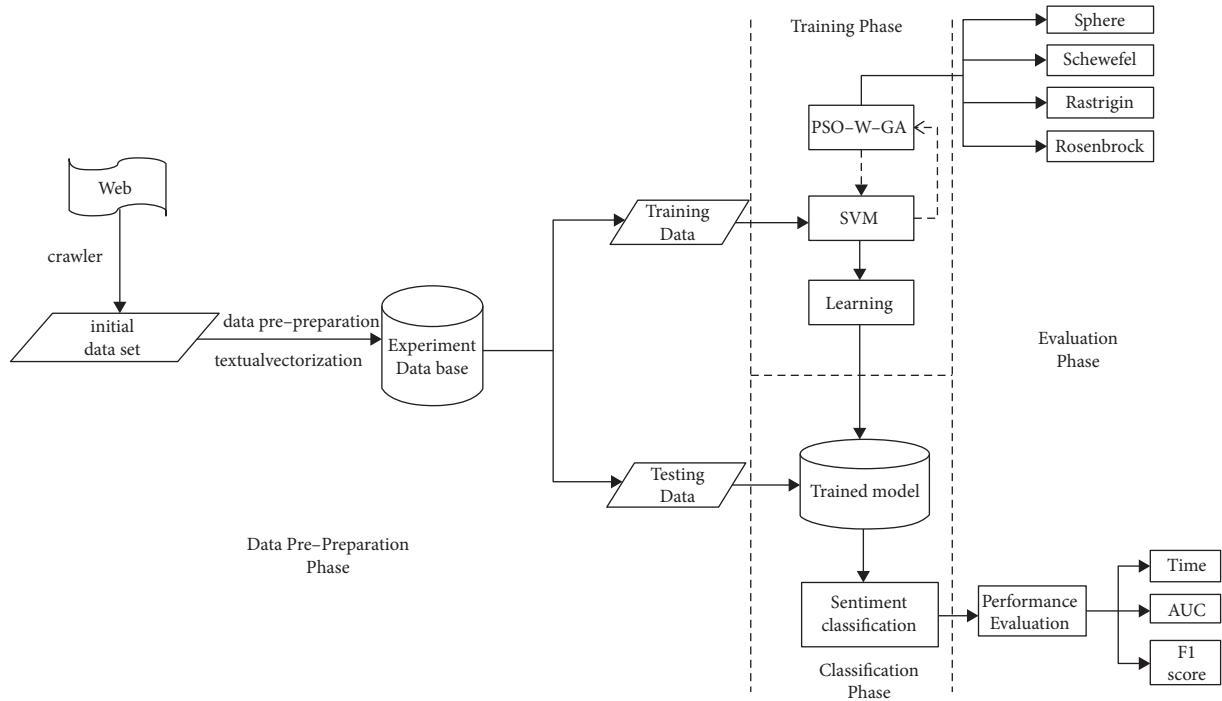


FIGURE 6: The structure of the proposed method.

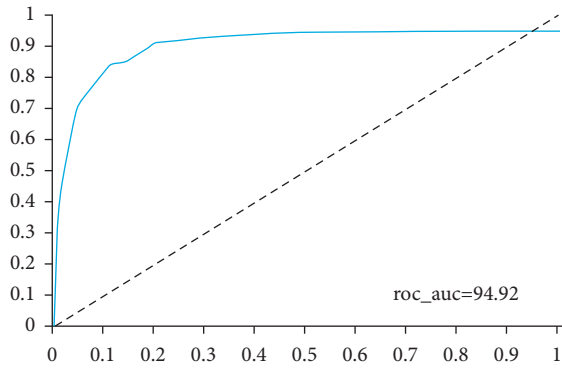


FIGURE 7: The AUC values of SVM-IPSO.

TABLE 3: Classification effect under different models.

Model	T (s)	Auc (%)	F1 (%)
Emotional dictionary	542	81.15	80.13
SVM	225	84.64	84.75
SVM + PSO	267	92.81	92.66
CNN	342	93.84	93.87
SVM + PSO-W-GA	283	94.92	94.82

proposed method has higher prediction accuracy and higher operation efficiency.

In terms of time consumption, emotion dictionary has the worst performance. Both SVM algorithm and our proposed algorithm are less than 300 s. Since we conduct parameter optimization on the basis of the SVM model, all time-consuming SVM algorithm is longer than the single SVM algorithm, and our proposed algorithm is significantly

better than other comparison algorithms in terms of accuracy and F1 score. This shows the effectiveness of our algorithm. In addition, the accuracy of CNN algorithm is also high. We will consider adding CNN algorithm into our combined model in future research to further improve the accuracy of our model for emotion classification.

6. Conclusion

In this research, we proposed an improved particle swarm optimization algorithm, and it is used to optimize SVM model parameters for Chinese text emotional classification. The kernel technique is used to learn the nonlinear model in SVM model, and the loss is reduced. The research results demonstrate that the SVM-IPSO makes up for the deficiency of traditional emotional dictionary which is affected by word order and different contexts and solve the problem of local optimization. Meanwhile, it avoids the problem of gradient disappearance or dispersion when using convolution, reduces the cost of parameter optimization and adjustment, has higher operation efficiency and accuracy, and can predict text emotion well. In the future, we will also continue to work on improving the algorithm to enhance the accuracy; at the same time, the experimental data in this study are all extracted from the Internet, so it is necessary to increase the data scale and verify the classification effect of the proposed model in large-scale data. This model has a good effect on binary classification problems, so we will consider extending the model to solve more complex classification problems. The limitations of our study is that the network comment text emotion classification may not be a second classification; we can set up more emotional

expression in mood for more accurate classification according to the quantitative, such as the design of the emotional scale to quantify the score values of emotions from low to high, so as to better provide effective decision support for managers.

Data Availability

The experimental data of this research are available upon request from the corresponding author.

Conflicts of Interest

All authors declared that they have no conflicts of interest regarding this study.

Acknowledgments

This work was supported by 2018 the backbone teachers Training Program of Henan Colleges and Universities (no. 2018GGJS183).

References

- [1] D. P. Morgan and C. L. Scofield, "natural language processing," *Neural Networks and Speech Processing*, vol. 8, pp. 245–288, Springer US, 1991.
- [2] H. Kaur and V. Mangat, "A survey of sentiment analysis techniques," in *Proceedings of the 2017 International Conference on I-SMAC (IoT in Social, Mobile, Analytics and Cloud) (I-SMAC)*, IEEE, Palladam, India, February 2017.
- [3] K. Dave, S. Lawrence, and D. M. Pennock, "mining the peanut gallery: opinion extraction and semantic classification of product reviews," in *Proceedings of the 12th international conference on World Wide Web*, ACM, NY, USA, May 2003.
- [4] A. Go, R. Bhayani, and L. Huang, "Twitter Sentiment Classification Using Distant supervision," pp. 1–6, 2009.
- [5] A. Joshi, A. R. Balamurali, and P. Bhattacharyya, "C-Feel-It: A Sentiment Analyzer for Micro-blogs," in *Proceedings of the International Conference on Networked Computing & Advanced Information Management*, IEEE Computer Society, Portland, Oregon, USA, June 2011.
- [6] M. Gamon, A. Aue, and S. Corston-Oliver, *Pulse: Mining Customer Opinions from Free Text*, Springer-Verlag, Heidelberg, Germany, 2005.
- [7] S. Li, C. R. Huang, and G. Zhou, "Employing personal/im-personal views in supervised and semi-supervised sentiment classification," in *Proceedings of the 48th Annual Meeting of the Association for Computational Linguistics*, DBLP, Uppsala Sweden, July 2010.
- [8] Y. G. Li, X. G. Zhou, Y. Sun, and Z. H. Guo, "Research and implementation of chinese microblog sentiment classification," *Journal of Software*, vol. 28, 2017.
- [9] R. Johnson and Z. Tong, "Effective use of word order for text categorization with convolutional neural networks," Eprint Arxiv, 2014, <https://arxiv.org/abs/1412.1058>.
- [10] X. Wei and L. Tao, "Aspect Based Sentiment Analysis with Gated Convolutional Networks," in *Proceedings of the Meeting of the Association for Computational Linguistics*, Melbourne, Australia, July 2018.
- [11] S. Parupalli, V. A. Rao, and R. Mamidi, "Bcsat: a benchmark corpus for sentiment analysis in Telugu using word-level annotations," *Student Research Workshop in 56th Annual Meeting of the Association for Computational Linguistics*, vol. 1, 2018.
- [12] S. Angelidis and M. Lapata, "Multiple instance learning networks for fine-grained sentiment analysis," *Transactions of the Association for Computational Linguistics*, vol. 6, pp. 17–31, 2017.
- [13] L. Gui, J. Hu, and Y. He, "A Question Answering Approach for Emotion Cause Extraction," in *Proceedings of the 2017 Conference on Empirical Methods in Natural Language Processing*, Copenhagen, Denmark, September 2017.
- [14] Y. Zhang, J. Riesa, D. Gillick, A. Bakalov, J. Baldrige, and D. Weiss, "A Fast, Compact, Accurate Model for Language Identification of Codemixed Text," 2018, <https://arxiv.org/abs/1810.04142>.
- [15] M. Bordoloi and S. K. Biswas, "Graph-Based Sentiment Analysis Model for E-Commerce Websites' Data," *Cognitive Informatics and Soft Computing. Advances in Intelligent Systems and Computing*, vol. 768, 2019.
- [16] M. Dong, Y. Li, X. Tang, J. Xu, S. Bi, and Y. Cai, "Variable convolution and pooling convolutional neural network for text sentiment classification," *IEEE Access*, vol. 8, no. 99, p. 1, 2020.
- [17] X. Liu, T. Tang, and N. Ding, "Social network sentiment classification method combined Chinese text syntax with graph convolutional neural network," *Egyptian Informatics Journal*, vol. 23, 2021.
- [18] T. Shoryu, L. Wang, and R. Ma, "A deep neural network approach using convolutional network and long short term memory for text sentiment classification," in *Proceedings of the 2021 IEEE 24th International Conference on Computer Supported Cooperative Work in Design (CSCWD)*, IEEE, Dalian, China, May 2021.
- [19] Y. Zhu, W. Zheng, and H. Tang, "Interactive dual attention network for text sentiment classification," *Computational Intelligence and Neuroscience*, vol. 2020, no. 3, pp. 1–11, Article ID 8858717, 2020.
- [20] Z. Bao and C. Wang, "A multi-agent knowledge integration process for enterprise management innovation from the perspective of neural network," *Information Processing & Management*, vol. 59, no. 2, Article ID 102873, 2022.
- [21] L. I. Rong-Yu, W. J. Zhang, and Z. Y. Zhou, "Improved PSO algorithm and its load distribution optimization of hot strip mills," *Computer Science*, vol. 45, 2018.
- [22] J. Kennedy, "Particle swarm optimization," in *Proceedings of the 1995 IEEE Int. Conf. Neural Networks*, vol. 4, no. 8, pp. 1942–1948, Perth, Australia, December 2011.
- [23] Y. Shi, "A Modified Particle Swarm Optimizer," in *Proceedings of the IEEE Icc Conference*, Anchorage, AK, USA, May 1998.
- [24] X.-F. Song, Y. Zhang, D.-W. Gong, and X.-Z. Gao, "A fast hybrid feature selection based on correlation-guided clustering and particle swarm optimization for high-dimensional data," *IEEE Transactions on Cybernetics*, pp. 1–14, 2021.
- [25] M. R. Rapaic and Z. Kanovic, "Time-varying PSO – convergence analysis, convergence-related parameterization and new parameter adjustment schemes," *Information Processing Letters*, vol. 109, no. 11, pp. 548–552, 2009.
- [26] J. L. F. Martínez and E. G. Gonzalo, "The PSO family: deduction, stochastic analysis and comparison," *Swarm Intelligence*, vol. 3, no. 4, pp. 245–273, 2009.
- [27] R. C. Eberhart and Y. Shi, "Tracking and optimizing dynamic systems with particle swarms," in *Proceedings of the 2001 Congress on Evolutionary Computation*, IEEE, Seoul, Korea (South), May 2001.

- [28] Y. H. Shi and R. C. Eberhart, "Empirical Study of Particle Swarm optimization," in *Proceedings of the Congress on Evolutionary Computation*, IEEE, Washington, DC, USA, August 2002.
- [29] J. J. Liang, B. Y. Qu, and P. N. Suganthan, "Problem definitions and evaluation criteria for the CEC 2014 special session and competition on single objective real-parameter numerical optimization," Technical report, Zhengzhou Univ, China, 2013.

Research Article

Research on Stock Price Time Series Prediction Based on Deep Learning and Autoregressive Integrated Moving Average

Daiyou Xiao ¹ and Jinxia Su²

¹*School of Finance, Central University of Finance and Economics, Beijing, China*

²*School of Business, Central University of Finance and Economics, Beijing, China*

Correspondence should be addressed to Daiyou Xiao; 2019110134@email.cufe.edu.cn

Received 7 December 2021; Revised 24 January 2022; Accepted 21 February 2022; Published 31 March 2022

Academic Editor: Hangjun Che

Copyright © 2022 Daiyou Xiao and Jinxia Su. This is an open access article distributed under the Creative Commons Attribution License, which permits unrestricted use, distribution, and reproduction in any medium, provided the original work is properly cited.

Different from traditional algorithms and model, machine learning is a systematic and comprehensive application of computer algorithms and statistical models, and it has been widely used in many fields. In the field of finance, machine learning is mainly used to study the future trend of capital market price. In this paper, to predict the time-series data of stock, we applied the traditional models and machine learning models for forecasting the linear and non-linear problem, respectively. First, stock samples that occurred from year 2010 to 2019 at the New York Stock Exchange are collected. Next, the ARIMA (autoregressive integrated moving average model) model and LSTM (long short-term memory) neural network model are applied to train and predict stock price and stock price subcorrelation. Finally, we evaluate the proposed model by several indicators, and the experiment results show that: (1) Stock price and stock price correlation are accurately predicted by the ARIMA model and LSTM model; (2) compared with ARIMA, the LSTM model performance better in prediction; and (3) the ensemble model of ARIMA-LSTM significantly outperforms other benchmark methods. Therefore, our proposed method provides theoretical support and method reference for investors about stock trading in China stock market.

1. Introduction

Stock market forecasting is a behavior to determine the future value of corporate stocks or other financial instruments traded on exchanges. Successful forecast of the future stock price can make considerable profit. According to EMH (efficiency market hypothesis), stock prices reflect all existing information, so any price changes not based on newly released information cannot be forecast. Although other people disagree with the hypothesis, some supporters of the view hold countless methods and techniques that supposedly allow them to access to future price information.

Stock market forecast is especially difficult, given the nonlinearity, volatility, and complexity of the market. Before the emergence of machine learning technology, stock market forecasts were generally realized through fundamental and technical analysis. With the computer technologies, such as machine learning, emerged and developed in business [1],

deep learning, especially neural network model, has become the current hot spot of stock prediction model. Meanwhile, stock market forecast has been more convenient and efficient due to these technologies [2]. At present, stock forecasting models usually fall into traditional linear models and models represented by deep learning. However, since the time series data have both linear and nonlinear parts, the forecasting results singly through forecasting models are usually not so reliable. Therefore, many experts and scholars combine various single models to significantly improve the accuracy and stability of the forecasting results.

In addition, the coefficient of association between the stock index and its constituent stocks can reflect the sensitivity of the constituent stocks to the changes of the stock index, that is, the correlation between the constituent stocks and the stock index (also known as “stock character”), which can be referred to by investors to adapt investment strategies. According to the market trend forecast, extraneous income

can be expected to gain by choosing different β coefficient of stocks. Moreover, the stock index and its constituent stock prices often keep trend in sync in the global stock market. Therefore, except for predicting stock index and single stock prices, better portfolio strategies can be worked out by forecasting the correlation coefficients of the expected constituent stock of the stock index for higher returns on investment.

Based on all of this, this paper takes the strong-enough representative S&P 500 stock index and its constituent stocks as the research object to forecast the future trend of the S&P 500 stock index through forecast models and then predict the correlation coefficient between its constituent stocks and the stock index, so as to formulate the optimal investment strategy for investors to refer to at a certain extent.

Over the past few decades, many social science researches have focused on predict social and economic development trends with quantitative methods. Many feasible methods in time-series analysis, both with advantages and disadvantages, can be interpreted as techniques for using past data to build forecasts and strategies on future value.

First, research about linear model: As early as the 1990s, the ARIMA (autoregressive integrated moving average) method has already been used by scholars to forecast in the capital market. Some researchers used the ARIMA and coefficients to predict stock market data [3], and in their experiments, researchers found that the experiment result was better than the prediction of the zero hypothesis of random fluctuations in the base value. The ARIMA model has been used in many fields including temperature prediction, prices prediction for electricity, and wind speed. Some studies adopted the process of ARIMA time in their research [4]. Yang et al. selected the Shanghai Composite Index to structure ARIMA model [5]. Kim and Sayama developed a new method aiming to forecasting the future trend of the S&P 500 index by establishing a complex network of time series of the index-foundation S&P 500 and then linking the network to the interconnected weights [6]. The study showed that adding network measurement results to the ARIMA can improve the prediction accuracy. Khashei and Hajirahimi believe that the time series in the hybrid model is divided into t linear and nonlinear two parts [7]. Therefore, ARIMA and MLP (multiparametric linear programming) are chosen to build hybrid models. They also found that on the whole, the ANN-ARIMA hybrid model can be adopted to achieve more accurate results. Unggara et al. used the Firefly algorithm to optimize the ARIMA (p, d, q) model and determined the best ARIMA model by looking for the smallest AIC (Akaike information criterion) value [8]. As a result, the ARIMA model optimized by the Firefly algorithm has a better forecasting performance.

Second, research about neural network model: The LSTM (long short-time memory) network, which has achieved further success in processing large data sets, is mainly used for deeper learning. Although LSTM model is limited in the number of inputs, Siami-Namini and Namin attempted to use the LSTM in financial data sets [9]. Experiment results indicate that the proposed method

performs well in predicting economic and financial time series. Other researchers put forward a stock price prediction method using deep learning models [10]: 14 different DL methods similar to LSTM are comprehensively adopted in S&P stocks; BSE-BANKEX stock index will be capable of forecasting one or even four steps ahead. It is found that the DL methods proposed in their research can obtain a good prediction results for stock price. Joo II and Seung-ho proposed a stock price forecast model of a two-way LSTM recurrent neural network, which adds a hidden layer in the opposite direction of the data flow to deal with the limited network through the previous model based on the RNN [11]. It was found that, compared with the nonbidirectional LSTM recurrent neural network, the stock price prediction model using the bidirectional LSTM recurrent neural network has higher accuracy. To get rid of high noise in stock data, researchers applied the wavelet threshold denoising method to preprocess the initial data sets [12]. In their study, the soft/hard threshold method used for data preprocessing has a significant effect on noise suppression. Based on this research, a new multi-optimal combination wavelet transform (MOCWT) was proposed, and the research finally showed that MOCWT is more accurate in forecasting than traditional methods. Researchers also proposed the LSTM model and employed it to intraday stock forecasts [13]. Chen and Ge made an exploration on the forecasting mechanism of stock price movement based on LSTM and found that it significantly improved the forecasting performance [14].

Third, the research on the hybrid model is as follows: Peter and Zhang used ARIMA and ANN hybrid method to study time series estimation [15]. Narendra Babu and Eswara Reddy proposed a linear hybrid model that can simultaneously maintain the prediction accuracy and the trend of the data [16]. Baek and Kim proposed a novel data enhancement method for stock market index prediction based on the ModAugNet framework [17]. The method includes the over-fitting prevention LSTM module and the predictive LSTM module and it is found from analysis that the test performance depends entirely on the latter. An ensemble method LSTM with GARCH is proposed [18]; it has high predictive ability and good applicability. Chen et al. proposed a new ensemble model to problems on portfolio selecting with skewness and kurtosis [19].

Through the analysis of recent literature, it can be found that domestic and foreign forecasting models can be roughly divided into linear, nonlinear, and hybrid models. In general, the current research status at home and abroad can be summarized as follows: The research on linear models mainly focuses on the ARIMA model. For recent researches, many researchers keep more belief in predictive performance of non-linear models than that of linear models. The hybrid model is the best predictive model in all. It can not only process the linear part of time series data, but also has better processing capabilities for its nonlinear part. Therefore, in our study, a single method is first used to predict the trend of stock indexes, and then a hybrid one is adopted to predict the correlation coefficients of stock indexes and their constituent stocks, so that provide investors with guidance to profit to a certain extent.

2. Methods

In this section, we first introduce ARIMA model and LSTM model, respectively, and finally introduce our proposed integration model.

2.1. Autoregressive Integrated Moving Average Model. ARIMA (p , d , and q), where p is the autoregressive term, q is the number of moving average terms, and d is the number of differences made when the time series becomes stationary. The prediction results can be adjusted by adjusting the aforementioned three parameters d , p , and q , so as to draw the optimal model. The model calculation formula is as follows:

$$y_t = \theta_0 + \Phi_1 y_{t-1} + \dots + \Phi_p y_{t-p} + \varepsilon_t - \theta_1 \varepsilon_{t-1} - \theta_2 \varepsilon_{t-2} - \dots - \theta_q \varepsilon_{t-q}, \quad (1)$$

where y_t and ε_t are the actual value and random error of the time period t , respectively; Φ_i ($i = 1, 2, \dots, p$) and θ_j ($j = 1, 2, \dots, q$) are the model parameters; p and q , the order of the model (p and q are integers), are also the model parameter mentioned earlier; the random error ε_t , whose mean value is 0, is assumed to be independent and obey the same distribution in the model. The variance of constant term is denoted as σ_2 . Equation (1) involves several important special cases of ARIMA series models. If $q = 0$, then equation (1) can be simplified to an AR model of order p . When $p = 0$, the model can be simplified to a q -order MA model. Among them, the model order (p, q) is the key link in ARIMA model construction, which determines the accuracy of model prediction. The parameters of the AR and MA operations are defined as (p) and (q), respectively. These two parameters need to be determined by the auto-correlation graph (ACF). ARIMA includes the following steps:

Step 1: Data diagnosis and check: In the first step, it is necessary to check the stationarity of the given time series data, which is essential to improve the accuracy of forecasting. A stationary time series is a time series whose statistical properties such as mean, variance, and covariance are related to time.

Step 2: Model parameter estimation: In order to stabilize the nonstationary time series, a proper degree of difference (d) is performed on it, and the stability test is performed again and this process is continued until a stable series is obtained. (d) is a positive integer that shows the degree of difference. If the difference operation is performed (d) times, the integration parameter of the ARIMA model is set to (d), and then the obtained stationary data are identified. In this process, the model (ACF graph) and partial auto-correlation graph (PACF graph) are determined.

Step 3: Model identification and selection: After ensuring that the input variable is a stationary series, the parameter d has been determined. Next, calculation algorithms are used to estimate the parameters to find the coefficients most suitable for the selected ARIMA model. And then the AIC standard or BIC standard is used to test the model and select the minimum

standard value. The essence of the two standards is maximum likelihood estimation or nonlinear least square estimation, and the AIC standard is chosen in this article.

Step 4: Model testing: Model testing is the test on whether the estimated model meets the norms of a stationary univariate process. In particular, the residuals of the model output should be independent of each other, and the mean value and the constant that changes with time should remain unchanged. If the estimate is insufficient, the modeling process must be resumed to build a better model.

Step 5: Data prediction: After the ARIMA model with the minimum AIC standard is obtained, the data can be input into the model to predict its linear part.

2.2. Long Short-Term Memory Model. Many researchers found that different models are good at dealing with different types of prediction problems. This provides a basis for using the ARIMA-LSTM hybrid model, which contains both linear and nonlinear parts, to produce better results than a single method. Figure 1 shows the LSTM neural grid stores the internal structure of cells.

Our study used the standard LSTM including the four interactive neural networks (forgetting gates, input gates, input candidate gates, and output gates).

$$f_t = \sigma(W_f \times [h_{t-1}, x_t] + b_f), \quad (2)$$

where σ represents the sigmoid activation function.

$$\sigma(X) = \frac{i}{1 + e^{-x}}. \quad (3)$$

And then, a new unit state C_t is obtained from the input gate, this state will be as an update unit state in the next time step. The input gate employed the σ as the activation function and i_t and \tilde{C}_t as outputs. i_t is employed to determine the feature in C_t to reflect \tilde{C}_t .

$$\begin{aligned} i_t &= \sigma(W_i \times [h_{t-1}, x_t] + b_i), \\ \tilde{C}_t &= \tanh(W_c \times [h_{t-1}, x_t] + b_c), \end{aligned} \quad (4)$$

σ function outputs a value in the range 0 to 1 and the \tanh outputs a value in the range -1 to 1.

Next, the value selected by the h_t activates O_t and C_t , which are decided by the output gate.

$$\sigma_t = \sigma(W_o \times [h_{t-1}, x_t] + b_o), \quad (5)$$

$$C_t = f_t \times C_{t-1} + i_t \times \tilde{C}_t, \quad (6)$$

$$h_t = o_t \times \tanh(C_t). \quad (7)$$

Equations (6) and (7) produce the C_t and h_t , and they will be passed to the next time step. The experiment in this article is a regression problem, and the range of output value of the proposed model is -1 to 1; therefore, the last element is activated by the \tanh function.

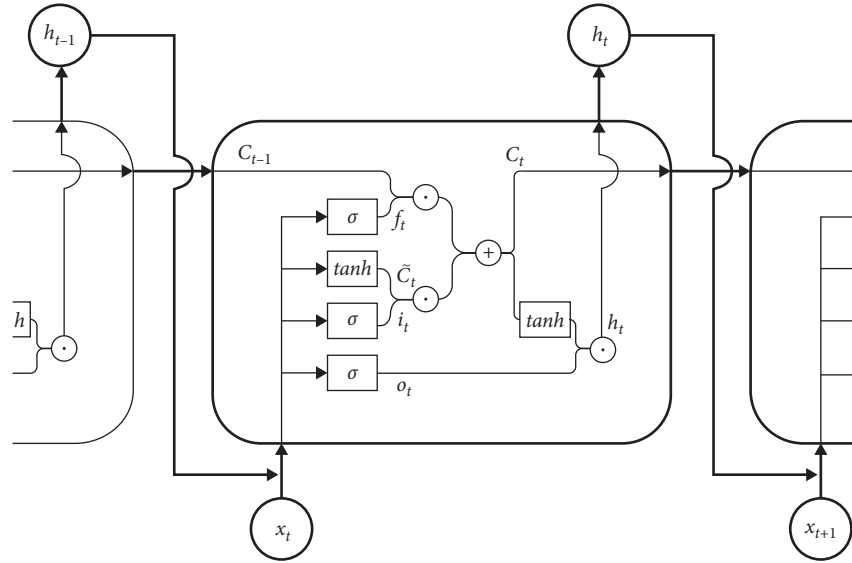


FIGURE 1: LSTM neural grid stores the internal structure of cells.

2.3. Ensemble Prediction Model. Unlike single algorithms, a combination of multiple methods can obtain higher estimation results [20]. These hybrid models are based on supervised machine learning algorithms, so they can be used for training and prediction purposes. Moreover, the ensemble methods improve the solving problem applicability and will obtain better performance [21, 22]. Traditional econometric models and machine-learning-based models have been widely used in the prediction research of time series. In our study, for the time series in the stock market, due to the existence of a large number of linear and nonlinear relations, the previous single model would be difficult to deal with this type of prediction. Therefore, in our study, we will make a combination prediction based on ARIMA and LSTM, respectively, for different characteristics of stock market data, in order to obtain better prediction effect. Recently, the ensemble method based on ARIMA and LSTM has been applied to some fields like business and energy and achieved great success [23–25].

Even if the results obtained using the mixed model and the results obtained using the model alone are not related to each other, it also demonstrates that it has reduced the prediction error. Therefore, the hybrid model is considered to be the most successful prediction task model [26]. To make predictions, many ensemble methods composed of linear and nonlinear models are employed by different researchers. In our experiment, historical data are used in the time series to predict the future. Figure 2 introduces the structure of the proposed ensemble method.

$$y_t = L_t + N_t. \quad (8)$$

Figure 2 shows the ARIMA-LSTM hybrid model. In our time series data sets, L_t represents the linear part and N_t represents the nonlinear part. In our hybrid model, the linear part L_t is calculated through the ARIMA at first, and then the LSTM is applied to predict the nonlinear part N_t . At last, the sum of the error values of the two models is obtained.

In the mixed model, the linear component L_t is calculated through the ARIMA model at first and then the LSTM model is used to predict the nonlinear component N_t of the time series. At last the sum of the error values of the two models is obtained. The formulas for calculating L_t and N_t are given in formulas (9) and (10):

$$\text{LSTM}_{\text{error}} = \text{LSTM_mean}[\text{error}], \quad (9)$$

$$\text{ARIMA}_{\text{error}} = \text{ARIMA_mean}[\text{error}]. \quad (10)$$

Calculate the weight of the model using the error values obtained in equations (11) and (12).

$$\text{ARIMA}_{\text{weight}} = \left(1 - \left(\frac{\text{LSTM}_{\text{error}}}{\text{LSTM}_{\text{error}} + \text{ARIMA}_{\text{weight}}} \right) \right) \times 2, \quad (11)$$

$$\text{ARIMA}_{\text{weight}} = 2 - \text{LSTM}_{\text{error}}. \quad (12)$$

Use the given equation (13) to obtain the weight value of the model and each predicted value of the final mixed model.

$$\text{Hybrid}_{\text{predict}}[i] = \frac{\text{LSTM}_{\text{weight}}[i] \times \text{LSTM}_{\text{error}}[i] + \text{ARIMA}_{\text{weight}}[i] \times \text{ARIMA}_{\text{error}}[i]}{2}. \quad (13)$$

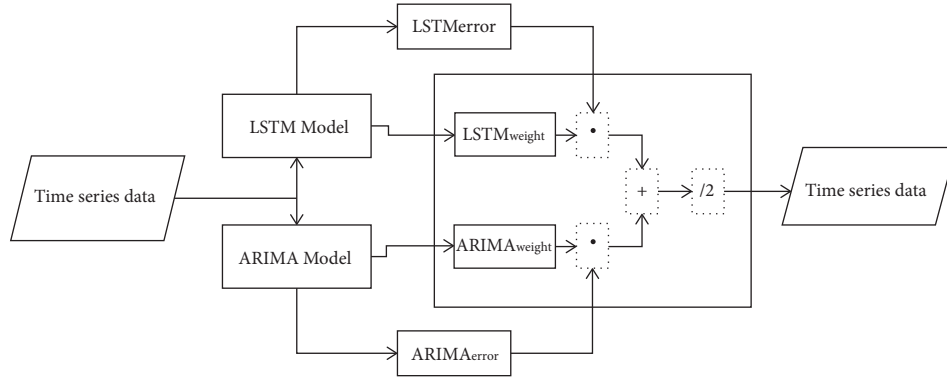


FIGURE 2: ARIMA-LSTM hybrid model.

3. ARIMA-LSTM Hybrid Model Design and Evaluation

To evaluate the performance of the proposed ensemble model, we employ some commonly used method such as MAE, MSE, and RMSE to compare and evaluate the ensemble method and several benchmark methods.

3.1. Data Set Selection and Preprocessing. In this study, two stock index forecasting models, ARIMA and LSTM, are constructed at first. The S&P 500 stock index is selected in the empirical data selects, and the daily trading data is selected in the data sample interval selects from January 1, 2010, to December 31, 2019, which are 2519 sets of data in total. Among them, the first 90% is used for model training, and the 10% is used for model prediction. The S&P 500 stock index sequence is shown in Figure 3. It can be found from the figure that within the selected time range, the S&P 500 Index generally shows a steady increasing trend.

3.2. Comparative Analysis of Stock Index Forecast Model Results. After obtaining the prediction data set, the aforementioned four test methods are used in this study to test the data of each forecasting method. The following table shows the different loss value obtained on the basis of the prediction of the four foreign exchange median prices and the ARIMA model and the RNN neural network model.

Table 1 shows the fitting results based on the loss values of the prediction results of each model under different loss functions. It can be seen from the table that the loss functions of the LSTM model are all smaller than the ARIMA model, which is because the LSTM model can not only describe the nonlinear relationship of time series data but also has certain processing capabilities for its linear part despite of its instability in comparison with the ARIMA model. However, generally speaking, both models have gained very low loss values, indicating that the two models are both relatively perform well in predicting accuracy. Figure 4 shows the predicted results using LSTM and ARIMA, respectively.

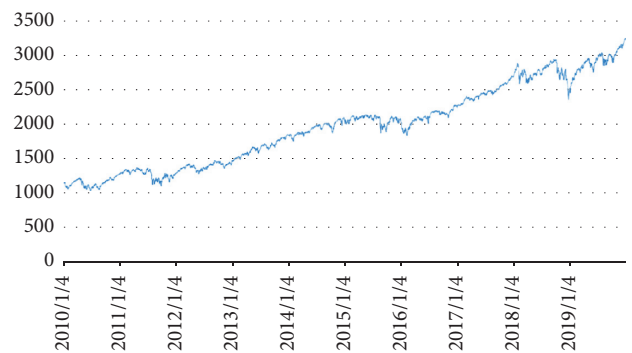


FIGURE 3: S&P Stock index closing sequence.

TABLE 1: The experiment results about ARIMA and LSTM model forecasting.

	MSE	MAE	RMSE
ARIMA	0.000101	0.007333	0.043788
LSTM	0.000096	0.007184	0.028828

3.3. The Design of Stock Price Correlation Coefficient Prediction Ensemble Model

3.3.1. The Design of ARIMA for Stock Price Correlation Coefficient Prediction

- (1) In the experiment of correlation coefficient prediction, the adjusted closing price of the constituent stocks of the S&P 500 index is selected, and the sample interval is still set from January 1, 2010, to December 31, 2019, on the New York Stock Exchange daily transaction receipts. Data are mainly acquired in the use of Python language’s Beautiful Soup function library through crawler technology. The trading data of the constituent stocks originates from the Quandl database, and the industry information of the constituent stocks is from Wikipedia.

After preprocessing the data, the program randomly generates 150 stocks from the remaining 446 assets, and calculates the correlation coefficient of each pair of assets in a 100-day time window. In order to diversify the data, 5 sets of data are set up in this

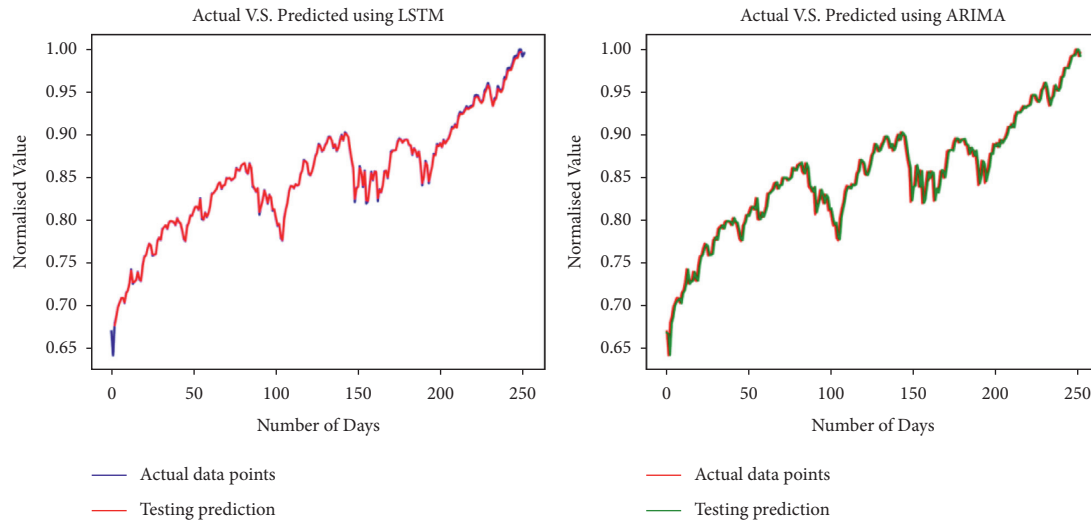


FIGURE 4: The predicted results using LSTM and ARIMA.

article with a starting value every 20 days: day 1; day 21; day 41; day 61; and day 81. Each value corresponds to a rolling 100-day window, advancing in 100-day time-steps until the end of the data set training. In this process, a total of 55,875 sets of time series data were trained, and each set has 24 time-steps. Development, test1, and test2 are produced using these $55,875 \times 24$ data sets. In the model evaluation stage, this paper divides the data as follows to achieve forward optimization.

- (2) The parameters of the model should be determined before fitting the ARIMA model. ARIMA (p, d, q) , where d is easiest to be determined. Data difference aims to making the last data used is a time series that tends to be stable, which can improve forecasting accuracy. As mentioned in the previous section, the S&P 500 Index and its constituent stocks generally show a steady increasing trend. The data will tend to be stable after a difference, so the parameter d here can be determined as the value 1. The determination of the parameters p and q needs to adopt the ACF and PACF of the data.

The ACF and PACF are set into zero after a certain order is called truncation. The running results show that most data sets show an oscillation trend, as shown in Table 2. There are also notable trends covering rising/falling trends, large drops occasionally when the correlation coefficient is stabilized, and stable periods with mixed oscillations. Although the ACF and PACF images show that most of the data sets are close to white noise, the images show that five groups of parameters can be effectively used in the prediction of the ARIMA model. These five sequences are used in this article to test the ARIMA model, and a total of 55,875 data sets are trained. What is more, for each data set, we will select the smallest AIC-value-based model after training.

AIC (Akaike information criteria) is a commonly used test standard for the prediction performance of ARIMA models. The expression of AIC calculation is as follows:

$$\text{AIC} = -2\ln(L) + 2N, \quad (14)$$

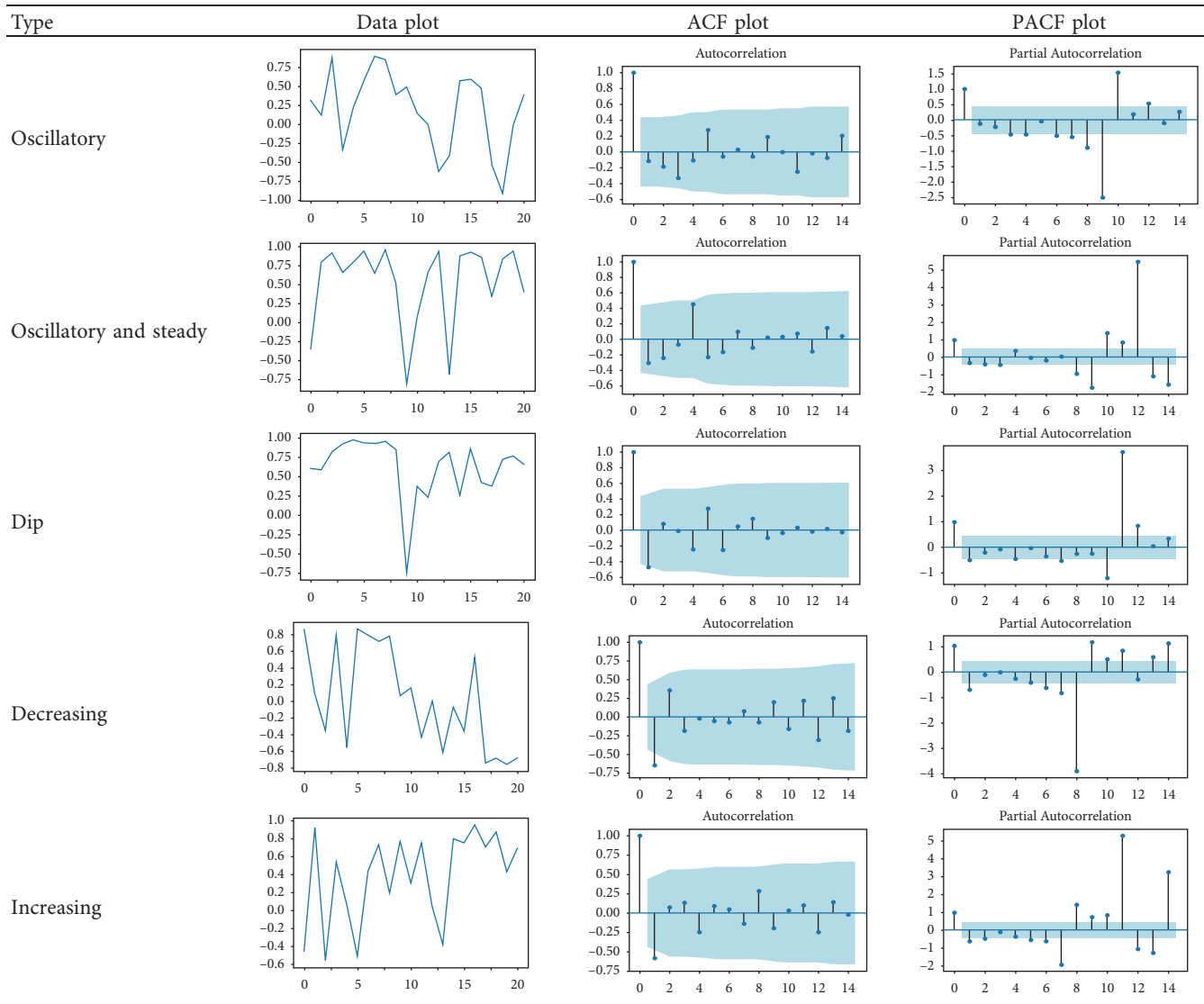
where L represents the maximum likelihood function and N represents the number of parameters.

The AIC standard was proposed by the Japanese statistician Akaike, so it is named directly after initials of his name. To evaluate the performance of the ARIMA model with the application of AIC standard, the maximum likelihood function and the model parameters are used to judge its prediction effect. Specifically, the larger the maximum likelihood function value, the higher the prediction effect; theoretically speaking, the more the number of model parameters is set, the lower the difficulty of fitting the data relationship or the better the fit will be. However, too many parameters will also complicate the model structure, which may lead to more difficulties in parameter estimation, thereby reducing the model prediction accuracy. Therefore, the ideal ARIMA model should be the optimal combination of maximum likelihood function and parameters. The AIC standard comprehensively considers the above two indicators and can perform comprehensively on evaluation of the ARIMA model. Therefore, when optimizing the ARIMA model, the parameter with the smallest AIC value will be selected.

If the ARIMA model is used to predict future data, the generated data are in the ARIMA model. In other words, the underlying process of generating the time series only has a linear correlation structure, but the nonlinear relationship in the experiment data cannot be described. The ARIMA method still has certain limitations in predicting complex real-world problems. In this regard, the NN model can be employed to analyze the nonlinear parts that the ARIMA model cannot deal with.

After fitting the ARIMA model to the linear part of the data, this article generates a new data set to calculate the residual value of the remaining non-linear part at every 21-time steps, as shown in Figure 5. Since the input is the nonlinear partial residuals processed by the ARIMA model, the residual distributions of the X and Y data sets all fall

TABLE 2: ARIMA model's ACF/PACF.



between 0 and 1. The newly generated X and Y segmentation data set will be used as the input value of the next nonlinear LSTM model for training.

3.3.2. Forecast Design Based on LSTM Stock Price Correlation Coefficient. (1) *Data Selection and Acquisition:* After the ARIMA model processes the linear part of 150 pairs of combined assets generated at any time, the remaining nonlinear part is calculated as the residual value and used as the input of the LSTM model, as shown in Figure 5.

The input data set of the LSTM model is also divided into X and Y trains, X and Y developments and two sets of X and Y test set 1 and test set 2. The input data are stored in the X and Y data sets as shown in Figure 6. Each x data set size is a $55,874 \times 20$ matrix, and each X time series corresponds to a Y data set.

(2) *Training for LSTM Model:* The model structure constructed in this paper is an improved LSTM model based

on RNN, which contains 25 units. The final output of the cells is combined into a value with a full-connection layer. This value is then output as a final predicted value through a \tanh activation function of a two-layer network. The \tanh activation function of the two-layer network can be simply understood as the \tanh function magnified by two times. Figure 7 shows the simplified architecture of the method.

3.4. Prediction Results Analysis

3.4.1. Forecasting Performance Evaluation. This paper aims to fit the parameters of the model so that the optimal parameters can be used to apply and predict various assets in different time periods. Therefore, only the first window is trained, and the trained model can be applied to the data training of the three time intervals of the validation set and the two test sets. In addition, when the prediction results of

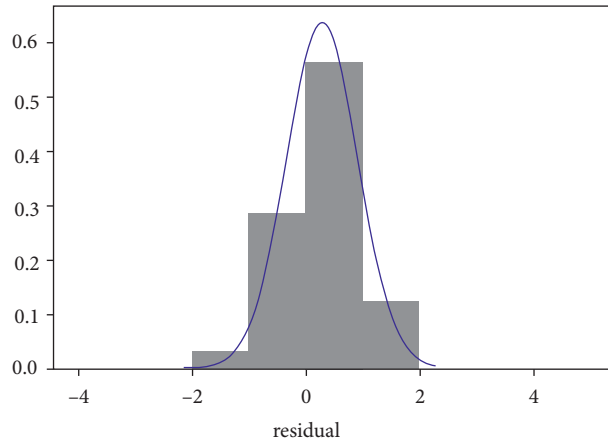


FIGURE 5: Residual data distribution of training set.

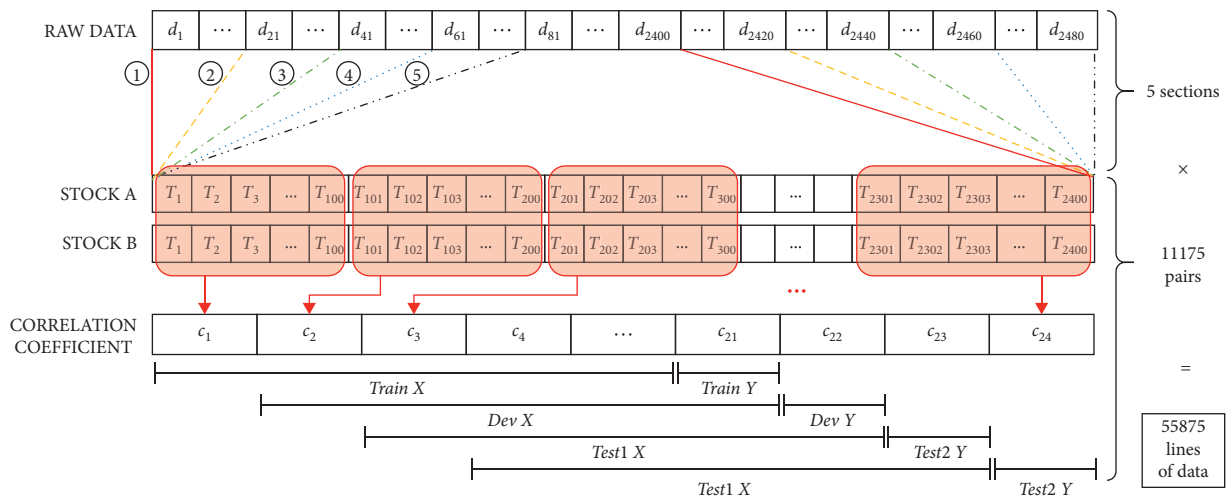


FIGURE 6: The input data for time series.

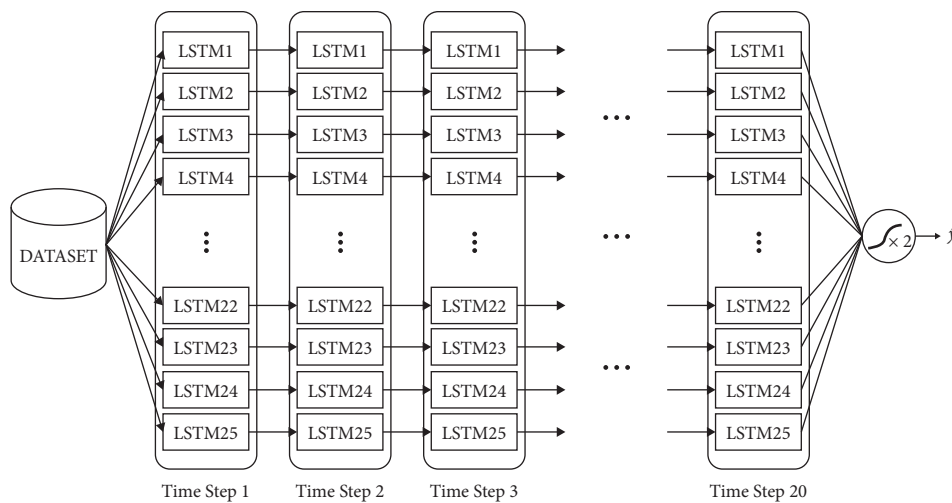


FIGURE 7: The structure of the LSTM model.

the correlation coefficient of the model in the two time periods are relatively ideal, some classic financial prediction models are selected to analyze the prediction effects of each

model to test the model in this article. The MSE and MAE values of four financial models are calculated in this article.

3.4.2. *Forecast Results and Analysis.* After the data are processed, in the hybrid model prediction experiment, the ARIMA method is first employed in this article to process the S&P 500 index component stocks in the aspect of linear as the first step, and then the nonlinear part of the data residual value processed at the first step is used as the input data of the LSTM model. Finally, model establishment, data training and testing is developed. The final prediction results of the correlation coefficient between the 150 randomly generated asset portfolios and the S&P 500 index in the next 20 time steps are shown in Figure 8.

3.5. *Control Group Forecasting Model.* Predicting the results by the hybrid model alone is not enough to show that the certain advantages of the model in the forecasting performance of research objects such as correlation coefficients. In order to make comparison between the proposed hybrid model proposed and other models for the accuracy of financial sequence forecasting, other commonly used forecasting models are introduced as the reference group. Many studies have shown that the full-sequence model is poor in prediction performance during the period of predicting financial sequences, so three other commonly used prediction models are also discussed, which are compared with the prediction results of hybrid models.

3.5.1. *Full-Sequence Model (FS).* Adopting the full-sequence algorithm is the easiest way to estimate the portfolio correlation. All the past correlation values are used in the model to predict the future correlation coefficient.

$$\hat{\rho}_{ij}^{(t)} = \frac{\beta_i \beta_j \sigma_m^2}{\sigma_i \sigma_j} \rho_{ij}^{(t)} = \hat{\rho}_{ij}^{(t-1)}. \quad (15)$$

However, compared with other equivalent models, the prediction quality of this model is relatively poor.

3.5.2. *Constant Coefficient Correlation Model (CCC).* The CCC model shows that the average value of the correlation coefficients of all asset portfolios can be regarded as the estimated value of the required predicted asset portfolio. Therefore, all assets in the portfolio in this model have the same correlation coefficient.

$$\rho_{ij}^{(t)} = \frac{\sum_{i>j} \rho_{ij}^{(t-1)}}{n(n-1)/2}. \quad (16)$$

3.5.3. *Single-Index Model (SI).* Adopting the single-index model is a simple way of asset pricing, which is usually used to evaluate the risk and return of stocks. To facilitate calculation and analysis, the single-index model acts with a kind of macro factor, such as the S&P 500 index, to measure the risk and return of stocks. The single-index model assumes that the rate of return on assets and the “single index,” that is, the market rate of return changes in the same

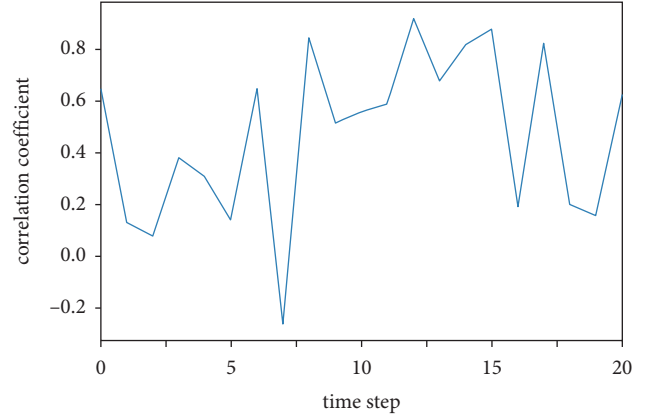


FIGURE 8: Prediction results of correlation coefficient.

direction. In order to quantify the volatility of assets and market returns, it is necessary to specify the market returns themselves. This specification is called the “market model.”

$$R_{i,t} = \alpha_i + \beta_i R_{m,t} + \varepsilon_{i,t}, \quad (17)$$

where $R_{i,t}$ represents the return of asset i at time t ; in the same way, $R_{m,t}$ represents the return of asset m at time t ; α_i represents the excess return of asset i after risk adjustment; β_i represents the impact of asset i on the market sensitivity; $\varepsilon_{i,t}$ represents the residual income of asset i at time t , also called the error term. So there is

$$\begin{aligned} E(\varepsilon_i) &= 0, \\ \text{Var}(\varepsilon_i) &= \sigma_{\varepsilon_i}^2, \\ \text{Cov}(R_i R_j) &= \rho_{ij} \sigma_i \sigma_j = \beta_i \beta_j \sigma_m^2, \end{aligned} \quad (18)$$

where σ_i and σ_j respectively represent the standard deviation of asset i and asset j ; σ_m represents the standard deviation of market returns. In a single-index model, the estimated value of the correlation coefficient $\hat{\rho}_{ij}^{(t)}$ can be expressed as,

$$\hat{\rho}_{ij}^{(t)} = \frac{\beta_i \beta_j \sigma_m^2}{\sigma_i \sigma_j}. \quad (19)$$

3.5.4. *Multisequence Model.* The industry sector of the asset is considered in the multisequence. The model assumes that assets generally have a trend of volatility in the same direction in the same industry, so it can be considered that the correlation coefficients of the asset portfolio are equal to the average value of the correlation coefficients of the industry. For example, there are company A and B that belong to industry sectors α and β , respectively; then, their correlation coefficients are equal to the average correlation coefficients of all asset portfolios in their respective industry sector combinations (α, β) . According to whether the two industrial sectors α and β are the same, the prediction formula is slightly different. The equation is as follows:

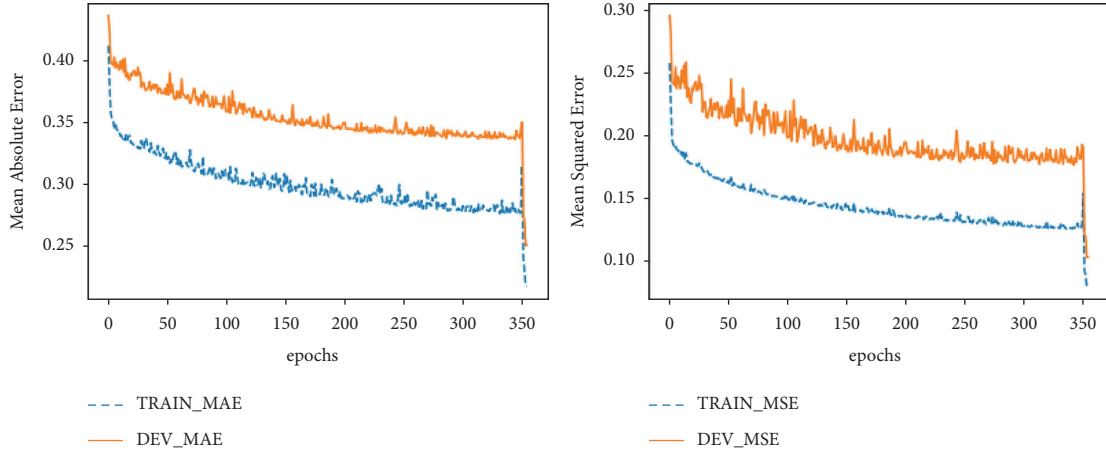


FIGURE 9: The learning curve of the ensemble model (ARIMA-LSTM).

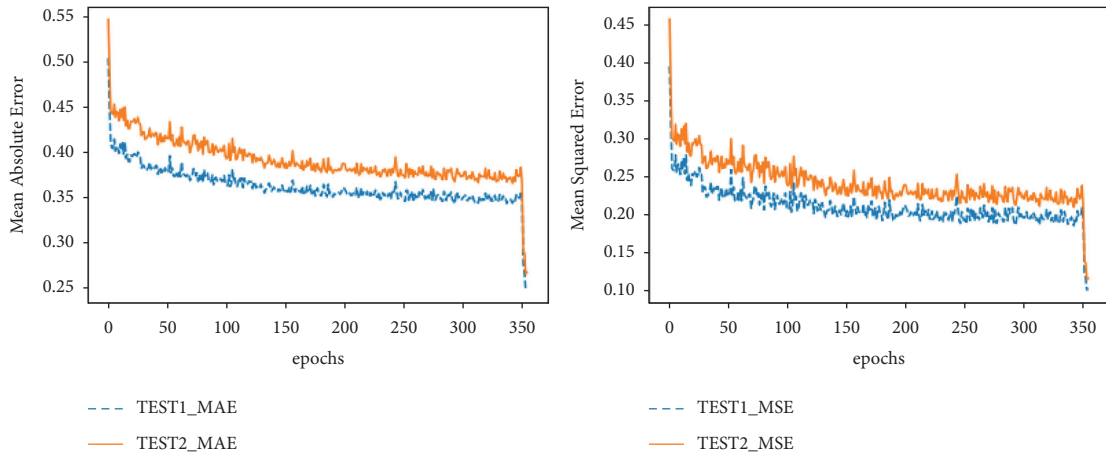


FIGURE 10: The prediction curve of the ensemble model (ARIMA-LSTM).

TABLE 3: ARIMA-LSTM mixed-model loss function evaluation table.

	Develop data set			Test1 data set			Test2 data set		
	MSE	RMSE	MAE	MSE	RMSE	MAE	MSE	RMSE	MAE
ARIMA-LSTM	0.103	0.320	0.250	0.101	0.319	0.248	0.116	0.341	0.266
Full history	0.479	0.692	0.558	0.463	0.681	0.554	0.432	0.657	0.523
Constant correlation	0.277	0.526	0.462	0.214	0.463	0.400	0.281	0.530	0.430
Single-index model	0.420	0.624	0.540	0.411	0.641	0.534	0.247	0.497	0.482
Multigroup	0.307	0.554	0.451	0.291	0.539	0.455	0.297	0.536	0.448

$$\left\{ \begin{array}{l} \frac{\sum_{ie\alpha}^{n\alpha} \sum_{j\epsilon\beta; i \neq j}^{n\beta} \rho_{ij}^{(t-1)}}{n_{\alpha}(n_{\beta} - 1)}, \quad \alpha = \beta, \\ \frac{\sum_{ie\alpha}^{n\alpha} \sum_{j\epsilon\beta; i \neq j}^{n\beta} \rho_{ij}^{(t-1)}}{n_{\alpha}n_{\beta}}, \quad \alpha \neq \beta, \end{array} \right. \quad (20)$$

where α and β respectively represent different industry sectors in the stock market; n_{α} and n_{β} represent the number of companies in the α plate and β plate, respectively.

3.6. Experimental Results and Evaluation. From Figures 9 and 10, it can be found that the learning curve of the train data set and the development data set after a certain period of learning and training (about 350 time steps) begin to converge, and the aforementioned two data sets have obtained smaller MSE and MAE loss function values.

Table 3 shows that the value of the Validation set (develop), test1, and test2 are all smaller than that of the compared models through the ARIMA-LSTM ensemble model designed in our study and calculation of the MSE, RMSE, and MAE for predicted values. Therefore, it could be considered that the

accuracy of the ensemble method has been improved, and the model can be extensively used to other applications of stock market prediction.

4. Conclusion

First, the two single models have good applicability to the data with single dimension. The loss function is used to calculate the prediction results of the proposed model, and we found that both ARIMA and LSTM model have lower loss function values in stock index prediction. By comparing the loss function values of all methods, it can indicate that the three loss function indexes of LSTM model are superior to ARIMA model. Moreover, the prediction accuracy of ARIMA-LSTM hybrid model is better than other financial models. In this paper, we proposed a hybrid model ARIMA-LSTM, linearity is filtered out in ARIMA modeling, and nonlinear trends are predicted in LSTM recursive neural networks. The loss function test results show that the MSE, MAE, and RMSE of ARIMA-LSTM hybrid model are smaller than those of other control models. Therefore, ARIMA-LSTM model is feasible to predict the correlation coefficient of portfolio optimization. Although the prediction results in this paper are basically consistent with the expected results before the experiment, the time series before 2010 is not considered for only the data after 2010 are selected. Therefore, the model's ability to predict the special financial situation before 2010 need to be further tested. What is more, as financial anomalies and noise are common, all special trends cannot be covered by the model. Therefore, in the next step, it is necessary for researchers to further study how to deal with Black Swan Theory in the financial world.

Data Availability

The experimental data of this research are available from the corresponding author upon request.

Conflicts of Interest

All the authors declared that they have no conflicts of interest regarding this study.

References

- [1] Z. Bao and C. Wang, "A multi-agent knowledge integration process for enterprise management innovation from the perspective of neural network," *Information Processing & Management*, vol. 59, no. 2, Article ID 102873, 2022.
- [2] S. Deng, X. Huang, J. Shen, H. Yu, and C. Wang, "Prediction and trading in crude oil markets using multi-class classification and multi-objective optimization," *IEEE Access*, vol. 7, no. 99, p. 1, 2019.
- [3] G. Caginalp and G. Constantine, "Statistical inference and modelling of momentum in stock prices," *Applied Mathematical Finance*, vol. 2, no. 4, 1995.
- [4] T. Zheng, J. Farrish, and M. Kitterlin, "Performance trends of hotels and casino hotels through the recession: an ARIMA with intervention analysis of stock indices," *Journal of Hospitality Marketing & Management*, vol. 25, no. 1, pp. 49–68, 2016.
- [5] B. Yang, C. Li, D. Wang, and X. He, "Research on the Risk of Shanghai Composite Index Based on VaR and GARCH Model," in *Proceedings of the 2017 3rd International Conference on Economics, Social Science, Arts, Education and Management Engineering (ESSAEME 2017)*, Huhhot, China, January, 2017.
- [6] M. Kim and H. Sayama, "Predicting stock market movements using network science: an information theoretic approach," *Applied Network Science*, vol. 2, no. 1, p. 35, 2017.
- [7] M. Khashei and Z. Hajirahimi, "A comparative study of series arima/mlp hybrid models for stock price forecasting," *Communications in Statistics-Simulation and Computation*, vol. 48, no. 9, pp. 2625–2640, 2019.
- [8] I. Unggara, A. Musdholifah, and K. S. Anny, "Optimization of ARIMA forecasting model using firefly algorithm," *IJCCS (Indonesian Journal of Computing and Cybernetics Systems)*, vol. 13, no. 2, 2019.
- [9] S. Siami-Namini and A. S. Namin, "Forecasting Economics and Financial Time Series: ARIMA vs. LSTM," *Papers*, 2018, <https://arxiv.org/abs/1803.06386>.
- [10] A. Jayanth Balaji, D. S. Harish Ram, and B. B. Nair, "Applicability of deep learning models for stock price forecasting an empirical study on BANKEX data," *Procedia Computer Science*, vol. 143, pp. 947–953, 2018.
- [11] T. Joo II and C. Seung-Ho, "Stock prediction model based on bidirectional LSTM recurrent neural network," *Journal of Korea Institute of Information, Electronics, and Communication Technology*, vol. 11, no. 2, pp. 204–208, 2018.
- [12] X. Liang, Z. Ge, L. Sun, M. He, and H. Chen, "LSTM with wavelet Transform based data preprocessing for stock price prediction," *Mathematical Problems in Engineering*, vol. 2019, Article ID 1340174, 8 pages, 2019.
- [13] S. Borovkova and I. Tsiamas, "An ensemble of LSTM neural networks for high-frequency stock market classification," *SSRN Electronic Journal*, vol. 01, 2018.
- [14] S. Chen and L. Ge, "Exploring the attention mechanism in," *LSTM-based Hong Kong Stock price Movement Prediction*, Taylor & Francis Journals, Milton Park, UK, 2019.
- [15] G. Peter and Zhang, "Time series forecasting using a hybrid ARIMA and neural network model," *Neurocomputing*, vol. 50, 2003.
- [16] C. Narendra Babu and B. Eswara Reddy, "Prediction of selected Indian stock using a partitioning-interpolation based ARIMA-GARCH model," *Applied Computing and Informatics*, vol. 11, no. 2, pp. 130–143, 2015.
- [17] Y. Baek and H. Y. Kim, "ModAugNet: a new forecasting framework for stock market index value with an overfitting prevention LSTM module and a prediction LSTM module," *Expert Systems with Applications*, vol. 113, no. DEC, pp. 457–480, 2018.
- [18] H. Y. Kim and C. H. Won, "Forecasting the volatility of stock price index: a hybrid model integrating LSTM with multiple GARCH-type models," *Expert Systems with Applications*, vol. 103, pp. 25–37, 2018.
- [19] B. Chen, J. Zhong, and Y. Chen, "A hybrid approach for portfolio selection with higher-order moments: empirical

- evidence from Shanghai Stock Exchange,” *Expert Systems with Applications*, vol. 145, Article ID 113104, 2019.
- [20] D. Opitz and R. Maclin, “Popular ensemble methods: an empirical study,” *Journal of Artificial Intelligence Research*, vol. 11, pp. 169–198, 1999.
- [21] J. J. Garcia Adeva, U. Cervino Beresi, and R. A. Calvo, “Accuracy and diversity in ensembles of text categorisers,” *CLEI Electronic Journal*, vol. 8, no. 2, pp. 1–12, 2005.
- [22] M. Oliveira and L. Torgo, “Ensembles for time series forecasting,” in *Proceedings of the Asian Conference on Machine Learning (ACML’2014)*, pp. 360–370, Nha Trang city, Vietnam, January, 2015.
- [23] E. Dave, A. Leonardo, M. Jeanice, and N. Hanafiah, “Forecasting Indonesia exports using a hybrid model ARIMA-LSTM,” *Procedia Computer Science*, vol. 179, no. 1, pp. 480–487, 2021.
- [24] Y. Deng, H. Fan, and S. Wu, “A hybrid ARIMA-LSTM model optimized by BP in the forecast of outpatient visits,” *Journal of Ambient Intelligence and Humanized Computing*, 2020.
- [25] Z. Wang, J. Qu, X. Fang, H. Li, T. Zhong, and H. Ren, “Prediction of early stabilization time of electrolytic capacitor based on ARIMA-Bi_LSTM hybrid model,” *Neurocomputing*, vol. 403, 2020.
- [26] M. Khashei and M. Bijari, “Improving forecasting performance of financial variables by integrating linear and non-linear ARIMA and artificial,” *QJER*, vol. 8, no. 2, pp. 83–100, 2008.

Retraction

Retracted: Analysis of Key Indicators Related to the Teaching of Floral Art Skills Competition Based on Fuzzy Hierarchical Model

Scientific Programming

Received 29 August 2023; Accepted 29 August 2023; Published 30 August 2023

Copyright © 2023 Scientific Programming. This is an open access article distributed under the Creative Commons Attribution License, which permits unrestricted use, distribution, and reproduction in any medium, provided the original work is properly cited.

This article has been retracted by Hindawi following an investigation undertaken by the publisher [1]. This investigation has uncovered evidence of one or more of the following indicators of systematic manipulation of the publication process:

- (1) Discrepancies in scope
- (2) Discrepancies in the description of the research reported
- (3) Discrepancies between the availability of data and the research described
- (4) Inappropriate citations
- (5) Incoherent, meaningless and/or irrelevant content included in the article
- (6) Peer-review manipulation

The presence of these indicators undermines our confidence in the integrity of the article's content and we cannot, therefore, vouch for its reliability. Please note that this notice is intended solely to alert readers that the content of this article is unreliable. We have not investigated whether authors were aware of or involved in the systematic manipulation of the publication process.

Wiley and Hindawi regrets that the usual quality checks did not identify these issues before publication and have since put additional measures in place to safeguard research integrity.

We wish to credit our own Research Integrity and Research Publishing teams and anonymous and named external researchers and research integrity experts for contributing to this investigation.

The corresponding author, as the representative of all authors, has been given the opportunity to register their agreement or disagreement to this retraction. We have kept a record of any response received.

References

- [1] N. Wu and J. Zhou, "Analysis of Key Indicators Related to the Teaching of Floral Art Skills Competition Based on Fuzzy Hierarchical Model," *Scientific Programming*, vol. 2022, Article ID 7765024, 8 pages, 2022.

Research Article

Analysis of Key Indicators Related to the Teaching of Floral Art Skills Competition Based on Fuzzy Hierarchical Model

Ningling Wu  and Jieliang Zhou

College of Plant Science and Technology, Hunan Biological Electromechanical Vocational Technical College, Changsha 410127, China

Correspondence should be addressed to Ningling Wu; 18674814086@hnbemc.edu.cn

Received 16 February 2022; Accepted 8 March 2022; Published 29 March 2022

Academic Editor: Wenming Cao

Copyright © 2022 Ningling Wu and Jieliang Zhou. This is an open access article distributed under the Creative Commons Attribution License, which permits unrestricted use, distribution, and reproduction in any medium, provided the original work is properly cited.

The art of floral arrangement has become an essential part of the curriculum to enhance students' professionalism. By studying the connotation of academic style construction and disciplinary skill competitions and the promotion of disciplinary skill competitions to academic style construction based on the fuzzy hierarchy model, we propose to keep abreast of the times and attach importance to the significance of disciplinary skill competitions; to deepen and improve the organizational structure; improve the evaluation and incentive mechanisms to create a brand; and to gradually form a multilevel management and long-term mechanism to build a disciplinary skill competition system. The aim is to deepen the construction of the university academic style and provide a solid platform for promoting the cultivation of skilled and comprehensive talents.

1. Introduction

The inclusion of traditional Chinese flower arranging in the second national list of intangible cultural heritage in 2008 means that the art of flower arranging has entered a new phase of conservation. As an educator in a vocational college, I am aware that in order to occupy a place in society, students in higher education institutions must be trained in all aspects of floral art, and that it is imperative to improve the quality of students' training, as well as their hands-on skills [1].

The art of flower arranging is so vast and profound that it is impossible to teach theoretical knowledge in a limited number of hours and at the same time have the students really master the skill [2]. The only way to make use of the limited number of hours we have is to motivate the students and bring floristry into their lives. In the teaching, the theoretical knowledge is divided into 10 hours, including the history of the development of floristry in the East and West, the understanding of flowers, color combinations, physical phenomena, and floral design, and the principle of "the master introduces the door, the practice depends on the individual." In the other 20 hours, the students' initiative is brought into full play, from imitating outstanding flower arrangements and gaining experience in the hand, to

discussing in small groups or proposing innovative designs, so that they can fully feel the sense of achievement when their work is completed [3].

The teaching of flower arranging is a hands-on discipline, and although there is theoretical knowledge, it is not a subject that can be completed by rote memorization. The course is therefore arranged in a ratio of 1 : 2 between theory and practice. In the first step, based on the theoretical knowledge and the examples of flower arrangements provided by the teacher in the classroom, the students are asked to work in groups to make flower arrangements, combining theory with practice [4]. For most of us who have never been involved in floral art before, the teacher has asked the students to imitate existing works, so that they can understand intuitively the structure of a flower arrangement and how to make it. The main methods of evaluation are through peer review and teacher summary [5]. The third step is to train students to be more creative and adaptable in the skills competition. This involves two types of training: (1) preparing flowers from which students can choose the type, color, and quantity of flower material to create their own ideas, which must be both beautiful and positive. (2) The students will be asked to think about the effect of the flower arrangement and to buy the necessary materials to make it.

And as the soul of a school, academic style refers to the attitude and ethos that students display in their studies and is the external expression of their inner qualities such as ideas, morals, interests, and qualities in their studies, which can promote and sustain their learning activities [6].

The construction of academic style not only affects the improvement of the overall teaching quality of the school and the realization of the teaching objectives of the university but also has a non-negligible role in the long-term planning of the school and the overall development of students [7]. It is of great practical significance to carry out various kinds of academic style construction activities and continuously deepen the construction of academic style in colleges and universities. Guiding students to participate in skills competitions can stimulate students' enthusiasm for learning, enhance their innovation consciousness and collaboration ability, and is one of the most effective ways to promote the overall improvement of students' comprehensive quality and build a good academic style.

2. The Connotation of Academic Style Building and Subject Skills Competition in Higher Education

The definition of "academic style" in the Chinese dictionary is "the ethos of a school, the collective character". Academic style in colleges and universities refers to "a more stable purpose, spirit, attitude, and method of governance formed by all teachers and students in colleges and universities in the process of long-term education practice, which is the expression of the group psychology and behavior of all teachers and students in governance" [8]. The construction of academic style is the key to university education, an important content of the construction of socialist spiritual civilization in universities, an important way to integrate the socialist core value system into national education, an important condition to realize the cultivation goal of socialist schools, and an important index to measure the level of a university [9]. As a kind of subtle and powerful spiritual force, a good academic style has a great influence on the creation and development of the academic atmosphere in colleges and universities and can inspire students to grow up healthily and develop comprehensively. The construction of academic styles in colleges and universities is directly related to the quality of talent cultivation.

The academic skills competition is a competition to examine students' ability to combine theory with practice and solve practical problems. It is a competition for the general public and is a powerful way to stimulate potential, enhance interest, cultivate a sense of innovation and collaboration, and provide a series of activities to enhance students' confidence in learning and work [10]. Let us take Hunan Agricultural University as an example. As an agricultural institution, the university has special advantageous majors such as tea science and ornamental horticulture, and actively organizes related skills competitions. In the past 23 years, it has hosted many tea competitions at all levels and won more than 20 national and provincial tea competitions.

The College of Horticulture and Landscape Architecture has been running a regular floral arrangement skills competition for students from the province since 2012, with a series of activities such as precompetition coaching, floral arrangement training, and master lectures at different levels [11]. On the one hand, the competitions enrich the students' lives after school, increase their motivation to study, enable them to learn and think about another skill to earn a living, and broaden the path of graduation competition for university students; on the other hand, the development of such subject skills competitions is a great support to the school's overall academic style construction work, which is of great importance.

3. Fuzzy AHP Integrated Evaluation of Competition Competitiveness

Fuzzy hierarchical analysis (AHP) is a kind of system analysis method combining qualitative and quantitative analysis. This method introduces the principle of affiliation, which can improve the shortcomings of the hierarchical analysis method in constructing the pairwise comparison judgment matrix with the subjectivity of human judgment and adjust the pairwise comparison matrix into a fuzzy consistency matrix, which overcomes the traditional hierarchical analysis method that requires several adjustments and tests to make the judgment matrix pass the consistency test. However, this method lacks the unified quantification of indicators in the overall evaluation of the target and is only used for the weight analysis of indicators in practical applications [12]. Therefore, the fuzzy hierarchical analysis method is combined with the fuzzy comprehensive evaluation method to evaluate the competitiveness of university students' competitions, i.e., the weights of each index are calculated by the fuzzy hierarchical analysis method first, and then the overall evaluation is carried out by the fuzzy comprehensive evaluation method [13].

3.1. General Steps of Fuzzy Hierarchical Analysis for Evaluation

3.1.1. Constructing a fuzzy consistency matrix

Definition 1. Let the matrix $R = (r_{ij})_{n \times n}$ if it satisfies $0 \leq r_{ij} \leq 1$ ($i = 1, 2, \dots, n, j = 1, 2, \dots, n$), then R is said to be a fuzzy matrix.

Definition 2. A fuzzy matrix R is said to be fuzzy complementary if the fuzzy matrix $R = (r_{ij})_{n \times n}$ satisfying $r_{ij} + r_{ji} = 1$ ($i = 1, 2, \dots, n; j = 1, 2, \dots, n$).

Definition 3. A fuzzy matrix F is said to be fuzzy consistent if the fuzzy complementary matrix $F = f(i, j)$ satisfies $r_{ij} + r_{ji} = 1$ ($i = 1, 2, \dots, n; j = 1, 2, \dots, n$) for any k .

- (1) Hierarchical single ranking, the root method was used to calculate the weights of each factor in the hierarchy and the weight indicators were normalized to

$$T_j^k = \frac{\bar{T}_j}{\sum_{j=1}^m \bar{T}_j}, \bar{T}_j = \left[\prod_{i=1}^m r_{ij}^k \right]^{1/m}. \quad (1)$$

(2) The total ranking of the levels, combining the weights of each level, gives the weight of the indicator level relative to the total objective, i.e.,

$$w_n^1 = \prod_2^{k=n} w_k^{k-1} = w_1^{n-1} w_2^{n-2} \cdots w_3^2 w_2^1. \quad (2)$$

(3) Comprehensive evaluation of the model using the fuzzy integrated evaluation method.

3.2. The Process of Implementing a Competition Competitiveness Evaluation Model for University Students

3.2.1. Calculation of Indicator Weights Using Fuzzy AHP. According to the calculation steps of the fuzzy analytic hierarchy process, the five primary indicators and 19 secondary indicators in the model are designed into a closed hierarchical model questionnaire with the Likert scale method. Through the network questionnaire star platform, some graduates of local undergraduate normal universities, competition instructors, practice base instructors, and student work managers, the person in charge of the employer conducts a questionnaire survey, converts the collected data with SPSS software, constructs a fuzzy consistency matrix, and sorts the hierarchy to obtain the weight of the corresponding indicators of each criterion level, as shown in the following tables: Table 1, Table 2, Table 3, Table 4, and Table 5.

From Table 1, the weights of the indicators in the criterion level are $w = (0.219, 0.272, 0.241, 0.268)^T$ and the weights of the indicators in the subcriterion level can be calculated as shown in Tables 1–5, which show that the fuzzy consistency matrix of the indicators and their relative weights to the objectives in the competition competitiveness model are knowledge and skills (B_2), redevelopment ability (B_4), morality and quality (B_3), and basic competitiveness (B_1). Among the indicators of “knowledge and skills”, teacher training skills, social practice skills, and academic achievement have relatively greater influence, followed by the ability to use modern technology, research and innovation, and academic competitions; among the indicators of “redevelopment ability”, the ability to combine learning and application has relatively greater influence. In the index factor of “moral and quality,” the influence of professional ethics and dedication is relatively more important, followed by honesty and trustworthiness, law-abiding, collective honor, and political performance; in the index factor of “basic competitiveness, among the “basic competitiveness” indicators, communication ability has a relatively higher weighting, followed by psychological quality, physical quality, and family background.

According to the overall hierarchical ranking formula $w_n^1 = \prod_2^{k=n} w_k^{k-1} = w_1^{n-1} w_2^{n-2} \cdots w_3^2 w_2^1$ out of $w_k^{k-1} = (w_k^k, w_2^k, \dots, w_n^k)$, the influence of 19 secondary indicators on the

TABLE 1: Fuzzy consistency matrix of primary indicators in competition competitiveness model and its relative weight to objectives.

Arrangement B	B_1	B_2	B_3	B_4	w
B_1	0.49	0.40	0.457	0.416	0.22
B_2	0.602	0.51	0.558	0.509	0.273
B_3	0.5554	0.444	0.51	0.452	0.242
B_4	0.595	0.493	0.55	0.51	0.269

TABLE 2: Fuzzy consistency matrix and relative weights for each secondary indicator in criterion B_1 in the competition competitiveness model.

Arrangement B_1	B_{11}	B_{12}	B_{13}	B_{14}	w_1
B_{11}	0.510	0.457	0.489	0.70	0.267
B_{12}	0.545	0.51	0.53	0.743	0.30
B_{13}	0.517	0.472	0.51	0.715	0.277
B_{14}	0.312	0.259	0.287	0.51	0.164

TABLE 3: Fuzzy consistency matrix and relative weights for each secondary indicator in criterion B_2 in the competition competitiveness model.

Arrangement B_2	B_{21}	B_{22}	B_{23}	B_{24}	B_{25}	w_2
B_{21}	0.51	0.466	0.458	0.497	0.469	0.162
B_{22}	0.536	0.49	0.493	0.532	0.504	0.178
B_{23}	0.544	0.509	0.51	0.54	0.509	0.179
B_{24}	0.505	0.47	0.462	0.51	0.472	0.166
B_{25}	0.533	0.498	0.491	0.53	0.60	0.176

TABLE 4: Fuzzy consistency matrix and relative weights for each secondary indicator in criterion B_3 in the competition competitiveness model.

Arrangement B_3	B_{31}	B_{32}	B_{33}	B_{34}	w_3
B_{31}	0.51	0.517	0.469	0.532	0.21
B_{32}	0.485	0.51	0.453	0.516	0.194
B_{33}	0.533	0.547	0.51	0.564	0.214
B_{34}	0.47	0.46	0.438	0.51	0.189

TABLE 5: Fuzzy consistency matrix and relative weights for each secondary indicator in criterion B_4 in the competition competitiveness model.

Arrangement B_4	B_{41}	B_{42}	B_{43}	B_{44}	w_4
B_{41}	0.49	0.45	0.455	0.495	0.237
B_{42}	0.561	0.51	0.515	0.556	0.267
B_{43}	0.545	0.487	0.51	0.55	0.26
B_{44}	0.516	0.117	0.47	0.51	0.24

overall target competition competitiveness is weighted as follows: learning ability, teamwork ability, self-improvement ability, communication ability, organization and management ability, psychological quality, physical quality, professional ethics and professionalism, honesty and trustworthiness, teacher training skills, compliance with the law, social practice ability, academic achievement, collective honor, political performance, modern technology ability,



FIGURE 1: The flower technology course.

research and innovation ability, discipline competition, and family background.

3.3. The Case of Fuzzy Comprehensive Evaluation Method for Evaluating the Competitiveness of University Students' competitions. The relative weights of the indicators in the competition competitiveness model calculated by the above fuzzy hierarchical analysis method can be used to calculate the overall competition competitiveness of students by using fuzzy comprehensive evaluation, and the combination of the two methods can comprehensively evaluate the competitiveness of students so as to improve the competition competitiveness of students in a targeted manner [14].

The evaluation team is composed of graduates, competition instructors, student work managers, representatives of practice base instructors, and some employers, and according to the observation points contained in each index, a set of comments $U = \{\text{strong, strong, fair, poor}\}$.

Let us determine the relationship matrix between the criterion level B and U, $B_1 = \{0.3, 0.5, 0.2, 0\}$, $B_2 = \{0.2, 0.2, 0.5, 0.1\}$, $B_3 = \{0.3, 0.4, 0.2, 0.1\}$, and $B_4 = \{0, 0.3, 0.5, 0.2\}$. The specific meaning is exemplified by the fact that 30% of the evaluation team considered the observation of the basic competitiveness indicator in the overall competition competitiveness of the class to be strong, 50% considered it to be strong, 20% considered it to be average, and 0% considered it to be poor. From this, the relationship matrix is obtained as follows:

$$R = \begin{pmatrix} B_1 \\ B_2 \\ B_3 \\ B_4 \end{pmatrix} = \begin{pmatrix} 0.3 & 0.5 & 0.2 & 0 \\ 0.2 & 0.2 & 0.5 & 0.1 \\ 0.3 & 0.4 & 0.2 & 0.1 \\ 0 & 0.3 & 0.5 & 0.2 \end{pmatrix}. \quad (3)$$

Based on the weights of the indicators at each level of the criterion layer calculated above $w = \{0.219, 0.272, 0.241, 0.268\}$. The weighted average fuzzy synthesis operator $M(\bullet, \oplus)$ is used to synthesize W and foot to obtain a fuzzy comprehensive evaluation result vector v , i.e., $v = w \circ R$. Here, " \circ " is the weighted average fuzzy synthesis operator $M(\bullet, \oplus)$, which is calculated as follows:

$$v_j = \min \left(1, \sum_{i=1}^p w_j r_{ij} \right), j = 1, 2, \dots, n. \quad (4)$$

Then there are

$$\begin{aligned} v = w \circ R &= (0.219, 0.272, 0.241, 0.268) \circ \begin{pmatrix} 0.3 & 0.5 & 0.2 & 0 \\ 0.2 & 0.2 & 0.5 & 0.1 \\ 0.3 & 0.4 & 0.2 & 0.1 \\ 0 & 0.3 & 0.5 & 0.2 \end{pmatrix} \\ &= \{0.1924, 0.3407, 0.362, 0.1049\}. \end{aligned} \quad (5)$$

The calculation results show that through the fuzzy comprehensive evaluation of the indicators, 19.24% of the students in the selected graduation class have strong competitive ability, 34.07% have strong competitive ability, 36.2% have average competitive ability, and 10.49% have poor competitive ability. According to the order of weighting of each observation, universities should develop corresponding countermeasures to improve the competitive ability of students with average and poor competitive ability when training talents.

4. Design Effect

Firstly, according to market demand, there is a division between flowers for personal consumption and flowers for weddings and business meetings. The students were asked to investigate the daily use of flowers, and the general demand was for loose flowers to decorate homes at wholesale, mainly in vases, or for people to use them for hobbies and cultivation, arranging flowers according to their own interests [15]. For weddings and conferences, the majority of flowers are used for the decoration of the venue, mainly in large groups, specifically for the decoration of the sign-in desk, the podium, and the guests' desk in the hotel venue, as well as for the local decoration of the floats, the new house, and the participants in the conference. As a teacher of floristry, the floristry course, shown in Figure 1, is



FIGURE 2: Example of flower arrangement.

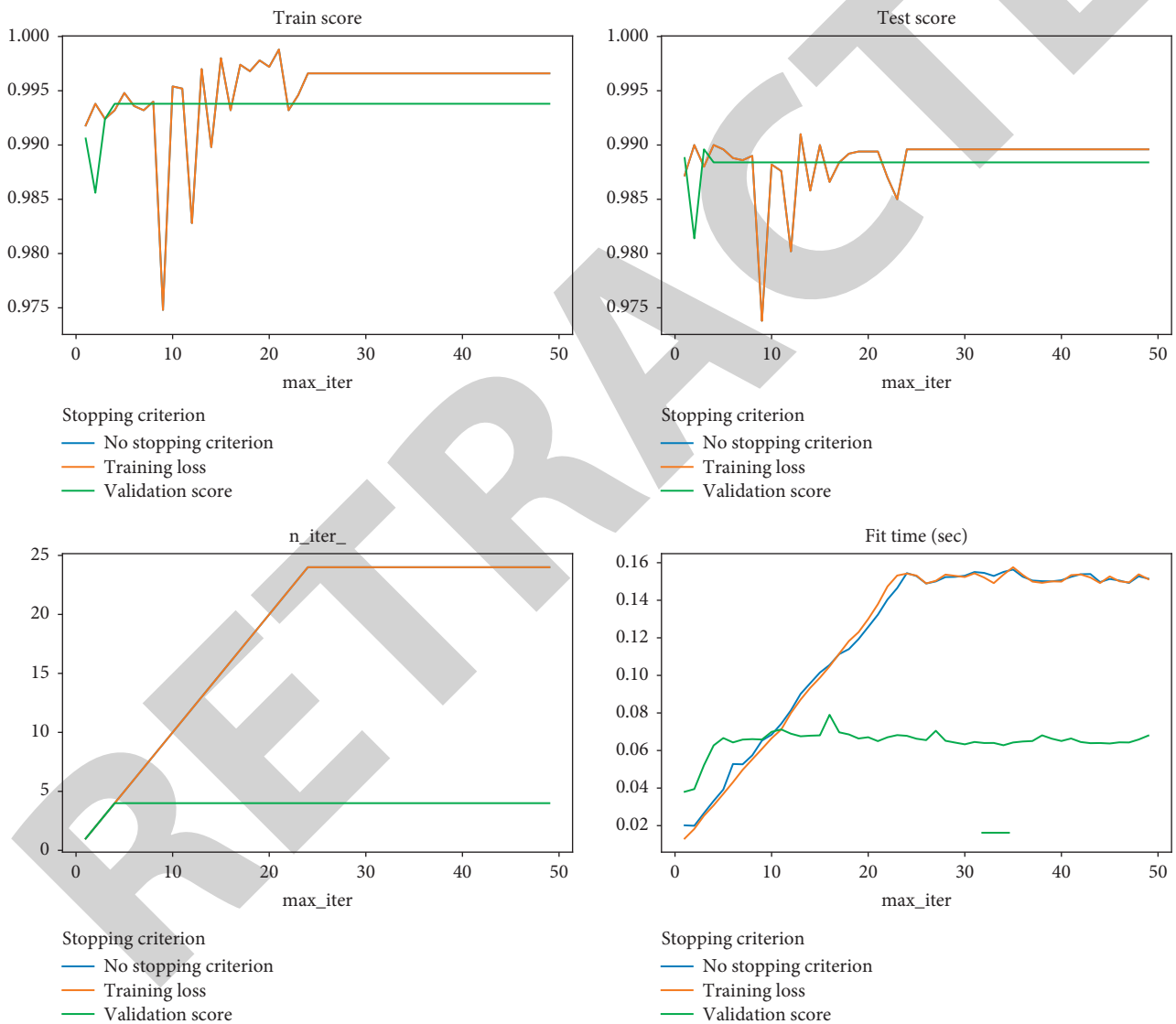


FIGURE 3: Effect of flower arrangement with different parameters.

designed to provide students with an in-depth understanding of the art of floral arranging, not only through the operation of floral arrangements in the training room but also through the process of planting and growing various floral materials.

Professional ethics are the most fundamental, basic, and minimum ethical concepts for those engaged in a certain

kind of work. As a florist, the most fundamental aspect of professional ethics is the use of floral art to work for human civilization, and for the sake of this civilization, I and my students are required to be highly disciplined in our professional ethics and to create works with a soul: to work in the art of floral arrangement, one must first love floral art and not dislike the hardships involved in its creation [16].

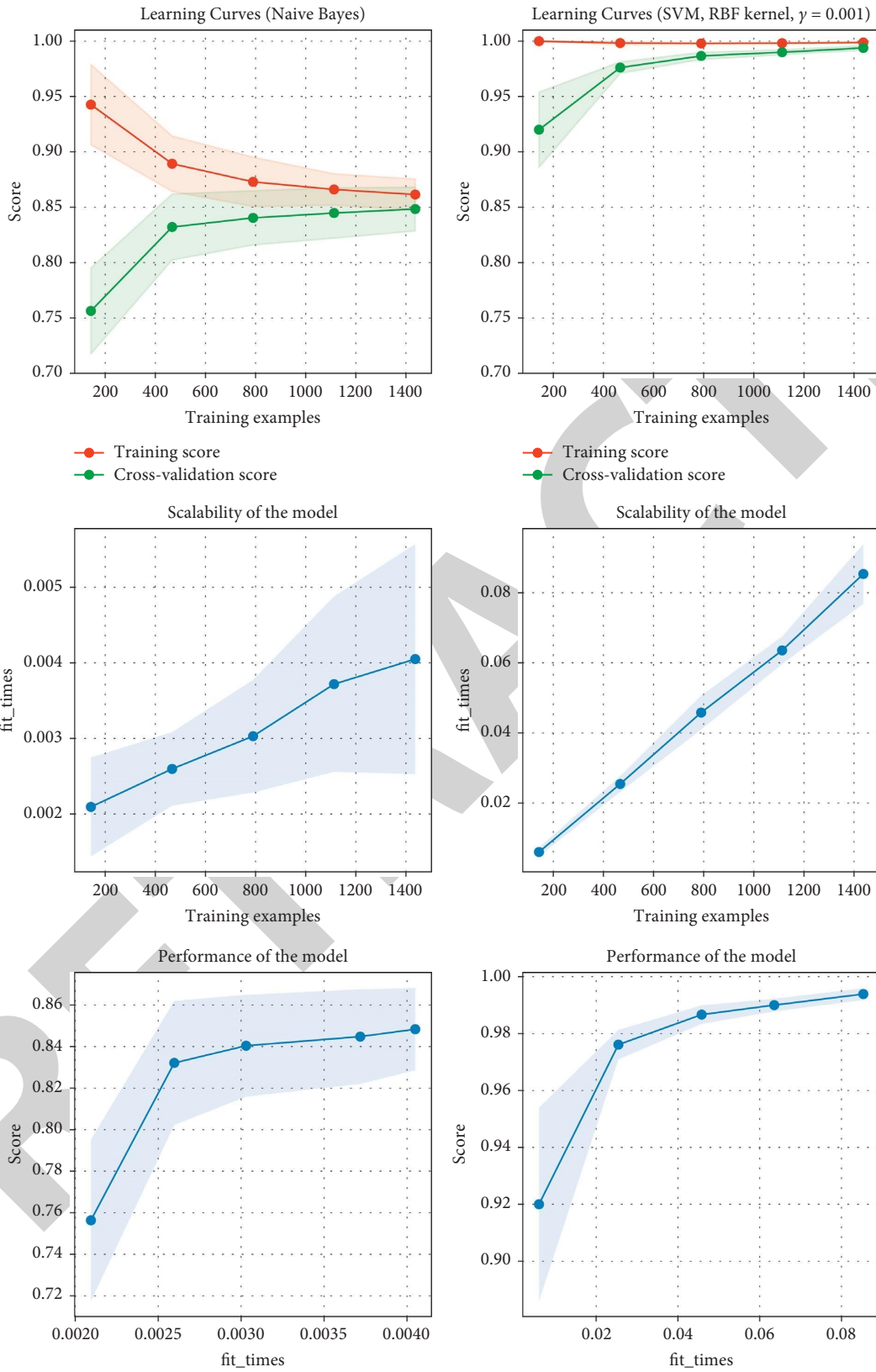


FIGURE 4: Teaching effects with different training effects.

The work of floral arrangement is a work of art. Floral artwork is all about beauty, but in practice, we flower arrangers have to do a lot of preliminary work before the flowers and plants become a work of art, as shown in Figure 2.

5. Case Studies

The academic skills competition is neither a matter for a few students nor the ultimate goal, but a link in the teaching system and a means to cultivate the innovative and practical ability of college students [17]. It is only by allowing all interested students to participate in it that we can fundamentally create a good academic atmosphere and contribute to the construction of an excellent academic style in universities. Therefore, first of all, it is necessary to move towards a profound understanding of the disciplinary skills competition from the ideological point of view, to realize the real meaning of the skills competition, and to create a harmonious atmosphere around the disciplinary skills competition with the scientific outlook on development as the guiding ideology. The effect of flower arrangement under different parameters, as shown in Figure 3, (a) perfect organizational structure and a sound evaluation and incentive mechanism are important guarantees for the smooth development of the discipline skills competition. The documents related to the competition are unified by the school, and the competition organization steering committee is unified in its deployment, which makes the organization work all based on evidence and responsibility to the people.

The university's academic affairs management department constantly standardizes the process of subject skills competitions, summarizes and recognizes them in a timely manner, and institutionalizes them, incorporating competition-related organization and coaching work into the assessment and evaluation system. As shown in Figure 4, the different teaching effects are rewarded with extra points for comprehensive assessment, Xiangnong youth quality development credits, and competition bonuses for the winning students; the instructors are rewarded with guidance bonuses, workload recognition, and tilted title assessment and the outstanding individuals and groups who have won awards are commended at the annual school-level commendation conference, which has comprehensively stimulated the enthusiasm and initiative of students and teachers for the subject skills competitions [18]. To a certain extent, the branding of subject skills competitions is a reflection of the characteristics of a university, and subject skills competitions with subject characteristics and professional features are an important opportunity to enhance teaching quality and promote innovation [19]. By promoting the multilevel management of disciplinary skills competitions, the disciplinary skills competitions can be developed on a large scale so as to realize the branding of high-quality disciplinary skills competitions with one specialty in one college and many products in one university.

In summary, the course is taught in groups, with free combinations, observation of students' performance, and a graded approach to teaching students according to their

abilities. In terms of credit assessment, the theoretical knowledge is assessed in the form of written questions and answers, accounting for 30% of the total grade; the practical production of floral artworks accounts for 40% of the total grade; and the usual performance accounts for 30% of the total grade so that a combination of various aspects can be achieved to arrive at an objective and fair overall grade for the students [20, 21].

6. Conclusions

As an important element in the development of comprehensive quality education activities in universities, it can not only stimulate the interest of university students in learning scientific knowledge and enthusiasm for learning and strengthen their hands-on ability, but also enhance the initiative and creativity of students in learning, which can contribute to the overall improvement of comprehensive quality education and talent quality training of university students, demonstrate the enterprising spirit of teachers and students, cultivate a group of innovative and entrepreneurial talents with high sensitivity to competition, and play a positive role in the construction of university academic style.

Data Availability

The experimental data used to support the findings of this study are available from the corresponding author upon request.

Conflicts of Interest

The authors declare that they have no conflicts of interest regarding this work.

Acknowledgments

1. Scientific and technological innovation team construction project of severe rocky desertification control mode of Hunan Biological Electromechanical Vocational Technical College (no. 18TD02). 2. Construction project of Teaching Resource Bank of leisure agriculture specialty in Hunan Province (no. xxny11).

References

- [1] A. Kamilaris and F. X. Prenafeta-Boldú, "Deep learning in agriculture: a survey," *Computers and Electronics in Agriculture*, vol. 147, pp. 70–90, 2018.
- [2] C. D. S. Garcia, A. Meinheim, E. R. Faria Junior et al., "Process mining techniques and applications - a systematic mapping study," *Expert Systems with Applications*, vol. 133, pp. 260–295, 2019.
- [3] H.-Y. Wu, H.-S. Wu, I.-S. Chen, and H.-C. Chen, "Exploring the critical influential factors of creativity for college students: a multiple criteria decision-making approach," *Thinking Skills and Creativity*, vol. 11, pp. 1–21, 2014.
- [4] D. Tien Bui, H. Shahabi, A. Shirzadi et al., "A novel integrated approach of relevance vector machine optimized by imperialist competitive algorithm for spatial modeling of shallow landslides," *Remote Sensing*, vol. 10, no. 10, p. 1538, 2018.

Research Article

Rule Analysis of Teaching Evaluation System Based on Data Mining under Web Platform

Jing Wang 

Faculty of Education, Southwest University, Chongqing 400715, China

Correspondence should be addressed to Jing Wang; wj6002@swu.edu.cn

Received 20 December 2021; Revised 20 January 2022; Accepted 28 January 2022; Published 29 March 2022

Academic Editor: Antonio J. Peña

Copyright © 2022 Jing Wang. This is an open access article distributed under the Creative Commons Attribution License, which permits unrestricted use, distribution, and reproduction in any medium, provided the original work is properly cited.

In order to understand the advantages of the teaching evaluation system to teachers and students more intuitively, according to the data analysis, the lowest total score of teachers is $\rightarrow 1.04$, and the five index values are all negative, so the relevant teaching contents should be changed according to the index factors of relevant teaching evaluation to make it easier for students to understand and accept. Through the analysis of the total evaluation scores of several teachers surveyed in each semester, we can see that the total evaluation scores of teachers 4 and 7 fluctuate greatly, so we should choose suitable teaching content for rectification. By classifying teachers, they are divided into three categories by means of discipline colleges, etc. It can be seen from the figure that the lowest total score of teachers in category 3 is $\rightarrow 2.12$, which shows that teachers in this category may have similar problems in teaching methods. By comparing the information entropy algorithm of teaching evaluation, we know that the information entropy under the AVF algorithm model takes about 1 ms to the teaching evaluation algorithm, while the greedy algorithm model takes about 20 ms to test the teaching evaluation system. We know that the teaching evaluation system based on the proposed algorithm information entropy algorithm and the teaching evaluation system under the AVF algorithm model and traditional information entropy all pass the test. However, combined with the images, the AVF algorithm model has the highest computational efficiency and the shortest time, followed by the proposed algorithm model. Compared with the traditional teaching evaluation algorithm, it is inefficient and takes a long time. When the number of requests is 1000, the average response time of the AVF algorithm method is 17 ms, and the longest time of the traditional method is 32 ms. Combined with images, when the number of requests is 1000, 1500, 200, 2500, 3000, 350, and 4000, the average response time increases with the increase of the number of requests, but the AVF algorithm method takes the shortest time and meets most teaching evaluation requirements. Combined with the success rate image, we can see that the success rate decreases slightly with the increase of request times, but the success rate of the AVF algorithm method is relatively stable, with the lowest of 99.6% when the request times are 3500. Through a large number of charts and analyses, we can see that the teaching evaluation under the AVF algorithm method has the highest efficiency and the shortest time.

1. Introduction

Through the research of data mining technology, we can get the related methods to improve data mining technology and establish and analyze the teaching evaluation system so as to improve the teaching evaluation system from many aspects. At the same time, the information entropy is calculated by the AVF algorithm, which can improve the efficiency and time of teaching evaluation.

The gene is transferred from its natural genome to the substitute of the same code, which becomes “codon

optimization” [1]. However, the scientific community lacks a systematic understanding of this method and puts forward the method of “synthetic gene designer” to solve this problem. In order to meet the needs of high-capacity wireless communication, engineers continue to develop technologies [2]. At the same time, students also need to know how to learn this technology. Literature [3] for efficient computation and analysis of 3DFD uses a web platform for related research. In order to complete 3DFD, it is necessary to combine CUDA with web GL and other emerging technologies. Literature [4] carries out learning tasks such as

genome comparison by annotating position sequences and studying gene models. This method is applied to sequence comparison by BLAST. *JBrowse* is easy to embed in a website or application. It is built in JavaScript and HTML5 [5], and it is much faster and more scalable. At the same time, *JBrowse* can distinguish pictures offline. As an independent web page, you can easily use plug-ins to add, analyze, and perform other operations. Literature [6] can describe the number of lymphocytes by RepSeg method. Lymphocytes can recognize specific antigens and have specificity. The application of Vidjil involves four steps. Through Witten and Frank's book on output knowledge [7], we understand the main methods of data mining. Literature [8] studies data mining through basic input, input algorithms, and schemes. Combining data mining with open source machine science and other data modeling and analyzing it with illustrations and tables to discuss its uses in-depth and also make the analysis more in-depth, more comprehensive, and efficient. Data mining, a hot topic, has been listed as a high-income mode by many companies [9], and at the same time, many researchers are taking data mining as a related research topic. Data mining technology has attracted many researchers' attention, and they want to better understand customer behavior through related data mining so as to increase business opportunities. Literature [10] has reported that data mining can dig out secrets from massive data. Data mining is very important for customer information and relationship management [11], but there are also some problems, such as a lack of relevant literature reviews. In order to improve the teaching quality, students, as the main body [12], should evaluate the teaching quality through questionnaires and interviews. Literature [13] evaluates and investigates 6395 students, including 3200 undergraduates and 300 postgraduates, and analyzes the overall teaching achievements. Then, according to the relevant reward and punishment system and the balance between teaching and research, the teaching system is discussed and formulated. In order to make dictation play an important role in foreign language teaching [14], and teaching evaluation analyzes the common mistakes in foreign language listening based on many years of English teaching experience and obtains some changes in nature and function. Literature [15] experiences its use in the learning environment by writing role-playing.

2. Model and Process Analysis

2.1. Web Platform Based on Revit Model. Revit models fall into two categories, users and administrators. Administrators log in to the web platform for user management, system messages, file processing, and other operations [16]. Revit file processing includes saving data into a database, obtaining Revit files, building 3D models, and other operations [17]. As shown in Figure 1.

Revit model has the following advantages as the core of system platform processing:

- Projects: each project has a separate database
- Family: contains all the information of the parameter model

Program interface: can create new functional modules and model construction

The overall operation of the web platform is as follows:

The web management system mainly includes login and then displaying the web interface, Revit file management, and the functions of the interface management and other functions.

Revit file processing plug-in mainly includes geometric parameter data conversion, attribute parameter data extraction, and other operational processes. As shown in Figure 2.

2.2. Platform Operation Diagram. The overall process of the platform is as follows: by logging in to the platform and carrying out the Revit file management interface, it can process data and content in many aspects, export data, and convert data. Finally, the data is logged in to the database and the process ends [18], as shown in Figure 3.

2.3. Web Services Platform Flow Chart. Users enter the login interface by sending login requests, enter the Web management system for file uploading and verification after successful login, and finally process files in the Revit file processing plug-in interface [19], as shown in Figure 4.

2.4. Teaching Evaluation System. By establishing a teaching evaluation system to investigate the teaching quality of teachers, the data can be obtained [20]. The low score of the teaching evaluation indicates that the teaching method is not suitable for students or the teaching difficulty coefficient is large, so the teaching scheme should be adjusted according to the specific teaching evaluation factors. The high score of the teaching evaluation indicates that most students are suitable for the teacher's teaching method, and the teaching quality is monitored normally through teaching evaluation so as to adjust the teaching plan [21], as shown in Figure 5.

2.5. Data Mining Technology. Data mining includes screening data, extracting target data, preprocessing data, mining data, evaluating related data, and finally transforming them into knowledge [22], as shown in Figure 6.

3. Data Mining and Teaching Evaluation Techniques

3.1. Data Mining

3.1.1. Apriori Basic Algorithm. X and Y are arbitrary itemsets, then

$$\text{sup}(X \cup Y) = \frac{|X \cup Y|}{|D|}. \quad (1)$$

Confidence is

$$\text{conf}(X \cup Y) = \frac{|X \cup Y|}{|X|}. \quad (2)$$

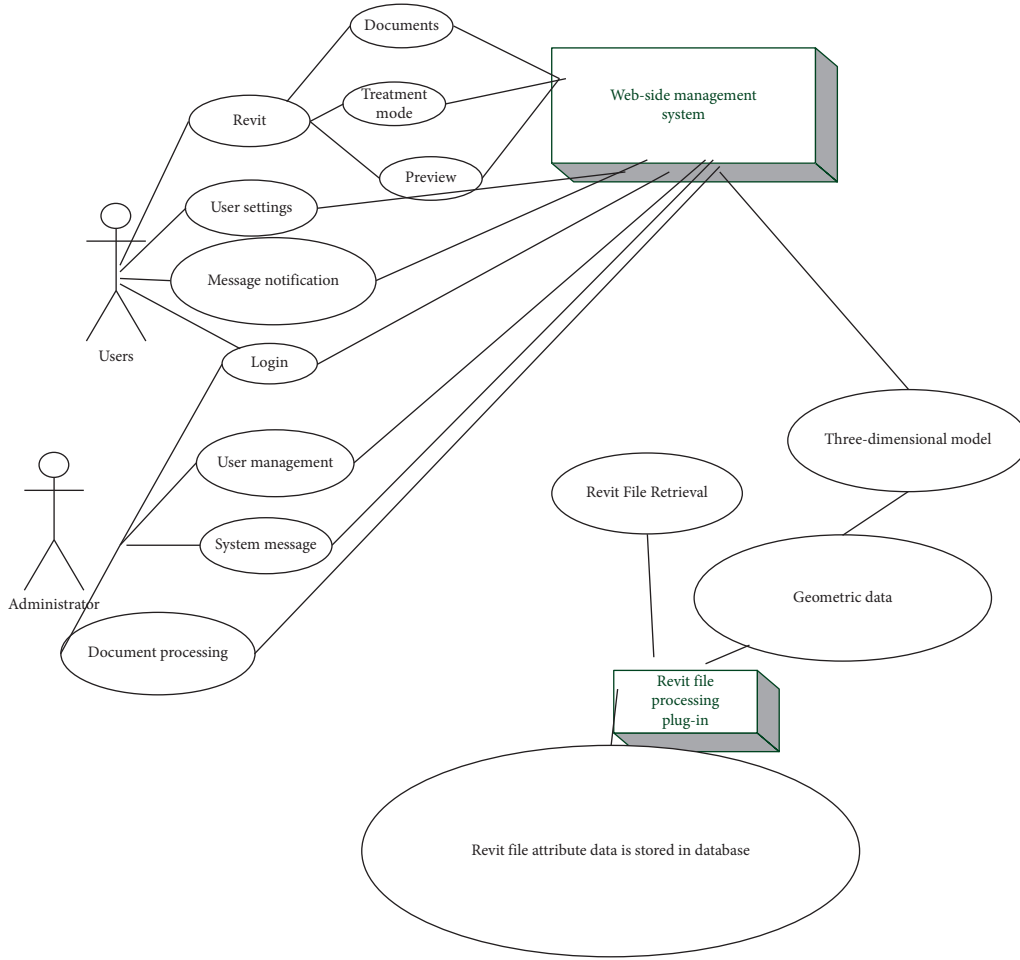


FIGURE 1: Web platform under Revit.

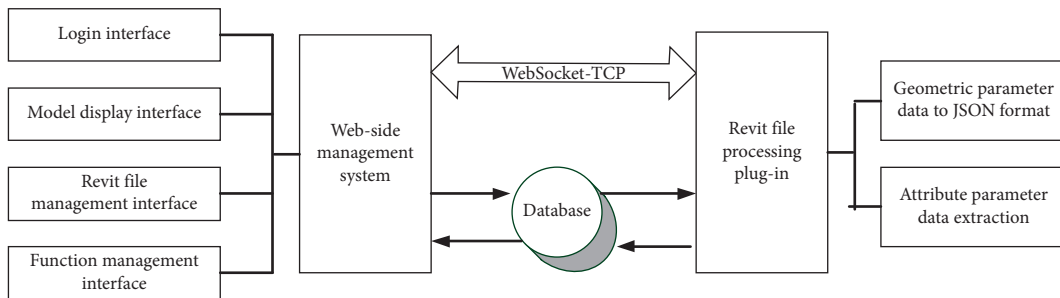


FIGURE 2: Overall diagram of the web platform.

3.1.2. *Weighting Factor Algorithm.* $w \sup_w(I)$ is the weighted minimum support and it is represented as follows:

$$w \sup_w(I) = \frac{1}{k-2} \sum_{i \in I} w_i \sup(I). \quad (3)$$

$w \text{ conf}_w I$ is the weighted minimum confidence and it is represented as follows:

$$(w \text{ conf}_w I \rightarrow J) = \frac{w \sup(I \cup J)}{w \sup(I)}. \quad (4)$$

3.2. *Information Entropy of Teaching Evaluation*

3.2.1. *Information Entropy Algorithm.* The probability is

$$P_i = \frac{x_i}{x}. \quad (5)$$

Sample classification information entropy

X is the set of data samples, and X is the number of X . C is the attribute class variable, n is the total number of classes, and x_i is the number of samples contained in the C_i class. Then

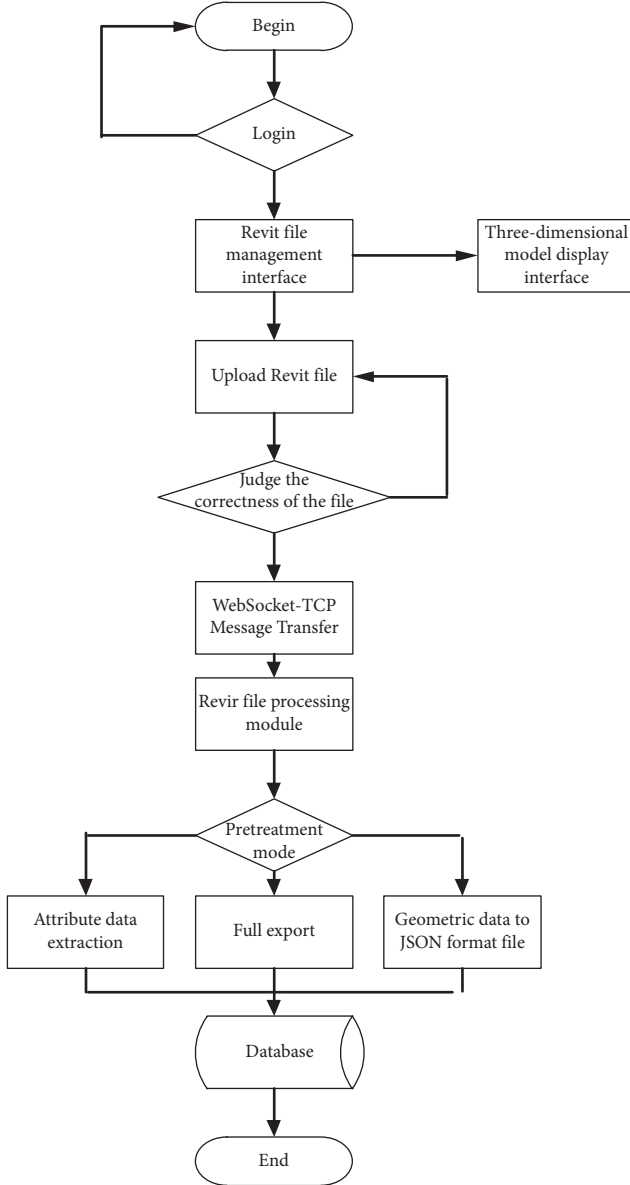


FIGURE 3: Overall flow chart of the platform.

$$I(x_1, x_2, \dots, x_n) = - \sum_{i=1}^n p_i \log_2 p_i. \quad (6)$$

The information entropy of Y is

$$E(Y) = \sum_{j=1}^m \frac{x_{1j} + x_{2j} + \dots + x_{nj}}{x} \times I(x_{1j}, x_{2j}, \dots, x_{nj}). \quad (7)$$

Information gain is calculated as

$$\text{Gain} = I(x_1, x_2, \dots, x_n) - E(Y). \quad (8)$$

3.2.2. Improvement of Information Entropy Algorithm

$$p_i = \frac{1 - s_i}{1 + s_i}. \quad (9)$$

From formula (9)

$$s_i = \frac{1 - p_i}{1 + p_i}. \quad (10)$$

The entropy of information brought into sample classification is

$$- \sum_{i=1}^n \frac{1 - s_i}{1 + s_i} \log_2 \frac{1 - s_i}{1 + s_i} = - \sum_{i=1}^n \frac{1 - s_i}{1 + s_i} \frac{\ln 1 - s_i / 1 + s_i}{\ln 2}. \quad (11)$$

The formula for calculating information entropy is

$$\frac{1}{x} \sum_{i=1}^n \frac{x_i (x^3 - x_i^3)}{(x + x_i)^3}. \quad (12)$$

3.2.3. Teacher-Driven Algorithm

(1) Through relevant teaching evaluation, teachers' driving force is divided into four entropies: excellent, good, medium, and poor [24].

$$E(X_{\text{Excellent}}) = 0,$$

$$E(X_{\text{Good}}) = 0.3,$$

$$E(X_{\text{Medium}}) = 0,$$

$$E(X_{\text{Difference}}) = - \left(\frac{1}{1} \right) \log_2 \left(\frac{1}{1} \right) = 0,$$

$$E(X_{\text{Teacher-driven}}) = \left(\frac{5}{10} \right) E(X_{\text{Excellent}}) + \left(\frac{3}{10} \right) E(X_{\text{Good}}) + \left(\frac{1}{10} \right) E(X_{\text{Medium}}) + \left(\frac{1}{10} \right) E(X_{\text{Difference}}) = 0.2. \quad (13)$$

(2) Participating in interaction (Boolean variable), then

$$E(X_{\text{Yes}}) = 0.3, \quad (14)$$

$$E(X_{\text{No}}) = 0.2.$$

The entropy obtained from the information entropy is

$$E(X_{\text{Doyouparticipateintheinteraction}}) = \left(\frac{3}{10} \right) E(X_{\text{Yes}}) + \left(\frac{7}{10} \right) E(X_{\text{No}}) = 0.3. \quad (15)$$

(3) Curriculum difficulty entropy includes four variables: easy, acceptable, hard, and difficult. They are expressed as

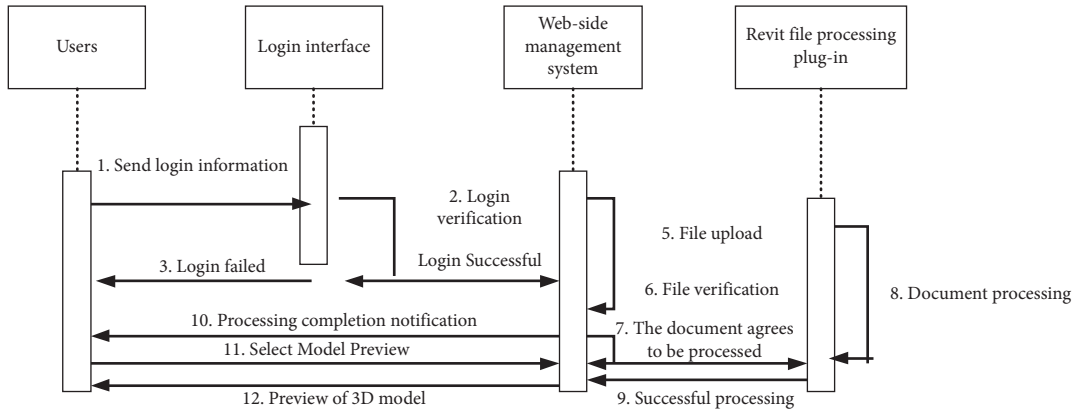


FIGURE 4: Web services flow chart.

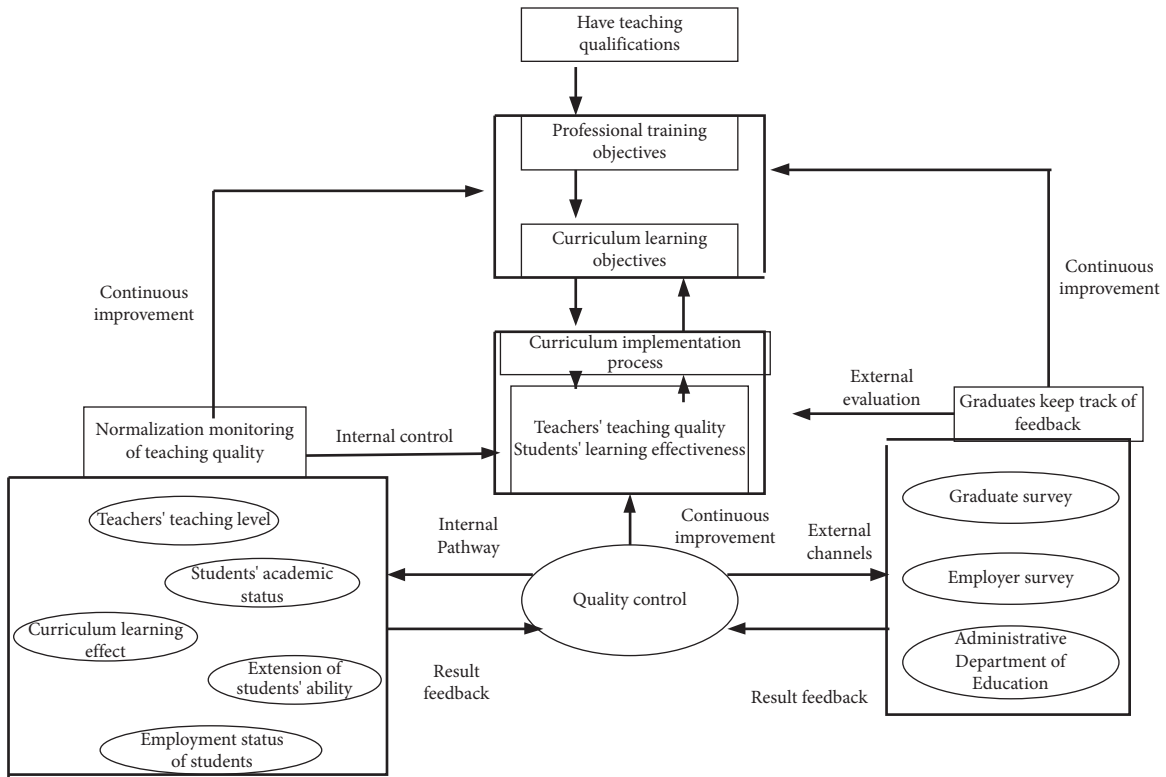


FIGURE 5: Model diagram of teaching evaluation system.

$$\begin{aligned}
 E(X_{\text{Easy}}) &= 0, \\
 E(X_{\text{Acceptable}}) &= 0.2, \\
 E(X_{\text{Hard}}) &= 0.1, \\
 E(X_{\text{Difficult}}) &= 0.3.
 \end{aligned}
 \tag{16}$$

$$\begin{aligned}
 E(X_{\text{Coursedifficulty}}) &= \left(\frac{2}{10}\right)E(X_{\text{Easy}}) + \left(\frac{3}{10}\right)E(X_{\text{Acceptable}}) \\
 &\quad + \left(\frac{2}{10}\right)E(X_{\text{Hard}}) \\
 &\quad + \left(\frac{3}{10}\right)E(X_{\text{Difficult}}) = 0.3.
 \end{aligned}
 \tag{17}$$

The characteristic entropy of course difficulty is:

(17)

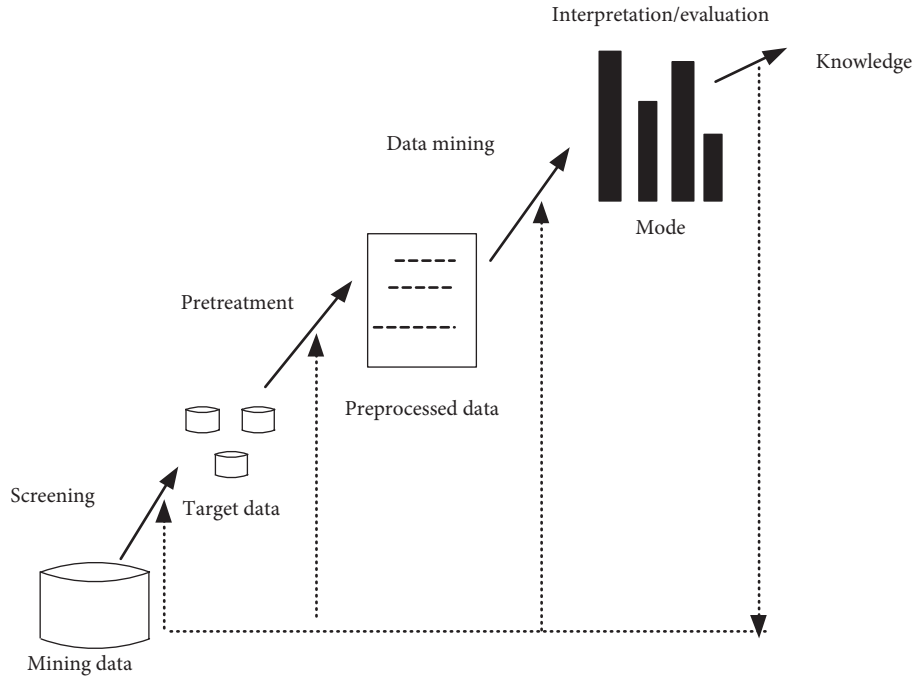


FIGURE 6: Data mining flow chart.

- (4) Curriculum neutralization evaluation entropy is divided into four attributes: excellent, good, medium, and poor [11]. They are expressed as

$$\begin{aligned}
 E(X_{\text{Excellent}}) &= 0, \\
 E(X_{\text{Good}}) &= 0.1, \\
 E(X_{\text{Medium}}) &= 0.5, \\
 E(X_{\text{Difference}}) &= 0.
 \end{aligned} \tag{18}$$

The entropy of curriculum attribute neutralization and evaluation is as follows:

$$\begin{aligned}
 &E(X_{\text{Comprehensiveevaluationofcurriculum}}) \\
 &= \left(\frac{3}{10}\right)E(X_{\text{Excellent}}) + \left(\frac{2}{10}\right)E(X_{\text{Good}}) + \left(\frac{5}{10}\right)E(X_{\text{Medium}}) \\
 &\quad + \left(\frac{0}{10}\right)E(X_{\text{Difference}}) = 0.1.
 \end{aligned} \tag{19}$$

4. Analysis of Teaching Evaluation System

4.1. Analysis of Teacher Evaluation Index

4.1.1. Analysis of Teachers' Indicators. According to the analysis of five indexes of nine teachers in a college in the following figure, the total score of teacher 1 is -1, of which the highest index 5 is -0.7 and the lowest index 2 is -1.2. The total score of teacher 2 is 0.68, among which the highest score of index 5 is 0.8 and the lowest scores of indexes 2 and 3 are 0.6. The total score of teacher 3 is 1.24, among which the lowest score of index 2 is 1.1 and the highest score of

index 5 is 1.4. The total score of teacher 4 is -0.24, and the lowest score is index 2 is -0.3. The total score of teacher 5 is 0.26 and the highest score of index 4 is 0.4. The total score of teacher 6 is -1.04 and the highest score of index 3 is -1. The total score of teacher 7 is 1.18 and the highest scores of indicators 1 and 4 are 1.3. The total scores of teachers 8 and 9 are 0.38 and 0.84, respectively. Compared with the total scores of 9 teachers, the highest total score of teacher 3 is 1.24, and the lowest total score of teacher 6 is -1.04. Through the analysis of the total score, it can be seen that among the 9 teachers, teacher 3 has a better teaching evaluation, and the teaching method may be more acceptable to students. At the same time, the total scores of teachers 1 and 6 are relatively low, and the teaching quality or methods need to be improved. The teaching evaluation index represents a comprehensive evaluation of teachers in many aspects, which can represent teachers' driving force, participation in class, course difficulty, teaching wit, teachers' dress, and so on, as shown in Figure 7.

4.1.2. Analysis of Teachers' Evaluation in Each Semester.

Through the analysis of the following figure, it can be seen that the total score of teacher 1 decreased slightly from the 123rd semester to the 125th semester and increased slightly from the 126th semester to the 127th semester, indicating that the teacher gradually found an adaptive teaching method after the 126th semester, and the total score of the teaching evaluation increased. The total score of teacher 2's teaching evaluation basically remained between -0.3 and 0.4, with little change. Teacher 4's total score of the teaching evaluation fluctuates greatly, falling to about -3.6 in the 127th semester. We should analyze the small scores of each index, adjust the relevant teaching methods as soon as

```

(i) Input: transaction set  $T$ , minimum support  $\text{min\_sup}$ , and minimum confidence  $\text{min\_conf}$  [23].
Output: frequent itemset  $L$ 
BEGIN
1)  $\forall T \neq \text{NULL}$ 
2)  $C_1 = \text{Generate\_}C_1(T)$ ;
3)  $L_1 = \{c \in C_1 | \text{sup}(c) \geq \text{min\_sup}\}$ ;
4)  $K = 2$ ;
5) While ( $L_k > 0$ )do
6)  $\{K++\}$ ;
7)  $C_k = \text{Generate\_}C_k(T_{k-1})$ ;
8)  $L_k = \{c \in C_k | \text{sup}(c) \geq \text{min\_sup}\}$ ;
9)  $L = \cup L_k$ ;
10)  $R = \text{Generate\_Rule}(L); // \text{min\_conf}$ 
END.
    
```

ALGORITHM 1: Apriori classical algorithm.

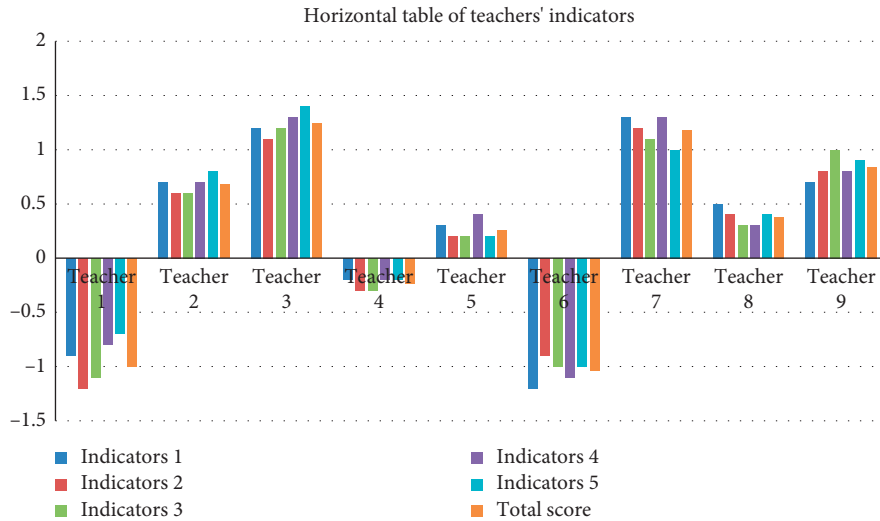


FIGURE 7: Horizontal analysis of teaching evaluation.

possible, and provide students with more suitable teaching content. The scores of teachers 6 and 8 fluctuate a little, and the total score of teachers 7 dropped to -1.4 in the 127th semester, so teaching methods should be improved as soon as possible. As shown in Figure 8.

4.1.3. *Analysis of Teacher Classification Index.* According to the disciplines and colleges taught by their teachers, teachers are divided into three categories. The total score of teacher category 1 is -0.68. The scores of indicators 1 to 5 are relatively average and do not fluctuate much, but indicators 1 to 5 are all negative. Teaching quality and students' acceptance should be improved through the analysis of various indicators. The total score of teacher category 2 is 0.68, and the scores of indicators 1–5 are relatively average. The lowest total score of teachers' category 3 is -2.12, and most of its indexes are lower than -1.7, which is low. Therefore, teaching

methods should be changed as soon as possible to improve the scores of each index. As shown in Figure 9.

4.2. *Comparison of Data Mining Algorithms.* As can be seen from Table 1, the total time consumption of the improved Apriori algorithm is 264, which saves more time than the other two data mining algorithms. The total time consumed by the Apriori algorithm is 443, the total time consumed by the improved Apriori algorithm is 264, and the total time consumed by the ID3 algorithm is 524. The analysis shows that the Apriori algorithm can save time and have higher efficiency than the ID3 algorithm. Compared with the traditional Apriori algorithm, the improved Apriori algorithm further shortens the data mining time and improves the efficiency again. Therefore, in order to improve the efficiency of data mining, the improved Apriori algorithm should be preferred.

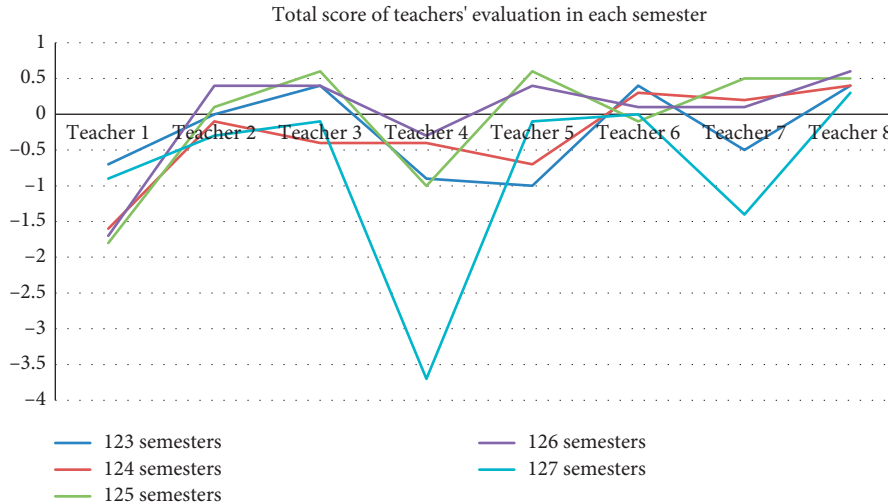


FIGURE 8: Analysis of the total score of teaching evaluation in each semester.

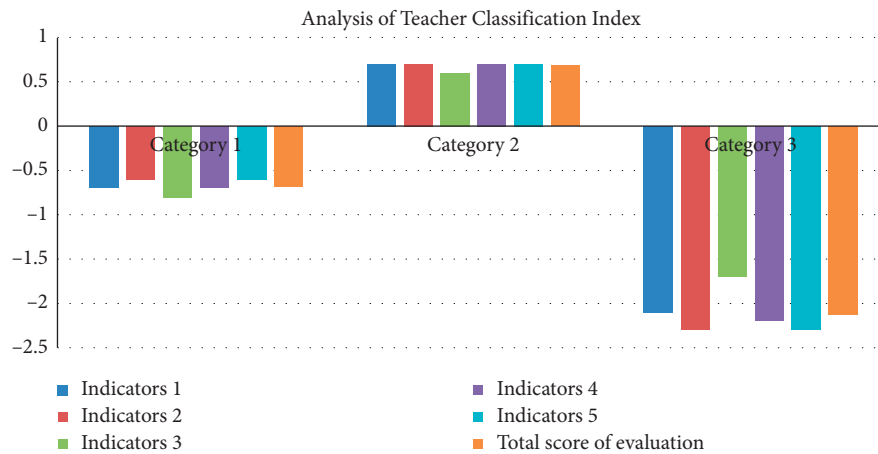


FIGURE 9: Classification index analysis.

TABLE 1: Comparison of data mining algorithms.

Algorithm	C ₁	C ₂	C ₃	C ₄	C ₅	C ₆	总耗时
Apriori algorithm	153	163	239	156	132	133	443
Improved Apriori algorithm	151	79	144	68	31	16	264
ID3 algorithm	164	152	248	173	158	147	524

Through image analysis in Figure 10, we can see that the curve trend of the Apriori algorithm is similar to that of the improved Apriori algorithm, but the improved Apriori algorithm takes less time, so the algorithm is preferred when selecting the algorithm.

4.3. Comparison of Information Entropy Algorithms in Teaching Evaluation. By comparing three kinds of information entropy in teaching evaluation, we can see that the longest running time of the information entropy calculation of greedy algorithm model is 20 ms, the longest running time of the information entropy calculation of the proposed

algorithm is about 4 ms, and the shortest running time of the information entropy calculation of the AVF algorithm is about 1 ms. In contrast, this method has the shortest running time and the highest efficiency, as shown in Figure 11.

4.4. System Test. The average response time and peak flow response time of the system are tested and analyzed by teaching evaluations of 1000, 2000, and 3000 people at the same time.

As can be seen from Table 2, in the teaching evaluation system based on the proposed algorithm information entropy algorithm, when the number of evaluators is 1000, the

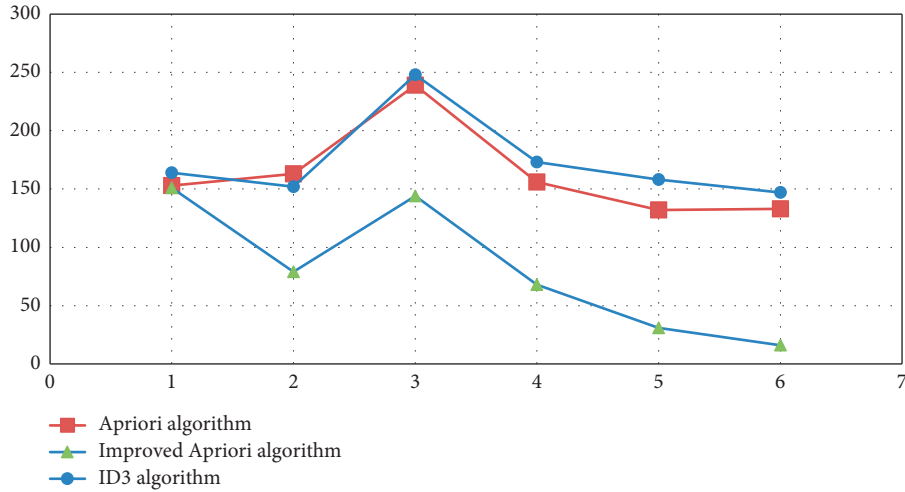


FIGURE 10: Comparison of data mining algorithms.

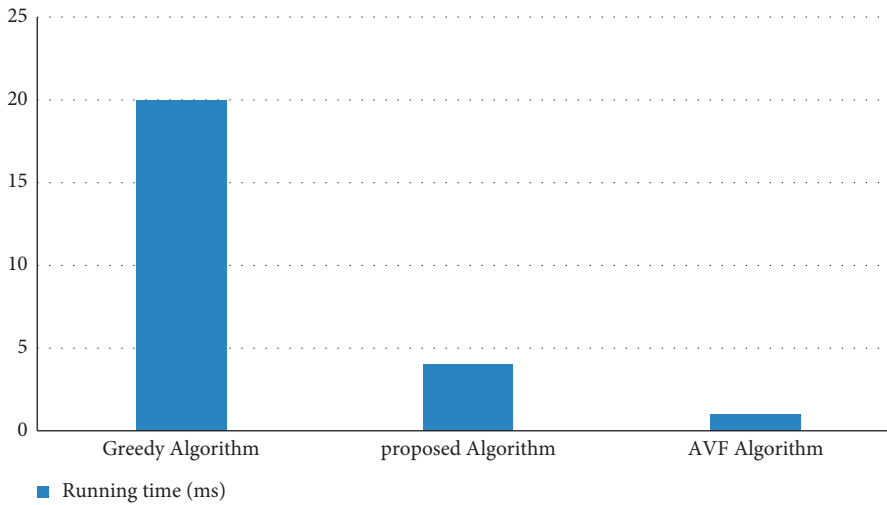


FIGURE 11: Comparison of information entropy operations.

TABLE 2: Proposed algorithm model analysis.

Number of evaluators	Average response time (ms)	Peak flow response time (ms)	Test conclusion
1000	1.323	1.468	Pass
2000	1.654	2.031	Pass
3000	2.346	2.447	Pass

average response time is 1.323 ms, and the peak flow response time is 1.468 ms; when the number of evaluators is 2000, the average response time is 1.654 ms, and the peak flow response time is 2.03 ms; and when the number of evaluators is 3000, the average response time is 2.346 ms, and the peak flow response time is 2.44 ms. The test results are all passed.

According to the data in the following Table 3, the average response time of the teaching evaluation system

based on the AVF algorithm information entropy algorithm is 0.656 ms, 1.212 ms and 1.99 ms respectively when the number of evaluators is 1000, 2000 and 3000; The peak response times were 0.785 ms, 1.454 ms and 2.107 ms, respectively. All three groups of evaluators passed the test.

It can be seen from Table 4 that the average response time of the traditional information entropy algorithm is 2.546 ms, 2.987 ms, and 3.231 ms, respectively, when the

TABLE 3: Teaching analysis under AVF model.

Number of evaluators	Average response time (ms)	Peak flow response time (ms)	Test conclusion
1000	0.656	0.785	Pass
2000	1.212	1.454	Pass
3000	1.996	2.107	Pass

TABLE 4: Teaching evaluation system based on traditional information entropy algorithm.

Number of evaluators	Average response time (ms)	Peak flow response time (ms)	Test conclusion
1000	2.546	2.878	Pass
2000	2.987	3.024	Pass
3000	3.231	3.546	Pass

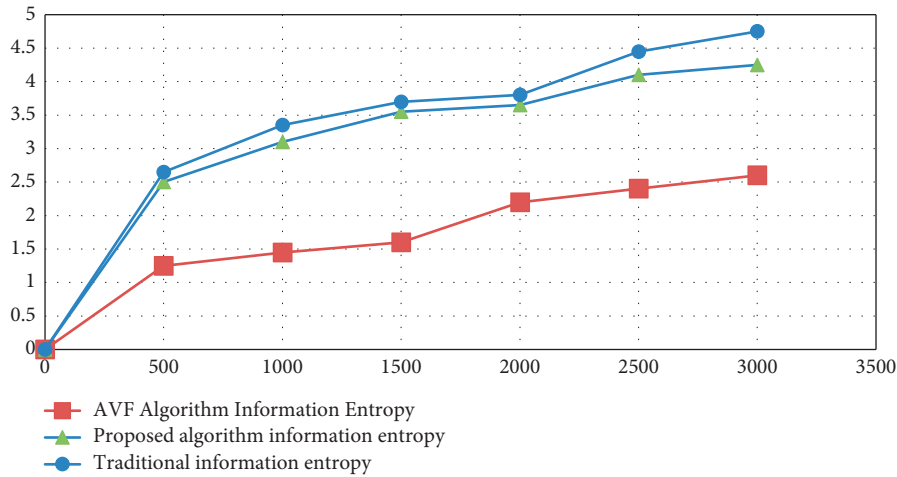


FIGURE 12: Comparison of teaching evaluation algorithms.

number of evaluators is 1000, 2000, and 3000. When the number of evaluators is 1000, the peak response time is 0.785 ms. The peak response time is 1.454 ms and 2.107 ms when the number of people is 2000 and 3000, respectively. The test results are all passed.

Through the analysis of the proposed algorithm model in Table 2, the teaching analysis under the AVF model in Table 3, and the teaching evaluation system table analysis based on the traditional information entropy algorithm in Table 4, it is known that the three methods compared in this paper have passed the system test. When the unified variable is 3000 people and the relevant teaching evaluation is carried out at the same time, the average response time of the proposed model is 2.346, and the peak response time is 2.447; the AVF model is 1.996, 2.107; the traditional algorithms are 3.231 and 3.546, respectively. In contrast, the teaching evaluation system based on the AVF algorithm information entropy algorithm needs the shortest time and the highest efficiency, while the traditional teaching evaluation system needs the longest time, as shown in Figure 12.

4.5. Comparison of Specific Function Tests of the System. The number of teaching evaluation requests is divided into seven groups: 1000, 1500, 2000, 2500, 3000, 3500, and 4000. As shown in Table 5.

By comparing the teaching evaluation system under the proposed algorithm method with the teaching system under the AVF algorithm method and the teaching evaluation system under the traditional method, we can see that the average response time increases with the increase of the number of evaluators at the same time, but the average response time required by the teaching evaluation system under the AVF algorithm method is shorter and the efficiency is higher, as shown in Figure 13.

It can be seen from Figure 14 that when the number of experimenters is 1000 to 4000, the lowest success rate of the teaching evaluation system under the AVF algorithm method is 99.6%, the lowest success rate of the teaching evaluation system under the proposed algorithm method is 98.7%, and the lowest success rate of the teaching evaluation system under the traditional method is 99%. The success rate and average response time of the teaching evaluation system

TABLE 5: System function test.

System	Number of evaluation requests	1000	1500	2000	2500	3000	3500	4000
Proposed algorithm method	Mean response time (ms)	21	37	69	113	167	198	236
	Success rate (%)	100	99.8	99.7	99.8	99.5	99.1	98.7
AVF algorithm method	Mean response time (ms)	17	32	43	82	101	146	187
	Success rate (%)	100	100	99.9	99.8	99.9	99.6	99.8
Traditional method	Mean response time (ms)	32	54	87	166	221	312	452
	Success rate (%)	100	99.6	99.4	99.2	99.2	99.2	99

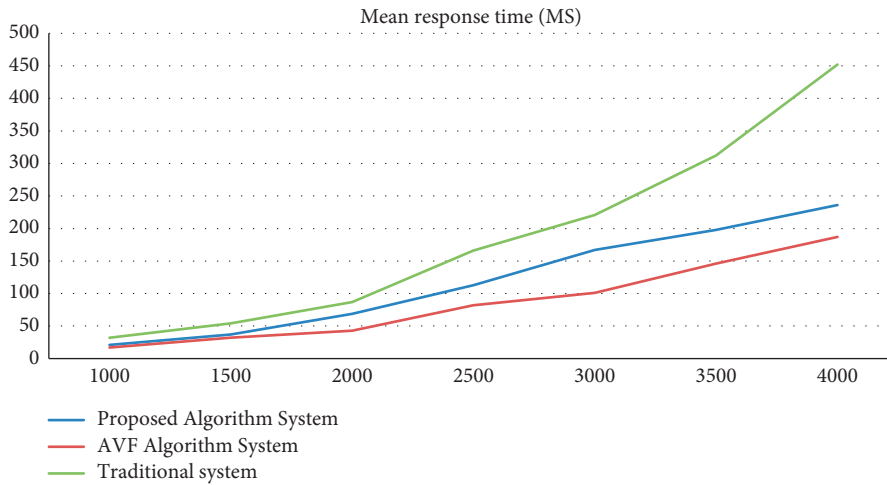


FIGURE 13: Average response time.

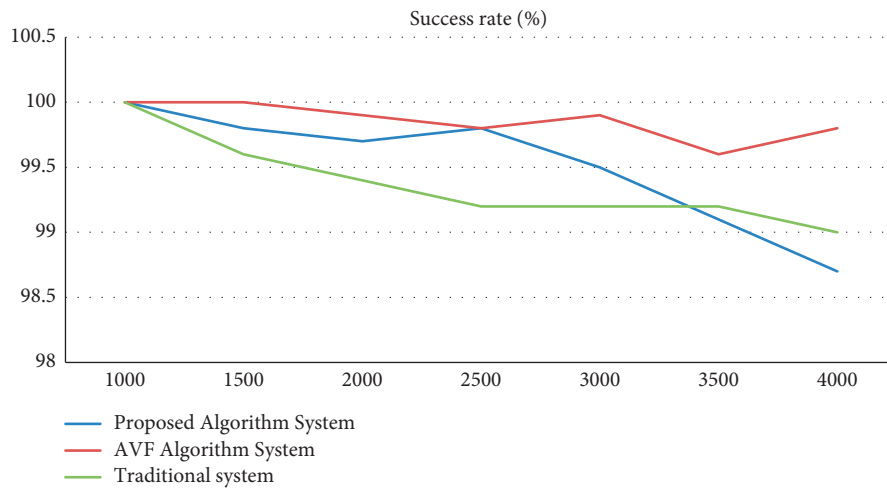


FIGURE 14: Success rate analysis chart.

based on the AVF algorithm are better than those based on traditional methods, so this method should be preferred.

5. Conclusion

By testing the efficiency and accuracy of data mining technology from a variety of calculation methods and improving the quality and efficiency of teaching evaluation through a variety of model methods, we can intuitively

analyze what problems exist in the teaching content and then improve it. Through the comparison of multimethod models, the improved Apriori method can improve the efficiency of data mining, and the information entropy algorithm of teaching evaluation under the AVF method can save more time. It can be seen that the teaching evaluation system can effectively improve efficiency. In the future, teaching evaluations based on data mining should give priority to teaching evaluations based on the AVF algorithm.

Data Availability

The experimental data used to support the findings of this study are available from the corresponding author upon request.

Conflicts of Interest

The authors declare that they have no conflicts of interest regarding this work.

Acknowledgments

This work was sponsored in part by Chongqing Social Science General Project, no.2019 YBJJ114.\\S1HCIFS01\DEMDData\16955\MYFILES\HINDAWI\SP\7133380\PROOF\COPYEDITING\gs1

References

- [1] W. Gang, N. Bashir-Bello, and S. J. Freeland, "The Synthetic Gene Designer: a flexible web platform to explore sequence manipulation for heterologous expression," *Protein Expression and Purification*, vol. 47, no. 2, pp. 441–445, 2006.
- [2] R. Giri and A. K. Das, "Indian Citation Index: a new web platform for measuring performance of Indian research periodicals," *Library Hi Tech News*, vol. 28, no. 3, pp. 33–35, 2013.
- [3] J. Jiménez, A. M. López, J. Cruz et al., "A Web platform for the interactive visualization and analysis of the 3D fractal dimension of MRI data," *Journal of Biomedical Informatics*, vol. 51, no. 31, pp. 176–190, 2014.
- [4] H. Ji, X. Dai, and X. Zhao, "PLAN: a web platform for automating high-throughput BLAST searches and for managing and mining results," *BMC Bioinformatics*, vol. 8, no. 1, pp. 1–10, 2007.
- [5] R. Buels, E. Yao, C. M. Diesh et al., "JBrowse: a dynamic web platform for genome visualization and analysis," *Genome Biology*, vol. 17, no. 1, pp. 66–24, 2016.
- [6] D. Marc, G. Mathieu, H. Ryan, T. Rocher, M. Salson, and F. Thonier, "Vidjil: a web platform for analysis of high-throughput repertoire sequencing," *PLoS One*, vol. 11, no. 11, Article ID e0166126, 2016.
- [7] I. H. Witten, E. Frank, and M. A. Hall, "Data mining," *Practical Machine Learning Tools & Techniques with Java Implementations*, vol. 13, no. 1, p. 1, 2005.
- [8] I. H. Witten and E. Frank, "Data mining: practical machine learning tools and techniques," *Acm Sigmod Record*, vol. 31, no. 1, pp. 76–77, 2011.
- [9] M. S. Chen, J. Han, and P. S. Yu, "Data mining: an overview from a database perspective," *IEEE Transactions on Knowledge and Data Engineering*, vol. 8, no. 6, pp. 866–883, 1997.
- [10] G. Chen, L. Wang, M. Alam, and M. Elhoseny, "Intelligent group prediction algorithm of GPS trajectory based on vehicle communication," *IEEE Transactions on Intelligent Transportation Systems*, vol. 22, no. 7, pp. 3987–3996, 2020.
- [11] E. Ngai, L. Xiu, and D. Chau, "Application of data mining techniques in customer relationship management: a literature review and classification," *Expert Systems with Applications*, vol. 36, no. 2p2, pp. 2592–2602, 2009.
- [12] M. Cai and Z. Li, "An investigation on university student involvement in teaching evaluation," *The Journal of Higher Education*, vol. 23, no. 5, pp. 98–123, 2005.
- [13] T. L.-P. Tang, "Teaching evaluation at a public institution of higher education: factors related to the overall teaching effectiveness," *Public Personnel Management*, vol. 26, no. 3, pp. 379–389, 1997.
- [14] L. S. . Shan, "Dictation: an effective means of FL teaching and teaching evaluation," *Journal of Pla University of Foreign Languages*, vol. 67, no. 5, pp. 109–128, 2001.
- [15] M. C. Alkin and C. A. Christie, "The use of role-play in teaching evaluation," *American Journal of Evaluation*, vol. 23, no. 2, pp. 209–218, 2002.
- [16] J. Stülke, L. A. Flórez, C. R. Lammers, and R. Michna, "CellPublisher: a web platform for the intuitive visualization and sharing of metabolic, signalling and regulatory pathways," *Bioinformatics*, vol. 26, no. 23, pp. 2997–2999, 2010.
- [17] M.-H. Abel, "Knowledge map-based web platform to facilitate organizational learning return of experiences," *Computers in Human Behavior*, vol. 51, pp. 960–966, 2015.
- [18] X. Ning, W. Li, B. Tang, and H. He, "BULDP: biomimetic uncorrelated locality discriminant projection for feature extraction in face recognition," *IEEE Transactions on Image Processing*, vol. 27, no. 5, pp. 2575–2586, 2018.
- [19] P. Maia, T. Batista, E. Cavalcante et al., "A web platform for interconnecting body sensors and improving health care," *Procedia Computer Science*, Elsevier B.V, vol. 40, , pp. 135–142, 2014.
- [20] C. K. Surratt and S. P. Desselle, "Pharmacy students' perceptions of a teaching evaluation process," *American Journal of Pharmaceutical Education*, vol. 71, no. 1, pp. 56–79, 2007.
- [21] X. Ning, K. Gong, W. Li, L. Zhang, X. Bai, and S. Tian, "Feature refinement and filter network for person re-identification," *IEEE Transactions on Circuits and Systems for Video Technology*, vol. 31, no. 9, pp. 3391–3402, 2021.
- [22] C. W. Barnett and H. W. Matthews, "Teaching evaluation practices in colleges and schools of pharmacy," *American Journal of Pharmaceutical Education*, vol. 8, no. 2, pp. 165–179, 2009.
- [23] G. Chen and S. Li, "Research on location fusion of spatial geological disaster based on fuzzy SVM," *Computer Communications*, vol. 153, pp. 538–544, 2020.
- [24] S. K. Pal, V. Talwar, and P. Mitra, "Data mining in soft computing framework: a survey," *IEEE Transactions on Neural Networks*, vol. 13, no. 1, pp. 3–14, 2002.

Research Article

Research on Simulation Analysis of Physical Training Based on Deep Learning Algorithm

Zhao Hui ¹, Chen Jing,² and Wang Taining³

¹Physical Education Institute of Qingdao University, Qingdao, Shandong, China

²Qingdao Badminton Swimming Sports Management Center, Qingdao, Shandong, China

³Binzhou University, Binzhou, Shandong, China

Correspondence should be addressed to Zhao Hui; qdqt@qdu.edu.cn

Received 29 December 2021; Revised 11 January 2022; Accepted 17 January 2022; Published 27 March 2022

Academic Editor: Man Fai Leung

Copyright © 2022 Zhao Hui et al. This is an open access article distributed under the Creative Commons Attribution License, which permits unrestricted use, distribution, and reproduction in any medium, provided the original work is properly cited.

Aging is the trend of the global population in the 21st century. Physical degradation of the elderly and related care is a major challenge in the face of an aging society. Exercise can delay physiological aging and promote the metabolism of body functions. Although aging is an irreversible natural law, proper physical training can help prevent aging. Therefore, relevant personnel attach great importance to the training of physical fitness. To this end, a 12-week elderly functional fitness training experiment was conducted with elderly residents in a village in Nanjing. In the detection process, the gait analysis system is mainly used for the subject's motion detection and recording and records the data into the gait analysis software system based on the improved deep learning algorithm for sports training simulation analysis. After completing the physical training simulation experiment, the RTM model is used for simulation analysis. The results were evaluated. The evaluation data show that the homogeneity test results of the designed physical training simulation experiment are very reasonable. Since the result is much larger than 0.10, it can be inferred that the results of the physical training simulation analysis have been expected and also meet the national GB/T 31054–2014 standard requirements.

1. Introduction

Physical fitness is the basis of all sports. Only when people have excellent physical fitness can they perform better technical movements and maintain their competitive ability. With the development of modern sports, people pay more and more attention to people's physical training (Li) [1]. Reasonable physical training for people can not only keep people enthusiastic about sports all the time but also lay a good foundation for people's future technical training and competitive ability. Nowadays, with the rapid development of modern science and technology, more and more new technologies have been introduced into physical fitness training, and its training theory has maintained a relatively rapid development speed (Qiu et al.) [2]. With the deepening of physical training, its research direction is not limited to the traditional training methods and testing methods. The research direction has become more extensive, and the

research system has become more abundant. More comprehensive and systematic research is carried out, and research work is no longer carried out for individual projects [3]. Moreover, physical training has become more focused on the comprehensive effects of its training, introducing more new ways of thinking and developing a lot of creative research directions. In the field of physical fitness training, it has attracted wide attention, which makes the traditional training mode suffer a great impact (Zhang) [4]. Nowadays, physical training is in a new period of development and transformation. Experts and scholars have different understandings of them, and they all have their own opinions. All kinds of new thinking modes have been introduced into physical training, which has completely changed the traditional physical training mode. It has injected a new direction of development into physical training, and the recognition of this new direction of development, considering that it is still in the initial stage. Neither theorists nor

front-line staff who are engaged in relevant research work have formed a unified and complete cognitive system for them, and they are still in the primary exploratory stage (Zhou and Chang-Hui) [5]. However, it can be confirmed that, with the development of modern sports, the traditional physical training mode can no longer meet the physical needs of people, especially for the elderly. Aging is the trend of global population in the 21st century, and the problems associated with the aging society follow. For example, the physical deterioration of the elderly, the care of the elderly, the health care of the elderly, and the social problems of the elderly are issues that need to be valued and considered. Physical degradation and related care for the elderly is a major challenge in the face of an aging society (Akhigbe et al.) [6]. Exercise can delay physiological aging and promote the metabolism of body function. Although aging is an irreversible natural law, proper physical training is beneficial to prevent aging. Therefore, we need a better physical training mode to help the elderly improve their physical fitness and to maintain a higher physical fitness for a longer period of time while not causing greater damage to the body.

Although physical training has developed to the present day, a large number of excellent research results have emerged, and physical training has undergone several generations of improvement. But with the development of sports and the improvement of sports level, traditional physical training has been unable to meet the current training needs. In the context of rapid development, physical training also needs to be developed rapidly to carry out technical iterations to meet real-world needs. It is urgent to improve the traditional physical training. Only further in-depth research on physical training can provide a solid foundation for the development of sports and better help people improve their physical quality. Therefore, based on the depth-oriented learning algorithm, the physical training is deeply analyzed, the physical training mode is improved, and the effect of physical training is comprehensively improved.

The deep learning technology is used to analyze the effects of 12-week elderly functional physical training with elderly residents in a village in Nanjing. Deep learning technology is mainly used in the processing of complex data models. In the process of research, it can be analyzed by program modeling. There are two common models: the basic model and the empirical model. The so-called basic model is based on the basic physics and chemical laws of the program. This mode is often caused by an internal organization that is too complex or where there are unknown or uncertain parameters that result in failure or unsatisfactory verification results. Therefore, there is an empirical mode. The empirical mode is to treat the program as a "black box" without any knowledge of the program organization under study. It is determined by mathematical techniques only by the input and output data of the program. The representative in the empirical mode is artificial intelligence technology. The so-called artificial intelligence technology is the technique of copying the thinking and operation of human beings. Among them, it can be divided into the neural network, the genetic algorithm, and the fuzzy theory, which are currently

more concerned about development. The deep learning technology mainly uses intelligent algorithms to train different network architectures such as optimization neural network link weights through the common factors of factor analysis and is used for the processing of abnormal data in the data model.

The paper mainly has the following innovations in several major areas: (1) Based on the deep learning algorithm, the multiangle analysis of physical training, using the technical advantages of deep learning algorithm, comprehensive analysis, and processing of various factors in physical training, it comprehensively improves the actual training effect of physical training and optimizes the physical training model to conduct targeted demonstration. (2) It improves the actual training effect of physical fitness training in an all-round way, optimizes the physical fitness training mode, and demonstrates the results.

The organizational structure is as follows. The first section mainly describes the research background and the organizational structure of the paper. The second section mainly describes the research status of deep learning technology in physical training. The third section mainly describes the design process of the algorithm model. The fourth section mainly describes the practical research of deep learning technology in the simulation analysis of physical training. The fifth section mainly summarizes the research results.

2. Related Work

In the early days, because sports were relatively simple, the requirements for physical training were relatively simple, and the demand for physical training was relatively simple. Most of them are training on a single quality requirement, and in the early stage, they lack the consideration of physical tolerance. As a result, unscientific training volume arrangement has brought a great load to the athletes' bodies and affected their physical function and health. Lian proposed that athletes should be trained in comprehensive physical fitness, not in a single technical movement or in a single part of the strength training, but in overall physical fitness training. Then, according to the different sports, we analyzed the physical weaknesses and made up for them with scientific training (Lian et al.) [7]. After this training idea was put forward, it was widely concerned and recognized by the industry. More and more scholars began to carry out various research work based on all-round physical training ideas. Cheng proposed that, in physical training, it is necessary to pay attention to the practice of self-balance control and strengthen the athlete's ability to control the stability of his body. As far as possible, based on itself, without the help of outside training equipment, the body is treated as a load to complete the training in order to achieve the ability of training to control the body's stability (Cheng et al.) [8]. Jia proposed that when performing physical training, it is necessary to take into account the acceleration or deceleration of the body when the athlete performs the training action. It is necessary to strengthen the athlete's control over his own stability according to the specific action (Jia et al.)

[9]. Yang proposed that physical training should be to train the overall physical fitness, and the training method should conform to the physiological structure of the human body and simulate the exercise mode of the actual sports as much as possible (Yang et al.) [10]. Li proposed that the main purpose of physical training is to enable trainees to have better physical performance in their normal life or to enable professional athletes to have better physical fitness when performing competition (Li et al.) [11].

The core of the training is not single muscle strength, but it is to allow the body strength to effectively cooperate and strengthen the actual control of the body, so it is not to train the muscles but to exercise.

Combined with the corresponding body movements, strengthen the body muscle fit, so that the body has a better balance and power (as shown in Figure 1).

The model of physical fitness training should not be too single, and reasonable movement design should be carried out for sports events. This can not only strengthen the body strength but also exercise the stability and coordination of the body and train the physical fitness suitable for the sport (Zhong et al.) [12]. In the process of training, we can use external training equipment to design training movements. We can also combine it with yoga, gymnastics, and other ways to exercise the coordination of the body. Through rich training forms, improve the enthusiasm of coaches, help them understand sports skills, and improve specific physical fitness. Scholars suggest that we can strengthen the whole body strength through scientific and perfect movement training without significantly enhancing the local muscle strength. Wu suggested that physical training should also be carried out to strengthen people's willpower. Through reasonable psychological hints, it can enhance the control ability of trainers to the body, promote the strengthening of body adaptability, and help trainers to improve their sports ability (Wu et al.) [13]. At the same time, for different groups of people, we should adopt different training methods, not completely in accordance with a standard; we should adjust the degree and difficulty of willpower training according to the actual situation. Guo-Qing argued that the human body did less movement in one direction and more comprehensive movement in many directions. In these movements, the body is accomplished mainly by rotation so the training movement cannot be a single direction of action. The body movements in the actual exercise to be considered and the training of the body's ability to rotate are enhanced to enhance the ability of the body to exercise in combination (Guo-Qing) [14] (as shown in Figure 2).

3. Algorithm Model Design

3.1. Deep Learning Technology. At present, deep learning technology is mainly used in the processing of complex data models. In the process of research, it can be analyzed by process modeling. There are two common patterns: Fundamental Model and Empirical Model. The representative of experience mode is artificial intelligence technology, and the so-called artificial intelligence technology is to imitate human thinking, operation, and other skills. It

can also be divided into Artificial Neural Network, Gene Algorithms, and Fuzzy Theorem, which are paid more attention to at present. The deep learning technology mainly uses intelligent algorithms to train different network architectures such as optimization neural network link weights through the common factors of factor analysis and is used for the processing of abnormal data in the data model (Yang et al.) [15]. The deep learning technique is a data calculus method that obtains a mathematical model by using an iterative random sampling method to extract and screen abnormal data. The implementation principle is mainly based on the assumption that there are two different data types in the sample data: (1) a normal data model; (2) a noise and anomalous data model. The algorithm believes that the reason why it cannot adapt to the mathematical model is mainly that the abnormal data may be caused by wrong assumptions in the process of mathematical model calculation (as shown in Figure 3). However, these erroneous data often lack enough parameters to restore them. For this reason, the algorithm restores its real data through multiple iterations. Its basic implementation process is as follows.

Firstly, we need to obtain the necessary data model information. The main way to obtain data is to traverse the SPSS data statistics software (as shown in Figure 4). According to the different domains of use, it can be divided into two kinds: one is spatial processing, and the other is frequency processing. The former deals directly with the data model itself, while the latter deals with the data model in a special way and carries out various calculations and analyses. The processing formulas for airspace are as follows:

$$g(x, y) = EH[f(x, y)]. \quad (1)$$

Among them, $f(\cdot)$ is the data model before enhancement, $g(\cdot)$ is the data model after enhancement, and EH represents the enhancement operation.

For a continuous function $f(x, y)$, its gradient at position (x, y) can be expressed as

$$\nabla f(x, y) = G(x, y) = [G_x G_y]^T = \left[\frac{\partial f}{\partial x} \frac{\partial f}{\partial y} \right]^T. \quad (2)$$

The gradient is a vector whose magnitude and direction angles are, respectively,

$$|\nabla f| = |G(x, y)| = [G_x^2 + G_y^2]^{1/2} \quad (3)$$

$$\phi(x, y) = \arctan\left(\frac{G_y}{G_x}\right)$$

The approximate expression of the gradient is as follows:

$$\begin{aligned} G_x &= f[i, j + 1] - f[i, j], \\ G_y &= f[i + 1, j] - f[i, j]. \end{aligned} \quad (4)$$

Usually, in order to reduce the amount of calculation, the absolute approximate gradient amplitude is often used to calculate.



FIGURE 1: The schematic diagram of the algorithm model.

$$|G(x, y)| = |G_x| + |G_y|. \quad (5)$$

When analyzing the data model, the approximation is usually calculated by using a small area template tape (as shown in Figure 5). For G_x and G_y , one template is used, which requires two templates. According to the size of different templates, the computational attributes are also different.

Then, it extracts the corner points of the data model which has completed the preliminary processing. Suppose that there are variables I_x and I_y used to represent the data and the first-order partial derivatives of the model I in two different aspects of the x -axis and the y -axis of Cartesian coordinates. Then, function $w(x, y)$ can be used to represent a two-dimensional Gaussian smoothing function on Cartesian coordinates. The calculation process of this function is shown in the following two formulas:

$$M = \sum_{x,y} w(x, y) \begin{bmatrix} I_x^2 & I_x I_y \\ I_x I_y & I_y^2 \end{bmatrix}. \quad (6)$$

Solving formula (4) can get the specific number of each corner R in the data model. Then, using the corner points calculated by the normalization idea to match, the data model corner point value can be obtained. The matching calculation equation is as follows:

$$NCC = \frac{\sum_i (I_1(x_i, y_i) - u_1)(I_2(x_i, y_i) - u_2)}{\sqrt{\sum_i (I_1(x_i, y_i) - u_1)^2 \sum_i (I_2(x_i, y_i) - u_2)^2}} \quad (7)$$

At the same time, the deep learning data analysis algorithm can be used to purify the data model corner values (as shown in Figure 6). In the process of purification, the data model needs to be purified according to the hierarchical

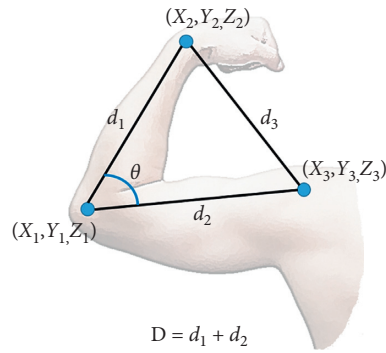


FIGURE 2: Network distance teaching based on streaming media technology has a wealth of research.

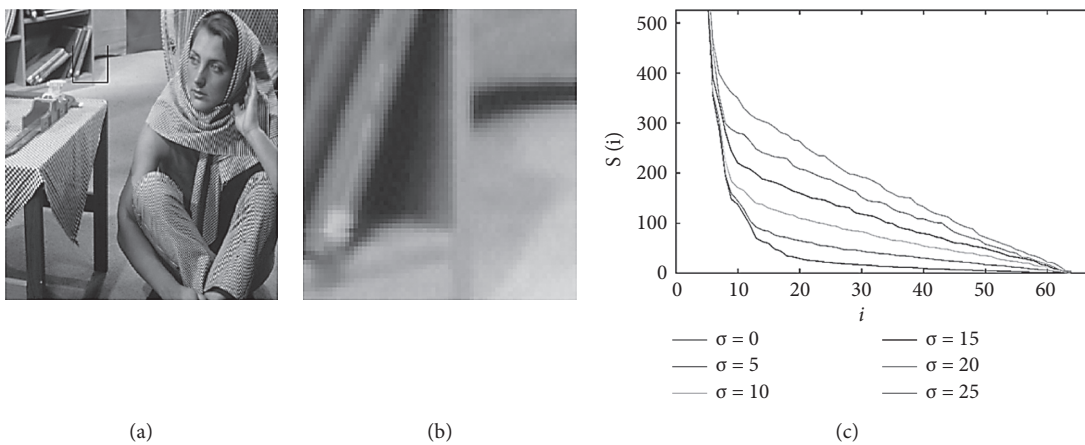


FIGURE 3: The healing of tendon injury was obtained by medical image analysis.

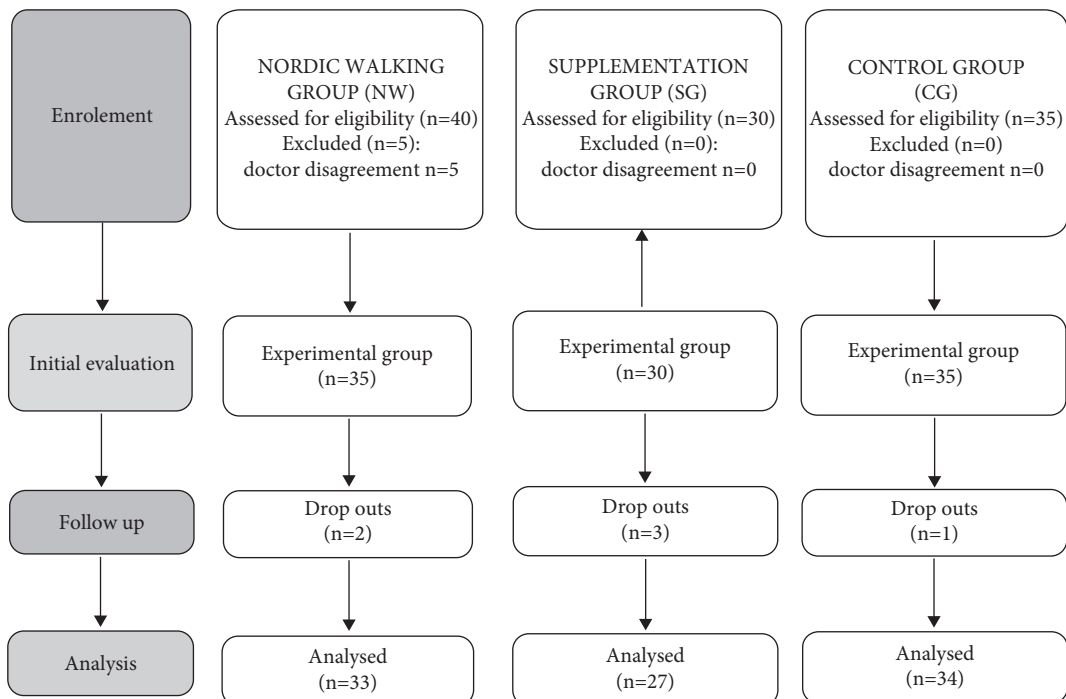


FIGURE 4: Local image information for the first derivative operator.

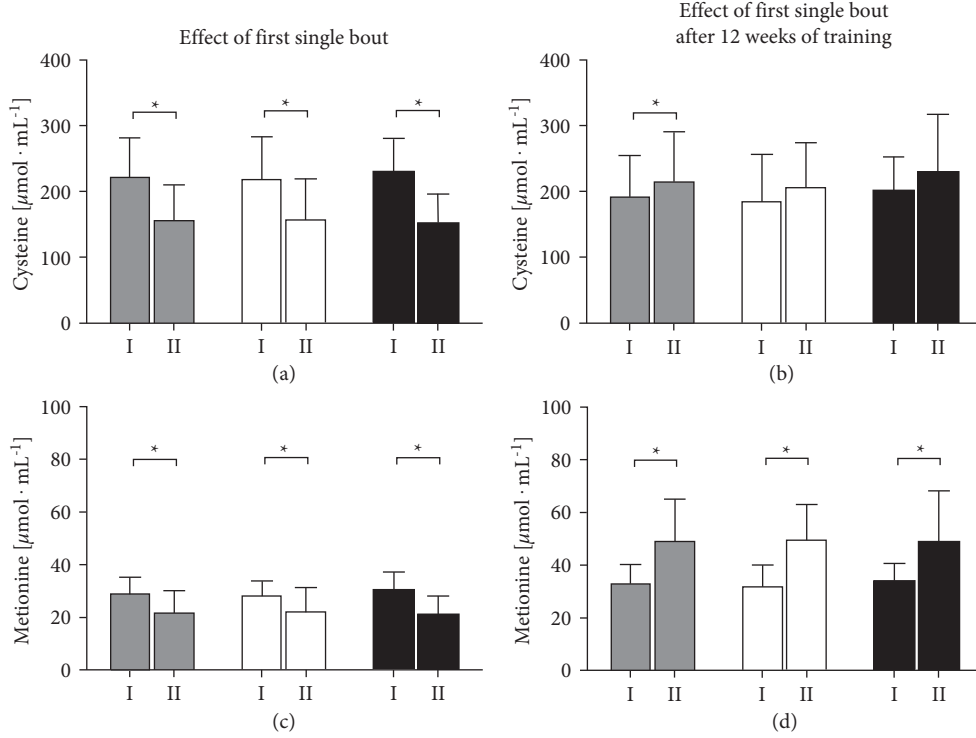


FIGURE 5: The operator approximates the amplitude of the continuous gradient of the edge point.

channel mode, so there is the following linear algebraic equation:

$$\begin{pmatrix} R_2 \\ G_2 \\ B_2 \end{pmatrix} = \begin{pmatrix} c_r & 0 & 0 \\ 0 & c_g & 0 \\ 0 & 0 & c_b \end{pmatrix} \cdot \begin{pmatrix} R_1 \\ G_1 \\ B_1 \end{pmatrix} + \begin{pmatrix} d_r \\ d_g \\ d_b \end{pmatrix}. \quad (8)$$

EKF truncates the Taylor expansion of nonlinear function by first-order linearization and ignores other higher-order terms so as to transform the nonlinear problem into linear. The Kalman linear filter algorithm can be applied to nonlinear systems. In this way, the nonlinear problem is solved. Although EKF is applied to nonlinear state estimation systems, it has been recognized by academia and is widely used. In order to solve the problem that the constant matrix cannot accurately describe the system noise of permanent magnet synchronous motor (PMSM) under different operating conditions, an adaptive extended Kalman filter algorithm (AEKF) based on innovation sequence and state residual is proposed. The simulation results show that, compared with the traditional extended Kalman filter algorithm, AEKF has better convergence speed and convergence accuracy and better parameter robustness.

In the above formula, variable R_2 , variable G_2 , and variable B_2 represent three different levels of channels of the data model, respectively. The variable (c, d) is mainly used to represent the transformation parameters of the linear equation.

The calculation is performed using the R channel as an example. It is assumed that there are corner data of different data models of group n , and variable d_n represents the absolute distance of different data points $(R_2, R_1)_n$ to straight

line (c, d) . At this point, the purification is done by iterative summation as follows:

$$E = \sum T(d_n^2). \quad (9)$$

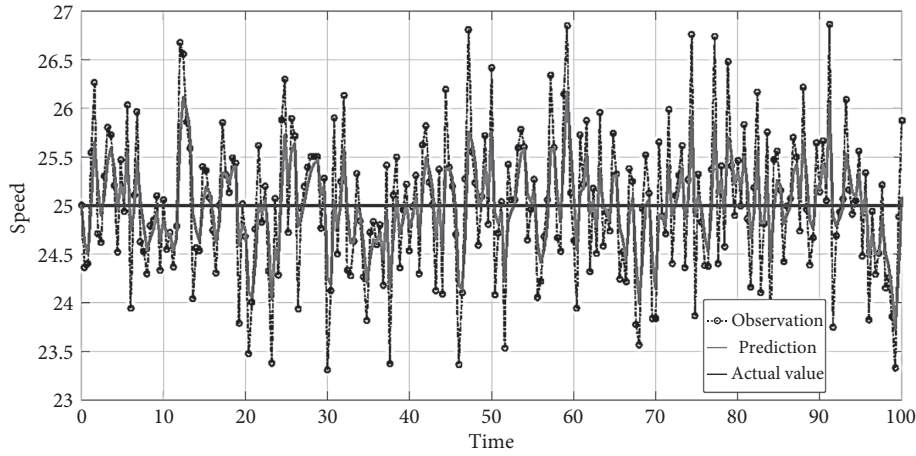
In the above formula, when the condition satisfies $d_n^2 < Thre^2$, then $T(d_n^2) = d_n^2$. Otherwise, $T(d_n^2) = Thre^2$. The corners of the data model satisfying the conditions are screened out, and the iterative calculation is continued. The whole purification process is completed until the value of E does not change significantly (as shown in Figure 7).

After the data model is segmented, the similarity between the data model and the established data model in the database is calculated and matched according to the calculated results. The matching result of the data model is very characteristic. The following functions are used to measure the similarity between T and f :

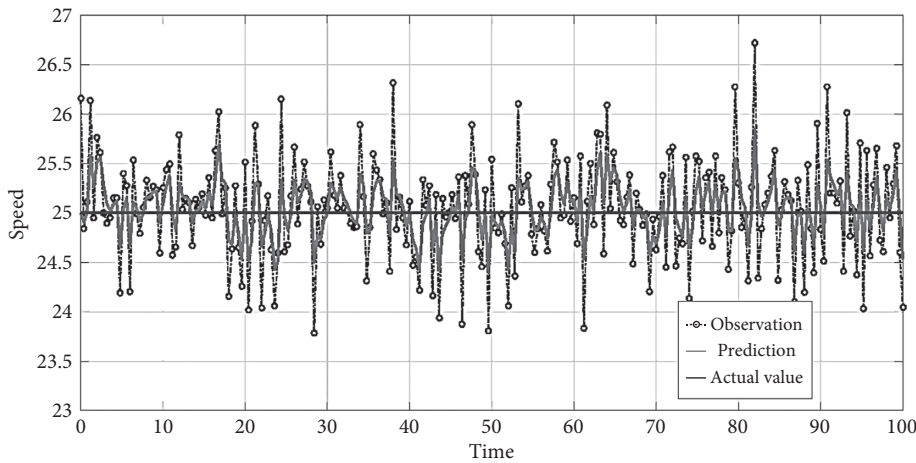
$$SE(x, y) = \sum_{i=1}^N \sum_{j=1}^N [f(x-i, y-j) - T(i, j)]^2. \quad (10)$$

Among them, the size of the data model is $N \times N$. The formula provides a measure of the degree of matching between the data model T and f at (x, y) coordinates. The matching result can be calculated by expanding the above formula:

$$SE(x, y) = \sum_{i=1}^N \sum_{j=1}^N f^2(x-i, y-j) - 2 \sum_{i=1}^N \sum_{j=1}^N f(x-i, y-j)T(i, j) + \sum_{i=1}^N \sum_{j=1}^N T^2(i, j). \quad (11)$$



(a)



(b)

FIGURE 6: In the process of purification, the image should be considered separately according to the red, green, and blue color channels. (a) EKF algorithm. (b) AEKF algorithm.

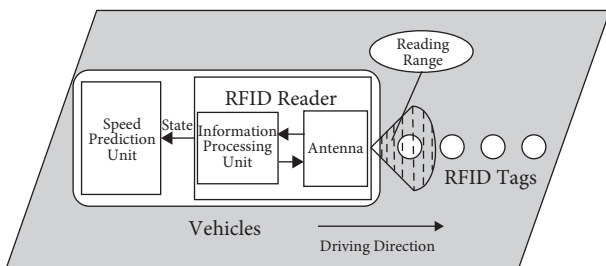


FIGURE 7: Image segmentation technique image segmentation technology.

3.2. *Deep Learning Algorithms.* At present, the common deep learning algorithms mainly include the following: conditional random fields, convolutional neural networks, recurrent neural networks, and memory networks. Conditional random fields (CRFs) in deep learning algorithms mainly belong to the field of natural language processing (NLP). Natural language processing is a very popular field in artificial intelligence. Named Entity Recognition (NER) is a subtask in the field of

natural language processing. Its main purpose is to classify unstructured text into predefined categories by identifying Named Entity, such as Personal Name (PER), Place Name (LOC), and Organizational Name (ORG). In the task of conditional random field (CRF) in Sequence Labeling of natural language, CRF is the choice of most people and is widely used. However, according to the research, conditional random field (CRF) can only capture a small range of article information, and the key limitation of CRF is to obtain the information in the whole article (as shown in Figure 8).

Convolutional neural networks (CNN) is a feed-forward neural network, which is usually composed of convolutional layer, pooling layer, and fully connected layer. Compared with other networks, convolutional neural network (CNN) needs fewer parameters, which makes it an attractive in-depth learning model. Convolutional neural network (CNN) has the advantage of automatically capturing adjacent features. Firstly, it is applied to sequential markup tasks in natural language processing, and good results have been achieved. Recently, the convolutional neural network (CNN) combined with the Gated Linear Unit (GLU) is used, and in

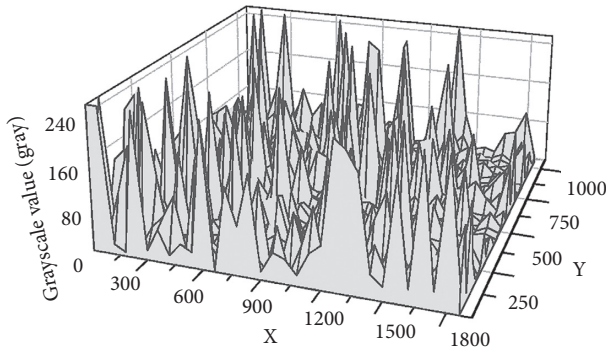


FIGURE 8: Receive feedback from participating nodes.

order to avoid the loss of text information, the pooling layer is abandoned and applied to the Chinese Word Segmentation task.

Natural language processing (NLP) usually considers the context before and after the article so as not to take the meaning out of context, in other words, to train the language model. If the context information can be provided to the model as training data, the effectiveness of the model will be improved. Therefore, recurrent neural network (RNN) is widely used in the deep learning method of natural language processing (NLP), which leads to the widespread use of recurrent neural network (RNN). Based on the universal use of recurrent neural network (RNN), many researchers have developed some changes in order to expand the function of RNN. The proposed LSTM (Long Short-Term Memories) uses memory as a reference factor to enhance current decision-making, while Gated Recurrent Units (GRUs) improves LSTM (Long Short-Term Memories). Recently, the concept of Bidirectional has been introduced to retrieve forward and backward information by using long-term and short-term memory (LSTM) in sequential tagging tasks. At the end of the model, combined with conditional random field (CRF), it has been applied to English data sets and achieved very good results. However, with the increase in the length of the input sentence, the efficiency will deteriorate. Although time series markers have been added, they still prefer adjacent character information and perform poorly in judgments involving remote context dependence. Because the traditional conditional random field (CRF) has no ability to capture the features of articles beyond a long range, the recursive neural network (RNN) is not very effective in long-distance article information retrieval. Therefore, memory network can be used to enhance the performance of retrieving features of long-range articles and applied to QA tasks. It proves that the increase of memory is essential for performing reasoning that requires constant-distance article information (as shown in Figure 9).

4. Practical Application

4.1. An Overview of Experiments. Aging is the trend of global population in the 21st century, and the problems associated with the aging society follow. For example, the

physical deterioration of the elderly, the care of the elderly, the health care of the elderly, and the social problems of the elderly are issues that need to be valued and considered. Physical degradation and related care for the elderly is a major challenge in the face of an aging society. Exercise can delay physiological aging and promote the metabolism of body functions. Although aging is an irreversible natural law, the timing of exercise intervention and the effect of mode on prevention will still cause differences. Based on the above background, the effects of 12-week old functional physical training were simulated using deep learning techniques (as shown in Figure 10).

The elderly residents of a village in Nanjing were used as subjects. They were over 65 years old. There were no serious illnesses or inconveniences in lower limbs. There were 14 subjects, 5 males and 9 females, with an average age of 72.5 years, an average height of 155.6 cm, and an average weight of 58.7 kg. The study was conducted from March 26 to June 16, 2018, for a total of 12 weeks. Research tools mainly include (1) tape measure, detecting the maximum balance range; (2) stopwatch, detecting open-eye standing, closed-eye standing, open-eye cushion standing, closed-eye cushion standing, and obstacle test completion time; (3) 30 cm ruler, detecting the predumping aids; (4) 15 cm high steps, detecting straddle aids; (5) gait analysis system (L2Sens-B Free4Act System, 4Act WALK versione Base e XL, LorAn, Castel Maggiore, Italia): detecting gait parameters for ten-meter gait and obstacle test; (6) improved gait analysis software system based on deep learning algorithm; (7) balance pad (3240 body-balance, Carnegie fitness, Tainan, Taiwan): detecting open-eye cushion standing and closed-eye padded standing aids; (8) obstacle: self-made test obstacles test.

4.2. Experimental Simulation. A briefing session was held before the experiment, and the consent form and experimental instructions were given to the subject, indicating the purpose and method of the experiment; the subject was asked to sign the consent form and then returned, indicating that they agreed to participate in the experiment. On the other day of the test, the subject is explained and answered with questions related to the experiment. In the experiment, the subject can ask questions at any time, but the subject is required to observe the test time: (1) Maintain daily routine during the experiment. (2) It is forbidden to drink any caffeine-containing alcoholic beverages before, during, and after the test; alcoholic beverages. (3) 30 minutes before the test, light clothes arrived at the test site, and researchers warmed up to participate in the experiment. (4) At the first class, the subject is required to wear a wrist unit and test the training intensity (as shown in Figure 11).

In the detection process, the different color exploration gait analysis system is used to detect and record the subjects' movement, and the data are recorded in the gait analysis software system based on the improved deep learning algorithm. Finally, the physical training simulation analysis is carried out through the incremental value (gray). Specifically,

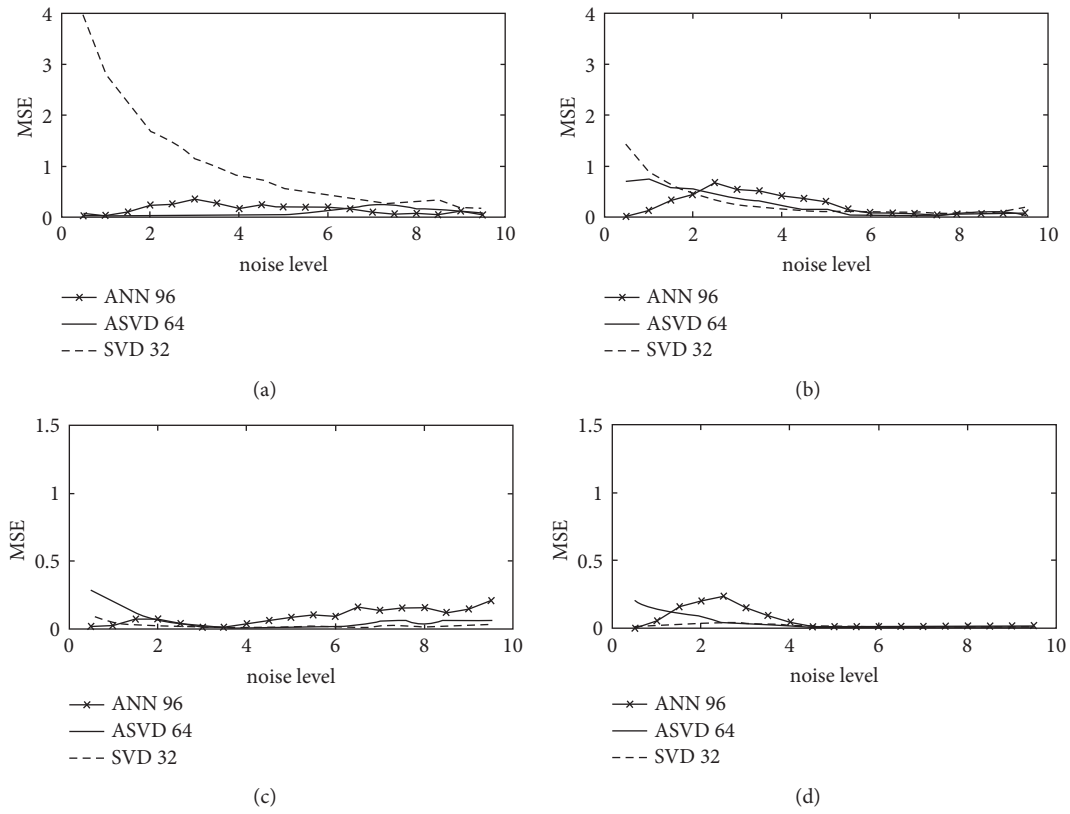


FIGURE 9: Multicast is the sending of data packets to a host group represented by a unique IP address.

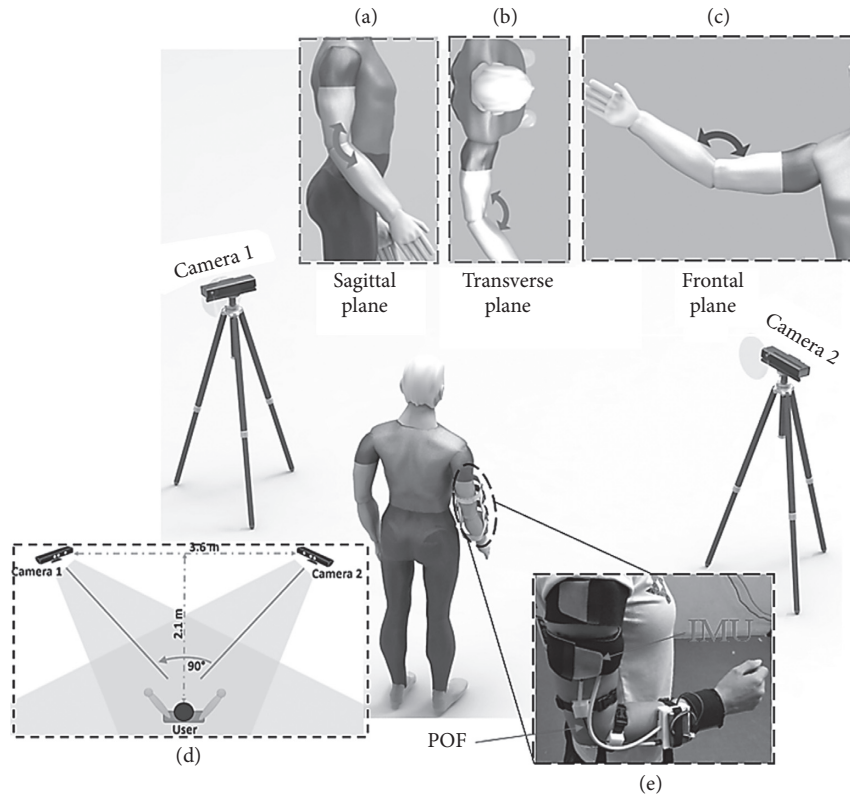


FIGURE 10: The expert model of building energy intelligent management is applied to the energy management of the building garden.

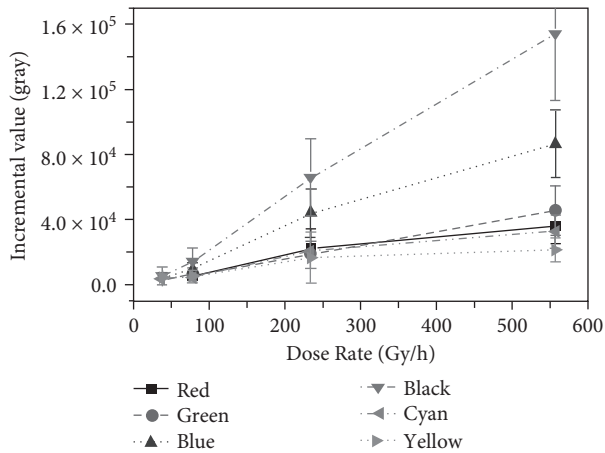


FIGURE 11: Actively issue abnormal energy consumption and alert to reduce wrong energy consumption.

it includes the following aspects: (1) Standing on one foot: subjects were lifted off the ground for a single second, with a maximum of 20 seconds, and scored. (2) Open eyes: the subjects stood naturally on both feet and embraced their chests with both hands. Measure open eyes, perform three times, and record time, each time limited to 30 seconds. (3) Close your eyes and stand on your legs. When the subject's heels are close together and when they close their eyes, they start timing at the same time. When the subject loses balance or opens both eyes, stop timing, time up to 30 seconds, and score. (4) Stand with your eyes closed. The subjects naturally stand on their feet, hold their chests with both hands, close their eyes when starting the test, measure the closed eyes, perform three times, and record the time to take the maximum value; each time is limited to 30 seconds. (5) Open the eye cushion. The subjects stood naturally on both feet and embraced their chests with both hands. Measure the opening of the eye station cushion, each item is executed three times, the time is recorded, and each time is limited to 30 seconds. (6) Closed-eye cushion standing: the subjects stood naturally on both feet and embraced their chests with both hands. Measure the closed-eye station cushions, perform three times each, record the time, each time limited to 30 seconds, and score. (7) Swinging head walking: the subject turned his head at a frequency of 100 beats/min and took a straight line ten steps forward to score. (8) Circling in place: subjects were asked to turn right 1 turn, pause at the original position, then turn left 1 turn to record the number of steps in the process, and score.

4.3. Experimental Evaluation. The elderly residents in a village in Nanjing were used as subjects, and the effects of 12-week-old functional physical training were simulated by deep learning techniques. In the detection process, the gait analysis system is mainly used for motion detection and recording of the subjects, the data is recorded into the gait analysis software system based on the improved deep learning algorithm for physical training simulation analysis, and the RTM model is used for simulation analysis.

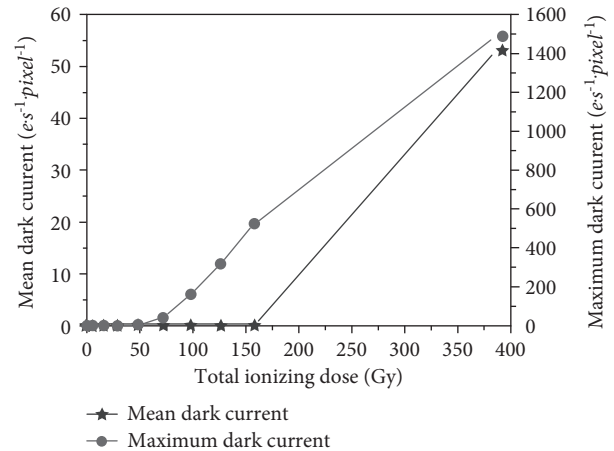


FIGURE 12: Precision instrument of watt-hour meter tester with fault in transmission system.

After completing the physical training simulation experiment, the RTM model was used to evaluate the analysis results. The execution steps are as follows: find different evaluation indicators of the evaluated objects and establish an evaluation weight matrix R . The product of each row element of the judgment matrix R is calculated, the actual weight value of the different indexes of the object to be evaluated can be obtained, and the evaluation score can be calculated by calculating the weight value and the evaluation content data.

The evaluation results can be obtained by calculating the data information recorded during the experiment according to the above calculation method (as shown in Figure 12). The data in the figure shows that the homogeneity test results of the designed fitness training simulation experiment are $P = 0.662 > 0.10$. Since the result is much larger than 0.10, it can be inferred that the results of the physical training simulation analysis have been expected and also meet the national GB/T 31054-2014 standard requirements.

5. Conclusion

In the face of an aging society, physical degradation and related care of the elderly is a major challenge. Appropriate physical exercise can help prevent aging. Therefore, relevant personnel attach great importance to the training of physical quality. Therefore, this paper conducted a 12-week functional fitness training experiment on elderly residents in a village in Nanjing. In the detection process, the gait analysis system is mainly used for motion detection and recording of subjects and records the data into the gait analysis software system based on the improved deep learning algorithm for motion training simulation analysis. After completing the sports training simulation experiment, the RTM model is used for simulation analysis. The results were evaluated. The evaluation data show that the homogeneity test results of the designed physical training simulation experiment are as follows. Since the result is far greater than 0.10, it can be inferred that the result of sports training simulation analysis is expected and meets the requirements of the national GB/T 31054-2014 standard. Based on the deep learning algorithm,

this paper makes a multiangle analysis of physical training and makes use of the technical advantages of deep learning algorithm to comprehensively analyze and deal with various factors in physical training, comprehensively improve the effectiveness of physical exercise, optimize the physical exercise mode, and carry out targeted demonstration, and comprehensively improve the actual training effect of physical training, optimize the physical training mode, and show the sports effect. However, this study does not conduct multiangle combined research and analysis on the subjects' living habits, which leads to the fact that the technical advantages of deep learning algorithm may not accurately grasp the focus of the research, which needs further analysis in future research.

Data Availability

The experimental data used to support the findings of this study are available from the corresponding author upon request.

Conflicts of Interest

The authors declare that they have no conflicts of interest regarding this work.

References

- [1] X. Li, "Research on text clustering algorithm based on K_means and SOM[J]," *Journal of Forestry*, vol. 51, no. 21, pp. 6499–6514, 2008.
- [2] H. Qiu and Y. Xiang, "Research on a method for building up a patent map based on k-means clustering algorithm[J]," *Remote Sensing*, vol. 7, no. 9, pp. 11125–11150, 2009.
- [3] W. Dai, C. Jiao, and T. He, "Research of K-means clustering method based on parallel genetic algorithm[J]," *Chinese Science Bulletin*, vol. 61, no. 33, pp. 3564–3571, 2007.
- [4] Q. Zhang, "Impact of policy change of RMB exchange rate on RMB cross-border businesses of commercial bank of China—based on analysis of VAR test[J]," *Journal of Luoyang Institute of Science & Technology*, vol. 9, no. 1, pp. 80–95, 2018.
- [5] X. L. Zhou and D. Chang-Hui, "Analysis on the influence and countermeasure of cross-border trade in RMB to China's foreign trade enterprises[J]," *Journal of Northeast Dianli University*, vol. 72, no. 3, pp. 961–980, 2012.
- [6] A. Akhigbe, A. D. Martin, and M. Newman, "Exchange rate exposure and valuation effects of cross-border acquisitions [J]," *Journal of International Financial Markets, Institutions and Money*, vol. 13, no. 3, pp. 255–269, 2004.
- [7] F. Lian and Q. I. Min-Jia, "Exchange rate marketization, macro prudential policy and cross-border capital flow:an analysis based on dynamic stochastic general equilibrium[J]," *Financial Theory and Practice*, vol. 90, no. 6, p. 441, 2014.
- [8] R. Cheng and Y. Jin, "A social learning particle swarm optimization algorithm for scalable optimization[J]," *Information Sciences*, vol. 291, no. 6, pp. 43–60, 2015.
- [9] W. Jia, D. Zhao, T. Shen, S. Ding, Y. Zhao, and C. Hu, "An optimized classification algorithm by BP neural network based on PLS and HCA[J]," *Applied Intelligence*, vol. 43, no. 1, pp. 1–16, 2015.
- [10] Y. Zhou, W. S. Xu, N. Wang, and W. H. Shao, "Multi-objective siting and sizing of distributed generation planning based on improved particle swarm optimization algorithm[J]," *Transactions of China Electrotechnical Society*, vol. 1, no. 9, p. 78, 2018.
- [11] Q. Li, X. Wang, and Q. Zhang, "Remote wireless of sensor networks technology applying in intelligence irrigation monitoring[J]," *Journal of Agricultural Mechanization Research*, vol. 63, no. 3, pp. 189–197, 2010.
- [12] D. Zhong and X. Tong, "Application research on hydraulic coke cutting monitoring system based on optical fiber sensing technology[J]," *Transactions of the Chinese Society for Agricultural Machinery*, vol. 31, no. 13, pp. 11–18, 2014.
- [13] M. Y. Wu, Y. H. Lin, and C. K. Ke, "WSN-based automatic monitoring management platform for plant factory[J]," *International Journal of Digital Content Technology & Its Applications*, vol. 8, no. 6, pp. 303–311, 2011.
- [14] D. U. Guo-Qing, "Discussion on new sensor technology for automatic monitoring of bridge structure deflection[J]," *Transportation Standardization*, vol. 31, no. 10, pp. 204–210, 2013.
- [15] J. C. Yang, W. M. Chen, M. Xu, H. Yang, and W. J. Yang, "New sensing technology used in bridge deflection automatic monitoring," *Journal of Chongqing University*, vol. 29, no. 4, pp. 15–18, 2006.

Research Article

Multiple Musical Instrument Signal Recognition Based on Convolutional Neural Network

Lei Lei 

Minjiang University CAI Jikun Conservatory of Music, Fuzhou 350108, China

Correspondence should be addressed to Lei Lei; 1989@mju.edu.cn

Received 25 November 2021; Revised 10 January 2022; Accepted 8 February 2022; Published 25 March 2022

Academic Editor: Hangjun Che

Copyright © 2022 Lei Lei. This is an open access article distributed under the Creative Commons Attribution License, which permits unrestricted use, distribution, and reproduction in any medium, provided the original work is properly cited.

To improve the accuracy of multi-instrument recognition, based on the basic principles and structure of CNN, a multipitch instrument recognition method based on the convolutional neural network (CNN) is proposed. First of all, the pitch feature detection technology and constant Q transform (CQT) are adopted to extract the signal characteristics of multiple instruments, which are used as the input of the CNN network. Moreover, in order to improve the accuracy of multi-instrument signal recognition, the benchmark recognition model and two-level recognition model are constructed. Finally, the above models are verified by experiments. The results show that the two-level classification model established in this article can accurately identify and classify various musical instruments, and the recognition accuracy is improved most obviously in xylophone. Compared with the benchmark model, the constructed two-level recognition has the highest accuracy and precision, which shows that this model has superior performance and can improve the accuracy of multi-instrument recognition.

With the rise of artificial intelligence technologies such as deep learning and the growth of massive music data, content-based music retrieval has become an urgent issue at present. In content-based music retrieval, how to identify music has become the focus of current music information retrieval research. Compared with the traditional speech signal, speech signal should have a richer spectrum, treble, and timbre. Therefore, based on the above characteristics, the recognition of music signal can be divided into recognition method, recognition accuracy, recognition time, and recognition scene. María and ValeroMas Jose applied the convolutional recursive neural network to music recognition, which greatly reduces the precision of musical note and number recognition [1]. Agarwal and Om applied the machine learning algorithm to music recognition and obtained the highest recognition accuracy by the improved method through the music emotion recognition of the ISMIR2012 dataset, NJU_V1 dataset, and self-built dataset [2]. Sarkar applied the deep learning algorithm to the recognition of music and audio by extracting MFCC features and finally using VGGNet for recognition. The

results show that the method has obvious advantages in three datasets [3]. Yan uses the genetic algorithm to improve the T-S cognitive neural network and applies the model to music recognition for higher accuracy and robustness [4]. Liang used machine learning algorithms to build prediction models among audio features, individuals, and emotions, so as to propose suggestions on emotional influence in music [5]. Wang and others accurately identified different emotions including happiness, anger, sadness, and fear by establishing CLDNN's musical instrument emotion recognition model [6]; ATILA Orhan proposed a speech emotion recognition model based on 3D CNN-LSTM and evaluated speech from the perspectives of accuracy, sensitivity, specificity, and F1, which provided a reference for speech evaluation [7]. Solanki et al. also use the convolutional neural network to recognize musical instruments, but mainly focus on extracting the characteristic parameters of musical instruments [8–10]. As can be seen, the above research provides reference for the music retrieval and identification. However, the above research is mainly aimed at the musical identification of a single

instrument. At present, there are relatively few references for the music identification of multiple instruments. In multi-instrument recognition of polyphony, not only the traditional single tone signal must be extracted, but also the tones of different instruments must be identified. Therefore, based on the reality of research, a convolutional neural network is used to identify the multi-instrument music signal. Therefore, this article attempts to identify the signals of different musical instruments by extracting and identifying the characteristics of musical instruments on the basis of traditional single instrument recognition.

1. Introduction to Convolutional Neural Network

CNN, a representative algorithm of deep learning, is a kind of feed-forward neural network, which includes convolution calculation and has depth structure [11]. CNN can learn the original data efficiently and quickly, so as to extract the features of the data, which means that it has the ability of representation learning. The specific structure is shown in Figure 1, which is mainly divided into five network layers and belongs to multilayer perceptron (MLP) [12]. The most important steps are convolution calculation and pooling operation.

1.1. Convolutional Layer. The convolution formula is as follows:

$$s(t) = x(t) * w(t) = \sum_{\tau=-\infty}^{\tau=+\infty} x(\tau)w(t - \tau), \quad (1)$$

where $s(t)$, $x(t)$, and $w(t)$ represent feature mapping, input features, and convolution cores, respectively. If it is two-dimensional matrices, it can be represented as

$$s(i, j) = \sum_{m=0}^M \sum_{n=0}^N (w_{m,n}x_{i+m} + w_b). \quad (2)$$

In the above formula, the size of convolution kernel is $M \times N$, which is shown in Figure 2 [13–15]. The advantages of convolution operation are mainly reflected in three aspects. Firstly, the realization of parameter sharing helps to reduce the size of the parameter set. Secondly, sparse connection reduces the number of parameters and improves the efficiency, which has certain advantages over full connection. Thirdly, because the same convolution kernel is used, when the value of input eigenmatrix changes, the corresponding result will change at the same position.

1.2. Pooling Layer. The pooling layer refers to the output of statistics for a specific region within the input eigenmatrix. Generally, two pooling methods can be adopted, namely, average pooling and maximum pooling. They take the mean and maximum values of the local region as the output, respectively. Except for these two methods, there is a random pooling, which selects neurons with greater probability values.

2. The Construction of Multi-Instrument Signal Recognition Model Based on Convolutional Neural Network

2.1. Multi-Instrument Signal Feature Extraction. In order to realize the recognition of multi-instrument signals, it is necessary to extract musical instrument signal features first. Conventional instrument signal extraction is usually only for a single instrument, which is relatively simple. It only needs to eliminate the instrument noise and then classify them. But for multi-instrument signals, it not only needs to deal with the noise, but also faces the knowledge of notes of different instruments. In other words, the conventional time-frequency feature extraction, such as MFCC, may not achieve the recognition effect. Therefore, on the basis of signal processing, the essential elements of music, such as pitch, harmony, and other signals, are combined to identify the signals of multiple instruments. The instrument signal characteristics are processed by pitch characteristic detection and constant Q transformation.

2.1.1. Pitch Feature Extraction. The multipitch detection based on a statistical model and spectral decomposition is the main method to extract pitch features. However, considering that an end-to-end neural network may have the problem of overfitting in the display feature extraction, filters are introduced to extract the time-frequency features of musical instrument signals in the primary feature extraction process of convolutional neural network. In other words, the first layer of the convolutional neural network is replaced by the filter, which can greatly reduce the overfitting problem. The specific extraction process is shown in Figure 3 [16–18].

The specific process is as follows:

Firstly, the audio frame X is normalized, that is, $X \rightarrow X/\|X\|^2$. The audible variables of each frame are standardized. Then, it is divided into T_p segments, and each segment is represented as x_t . The number of sampling points is s , which means $x_t = (x_{t_1}, x_{t_2}, \dots, x_{t_s})$. To map X , it needs to use the filter banks in the log-frequency domain, including cosine and sine filters, and the total number is $n_p = 511$. Thus, the logarithmic frequency-time matrix ($n_p \times T_p$) can be formed, and the log-frequency domain is $\log f_L$ to $\log f_H$. Then, the parameter of sine filter i is shown as follows [19]:

$$w_{i, \sin} = (\sin 2\pi f_i t_1, \dots, \sin 2\pi f_i t_s). \quad (3)$$

The parameters of cosine filter i are shown as follows:

$$w_{i, \cos} = (\cos 2\pi f_i t_1, \dots, \cos 2\pi f_i t_s). \quad (4)$$

In the above formula, $f_i = 10^{\log f_L + i(\log f_H - \log f_L/n)}$, according to the normalized amplitude $x_t = (x_{t_1}, x_{t_2}, \dots, x_{t_s})$, the position t_1, t_2, \dots, t_s at each time can be determined.

Then, let x_t do the inner product calculation with $w_{i, \sin}$ and $w_{i, \cos}$. Next, the square and the sum of the two can be calculated. So the output of filter i can be obtained as follows [20–22]:

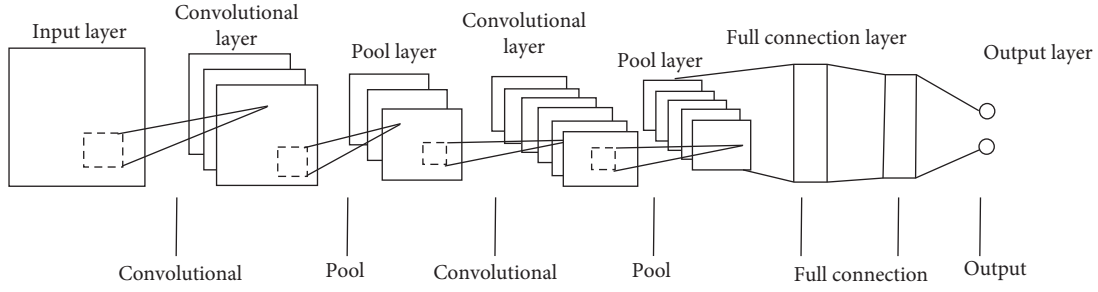


FIGURE 1: CNN neural network structure.

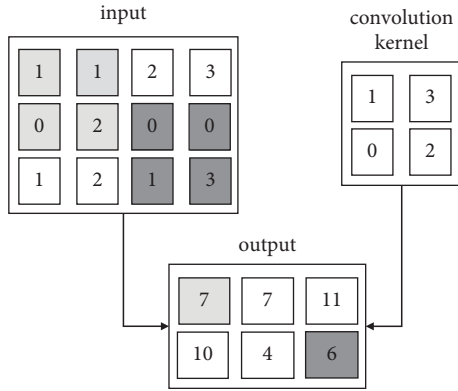


FIGURE 2: Example of convolution operation.

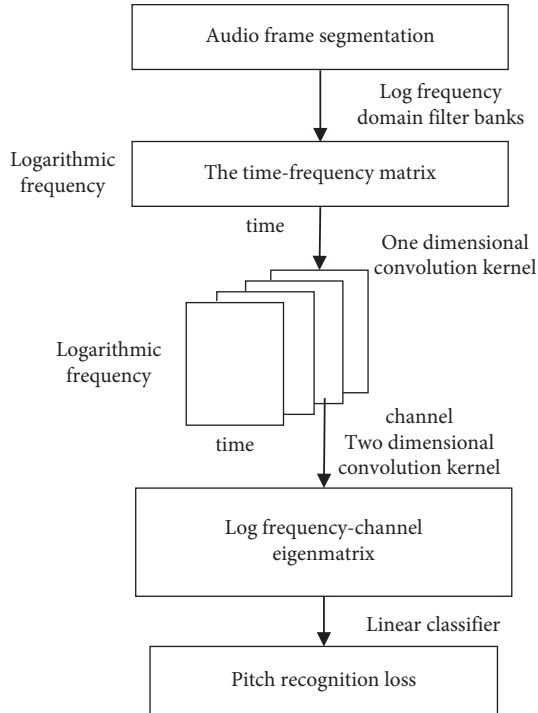


FIGURE 3: Pitch feature extraction process.

$$\text{filter}_i = (w_{i,\sin}^T x_t)^2 + (w_{i,\cos}^T x_t)^2. \quad (5)$$

If the number of filters is n_p , the corresponding outputs are $\text{filter}_1, \dots, \text{filter}_{n_p}$. Dividing the audio frames into

segments, if the number of segments is T_p , the logarithmic frequency-time matrix is $n_p \times T_p$.

Secondly, processing the above matrix, the tensor of logarithmic frequency-time-channel can be obtained after convolution. The first layer of the convolutional network is the matrix obtained in the first step. However, setting up the mapping of the second layer is to do the convolution computation for the logarithmic frequency axis. The step size is set to 3, and the convolution kernel 128×1 is selected. The matrix after convolution is mapped to channels, and the tensor of $128 \times T_p \times C_1$ is obtained, where C_1 represents the number of channels.

Thirdly, continue the two-dimensional convolution for the tensor obtained in the previous step, so that the logarithmic frequency-channel matrix can be obtained. Mapping to the third layer with the same method, the height of convolution kernel ($T_p \times C_2$) is 1; thus, the matrix of $128 \times C_2$ can be obtained, where C_2 represents the number of channels.

The full connection processing of the matrix obtained in the previous step is performed, and the corresponding pitch recognition vector can be obtained. It is necessary to connect the lines of the matrix in the previous step with the linear classifier. The number of pitch frequency is m_1 . If the number of valid elements is the same, the vector is 1. If the number is different, the vector is 0.

After the frame segmentation is completed, each audio frame is processed based on the above process. The corresponding pitch feature matrix can be obtained. If the pitch frequency in the pitch set is M_p , and the number of frame is N_p , so the corresponding matrix size is expressed as $M_p \times N_p$.

2.1.2. Constant Q Transform. In order to better display the pitch frequency on the spectrum space of DFT or STFT, the constant Q transform (CQT) is adopted in this study to transform the time-frequency of music signal analysis. The specific steps are as follows [23–25]:

- (1) Find the spectral kernel matrix corresponding to the octave with the highest frequency.
- (2) The corresponding CQT frequency band of the input signal $x(n)$ is calculated by the DFT transform vector, and the input signal $x(n)$ is marked as $x_0(n)$.
- (3) Sample the signal.

- (4) Calculate the CQT frequency band by the corresponding DFT transform vector of the next octave.
- (5) Repeat steps (3) and (4) until the calculation is complete, as shown in Figure 4.

In Figure 4, $G(f)$ represents the low-pass filter, and $\downarrow 2$ represents downsampling with a downsampling factor of 2. Here, the downsampling of $x_d(n)$ is $f_s/2d$ ($d \geq 1$), and the CQT transform X_d^{CQ} of each octave is

$$X_d^{CQ} = A^* X_d, \quad (6)$$

where A^* represents the conjugate transpose of the complex numerical spectrum kernel matrix, which is usually used to calculate the CQT of octaves.

2.2. Construction of Multi-Instrument Signal Recognition Model

2.2.1. Construction of Benchmark Model.

First of all, the benchmark model needs to be established, and then the modification and improvement can be achieved on this basis. In this article, combining the convolutional network model designed by liu and Yang, the model can realize automatic music labeling. The data used in this training have a frame-level accuracy label, which is used as a supervisory signal.

This model is divided into multiple layers, including the batch standardization layer, convolution layer, pooling layer, etc., and the specific structure is shown in Figure 5 [26].

Due to the problem of internal covariable offset in the training process of the convolutional network, the batch standardization layer can be used to deal with it. It is necessary to ensure the consistency in the distribution of training and test data, and it is helpful to improve generalization ability. However, when there are many parameters and the number of network layers increases, the data distribution will change after the parameter update. At this time, the difficulty of training will increase. To solve the above problems, the batch standardization can be adopted to adjust the data distribution. It makes the intermediate characteristic data become normal distribution, which is realized by processing the input or output data of the intermediate hidden layer. This is a standardized processing procedures, and its formula is shown as follows [27]:

$$a_i^n = \gamma_i \times \frac{a_i - \mu}{\sigma} + \beta_i. \quad (7)$$

Here, β_i and γ_i represent translation and zoom factor, respectively; a_1 represents initial activation value; μ and σ are as follows, respectively:

$$\mu = \frac{1}{m} \sum_{k=1}^m a_k, \quad k \in S, \|S\| = m, \quad (8)$$

$$\sigma = \sqrt{\frac{1}{m} \sum_{k=1}^m (a_k - \mu)^2 + \varepsilon}, \quad k \in S, \|S\| = m.$$

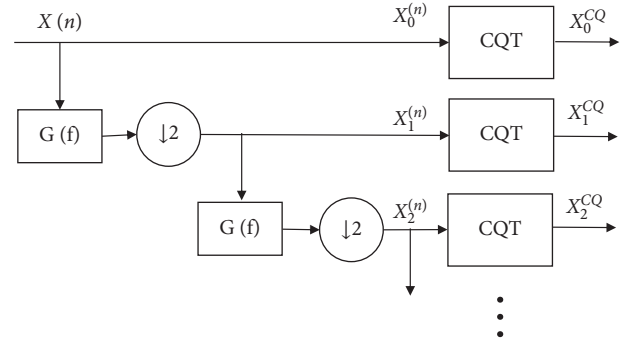


FIGURE 4: The method of CQT calculation for each octave.

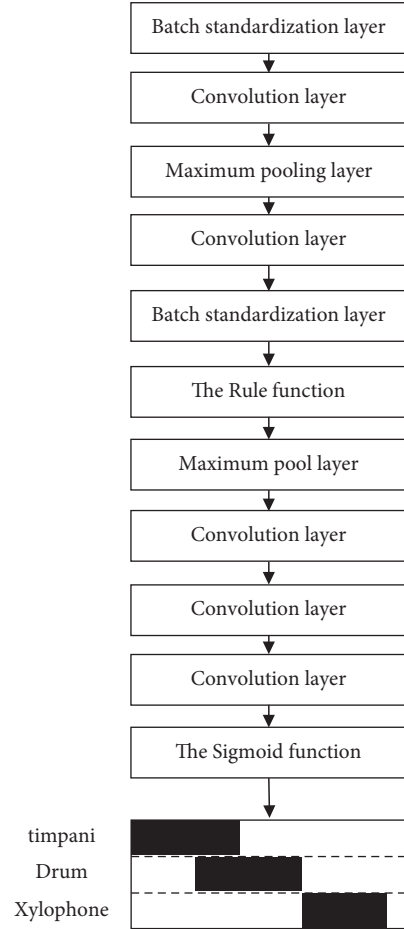


FIGURE 5: Network structure of the benchmark model.

In the formulas, S represents the neuron set with a size of M , but it has different meanings for different networks. If it is a convolutional network, m actually represents the total

number of all activation values formed based on the convolutional kernel channel. For a fully connected network, it represents the number of activation values formed by all instances in a particular batch. ε represents the constants related to training stability.

Batch standardization is a key process. The problem of gradient explosion can be solved by adjusting data distribution, because the noise caused by scaling and other operations can help to get the parameters with higher generalization performance. In addition, to improve the efficiency of convergence, a relatively large learning step can be set.

Except for the above layers, the function of the convolution layer is to extract the required intermediate features. The maximum pooling layer is an important part, which can realize the function of compression features. And it can reduce the difficulty of calculation. Specifically, the maximum value dividing the pooling area is taken as the output value. ReLu function is adopted in the middle, and the specific form is as follows [28].

$$f(x) = \begin{cases} x, & x > 0, \\ 0, & x \leq 0, \end{cases} \quad (9)$$

where some activation values of output are equal to zero, which makes the network sparse. Compared to the Sigmoid function, a higher convergence speed can be achieved. The output layer is mainly applied, and its form is shown as follows [29]:

$$f(x) = \frac{1}{1 + \exp(-x)}. \quad (10)$$

Based on the function, the normalization has been achieved. The output value of the instrument recognition model is placed in the range of 0–1, namely, the existence probability of various musical instruments. Then, the binarization method can be adopted to determine instruments' existing situation. This process depends on the proper threshold. If the threshold is set to 0.5, there is no guarantee for good performance. Therefore, a kind of threshold selection algorithm is designed. It means that the method of maximizing the F1 score of the training set is used to set the threshold value. There are 99 candidates' threshold values, which are 0.1, 0.2, . . . , 0.99, respectively.

The loss function adopted in the training is binary cross-entropy, and the specific form is shown as follows [30]:

$$l = - \sum_{k=1}^{11} \hat{y}_k \log y_k + (1 - \hat{y}_k) \log (1 - y_k). \quad (11)$$

Here, k represents the specific musical instrument category, and y_k and \hat{y}_k represent the identification of each time frame and real label. Considering the imbalance of categories, a certain weight is set for each category, which is expressed as ω_k . The specific form is shown as follows [30]:

$$\omega_k = \left(\frac{\bar{p}}{p_k} \times \frac{1 - p_k}{1 - \bar{p}} \right)^\eta. \quad (12)$$

In the formula, η represents the hyperparameter, which is generally valued at 0.3; \bar{p} represents the mean value of all of p_k ; and p_k represents the proportion occupied by category k . l_{ban} is expressed as follows:

$$l_{\text{ban}} = - \sum_{k=1}^{11} \omega_k [\hat{y}_k \log y_k + (1 - \hat{y}_k) \log (1 - y_k)]. \quad (13)$$

According to the above analysis, the weights need to be set in conjunction with the proportion size occupied by a specific categories of instruments. For example, when the proportion occupied by a specific categories of instruments is low, a higher weight should be set to improve the accuracy of instrument recognition results. So when the frequency of occurrence is not high, the effective recognition even can be ensured. The momentum algorithm is adopted in the calculation, in which weight attenuation factor, learning rate, and batch are 2×10^{-4} , 0.01, and 80, respectively.

2.2.2. Multi-Instrument Signal Recognition Based on Two-Level Classification. When multiple instruments are played at the same time, the traditional classification model based on the attention network has a poor recognition effect on harmonic instruments. The main reason is the category imbalance, which means that the difference in the proportion of different categories interferes with the learning of model parameters. Therefore, combined with the basic principle of undersampling or oversampling, the two-level classification model is proposed. This model is mainly divided into the first-level and the second-level convolutional neural network classification models.

The first-level classification model takes the constant Q transform matrix as the input feature. Firstly, the instrument families in audio signals are rough classified. The constant Q transform matrix reflects the time-frequency energy distribution of audio signals, and it can be used as an effective feature of rough classification.

The second-level classification model is composed of three residual network models with the same architecture. Each residual network model is specially trained to identify various instruments under a certain musical instrument family. There is a special network model for each of the three musical instrument families. The specific process of the two-level classification model is as follows [30, 31].

Figure 6 shows the network architecture of first-level classification model. From the top to the bottom, there are batch standardization layer, convolution layer, batch standardization layer, convolution layer, convolution layer, batch standardization layer, ReLu layer, maximum pooling layer, convolution layer, and Sigmoid layer.

Figure 7 shows the residual network model architecture of three same structures in the second-level classification model. From the top to the bottom, there are batch standardization layer, convolution layer, residual block, maximum pooling layer, residual block, convolution layer, maximum pooling layer, batch standardization layer, ReLu layer, convolution layer, and Sigmoid layer.

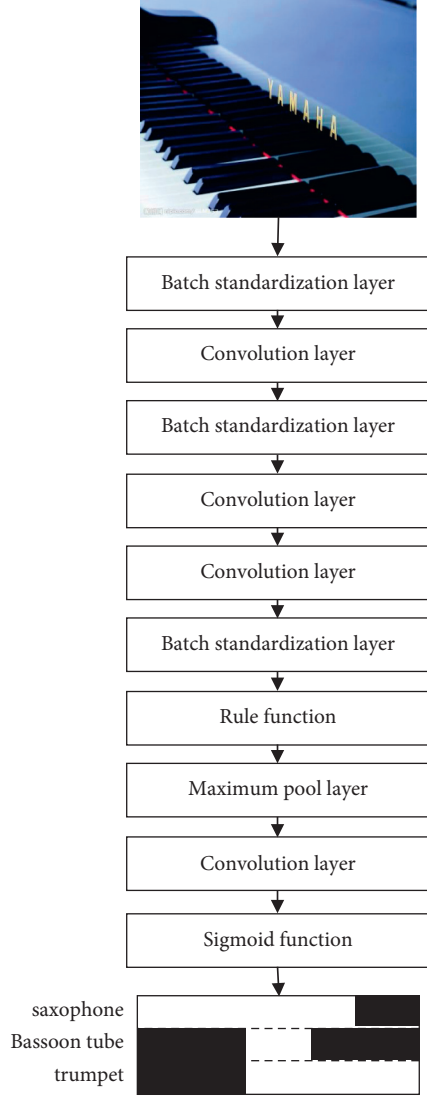


FIGURE 6: The network structure of the first-level classification model in the two-level classification model.

The residual block is divided into two parts. The first part includes batch standardization layer, convolution layer, batch standardization layer, ReLu layer, convolution layer, and batch standardization layer. And the second part is a convolution layer. The input of the residual block enters these two parts to obtain the output, and the output of two parts is summed as the final output of the residual block.

The residual structure of the residual network can effectively solve the problem of gradient disappearance in deep network. In this article, it is applied to detect and recognize the time-frequency characteristic spectrum, and the intermediate feature extraction of musical instrument recognition is realized successively.

The loss function is expressed as

$$\zeta'_{\text{ban}} = - \sum_{k=1}^K \omega_k [\hat{y}_k \log y_k + (1 - \hat{y}_k) \log (1 - y_k)]. \quad (14)$$

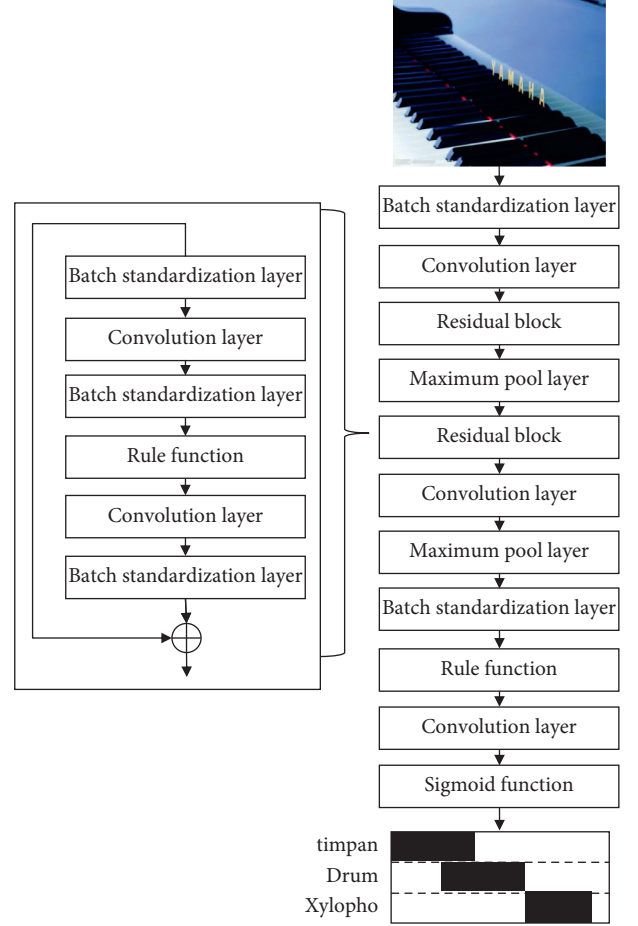


FIGURE 7: Structure of three residual network models with the same structure in the second-level classification model.

In the first-level classification model, the K of equation (14) is valued at 3, representing the three musical instrument family categories of string, wind, and percussion. In the second-level classification model, the K in the string music classification network is valued at 5, representing piano, violin, viola, guitar, and bass. In the wind music classification network, the K is valued at 3, representing saxophone, bassoon, and trumpet. The value of K in the percussion classification network is valued at 3, representing timpani, small drum, and xylophone.

3. Simulation Verification

3.1. Experimental Environment. In order to achieve better experimental results, Intel i7-7800X CPU is selected as the hardware system in this experiment. The main frequency is 3.5 GHz, and the farce frequency is 4.0 GHz. It uses 6 cores and 12 threads. The memory is 16 GB, and the graphics card is an NVIDIA GTX 2080 dual-channel GPU.

Software system: Ubuntu 16.04, 64 bit operating system, Anaconda3-4.4.0, deep learning framework PyTorch0.4.1, and acceleration module CUDA 10.0.

3.2. Dataset Sources. At present, the commonly used dataset includes Bach10 dataset, MedleyDB dataset, and MIXING SECRETS dataset. Among them, Bach10 dataset includes ten large choral works by J.S.Bach, each of which contains four monophonic parts. The audio recordings of each monophonic part are performed by violin, clarinet, saxophone, and bassoon; the MedleyDB dataset consists of 122 songs, in which 108 songs are vocal and instrumental melodies; the MIXING SECRETS dataset contains 258 multitrack audio songs, and there are a variety of music genres involved. However, the scale of the above three public datasets is still not large, and there is no note label in the MIXING SECRETS dataset, only instrument label. Moreover, there are 14 songs in the Medley DB dataset and no note label. In order to solve the above problems, the label annotation information of the MIDI score in an open-source music platform is aligned to the original audio by means of self-built dataset, and then, it is manually calibrated by people with professional music background. Finally, there are 307 useable extended datasets obtained, including various musical instruments and music types, and every frame has the annotation label.

3.3. Processing of Pitch Feature Matrix. Musical instruments of the same family have certain similarities in pitch range. In order to better identify, the energy ratio of harmonics needs to be considered. Therefore, based on the extracted pitch feature matrix, lines 7–94 of the extracted matrix are expressed as Y_1 . According to available information, the matrix is sparse. Then, the fundamental frequency position value within Y_1 is moved to 12 grids $2^{(12/12)} = 2$ distance from it. Thus, the matrix Y_2 is formed. Using the same way to move to 19 grid $2^{(19/12)} = 3$, 24 grid $2^{(24/12)} = 4$, 28 grid $2^{(28/12)} = 5$, and 31 grid $2^{(31/12)} = 6$ in turn, the matrix is respectively represented as Y_3 , Y_4 , Y_5 , and Y_6 .

The basic form of harmonic sequence matrix is as follows:

$$S_n = Y_1 + Y_2 + \dots + Y_n. \quad (15)$$

The matrix actually represents a sequence combination of fundamental frequencies and corresponding harmonics. Therefore, when determining the meaning of Y_6 , S_1 – S_6 matrices can be obtained, which are the input feature of the CNN.

3.4. Experimental Results and Analysis

3.4.1. Multi-Instrument Recognition Results under Benchmark Model. There are ten kinds of musical instruments, which are divided into three categories: percussion instruments, string instruments, and wind instruments. The percussion instruments are xylophone, timpani, trumpet, and the string instruments are guitar, piano, bass, viola, and violin. In addition, the wind instruments are bassoon and saxophone. In the experiment, an appropriate experimental environment should be configured first, which is basically consistent with the previous pitch feature extraction experiment. The dataset is divided into two parts, namely,

training set and test set. The ratio of the two parts is 9:1. Moreover, the possibility of the inexistence and unlabeled instruments in the training set should be considered.

The extracted constant Q transform matrix X^{CQ} (88×165) is processed, which is spliced with S_1 – S_6 . The corresponding input matrices can be obtained, which can be represented as I_1 – I_6 , namely, the harmonic mapping matrix. Then, they are input into the model, and the corresponding class-time series matrix can be obtained. The feature changes in the benchmark model are shown in Table 1.

The experimental results are obtained according to Table 2. The instrument-type recognition results are evaluated through F1. In the total number of instrument recognition, there are three cases of unrecognized, misrecognized, and correct recognition. It can be seen that the overall accuracy can identify the proportion of accuracy times.

The real pitch label matrix is adopted to design the harmonic mapping matrix I_n^g (n is 1–6). At this time, the values in Y_1 are all accurate. According to the information in Tables 2 and 3, it can be clearly seen that compared with the estimated pitch labels, the harmonic mapping matrix obtained by using real labels can achieve higher overall accuracy and F1 value. In addition, compared with xylophone and timpani, the recognition results of estimated and real pitch of a small drum are basically the same, which is mainly related to the unfixed pitch. In this study, the pitch features are mainly used to recognize the musical instruments. So the recognition scores of different types of musical instruments are different. Compared with percussion instruments, the recognition scores of orchestral instruments are higher, which verifies the effectiveness of pitch feature extraction.

3.4.2. Multi-Instrument Classification Results under Two-Level Recognition. Firstly, the configuration of the experimental environment is consistent with the previous section. The momentum algorithm (0.9) is adopted, where the weight attenuation factor, learning rate, and batch are $2 * 10^{-4}$, 0.05, and 60, respectively. In this experiment, a tensor is input, including I_1 – I_6 . Furthermore, the output result is class-time series matrix. The specific characteristic changes are shown in Table 4.

I_3 and I_5 as the benchmark model of input are represented as BI_3 and BI_5 , respectively. The classification model is represented as MA. According to the information in Table 5, it can be seen that compared with the previously adopted benchmark model, a higher overall accuracy is achieved by adopting the attention network model, and the recognition scores of all instruments except xylophone are improved.

Based on the analysis of the above phenomenon, it is found that the attention network actually is to set the appropriate weights for the intermediate feature graph. Compared with the other types of musical instruments, the melodic instrument features are more conducive to recognition, which means the weights are higher. The common melodic instruments are piano and guitar, and the xylophone is rarely used as a melodic instrument. Therefore, if it exists at the same time with other instruments, the

TABLE 1: Change process of the feature size in the benchmark model.

Input size	Operation	Output size
$176 \times 165 \times 1$	2×1 Convolution kernel, 352 channels	$352 \times 164 \times 1$
$352 \times 164 \times 1$	3×1 Maximum pooling	$352 \times 54 \times 1$
$352 \times 54 \times 1$	3×1 Convolution kernel, 704 channels	$704 \times 52 \times 1$
$704 \times 52 \times 1$	3×1 Channels	$704 \times 17 \times 1$
$704 \times 17 \times 1$	2×1 Channels, 704 channels	$704 \times 8 \times 1$
$704 \times 8 \times 1$	1×1 Channels, 11 channels	11×8

TABLE 2: F1 and overall accuracy of ten instruments under the benchmark model (using estimated pitch).

Harmonic mapping matrix order	Piano	Violin	Viola	Guitar	Saxophone	Bassoon tube	Timpani	Xylophone	Bass	Trumpet	Overall accuracy
I_1	0.88	0.88	0.84	0.88	0.82	0.82	0.76	0.73	0.77	0.80	0.77
I_2	0.89	0.89	0.84	0.89	0.84	0.83	0.78	0.75	0.73	0.81	0.77
I_3	0.90	0.90	838.00	0.892	0.83	0.836	0.78	0.76	0.80	0.74	0.77
I_4	0.90	0.40	832.00	0.89	0.84	0.84	0.79	0.75	0.75	0.79	0.77
I_5	0.89	0.89	0.84	0.89	0.85	0.85	0.80	0.77	0.80	0.76	0.77
I_6	0.89	0.89	0.83	0.89	0.85	0.85	0.04	0.77	0.77	0.79	0.78

TABLE 3: F1 scores and overall accuracy of ten instruments under the benchmark model (using real pitch).

Harmonic mapping matrix order	Piano	Violin	Viola	Guitar	Saxophone	Bassoon tube	Timpani	Xylophone	Bass	Trumpet	Overall accuracy
I_1^g	0.90	0.90	0.85	0.89	0.84	0.83	0.77	0.74	0.77	0.83	0.80
I_2^g	0.91	0.91	0.86	0.89	0.85	0.83	0.80	0.76	0.75	0.85	0.80
I_3^g	0.91	0.91	0.85	0.91	0.85	0.84	0.79	0.77	0.76	0.84	0.80
I_4^g	0.91	0.91	0.85	0.90	0.85	0.86	0.81	0.78	0.77	0.85	0.81
I_5^g	0.91	0.91	0.84	0.90	0.86	0.87	0.82	0.79	0.80	0.81	0.80
I_6^g	0.91	0.91	0.85	0.90	0.86	0.87	0.77	0.78	0.79	0.82	0.80

TABLE 4: Changes of feature size in the classification model based on the attention network.

Input size	Operation	Output size
$176 \times 165 \times 6$	2×1 Convolution kernel, 352 channels	$352 \times 164 \times 6$
$352 \times 164 \times 6$	3×1 Maximum pooling	$352 \times 54 \times 6$
$352 \times 52 \times 6$	3×1 Convolution kernel, 704 channels	$704 \times 52 \times 6$
$704 \times 52 \times 6$	3×1 Channels	$704 \times 17 \times 6$
$704 \times 17 \times 6$	2×1 Channels, 11 channels	$11 \times 8 \times 6$
$704 \times 17 \times 6$	Attention subnet	Six attention weights
$11 \times 8 \times 6$	The sum using the weighting of attention weight	11×8

TABLE 5: F1 and overall accuracy and comparison of ten musical instruments based on the attention network classification model.

	Piano	Violin	Viola	Guitar	Saxophone	Bassoon tube	Timpani	Xylophone	Bass	Trumpet	Overall accuracy
BI_3	0.90	0.90	0.84	0.89	0.83	0.84	0.78	0.76	0.81	0.73	0.77
BI_5	0.89	0.89	0.84	0.89	0.85	0.85	0.80	0.77	0.76	0.88	0.77
MA	0.91	0.90	0.85	0.91	0.86	0.86	0.81	0.74	0.80	0.86	0.83

characteristics that need to be recognized can be easily masked. In this perspective, after adding the attention network, it is beneficial for melody instrument recognition, which is helpful to improve the overall accuracy. However, it is not possible to improve all instrument recognition scores, which needs to be further studied.

In this article, the constant Q transform matrix of the first-level classification model is used as input and output instrument family-time series matrix. In the second-level classification model, the third-order harmonic mapping

matrix I_3 , the fifth-order harmonic mapping matrix I_5 , and the sixth-order harmonic mapping matrix I_6 are used as the input features of the string music classification network, wind music classification network, and percussion music classification network, respectively. Then, the output of the three networks is summarized to obtain the final instrument class-time series matrix. The recognition scores and overall accuracy of various musical instruments in the two-level classification model (MT) are obtained, and the comparison is shown in Table 6.

TABLE 6: Comparison of F1 and overall accuracy of ten musical instruments in the two-level classification model.

	Piano	Violin	Viola	Guitar	Saxophone	Bassoon tube	Timpani	Xylophone	Bass	Trumpet	Overall accuracy
BI_3	0.90	0.90	0.84	0.89	0.83	0.84	0.78	0.76	0.79	0.75	0.77
BI_5	0.89	0.89	0.84	0.89	0.85	0.85	0.80	0.77	0.71	0.83	0.77
MA	0.91	0.90	0.85	0.91	0.86	0.86	0.81	0.74	0.75	0.91	0.83
MT	0.91	0.90	0.85	0.91	0.86	0.87	0.82	0.81	0.83	0.89	0.86

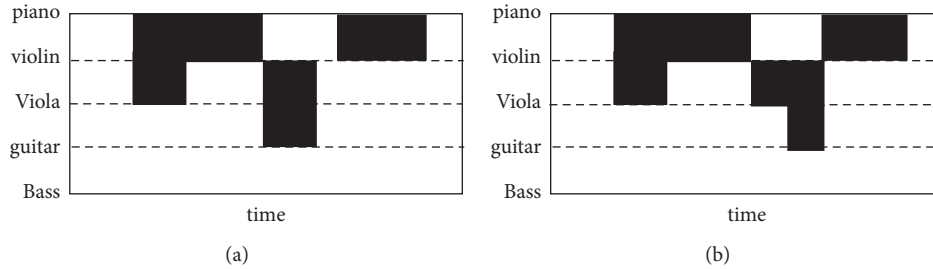


FIGURE 8: Recognition effect of string music classification network in the second-level classification model.

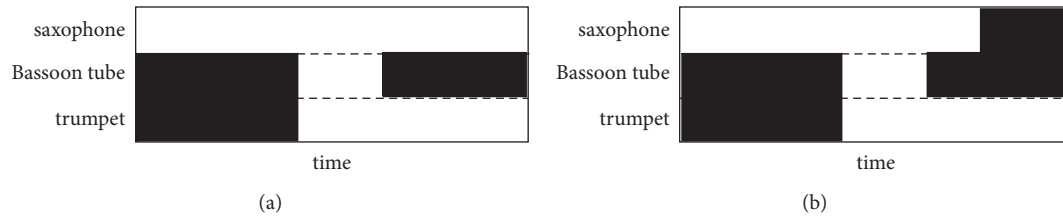


FIGURE 9: Identification effect of the wind music classification network in the second-level classification model.

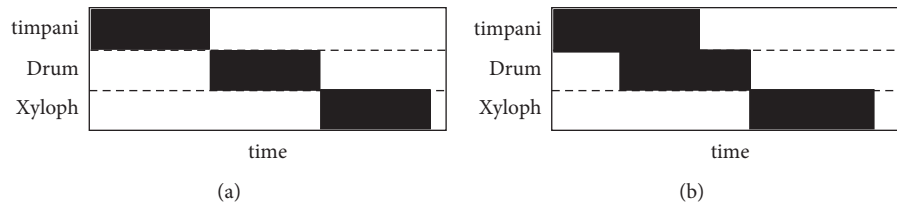


FIGURE 10: Recognition effect of the percussion classification network in the second-level classification model.

After comprehensively analyzing the charts, what can be found is that the recognition scores of most musical instruments are improved, especially xylophone. And it can be seen that the two-level classification model proposed in this article can balance the classification of musical instruments well, and the overall accuracy is further improved.

Figure 8 is the recognition effect diagram of the string music classification network. The upper part (a) represents the real label, the lower part (b) represents the recognition result, and the black part represents the existence of musical instruments.

As can be seen intuitively from the figure above, piano and violin can be accurately identified, while there is confusion in the viola, and the recognition accuracy needs to be improved.

Figure 9 is the identification effect diagram of the wind music classification network. As can be seen from the

picture, the trumpet can be identified accurately, while there are confusions in the the other two instruments, and the recognition accuracy needs to be improved.

Figure 10 is the identification effect diagram of the percussion music classification network. It can be clearly seen from the figure that all three musical instruments have been accurately identified, which means that there are obvious differences between these three musical instruments, so that they can be well identified and classified.

The comprehensive analysis shows that the two-level classification model constructed in this article has the best comprehensive performance, and it has the more accurate recognition effect.

To further verify the effectiveness of the proposed method, the experiment compares the accuracy of the proposed model with that of the existing duets, trios, and quartet, and the obtained comparison results are shown in Table 7.

TABLE 7: Comparison between the proposed model and existing methods.

	Piano	Violin	Viola	Guitar	Saxophone	Bassoon tube	Timpani	Xylophone	Bass	Trumpet	Overall accuracy
MA	0.912	0.903	0.849	0.908	0.855	0.859	0.809	0.743	0.762	0.889	0.825
Bipolar classification model	0.913	0.901	0.853	0.907	0.863	0.866	0.822	0.811	0.834	0.880	0.857
Duet	0.827	0.881	—	0.829	—	—	—	—	—	—	0.841
Trio	0.683	0.825	—	0.828	—	—	—	—	—	—	0.778
Quartet	0.573	0.799	—	0.791	—	—	—	—	—	—	0.731

As can be seen from the above table, compared with the other three methods, the recognition accuracy of the two-level classification model proposed in this article is as high as 85.7%. The recognition accuracy of duet is 84.1%. There are 77.8% for trio, and there are 73.1% for quartet. The method proposed in this article is much higher than the other three methods, which shows that the method proposed in this article has a higher recognition accuracy and better performance.

4. Conclusion

In conclusion, the two-level classification model based on the convolutional neural network proposed in this article has a good classification effect and recognition accuracy. It has certain validity. Through comparative experiments, it is found that the recognition accuracy of the proposed method is 1.6%, 8.1%, and 13.4% higher than that of the method of duet, trio, and quartet. So the recognition accuracy and classification effect of the proposed method are better. The validity of the proposed classification model is further verified by comparing the benchmark classification model with the classification model based on the attention network. However, due to the lack of experience and adequate experimental conditions, the research needs to be further improved and perfected. Specifically, the original audio and scores of various musical instruments can be added to obtain more datasets, so as to further improve the experiment scientificity.

Data Availability

The experimental data are available from the corresponding author upon request.

Conflicts of Interest

The author declares that there are no conflicts of interest regarding this work.

Acknowledgments

This project was funded by the First-class Undergraduate Curriculum Development Program of Minjiang University (MJU2021KC314).

References

- [1] A. C. María and J. ValeroMas Jose, "Exploiting the two-dimensional nature of agnostic music notation for neural optical music recognition," *Applied Sciences*, vol. 11, no. 8, p. 3621, 2021.
- [2] G. Agarwal and H. Om, "An efficient supervised framework for music mood recognition using autoencoder-based optimised support vector regression model," *IET Signal Processing*, vol. 15, no. 2, pp. 98–121, 2021.
- [3] R. Sarkar, S. Choudhury, S. Dutta, A. Roy, and S. Saha, "Recognition of emotion in music based on deep convolutional neural network," *Multimedia Tools and Applications*, vol. 79, no. 1, pp. 765–783, 2020.
- [4] F. Yan, "Music recognition algorithm based on T-S cognitive neural network," *Translational Neuroscience*, vol. 10, no. 1, pp. 135–140, 2019.
- [5] X. Liang, L. Xu, X. Wen, J. Shi, S. Li, and X. Qian, "Effects of individual factors on perceived emotion and felt emotion of music: based on machine learning methods," *Psychology of Music*, vol. 49, no. 5, pp. 1069–1087, 2021.
- [6] J. Wang, Q. Wang, and H. Liu, "Emotion recognition of musical instruments based on convolution long short time memory depth neural network," *Journal of Physics: Conference Series*, vol. 1976, no. 1, 2021.
- [7] A. Orhan and Ş. Abdulkadir, "Attention guided 3D CNN-LSTM model for accurate speech based emotion recognition," *Applied Acoustics*, vol. 182, 2021.
- [8] A. Solanki and S. Pandey, "Music instrument recognition using deep convolutional neural networks," *International Journal of Information Technology*, pp. 1–10, 2019.
- [9] I. Maliki, "Musical instrument recognition using mel-frequency cepstral coefficients and learning vector quantization," *IOP Conference Series: Materials Science and Engineering*, vol. 407, no. 1, 2018.
- [10] K. Patil and M. Elhilali, "Biomimetic spectro-temporal features for music instrument recognition in isolated notes and solo phrases," *EURASIP Journal on Audio Speech and Music Processing*, vol. 2015, no. 1, 27 pages, 2015.
- [11] V. Gupta, S. Juyal, G. P. Singh, C. Killa, and N. Gupta, "Emotion recognition of audio/speech data using deep learning approaches," *Journal of Information and Optimization Sciences*, vol. 41, no. 6, pp. 1309–1317, 2020.
- [12] T. Y. Chin, B. N. I. Eskelson, K. Martin, and V. LeMay, "Automatic bird sound detection: logistic regression based acoustic occupancy model," *Bioacoustics*, vol. 30, no. 3, pp. 324–340, 2021.
- [13] E. N. N. Ocquaye, Q. Mao, Y. Xue, and H. Song, "Cross lingual speech emotion recognition via triple attentive asymmetric convolutional neural network," *International Journal of Intelligent Systems*, vol. 36, no. 1, pp. 53–71, 2020.
- [14] Y. Yin, D. Tu, W. Shen, and J. Bao, "Recognition of sick pig cough sounds based on convolutional neural network in field situations," *Information Processing in Agriculture*, vol. 8, no. 3, pp. 369–379, 2021.
- [15] Mustaqeem and S. Kwon, "Optimal feature selection based speech emotion recognition using two-stream deep convolutional neural network," *International Journal of Intelligent Systems*, vol. 36, no. 9, pp. 5116–5135, 2021.

- [16] T. Anvarjon, J. Y. Choeh, and S. Kwon, "Age and gender recognition using a convolutional neural network with a specially designed multi-attention module through speech spectrograms," *Sensors*, vol. 21, no. 17, p. 5892, 2021.
- [17] D.-H. Jung, N. Y. Kim, S. H. Moon et al., "Deep learning-based cattle vocal classification model and real-time livestock monitoring system with noise filtering," *Animals*, vol. 11, no. 2, p. 357, 2021.
- [18] F. Misbah, M. Farooq, F. Hussain, N. Baloch, F. Raja, and Y. Zikria, "Impact of feature selection algorithm on speech emotion recognition using deep convolutional neural network," *Sensors*, vol. 20, no. 21, p. 6008, 2020.
- [19] W. C. Yin, W. Ei Hlaing, and M. Myo Khaing, "Myanmar continuous speech recognition system using convolutional neural network," *International Journal of Image, Graphics and Signal Processing*, vol. 13, no. 2, pp. 44–52, 2021.
- [20] K. Mukul, M. Kumar, N. Katyal, N. Ruban, E. Lyakso, and G. Richard, "Transfer learning based convolution neural net for authentication and classification of emotions from natural and stimulated speech signals," *Journal of Intelligent and Fuzzy Systems*, vol. 41, no. 1, pp. 2013–2024, 2021.
- [21] X. Chen, "Simulation of English speech emotion recognition based on transfer learning and CNN neural network," *Journal of Intelligent and Fuzzy Systems*, vol. 40, no. 2, pp. 2349–2360, 2021.
- [22] M. Seo and M. Kim, "Fusing visual attention CNN and bag of visual words for cross-corpus speech emotion recognition," *Sensors*, vol. 20, no. 19, p. 5559, 2020.
- [23] V. Passricha and R. K. Aggarwal, "PSO-based optimized CNN for Hindi ASR," *International Journal of Speech Technology*, vol. 22, no. 4, pp. 1123–1133, 2019.
- [24] G. Wang, W. Li, L. Zhang, L. Sun, and X. Ning, "Encoder-X: solving unknown coefficients automatically in polynomial fitting by using an autoencoder," *IEEE Transactions on Neural Networks and Learning Systems*, 2021.
- [25] V. Passricha and R. K. Aggarwal, "Convolutional support vector machines for speech recognition," *International Journal of Speech Technology*, vol. 22, no. 3, pp. 601–609, 2019.
- [26] S. Wang, T. H. Wu, T. Shao, and Z. X. Peng, "Integrated model of BP neural network and CNN algorithm for automatic wear debris classification," *Wear*, vol. 426–427, pp. 1761–1770, 2019.
- [27] Q. Zheng, P. Zhao, Y. Li, H. Wang, and Y. Yang, "Spectrum interference-based two-level data augmentation method in deep learning for automatic modulation classification," *Neural Computing & Applications*, vol. 33, no. 13, pp. 7723–7745, 2020.
- [28] C. Lin, Y. Shi, J. Zhang, C. Xie, W. Chen, and Y. Chen, "An anchor-free detector and R-CNN integrated neural network architecture for environmental perception of urban roads," *Proceedings of the Institution of Mechanical Engineers - Part D: Journal of Automobile Engineering*, vol. 235, no. 12, pp. 2964–2973, 2021.
- [29] R. Vidhya and G. Vadivu, "Towards developing an ensemble based two-level student classification model (ESCM) using advanced learning patterns and analytics," *Journal of Ambient Intelligence and Humanized Computing*, vol. 12, no. 7, pp. 7095–7105, 2020.
- [30] J. Ma and T. W. S. Chow, "Label-specific feature selection and two-level label recovery for multi-label classification with missing labels," *Neural Networks*, vol. 118, pp. 110–126, 2019.
- [31] S. Qi, X. Ning, G. Yang et al., "Review of multi-view 3D object recognition methods based on deep learning," *Displays*, vol. 69, no. 1, 2021.

Research Article

Deep Collaborative Online Learning Resource Recommendation Based on Attention Mechanism

Cuiping Hao and Ting Yang 

Yulin University, Yulin 719000, Shanxi, China

Correspondence should be addressed to Ting Yang; yt1028@yulinu.edu.cn

Received 6 January 2022; Revised 14 February 2022; Accepted 1 March 2022; Published 24 March 2022

Academic Editor: Hangjun Che

Copyright © 2022 Cuiping Hao and Ting Yang. This is an open access article distributed under the Creative Commons Attribution License, which permits unrestricted use, distribution, and reproduction in any medium, provided the original work is properly cited.

In view of the lack of hierarchical and systematic resource recommendation caused by rich online learning resources and many learning platforms, an attention-based ADCF online learning resource recommendation model is proposed by introducing the attention mechanism into a deep collaborative DCF model. Experimental results show that the proposed ADCF model enables an accurate recommendation of online learning resources, reaching 0.626 and 0.339 on the HR and NDCG metrics, respectively, compared to the DCF models before improved, up by 1.31% and 1.25%, and the proposed ADCF models by 1.79%, 2.17%, and 2.32%, respectively, compared to the IUNeu and NeuCF models.

1. Introduction

In recent years, the application of the Internet has promoted education from offline to online. Online education has become a trend in today's education development and occupies a place in the huge education market. Data show that the number of online education users in China's in 2020 grew from 90.992 million in 2015 to 182.492 million, an increase of 50.14%. With the infiltration of online education methods, online education and learning resources are increasingly rich, which not only brings the balanced development and multidirectional development of education but also brings great difficulties to the recommendation of learning resources. On the one hand, there are more online education platforms, and the curriculum types of each platform are complex and the curriculum quality is poor, making it difficult for learners to choose by themselves; on the other hand, online education and learning resources lack understanding of learners, which makes it difficult for the platform to recommend personalized courses to learners. Therefore, it is necessary to integrate and analyze the online learning resources and recommend them according to learners' needs. To achieve this purpose, the relevant scholars conduct research. According to the different

characteristics of students, Hu and others select a small piece of content course knowledge points in the learning resources, take the course knowledge as the recommendation point, and realize the recommendation of personalized online learning resources by designing personal personalized learning mechanism recommendation [1]. In order to solve the problem of sparse data and poor scalability in collaborative filtering algorithms, Honggang Wang and others optimized them using dynamic k close neighbors and slope one algorithms, and analyzed the sparsity of learning resource data in the network based on the neighbor selection results. Two-way self-equilibrium of stage evolution is adopted to improve the personalized recommendation of resource push, and the fuzzy adaptive binary particle group optimization algorithm based on evolutionary state judgment is adopted to solve the optimal sequence recommendation problem, thus to realize the personalized recommendation of learning resources and improve the matching degree and recommendation speed of online learning resources [2, 3]. Yuan studies link prediction methods in network education, builds a suitable model for network education, and proposes an improved path sorting algorithm based on the neural network sorting method through an improved analysis of traditional methods.

Meanwhile, the random-walk model and the neural network-path sorting algorithm are used to realize the link prediction problem in the online learning knowledge base [4]. Xie et al. proposed a user interaction-based recommendation framework that explores real-time interest from immediate feedback, and experiments on real datasets show that the algorithm achieves more accurate prediction results and higher recommendation efficiency [5]. Liang et al. proposed a learning style model, AROLS model, to represent the characteristics of online learners, realize learning resource adaptation by mining behavioral data of learners, and improve the recommendation effect of online learning resources [6]. Antequera et al. present a novel approach to providing fast, automatic, and flexible resources for application owners with limited expertise in building and deploying appropriate cloud architectures; compared to existing schemes, the scheme improves resource recommendation accuracy in manufacturing scientific gateway applications by 21% [7, 8]. Through the above research, it can be found that the existing online learning resource recommendation is limited to the recommendation of courses on their own platforms and does not integrate and comprehensively recommend similar courses on other platforms, resulting in often the accurate recommendation of courses to learners. To solve this problem, this paper constructs an ADCF recommendation model based on the existing DCF model, by integrating the whole-platform online learning resources and introducing the attention mechanism to allocate the weight to the resources so as to realize the accurate recommendation of online learning resources.

2. Basic Approach

2.1. Brief Introduction of the DCF Model. The DCF model is a deep learning collaborative filter recommendation model developed based on the neural collaborative filter recommendation (NeuCF) model, which solves the problem of few input feature types of the NeuCF model and effectively improves the feature combination ability and nonlinear ability of the model. Its basic architecture is similar to that of NeuCF model architecture, mainly composed of multilayer perceptron (MLP) and generalized matrix decomposition (GMF), including input layer, coding layer, embedding layer, embedding layer, feature extraction layer, pooling layer, feature splicing layer, neural network layer, and output layer, as shown in Figure 1 [9, 10].

The model input layer is mainly responsible for inputting the relevant information and its auxiliary information into the model for training. The coding layer is responsible for coding input feature information. The embedding layer is responsible for converting the encoding into a corresponding feature representation, often including two types for the linear model GMF and for the nonlinear model MLP. The feature extraction layer is responsible for extracting feature relationships, where GMF is used to extract linear feature relationships, and MLP is used to extract nonlinear relationships [10]. The pooling layer is responsible for adjusting the feature size to facilitate feature splicing,

including maximum pooling and mean pooling [11]. The feature splicing layer is responsible for integrating the feature information extracted from GMF and MLP, mainly by adding or splicing the extracted features. The neural network layer is responsible for training the model and model parameter tuning, and uses the cross-entropy loss function to adjust the network weight. The output layer maps the output value to a specific range through the activation function. The sigmoid function is selected as the activation function, and its mathematical expression is as follows [12]:

$$f(x) = \frac{1}{1 + e^{-x}}. \quad (1)$$

In the formula, the value range of $f(x)$ is $[0, 1]$.

The DCF model can extract nonlinear and linear features of information and has strong personalized recommendation ability, but the model believes that all features have the same impact on the final recommendation results and do not have the importance of distinguishing between different features. In practice, different characteristic factors contribute differently to the model prediction results, so it is necessary to improve the model. In this paper, the recommendation effect of the model is improved by introducing an attention mechanism into the model to distinguish between the importance of different features.

2.2. DCF Model Refinement. The improvement of the DCF model in this paper is the introduction of the attention mechanism into the model to improve the model recommendation effect by adding the importance of distinguishing attention layers between the feature splicing layer and the neural network layer. The attention mechanism in the DCF model is mainly attached to the framework of the encoder and decoder, and the essence is a thought model, formulas (2) ~ (4), by allowing the neural network in the DCF model to only focus on the partial information of the input and select specific inputs [13].

$$a = f(X_N), \quad (2)$$

$$Z_a = a \odot X_n, \quad (3)$$

$$\text{st: } a \in (0, 1). \quad (4)$$

In the formula, X_n represents the n-dimensional eigenvector input attention layer, $f(x)$ indicates the attention mechanism network, a represents the attention corresponding to the n-dimensional eigenvector through $f(x)$, and Z_a represents the output layer output result. At that time, $f(x) = \text{Soft max}(X_n)$, the value range of a was $(0, 1)$; when a is constant 1, the attention network helps fit the complex function model when the model degenerated into a DCF model.

The attention mechanism layer of the DCF model (hereinafter referred to as the ADCF model) obtains the weight of each feature dimension through equations (5) ~ (7) [14]. Computing the attention of each feature dimension using softmax, then interacting with the corresponding

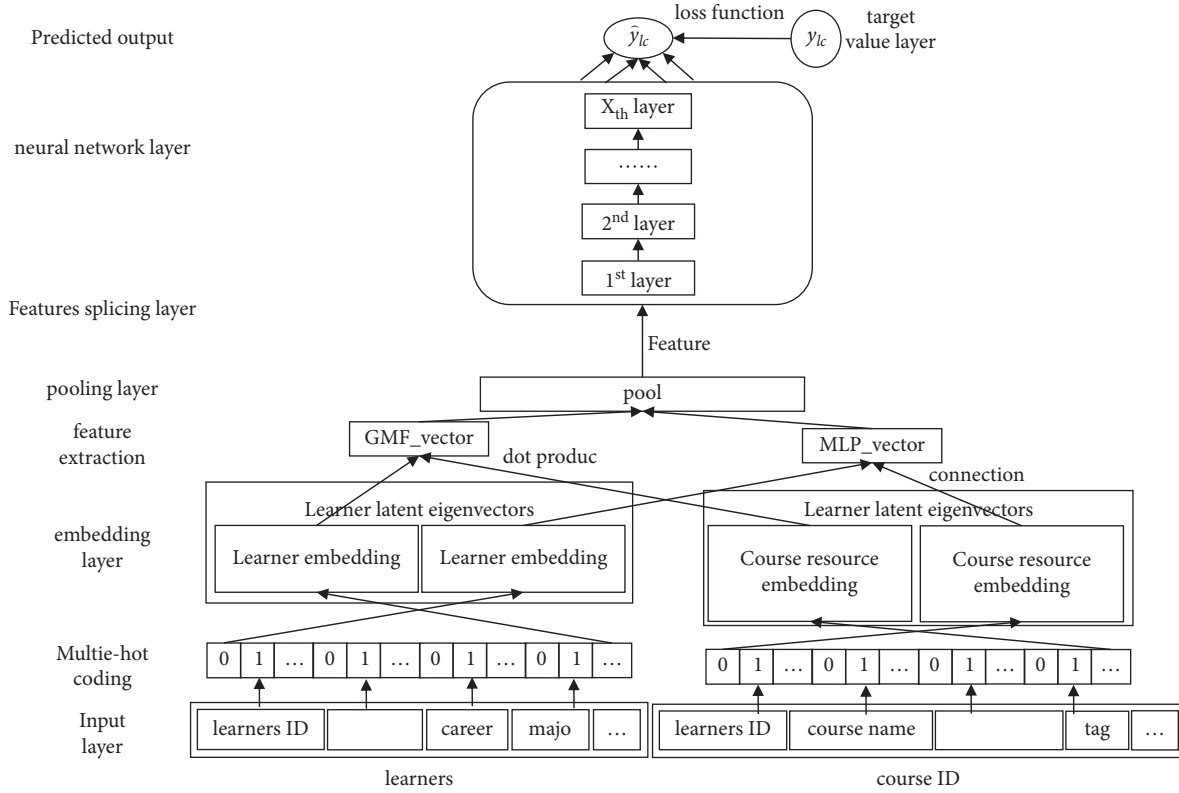


FIGURE 1: The DCF model structure.

features for a point-multiply input deep neural network, and finally the predictive values can be obtained through iterative training.

$$\text{Soft max}(Z_i) = \frac{e^{z_i}}{\sum_{i=1}^k e^{z_i}}, \quad (5)$$

$$A_n = \text{Soft max}(X_n), \quad (6)$$

$$A_{\text{out}} = A_n \otimes X_n. \quad (7)$$

In the formula, Z_i represents the i th element input by the softmax function, $\text{soft max}(Z_i)$ represents the corresponding softmax value of this element, and X_n represents the output value of the feature splicing layer. \otimes indicates point multiplication; A_n represents the corresponding value calculated by softmax, and A_{out} represents the attention layer output value.

The ADCF model, by introducing the attention layer into the DCF model, can distinguish the degree of contribution of different feature information to the predicted recommendation results and then improve the model recommendation effect. Therefore, this paper proposes a new online resource recommendation method based on the ADCF model.

3. Recommended Methods for Online Learning Resources Based on ADCF

3.1. ADCF Mathematical Model. The mathematical model of the ADCF model is as follows:

$$\begin{aligned} P_c^{GMF} &= (c_0^{GMF} \oplus c_1^{GMF} \oplus c_2^{GMF} \oplus c_3^{GMF}), \\ P_l^{GMF} &= (l_0^{MLP} \oplus l_1^{MLP} \oplus l_2^{MLP} \oplus l_3^{MLP}), \\ q_c^{MLP} &= (c_0^{MLP} \oplus c_1^{MLP} \oplus c_2^{MLP} \oplus c_3^{MLP}), \\ \varphi^{GMF} &= P_l^{GMF} \otimes q_c^{GMF}, \\ \varphi^{MLP} &= \partial_L W_L^T \left(\partial_{L-1} \left(\dots \partial_2 \left(W_2^r \begin{bmatrix} P_l^{MLP} \\ q_c^{MLP} \end{bmatrix} + b_2 \right) \dots \right) \right) + b_L, \\ A_{\text{out}} &= \text{Soft max} \left(\begin{bmatrix} \varphi^{EGMF} \\ \varphi^{MLP} \end{bmatrix} \right) \otimes \begin{bmatrix} \varphi^{EGMF} \\ \varphi^{MLP} \end{bmatrix}, \\ \hat{y}_k &= \sigma(h^T A_{\text{out}} + b). \end{aligned} \quad (8)$$

In the formula, \oplus represents connections; liGMF and liMLP represent the learner eigenvectors of the GMF and MLP models, $\{l_0, l_1, l_2, l_3\}$, respectively, corresponding to {learner_id, sex, profession, job}; ciGMF and ciMLP represent the course resource eigenvectors of the models, $\{c_0, c_1, c_2, c_3\}$, respectively, corresponding to {curriculum_id, name, complexity, label}; the piGMF, piMLP, qcGMF, and qcMLP represent the learner and course resource feature vector with auxiliary information for the GMF and MLP models; φ^{MLP} and φ^{EGMF} , respectively, represent the underlying feature relationships learned through the MLP and GMF models. From the model, the whole model process uses the learner and course auxiliary information, which jointly determines the prediction recommendation performance of the model.

3.2. Online Learning Resource Recommendation Based on ADCF. From the above analysis, the online learning resource recommendation model based on ADCF is designed, as shown in Figure 2. The model input layer includes the relevant information of the learner and the course, whose input form is the behavioral sequence of the learner-course $X = \{X_1, X_2, X_3, \dots, X_N\}$. Among these, X_i represents the i th behavior $\langle \text{Learner}_i, \text{Course}_i \rangle$. Learner_i contains information about learners' ID, gender, occupation, and Course_i contains course ID, label, name, etc.

The encoding layer transforms input information via one-hot to embedding feature demo [15]. Taking learner sex as an example, male is coded as [1, 0] and female as [0, 1].

The embedding layer first initializes a embedding matrix about sex, with a matrix size of $2 * d$, where 2 indicates possible sex values and d indicates the embedding dimension. With the above operation, the intractable category feature is able to be converted into tractable vectors. For course and learner features, encoding includes course ID, name, complexity, tag, and learner ID, gender, major, occupation. Embedding corresponds to a length of 16, so the total embedding length is $16 * 8 = 128$ and the output matrix dimension is $1 * m * n$. Then, the auxiliary information $(m - 1) * n$ is added through the flattening operation to extend the length to $m * n$, where m represents the input length, n indicates the potential feature length, and the embedding layer input scale extends from $(1, 1, n)$ to $(1, m, n)$.

The feature extraction layer uses GMF and MLP to extract linear and nonlinear relationships between the learners and the course, the GMF model takes the implicit feature vector point multiplication of the user and the project as the output result, and the MLP model connects the flattening results beginning to end as the output results into the neural network. The activation function of the neural network adopts the ReLU function [16].

The pooling layer adopts the maximum pooling adjusted feature size so that the output vector of the GMF model and the MLP model reaches the same size through the pooling layer.

The feature splice layer was splicing to splicing the feature information extracted from the GMF and MLP models. The attention layer assigns the splice weights and inputs the assignment results into the neural network layer. The neural network layer loss function follows the cross-entropy loss function of the DCF model, adjusted for by backpropagation of the weights of each layer [17]. The output layer follows the sigmoid function as an activation function and maps the output values to a certain range for recommendation.

4. Simulation Experiment

4.1. Experimental Environment Construction. This experiment was carried out on the NVIDIA distributed framework and CUDA parallel computing platform with Selenium + Web Driver, installation of Chrome80.03987.132, compilation environment Python3.6, compiler PyCharm, and dependent module Requests2.21.0, Beautiful Soup, Selenium, etc.

4.2. Data Preprocessing. Considering the large number of crawled datasets, computer-class-related data were selected to construct experimental datasets, and learners with interactions greater than 20 were selected as the main study subjects. Through statistical collation, 878 computer courses, 3,066 learners, and 203,987 learner history data were obtained. The distribution of course interaction number and number of learners is shown in Figure 3.

4.3. Dataset Construction. Online learning resource recommendation is actually a disclassification problem of predicting whether a learner will learn course [18]. Online learning resource recommendation is actually a disclassification problem of predicting whether a learner will learn course [18, 19]. If the missing samples in the dataset are taken by default to positive samples, it can easily lead to an unbalanced dataset. Therefore, to solve this problem, this paper selects some samples as negative samples by random uniform sampling from the missing values.

Considering the certain sequence relationship between learner history learning records, the first $n - 1$ records were used as the training set and the last effective interaction n as the test set. The model was trained by using the training set, and its performance was detected using the validation set. The validation set consists of 100 courses and splicing test set data randomly drawn from the no-interaction course. For experimental convenience, the batch size trained by the model is set to the effective number of interactions $n - 1$ per learner.

4.4. Evaluating Indicator. Hit Ratio, HR and Normalized Discounted Cumulative Gain, and NDCG were used as the indicators to evaluate model performance, calculated as formula (9) and formula (10) [20–22]:

$$\text{HitRatio@K} = \frac{\text{Number Of Hits@K}}{|GT|} \times 100\%, \quad (9)$$

$$\text{NDCG}_k = \frac{\text{DCG}_k}{\text{IDCG}_k}, \quad (10)$$

$$\text{IDCG}_k = \sum_{i=1}^k \frac{1}{\log_2^{1+i}}, \quad (11)$$

$$\text{DCG}_k = \sum_{i=1}^k \frac{2^{\text{reli}} - 1}{\log_2^{i+1}}, \quad (12)$$

$$\text{CG}_k = \sum_{i=1}^k \text{reli}. \quad (13)$$

In equation (9), HitRatio @K represents the hit rate, the number of tests predicted in the Top-k list per learner, and the denominator represents the number of test sets. In equation (10) ~ equation (13), i represents the position in the recommended list; k represents the k value in Top-k; CG_k represents the cumulative gain; and reli represents the correlation of the

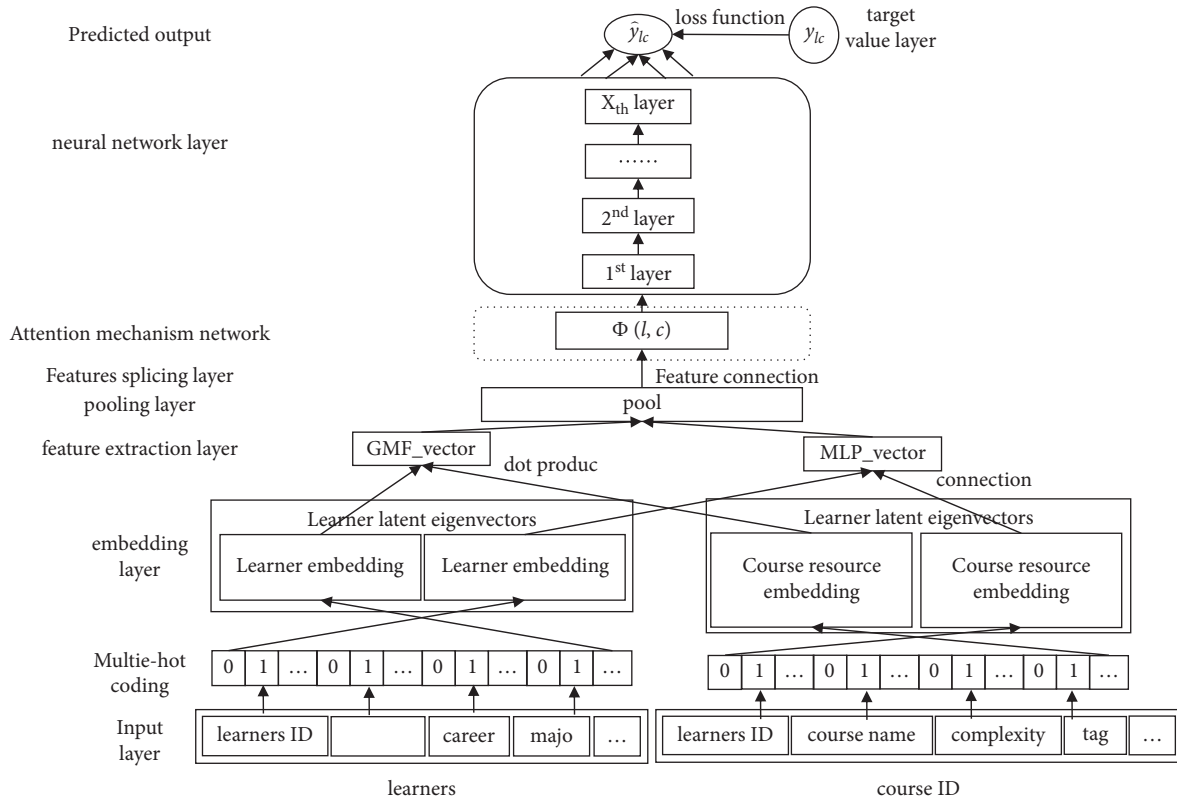


FIGURE 2: Resource recommendation based on ADCF.

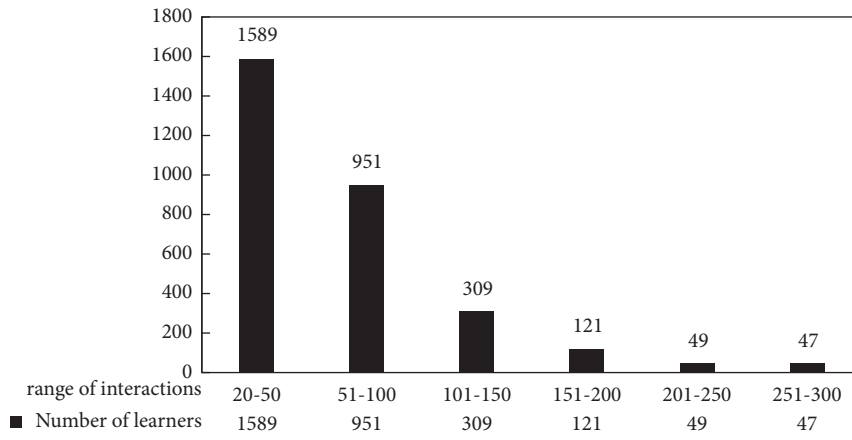


FIGURE 3: The number of learners distributed across the range of interaction numbers.

recommended result in position i . In this paper, $reli = 1$ indicates hits, and $reli = 0$ indicates misses. DCG_k represents the cumulative damage gain, so when $reli = 1$, DCG_k is calculated as formula (14) and when $reli = 0$, DCG_k is calculated as formula (15). $IDCG_k$ represents the idealized loss gain, with all predicted hits, $reli = 1$, so the $IDCG_k$ calculation method can be rewritten as in formula (16).

$$DCG_k = \sum_{i=1}^k \frac{2^i - 1}{\log_2^{i+1}} = \sum_{i=1}^k \frac{\log 2}{\log(i+1)}, \quad (14)$$

$$DCG_k = \sum_{i=1}^k \frac{2^0 - 1}{\log_2^{i+1}} = 0, \quad (15)$$

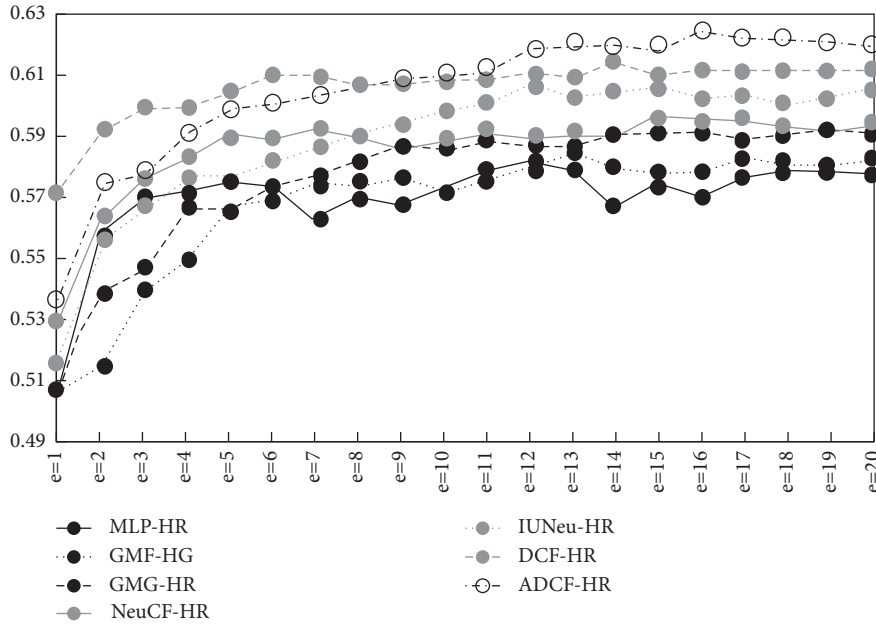


FIGURE 4: The effect of different iterations on model HR.

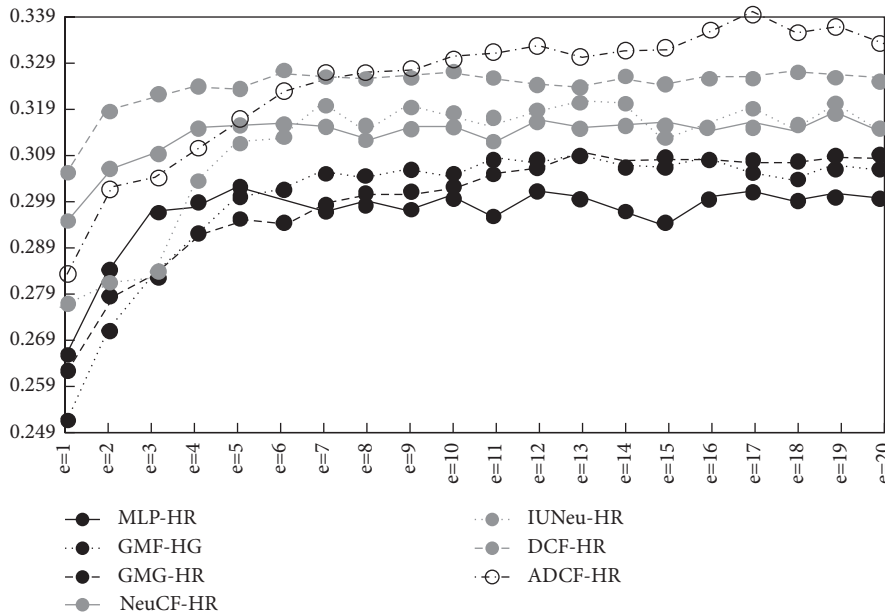


FIGURE 5: Effect of the different iterations on model NDCG.

$$IDCG_k = \sum_{i=1}^k \frac{1}{\log_2^{1+i}}. \quad (16)$$

$$L(Y, P(Y|X)) = -\log P(Y|X) = -\frac{1}{N} \sum_{i=1}^N \sum_{j=1}^M y_{ij} \log(p_{ij}). \quad (17)$$

4.5. Parameter Setting. In this experiment, the model learning rate was set at 0.001, the number of iterations was 20, and the predicted number was $k = 10$. The model adopts the cross-entropy loss function, which is calculated by the formula as follows [23, 24]:

In the formula, X represents the input variable, Y the output variable, L the loss function, N the input sample size, and M the number of possible categories. The y_{ij} is a binary indicator indicating whether the category j enters the real category of the instance x_i . The p_{ij} represents the probability that the model predicts that the input instance x_i belongs to

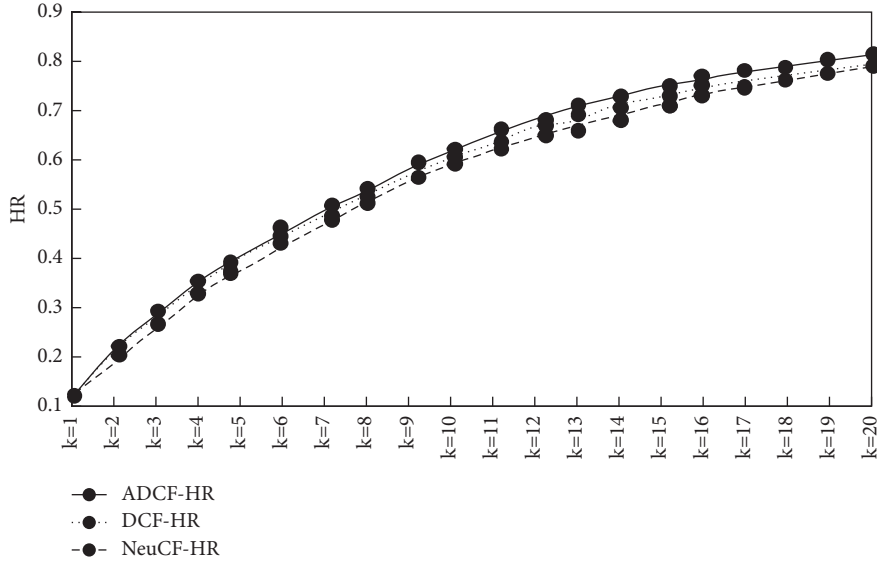


FIGURE 6: Index comparison of HR Model at different k values.

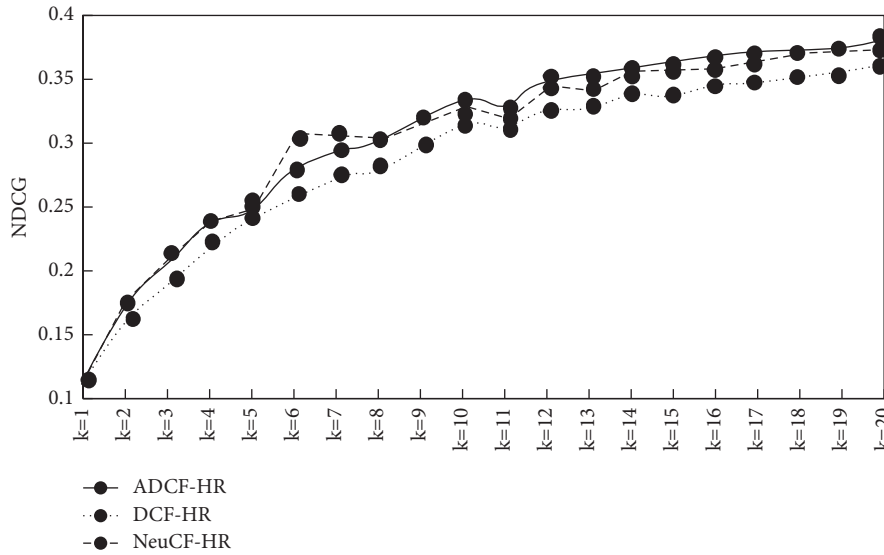


FIGURE 7: Comparison of the model NDCG indicators at different k values.

the category j . In this paper, the recommendation results include recommendations and disapproval, which are indicated by 1 and not by 0. Thus, formula (17) can be overwritten as

$$L(\text{loss}) = \frac{1}{N} \sum_{i=1}^N (y_i \log p_i + (1 + y_i) \log(1 - p_i)). \quad (18)$$

In the formula, y_i represents the real category of the input instance x_i , p_i indicates the probability that the predicted input instance x_i belongs to category 1, and $L(\text{loss})$ represents the logarithmic loss average for each sample. The cross-entropy function is used to measure the similarity of y_i and p_i .

4.6. Experimental Result

4.6.1. *Analysis of Parameters on Model Performance.* This experiment was used to explore the influence of different parameters on the model performance. Figures 4 and 5 are the changes in the HR and NDCG indicators at the different number of iterations, respectively. According to the figure, with the same number of iterations, the DCF and ADCF models performed better on the HR and NDCG indicators compared to the IUNeu and NeuCF models, and the DCF and ADCF models also showed better and more stable performance with the number of iterations increasing. The proposed ADCF model adds the attention mechanism to extract the features and perform the best.

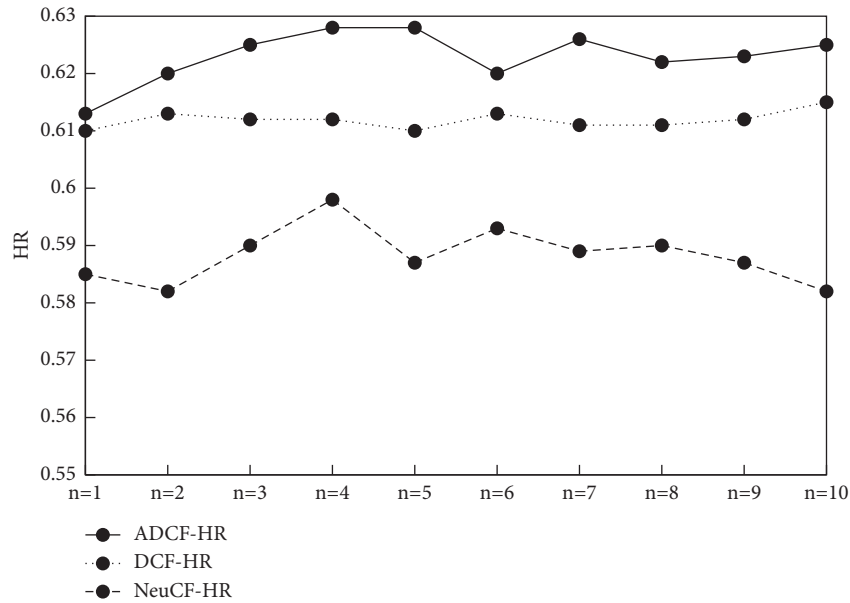


FIGURE 8: The effect of the different num-neg on model HR.

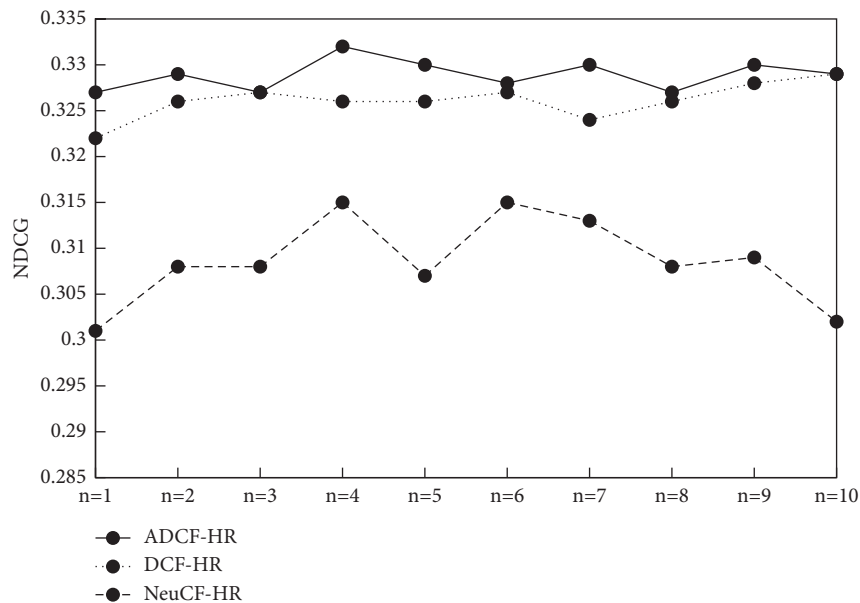


FIGURE 9: Effects of the different num-neg on model NDCG.

For different recommended courses k , the recommended performance of different models is Figures 6 and 7. As shown in the figure, increased with k values, the HR and NDCG metrics of the ADCF, DCF, and NeuCF models were gradually increased, showing that the model recommendation effect is getting better. At the same k values, the ADCF model outperformed the DCF model than the NeuCF and the IUNeu model and the ADCF model, showing that the ADCF model recommended the best effect. Thus, it shows that the proposed ADCF model recommends the best performance.

HR and NDCG indicators for different models under different negative sampled num-neg values are compared in Figures 8 and 9, respectively. From the figure, the value

range of negative sampling n is $[1, 10]$, and the recommended effect of different models is optimal when $n = 4$. Overall, the proposed ADCG model has smaller fluctuations in the HR and NDCG metrics as compared to the DCF and NeuCF models. This shows that the overall ADCF model generally has better recommended performance.

4.6.2. Model Performance Analysis. To validate the performance of the proposed model, the test results of different models such as IUNeu, NeuCF, and DCF were tested with the proposed models on the experimental dataset, as shown in Table 1. According to the table, the

TABLE 1: Comparison of the results of the different algorithms on the experimental datasets.

Serial number	Algorithm	HR@10	NDCG@10	Loading data time (s)	Time
1	ADCF	0.626	0.339	14.3	12.9 s (training) + 2.3 s (test)
2	DCF	0.613	0.326	12.5	12.4 s (training) + 1.8 s (test)
3	IUNeu	0.608	0.320	12.3	11.4 s (training) + 2.1 s (test)
4	NeuCF	0.598	0.317	11.1	11.2 s (training) + 1.4 s (test)
5	ConvNCF	0.546	0.292	16.9	16.9 s (training) + 2.6 s (test)

proposed model performs best on the HR and NDCG indicators, reaching 0.626 and 0.339, compared to the IUNeu model, respectively; HR and NDCG indicators increased 1.79% and 1.86%, respectively; compared with the NeuCF, it was increased by 2.17% and 2.32% on the HR and NDCG indicators, respectively; compared to the DCF models, it was increased by 1.31% and 1.25%, respectively.

In terms of time indicators, the proposed ADCF model has improved both the training time and the validation time of the dataset compared to the comparison model; compared to the DCF and NeuCF models, the average total training time increased by 1 s and 2.6 s, the average total validation time per iteration was increased by 0.5 s and 0.2 s, respectively. The reason for the analysis is that the proposed model introduces an attention mechanism in the characteristic splicing layer, so its temporal performance decreases, but the overall effect is small.

5. Conclusion

In this paper, an attention-based deep collaborative online learning resource recommendation method is proposed; it can realize the accurate recommendation of online learning resources. Compared with the proposed former DCF model, the proposed ADCF model was improved by 1.31% and 1.25% on the HR and NDCG indicators, respectively; compared with the IUNeu and NeuCF models, the proposed ADCF model was improved by 1.79% and 1.86%, 2.17%, and 2.32% on the HR and NDCG metrics, respectively, which has some practical application value. This paper presents a preliminary study of online learning resource recommendation, but the study is still in its infancy, and there are some problems to be improved. For example, when there is one feature fusion method, a splicing method is adopted, while there are many feature fusion methods, different fusion methods are suitable for different models. Therefore, multiple ways should be explored to choose the best fusion methods. Next step, it will be optimized from the above deficiencies to further improve the recommendation effect of online learning resources.

Data Availability

The experimental data used to support the findings of this study are available from the corresponding author upon request.

Conflicts of Interest

The authors declare that they have no conflicts of interest.

References

- [1] X. Hu, Y. Wang, Q. B. Chen, Q. Liu, and X. Fan, "Research on personalized learning based on collaborative filtering method," *Journal of Physics: Conference Series*, vol. 1757, no. 1, pp. 012050–012055, 2021.
- [2] H. Wang and W. Fu, "Personalized Learning Resource Recommendation Method Based on Dynamic Collaborative Filtering," *Mobile Networks and Applications*, vol. 26, pp. 1–15, 2020.
- [3] N. Sokolov Milovančević and A. Gračanac, "Time and ontology for resource recommendation system," *Physica A: Statistical Mechanics and Its Applications*, vol. 525, pp. 752–760, 2019.
- [4] I. Yuan, "Network education recommendation and teaching resource sharing based on improved neural network," *Journal of Intelligent and Fuzzy Systems*, vol. 39, no. 4, pp. 1–10, 2020.
- [5] Q. Xie, Y. Zhu, F. Xiong, L. Li, Z. Bao, and Y. Liu, "Interactive resource recommendation with optimization by tag association and significance analysis," *Neurocomputing*, vol. 391, pp. 210–219, 2020.
- [6] Q. Liang, X. Zheng, Y. Wang, and M. Zhu, "O3ERS: an explainable recommendation system with online learning, online recommendation, and online explanation," *Information Sciences*, vol. 562, pp. 94–115, 2021.
- [7] R. B. Antequera, P. Calyam, A. A. Chandrashekhara, and R. Mitra, "Recommending heterogeneous resources for science gateway applications based on custom templates composition," *Future Generation Computer Systems*, vol. 100, pp. 281–297, 2019.
- [8] D. Mo, X.-G. Chen, S. Duan et al., "Personalized resource recommendation based on collaborative filtering algorithm," *Journal of Physics: Conference Series*, vol. 1302, no. 2, p. 022025, 2019.
- [9] Y. He, G. Xia, Y. Luo et al., "DVFENet: dual-branch voxel feature extraction network for 3D object detection," *Neurocomputing*, vol. 459, pp. 201–211, 2021.
- [10] L. Dai, X. Liu, Y. Liu et al., "Enhancing two-view correspondence learning by local-global self-attention," *Neurocomputing*, vol. 459, pp. 176–187, 2021.
- [11] Y. L. Wang, Z. J. Zhao, S. Y. Hu, and F. L. Chang, "CLCU-Net: cross-level connected U-shaped network with selective feature aggregation attention module for brain tumor segmentation," *Computer Methods and Programs in Biomedicine*, vol. 207, pp. 106154–106155, 2021.
- [12] Y. Shi, Q. Huang, and T. Hain, "H-VECTORS: improving the robustness in utterance-level speaker embeddings using a hierarchical attention model," *Neural Networks*, vol. 142, pp. 329–339, 2021.
- [13] W. Zheng, L. Yan, C. Gou et al., "Pay attention to doctor-patient dialogues: multi-modal knowledge graph attention image-text embedding for COVID-19 diagnosis," *Information Fusion*, vol. 75, pp. 168–185, 2021.

- [14] M. Chen, Y. Li, and X. Zhou, "CoNet: Co-occurrence neural networks for recommendation," *Future Generation Computer Systems*, vol. 124, pp. 308–314, 2021.
- [15] J. Zhenyan, M. Wu, H. Yang, and J. E. A. Inigo, "Temporal sensitive heterogeneous graph neural network for news recommendation," *Future Generation Computer Systems*, vol. 125, pp. 324–333, 2021.
- [16] J. Wang, "An intelligent computer-aided approach for atrial fibrillation and atrial flutter signals classification using modified bidirectional LSTM network," *Information Sciences*, vol. 574, pp. 320–332, 2021.
- [17] F. Xue, S. Pan, M. Yan et al., "Dynamic prediction of late noninvasive ventilation failure in intensive care unit using a time adaptive machine model," *Computer Methods and Programs in Biomedicine*, vol. 208, pp. 106290–106298, 2021.
- [18] H. Lin, S. Xie, Z. Xiao, X. Deng, H. Yue, and K. Cai, "Adaptive recommender system for an intelligent classroom teaching model," *International Journal of Emerging Technologies in Learning (iJET)*, vol. 14, no. 5, pp. 51–63, 2019.
- [19] Y. Oh and Y. Kim, "A resource recommendation method based on dynamic cluster analysis of application characteristics," *Cluster Computing*, vol. 22, no. 1, pp. 175–184, 2019.
- [20] H. Zhang, T. Huang, Z. Lv, S. Liu, and H. Yang, "MOOCRC: a highly accurate resource recommendation model for use in mooc environments," *Mobile Networks and Applications*, vol. 24, no. 1, pp. 34–46, 2019.
- [21] H. Liu, "Resource recommendation via user tagging behavior analysis," *Cluster Computing*, vol. 22, no. 1, pp. 885–894, 2019.
- [22] *Studies from Wuhan University of Technology Yield New Information about Algorithms (Interactive Resource Recommendation Algorithm Based on Tag information)*, Internet Weekly News, UK, pp. 382–386, 2018.
- [23] Q. Xie, F. Xiong, T. Han, Y. Liu, L. Li, and Z. Bao, "Interactive resource recommendation algorithm based on tag information," *World Wide Web*, vol. 21, no. 6, pp. 1655–1673, 2018.
- [24] J. H. Park, "Resource collaboration system based on user history and the psychological mode," *Journal of Ambient Intelligence and Humanized Computing*, vol. 9, no. 5, pp. 1683–1691, 2018.

Research Article

Construction and Simulation of the Market Risk Early-Warning Model Based on Deep Learning Methods

Yuchen Lei¹ and Yinghui Li² 

¹School of Finance, Shandong University of Finance and Economics, Jinan 250000, China

²Henan Finance University, Zhengzhou 450046, China

Correspondence should be addressed to Yinghui Li; liyingshui@hafu.edu.cn

Received 21 January 2022; Accepted 23 February 2022; Published 24 March 2022

Academic Editor: Man Fai Leung

Copyright © 2022 Yuchen Lei and Yinghui Li. This is an open access article distributed under the Creative Commons Attribution License, which permits unrestricted use, distribution, and reproduction in any medium, provided the original work is properly cited.

To address the problem of low efficiency of existing forecasting models for market risk warning, a market risk early-warning model based on improved LSTM is suggested utilizing the whale optimization algorithm (WOA) to optimize the number of hidden layer neurons and time step parameters of long short-term memory. The proposed market risk early-warning model is validated by using 40 real estate companies as the research subjects and 20 relevant variables such as gross operating income, net profit asset growth rate, and total asset growth rate as indicators. The results demonstrate that the proposed model's prediction accuracy for market risk is greater than 96% and that when compared to the standard CNN and LSTM models, the suggested model's prediction accuracy for corporate finance from 2012 to 2019 is increased by 14% and 12%, respectively, and the prediction accuracy for corporate finance in 2020 is improved by 22% and 7%, respectively, which has certain practical application value and superiority.

1. Introduction

In recent years, affected by the trade war between China and the USA and the global coronavirus pandemic, the real estate industry across the country has been severely impacted and caused varying degrees of bubbles and other problems, putting the real estate market and the entire national economy in jeopardy. To ensure a healthy and stable development, macroregulation based on early-warning information provided by the real estate market is crucial. To this end, based on Internet big data, Jiang et al. suggested a support vector machine-based (SVM) real estate market risk early-warning model [1]. China A-share listed real estate companies in 2019 are used as the study subjects. Using the random forest algorithm to select five important feature dimensions, current ratio, equity financing ratio, operating income, current liability ratio, and receivables' turn, the financing risk prediction of real estate companies is achieved by collecting the relevant companies' financial information from 2010 to 2019 and supplementing the risk sample data from 2005 to 2010. Using Philadelphia as the study object,

Junchi et al. suggested an improved regression tree (BRT) for merging urban data, including metadata and image data, with home features to estimate the market value of Philadelphia housing at the projected level [2]. Alvarez et al. proposed to forecast house values, using publicly available information on geography, city characteristics, traffic, and real estate for sale by a tree-based incremental learning model and allowing for early warning of real estate risk. Using massive datasets for training and incremental learning to deliver accurate price projections on a daily basis, the model's prediction accuracy was enhanced [3]. García-Magariño and Lacuesta analyzed and predicted the possible buying and selling behavior in the real estate market based on agent's simulation tool, by taking Spanish real estate as a research object and simulating real estate transactions, which can effectively warn the market risk in the real estate industry [4]. Zhou et al. assessed the real estate market's internal and external environments and a PSO-SVM model-based, and the real estate risk early-warning model was proposed, which accurately predicts cyclical real estate risk in Beijing and has good early-warning performance [5].

Based on the DEA-Malmquist method, Chen et al. predicted corporate assets by analyzing the inventory manifestation of the Chinese real estate industry from 2005–2015, concluding that there may be zombie enterprises and the risk of future unemployment [6]. Kamara et al. proposed a new hybrid neural network model with CNN attention (CNNA) and bidirectional LSTM (BLSTM)-based modules to extract features to tackle the Day-of-Market (DOM) prediction problem [7]. According to the estimated distribution of the characteristics, confidence intervals for the four properties in the dataset were derived from percentile Bootstrap confidence intervals (CI) or percentile bias-corrected accelerations' (BCA) Bootstrap CI. Finally, proposed method's superiority to the DOM prediction problem was demonstrated and the prediction accuracy reached 87% by conducting experiments on the dataset of a well-known real estate agency in Shanghai. By investigating the association between financial stability and real estate price volatility in China and utilizing detrended cross-correlation analysis, Liu et al. proved the interrelationship between financial stability and the real estate market [8]. We use multiple fractals' asymmetric detrended cross-correlation analysis (MF-ADCCA) to assess scalar features of the correlation between financial stability and estates' price volatility to achieve monitoring and early warning of that. According to the above related research results, it is clear to observe that deep learning-based early-warning models have advantages in real estate market risk warning and can predict real estate market risk more accurately, with an overall prediction accuracy of about 80%, but its prediction accuracy still needs to be improved. Therefore, this research provides an enhanced LSTM real estate market risk early-warning model based on the LSTM model that utilizes WOA algorithm to maximize the number of hidden neurons and time step for increasing prediction accuracy.

2. Basic Methods

2.1. Introduction to LSTM Networks. LSTM is a temporal recurrent neural network that uses a "gate" structure to overcome the difficulties of gradient disappearance and long-term reliance in recurrent neural network (RNN) [9]. Its basic structure is shown in Figure 1, which consists of input gate, output gate, and forget gate.

In Figure 1, x_t denotes the network input at moment t , h_{t-1} and C_{t-1} denote network output and cell state output at $t-1$ moment, δ denotes sigmoid function, and the mathematical expression is shown as (1), \tanh denotes activation function, and the mathematical expression is shown as (2), and \odot and \oplus denote the Hadamard product and summation, respectively:

$$s(x) = \frac{1}{1 + e^{-x}}, \quad (1)$$

$$\begin{aligned} \tanh x &= \frac{\sinh x}{\cosh x} \\ &= \frac{e^x - e^{-x}}{e^x + e^{-x}}. \end{aligned} \quad (2)$$

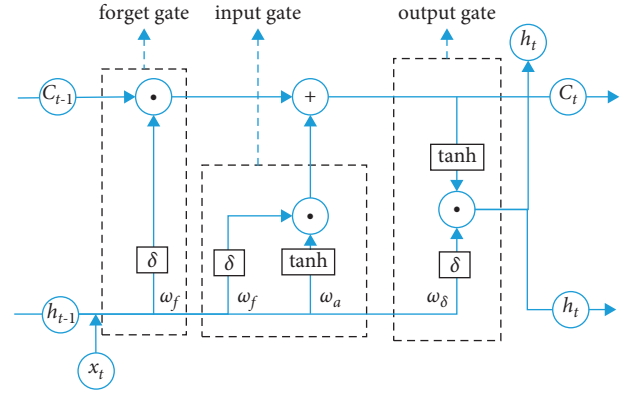


FIGURE 1: LSTM network structure.

The network output at moment t is as follows [10, 11].

Input gate:

$$i_t = \text{sigmoid}(W_{xi}x_t + W_{hi}h_{t-1} + W_{ci}C_{t-1} + b_i). \quad (3)$$

Forget gate:

$$f_t = \text{sigmoid}(W_{xf}x_t + W_{hf}h_{t-1} + W_{cf}C_{t-1} + b_f). \quad (4)$$

Cell state:

$$C_t = f_t C_{t-1} \odot i_t \tanh(W_{xc}x_t + W_{hc}h_{t-1} + b_c). \quad (5)$$

Output gate:

$$o_t = \text{sigmoid}(W_{xo}x_t + W_{ho}h_{t-1} + W_{co}C_{t-1} + b_o). \quad (6)$$

Network output:

$$h_t = o_t \tanh(C_t). \quad (7)$$

In which, W and b are the relative weight coefficient matrices and bias vectors.

The LSTM model is highly efficient, but it is difficult to find the best combination of parameters due to the large number of model parameters and the large amount of computational resources required to combine the relevant parameters, which in turn leads to poor model prediction performance [12]. Therefore, this study employs the whale optimization approach to improve the model prediction performance by optimizing the LSTM model parameters.

2.2. LSTM Network Improvements

2.2.1. An Introduction to the WOA Algorithm. The WOA algorithm is an optimization algorithm presented by Seyedali Mirjalili et al. to model humpback whale hunting behavior [13]. The algorithm uses a hypothetical method to represent the optimal solution, mathematically expressed as follows [14]:

$$\vec{D} = |\vec{C} \vec{X} * (t) - \vec{X}(t)|, \quad (8)$$

$$\vec{X}(t+1) = \vec{X} * (t) - \vec{A} \cdot D^{-\vec{r}}, \quad (9)$$

where t is the current iteration, \vec{A} and \vec{C} denote the coefficient vector, \vec{X} and X^* denote the position vectors of the

current solution and the optimal solution, respectively, denotes taking the absolute value, and \cdot denotes the element product. When the iteration produces an optimization solution, X^* will update, and then, \vec{A} and \vec{C} can be calculated by (8) and (9):

$$\begin{aligned}\vec{A} &= 2\vec{a} \cdot \vec{r} - \vec{a}, \\ \vec{C} &= 2 \cdot \vec{r},\end{aligned}\quad (10)$$

in which the linearity drops from 2 to 0 during the \vec{a} operation, which denotes that random vectors take values in the range [0,1].

As illustrated in Figure 2, the WOA algorithm's search mechanism and spiral updating position. The specific calculation method of the spiral updating position is to prioritize the distance between the whale's position (X, Y) and its prey (X^+, Y^+) to simulate the whale's spiral movement by establishing the spiral equation [15]:

$$\vec{X}(t+1) = \vec{D}^t \cdot e^{bl} \cdot \cos(2\pi l) + \vec{X}^*(t), \quad (11)$$

where e^{bl} denotes logarithmic spiral, b denotes constants, and l denotes random numbers taking values in the range [-1,1].

Assuming that the probability of choosing one of the search mechanisms is 0.5, then [16]

$$\vec{X}(t+1) = \begin{cases} \vec{X}^*(t) - \vec{A} \cdot \vec{D}, & \text{if } p < 0.5, \\ \vec{D}^t \cdot e^{bl} \cdot \cos(2\pi l) + \vec{X}^*, & \text{if } p \geq 0. \end{cases} \quad (12)$$

In addition, the WOA algorithm can search for targets based on random shapes, variables, and vectors. This search mechanism is consistent with $\vec{A} > 1$, emphasizes exploration, and allows the execution of global searches, as modeled below [17]:

$$\vec{D} = |\vec{C} \cdot \vec{X}_{\text{rand}} - \vec{X}|, \quad (13)$$

$$X(t+1) = \vec{X}_{\text{rand}} - \vec{A} \cdot \vec{D}, \quad (14)$$

where \vec{X}_{rand} is the position vector in the whale population.

The WOA algorithm has fast convergence speed and strong search capability [18], so it is used in this paper to optimize the LSTM parameters.

2.2.2. WOA-Based LSTM Parameter Optimization. The prediction accuracy in LSTM networks is mainly affected by the number of hidden layer's neurons m and the time step c [19], so the optimization of LSTM parameters by WOA is mainly for m and c . Currently, the number of m is usually determined as an approximate range according to the empirical (13), and the value of c is usually set empirically [20]:

$$m = \sqrt{(a + \beta)} + q, \quad (15)$$

where a and β denote the number of output and input layer nodes and q is a constant taking values between [0,10].

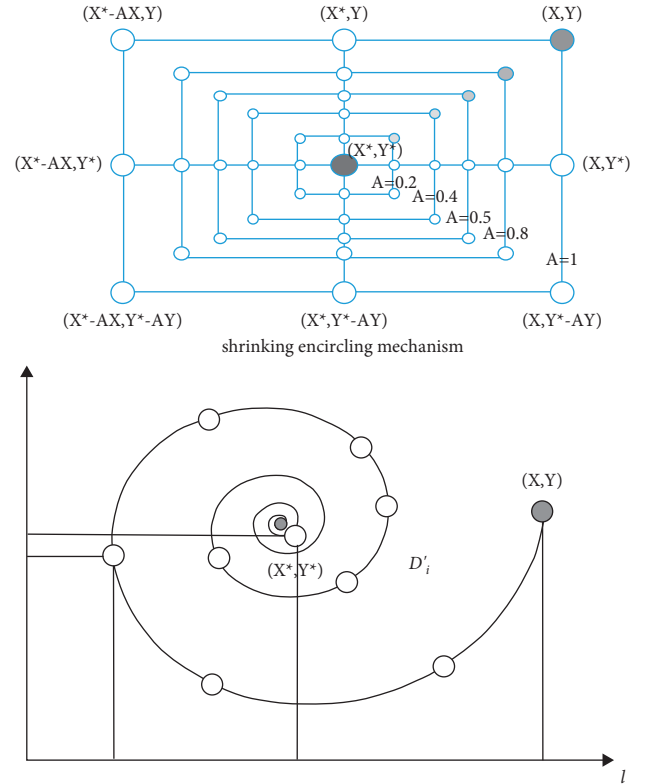


FIGURE 2: WOA algorithm search mechanism.

The optimization process of the LSTM network parameters m and c by using WOA is shown in Figure 3.

3. Market Risk Early-Warning Model Based on Improved LSTM

Based on the above improved LSTM model, the market risk early-warning model and its prediction process are designed in this study as Figure 4. The specific operation is as follows.

- Step 1: (data collection): collect relevant factor variables affecting the early warning of enterprise market risk, which is preprocessed by one-hot encoding and normalization
- Step 2: divide the data into training and test sets according to a certain ratio
- Step 3: create and train an LSTM model; then, store the LSTM model with the best prediction accuracy
- Step 4: use the WOA algorithm to optimize the number of hidden layer's neurons m and time step c
- Step 5: construct the WOA-LSTM model for prediction and output the results

4. Simulation Experiments

4.1. Experimental Environment Construction. The proposed model and comparison model are constructed in MATLAB 2019 for this experiment, running on a 64bit Windows 7 Professional system with Intel(R) Xeon(R) E5-2620V3

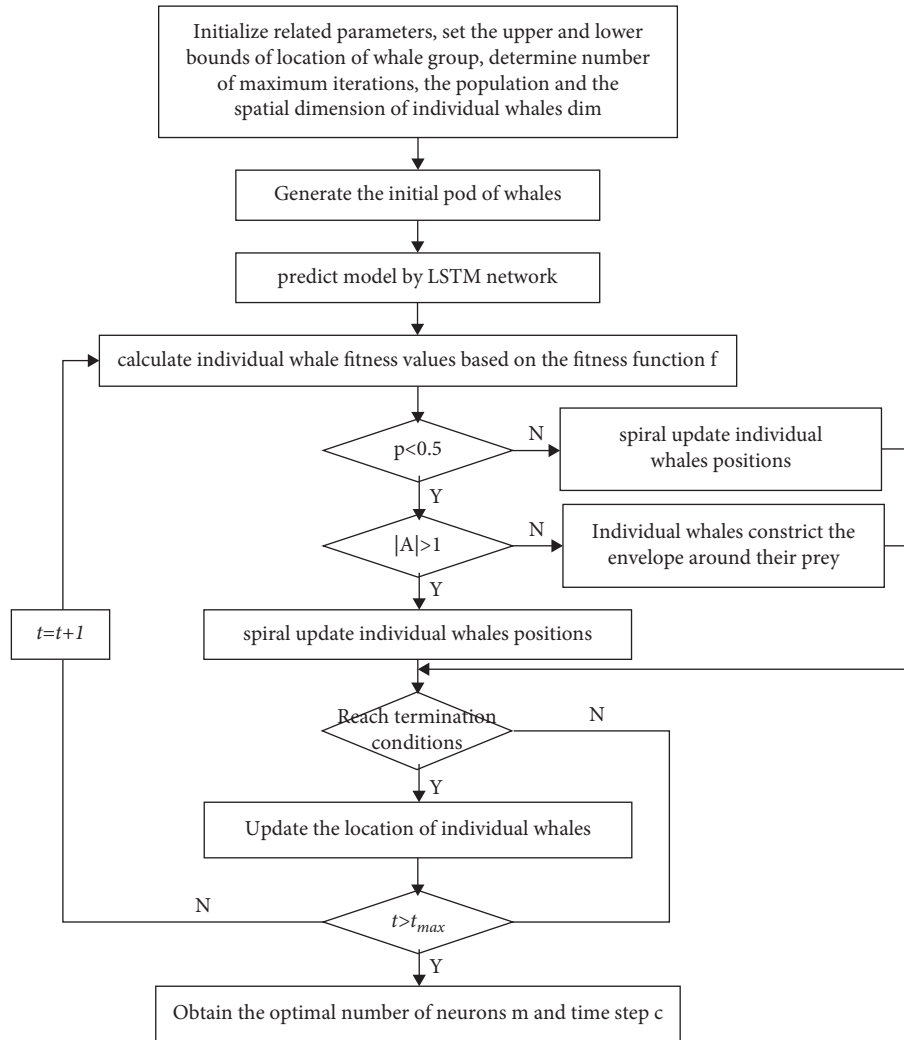


FIGURE 3: WOA optimization LSTM parameter flow.

2.40 GHz CUP, Tesla K80 GPU, and 8G memory, and the data are preprocessed by using SPSS software.

4.2. Data Sources and Preprocessing

4.2.1. Data Sources. In this experiment, 40 real estate companies listed on the Shanghai Stock Exchange from 2012 to 2020 are used as research subjects, among which 5 companies are in financial crisis and the remaining 35 companies are financially healthy. For the crisis sample, if the sample crisis time period is T , the study period for this experiment is $T-1$ years [21]. The listed companies selected for this experiment include five real estate companies such as Songjiang Group and Yin Yi Group. For the normal sample, 35 real estate companies, such as China Fortune Land Development and NACITY PROPERTY SERVICE GROUP, were selected while ensuring the same study period. Combining the current situation of real estate enterprises in China and related literature [22, 23], the relevant variables selected for this experiment are indicated in Table 1.

4.2.2. Data Preprocessing. Among the above variables, different variables have different degrees of influence on the prediction of corporate financial market risk, while variables that have less influence on the prediction results add data dimension and reduce the running speed of the model [24, 25]. Therefore, to solve this problem, this experiment uses factor analysis to analyze the variables and achieve a reduction in data dimension and increase the running speed of the model by removing factors with low commonality. The findings of factor analysis on the following 23 variables are reported in Table 2. The factor commonality of interest coverage multiple, operating income growth rate, and net profit growth rate is less than 0.5, indicating that the information on the impact of corporate financial market risk cannot be basically extracted from these variables. Therefore, the three variables were removed from this experiment, and 20 variables were finally obtained.

In order to expand the features, the variables were treated in this experiment by one-hot encoding. First, expand the data discrete features to the Euclidean space, and then, encode them using one-hot to obtain continuous features. Considering that different variables have different data magnitudes, all data

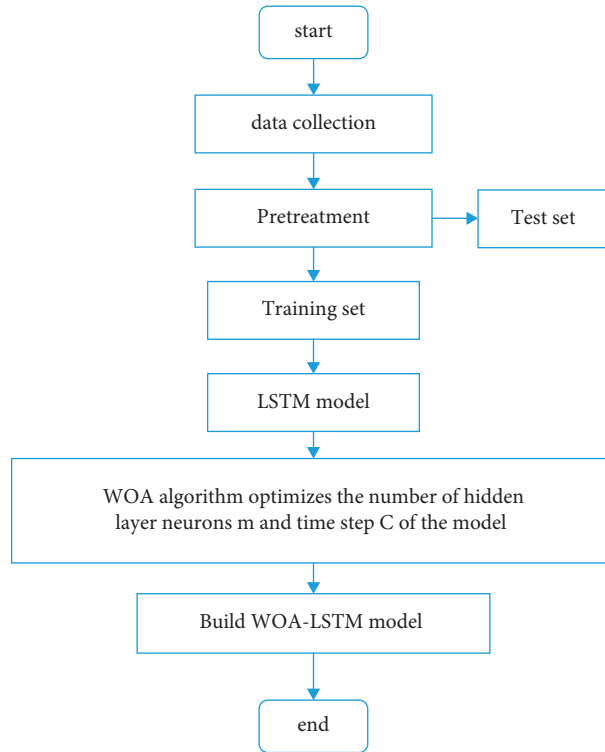


FIGURE 4: Market risk early-warning process based on improved LSTM.

TABLE 1: Index selection.

Index types	The first grade indexes	Secondary variables	Variable representations
Financial indexes	Repaying capability	Interest coverage ratio	Interest coverage ratio, _Intcvr
		Current ratio	Current ratio (%), _Currtr
		Long-term liability rate	Percentage of long-term liabilities. ()_LongDebtRt
		Asset-liability ratio	Asset-liability ratio (%), _Dbastrt
Nonfinancial indexes	Profitability	Return on assets	Return on assets (%), _ROAEBIT
		Cash ratio	Cash ratio (%), _CashRt
		Adjusted earnings per share (yuan)	Earnings per share, _BasieEPS
		Return on equity	Return on equity (diluted) (%), _ROE
		Quick ratio	Quick ratio (%), _Qckrt
	Development capacity	Ratio of profits to cost	Ratio of profits to cost (%), _Totprfcosttr
		Rate of return on sale	Rate of return on sale (%), _ROAEBIT
		Inventory turnover	Inventory turnover (second), Inventory Gross revenue
		Operating revenue	Operating revenue growth rate
		Net profit growth rate	Total assets' growth rate overhead rate
Operating capacity	Growth rate of main business revenue	Operating revenue growth rate	
	Fixed assets' turnover	Fixed assets' turnover	
	Total assets' turnover	Total assets' turnover	
		Operating profit margin	Operating profit margin

magnitudes are normalized in this study to facilitate the analysis. Finally, the data from 2012 to 2019 were divided into a training set and a test set in the ratio of 4:1, and the four quarterly values for 2020 were predicted.

coefficient of determination (R^2), which are calculated as follows:

$$MAE = \frac{1}{N} \sum_{t=1}^N |y_t - \hat{y}_t|, \quad (16)$$

$$MSE = \frac{1}{N} \sum_{t=1}^N (y_t - \hat{y}_t)^2, \quad (17)$$

4.3. *Evaluation Indexes.* The evaluation indexes for this experiment are mean absolute error (MAE), mean square error (MSE), root mean square error (RMSE), and

TABLE 2: Variable results of factor analysis.

Name	Communality
BasicEPS	0.796
ROE	0.57
ROAEBIT	0.754
Netprfrit	0.946
Opeprfrit	0.944
Totprfcostrt	0.747
Currt	0.818
Qckrt	0.790
LongDebtRt	0.683
CashRt	0.778
Totassgrrt	0.777
Invtrrat	0.835
Totassrat	0.738
Dbastrt	0.632
Total operating income	0.62
Fixassrat	0.479
Intcvr	0.096
Netprfgrrt	0.393
Opeinmgrrt	0.234

$$\text{RMSE} = \sqrt{\frac{1}{N} \sum_{t=1}^N (y_t - \hat{y}_t)^2}, \quad (18)$$

$$R^2 = 1 - \frac{\sum (y - \hat{y})^2}{\sum (y - \bar{y})^2}. \quad (19)$$

In (19), R^2 takes a range of (0,1), and the larger the value, the better the model performance.

4.4. Experimental Results

4.4.1. Model Validation

(1) *Operating Margin Forecast Results.* Taking the operating margin of Centralcon Holding as an example, the training set is used to train the improved LSTM model, and the training results are compared to the test set, as shown in Figure 5. The anticipated values are consistent with the change trend of the actual values, and the overall fitting effect is good, indicating that the proposed algorithm has good prediction effect.

The experience enters the indices except the operating profit margin into the prediction model and constructs the prediction model with the operating profit margin as the output for quantitatively analyzing the prediction performance of the proposed model. The model's prediction performance is shown in Table 3. From the table, the suggested model's prediction accuracy is 98%, showing that it has a high prediction accuracy and can better forecast the impact of each index on the operating margin.

(2) *Predicted Results for Each Variable.* Using quarterly data from 2012 to 2019 as model inputs and various indexes (operating margin as an example) as model outputs, Table 4 represents the predictive performance of the model, and its

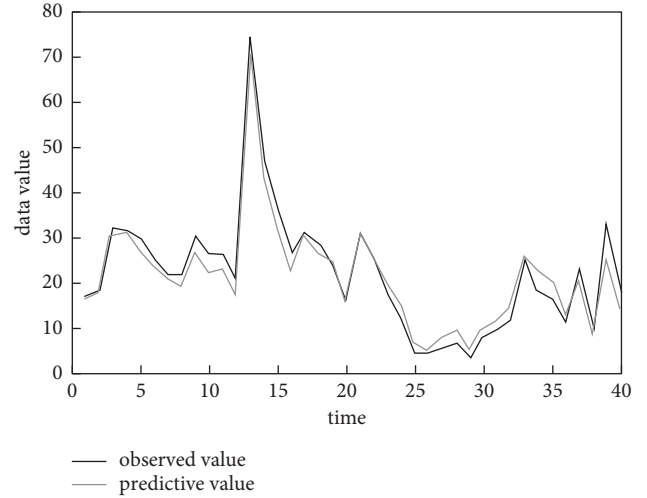


FIGURE 5: Multivariable input prediction trend of operating profit margin of the improved LSTM model.

TABLE 3: Prediction performance of operating profit margin of the improved LSTM model.

Performance evaluation index	Value
MSE	23.97
MAE	3.76
RMSE	4.89
R^2	0.97

TABLE 4: Prediction performance of operating profit margin of the improved LSTM model.

Performance evaluation index	Value
MSE	3.83
MAE	17.79
RMSE	19.37
R^2	0.96

fit and iteration plots are shown in Figure 6. The revised LSTM model has an excellent prediction effect, attaining a prediction accuracy of 96%, and the overall fitting effect between the predicted and observed values is good, as shown by the prediction results.

4.4.2. *Comparison of Models.* The studies evaluated the prediction effect of the proposed model with CNN and LSTM models for each index for each quarter from 2012 to 2019 to ensure that the proposed model is effective, with the finding displayed in Figure 7. From Figure 7, the suggested algorithm outperforms the comparison algorithm in all indexes, and the prediction accuracy is likewise greater, which is improved compared with the CNN model and LSTM model, respectively. This indicates that the proposed model can enhance its prediction accuracy by improving the LSTM algorithm, thus improving the prediction performance to some extent.

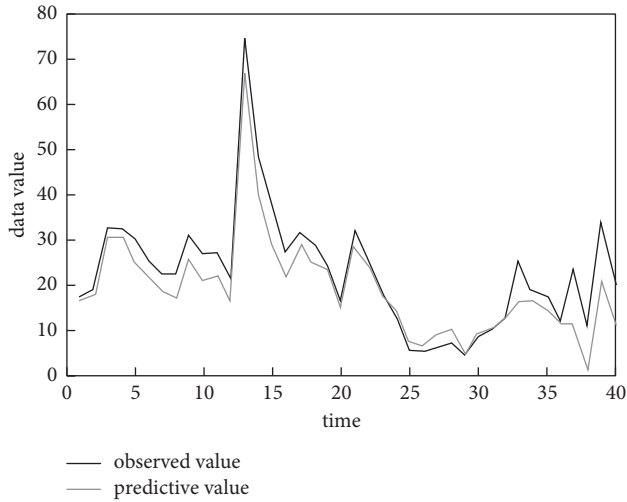


FIGURE 6: Univariate fitting diagram of operating profit margin of the improved LSTM model.

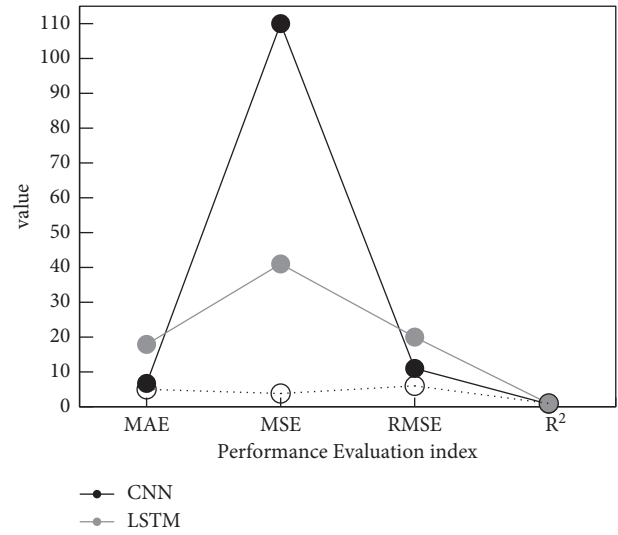


FIGURE 8: Performance comparison of different models.

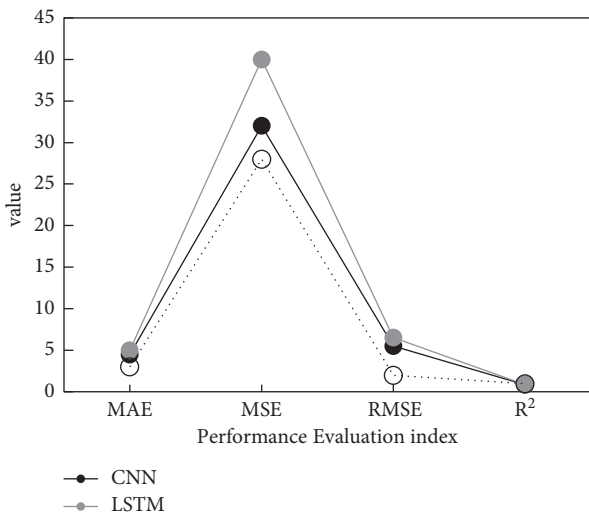


FIGURE 7: Performance comparison of different models.

For further verification of the validity of the proposed model, the experiments compare its prediction effects with the CNN model and the LSTM model for four quarters in 2020, and the results are shown in Figure 8. As shown in the table, the proposed model outperforms the comparison model in all performance metrics, and the proposed model improves the prediction accuracy by 22% compared to the CNN model and 7% compared to the LSTM model. The reason is that the upgraded LSTM model optimizes the LSTM network parameters using the WOA algorithm, which improves the model’s global optimization capabilities and prediction performance. This shows that the model described in this study has certain effectiveness and superiority to identify and warn market risks in advance and take corresponding measures according to the risks to ensure the healthy operation of the enterprise.

5. Conclusion

In summary, the predictive accuracy of the improved LSTM-based market risk warning model can be improved by optimizing the number of hidden layer’s neurons and the time step of the LSTM using the WOA algorithm, and the prediction accuracy can reach more than 96%, resulting in high-precision early warning of market risks. The proposed model improves the prediction accuracy of corporate finance from 2012 to 2019 to different degrees, by 14% and 12%, respectively. In addition, it improves the prediction accuracy of corporate finance in 2020 by 22% and 7%, respectively. And compared with the traditional CNN and LSTM models, it has certain superiority. The innovation of this study is to use WOA algorithm to improve LSTM and change the previous LSTM parameter optimization method, so as to better improve the prediction accuracy of the algorithm, which is also an innovation of this research [26].

Data Availability

The experimental data used to support the findings of this study are available from the corresponding author upon request.

Conflicts of Interest

The authors declare that they have no conflicts of interest regarding this work.

References

- [1] L. Jiang, Y. Tan, and A. Zhang, “The application of Internet big data and support vector machine in risk warning,” *Journal of Physics: Conference Series*, vol. 1952, no. 4, Article ID 042030, 2021.
- [2] B. Junchi, G. Bryan, L. Eric, and L. Zheng, “Multi-source urban data fusion for property value assessment: a case study in Philadelphia,” *Neurocomputing*, vol. 404, no. prepublsh, pp. 70–83, 2020.

- [3] F. Alvarez, E. Roman-Rangel, and V. Montiel Luis, "Incremental learning for property price estimation using location-based services and open data," *Engineering Applications of Artificial Intelligence*, vol. 107, pp. 68–76, 2022.
- [4] I. Garcia-Magariño and R. Lacuesta, "Agent-based simulation of real-estate transactions," *Journal of Computational Science*, vol. 21, pp. 60–76, 2017.
- [5] W. Zhou, M. Chen, Z. Yang, and X. Song, "Real estate risk measurement and early warning based on PSO-SVM," *Socio-Economic Planning Sciences*, vol. 63, Article ID 101008, 2020.
- [6] K. Chen, Y. Y. Song, J. F. Pan, and G. L. Yang, "Measuring destocking performance of the Chinese real estate industry: a DEA-Malmquist approach," *Socio-Economic Planning Sciences*, vol. 69, no. C, Article ID 100694, 2019.
- [7] A. F. Kamara, X. Pan, Q. Liu, and E. Chen, "A hybrid neural network for predicting Days on Market a measure of liquidity in real estate industry," *Knowledge-Based Systems*, vol. 208, no. prepublish, pp. 79–83, 2020.
- [8] C. Liu, Y. Zheng, Q. Zhao, and C. Wang, "Financial stability and real estate price fluctuation in China," *Physica A: Statistical Mechanics and Its Applications*, vol. 540, no. C, Article ID 122986, 2020.
- [9] C. Wu, X. Zhang, W. Wang et al., "Groundwater level modeling framework by combining the wavelet transform with a long short-term memory data-driven model," *The Science of the Total Environment*, vol. 783, Article ID 146950, 2021.
- [10] Z. Peng, J. Dang, M. Unoki, and M. Akagi, "Multi-resolution modulation-filtered cochleagram feature for LSTM-based dimensional emotion recognition from speech," *Neural Networks*, vol. 140, pp. 261–273, 2021.
- [11] U. Emine, Ü. Atila, M. Uçar, and K. Akyol, "Automated detection of Covid-19 disease using deep fused features from chest radiography images," *Biomedical Signal Processing and Control*, vol. 69, Article ID 102862, 2021.
- [12] L. Liu, Q. Wang, Q. Wang, and Y. Li, "Improved Chinese sentence semantic similarity calculation method based on multi-feature fusion," *Journal of Advanced Computational Intelligence and Intelligent Informatics*, vol. 25, no. 4, pp. 442–449, 2021.
- [13] D. B. Prakash and C. Lakshminarayana, "Optimal siting of capacitors in radial distribution network using whale optimization algorithm," *Alexandria Engineering Journal*, vol. 56, no. 4, pp. 499–509, 2017.
- [14] J. Vimpari and S. Junnila, "Estimating the diffusion of rooftop PVs: a real estate economics perspective," *Energy*, vol. 172, pp. 1087–1097, 2019.
- [15] W.-C. Wang, Y.-J. Chang, and H.-C. Wang, "An application of the spatial autocorrelation method on the change of real estate prices in taitung city," *ISPRS International Journal of Geo-Information*, vol. 8, no. 6, pp. 249–256, 2019.
- [16] V. D. Giudice, P. D. Paola, T. Francesca, P. J. Nijkamp, and A. Shapira, "Real estate investment choices and decision support systems," *Sustainability*, vol. 11, no. 11, pp. 3110–3116, 2019.
- [17] P. McAllister and I. Nase, "The impact of minimum energy efficiency standards: some evidence from the london office market," *Energy Policy*, vol. 132, pp. 714–722, 2019.
- [18] R. P. Dahal, R. K. Grala, J. S. Gordon, I. A. Munn, D. R. Petrolia, and J. R. Cummings, "A hedonic pricing method to estimate the value of waterfronts in the Gulf of Mexico," *Urban Forestry and Urban Greening*, vol. 41, pp. 185–194, 2019.
- [19] F. Andrea and R. Daniele, "Revealing Pairs-trading opportunities with long short-term memory networks," *European Journal of Operational Research*, vol. 295, no. 2, pp. 772–791, 2021.
- [20] F. Gauger, J. O. Strych and A. Pfnür, "Linking real estate data with entrepreneurial ecosystems: coworking spaces, funding and founding activity of start-ups," *Data in Brief*, vol. 37, Article ID 107185, 2021.
- [21] J. Wang, "An intelligent computer-aided approach for atrial fibrillation and atrial flutter signals classification using modified bidirectional LSTM network," *Information Sciences*, vol. 574, pp. 320–332, 2021.
- [22] P. Yuan, C. Hu, Y. Lu, Y. Wu, Q. Zeng, and Z. Lei, "Load forecasting of refrigerated display cabinet based on CEEMD-IPSO-LSTM combined model," *Open Physics*, vol. 19, no. 1, pp. 360–374, 2021.
- [23] J. D. Domingo, J. Gómez-García-Bermejo, and E. Zalama, "Optimization and improvement of a robotics gaze control system using LSTM networks," *Multimedia Tools and Applications*, vol. 49, pp. 1–18, 2021.
- [24] S. Zhang and A. S. Hassan, "Language processing model construction and simulation based on hybrid cnn and lstm," *Computational Intelligence and Neuroscience*, vol. 2021, Article ID 2578422, 11 pages, 2021.
- [25] D. Zhu, "Research and analysis of a real estate virtual E-commerce model based on big data under the background of COVID-19," *Journal of Organizational and End User Computing*, vol. 33, no. 6, pp. 1–16, 2021.
- [26] B. Hamid, "Forecasts of growth in US residential investment: accuracy gains from consumer home-buying attitudes and expectations[[]]," *Applied Economics*, vol. 53, no. 32, pp. 3744–3758, 2021.

Research Article

Data Analysis and Prediction Modeling Based on Deep Learning in E-Commerce

Lei Feng 

School of Digital Commerce, Beijing Information Technology College, Beijing 100018, China

Correspondence should be addressed to Lei Feng; fengl@bitc.edu.cn

Received 15 December 2021; Revised 27 December 2021; Accepted 25 January 2022; Published 24 March 2022

Academic Editor: Hangjun Che

Copyright © 2022 Lei Feng. This is an open access article distributed under the Creative Commons Attribution License, which permits unrestricted use, distribution, and reproduction in any medium, provided the original work is properly cited.

Due to the low efficiency of traditional data analysis methods for massive e-commerce data analysis, an e-commerce data analysis and prediction method based on the GBDT deep learning model was proposed. Purchase behavior is divided into another category, which transforms the problem of e-commerce data analysis and prediction into a binary classification problem. At the same time, we extract 107 features that can reflect the user behavior and construct the GBDT model. The characteristics include counting class, sorting class, time difference class, conversion rate class, and so on. It follows from the above that the analysis and prediction of e-commerce data are realized. In addition, the results show that when the learning rate of GBDT model parameters is 0.05, the number of basic learners is 200, the tree depth is 20, the threshold is 0.5, the model prediction effect is best, and the F1 value can reach 0.12. Compared with the traditional prediction model based on logistic regression and neural network, the proposed GBDT model is more suitable for e-commerce data analysis and prediction.

1. Related Work

The development of computer technology and Internet technology has accelerated the construction and popularization of e-commerce platform. In the era of economic globalization, e-commerce has played a positive role in national economic and social development. Therefore, the use of e-commerce can improve business efficiency and promote sustained and healthy economic development, which is the focus and difficulty of current economic research. The premise of using e-commerce to improve business efficiency is to fully understand the e-commerce platform, which requires the analysis and prediction of e-commerce data. At present, the analysis and prediction methods for data mainly include two categories based on logistic regression and neural network, and the analysis and prediction of data can be realized by constructing the corresponding optimal prediction model using training sets. For example, Ozgur and Franklin analyzed multiple linearity in independent variables of the logistic regression model and applied it to actual data analysis cases [1]. The

results show that the logistic regression model is easy to operate in data analysis and can obtain relatively comprehensive prediction results. Cioci et al. and Rekha et al. believed that multiple logistic regression (MLR) used to analyze categorical variables or continuous variables has a positive impact on the single dichotomy by reviewing the statistical methods of adjusting baseline differences in nonrandom studies [2, 3]. It can be seen that the data analysis can be realized according to the data format. [4] realized the prediction of Indian stocks by analyzing the data of Indian stocks based on the advantages of machine learning, especially the recurrent neural network, which can better extract the features of text and data [4, 5]. On the basis of deep learning, Son et al. and Jin et al. adopted the LSTM model to achieve spatiotemporal data prediction and conducted visual analysis [6, 7]. Guo et al. and Agafonov realized the prediction of microinternal leakage by analyzing the data of hydraulic cylinder based on the neural network model [8, 9]. The above method has made some research results in data analysis and prediction. However, due to the huge amount of e-commerce data, the data

structure is complex and the data characteristics are rich; if the above method is used to analyze e-commerce data, there is usually a problem of the low efficiency of data analysis, prediction, or the accuracy of prediction. In order to solve the above problems, this paper, with the help of the gradient boosting decision tree (GBDT) model, which has the advantages of high prediction accuracy, few parameters, and stable training process, an e-commerce data analysis and prediction method based on GBDT deep learning model is proposed.

2. Introduction to GBDT Model

The GBDT model is an iterative decision tree algorithm, consisting of multiple decision trees as the base learner. The accuracy of the whole model is improved by trying to reduce the deviation of each decision tree. For the regression and classification problems, the decision trees adopted by the GBDT model are CART regression trees [9]. The CART regression tree is generated by traversing all the data features and dividing the data set into nodes in turn. Firstly, the features are selected according to the least square error, then each region is divided into two regions, and finally, the mean value of the current region is output to establish a regression tree [10]. The steps are as follows:

- (1) Suppose the training dataset is D , the feature with the least square error is j , and the corresponding partition node is s . Solve (1) to obtain the optimal partition feature.

$$\min_{j,s} \left[\min_{c_1} \sum_{x_i \in R_1(j,s)} (y_i - c_1)^2 + \min_{c_2} \sum_{x_i \in R_2(j,s)} (y_i - c_2)^2 \right]. \quad (1)$$

- (2) Select the best (j , s) to divide regions and output corresponding region values:

$$R_1(j, s) = \{x | x^{(j)} \leq s\}, R_2(j, s) = \{x | x^{(j)} > s\}$$

$$\hat{c}_m = \frac{1}{N_m} \sum_{x_i \in R_m(j,s)} y_i, \quad x \in R_m, m = 1, 2. \quad (2)$$

- (3) Repeat the above operations for the two divided regions until the termination conditions are met.
- (4) Divide the input space into R_1, R_2, \dots, R_M subregions, where M is the number of subregions, and the final decision tree is generated.

$$f(x) = \sum_{i=1}^M \hat{c}_m I(x \in R_m). \quad (3)$$

2.1. Gradient Boosting Tree. The GBDT model usually adopts gradient boosting tree to optimize the model learning process. Using the negative gradient of loss function as the

descent mode, the regression tree can be constructed rapidly. The generation method of gradient boosting tree is as follows:

- (1) Set input training dataset as $T = \{(x_1, y_1), (x_2, y_2), \dots, (x_N, y_N)\}$ and loss function as $L(y, f(x))$. Then, initialize $f_0(x) = 0$.
- (2) Calculate the pseudo-residual of sample $i = 1, 2, \dots, N$ according to the following formula [11]:

$$r_{mi} = - \left[\frac{\partial L(y, f(x_i))}{\partial f(x_i)} \right]_{f(x) = f_0(x)}. \quad (4)$$

- (3) Conduct fitting learning for the residuals and then obtain a regression tree $h_m(x)$, $m = 1, 2, \dots, M$.
- (4) Update:

$$f_m(x) = f_{m-1} + h_m(x). \quad (5)$$

- (5) Finally, get the gradient boosting tree:

$$f_M(x) = \sum_{m=1}^M h_m(x). \quad (6)$$

2.2. Selection of Loss Function. Common loss functions include squared error, hinge loss, and logistics regression loss. The mathematical expressions are shown in formulas (7)–(9) [12]. Among them, squared error loss function is mainly used for regression model, and hinge loss function is mainly used for SVM classifier. Therefore, this paper adopts logistics regression loss function as GBDT model loss function.

$$L(y, f(x)) = \sum_{i=1}^n (f(x_i) - y_i)^2$$

$$L(x, f(x)) = \sum_{i=1}^n \max(0, 1 - y_i * f(x_i)) \quad (7)$$

$$L(y, f(x)) = \sum_{i=1}^n \log(1 + \exp(-y_i * f(x_i))).$$

2.3. Classification Method of GBDT Model. Above all, the classification calculation process of GBDT model using logistics regression loss function can be summarized as follows:

- (1) Let the training dataset be $T = \{(x_1, y_1), (x_2, y_2), \dots, (x_N, y_N)\}$, and the loss function be $L(y, f(x)) = \ln(1 + \exp(-2yf(x)))$, $y \in \{0, 1\}$; initialize:

$$f_0(x) = \frac{1}{2} \ln \frac{P(y=1|x)}{P(y=0|x)}. \quad (8)$$

- (2) Calculate the pseudo-residual of sample $i = 1, 2, \dots, N$:

$$r_{mi} = \frac{2y_i}{1 + \exp(2y_i f_{m-1}(x_i))}. \quad (9)$$

- (3) Adopt regression tree to fit (12) and then obtain the leaf node region R_{mj} , $j = 1, 2, \dots, J$ of m trees.

$$\{(x_1, r_{m1}), (x_2, r_{m2}), \dots, (x_N, r_{mN})\}. \quad (10)$$

- (4) Calculate $j = 1, 2, \dots, J$, $i = 1, 2, \dots, N$:

$$c_{mj} = \frac{\sum_{x_i \in R_{mj}} r_{mj}}{\sum_{x_i \in R_{mj}} |r_{mj}| (2 - |r_{mj}|)}, \quad (11)$$

where $m = 1, 2, \dots, M$.

- (5) Update:

$$f_m(x) = f_{m-1}(x) + \sum_{j=1}^J c_{mj} I(x \in R_{mj}). \quad (12)$$

- (6) Finally, get the classification tree:

$$f(x) = \sum_{m=1}^M \sum_{j=1}^J c_{mj} I(x \in R_{mj}). \quad (13)$$

- (7) Use the difference between the predicted category probability value and the real probability value to fit the loss, then obtain the probability of different categories, and select the prediction category with high probability [13].

$$P(y = 1|x) = \frac{1}{1 + \exp(-2f(x))}, \quad (14)$$

$$P(y = 0|x) = \frac{1}{1 + \exp(2f(x))}.$$

3. E-Commerce Data Analysis and Prediction Model Based on GBDT

Based on the above GBDT model analysis, the design of the e-commerce data analysis and prediction method is as follows:

- (1) Firstly, delete missing values and desensitize all selected e-commerce data. Then, for better data analysis and prediction, the overall distribution of the data is described to obtain the distribution of user behavior.
- (2) User browsing, collection, and additional purchase behavior are divided into one category. Purchase behavior is divided into another category. In addition, the problem is converted into binary classification problem.
- (3) Select the features that can reflect the data to build the GBDT model and initialize the parameters of GBDT model, including learning rate, the number of base learners, thresholds, and others.

- (4) Use the training set to train the GBDT model and tune the model parameters by random search [14]. When the model reaches the maximum number of iterations or optimal parameters, the training is stopped, and the optimal model is output.
- (5) Use the optimal model obtained by training to predict the data to predict and then output the prediction result. Thus, the analysis and prediction of e-commerce data are realized.

4. Simulation Experiment

4.1. Construction of Experimental Environment. This experiment is carried out on 64bit Windows 7 operating system, and the GBDT model is constructed on Python and TensorFlow framework. The CPU is Intel(R)Core(TM) i7-7770hq 2.8 GHz with 8 GB memory.

4.2. Data Sources and Processing

4.2.1. Data Sources. Select tianchi offline competition data as the experimental dataset to predict user purchase data on December 19, 2014. This dataset includes the historical e-commerce behavior data of 20,000 users on the complete collection of goods from November 18 to December 18, 2014 [15]. Its source data include user behavior dataset D and product subset P on the complete collection of goods. Dataset D contains 4758484 kinds of commodities and 4 behavior types where a total of 9557 commodity categories are missing commodity spatial identification [16]. The field description is shown in Table 1, and some data are shown in Table 2. Dataset P contains 422858 kinds of commodities. Here, the spatial identification of 1,054 commodity categories is missing. The field description is shown in Table 3, and some data are shown in Table 4.

4.2.2. Data Description. For better data analysis and prediction, it is necessary to understand the overall distribution of data. First, the operational purchase conversion rate of the data is calculated, that is, the proportion of the user's purchase behavior to its total behavior [17]. Through calculation, the complete behavior distribution of commodities is obtained as shown in Figure 1. It can be seen from the figure that users' browsing behavior on the complete collection of goods accounts for the largest proportion among all behaviors. Except for the abnormal behavior on December 12, the user's behavior on other days is relatively stable. The analysis of the reason for the abnormal behavior on December 12 is related to the promotion of "Double 12" on e-commerce platform.

Figure 2 shows the behavior distribution of users on a subset of goods. It can be seen from the figure that the user's behavior on the subset of goods is mainly browsing. The number of behaviors on December 12 is higher than that on other dates, which is related to the promotion of "Double 12" e-commerce platform. Compared with the user's behavior on the complete collection of goods, the user's behavior on the subset of goods varies greatly.

TABLE 1: Field description of dataset D.

Field	Meaning	Note
User_id	User ID	Be unique
Item_id	Commodity identification	Be unique
Behavior_type	There is a many-to-one relationship with commodities	Browse Collection Add shopping cart 4-purchase order
User_geohash	The product category ID of the longitude and latitude area encoded by geohash where the user is located	Encoded by the GeoHash algorithm
Item_category		There is a many-to-one relationship with commodities
Time	Time	The format is year/month/day/hour

TABLE 2: Partial data examples of dataset D.

Item_id	Behavior_type	Item_category	Time
275254735	1	4076	2019-12-08
436**9947	1	5503	2019-12-12
436**8907	1	5503	2019-12-12
536**6768	1	9762	2019-12-02
151**6952	1	5232	2019-12-12
536***76	4	9762	2019-12-02
2900**061	1	5503	2019-12-12
2983**524	1	10894	2019-12-12
3210**425	1	6513	2019-12-12

TABLE 3: Field description of dataset P.

Field	Meaning	Note
Item_id	Commodity identification	Be unique
Item_geohash	The product category ID of the longitude and latitude area encoded by geohash where the user is located	Encoded by the GeoHash algorithm
Item_category		There is a many-to-one relationship with commodities

TABLE 4: Partial data examples of dataset P.

Item_id	Item_category
100**2303	3368
100**3592	7995
100**6838	12530
1000**089	7791
100**2750	9614
10****072	1032
10****63	9023
10****387	3064
10**23812	6700
1003****7	5827

Since the purpose of this paper is to predict the user's purchase behavior on e-commerce platforms to achieve accurate product recommendation, this paper focuses on the distribution of users' purchase behavior. Figure 3 shows the user's purchase behavior on the complete collection of goods, and Figure 4 shows the user's purchase behavior on the subset of goods. It can be seen from Figure 5 that the distribution of users' purchasing behaviors on the complete collection of goods is relatively stable, stable at about 7000. The number of purchases jumped to 30,000 on December 12th. It can be seen from Figure 5 that the fluctuation range of users' purchasing behavior distribution on the subset of goods is larger than

that on the complete collection of goods. The purchasing behavior of users on November 22, November 28, and December 22 is quite different from the usual purchasing behavior, reaching more than 4000.

To further analyze the user behavior, this paper studies the user behavior distribution in 24 hours from the vertical time dimension. The user's behavior distribution in the complete collection of goods is shown in Figure 4, and the behavior distribution in the subset of goods is shown in Figure 6. It can be seen from the figure that the number of user behaviors is related to the user's daily life rules [18]. The number of user behaviors is less in rest time (00:00–08:00), more balanced in working time (09:00–18:00), and reaches the peak in the evening (19:00–23:00) during leisure time.

Figure 7 shows the distribution of user's purchasing behavior on the complete collection and subset of goods, respectively. It can be seen from Figure 7 that the users' purchase behaviors are relatively low during 16:00–18:00, and the number of purchase behaviors is generally flat between day and night. This shows that in the complete collection of goods, users have clear intention to purchase goods during working hours, and the purchase conversion rate is high. The purchase conversion rate is lower due to the longer time in the evening. As can be seen from Figure 8, in the subset of goods, the purchasing power of users is lower in

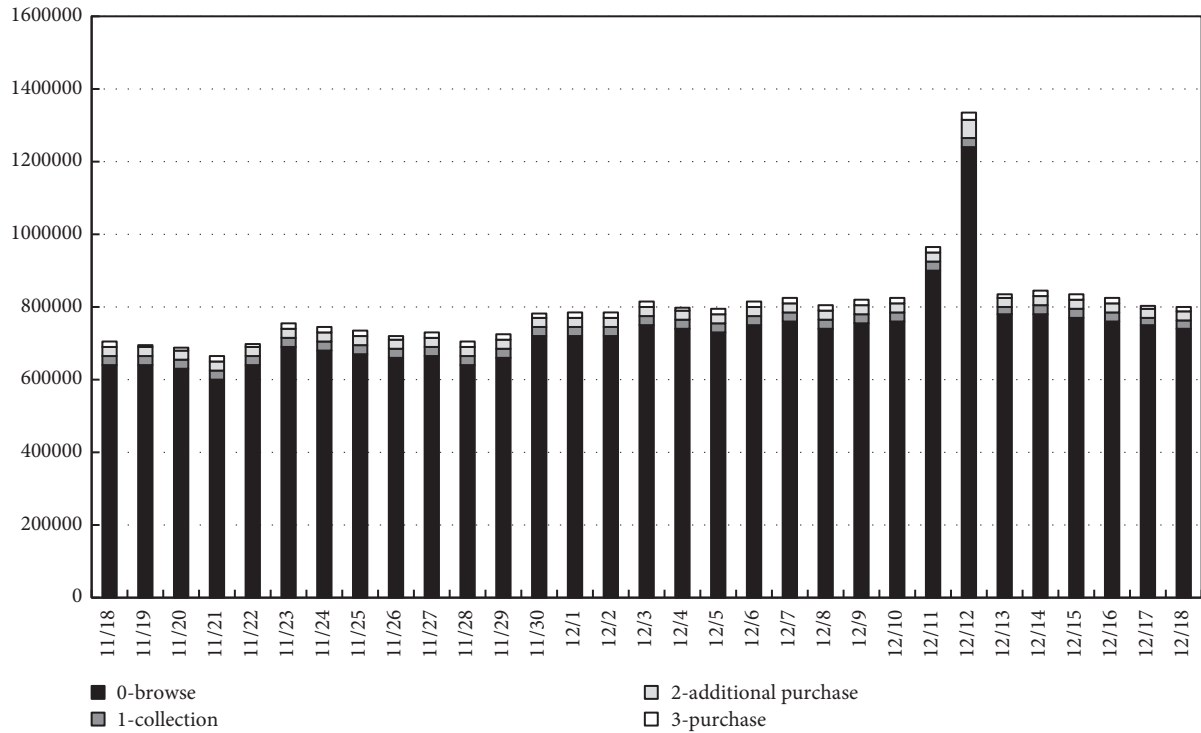


FIGURE 1: Distribution of user behavior in the complete collection of goods.

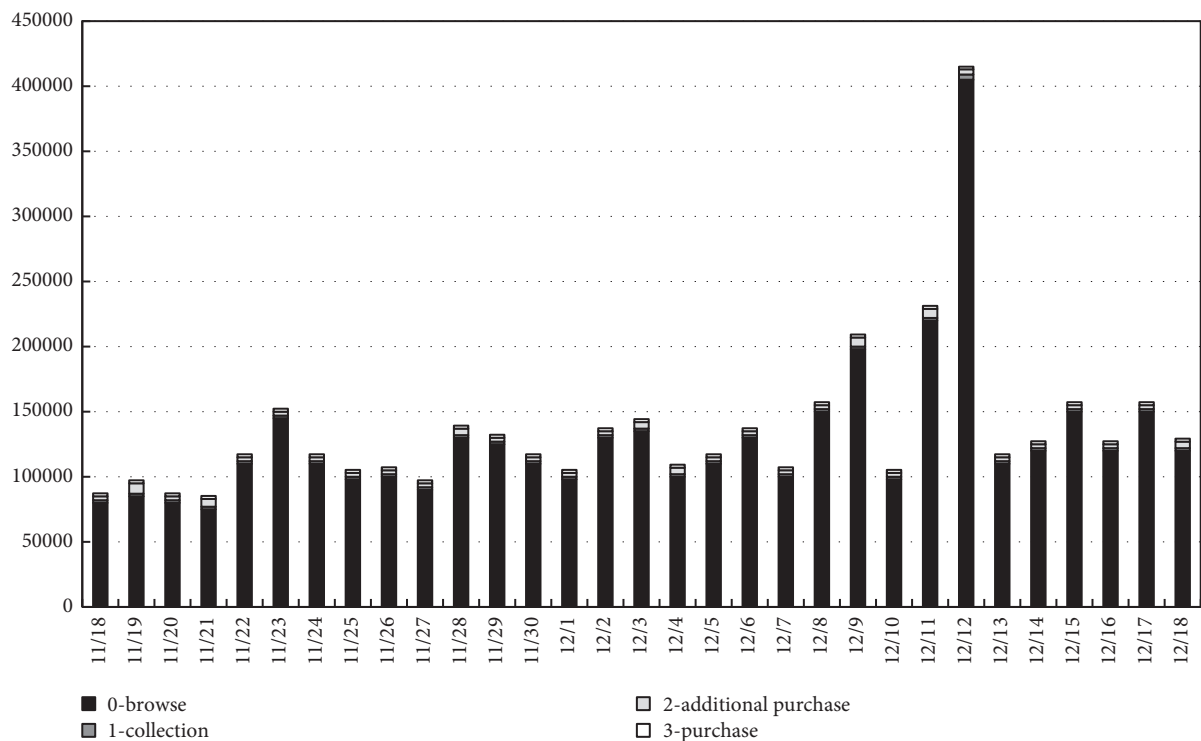


FIGURE 2: Distribution of user behavior in the subset of goods.

the daytime than in the evening, but it will reach a maximum point in the daytime. Compared with the complete collection of goods, the distribution of users' purchasing behavior on the subset of goods is not stable.

4.2.3. *Data Processing.* To better predict the user purchase data on December 19, this paper selects the purchase data on December 18, which is close to the date, as the basis and constructs the data characteristic cycle by analyzing the

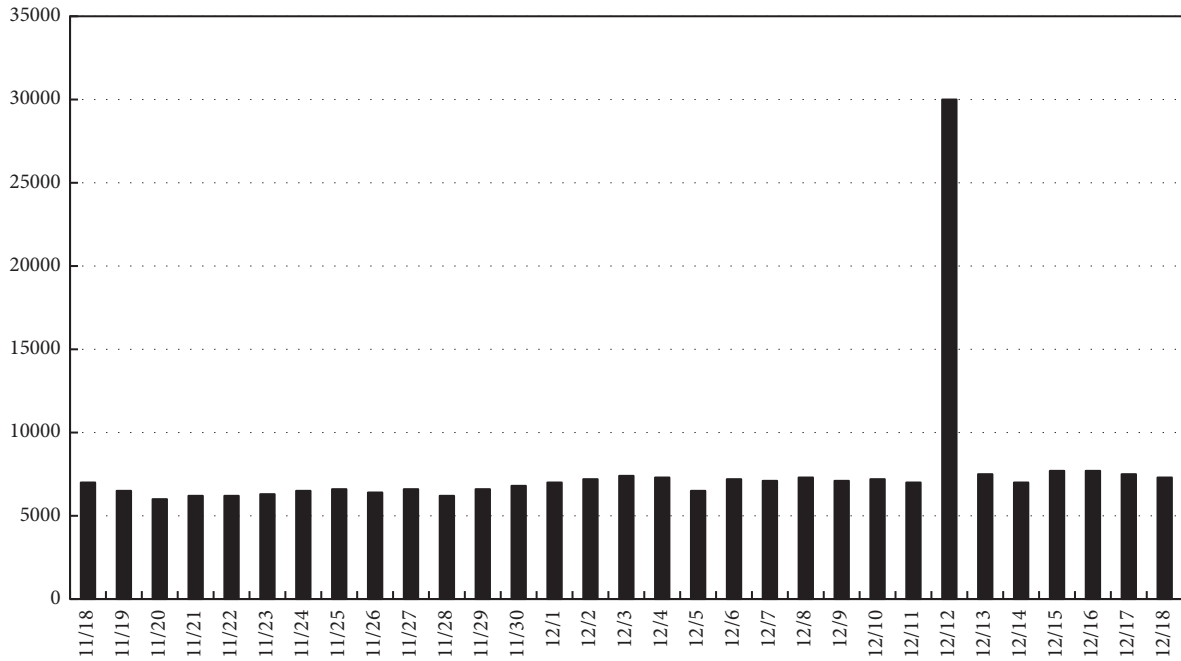


FIGURE 3: Distribution of user's purchasing behavior on the complete collection of goods.

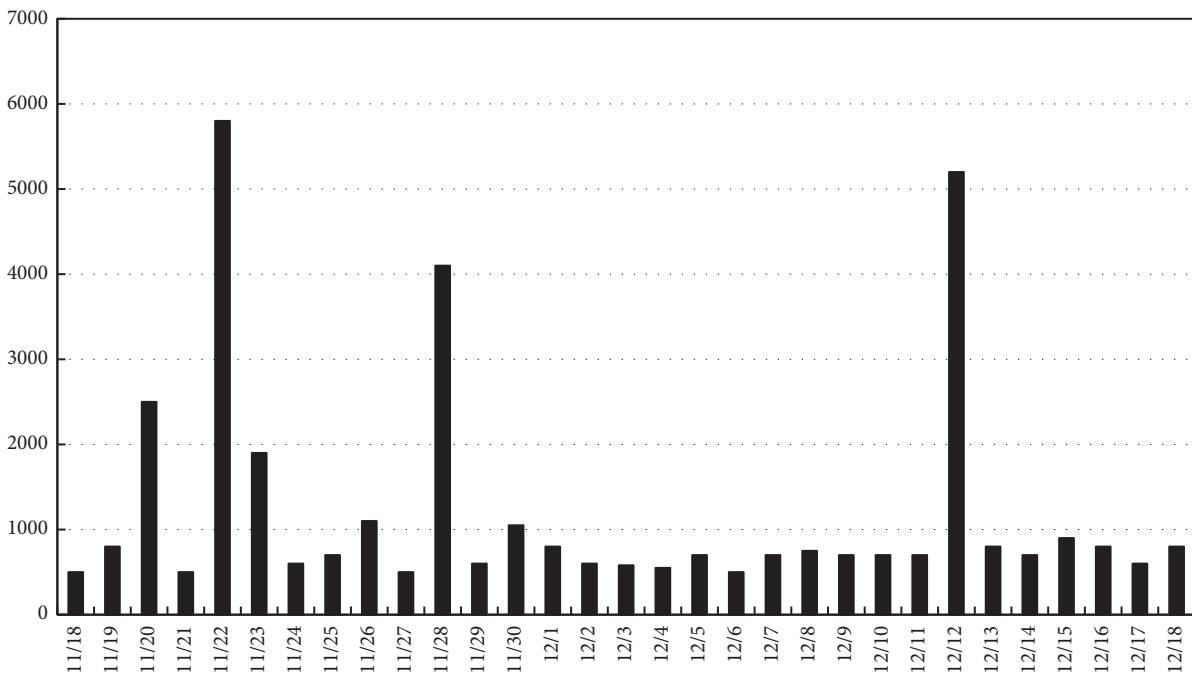


FIGURE 4: User's behavior distribution in the complete collection of goods (h).

interaction between the purchase behavior on December 18 and other dates. There are 6,925 items of purchase data on December 18, among which 4,662 items cannot be matched with the historical data of one month, and the remaining data can be matched with the historical data of one month. Figure 9 shows the historical data distribution that interacts with the behavior that existed on December 18. As can be seen from the figure, the number of interaction data increases significantly in the week before December 18 and

reaches the maximum value on December 17. Therefore, this paper adopts the data of one week before the forecast date to predict it.

Considering that part of the user's purchase behavior on December 18 comes from the direct purchase on that day, there is no interaction with the previous period. There is no positive effect on the user's purchase behavior prediction. The previous browsing, collecting, additional purchasing, and purchasing behavior have a positive impact on the

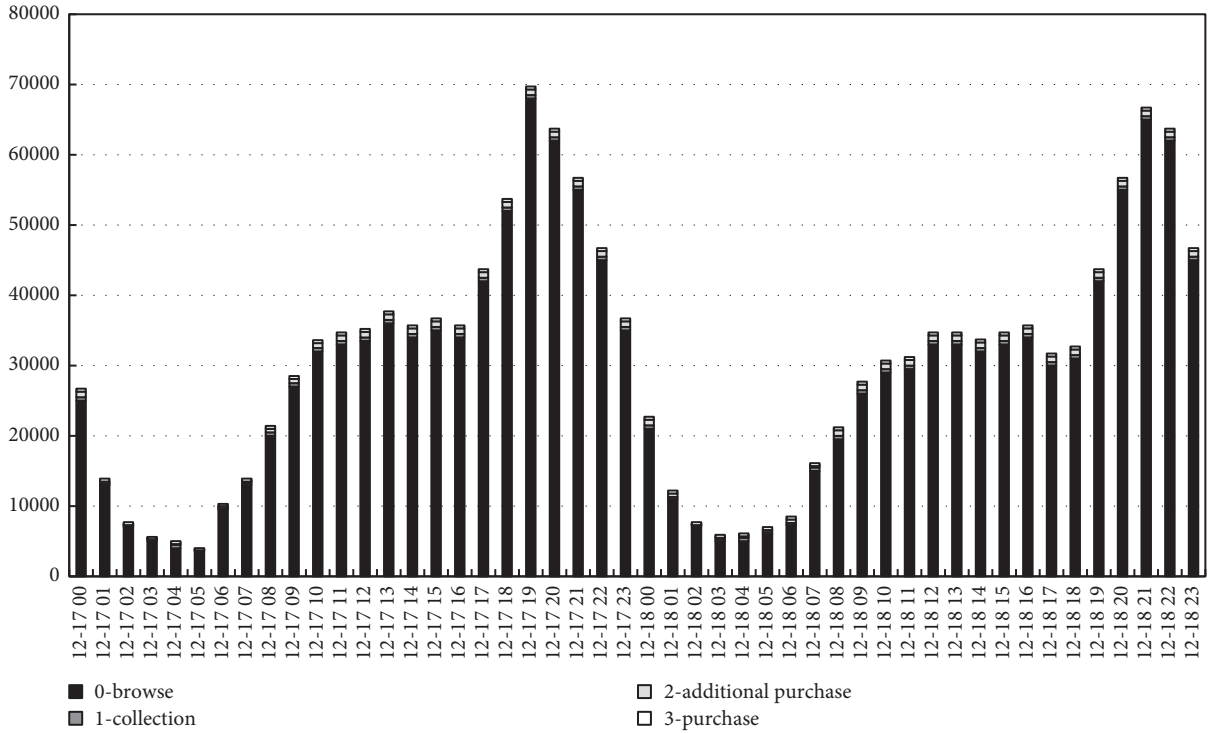


FIGURE 5: Distribution of user’s purchasing behavior on the subset of goods.

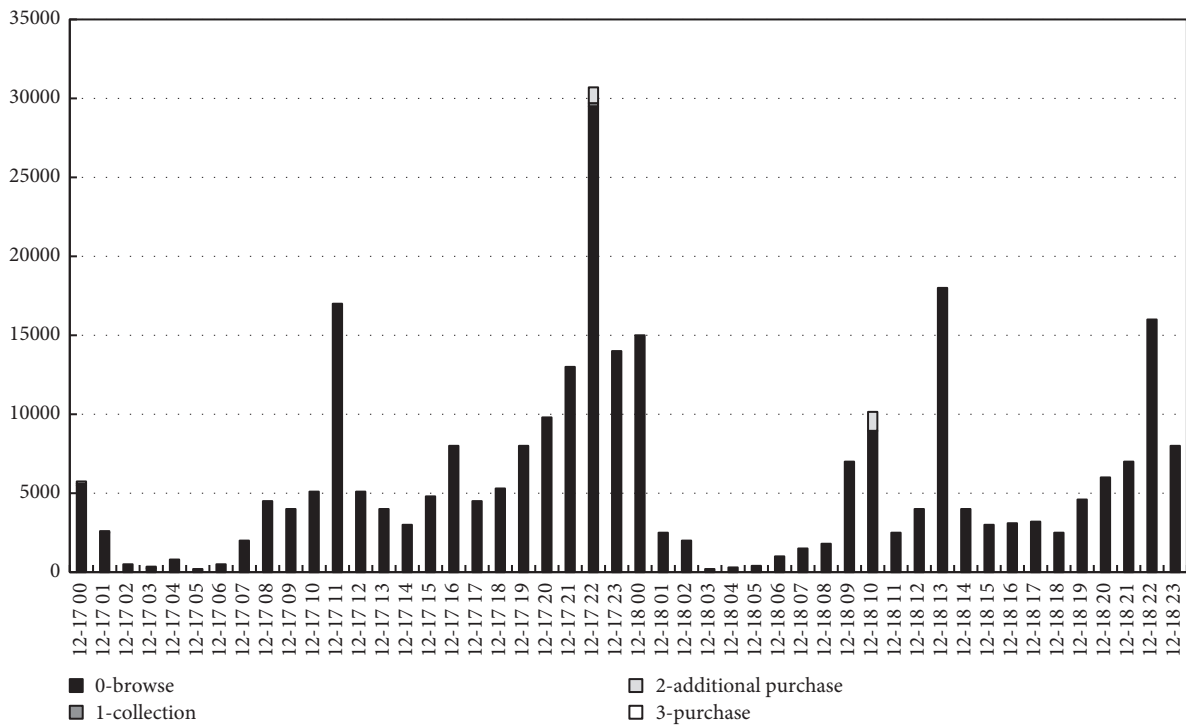


FIGURE 6: User’s behavior distribution in the subset of goods (h).

prediction of the day. Therefore, this part is selected as the main target of this paper for prediction.

To sum up, this experiment divides the longitudinal dimension according to the data weeks, and the horizontal dimension takes Friday data as the goal to build the model.

November 22nd to November 28th, November 29th to December 5th, and December 6th to December 12th are split into training sets. Meanwhile, December 13th to December 18th are split into test sets. Then, the problem is transformed into a binary classification problem by taking the user’s

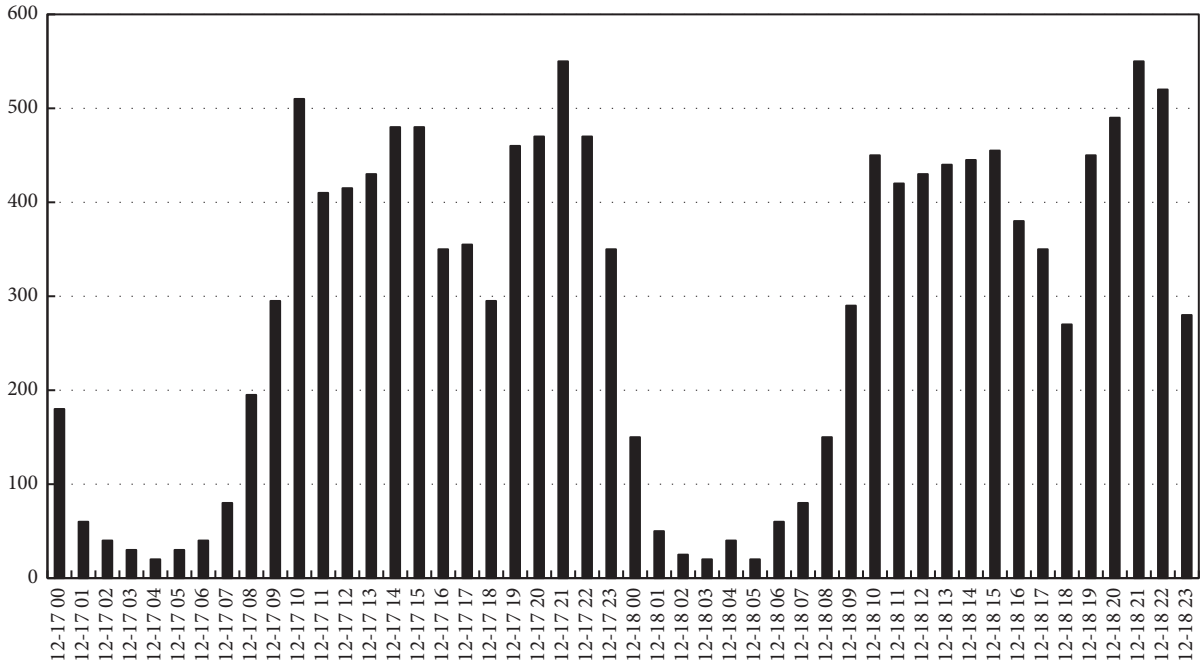


FIGURE 7: Distribution of user's purchasing behavior on the complete collection of goods (h).

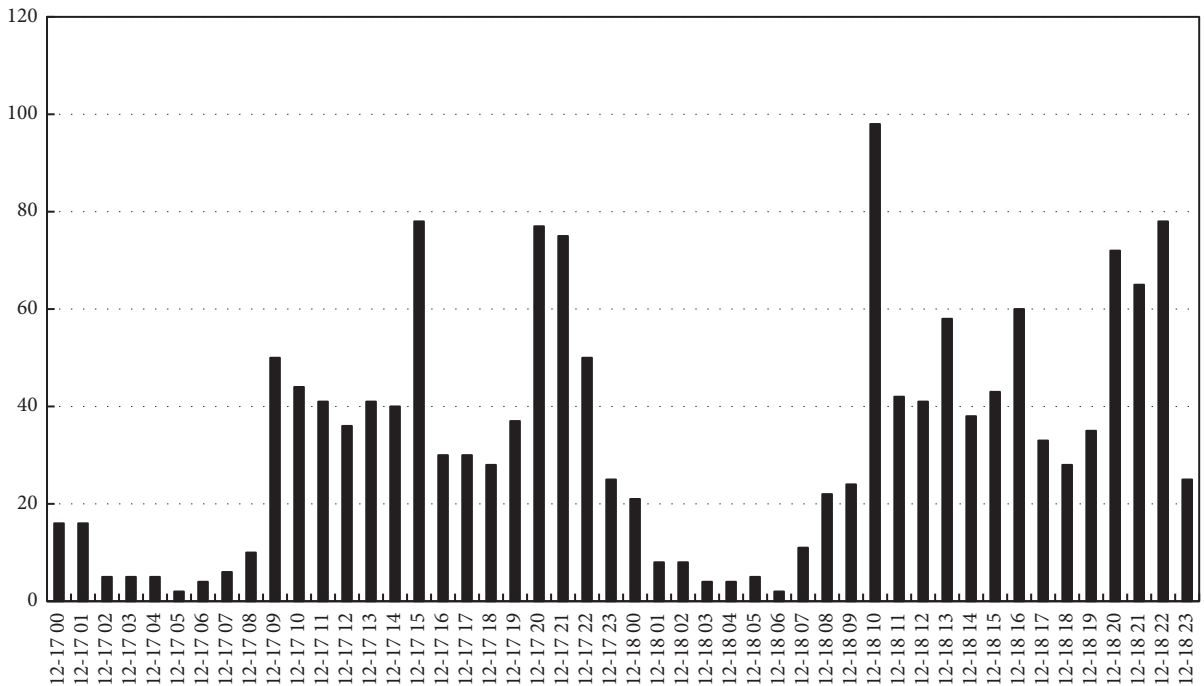


FIGURE 8: Distribution of user's purchasing behavior on a subset of goods (h).

browsing, collection, and additional purchase behavior as one category and the purchase behavior as another category. In addition, because the data on December 12 are obviously abnormal, they are deleted in order to avoid the influence of the data on the predicted results [19].

4.2.4. Feature Extraction. It is difficult to mine information from the existing feature dimensions because the dataset includes users, commodities, commodity categories, user

behavior types, operation time, and other data [20]. Therefore, in order to better mine useful information from data, the 107 features of counting class, sorting class, time difference class, and conversion rate class are selected from the aspects, such as commodities, commodity categories, user-commodity interaction, user-commodity category interaction, and commodity-commodity category interaction, to construct the model [21, 22]. The characteristics of each category and their meanings are shown in Table 5. At the same time, according to the purchase situation of the

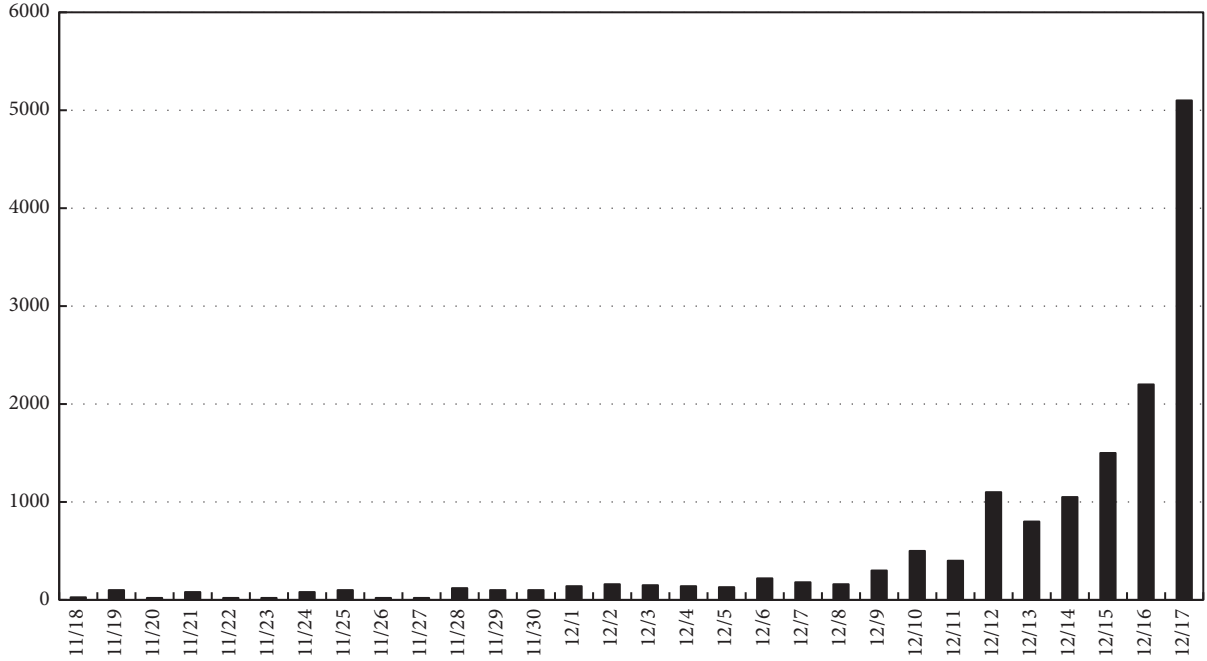


FIGURE 9: Number of interactions.

TABLE 5: Feature description.

Characteristic category	Characteristic meaning	Characteristic number
Counting	Number of behaviors of user/product/product category and interaction on 1/3/6 days prior to the inspection date	81
Sorting	Sorting of commodities and user-commodity interactions	12
Time difference	Average time difference between user/product/product category click purchase and interactive product behavior, and check the time difference of date	11
Conversion rate	User/product/product category click-to-buy conversion rate	3

corresponding group on the last day, the data are labeled as follows: 0 means no purchase and 1 means purchase.

4.3. *Evaluation Indicators.* The F1 value is adopted as an indicator to evaluate the e-commerce data analysis and prediction model, and its calculation method is as follows [23]:

$$\begin{aligned}
 \text{precision} &= \frac{|\cap (\text{prediction set}, \text{reference set})|}{|\text{prediction set}|}, \\
 \text{recall} &= \frac{|\cap (\text{prediction set}, \text{reference set})|}{|\text{reference set}|}, \\
 \text{F1} &= \frac{2 \times \text{precision} \times \text{recall}}{\text{precision} + \text{recall}},
 \end{aligned} \tag{15}$$

where prediction set represents the predicted purchase data and reference set represents real purchase data.

4.4. *Experimental Result*

4.4.1. *Parameter Setting.* There are many parameters involved in the training process of GBDT model, and different parameters have some influence on model training and

prediction. In order to determine the best model parameters, the control variable method is used to carry out experiments on the positive and negative sample ratio, learning rate, number of base learners, tree depth, and threshold that affect the model fitting results. However, because there is an extreme imbalance between positive and negative samples of e-commerce data and this factor has a great influence on the model fitting results, the positive and negative sample ratio needs to be determined first. Then, the learning rate of the model itself and the number of base learners are determined. Finally, the depth and threshold of the tree are determined.

Figure 10 shows the F1 value changes of the model under different ratios of negative samples and positive samples. As can be seen from the figure, when the ratio of negative samples to positive samples is less than 50, the F1 value increases gradually. When the ratio of negative samples to positive samples is between 50 and 100, the F1 value begins to fluctuate. When the ratio of negative samples to positive samples is greater than 100, the F1 value decreases gradually. The reason is that when the negative and positive samples are less than 50, the F1 value of the model is gradually increased as the number of iterations increases and the model underfitting is reduced. When the negative and positive

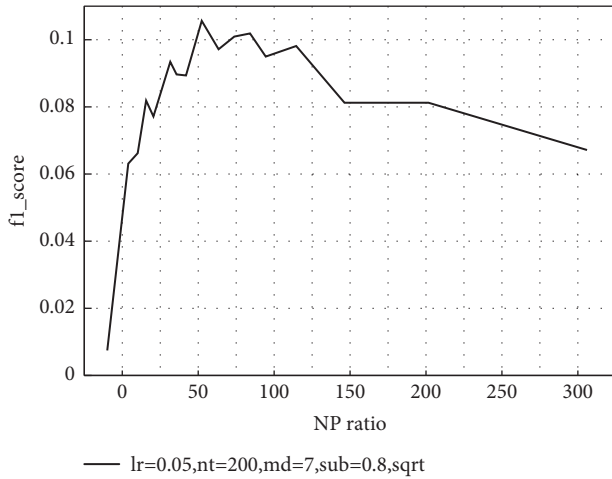


FIGURE 10: Influence of different negative sample/positive sample ratios on the model.

samples are larger than 100, the model is subject to overfitting, which leads to the reduction of its generalization ability. After comprehensive comparison, the negative and positive sample ratio of the input model selected in this paper is 60.

Figure 11 shows the influence of different learning rates on the predicted results of the model. As can be seen from the figure, different learning rates have different influences on the F1 value of the model. When the learning rate is 0.05, the F1 value of the model is the maximum, and with the increase of the learning rate, the F1 value of the model gradually decreases. Therefore, the learning rate of the proposed model is set at 0.05 in this experiment.

After determining the learning rate of 0.05, the number of base learners of the model is determined, and the results are shown in Figure 12. As can be seen from the figure, with the increase of number of base learners, the F1 value of the model begins to fluctuate and decrease after it starts to rise. When the number of base learners is 30, the F1 value of the model begins to fluctuate. When the number of base learners is 400, the F1 value of the model begins to decline. Therefore, it can be determined that the number of base learners of the model is between 30 and 400, and the median 200 is taken as the number of model base learners in this paper.

Figure 13 shows the influence of different tree depths on the model. It can be seen from the figure that with the increase of tree depth, the F1 value of the model rises first and then decreases. When the tree depth reaches a certain value, the F1 value of the model finally shows an upward trend. The final selected tree depth in this paper is 20.

Figure 14 shows the influence of different thresholds on the model. As can be seen from the figure, when the threshold is less than 0.4, the F1 value of the model rises gradually with the increase of the threshold. When the threshold value is between 0.4 and 0.9, the F1 value of the model fluctuates between 0.130 and 0.135. When the threshold value is greater than 0.9, the F1 value of the model decreases rapidly. Finally, the threshold of the model is determined to be 0.5.

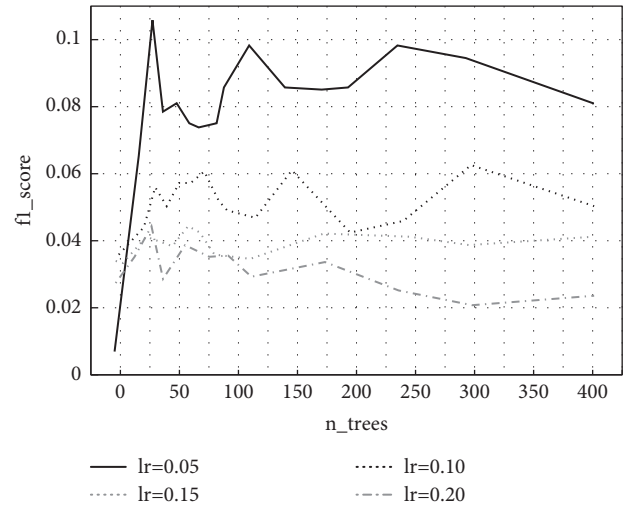


FIGURE 11: Influence of different learning rates on the model.

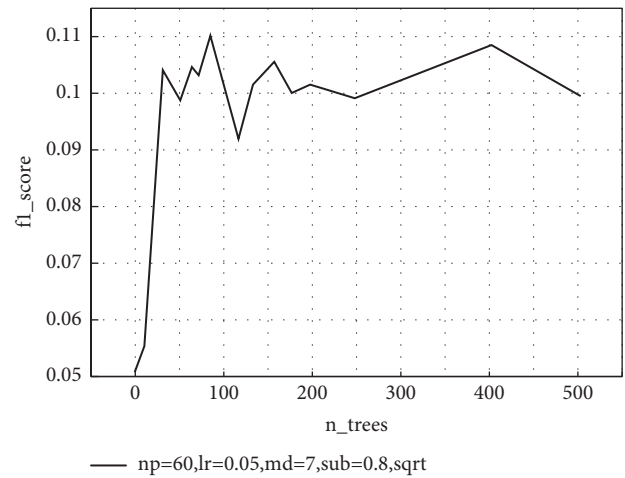


FIGURE 12: Influence of different number of base learners on the model.

In summary, the parameters of the proposed GBDT model are set as follows: learning rate = 0.05, base learner number = 200, tree depth = 20, and threshold = 0.5.

4.4.2. Comparison of Prediction Results. To further verify the effectiveness of the proposed model, the experiment compares the prediction effect of the proposed model with the traditional logic regression-based prediction model and the neural network-based prediction model. The GBDT model parameters are set according to the parameter setting. Meanwhile, the prediction model parameters based on logical regression of the comparison model are set to the threshold of 0.6. The prediction model parameters based on neural networks are set to the maximum number of iterations of 300. The single training samples are 64, and there are two layers of hidden layers. In addition, the number of nerve nodes per layer is 65.

The GBDT model and comparison model are trained on the training set with a ratio of negative samples to positive

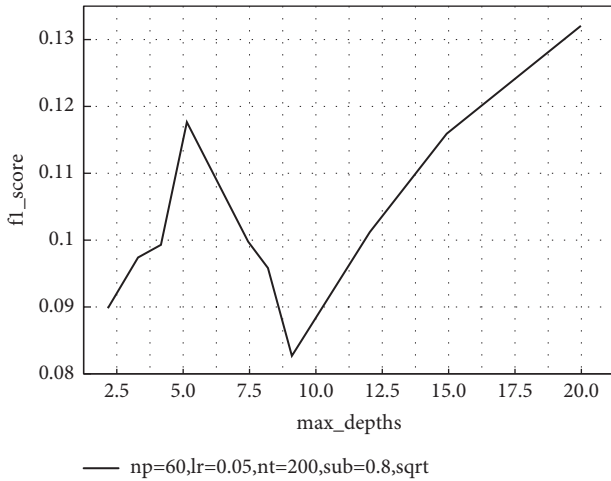


FIGURE 13: Influence of different tree depths on the model.

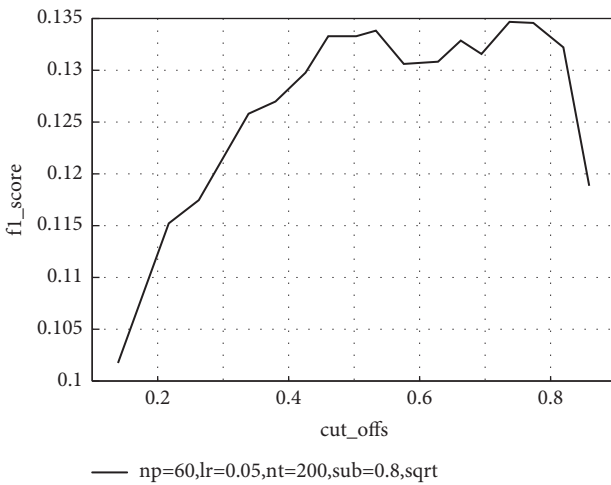


FIGURE 14: Influence of different model thresholds on the model.

TABLE 6: Comparison of prediction results.

Model	F1 score
Logistic regression	0.06
Neural network	0.06
GBDT	0.12

samples of 55, and the test set with a ratio of negative samples to positive samples of 60 is used for testing. The results are shown in Table 6. As can be seen from the table, compared with the comparison model, the proposed GBDT model has the highest F1 score of 0.12, which increases about 50%. Therefore, the proposed GBDT model is more suitable for data analysis and prediction in e-commerce.

5. Conclusion

To sum up, the e-commerce data analysis and prediction method based on GBDT model is proposed in this paper. It can be seen that the e-commerce data are preprocessed with missing values, desensitization, etc. At the same time, according to the user behavior, the browsing, collecting, and

additional purchase behavior are divided into one category, and the purchase behavior is divided into another category. The problem of e-commerce data analysis and prediction is transformed into a binary classification problem. Then, a total of 107 characteristics of counting class, sorting class, time difference class, and conversion rate class that can reflect the users' behavior characteristics are extracted to build a GBDT model. Finally, the efficient analysis and prediction of e-commerce data are realized. Compared with the traditional prediction model based on logical regression and based on neural network, the proposed GBDT model is more suitable for e-commerce data analysis and prediction. Also, when the learning rate of the GBDT model is 0.05, the number of basic learners is 200, the tree depth is 20, and the threshold is 0.5, and the prediction effect of the proposed model is best. Meanwhile, the F1 value can reach 0.12. Although this paper has obtained some research results, there are still some deficiencies, which are that the random search method is adopted to tune the GBDT model parameter, whose time cost is higher, and the efficiency generally needs to be improved. Therefore, the model automatic tuning parameter can be adopted in the future to improve the efficiency of model training, so as to realize higher precision analysis and prediction of e-commerce data [24, 25].

Data Availability

The experimental data used to support the findings of this study are available from the corresponding author upon request.

Conflicts of Interest

The author declares that there are no conflicts of interest.

References

- [1] B. E. Ozgur and D. Franklin, "Multicollinearity in logistic regression models[J]," *Anesthesia & Analgesia*, vol. 133, no. 2, pp. 362–365, 2021.
- [2] A. C. Cioci, A. L. Cioci, A. M. A. Mantero, J. P. Parreco, D. D. Yeh, and R. Rattan, "Advanced statistics: multiple logistic regression, cox proportional hazards, and propensity scores," *Surgical Infections*, vol. 22, no. 6, pp. 604–610, 2021.
- [3] D. Rekha, J. Sangeetha, and V. Ramaswamy, "Digital document analytics using logistic regressive and deep transition-based dependency parsing," *The Journal of Supercomputing*, vol. 78, pp. 1–17, 2021.
- [4] J. Singh and A. Chhabra, "Indian stock markets data analysis and prediction using macroeconomics indicators in machine learning," *International Journal of Innovative Technology and Exploring Engineering*, vol. 9, no. 10, pp. 484–486, 2020.
- [5] F. Halawa, S. Al-Hihi, W. Shen, and D. Won, "A model-based approach of data analysis and prediction in chronic kidney diseases (CKD)," in *Proceedings of the 2017 Industrial and Systems Engineering Conference*, Pittsburgh, PA, USA, 2017.
- [6] H. Son, S. Kim, H. Yeon, Y. Kim, Y. Jang, and S.-E. Kim, "Visual analysis of spatiotemporal data predictions with deep learning models," *Applied Sciences*, vol. 11, no. 13, 5853 pages, 2021.

- [7] X.-B. Jin, J.-H. Zhang, T.-L. Su, Y.-T. Bai, J.-L. Kong, and X.-Y. Wang, "Modeling and analysis of data-driven systems through computational neuroscience wavelet-deep optimized model for nonlinear multicomponent data forecasting," *Computational Intelligence and Neuroscience*, vol. 2021, 2021.
- [8] Y. Guo, G. Xiong, L. Zeng, and Q. Li, "Modeling and predictive analysis of small internal leakage of hydraulic cylinder based on neural network," *Energies*, vol. 14, no. 9, 2456 pages, 2021.
- [9] A. A. Agafonov, "Short-term traffic data forecasting: a deep learning approach," *Optical Memory & Neural Networks*, vol. 30, no. 1, pp. 1–10, 2021.
- [10] S. Omer and R. Lior, "Approximating XGBoost with an interpretable decision tree," *Information Sciences*, vol. 572, pp. 522–542, 2021.
- [11] Y. Zou, Y. Chen, and H. Deng, "Gradient boosting decision tree for lithology identification with well logs: a case study of zhaoxian gold deposit, shandong peninsula, China," *Natural Resources Research*, vol. 30, no. 5, pp. 1–21, 2021.
- [12] T. Syed AsSadeq and Y. Chen, "Analysis of severe injuries in crashes involving large trucks using K-prototypes clustering-based GBDT model," *Safety Now*, vol. 7, no. 2, p. 32, 2021.
- [13] W. Zhang, J. Yu, A. Zhao, and X. Zhou, "Predictive model of cooling load for ice storage air-conditioning system by using GBDT," *Energy Reports*, vol. 7, pp. 1588–1597, 2021.
- [14] W. Qiu, Z. Lv, Y. Hong, J. Jia, and X. Xiao, "BOW-GBDT: a GBDT classifier combining with artificial neural network for identifying GPCR–drug interaction based on wordbook learning from sequences," *Frontiers in Cell and Developmental Biology*, vol. 8, 2021.
- [15] B. Zhang, J. Ren, Y. Cheng, B. Wang, and Z. Wei, "Health data driven on continuous blood pressure prediction based on gradient boosting decision tree algorithm," *IEEE ACCESS*, vol. 7, pp. 32423–32433, 2019.
- [16] X. Ye, J. Wang, T. Wang, X. Yan, Q. Ye, and J. Chen, "Short-term prediction of available parking space based on machine learning approaches," *IEEE ACCESS*, vol. 8, pp. 174530–174541, 2020.
- [17] J. Yang, Y. Sheng, and J. Wang, "A GBDT-paralleled quadratic ensemble learning for intrusion detection system," *IEEE ACCESS*, vol. 8, pp. 175467–175482, 2020.
- [18] G. Rong, S. Alu, K. Li et al., "Rainfall induced landslide susceptibility mapping based on bayesian optimized random forest and gradient boosting decision tree models—a case study of shuicheng county, China," *Water*, vol. 12, no. 11, 2020.
- [19] J. Zhang, Q. Feng, X. Zhang, Q. Hu, J. Yang, and N. Wang, "A novel data-driven method to estimate methane adsorption isotherm on coals using the gradient boosting decision tree: a case study in the qinshui basin, China," *Energies*, vol. 13, no. 20, pp. 5369–5379, 2020.
- [20] G. He, "Enterprise E-commerce marketing system based on big data methods of maintaining social relations in the process of E-commerce environmental commodity," *Journal of Organizational and End User Computing*, vol. 33, no. 6, pp. 1–16, 2021.
- [21] Y. Kim, H. J. Lee, and J. Shim, "Developing data-conscious deep learning models for product classification[J]," *Applied Sciences*, vol. 11, no. 12, 2021.
- [22] S. P. Goldman, H. van Herk, T. Verhagen, and J. W. Weltevreden, "Strategic orientations and digital marketing tactics in cross-border e-commerce: comparing developed and emerging markets," *International Small Business Journal: Researching Entrepreneurship*, vol. 39, no. 4, pp. 350–371, 2021.
- [23] M. Zhu, "Implementation of support-vector machine algorithm to develop a model for electronic commerce energy regulatory system," *Energy Reports*, vol. 7, pp. 2703–2710, 2021.
- [24] N. Sharma, A. Raj, V. Kesireddy, and P. Akunuri, "Machine learning implementation in electronic commerce for churn prediction of end user," *International Journal of Soft Computing and Engineering*, vol. 10, no. 5, pp. 20–25, 2021.
- [25] J. Hou, Q. Li, Y. Liu, and S. Zhang, "An enhanced cascading model for E-commerce consumer credit default prediction," *Journal of Organizational and End User Computing*, vol. 33, no. 6, pp. 1–18, 2021.

Research Article

Student Performance Prediction in Mathematics Course Based on the Random Forest and Simulated Annealing

Shaohai Huang¹ and Junjie Wei^{2,3} 

¹Mathematics and Computer Department, Fuzhou Preschool Education College, Fuzhou 344000, China

²Henan Polytechnic University, Jiaozuo 454003, Henan, China

³School of Intelligent Engineering, Shandong Management University, Jinan 250357, China

Correspondence should be addressed to Junjie Wei; 111801010008@home.hpu.edu.cn

Received 18 December 2021; Revised 21 January 2022; Accepted 8 February 2022; Published 23 March 2022

Academic Editor: Hangjun Che

Copyright © 2022 Shaohai Huang and Junjie Wei. This is an open access article distributed under the Creative Commons Attribution License, which permits unrestricted use, distribution, and reproduction in any medium, provided the original work is properly cited.

Educational data mining is becoming a more and more popular research field in recent years, mainly with the help of cross research conducted by various disciplines, so as to solve various difficult problems in the teaching and education process. In this paper, we proposed a hybrid approach for student performance prediction. We collected the dataset, including 15 characteristics of students from three categories (individual basic information, individual education information, and individual behavior information). Based on the random forest (RF) and simulated annealing (SA) algorithms, we binary encode the relevant parameters (number of features, tree size, and tree decision weights) as the target variables for algorithm optimization, use the out-of-bag error as the optimization objective function, and then propose the IRFC (improved random forest classifier) algorithm in this paper. Compared with other mainstream improved random forest algorithms, the research results demonstrate that the proposed algorithm in this paper has higher generalization ability and smaller OOB error. This study provides a methodological reference for the prediction of student achievement and also makes a marginal contribution to student management work.

1. Introduction

At present, universities have accumulated a large amount of obvious data in the education of students, such as the basic information of students, their family situation, and their grades and scores in various subjects, as well as the specific information of students' speech rate and correct rate in answering questions in the classroom and their attendance in the classroom. Obviously, these data in the field of education are constantly changing and will grow explosively with the development of education informatization, so how to extract useful information from these complex and tedious data for data analysis will have a good research value.

It is not an easy task to use modern technology to process the data resources with huge data size education data and discover the hidden knowledge accurately. The emergence of data mining technology in recent years has provided powerful technical support for solving such challenges. The

use of data mining technology to discover valuable data or relevant knowledge law information from a large amount of data and the analysis and mining results applied to the teaching management will have far-reaching significance to improve the quality of school teaching and education management level.

Data parallelization processing has become one of the important issues of the current era. How to combine data mining work with data parallel processing mechanism for processing is also one of the major challenges for data mining work. The combination of data mining algorithm and data parallelism mechanism can make full use of the parallelism mechanism to accelerate the fast processing of data and also to dig the hidden rules or principles behind the massive data according to a deeper level so as to understand the nature of things more deeply.

Educational data mining is becoming a more and more popular research field in recent years, mainly with the help of

cross research conducted by various disciplines (such as computer science, education, and statistics), so as to solve various difficult problems in the teaching and education process [1–3]. In the context of the big data era, educational data mining research will take a new watershed. Educational data mining involves more working levels, including student performance prediction, teaching deficiency analysis, student adaptive learning ability analysis, automatic student performance discrimination, and other subdomains [4–7], and the scope of this paper will be limited to student performance prediction.

The educational data mining for the specific direction of student achievement prediction consists of two stages. The first period was the last century, when researchers used data mining techniques for education only in a simple way, and the scope of application was narrow due to the limitation of the technology level at that time. The second period is the rapid development of the last two decades, with the use of Internet technology to trigger a change in educational technology, using a variety of data mining techniques to promote the development of educational informatization [8]. EDUCAUSE, the US Association for Information Technology in Higher Education, has proposed a definition of educational data mining in the new era of educational challenges as the ability to use data-based methods to predict student learning progress and outcomes and to act on them.

In recent years, many researchers at home and abroad have used data mining technology to study and analyze curriculum score data. Ei-Halees used a data mining method to study students' learning habits and put forward specific suggestions for improving students' performance. Ayesha used the k-means clustering method to predict students' course understanding level on the basis of students' test score set, thus providing a data basis for the construction of final exam questions. Overall, course data mining research has attracted a large number of scholars to explore [9, 10].

In this research, the random forest algorithm based on the decision tree algorithm is mainly used. The decision tree is a very efficient supervised learning algorithm with easy to interpret characteristics. The key to decision tree construction is to choose which attribute as the basis of classification, and the typical construction algorithms are ID3 [11], C4.5 [12], and CART [13], respectively.

The random forest algorithm uses the bootstrap sampling method for M rounds of training and constructs M decision trees by classifiers (decision trees, SVM, logistic regression, etc.) to build a random forest and determine the final attribution classification of the data by voting results [14]. The random forest performs well on the dataset and does not easily fall into overfitting than neural network [15] while having good noise resistance. Random forests can handle very high dimensional (large feature size) data and do not have to make feature selection; they can handle both discrete and continuous data. Random forests are also highly adaptable to the dataset; the input dataset does not need to be normalized. Many studies have shown that combined classifiers are better at classification, which makes the random forest algorithm extremely important in both regression and classification. 2014 E Cernadas compared the

actual results of different classifiers on different datasets and showed that the random forest algorithm was on average the strongest, getting first place on 9.9% of the datasets. Fernandez-Delgado M et al. compared various 179-class classification algorithms on 121 UCI datasets, including excellent classification algorithms such as the random forest algorithm, decision tree algorithm, and SVM algorithm, and the experimental results confirmed that the random forest algorithm was optimal among all the algorithms [16].

Although the rapid rise of data parallel processing platforms has enabled machine learning algorithms to be widely used, many machine learning algorithms are black-box models that cannot be adapted to certain special prediction research fields. As an important mining algorithm in the aspect of ML, the RF algorithm can detect data characteristics such as interactions and nonlinear relationships between data without any preconceptions while having low generalization errors in many practical application scenarios and problem solutions. More significantly, the random forest algorithm is interpretable and can be explained as the effect of certain importance measures, binary measures or multivariate dependencies, and other relevant factors.

This paper focuses on the practical problem of student performance prediction and academic performance prediction and tries to find out the influencing factors and prediction models about student performance from them through the analysis of educational big data.

In this paper, we proposed a hybrid approach for student performance prediction. We collected the dataset, including the characteristics of students from three categories. Based on the random forest (RF) and simulated annealing (SA) algorithm, we binary encode the relevant parameters (number of features, tree size, and tree decision weights) as the target variables for algorithm optimization, use the out-of-bag error as the optimization objective function, and then propose the IRFC (improved random forest classifier) algorithm in this paper. The results of this study will be useful for educational management, teaching participants, and individual students and will provide methodological support for improving student performance. In addition, the results of our research can be further extended, for example, to build an early warning identification system and early prevention and control system based on our research results or to personalize the curriculum by predicting student performance and to intervene in the teaching process in order to obtain an overall improvement of student performance.

2. Method

2.1. Random Forest. Compared with ANN, regression tree, and SVM, the random forest algorithm has been proven to be more stable and robust while also maintaining a high level of classification in scenarios with missing data [17].

2.2. Standard Random Forest. The standard RF algorithm is an ensemble of algorithms such as Bagging and CART, which mainly performs diverse combinations by using

decision trees as the basic unit; the final classification result is output by voting for most single classifiers.

To summarize, there are two parts of the RF classification; one is the random generation of input data for each single classifier by using the Bagging method; the second is the random selection of feature subsets to obtain the best classification features through information gain.

In the following, the Bagging method and CART model of the RF are explained in detail, followed by a detailed description of the entire workflow of the random forest algorithm. Subsequently, this paper enhanced the classification results on the above foundation.

2.3. Bagging Method. The key point of the Bagging method is that the process of calculating any classification does not rely on any previous classification calculation process. In each rating calculation process, a part of data shall be selected for independent operation based on the original dataset, and the results of each classification shall be effectively aggregated to enhance the classification accuracy of the algorithm and avoid aggregation of unstable learning algorithms [18, 19].

2.4. CART Algorithms. In this study, we first explain the CART model in detail. The CART algorithm is a decision tree algorithm proposed by Breiman and Friedman. CART usually generates a binary decision tree through the Gini index; it uses a binary recursive model for binary tree construction; each division will divide the entire dataset into two sets, resulting in two branching subtrees. The Gini index is mostly employed to indicate the impurity of the dataset. Sample set D 's Gini index is defined as

$$\text{Gini}(D) = 1 - \sum_{i=1}^m p_i^2, \quad (1)$$

where p_i denotes the probability that the data in D belongs to category C_j . If the binary division of D based on attribute A will be divided into two subsets, D_1 and D_2 , the Gini index based on this division can be calculated as a weighted sum of the impurity of each partition:

$$\text{Gini}_A(D) = \frac{|D_1|}{|D|} \text{Gini}(D_1) + \frac{|D_2|}{|D|} \text{Gini}(D_2). \quad (2)$$

By the above calculation, it is known that the reduction of impurity due to the binary division based on attribute A is

$$\Delta \text{Gini}(A) = \text{Gini}(D) - \text{Gini}_A(D). \quad (3)$$

During the execution of the CART algorithm, the attribute maximizes the impurity reduction.

Out-of-bag (OOB) error calculation is often used as a common algorithm evaluation metric for classification performance assessment of random forest algorithms because it is an unbiased estimate, an alternative to the dataset cross-validation method, and a practical experience which represents that its measured values are generally of great nicety.

The smaller the value of OOB error, the better the classification result of the RF, which is usually expressed as

$$\text{OOB error} = \frac{\sum_{i=1}^K \text{OOB error}_i}{k}. \quad (4)$$

2.5. Random Forest Algorithm Flow. Combining the above Bagging method and CART algorithm, we will explain the workflow of the RF in detail. The detailed execution process of the RF is shown in Figure 1, and the specific execution process of the RF is shown as follows:

Symbol description: the original training dataset is represented by D , which is composed of M base attributes and a classification outcome attribute Y .

Input: original training set D and decision tree size K .

Output: classifier model and classification results.

Process:

Step 1: generate training subsets. Using the Bagging algorithm for the original training set D , N times repeated random sampling is performed to obtain a training subset of size N (where there may be duplicate data). The above process is repeated K (such as 10, 15, and 20) times to obtain the training subset $\{D_1, D_2, D_3, \dots, D_x\}$. The feature selection is also performed for M base attributes and O ($0 \leq M$, such as 1, 2, 3, ..., M) attributes for analysis.

Step 2: for each training subset D_i ($1 < i < K$), the CART is employed to produce an unpruned dichotomous decision tree recursion. At each intermediate node of the decision tree, it needs to follow the following rules: instead of selecting the optimal segmentation features from all the features, a subset of features is constructed from a random selection of m features ($m \leq M$), and then the features corresponding to the best segmentation form (with the largest Gini measure) are selected from the subset of features. CART trees need to continue the above process for node splitting. The corresponding decision tree h_i (D_i) is finally produced for each D_i .

Step 3: combine the decision trees produced in the last step to form an RF $\{h_1(D_1), h_2(D_2), \dots, h_i(D_i)\}$ and test it based on the measured set of samples X to get the corresponding results.

Step 4: final results for test data X are determined using the majority voting method and the weighted voting method for the K -tree classification results, and the classification error OOB error needs to be calculated. The weighted voting method is mainly for the results of each decision tree weighted statistics, S_c represents the total number of votes, and it can be calculated as

$$S_c = \sum_{t=1}^K (T_{c,x}(X)W_t), \quad (5)$$

where $T_{c,x}(X)$ takes the value of 1 or 0. If sample X results in class c after classification by decision tree, it takes the value of 1; otherwise, it takes the value of 0.

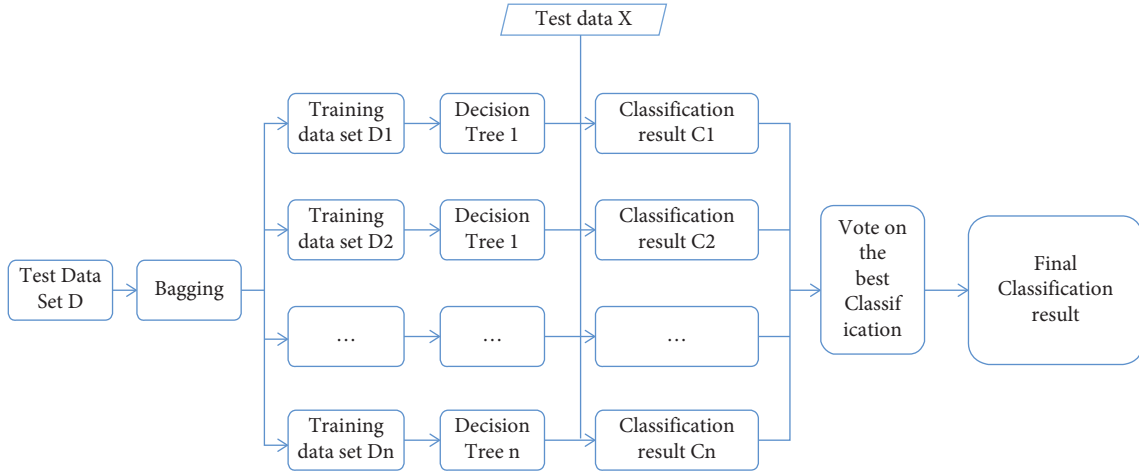


FIGURE 1: Basic workflow of random forest algorithm.

After counting by the weighted voting method, the class with the most votes is selected as the final output classification result of sample X .

The algorithm ends.

A point worth stating is that, throughout the operation of the algorithm, the individual variables, such as the number of resampling N , the decision tree size K , feature selection value O , and decision weight Wt , remain independent of each other and do not have any dependency.

2.6. Simulated Annealing Algorithm. Metropolis first proposed the simulated annealing (SA) algorithm, and then SA was applied to combinatorial optimization algorithms by Kirkpatrick, with the main goal of solving the problems of overcoming initial value dependence [20, 21]. The calculation steps of the simulated annealing are as follows:

Phase 1: generate a random initial solution x_0 such that $x_{best} = x_0$, calculate the objective function value $E(x_0)$, and set $k = 0$ and initial temperature $t_0 = t_{max}$.

Phase 2: if the temperature reaches the stop condition then skip to phase 3, or else choose x_{best} randomly from the neighborhood $Nv(x_{best})$ of the current optimal solution x_{new} and calculate the associated objective function value $E(x_{new})$, from which the associated incremental value $\Delta E = E(x_{new}) - E(x_{best})$ is derived. Update x_{best} by the following equation:

$$x_{best} = \begin{cases} x_{new, \Delta E \leq 0} & \\ x_{new, \Delta E > 0} & \text{and } e^{-\frac{\Delta E}{t_k}} > \text{random}(0, 1), \\ x_{best}, \text{ other situations} & \end{cases} \quad (6)$$

Phase 3: set $t_{k+1} = d(t_k)$; $k = k + 1$. If the output value meets eventually the stop condition, the computation is terminated, or else return to phase 2 to continue the execution. Finally, the optimal solution x_{best} is output.

As a general optimization algorithm, the simulated annealing algorithm has already been widely employed in many optimization field problems, such as in industrial shop layout optimization problems, transportation network optimization, supply chain optimization problems, atmospheric radiation equation solution problems, loan problem optimization solutions, and other application levels, which have good application effect, and in many cases can find the global optimal point.

2.7. Improved Algorithm

2.7.1. Improvement Ideas. Although the original random forest algorithm has been able to achieve better operational results compared with other classification algorithms, there are still several problems in itself. First, the default parameters are not optimal choices, especially the weighted weight parameters, while the traditional grid search method for optimal parameter decisions is too time-consuming for practical applications. Second, the algorithm OOB error will be reduced further and used as algorithm objective function definition; the number of algorithms for feature selection is usually predetermined, which may be far from the exact value. The IRF proposed in our chapter is mostly for the above problems to correct.

In recent years, many scholars have also incorporated intelligent algorithms into random forest algorithms to achieve good research results; for example, some researchers combined genetic algorithm and random forest algorithm for fault detection to reduce OOB outside the bag error [22]; a combination of particle algorithm and random forest algorithm is proposed for feature selection research and has good experimental results [23]; researchers incorporated AFSA into random forest algorithm for feature selection as well as parameter optimization [24], and the simulation experimental results prove that the algorithm OOB error is generally small and the generalization ability is relatively strong, which provides an effective guidance method for random forest algorithm feature selection and parameter estimation.

In our study, the IRFC is proposed for parameter optimization, weight correction, and feature selection to finally achieve two classifications or multiple classifications. O value, the more commonly used value, includes \sqrt{M} , $2\sqrt{M}$, and $\log_2(\sqrt{M}) + 1$, and it is found in the experimental data that when the value of M is relatively small, the algorithm classification effect is the best when the hyperparameter O chooses $\log_2(\sqrt{M}) + 1$, but it cannot obtain the optimal effect at any time. Many studies have started to use KNN methods, minimization of OOB errors, random combination of input variables, and other methods to carry out the optimal value solution of hyperparameter X , with relatively good classification results and with short computation time and small storage space compared with traditional methods.

For the output sample classification results, the random forest algorithm will take the output results of most decision trees as the basis. In our study, we will give different weights to the decision trees to further improve the shortcomings of the traditional algorithm so as to improve the classification accuracy.

2.8. Improved Algorithm Flow. For the above parameter optimization, our study proposes a new method for integrated optimization based on the previous study, mainly by incorporating the SA into the RF execution process, and the parameters are combined and optimized. In our proposed method, the objective function is introduced:

$$f(K^*, O^*, \{\text{Attribute}_i | i = 1, 2, \dots, M\}, \{w_j | j = 1, 2, \dots, K\}), \\ = \arg \min (\text{avg OBB error}). \quad (7)$$

Optimization variables are as follows: K , O , $\{\text{Attribute}_i | i = 1, 2, \dots, M\}$, $\{w_j | j = 1, 2, \dots, K\}$, where K , O are real numbers, K takes values in the range $[0, 500]$, and w_j is an integer taking values in the range $[0, 15]$. Attribute is a 01 variable. Figure 2 introduces the optimization variables, which are represented using a binary code and consist of four parts.

On the basis of the above binary encoding of variables, the flow of our planned improved random forest algorithm IRFC is shown in Figure 3, and its corresponding flow is shown as follows:

Phase 1: set the initialization temperature $t = t_{\max}$, $k = 1$, generating a random initial solution X , and let $X_{\text{best}} = X_0$.

Phase 2: calculate $F = \max(1/f)$ with RF algorithm.

Phase 3:

- (1) If the temperature is achieved the inner loop stopping condition, then skip to (2), or else choose x_{new} randomly from the neighborhood $N(x_{\text{best}})$ of the current optimal solution x_{best} and calculate the associated objective function value $f(x_{\text{new}})$, from which the associated incremental value $\Delta F = f(x_{\text{new}}) -$

$f(x_{\text{best}})$ is derived. Update X best by the following equation:

$$X_{\text{best}} = \begin{cases} X_{\text{new}}, \Delta F < 0 \\ X_{\text{new}}, \Delta F > 0 \text{ and } e^{-\frac{\Delta F}{t_k}} > \text{random}(0, 1). \\ X_{\text{best}}, \text{other situations} \end{cases} \quad (8)$$

- (2) Set $t_{k+1} = d(t_k)$; $k = k + 1$; if the eventually stopping condition is satisfied, the computation is terminated and the x_{best} is output, or else return to (1).

Phase 4: if $gen > \max gen$, output the best $X^* = (K, O, \text{Attribute}, W)$. Or else, return to phase 2.

3. Experiment Design

3.1. Data Introduction. Students' course performance depends on many elements, including their own learning characteristics, their own professional orientation, the degree of study in the course, the degree of review after class, the teacher of the class, and other factors. This course will incorporate the improved random forest algorithm into the student course prediction data through the IRFC to enhance the predicted results for the students' achievement in each course; based on this, managers can pay attention to the factors that affect student performance and pay attention to these factors in the course teaching process [25, 26]. By continuously cycling this predict-practice-improve approach, we can enhance the teaching and learning reform efforts to make it more scientific and efficient and at the same time make students' performance better and enhance their competitiveness in job opportunities after graduation.

The dataset for conducting experiments in this section is the student performance dataset, which is student characteristics collected from our school's advanced mathematics course. The dataset includes 15 characteristics of students, which consists of three parts: individual basic information, individual education information, and individual behavior information. The classification of student statistical features includes features such as birthplace, gender (male or female), place of entrance examination, and direct contact (father or mother) [27–30]. The classification of individual education information includes characteristics such as student grade level, teaching semester, teaching classroom, student major, faculty members, and student course subtest scores (in-class exam scores, midterm exam scores, and practical scores).

The dataset was obtained by the authors from their class teaching, which involved a many dimensions collection of raw data. The work involved a long time frame and a relatively large amount of work. Subsequently, data preprocessing was performed on the raw data, including data cleaning, data discretization work, and data filtering. Due to the variability and diversity of the collected data expressions, data preprocessing was required: for data with characteristics such as "student course activity level," the data were



FIGURE 2: Optimization variables of binary encoding.

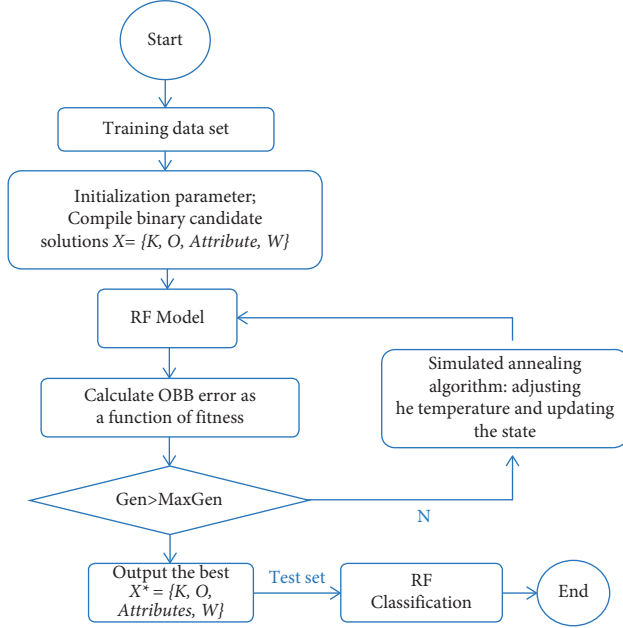


FIGURE 3: The overall flowchart of the algorithm of the improved random forest algorithm IRFC.

discretized and normalized, and we also cleaned up some of the abnormal data.

Table 1 introduces the feature information of the student performance, where the English name, Chinese meaning, and the result of each feature are explained in detail. Based on the historical records and student behavior subjects, we choose the first two years as a training set and trained the prediction model with the improved random forest algorithm, and then, we employed the the last years of data as a test set for performance prediction and made comparative analysis with the real performance. The size of the student achievement dataset (three years) is 2002.

3.2. Feature Normalization. First, we normalized the data features. The feature normalization method aims to reduce the numerical difference in the range of values taken by different features and reduces the impact of the training model on the units of measure. The feature normalization mostly employs linear transform, log transform, or tan transform to normalize the initial data, thus transforming it into a smaller public space.

About the student performance dataset, the feature variables that require feature programming include student activity in class, student absenteeism, and student course satisfaction features, while other feature variables are calculated using raw values, such as birthplace using coded values and gender using the Boolean values coded as 0 or 1.

For the student absenteeism count feature, the feature programming method is mainly a mnemonic linear transformation using the maximum-minimum normalization method. In the following, we choose the most representative example of student classroom activity for a complex feature normalization illustration.

For the characteristics of students' classroom activity, the number of times users raise their hands to answer questions, the number of times they communicate in class, and the degree of personal concentration in class are collected for comprehensive evaluation. In the process of implementation, the discrete data are first normalized to $[0, 1]$ based on the log function normalization method, and each factor is assigned a corresponding weight coefficient to obtain the student classroom activity data. The expression of the student classroom activity level is

$$\text{KTScore} = \frac{W_{js} * \log_{10}(JSx)}{\log_{10}(\max JS)} + \frac{W_{jl} * \log_{10}(JLx)}{\log_{10}(\max JL)} + W_{zz} * \text{ZZFactor}. \quad (9)$$

W_{js} , W_{jl} , and W_{zz} denote the weighting factors of the three factors, which are set by default at 0.4, 0.3, and 0.3; ZZFactor denotes the teacher's subjective evaluation score of students' concentration; the range of it is 0-1.

3.3. Classification Algorithm Evaluation Indicator. After proposing an improved random forest model, an overall evaluation of the performance of the whole model is needed. The more common performance evaluation metrics include accuracy, precision, recall, F-value, ROC curve, and AUC value.

First, we make some assumptions about the evaluation criteria: TP (True Positive) represents the correctly classified positive class, FP (False Positive) indicates the incorrectly classified negative class, FN (False Negative) denotes the incorrectly classified positive class, and TN (True Negative) is on behalf of the correctly classified negative class. $N = TP + FN + FP + TN$ denotes the total amount of sample data.

Accuracy, which represents the overall classification accuracy inside the total sample data, is calculated as follows:

$$\text{accuracy} = \frac{TP + TN}{N}. \quad (10)$$

Accuracy is the most important basic index among all evaluation indexes, which directly evaluates the efficiency of the model. The higher the value, the better the classification effect.

Recall is mainly the classification accuracy of all sample data for positive classes, which means the proportion of

TABLE 1: Detailed information on the characteristics of the student performance.

No.	Name	Feature	Introduction of the values
1	Birthplace	Birthday	National province dictionary
2	Gender	Gender	{0: male; 1: female }
3	Place of entrance examination	Exam location	National identity dictionary
4	Direct contact	Contact person	{0: father; 1: mother; 2: other }
5	Student's grade level	Grade	{1, 2, 3, 4}
6	Teaching semester	Semeter	{1, 2}
7	Teaching classroom	Classroom	Classroom dictionary
8	Student's major	Major	Professional dictionary
9	Faculty staff	Teacher	Faculty dictionary
10	Student course quiz results	Quiz test	Average score/100
11	Students' activity in class	Activity	Normalize to [0, 1]
12	Student absence	Absence	Normalize to [0, 1]
13	Number of times students access teaching resources after class	Visit resouces	Normalize to [0, 1]
14	Number of student discussions in the course	Discussion	Normalize to [0, 1]
15	Student course satisfaction	Satisfaction	Normalize to [0, 1]

correctly classified positive samples occupying all correctly classified samples, and the corresponding calculation formula is as follows:

$$\text{recall} = \frac{TP}{TP + TN}. \quad (11)$$

Precision mainly indicates the proportion of correctly classified positive samples to all predicted positive samples and is calculated as follows:

$$\text{precision} = \frac{TP}{TP + FP}. \quad (12)$$

The F-value is a comprehensive performance metric used to evaluate the imbalance of the dataset, mainly based on the combination of precision and recall, where β is used to indicate the importance of precision rate and recall rate. Only when both precision and recall are high, the F-value is higher and also indicates better classification results.

$$F = \frac{(1 + \beta^2) * \text{precision} * \text{recall}}{\beta^2 * \text{precision} + \text{recall}}. \quad (13)$$

ROC (Receiver Operating Characteristic) is an important criterion for judging the performance of classification models and is well suited for evaluating imbalance. When the ROC is closer to the upper left corner, it indicates better classification results. The area under the ROC is called the AUC (Area Under Curve); AUC can also be used to indicate the criterion for the superiority of the classifier; the higher the AUC, the better the classification results.

4. Experiment Evaluation

4.1. Comparison of Traditional Algorithm Results. Table 2 and Figure 4 show our comparative classification using a variety of basic data mining algorithms in an attempt to analyze the differences between the various data mining methods. Our comparison results indicate that the RF has a slight advantage over other data algorithms on the student feature dataset but is not significantly different overall.

TABLE 2: Comparison of classification results of student grades dataset on each base algorithm.

	LR	NB	SVM	GRNN	RF
TP	231	214	223	216	230
FN	15	32	13	22	15
FP	28	24	42	34	40
TN	84	88	80	86	77

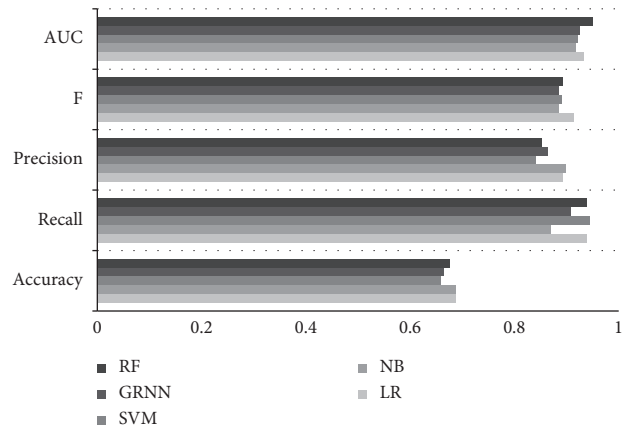


FIGURE 4: The result of different algorithms of student grades.

4.2. Algorithm Basic Evaluation. we can find that in every index level, the improved random forest algorithm has obtained almost the minimum OOB error, which shows the proposed algorithm has strong generalization ability and higher classification accuracy. Table 3 and Figure 5.

5. Conclusion

In this study, based on random forest, a new method, IRFC, is proposed, which is proven to have a high classification accuracy in order to predict students' performance in university courses. To enhance the execution efficiency of the method, the parallelization of the improved random forest algorithm is subsequently carried out on a big data platform

TABLE 3: Comparison of classification results of student grades on different random forest algorithms.

	RF_1	RF_2	RF_3	RF_4	GRNN	IRFC
N	100	100	100	100	—	339
K	1	14	4	5	—	9
Num (attribute)	14	14	14	14	—	12
Avg (W)	8	8	8	8	—	6.7

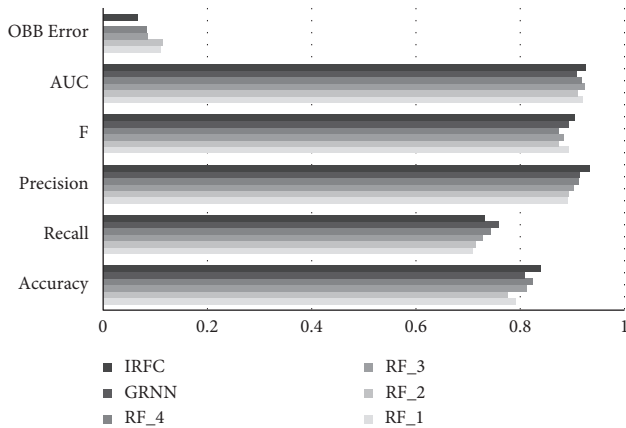


FIGURE 5: The result of different random forest algorithms of student grades.

to shorten the execution time of the algorithm. The main work of this paper is shown in the following: the hybrid algorithm IRFC, which combines a simulated annealing algorithm with RF, is proposed to optimize the performance of RF comprehensively. This paper analyzes the current research status of the random forest algorithm, binary encodes the relevant parameters (number of features, tree size, tree decision weights) as the target variables for algorithm optimization, uses the out-of-bag error as the optimization objective function, and then proposes the IRFC algorithm in this paper. Compared with other mainstream improved random forest algorithms for comparison, our results demonstrate that the IRFC algorithm has higher generalization ability with smaller OOB error.

This paper also focuses on the parameter impact analysis of the improved RF algorithm on the student performance dataset, and the validation results confirm that the application of SA provides auxiliary effects on the effective performance of our model, which will help to carry out teaching curriculum reform. In this paper, we have completed the design and experiments of the improved random forest algorithm and fully verified the effectiveness and reliability of the improved algorithm in this paper. However, there are some shortcomings in our work; for example, the parallelization strategy is not the most fine-grained parallel working model. We will improve this in future work.

Data Availability

The experimental data used to support the findings of this study are available from the corresponding author upon request.

Conflicts of Interest

The authors declare that they have no conflicts of interest regarding this work.

References

- [1] X. Du, J. Yang, J. L. Hung, and B. Shelton, "Educational data mining: a systematic review of research and emerging trends," *Information Discovery and Delivery*, vol. 48, no. 4, pp. 225–236, 2020.
- [2] R. S. Baker and P. S. Inventado, *Educational Data Mining and Learning Analytics*, Wiley, New Jersey, USA, 2014.
- [3] A. A. Anjewierden, B. Kollöffel, and C. Hulshof, "Towards educational data mining," *Using data mining methods for automated chat analysis and support inquiry learning processes*, 2007, <https://core.ac.uk/display/20962888>.
- [4] K. Havstad, "A study on feature selection techniques in educational data mining," *Intergovernmental Relations Series*, <https://arxiv.org/abs/0912.3924>, 2009.
- [5] M. N. Injadat, A. Moubayed, A. B. Nassif, and A. Shami, "Multi-split optimized bagging ensemble model selection for multi-class educational data mining," *Applied Intelligence*, vol. 50, no. 12, pp. 4506–4528, 2020.
- [6] T. M. Ogwoka, W. Cheruiyot, and G. Okeyo, "A model for predicting students' academic performance using a hybrid of K-means and decision tree algorithms," *International Journal of Computer Applications Technology and Research*, vol. 4, no. 9, pp. 693–697, 2015.
- [7] V. T. Tampakas, "Predicting secondary school students' performance utilizing a semi-supervised learning approach," *Journal of Educational Computing Research*, vol. 57, 2019.
- [8] E. A. Amrieh, T. Hamtini, and I. Aljarah, "Mining educational data to predict student's academic performance using ensemble methods," *International Journal of Database Theory and Application*, vol. 9, no. 8, pp. 119–136, 2018.
- [9] A. El-Halees, "Mining students data to analyze learning behavior: a case study," in *Proceedings of the The 2008 international Arab Conference of Information Technology (ACIT2008) – Conference Proceedings*, p. 137, University of Sfax, Hammamet, Tunisia, December 2008.
- [10] S. Ayesha, T. Mustafa, A. Sattar, and I. Khan, "Data mining model for higher education system[J]," *European Journal of Scientific Research*, vol. 43, no. 1, pp. 24–29, 2018.
- [11] L. Wei, *Application and Practice of ID3 Algorithms in College Students' Education*, Springer, Berlin, Germany, 2020.
- [12] A. Joshuva, R. S. Kumar, S. Sivakumar, G. Deenadayalan, and R. Vishnuvardhan, "An insight on VMD for diagnosing wind turbine blade faults using C4.5 as feature selection and discriminating through multilayer perceptron," *AJ - Alexandria Engineering Journal*, vol. 59, no. 5, 2020.
- [13] R. Tang and X. Zhang, "CART decision tree combined with boruta feature selection for medical data classification," in *Proceedings of the 2020 5th IEEE International Conference on Big Data Analytics (ICBDA)*, May 2020.
- [14] L. H. Alamri, R. S. Almuslim, M. S. Alotibi, D. K. Alkadi, and I. U. Khan, "Predicting student academic performance using support vector machine and random forest," in *Proceedings of the 3rd International Conference on Education Technology Management*, London, UK, December 2020.
- [15] Z. Bao and C. Wang, "A multi-agent knowledge integration process for enterprise management innovation from the

- perspective of neural network,” *Information Processing & Management*, vol. 59, no. 2, 2022.
- [16] M. Fernández -Delgado, E. Cernadas, S. Barro, and D. Amorim, “Do we need hundreds of classifiers to solve real world classification problems,” *Journal of Machine Learning Research*, vol. 15, no. 1, pp. 3133–3181, 2014.
- [17] S. Deng, C. Wang, Z. Fu, and M. Wang, “An intelligent system for insider trading identification in Chinese security market [J],” *Computational Economics*, vol. 57, no. 6, 2021.
- [18] R. H. Dong, H. H. Yan, and Q. Y. Zhang, “An intrusion detection model for wireless sensor network based on information gain ratio and bagging algorithm,” *International Journal on Network Security*, vol. 22, no. 2, pp. 218–230, 2020.
- [19] T. Xia, P. Zhuo, L. Xiao, S. Du, D. Wang, and L. Xi, “Multi-stage fault diagnosis framework for rolling bearing based on OHF elman AdaBoost-bagging algorithm,” *Neurocomputing*, vol. 433, 2021.
- [20] H. Samma, J. Mohamad-Saleh, S. A. Suandi, and B. Lahasan, “Q-learning-based simulated annealing algorithm for constrained engineering design problems,” *Neural Computing & Applications*, vol. 32, no. 9, pp. 5147–5161, 2020.
- [21] T. A. Shaikh and R. Ali, “An intelligent healthcare system for optimized breast cancer diagnosis using harmony search and simulated annealing (HS-SA) algorithm,” *Informatics in Medicine Unlocked*, vol. 21, Article ID 100408, 2020.
- [22] H. Norouzi, A. A. Moghaddam, F. Celico, and J. Shiri, “Assessment of groundwater vulnerability using genetic algorithm and random forest methods (case study: miandoab plain, NW of Iran),” *Environmental Science and Pollution Research*, vol. 28, no. 1, pp. 1–16, 2021.
- [23] M. Zhou, F. Lin, Q. Hu, Z. Tang, and C. Jin, “AI-enabled diagnosis of spontaneous rupture of ovarian endometriomas,” *A PSO Enhanced Random Forest Approach*, IEEE Access, vol. 8, no. 99, 2020.
- [24] D. Jia, Z. Li, and C. Zhang, “A parametric optimization oriented, AFSA based random forest algorithm: application to the detection of cervical epithelial cells,” *IEEE Access*, vol. 8, pp. 64891–64905, 2020.
- [25] W. Lin, Z. Wu, L. Lin, A. Wen, and J. Li, “An ensemble random forest algorithm for insurance big data analysis,” *Ieee Access*, vol. 5, pp. 16568–16575, 2017.
- [26] N. S. Ahmed and M. H. Sadiq, “Clarify of the random forest algorithm in an educational field,” in *Proceedings of the 2018 International Conference on Advanced Science and Engineering (ICOASE)*, pp. 179–184, IEEE, Duhok, Iraq, October 2018.
- [27] M. Zhu, J. Xia, X. Jin et al., “Class weights random forest algorithm for processing class imbalanced medical data,” *IEEE Access*, vol. 6, pp. 4641–4652, 2018.
- [28] S. K. Lakshmanaprabu, K. Shankar, M. Ilayaraja, A. W. Nasir, V. Vijayakumar, and N. Chilamkurti, “Random forest for big data classification in the internet of things using optimal features,” *International Journal of Machine Learning and Cybernetics*, vol. 10, no. 3, pp. 1–10, 2019.
- [29] Q. Wu, H. Wang, X. Yan, and X. Liu, “MapReduce-based adaptive random forest algorithm for multi-label classification,” *Neural Computing & Applications*, vol. 31, no. 3, pp. 1–14, 2018.
- [30] C. A. Tawiah and V. S. Sheng, “Empirical comparison of multi-label classification algorithms,” in *Proceedings of the 27th national conference on artificial intelligence (AAAI)*, pp. 1645–1646, Bellevue, Washington, USA, 2013.

Retraction

Retracted: Dynamic Correlation between Ozone and Volatile Organic Compounds in the Southeastern Coastal Region

Scientific Programming

Received 29 August 2023; Accepted 29 August 2023; Published 30 August 2023

Copyright © 2023 Scientific Programming. This is an open access article distributed under the Creative Commons Attribution License, which permits unrestricted use, distribution, and reproduction in any medium, provided the original work is properly cited.

This article has been retracted by Hindawi following an investigation undertaken by the publisher [1]. This investigation has uncovered evidence of one or more of the following indicators of systematic manipulation of the publication process:

- (1) Discrepancies in scope
- (2) Discrepancies in the description of the research reported
- (3) Discrepancies between the availability of data and the research described
- (4) Inappropriate citations
- (5) Incoherent, meaningless and/or irrelevant content included in the article
- (6) Peer-review manipulation

The presence of these indicators undermines our confidence in the integrity of the article's content and we cannot, therefore, vouch for its reliability. Please note that this notice is intended solely to alert readers that the content of this article is unreliable. We have not investigated whether authors were aware of or involved in the systematic manipulation of the publication process.

Wiley and Hindawi regrets that the usual quality checks did not identify these issues before publication and have since put additional measures in place to safeguard research integrity.

We wish to credit our own Research Integrity and Research Publishing teams and anonymous and named external researchers and research integrity experts for contributing to this investigation.

The corresponding author, as the representative of all authors, has been given the opportunity to register their agreement or disagreement to this retraction. We have kept a record of any response received.

References

- [1] H. Li and X. Nie, "Dynamic Correlation between Ozone and Volatile Organic Compounds in the Southeastern Coastal Region," *Scientific Programming*, vol. 2022, Article ID 8566454, 9 pages, 2022.

Research Article

Dynamic Correlation between Ozone and Volatile Organic Compounds in the Southeastern Coastal Region

Hao Li¹ and Xing Nie ^{2,3}

¹Hu'nan Chenzhou Ecological and Environmental Monitoring Center, Chenzhou 423000, China

²Basic school of Hunan food and Drug Vocational College, Changsha 410000, China

³Yangtze University College of Chemistry & Environmental Engineering, Jingzhou 430000, China

Correspondence should be addressed to Xing Nie; 202001310@yangtzeu.edu.cn

Received 10 February 2022; Revised 28 February 2022; Accepted 1 March 2022; Published 23 March 2022

Academic Editor: Man Fai Leung

Copyright © 2022 Hao Li and Xing Nie. This is an open access article distributed under the Creative Commons Attribution License, which permits unrestricted use, distribution, and reproduction in any medium, provided the original work is properly cited.

In order to investigate the sources and effects of atmospheric volatile organic compounds (VOCs) in the southeast coastal region and to formulate effective ozone control policies, 96 VOCs were measured in the southeast coastal region from September to October 2016 using an online gas chromatograph-mass spectrometer/flame ionization detector (Online-GC-MS/FID). The composition, daily trends, sources, and contribution to ozone production of 96 VOCs in the southeast coastal region were analyzed. The results of the study showed that the volume mixing ratio of alkanes was the highest, followed by aromatic hydrocarbons; the daily variation trend of alkanes and aromatic hydrocarbons was obvious, with a double-peaked feature; propane, isoprene, and aromatic hydrocarbons in the atmosphere of the southeast coastal region came from liquefied petroleum gas (LPG), natural sources, and industrial emissions, respectively. The analysis of the activity of VOCs shows that aromatic hydrocarbons and alkanes are the most important contributors to OFP in the southeast coastal region, with toluene, m-/paraxylene, and ethylene being the species that contribute the most to OFP. Therefore, the control of VOC emissions from anthropogenic sources is a priority for ozone pollution control in the southeast coastal region in the future.

1. Introduction

VOCs can be divided into natural source VOCs and anthropogenic VOCs. Reference [1] estimated global emissions of natural source VOCs at 1150 Tg, which is much greater than that of anthropogenic VOCs [2]. Studies have shown that natural sources of VOCs are involved in plant growth, reproduction, and defense and have important effects on other biological, atmospheric chemical, and physical processes [3]. BVOCs are present in low concentrations in the atmosphere compared to other gases in the atmosphere, but most of them are highly reactive and can react chemically with anthropogenic pollutants (especially nitrogen oxides) under certain temperature and light conditions, resulting in significant photochemical pollution [4].

At present, the representative models of BVOCs are BEIS, G95, BEIS2, GLOBEIS, MEGAN, etc. In this study, the

MEGAN2.1 model, which is widely used internationally, is a model for the emission of gaseous pollutants and aerosols from natural sources, based on a large amount of experimental data and the G95 algorithm, and further refining the mechanism and surface data [5].

The MEGAN model is not only a good replacement for the previous model but also has higher resolution and can meet the requirements of both regional and global scale simulations and has been commonly used in BVOCs emission studies at home and abroad. Many scholars have previously estimated BVOCs emissions in China using different modeling algorithms, and some studies have simulated some regions in China, such as Beijing, Hong Kong, Pearl River Delta, and Yangtze River Delta, but few studies have been conducted on BVOCs emissions with high spatial and temporal resolution for the northern inland regions of China. Therefore, in this study, the high-resolution leaf area index

(LAI) and vegetation functional type (PFT) data of the southeast coastal region were obtained from MODIS remote sensing images, and the meteorological data of the study area were modeled with the help of WRF model, and the final simulation was carried out by MEGAN2.1 model to obtain the high spatial and temporal resolution BVOCs emission inventory of the southeast coastal region [6]. The results of this study can provide a basis for future atmospheric research on photochemical pollution and ozone formation and will help to improve the atmospheric quality in northern China and further reduce the impact of atmospheric pollution on the ecological environment and human health.

The atmosphere on the Earth's surface determines the climate and environment on the planet, and it has a significant impact on biological and life processes on the Earth's surface; the composition and content of various chemical components in the atmosphere and their inter-conversion directly affects the environmental conditions on the Earth's surface, where the distribution of certain chemicals in the atmosphere (e.g., acid rain, ozone) on the Earth's surface has a direct impact on the biosphere and has become a major local environmental problem in some regions [7]. Nonmethane hydrocarbons (NMHCs) are trace gases produced by a variety of biological and geological processes on Earth, and although, they are present in small amounts in the atmosphere, they are decisive for certain atmospheric chemical processes. The amount of NMHC released is $1.273 \text{ Tg C} \cdot \text{yr}^{-1}$ ($1.273 \times 10^{12} \text{ g C}$ content per year), and in densely populated urban and industrialized areas, anthropogenic releases of NMHC occupy an undervalued position, but globally, the vast majority of NMHC is released from nature [8], with only a small fraction coming from the oceans and most of the rest from terrestrial ecosystems. The majority of the rest comes from vegetation in terrestrial ecosystems, especially woody plants, which contribute more than 90% ($1,150 \text{ Tg C} \cdot \text{yr}^{-1}$) of the global NMHC emissions [9]. Plant VOCs are mainly volatilized into the atmosphere through the foliage of plants and have hundreds of components and structures, but two groups of compounds account for more than half of them: isoprene (C_5H_8), which contains five carbon atoms, and monoterpenes, which contain ten carbon atoms, such as α -pinene; the two types of volatile compounds released from plants total 500 and $125 \text{ Tg C} \cdot \text{yr}^{-1}$ [10], respectively.

Many plants are capable of releasing VOCs under certain natural conditions and these compounds play a key role in the succession of ecosystems, for example, to mitigate heat stress [11], to protect against insect predation [12], and to meet the nitrogen requirements of the early stages of ecosystem succession by taking gaseous nitrogen from the air [13]. VOCs are chemically active and can undergo complex chemical reactions with atmospheric HO and H_2O , etc. The rate of VOC release from plants and their atmospheric content control the concentration of OH ions in the atmosphere, which in turn determines the atmospheric concentration of methane (CH_4) and CO, which in turn influences the radiative balance in the atmosphere and hence the spatial and temporal distribution of global heat and precipitation, with a strong impact on the regional and

global environment and climate [14]. On the other hand, numerous studies have confirmed [15] that VOC has a significant impact on the photochemical synthesis of ozone in the near-earth troposphere and that the increase of ozone concentration in the troposphere can lead to serious ecological consequences such as forest decline and crop yield reduction [16]; atmospheric VOC also plays an important role in the global carbon cycle [17]. Therefore, the determination of atmospheric biogenic volatile compounds (BVOCs), especially the fluxes of VOC released by plants in various ecosystems, is important for the successful implementation of tropospheric ozone control.

Different plant taxa release different types and amounts of VOCs. For example, isoprene is one of the most abundant VOCs released by plants, and its release is dependent on sufficient light and high temperatures [18]. Among the angiosperms, *Quercus*, *Platanus*, *Populus*, *Rhamnus*, *Salix*, and *Eucalyptus* are typical isoprene releasers, while *Acer*, *Citrus*, and *Magnolia* are the main terpene releasers. Moreover, other genera mainly release terpenoids. Studying the phylogeny of plants and their interrelationship with VOC release developed a global VOC release model that provides a good explanation of the inter-relationship between the structure of temperate ecosystems and their atmospheric environment. However, this model is based on the species and capacity of different plant groups to release VOCs, requiring field and laboratory testing and analysis of a large number of plant species, which is not only a large amount of work but also results in large differences in the amount released due to different testing conditions and environments.

Studies in several regions have shown that VOC release is significantly correlated with the ecosystem type and closely related to the environmental conditions in which the ecosystem is located [19]. Further studies have also shown that plant VOC release in various ecosystems has an ecosystem succession-related pattern, with early to middle successional stages of ecosystems having a strong capacity to release isoprene, and plants with strong isoprene release mostly being the main components of this successional stage [20], while later successional plant species are mostly terpene releasers [21]. Succession is a process of ecosystem development that results in a constant turnover of vegetation types with different community structure and species composition (different successional stages). During the succession of an ecosystem, its productivity, biomass, nutrient cycling, and energy flow are widely predictable [6]. If VOC release is linked to ecosystem succession, then a systematic pattern of VOC release can be identified along the ecosystem succession sequence, and this pattern can be used to develop a succession-based VOC release model that can replace the cumbersome species-based VOC release model.

2. Research Methodology and Driving Data (Methods and Data)

2.1. Study Area and Emission Model. The southeastern coastal region is located at longitudes $113^{\circ}27'$ to $119^{\circ}50'$ E and latitudes $36^{\circ}05'$ to $42^{\circ}40'$ N, with a north-south length

of 735 km and an east-west width of 576 km, and a temperate monsoon climate. The study area was divided into 245×192 grids at a distance of 3 km.

The MEGAN model, version 2.1, which is widely used internationally, was used to estimate BVOCs in agricultural, rural, and urban ecosystems. MEGAN2.1 was updated from MEGAN2.0 and MEGAN2.02, which not only expanded the emission categories but also added model control processes [7]. Previous models for estimating emissions of BVOCs have included one or more “other VOCs” in an attempt to include all emissions. However, “other VOCs” cannot be converted to known compound classes, or even from mass to substance, so this approach has significant limitations. To address this issue, the MEGAN2.1 model removes the category “other VOCs” and converts “other VOCs” into 73 specific categories of compounds. F_i is calculated as follows:

$$F_i = \gamma_i \sum \varepsilon_{i,j} \chi_j \rho, \quad (1)$$

where $\varepsilon_{i,j}$ is the standard condition for vegetation type j (leaf area index LAI = 5, solar altitude angle of 60° , atmospheric light quantum flux transmittance of 0.6, air temperature of 303 K, air humidity of $14 \text{ g} \cdot \text{kg}^{-1}$, wind speed of $3 \text{ m} \cdot \text{s}^{-1}$, soil moisture of $0.3 \text{ m}^3 \cdot \text{m}^{-3}$, and sunrise photon flux of $200 \mu\text{mol} \cdot \text{m}^{-2} \cdot \text{s}^{-1}$ for the past 24 to 240 h). χ_j is the proportion of this vegetation type in the corresponding grid; ρ is the fugacity factor, usually taken as a constant 1; γ_i is the emission activity factor, which is used to correct vegetation emissions according to changes in surrounding meteorological conditions (temperature, light, humidity, etc.), according to the following algorithm:

$$\gamma_i = C_{CE} \cdot \text{LA} \cdot \gamma_{P,i} \cdot \gamma_{T,i} \cdot \gamma_{A,i} \cdot \gamma_{SM,i} \cdot \gamma_{C,i}, \quad (2)$$

where CCE is the canopy environmental coefficient, taken as 0.57 in MEGAN; LAI is the leaf area index; $\gamma_{P,i}$ represents the environmental regulation parameter related to light radiation; $\gamma_{T,i}$ represents the regulation parameter related to temperature; $\gamma_{A,i}$ represents the regulation parameter related to leaf age; $\gamma_{SM,i}$ represents the regulation parameter related to soil moisture, which is only used for estimating isoprene and is defaulted to 1.0 for other emission categories; $\gamma_{C,i}$ represents the emission parameter related to CO_2 . The technical route of this paper is shown in Figure 1.

2.2. Data Preparation

2.2.1. LAI Profile. In this study, the 2017 MODIS leaf area index standard product MOD15A2H was used with a spatial resolution of 500 m and a temporal resolution of 8 d. Arcgis10.2 was used to stitch, reproject, crop, and resample the maps, and then ENVI5.3 was used to convert the output to obtain LAI data files in the study area.

2.2.2. Types of Vegetation Function. PFT The vegetation functional types in this study were classified using the MODIS land use standard product MCD12Q1 at a spatial resolution of 500 m. The images were stitched, reprojected, cropped, and resampled using Arcgis10.2, then were

converted and exported using ENVI5.3 to form a 3 km resolution grid, with the proportion of each vegetation type calculated separately within each grid. The proportion of each vegetation type was calculated for each grid. Table 1 shows the area distribution of various vegetation types in the southeast coastal area.

2.2.3. Determination of EF Emission Factors. The model applied in this study is MEGAN2.1, where the emission factors are measured under standard conditions, and the national emission factor averages [8] are used for the emission rates of specific categories of isoprene, monoterpene, and hemiterpene, while the default values in the model are used for the emission rates of specific categories of other VOCs. The emission factor unit in the MEGAN model is $\mu\text{g} \cdot \text{m}^{-2} \cdot \text{h}^{-1}$, whereas the emission factor unit in the literature is $\mu\text{g}(c) \cdot \text{g}^{-1} \cdot \text{h}^{-1}$ (in dry weight). So, this paper uses leaf biomass density ($\text{g} \cdot \text{m}^{-2}$, in dry weight) for conversion.

2.2.4. Meteorologically Driven Data. This study uses the latest release of WRF4.0 model data in 2018 as the meteorological driver data. MCIP was used to convert the WRF data into the standard input data of MEGAN2.1, where the projection of the MEGAN model is by default the same as the meteorological data, the Lambert equirectangular projection. The variables include temperature data (canopy temperature at 2 m above ground level and surface temperature for differential soil temperature), air humidity data (air humidity data at 2 m above ground level), wind speed data (canopy wind speed), soil data (soil moisture, soil temperature), solar radiation (downward shortwave radiation), etc.

3. Results and Discussion

3.1. Characteristics of Atmospheric VOC Concentration Levels and Composition in the Southeast Coastal Region. The composition of the VOCs varied considerably, with alkanes accounting for the largest proportion (56%), followed by OVOCs (13%) and aromatic hydrocarbons (12%). The top 10 compounds in terms of concentration were propane, n-butane, acetone, isobutane, toluene, isopentane, ethane, methylene chloride, acetylene, and n-pentane (Figure 2).

Table 2 shows the comparison of VOC concentrations in the southeastern coastal region and some major cities in China and abroad, and it can be seen that propane and toluene have the highest concentrations in each city. The concentrations of these species in the southeast coastal region are closer to those in Guangzhou and Hong Kong, and the high concentrations of propane, isobutane, and n-butane compared to other cities are related to the high number of buses and taxis using LPG (liquefied petroleum gas) fuels in the Hong Kong-Zhuhai-Macao region. Compared to Hong Kong and other cities in the PRD region, isopentane and methylene chloride concentrations in atmospheric VOCs are also high in the southeast coastal region, suggesting that oil volatilization and the chemical industry contribute to

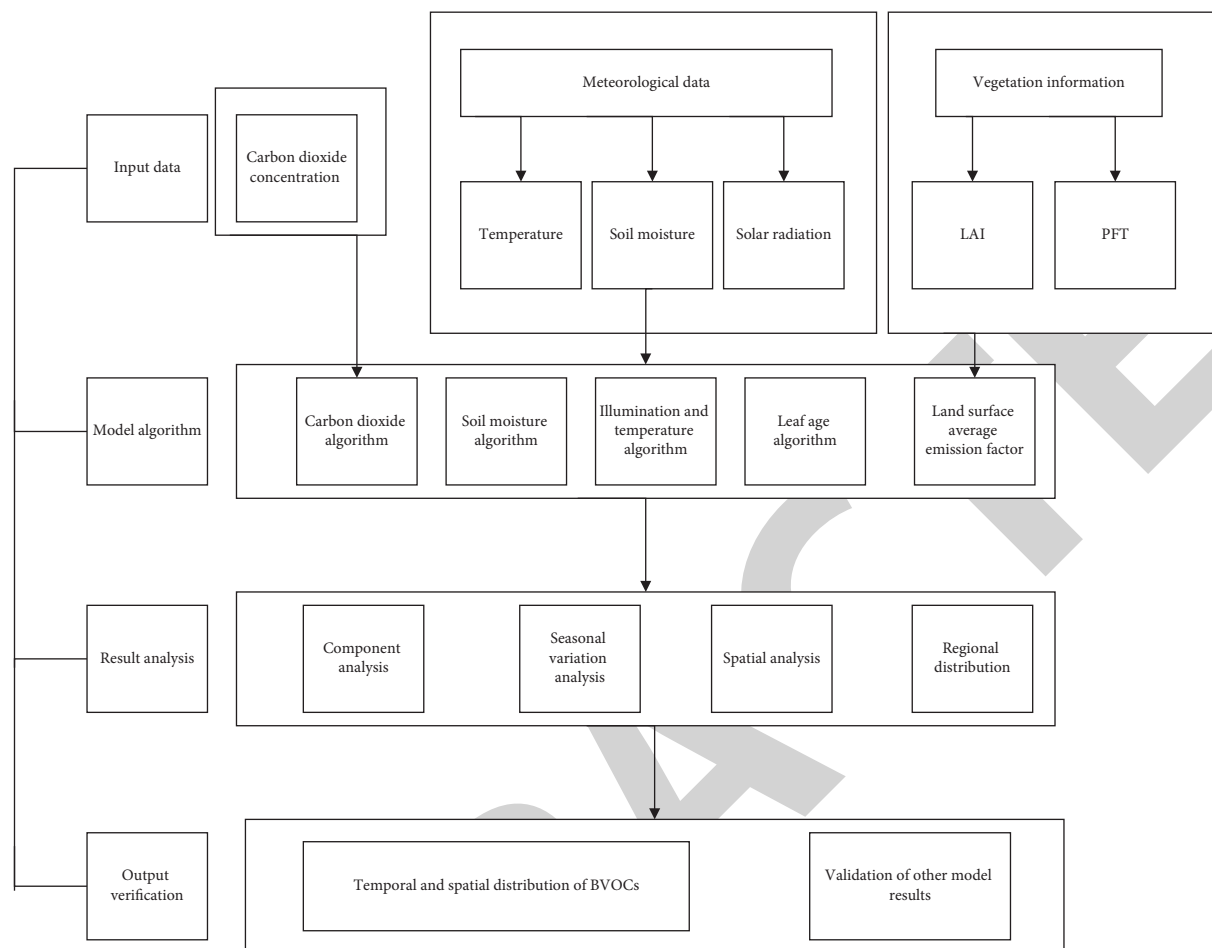


FIGURE 1: Technology roadmap for this study.

atmospheric VOCs in the southeast coastal region. The gasoline used in the PRD is mainly composed of lighter C4–C7 hydrocarbons, of which toluene and isopentane are the most abundant species, and atmospheric isopentane in the southeast coastal region may also come from the evaporation of gasoline fuels during the production process of the petrochemical industry. In addition, the source of methylene chloride may be the storage tank emissions from the chlorination plant. It can be seen that changes in atmospheric VOC concentrations in the southeast coastal region are influenced by various sources such as LPG exhaust, oil and solvent volatilization, and industrial production .

3.2. VOCs' Daily Variation Characteristics. The daily variation of alkanes, most olefins, and aromatic hydrocarbons in atmospheric VOCs in the southeastern coastal region shows a typical bimodal feature, with high concentrations in the morning and evening and lower concentrations at noon, see Figure 3. The strong convection in the midday, the boundary layer is elevated, which is conducive to the dilution and mixing of VOCs, and the strong sunlight in the midday consumes a large amount of VOCs in photochemical reactions, resulting in lower concentrations in the midday [9].

Acetonitrile (CH₃CN), a tracer of biomass burning [10], did not vary significantly from day to day, but its concentration tended to increase in the evening, as shown in Figure 3. The concentration of acetonitrile increased significantly in individual evening sampling periods, with high values reaching 2.67×10^{-9} , much higher than the average concentration level, indicating that episodic biomass burning occurred in the evening.

Isoprene is an important indicator of emissions of biogenic (plant-derived) VOCs and its emission rate is dependent on light and temperature [11]. Isoprene is an important indicator of VOCs emissions from biogenic sources (plant sources). The regression results of MACR and MVK with 1,3-butadiene were 0.003 and 0.09, respectively, excluding the factor of motor vehicle exhaust emissions [12], indicating that isoprene and its oxidation products in atmospheric VOCs in the southeast coastal region are mainly from natural sources. The results of the regressions were 0.003 and 0.09, respectively, excluding motor vehicle emissions.

The daily variation of OVOCs (aldehydes and ketones) is characterized by single peaks, with high values lasting for a long time, with higher concentrations between 8:00 and 18:00 and lower concentrations at night, and with little variation in concentration, see Figure 3. For example, acetone is

TABLE 1: Vegetation types and areas in the southeastern coastal zone.

ID	Vegetation type	km ²
1	Evergreen coniferous forest	4
3	Deciduous coniferous forest	3
4	Deciduous broad-leaved forest	9563
5	Thicket	1542
6	Grassland	81998
7	Cultivated land	101681

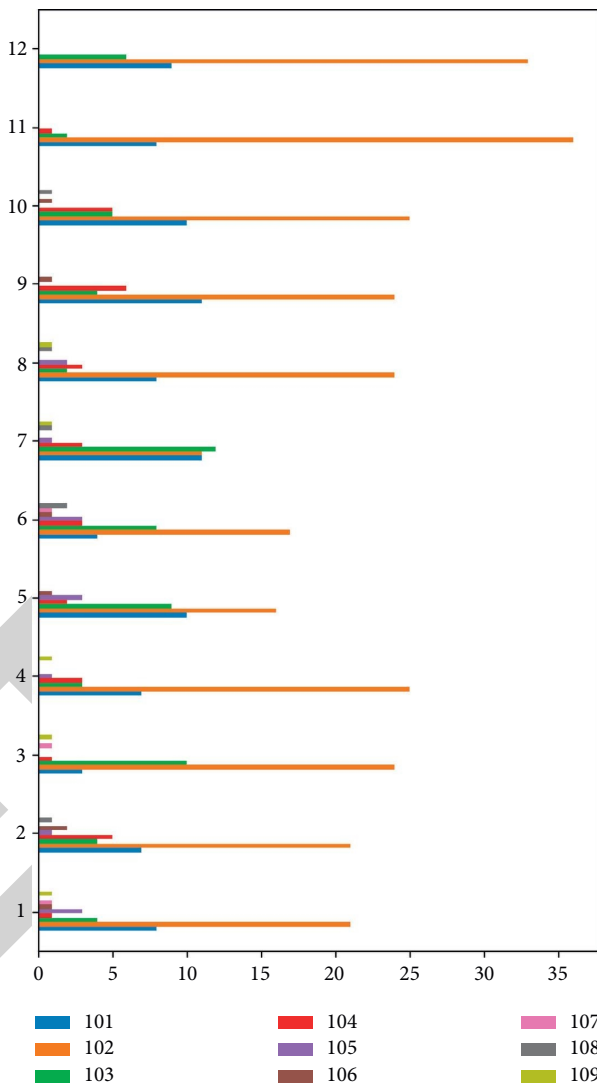


FIGURE 2: Top 10 VOC species in Zhuhai.

the species with the highest volumetric mixing ratio of atmospheric OVOCs in the southeast coastal region, and its source is both primary emissions from petroleum refining and petrochemical compounding processes [13] and secondary production from atmospheric oxidation of

precursors such as propane [14]. Due to the subtropical location of the southeastern coastal region, the strong midday light, long light hours, high temperatures, and strong photochemical reactions, and the long duration of high values of OVOCs, it is suggested that OVOCs in the

TABLE 2: Comparison of VOCs species concentrations between the southeast coastal region and selected cities in China and abroad.

Species	Our study	Guangzhou	Hong Kong	Shanghai	Nanjing	Beijing
Ethane	1.58	3.36	2.34	-	6.97	3.37
Propane	6.05	6.32	3.35	4.81	3.28	3.22
Isobutane	1.88	3.01	2.6	1.43	1.51	1.6
N-butane	3.25	3.69	4.34	2.04	1.69	1.7
Isopentane	1.62	1.05	0.66	2.29	1.12	1.99
N-hexane	0.4	0.62	0.23	0.68	0.67	0.23
2-Methylpentane	0.4	0.61	0.23	0.68	0.34	0.14
Ethylene	1.08	2.78	1.86	-	5.67	4.25
Propylene	0.27	0.69	0.54	0.84	2.45	0.53
Isoprene	0.16	0.07	-	0.12	0.54	0.47
Benzene	0.39	0.95	0.73	1.81	3.14	0.75
Toluene	1.85	4.83	2.56	4.7	2.2	1.02
M/p-Xylene	0.75	0.94	0.60	1.5	0.95	0.29
Dichloromethane	1.42	—	0.90	0.95	—	—
Acetaldehyde	0.70	—	1.92	—	—	—
Acetylene	1.13	2.5	—	—	3.13	—
Acetone	2.59	—	4.15	—	—	—

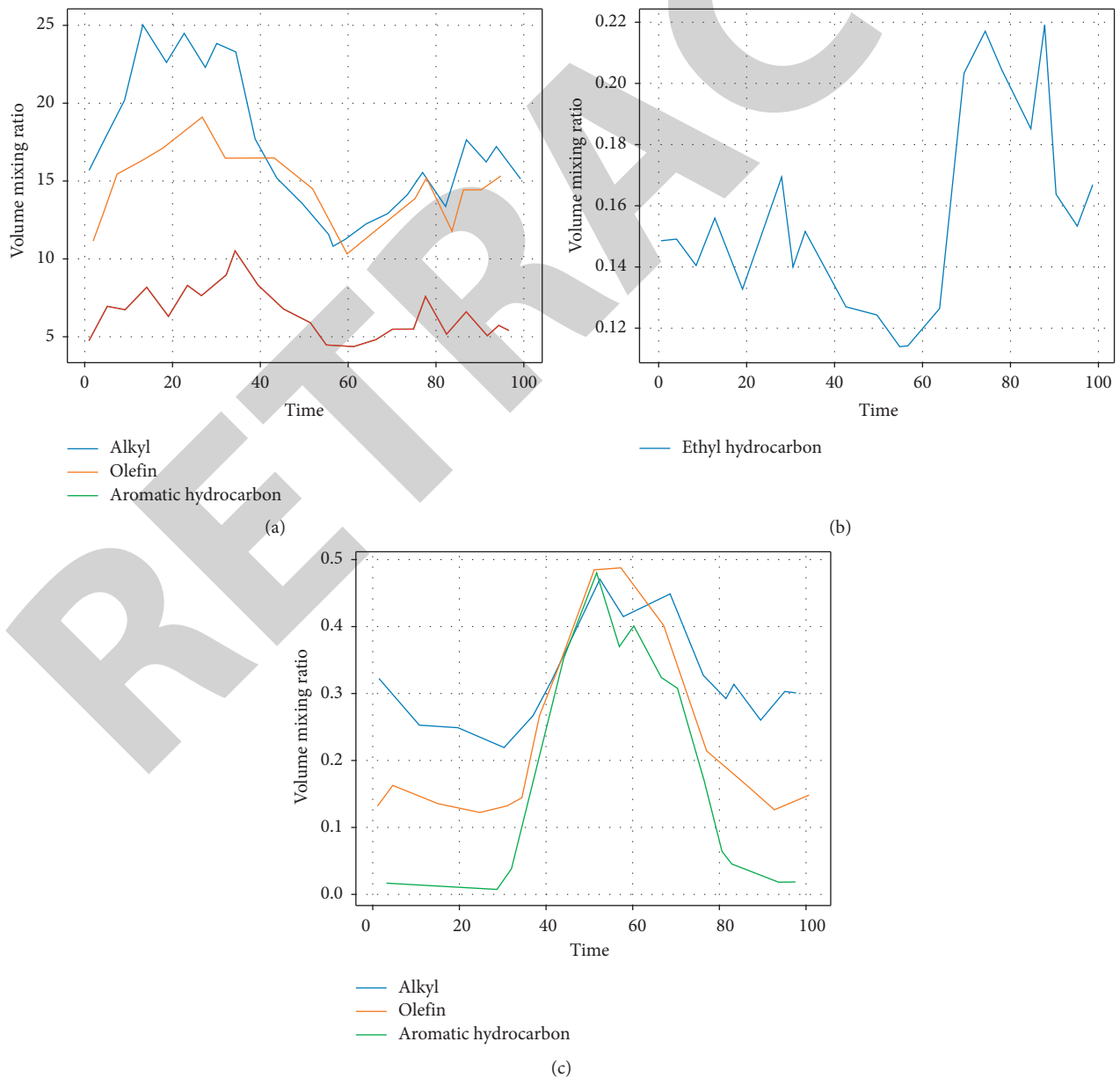


FIGURE 3: Diurnal variation of VOC species in Zhuhai.

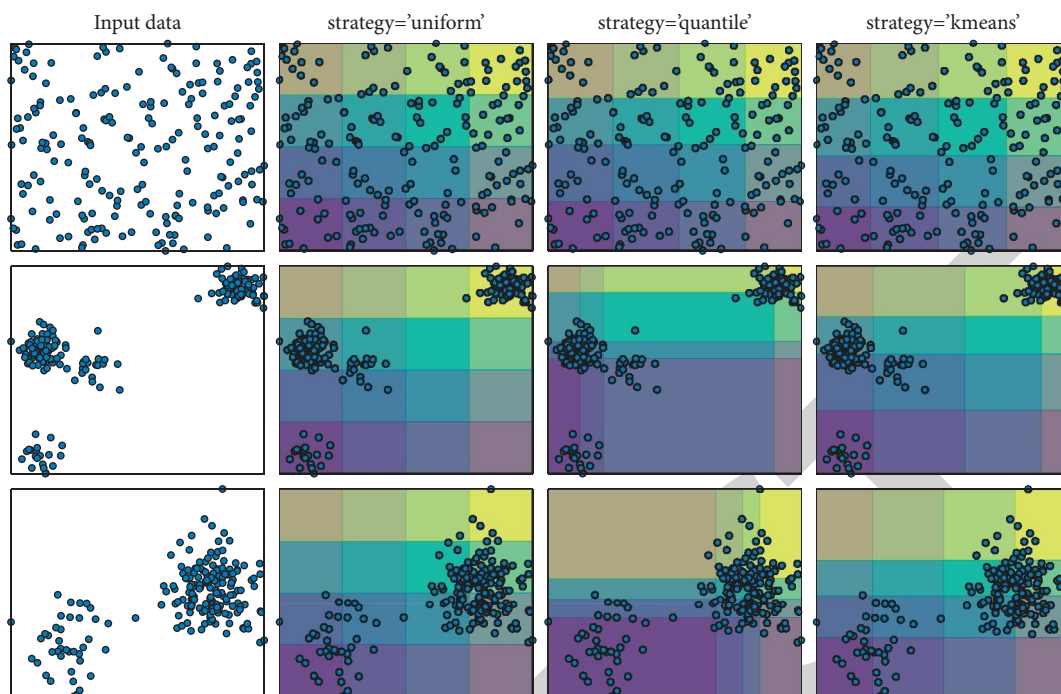


FIGURE 4: Regression analysis between selected species.

southeastern coastal region are mainly derived from secondary production by photochemical reactions, in addition to the effects of primary emissions.

3.3. Source Analysis

3.3.1. Species-Specific Regression Analysis. Studies have shown that the main sources of VOCs can be determined from the regression analysis of tracer compounds and compounds with different lifetimes [15]. Propane is the most concentrated VOC in the atmosphere in the southeast coastal region, with a mean volume mixing ratio of $(6.0 \pm 4.4) \times 10^{-5}$. The regression results between propane and n-butane and isobutane are shown in Figure 4, with R^2 0.57 and 0.78, respectively, and those between ethylene and acetylene (characteristic compounds of combustion and industrial emissions) are shown in Figure 4, with R^2 0.40 and 0.19. Since propane, isobutane and n-butane are all important components of LPG, it is clear that propane in the atmosphere of the Southeast Coastal Region is mainly derived from LPG. volatilization of liquefied petroleum gas (LPG) [16].

Isoprene is mostly emitted from natural sources, with some contribution from motor vehicle exhaust, and 1,3-butadiene is often seen as a marker for motor vehicle emissions. 1,3-butadiene regression results with isoprene are shown in Figure 4, $R^2 = 0.02$, indicating that isoprene in the

atmosphere in the southeast coastal region is mainly emitted from natural sources.

3.3.2. Reverse Trajectory Analysis. The HYSPLIT4.9 inverse trajectory model was used to analyze the inverse trajectories of the air masses during the sampling period. According to the time resolution of the sampling, one track was calculated every 1 h. The inversion time was 72 h and the altitude was 500 m. The track curves during the sampling period were clustered and analyzed, and five types of inversion tracks were obtained. The inland air masses in the northeastern direction dominated the sampling period, accounting for 33% of the total. The proportion of alkanes, olefins, aromatic hydrocarbons, OVOCs, and other VOCs in each trajectory was calculated and the results are shown in Figure 5. The lowest concentration was olefins, which were around 5%. The total concentrations of VOCs measured were significantly higher when the air masses were from inland (Tracks I and II) than when the air masses were from the sea (Tracks III and V). Moreover, anthropogenic VOCs such as aromatic hydrocarbons are higher in absolute concentration and proportion than marine air masses when the air masses are from inland. This indicates that the contribution of inland air masses to VOCs in the southeast coastal region is higher than that of marine air masses and that the influence of inland areas,

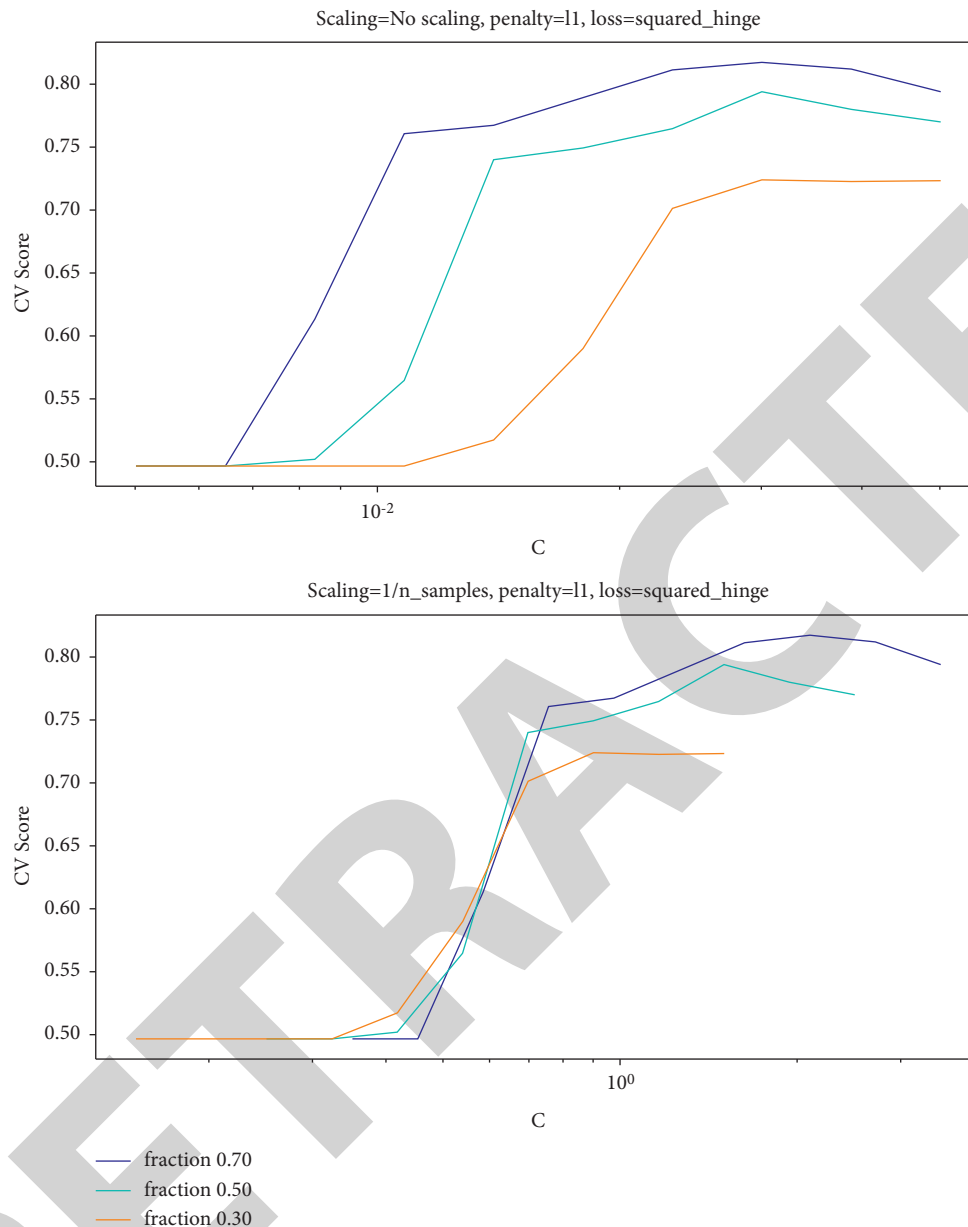


FIGURE 5: Proportion of each VOCs species at different trajectories.

especially the Pearl River Delta region (air mass I), on anthropogenic VOCs in the southeast coastal region is particularly pronounced.

4. Conclusions

In this paper, 96 VOCs were measured in the atmosphere of the southeast coastal region, and their composition, daily trends, sources, and contribution to ozone production were analyzed. The results of the study show that the volume mixing ratio of alkanes is the highest, followed by aromatic hydrocarbons; the daily variation trend of alkanes and aromatic hydrocarbons is obvious, with a bimodal characteristic, and their influence on the ozone potential (OFP) is mainly from aromatic hydrocarbons.

Data Availability

The experimental data used to support the findings of this study are available from the corresponding author upon request.

Conflicts of Interest

The authors declare that they have no conflicts of interest regarding this work.

References

- [1] Z. Niu, H. Zhang, Y. Xu, X. Liao, L. Xu, and J. Chen, "Pollution characteristics of volatile organic compounds in the atmosphere of haicang district in xiamen city, southeast China," *Journal of Environmental Monitoring: Journal of Electron Microscopy*, vol. 14, no. 4, pp. 1145–1152, 2012.

Research Article

Analysis of Aerobics Auxiliary Training Based on Deep Learning

Can Li 

Sports Department of Fuzhou University, Fuzhou 350002, China

Correspondence should be addressed to Can Li; lican1976@fzu.edu.cn

Received 27 January 2022; Revised 11 February 2022; Accepted 14 February 2022; Published 22 March 2022

Academic Editor: Hangjun Che

Copyright © 2022 Can Li. This is an open access article distributed under the Creative Commons Attribution License, which permits unrestricted use, distribution, and reproduction in any medium, provided the original work is properly cited.

With the in-depth integration of information technology and subject teaching, it is also an inevitable trend to apply modern information technology to aerobics teaching. In this paper, the N-best algorithm is used in the video and real-time camera in aerobics, so that the human posture parameters in a single-frame image can be estimated. By using the relative position and motion direction of each part of the human body to describe the characteristics of aerobics, the Laplace scoring method is used to reduce the dimension of the data, and the discriminant human motion feature vector with a strong local topological structure is obtained. Finally, the iterative self-organizing data analysis technology (ISODATA algorithm) is used to dynamically determine the keyframe. In the aerobics video keyframe extraction experiments, the ST-FMP model improves the recognition accuracy of nondeterministic body parts of the flexible hybrid articulated human model (FMP) by about 15 percentage points and achieves 81% keyframe extraction accuracy, which is better than the keyframe algorithms of KFE and motion block. The proposed algorithm is sensitive to human motion features and human pose and is suitable for motion video annotation review.

1. Introduction

In the twenty-first century, modern information technology has been widely used in the field of teaching, and multimedia and network technologies have played a role in achieving educational teaching reform, which has brought opportunities for today's physical education teaching reform [1]. In the practice of physical education, giving full play to the advantages of digitalization, networking, intelligence, and multimedia of information technology has given life to physical education classroom teaching, stimulated students' enthusiasm, and autonomy in learning physical education knowledge and skills and has had a multiplier effect on improving the quality of physical education classroom teaching. Modern information technology serves physical education classroom teaching, which plays a very important role in implementing the new curriculum standards for physical education and improving the quality of physical education classroom teaching [2].

Aerobics is an important element in physical education. The teaching of aerobics is a very technical and contemporary practical class. The use of modern information technology can disseminate information to students through

a variety of media such as images, sound, animation, and text, thus making the process of teaching aerobics simple, difficult, and easy, and showing students the teaching content that teachers cannot teach with words in a vivid way, and can also open up students' horizons [3].

Demonstration is a method often used in aerobics teaching, and it is the teacher rehearses the action for students to see, so that students have a visual impression of the action, to facilitate students to imitate and learn the common method [4].

The use of multimedia means to improve the teaching of movement demonstration can make a fundamental change in the demonstration. The use of multimedia demonstration teaching not only has the characteristics of image, intuitive, vivid, and can be achieved through the media size, distance, fast, and slow changes for students to understand the teaching demonstration, but also has the teacher in the aerobics theory class teaching difficult to say clearly that students are not easy to grasp, difficult to understand the content of aerobics knowledge in front of the students, which helps to teach the key and difficult points to reach and solve [5, 6].

It is not easy for students to capture the details of the action. Therefore, to understand the essence of these actions,

multimedia technology needs to be used to assist students in understanding. The use of multimedia technology to assist teaching can visually show the decomposition and overall movements for students and synchronized with the teacher's detailed language explanation, and students can easily understand the main points of the movement, laying the foundation for mastering the movement technology [7, 8]. Therefore, teachers inevitably encounter difficulties in the actual work of teaching perfunctory or errors. The application of modern information technology for teaching can avoid the above problems, reduce the teacher's work intensity and pressure, make up for the teacher's own lack of ability, present to students a modern, advanced, and accurate demonstration of technical movements, and give full play to the teacher's leading role in teaching.

The use of modern information technology in aerobics teaching can create a good teaching atmosphere, a high level of competitive technology, a beautiful demonstration of movement techniques, vivid images, and so on, making teaching vivid, lively, and fashionable, leaving a deep and unforgettable impression on students, stimulating their interest in learning and desire for knowledge, making the learning content intuitive and easy to understand, and reducing the difficulty of learning [9]. For the video and real-time camera of aerobics, this paper uses the N-best algorithm to estimate the human pose parameters in a single frame; the iterative self-organizing data analysis technique (ISODATA) algorithm is used to determine the keyframes dynamically. In the aerobics video keyframe extraction experiments, the ST-FMP model improves the recognition accuracy of nondeterministic body parts of the flexible hybrid articulated human model (FMP) by about 15 percentage points [10].

2. Combination of Aerobics Knowledge

2.1. Teaching Tasks of Aerobics. Task design and establishment are the first step in building the network teaching mode of college aerobics, using the teaching content to the network platform to design various teaching tasks. Here, taking the teaching of mass aerobics as an example, the teacher can introduce the collective competition mode in the teaching process, combining with the competition mode to first stimulate students' enthusiasm for learning aerobics [11]. First of all, the teacher will make a microvideo according to the requirements of the designed group competition mode, show it to the students through the multimedia platform, so that the students can understand the aerobics learning tasks intuitively, and, at the same time, give the students time to discuss and ask questions to the teacher, increasing the interactive communication link before the class.

The teacher will then design a teaching module to show all the decomposition teaching videos of each movement of the aerobics course, and let students watch the decomposition movements of aerobics through the operation of the computer learning platform, choose their favorite and suitable group of aerobics movements, and give feedback to the teacher by voting, while the teacher will choose which

group of aerobics movements to teach in class according to the students' voting results. After the movements are taught, competition protocols are created. Movement routines are choreographed for students, and competitions are organized to develop more in-depth teaching content [12].

2.2. Competition Process. After specifying the designated tasks, we should prepare to start the competition process, determine a reasonable competition plan for students, decompose aerobics movements around specific knowledge points and considerations, and develop independent aerobics competition protocols and competition rules for students. Finally, the most organized teaching program is chosen to start the competition protocol, and the subtask classification menu of aerobics teaching is set in combination with the Internet search process, and the process related to aerobics competition is clarified in combination with the menu content to ensure the independence of the teaching design program [13].

2.3. Optimized Movement Choreography. After completing the teaching preparation phase on the Internet platform, students should be grouped heterogeneously according to their actual learning status, and each group should form a team to participate in the teacher-designed competition. After the grouping, students also have to rehearse through aerobics microvideo demonstration teaching to form a tacit understanding between each other and to guide them in the aerobics training practice process [14]. After watching the demonstration video, the teacher will give a focused lecture for the students, combined with offline teaching, to form an intuitive impression of aerobics-related movements through hands-on demonstration and optimize the students' aerobics-related skills ability by combining online and offline [15].

2.4. Completion of the Contest Content. In the final aerobics competition stage, the teacher will realize to explain the rules and precautions related to the competition for students and emphasize the importance of joint cooperation within the group by mobilizing the participation of group students. After the competition, the teacher will enter all students' competition results into the online platform database for subsequent teaching assessment use [16].

3. Data Acquisition

Students' formation and mastery of motor skills are a direct reflection of the effect of aerobics teaching. Therefore, it is the key and difficult point in teaching to let students master technical movements and develop motor skills as soon as possible. Traditional teaching uses demonstration, explanation, and practice, but it is difficult to break through the detailed part of each link, and the teaching effect is not good. If modern information technology is used to assist teaching, it can make up for the

shortcomings of traditional teaching, taking the teaching experiment as an example: the following is the result of the comparison experiment between teaching with modern information technology (1 group) and traditional teaching (2 groups) as shown in Table 1.

The above experimental results prove that, with no significant difference in the students' own quality between the two groups, the performance of group 1 students' assessment is significantly better than that of group 2. We can clearly see the advantages of using multimedia information technology to assist teaching.

In the learning process of motor skills, the application of information technology discipline integration can increase the amount of teaching information, stimulate students' senses in many aspects such as visual, auditory, and tactile senses, and deepen students' understanding and mastery of the structure of technical movements and the inner connection between movements, thus promoting the formation and mastery of students' motor skills [17]. In addition, students can also improve their ability to analyze and solve problems on the basis of understanding movement techniques and develop their ability to investigate and learn [18].

The teaching of aerobics is highly flexible and requires high sensitivity, coordination, and appreciation of students. The teaching process should take students as the starting point, keep abreast of students' need and acceptability, adjust the teaching plan at any time, and feedback any new problems found [19]. It is important to be relevant to different individuals, rather than relying too much on modern information technology and indoctrination in a uniform manner. The teaching of aerobics is mainly through the teacher's body language explanation, demonstration, and students' repeated physical exercises to develop the body and enhance physical fitness, the course is practical, and the teaching process includes the teacher's emotional expression and the emotional communication between teachers and students, which is the reason why the traditional teaching mode cannot be completely replaced [20]. The use of modern information technology in classroom teaching is very significant, and the effect is quite obvious. At the same time, the use of modern information technology in the teaching of aerobics class must take into account its advantages and disadvantages [21]. Therefore, only by reasonably combining the two can we create a lively classroom teaching atmosphere, stimulate students' interest in learning, breakthrough teaching difficulties, enable students to acquire knowledge through multiple senses, enhance understanding and memory, provide feedback to improve motor skills, and improve students' self-improvement, so that modern information technology can better serve aerobics teaching and bring a qualitative leap to aerobics teaching [22].

3.1. Program of This Article. In this paper, we propose a motion video keyframe extraction process based on the ST-FMP model and dynamic clustering, referred to as the ST-FMP algorithm.

First, the ST-FMP model is used to estimate the human pose parameters of the r th frame image to obtain the set of human parts $p = \{p_u | u \in V\}$ by Eq. and obtain the human motion vector by using Eq., and that is,

$$f_r = (f_{r1}, f_{r2}, \dots, f_{rK}), \quad (1)$$

where K equals to $3d$; f_{ri} denotes the number of motion features; I_r denotes the motion feature of the i -th body part in the motion video.

Then, all motion vectors of the motion video are combined to obtain the combined vector of motion features; that is,

$$f_{\text{com}} = (f_1, f_2, \dots, f_{KT}), \quad (2)$$

where T denotes the number of frames of the motion video. Then, the LS algorithm is used to calculate the Lr score of f_{com} to obtain the discriminative motion feature vector, denoted as f_{sub} .

Finally, the feature curve of f_{sub} is constructed by using the Lr component vector, and the local extreme points on the feature function are selected as the set of candidate keyframes by the principle of extreme value determination, which is denoted as \tilde{f}_c .

In practice, it has been found that when the time interval between some candidate keyframes in \tilde{f}_c is short or the difference in pose parameters is small, it leads to a large amount of redundant data in f_{com} ; conversely, it reduces the motion representation capability of \tilde{f}_c . Therefore, a keyframe selection process is needed to filter out keyframes. Considering the good adaptiveness of the dynamic clustering method ISODATA algorithm [23], this paper selects this algorithm for \tilde{f}_c clustering selection.

4. Experimental Results and Analysis

In this paper, the keyframes of aerobics action video are used as an example for simulation experiments, and the experimental results are compared with the manual extraction and the extraction results of the latest motion video keyframe algorithm [24].

4.1. Experimental Data Samples and Feature Training.

First, three students were invited to perform 120 s of popular aerobics movements twice, and the videos were recorded with a resolution of 640×480 using a common webcam at a sampling rate of 20 frames/s. Then, 300 frames from each of the six sets of videos were selected as experimental data starting from the 10th rhythmic beat; finally, each joint position was manually marked in 1,800 frames as shown in Figure 1. Finally, 13 joint positions of each aerobic movement were marked manually in 1,800 frames as shown in Figure 1. In the simulation experiment, 900 frames of each of the first and second movements were selected as the training sample data set and the test sample data set.

In the training process, in order to enrich the human action characteristics of the positive samples, first, image operations such as rotation (at four angles of -15° , -7° , 5° , 7° , 5° , and 15°) and mirror image are used to expand 900 training samples to

TABLE 1: Comparison table of aerobics technical assessment results.

Group	Total number	Excellent		Good		Secondary		Pass		Fail	
		Number of people	%	Number of people	%	Number of people	%	Number of people	%	Number of people	%
Group 1 technology	40	10	24	10	26	12	30	7	18	1	2
Group 2 traditional	40	5	14	5	14	9	19	14	35	7	18

10×900 frame positive sample set, recorded as Φ_p^* . Then, by adding key points at the midpoint of two adjacent joint positions, the coordinates of 26 flexible human body parts of each image in Φ_p^* are calculated. Finally, the ho g feature of each human body part is calculated with a ho g unit of 5×5 pixels, and the parameters such as $\varphi(I, l_u)$ and $\psi(l_u - l_v)$ in equation (3) are determined by linear support vector machine.

4.2. Evaluation Criteria. All keyframes in the test sample set are manually extracted, and the commonly used keyframe extraction accuracy as the algorithm performance evaluation criterion, that is,

$$\text{accuracy} = \frac{\sum_{i=1}^m \delta(f_i, r_i)}{n}, \quad (3)$$

where n and m represent the number of manually and algorithmically extracted keyframes, respectively; f_i and r_i represent the algorithmically and manually extracted keyframes; $\delta(\cdot)$ is the similarity function between f_i and r_i ; and the value of $\delta(\cdot)$ is 1 when f_i and r_i are the same; otherwise, it is 0.

4.3. Analysis of Experimental Results

4.3.1. Comparison of the Effectiveness of Spatio-Temporal Feature Embedding in Nondeterministic Parts. In order to test the accuracy of the human body parts in video with the embedding of spatio-temporal features of nondeterministic parts, three different ST-FMP model implementations were used to conduct comparative experiments for two human body parts, elbow, and knee, according to different error pixel thresholds, and the experimental results are shown in Figure 2.

Compared with the FMP model, the accuracy of nondeterministic parts within a certain pixel error range is significantly improved when the ST-FMP algorithm is used for human pose estimation in motion video. For example, with an error threshold of 20 pixels, the accuracy of the ST-FMP algorithm for the elbow and knee is about 15 and 19 percentage points higher than that of the FMP model, respectively. However, the difference in accuracy is not significant when the pixel error threshold is larger (e.g., greater than 40 pixels) or smaller (e.g., greater than 10 pixels). Figure 2 also shows that the recognition accuracy of the elbow and wrist (knee and ankle) is higher than that of the direct FMP model but lower than that of the ST-FMP algorithm when only the temporal continuity of the nondeterministic parts of the upper (lower) limbs is maintained. The experimental results show that the ST-FMP algorithm



FIGURE 1: Aerobics posture.

significantly improves the recognition performance of nondeterministic parts in motion videos by optimizing the body part recognition results with the local time continuity constraint of body parts.

This paper also compares the performance of the FMP model [25] and the ST-FMP [26] models and their different implementations for motion video keyframe extraction. The experimental results are shown in Figure 3. From Figure 3, we can find that (1) when the accuracy error is less than 30 pixels, the accuracy of the ST-FMP algorithm is higher and more stable, with an average improvement of about 11 percentage points than the keyframe algorithm using FMP, and the keyframe extraction accuracy of the FMP model is still improved by about 3 percentage points when only the temporal continuity constraint of the nondeterministic parts of the upper limb (lower limb) is added; (2) when the error accuracy is greater than 35 pixels, the accuracy of ST-FMP algorithm is more stable than that of the FMP algorithm; (3) when the error accuracy is greater than 35 pixels, the performance of ST-FMP algorithm still improves compared with the FMP model, but the accuracy is reduced by about 15 percentage points.

Meanwhile, when the accuracy error is 30 pixels and the keyframes are extracted by the ST-FMP algorithm with a different number of motion features, the accuracy curve of the algorithm does not fluctuate drastically in the interval from 15 to 60 motion features, and the performance is stable, as shown in Figure 4.

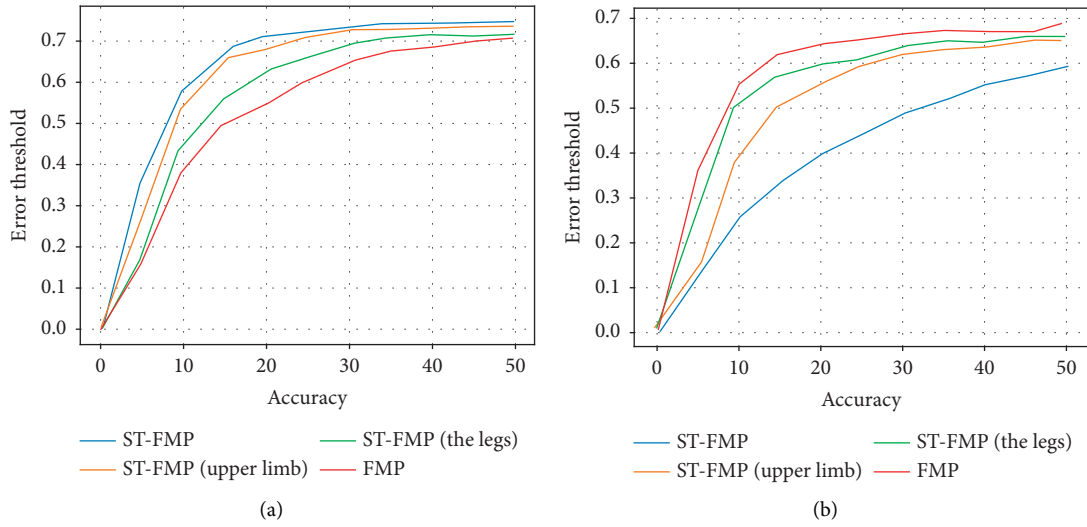


FIGURE 2: Comparison of body part recognition accuracy under different ST-FMP implementations.

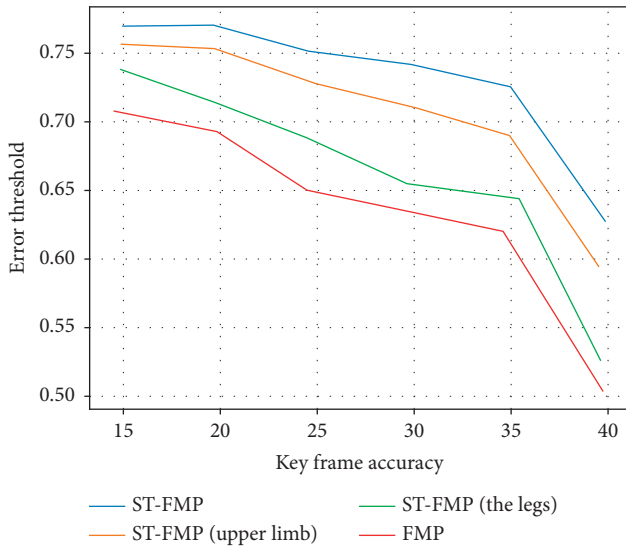


FIGURE 3: Experimental results of keyframe extraction based on FMP and ST-FMP.

The above experimental results show that the ST-FMP algorithm is sensitive to the human pose estimation results and the local topology of the human body, and the spatio-temporal constraint of the nondeterministic parts is maintained for the keyframe extraction performance.

4.3.2. Keyframe Algorithm Performance Comparison. In order to compare the performance of the keyframe algorithm, the simulation experimental results of the ST-FMP algorithm are compared with the running results of the priority-based action video keyframe extraction algorithm (abbreviated as KFE algorithm) of the literature [26] and the motion block keyframe extraction algorithm (abbreviated as motion block algorithm) of the literature [27], as shown in Table 2. The experimental results in Table 2 show that the ST-FMP algorithm outperforms the

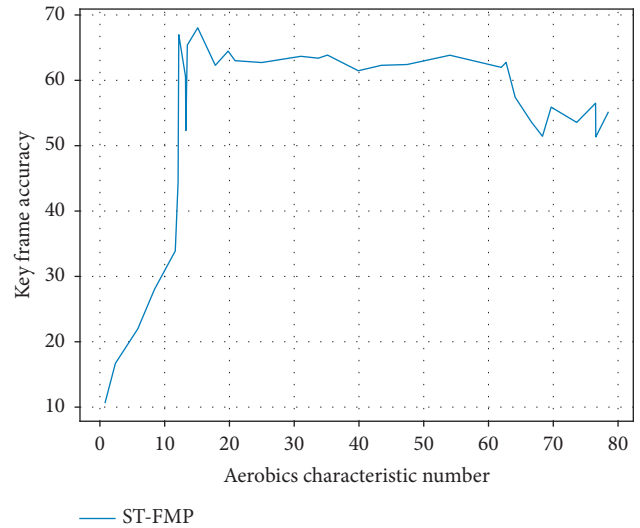


FIGURE 4: Comparison of keyframe accuracy with a different number of motion features.

other two algorithms in terms of accuracy and recall. First, the accuracy of the ST-FMP algorithm is about 18 and 26 percentage points higher than that of the KFE algorithm and the motion block algorithm, respectively; the KFE algorithm uses the motion direction of 16 predefined blocks to represent human motion features, while the ST-FMP algorithm uses the first 15 LS human motion pose feature values of each action video to represent human motion. Therefore, the ST-FMP algorithm uses motion feature vectors with less redundancy, less noise, and accurate local motion representation of human parts, which are beneficial for improving the accuracy of keyframe and action recognition [28].

Secondly, Table 2 also shows that the recall rate of the ST-FMP algorithm is also significantly better than the other two algorithms, with an average of about 23 and 13 percentage points higher, respectively. Kph algorithm and motion block

TABLE 2: Performance comparison of different keyframe extraction algorithms.

Algorithm	Accuracy	Recall
ST-FMP algorithm	0.81	0.82
KFE algorithm	0.63	0.59
Motion block algorithm	0.55	0.69

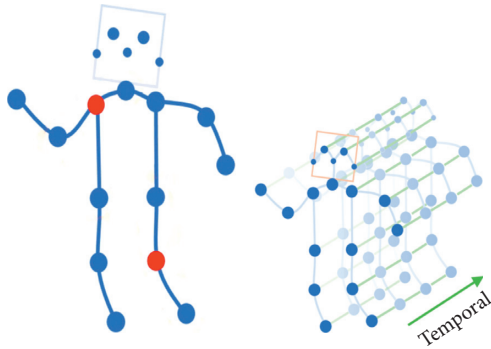


FIGURE 5: Effect of aerobics joint recognition.

algorithm are both keyframe techniques based on the difference of underlying image features, and they filter keyframes by comparing motion changes in different regions of the image using specific thresholds. The ST-FMP algorithm describes the local motion characteristics of human body parts, which is essentially a semantic model that can analyze and understand human body movements in motion videos at a higher level, such as the participating parts of human body movements and their motion change trends, and use semantic rules such as human pose similarity to filter keyframes, which can obtain more accurate keyframe results in line with people's cognitive process [29, 30].

4.3.3. Aerobics Auxiliary Effect. As illustrated in Figure 5 aerobics results, the ST-FMP algorithm is closer to the manual extraction results and more suitable for keyframe-based action video review because it not only has a strong ability to express the local topology of body part actions but also has the ability to support keyframe screening based on semantic rules. At the same time, ST-FMP splits the human body parts into different flexible components, recognizes the human pose through the local topology of the flexible components, and reduces the continuous error of human pose estimation with the help of temporal feature edge constraints, so it has strong robustness in complex scenes.

5. Conclusions

For aerobics video and real-time camera, the N-best algorithm is used to estimate the human pose parameters in a single frame; in the aerobics action video keyframe extraction experiment, the ST-FMP model improves the recognition accuracy of nondeterministic body parts of the flexible hybrid articulated human model (FMP) by about 15 percentage points and achieves 81% keyframe extraction accuracy.

Data Availability

The experimental data used to support the findings of this study are available from the corresponding author upon request.

Conflicts of Interest

The authors declare that they have no conflicts of interest regarding this work.

References

- [1] B. A. Martin, R. H. Bruskiwitz, and B. A. Chewning, "Effect of a tobacco cessation continuing professional education program on pharmacists' confidence, skills, and practice-change behaviors," *Journal of the American Pharmacists Association*, vol. 50, no. 1, pp. 9–18a, 2010.
- [2] C. R. Dass, "Lipoplex-mediated delivery of nucleic acids: factors affecting in vivo transfection," *Journal of Molecular Medicine*, vol. 82, no. 9, pp. 579–591, 2004.
- [3] Y. Rice, M. Deletter, L. Fryman, E. Parrish, C. Velotta, and C. Talley, "Implementation and evaluation of a team simulation training program," *Journal of Trauma Nursing*, vol. 23, no. 5, pp. 298–303, 2016.
- [4] G. Maria, G. Dimitrios, and Y. Georgia, "The psychological mood of adult participants in aerobics, Greek traditional dances and muscle strengthening programs," *International Journal of Sport Management Recreation & Tourism*, vol. 4, no. c, pp. 40–51, 2009.
- [5] M. R. Maurya, S. Dhaka, and F. Avecilla, "Synthesis, characterization, reactivity and catalytic activity of dioxidomolybdenum(VI) complexes derived from tribasic ONS donor ligands," *Polyhedron*, vol. 81, pp. 154–167, 2014.
- [6] J. Masahiro and T. Kikushima, "The implementation and evaluation of a training program for developing undergraduates' critical thinking and attitudes," *Educational technology research*, vol. 41, no. 1, pp. 91–103, 2019.
- [7] J.-P. Hatala and J. C. Gumm, "Managing organizational cultural influences during the implementation of competency-based training," *Advances in Developing Human Resources*, vol. 8, no. 2, pp. 229–246, 2006.
- [8] M. Baruth, S. Wilcox, M. Laken, M. Bopp, and R. Saunders, "Implementation of a faith-based physical activity intervention: insights from church health directors," *Journal of Community Health*, vol. 33, no. 5, pp. 304–312, 2008.
- [9] P. Runkle, L. Carin, and L. Couchman, "Multiaspect target identification with wave-based matched pursuits and continuous hidden Markov models," *IEEE Transactions on Pattern Analysis and Machine Intelligence*, vol. 21, no. 12, pp. 1371–1378, 2002.
- [10] M. Marilyn, S. A. Billinger, J. J. Eng, and R. Macko, "Aerobic exercise recommendations to optimize best practices in care after stroke: AEROBICS 2019 update," *Physical Therapy*, no. 1, p. 1, 2019.
- [11] I. A. Doush, F. Alkhateeb, and A. H. Gharaibeh, "A novel Arabic OCR post-processing using rule-based and word context techniques," *International Journal on Document Analysis and Recognition*, vol. 21, no. 1-2, pp. 77–89, 2018.
- [12] J. D. Brusenhan and M. T. Saul, "Aerobics to the rescue," *Pollution Engineering*, vol. 38, no. 1, pp. 16–17, 2006.
- [13] H. Rahimian, M. Kazemi, and A. Abbaspour, "Design, explanation, and evaluation of training model structures based on learning organization—in the cement industry with a

- nominal production capacity of ten thousand tons,” *International Education Studies*, vol. 10, no. 1, 2016.
- [14] B. Hoare and A. A. Tseytlin, “On integrable deformations of superstring sigma models related to $AdS_n \times S_n$ supercosets,” *Nuclear Physics B*, vol. 897, no. C, pp. 448–478, 2015.
- [15] L. M. Schnapp, M. Vaught, D. R. Park, G. Rubinfeld, R. B. Goodman, and L. D. Hudson, “Implementation and impact of a translational research training program in pulmonary and critical care medicine,” *Chest*, vol. 135, no. 3, pp. 688–694, 2009.
- [16] O. Dangles, F. C. Carpio, M. Villares et al., “Community-based participatory research helps farmers and scientists to manage invasive pests in the Ecuadorian andes,” *Ambio*, vol. 39, no. 4, pp. 325–335, 2010.
- [17] D. Woodruff and S. Yekhanin, “A geometric approach to information-theoretic private information retrieval,” *SIAM Journal on Computing*, vol. 37, no. 4, pp. 1046–1056, 2007.
- [18] S. A. Abhayawansa and A. Subhash, “A review of guidelines and frameworks on external reporting of intellectual capital,” *Journal of Intellectual Capital*, vol. 15, no. 1, pp. 100–141, 2014.
- [19] S. Khan, O. Kintzel, and J. Mosler, “Experimental and numerical lifetime assessment of Al 2024 sheet,” *International Journal of Fatigue*, vol. 37, pp. 112–122, 2012.
- [20] C. Sezer, “An analysis on relations between implementation of training activities and HRM organization in service businesses: a sample in hotels,” *Procedia - Social and Behavioral Sciences*, vol. 1, no. 1, pp. 2385–2389, 2009.
- [21] S. Supari, I. Syafaruddin, I. M. Y. Negara, M. Ashari, and T. Hiyama, “RBFN based efficiency optimization method of induction motor utilized in electrically driven marine propellers,” *IEEE Transactions on Industry Applications*, vol. 131, no. 1, pp. 68–75, 2011.
- [22] V. Podrázsk, R. ermák, D. Zahradník, and J. Koba, “Production of Douglas-Fir in the Czech Republic based on national forest inventory data,” *Journal of Forest Science*, vol. 59, no. 10, pp. 398–404, 2013.
- [23] L. C. Frattarelli and R. Kasuya, “Implementation and evaluation of a training program to improve resident teaching skills,” *American Journal of Obstetrics and Gynecology*, vol. 189, no. 3, pp. 670–673, 2003.
- [24] M. S. Węglowski and S. Dymek, “Badanie procesu tarciowej modyfikacji warstwy wierzchniej odlewniczego stopu aluminium AlSi9Mg,” *Inzynieria Materiaowa*, vol. 32, pp. 785–788, 2011.
- [25] M. Bopp, S. Wilcox, M. Laken et al., “Using the RE-AIM framework to evaluate a physical activity intervention in churches,” *Preventing Chronic Disease*, vol. 4, no. 4, p. A87, 2007.
- [26] R. G. Tabak, M. M. Padek, J. F. Kerner et al., “Dissemination and implementation science training needs: insights from practitioners and researchers,” *American Journal of Preventive Medicine*, vol. 52, no. 3, pp. S322–S329, 2017.
- [27] R. Dittmann, F. Froehlich, R. Pohl, and M. Ostrowski, “Optimum multi-objective reservoir operation with emphasis on flood control and ecology,” *Natural Hazards and Earth System Sciences*, vol. 9, no. 6, pp. 1973–1980, 2009.
- [28] P. Rouby, A. Hollebecque, R. Bahleda et al., “Communication en oncologie dans le cadre d’essais thérapeutiques de phase I: mise en œuvre et évaluation d’un programme de formation,” *Bulletin du cancer*, vol. 102, no. 2, pp. 174–181, 2015.
- [29] D. R. Burwen, D. H. Galusha, J. M. Lewis et al., “National and state trends in quality of care for acute myocardial infarction between 1994-1995 and 1998-1999,” *Archives of Internal Medicine*, vol. 163, no. 12, pp. 1430–1439, 2003.
- [30] C. Chen, “Research on aerobics training and evaluation method based on artificial intelligence-aided modeling,” *Scientific Programming*, vol. 2021, Article ID 9545909, 10 pages, 2021.

Research Article

Research on System Economic Operation and Management Based on Deep Learning

Wangtao,¹ Zhenzhu Zheng,² Peiyuan Wang,³ and Xiaobin Liu ^{4,5}

¹National University of Malaysia, Bangi Selangor 43600, Malaysia

²University of Malaysia, Kuala Lumpur 59200, Malaysia

³Wenzhou-KEAN University, Wenzhou 325000, China

⁴Qingdao Conson Development (Group) Co.,Ltd, Qingdao 266071, China

⁵Shandong University, Jinan 250100, China

Correspondence should be addressed to Xiaobin Liu; zrwang@sdu.edu.cn

Received 17 December 2021; Revised 10 February 2022; Accepted 11 February 2022; Published 19 March 2022

Academic Editor: Hangjun Che

Copyright © 2022 Wangtao et al. This is an open access article distributed under the Creative Commons Attribution License, which permits unrestricted use, distribution, and reproduction in any medium, provided the original work is properly cited.

It is of great significance to accurately predict the operation of the system economy, analyze the gains and losses of macrocontrol policies, evaluate the operation quality of the economic system, and correctly formulate the future development plan and strategy. This paper introduces the deep belief network, which has attracted much attention in the field of deep learning in recent years, into the research of system economic operation and management. This method solves the problems of slow training and learning speed, easy to fall into local minima and insufficient generalization of BP artificial neural network in the research of system economic operation and management. Taking the consumer price index and total import and export volume of F Province as the research object, the experiment proves that DBN has better application in system economic operation and management than BP neural network and vector autoregressive analysis. This paper analyzes and compares the modeling performance of DBN, BP neural network, and VaR method from many aspects, such as prediction accuracy, training convergence speed, and pretraining with or without samples. Relevant empirical results show that DBN has better economic prediction performance than BP neural network and ver. On the other hand, DBN can effectively use nonstandard samples to pretrain network weight parameters. Therefore, DBN is a better operation and management modeling means of economic system, with excellent practicability and application, and is expected to be popularized and applied in the field of economic forecasting.

1. Introduction

In order to correctly judge the trend of system economy, analyze the gains and losses of macrocontrol policies, evaluate the operation quality of economic system, and correctly formulate future development plans and strategies, it is also of guiding value to the investment plans of enterprises and individuals [1]. Especially this year is the beginning year of the “14th Five-Year Plan,” and China’s economy is in an important period of “climbing over the ridge” and “tackling key problems and transforming.” The economic pressure is still relatively large, and the uncertain factors facing economic operation and management are increasing. In such an important period, through the

establishment of scientific prediction model, the current economic development trend is quantitatively analyzed and predicted by using historical data. However, most of the traditional economic models are linear models [2]. This model has certain economic forecasting ability, but it also has obvious shortcomings that it is difficult to reflect the nonlinear relations widely existing in economic systems. Economic system is very complex, with many internal influencing factors, strong combination, time-varying, nonlinear and other characteristics, which is very challenging for modeling and forecasting of economic system. Deep learning embodies characteristic learning, and maps samples to new spaces through characteristic transformation of each layer to promote prediction. Features obtained

through deep learning are more profound in the nature of data, so they can effectively improve the performance of applications, such as regression and classification or prediction. Therefore, it is of more practical significance to establish a scientific prediction model through deep learning [3] and use historical data to quantitatively predict the current economic development trend of the system, which is convenient for the operation and management research of the system economy.

Research and investment are the foundation of economic development, so it is particularly important to measure economic well-being comprehensively and accurately. There is no similar measure in many local-level regions. We use the training deep learning model to predict 20,000 African villages to investigate their asset estimates [4]. Macroeconomic forecasting can predict the future economic situation, and also play a directional role in the formulation and implementation of economic policies, so its accuracy is required. There are many prediction models in previous studies, but they are not well used because of their low accuracy and narrow application area. In order to better predict the future global economic prospects, we put forward a new GDP growth prediction model. In the experiment, we collected 70 countries as samples and adopted different methods to realize a high-precision model, that is, deep neural decision tree. The results show that this model has a potential impact on the adequacy of macroeconomic policies and creates a new method and breakthrough for GDP growth prediction [5].

Compared with the traditional machine learning model, the deep learning model has better prediction performance, and it is undergoing great changes at present. However, there are not many works using deep learning in our actual science, so we urgently need to review the research of deep learning in various fields, let researchers and actual operators know its advantages, and then encourage its use. In this process, we provide them with guidance and enlightenment on the business analysis ability of deep learning [6]. In this paper, the proposed method is described according to the corresponding theoretical requirements, and the solution of deep learning model is adopted to solve it. However, the deep learning method in the experiment has good experimental results, and all the proposed methods are based on the deep learning method to explain the theoretical model in detail.

2. Deep Learning

2.1. Neural Networks. The human brain is made up of tens of billions of nerves. The human brain does not superimpose the received information, but after the sum of the superimposed values exceeds the set threshold, neurons send their own energy to other connected neurons. Our human brains learn by regulating the number and intensity of connections between neurons. In the field of machine learning, a neural network model is developed according to the nervous system structure and working mechanism of human brain, which is suitable for multielement nonlinear fuzzy problems, such as distributed memory, parallel computing and adaptive

learning ability [7]. Therefore, it is especially suitable for the research in the field of system economic operation and management.

Compared with previous methods, deep learning has been greatly improved in the fields of sound, image and pattern recognition [8]. This is an integral part of learning multiple features, and each level learns the form of feature expression. In recent years, Deep Belief Networks have been widely used and achieved very good results [9]. In order to better understand the following chapters, this chapter provides the basic principles of BP neural network and convinced network.

2.2. Principle of BP Neural Network. In 1989, Robert proved that the continuous function existing in the closed interval can be approximately represented by BP neural network including hidden layer [10,11], so BP neural network including three layers allows the construction from arbitrary input (m-dimension) to output (n-dimension) as shown in Figure 1.

BP algorithm is the most commonly used algorithm in neural network model learning. BP algorithm is based on supervised learning algorithm [12, 13].

The specific process is as follows:

It is assumed that the neural network is an I input unit and a K output unit, the implicit layer is a layer, and the J unit is shared. The formula for the sum of squared errors is as follows.

$$E = \frac{1}{2} \sum_{k=1}^k (d_k - o_k)^2. \quad (1)$$

Here, $o_k = f(\text{net}_k)$ is the actual output value of neuron k in the output layer; d_k is the expected output value of neuron k in the output layer; and y_j is the output value of hidden layer neuron j .

For the E value, in order to achieve the goal of the ideal value, it is necessary to change the weight value of the network. First, adjust the connection weights between the implicit layer and the output layer.

$$w_{kj}(t+1) = w_{kj}(t) + \Delta w_{kj}. \quad (2)$$

In the above formula, the value obtained by the gradient method is the adjusted value of the connection weight between the implicit layer and the output layer.

$$\Delta w_{kj} = -\eta \frac{\partial E}{\partial w_{kj}} = \eta (d_k - o_k) f'(\text{net}_k) y_j. \quad (3)$$

In the above formula η is the normal value, which is expressed as the iteration step.

In a similar manner, you can adjust the join weights between the input layer and the implicit layer. Formula adjustment:

$$v_{ji}(t+1) = v_{ji}(t) + \Delta v_{ji}. \quad (4)$$

In the above formula, Δv_{ji} is the adjustment amount for determining the connection weight between the input layer

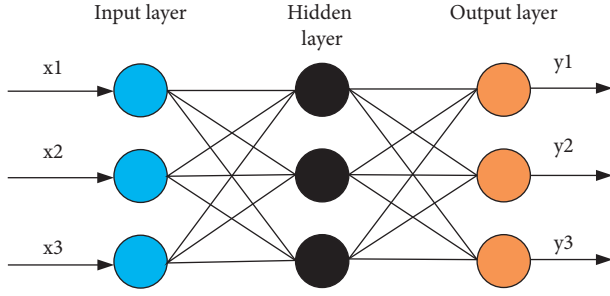


FIGURE 1: Structure diagram of BP neural network.

and the implicit layer by the gradient method. It can be obtained from the following formula:

$$\Delta v_{ji} = -\eta \frac{\partial E}{\partial v_{ji}} = \eta \sum_{k=1}^k (d_k - o_k) f'(\text{net}_k) w_{kj} f'(\text{net}_j) x_i. \quad (5)$$

When there are samples, if there are P training samples, the total error sum form of the above calculation method is defined as

$$E_p = \frac{1}{2} \sum_{p=1}^P \sum_{k=1}^K (d_k - o_k)^2. \quad (6)$$

As long as the operation is repeated for P samples as described above, E_p reaches the minimum requested value, and the algorithm ends.

The following introduces the principle derivation of the two processes of BP neural network [14,15].

2.2.1. Forward Propagation of BP Neural Network. The connection weight between the two nodes is w_{ij} the offset of the nodes is b_j the output value of each node is x_j and the output value of the node is calculated based on all the nodes in the previous layer and the offset of the current layer. The calculation is as follows:

$$S_j = \sum_{i=0}^{m-1} w_{ij} x_i + b_j, \quad (7)$$

$$x_j = f(S_j). \quad (8)$$

where f is the activation function, which is usually the sigmoid function:

$$f(x) = \frac{1}{1 + \exp(-x)}. \quad (9)$$

In BP neural network, only the input layer of the network has no bias term.

2.2.2. Error back Propagation. Compared with forward propagation, the back propagation of error is complex and is based on Widrow-Hoff rule. If the output result of the output layer is defined as d , the following error function is defined:

$$E(w, b) = \frac{1}{2} \sum_{j=0}^{n-1} (d_j - y_j)^2. \quad (10)$$

By continuously modifying the weight matrix and offset, the BP neural network is gradually reduced to reduce the error function.

2.2.3. Disadvantages of Neural Network. BP neural network is widely used, but it also has some shortcomings [16]:

- (1) It is easy to fall into local minimum, and the global minimum cannot be obtained. Because there are many minimums in the network, it is easy to enter local minimum. For this problem, better initialization is needed, but it is difficult to get a good initial value.
- (2) The learning efficiency during training is very low, and it is still very long until the end of the network.
- (3) The number of hidden layers and the number of neurons in each hidden layer are lack of effective theoretical guidance.

BP neural network including hidden layer can approximate any function in theory, but it has no good effect in practical application.

2.3. Principle of Deep Belief Network (DBN). Deep Belief Network (DBN) is different from the neural network belonging to the previous discriminant model, which is a probability generation model. The probability generation model calculates P (observation label) and P (label observation) while modeling the cooperative distribution between samples and labels, and the discriminant mode only calculates (label observation).

2.3.1. Principle of 1 Deep Belief Network (DBN). Deep Belief network (DBN) can obtain the connection weights between neurons by iterative optimization, and can generate the trained network according to the benchmark of maximum probability as shown in Figure 2:

DBN is composed of restricted Boltzmann machines (RBM). DBN is trained for each layer. During training, the input layer is the input layer of the first RBM in units of RBM, and the output layer of the first RBM is the input layer of the second RBM. Inference is made for each layer.

The structure of RBM is shown in Figure 3.

2.3.2. DBN Training Process. The training process of RBM is basically to find the most possible distribution form of generating training samples [17].

The training method of Deep Belief Network is as follows: firstly, the initialization weight of the network is obtained by the training method of each nonmonitoring layer, and then the subsequent network optimization is realized by error inverse adjustment.

- (1) Training the first RBM until the error converges

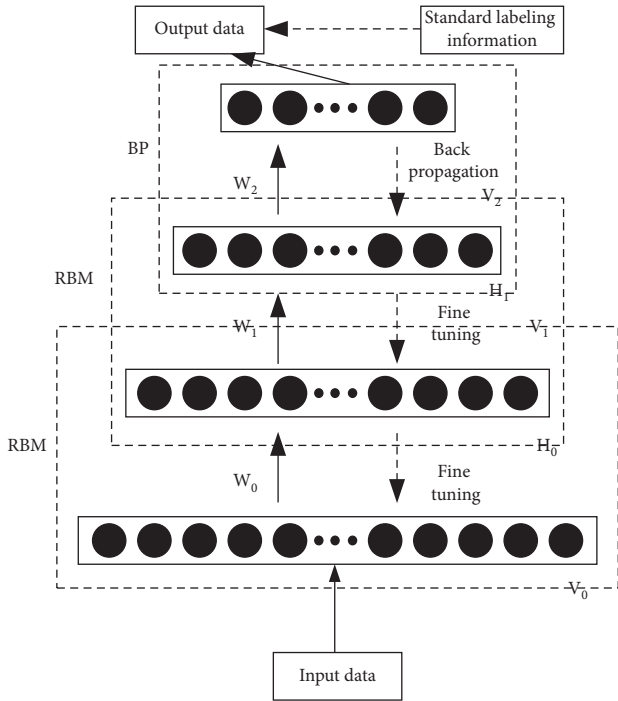


FIGURE 2: Schematic diagram of Deep Belief Network structure.

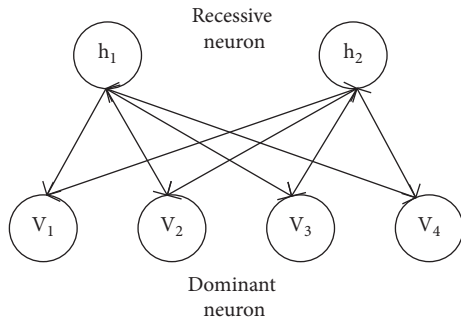


FIGURE 3: Schematic diagram of RBM structure.

- (2) Fixing weights and offsets of the RBM trained in the previous step, and calculating an output of the RBM as an input vector of the second RBM
- (3) Before error convergence, the output layer of the second RBM is trained as the output layer of the whole network, and the output layer of the first network is operated as the hidden layer of the whole network
- (4) repeat the above steps until all layers are trained
- (5) If the whole network is a supervised network with labels, the weight method used to train the last layer network initializes all connections, and the number of neurons in the last output layer is 5 neurons, which is gradually optimized by using the error inverse adjustment algorithm until the error converges

The model proposed in this paper has good forecasting effect and practical application. From the experiment, DBN

is a better modeling method for economic system operation and management, which has excellent practicability and applicability, and is expected to be popularized and applied in the field of economic forecasting.

3. Research on System Economic Operation and Management Based on Deep Belief Network

Economic system is a relatively complex nonlinear system. There are many influencing factors in the system, such as resources, consumption, investment, industrial structure. These factors also influence and restrict each other. The characteristics of high nonlinearity and time-varying bring great obstacles to economic operation and management. It can be seen from the explanation in the previous chapter that artificial neural network has strong nonlinear approximation ability. Theoretical research shows that artificial neural network can approximate any nonlinear function and can deal with difficult problems such as economic prediction. In recent years, the deep learning method proposed by the academic circles provides a good initial value for the neural network through the hierarchical pretraining method [18, 19], which overcomes the existing shortcomings and activates new vitality to a certain extent.

This chapter focuses on several variables reflecting the macroeconomic development of F province, such as consumer price index, fiscal expenditure, tax revenue, total exports and total imports, as the forecast of consumer price index and total imports. The error propagation neural network, deep belief network, and vector self-regression (VAR) are verified [20], and the prediction accuracy of DBN deep learning method, the limitation of target sample size and the performance of training and learning speed are studied.

3.1. Construction and Selection of Economic Forecast Index System. Use neural network or deep learning method to predict the actual economy, In essence, the highly nonlinear function between dependent variable economic indicators and independent variable economic indicators is learned through training samples, and introduce new independent variable economic indicators, use nonlinear function to forecast the corresponding variable economic indicators. Because of the highly nonlinear characteristics of economic development, the relationship between economic indicators is very different. Therefore, for different variable economic indicators, appropriate independent variable economic indicators should be selected as input. Choosing different index variables for forecasting will have a great impact on the forecasting results. If the selected variable forecasting indicators cannot reflect the economic goals we want to predict and cannot achieve the best algorithm, we can only evaluate enough independent variable economic indicators according to experience and experimental results.

3.1.1. Selection of Indicators. Accord to that basic principles of construct the above indicators, This paper selects several indicators, which can reflect the local macroeconomic

development of F province, analyzes their correlation, predicts their time correlation, and selects some economic indicators closely related to the local economic development trend. The economic indicators proposed in this paper include public finance, foreign trade and residents' life. This paper studies the application of DBN deep learning model in the field of economic forecasting [21,22]. Specific indicators are tax expenditure, tax revenue, total imports, total exports and consumer price index.

3.2. Selection and Preprocessing of Data Samples. Based on the abovementioned index construction principles, this paper collects relevant source data and establishes relevant economic forecasting index system. The source data used in this paper comes from China Economic Database. The time span of data collection is the economic data of F province from January 2005 to February 2015. The collected index source data mainly include important index data of regional economic development, such as fiscal revenue, total import, total export and consumer price index. Selecting the source data of the above indicators is mainly considering that the data of relevant indicators during this period is relatively complete, which can basically meet the training and testing needs of sample quantity. Please refer to Table 1 for specific source data.

The absolute quantity of the abovementioned economic indicators and the overall trend changing with time are similar to linear monotone curves. If the absolute value of the abovementioned indicators is directly taken as the index quantity of economic prediction, it is rare for them to reappear in the past numerical position because of their monotony, that is to say, history will not repeat itself. Therefore, this paper takes the growth rate of each economic index as the input and output of the economic prediction function, and the absolute quantity prediction of specific economic indicators is converted from the predicted growth rate. In this paper, the calculation formula of the corresponding growth rate obtained from the absolute quantity of economic indicators is as follows:

$$y^t = \frac{x^t - x^{t-1}}{x^{t-1}} \quad (11)$$

where t is time value; x^t and x^{t-1} are the absolute quantity of a certain economic index at the current moment and the previous moment; y^t is the growth rate of this economic indicator at the current time.

Using this formula, we can obtain the growth rate of each economic index in Table 1.

In addition, because different economic indicators or their growth rates have different acquisition ranges, the numerical range of input quantities of neural networks or deep networks is usually required between $[0, 1]$ or $[1,1]$. Therefore, this paper normalizes the growth rate of economic indicators obtained in (11). In this paper, the maximum and minimum value normalization method is adopted, and the growth rate of all indexes is normalized to $[0, 1]$. The maximum value corresponds to 1 and the minimum value corresponds to 0. The specific normalization formula is as follows.

$$y_nor = \frac{y - \min(y)}{\max(y) - \min(y)} \quad (12)$$

where y_nor is the normalized index growth rate data; $\max(y)$ is the maximum value of the index growth rate; and $\min(y)$ is the minimum of the index growth rate.

3.3. Model Parameter Setting and Model Training and Learning. In this study, DBN deep learning method, BP neural network and VAR method are used to predict the consumer price index of F province, but DBN deep learning method adopts single hidden layer network [23]. The number of neurons in the input layer is 30, the number of neurons in the hidden layer is 15, and the number of neurons in the output layer is 1. The network structure is shown in Figure 4.

3.3.1. Sample Set. In this thesis, we use two training groups: standard sample training group and nonstandard sample training group. The standard sample set includes variable and parameter pairs. In order to distinguish between labeled samples and unlabeled sample sets, capital letters A and B are used here, respectively, and $T1$ and $T2$ are the number of samples in the sample set.

3.3.2. DBN Network Weight Initialization. A contrast divergence algorithm is used to pretrain weights between input layer and implicit layer elements to obtain initial weights. The pretraining process of CD algorithm does not need to add variable samples to output, that is, the unsampled set is selected as the pretraining samples. Because only input variables are provided, no output variables are provided.

3.3.3. Weight Learning of DBN Network. After initialization, the DBN network can update the weights by BP algorithm and constant sample set training, and the corresponding parameters can be optimized by intelligent optimization algorithm [24,25]. The research on the forecast of consumer price index in F province is still in its initial stage. Unlike the startup phase, there is no need to output variables at startup. BP algorithm needs to participate in output variables. The weights in the pretraining stage only provide the best initial value for BP training. The parameters of BP weight updating stage are 0.001 steps, 1000 repetitions, and 50 batches.

3.3.4. Weight Learning of BP Neural Network. In this study, BP neural network adopts the same training samples and network structure as DBN. The weights of BP neural network are initialized randomly in the guiding stage, and the weights are updated by error reappearance algorithm.

4. Experiment

4.1. Performance Comparison between DBN Deep Learning Model and BP Neural Network. Parameters such as network

TABLE 1: Economic data of F Province (Millions of RMB).

Consumer price index	Export	Import	Fiscal revenue	Fiscal expenditure
102.5	2433.29	1465.92	4274.00	3741.00
104.2	1956.58	1197.10	2566	3031
103.1	2953.14	1731.80	3158	4566
101.9	2894.11	1776.27	3945	3982
102.7	2590.99	1523.70	3110	3587
103.3	3161.81	1707.53	3066	5963
102.9	2942.86	1613.87	3467	3753
102.2	3355.52	1815.29	2788	4261
100.8	2965.89	1695.66	6107	5548
101.2	2971.69	1530.81	3994	4337
101	3116.78	1723.01	2898	5319
100.9	3524.29	1761.69	3887.03	11254.33
101	3063.88	1603.51	5885.00	4360.00
99.4	2184.00	1494.82	3525	3244
99.2	3344.93	1876.25	3891	5596
100.4	3566.12	1869.71	5754	5842
100.4	3346.03	1610.96	4118	3746
101	3413.19	1753.50	4560	5699
100.9	3442.79	1733.58	4989	4914
101	3739.88	1907.23	3884	5387
100.9	3538.27	2035.81	4127	6339
100.4	3702.18	1654.73	5124	4521
101.5	3765.89	1895.45	3357	7359
103.5	4236.04	1965.64	4903.07	15862.73
103.3	3684.97	1722.87	7659.00	4360.00
105.2	3336.26	1393.18	4896	4748
104.9	3187.52	1962.44	5128	6261
103.6	3973.39	2006.85	7490	6239
103.7	3946.61	1868.55	5127	5628
104.6	4835.46	2002.00	5718	7248
105.8	4154.41	2171.71	6583	6034
106.6	4271.86	2173.26	4966	6325
106.4	4519.39	2335.19	5420	8617
106.6	4332.73	2109.07	6443	7501
106.8	4690.83	2376.98	4160	8828
105.1	5020.48	2361.34	6355.77	19275.46
105.3	4634.58	2343.48	10104	7374.00
106.8	3498.13	2017.10	5902	4378
106.9	4393.20	2614.80	6322	7417
107.2	5090.21	2595.59	8767	8498
106.6	4915.64	2548.41	6608	8309
105.5	4817.22	2364.93	7445	8260
104.8	5266.06	2678.15	7850	9479
103.6	5389.98	2539.06	5377	6784
103.4	5171.11	2466.40	5964	8349
103.1	4932.37	2204.93	7754	7631
...

weights are determined, that is, a fixed prediction model is obtained. In order to compare the modeling performance of the two models, the above two models are used for training in this experiment. The network output is the normalized growth rate y_{nor} , and the formula for transforming y_{nor} into growth rate is as follows:

$$y = y_{nor} \times \max(y) + \min(y) \quad (13)$$

Here, y_{nor} is normalized growth rate; y is growth rate; $\max(y)$ is maximum growth rate of the indicator; $\min(y)$ is the minimum value of the index growth rate.

4.1.1. Comparison of Prediction Results. DBN deep learning model is better than BP neural network model, that is, DBN is a better modeling method than BP. Compared with VAR model, DBN deep learning model can predict the change of growth rate more effectively, and VAR tends to learn slower linear mapping in Figure 5.

Figure 5 shows that, The predicted DBN and BP values deviate from the actual growth rate to a certain extent in the local high frequency oscillation part, but in the overall growth rate change trend, the predicted values can effectively track the change behavior of the actual value, which reflects that both DBN deep learning model and BP neural network

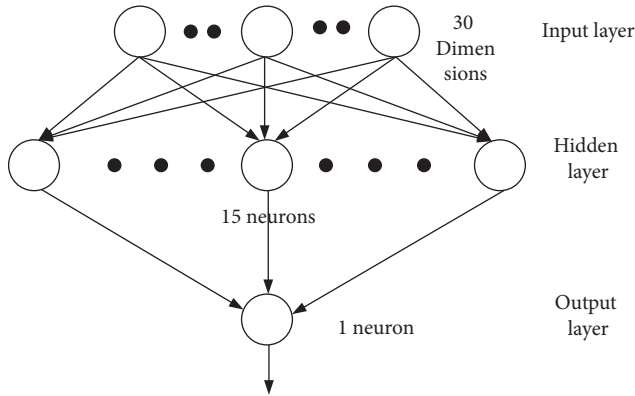


FIGURE 4: Network structure diagram adopted by DBN and BP.

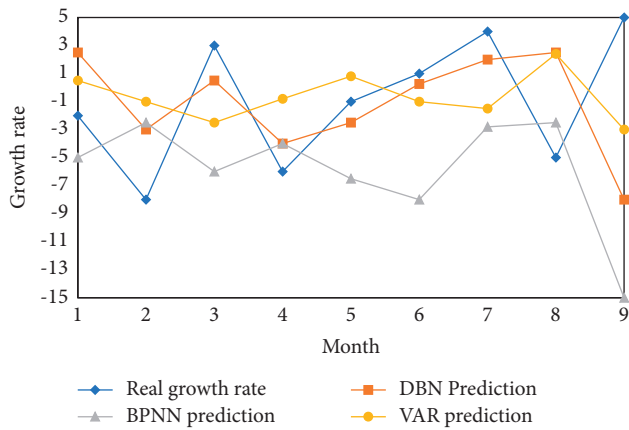


FIGURE 5: Forecast comparison of growth rate of consumer price index in F province.

model can effectively establish nonlinear problem models about economic prediction.

Using the predicted growth rate of the consumer price index of F province, the predicted value of the consumer price index of F province next month can be calculated from (13).

$$x^t = x_{true}^{t-1} \times (1 + y^t) \quad (14)$$

Here, x^t is current projected indicator values; x_{true}^{t-1} is the actual index value at the previous moment; and y^t is current projected indicator growth rate.

The results of the consumer price index of F province from June 2014 to February 2015 predicted by formula (13) are shown in Figure 6:

Figures 6 and 7 show that compared with BP neural network model and VER model, DBN deep learning model can more accurately predict the consumer price index and import growth rate of F province.

The expected import growth rate can be used to calculate the total import volume next month. Figure 8 shows a comparison between the projected total imports and the actual value of total imports from June 2014 to February 2015, based on different methodologies.

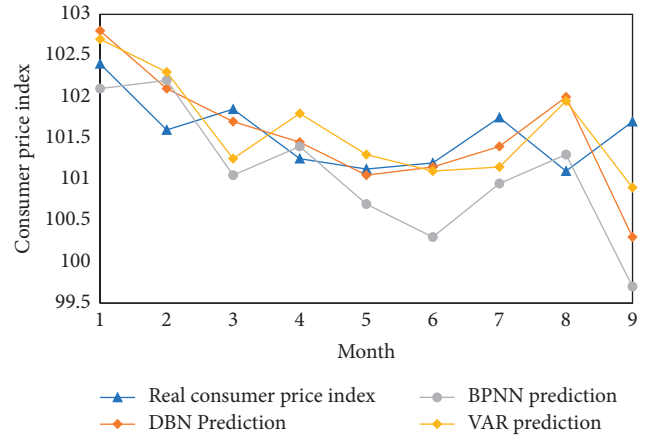


FIGURE 6: Comparison of consumer price index forecasts in F province.

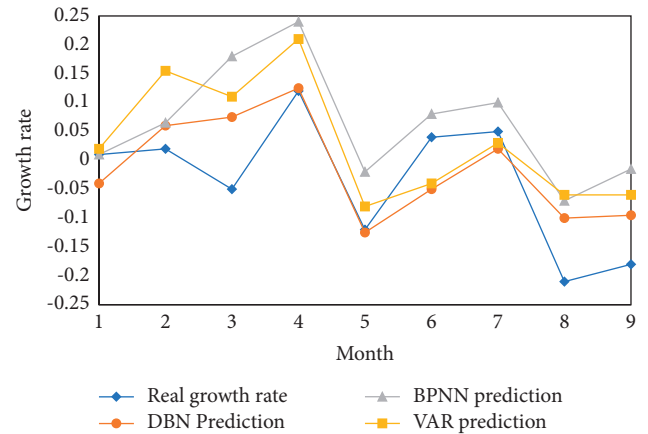


FIGURE 7: Forecast comparison of total import growth rate in F province.

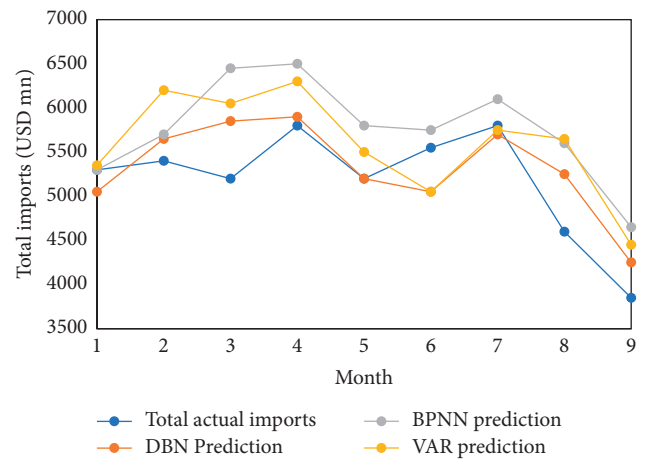


FIGURE 8: Comparison of forecast of total import in F province.

4.1.2. Comparison of Quantitative Prediction Accuracy. In order to quantitatively compare the prediction performance of DBN, BP and VAR, the following three indexes are

used to determine the prediction accuracy. The definition formula is as follows.

$$MAE = \frac{\sum_{t=1}^N |y^t - y_{true}^t|}{N}, \quad (15)$$

$$MSE = \frac{\sum_{t=1}^N (y^t - y_{true}^t)^2}{N}, \quad (16)$$

$$\text{average relative error} = \frac{\sum_{t=1}^N |y^t - y_E^t| / y_{true}^t}{N}. \quad (17)$$

The comparison results of prediction accuracy of DBN, BP, and VAR models are shown in Table 2. Bold numbers indicate the metrics corresponding to the most suitable method.

The three methods in Table 2 have little error and can predict the consumer price index of F province with certain accuracy, reflecting the change behavior of the price index. Among them, DBN performs best in absolute error (MAE) and average relative error, reflecting the excellent prediction accuracy of DBN.

According to Figure 6, the forecast period is from June 2014 to February 2015, and the actual consumer price index of F Province decreases slightly and tends to be stable. The forecast results of DBN model can be followed up more closely according to the downward trend of consumer price index of F Province in the first six months, which is consistent with the actual situation. Both BP and VAR forecasts show that in the first seven months, the consumer price index of F province will follow a downward trend, which is different from the actual situation. The former is beneficial for the government to prevent inflation immediately, while the latter may lose control of inflation.

From Table 3, we can see that the absolute mean error (MAE), mean square error (MSE) and average relative error of DBN are smaller than the other two methods. DBN not only has a relatively correct average prediction level, but also has a small error range. The reason why all indicators are lower than the consumer price index is that the total import base is large and the prediction error is large. In addition, the change of total imports is very large, which is difficult to predict. Therefore, the relative error is also very large.

4.1.3. Convergence Rate Comparison. Figure 9 shows the error convergence curves of DBN deep learning model and BP neural network in training and learning stages. As far as convergence speed is concerned, DBN is faster than BP neural network and has less fluctuation. This is mainly because the pretraining and learning methods adopted by DBN provide a good initial value of the network. On the other hand, because BP neural network uses random parameters to initialize the network, the starting point of error curve becomes higher, the convergence time becomes longer, and fluctuation may occur, which is also one of the reasons for the degradation of BP prediction performance. VAR does not need repeated training and learning, so there is no convergence speed problem.

TABLE 2: Comparison of forecast accuracy of consumer price index in F province.

Method	MAE	MSE	Average relative error (%)
DBN	0.425	0.323	0.418
BPNN	0.690	0.752	0.679
VAR	0.492	0.291	0.484

TABLE 3: Comparison of forecast accuracy of total import volume in F province.

Method	MAE	MSE	Average relative error (%)
DBN	314.14	145569.09	6.303
BP	529.78	413963.91	10.626
VAR	466.64	303774.48	9.313

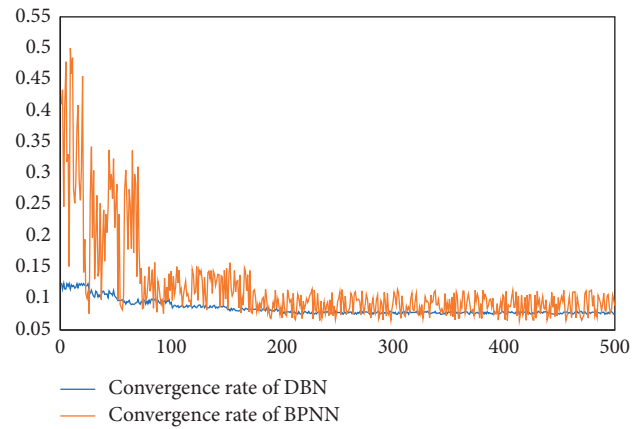


FIGURE 9: Convergence curves of DBN and BP.

Figure 10 shows the convergence curve of DBN and BP training of F province's total import prediction model. DBN has faster convergence speed, higher convergence accuracy and better practicability.

The prediction results of this paper show that the model can more accurately predict the phenomenon that the consumer price index of F province has a slight decline in the second half of 2014, and predict the stable fluctuation state after the decrease. By predicting this downward trend in advance, the government can estimate the effect of current policy adjustment in advance, so as to maintain or adjust the current monetary policy and keep the consumer price index at a stable level.

From the experimental results of this paper, the results obtained by using different deep learning models have obvious advantages. The simulation results of several models are analyzed and compared from the aspects of prediction accuracy, training convergence speed, pretraining with or without samples, etc. The results show that DBN has certain advantages. The scientific significance of this paper is to introduce deep learning model to predict the efficiency of economic operation and management. Therefore, scientific research is of great significance, which can find out the problems in the process of economic development and reflect the changes of residents' consumption and living index.

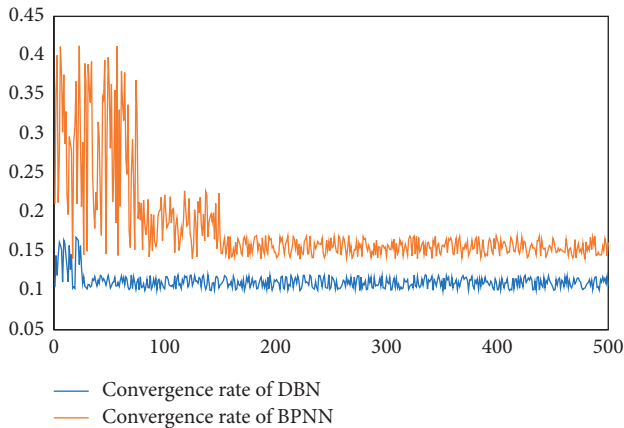


FIGURE 10: Training convergence curve of DBN and BP total import prediction model.

5. Conclusion

The model in this paper can predict the decline of total imports more accurately, so the relevant management departments can study the countermeasures in advance. While enterprise managers prevent the impact of the reduction of import volume on enterprise operation, enterprises relying on imports must plan in advance in order to maintain the normal production operation and market supply of enterprises. On the other hand, in order to prevent the decline of imported goods from affecting the prices and economic variables in the local market, government managers should take countermeasures as soon as possible. Actively take countermeasures to protect enterprises and consumers from the impact of import reduction. Specifically, for enterprises, the total import volume is expected to decrease. Through further analysis, we can investigate the reasons for the possible decrease in the total import volume.

Data Availability

The experimental data used to support the findings of this study are available from the corresponding author upon request.

Conflicts of Interest

The authors declared that they have no conflicts of interest regarding this work.

References

- [1] Z. Min, S. Jian, C Li, Z Bin, ZS. Liang, and H. Zhe, "Status evaluation of smart substation measurement and control device," *IOP Conference Series: Materials Science and Engineering*, vol. 563, no. 4, Article ID 042077, 2019.
- [2] T. Min, "Estimable group effects for strongly correlated variables in linear models [J]," *Journal of Statistical Planning and Inference*, vol. 198, pp. 29–42, 2019.
- [3] X Zhang, "Research on forecasting method of aviation traffic based on social and economic indicators [J]," *IOP Conference*

- Series: Materials Science and Engineering*, vol. 780, Article ID 062038, 2020.
- [4] C. Yeh, A. Perez, A. Driscoll, G. Azzari, Z. Tang, and D. Lobell, "Using publicly available satellite imagery and deep learning to understand economic well-being in Africa," *Nature Communications*, vol. 11, no. 1, p. 2583, 2020.
 - [5] D Alaminos, MB Salas, and MA Fernández-Gámez, "Quantum computing and deep learning methods for GDP growth forecasting [J]," *Computational Economics*, vol. 59, no. 2, pp. 1–27, 2021.
 - [6] M. Kraus, S. Feuerriegel, and A. Oztekin, "Deep learning in business analytics and operations research: models, applications and managerial implications," *European Journal of Operational Research*, vol. 281, no. 3, pp. 628–641, 2020.
 - [7] S Panigrahi and HS Behera, "A study on leading machine learning techniques for high order fuzzy time series forecasting [J]," *Engineering Applications of Artificial Intelligence*, vol. 87, Article ID 103245, 2020.
 - [8] X Sun, Q, Zhu, and Q Qin, "A multi-level convolution pyramid semantic fusion framework for high-resolution remote sensing image scene classification and annotation," *IEEE Access*, vol. 9, pp. 18195–18208, 2021.
 - [9] L Zhou and Q Zhang, "Recognition of false comments in E-commerce based on deep learning confidence network algorithm," *J. Information Systems and e-Business Management*, pp. 1–18, 2021.
 - [10] J. Yang, K Zhang, C Zhang, C Fu, and G Tian, "Reservoir characterization using multi-component seismic data in a novel hybrid model based on clustering and deep neural network[J]," *Natural Resources Research*, vol. 30, no. 5, pp. 1–26, 2021.
 - [11] X. Fang, J. Huang, and R Zhang, F Wang, Q Zhang, and G Li, Convolution neural network-based prediction of protein thermostability[J]," *Journal of Chemical Information and Modeling*, vol. 59, no. 11, 2019.
 - [12] FM Yin, HH Xu, and HH Gao, "Research on weibo public opinion prediction using improved genetic algorithm based BP neural networks," *Journal of Forests*, vol. 30, no. 3, pp. 82–101, 2019.
 - [13] D. Zhang and S. Lou, "The application research of neural network and BP algorithm in stock price pattern classification and prediction," *Future Generation Computer Systems*, vol. 115, pp. 872–879, 2021.
 - [14] Z Uykan, "On the working principle of the hopfield neural networks and its equivalence to the GADIA in optimization," *IEEE Transactions on Neural Networks and Learning Systems*, vol. 31, no. 9, pp. 3294–3304, Sept. 2020.
 - [15] D Zhang, W Li, X Wu, and X Lv, "Application of simulated annealing genetic algorithm optimized back propagation (BP) neural network in fault diagnosis [J]," *International Journal of Modeling Simulation & Scientific Computing*, vol. 10, no. 4, pp. 46–49, 2019.
 - [16] Y Jin, Z Li, Y Han, X Li, P Li, G Li et al., "A research on line loss calculation based on BP neural network with genetic algorithm optimization [J]," *IOP Conference Series: Earth and Environmental Science*, vol. 675, no. 1, Article ID 012155, 2021.
 - [17] P Qin, Z Cheng, Y Cui, J Zhang, and Q Miao, "Research on image colorization algorithm based on residual neural network," *Communications in Computer and Information Science*, vol. 771, pp. 608–621, 2017.
 - [18] X. Peng, H. Wang, J Lang et al., "EALSTM-QR: interval wind-power prediction model based on numerical weather prediction and deep learning," *Journal of Energy*, vol. 220, no. 3, Article ID 119692, 2020.

- [19] L Fang, X Cheng, H Wang, and L Yang, "Idle time window prediction in cellular networks with deep spatiotemporal modeling," *IEEE Journal on Selected Areas in Communications*, vol. 37, no. 6, pp. 1441–1454, June 2019.
- [20] Z Zhang, WC, Hong, and J Li, "Electric load forecasting by hybrid self-recurrent support vector regression model with variational mode decomposition and improved cuckoo search algorithm," *IEEE Access*, vol. 8, pp. 14642–14658, 2020.
- [21] Y. Guo and X. Wang, "Applying TS-DBN model into sports behavior recognition with deep learning approach [J]," *The Journal of Supercomputing*, no. 5–7, pp. 12192–12208, 2021.
- [22] NA. Kallioras and ND. Lagaros, "DL-Scale: deep Learning for model upgrading in topology optimization," *Procedia Manufacturing*, vol. 44, pp. 433–440, 2020.
- [23] S. Deb, "VAR model based clustering method for multivariate time series data," *Journal of Mathematical Sciences*, vol. 237, no. 6, pp. 754–765, 2019.
- [24] W. H. Bangyal, A. Hameed, W. Alosaimi, and H. Alyami, "A new initialization approach in particle swarm optimization for global optimization problems," *Computational Intelligence and Neuroscience*, vol. 2021, pp. 1–17, 2021.
- [25] WH. Bangyal, K. Nisar, AABA. Ibrahim, MR Haque, JJPC Rodrigues, DB. Rawat et al., "Comparative analysis of low discrepancy sequence-based initialization approaches using population-based algorithms for solving the global optimization problems," *Applied Sciences*, vol. 11, no. 16, p. 7591, 2021.

Research Article

Analysis of the Coupling and Coordination Relationship between the Evolution of Enterprise Spatial Structure and Economic Development Based on the Deep Learning Model

Lei Wang,¹ Yuan He,² and Yao Qi³ 

¹School of Economics and Management, Jiaozuo Normal College, Jiaozuo 454000, China

²Department of Finance and Business, Henan College of Industry & Information Technology, Jiaozuo 454000, China

³School of Business Administration, Henan Polytechnic University, Jiaozuo 454000, China

Correspondence should be addressed to Yao Qi; qiyao@hpu.edu.cn

Received 4 January 2022; Revised 24 January 2022; Accepted 16 February 2022; Published 18 March 2022

Academic Editor: Hangjun Che

Copyright © 2022 Lei Wang et al. This is an open access article distributed under the Creative Commons Attribution License, which permits unrestricted use, distribution, and reproduction in any medium, provided the original work is properly cited.

This study is based on the unsupervised learning-based enterprise spatial structure evolution and economic coupling coordination relationship situation assessment method. Pattern recognition has high-precision characteristics, but it is necessary to train the evaluation model for the enterprise spatial structure evolution in advance and then carry out economic coupling coordination based on the trained model. The conclusions are as follows: (1) through the RC1, RC2, RC3, RC4, RC5, and RC6 evaluation indicators to evaluate the situation evaluation method based on the unsupervised learning of the evolution of the enterprise spatial structure and the economic coupling and coordination relationship, it is found that the main component characteristics as a whole meet the standard. The optimal RC is RC6: profit = -0.0885, highest = -0.0809, lowest = -0.0932, WR.WR2 = 0.0038, MA.MA3 = -0.0782, MTM.MTM = -0.0427, OSC.OSC = -0.0355, ROC.MAROC = 0.0105, SKDJ.D = -0.0268, BIAS-QL.BIAS = -0.01, WIDTH.WIDTH = 0.2408, CYD.CYDN = -0.0961, FSL.SWL = -0.0868, ADTM.ADTM = -0.0379, ATR.ATR = -0.0278, DMA.DIFMA = -0.0358, DMI.ADX = 0.8516, DMI.ADXR = 0.854, EMV.EMV = -0.0942, VMACD.DIF = 0.3312, and UOS.MAUOS = -0.0846.2. Based on the deep learning model of the coupling and coordination relationship between the evolution of the spatial structure of the enterprise, the time-dependent matrix comparison experiment is divided into directed + self, directed, undirected + self, and undirected time for comparison. The experimental results on directed + self are the best; with various indicators, the upward improvement is above 10%: CP = 0.8611, CR = 0.9353, C-F1 = 0.8967, EP = 0.8865, ER = 0.857, E-F1 = 0.917, OP = 0.856, OR = 0.9845, and O-F1 = 0.99.3. The time cost, profit, and transaction volume data of the company are collected for a certain period of time, and simulation experiments are conducted to get a small difference between the predicted result and the actual data. The January data are closest to the true value: cost = 30.78, profit = 30.11, highest = 30.1, lowest = 29.7, WR.WR1 = 81.21, WR.WR2 = 45.62, AMV.AMV2 = 32.67, AMV.AMV3 = 34.95, and MCST.MCST = 36.08.4. In the model score, the best performance of LSTM data is CP = 0.3829, CR = 0.3664, C-F1 = 0.3744, EP = 0.3726, ER = 0.3004, E-F1 = 0.3326, OP = 0.9155, OR = 0.9316, and O-F1 = 0.9234, which is better than the BiLSTM model with CP = 0.3648, CR = 0.3319, C-F1 = 0.3392, EP = 0.4402, ER = 0.391, E-F1 = 0.4145, OP = 0.9215, OR = 0.9318, and O-F1 = 0.9266.

1. Introduction

Deep learning (DL) network, also known as deep neural network, derived from the artificial neural network, simulates the human brain to learn and perceive the outside world, and its core neurons are a new field in machine learning research. Both deep learning and shallow learning

methods simulate the human brain to perceive the outside world. The difference between the two is that the deep learning model can transform high-dimensional complex feature data into higher levels and more through deep and simple linear and nonlinear network structures. Abstract representation was used to carry out deep learning algorithms such as deep self-encoding networks. It has good

characterization ability for high-dimensional complex deep self-encoding network [1–3]. Deep self-encoding networks can have outstanding advantages in processing large-scale, nonlinear, and multidimensional data. The gated recurrent unit neural network in the rise of deep neural networks has the function of data security situation assessment and is suitable for processing deep neural network time series data. Generative adversarial network (GAN) has a good effect in the field of intelligent robot data generation under wireless connection. Based on deep learning, an adaptive feature quantitative evaluation method of intelligent robot clusters based on convolutional neural network (CNN) under wireless connection has emerged. This method combines the coupling and coordination relationship of the evolution of enterprise spatial structure with the characteristics of CNN and realizes a comprehensive quantitative evaluation of deep neural networks through self-adaptive deep self-encoding features such as online learning. Artificial intelligence researchers use neural networks as a way to express complex problems in a nonlinear way. In recent years, they have been applied in the field of biological theory and artificial intelligence. The research of neuron perceptron has received extensive attention [4–6]. Deep neural networks are derived from neural networks and are superior to traditional neuron perceptron networks. Artificial intelligence research using deep neural networks will be a very promising research direction. Artificial intelligence researchers have designed the neuron unit in the artificial neural network in the deep self-encoding network, also known as the high-dimensional complex deep self-encoding network perceptron, which receives the information input of the high-dimensional complex deep network and after time series data processing outputs the result. Since the human body's perception of the external world is realized by interconnecting deep autoencoding networks formed by hundreds of neurons, the artificial neural network designs perceptrons of high-dimensional complex deep autoencoding networks to connect them to each other. According to the high-dimensional complex deep self-encoding network signal processing flow, it is divided into a data security input layer, a time series hidden layer, and a self-encoding network output layer. The perceptron layer that initially senses the incoming signal is called the input layer [5–9]. The perceptron layer that processes internal signals and continues to output internal signals is called the hidden layer, and the signal that is responsible for the final output of the relationship between the evolution of the enterprise's spatial structure and the economic coupling is called the output layer. Deep neural network, as an extension of artificial neural network vector machine and feature gravity search algorithm, adds more vector machine feature search on its basis. The neurons in the data security input layer, the time series hidden layer, and the output layer of the self-encoding network are fully connected. As the number of output layers of the self-encoding network increases, deep neural networks have stronger learning output capabilities. In order to solve the parameter selection problem of deep self-encoding network and high-dimensional complex deep self-encoding network in machine learning technology, support vector

machine and feature gravity search algorithm (GSA) can be combined based on parameter optimization, so that the neural network security situation assessment system has better global optimization function. A cyberspace method based on an improved feature gravity search algorithm can be optimized using high-dimensional complex deep self-encoding network learning strategies and simulation methods, which significantly improves the accuracy of the feature gravity search algorithm and the computational efficiency of the cyberspace method. The neural network method that optimizes the network space method of the feature gravity search algorithm can be used to perform an adaptive mechanism of neural network training efficiency through the cuckoo neural network algorithm. In this paper, the method of sequential data processing based on conjugate gradient is introduced [10–13].

With the development of machine learning technology, pattern recognition methods such as deep autoencoding networks, high-dimensional complex deep autoencoding networks, data security situation assessment functions, and time series data vector machines have also been widely used in the coordination of the evolution of enterprise spatial structure and economic coupling. Based on the characteristics of deep autoencoder (DAE) and deep neural network (DNN) [14, 15], a method for analyzing the relationship between the evolution of enterprise spatial structure and economic coupling is proposed, which improves the accuracy of identifying the evolution of the enterprise's spatial structure and the flexibility of the relationship between economic coupling and coordination. On the basis of the traditional hierarchical model, unsupervised learning is performed by using neurons to perceive signal data through synapses, combined with a variational autoencoder (VAE) to process new output signals. Finally, a method for evaluating the situation of the coordination relationship between the evolution of the spatial structure of the enterprise and the economic coupling based on unsupervised learning is formed. Pattern recognition based on unsupervised learning-based enterprise spatial structure evolution and economic coupling coordination relationship situation assessment method has high-precision characteristics, but it is necessary to train the evaluation model for the enterprise spatial structure evolution in advance and then carry out economic coupling coordination based on the trained model.

2. Evolution of Enterprise Spatial Structure and Economic Development

2.1. Deep Learning Model. The deep learning model is a network model that is further developed on the basis of deep neural networks. It can greatly reduce the number of parameters through weight sharing. At the same time, convolutional neural networks can process multidimensional input data of the evolution of the enterprise's spatial structure and the coordination relationship between economic coupling and retention. The original local spatial information of the input data of the deep self-encoding network in the machine learning technology has been greatly

improved, and its feature extraction ability has also been greatly improved. It is mainly used in the processing of enterprise spatial structure evolution and economic coupling recognition. The nodes between the various convolutional neural layers of the deep learning model are connected to each other to make it have the memory function of the network model. It can obtain the hidden layer state of the spatial structure evolution and then calculate the output of the hidden layer at the current time according to the output of the input layer at the current time. It solves the problem that the fully connected deep neural network cannot model time series data. It is mainly used to deal with the evolution of the enterprise spatial structure and the identification of economic coupling. The deep learning model is shown in Figure 1 [16–18].

2.2. Coupling and Coordination Relationship of the Evolution of Enterprise Spatial Structure Based on the Deep Learning Model. The deep learning model-based corporate spatial structure evolution coupling coordination relationship model includes corporate structure filtering algorithms, as well as deep learning model resource recommendation and resource display algorithms. Therefore, it is necessary to design the algorithms required for the coupling and coordination relationship model of the evolution of the enterprise space structure, and at the same time, through experiments, adjust the parameters of the deep learning models designed by different companies, select better parameters, and finally coordinate the relationship through the evolution of the enterprise space structure. The real dataset is compared with the classic algorithm to verify the feasibility and rationality of the designed algorithm. The coupling and coordination relationship model of the evolution of the enterprise spatial structure includes the data layer, the evaluation layer, and the knowledge layer, as shown in Figure 2. The evolution of the spatial structure of an enterprise cannot be done without the support of big data for the development of the coupling and coordination relationship, and big data cannot do it without the deep learning model technology. Therefore, data processing technology plays an important role in resource recommendation and resource display algorithms. Datasets usually need to be preprocessed [19]. Especially for the dataset in the field of enterprise spatial structure, preprocessing the dataset can filter out the impurity information of the evolution of the silent structure of the enterprise to a certain extent.

2.3. Data Processing Technology. Data processing refers to the evolution of the enterprise's spatial structure, coupling and coordinating relational data acquisition, data cleaning, data processing, and data visualization. The significance of data processing is to transform the company's messy data source processing into information useful for deep learning model resource recommendation and resource display algorithms. The filtering algorithm deletes outlier data and duplicate data and normalizes and standardizes the data, so that we can store, search, analyze, and reuse the outlier data and duplicate data. Data processing technology is the deep

learning technology to realize the automation of data processing. Instead of manual work, it can relatively easily process the evolution of the enterprise's spatial structure, coupling and coordinating relational data, effectively saving the cost and time of data processing. For large-scale enterprise spatial structure evolution, coupling and coordinating relational data processing are quite complicated, and it is difficult to complete it manually. Therefore, corresponding tools or technical means are needed to complete data processing tasks.

3. Application of the Deep Learning Model in Enterprise Economic Development

3.1. LSTM [20–22].

$$X = \{x_1, x_2 \dots x_n\}. \quad (1)$$

The deep learning model is defined as follows:

$$\begin{aligned} h_t &= f(Ux_t + Wh_{t-1}), \\ o_t &= g(Vh_t). \end{aligned} \quad (2)$$

The number of parameters is defined as follows:

$$o_t = g(Vf(Ux_t + Wh_{t-1})). \quad (3)$$

3.1.1. Analysis on the Coordination Relationship between the Evolution of Enterprise Spatial Structure and Economic Coupling.

$$\begin{aligned} o_t &= g(Vf(UX_t + Wf(Ux_{t-1} + Wh_{t-2}))), \\ z_t &= \sigma(W_z \cdot [h_{t-1}, x_t]), \\ r_t &= \sigma(W_r \cdot [h_{t-1}, x_t]). \end{aligned} \quad (4)$$

Input data are defined as follows:

$$\begin{aligned} h' &= \tanh(W \cdot [r_t * h_{t-1}, x_t]), \\ h_t &= (1 - z_t) * h_{t-1} + z_t * h'_t, \\ Z^{l+1}(i, j) &= [Z^l \otimes w^{l+1}](i, j) + b. \end{aligned} \quad (5)$$

3.2. BiLSTM [23].

$$Z^{l+1}(i, j) = \sum_{k=1}^{kl} \sum_{x=1}^f \sum_{y=1}^f [Z_k^l(s_o i + x, s_o j + y) + b]. \quad (6)$$

Machine learning technology is defined as follows:

$$\begin{aligned} (i, j) &\in \{0, 1, \dots, L_{l+1}\}, L_{l+1} = \frac{L_l + 2p - f}{s_o}, \\ g_v &= \text{ReLU} \left(\sum_{u \in N(v)} h_u \cdot W_{L(u,v)} \right), \\ E &= - \sum_{i=0}^n X_i \log P(X_i). \end{aligned} \quad (7)$$

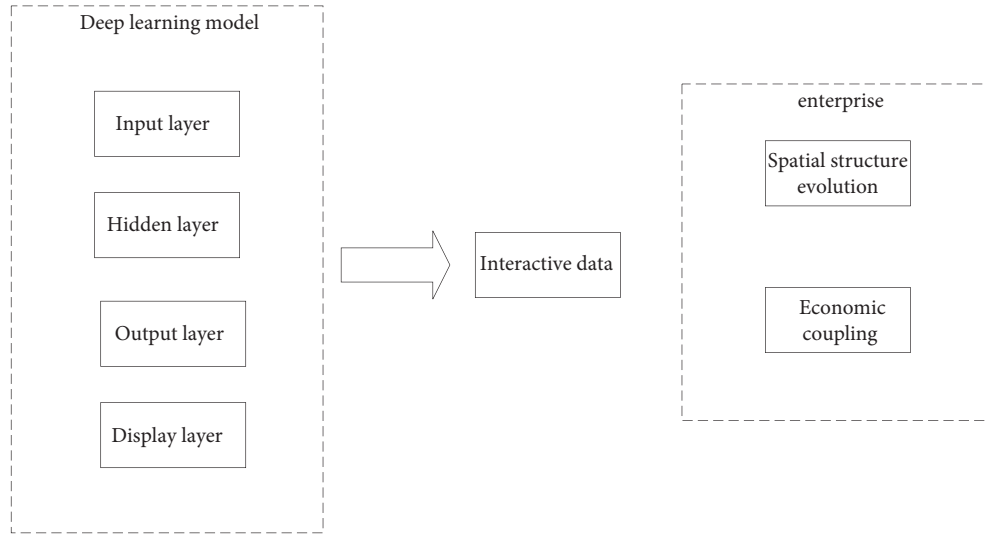


FIGURE 1: Deep learning model.

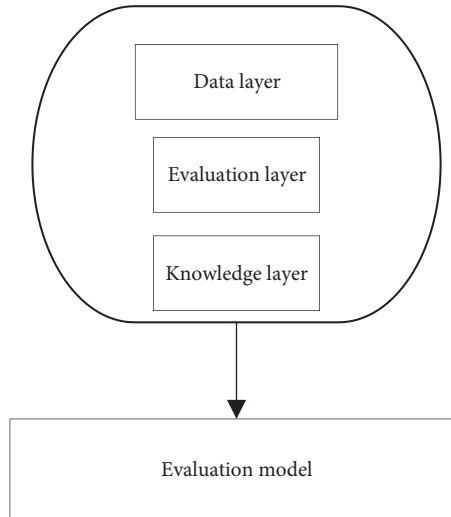


FIGURE 2: Coupling and coordination relationship model for the evolution of enterprise spatial structure.

Deep autoencoding network is defined as follows:

$$\begin{aligned}
 E &= - \sum_{i=0}^2 X_i \log P(X_i), \\
 \hat{\beta} &= \arg \min_{\beta \in R^d}, \\
 \beta &= \arg \min_{\beta \in R^d} \|Y - X\beta\|^2 \text{ s.t.}, \\
 \sum_{j=1}^d |\beta_j| &\leq t, \quad t \geq 0.
 \end{aligned} \tag{8}$$

Enterprise spatial structure evolution is defined as follows:

$$\begin{aligned}
 \beta &= \arg \min_{\beta \in R^d} (\|Y - X\beta\|^2 + \lambda \sum_{j=1}^d |\beta_j|), \\
 t_0 &= \sum_{j=1}^d |\beta_j(\text{OLS})|.
 \end{aligned} \tag{9}$$

3.3. GCN [15, 24–26].

$$X = (X_1, X_2, X_3, \dots, X_p)^T,$$

$$Z_{ij} = \frac{x_{ij} - \bar{x}_j}{s_j}. \quad (10)$$

3.3.1. Analysis on the Coupling and Coordination Relationship of Enterprise Economy.

$$i = 1, 2, \dots, n,$$

$$j = 1, 2, \dots, p. \quad (11)$$

3.3.2. The Evolution of Enterprise Spatial Structure Based on the Deep Learning Model.

$$\bar{x}_j = \frac{\sum_{i=1}^n x_{ij}}{n},$$

$$s_j^2 = \frac{\sum_{i=1}^n (x_{ij} - \bar{x}_j)^2}{n-1}. \quad (12)$$

Financial analysis is defined as follows:

$$R = [r_{ij}]_p \times P = \frac{Z^t Z}{n-1}, \quad (13)$$

$$U_{ij} = z_i^T b_j^o, \quad j = 1, 2, \dots, m.$$

4. Simulation Experiment

4.1. Principal Component Feature Analysis. RC1, RC2, RC3, RC4, RC5, and RC6 are used to evaluate the situation evaluation method based on the unsupervised learning of the evolution of the spatial structure of the enterprise and the economic coupling and coordination relationship, and it is found that the main component characteristics as a whole meet the standard. The optimal RC is RC6: profit = -0.0885, highest = -0.0809, lowest = -0.0932, WR.WR1 = 0.0038, MA.MA3 = -0.0782, MTM.MTM = -0.0427, OSC.OSC = -0.0355, ROC.MAROC = 0.0105, SKDJ.D = -0.0268, BIAS-QL.BIAS = -0.01, WIDTH.WIDTH = 0.2408, CYD.CYDN = -0.0961, FSL.SWL = -0.0868, ADTM.ADTM = -0.0379, ATR.ATR = -0.0278, DMA.DIFMA = -0.0358, DMI.ADX = 0.8516, DMI.ADXR = 0.854, EMV.EMV = -0.0942, VMACD.DIF = 0.3312, and UOS.MAUOS = -0.0846, as shown in Table 1 and Figure 3.

4.2. Evaluation Indicators for the Coupling and Coordination Relationship of the Evolution of Enterprise Spatial Structure Based on the Deep Learning Model. Based on the deep learning model of the enterprise spatial structure evolution coupling and coordination relationship model, the principal component evaluation index algorithm is included. It is necessary to design the principal component evaluation indicators of the enterprise spatial structure evolution

coupling coordination relationship model and, at the same time, through experiments, to design the principal components of different companies. The evaluation index is adjusted, and finally the principal component evaluation index is obtained through the coupling and coordination relationship of the evolution of the enterprise's spatial structure. Indicators CP, CR, C-F1, EP, ER, E-F1, OP, OR, O-F1, PCNT.PCNT, PCNT.MAPCNT, AMO.AMO2, VRSI.RSI3, AMV.AMV2, AMV.AMV3, and MCST.MCST are used to evaluate the model. It is found that, in the coupling and coordination relationship of the evolution of enterprise spatial structure based on the deep learning model, when RC=6, the indicators are optimal: CP = -0.0184, CR = -0.0933, C-F1 = -0.3346, EP = -0.0051, ER = 0.1221, E-F1 = 0.0195, OP = -0.5153, OR = 0.1523, O-F1 = -0.113, PCNT.PCNT = -0.0023, PCNT.MAPCNT = -0.018, AMO.AMO2 = -0.022, VRSI.RSI3 = 0.2018, AMV.AMV2 = -0.076, AMV.AMV3 = -0.0543, and MCST.MCST = 0.0148, as shown in Table 2 and Figure 4.

4.3. Time-Dependent Matrix Comparison Experiment.

Based on the deep learning model of enterprise spatial structure evolution coupling coordination relationship model, the time-dependent matrix comparison experiment is divided into directed + self, directed, undirected + self, and undirected time for comparison. The experimental result on directed + self is the most effective. The indicators are improved by more than 10%: CP = 0.8611, CR = 0.9353, C-F1 = 0.8967, EP = 0.8865, ER = 0.857, E-F1 = 0.917, OP = 0.856, OR = 0.9845, and O-F1 = 0.99, as shown in Table 3 and Figure 5.

4.4. Simulation Experiments in Different Companies. The time cost, profit, and transaction volume data of the company are collected for a certain period of time, and simulation experiments are conducted to get a small difference between the predicted result and the actual data. The January data are closest to the true value: cost = 30.78, profit = 30.11, highest = 30.1, lowest = 29.7, WR.WR1 = 81.21, WR.WR2 = 45.62, AMV.AMV2 = 32.67, AMV.AMV3 = 34.95, and MCST.MCST = 36.08, as shown in Table 4 and Figure 6.

Then, different models are compared to predict the economic development of the company. In the LSTM model, A company = -1.03, B company = -0.9, C company = -0.95, D company = -0.94, E company = -0.96, F company = -0.68, G company = -0.67, H company = -0.59, I company = -0.49, and J company = -0.56. The LSTM model is obtained as the optimal model, as shown in Table 5 and Figure 7.

4.5. Scoring of Different Models. The scoring standards include accuracy (P), recall (R), and F1 scoring experiment results. The best performance of LSTM data is CP = 0.3829, CR = 0.3664, C-F1 = 0.3744, EP = 0.3726, ER = 0.3004, E-F1 = 0.3326, OP = 0.9155, OR = 0.9316, and O-F1 = 0.9234, which is better than the BiLSTM model with CP = 0.3648, CR = 0.3319, C-F1 = 0.3392, EP = 0.4402,

TABLE 1: Principal component analysis.

	RC1	RC2	RC3	RC4	RC5	RC6
Profit	0.9452	0.195	0.2122	0.0049	-0.0289	-0.0885
Highest	0.9448	0.1982	0.2196	0.058	-0.006	-0.0809
Lowest	0.9413	0.1962	0.2103	0.0511	-0.0609	-0.0932
WR.WR2	-0.001	-0.2737	0.0275	-0.0395	0.0512	0.0038
MA.MA3	0.9734	-0.1121	0.1559	-0.0541	-0.0241	-0.0782
MTM.MTM	-0.0032	0.8769	0.1252	0.2854	-0.0061	-0.0427
OSC.OSC	-0.0011	0.8331	0.1869	0.4332	-0.0202	-0.0355
ROC.MAROC	0.0338	0.8914	0.3031	-0.0275	0.0344	0.0105
SKDJ.D	0.0389	0.8678	0.0432	0.106	-0.0683	-0.0268
BIAS-QL.BIAS	-0.0362	0.3561	0.0002	0.8862	-0.0239	-0.01
WIDTH.WIDTH	0.1058	0.014	0.021	0.0285	0.7291	0.2408
CYD.CYDN	0.1315	0.3727	0.2886	0.3361	-0.5788	-0.0961
FSL.SWL	0.9611	0.1197	0.215	-0.0159	-0.0272	-0.0868
ADTM.ADTM	0.0591	0.5492	0.6507	0.0818	-0.1677	-0.0379
ATR.ATR	0.6541	-0.0014	0.2166	0.0058	0.5668	-0.0278
DMA.DIFMA	0.2072	0.098	0.8759	-0.0667	0.0374	-0.0358
DMI.ADX	-0.0985	-0.0335	0.008	-0.0152	0.1862	0.8516
DMI.ADXR	-0.1379	-0.0591	0.0294	0.0072	0.2531	0.854
EMV.EMV	0.0275	0.8208	0.2628	0.1308	-0.0963	-0.0942
VMACD.DIF	-0.0466	0.6583	0.1273	0.1629	0.113	0.3312
UOS.MAUOS	0.0941	0.8208	0.2045	0.1164	0.027	-0.0846

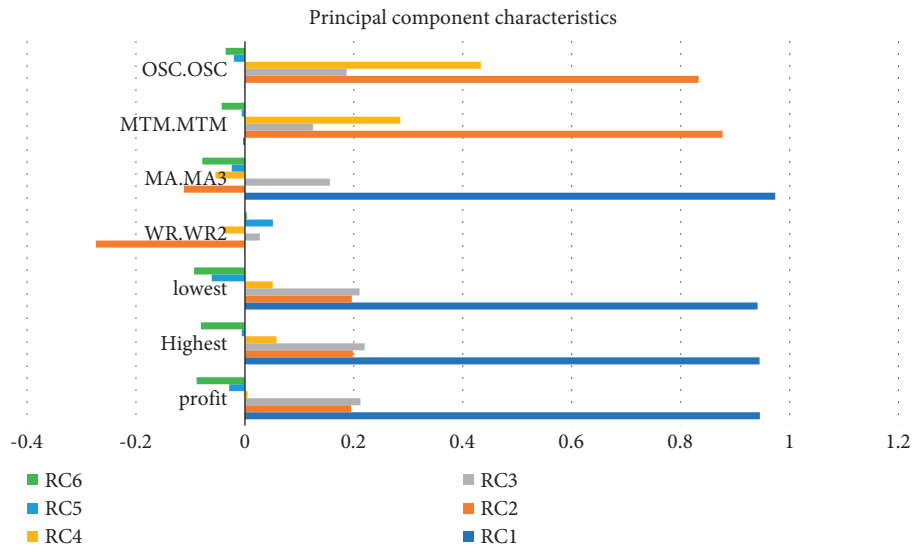


FIGURE 3: Principal component feature analysis.

TABLE 2: Main component evaluation index.

	RC1	RC2	RC3	RC4	RC5	RC6
CP	0.1535	0.3535	0.7474	-0.0868	0.1219	-0.0184
CR	0.2483	0.5096	0.536	0.4017	-0.256	-0.0933
C-F1	0.2981	0.1999	0.689	0.0047	0.2559	-0.3346
EP	0.0071	-0.0265	-0.1641	0.2175	0.0069	-0.0051
ER	0.1411	0.4014	0.6578	0.1225	-0.294	0.1221
E-F1	0.1891	0.0036	0.9024	-0.0307	0.0437	0.0195
OP	0.3858	-0.2712	0.2265	0.0165	0.304	-0.5153
OR	0.129	0.4455	0.7093	-0.0163	-0.0791	0.1523
O-F1	0.3228	0.0114	0.0387	0.011	-0.4751	-0.113
PCNT.PCNT	-0.0489	-0.0036	0.042	0.8405	-0.0144	-0.0023
PCNT.MAPCNT	-0.0476	0.4017	0.0211	0.8841	-0.0426	-0.018

TABLE 2: Continued.

	RC1	RC2	RC3	RC4	RC5	RC6
AMO.AMO2	0.4653	0.3189	0.4335	-0.0185	0.577	-0.022
VRSL.RSI3	-0.0397	0.4054	0.0615	0.3812	0.0391	0.2018
AMV.AMV2	0.9664	-0.0094	0.2118	-0.0614	-0.0229	-0.076
AMV.AMV3	0.978	-0.1596	-0.0036	-0.0347	0.0163	-0.0543
MCST.MCST	0.9613	-0.1087	-0.1285	-0.0628	0.0471	0.0148

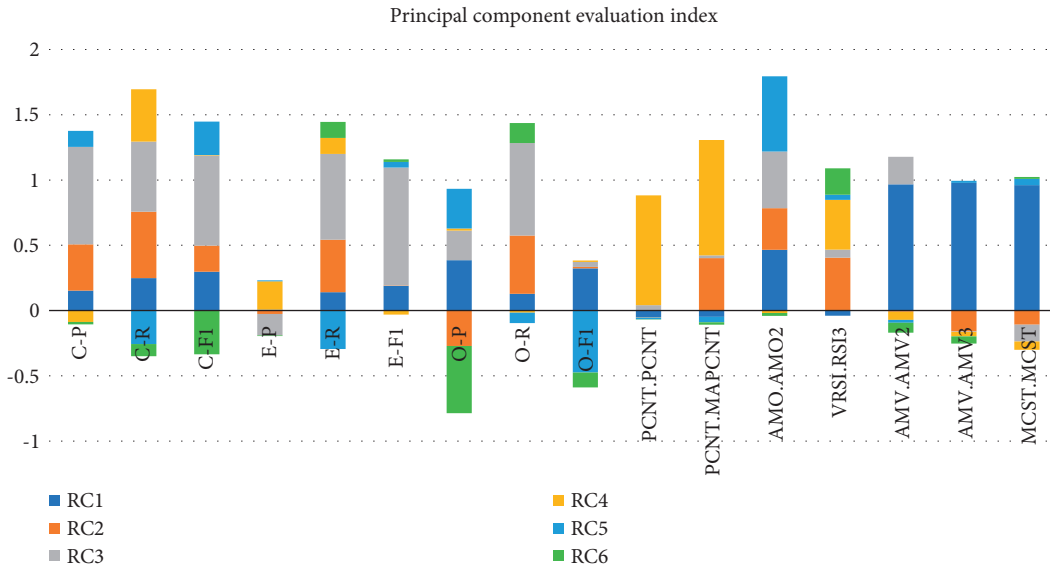


FIGURE 4: Principal component evaluation index.

TABLE 3: Time-dependent comparative experiment.

Time-dependent matrix type	CP	CR	C-F1	EP	ER	E-F1	OP	OR	O-F1
Directed + self	0.8611	0.9353	0.8967	0.8865	0.9506	0.9174	0.9956	0.9845	0.99
Directed	0.8381	0.8922	0.8643	0.8706	0.9468	0.9071	0.9939	0.983	0.9884
Undirected + self	0.6977	0.7759	0.7347	0.7826	0.7529	0.7674	0.991	0.9865	0.9888
Undirected time	0.6395	0.8103	0.7148	0.7309	0.692	0.7109	0.9974	0.9836	0.9904

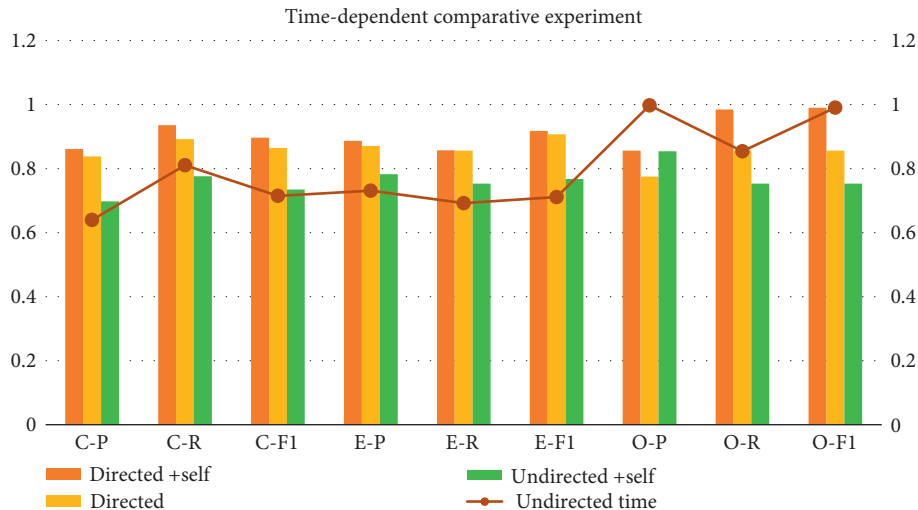


FIGURE 5: Time-dependent comparative experiment.

TABLE 4: Enterprise simulation experiment.

Time	Cost	Profit	Highest	Lowest	WR.WR1	WR.WR2	AMV.AMV2	AMV.AMV3	MCST.MCST
2020.01	30.78	30.11	30.1	29.7	81.21	45.62	32.67	34.95	36.08
2020.02	31.97	30.75	32.08	30.37	60.23	34.44	32.28	34.78	35.95
2020.03	31.56	31.97	32.2	31.4	31.23	24.62	31.96	34.69	35.88
2020.04	31.58	31.43	31.96	31.36	23.85	24.8	31.75	34.62	35.83
2020.05	31.92	31.58	32.56	31.38	21.62	22.38	31.46	34.5	35.73
2020.06	35.18	35.52	35.99	35.16	86.79	74.86	38.62	44.68	43.19
2020.07	35.16	35.84	35.86	35.13	87.09	75.43	38.04	44.61	43.05
2020.08	34.01	34.79	34.79	33.01	81.72	76.13	37.36	44.44	42.82
2020.09	34.1	34.47	34.78	34.07	79.2	73.99	36.86	44.3	42.7
2020.10	34.83	34.1	35.48	34	62	56.56	36.29	44.06	42.5

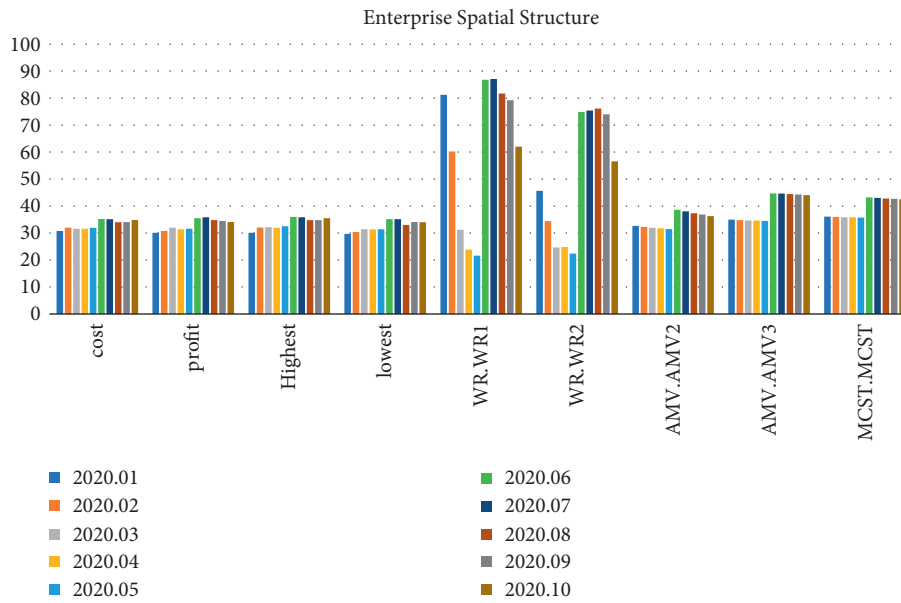


FIGURE 6: Enterprise simulation experiment.

TABLE 5: Enterprise economic forecast.

LSTM	BiLSTM	BiLSTM + GCN (dependency)	BiLSTM (WordNet)	BiLSTM + GAT	BLTGM (noNor)	BLTGM (nor)	BLTGM2	BLTGM3	MCST.MCST
-1.03	-1.1	-1.05	-1.09	-0.26	1.04	-0.17	-0.65	-0.61	-0.74
-0.9	-1.03	-0.95	-1.02	0.043	0.311	-1.59	-0.67	-0.63	-0.755
-0.95	-0.9	-0.94	-0.9	-0.5	-0.69	-0.89	-0.68	-0.64	-0.76
-0.94	-0.96	-0.96	-0.91	-0.79	-0.94	-0.89	-0.68	-0.65	-0.77
-0.96	-0.94	-0.9	-0.9	-0.07	-1.03	-0.97	-0.7	-0.67	-0.78
-0.68	-0.59	-0.66	-0.72	-0.18	1.06	0.87	0.45	0.4	0.17
-0.67	-0.62	-0.66	-0.6	-0.64	0.97	0.8	0.44	0.4	0.15
-0.59	-0.66	-0.59	-0.61	-0.16	0.37	0.2	0.41	0.39	0.13
-0.49	-0.62	-0.55	-0.56	0.21	-0.29	-1.46	0.37	0.39	0.09
-0.56	-0.49	-0.57	-0.52	-0.31	-0.01	-0.78	0.34	0.38	0.07

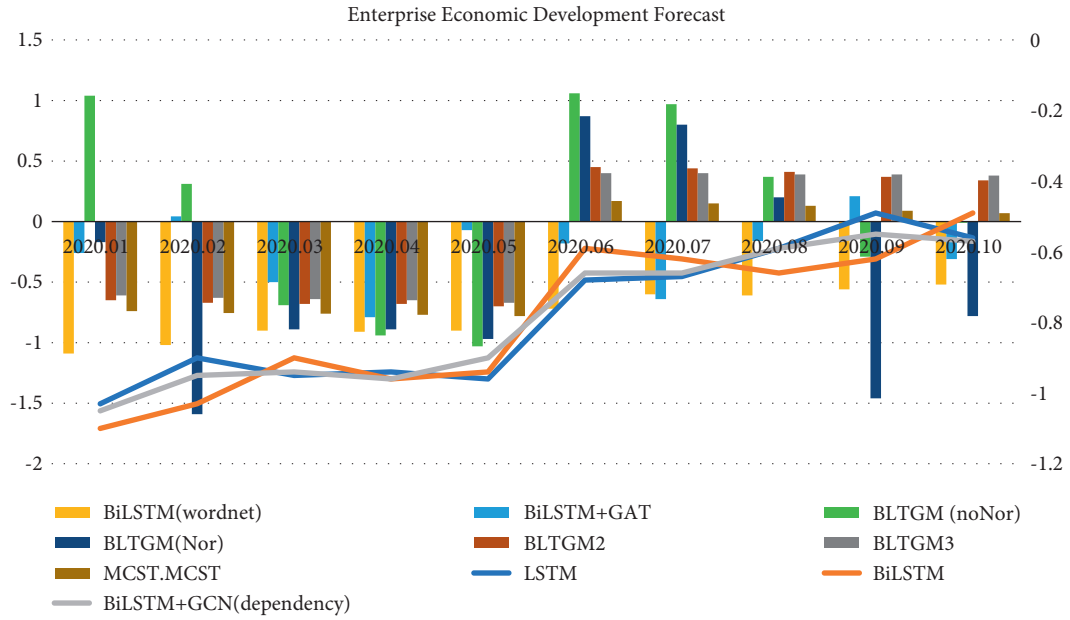


FIGURE 7: Enterprise economic forecast.

TABLE 6: Scores of different models.

Model	CP	CR	C-F1	EP	ER	E-F1	OP	OR	O-F1
LSTM	0.3829	0.3664	0.3744	0.3726	0.3004	0.3326	0.9155	0.9316	0.9234
BiLSTM	0.3648	0.3319	0.3392	0.4402	0.3916	0.4145	0.9215	0.9318	0.9266
BiLSTM + GCN (dependency)	0.3897	0.3578	0.373	0.4889	0.4183	0.4508	0.9247	0.9399	0.9322
BiLSTM (WordNet)	0.474	0.3922	0.4292	0.5	0.5209	0.5102	0.9355	0.9433	0.9394
BiLSTM + GAT	0.6882	0.8276	0.7515	0.7749	0.7985	0.7865	0.9997	0.9839	0.9917
BLTGM (noNor)	0.8375	0.8664	0.8517	0.8863	0.8593	0.8726	0.9853	0.9853	0.9853
BLTGM (Nor)	0.8611	0.9353	0.8967	0.8865	0.9506	0.9174	0.9956	0.9845	0.99
BLTGM2	0.8488	0.944	0.8939	0.9182	0.9392	0.9286	0.9951	0.9859	0.9905
BLTGM3	0.8065	0.9698	0.8806	0.9094	0.9544	0.9314	0.9994	0.9822	0.9907

TABLE 7: Principal component feature analysis of the LSTM model.

	RC1	RC2	RC3	RC4	RC5	RC6
SS loadings	8.63	6.91	5.21	3.84	2.25	2.18
Proportion var	0.23	0.19	0.14	0.1	0.06	0.06
Cumulative var	0.23	0.42	0.56	0.66	0.73	0.78
Proportion explained	0.3	0.24	0.18	0.13	0.08	0.08
Cumulative proportion	0.3	0.54	0.71	0.85	0.92	1

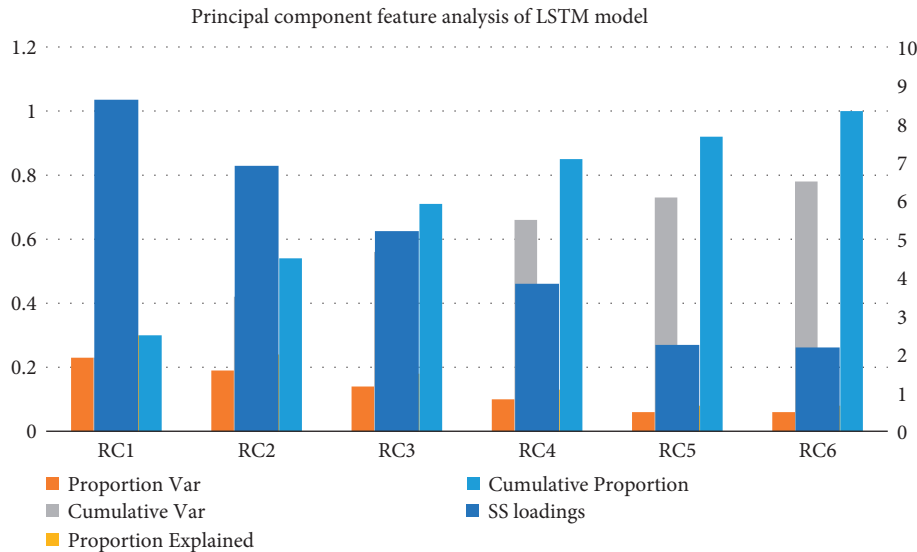


FIGURE 8: Principal component feature analysis of the LSTM model.

ER = 0.391, E-F1 = 0.4145, OP = 0.9215, OR = 0.9318, and O-F1 = 0.9266, as shown in Tables 6 and 7 and Figure 8.

Analyzing the principal component characteristics of LSTM, all data indicators meet the standards, and the best performance in the cumulative ratio is RC1 = 0.3, RC2 = 0.54, RC3 = 0.71, RC4 = 0.85, RC5 = 0.92, and RC6 = 1.

5. Conclusion

This study is based on the unsupervised learning-based enterprise spatial structure evolution and economic coupling coordination relationship situation assessment method. Pattern recognition has high-precision characteristics, but it is necessary to train the evaluation model for the enterprise spatial structure evolution in advance and then carry out economic coupling coordination based on the trained model.

Data Availability

The experimental data used to support the findings of this study are available from the corresponding author upon request.

Conflicts of Interest

The authors declare that they have no conflicts of interest regarding this work.

Acknowledgments

This work was supported by the Key Project of Chinese Ministry of Education of the 14th Five-Year Plan of the National Education Sciences Planning (DIA210365): Study on the Interactive Relationship between Spatial Structure of Local Enterprise and Supply of Talent in Local Colleges from the Perspective of Urban Transformation.

References

- [1] M. Ochodek, S. Koczyńska, and M. Staron, "Deep learning model for end-to-end approximation of COSMIC functional size based on use-case names," *Information and Software Technology*, vol. 123, Article ID 106310, 2020.
- [2] Z. Zhuang, G. Liu, and W. Ding, "Cardiac VFM visualization and analysis based on YOLO deep learning model and modified 2D continuity equation," *Computerized Medical Imaging and Graphics*, vol. 82, Article ID 101732, 2020.
- [3] G. Chen, Q. Pei, and M. M. Kamruzzaman, "Remote sensing image quality evaluation based on deep support value learning networks," *Signal Processing: Image Communication*, vol. 83, Article ID 115783, 2020.
- [4] L. Carvelli, O. An, A. Brink-Kjær, E. B. Leary, and P. Jennum, "Design of a deep learning model for automatic scoring of periodic and non-periodic leg movements during sleep validated against multiple human experts," *Sleep Medicine*, vol. 69, pp. 109–119, 2020.
- [5] Z. Song, T. Liu, and L. Shi, "The deep learning model combining CT image and clinicopathological information for predicting ALK fusion status and response to ALK-TKI therapy in non-small cell lung cancer patients," *European Journal of Nuclear Medicine and Molecular Imaging*, vol. 48, no. 2, pp. 361–371, 2021.
- [6] G. Chen and S. Li, "Network on chip for enterprise information management and integration in intelligent physical systems," *Enterprise Information Systems*, vol. 15, no. 7, pp. 935–950, 2021.
- [7] R. Ghosh, "A Recurrent Neural Network based deep learning model for offline signature verification and recognition system," *Expert Systems with Applications*, vol. 168, no. 5, 2020.
- [8] F. M. Howard, J. Dolezal, S. Kochanny, J. Schulte, and A. T. Pearson, "The impact of site-specific digital histology signatures on deep learning model accuracy and bias," *Nature Communications*, vol. 12, no. 1, 2021.
- [9] F. Niemeyer, F. Galbusera, Y. Tao, A. Kienle, and H. J. Wilke, "A deep learning model for the accurate and reliable classification of disc degeneration based on MRI data," *Investigative Radiology*, vol. 8, no. 12, pp. 61–71, 2020.

- [10] J. Zaucha, C. A. Softley, M. Sattler, D. Frishman, and G. M. Popowicz, "Deep learning model predicts water interaction sites on the surface of proteins using limited-resolution data," *Chemical Communications*, vol. 56, 2020.
- [11] E. Choi, S. Cho, and D. K. Kim, "Power demand forecasting using long short-term memory (LSTM) deep-learning model for monitoring energy sustainability," *Sustainability*, vol. 12, 2020.
- [12] J. S. Raj, S. J. Shobana, I. V. Pustokhina, D. A. Pustokhin, and K. K. Shankar, "Optimal feature selection-based medical image classification using deep learning model in internet of medical things," *IEEE Access*, vol. 8, pp. 58006–58017, 2020.
- [13] N. Shivsharan and S. Ganorkar, "Diabetic retinopathy detection using optimization assisted deep learning model: outlook on improved grey wolf algorithm," *International Journal of Image and Graphics*, vol. 21, Article ID 2150035, 2021.
- [14] H. Shahabi, A. Shirzadi, S. Ronoud et al., "Flash flood susceptibility mapping using a novel deep learning model based on deep belief network, back propagation and genetic algorithm," *The Journal*, vol. 12, no. 3, p. 23, 2021.
- [15] S. J. Im, N. D. Viet, and A. Jang, "Real-time monitoring of forward osmosis membrane fouling in wastewater reuse process performed with a deep learning model," *Chemosphere*, vol. 275, Article ID 130047, 2021.
- [16] G. Foo, S. Kara, and M. Pagnucco, "Screw detection for disassembly of electronic waste using reasoning and re-training of a deep learning model," *Procedia CIRP*, vol. 98, no. 8, pp. 666–671, 2021.
- [17] L. Cong, W. Feng, Z. Yao, X. Zhou, and W. Xiao, "Deep learning model as a new trend in computer-aided diagnosis of tumor pathology for lung cancer," *Journal of Cancer*, vol. 11, no. 12, pp. 3615–3622, 2020.
- [18] X. Pan, Z. Lu, H. Huang, M. Wang, and H. Chen, "Improving nowcasting of convective development by incorporating polarimetric radar variables into a deep learning model," *Geophysical Research Letters*, vol. 48, 2021.
- [19] H. Tanyildizi, A. Engür, Y. Akbulut, and M. Ahin, "Deep learning model for estimating the mechanical properties of concrete containing silica fume exposed to high temperatures," *The Journal*, vol. 14, no. 6, p. 15, 2020.
- [20] X. Yang, Y. Fu, Y. Lei, S. Tian, and T. Liu, "Deformable MRI-TRUS registration using biomechanically constrained deep learning model for tumor-targeted prostate brachytherapy," *International Journal of Radiation Oncology, Biology, Physics*, vol. 108, no. 3, p. e339, 2020.
- [21] A. Muhammad, S. Hong, and J. M. Lee, "A multi-layer perceptron based deep learning model to quantify the energy potentials of a thin film a-Si PV system," *Energy Reports*, vol. 6, pp. 1331–1336, 2020.
- [22] S. M. Chiu, Y. C. Chen, and C. Lee, "Estate price prediction system based on temporal and spatial features and lightweight deep learning model," *Applied Intelligence*, vol. 52, pp. 808–834, 2022.
- [23] W. M. Alenazy and A. S. Alqahtani, "Gravitational search algorithm based optimized deep learning model with diverse set of features for facial expression recognition," *Journal of Ambient Intelligence and Humanized Computing*, vol. 12, no. 10, 2021.
- [24] X. Ning, W. Li, B. Tang, and H. He, "BULDP: biomimetic uncorrelated locality discriminant projection for feature extraction in face recognition," *IEEE Transactions on Image Processing*, vol. 27, no. 5, pp. 2575–2586, 2018.
- [25] A. Onan and S. Korukoğlu, "A feature selection model based on genetic rank aggregation for text sentiment classification," *Journal of Information Science*, vol. 43, no. 1, pp. 25–38, 2017.
- [26] S. K. AytuğOnana and H. Bulut, "Ensemble of keyword extraction methods and classifiers in text classification," *Expert Systems with Applications*, vol. 57, pp. 232–247, 2016.

Retraction

Retracted: Analysis and Optimization of Online Music Teaching System Based on Dynamic Model

Scientific Programming

Received 8 August 2023; Accepted 8 August 2023; Published 9 August 2023

Copyright © 2023 Scientific Programming. This is an open access article distributed under the Creative Commons Attribution License, which permits unrestricted use, distribution, and reproduction in any medium, provided the original work is properly cited.

This article has been retracted by Hindawi following an investigation undertaken by the publisher [1]. This investigation has uncovered evidence of one or more of the following indicators of systematic manipulation of the publication process:

- (1) Discrepancies in scope
- (2) Discrepancies in the description of the research reported
- (3) Discrepancies between the availability of data and the research described
- (4) Inappropriate citations
- (5) Incoherent, meaningless and/or irrelevant content included in the article
- (6) Peer-review manipulation

The presence of these indicators undermines our confidence in the integrity of the article's content and we cannot, therefore, vouch for its reliability. Please note that this notice is intended solely to alert readers that the content of this article is unreliable. We have not investigated whether authors were aware of or involved in the systematic manipulation of the publication process.

Wiley and Hindawi regrets that the usual quality checks did not identify these issues before publication and have since put additional measures in place to safeguard research integrity.

We wish to credit our own Research Integrity and Research Publishing teams and anonymous and named external researchers and research integrity experts for contributing to this investigation.

The corresponding author, as the representative of all authors, has been given the opportunity to register their agreement or disagreement to this retraction. We have kept a record of any response received.

References

- [1] M. Miao, "Analysis and Optimization of Online Music Teaching System Based on Dynamic Model," *Scientific Programming*, vol. 2022, Article ID 4426555, 9 pages, 2022.

Research Article

Analysis and Optimization of Online Music Teaching System Based on Dynamic Model

Miao Miao 

Music and Dance College, Liaocheng University, Liaocheng 252000, China

Correspondence should be addressed to Miao Miao; miaojing@lcu.edu.cn

Received 23 December 2021; Revised 21 January 2022; Accepted 27 January 2022; Published 17 March 2022

Academic Editor: Hangjun Che

Copyright © 2022 Miao Miao. This is an open access article distributed under the Creative Commons Attribution License, which permits unrestricted use, distribution, and reproduction in any medium, provided the original work is properly cited.

The online teaching system is based on a high-tech framework to realize the integration and utilization of existing resources. Applying the online teaching system to distance learning education will help practitioners or self-study people to obtain learning resources more conveniently and quickly. With the development of technology and the social environment, more and more people are participating in online teaching. This has led to rapid growth in online teaching. However, when users use it, there are still problems, such as poor system interaction performance, and cumbersome interface. The construction of a system dynamics model is based on powerful system dynamics methodology and rules to analyze and solve complex problems and make optimal judgments. Through this research, we can get (1). to design the dynamic model music online teaching components: student user table, teacher user table, administrator table, virtual classroom, electronic courseware table, and multimedia music library table. (2). To correct the audio quality, audio speed, audio height, initial efficiency, initial efficiency parameters, video quality, and video traffic. The 3A-10 group has the best effect ($k = 13.9$, $c = 0.30$, $A = 3.27$, $\alpha = 0.80$, $B = 1.67$, and $\gamma = -4.31$). (3). During the appreciation of different music types (groups A, B, C, D, E, and F), the scores were evaluated according to the dynamic model, and the scores were found to be better than 10^6 . (4). The comparison of kinetic equations, Kuramoto, and LIF shows that the scores of the kinetic equations are significantly better than the other two models. In the kinetic model, $F-s = 0.81$, $F-c = 0.66$, $D-s = 0.81$, $D-c = 0.71$, $H-s = 0.72$, $H-c = 0.56$, $V-s = 0.65$, and $V-c = 0.75$.

1. Introduction

In 2019, due to the impact of the coronavirus disease (COVID-19) pandemic, many schools around the world have to carry out online teaching. The Ministry of Education of China has also proposed a plan to transform offline education into online teaching to deal with the impact of the epidemic on teaching. Through the use of Tencent conferences and DingTalk software, etc., a small-scale personal education online course (SPOC) model was established to solve the needs of students to attend classes and perfectly deal with the obstacles of the epidemic to teaching. The small-scale personal education online course model is based on “video courses as the main body, supplemented by online questions and answers” [1–3]. The system also has feedback and improvement links such as online discussions and chapter tests. The teaching quality and effectiveness are evaluated through student group presentations, course examinations, and questionnaire surveys. The online teaching

system is also of great help to the education of the elderly. The online teaching system is a combination of web-based modules or courses, other distance learning technologies, and traditional learning methods. The online teaching system can also provide unified training for rural teachers and update the course content in time. We try to narrow the gap between urban and rural schools as much as possible [4]. The online teaching system is based on a high-tech framework to realize the integration and utilization of existing resources. Applying the online teaching system to distance learning education will help practitioners or self-study people to obtain learning resources more conveniently and quickly. With the development of technology and the social environment, more and more people are participating in online teaching. This has led to signs of rapid growth in online teaching [5–7]. The online teaching system is most related to distance education, but it also appears in classroom education in the form of blended learning. In this period of growth in online teaching, there is time to develop

standards to ensure its quality. Online classrooms are derivatives of traditional classroom teaching standards. There are no specific requirements or rules for online education. Due to its appearance too early, various systems may still have some defects, which requires us to follow-up to improve them. The most useful help for online teachers does not come from the education sector, but from the technical support services of the industrial sector, especially the IT industry. The online teaching system also plays an important role in the online teaching of music, making music teaching more intelligent and personalized, providing technical support for the offline and online teaching of the majority of music teachers, and enriching the means of music teaching. The chain reaction produced by scientific and technological progress has caused corresponding changes in the music teaching model [8]. The traditional music teaching model emphasizes the role of the teacher. Without a balanced relationship between the teacher and the student, the student's independent learning ability and the ability to explore and innovate are restricted. The development of modern information technologies such as mobile Internet technology, artificial intelligence, and big data has made new teaching models more and more abundant. The diversification of teaching methods, tools, and forms not only affects the development of social music teaching but also affects the teaching of music classrooms in primary and secondary schools. The dynamic model also plays an important role in online music teaching [9] involving systematic self-learning, model optimization, checking for omissions and filling vacancies, etc. Generally, there are two mathematical forms used to describe system dynamics, namely differential equations and iterative mapping. Differential equations are used to describe time-continuous dynamic systems, while iterative mapping describes time-discrete systems. There are many universities across the country, and the academic resources and other online resources of the libraries of these universities are very complicated to manage. Generally speaking, it is a very unscientific method to measure which resources the school must purchase more of and which are excess resources. It only depends on the ratio of teachers to students in the school. Some resources will be extremely short-term [10–14]. In order to provide schools with more accurate predictions, it is necessary to introduce system dynamics models. The system dynamics model can be used to measure the distribution and occupation of educational resources to meet the needs of college students' academic activities. The system dynamics method is a powerful computer simulation technology that can bring convenience to people in real life and at work. The construction of a system dynamics model is based on powerful system dynamics methodology and rules to analyze and solve complex problems and make optimal judgments. System dynamics modeling technology can also provide certain assistance to the management and development of enterprises. The cross-impact analysis (CIA) method can be used to construct a system dynamics model [15]. The use of system dynamics can realize the collaborative office of company and enterprise employees and provide convenient conditions for online offices and freelancers. This research will demonstrate

its support for online music education by optimizing the system dynamics model.

2. Technical Analysis of Music Teaching System

2.1. Streaming Media Technology. Streaming media technology is used to enable digital transmission and playback of audio and video. After the video and audio are compressed and decoded, they can be played on the designated server and storage unit, which can achieve the effect of playing while downloading, instead of waiting for 100% of all audio and video downloads to enjoy and watch. Streaming media technology brings together some of the characteristics of the computer field, including data collection, data compression, data storage, and network communications. Sequential streaming can transmit data in real-time, and audio pictures can be transmitted in real-time. Teachers can record their lectures in advance, upload them to the proprietary streaming media database, and then transcode, translate, and re-encode them through the Windows Media Encoder, finally showing lossless sound quality and high-definition picture playback. Windows Media and PowerPoint can combine audio and video [16–18]. You can use the screen recording function and save audio and video as resynthesis in Figure 1.

2.2. Video Live Broadcast Technology. Using the Microsoft streaming information broadcasting program, can realize the promotion and dissemination of audio and video tutorials. Based on the current Internet technology, the rapid dissemination of multimedia data can be realized. The existing technologies basically require users to download impact resources on a dedicated player or the Internet and use dedicated video decoding players or plug-ins to browse and watch audio and video. Therefore, the problem we are facing is that the consumption of downloading the original data is relatively large, time-consuming, and labor-intensive, and occasionally the download is interrupted, which makes users miserable. After a long time of downloading, it may be necessary to perform decoding operations and so on. There is also an important storage issue. When files are downloaded locally, it will be a burden for mobile terminal devices, occupying a large amount of storage resources on mobile phones and computers. This will cause the burden of ordinary users to increase, and the memory may become full and the computer may crash for a long time. Therefore, we optimize the system, increase the threads of the system, perform multithreaded connections and operations, and develop the maximum energy of the server and use the equipment. We count the needs of users, provide peer-to-peer services, and carry out relevant courses according to the students' own learning plans and learning needs. They can learn and work independently in the VOD mode no matter where and when. The control of the node can be operated on its own mobile terminal [19–21].

2.3. Online Music Teaching Module. This online teaching system is based on computer hardware and integrates communication technology, streaming media technology,

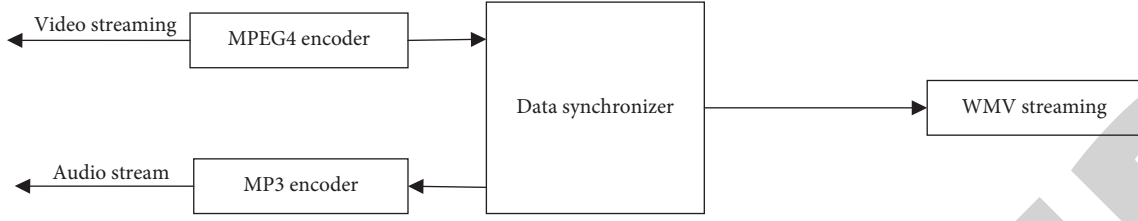


FIGURE 1: Streaming media production method.

network video technology, and cross-cooperation in multiple fields to provide users with an online teaching system. This system is divided into three modules, 1. student space (as shown in Figure 2 online music teaching student space), the student space module includes autonomous learning space, real-time learning, examination learning, and collaborative learning. We use these learning modes to understand and learn unknown knowledge, and the final detection method is answer detection. 2. Virtual classroom (Figure 3 online music teaching virtual classroom), the virtual classroom module is divided into performance and appreciation of music stories, live classroom, grading courses, discussion, and exchanges, through the appreciation and understanding of music, online questions to test the teaching of this lesson quality. 3. Teacher space (Figure 4 online music teaching teacher space). The teacher space module is divided into electronic courseware, live teaching, discussion management, and examination management.

2.4. Dynamic Model Music Online Teaching Composition. Dynamic model music online teaching is divided into student user tables, teacher user tables, administrator tables, virtual classrooms, electronic courseware tables, and multimedia music library tables. The student table is to collect some information about the student, as shown in Table 1(dynamic model music online teaching student user table), including the student's name, set ID, initial password, and other information. The teacher information form needs to fill in some information about the teacher, and its basic information is similar to that in Table 2. The administrator table includes information such as the administrator number, password, last login time, and last login IP. The virtual classroom includes information such as a classroom number and a classroom type. The electronic courseware table, as shown in Table 3, includes courseware number, courseware type, producer, class to which it belongs, courseware content, courseware duration, number of viewers, etc. The multimedia music library table includes file type, file path, upload time, performance skills, number of listening times, and number of collections.

3. Application of Dynamic Model in Online Music Teaching

3.1. LIF (Leaky Integrate Fire) Model [22, 23]. For a dynamic system, the state variable X can be used to characterize the system as

$$X = (x_1, x_2, \dots, x_n). \quad (1)$$

Continuous time music appreciation ability is

$$X'(t) = f[X(t)], \quad x \in R^n. \quad (2)$$

Dynamic equations of time-discrete systems

$$x(t+1) = g[x(t)]. \quad (3)$$

Online teaching system parameters are

$$x_0 = (x_{0,1}, \dots, x_{n,0}). \quad (4)$$

Music node bifurcation (saddle-node bifurcation) is

$$\dot{x} = r - x^2 \quad (x_1 = \sqrt{r}, x_2 = -\sqrt{r}). \quad (5)$$

Treble frequency is

$$\dot{x} = rx - x^2. \quad (6)$$

Online teaching system is expressed as follows:

$$\begin{aligned} \dot{x} &= rx - x^3, \\ \dot{z} &= (r + iw - |z|^2)z. \end{aligned} \quad (7)$$

Node degree is

$$k_i = \sum_{j=1}^N a_{ij} \sqrt{a^2 + b^2}. \quad (8)$$

3.2. Kuramoto Model.

$$\dot{\theta} = \omega_i + \frac{K}{N} \sum_{j=1}^N \sin(\theta_j - \theta_i), \quad i = 1, 2, \dots, N. \quad (9)$$

Natural audio frequency is

$$\dot{\tilde{\theta}} = \omega_i + \frac{K}{N} \sum_{j=1}^N \sin(\tilde{\theta}_j - \tilde{\theta}_i). \quad (10)$$

White noise is as follows:

$$re^{i\tilde{\psi}} = \frac{1}{N} \sum_{j=1}^N e^{i\tilde{\theta}_j}. \quad (11)$$

Kuramoto model fitting online music teaching system is expressed as follows:

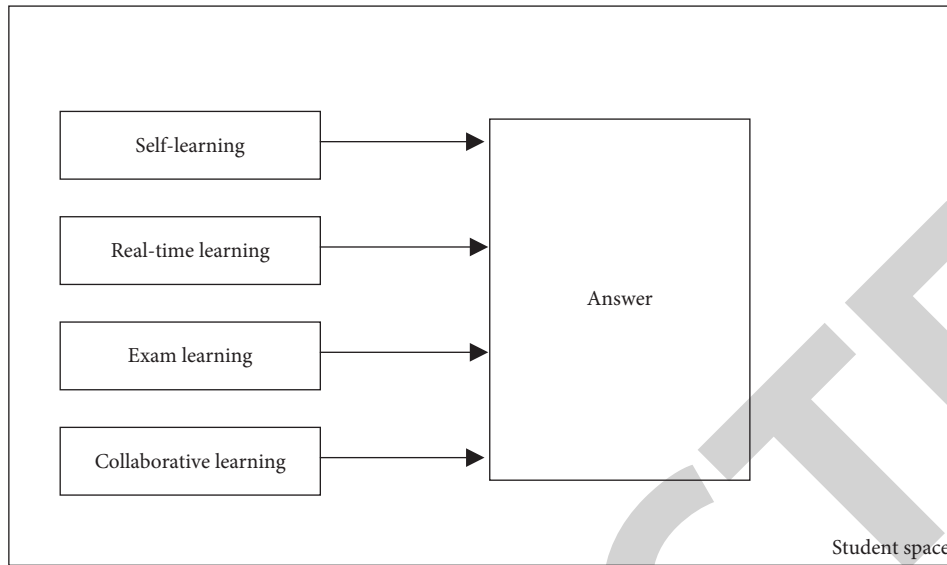


FIGURE 2: Online music teaching student space.

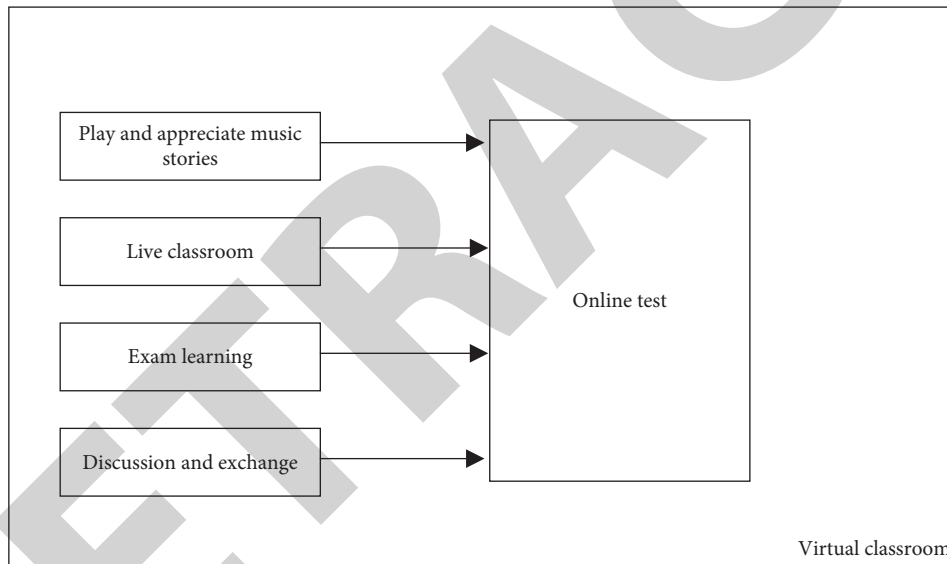


FIGURE 3: Online music teaching virtual classroom.

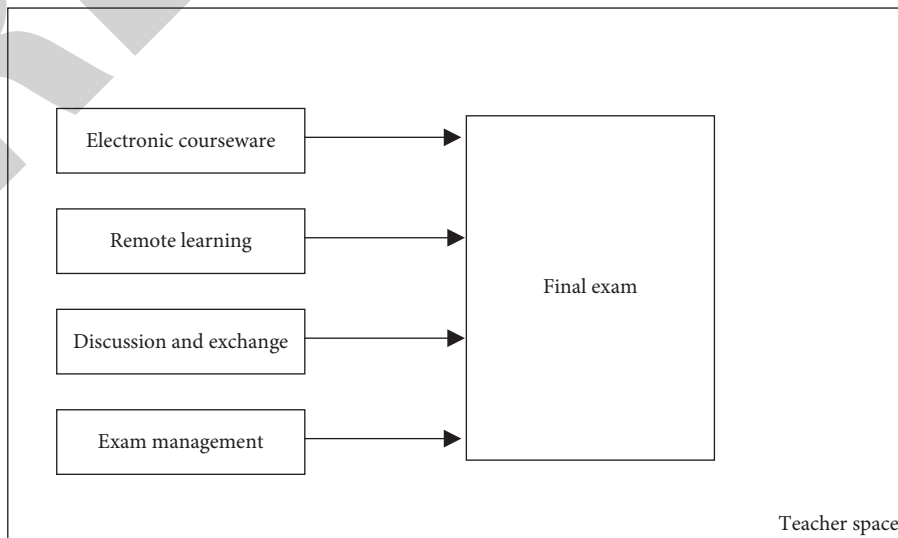


FIGURE 4: Online music teaching teacher space.

TABLE 1: Dynamic model music online teaching student user list.

Field name	Type	Primary key	Foreign key	Can it be empty	Illustrate
StudentID	Int	Y	N	N	Student ID
Name	Varchar (50)	N	N	N	Name
Password	Varchar (50)	N	N	N	Password
Nickname	Varchar (50)	N	N	N	Nick name
Sex	Varchar (5)	N	N	N	Gender
Age	Int	N	N	N	Age
E-mail	Varchar (50)	N	N	Y	E-mail
Address	Varchar (50)	N	N	Y	Contact address
Telephone	Varchar (20)	N	N	Y	Contact number
PicPath	Varchar (100)	N	N	Y	Photo path
Balanced	Int	N	N	N	Point card balance
Grade	Int	N	N	N	User level
RegTime	Date	N	N	N	Registration time
Comments	Varchar (200)	N	N	Y	Remark

TABLE 2: Dynamic model music online teaching multimedia library list.

Field name	Type	Primary key	Foreign key	Can it be empty	Illustrate
MusicID	Int	Y	N	N	Song number
MusicName	Varchar (50)	N	N	N	name
MusicType	Varchar (20)	N	N	N	Type
Author	Varchar (20)	N	N	N	Author
FileType	Int	N	N	N	File type
FilePath	Varchar (50)	N	N	N	File path
UpdateID	Int	N	Y	N	Uploaded by
UpdateTime	Data	N	N	N	Upload time
PlaySkill	Varchar (200)	N	N	Y	Musical skills
PlayCount	Int	N	N	N	Number of listens
CollectCnt	Int	N	N	N	Favorites
Comments	Varchar (200)	N	N	Y	Remark

TABLE 3: Dynamic model music online teaching electronic courseware list.

Field name	Type	Primary key	Foreign key	Can it be empty	Illustrate
VideoNum	Int	Y	Y	N	Courseware number
VideoType	Int	N	N	N	Courseware type
Author	Int	N	Y	N	Maker
CourseID	Varchar (20)	N	Y	N	Belonging to the course
CourseCN	Varchar (200)	N	N	Y	Courseware content
Time	Time	N	N	N	Courseware duration
PlayCount	Int	N	N	Y	Viewers
Comments	Varchar (200)	N	N	Y	Remark

$$r e^{i\tilde{\psi}} = r = \frac{1}{N} \sum_{j=1}^N e^{i\theta_j}, \quad (12)$$

$$\dot{\theta} = \omega_i + Kr \sin(\varphi - \theta_i) = \omega_i + Kr \sin \theta_i.$$

Different types of music inputs are

$$\frac{\partial_\rho}{\partial_t} + \frac{\partial_{(\rho v)}}{\partial_t} = \frac{\partial_\rho}{\partial_t} + \frac{\partial_\rho(\omega - Kr \sin \theta)}{\partial_\theta}, \quad (13)$$

$$Z = \iint d\theta d\omega e^{i\theta} g(\omega) \rho(\theta, \omega, t).$$

$$\rho(\omega, \theta) = \frac{c(\omega)}{|\omega - r \sin \theta|}. \quad (14)$$

The sequence parameter value is calculated as follows:

$$Z = \iint d\theta d\omega e^{i\theta} g(\omega),$$

$$\frac{\partial_{(\rho v)}}{\partial_t} = \frac{\partial_\rho(\omega - Kr \sin \theta)}{\partial_\theta},$$

$$r = \iint d\omega d\theta g(\omega) \delta\left(\theta - \arcsin\left(\frac{\omega}{kr}\right)\right) \quad (15)$$

$$= \int_{-\gamma}^{\gamma} d\omega g(\omega) \sqrt{1 - \left(\frac{\omega}{\gamma}\right)^2}.$$

3.3. Kinetic Model KE (Kinetic Equations). The parameter input of the dynamic model to music online teaching [24–26] is as follows:

TABLE 4: Initial simulation parameters.

Initial simulation parameters	Numerical value
Audio quality	5000
Audio speed	3000
Audio height	460
Initial efficiency	6
Initial efficiency parameter	1.29
Video quality	78.5
Video flow coefficient	0.8

TABLE 5: Calibration results of $k, c, A, \alpha, \beta, \gamma$ and other parameters.

f/Hz	-3A		-1A		1A		3A	
	4	10	4	10	4	10	4	10
k	21.5	22.1	18.9	19.1	17.8	16.8	13.9	14.9
c	0.53	0.48	0.42	0.39	0.37	0.36	0.30	0.31
A	5.61	5.57	4.85	4.53	4.10	3.80	3.27	2.93
α	0.32	0.34	0.52	0.54	0.64	0.63	0.80	0.83
β	2.84	3.16	0.42	1.92	3.54	3.31	1.67	3.94
γ	-5.05	-6.51	-6.48	-5.41	-6.23	-6.59	-4.31	-5.06

Balance equation is expressed as follows:

$$\int_0^{2\pi} d\theta \frac{c(\omega) \sin \theta}{|\omega - r \sin \theta|} \quad (16)$$

The fitting of a dynamic model to music online teaching is expressed as follows:

$$r = \int_0^\infty d\omega g(\omega) \omega + \int_{-\infty}^{-\gamma} d\omega g(\omega) \sqrt{\omega^2 - \gamma^2} - \int_{\gamma}^\infty d\omega g(\omega) \sqrt{\omega^2 - \gamma^2}. \quad (17)$$

Kinetic function is

$$\begin{aligned} f(u, v) &= u(a - u)(u - 1) - v, \\ g(u, v) &= bu - \gamma v, \end{aligned} \quad (18)$$

$$\frac{d}{dt} \left(\sum_{i=1}^n X_i \right) = \left(DF + \frac{x - \mu}{\sigma} \right).$$

Model evaluation is

$$\frac{d\sigma x_i}{dx} = DF\sigma x_i + \epsilon_1 \sum_{j=1}^N M_{ij}^1 B^1 + \epsilon_2 \sum_{j=1}^N M_{ij}^2 B^2 \sigma x_i. \quad (19)$$

4. Simulation Experiment

4.1. Initial Parameter Settings. At the beginning of the experiment, the initial simulation parameters of the experiment were set, and the audio quality, audio speed, audio height, initial efficiency, initial efficiency parameters, video

quality, and video flow coefficient were set. The results are shown in Table 4 as the initial simulation parameters.

4.2. Using Bouc–Wen Model to Calibrate the Online System. The $k, c, A, \alpha, \beta,$ and γ parameters correct the audio quality, audio speed, audio height, initial efficiency, initial efficiency parameters, video quality, and video traffic. As shown in Table 5 and Figure 5, the Bouc–Wen model is used to analyze the parameter sensitivity of the online system. Grouping into -3A, -1A, 1A, 3A, the 3A-10 group has the best effect ($k = 13.9, c = 0.30, A = 3.27, \alpha = 0.80, \beta = 1.67,$ and $\gamma = -4.31$).

4.3. Evaluation of Dynamic Model of Music Online Teaching. The scoring of the model is shown in Figure 6.

We group the music online classes into six groups: A, B, C, D, E, and F and appreciate different music types (diplomacy, military, politics, technology, sports, and livelihood) in Table 6, and then scored according to the dynamic model evaluation and found that the score fit is higher than 10^6 .

Among them, the various types account for diplomacy = 7%, military = 18%, politics = 26%, technology = 10%, sports = 17%, and livelihood = 22% as shown in Figure 7.

As shown in Table 7(model optimization comparison) and Figure 8 (model comparison), use $F-s, F-c, D-s, D-c, H-s, H-c, V-s,$ and $V-c$ to evaluate and compare the models. Comparing the three models of kinetic equations, Kuramoto, and LIF, it is found that the scores of the kinetic equations are significantly better than the other two models. In the kinetic model, $F-s = 0.81, F-c = 0.66, D-s = 0.81, D-c = 0.71, H-s = 0.72, H-c = 0.56, V-s = 0.65,$ and $V-c = 0.75$.

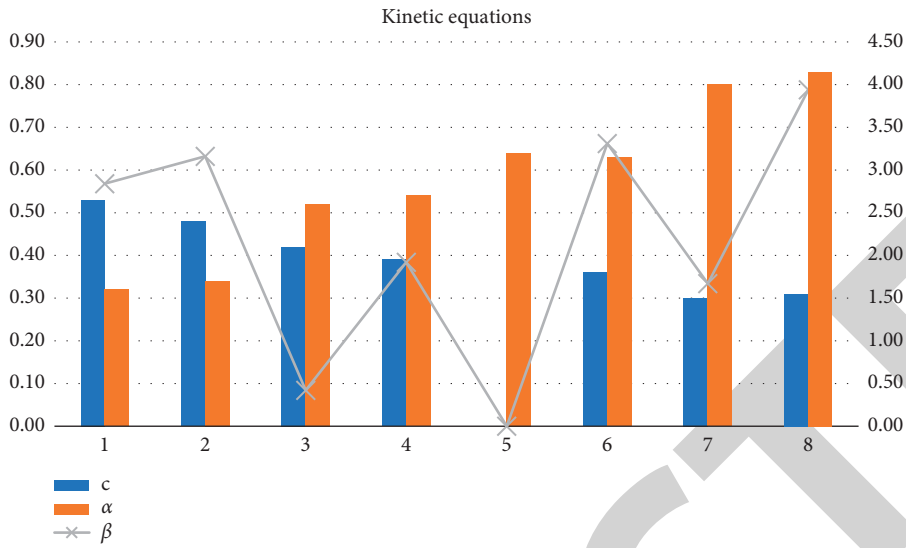


FIGURE 5: Correction results of (c) α and β parameters.

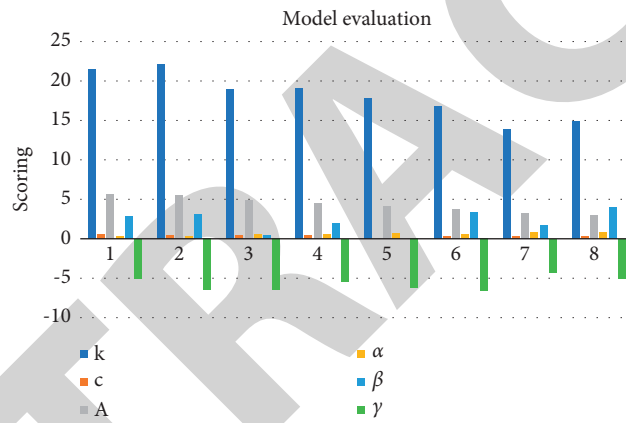


FIGURE 6: Model scoring.

TABLE 6: Dynamic appreciation scores of different music types.

Serial number	Category	Content	value
A	Diplomacy	China and the United States agree not to impose new tariffs	1159691
B	Military	U.S. withdrawal from Syria	3144622
C	Politics	Speech at the 40th anniversary of reform and opening up	4462115
D	Technology	Blackmail virus requiring WeChat to pay ransoms	1829246
E	Sports	Ke Jie defeated Korean players	2866745
F	Livelihood	Yueqing boy lost incident	3783792

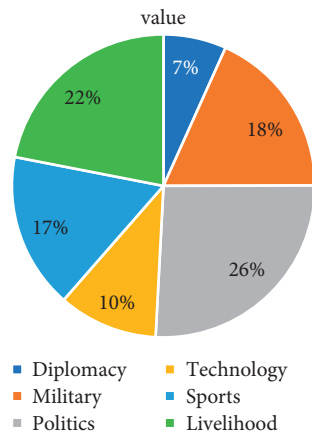


FIGURE 7: Proportion of various types of music.

TABLE 7: Model optimization comparison.

	$F-s$	$F-c$	$D-s$	$D-c$	$H-s$	$H-c$	$V-s$	$V-c$
Kinetic equations	0.81	0.66	0.81	0.71	0.72	0.56	0.65	0.75
Kuramoto	0.78	0.62	0.74	0.58	0.64	0.56	0.45	0.62
LIF	0.74	0.59	0.72	0.56	0.16	0.32	0.21	0.25

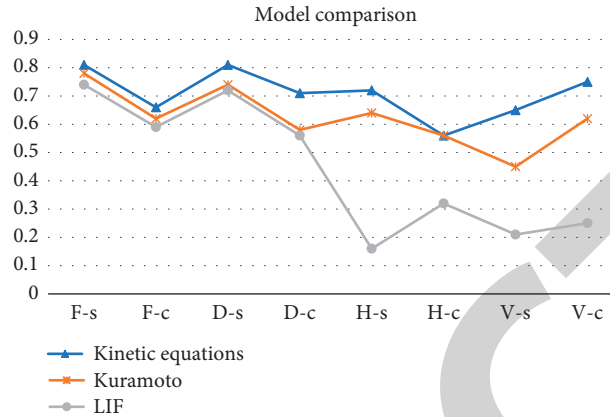


FIGURE 8: Model comparison.

5. Conclusion

In this study, by setting the initial parameters of the kinetic model, the kinetic model can better fit the music online teaching system. And we use the Bouc–Wen model to detect and modify the online system. Finally: (1). we designed the dynamic model for music online teaching components: student user table, teacher user table, administrator table, virtual classroom, electronic courseware table, multimedia music library table. (2). We corrected the audio quality, audio speed, audio height, initial efficiency, initial efficiency parameters, video quality, and video traffic. The 3A-10 group has the best effect ($k=13.9$, $c=0.30$, $A=3.27$, $\alpha=0.80$, $B=1.67$, and $\gamma=-4.31$). (3). In the appreciation of different music types (groups A, B, C, D, E, and F), the scores were evaluated according to the dynamic model, and the scores were found to be better than 10^6 . (4). The three models, kinetic equations, Kuramoto, and LIF, are compared, and it is found that the scores of the kinetic equations are significantly better than the other two models. In the kinetic model, $F-s=0.81$, $F-c=0.66$, $D-s=0.81$, $D-c=0.71$, $H-s=0.72$, $H-c=0.56$, $V-s=0.65$, and $V-c=0.75$. The main research work in the future focuses on the characteristics and efficiency of online music communication and puts forward the analysis of relevant online music communication paths. The main propagation models in different application scenarios are deeply studied, and the key propagation nodes and function analysis of different algorithms are proposed.

Data Availability

The experimental data used to support the findings of this study are available from the corresponding author upon request.

Conflicts of Interest

The author declares that there are no conflicts of interest regarding this work.

References

- [1] W. Wang, Y. Zhang, K. Tang et al., “Exploration and practice of online teaching system of medical immunology based on small private online course (SPOC) model during coronavirus disease 2019 (COVID-19) pandemic,” *Chinese journal of cellular and molecular immunology*, vol. 36, no. 4, pp. 376–382, 2020.
- [2] Xi Bao, F. Yu, M. Yi, and Z. Xue, “Standards for online teaching: lessons from the education, health and IT sectors,” *Nurse Education Today*, vol. 25, no. 1, pp. 23–30, 2005.
- [3] R. M. K. Medeiros, R. C. Teixeira, A. B. Nicolini, A. S. Alvares, Á. C. d. P. Corrêa, and D. P. Martins, “Cuidados humanizados: a inserção de enfermeiras obstétricas em um hospital de ensino,” *Revista Brasileira de Enfermagem*, vol. 69, no. 6, pp. 1091–1098, 2016.
- [4] Z. D. Sun, D. Y. Ran, M. A. Dong-Dong, B. Wang, and S. L. Song, “Design of online teaching system for passing levels engine repair,” *Education Teaching Forum*, vol. 11, no. 23, pp. 51–62, 2019.
- [5] S. Wang and M. Mu, “Exploring online intelligent teaching method with machine learning and SVM algorithm,” *Neural Computing & Applications*, vol. 36, no. 6, pp. 1–14, 2021.
- [6] W. Y. J. Ho and K. W. H. Tai, “Doing expertise multilingually and multimodally in online English teaching videos,” *System*, vol. 94, no. 3, Article ID 102340, 2020.
- [7] C. S. Pedamallu, L. Ozdamar, G. W. Weber, and E. Kropatd, “A system dynamics model to study the importance of infrastructure facilities on quality of primary education system in developing countries,” in *Proceeding of the AIP Conference Proceedings*, vol. 1239, no. 1, pp. 321–325, American Institute of Physics, College Park, MA, USA, June 2010.

Retraction

Retracted: Influence of Management Efficiency of Sports Equipment in Colleges and Universities Based on the Intelligent Optimization Method

Scientific Programming

Received 29 August 2023; Accepted 29 August 2023; Published 30 August 2023

Copyright © 2023 Scientific Programming. This is an open access article distributed under the Creative Commons Attribution License, which permits unrestricted use, distribution, and reproduction in any medium, provided the original work is properly cited.

This article has been retracted by Hindawi following an investigation undertaken by the publisher [1]. This investigation has uncovered evidence of one or more of the following indicators of systematic manipulation of the publication process:

- (1) Discrepancies in scope
- (2) Discrepancies in the description of the research reported
- (3) Discrepancies between the availability of data and the research described
- (4) Inappropriate citations
- (5) Incoherent, meaningless and/or irrelevant content included in the article
- (6) Peer-review manipulation

The presence of these indicators undermines our confidence in the integrity of the article's content and we cannot, therefore, vouch for its reliability. Please note that this notice is intended solely to alert readers that the content of this article is unreliable. We have not investigated whether authors were aware of or involved in the systematic manipulation of the publication process.

Wiley and Hindawi regrets that the usual quality checks did not identify these issues before publication and have since put additional measures in place to safeguard research integrity.

We wish to credit our own Research Integrity and Research Publishing teams and anonymous and named external researchers and research integrity experts for contributing to this investigation.

The corresponding author, as the representative of all authors, has been given the opportunity to register their agreement or disagreement to this retraction. We have kept a record of any response received.

References

- [1] S. Wang, "Influence of Management Efficiency of Sports Equipment in Colleges and Universities Based on the Intelligent Optimization Method," *Scientific Programming*, vol. 2022, Article ID 7126743, 8 pages, 2022.

Research Article

Influence of Management Efficiency of Sports Equipment in Colleges and Universities Based on the Intelligent Optimization Method

Shuai Wang 

Physical Education Teaching and Research Department of Heilongjiang University, Harbin 150080, China

Correspondence should be addressed to Shuai Wang; 2004114@hlju.edu.cn

Received 22 January 2022; Revised 11 February 2022; Accepted 14 February 2022; Published 14 March 2022

Academic Editor: Hangjun Che

Copyright © 2022 Shuai Wang. This is an open access article distributed under the Creative Commons Attribution License, which permits unrestricted use, distribution, and reproduction in any medium, provided the original work is properly cited.

China has always considered the improvement of youth physical quality as one of the key steps in the talent training program, and universities have always followed the national policy to change the quantity and quality of sports equipment. This study mainly focuses on the development of sports equipment management system in colleges and universities. By building a scientific sports equipment management system, the efficiency of sports equipment management process is improved and the difficulty of managers' work is reduced. The construction of the sports equipment management system is a comprehensive information service platform created specifically for sports administrators. The main function is to help sports equipment administrators obtain information on equipment management, and it is an electronic system that can obtain the status of sports equipment use through certain instructions, providing an example for sports equipment management in China's universities.

1. Introduction

Along with the accelerated pace of economic development, the quality education advocated by the Ministry of Education in all colleges and universities has received wide attention from all walks of life, especially in the field of physical education, in order to quickly improve the quality of teaching. The equipment of hardware has increased significantly [1]. Then, about the use of this equipment, the construction of scientific and reasonable rules and regulations as well as the effective realization of the rational application of resources in teaching to achieve the improvement of quality must become the issue that needs to be considered at present. Today, with the increasingly rapid development in the field of information technology, it is possible to solve precisely the problems described above [2]. The use of information technology as a medium to achieve electronic system management of sports equipment can achieve efficient and convenient management [3].

As a part of fixed asset management, traditional sports equipment management is carried out manually, which

requires sports equipment managers to be on standby every day, making sports equipment management a headache that wastes both human and financial resources and is not favored. This problem is especially obvious in our unit [4].

First of all, as the size of the school continues to expand and develop, the sports equipment assets continue to expand and become more frequently used, and the number of sports equipment in the school is correspondingly much larger than the general number of schools and colleges, thus making it more difficult to manage. Furthermore, under the contradiction of one set of management system of two units, the school is divided into two parts in the management of fixed assets of sports equipment, College A and Branch B [5]. However, in the process of use, the two levels can use each other, which invariably increases the difficulty of sports equipment management and scheduling.

Secondly, there is no fixed position of sports equipment manager in our unit, it is done by physical education teachers on a part-time basis, and each physical education teacher has classes to attend and teaching tasks to complete. In response to the above phenomenon, at least two teachers

need to take turns to sit on duty to manage the assets and loan of physical education equipment, which increases the burden of teachers [6, 7].

Again, the use and management of physical education equipment in colleges and universities are characterized by many types, large quantities and decentralized departments, so it is impossible to take physical inventory regularly, which leads to the management of obsolescence; obsolescence and renewal of equipment often cannot be reflected and updated in time, which often causes discrepancies between accounts and reality and cannot objectively and truly reflect the status of assets [8].

Finally, the school has to fill out forms and apply and record the use of sports equipment in a detailed manner. These steps of approval and record-keeping consume the working time of the management staff and lead to the reduction of enthusiasm of students and related departments due to the complicated steps of loaning and returning equipment. Therefore, it is important to simplify the rental procedures and streamline the rental process [9].

The abovementioned reasons have brought a lot of trouble to the management of sports equipment in units. As the number and types of school sports equipment continue to increase, its utilization rate also gradually increases. In order to effectively manage school sports equipment, increase the purchase of sports equipment in a timely manner, keep track of the loan of sports equipment, and reflect the true information of fixed assets; it is imperative to develop an efficient sports equipment management system [10].

The purpose of developing and using a PE equipment management system is to free managers from the tedious manual registration work and to devote their energy to improving the efficiency of PE equipment management and facilitating the use of PE equipment, thus making PE equipment management more efficient and convenient and better serving the overall school teaching [11].

2. Overall Design of Sports Equipment Management System in High School

The development of the sports equipment management system in colleges and universities is conducive to the expansion of new ideas in the management of sports equipment in colleges and universities. Administrators can make real-time inquiries about sports equipment borrowing and returning information within the system, supervise students who have not returned their equipment after the deadline, and set up compensation and other management operations through the sports equipment management system. With the assistance of the sports equipment management system, the sports management department can have the remaining time to perform other tasks in their positions. The construction of a sports equipment management system in higher education provides a good working atmosphere and an efficient form of work for the sports equipment management department [12].

Management information system (hereinafter referred to as MIS) must be human-centered in the process of realization; of course, hardware and network equipment and computer software are essential, mainly for the specific

transfer, processing, collection, and processing of information on the target to be able to ensure the efficiency of management [13]. Management information systems are very different from other systems mainly because this system is mostly focused on the analysis of operations. While in specific academic studies, systems of decision automation and decision support are the collective term for information management methods (e.g., decision support systems, expert systems, and supervisory support systems) [13].

The functions of management information systems are very numerous and are inextricably related to each other, as well as to the combined situation of an organism dedicated to the realization of the overall functionality. The specific functions are described below: data processing, that is, the processing of data for storage, collection, transmission, processing, and input and other processes transaction processing, mainly focused on the assistance of the content of the work of managers, who, with the relevant research, are well able to free themselves from the mental and physical labor of the past, greatly improving the efficiency of work and increasing the creativity of the staff [14]. The forecasting function, which can analyze the future situation by means of data formulas and realistic simulations, enables rational planning; the planning function can plan the work of the department in advance and control the final execution by means of relevant monitoring systems; the control function, which can control the management and analyze the causes of loopholes, plays a role in supporting the staff. The auxiliary decision-making function can improve the scientific nature of decision-making, especially in terms of the accuracy of mathematical models.

Management information system (MIS) is a type of information that uses computer terminals and network communication devices, businesses, schools, and government departments, such as collecting, transmitting, sharing and maintaining a specific range of information, and interacting with relevant system operators [15]. Management information systems in order to the ultimate goal to improve management efficiency and thus improve the market competitiveness of enterprises. The project is shown in Figure 1.

The integrated management information system consists of six parts, which are mainly collected, processed, stored, transmitted, maintained, and used [16]. A well-developed management information system allows the user to first specify exactly what information is needed, to purposefully collect relevant information and convert it into a format that accepts the user on this basis, in addition to information management.

The process of carrying out the development of the system should pay great attention to the workflow, and it is necessary to achieve precise transformation in the specific workflow so that it is possible to constantly innovate the management mechanism, which is significant in terms of establishing reasonable rules and regulations, as well as stable production procedures, and constantly broadening the management practices in management, promoting the upgrading of the management system, and greatly simplifying the workflow, and in terms of improving the efficiency of work, the significance is significant [17].

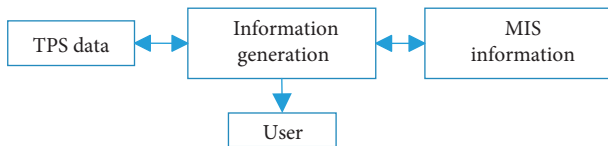


FIGURE 1: Working principle diagram.

The development of the management information system must pay attention to the requirements and make a fairly detailed analysis of the requirements in order to be able to achieve the target. From the beginning, it is important to have a big picture view, to be able to face the management object from a certain level, to be able to analyze the main issues and details, and to follow the top-down principle. At the development level, it should be compatible and adaptable to the later development and maintenance of the system. The code should be readable, modular, and pluggable and have the ability to adapt to changes in requirements as they occur. Training documents and trainers are available during the application phase. Users are enabled to have some knowledge of the benefits of the system and to manage it, so that the use of the system can be promoted smoothly [18].

3. Sports Equipment Management

3.1. School Sports Equipment. School sports equipment refers to school sports training, various equipment, sports equipment and teaching materials, sports competitions, and extracurricular sports activities and uses. It is a task to complete school sports and to achieve the basic premise and material basis, the purpose of school sports. Physical education supervision is an important part of the development of school physical education, and it measures the standardization of school physical education.

3.1.1. According to the Classification of Sports Items. After the classification of sports, it is also possible to achieve the classification of equipment, such as track and field track and field equipment, weightlifting equipment, and ice and snow equipment.

3.1.2. Classification according to the Nature of Sports Equipment. The current classification is mainly based on four categories: self-provided equipment, designated equipment, field equipment, and other equipment.

When the two sides of the competition often specify the manufacturers, trademarks, and specifications of the equipment, which is a good way to avoid conflicts, self-provided equipment is the equipment carried by the athletes themselves, for example, some sports are brought by themselves, such as ball bats, sports clothing and related shoes, hats, and protective gear and some are items in the venue, such as goals, stoppers, and timers. Of course, there are some nonfield information, mainly including physical training, fitness activities, and sports and recreation equipment.

3.2. The Concept of Sports Equipment Management. In "Management," that is, the specific management process, there are many interpretations of the concept of management, and the following definition is made by summarizing the conceptual theories of most scholars: the manager is the subject of management, mainly based on the understanding of the objective laws of the accident, using a rational approach and an orderly, rational, and scientific analysis of the relevant processes, which may contain a lot of planning and control in the process. The main purpose is to regulate the flow of activities and the integration of resources so as to achieve the target process [9, 10].

Based on the understanding of the concept of management, the definitive conclusion about the management of physical education equipment is made in this study: the school should take into account the condition of the equipment itself and adopt reasonable means and procedures in conducting the use of physical education equipment. The methods are controlled so that the sports equipment can play its proper role and can achieve the coordination of all aspects, which is significant for the use of sports equipment.

4. Design of Sports Equipment Management System in High School

4.1. Overall System Design. Layered architectures are very common in software architecture planning, and they are also a very important class of constructs. A hierarchical model can often have three main layers, roughly from bottom to top: the domain layer, the data access layer, and the representation layer [6], as shown in Figure 2.

The role of each level is as follows.

The access data layer is mainly a class of operations on the initial numbers (database or a series of files and other types of storage of numbers), but not the initial class of data alone. We can also say that it is related to the operation of the numbers, specifically the transaction logic layer or the related services provided on behalf of the class.

The logical layer of the transaction: it is mainly for the operation of the problem, which can also be understood as the operation of the data and the logical processing of the data transaction. If the building blocks are the data layer, then the building blocks are the logical layer.

Representation layer: the main representation WEB way can also be expressed as WINFORM way. WEB way can also be expressed as aspx; if the logic layer is quite powerful and perfect, no matter how the performance layer is defined and changed, the logic layer can be perfect to provide services.

This system administrator C/S structure to achieve the overall architecture design is shown in Figure 3.

The technical route of system development adopts J2EE development technology and follows J2EE1.4 specification.

C/S structure part of the implementation of the interface representation layer using java application swing components to achieve GUI graphical user interface and to achieve database connection using JDBC-ODBC bridge.

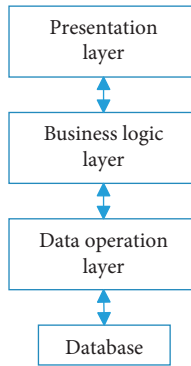


FIGURE 2: C/S three-tier architecture diagram.

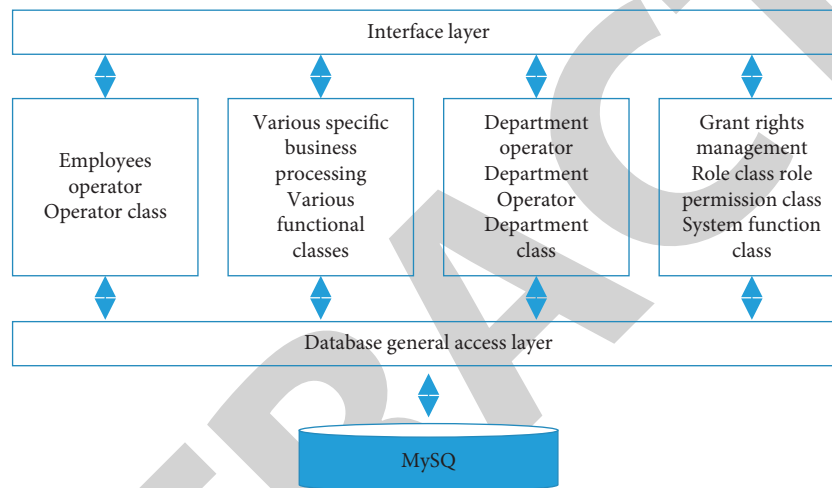


FIGURE 3: C/S implementation three-tier architecture diagram.

4.2. System Functional Module Design. In accordance with the top-down, step-by-step approach, the top-level modules are designed to design their subordinate modules for each module. The structure diagram of several important modules is shown in Figure 4:

As seen in Figure 5, loan registration is the top-level module and borrower information and device information are its subordinate modules, while borrower number and borrowing time are the subordinate modules of borrower, and device level, quantity, and device name are the subordinate modules of device information.

In Figure 6 of the structure of the “return device” module, the return registration is the top module for the borrower information and the device information; the borrower information is also the top module for the borrower number and the return time, and the device information is the top module for selecting the returned device.

In Figure 7 of the ‘request device’ module structure, the request registration is the top-level module and its subordinate modules are borrower information, submission time, and device information. The borrower information is the top module for the borrower number and the borrowing time; the device information is the top module for the quantity and the selected device name.

In the structure diagram of the “approval application” module, the approval result is the top-level module for approval, the approval is the top-level module for viewing the application record, and the viewing application record is the top-level module for borrower information and equipment information.

The software design of the university sports equipment management system is mainly divided into three layers: information display layer, business processing layer, and data storage layer [3].

The information display layer is the interaction interface between the equipment management system and the user, and its main function is to display the information of equipment borrowing and returning. For example, if a device borrower forgets the login password when logging into the device management system, he/she can log in or reset the password in the form of a dynamic verification code to ensure the security of the system.

The business processing layer can play a role between the information display layer as well as the data storage layer. When sports equipment borrowers and returners initiate business processing or inquiries in the information display layer, the processing results can be retrieved to the processing center of the data to retrieve the user’s information,

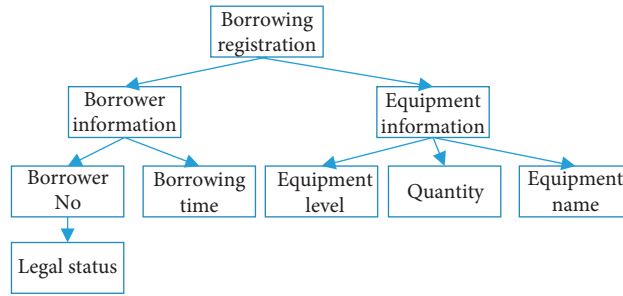


FIGURE 4: Structure of the “loaner” module.

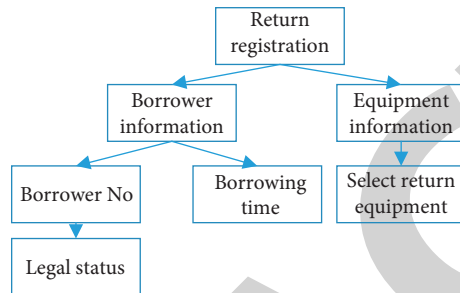


FIGURE 5: Structure of the “return of equipment” module.

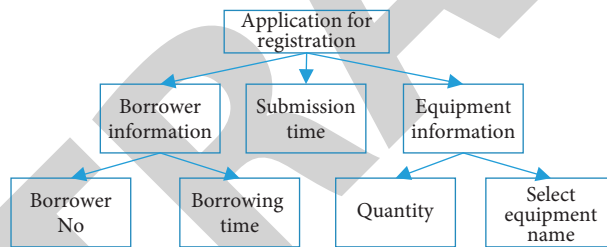


FIGURE 6: Structure of the “request device” module.

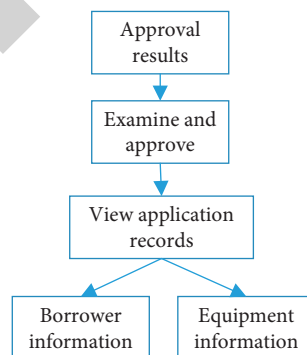


FIGURE 7: Structure of “approval application” module.

and the results can be fed back to the representation layer. When designing the core business processing layer that is in the whole software system, the rules and regulations and system application processes developed in the early stage should be placed in this layer to avoid code errors in the application process of the sports equipment management system. When certain sudden code errors appear, the business processing layer will provide timely feedback to the

information display layer. When designing the business processing layer, attention needs to be focused on the problem of anomalous phenomena and the system crash caused by network virus problems.

The data storage layer is mainly responsible for changing the data storage content and the output method of the data, and the data can be retrieved, passed, and deleted in the college sports equipment management system. After the original data

are basically determined in the early stage of system data setting, the original data will not be changed in the later stage. In order to improve the sense of the later use of the whole equipment management system, this study provides a more convenient data storage layer operation method for the third layer system.

5. Database Design of Sports Equipment Management System in Colleges and Universities

5.1. Sports Equipment Management System Design Process. Database design can be arranged into five main stages: user requirements analysis, system conceptual design, data structure design, software design, and post-operation and maintenance. In the preliminary stage of database development, the user requirements and system conceptual design are the most important.

5.2. Conceptual Structure Design of Sports Equipment Management System. E-R diagram, proposed by P.P. Schen in 1976, is one of the effective methods of initial conceptual analysis of database modules of sports equipment management systems [5]. In the sports equipment management system of universities, the main design idea should be followed to build a relational model system that reflects the real phenomenon. In the corresponding sports equipment management system, the relationship between individual entities is closer, and it can be seen that when designing the core terminal of the system, it is necessary to take into account the problem of data attributes and realize real-time query, modification, and deletion operations between subjects.

5.3. Sports Equipment Management System Process Structure Design. In the data storage system of college sports equipment management system, teachers need to be granted the authority to manage the system firstly, which can be mainly divided into the following categories: system management teachers, sports equipment management teachers, and teachers in charge of sports equipment management. Mainly through the system management teacher for permission allocation work, the teacher table is the main data source for system login and equipment check-in/check-out.

When a class needs to borrow sports equipment, they need to present their student ID card to the sports equipment manager and check their personal information against the class form to complete the loan.

In the college sports equipment management system, the class and teacher's class schedule is stored, and when a class needs to borrow sports equipment, this form can be used to verify the information. The management of the schedule is a little more complicated, as the schedule needs to be updated every semester according to the teaching schedule, so the system administrator needs to make real-time changes to the schedule.

In the PE equipment management system of the university, teachers need to apply for the loan of PE equipment according to the regulations issued by the PE equipment

room. It is important to note that, in order to regulate the equipment borrowing behavior of teachers, the number of sports equipment that can be borrowed at a time should be specified. For example, teachers may only borrow three types of physical education equipment at a time and students may borrow one type of physical education equipment at a time. When the borrower returns the equipment after use, the administrator then modifies and records the corresponding fields in this table. The details are shown in Figure 8.

When teachers or students return sports equipment, the system automatically updates the data in real time and analyzes the loan record table together with this table. When the system makes a regular inquiry for the users who have not yet returned the sports equipment, if the teacher or student is found to be the one who returned the sports equipment, the system will automatically remind the teachers and students who have not yet returned the sports equipment to try to return it at once. The details are shown in Figure 9.

6. Performance Test

According to the communication and research with other colleges and universities, some specialized sports colleges and universities, such as Tianjin Sports Institute, have just developed their own sports equipment management information system. Although the sports equipment management system developed by each university is only successfully developed and put into use in these two years, the history is not too long, but it shows that this issue has already attracted the attention of each university on fixed assets' management in sports equipment management. These sports equipment management systems developed by colleges and universities are mainly used for a number of purposes, approving the borrowing of the equipment concerned, statistical management of the total classification, reporting and updating, etc., which basically solve the basic functions required by most colleges and universities in need of such systems, as shown in Figure 10.

However, the sports equipment management system developed by these sister schools and colleges cannot fully meet the needs of sports equipment recall and management under the unique system of "two levels of schools and colleges with one set of management mechanism" in the light of the actual management situation of the school. Different equipment management systems focus on different functional points, and this system is mainly intended to solve the borrowing and returning of sports equipment for two levels of schools, including College A and Branch B. There are major differences between the management process and ideas of sports equipment and other equipment management systems, for example, in the number of returns and the time nodes of returns, as shown in Figure 11.

The difference in categories leads to differences in borrowing and lending. For sports equipment, borrowers are usually teachers, and at some point in time, the number of one-time borrowing and returning is larger. From the security point of view, other systems, especially those involving the military, generally have more security and confidentiality design to consider, while the sports equipment management system is a civilian, relatively less in terms of security.

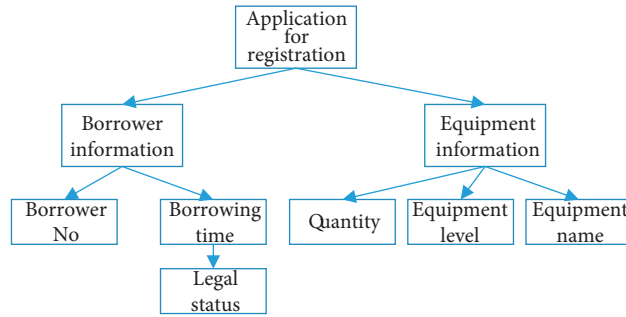


FIGURE 8: Structure of the loaner device module.

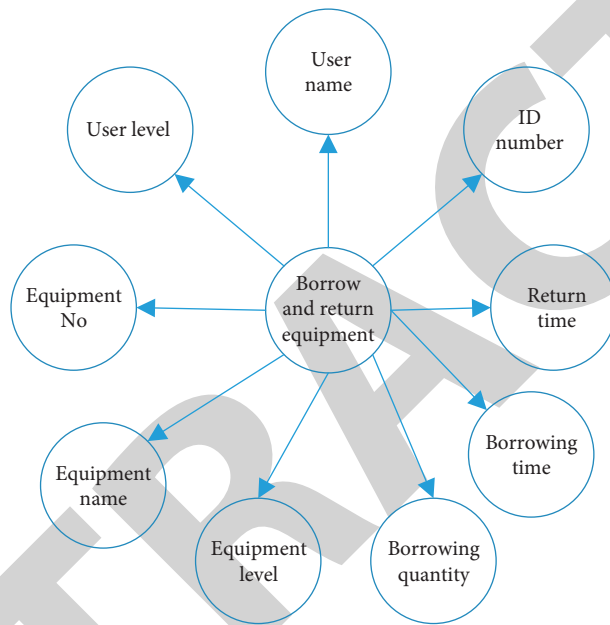


FIGURE 9: Property diagram of the loan and return information entity.

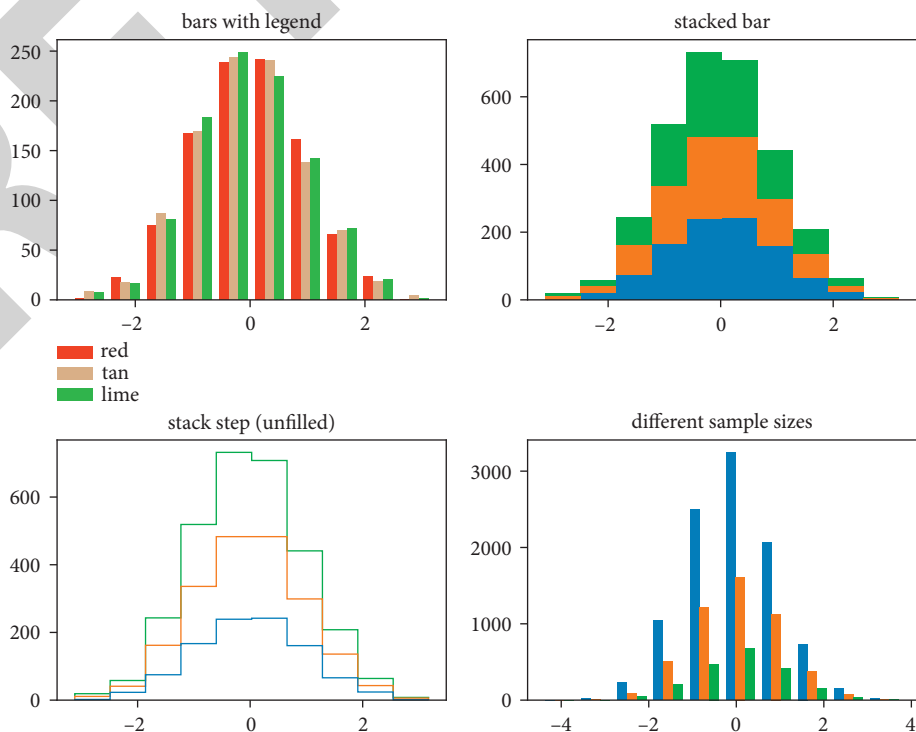


FIGURE 10: Different management effects.

Research Article

Construction and Simulation of Market Risk Warning Model Based on Deep Learning

Li Zhao, Yafei Gao , and Dongwei Kang

Dongwei Kang School of Management Engineering and Business, Hebei University of Engineering, HanDan 056038, China

Correspondence should be addressed to Yafei Gao; gaoyafei@hebeu.edu.cn

Received 15 December 2021; Revised 17 January 2022; Accepted 31 January 2022; Published 12 March 2022

Academic Editor: Hangjun Che

Copyright © 2022 Li Zhao et al. This is an open access article distributed under the Creative Commons Attribution License, which permits unrestricted use, distribution, and reproduction in any medium, provided the original work is properly cited.

The market is intricate and complicated, and the existing risk warning models have problems of low efficiency and poor generalization in predicting market risk data. Aiming at the problems, this study takes stock market risk warning as the research object and proposes a market risk warning model based on LSTM-VaR. 15 variables in the three categories of basic transaction data, statistical technical indicators, and moving interval data are selected as the stock market characteristic indicators, the LSTM(Long Short Term Memory) prediction model is constructed and the standard deviation of stock returns is predicted. Based on the predicted results, the probability distribution of return rate under the conditional distribution is obtained, and the VaR(Value at Risk) is calculated. 1% and 5% sample quantiles are taken as the warning line, and the LSTM-VaR warning model is obtained. The results show that the RMSE value of the model is the smallest, which is 0.013762, when the activation function of the LSTM-VaR model is the Leaky ReLU function, the training periods epochs are 10, the time window length N is 9, the batch size is 8, the number of neurons in each layer is 50, the dropout probability is 0.1, and adam is used as the optimizer. Compared with traditional prediction models such as MLP, the proposed model has better performance and can well realize market risk warning.

1. Introduction

The influencing factors of the market are complex and changeable, and it is usually difficult to master the rules. In recent decades, market crises occurred frequently. For example, the global economic crisis in 2008 triggered economic turmoil around the world, resulting in unemployment of tens of millions of laborers worldwide, an increase of 50 million poverty population, and irreparable losses [1]. This shows the significance of market risk warning in the global economy. At present, with the progress of artificial intelligence technology, deep learning, with good nonlinear mapping ability and fitting generalization ability, is widely used in market dynamic prediction. For instance, prediction methods based on artificial neural networks have achieved good prediction results in dealing with market non-linearity and time series dependence. Lin Wenhao and Chen Xuebin et al., combined with the relevant data of Shanghai Securities, proposed a stock market risk prediction method based on GARCH(Generalized Autoregressive

Conditional Heteroskedasticity model), which effectively realized the prediction of stock market risk [2, 3]; Li Xinxin and Liu Chengcheng et al. built a risk prediction model with generalized vector autoregressive model [4, 5]; Guo Jing and Liu Wenchao et al. evaluated the inherent volatility risk of the stock market through implied tail risk, greatly improving the risk warning ability [6, 7]; Zhou Wenhao and Tian Chongwen et al., constructed a customer default model of banks on the basis of commercial banks data and the logistic regression, so as to improve the identification ability of customer risks of banks; However, the above methods are mainly through quantitative risk analysis [8, 9]. With the application of neural network, It has begun to be applied to risk prediction. For example, Ren Ni et al. applied deep learning algorithm to financial risk prediction, providing reference for the application of deep learning algorithm in risk prediction [10]. Zhang Qun et al. applied LSTM algorithm to wind forecasting, which is characterized by fitting with time series data. In the above studies, the focus is how to improve the accuracy of risk prediction [11]. Therefore, in

order to solve the above problems, based on extensive review of relevant literature, this study takes stock market risk warning as the research object, and proposes a LSTM-VaR market risk warning model in the basis of the LSTM(Long Short Term Memory) and the VaR(Value at Risk). By using LSTM network to predict standard deviation of stock returns and VaR to measure value at risk, the stock market risk warning can be realized.

2. Basic Methods

2.1. LSTM Model Introduction. LSTM model is a variant of recurrent neural network (RNN). By replacing the neuron structure of RNN with a three-layer “gate” structure of input gate, output gate and forgetting gate, the problem of gradient disappearance of RNN network loss function and long-term dependence can be solved. Figure 1 is the LSTM network model structure, showing the processing flow of data through the memory unit and gate structure. In the figure, i_t represents the input gate, f_t represents the forgetting gate, O_t represents the output gate, C_t represents the hidden layer neuron state, l_t represents the candidate value generated by inputting Z_t , $[h_{t-1}, z_t]$ represents the connection vector between the hidden layer output at time $t - 1$ and the input at time t , and w_f, b_f respectively represent the weight matrix of the forgetting gate and bias, w_i, b_i respectively represent the weight matrix of the input gate weight matrix and bias, w_o, b_o respectively represent the weight matrix of the output gate weight matrix and bias, w_1, b_1 respectively represent the weight matrix of the current state value weight matrix and bias.

The status update mode of the LSTM network model is shown in (1)–(5)

$$f_t = \sigma(w^f [h_{t-1}, z_t]) + z^f, \quad (1)$$

$$o_t = \sigma(w^o [h_{t-1}, z_t]) + b^o, \quad (2)$$

$$l_t = \tan h(W^l [h_{t-1}, z_t]) + b^l, \quad (3)$$

$$c_t = f_t \cdot c_{t-1} + i_t \cdot l_t, \quad (4)$$

$$h_t = o_t \cdot \tan h(c_t), \quad (5)$$

2.2. VaR Model Introduction. The VaR model, value-at-risk model, can be calculated by formula (6)

$$P(\Delta P > VaR) = 1 - a. \quad (6)$$

In the formula, P stands for probability measurement; ΔP stands for value loss; a stands for confidence level, the larger the value, the more disgusted the separation. The meaning of the above formula is that within a period of time in the future, the probability loss of the asset portfolio $1 - \alpha$ will not exceed the VaR value. For VaR measurement, it is usually calculated by the empirical distribution of the rate of return based on historical data, as shown in formulas (7) and (8) [12].

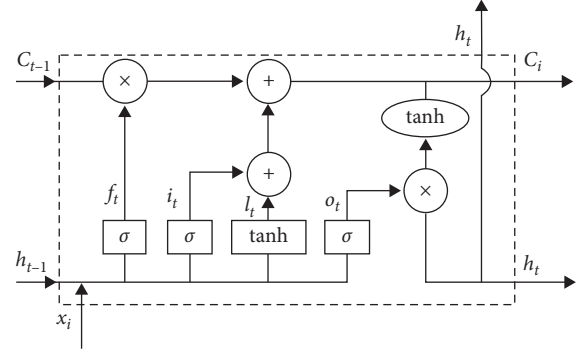


FIGURE 1: Schematic diagram of LSTM network structure.

$$(R_t | \Omega_{t-1}) \sim N(\mu_t, \sigma_t^2). \quad (7)$$

In the formula, R_t is the rate of return; μ_t is the average rate of return; σ_t is standard deviation of return rate; Ω_{t-1} is the information set at time $t-1$.

According to the above LSTM and VaR model introductions, LSTM has strong nonlinear mapping capabilities [13], VaR model is a risk management method to measure market risk, and it is easy to handle and fast in calculation [14]. Therefore, combining LSTM model and VaR model, this study proposes a market risk warning model based on LSTM-VaR.

3. Market risk warning model based on LSTM-VaR

3.1. Characteristic variables selection. The selection of characteristic variables is a prerequisite for realizing market risk warning. This paper takes stock as the research object, and constructs a market risk warning model based on optimized LSTM model. According to literature and the nonlinear characteristics of stock data [15], this paper selects representative indicators from basic transaction data, statistical technical indicators and moving interval data as characteristic index variables, as shown in Table 1.

3.2. LSTM-VaR model construction

3.2.1. Activation function. In order to strengthen the learning ability of the network, an activation function is introduced into the network. The Sigmoid function is the designated activation function of the logistic regression model. It has the advantage of being easy to derive, but it is prone to the problem of gradient disappearance. Its mathematical expression is as formula (8). Tanh function is a saturated activation function, and there is still the problem of gradient disappearance. Its mathematical expression is as formula (9), and the calculation is simplified as formula (10). Relu function has certain advantages in solving the problem of gradient disappearance, and its mathematical expression is shown in formula (11). The Leaky Relu function is an expanded and improved activation function of Relu function [16], which can better solve the problem of gradient disappearance. Therefore, this study selects the Leaky Relu function as the activation function of the LSTM-VaR model.

TABLE 1: Characteristic index variables.

Categories of characteristics	Characteristic variables
Basic transaction data	Opening price
	Closing price
	Intraday ceiling price
	Intraday bottom price
	Volume
Statistical technical indicators	Turnover
	Average price
	Spread
	Price-to-earnings ratio (P/E Ratio)
Moving interval data	Rate of return
	5-day yield
	10-day yield
	Circulation market value
	5-day circulation market value
	10-day circulation market value

$$\sigma_s = \frac{1}{1 + e^{-z}}, \quad (8)$$

$$\tanh h = \frac{e^x - e^{-x}}{e^x + e^{-x}}, \quad (9)$$

$$\tanh h(x) = \frac{2}{1 + e^{-2x}} - 1, \quad (10)$$

$$\text{ReLU} = \max(0, x). \quad (11)$$

3.2.2. Loss function selection. Loss function is a method to solve the problem of model overfitting. By not allowing parameters to pass through all neurons, it can reduce neuronal computation, improve computational efficiency, and reduce network scale. This research reduces the network scale by adding a loss function at the dropout layer of the LSTM-VaR network. Commonly used loss functions include 0-1 loss function, absolute loss, logarithm and root mean square error (RMSE), whose mathematical expressions are as follows: (12)–(14). Since the root mean square error function has a better solution to the fitting phenomenon, this study chooses it as the loss function of the LSTM-VaR network model [17].

$$L(Y, f(X)) = \begin{cases} 1, Y \neq f(X) \\ 0, Y = f(X) \end{cases}, \quad (12)$$

$$L(Y, f(x)) = |Y - f(x)|, \quad (13)$$

$$L(Y, P(Y|X)) = -\log P(Y|X), \quad (14)$$

$$\text{RMSE} = \sqrt{\frac{1}{n} \sum_{i=1}^n (y_i - \hat{y}_i)^2}. \quad (15)$$

In the formula (15), n represents quantity, y_i represents the true value and \hat{y}_i represents the predicted value.

3.2.3. Sliding windows. The input of market risk warning model based on LSTM-VaR is time series data, while sliding Windows are usually used in time series prediction [18]. The sliding window realizes data statistics by dividing a period of time into multiple windows, and sliding each window with equal length, taking the window data as the unit. By using the sliding window, more relevant and time-sensitive data information can be extracted. Figure 2 is a schematic diagram of an instant sliding window. As the window slides, the previous window becomes invalid, and a new window is generated accordingly.

3.2.4. Dropout layer. LSTM-VaR model contains a large number of parameters which are prone to over-fitting during model training, resulting in poor fitting effect of data samples on training set and test set [18]. Therefore, this paper adds a dropout layer to the model to solve this problem. The process of dropout node units is to randomly select neurons for temporary hiding in a loop, and perform looping and optimization [19]. Repeat the operation until the end of the training.

3.3. Market risk warning process based on LSTM-VaR. Based on the above analysis, the risk warning process of the stock market is summarized as follows: Firstly, missing values and standardized processing are carried out on the collected stock market data, then the risk measurement on the processed data. Secondly, the data after risk measurement is input into LSTM-VaR model, and the deep learning model LSTM is used to predict the stock market risk, and the prediction results are output. Finally, the prediction results are measured by VaR to realize risk warning. The above process can be illustrated in Figure 3.

4. Simulation experiment

4.1. Experimental environment construction and data sources. This experiment was carried out in Python, TensorFlow and keras environment. The experiment takes the stock market risk warning as the research object, takes day as the unit, selects the relevant data of the Shanghai and Shenzhen 300 Index of Oriental Fortune from October 5, 2009 to August 5, 2020 as the experimental data. The CSI 300 yield trend is shown in Figure 4 [20, 21].

Considering the problem of missing data in the collected data, in order to avoid the impact of missing data on the risk prediction results, the study performed deletion preprocessing on missing data. In addition, due to the large differences in the magnitude and dimension of different indicators, this experiment standardized the data by formula (16) [22]. In the end, this study obtained a total of 2,917 sets of historical data for stock market risk prediction.

$$X' = \frac{X - \text{mean}(X)}{\text{std}(X)}. \quad (16)$$



FIGURE 2: Sliding Windows.

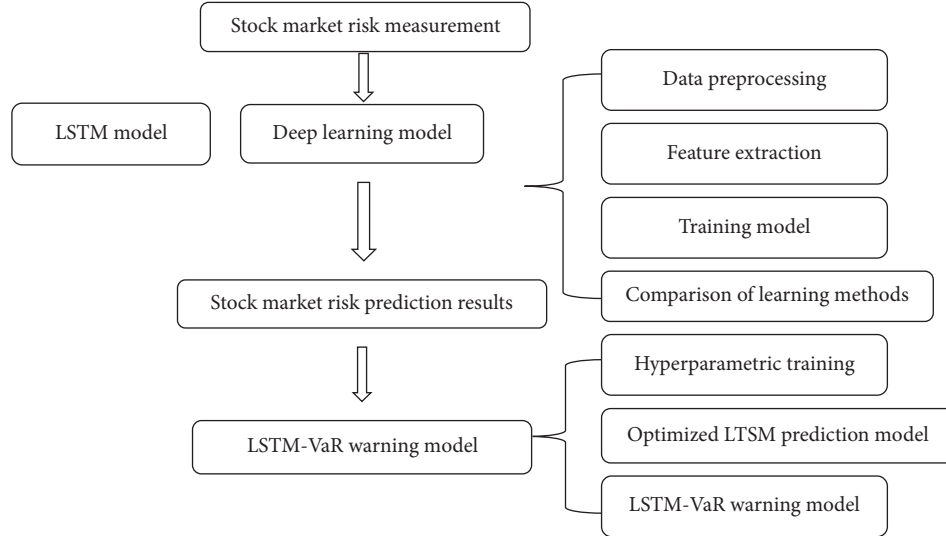


FIGURE 3: LSTM-VaR model warning process.

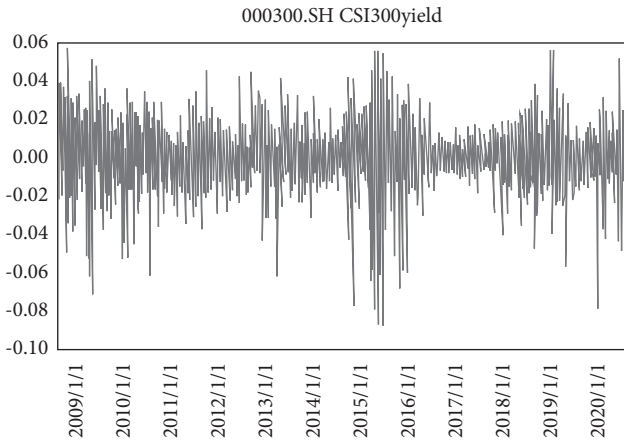


FIGURE 4: The CSI 300 yield trend.

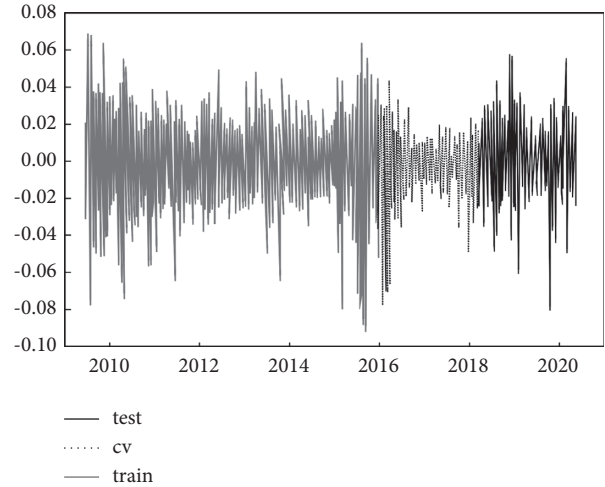


FIGURE 5: Division results of stock return data set.

The pre-processed data were divided into training set, test set and verification set in a ratio of 3:1:1, and the specific distribution was shown in Figure 5.

4.2. Evaluation Indicators. In this experiment, root mean square error (RMSE) was used as an indicator to evaluate model performance, as shown in formula (17). The smaller the value is, the better the prediction effect is [23].

$$RMSE = \sqrt{\frac{1}{n} \sum_{i=1}^n (y_i - \hat{y}_i)^2}. \quad (17)$$

According to the definition of VaR, stock rate of return is a significant indicator affecting value-at-risk prediction. Therefore, it is selected as the warning indicator of stock market risk in this experiment. Stock return rate is usually expressed by relative return rate, as shown in formula (18) [24]:

$$R_{i,t} = \ln P_{i,t} - \ln P_{i,t-1}. \quad (18)$$

In the formula, $R_{i,t}$ represents the price return rate of index i on day t ; $P_{i,t}$ represents the daily closing price of the index on day t ; and $P_{i,t-1}$ represents the daily closing price of the index on day $t-1$.

4.3. Parameter Settings. In this experiment, the initial parameters of the LSTM model were set as follows: training periods epochs were 10, time window length N was 9, Batch size was 8, the number of neurons in each layer was 50, and the dropout probability was 0.1. Tanh function was selected as the activation function and Adam as the optimizer [25]. To obtain the optimal LSTM model, the optimal parameters are determined by experimentally observing the RMSE value of the model. Firstly, different epochs are selected to train the LSTM model when other parameters remain unchanged, and RMSE corresponding to different epochs values are obtained as shown in Table 2. According to the table, when epochs = 10, RMSE is the smallest. As the epochs increase, the RMSE value gradually increases, indicating that the model overfits when epochs >10. Therefore, epochs were set to 10 in this experiment

Secondly, under the condition that other parameters remain unchanged, different Batch sizes are selected for training of LSTM models, and RMSE corresponding to different batch size values are obtained as shown in Table 3. In order to display the relationship between batch sizes and RMSE more intuitively, the table is drawn into a line chart, as shown in Figure 6. As can be seen from the figure, RMSE of the model fluctuates with the increase of batch size values. When Batch size is 8, RMSE value corresponding to the model is the minimum. Therefore, batch size was set to 8 in this experiment.

In the same way, the controlled variable method was used to experiment with the length of the time window of the LSTM model, the number of neurons in each layer, and the dropout probability value. While other parameters remain unchanged, RMSE of the model under different time window lengths (N), number of neurons at each layer, and dropout probability values are shown in Figure 7 and Figure 8.

Figure 7 shows that the RMSE value of the model fluctuates with the increase of N . When N is 16, the RMSE of the model is the minimum. Therefore, the time window length was set as 16 in this experiment.

It can be seen from Figure 8 that the RMSE value of the model is the smallest when the number of neurons in each layer is 100.

As shown in Figure 9, the RMSE value of the model is minimal when the dropout probability value is 0.5. Therefore, the dropout probability of the model was set to 0.5 in this experiment.

Finally, for purpose of testing the impact of different activation functions on the model, on the basis of the above optimal parameters, Leaky ReLu, TANH and ReLu functions were selected as the activation functions of the LSTM model, and RMSE values of the model under different activation functions were obtained, as shown in Table 4. According to the table, when the activation function is Leaky ReLu, the RMSE of the model is the smallest. Therefore, Leaky ReLu function was selected as the activation function of the LSTM model in this experiment.

Through the above operations, the parameter settings of the experimental model are shown in Table 5.

TABLE 2: RMSE comparison of different epochs.

Epochs	RMSE
10	0.014473
20	0.014570
30	0.014663
40	0.014657
50	0.014546

TABLE 3: RMSE comparison of different batch sizes.

Epochs	RMSE
8	0.014473
16	0.014591
32	0.014528
64	0.014608
128	0.014578

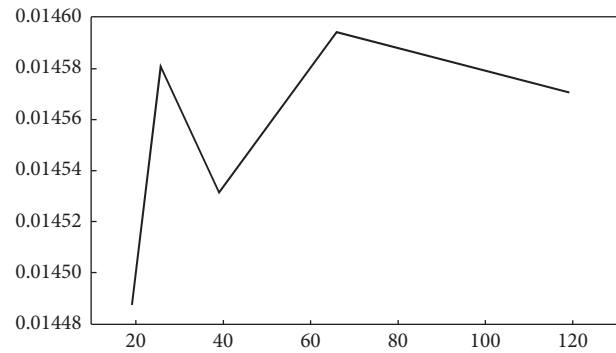


FIGURE 6: RMSE line chart of different batch sizes.

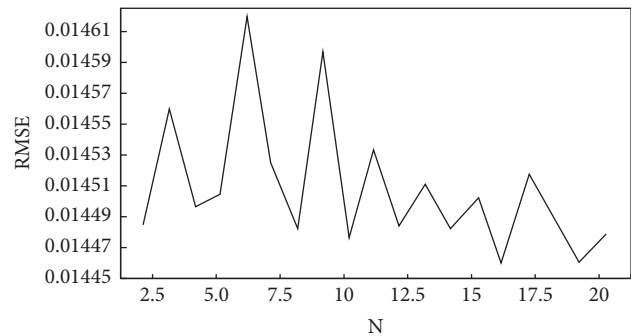


FIGURE 7: RMSE line chart of different time window lengths.

4.4. Experimental Results

4.4.1. LSTM model verification. In order to verify the performance of the LSTM model with optimized parameters, this study compared the prediction results with the LSTM prediction results before parameter optimization and the prediction results of common prediction methods such as MLP (multi-layer perceptron), as shown in Table 6. As can be seen from the table, the optimized LSTM model has the lowest RMSE value compared with the other prediction method. Therefore, the optimized LSTM model proposed in this study can effectively and well predict the stock return rate, which has certain advantages.

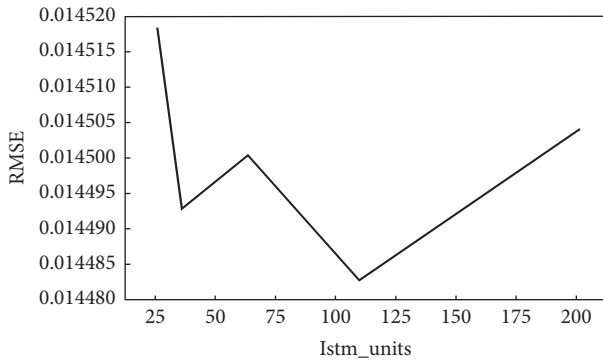


FIGURE 8: RMSE line chart of different number of neurons.

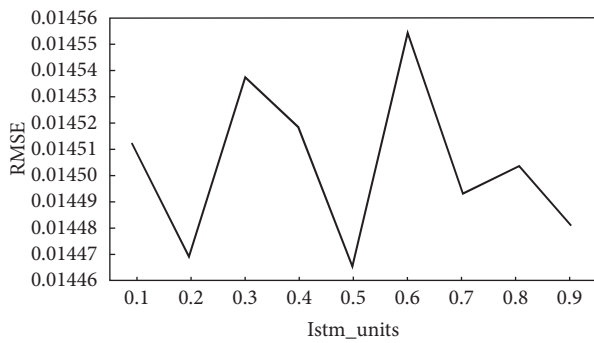


FIGURE 9: RMSE line chart of different dropout probability.

TABLE 4: RMSE comparison of different activation functions.

Activation	RMSE
Leaky ReLu	0.014479
Tanh	0.146065
Relu	0.014501

TABLE 5: Optimal parameter Settings of the model.

Parameter Variable	Value
Epochs	10
Batch size	8
N	16
Istm units	100
Dropout	0.5
Activation	Leaky Relu

TABLE 6: Comparison of prediction results of different prediction methods.

Prediction Method	RMSE
The day value as predicted value	0.021977
Moving average as predicted value	0.016104
MLP (multilayer perceptron)	0.014509
LSTM	0.014804
LSTM (optimized)	0.013762

The residual sequence histogram of the LSTM model is shown in Figure 10. As the figure shows, the residual sequence follows normal distribution. Descriptive statistics were made in Table 7. The table shows that the residual mean, standard

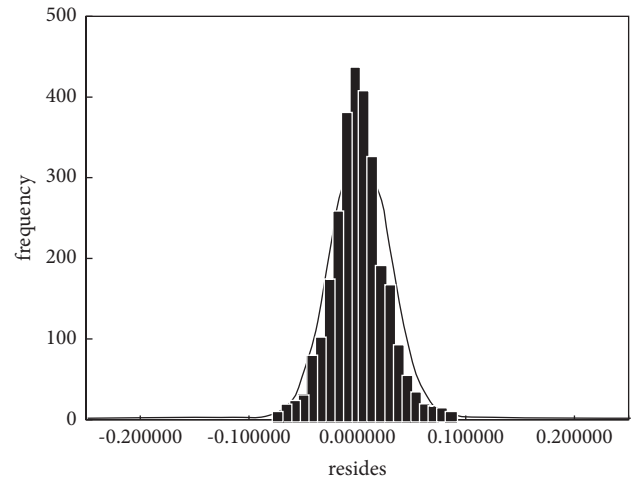


FIGURE 10: Histogram of residual distribution.

TABLE 7: Residual description.

Variable	Value
Average	-0.0011642
Standard deviation	0.0245195
Maximum	0.144568
Minimum	-0.0170837
Skewness	-0.027
Kurtosis	3.321

TABLE 8: Standard deviation σ_t prediction model.

Parameter	Value
Epochs	10
Batch size	8
N	9
Istm units	100
Optimizer	Adam
Dropout	0.1
Activation	Tanh

deviation and skewness are approximately 0, and the kurtosis is close to the kurtosis value of the standard normal distribution.

Then, the standard deviation of return rate σ_t was predicted by rolling, and LSTM model parameters were obtained, as shown in Table 8. Using this parameter to predict the standard deviation, the fitted broken line is shown in Figure 11. It can be seen from the figure that the model has a good fitting effect and can well fit the standard deviation trend.

4.4.2. VaR measurement results. Using VaR to calculate the test set, some results are shown in Figure 12. As can be seen from the figure, VaR fluctuates sharply in the stock market.

The sample quantiles with stock return rate of 1% and 5% are taken as the warning line of stock market risk. When the VaR is lower than the warning line, the warning model indicates. Figure 13 shows the warning diagram. The figure shows that VaR was in the trough in April 2020. Enlarged area is got in Figure 14 As Figure 14 shows, VaR was below the warning line of 1% sample quantile from March 13 to April 1 2020.

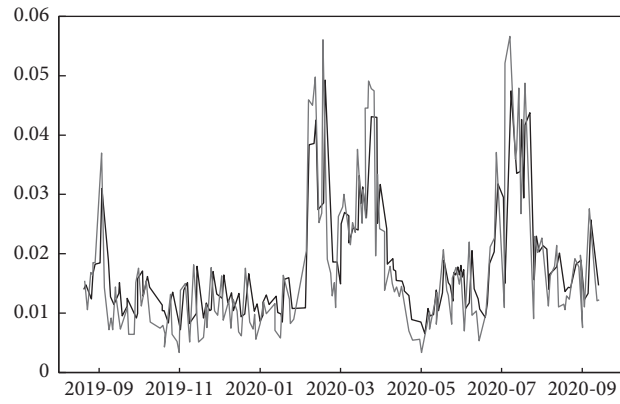


FIGURE 11: Standard deviation fitting graph.

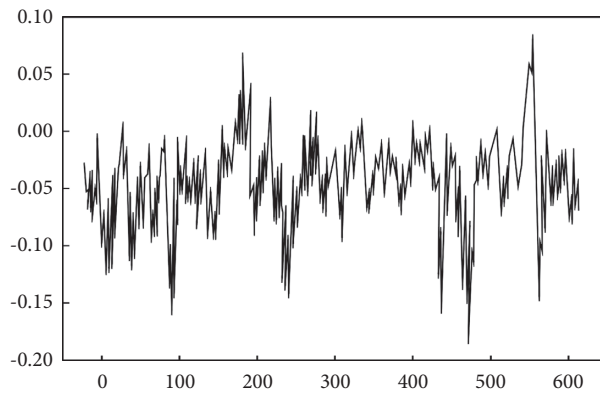
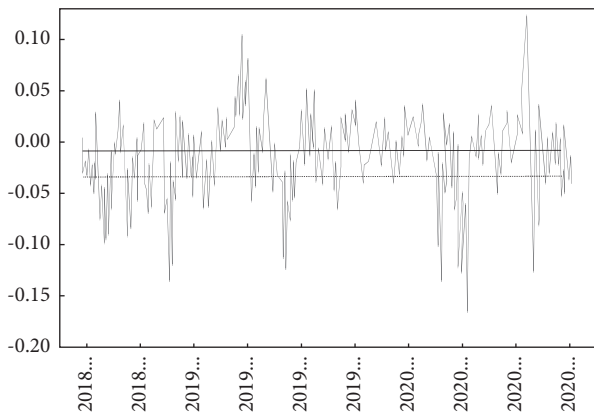
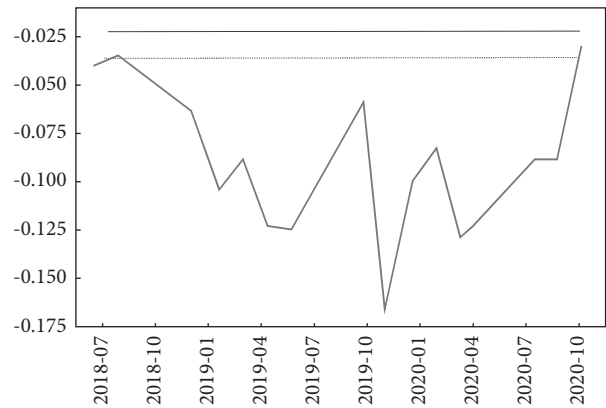


FIGURE 12: VaR trend chart.



— 5%warning line
..... 1%warning line
— VaR

FIGURE 13: Risk warning diagram.



— 5%warning line
..... 1%warning line
— VaR

FIGURE 14: Risk warning interval diagram.

5. Conclusion

To sum up, the proposed model predicts the standard deviation of stock return rate with LSTM model. Taking Leaky Relu function as the activation function, training period epochs were 10, time window length N was 9, batch size was 8, the number of neurons in each layer was 50, and the dropout probability was 0.1, and Adam as the optimizer, the standard deviation of stock return rate can be effectively realized. In this case, the RMSE value of the model is the minimum, which is 0.013762. The stock market risk warning can be realized by measuring VaR and taking 1% and 5% sample quantile as warning line. Compared with traditional prediction models such as MLP, the LSTM-VAR model proposed in this study has a better effect on market risk warning and can realize the warning well. However, there are still some shortcomings in the research process, such as the selection of characteristic variables, which are all structured data. It is recommended to add unstructured data to enrich data features to better capture market sentiment characteristics. In addition, due to the limitations of equipment conditions and the long time-consuming model training parameters, the model was only trained once, so there may be some errors in the results. It is suggested to train the model for several times if conditions permit, or to reduce the training duration by optimizing the model. In the next step, researches should be improved from the above shortcomings to increase the breadth of the research.

Data Availability

The experimental data used to support the findings of this study are available from the corresponding author upon request.

Conflicts of Interest

The authors declared that they have no conflicts of interest regarding this work.

Acknowledgments

This work is supported by the social science development research project of Hebei Province (20210201118) "Research on the industrialization of housing decoration and the selection of supply logistics mode in Hebei Province".

References

- [1] W. Hu, "Construction of early-warning mechanism for identification of default risk of credit bonds and management of market entities' behavior," *Northern Finance*, vol. 2021, no. 05, pp. 45–52, 2021.
- [2] W. Lin, M. Chen, L. Zhou, and X. X. Meng, "Analysis of Chinese stock market risk prediction ability based on VaR-GARCH model family," *Statistics & Decisions*, vol. 35, no. 21, pp. 151–155, 2019.
- [3] X. Chen, J. Wu, and M. Xu, "The measurement and prevention of individual default risk of my country's credit bonds—based on the LSTM deep learning model," *Journal of Fudan University (Social Science)*, vol. 63, no. 03, pp. 159–173, 2021.
- [4] X. Li, "The application of artificial intelligence in corporate financial risk prevention and control—based on a big data environment," *Communication of Finance and Accounting*, vol. 2021, no. 22, pp. 137–142, 2021.
- [5] C. Liu, Z. Su, and P. Song, "Measurement, supervision and warning of risk contagion among global stock markets," *Financial Research*, vol. 2020, no. 11, pp. 94–112, 2020.
- [6] J. Guo, Z. Ni, and J. Xiao, "An analysis of the early warning capability of the implied volatility risk of SSE 50ETF options on capital market risks," *Statistics and Information Forum*, vol. 36, no. 04, pp. 60–71, 2021.
- [7] W. Liu, Y. An, and F. Rui, "The extreme risk spillover effect and early warning effect of stock index futures on the stock market: empirical evidence based on high-frequency data of the Shanghai and Shenzhen 300 Index," *China Securities Futures*, vol. 11, no. 01, pp. 4–19, 2021.
- [8] W. Zhou, Q. Wang, H. Zhang, and L. Wang, "Research on the long memory recognition and risk measurement of Shanghai composite index volatility based on the realized extremely poor," *Journal of Southwest University (Natural Science Edition)*, vol. 43, no. 11, pp. 142–150, 2021.
- [9] C. Tian, "Analysis of substantial default factors and warning of substantial default risk in the bond market based on logistic regression algorithm," *Marketing Circles*, vol. 10, no. 26, pp. 41–45, 2021.
- [10] J. Liu, L. Zheng, and H. Liu, "Research on monitoring and early warning of extreme risk spillover in China's financial market—based on the implementation of MVMQ-CAViAR method," *Economics and Management Research*, vol. 41, no. 02, pp. 19–29, 2020.
- [11] N. Ren, B. Tong, G. Shen, and T. Guo, "Research on fine-grained named entity recognition based on deep learning—take tomato diseases and pests as an example," *Information Science*, vol. 39, no. 11, pp. 96–102, 2021.
- [12] Q. Zhang, Z. Tang, and W. Gong, "etc. Ultra-short-term wind power prediction model based on long and short-term memory network," *Acta Energetica Sinica*, vol. 42, no. 10, pp. 275–281, 2021.
- [13] J. Fan, Y. Guo, X. Wu, X. Chen, and Y. Lin, "Fault diagnosis of planetary gearbox based on LSTM neural network and enhanced fault feature," *Journal of Vibration and Shock*, vol. 40, no. 20, pp. 271–277, 2021.
- [14] J. Shi and L. Hou, "Fault diagnosis of rolling bearing based on two-way gated cyclic unit network[J]," *Electric Power Science and Engineering*, vol. 37, no. 10, pp. 64–70, 2021.
- [15] X. Han and X. Xu, "Establishment and standard analysis of market risk early warning indicator system for rare earth enterprises," *Science & Technology and Economy*, vol. 33, no. 04, pp. 106–110, 2020.
- [16] Y. Zhang, F. Lu, and L. Bo, "The construction and innovation of the early warning mechanism of Yunnan Pu'er tea market," *Chinese Market*, vol. 29, no. 26, pp. 49–50, 2020.
- [17] H. Bai, S. Liu, X. Luo, L. L. Liu, and W. Y. Hao, "Research on my country's systemic financial risk measurement and early warning based on the real estate market," *Financial Research*, vol. 29, no. 08, pp. 54–73, 2020.
- [18] J. Li, "Analysis of the establishment of an early warning mechanism for corporate financial risks in the new era," *Contemporary Accounting*, vol. 8, no. 22, pp. 35–36, 2019.
- [19] K. Yang, W. Yu, and J. Ma, "Research on the risk warning of stock market style asset portfolio based on vine copula," *Wuhan Finance*, vol. 38, no. 11, pp. 51–59, 2019.

- [20] M. Sui and X. Yuan, "Analysis of influencing factors of my country's cross-border RMB settlement business—based on VAR model," *Business Economics*, vol. 28, no. 11, pp. 176–180, 2021.
- [21] H. Yang and X. Sun, "VAR-based analysis of influencing factors of operating profit of my country's real estate enterprises," *Journal of Wuhan University of Technology*, vol. 34, no. 04, pp. 96–103, 2021.
- [22] H. Wang, J. Li, W. Zheng, Z. Y. Fan, and K. Chen, "Ecological stoichiometric characteristics of litter in the fir forest of Sejlaji and long buds," *Plateau Agriculture*, vol. 33, no. 05, pp. 433–443+459, 2021.
- [23] Y. Tian and S. Xu, "An empirical study on the relationship between China's financial efficiency and economic growth," *Technical Economy and Management Research*, vol. 2021, no. 10, pp. 86–91, 2021.
- [24] Z. Liang and X. Guo, "Research on stock market risk early warning based on implied volatility of options," *Shanghai Finance*, no. 07, pp. 39–44, 2020.
- [25] Y. Liu and W. Zhang, "Analysis of the impact of mortgage interest rate policy reform," *Journal of Qufu Normal University (Natural Science Edition)*, vol. 47, no. 04, pp. 51–59, 2021.

Research Article

The Motor Action Analysis Based on Deep Learning

TianYu Zhang 

Sanjiang University, Ministry of Sports, Nanjing 210000, China

Correspondence should be addressed to TianYu Zhang; 2009040141@st.btbu.edu.cn

Received 7 December 2021; Revised 27 December 2021; Accepted 11 January 2022; Published 10 March 2022

Academic Editor: Hangjun Che

Copyright © 2022 TianYu Zhang. This is an open access article distributed under the Creative Commons Attribution License, which permits unrestricted use, distribution, and reproduction in any medium, provided the original work is properly cited.

For the slow speed and low accuracy of slow motor action recognition methods, this study proposes a motor action analysis method based on the CNN network and the softmax classification model. First, in order to obtain motor action feature information, by using static spatial features of BN-inception based on CNN network extracted actions and high-dimensional features of 3D ConvNet, then based on softmax classifier structure and realizing taxonomic recognition of the motor actions. Finally, through the decision-layer fusion and time semantic continuity optimization strategy, the motion action recognition accuracy is further improved and the more efficient motion action classification recognition is realized. The results show that the proposed method can complete the motor action analysis and achieve the classification recognition accuracy to 83.11%, which has certain practical value.

1. Related Work

Movement action analysis is an important branch of computer vision, which also involves data mining, image processing, and other content, and is widely used in sports, music playing, and many other scenes. Due to the complex patterns of movement action and the big differences in movement rules of different individuals, the movement action recognition analysis is somewhat challenging and has attracted the keen attention of relevant researchers. At present, motion action analysis mainly focuses on motion detection and recognition and has achieved remarkable research results. For example, Hua-xin Zhang et al. realized the estimation of human posture by capturing 3D motion [1]. In addition, Xiaoqiang Li et al. applied the convolutional neural network to action recognition. The results show that the action recognition results of a convolutional neural network with the dual-attention mechanism are comparable to the recognition results of the latest algorithm [2]. Haohua Zhao et al. extracted intraframe feature vectors by deep network training to form a multimode feature matrix. The matrix is input into CNN to achieve feature classification. The results show that the proposed method has better performance than the existing LSTM in video action recognition [3]. Ran Cui et al. analyzed the motion by

constructing skeletal joints and static and dynamic features. The prediction of motion is realized through motion recognition [4]. Manikandaprabu et al. detected the ROI of the human body using the combination of background subtraction and frame subtraction [5]. Then the CAMShift algorithm is adopted for recognition. The results show that this method has good precision and has great advantages compared with the most advanced algorithms. It can be seen from the above studies that convolutional neural networks are widely used in action recognition, among which the CNN attracts more attention due to its unique characteristics.

Despite the great progress in motor motion analysis, its overall performance still needs to be improved, mainly due to the blurred boundary of motor motion, which increases the difficulty of the study. For the difficulties, this study applies powerful deep learning capabilities, based on the CNN network and the softmax classifier, and proposes a deep learning-based motion action analysis method.

2. Basic Methods

2.1. Network Profile. The CNN network is a representative algorithm of deep learning, which is commonly used in image processing, video image recognition, and other fields,

with the characteristics of simple structure and strong expansion performance. Its basic module includes a convolution layer, a pooling layer, and a full connection layer, as shown in Figure 1. The convolution layer is responsible for extracting the local features of the input image to obtain different feature maps; the pooling layer reduces the dimension of the extracted features of the convolution layer to retain important information while reducing the risk of overfitting due to nonessential information. Common pooling layer settings include average pooling and maximum pooling; the full connection layer plays a classification role in the network and enables sample data classification by mapping the learned feature data to the space of sample markers [6–11].

In recent years, with the deepening of deep learning research, a huge breakthrough in CNN network structure has been made. In terms of spatial feature extraction, the network continuously deepens, forms the inception structure module, as shown in Figure 2, which greatly reduces the quantities of network parameters, realizes the multiscale processing fusion of images, and obtains a better feature representation [12–15].

In terms of spatiotemporal feature extraction, a 3D ConvNet network emerged, acquiring spatiotemporal features by performing both convolutional and pooling operations in time and space simultaneously, further improving the model performance.

2.2. Softmax Model Introduction. The softmax model is a multiclassifier based on the logistic regression model that can handle multiclassification problems. In the softmax model, for a given input x , the hypothetical function $h_\theta(x)$ was used to estimate the probability value of each category j , $p(y=j|x)$, i.e., estimating the probability of each classification result of x . Suppose the k -dimensional vector output by the function is the probability of these estimated k values. The $h_\theta(x)$ form is as follows:

$$h_\theta(x^{(i)}) = \begin{bmatrix} p(y^{(i)} = 1|x^{(i)}; \theta) \\ p(y^{(i)} = 2|x^{(i)}; \theta) \\ \vdots \\ p(y^{(i)} = k|x^{(i)}; \theta) \end{bmatrix} = \frac{1}{\sum_{j=1}^k e^{\theta_j^T x^{(i)}}} \begin{bmatrix} e^{\theta_1^T x^{(i)}} \\ e^{\theta_2^T x^{(i)}} \\ \vdots \\ e^{\theta_k^T x^{(i)}} \end{bmatrix}. \quad (1)$$

In the formula, $\theta_1, \theta_2, \dots, \theta_k \in \mathfrak{R}^{n+1}$ represents model parameters, $1/\sum_{j=1}^k e^{\theta_j^T x^{(i)}}$ is to normalize the probability distribution so that the sum of all probabilities is one.

Thus, the probability that softmax classifies x into category j can be expressed as [16–18]

$$p(y^{(i)} = j|x^{(i)}; \theta) = \frac{e^{\theta_j^T x^{(i)}}}{\sum_{l=1}^k e^{\theta_l^T x^{(i)}}}. \quad (2)$$

Motor action analysis is a multitaxonomic recognition process. According to the above analysis, in order to better analyze motor actions, this paper first used the feature extraction method to acquire motor representation based on

the CNN network and then identified by the softmax classifier to realize the analysis of motor actions.

3. Motor Motion Analysis Method Based on Deep Learning

3.1. Characteristic Extraction Based on CNN Network. The analysis of motor actions includes the appearance features and action context information of the data. In order to obtain well robust action characteristics, this study, based on the CNN network, represents the motion action appearance features and motion features by extracting the low-dimensional static features and high-dimensional spatial and temporal features of the data, respectively, to represent the motion action features, as shown in Figure 3.

3.1.1. Static Spatial Characteristic Extraction. In this paper, the BN-inception network with high accuracy and efficiency extracts the static spatial features of motion action, whose network structure is shown in Table 1. Specific extraction steps are as follows [19–22]:

Step 1: pretreatment for image cutting, motion action images, and image level flipping to obtain a matrix that meets the BN-Inception network input

Step 2: tacking the input matrix through a pretrained BN-inception model with feature extraction and calculating the feature average of each dimension of different image parts according to equation (3)

$$d_j = \frac{1}{M} \sum_{i=1}^M fea_{i,j}, \quad j = \{1, 2, \dots, 10\}, j = \{1, 2, \dots, 1024\}. \quad (3)$$

Step 3: obtaining final feature representation of a single-frame image, as in formula (4)

$$\text{Static}_{\text{fea}} = (d_1, d_2, \dots, d_{1024}). \quad (4)$$

Decreasing $f = \text{Static}_{\text{fea}}$, a characteristic representation of a sample of motion action data is a two-D matrix $F = \{f_1, f_2, \dots, f_N\}$ of $N \times D$. In it, N represents the total number of motion action video segment frames, fn represents the single-frame image feature, and D represents the feature dimension size. And so forth, all the static spatial features of the motor movement can be obtained.

3.1.2. Dynamic Spatiotemporal Feature Extraction. In this paper, 3D ConvNet high-dimensional spatial features and the network structure are shown in Figure 4. The specific extraction method is as follows:

Step 1: A multiscale frame sequence is entered and divides the video into different scale segments according to the set window size

Step 2: the spatiotemporal feature representation of each segmentation timing segment fc6 layer is extracted by network forward propagation, such as follows:

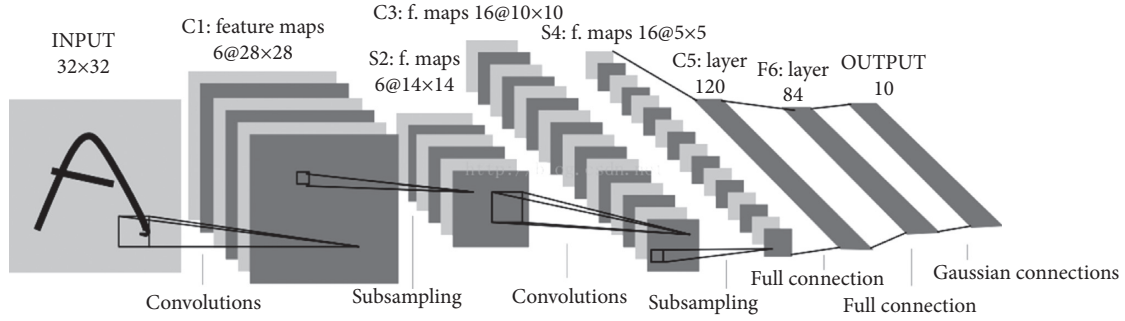


FIGURE 1: Standard CNN network structure.

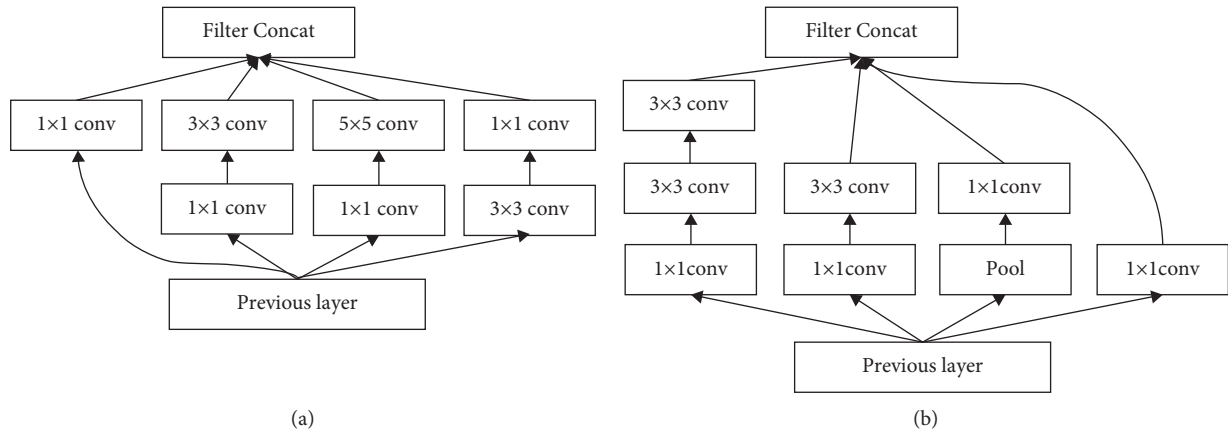


FIGURE 2: Structural representation of inception. (a) Inception v1 module. (b) Inception v2 module.

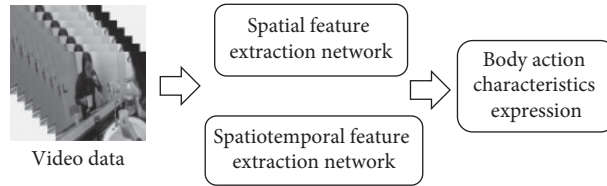


FIGURE 3: Structured flowchart of deep feature extraction.

TABLE 1: BN-inception network structure.

Type	Kernel size/step	Output size
Convolution	$7 \times 7/2$	$112 \times 112 \times 64$
Max pool	$3 \times 3/2$	$56 \times 56 \times 64$
Convolution	$3 \times 3/1$	$56 \times 56 \times 192$
Max pool (3a)	$2 \times 3/2$	$28 \times 28 \times 192$
Inception (3b)		$28 \times 28 \times 256$
Inception (3a)		$28 \times 28 \times 320$
Inception (3c)	stride2	$14 \times 14 \times 576$
Inception (3a)		$14 \times 14 \times 576$
Inception (4a)		$14 \times 14 \times 576$
Inception (4b)		$14 \times 14 \times 608$
Inception (4c)		$14 \times 14 \times 60 \times$
Inception (5a)	stride2	$7 \times 7 \times 1056$
Inception (5b)		$7 \times 7 \times 1024$
Inception (5c)		$7 \times 7 \times 1024$
Avg pool	$7 \times 7/1$	$1 \times 1 \times 1024$

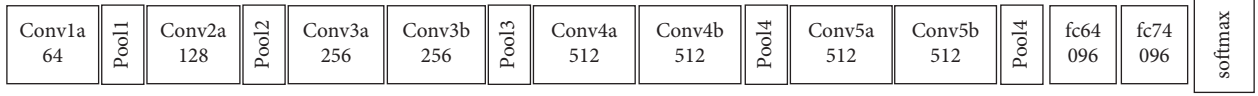


FIGURE 4: 3D ConvNet network structure block diagram.

$$\text{Dynamic}_{\text{fea}} = (d_1, d_2, \dots, d_{4096}). \quad (5)$$

Decreed $f = \text{Dynamic}_{\text{fea}}$, for a sample of motion action video data with a total frame number as N , if the time overlap is 50%, the extracted action feature representation $F = (f_1, f_2, \dots, f_K)$ is a $K \times D$ 2D matrix. Where $K = \lfloor (N - (w_i/2)) / (w_i/2) \rfloor$, f_k represents the input fragment features, and D represents the dimension size. With the above operation, the spatio-temporal features of all motion action video samples are extracted.

3.2. Classification Identification of Motion Actions Based on the Softmax Model

3.2.1. Model Structure Construction. Based on the above feature extraction, the softmax model structure was designed as shown in Figure 5 in this study. This classification network includes three fully connected layers for selecting parameters, one dropout layer to prevent overfitting, and finally, connecting the softmax loss. During training, the parameters were optimized by using small-batch gradient descent [23–25].

Considering that CNN network-based features include low-dimensional static features extracted by BN-inception and high-dimensional spatiotemporal features extracted from C3D, to improve the classification effect, different dimensions were trained separately in the study. To set the number of full connected-layer neurons of the low-dimensional feature softmax classification network for $\text{fc1} = 512$, $\text{fc2} = 256$, $\text{fc3} = 6$, and $\text{fc1} = 1024$, $\text{fc2} = 512$, and $\text{fc3} = 6$, while the high-dimensional feature softmax classification network for $\text{fc1} = 1024$, $\text{fc2} = 512$, $\text{fc3} = 6$.

3.2.2. Model Training and Testing. Specific procedures of training and testing of the above softmax model are as follows:

Step 1: The feature matrix of the training sample data is built. Assuming training sample QTY is M , the feature matrix of sample i ($i = 1, 2, 3, \dots, M$) is $F_i = N \times D$, N represents the number of training sample frames, and D represents the size of the feature dimension extracted per frame. The total number of M samples can be represented as

$$F = \sum_{i=1}^M F_i. \quad (6)$$

To train the soft model by the network structure in Figure 5, the number of fc3 output neurons is the same as in the categorical category C and the output vector

$X = \{x_j\}, j = 1, 2, \dots, C$. Therefore, the corresponding marker probability y_j for the output value x_j obtained by the softmax function can be expressed as [26]

$$y_j = \text{softmax}(x_j) = \frac{\exp(x_j)}{\sum_{j=1}^C \exp(x_j)}. \quad (7)$$

Step 2: to minimize the loss, a cross-entropy loss function was used, as shown in equation (8) to minimize the loss during training.

$$H_y(y) = -\sum_j y_j \log(y_j). \quad (8)$$

In the abovementioned formula, y_j represents the score distribution of classification by softmax; and y_j represents the target true value. Thus, the C category final-loss-value loss is the average of the cross-entropy loss for each category, as in the following formula[27]:

$$\text{Loss} = \text{mean}(H_y(y)). \quad (9)$$

Step 3: after optimizing the training parameters to speed up the model training, the model parameters were optimized by using M-BGD. During optimization, weight optimization is as in formula (10)–(14) [28].

$$\text{errors} = y_j - \text{softmax}(x_j). \quad (10)$$

$$\Delta w = \alpha \times x_j \times \text{errors}, \quad (11)$$

$$\Delta \beta = \alpha \times \text{errors}, \quad (12)$$

$$w = w - \Delta w, \quad (13)$$

$$\beta = \beta - \Delta \beta, \quad (14)$$

where errors represent the weight error, α represents the learning rate, w represents the weight, and β represents the deviation.

Step 4: model testing is performed. The best softmax classification model obtained by training is selected to classify and identify the test dataset, and the corresponding action category of the maximum classification score in C categories output from the following layer is selected as the classification result of the test data, and it is expressed as follows:

$$\text{class} = \text{index}(\max\{y_1, y_2, \dots, y_c\}). \quad (15)$$

3.3. Decision-Making Layer-Based Fusion. Considering the diversity, complexity, and ambiguity among motor

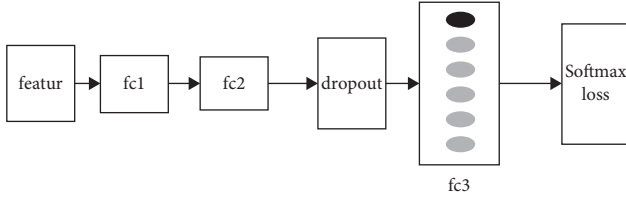


FIGURE 5: Structure diagram of the classification network based on softmax.

movements and the different key movements, different movement performance modes need to be mixed together to improve the classification and recognition accuracy of motor movements. Currently, common fusion methods include feature-based and decision-based fusion. Since feature-based fusion stitched and fused the features, it may lead to mutual interference among features and learning efficiency. In contrast, the fusion method based on the decision-layer only needs to determine action categories based on different classification confidence sizes, which is efficient and simple. Therefore, this paper fuses the classification results in a decision-layer fusion-based manner.

The fusion structure based on the decision-layer fusion mode is shown in Figure 6. Assuming the number of classified motor action categories is C , for individual test data X , the classification result is where $\text{result}(X) = \{s_1, s_2, \dots, s_C\}$, in it, s_i represents the classification score of category i , $i \in \{1, 2, \dots, C\}$, the N road classification identification results can be summarized according to formula (16).

$$\text{result}(X'_i) = \frac{1}{N} \sum_{n=1}^N \text{result}(X_n^i), \quad n \in \{1, 2, \dots, N\}. \quad (16)$$

Then to sum and average the data to obtain the final classification results

$$\text{result}(X)' = \{s'_1, s'_2, \dots, s'_3\}. \quad (17)$$

In the formula, X_n^i represents the classification score of sample X in the classifier n , and X'_i is the classification score of X is category i after fusion. The classification result based on $\text{result}(X)'$ maximum is the final classification category of sample X , as in the following formula:

$$\text{label} = \max\{\text{result}(X'_i)\}, \quad i \in \{1, 2, \dots, C\}. \quad (18)$$

3.4. Time-Based Semantic Continuity Optimization.

Movement actions have a certain time sequence, so there are a large number of redundant and incomplete trivial fragments during sequential action detection. To further improve the detection performance of the method according to temporal semantic continuity, this study proposes an optimization strategy based on the characteristics of motion action.

First, to model the motion action time sequence semantics and time sliding window classification at different scales, initial detection results are taken. Defined all detection results of a motor action as X , $\text{seg}(c_i, w_k)$ indicated a

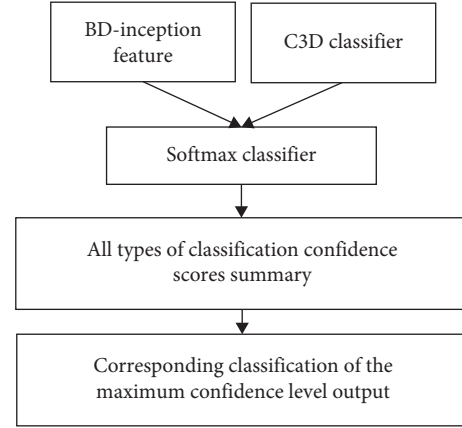


FIGURE 6: Fusion structure block diagram.

category of c_i in X , and a set of tests with a sliding window size of w_k can be represented as

$$X = \{\text{seg}(c_i, w_k)\}, \quad (19)$$

$$\text{seg}(c_i, w_k) = \{(s_n, e_n, g_n)\}_{n=1}^{N_{i,k}}. \quad (20)$$

In the formula, C represents the total number of categorical categories; K represents the total number of sliding windows; $N_{i,k}$ is the number of action time segments detected in c_i and w_k ; s_l, e_l are the start and end times of detected action segments; and g_n represents the classification score.

Then to calculate the classification score, the temporal overlap values of different time periods, as in equations (21) and (22), and compare them with the set threshold.

$$|g_l - g_s| < \theta, \quad (21)$$

$$\text{IOU}(p_l, p_s) \geq U \times \min(T_l, T_s), \quad l, s \in \{1, 2, \dots, N_{i,k}\}, \quad l \neq s. \quad (22)$$

In the formula, $P = \text{seg}(c_i, w_k)$ represents the detection results of the same category c_i and the same scale w_k , $pl = (sl, el, gl)$, and $ps = (ss, es, gs)$ both are one detection fragment of P ; $|g_l - g_s|$, $\text{IOU}(p_l, p_s)$ represent the score difference and time overlap value, respectively; $T_l = e_l - s_l$, $T_s = e_s - s_s$ the execution time of two actions, and θ, U the set threshold.

The two action segments were integrated if the two action segment classification scores were less than the set threshold and the time overlap was greater than the threshold.

Considering that the motion action obtained by the above operation is synthesized from multiple incomplete fragments, which partially destroys the spatiotemporal structure of the action, it also needs to conduct classification detection. This study uses a 3D convolutional neural network with good classification performance for reclassification. Furthermore, to ensure more accurate classification results and reduce the classification impact of sliding windows on motor movements, it statistically calculated the weight scores of different sliding windows for different

categories, further adjusted the classification confidence scores, and trained classification models by softmax classifier and overlap loss function.

Finally, to reduce redundancy detection in the presence of sliding windows at different scales, they were processed by nonmaximum inhibition to bring the final results close to the start and end of the motor action.

4. Simulation Experiment

4.1. Data Source and Preprocessing. The project dataset and the Thoumos14 publicdata set were used for this experiment. The project dataset contains 72 video action segments of six action categories, including brushing, mouthwash, and cleaning, with the characteristics of complex background, variable perspective, and an obvious difference in action execution speed. Its specific description is shown in Table 2. The Thoumos14 public dataset includes 2,755 clips in 20 sports action categories, with a total of 212 test videos annotated with timing. Because there were two mislabels of “270” and “1496” in this dataset, the remaining 210 annotated timing videos were selected for this experiment.

4.2. Parameter Settings

4.2.1. BN-Inception Network Parameter Settings. The BN-inception network parameters of this experiment are set as in Table 3.

4.2.2. 3D ConvNet Network Parameter Settings. In this experiment, the 3D ConvNet network parameters were set as follows: the convolutional kernel size was $3 \times 3 \times 3$, the step size was $1 \times 1 \times 1$, the size of the first pooling layer was $1 \times 2 \times 2$, and the size of the remaining pooling layers to $2 \times 2 \times 2$ with maximum pooling.

4.2.3. Softmax Classifier Parameter Selection. The M-BGD optimized softmax classifier parameters were used for this experiment. First, the batch-size size of the softmax classifier was selected. The average accuracy change curve on the project dataset test set under the same number of iterations when different batch-size values are taken in Figure 7. It is known from Figure 7(a) that when batch-size = 64, the test had the highest average accuracy, hence batch-size = 64 is set. Second, the number of iterations is selected. The effect of the different number of iterations on the identification results during training is shown in Figure 7(b). As Figure 7(b) shows that the highest identification result was achieved when the number of iterations was 20000, so the number of iterations was set at 20000.

During the training session, the loss change curves are shown in Figure 8. This figure shows that the loss values gradually decrease and tend to 0 during training.

4.2.4. Thresholding Selection Based on Temporal Semantic Continuity. The choice of score difference optimized threshold θ has a certain impact on the integration speed of the detection

window. If θ value is too large, it will easily lead to excessive integration of the detection window; if θ value is too small, it will lead to the integration time fragments cannot being merged, and there are still too many incomplete time fragments. Therefore, this experiment determined reasonable values by analyzing the influence of different θ values on mAP. Figure 9 shows the mAP taking different values at different temporal overlap thresholds on the Thoumos14 public dataset. And the highest mAP value is when $\theta = 0.5e-3$. Therefore, this experiment was set $\theta = 0.5-3$.

Considering the time continuity of motion movements and the variability of sliding windows at different scales, the time overlap threshold was set for $U = 2/3$.

4.3. Results and Analyses

4.3.1. Softmax Classified Network Performance Analysis. To validate the performance of the proposed softmax classification network, this study was validated on the project dataset and compared with the SVM classification network, and the results are presented in Table 4. According to the table, compared with the SVM classifier, the softmax classifier has a better effect, achieves a classification identification accuracy of 78.52%, and improves by 12.22%. Moreover, with the same classification recognition accuracy, the proposed softmax network in this study has a shorter training time and looks about 10 times shorter than the SVM classifier. This shows that the softmax classification network proposed in this study performs better and is more conducive to motion action analysis.

4.3.2. Fusion Result Analysis Based on the Decision Layer. To verify the effectiveness of the decision-layer-based fusion method proposed in this study, the study was validated on the project dataset and compared with the prefusion classification identification results, results are shown in Table 5. According to the table, the average classification recognition accuracy reached 79.89%, an improvement of 1.38% compared with before the fusion method, indicating that the fusion method has some effectiveness.

4.3.3. Validation Based on the Temporal Semantic Continuity Optimization Method. To further verify the effectiveness of this temporal semantic-based continuity optimization method, the study was validated on the project dataset and compared the identification results of partial test samples before and after optimization, as shown in Table 6 and Table 7. According to the table, this proposed method in this study can effectively improve the recognition accuracy from 79.89% to 83.11%.

In the test dataset, the mAP values at different time overlap thresholds are shown in Table 6. According to the table, when $\alpha = 0.5$, the average detection accuracy of the present study is 60.2%.

4.3.4. Classification Identification Results Analysis. To verify the effectiveness of the proposed method, this study visualized the method classification identification results in

TABLE 2: Project dataset description.

Difficulties	Description
Background noise	Different individual clothing changes, relationships with the environment, etc
Action nonstandardized	There are interruptions in the process of action execution, disorderly order, property management action, etc
Speed difference of action execution	Differences in speed and performance time during action execution occur due to the behavioral habits of different individuals
Different perspectives	Camera location, different angles, etc
Shelter	Cameras and their own occlusion problems
Lens movement	There are varying degrees of lens movement during the dataset recording process

TABLE 3: BN-inception network parameter settings.

type	Depth	#1 × 1	#1 × 1 reduce	#3 × 3	#3 × 3 reduce	Double #3 × 3	Pool + proj
Convolution	1						
Max pool	0						
Convolution	1	64	192				
Max pool	0						
Inception (3a)	3	64	64	64	64	96	Avg + 32
Inception (3b)	3	64	64	96	64	96	Avg + 64
Inception (3c)	3	0	128	160	64	96	Max + pass
Inception (4a)	3	224	64	96	96	128	Avg + 128
Inception (4b)	3	192	96	128	96	128	Avg + 128
Inception (4c)	3	160	128	160	128	160	Avg + 128
Inception (4d)	3	96	128	192	160	192	Avg + 128
Inception (4e)	3	0	128	192	192	256	Max + pass
Inception (5a)	3	352	192	320	160	224	Avg + 128
Inception (5b)	3	352	192	320	192	224	Max + 128
Avg pool	0						

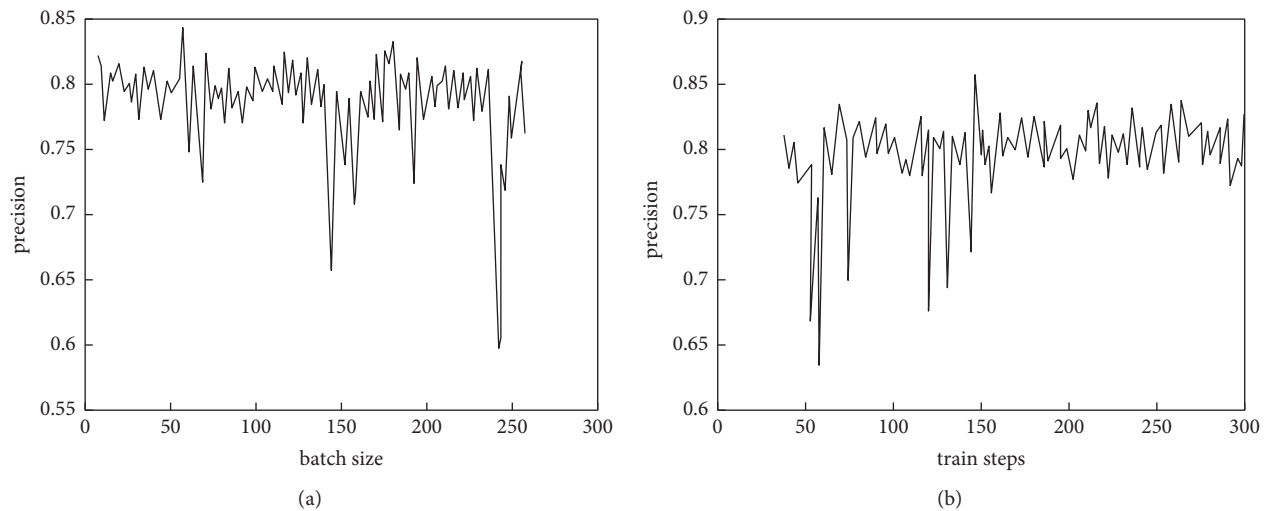


FIGURE 7: Selection of training parameters. (a) Effect on the identification results. (b) Effect of the number of training iterations on the identification results.

Figure 10. Figure 10(a) is the input video stream identification result, where the abscissa is the video frame, and the ordinate is the identification accuracy with the highest classification score for each frame. Figure 10(b) is the action performed at different time periods in the video stream, the abscissa represents the video stream, and the ordinate is the action category. Since the project dataset used for the

experiment includes six action categories, each color in the figure corresponds to one action category, so there are six colors in Figure 10. According to the figure, the proposed method has the highest accuracy of the actions in the process. The recognition accuracy of different actions decreased due to the vague beginning and end of the operation type and time location. In Figure 10(b), green presents for

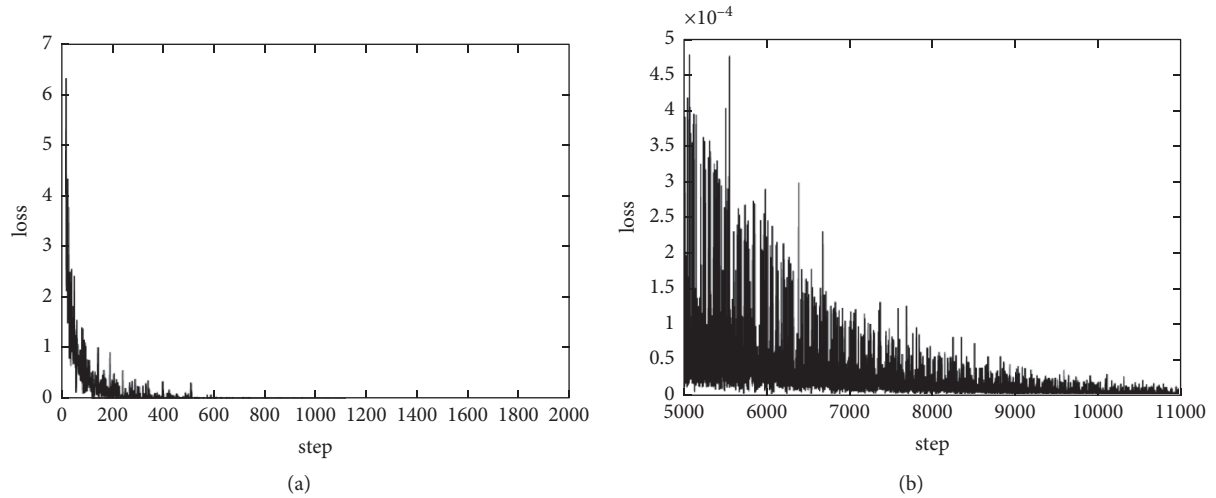


FIGURE 8: Loss curves of different iteration times. (a) The loss change with 0–2,000 iterations. (b) The loss change with 50000–11,000 iterations.

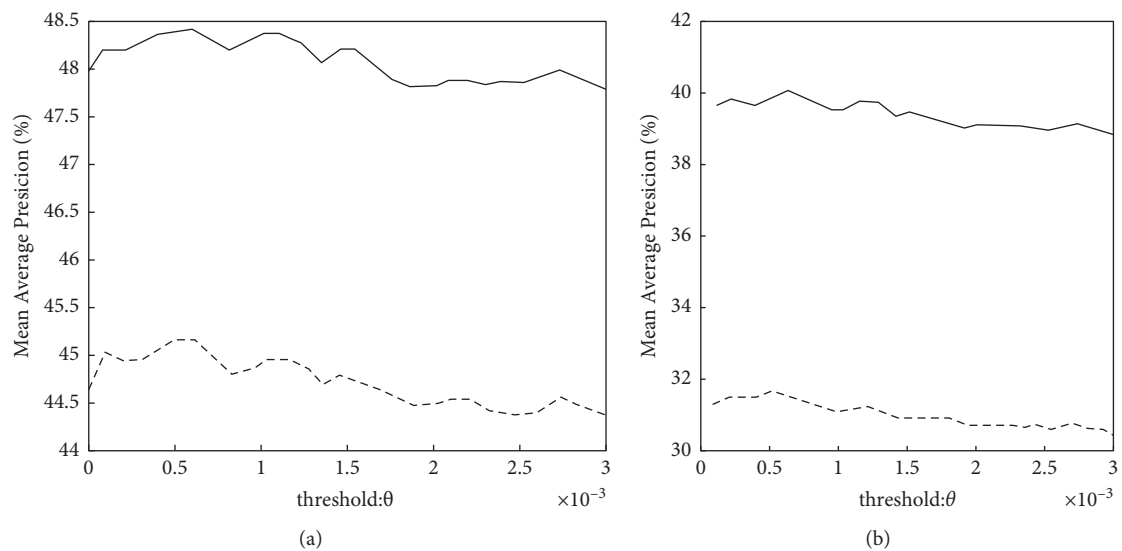


FIGURE 9: Different thresholds θ impact on mAP. (a) θ changing curves with mAP when A is 0.1,0.2. (b) θ changing curves with mAP when A is 0.3,0.4.

TABLE 4: Comparison of classification and recognition results of different classifiers.

Features test videos	Softmax	SVM
P1	76.84	58.73
P2	80.33	59.51
P3	51.25	72.07
P4	86.39	84.24
P5	76.29	33.33
P6	943.6	94.21
P7	93.34	61.82
P8	71.69	72.82
P9	82.80	58.42
P10	71.88	67.91
AVG	78.52	66.30

TABLE 5: Fusion experimental results.

classifier Features test video	Softmax classifier		Class score confusion
	BN-inception features (%)	C3D features (%)	
P1	76.84	58.73	75.91
P2	80.33	59.51	81.63
P3	51.25	72.0	63.26
P4	86.39	84.24	86.13
P5	76.29	33.33	74.29
P6	94.36	94.21	94.43
P7	93.34	61.82	94.52
P8	71.69	72.82	76.17
P9	82.80	58.42	84.41
P10	71.88	67.91	68.23
AVG	78.51	66.30	79.89

TABLE 6: Comparison of results before and after optimization.

Methods test videos	Class score confusion (%)	Action continuity and temporal integrated (%)
P1	75.91	81.18
P2	81.63	81.39
P3	63.26	76.97
P4	86.13	83.81
P5	74.2 V	72.02
P6	94.43	94.62
P7	94.52	95.24
P8	76.17	80.46
P9	84.41	89.78
P10	68.23	75.61
AVG	79.89	83.11

TABLE 7: Comparison of map values at different time overlapping thresholds.

α	0.5	0.6	0.7	0.7	0.8	0.9
mAP (%)	60.2	45.1	35.3	35.3	27.1	14.3

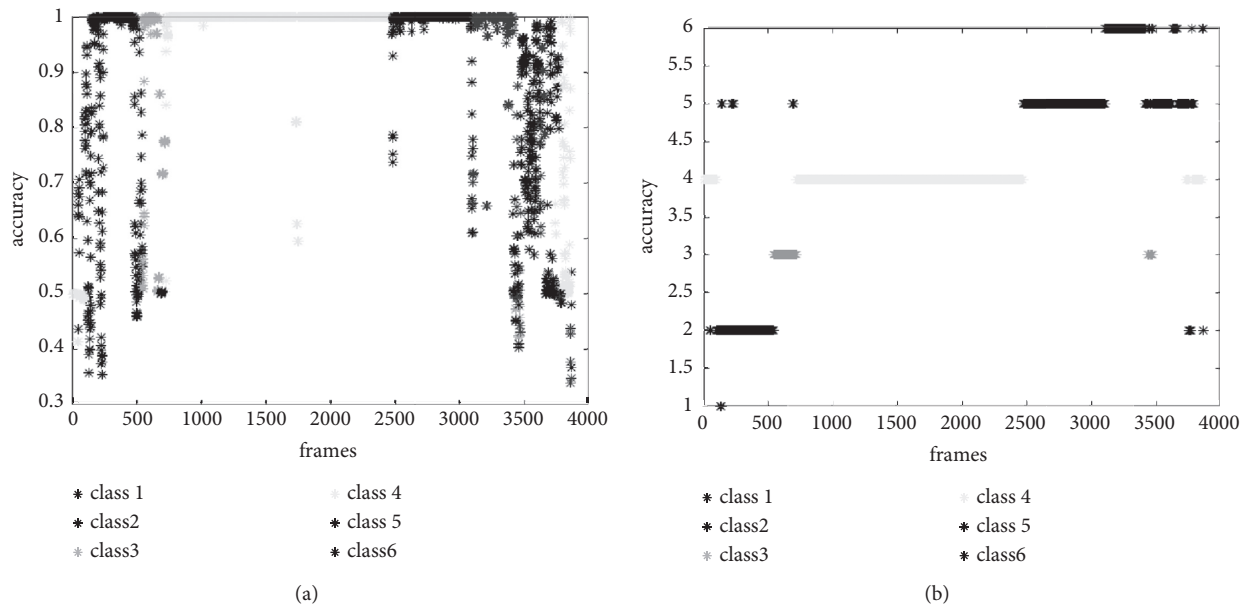


FIGURE 10: Visualization of classification recognition results. (a) Optimal visualization results of single frames in a video stream. (b) Classification results in the action timing flow.

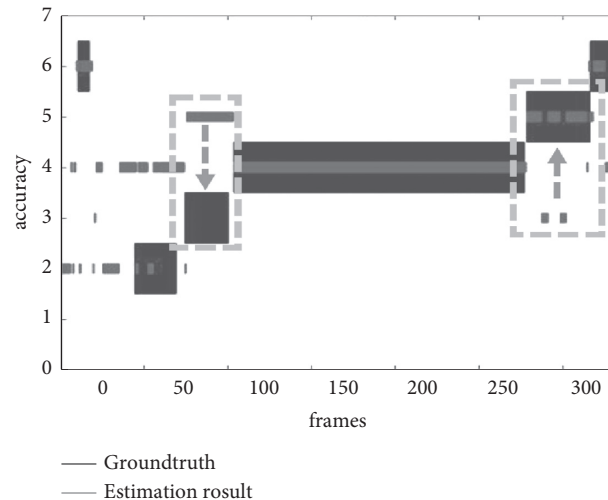


FIGURE 11: Visualization of classification recognition results.

the third action category. The proposed method presents the detection results (545,687), (697,672), and (3440,3468) frames, consistent with actual conditions.

To further analyze the classification and recognition effects of the similarity action, a study performed taxonomic identification of a test sample, and the results were shown in Figure 11. In the figure, abscissa represents video streams, the ordinate represents action categories, blue represents true values, red represents predictive values, and green boxes represent misclassification caused by similarity actions. According to the figure, considering the action time timing structure is conducive to the analysis of motion movements.

5. Conclusion

In summary, using the deep-learning-based motor action analysis method proposed in this study, static spatial features of the motion action are extracted by using BN-inception and high-dimensional spatiotemporal features of motor movements are extracted by 3D ConvNet. A characteristic representation containing the spatiotemporal information of the motor movements is obtained. By using the softmax classifier and integrating the extracted features with the fusion based on decision layers, the accuracy of motion action classification and recognition was improved, so that the average motion action classification and recognition accuracy reached 79.89%. Through the time-based semantic continuity optimization strategy, the recognition accuracy of motion movements was further improved, and the average motion action classification recognition accuracy reached to 83.11%, realizing the efficient recognition of motion actions. However, there are still some deficiencies in this study, mainly manifested in feature extraction. The BN-inception network and 3D ConvNet network used in the study trained the model in advance for the public dataset and did not fine-tune the model structure according to the research content, so its robustness needs to be further improved.

Data Availability

The data used in this experiment are available from the corresponding author upon request.

Conflicts of Interest

The author declares that there are no conflicts of interest regarding this work.

References

- [1] X. Li, M. Xie, Y. Zhang, G. Ding, and W. Tong, "Dual attention convolutional network for action recognition," *IET Image Processing*, vol. 14, no. 6, pp. 1059–1065, 2020.
- [2] H.-X. Zhang and L. Su, "An improved approach for human motion simulation and sports analysis based on dynamic image analysis[J]," *International Journal of Frontiers in Sociology*, vol. 0, no. 4, p. 2, 0, 2020.
- [3] H. Zhao, W. Xue, X. Li, Z. Gu, L. Niu, and L. Zhang, "Multi-mode neural network for human action recognition," *IET Computer Vision*, vol. 14, no. 8, pp. 587–596, 2020.
- [4] R. Cui, A. Zhu, J. Wu, and G. Hua, "Skeleton-based attention-aware spatial-temporal model for action detection and recognition," *IET Computer Vision*, vol. 14, no. 5, pp. 177–184, 2020.
- [5] N. Manikandaprabu and S. Vijayachitra, "Moving human target detection and tracking in video frames[J]," *Studies in Informatics and Control*, vol. 30, no. 1, pp. 119–129, 2021.
- [6] M. Khan, Mustaqeem, A. Ullah et al., "Human action recognition using attention based LSTM network with dilated CNN features[J]," *Future Generation Computer Systems*, vol. 125, pp. 820–830, 2021.
- [7] A. V. Anant, S. C. Gupta, D. Kumar, and Savita, "Human action recognition using CNN-SVM model[J]," *Advances in Science and Technology*, vol. 6258, pp. 282–290, 2021.
- [8] A. K. S. Kushwaha and R. Khurana, "Fusing dynamic images and depth motion maps for action recognition in surveillance systems," *International Journal of Sensors, Wireless Communications & Control*, vol. 11, no. 1, pp. 107–113, 2021.
- [9] N. S. Russel and A. Selvaraj, "Fusion of spatial and dynamic CNN streams for action recognition[J]," *Multimedia Systems*, vol. 27, no. 5, pp. 1–16, 2021.

- [10] S. K. Park, J. H. Chung, T. K. Kang, and M. T. Lim, "Binary dense sift flow based two stream CNN for human action recognition[J]," *Multimedia Tools and Applications*, vol. 80, no. 28-29, pp. 35697-35720, 2021.
- [11] D. zheng, H. Li, H. Li, and S. Yin, "Action recognition based on the modified twostream CNN," *International Journal of Mathematics and Soft Computing*, vol. 6, no. 6, pp. 15-23, 2020.
- [12] L. Xiao, T. Lan, D. Xu, W. Gao, and C. Li, "A simplified CNNs visual perception learning network algorithm for foods recognition," *Computers & Electrical Engineering*, vol. 92, p. 107152, 2021.
- [13] G. Li and C. Li, "Learning skeleton information for human action analysis using Kinect," *Signal Processing: Image Communication*, vol. 84, p. 115814, 2020.
- [14] Y. Ji, Y. Yang, F. Shen, H. T. Shen, and X. Li, "A survey of human action analysis in HRI applications," *IEEE Transactions on Circuits and Systems for Video Technology*, vol. 30, no. 7, pp. 2114-2128, 2020.
- [15] Q. Wu, A. Zhu, R. Cui et al., "Pose-Guided Inflated 3D ConvNet for action recognition in videos," *Signal Processing: Image Communication*, vol. 91, p. 116098, 2021.
- [16] W. Li, N. Xu, G. Liu, L. Zhao, and X. Fang, "Segments-based 3D ConvNet for action recognition," *Journal of Physics: Conference Series*, vol. 1621, no. 1, p. 012042, 2020.
- [17] E. Barnefske and H. Sternberg, "PCCT: pcct: a point cloud classification tool to create 3D training data to adjust and develop 3D convnet," *The International Archives of the Photogrammetry, Remote Sensing and Spatial Information Sciences*, vol. XLII-2/W16, pp. 35-40, 2019.
- [18] M. Lkhagvadorj, K. H. Ryu, O.-E. Namsrai, and N. Theera-Umpon, "A partially interpretable Adaptive softmax regression for credit scoring[J]," *Applied Sciences*, vol. 11, no. 7, p. 3227, 2021.
- [19] J. Luo, W. Shi, N. Lu et al., "Improving the performance of multisubject motor imagery-based BCIs using twin cascaded softmax CNNs," *Journal of Neural Engineering*, vol. 18, no. 3, p. 036024, 2021.
- [20] D. M. Vo, D. M. Nguyen, and S.-W. Lee, "Deep softmax collaborative representation for robust degraded face recognition," *Engineering Applications of Artificial Intelligence*, vol. 97, p. 104052, 2021.
- [21] S. S. S. Palakodati, V. R. Chirra, Y. Dasari, and S. Bulla, "Fresh and rotten fruits classification using CNN and transfer learning[J]," *Revue d'Intelligence Artificielle*, vol. 34, no. 5, pp. 617-622, 2020.
- [22] R. Deepa, H. Rajaguru, and C. Ganesh Babu, "Analysis on wavelet feature and softmax discriminant classifier for the detection of epilepsy," *IOP Conference Series: Materials Science and Engineering*, vol. 1084, no. 1, p. 012036, 2021.
- [23] F. Gao, B. Li, L. Chen, Z. Shang, X. Wei, and C. He, "A softmax classifier for high-precision classification of ultrasonic similar signals," *Ultrasonics*, vol. 112, p. 106344, 2021.
- [24] C. V. R. Reddy, K. K. Kishore, U. S. Reddy, and M. Suneetha, "Person identification system using feature level fusion of multi-biometrics," in *Proceedings of the 2016 IEEE International Conference on Computational Intelligence and Computing Research*, pp. 1-6, Chennai, India, 15-17 Dec. 2016.
- [25] V. Chirra, S. ReddyUyyala, and V. KishoreKolli, "Deep CNN: a machine learning approach for driver drowsiness detection based on eye state," *Revue d'Intelligence Artificielle*, vol. 33, no. 6, pp. 461-466, 2019.
- [26] L. M. R. Azizah, S. F. Umayah, S. Riyadi, and N. A. Utama, "Deep learning implementation using convolutional neural network in mangosteen surface defect detection," in *Proceedings of the 2017 7th IEEE International Conference on Control System, Computing and Engineering (ICCSCE)*, pp. 242-246, Penang, Malaysia, 24-26 Nov. 2017.
- [27] A. Wu, J. Zhu, and T. Ren, "Detection of apple defect using laser-induced light backscattering imaging and convolutional neural network," *Computers & Electrical Engineering*, vol. 81, p. 106454, 2020.
- [28] A. Kamilaris and F. X. Prenafeta-Boldú, "Deep learning in agriculture: a survey," *Computers and Electronics in Agriculture*, vol. 147, pp. 70-90, 2018.

Research Article

Study on Machine Learning Applications in Ideological and Political Education under the Background of Big Data

Yanjie Li¹ and He Mao² 

¹*Xi'an Siyuan University, Xi'an, Shaanxi 330022, China*

²*Suzhou University of Science and Technology, Suzhou, Jiangsu 215000, China*

Correspondence should be addressed to He Mao; 1603@mail.usts.edu.cn

Received 8 December 2021; Revised 26 January 2022; Accepted 10 February 2022; Published 10 March 2022

Academic Editor: Man Fai Leung

Copyright © 2022 Yanjie Li and He Mao. This is an open access article distributed under the Creative Commons Attribution License, which permits unrestricted use, distribution, and reproduction in any medium, provided the original work is properly cited.

With the development of big data and data mining technology, machine learning has been applied in many fields. However, there are a large number of difficulties for students who majored in ideological and political education. It is very necessary for those students to integrate machine learning technology into ideological and political education courses. In this paper, we introduced how to integrate machine learning into ideological and political education courses in class. Firstly, we explained what teachers should do before/in/after class for teaching machine learning courses and what students should prepare. Secondly, we took the introduction section of machine learning courses as an example to connect each content with ideological and political education and illustrate them in the way of ideological and political education. Thirdly, we took the decision tree algorithm that belongs to machine learning as an example to explore the ideological and political education philosophy in the decision tree algorithm. Finally, we make a questionnaire from the perspective of learning attitude, learning influence, and learning effect to investigate the outcomes of students with our teaching way. Our results presented valuable meaningful information for students who majored in not only computer science but also ideological and political education, thus promoting the progress of interdisciplinary and making machine learning courses understood more easily in the class of ideological and political education.

1. Introduction

Big data has the characteristics of various types, huge capacity, fast processing speed, and low-value density [1]. From the perspective of searching, storing, and processing data, machine learning algorithms have improved data collection, but traditional algorithms have been unable to mine large-scale heterogeneous data. Therefore, in the era of big data, a comprehensive study of the application of machine learning in data mining has promoted the sustainable development of China's information society. Big data technology refers to a technical system including big data collection, preprocessing, storage, analysis, and visualization. Big data technology refers to quickly obtaining valuable information from massive data resources [2]. According to different levels, it can be roughly divided into six categories: big data collection, storage, management, big data analysis

and mining, big data interpretation, and application. Currently, cloud computing is a core principle of big data analysis and processing technology, and it is also the basic platform and supporting technology for big data analysis and application. The most typical cloud computing is the big data processing technology represented by distributed file system GFS, batch processing technology MapReduce, distributed database Big Table, and the open-source data processing platform Hadoop generated on this basis [3]. The key technology of big data mainly includes the following: (1) The integration of multisource data: multisource data fusion integration refers to the accurate, effective, and rapid integration of heterogeneous data from different sources, different storage formats, and different coordinate systems to make it a unified format, convenient management, and data set that can directly face data analysis applications. (2) Data transmission and storage protocol: with the evolution

of big data technology, large-scale and long-distance distributed storage technology has emerged and become popular. A distributed storage system is a logically unified data storage system that uses a computer network to connect multiple physically dispersed data storage units to form a logically unified data storage system. Compared with traditional centralized storage systems, distributed storage systems have the advantages of strong scalability, high fault tolerance, high availability, and quick response to client data operation requests. (3) Data dynamic monitoring and risk identification: data dynamic monitoring and risk identification is a way of using data for measurement. It dynamically observes the development and operation of a certain field in real time by monitoring the abnormal changes of certain characteristics of the data so as to grasp the trend, predict the trend, and discover the problem [4].

The massive amount of big data, the complex information attributes, and the high-end, cutting-edge technical attributes are all influencing people's way of thinking about observing, analyzing, grasping, and transforming the world. The way of thinking is the rational way of cognition of people in a certain era, and it is a relatively stable mode of thinking that combines the elements of thinking according to a certain structure, method, and procedure [5]. In the perspective of the Marxist theory, thinking is a historical category, which is determined by the way of practice and existence of people in a certain era, and at the same time, it is affected by the level of scientific and technological development of the era. Big data has brought about huge ideological emancipation and conceptual change, which has enabled people to form a new way of thinking, that is, using data to speak, make decisions, manage, and innovate big data thinking [6]. In essence, big data thinking refers to a new concept system that was born in the era of big data and based on big data technology. The so-called big data thinking refers to the consciousness that once public data is handled properly, it can provide answers to the urgently needed problems for millions of people. Big data thinking is a way of thinking that uses data to view and solve problems, that is, to use data and quantitative methods to understand, think, and solve problems, and to explore and reveal the law of development of things [7]. Big data has transformed human thinking from single linear thinking to systematic thinking. Big data system thinking presents diversified thinking characteristics such as holistic thinking, precise thinking, connected thinking, forward-looking thinking, open thinking, efficiency thinking, innovative thinking, dynamic thinking, and intelligent thinking. In other words, the big data system reflects the dialectical unified relationship between the diversity of cognitive thinking and the multiple attributes of cognitive objects [8].

Data mining can analyze and process the data in an all-round way, and it can also summarize the law of development in the processing of the data [9]. The main steps involved are to (1) prepare the corresponding data in advance, (2) find out the characteristics and changing laws of the data by analyzing the given data, and (3) analyze, summarize, and draw the conclusion and reveal the law. In the era of big data, the development of society is inseparable

from data mining, and the application scope of data mining has become wider. Machine learning is an important part of artificial intelligence, and its purpose is to study how to use experience E to improve its performance in task T through calculation [10]. The main tasks of machine learning include the following: (1) Classification: it mainly adopts the built models to classify various data. The learning data plays an important role in the process of constructing the model. (2) Regression analysis [11]: it uses scientific methods to analyze and summarize different data variables and their relationships and finally get an expression with functional properties. In the specific practice of data analysis, knowledge of the statistical category in advanced mathematics is mainly used to complete the task of estimating data. The rational use of the above methods can greatly improve the efficiency of data mining [12]. (3) It is necessary to adopt the method from constructing the model to complete the regression analysis of the data. There are many ways to build a model, and artificial neural network is one of the commonly used methods. (4) Association rule: it is mainly used in transactional data, and finally, a frequent item set can be constructed. Its function is mainly to predict the probability of occurrence of a certain thing [13]. (5) Clustering: specifically, it refers to the collection of data in different clusters. Artificial intelligence technology is used in machine learning. This technology can be used to find a large amount of data, including the knowledge and information you need, integrate the information efficiently, and use other algorithms to classify the data [14].

There are large advantages to machine learning used in data mining [15]. And it is applied in many fields, for example, medicine, agriculture, hydrology, and economy. In the past, the main form of traditional machine learning algorithms was based on memory [16]. Therefore, many algorithms simply cannot meet the requirements of current data mining. Only by continuously improving and optimizing machine learning algorithms can we adapt to the development of the big data era. The artificial neural network method is a kind of machine learning algorithm, which can construct different artificial neural network models with excellent description function and excellent precision control [17]. Traditional machine learning requires independence and distribution, and it is almost impossible to play a role. The application of machine learning in big data can greatly improve its own classification function [18]. In the context of big data, machine learning has been out of the scope of conceptual learning and continues to evolve in the direction of complex knowledge learning and processing. It is an important way to improve and optimize data mining. Optimizing computer performance is the main goal of machine learning [19]. To achieve this, we need to continuously accumulate experience in computer programs. After accumulating to a certain degree in quantity, it will naturally change in the quality and improve the efficiency of information processing. Computer learning algorithms can be roughly divided into three parts (Figure 1). Its main function is to test the effect of the algorithm after it is executed [20]. During the test, the knowledge base is mainly used as the reference standard, and the completeness of the

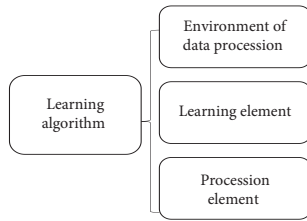


FIGURE 1: Computer learning algorithm model.

database content can also be analyzed through the final test results. In this way, more accurate suggestions can be provided for future learning [21].

A series of new changes are taking place in the background, objectives, and tasks of daily ideological and political education of college students. These new changes have brought not only new opportunities for college students' daily ideological and political education but also new challenges and issues [22]. On the other hand, the rapid development of a new round of information technology revolution with digitization, networking, and intelligence as its core features and its extensive integration with the economy and society provide new carriers and new means for college students' daily ideological and political education [23]. As far as the new challenges are concerned, the current international and national situations continue to undergo profound and complex changes. The ideological and cultural fields and ideological fields of colleges and universities are facing more complex situations, and the difficulty of daily ideological and political education for college students is increasing. In terms of the new faced issues faced, on the one hand, the Communist Party of China and the country's task of cultivating newcomers of the era who will take on the responsibility of national rejuvenation has given college students a new historical mission in their daily ideological and political education, and college students' daily ideological and political education has ushered in new development points. On the other hand, the new changes and characteristics of contemporary college students put forward new requirements for the daily ideological and political education of college students [24]. Big data empowers college students' daily ideological and political education innovation and development. Big data technology is a new assistant for college students' daily ideological and political education [25].

Big data thinking will also help college students' daily ideological and political educators to establish complex, dynamic, and intelligent thinking. On the one hand, big data thinking highly meets the needs of college students' daily ideological and political education [26]. The hybrid performance enhances the authenticity and relevant performance of ideological and political work objects, improves the foresight and unlimited performance of ideological and political work, and improves the continuity of the potential value of data mining. On the other hand, big data thinking is of great significance to the innovation of college students' daily ideological and political education concepts. The embedding and internalization of big data thinking in the daily ideological and political education of college students

help educators to pay more attention to objectivity and regulation in the development of work. To pay more attention to integrity, so as to provide new perspectives, ideas, and methods for the development and innovation of college students' daily ideological and political education [27]. At present, the methods connect ideological and political education with big data mainly through the following: (1) Literature research: before writing the thesis, read a large number of journal papers, academic papers, and books related to big data, systematically sort out and summarize the relevant theoretical points of big data and the precision of ideological and political education in colleges and universities, and pay close attention to the academic frontier in time. (2) Comprehensive analysis and research: the thesis analyzes the opportunities and challenges brought by big data to ideological and political education in colleges and universities. The first is to recognize the opportunities brought by big data. Traditional ideological and political education methods in colleges and universities have certain limitations. Therefore, the precision of ideological and political education has a profound practical necessity. The second is that the application of big data also provides ideological and political education in colleges. Development has brought a series of problems; data and information security is a big hidden danger. Therefore, we must actively explore effective practical paths to make research more scientific. (3) Linking theory with practice method: the subject of ideological and political education is a unity of theory and practice. Ideological and political education in colleges and universities plays an important role in guiding students to establish a correct world outlook, outlook on life, and values and is responsible for the important mission of cultivating socialist builders and successors. Therefore, the specific implementation path of the precision of ideological and political education in colleges and universities should combine students and teaching practice and put forward specific measures with strong operability.

In the era of big data, the new changes in the teaching methods of ideological and political courses are mainly manifested in that teachers of ideological and political courses carried out ideological and political course teaching with the help of a mixed teaching mode; that is, teachers of ideological and political courses rely on network teaching, classroom teaching, and practical teaching. The teaching method adopts the teaching mode of online and offline mixed teaching, combines teaching inside and outside the classroom, flood irrigation, and drip irrigation, and integrates the teaching methods of ideological and political courses to bring out the best teaching effect. Online teaching is manifested in the implementation of corresponding teaching methods to carry out ideological and political teaching with the help of online teaching methods such as MOOCs and microcourses, while offline teaching is manifested in teaching through classroom teaching and practical teaching. The combination of online and offline teaching modes is a concrete manifestation of the combination of inside and outside the classroom, flood irrigation, and drip irrigation. Teachers of ideological and political courses adopt different teaching methods according to the complexity of

teaching content and innovate teaching methods with the help of big data technology. The teaching method of ideological and political courses in the era of big data extends the classroom with the help of new teaching methods, breaks through the limitations of physical time and space, and can achieve precise teaching. But this does not mean that it is a negation of the teaching methods of ideological and political courses in the era of small data but inherits and develops the teaching methods of ideological and political courses in the era of small data. At the same time, ideological and political courses are a complex system. It is necessary to use online teaching methods such as MOOCs to divide ideological and political courses into several knowledge points and then use offline teaching, such as classroom teaching and practical teaching, to systematically spread ideological and political courses and internalize them in the heart and externalized them in the line. In the era of big data, where “everything can be digitized,” ideological and political teachers can use big data technology to collect and analyze the data of students’ learning on these platforms, predict students’ learning and other situations, and combine the teaching guidance of ideological and political teachers. Experience guides students in a focused manner. However, there are still some shortages in teaching methods under the background of big data, such as single teaching method, unreasonable method, poor compatibility, and insufficient function.

In our study, we take the introduction part of the professional course machine learning as an example. Based on the sorting out of the teaching content, the ideological and political elements are deeply explored, and the ideological and political construction of the course is promoted. Then, we take the decision tree in machine learning as an example to explore the organic integration of ideological and political education, quality education, and moral education and integrate them into the new teaching ideas of the first classroom of machine learning and ideas on other professional courses in computer science political elements and case design that have a certain reference significance and practical value. Section 2 aims to show the connection of ideological and political education with machine learning, and we present three ways to accomplish it. Section 3 mainly presents an ideology theory in machine learning and how students should understand it in learning courses.

2. Design Procedure

Machine learning courses are designed and constructed in accordance with OBE (Outcomes-Based Education) teaching concepts. The course objectives are divided into six dimensions: knowledge, application, integration, emotion, value, and learning. Among them, the knowledge dimension is to enable students to have the ability to correctly select and use common machine learning algorithms; the application dimension is to be able to select appropriate machine learning algorithms based on training data, test data, and actual needs and to use labeled data and unlabeled data to solve the classification, evaluating the effective conclusion obtained. Combining literacy and the spirit of innovation is organically unified, discovering new problems in the

professional field, generating new ideas, and creating new solutions or new products; the emotional dimension is to recognize the importance and significance of applying the knowledge learned to solve practical social problems; the value dimension is to allow students to correctly understand the relationship between human and machine learning technology, which can be reflected in the technical solutions to solve complex engineering problems. The idea of the harmonious development between human and machine learning technology, it is need to establish the value of machine learning technology. The learning dimension is to enable students to develop the habit of using various online and offline resources to learn independently before and after class and to develop learning in engineering practice. The six dimensions of the curriculum objectives are organically integrated and complementary and support the ability of professional engineering knowledge, research, and analysis to solve complex engineering problems, communication skills, and lifelong learning capabilities in the graduation indicators, as shown in Figure 2. Based on advanced mathematics, linear algebra, probability theory and mathematical statistics, high-level language programming, and so on, this course introduced the principles, techniques, and algorithms of commonly used machine learning analysis. The course content mainly includes model evaluation and selection, linear model, support vector machine, K-nearest neighbor method, clustering, decision tree, neural network, Bayesian classifier, and reinforcement learning.

The core design idea between the machine learning and course ideological and political is to integrate the three spirits of the basic principles of being a person and doing things, the fundamental requirements of socialist core values, and the ideal and responsibility of realizing national rejuvenation into the course teaching process. Curriculum ideological and political courses are different from ideological and political courses. Ideological and political courses are direct and clear ideological education, while curriculum ideological and political courses are to integrate ideological and political elements into professional courses to achieve genetic integration, three-dimensional penetration, and immersive interpretation. In recent years, as the core technology in the field of artificial intelligence [28], machine learning has played an active role in various application fields [29], such as technological progress, social and people’s livelihood, national defense and security, and national strategy. The ideological and political integration design of this course is a breakthrough point, including the following three levels: (1) Strategy to strengthen students’ scientific and technological self-confidence and learning motivation: as a new engineering professional course, the students will be the country’s new force of science and technology. (2) The direction of the application of science and technology to cultivate students’ country feelings and a sense of social responsibility: incorporating elements of the application of science and technology into the curriculum ideology guides students to pay attention to society and people’s livelihood around them and explain how machine learning technology can efficiently summarize and analyze epidemic data in the fight against the new crown pneumonia epidemic, which is

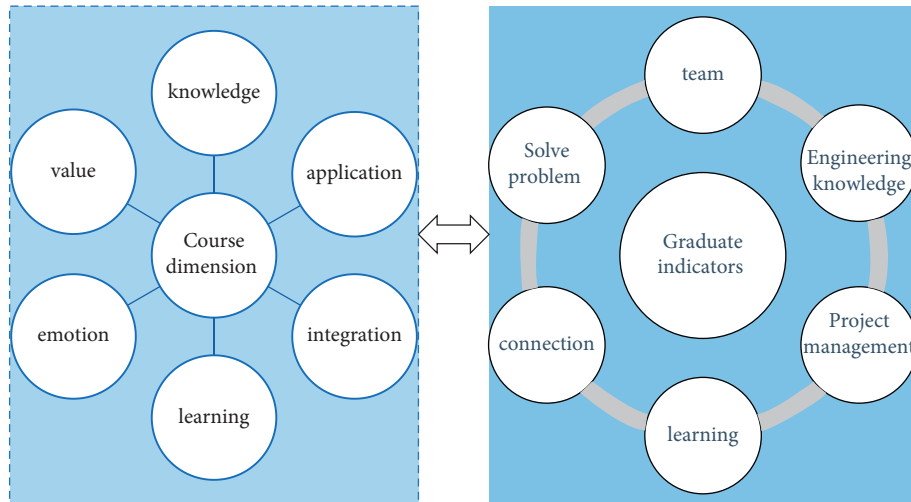


FIGURE 2: Connection between the course dimension and graduate aim.

the important role played in the decision-making of measures such as the adoption of using GIS (Geographic Information System) and spatial clustering analysis algorithms to master the laws and patterns of the spatial distribution of the epidemic and adopt different protection modes and protection preparations for different regions. The World Health Organization currently uses machine learning from a large amount of online data to detect alerts for new public health events and uses the open-source Infectious Disease Intelligence (EIOS) platform to use natural language processing technology for data processing, classification, and combination. (3) Dedication to cultivating the craftsman spirit of students: in the face of each machine learning algorithm, it is necessary to explore its theoretical basis, derivation process, applicable scenarios, optimization direction, and so on. These required a meticulous attitude and practical practice, as well as patience, concentration, and heart. For example, in the process of teaching and learning KNN (K-nearest neighbor algorithm), in order to obtain a suitable optimization model, the parameters of the model need to be repeatedly trained and continuously adjusted. In this process, students should focus on the main points of each training result and parameter adjustment and constantly seek the direction of success amidst setbacks.

3. Results and Discussion

3.1. Ideological and Political Course Integration Steps in Machine Learning. The implementation of the curriculum ideological and political education was planned and step-by-step. It is necessary to make great efforts in the design and practice of ideological and political education to implement. The ideological and political implementation of the machine learning course can be divided into three steps: before class, during class, and after class, as shown in Figure 3.

- (1) Before class, teachers are educated first and constantly improve their professional knowledge, ideology, patriotism, and other aspects of literacy and ability. For new engineering courses, teachers

continue to adapt to the development needs of the times and to learn and delve into cutting-edge technologies and problems of science and technology, which is also a kind of precept and deeds for students to climb the peak of science and technology. In the process of preparing lessons, dig deeper into ideological and political elements and integrate them into the curriculum reasonably. In the classroom, the ideological and political elements such as the power of science and technology and the feelings of home are integrated into the knowledge explanation in the way of spring weather. Through case analysis and discussion, the students' ability to analyze problems and distinguish right from wrong was improved. The integration of curriculum ideology and politics is reflected not only in the combination of ideological and political elements and curriculum content but also in the tone, facial expressions, and body language of the teacher's explanation. It is a natural process. After class, by assigning research assignments to experience the development of society, people's livelihood, and technology, students will be cultivated to pay attention to society, find and solve problems, and at the same time improve their teamwork and self-learning ability so that students can continue to accumulate a sense of social responsibility and responsibility and feel the power of technology.

In order to further understand the recognition and feelings of the students in the above step of teaching, after the teaching experiment, the students in the experimental group were tested by means of a feedback questionnaire, and the results are shown in Table 1.

After the teaching experiment, the attitude of the students in the experimental group was as follows: very welcome (50%), welcome (25%), not very welcome (15%), and not welcome at all (15%). Overall, most students accept this kind of teaching way. This kind of teaching method can bring students a certain sense of situational substitution and

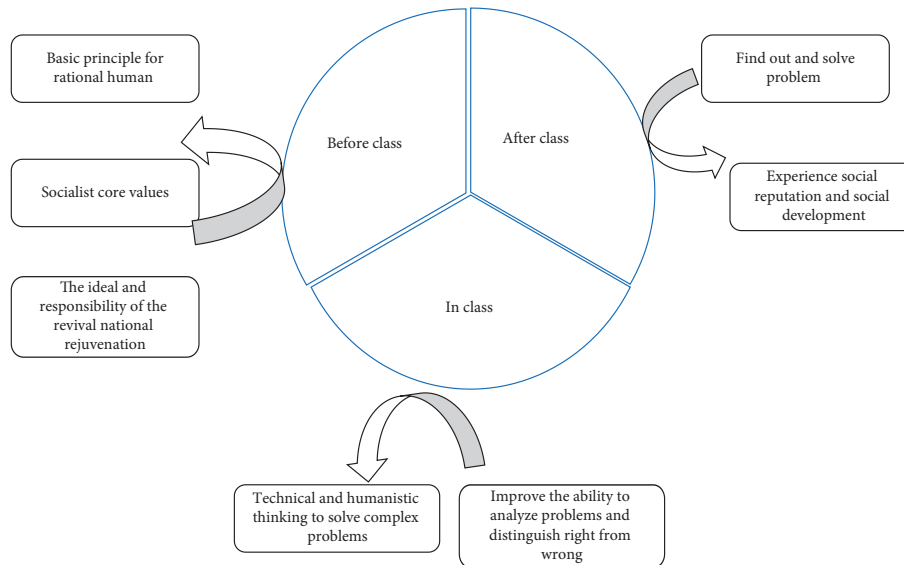


FIGURE 3: Ideological and political course implementation steps.

TABLE 1: Attitude of students on machine learning integrated with the ideological and political course.

Attitude	Very welcome	Welcome	General	Not very welcome	Not welcome at all
Percentage	50	25	15	10	0

interest, making it interesting for students to study ideological and political courses or machine learning, improving the learning effect of students, solving the boring learning state in the traditional classroom to a certain extent, and enriching the classroom teaching.

3.2. Design for Incorporating Ideological and Political Elements into Machine Learning. Machine learning focuses on overview, basic terms, two theorems, development process, and current status of machine learning applications. The ideological and political elements involved in a journey of a thousand miles begin with a single step, step-by-step learning, looking at problems dialectically, educating on frustration, enhancing national pride, strengthening the four self-confidences, and so on (Figure 4).

Before the course, this stage mainly allows students to understand the content to be explained in this lesson and have a basic overall understanding of the content of the lecture. The teacher draws the lectured content into a mind map and uploads it to the blackboard teaching platform to help students conduct preclass learning in an orderly and targeted manner, stimulate students' interest in learning, and guide students to think deeply. Teachers also set up a teaching platform that combines social current affairs thinking issues to enhance students' practical ability to find and solve problems and to ensure that ideological and political elements are effectively integrated into the classroom. In class, guide students to use analogy and reasoning about the process of human learning and thinking to get the concept of machine learning. Teach students about data-related terms: samples, attributes, features, and so on; learn about the classification of machine learning algorithms:

supervised learning and unsupervised learning. Students will feel boring in this part of the study, permeating the students' thinking of "learning to walk first, then learning to run." Nowadays, many cutting-edge machine learning researches, such as deep learning and natural language processing, stimulate students' interest to take the initiative to practice. Occam's Razor Principle is one of the most basic principles in natural science research. Its idea is to choose the simplest one if there are multiple hypotheses that are consistent with observations. When learning, the idea of "simplification" is introduced, and the decision tree is used as an example to explain. When the redundant branches are subtracted, the model can often get better generalization ability. After class, teachers publish coursework on the blackboard teaching platform. Combined with the content of the classroom, students in groups of 6 to 8 will submit the mind map of the knowledge points of the course, cultivate the students' spirit of cooperation, consolidate the content taught in the classroom, and truly integrate the classroom ideology and politics into the daily life of the students.

We also investigated the attention of students on ideological and political courses; see Table 2. Results show the effect of students' attention on learning in the experimental group: 55% of the students considered it very favorable, 30% considered it favorable, 10% of the students said they were uncertain, and 5% of the students said it was unfavorable. Therefore, most students believe that the introduction of machine learning can help focus attention, and at the same time, they can obtain a short-term immersion experience. For students who express their disadvantage, it may be that they will feel fatigued after a long study time and lose interest in short-term learning. Of course, this is a problem of the human mind. In conclusion, the teaching of

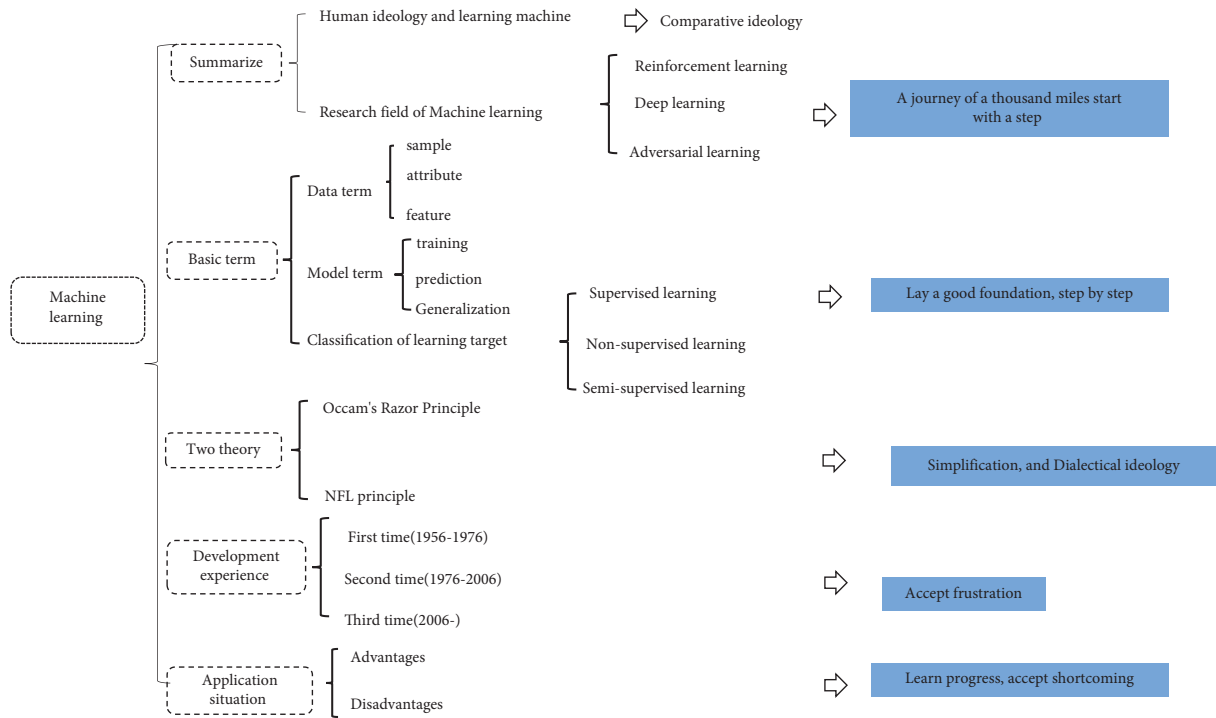


FIGURE 4: Relationships between the machine learning course and ideological and political course.

TABLE 2: Influence of machine learning integrated with the ideological and political course on students’ learning skills.

Influence	Very positive	Positive	Not sure	Negative	Very negative
Percentage	55	30	10	5	0

machine learning is significant for improving students’ attention.

3.3. *Decision Tree and Ideological and Political Elements.* According to the chapter of the decision tree, we sorted out the key points of learning and at the same time carried out detailed design and planning on how to integrate ideological and political elements into it, as shown in Figure 5.

The basic algorithm of the decision tree follows the strategy of simple and intuitive divide and conquer, which means that a problem is decomposed into two or more subproblems of the same or related types until these problems can be solved easily and directly. Here, we guide students to understand that in their study and life. Students should not shrink back and give up easily when encountering difficulties. Instead, they should continue to decompose the problem according to their existing abilities. Starting from what they can do, they should continuously optimize the way to solve the problem and train students to be the craftsman spirit of giving up and being lean and focused. When writing decision tree algorithms, the programming software python encapsulates many ready-made functions. It is easy to call these functions, and it is very convenient to implement the corresponding functions. However, students should be guided to fully learn from its

internal implementation; some implementation processes are regarded as learning paths, try to understand and master the algorithmic thinking contained therein, and constantly practice them to cultivate their own code writing ability; encourage students to compare the code debugged by themselves, analyze the pros and cons, and learn from each other in groups. Taking the essence and discarding the dross, cultivate students’ lean and rigorous scientific attitude.

The three methods of division selection are information gain, gain rate, and Gini index, and their corresponding algorithms are ID3, C4.5, and CART, respectively. These three algorithms can solve the problem of optimal attribute partitioning, and each has its own advantages and disadvantages. In actual application, specific analysis can be carried out according to the problem to be solved, and then the most suitable algorithm can be selected. Here, we guide students to insist on using scientific and dialectical viewpoints and methods of thinking to understand things and analyze problems comprehensively and objectively. It is necessary to observe the interrelationships between things but also to pay attention to the differences between things. When analyzing problems, they must comprehensively consider and pay attention to the relationship between their various constituent factors so as to avoid neglecting one and the other.

There are two methods of pruning strategy, “prepruning” and “postpruning.” The two methods are explained and analyzed. The former focuses on estimating whether the current division of each node can improve the generalization performance of the decision tree before dividing; the latter starts from the complete decision tree and examines whether nonleaf nodes are replaced by leaf nodes from the bottom to the top, thus helping to improve generalization performance. The basic theoretical knowledge mastered through

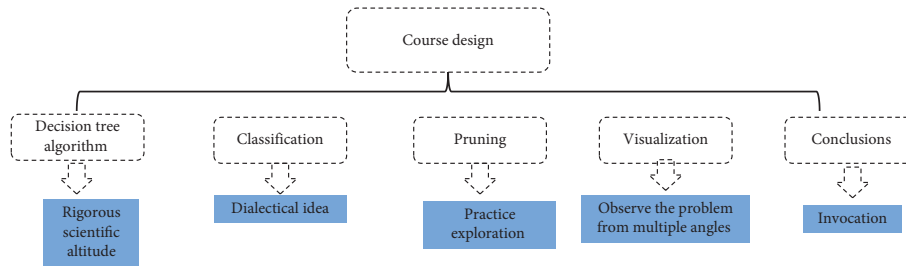


FIGURE 5: Integration decision tree into the ideological and political course.

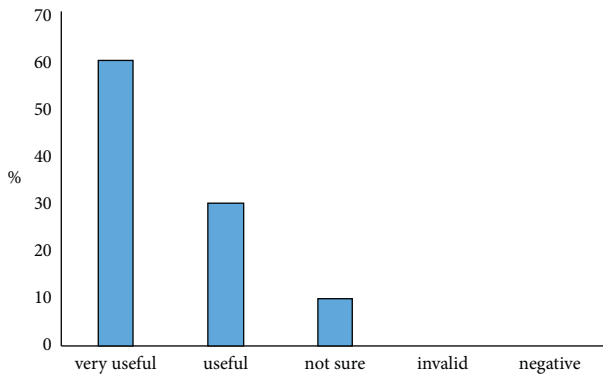


FIGURE 6: Learning effect of students on machine learning integrated with the ideological and political course.

practice will be more attractive to students, and students will be more interested, and through the process of practical operation, students will have a firmer grasp of basic theoretical knowledge. When describing the basic principles and strategies of pruning, on the one hand, it is necessary to integrate the spirit of practice and exploration to cultivate students' scientific spirit of seeking truth and being pragmatic; on the other hand, for the same problem, the conclusions obtained by different methods will be different, leading students to master the principle of nonuniqueness of solutions and cultivate their truth-seeking spirit of "practice is the only criterion for testing truth."

The teacher summarizes the main knowledge points in the decision tree chapter to guide the students to look at the problem in a comprehensive and holistic way. Through group collaboration within the group, the decision tree and visualization technology are used to solve more problems, such as wine classification and weather prediction. On the one hand, communication activities are carried out to enhance students' research interest, innovation ability, teamwork ability, and divergent thinking ability; on the other hand, improving students' professional quality in exploratory spirit and practical ability to help students career growth, realize the value of life as soon as possible.

To test the learning effect of students to the teaching way we introduced, we make a questionnaire to reach it; results are shown in Figure 6. Results show that after students learn through this teaching method, 55% of the students think it is very effective, 35% of the students think it is effective, and 10% of the students are uncertain. In a word, the introduction of machine learning into the teaching of ideological

and political courses has improved the enthusiasm of course learning and promoted the mastery of ideological and political courses and machine learning courses. Therefore, this teaching method has a positive impact on improving students' course learning outcomes.

4. Conclusions

In our study, we analyzed incorporating ideological and political courses into the application of machine learning under the background of big data. Firstly, we talk about what we should do for teachers before/in/after class. Making good use of machine learning technology, cultivating new era and new engineering talents with both ability and political integrity is the direction for the continuous advancement of the ideological and political teaching reform of the "machine learning" course. Secondly, we took the introduction part of machine learning as an example. On the basis of combining the content, we deeply explored the ideological and political elements, promoted the ideological and political construction of the curriculum, and guided the core socialist values in knowledge transfer and ability training. Thirdly, we took the decision tree in machine learning as an example, explored the organic integration of ideological and political education, quality education, and moral education, and integrated them into the new teaching ideas of the first classroom of machine learning, and the ideological and political elements of other professional courses in computer and case design have a certain reference significance and practical value. We finally make a questionnaire from the perspective of learning attitude, learning influence, and learning effect to investigate the outcomes of students with our teaching way. Overall, our teaching way promotes the learning ability and interest of students, and the learning efficiency will be modified significantly through this way.

Data Availability

The experimental data used to support the findings of this study are available from the corresponding author upon request.

Conflicts of Interest

The authors declare that they have no conflicts of interest to report regarding this paper.

References

- [1] E. Letouze, “Big data for development: challenges and opportunitise,” 2012, http://www.Unglobalpulse.Org/projects/Big_data_for_development UN Global Pulse.
- [2] T. Cass, “A handler for big data,” *Science*, vol. 282, no. 5389, Article ID 636, 1998.
- [3] M. Minnesota, “Big data:Science in the petabyte era,” *Nature*, vol. 455, no. 7209, pp. 1–136, 2008.
- [4] J. Manyika, M. Chui, B. Brown et al., “Big data:the next frontier for innovation, Competition,and productivity,” 2011-05-21, <https://www.mckinsey.com/business-functions/mckinsey-digital/our-insights/big-data-the-next-frontier-for-innovation> MCK insey Global Institute.
- [5] M. Hilbert and P. Lopez, “The world’s technological capacity to store, communicate and compute information,” *Science*, vol. 332, no. 6025, 2011.
- [6] J. Shaw, “Why“Big Data”Is a big deal,” 2014, https://Harvard_magzine.com/2014/03/why-big-data-is-a-big-deal.
- [7] H Haken, *Information and Self-Organization:A Macroscopic Approach Systems*, p. 11, Springer-Verlag, Berlin, 1988.
- [8] T. Devasia, R. Raje-Sha, T. P. Vinushree, and V. Hegde, “Prediction of students performance using educational data mining,” in *Proceedings of the 2016 International Conference on DataMining and Advanced Computing (SAPIENCE)*Piscataway, March 2016.
- [9] Z. Zhao, Z. Jian, G. S. Gaba, R. Alroobaea, M. Masud, and S. Rubaiee, “An improved association rule mining algorithm for large data,” *Journal of Intelligent Systems*, vol. 30, no. 1, 2021.
- [10] Y. Zhu and J. Chen, “Research on system of data mining technology based on computer,” *Journal of Physics: Conference Series*, vol. 1952, no. 4, 2021.
- [11] J. He, “A study on the integration of computer network information security prevention and web data mining technology,” *Journal of Physics: Conference Series*, vol. 1915, no. 3, 2021.
- [12] A. S. Ejaz, “Statistical and machine-learning data mining: techniques for better predictive modelling and analysis of big data[.],” *Technometrics*, vol. 63, no. 2, 2021.
- [13] M. C. SáizManzanares, J. J. RodríguezDíez, J. F. DíezPastor, S. RodríguezArribas, R. MarticorenaSánchez, and P. Jiyi, “Monitoring of student learning in learning management systems: an application of educational data mining techniques,” *Applied Sciences*, vol. 11, no. 6, 2021.
- [14] K. Qu and L. Wang, “Research on visual data mining technology,” *Journal of Physics: Conference Series*, vol. 1748, no. 3, 2021.
- [15] K. G. Devi, K. Balasubramanian, and L. A. Ngoc, *Machine Learning and Deep Learning Techniques for Medical Science*, CRC Press, 2021.
- [16] B. A. J. Tallón, *Modern Management Based on Big Data II and Machine Learning and Intelligent Systems III*, IOS Press, 2021.
- [17] N. Mohan, R. Singla, P. Kaushal, and S. Kadry, *Artificial Intelligence, Machine Learning, and Data Science Technologies: Future Impact and Well-Being for Society 5.0*, CRC Press, 2021-10-09.
- [18] The European Parliament and The Council of the European Union, “Regulation(EU) 2016/679 of the European Parliament and of the Council of 27 April 2016on the protection of natural persons with regard to the processing of personal data and on the free movement of such data, and repealing Directive 95/46/EC (GeneralData Protection Regulation),” *Journal of European Union*, vol. 59, no. L119, pp. 1–88, 2016.
- [19] B. McMahan, E. Moore, D. Ramage, S. Hampson, and B. A. y Arcas, “Communication-efficient learning of deep networks from decen-tralized data,” ArXiv preprint arXiv:1602.05629, 2016.
- [20] K. Bonawitz, V. Ivanov, and B. Kreuter, “Practical secure aggregation forprivacy-preserving machine learning,” in *Proceedings of the 2017 ACM SIGSACConference on Computer and Communications Security*, pp. 1175–1191, Dallas, TX, USA, 2017.
- [21] C. Zhang, P. Zhao, S. Hao et al., “Distributed multi-task classification: a decentralized online learning approach,” *Machine Learning*, vol. 107, no. 4, pp. 727–747, 2018.
- [22] H. Li, A. Kadav, I. Durdanovic, H. Samet, and H. P. Graf, “Pruning filters for efficient convnets,” 2016, <https://arxiv.org/abs/1608.08710>.
- [23] Y. H. Hen, T. Krishna, J. S. Emer, J. S. Emer, and V. Sze, “Eyeriss: an energy-efficient recon-figurabe accelerator for deep convolutional neural networks,” *IEEE Journal of Solid-State Circuits*, vol. 52, no. 1, pp. 127–138, 2016.
- [24] S. Han, J. Pool, J. Tran, and W. J. Dally, “Learning both weights and connections for ef-ficient neural network,” *Advances in Neural Information Processing Systems*, pp. 1135–1143, 2015.
- [25] S. Gupta, A. Agrawal, K. Gopalakrishnan, and P. Narayanan, “Deep learning withlimited numerical precision,” in *Proceedings of the International Conference on Machine Learning*, pp. 1737–1746, 2015.
- [26] Y. Qu, H. Cai, K. Ren et al., “Product-based neural networks for user response pre-diction[,” in *Proceedings of the 2016 IEEE 16th International Conference on Data Mining (ICDM)*, pp. 1149–1154, Barcelona, Spain, December 2016.
- [27] P. Sidhu, M. Bhatia, and A. Bindal, “Empirical support for weighted Majority,Early drift detection method and dynamic weighted majority,” in *Proceedings of the 2013 International Conference on Machine In-telligence and Research Advance-ment (ICMIRA)*, pp. 623–627, Katra, India, December 2013.
- [28] J. Duchi, E. Hazan, and Y. Singer, “Adaptive subgradient methods for online learning and stochastic optimization,” *Journal of Machine Learning Research*, vol. 12, no. 7, pp. 257–269, 2011.
- [29] H. Sahour, V. Gholami, M. Vazifedan, and S. Saeedi, “Machine learning applications for water-induced soil erosion modeling and mapping,” *Soil and Tillage Research*, vol. 211, 2021.

Research Article

E-Commerce Precision Marketing Model Based on Convolutional Neural Network

Xia Liu 

Shandong University of Finance and Economics, Shandong, Jinan, China

Correspondence should be addressed to Xia Liu; 20088532@sdufe.edu.cn

Received 23 December 2021; Revised 18 January 2022; Accepted 26 January 2022; Published 7 March 2022

Academic Editor: Hangjun Che

Copyright © 2022 Xia Liu. This is an open access article distributed under the Creative Commons Attribution License, which permits unrestricted use, distribution, and reproduction in any medium, provided the original work is properly cited.

With the rapid development of network and informatization of the consumer market in my country, the application and maturity of technologies such as the Internet, terminal equipment, logistics, and payment and the continuous improvement of people's consumption concepts, online shopping has gradually become the mainstream purchase method for Chinese consumers, and e-commerce has gradually become one of the important driving forces to promote the sustained and vigorous development of China's economy. Under the traditional marketing model, companies do not fully understand the needs of users. The sales staff's thinking is only how to sell products to users. They do not know the specific consumer needs, so they can only focus on the product. Based on these foundations, this research uses convolutional neural networks and applies this model to precision marketing to obtain accurate portraits of consumers, thereby increasing the company's turnover. After comparing different models and conducting some experiments, it is concluded that (1) through the collection and analysis of W enterprise data, the training and testing conditions of the CNN model, LSTM model, LSTM attention model, and CNN + LSTM attention model are compared. It is concluded that the CNN + LSTM attention model and the LSTM attention model perform better, and the accuracy of testing and training is higher. (2) Through the fitting of the model, it is found that $Sn(\%) = 70.71$, $Sp(\%) = 86.25$, $Acc(\%) = 81.07$, and $MCC = 0.752$ of the CNN + LSTM attention model are the best fitting models. The men and women stratification and gender stratification of users are predicted, and it is found that men in the W company are the main purchasing power, and in the age stratification, it is found that the population of 41–50 accounts for the highest proportion. (3) The average accuracy rate of the LSTM attention model is as high as 66.6%, the average recall rate is 82.3%, and the F1 score is 73.1%. This model has met expectations for precision marketing forecasts. (4) Using the CNN + LSTM attention model to predict the marketing input for the next year, it is found that the use of precision marketing will increase the profit of W company. The average annual data show that the monthly revenue of precision marketing has increased by 73.5%.

1. Introduction

In the past ten years, with the rapid development of network and informatization of China's consumer market, the application and maturity of technologies such as the Internet, terminal equipment, logistics, and payment and the continuous improvement of people's consumption concepts, online shopping has gradually become the mainstream purchase method for Chinese consumers. E-commerce has gradually become one of the important driving forces to promote the sustained and vigorous development of China's economy [1, 2]. Based on the analysis and statistics of the marketing models that currently exist in our society, it is

concluded that the growth rate of e-commerce online marketing is getting faster and faster. The refined and precise marketing model will be the mainstream model in the future. Literature [3] only makes good use of big data to paint portraits of consumers. The precision marketing model can greatly promote offline marketing and online marketing. The function of marketing is to act as a communication bridge between the company and consumers. It can not only help consumers understand the company and make these consumers become loyal customers of the company but also play a role in publicity, allowing the company to better understand its audience. Therefore, it is necessary to learn and improve marketing concepts and transform from ordinary

marketing to precision marketing. Precision marketing is a concept that may help promote collective thinking and understanding of the criteria used for segmentation and positioning. The purpose is to better serve customers, thereby highlighting the competitiveness of products and bringing profits to the company. Only by formulating sales strategies from person to person can the effect of precision marketing be maximized. Control the results and costs of communication as much as possible, give scientific standards, and avoid randomness. Convolutional neural networks are used to predict the detection index system of multilabel systems. The prediction model is superior to other existing prediction models in almost all five indicators of performance. The most outstanding performance in the "absolute truth" rate and "absolute truth" rate [4]. A multilabel classifier system is based on deep learning features of convolutional neural network to infer the classification of goods. The system is based on the two-dimensional representation of the sample: first, obtain a one-dimensional feature vector, extract the characteristics of the marketing amount and marketing model, find out the interaction and the structure and feature similarity information with other products of different categories, and then reshape the original one-dimensional feature vector to obtain a two-dimensional matrix table of commodities. Finally, using feature extractors, two general classifiers designed for multilabel classification are trained using deep learning features. The scores obtained are fused by the average rule [5, 6]. With the continuous breakthroughs in computer technology, deep neural networks and other technologies are becoming more and more widely used in our daily life applications. People process the acquired information with computer algorithms. Convolutional neural networks (CNN) are currently the mainstream computer network analysis means. Convolutional neural networks can be used to automatically learn structured data, extract effective features, and then use the extracted effective features to make predictions and make correct decisions, which can help manage company employees, predict consumer preferences, etc. Predictive classification of unknown consumers is of great significance to existing research. The ATC system is a multilabel classification system that classifies consumers according to their consumption preferences. The system includes five levels, and each level includes several levels; the first level includes 14 main overlapping categories. The ATC classification system also considers the distribution of population characteristics, brings into the model effect characteristics, and predicts unknown problems in its category. Such predictions can be used not only to infer the active ingredients of system performance but also to infer other possible active ingredients. Due to the high variability of samples and the overlap between classes, the problem of automatic prediction is very random, and there may be multiple prediction deviations and the complexity of machine learning. Convolutional neural networks are also widely used in the field of biomedical engineering. Medical image analysis is one of the most popular research and development fields. Deep learning has been successfully used as a machine learning tool. Neural networks have the ability

to automatically learn features [7]. The rapid growth of data has enabled statistical modeling and machine learning methods to predict the information of some compounds in bioinformatics and chemoinformatics and contribute to various applications of metabolic engineering and drug discovery [8]. Convolutional neural networks have been successfully applied to network big data predictions. Using four different experimental network models and dual graphs with different sparsity and degree distributions, high prediction performance is achieved in the case of relatively dense, but the performance becomes worse in the case of extreme sparseness. Human decision-making processes usually rely on the use of visual information from different perspectives or perspectives. However, in image classification based on machine learning, we usually only infer the category of the object from a single image showing the object. Especially for challenging classification problems, the visual information conveyed by a single image may not be enough to make accurate decisions. The optimization scheme relies on the fusion of visual information captured by images depicting the same object from multiple angles [9]. Convolutional neural networks are used to extract and encode visual features from multiple views, to fuse this information to study the feature maps of different network depths for fusion convolution, to fuse potential bottlenecks before classification, and to score fusion. These strategies were systematically evaluated on three data sets from different fields. The discovery emphasizes the benefits of integrating information fusion into the network instead of performing it through the postprocessing of classification scores [10–13]. A case study that has been trained proves that the network can be easily expanded through the best fusion strategy, which is much better than other methods. The CNN model can be used to decode the hidden focus of attention related to EEG events in the object selection process. It compares the performance of CNN and the commonly used linear discriminant analysis (LDA) classifier, applies it to different dimensional data sets, and analyzes the transfer learning ability. Using CNN can conduct in-depth analysis of e-commerce data, convert the characteristics of each product into recognizable computer instructions, and use these characteristics to predict sales. The impact of individual model components can be verified by systematically changing the model, and the saliency map can be used as a tool to visualize the spatial and temporal characteristics that drive the output of the model. The effect of different attribute training sets on the sparse rate of the CNN output feature matrix is verified, and the improved Grad-CAM algorithm is used to train the key features to improve the stability and accuracy of the CNN model. Convolutional neural networks were originally discovered in biological laboratories. They were computer simulations and transformations of neural networks of humans or animals with brains. With the continuous exploration of science and technology by human beings, CNN is also undergoing continuous innovation and transformation, with more extensive applications and continuous enhancement of computing capabilities [14, 15].

2. Materials and Methods

2.1. Convolutional Neural Network (CNN). The basic composition of the existing neural network model group is composed of the following parts: the input layer (100×1) is used for the input of the original data grid conversion and the convolutional layer 1 is the basic data grid layer of the model. Data filtering and sorting play an important role, and the specific parameters are shown in Figure 1. Convolutional layer 2 (Conv2) is to perform secondary sorting and reverse confirmation on the data grid of the first layer [16–18]. The residual network and the expansion convolution are performed in the stretching layer, and the accuracy of the ConvNet architecture predicting contact is judged by the F1 connection layer. The basic flow of the experiment is shown in Figure 1.

2.2. Data Grid Conversion. Data grid conversion is to classify data in ascending dimensions to facilitate data extraction for subsequent research. Use the DNCON2 data set (V1, V2, and V3) for training and test on the CASP12 data set (V4, V5, and V6). The structural equation model is shown in Figure 2, which has strong connections and close connections. ‘S association. A, B, and C are hidden variables, and A and B correspond to neurons in the convolutional layer. Y1 and Y2 are also observed variables. Figure 3 shows a convolution process diagram with a convolution kernel size of 1×3 . This convolution process can simulate the convolution process of the first two layers, and the input related variables can be constructed as latent factors.

2.3. Precision Marketing and Convolutional Neural Network. In the W enterprise, a large amount of personal data is collected, extracted from the enterprise database, and then simulated by a convolutional neural network to simulate accurate consumer portraits. For a small number of anonymous users who cannot obtain accurate data, through simulation and prediction of previous data sets, the hidden data are extracted by looping and replying experiments. Integrate centralized data resources, establish an enterprise-level big data center, and realize “normalization” and “resourceization.” Convolutional neural networks can be used to assist companies in precision marketing models. The general process is to sort out the collected raw data and check the data, including the adjustment of the content format and the change of logic errors. In the rewriting of the basic label, the basic customer information is rewritten, and the threshold is set [19–21]. Perform label classification on the basis of basic label rewriting, based on characteristics such as crowd consumption habits. Then, use the convolutional neural network to predict the customer’s behavior to form a three-dimensional label. The last is the output of the results, providing customers with personalized services and exporting detailed information items.

3. Application of Convolutional Neural Network in Precision Marketing

3.1. CNN Model

$$\begin{aligned}\mu_1 &= v_1 w_1, v_2 w_2, v_3 w_3, \\ \mu_2 &= v_4 w_1, v_5 w_2, v_6 w_3.\end{aligned}\quad (1)$$

Euclidean distance

$$d_{ij} = \left(\sum_{k=1}^n (X_{ki} - X_{kj})^2 \right)^{1/2}. \quad (2)$$

Pearson correlation distance

$$d_{ij} = 1 - |\rho_1 A_i|. \quad (3)$$

Let D_X denote a matrix composed of elements d_{ij} :

$$p_{ij} = \sqrt{(r_i - r_j)^2 + (c_i - c_j)^2}. \quad (4)$$

Let D_Y represent the matrix composed of elements p_{ij} :

$$\bar{D}_x = \frac{D_x}{\max(D_x)}, \quad (5)$$

$$\bar{D}_y = \frac{D_y}{\max(D_y)}. \quad (6)$$

Formula (5) calculates the number of users before correction, and formula (6) calculates the number of users after correction.

The convolution operation can be expressed by the following formula:

$$Y^{[l]} = f \left(\sum_{n=1}^{n^{[l]}} W^{[l]} + b^{[l]} \right), \quad (7)$$

where y_c represents the marketing forecast profit, and the calculation method is as follows:

$$y_c = \frac{\exp(z_c)}{\sum_j \exp(z_j)}, \quad c = 1, 2, \dots, c. \quad (8)$$

3.2. LSTM Model

$$Y_{conv} = f \left(\sum_{j=0}^{J=1} \sum_{i=0}^{I=1} x_{m+i,n+j} w_{ij} + b \right). \quad (9)$$

The value range of n in formula (9) is $(0, n)$.

Among them, the interval of the activation parameter m is between positive and negative m , f is the activation function; b is the additional offset (or offset); Y_{conv} is its output.

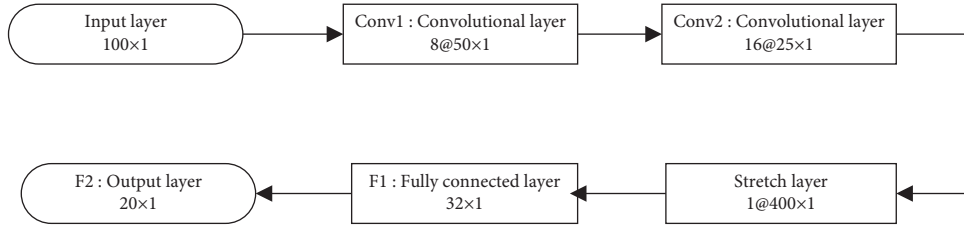


FIGURE 1: Convolutional neural network model.

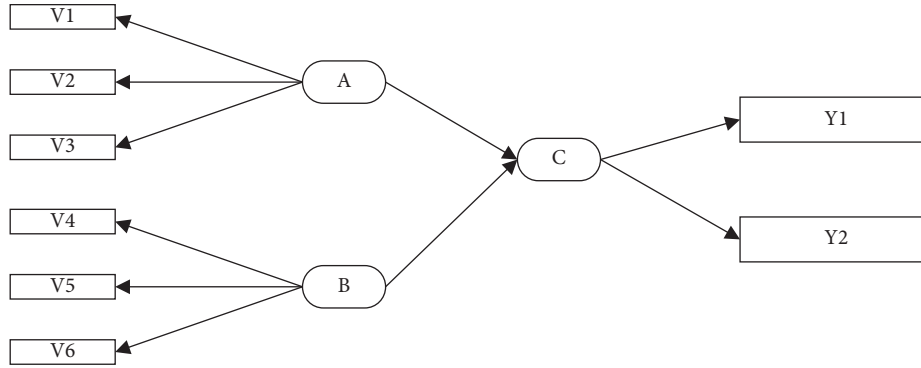


FIGURE 2: Structural equation simulation path diagram.

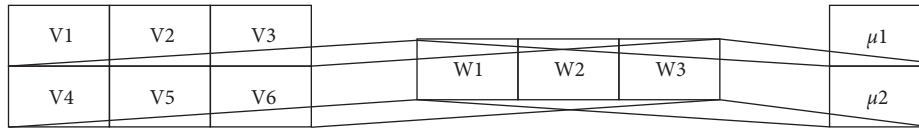


FIGURE 3: Convolution process with a 1x3 convolution kernel.

$$F_i = \frac{1}{N} = \sum_{x=1}^N f_i(x), \quad (10)$$

where $f_i(x)$ is the monthly profit income of W enterprise and N is the quarterly total profit income.

$$s_c = \sum_{i=1}^M F_i \times w_i^c. \quad (11)$$

The output of Softmax σ (S prediction result represents the gender and age of the consumer group).

$$\sigma(S_c) = \frac{e^{s_c}}{\sum_{j=1}^c e^{s_j}} \text{ for } c = 1, \dots, c, s = (S_1, \dots, S_c) \in \mathbb{R}^c. \quad (12)$$

In order to avoid overfitting, a regularized model is used to constrain

$$\text{loss} = -\frac{1}{n} \sum_{n=1}^N [y_n \log \hat{y}_n + (1 - y_n) \log(1 - \hat{y}_n)] + \lambda \|w\|^2. \quad (13)$$

Comprehensive judgment of the model

$$s_c = \sum_{i=1}^M F_i \times w_i^c = \frac{1}{N} \sum_{x=1}^N \sum_{i=1}^M w_i^c \times f_i(x), \quad (14)$$

$$M_c(x) = \sum_{i=1}^M w_i^c \times P_i(x),$$

The specific formula for the maximum sales of an enterprise is as follows:

$$f_{pool} = \text{Max}(x_{m,n}, x_{m,n+l}, x_{m+l,n+l}), \quad (15)$$

where f_{pool} is the predicted result of the largest sales.

ReLU is a consumer characteristic factor:

$$f_{(x)} = \max(0, x). \quad (16)$$

3.3. LSTM Attention Model. Correlation coefficient of two vectors:

$$\begin{aligned}
PCC(\vec{X}, \vec{Y}) &= \frac{s_{\vec{X}\vec{Y}}}{s_{\vec{X}}s_{\vec{Y}}}, \\
s_{\vec{X}\vec{Y}} &= \frac{1}{N-1} \sum_{k=1}^N (x_k - \bar{x})(y_k - \bar{y}), \\
s_{\vec{X}} &= \sqrt{\frac{1}{N-1} \sum_{k=1}^N (x_k - \bar{x})^2}, \\
s_{\vec{Y}} &= \sqrt{\frac{1}{N-1} \sum_{k=1}^N (y_k - \bar{y})^2}, \\
\bar{x} &= \frac{1}{N} \sum_{k=1}^N x_k, \\
\bar{y} &= \frac{1}{N} \sum_{k=1}^N y_k.
\end{aligned} \tag{17}$$

Here, x_k and y_k are the k th element of the vector. Finally, the precise demand profile of consumers is simulated [22].

3.4. *CNN + LSTM Attention Model.* Euclidean distance for two features

$$ED(\vec{X}, \vec{Y}) = \sqrt{\sum_{k=1}^N (x_k - y_k)^2}. \tag{18}$$

The maximum distance is recorded as

$$\max MD_i = ED_i (1 \leq i \leq M). \tag{19}$$

The F-score of consumer demand characteristics is defined as

$$F\text{-score}(j) = \frac{(\bar{x}_j^{(+)} - \bar{x}_j)^2 + (\bar{x}_j^{(-)} - \bar{x}_j)^2}{1/m^+ - 1 \sum_{k=1}^{m^+} (\bar{x}_{k,j}^{(+)} - \bar{x}_j^{(+)})^2 + 1/m^- - 1 \sum_{k=1}^{m^-} (\bar{x}_{k,j}^{(-)} - \bar{x}_j^{(-)})^2}. \tag{20}$$

\bar{x}_j , $\bar{x}_j^{(+)}$, and $\bar{x}_j^{(-)}$, respectively, represent the average value of all, positive, and negative predictions and actual eigenvalues. m^+ and m^- are the error interval between forecast and actual. The larger the value, the more obvious the consumer's demand characteristics, and q_i is the frequency of appearance.

$$q_i = \frac{m_i}{M}. \tag{21}$$

M is the total number of consumer features in all training data sets [23]. The probability in the male population and the female population can be defined as

$$p(n_{1,j}) = \sum_{m=n_{1,j}}^{N_j} \frac{N_j!}{m!(N_j - m)} q_i^m (1 - q_i)^{N_j - m}, \tag{22}$$

$$p(n_{-1,j}) = \sum_{m=n_{-1,j}}^{N_j} \frac{N_j!}{m!(N_j - m)} q_i^m (1 - q_i)^{N_j - m}.$$

where $n_{1,j}$ and $n_{-1,j}$ is the number of users.

Finally, according to the following formula, the company's turnover through precision marketing is predicted:

$$P_j = \min(p(n_{1,j}), p(n_{-1,j})). \tag{23}$$

4. Simulation Experiment

4.1. *Training and Testing of the Model.* As shown in Table 1, the training and testing of the CNN model, LSTM model, LSTM attention model, and CNN + LSTM attention model are compared in detail. The data source is the commercial marketing data of W company. After filtering the data, we input it to our model. Choose from July to July, July to August, July to September, July to October, July to November, August to August, August to September, August to October, August to November, and September to September. Data from different months are used; data from September to October are used for testing, and data from September to November are used for training. Based on the results of several models, the CNN + LSTM attention model and the LSTM attention model perform better, and the accuracy of testing and training is higher.

Figure 4 visualizes the training and testing comparison of the CNN model. The training and testing comparison of the LSTM Train model is shown in Figure 5. Figure 6 is the training and testing comparison of the LSTM attention model after LSTM optimization. The comparison of training and testing of the CNN+ LSTM attention model is shown in Figure 7. The comprehensive icon result CNN + LSTM attention model is the optimal model [24–27].

TABLE 1: Comparison of training and testing of different models.

Month	CNN		LSTM		LSTM attention		CNN + LSTM attention	
	Train	Test	Train	Test	Train	Test	Train	Test
7-7	0.75	0.74	0.69	0.68	0.71	0.73	0.72	0.72
7-8	0.61	0.62	0.53	0.52	0.58	0.56	0.59	0.57
7-9	0.62	0.63	0.61	0.6	0.69	0.68	0.69	0.69
7-10	0.65	0.64	0.6	0.59	0.69	0.68	0.67	0.69
7-11	0.61	0.62	0.65	0.64	0.66	0.65	0.66	0.65
8-8	0.75	0.76	0.77	0.76	0.78	0.77	0.77	0.79
8-9	0.81	0.8	0.79	0.78	0.8	0.81	0.84	0.8
8-10	0.76	0.77	0.75	0.74	0.76	0.78	0.77	0.77
8-11	0.75	0.74	0.72	0.71	0.73	0.74	0.73	0.74
9-9	0.85	0.84	0.8	0.79	0.81	0.81	0.83	0.79
9-10	0.74	0.73	0.75	0.74	0.76	0.74	0.75	0.76
9-11	0.65	0.69	0.68	0.67	0.69	0.7	0.68	0.7

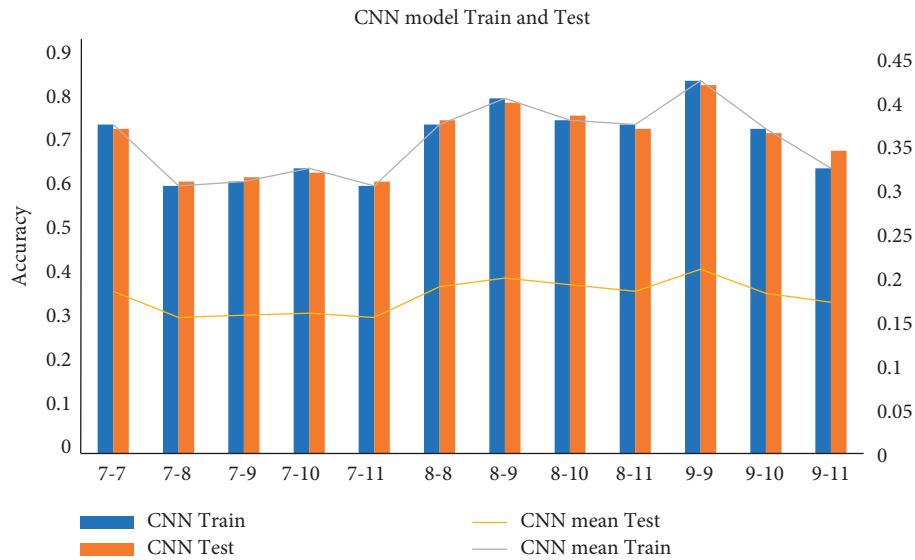


FIGURE 4: Comparison of training and testing of CNN model.

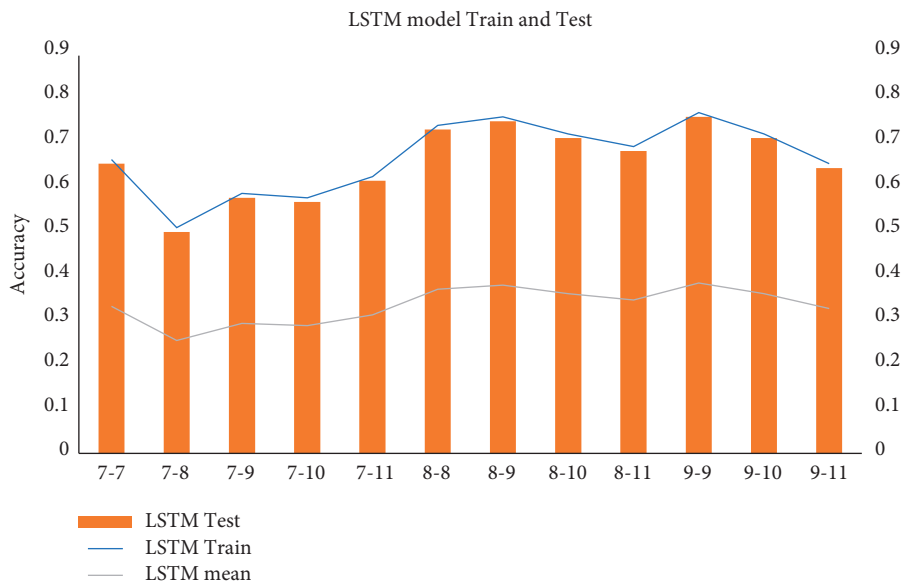


FIGURE 5: Comparison of training and testing of LSTM train model.

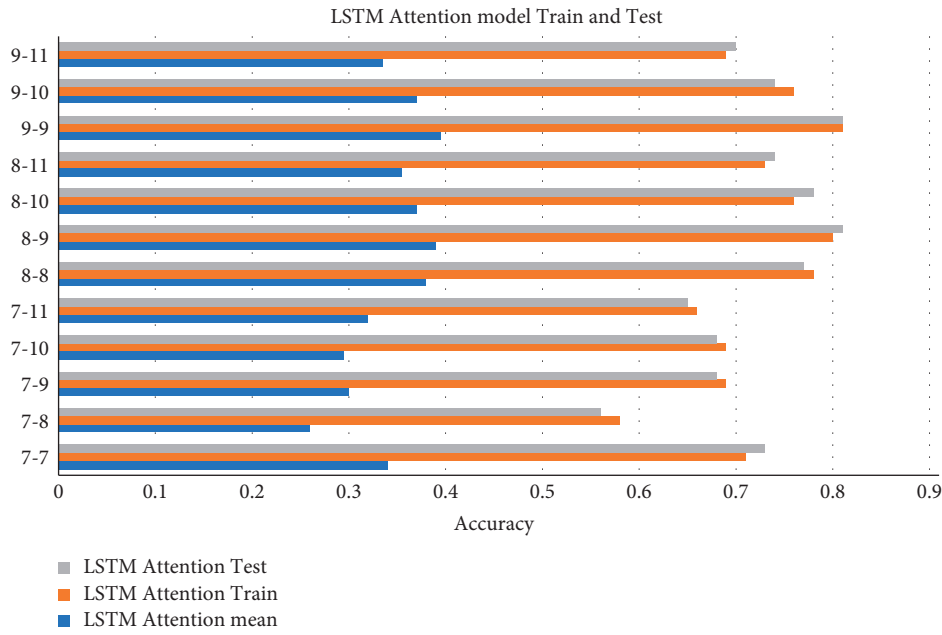


FIGURE 6: Comparison of training and testing of LSTM attention model.

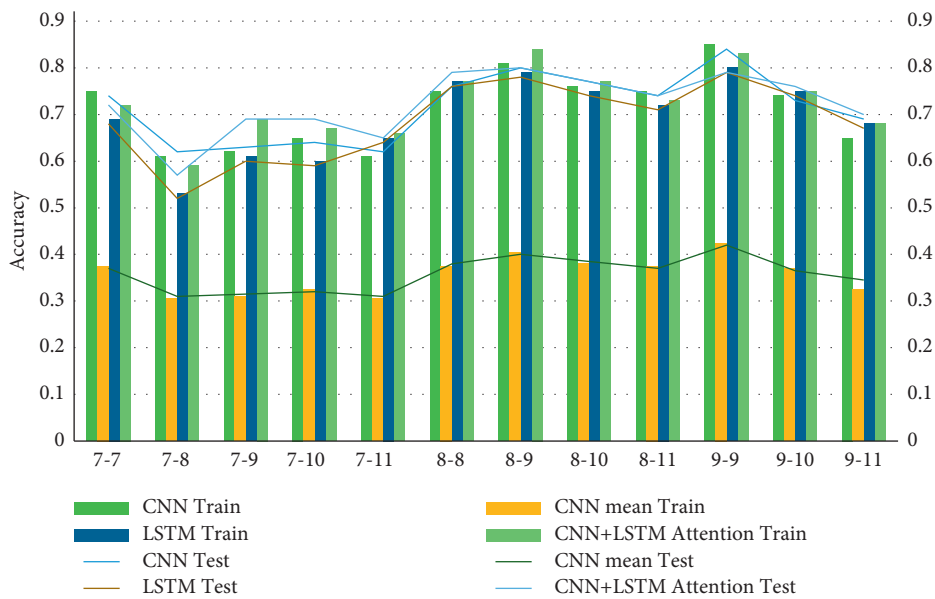


FIGURE 7: Comparison of training and testing of CNN + LSTM attention model.

4.2. Use Models to Fit Marketing Data. Using the marketing data of W company in previous years, bring in CNN model, LSTM model, LSTM attention model, and CNN + LSTM attention model, and evaluate the model using Sn(%), Sp(%), Acc(%), and MCC indicators. As shown in Table 2 and Figure 8, looking at the four indicators of Sn (%), Sp (%), Acc (%), and MCC, the Sn (%) of the CNN + LSTM attention model = 70.71, Sp (%) = 86.25, Acc(%) = 81.07, and MCC = 0.752 is the best fitting model.

As shown in Table 3, using CNN + LSTM attention to filter user tags, it is predicted that those users have greater buying potential.

As shown in Table 4, the users are classified by gender and gender, and it is found that men in the W company are the main purchasing power, and in the age stratification, it is found that the population of 41–50 accounts for the highest proportion. It can be seen from this that when performing precision marketing, the gender and age of the population must be precisely controlled.

4.3. Prediction of Precision Marketing and General Marketing. As shown in Table 5 and Figure 9, in the marketing input forecast for the next year, it is found that the use of precision

TABLE 2: Fitting of the model to marketing data.

Method	CNN	LSTM	LSTM attention	CNN + LSTM attention
Sn(%)	69.64	63.57	46.07	70.71
Sp(%)	90	94.46	93.92	86.25
Acc(%)	83.21	84.16	77.97	81.07
MCC	0.756	0.708	0.384	0.752

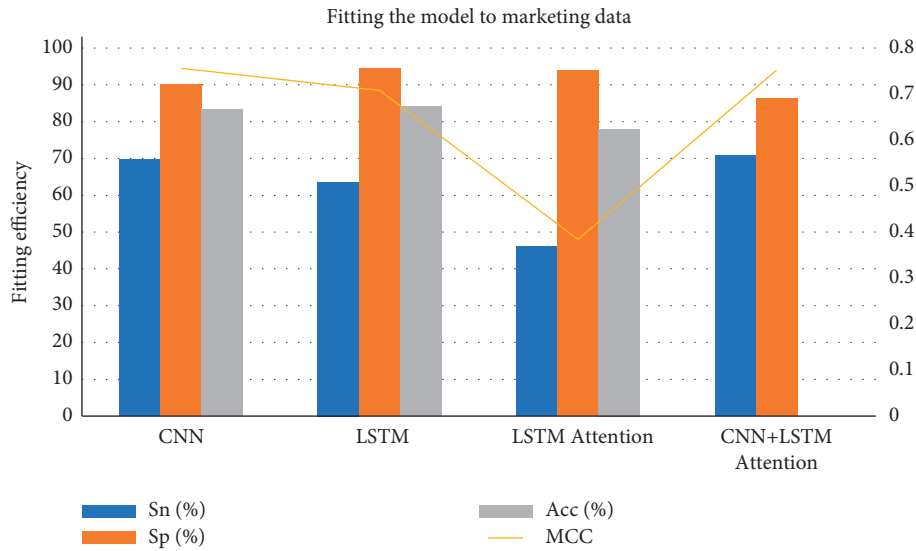


FIGURE 8: Fitting of the model to marketing data.

TABLE 3: Using CNN + LSTM attention to predict the number of users.

Serial number	Original log size (G)	Number of original tags	Number of filtered tags	User number
1	19.82	2319905	487180	154727
2	40.35	4450395	934583	297493
3	59.64	6879890	1444777	458726
4	78.92	8812650	1938783	587510
5	101.52	11300270	2486059	747618
6	120.08	13298965	3058762	887931
7	141.28	15470470	3094094	1031298

TABLE 4: Using CNN + LSTM attention to predict the number of users (male and female stratification and age stratification).

	Attribute value	User number	Percentage of generated data (%)	Proportion of original data (%)
Gender	Man	59190070	59.19	59.19
	Woman	32272265	32.27	32.47
	Others	8537665	8.54	8.54
Age	0-24	17879563	17.88	17.88
	25-30	15928089	15.93	15.93
	31-35	10995266	11.00	11.00
	36-40	9691802	9.69	9.69
	41-50	19059443	19.06	19.06
	>50	17924356	17.92	17.92
	Others	8521481	8.52	8.52

marketing will increase the profit of W enterprise. The average annual data shows that the monthly income of precision marketing is 0.735, while that of ordinary marketing is only 0.567.

4.4. *Practical Effects of the Model.* After downloading the data of W company from July 1 to November 30, 2020, the original data of W company’s marketing income through different methods is classified, and the comparative

TABLE 5: Prediction of precision marketing and general marketing.

Month	Precision marketing	General marketing
1	0.73	0.5
2	0.75	0.51
3	0.68	0.51
4	0.65	0.49
5	0.77	0.68
6	0.81	0.66
7	0.78	0.62
8	0.74	0.59
9	0.81	0.71
10	0.74	0.58
11	0.72	0.56
12	0.64	0.4

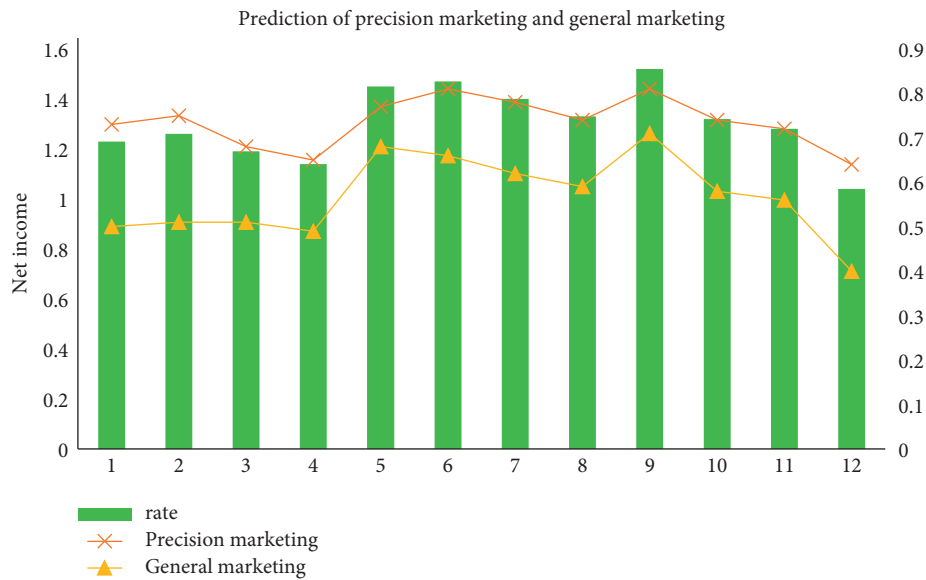


FIGURE 9: Prediction of precision marketing and general marketing.

TABLE 6: Practical effects of the model.

Months	Precision %	Recall %	F1-score %
7	73.1	77.6	75.2
8	61	72.3	66.2
9	55.9	91.6	69.4
10	78.3	84.1	81.1
11	64.9	85.7	73.8
Mean	66.6	82.3	73.1

analysis and supplementary analysis are applied to the optimization model. As shown in Table 6 and Figure 10, the results of comparative analysis and supplementary analysis are displayed. Precision, recall, and F1 scores are used to evaluate the comparative analysis and supplementary analysis, and the comparative analysis and supplementary analysis are simulated. The average accuracy rate of additive analysis is as high as 66.6%, the average

recall rate of comparative analysis and complementary analysis is 82.3%, and the F1 score of comparative analysis and complementary analysis is 73.1%. This model has met expectations for precision marketing forecasts. Using precision, recall, and F1 scores to predict the W company, it is found that the CNN + LSTM attention model can increase monthly revenue by 50% in peak seasons and about 20% in off-season.

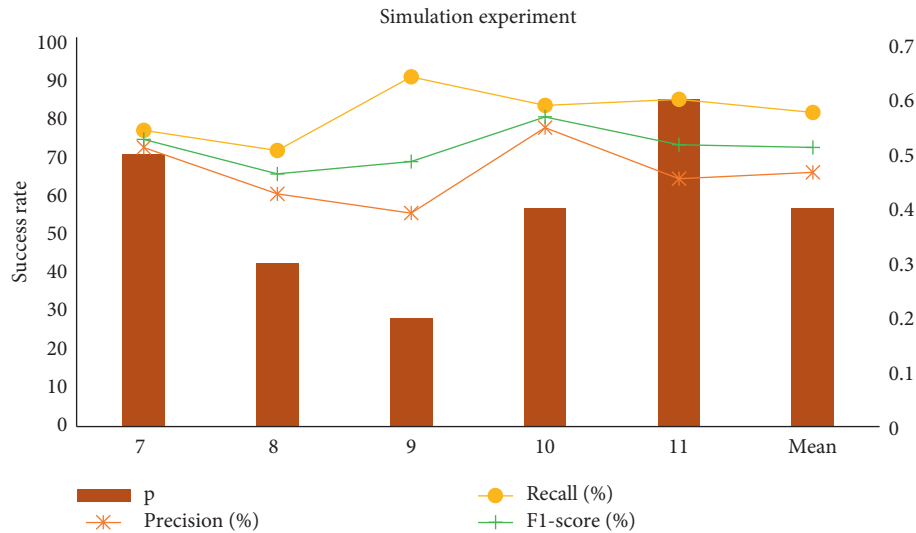


FIGURE 10: The practical effect of the model.

5. Conclusion

This research is based on curling neural networks, precision marketing, model optimization and construction, comparative analysis, and supplementary analysis and proposes precision marketing in response to the problems of existing marketing methods. Optimize the existing curl neural network model and apply it to e-commerce precision marketing. Through the collection and analysis of W enterprise data, the training and testing of CNN model, LSTM model, LSTM attention model, and CNN + LSTM attention model are compared, and the performance of CNN + LSTM attention model and LSTM attention model is obtained. Better, the accuracy of testing and training is higher. By fitting the model, it is found that $Sn(\%) = 70.71$, $Sp(\%) = 86.25$, $Acc(\%) = 81.07$, and $MCC = 0.752$ of the CNN + LSTM attention model are the best fitting models. The men and women stratification and gender stratification of users are predicted, and it is found that men in the W company are the main purchasing power, and in the age stratification, it is found that the population of 41–50 accounts for the highest proportion. Using the CNN + LSTM attention model to predict the marketing input for the next year, it is found that the use of precision marketing will increase the profit of W company. Using the CNN + LSTM attention model to predict the marketing input for the next year, it is found that the use of precision marketing will increase the profits of W companies. The average annual data show that precision marketing will increase monthly revenue by 42.5%. The simulation shows that the average accuracy rate of comparative analysis and supplementary analysis is as high as 66.6%, the average recall rate of comparative analysis and supplementary analysis is 82.3%, and the F1 score of comparative analysis and supplementary analysis is 73.1%. The model predicts precision marketing as expected.

Data Availability

The experimental data used to support the findings of this study are available from the corresponding author upon request.

Conflicts of Interest

The author declares no conflicts of interest regarding this work.

Acknowledgments

This work was sponsored in part by the National Social Science Foundation(20BGL176).

References

- [1] X. I. Xian-Ming and L. Wang, "The era of E-commerce marketing development," *Journal of Harbin University of Commerce(Social Science Edition)*, vol. 93, no. 5, pp. 58–67, 2006.
- [2] M. Sawhney, "Precision marketing: the new rules for attracting, retaining, and leveraging profitable customers," *Akuntansi Pegawai*, vol. 93, no. 3, pp. 158–165, 2004.
- [3] Z. Y. Liu, "Study on precision marketing method," *Journal of Shanghai Jiaotong University*, vol. 56, no. 65, pp. 32–45, 2007.
- [4] Z. Zhuo, S. Chen, and K. Y. Chau, "A new model of manufacturer's optimal product supply strategy in the context of precision marketing: based on real demand pattern," *Mathematical Problems in Engineering*, vol. 59, no. 02, pp. 62–98, 2020.
- [5] Z. Tian, "Research and analysis of automobile precision marketing based on big data:taking the construction of Audi car user portrait as an example," *Journal of Fujian University of Technology*, vol. 17, no. 4, pp. 391–397, 2019.
- [6] T. Cai and Z. Zhao, "Convolutional neural network-based surgical instrument detection," *Technology and Health Care*, vol. 28, no. S1, pp. 81–88, 2020.
- [7] S. Harada, H. Akita, M. Tsubaki et al., "Dual graph convolutional neural network for predicting chemical networks," *BMC Bioinformatics*, vol. 21, no. Suppl 3, p. 94., 2020 Apr 23.
- [8] K. Zhao and C. Wang, "Sales forecast in E-commerce using convolutional," *Neural Network[J]*, vol. 156, no. 51, pp. 21–46, 2017.
- [9] J. Hochuli, A. Helbling, T. Skaist, M. Ragoza, and D. R. Koes, "Visualizing convolutional neural network protein-ligand

- scoring,” *Journal of Molecular Graphics and Modelling*, vol. 84, pp. 96–108, 2018 Sep.
- [10] S. M. Anwar, M. Majid, A. Qayyum, M. Awais, M. Alnowami, and M. K. Khan, “Medical image analysis using convolutional neural networks: a review,” *Journal of Medical Systems*, vol. 42, no. 11, p. 226, 2018 Oct 8.
- [11] Z. Cao, S. Mu, and M. Dong, “Two-attribute e-commerce image classification based on a convolutional neural network,” *The Visual Computer*, vol. 94, no. 55, pp. 158–172, 2020.
- [12] H. Pan and H. Zhou, “Study on convolutional neural network and its application in data mining and sales forecasting for E-commerce,” *Electronic Commerce Research*, vol. 12, no. 154, pp. 123–142, 2020.
- [13] A. Jx and B. Lw, “Collaborative innovation of E-Commerce enterprises based on FPGA and convolutional neural network - ScienceDirect,” *Microprocessors and Microsystems*, vol. 12, no. 154, pp. 13–35, 2020.
- [14] A. Sun, X. Zhao, and C. Hu, “A novel convolutional neural network approach to improve the multi-product image based classification IN e-commerce,” *Journal of Shanxi Normal University (Philosophy and Social Sciences edition)*, vol. 12, no. 4, pp. 36–59, 2018.
- [15] A. Schindler, T. Lidy, and S. Karner, “Fashion and apparel classification using convolutional neural networks,” *Computer Vision and Pattern Recognition*, vol. 5, no. 5, pp. 3–34, 2018.
- [16] A. Krizhevsky, “One weird trick for parallelizing convolutional neural networks,” *Eprint Arxiv*, vol. 12, no. 14, pp. 62–98, 2014.
- [17] G. Suman, A. Panda, P. Korfiatis, and A. H. Goenka, “Convolutional neural network for the detection of pancreatic cancer on CT scans,” *The Lancet Digital Health*, vol. 2, no. 9, p. e453, 2020 Sep.
- [18] W. Yin, H. Schütze, and B. Xiang, “ABCNN: attention-based convolutional neural network for modeling sentence pairs,” *Computer Science*, vol. 12, no. 5, pp. 98–122, 2015.
- [19] V. Lebedev, Y. Ganin, and M. Rakhuba, “Speeding-up convolutional neural networks using fine-tuned CP-decomposition,” *Computer Science*, vol. 11, no. 14, pp. 123–142, 2014.
- [20] A. Dosovitskiy, P. Fischer, and J. T. Springenberg, “Discriminative unsupervised feature learning with exemplar convolutional neural networks,” *IEEE Transactions on Pattern Analysis and Machine Intelligence*, vol. 38, no. 9, pp. 1734–1747, 2014.
- [21] C. Santos, X. Bing, and B. Zhou, “Classifying relations by ranking with convolutional neural networks,” *Computer Science*, vol. 86, no. 86, pp. 132–137, 2015.
- [22] P. Molchanov, S. Tyree, T. Karras, T. Aila, and J. Kautz, “Pruning convolutional neural networks for resource efficient transfer learning,” *Machine Learning*, vol. 5, no. 4, pp. 048–067, 2017.
- [23] G. Chen and S. Li, “Research on location fusion of spatial geological disaster based on fuzzy SVM,” *Computer Communications*, vol. 153, pp. 538–544, 2020.
- [24] G. Sun, C.-C. Chen, and S. Bin, “Study of cascading failure in multisubnet composite complex networks,” *Symmetry*, vol. 13, no. 3, p. 523, 2021.
- [25] K. Kang, H. Li, and J. Yan, “T-CNN: tubelets with convolutional neural networks for object detection from videos,” *IEEE Transactions on Circuits and Systems for Video Technology*, vol. 28, no. 10, pp. 2896–2907, 2018.
- [26] S. Li and A. B. Chan, “3D human pose estimation from monocular images with deep convolutional neural network,” *Asian Conference on Computer Vision*, vol. 12, no. 15, pp. 56–72, 2014.
- [27] P. Lakhani and B. Sundaram, “Deep learning at chest radiography: automated classification of pulmonary tuberculosis by using convolutional neural networks,” *Radiology*, vol. 3, no. 5, pp. 23–51, 2017.

Research Article

Agricultural Product Sales Prediction of ICM Neural Network Improvement by Sparse Autoencoder

YingHui Li 

Henan Finance University, Zhengzhou 450046, China

Correspondence should be addressed to YingHui Li; liyingshui@hafu.edu.cn

Received 5 December 2021; Revised 30 December 2021; Accepted 21 January 2022; Published 4 March 2022

Academic Editor: Hangjun Che

Copyright © 2022 YingHui Li. This is an open access article distributed under the Creative Commons Attribution License, which permits unrestricted use, distribution, and reproduction in any medium, provided the original work is properly cited.

With the rapid development of agricultural product sales data, the traditional prediction model cannot meet the processing needs. Based on deep learning theory, an improved ICM agricultural product sales prediction model using the softmax classifier is proposed. Introducing the sparse autoencoder in ICM can reduce feature loss. The features also can be extracted. In addition, using the pretreatment mode based on fuzzy membership theory, we can obtain the fuzzy correspondence of considerations and grades of agricultural product sales. At the same time, the precision of prediction for the model is further optimized. It can be seen that the agricultural product sales prediction model based on improved ICM can realize the real-time prediction of agricultural product sales. The maximum classification accuracy of the model can reach 80.98%, which means that it has certain practical application value.

1. Related Work

Agricultural products are necessities of daily life. With the increase of sales platform, the agricultural product sales model is more diversified, and the online sales model has gradually become the mainstream sales model of agricultural products. However, because of the particularity of its products, the agricultural products have a strict shelf life. Therefore, to reduce the waste of agricultural product resources during the shelf life of agricultural products, the accurate sales of the online agricultural products sales platform need to be achieved, which is an urgent problem for the online sales of agricultural products. The current online precision sales of agricultural products are mainly through the shallow-layer deep learning network model. Also, it extracts the value information from the massive agricultural product sales data to predict the trend of sales changes, so as to help merchants adjust the sales strategy in real time. For example, Grasman and Kornelis [1] and de Souza et al. [2] used the Bass model and agricultural product sales data to estimate the future agricultural product sales, so as to achieve the inventory management. Meanwhile, the confidence interval is used to process and obtain the required

exact expression. Xiang and Cho et al. analyzed the essential characteristics of the self-service. Also, the importance and significance of building a self-service network marketing system are expounded. Therefore, a new sales model is proposed, which combines independent marketing and online customization. Her-e, merchants, businesses, and consumers collaborate to complete production and sales, so as to realize the precise services for consumers [3, 4]. Tsoumakas and Chen et al. realized accurate short-term sales prediction by reviewing video sales and applying machine learning. It enables the company to minimize in-store inventory and expired products. At the same time, it helps to avoid missing sales [5, 6]. Chen et al. and Eric et al. implemented online sales prediction of agricultural products by using multitask recursive neural network based on trend alignment [7, 8]. However, the prediction performance of the shallow-layer model is limited, so the real-time analysis processing of agricultural product trading data cannot be realized. At the same time, considering that agricultural sales data are growing exponentially every day, the semi-supervised learning model is the main means of predicting such rapid growth data. So, this paper selects the semi-supervised deep learning model as the sales prediction

model of agricultural products. Also, it puts forward a super-imperial crown model based on the ICM to predict the agricultural product sales.

2. Basic Methods

2.1. Introduction to ICM Model. The ICM model is an autoencoder network model, which contains two hidden layers. In addition, its structure of the input node is same with the feature vector structure used for prediction. Because the self-coding network model only learns the predicted feature vectors but does not classify them, this feature enables the classification prediction function of the model by adding a classifier on the top layer. Typically, the ICM classifier can be selected to achieve the classification effect and can get the softmax classifier and the corresponding probability values.

If the input sample set is L , the hypothesis function method is used to analyze each type of j belonging to different classification probability value $p = (y=j|x)$, and the hypothesis function can be expressed as [9]

$$h_{\theta}(x^{(i)}) = \begin{bmatrix} p(y^{(i)} = 1|x^{(i)}; \theta) \\ p(y^{(i)} = 2|x^{(i)}; \theta) \\ p(y^{(i)} = 3|x^{(i)}; \theta) \\ p(y^{(i)} = 4|x^{(i)}; \theta) \end{bmatrix}, \quad (1)$$

$$= \frac{1}{\sum_{j=1}^4 e^{\theta_j^T x^{(i)}}} \begin{bmatrix} e^{\theta_1^T x^{(i)}} \\ e^{\theta_2^T x^{(i)}} \\ \vdots \\ e^{\theta_k^T x^{(i)}} \end{bmatrix},$$

where $\theta_1, \theta_2, \dots, \theta_k$ represent the model parameters to be obtained. The cost function is defined as [10]

$$J(\theta) = -\frac{1}{m} \left[\sum_{i=1}^m \sum_{j=1}^k \{y^i = j\} \log \frac{e^{\theta_j^T x^{(i)}}}{\sum_{l=1}^k e^{\theta_l^T x^{(i)}}} \right]. \quad (2)$$

Add the self-coding network classified by softmax, and the structure of the ICM model is shown in Figure 1.

The steps for training the ICM model are as follows.

Firstly, the training samples are input into the model. Also, the two hidden layers are adopted to conduct unsupervised training on the training samples. So, the unlabeled output results are obtained. Secondly, the unlabeled output results are input into softmax classifier. At the same time, the labeled samples are used to train the softmax classifier. Thirdly, the values of some functions are solved, such as hidden layer kernel function, reconstruction error function, softmax classifier cost function, and the partial derivatives of all parameters. Finally, the parameters obtained in the above steps are utilized to initialize the model parameters.

Furthermore, the BP algorithm is used to solve the optimum parameters, so as to carry out the supervised training.

2.2. Improved ICM Model. It can be seen from the above analysis that it is easy for the ICM model to ignore the reconstruction of original non-linear data during prediction, which will affect the prediction results. In order to solve this problem, the sparse autoencoder is introduced into ICM and an improved ICM model is proposed.

Sparse autoencoder is an unsupervised learning method. Linear representation of vectors can be achieved by using a set of basis vectors \varnothing_i in the input vector [11]:

$$X = \sum_{i=1}^k a_i \varnothing_i \quad (i = 1, 2, \dots, k). \quad (3)$$

As can be seen from formula (3), k stands for the number of the input nodes and a_i stands for the linear correlation coefficient.

The average activation value of hidden layer unit j is [12]

$$\hat{\rho}_j = \frac{1}{m} \sum_{i=1}^m a \left[\sum_j^{(2)} (x^i) \right]. \quad (4)$$

Here, $i = 1, 2, \dots, m$, $m = k$; $a_j^{(2)}(x^i)$ represent the hidden layer unit activation amount when the input is X .

Set the sparseness parameter to ρ , make $\hat{\rho}_j = \rho$, and use KL to optimize the penalty factor, such as formula (5). So, the neuron activity of hidden layer is controlled near ρ .

$$KL(\rho \|\hat{\rho}) = \rho \log \frac{\rho}{1-\hat{\rho}} + (1-\rho) \log \frac{1-\rho}{1-\hat{\rho}_j}. \quad (5)$$

Therefore, the global cost function of sparse autocoding networks is [13]

$$J_{\text{sparse}}(w, b) = J(w, b) + \mu \sum_{j=1}^{s_2} KL(\rho \|\hat{\rho}_j), \quad (6)$$

where μ represents the punishment coefficient, and the larger its value is, the greater the punishment intensity is. Here $J(w, b)$ represents the global loss function. It can be calculated by formula (7). λ is responsible for avoiding overfitting [14].

$$J(w, b) = \left[\frac{1}{m} \sum_{i=1}^m J(W, b; x^i, y^i) \right] + \frac{\lambda}{2} \sum_{l=1}^{n_l-1} \sum_{l=1}^{s_l} \sum_{j=1}^{s_{l+1}} (W_{ji}^l)^2. \quad (7)$$

$J(W, b; x^i, y^i)$ represents the unit function:

$$J(W, b; x^i, y^i) = \frac{1}{2} \|h - y\|^2. \quad (8)$$

The output error can be obtained from formula (8).

$$\begin{aligned} \delta_i^{(3)} &= \frac{\partial}{\partial r_i^{(3)}} \frac{1}{2} \|h - y\|^2 \\ &= -(y_i - \alpha_i^{(3)}) f'(r_i^{(3)}). \end{aligned} \quad (9)$$

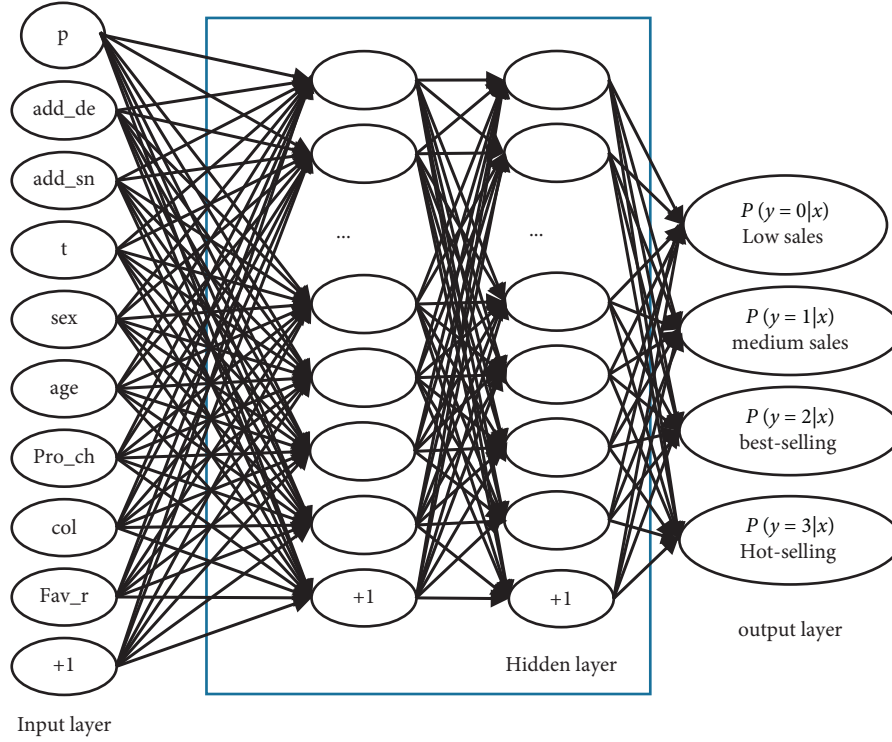


FIGURE 1: Structure of the ICM model.

It can be seen from formula (8) that $\delta_i^{(3)}$ represents the error of output layer; $a_i^{(3)}$ represents the active function.

$$r_i^{(3)} = W_i^{(2)} a_i^{(3)} + b^{(2)}. \quad (10)$$

Thus, the hidden layer element error can be obtained as

$$\delta_i^{(2)} = \left(\left(\sum_{j=1}^{s_2} W_{ji}^{(2)} \delta_j^{(3)} \right) + \mu \left(\frac{-\rho}{\hat{\rho}_J} + \frac{1-\rho}{1-\hat{\rho}_J} \right) \right) f'(r_i^{(2)}). \quad (11)$$

The SICM model introducing sparse autoencoder is implemented as follows:

Step 1. Randomly classify all data into training dataset and testing dataset in a ratio of 4:1

Step 2. Label the testing dataset and randomly select some data to train the SICM model. Furthermore, the remaining data are used to verify the improved ICM model.

Step 3. Use the repeated experiment method to determine the hidden layers and the nodes of each layer in the sparse self-coding network.

Step 4. Select the training dataset as the input vector of sparse autocoding network for unsupervised pre-training and input the labeled and unlabeled data into softmax classifier for training.

Step 5. Adopt BP algorithm to tune network parameters. The global optimal parameters can be obtained. As can be seen from formula (12), when $\lambda \neq 0$, the weight decay function is activated, so as to update the weight [15].

$$\Delta W_{ij} = \frac{\eta \partial J}{\partial \Delta W_{ij}}. \quad (12)$$

The formula shows that $\eta = 0.05$ which represents the learning rate [16].

The weight updating formula can be expressed as

$$\begin{aligned} \Delta W^{(l)} &= \Delta W^{(l)} + \nabla_{W^{(l)}} J(W, b; x, y), \\ \Delta b^{(l)} &= \Delta b^{(l)} + \nabla_{b^{(l)}} J(W, b; x, y). \end{aligned} \quad (13)$$

Here, $\Delta W^{(l)} = \Delta b^{(l)} = 0$ represents the initial value, and the weight can be obtained according to formulas (14) and (15) [17].

$$W^{(l)} = W^{(l)} - \alpha \left[\left(\frac{1}{m} \Delta W^{(l)} \right) + \lambda W^{(l)} \right], \quad (14)$$

$$b^{(l)} = b^{(l)} - \alpha \left(\frac{1}{m} \Delta b^{(l)} \right). \quad (15)$$

The above process can be represented in Figure 2.

3. Sales Prediction of Agricultural Products Based on Improved ICM

3.1. Building Improved ICM Model

3.1.1. Parameter Selection. The improved ICM model parameter is selected by the characteristic variables of the sales influencing factors of agricultural product. According to literature [18], the characteristic variables affecting the sales of

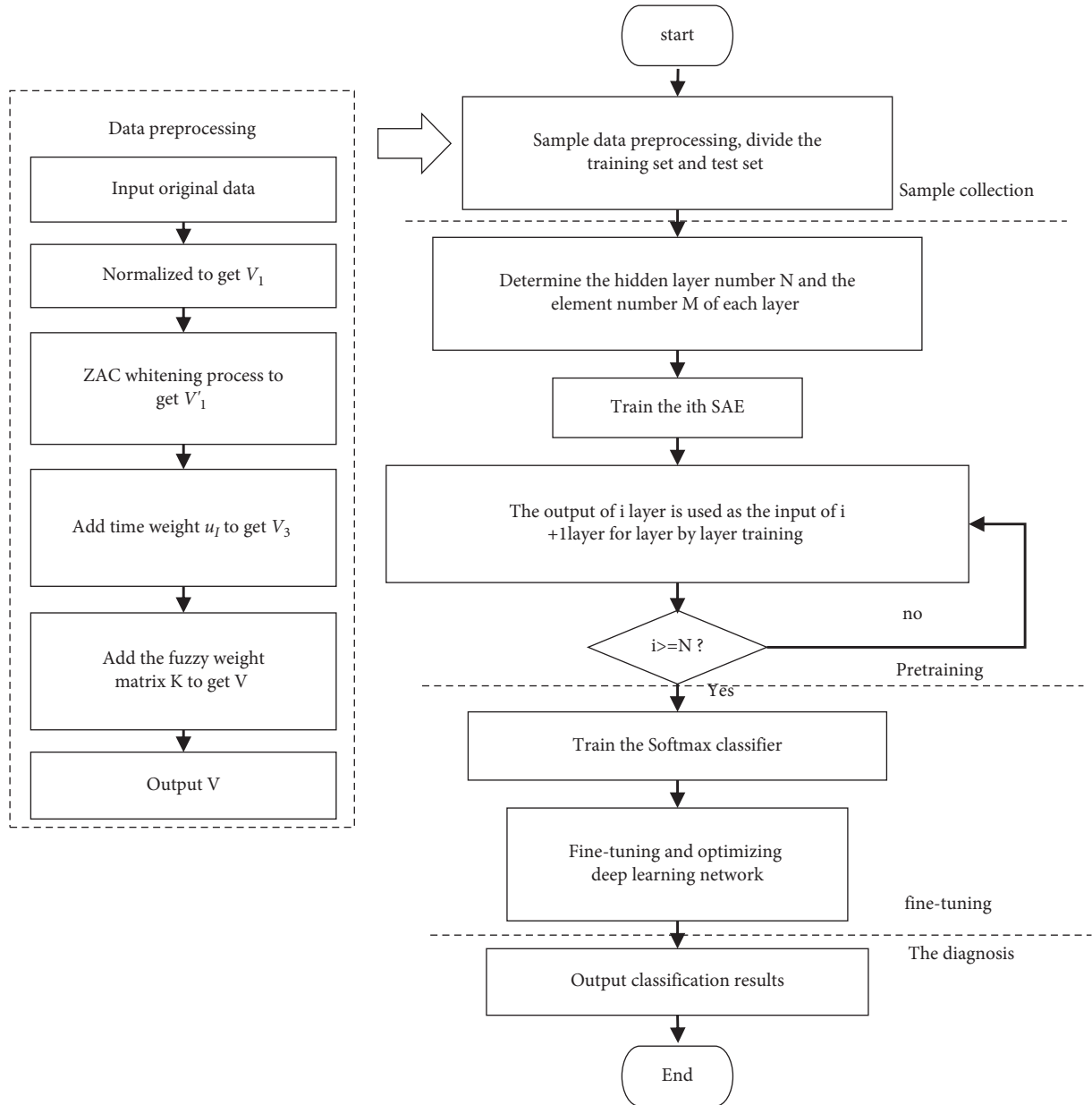


FIGURE 2: Improved ICM model implementation process.

agricultural products mainly include the attribute parameters of agricultural products, the personal factors of buyers, and nine-dimensional characteristic vector formed by promotion channels. Therefore, the parameters of the improved ICM model in this study use $V = [p, \text{add_de}, \text{add_sh}, t, \text{sex}, \text{age}, \text{pro_ch}, \text{col}, \text{fav_r}]$ to represent the 9-dimensional input vector, which is used for feature learning. Also, the preprocessed vector is expressed as $V = [pI, \text{add_de}, \text{add_sh}, tI, \text{sex}, \text{ageI}, \text{pro_chI}, \text{col}, \text{fav_rI}]$.

3.1.2. Classifier Design. The improved ICM model classifier uses the softmax classifier of the ICM model. As the cost function of the softmax classifier of ICM is a non-strict convex function, it is easy to fall into local optimum [19]. Therefore, this paper adds a weight attenuation term to the

cost function and penalizes the parameters whose weights are too large, so that the parameters can easily converge to the global optimal. The cost function added weighted attenuation term can be expressed as [20]

$$J(\theta) = -\frac{1}{m} \left[\sum_{i=1}^m \sum_{j=1}^k \{y^i = j\} \log \frac{e^{\theta_j^i x(i)}}{\sum_{k=1}^k e^{\theta_k^i x(i)}} \right] + \frac{\lambda}{2} \sum_{i=1}^k \sum_{j=1}^{n-1} \theta_{ij}^2. \quad (16)$$

The optimal parameter value can be obtained by minimizing $J(\theta)$, and the classifier can be used for the improved ICM model of agricultural product sales prediction.

3.1.3. Model Structure. There are two parts for the improved ICM model used for agricultural product sales prediction, namely, data preprocessing and deep learning network. The

specific structure is shown in Figure 3. The input vector of the model refers to the preprocessed data X , and the input cell number of SAE is $N + 1$, where N represents variable and 1 represents offsets. By processing the input vector through the hidden layer, the feature vector for classification can be obtained. Consider that SAE only digs deep features of sample feature vectors to obtain weight parameters of the hidden layer. The softmax classifier is needed to classify the processed data of hidden layers, so as to obtain all deep features [21]. In addition, the softmax classifier is added to the top layer of the model to obtain a complete improved ICM model. The output vector Y is the prediction result of agricultural product sales by the model.

3.2. Agricultural Product Sales Prediction Process Based on Improved ICM. The improved ICM model is applied to the sales forecasting of agricultural products. First of all, the sales data of agricultural products are preprocessed. Also, the sparse autocoding network is adopted to select representation samples with common features from the sales data of unlabeled agricultural products, so as to realize the adaptive feature extraction. After that use the labeled and unlabeled data training classifier to classify the agricultural product sales level. Furthermore, the parameters of each layer are tuned according to the backpropagation algorithm and strictly convex function to obtain the global optimal parameter values. Thus, we can get an accurate classification prediction improved ICM model which can realize the sales prediction of agricultural products. Finally, the data are input into the prediction model, and the output data are the prediction result. The specific process of agricultural product sales prediction based on Improved ICM is shown in Figure 4.

4. Simulation Experiment

4.1. Simulation Environment and Data Source

4.1.1. Experimental Environment Construction and Data Collection. This experiment is simulated on 64 bit Windows 7 system and coded on i386 platform. Crawler technology is used to obtain 5000 sets of data from Taobao egg agricultural products trading data; each set of data includes 20 samples.

4.1.2. Data Preprocessing. Considering that there are noise, incompleteness, and inconsistency in the crawled original data, this paper performs normalization, zero-phase component analysis, and fuzzy preprocessing for the original data before the experiment.

- (1) Normalization: carry out normalized preprocessing for experimental data to reduce the influence of data polarization on the final prediction results, which is shown in the following formula [22]:

$$X_n = \frac{Y_n}{z}, \quad (17)$$

where X_n represents the weight of an attribute total parameters in the total samples; Z indicates the total samples; and Y_n indicates sample feature vector with a total number n of an attribute.

- (2) Zero-phase component analysis: perform zero-phase component analysis for the normalized data. M sample data are selected to convert the original data into matrix $X_1 = V_1$. Set the single sample dimension to 9 and perform ZCA whitening processing on dataset. The specific process can be shown as follows:

- ① Set X_1^T as the numerical matrix with original data of $9 * m$. G represents the matrix after normalizing X_1^T , and the average value of each attribute in G matrix is 0.

- ② Calculate the sample covariance matrix Σ of G to obtain the corresponding eigenvalues and eigenvectors and rank them in order from large to small. The eigenvalues are denoted as $\gamma_1, \gamma_2, \dots, \gamma_9$, and the corresponding eigenvectors are $U = [u_1, u_2, \dots, u_9]$.

- ③ Multiply V_1^T and U^T to obtain the rotation matrix [23]:

$$V_{1rot}^T = U^T V_1^T = \begin{bmatrix} u_1^T x_1 & \cdots & u_1^T x_m \\ \vdots & \ddots & \vdots \\ u_9^T x_1 & \cdots & u_9^T x_m \end{bmatrix}. \quad (18)$$

Make the rotation matrix attribute values with unit variance:

$$V_{1rot}^T = \frac{1}{\sqrt{\gamma_i + 0.1}} V_{1rot}^T \quad (i = 1, 2, \dots, 9). \quad (19)$$

The unit variance per attribute in the rotation matrix is obtained by multiplying $1/\sqrt{\gamma_i}$ ($i = 1, 2, \dots, 9$) with each element of row i ($i = 1, 2, \dots, 9$) in V_{1rot}^T , and denote the obtained matrix as V_{1rot}'' , where $1/\sqrt{\gamma_i + \varepsilon}$ is used to replace $1/\sqrt{\gamma_i}$, which deals with the numerical fluctuation or overflow phenomenon when r_i approaches 0.

- ④ The results of ZCA whitening processing are as follows:

$$X_1^{T'} = U X_{1rot}^{T'} \quad (20)$$

- (3) Fuzzy processing: conduct fuzzy processing for the data by fuzzy membership theory, so the obtained data can be used in the experiment. The method based on fuzzy processing is as follows:

- ① Let $V_2 = [TS, pI, add_deI, add_sh1, t1, sex1, age1, pro_ch, col, fav_r1]$. The time TS in the vector V_2 represents the distance between the time of collecting sample data and the time of the system. Data are selected in a random way, and weights are marked for data in different states:

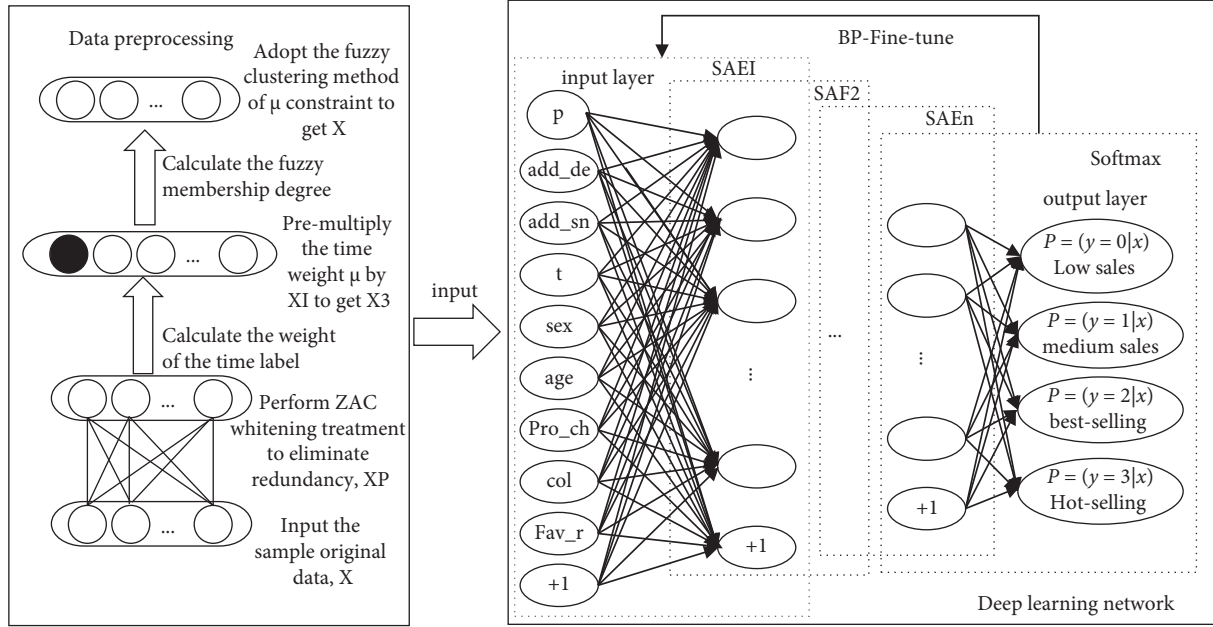


FIGURE 3: The improved ICM model structure.

$$TS = \frac{TS_n - TS_e}{30}, \quad (21)$$

where TS_n represents the current system time when data are processed and TS_e represents the time of data sample collection. The time label format is year-month-day.

② Use the fuzzy subset weight coefficient method to deal with the time weight and use the expert comment set method to set the weight of sample data at different distances:

$$\mu_1 = \begin{cases} 0.4, & TS < 1, \\ 0.31, & 1 \leq TS < 5, \\ 0.20, & 5 \leq TS < 9, \\ 0.08, & 9 \leq TS < 12, \\ 0, & TS \geq 12. \end{cases} \quad (22)$$

③ Determine the membership function. Set V'_1 as the weight in the sales prediction of each data obtained according to TS in V_2 , namely, $V_3 = \mu_1 V'_1$. It can be seen that the factor set V_3 , the judgment set Y , and the weight matrix K select the membership function of trapezoidal distribution as

$$\mu(x_i) = \begin{cases} 0, & x_i < a, \\ \frac{x_i - a}{b - a}, & a \leq x_i \leq b, \\ 1, & x_i > b. \end{cases} \quad (23)$$

Here, x represents the feature vector in V_3 ; t represents the value at t ($t = 1, 2, \dots, m$) in the eigenvector x ; and a and b can be determined by different characteristic attributes.

④ Obtain V_3 by applying V'_1 in step ①, and the input vector $V = \mu(x_t)_K V_3$ of SAE can be obtained by applying V_3 in step ②, which is as follows:

$$V = \{p, add_de, add_sh, t, sex, age, pro_ch, col, fav_r\}. \quad (24)$$

The experimental data for this study can be finally obtained by the above preprocessing. Some of the data are shown in Table 1.

As can be seen from the improved ICM model prediction process, part of the sample data is utilized to train the autoencoding network, so as to obtain the kernel function, cost function, and derivative function. Also, a part of the sample data is adopted to train the softmax classifier. Therefore, the preprocessed experimental data should be divided into feature learning and classification learning. To ensure general applicability of the improved ICM model, 3000 samples are randomly selected from the experimental dataset to be the feature learning subset, and 1000 samples are selected as classification learning subset, including 600 softmax classifier training sets and 400 test sets.

4.2. Parameter Settings

4.2.1. Determination of Hidden Layers. Set hidden layers to 1~10 and input 500 groups of samples to obtain the classification accuracy of the model [24], as shown in Figure 5. The figure shows that if the number of hidden layers is less than 3, the classification accuracy of the model will be gradually improved with the increase of hidden layers. If the number of hidden layers is greater than 3, the model classification accuracy does not change with the increase of hidden layers. So, it indicates that when there are 3 hidden layers, the model has reached the optimal classification

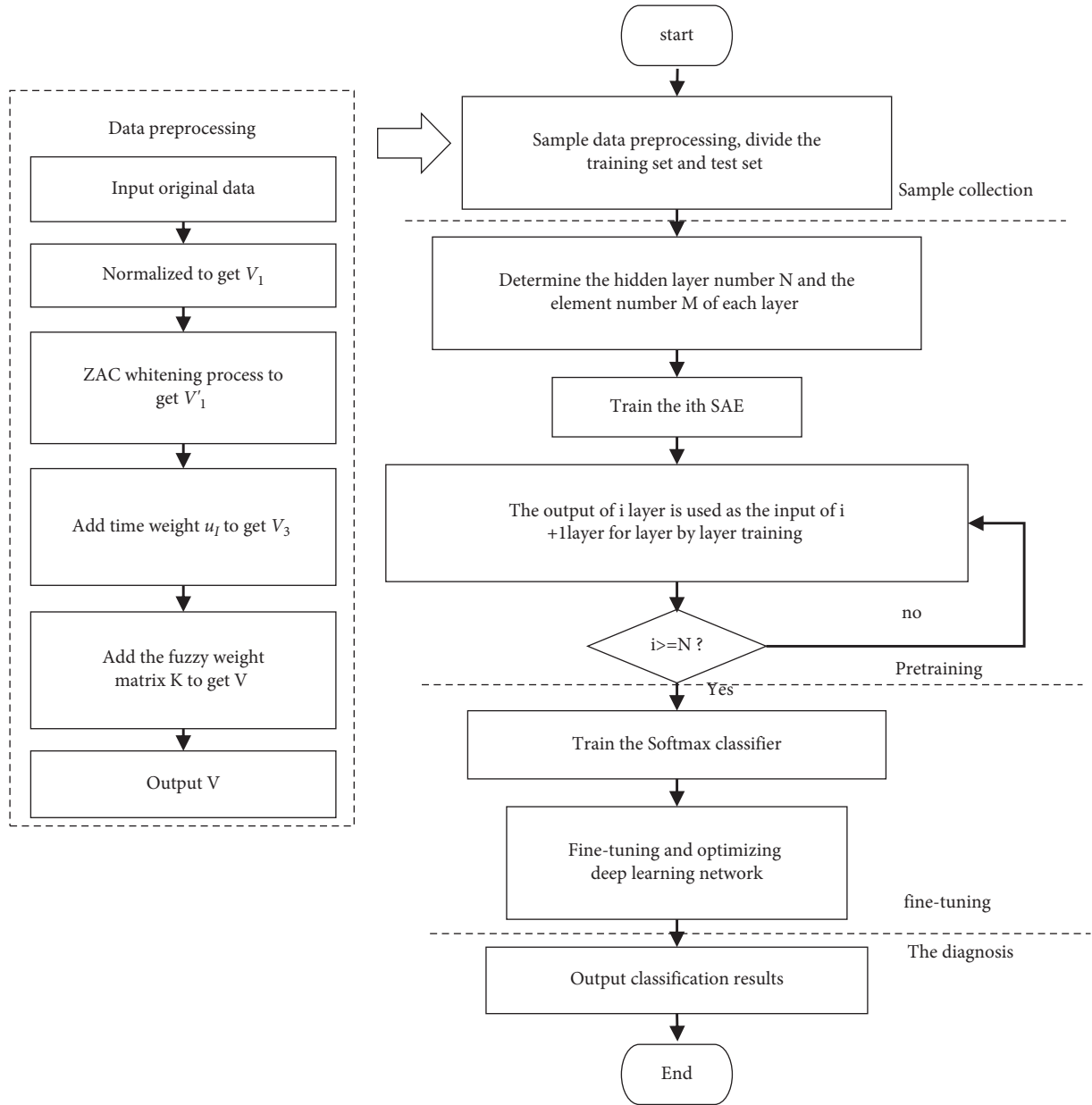


FIGURE 4: The prediction process of agricultural product sales based on improved ICM.

accuracy. Therefore, the hidden layer number of the model is set as 3 in this paper.

4.2.2. *Determination of the Unit Number of Hidden Layers.* Set iterations to 100, hidden layers to 3, and the sparsity parameter to 0.05. Meanwhile, input 1200 sets of data and increase units of the three hidden layers in a ratio of 3 : 2 : 2, and the results are shown in Figure 6. Here, when the unit of hidden layer in the second and third layers changes, the classification accuracy changes accordingly. When the units of each hidden layer are 6, 4, and 4, the classification accuracy of the model is the highest. Therefore, the units of hidden layer is set to 6, 4, and 4, respectively.

4.3. *Evaluation Index.* Precision and recall are used to evaluate model classification performance in this paper, and false positive rate (FPR) and false negative rate (FNR) are used to evaluate risk. The specific calculation methods are shown in formulas (25)–(28).

$$P = \frac{\text{the number correctly divided into this class}}{\text{the number actually divided into this class}}, \quad (25)$$

$$R = \frac{\text{the number correctly divided into this class}}{\text{the number actually divided into this class}}, \quad (26)$$

$$\text{FPR} = \frac{\text{the number incorrectly divided into this class}}{\text{the number actually divided into this class}}, \quad (27)$$

TABLE 1: Examples of preprocessed experimental specification data.

Id	P	Add_de	add_sh	Sex	Age	pro_ch	Col	fav_r
1	0.17	0.61	0.25	0.1	0.21	0.25	0.12	0.09
2	0.45	0.61	0.25	0.9	0.21	0.09	0.12	0.09
...
30	0.29	0.61	0.04	0.9	0.3	0.47	0.24	0.11

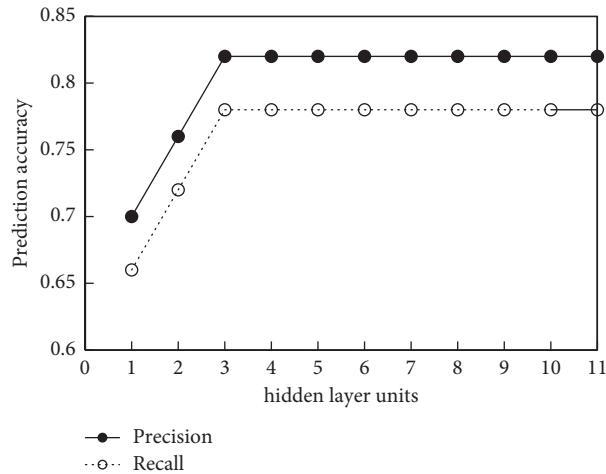


FIGURE 5: Influence of hidden layers on model classification accuracy.

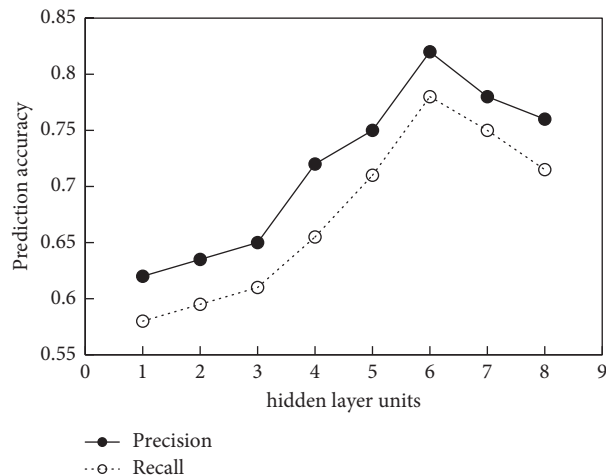


FIGURE 6: Influence of hidden layer units on model classification accuracy.

$$\text{FNR} = \frac{\text{the number not divided into this class}}{\text{the number actually divided into this class}}. \quad (28)$$

4.4. Experimental Result

4.4.1. Model Performance Verification. To verify the performance of the proposed model, the improved ICM is used to classify experimental datasets of different sizes, and its classification accuracy is compared with that of SVM and softmax classifier. The results are shown in Table 2. The table shows that with the increase of data scale, the classification precision and recall of each model are improved, and the

classification time increases accordingly. Compared with SVM and softmax classifier, the improved ICM has higher accuracy and shorter classification time under the same data scale. Furthermore, the advantage becomes more obvious with the increase of data scale. Therefore, there is strong self-learning ability for the proposed model to the massive and variable agricultural product sales data, where the high classification accuracy can be achieved, and the classification prediction advantage is obvious.

To verify the classification precision of the proposed model before and after optimization, in this paper, the classification accuracy of the model before and after optimization is determined by the number of iterations, which is shown in Table 3. The table shows that the classification

TABLE 2: Comparison of classification accuracy of different models.

Number of samples	Algorithm	Precision	Recall	Time
1000	Improved ICM	0.721	0.695	7.5
	SVM	0.646	0.628	8.6
	Softmax	0.425	0.406	8.8
2000	Improved ICM	0.763	0.743	12.1
	SVM	0.691	0.667	15.5
	Softmax	0.546	0.528	14.8
3000	Improved ICM	0.813	0.789	20.5
	SVM	0.715	0.709	25.2
	Softmax	0.551	0.538	25.9

TABLE 3: Precision changes of model classification.

Softmax iteration (times)	SAE1 iteration (times)	SAE2 iteration (times)	SAE3 iteration (times)	Fine-tuned iteration (times)	Precision (%)
10	—	—	—	—	62.9
100	—	—	—	—	64.1
100	100	—	—	—	68.8
100	100	100	—	—	73.4
100	100	100	100	—	79.3
100	100	100	100	100	81.3

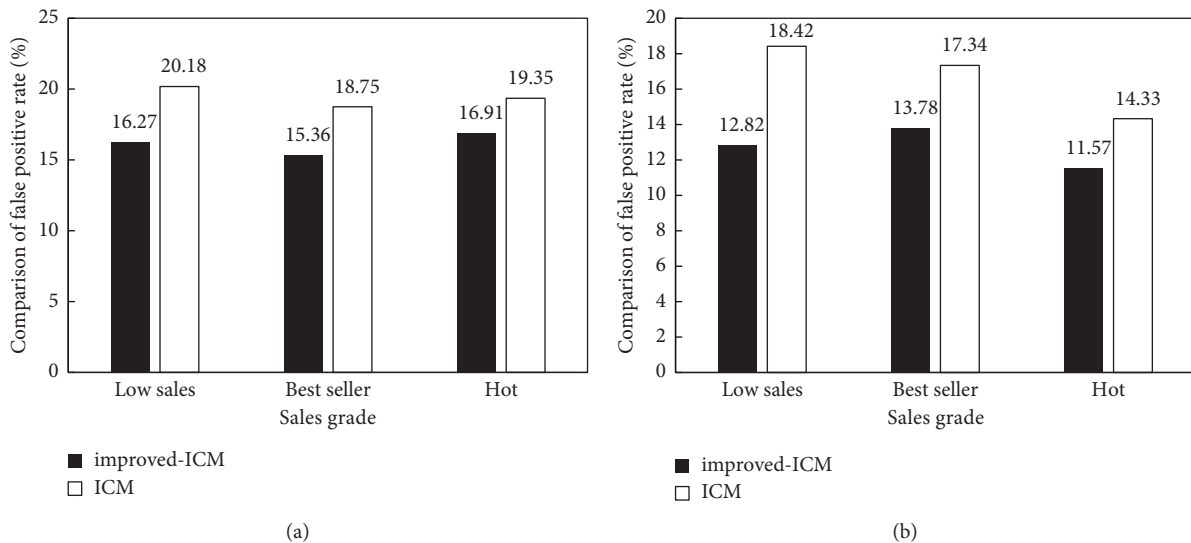


FIGURE 7: Comparison of model classification results. (a) Comparison of false positive rate. (b) Comparison of false negative rate.

accuracy before the proposed model optimization is 62.98%, and the classification accuracy after optimization is 80.98%, which increases by 18%. Therefore, the classification accuracy can be improved by fine-tuning the model.

4.4.2. Model Comparison. To verify the processing ability of the proposed model for fuzzy information, the improved ICM model is used to classify and predict 4000 sets of data, which are randomly selected from experimental samples. The false positives and false negatives of the two models are obtained by comparing the classification results with the ICM model, which are shown in Figure 7. The figure shows

that the false positive rate and false negative rate of the proposed model are obviously lower than those of the ICM model, which indicates that the proposed model can improve the classification and recognition ability of the model through fuzzy data preprocessing.

In order to further verify the classification performance of the improved ICM model, the improved ICM and ICM models are used for classification under different data scales, which are shown in Table 4. The table shows that the improved ICM model has better classification accuracy, recall, and classification time indexes than the ICM model under different data scales. Also, this advantage becomes more obvious with the increase of data scale. The reason is that the

TABLE 4: Comparison of model classification accuracy under different data sizes.

Number of samples	Algorithm	Precision	Recall	Time
1000	Improved ICM	0.73	0.71	7.11
	ICM	0.65	0.62	7.93
2000	Improved ICM	0.75	0.73	12.3
	ICM	0.72	0.69	13.8
3000	Improved ICM	0.82	0.79	22.9
	ICM	0.72	0.71	23.7

improved ICM model adopts sparse autocoding on the basis of the ICM model to reduce the loss of data features as much as possible. Compared with ICM autoencoder, the improved ICM model has stronger feature learning ability. In addition, the theory of fuzzy membership degree is added to the data preprocessing of the improved ICM model. It solves the problem that the ICM model ignores the fuzzy correspondence between the influencing factors and the grades of agricultural product sales. Therefore, the improved ICM model is superior to the ICM model in classification prediction of agricultural product sales.

5. Conclusion

To sum up, the proposed prediction method of agricultural product sales based on deep learning uses sparse autocoding to reduce the loss of data feature as much as possible. Meanwhile, we use the preprocessing agricultural product sales data based on fuzzy membership theory to build the improved ICM classification prediction model, which can effectively achieve the sales prediction of agricultural products. Compared with the ICM model, SVM, and softmax classifier, the model has higher sales prediction accuracy. When the number of hidden layers of the model is 3 and the units of hidden layers are 6, 4, and 4, the maximum classification accuracy of the model can reach 80.98%, which can be used to predict the actual sales of agricultural products. Although some achievements have been made, there are still some shortcomings, such as limitations in data sample acquisition, small size of data, and no verification of data processing capability with a lot of noise. So, the next step is to further discuss the classification and prediction performance of the improved ICM for massive data, which makes the model have stronger universality.

Data Availability

The experimental data used to support the findings of this study are available from the corresponding author upon request.

Conflicts of Interest

The author declares that there are no conflicts of interest.

Acknowledgments

This study was sponsored in part by Research on the Development of Culture and Tourism Industry in Ethnic

Minority Areas under the Background of Rural Revitalization (2021-GMB-020).

References

- [1] J. Grasman and M. Kornelis, "Forecasting product sales with a stochastic Bass model," *Journal of Mathematics in Industry*, vol. 9, no. 1, pp. 1–10, 2019.
- [2] M. P. de Souza, M. Hoeltz, P. D. Gressler, L. B. Benitez, and R. C. S. Schneider, "Potential of Microalgal Bioproducts: General Perspectives and main Challenges," *Waste and Biomass Valorization*, vol. 10, no. 8, pp. 2139–2156, 2019.
- [3] Y. Xiang, "Set self-service sales and online customization in one of the product network marketing system construction and management research," *Cluster Computing: the Journal of Networks, Software Tools and Applications*, vol. 22, no. 12, pp. 8803–8809, 2019.
- [4] Y. S. Cho, W. S. Na, and S. C. Moon, "Periodicity analysis using weighted sequential pattern in recommending service," *Cluster Computing*, vol. 22, no. 4, pp. 1049–1056, 2019.
- [5] G. Tsoumakas, "A survey of machine learning techniques for food sales prediction," *Artificial Intelligence Review*, vol. 52, no. 1, pp. 441–447, 2019.
- [6] K. Chen, P. Luo, and H. Wang, "Investigating transitive influences on WOM: from the product network perspective," *Electronic Commerce Research*, vol. 17, no. 1, pp. 149–167, 2017.
- [7] T. Chen, H. Yin, H. Chen, and H. Wang, "Online sales prediction via trend alignment-based multitask recurrent neural networks," *Knowledge and Information Systems*, vol. 62, no. 7, pp. 1–29, 2019.
- [8] W. K. Eric, See-To, and E. W. T. Ngai, "Customer reviews for demand distribution and sales nowcasting: a big data approach," *Annals of Operations Research*, vol. 270, no. 1–2, pp. 415–431, 2018.
- [9] S. K. Sharma, S. Chakraborti, and T. Jha, "Analysis of book sales prediction at Amazon marketplace in India: a machine learning approach," *Information Systems and E-Business Management*, vol. 17, no. 2–4, pp. 261–284, 2019.
- [10] H. Yuan, W. Xu, Li Qian, and R. Lau, "Topic sentiment mining for sales performance prediction in e-commerce," *Annals of Operations Research*, vol. 270, no. 1–2, pp. 553–576, 2018.
- [11] L. Wen and X. Yuan, "Forecasting the annual household electricity consumption of Chinese residents using the DPSONBP prediction model," *Environmental Science and Pollution Research*, vol. 27, no. 1, pp. 22014–22032, 2020.
- [12] Y. Zhang and G. Pan, "A hybrid prediction model for forecasting wind energy resources," *Environmental Science and Pollution Research*, vol. 27, no. 2, pp. 19428–19446, 2020.
- [13] Yu-J. Choe and J.-H. Yom, "Improving accuracy of land surface temperature prediction model based on deep-

- learning,” *Spatial Information Research*, vol. 28, no. 8, pp. 377–382, 2020.
- [14] V. Koolwal and K. K. Mohbey, “A comprehensive survey on trajectory-based location prediction,” *Iran Journal of Computer Science: International Journal*, vol. 3, no. 1, pp. 65–91, 2020.
- [15] Z. Lei, “Research and analysis of deep learning algorithms for investment decision support model in electronic commerce,” *Electronic Commerce Research*, vol. 20, no. 1–2, pp. 275–295, 2020.
- [16] H. H. Elmousalami and M. Elaskary, “Drilling stuck pipe classification and mitigation in the Gulf of Suez oil fields using artificial intelligence,” *Journal of Petroleum Exploration and Production Technology*, vol. 10, no. 10, pp. 2055–2068, 2020.
- [17] K. Priya, N. Goel, and V. K. Garg, “Human age prediction using DNA methylation and regression methods,” *International Journal of Information Technology: An Official Journal of Bharati Vidyapeeth’s Institute of Computer Applications and Management*, vol. 12, no. 2, pp. 373–381, 2020.
- [18] T. Izui and G. Venture, “Correlation analysis for predictive models of Robot User’s Impression: a study on Visual medium and Mechanical noise,” *International Journal of Social Robotics*, vol. 12, no. 5, pp. 425–439, 2020.
- [19] Y. Gao, “Forecast model of perceived demand of museum tourists based on neural network integration,” *Neural Computing & Applications*, vol. 33, no. 4, pp. 1–11, 2020.
- [20] D. Li, T. Nian, H. Wu, F. Wang, and L. Zheng, “A predictive model for the geometry of landslide dams in V-shaped valleys,” *Bulletin of Engineering Geology and the Environment*, vol. 79, no. 2, pp. 1–14, 2020.
- [21] J. N. Swerdel, J. M. Repts, D. Fife, and P. B. Ryan, “Developing predictive models to determine Patients in End-of-life Care in Administrative datasets,” *Drug Safety: The Official Journal of the International Society of Pharmacovigilance [ISoP]*, vol. 43, pp. 447–455, 2020.
- [22] L.-Y. Xue, Z.-Y. Jiang, T.-T. Fu et al., “Transfer learning radiomics based on multimodal ultrasound imaging for staging liver fibrosis,” *European Radiology*, vol. 30, no. 5, pp. 2973–2983, 2020.
- [23] W. Zhao, R. Zhang, Y. Lv, and J. Liu, “Quantile regression and variable selection of single-index coefficient model,” *Annals of the Institute of Statistical Mathematics*, vol. 69, no. 4, pp. 761–789, 2017.
- [24] M. Kim, K. M. Jang, J.-H. Kim et al., “Differentiation of mass-forming focal pancreatitis from pancreatic ductal adenocarcinoma: value of characterizing dynamic enhancement patterns on contrast-enhanced MR images by adding signal intensity color mapping,” *European Radiology*, vol. 27, no. 4, pp. 1722–1732, 2017.

Research Article

Research on Aided Judgment of Rural Sports Posture Based on Deep Learning

Hao Guo¹ and Qi Hao ^{2,3}

¹Chongqing College of Humanities, Science & Technology, Chongqing 401524, China

²Department of Sports and Health, Linyi University, Linyi 276000, China

³Department of Leisure-Sports, Pai Chai University, Daejeon 35345, Republic of Korea

Correspondence should be addressed to Qi Hao; haoqi@lyu.edu.cn

Received 8 November 2021; Revised 21 December 2021; Accepted 31 December 2021; Published 4 March 2022

Academic Editor: Man Fai Leung

Copyright © 2022 Hao Guo and Qi Hao. This is an open access article distributed under the Creative Commons Attribution License, which permits unrestricted use, distribution, and reproduction in any medium, provided the original work is properly cited.

With the rapid development of computer technology, people have begun to combine virtual reality and other technologies to achieve scientific sports auxiliary training, to get rid of the state of traditional sports training purely relying on experience. The article proposes a deep learning BP neural network human body posture recognition algorithm and briefly introduces the human body motion posture. The purpose of this research was to use the powerful data processing, mining, and analysis functions of deep learning to train the massive data generated in competitive sports training and apply it to competitive sports training. It is committed to promoting the accuracy and analysis of competitive sports training. Refinement provides technical guidance for athletes' training, promotes the scientific and informatized development of competitive sports training in China, and provides some reference methods for the research and application of deep learning in competitive sports training. The article's research results show that (1) taking a rural area as an example, we recorded the exercise postures of rural athletes in five different states: static, upstairs, downstairs, walking, and running. Comparing the recognition rate and training time of The BP neural network algorithm, ABC-BP algorithm, AFS-BP algorithm, and ABC-AFS-BP algorithm, it can be found that in terms of recognition rate, ABC-AFS-BP algorithm, AFS-BP algorithm, and ABC-BP algorithm are better than traditional BP algorithm. Among them, the recognition rate of the ABC-AFS-BP algorithm is higher than that of the ABC-BP algorithm, but it takes slightly more time than the ABC-BP algorithm. In terms of training time, the ABC-BP algorithm takes less time, but the accuracy is lower than the ABC-AFS-BP algorithm; the ABC-AFS-BP algorithm has a greater improvement in time consumption than the AFS-BP model and can guarantee the recognition rate and accuracy, and the error rate curves of the four algorithms show that after 500 iterations of the training part, the iteration error value of the ABC-AFS-BP algorithm is the smallest. (2) We evaluated sports postures of athletes from a certain rural team and concluded that bad postures will have a certain impact on the body. Among them, more than 85% of athletes in football and basketball have pelvic rotation. The problem is that football players have reached 90% of the test sample. 60% of football players and basketball players have the problem of collapsed foot. The main problem of aerobic athletes is flat back and collapsed foot. More than 90% of badminton players have high and low shoulder problems, and more than 80% of them have neck problems, which is a very serious body posture problem. (3) Detecting the flexibility experiment of the BP posture detection algorithm, compared with the traditional motion posture recording method, we tested from the three aspects of recording motion accuracy, missed detection rate, and recording time. The result shows BP posture detection. The missing detection rate of the algorithm is low, basically maintained at about 2.0, the accuracy of recording actions is relatively high, generally maintained above 98%, and the highest is 99.15%, and the recording time is short, maintained at 3–4 minutes; comparing traditional posture detection with the BP attitude detection algorithm, the missed detection rate of the algorithm is relatively high, kept at 4–6, the action accuracy is lower than that of the BP attitude detection algorithm, generally kept at about 95%, and the recording time is kept at 5–6 minutes. The posture detection algorithm is more efficient.

1. Introduction

Moving target recognition and analysis is an important research direction in the field of computer vision, which is widely used in our lives, such as intelligent robots, video surveillance, medical education, sports competitions, national defense security, and other fields. Sports applications are also very smart. With the continuous development of computer technology, based on deep learning methods, a sports video key gesture extraction system can be designed to extract the key gestures of athletes in competitive sports training videos to assist athletes and coaches in training reasonably and efficiently and avoid complexity. The interference of the environment on the extraction improves the inaccurate situation of traditional coaches in judging and extracting key gestures based on experience. Target detection and tracking based on deep learning, first, is the problem of target detection, that is, determining the position of the target object in the image or scene, which is generally determined by the bounding box of the object. In response to such problems, the literature [1] proposed that RCNN adopts the method of selecting the domain to obtain the local candidate regions where the detection target may exist in the image, and then, these candidate regions are input into the convolutional neural network to obtain their characteristics, and the classifier is connected to feature map, whether the corresponding area belongs to the target to be detected is judged, and finally, regression is performed on the calibration frame to correct the position of the prediction frame, but RCNN has the problem of repeated calculation. Literature [2] introduced the spatial pyramid pooling layer into CNN and proposed SPP-Net, which reduces the limitation of the CNN network on the size of the input image and improves the accuracy. Literature [3] proposed to use inertial sensors to collect information about human motion and apply the collected information to analyze and recognize human motion. Literature [4] discussed the theoretical framework for studying the coordination strategy of standing posture. The framework consists of a musculo-skeletal model of the lower limbs of the human body in the sagittal plane and a technology that geometrically visualizes how the constraints inside and outside the body affect movement. Literature [5] designed an action recognition method based on depth images. The algorithm projects the depth image in three projection planes, extracts the Gabor features from the three projection images, and uses these features to train the extreme learning machine classifier. The calculation efficiency of the algorithm is high, but the performance of recognition of small amplitude actions is not ideal. Literature [6] proposed a time-series deep belief network that can complete online human action recognition. This model solves the problem that the current deep belief network model can only recognize static images, but the training process of this model takes a long time to process, which affects the application performance of the algorithm for large-scale data sets, in addition to the time efficiency issue for large-scale data sets. Literature [7] used asymmetrical system deviation to model human movement information, and the algorithm introduces a posture labeling

mechanism to further improve the recognition performance of small movements. To meet the recognition of large-scale data sets and small-scale actions at the same time, a human action recognition algorithm based on multifeature fusion and motion information is designed. Literature [8] learned manual features and deep learning features, and the manual features adopted an improved dense trajectory. Literature [9] used a convolutional neural network based on motion information. High recognition accuracy is achieved for small-range actions, but the amount of features that need to be analyzed is large, and it is difficult to apply to large-scale data sets. Literature [10] used an inverted double pendulum to simulate the human body in an upright posture. The human body posture is a more complicated problem in biomechanics. The model proposed in this article can effectively distinguish the different parameters of the body and effectively control the body's movement posture. Literature [11] analyzed the experimental data, established a human body model, and conducted a simulation experiment on the OSG platform. When a person is exercising, there will be an angle between the limbs and the body. The accelerator is fixed on the arm, and the arm and torso can be calculated in real time. In recent years, athlete performance analysis has received widespread attention as a new anti-doping auxiliary judgment strategy, but many researchers have not had a clear understanding of this strategy in theory and practice. Literature [12] conducted in-depth research on performance analysis through literature review and inductive research methods. The literature takes some well-known athletes as examples and analyzes the results. The results show that whether there are athletes using doping can be quickly distinguished from the performance of the athletes, which can improve the efficiency of sports excitement detection. The purpose of the literature [13] is to determine which morphological indicators and how to affect postural stability and control through special tests. The results of the literature [14] can be used to enhance the digital human modeling motion generated for human motion simulation. Literature [15] analyzed the EMG response and joint movement of the legs in subjects who stood on a sinusoidal treadmill with their eyes closed.

2. Theory Introduction

2.1. The Status Quo of Rural Sports Development. At present, China's rural sports venues are few and of low quality, and some areas even lack suitable venues for villagers' activities. Rural sports venues and infrastructure are generally in poor condition; some villages have stadiums, but they have been idle for too long and no one is used. Even crops have already been planted, and the overall situation is not optimistic. This also causes farmers to watch TV as their main activity during leisure time, so conditions are not allowed to a certain extent, which limits the enthusiasm of villagers to participate in sports. Therefore, the relevant departments must take measures to solve these problems. The villagers do not have a deep understanding of the problem of sports and cultural exercises, and it is generally young people who participate in sports. Relevant governments have taken measures to solve

these problems, but despite this, rural sports activities are still a weak link in China's sports industry. The increasing sports health requirements in rural areas and the serious shortage of public sports venues in rural areas have restricted rural sports.

2.2. Classification of Human Motion Posture. The posture of the human body movement is the form displayed by the human body in the process of daily life activities. Whether a person's body is healthy or not is closely related to the posture of the human body movement, so the posture of the human body movement has been widely concerned by the majority of researchers. The increase in user needs and people's requirements for the quality-of-life force researchers to speed up the research on human body movement postures. These studies are of great significance to the timely discovery of the human body's health [16]. The basic forms displayed by the human body in the process of daily life activities include lying, standing upright, sitting, walking, and running. In some complicated situations, it may be due to some irresistible external factors, or some injury or illness, etc., which may cause people to fall. Under normal circumstances, people call the most basic postures displayed by the human body in the process of daily life activities, including lying, standing upright, sitting, walking, and running, as ADL. In the process of life activities, some basic activities have to be carried out to take care of themselves and their families, protect the family and social environment, or participate in some social activities. These activities of daily life are basic life postures that human beings must always repeat to survive and live in this society. Each posture can be subdivided into many types, such as standing posture, which can be subdivided into standing upright, standing tilted forward, and standing tilted backward; lying flat includes lying on your back, lying on the left, lying on the right, and lying on the left and right sides. Sitting posture can be subdivided into sitting upright, leaning forward when sitting, leaning backward when sitting, and so on. Like walking, running is also affected by the surrounding environment, road conditions, and the physical condition of the runner. Running can also be subdivided into even running, slow running, and fast running. In some special circumstances, due to some complicated reasons, it may be due to some irresistible external factors, or some injuries or illnesses, etc., which may cause people to fall. The fall mentioned here refers to the uncontrolled fall of the body to the ground or to another plane that is not controlled by humans, occurs suddenly without preparation, or falls to another plane [17]. The World Health Organization has classified "falls" (including falls), as shown in Table 1.

2.3. Human Body Motion Posture Detection Algorithm. To carry out a three-dimensional simulation of the athlete's movement posture to adjust the training method and improve the training level, this study studies the application of unlabeled 3D pose estimation method in training assistance system [18, 19]. While athletes interact with the computer through limb movement, it is difficult to establish a human

body posture database because there is no corresponding marking technology support to provide a robust observation method for the computer. Therefore, this article adopts a partial estimation method, which divides the athlete's overall posture into multiple partial postures, and estimates the posture of each part separately. The algorithm block diagram is shown in Figure 1.

3. Method

3.1. Deep Learning Features Based on Motion Information. Deep learning has been widely used in recent years [20, 21]. The time template can extract all the motion sequences of an image frame, and the difference between the video frames is used to calculate the motion information between the frames. The calculation formula of the time template is as follows [19]:

$$TT = \left(\frac{1}{255}\right) \sum_{i=2}^n \omega_i \cdot m(i). \quad (1)$$

Among them, n represents the number of video frames, $m(i)$ represents the motion information of the i th frame, ω_i represents the weight value of the i th frame [22], and the value range of the weight value is $[0, 255]$. Formula (1) is transformed to get the following:

$$TT = \sum_{i=2}^n \left(\frac{\omega_i}{255}\right) \cdot m(i). \quad (2)$$

A fuzzy membership function $\mu(i)$ is replaced to get the following:

$$TT = \sum_{i=2}^n \mu(i) \cdot m(i). \quad (3)$$

The appropriate $\mu(i)$ is selected, to enhance the saliency of the temporal motion information in the time template [23]; the model diagram of $\mu(i)$ is shown in Figure 2.

Four $\mu(i)$ are set to $\mu_1 \sim \mu_4$, defined by the following formulas:

$$\mu_1(i) = 1, \quad \forall i \in [0, n], \quad (4)$$

$$\mu_2(i) = \frac{i}{n}, \quad \forall i \in [0, n], \quad (5)$$

$$\mu_3(i) = 1 - \frac{i}{n}, \quad \forall i \in [0, n], \quad (6)$$

$$\mu_4(i) = \begin{cases} \frac{2i}{n}, & 0 \leq i \leq \frac{n}{2} \\ 2 - \frac{2i}{n}, & \frac{n}{2} \leq i \leq n. \end{cases} \quad (7)$$

3.2. Human Motion Gesture Recognition. The motion detection of the human body is carried out by detecting the confidence map S of the joint points of the human body and the affinity domain L of the human joint points of a two-

TABLE 1: Classification of falls.

Fall classification	Fall classification
Fall on the same plane of ice and snow	Falls and falls on stairs and steps
Sliding, tripping, and falling on the same plane	Falls and falls on the ladder
Falling while skating, skiing, or roller skating	Falls and falls on scaffolding
Other falls on the same plane caused by being hit or pushed by others	Falling or falling out of the house or building structure
Falling while being transported or supported by others	Injuries caused by diving or diving, excluding drowning and sinking
Fell on wheelchair	Other drops from one plane to another
Falling in bed	Other falls on the same plane
Falling on the chair	Falling on sports facilities
Falling on other furniture	Unspecified fall

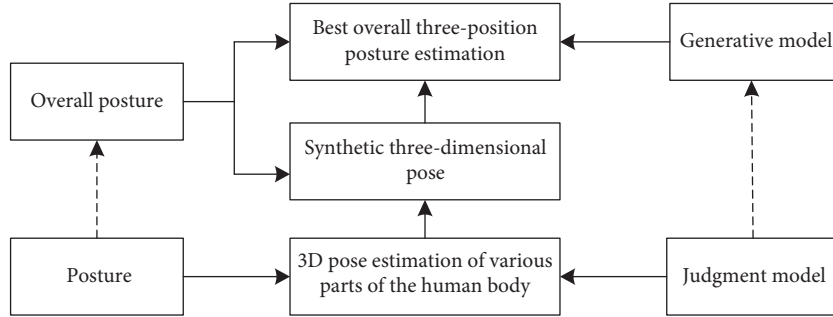


FIGURE 1: Frame diagram of a three-dimensional pose estimation method.

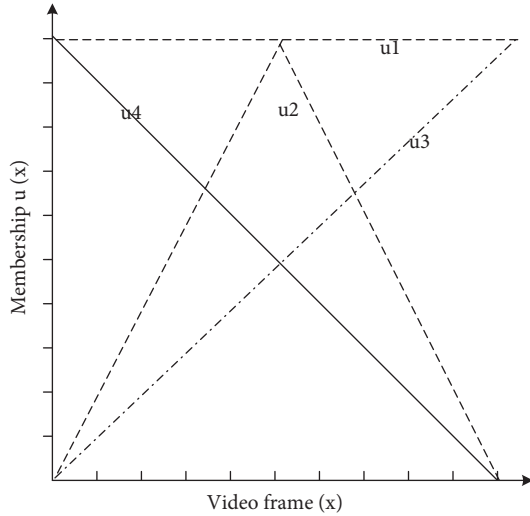


FIGURE 2: Graphs of 4 fuzzy membership functions.

dimensional vector [24], and the calculation formula is as follows:

$$\begin{aligned} S^t &= \rho^t(F^t, S^{t-1}, L^{t-1}), \quad \forall t \geq 2, \\ L^t &= \rho^t(F^t, S^{t-1}, L^{t-1}), \quad \forall t \geq 2. \end{aligned} \quad (8)$$

Each loss function is weighted, and the loss function is as follows:

$$f_S^t = \sum_{j=1}^J \sum_P w(p) \cdot \|S_j^t p - S_j^*(p)\|_2^2, \quad (9)$$

$$f_L^t = \sum_{c=1}^C \sum_P w(p) \cdot \|S_c^t p - S_c^*(p)\|_2^2.$$

Among them, $S_j^*(p)$ and $S_c^*(p)$ are the actual labeled values, and the final objective function is as follows:

$$f = \sum_{t=1}^T (f_S^t + f_L^t). \quad (10)$$

3.2.1. Confidence Graph Detection of Nodes. First, the confidence map of the k th person is $S_{jk}^*(p)$, and $x_{j,k}$ is the true value of the k th joint point for the j th person, and the predicted value $S_{jk}^*(p)$ at the p point is expressed as a Gaussian function [25]:

$$S_{j,k}^*(p) = \exp - \frac{\|p - x_{j,k}\|_2^2}{\sigma^2}, \quad x_{j,k} \in R^2. \quad (11)$$

The maximum operation is performed:

$$S_j^*(p) = \max_k S_{j,k}^*(p). \quad (12)$$

As shown in Figure 3, $x_{j_1,k}$, $x_{j_2,k}$ represent the real position of the k th person's joint point j_1 and joint point j_2 on the limb c , and the vector field [26] at p is as follows:

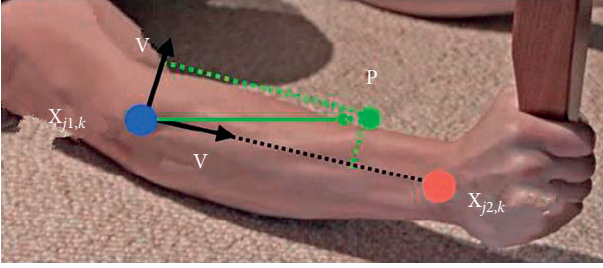


FIGURE 3: Connection diagram of key nodes.

$$L_{c,k}^*(p) = \begin{cases} V, & \text{If point } p \text{ is on limb } bc, \\ 0, & \text{else.} \end{cases} \quad (13)$$

Here,

$$V = \frac{(x_{j2,k} - x_{j1,k})}{\|x_{j2,k} - x_{j1,k}\|_2}. \quad (14)$$

The unit vector p representing the direction of the limbs satisfies the formula:

$$\begin{aligned} 0 &\leq V \cdot (p - x_{j1,k}) \leq l_{c,k}, \\ |V_{\perp} \cdot (p - x_{j1,k})| &\leq \sigma_l. \end{aligned} \quad (15)$$

Limb length $l_{c,k}$ is calculated as follows:

$$l_{c,k} = \|x_{j2,k} - x_{j1,k}\|_2. \quad (16)$$

Mean processing is calculated as follows:

$$L_c^*(p) = \frac{1}{n_c(p)} \sum_k L_{c,k}^*(p). \quad (17)$$

The link reliability of the affinity domain L_c along the line segment between two points E is calculated as follows:

$$E = \int_{u=0}^{u=1} L_c(u) \cdot \frac{d_{j2} - d_{j1}}{\|d_{j2} - d_{j1}\|_2} du, \quad (18)$$

$$p(u) = (1-u)d_{j1} + ud_{j2}.$$

Limb prediction results are as follows:

$$\max_Z E = \sum_{c=1}^c \max_{Z_c} E_c. \quad (19)$$

3.2.2. Human Motion Gesture Recognition. For the training data set (x, y) , where each sample x includes n -dimensional feature, namely $x = (x_1, x_2, \dots, x_n)$, the class label set has k categories, namely $y = (y_1, y_2, \dots, y_k)$ [27]; according to Bayes' theorem:

$$p(y_k | x) = \frac{p(x | y_k)p(y_k)}{p(x)}. \quad (20)$$

According to the total probability formula:

$$p(y_k | x) = \frac{p(x | y_k)p(y_k)}{\sum_k p(x | y_k)p(y_k)}. \quad (21)$$

$p(x | y_k)$ can be converted to:

$$p(x | y_k) = p(x_1, x_2, \dots, x_n | y_k) = \prod_{i=1}^n p(x_i | y_k). \quad (22)$$

The naive Bayes classification model is as follows:

$$\begin{aligned} f(x) &= \operatorname{argmax}_{y_k} p(y_k | x) \\ &= \operatorname{argmax}_{y_k} p(y_k) \frac{\prod_{i=1}^n p(x_i | y_k)}{\sum_k p(y_k) \prod_{i=1}^n p(x_i | y_k)}. \end{aligned} \quad (23)$$

It is converted to:

$$f(x) = \operatorname{argmax}_{y_k} p(y_k) \prod_{i=1}^n p(x_i | y_k). \quad (24)$$

4. Simulation Experiment and Data Analysis

4.1. Data Preprocessing. The article proposes a human body gesture recognition algorithm based on BP neural network, as well as the modified AEC-BP, ABC-BP, and ABC-AEC-BP algorithms. AEC-BP regards continuous video frames as a box and uses a three-dimensional convolution kernel for convolution. Through this structure, action information can be captured; ABC-BP uses single frame data and optical flow data, thus capturing motion information; ABC-AEC-BP is a convolutional neural network using two data streams for video behavior recognition. The video is divided into a static frame data stream and an inter-frame dynamic data stream. The static frame data stream can use single frame data, the inter-frame dynamic data stream uses optical flow data, and each data use a deep convolutional neural network for feature extraction. The BP algorithm is used to record the body's action decomposition during walking and running, as shown in Figures 4 and 5.

Taking a certain rural area as an example, we recorded the sports postures of rural athletes in five different states: stationary, going upstairs, going downstairs, walking, and running. The recognition results are as follows:

- AFC-BP algorithm in Table 2
- ABC-BP algorithm in Table 3
- ABC-AFC-BP algorithm in Table 4

Comparing the recognition rate and training time of the BP neural network algorithm, ABC-BP algorithm, AFS-BP algorithm, and ABC-AFS-BP algorithm, it can be seen from Table 5 that in terms of recognition rate, ABC-AFS-BP algorithm, AFS-BP algorithm, and ABC-BP algorithm are better than the traditional BP algorithm. Among them, the recognition rate of ABC-AFS-BP algorithm is higher than that of ABC-BP algorithm, but it takes slightly more time than the ABC-BP algorithm. In terms of training time, the ABC-BP algorithm takes less time, but the accuracy is lower than the ABC-AFS-BP algorithm. The error curves of the four algorithms are shown in Figure 7.

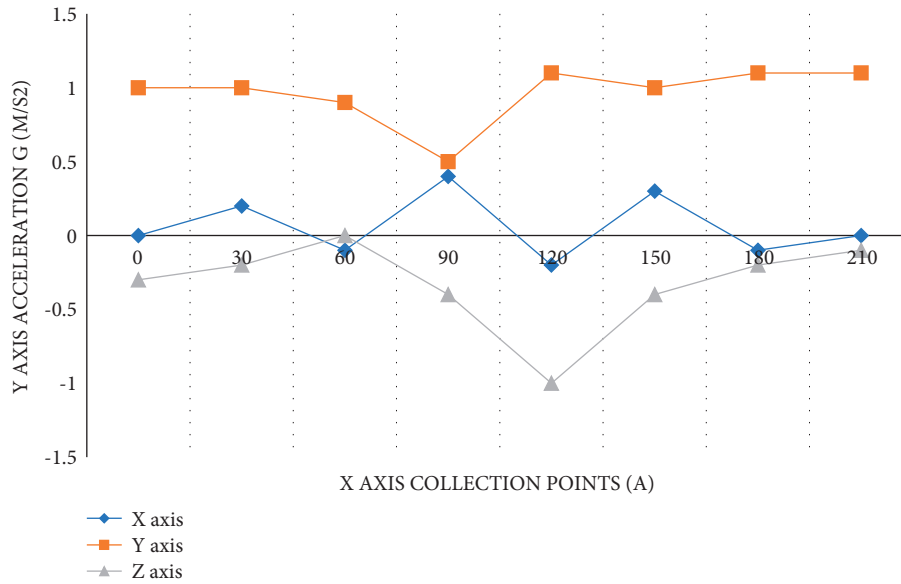


FIGURE 4: Exploded view of walking action.

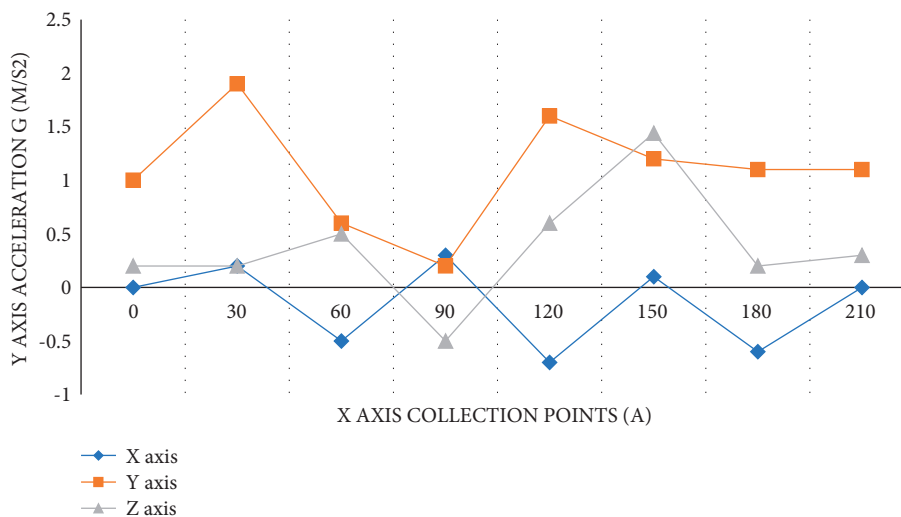


FIGURE 5: Exploded view of running action.

TABLE 2: AFC-BP recognition results.

Sports posture	Standstill	Go upstairs	Go downstairs	Walk	Run
Still	189	5	2	2	3
Go upstairs	3	114	6	4	4
Go downstairs	2	15	185	10	5
Walk	1	9	5	161	6
Run	2	6	11	5	218

TABLE 3: ABC-BP recognition results.

Sports posture	Standstill	Go upstairs	Go downstairs	Walk	Run
Still	190	5	2	1	3
Go upstairs	3	115	7	2	4
Go downstairs	2	13	189	6	7
Walk	2	5	3	164	8
Run	1	8	7	8	218

Through the comparison of Figure 7, it can be found that after 500 iterations of the training part, the iteration error value of the ABC-AFS-BP algorithm is the smallest, reaching the set accuracy, and the local searchability is strong, followed by BP neural network. The algorithm has the largest iterative error value, which is much different

from the set accuracy, and the searchability is poor, which proves that the error is smaller when the ABC-AFS-BP algorithm neural network is used for data training and the training effect is better. At the same time, the ABC-AFS-BP algorithm and the ABC-BP algorithm curve decline faster, and a smaller error value is reached after fewer

TABLE 4: ABC-AFC-BP recognition results.

Sports posture	Standstill	Go upstairs	Go downstairs	Walk	Run
Still	191	3	2	2	3
Go upstairs	1	120	5	2	3
Go downstairs	3	6	203	3	2
Walk	0	3	3	171	5
Run	1	9	9	5	222

We recorded the recognition rate and training time of different algorithms, as shown in Table 5 and Figure 6.

TABLE 5: Recognition rate and recognition results of the algorithm.

Classification algorithm	Recognition rate (%)	Training time
BP	86.23	00:18:83
ABC-BP	90.03	00:08:36
AFC-BP	89.11	00:33:26
ABC-AFC-BP	93.21	00:10:12

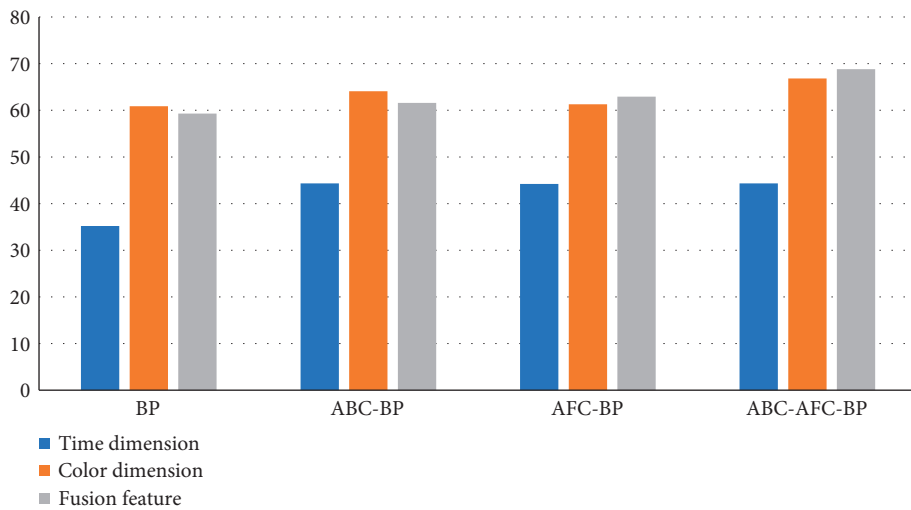


FIGURE 6: Recognition accuracy rate of different dimensions.

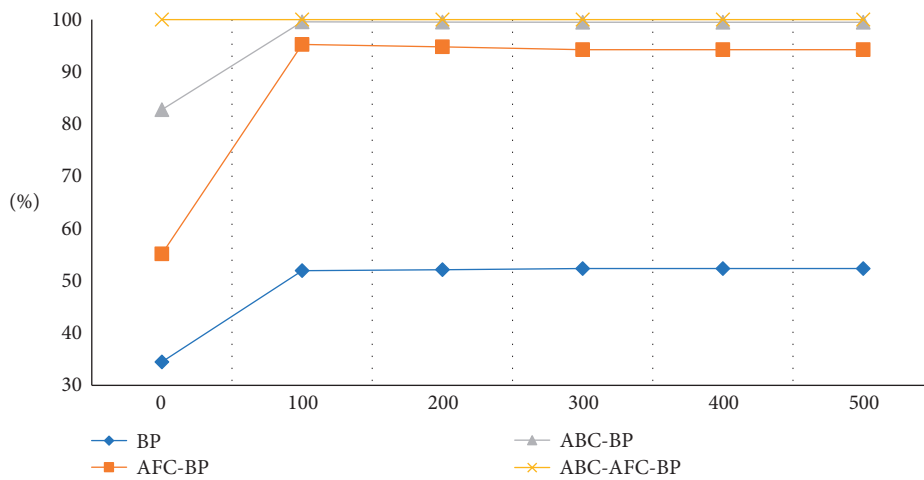


FIGURE 7: Error curve of the algorithm.

TABLE 6: Basic situation of athletes in different sports.

Sports	Source	Number of people	Age	Height (cm)	Weight (kg)	Sports years (years)
Football	Village 1	50	21.5	173.8	60.3	3.2
Basketball	Village 2	50	20.4	174.3	65.5	3.8
Aerobics	Village 3	50	20.8	166.4	50.4	3.4
Badminton	Village 4	50	21.2	170.7	53.4	2.8

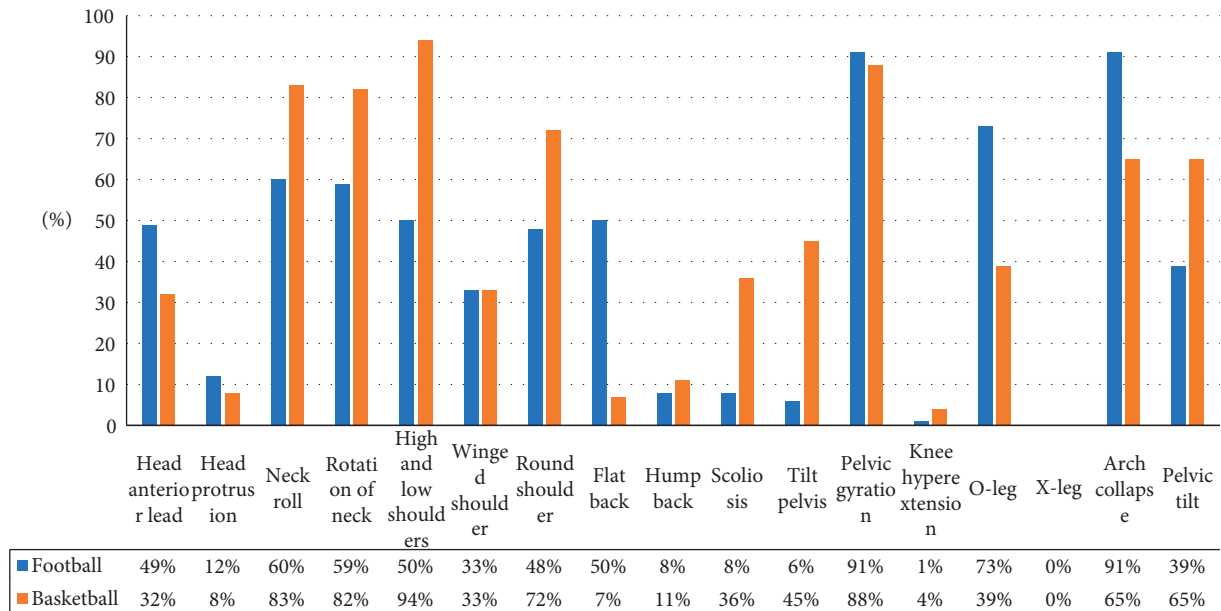


FIGURE 8: Total evaluation of abnormal posture results.

iterations. The simulation results confirm that the ABC-AFS-BP algorithm has better stability. The flexibility, fast convergence speed, and small error can largely avoid the problem of the BP neural network falling into local extreme value.

4.2. Simulation Experiment. We conducted a posture assessment of sports athletes from a certain team in rural areas. Because different sports have different power points, we selected football and basketball that consume more energy, as well as aerobics and badminton that consume relatively less energy. These 4 sports are taken as examples to study the effects of bad posture on the body in sports. We selected a total of 200 athletes. The experiment selected athletes whose gender, age, height, and weight were roughly the same, ignoring the influence of factors such as age, gender, and years of exercise on the athletes. The specific situation is shown in Table 6.

From the statistical data in Figure 8, we can conclude that bad postures in sports will have a certain impact on the athletes' bodies. Among them, more than 85% of athletes in football and basketball have the problem of pelvic rotation. The problem is more with football players; in 90% of the test sample, 60% of football players and basketball players have collapsed arches. Football players even reach 90% of the test sample, 77% of football players and 37% of basketball players have O-legs.

From the data in Figure 9, we can conclude that the main problems of aerobic athletes are flat backs and collapsed arches. More than 90% of badminton athletes have high and low shoulder problems, and more than 80% have neck problems. Serious body posture problems and wrong exercise posture can cause damage to the body, so in the daily training process, you should pay attention to these problems.

4.3. Comparative Experiment. To test the flexibility of the BP posture detection algorithm proposed in the article, we have compared it with the traditional motion posture recording method. We tested the accuracy of recorded motion, missed detection rate, and recording time. The experimental results are shown in Table 7 and Table 8.

From the data in Figures 10 and 11, we can conclude that the missed detection rate of the BP attitude detection algorithm is low, basically maintained at about 2.0, and the accuracy of recording actions is relatively high, generally maintained above 98%, with a maximum of 99.15%. The recording time is shorter, keeping it at 3-4 minutes; the missed detection rate of the traditional attitude detection algorithm is relatively high compared with the BP attitude detection algorithm, which is kept at 4-6, and the accuracy of action is lower than that of the BP attitude detection algorithm. It is generally maintained at about 95%, and the recording time is maintained at 5-6 minutes. The BP detection algorithm is faster and more efficient.

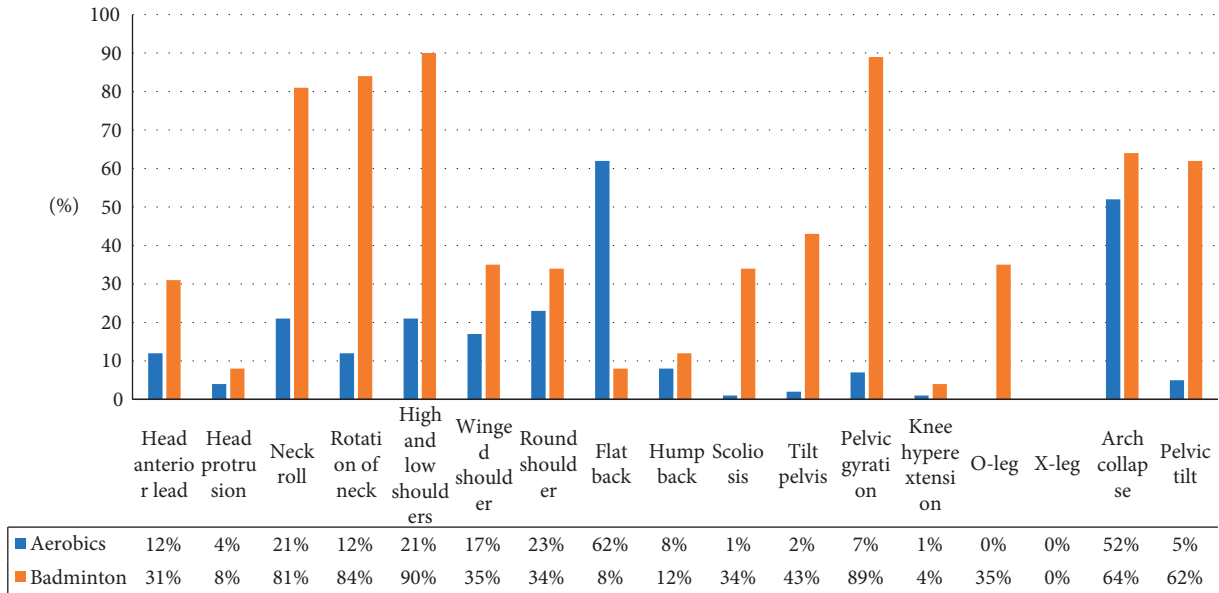


FIGURE 9: Total evaluation of abnormal posture results.

TABLE 7: BP attitude detection algorithm.

Target number	Goal 1	Goal 2	Goal 3	Goal 4	Goal 5	Goal 6	Goal 7	Goal 8
Total number of frames	752	752	752	752	752	752	752	752
Number of missed inspections	15	11	5	14	11	11	9	16
Missed detection rate (%)	2.0	1.5	0.7	1.9	1.5	1.5	1.2	2.1
Action accuracy	98.0%	98.6%	98.7%	98.6%	98.6%	98.9%	99.0%	99.15%
Recording time (minutes)	3.1	2.9	3.2	3.6	3.5	3.8	3.7	3.9

TABLE 8: Traditional pose detection algorithm.

Target number	Goal 1	Goal 2	Goal 3	Goal 4	Goal 5	Goal 6	Goal 7	Goal 8
Total number of frames	204	204	204	204	204	204	204	204
Number of missed inspections	9	11	12	10	13	8	7	9
Missed detection rate (%)	4.6	5.4	5.9	4.9	6.4	3.9	3.4	4.4
Action accuracy	95.0%	93.6%	94.7%	94.6%	93.6%	93.9%	94.0%	95.1%
Recording time (minutes)	5.1	5.3	5.5	5.4	5.5	5.7	5.9	5.8

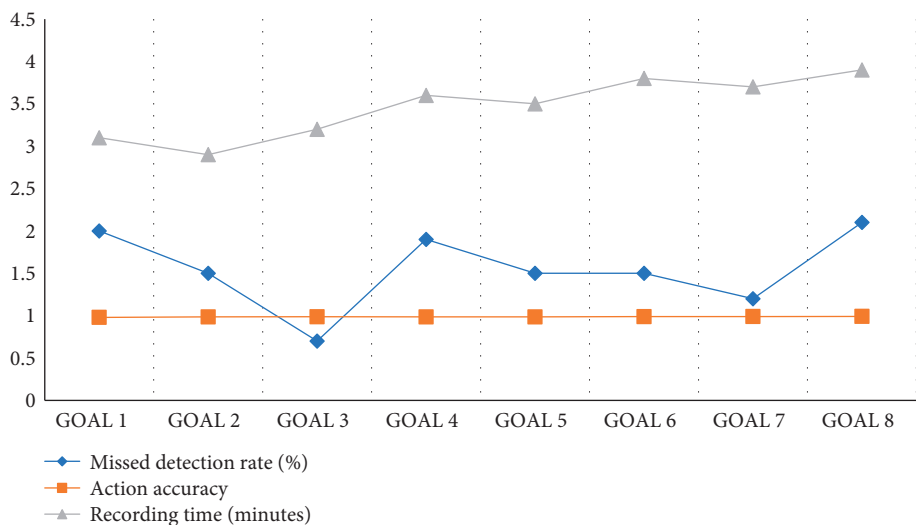


FIGURE 10: BP attitude efficiency graph.

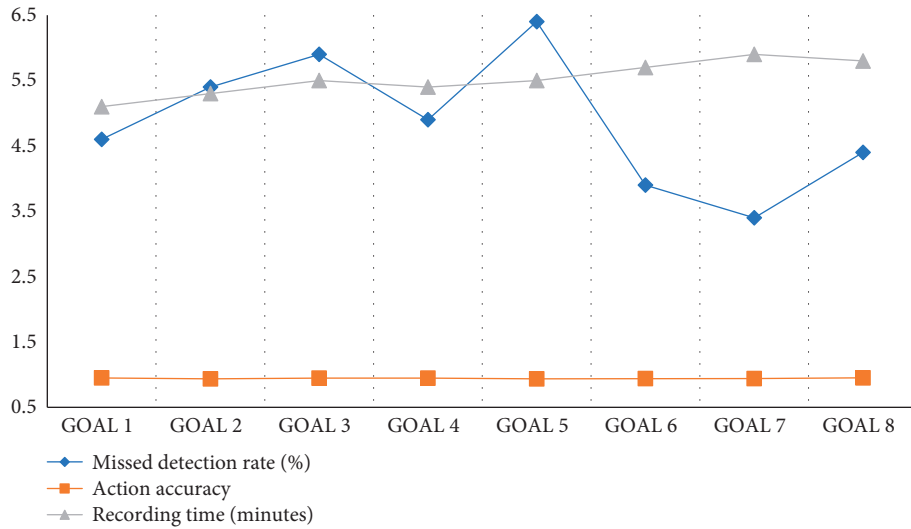


FIGURE 11: Traditional attitude efficiency graph.

5. Conclusion

The integrated development of urban and rural sports is the basic basis for the development of sports in China. Urban sports should promote the citizenization of migrant workers with its inclusiveness, and rural sports should attract urban residents to the countryside with its ecological nature, to meet the different needs of urban and rural residents for a better life. At this stage, focusing on creating rural ecological sports, promoting the two-way flow of urban and rural sports resources, then promoting the integrated development of urban and rural sports, and contributing to rural revitalization and the construction of new urbanization are the historical responsibility given to us by the new era. The model proposed in the article uses the powerful data processing, mining, and analysis functions of deep learning to train the massive data generated in competitive sports training and apply it to competitive sports training. It is committed to promoting the accuracy and analysis of competitive sports training. Refinement provides technical guidance for athletes' training, promotes the scientific and information development of competitive sports training in China, and provides some reference methods for the research and application of deep learning in competitive sports training. The human body poses that estimation has a good application prospect in sports analysis, but the truly appropriate matching method still needs to be adjusted according to specific data sets and specific applications. In addition, how to effectively use these data after getting the key points of the human body is also a question that requires in-depth thinking. The article only applies basic mathematical operations to get some simple metrics, which is relatively rough. There can be two directions for further research: one is to continue to improve the accuracy of key point extraction, the other is to fully tap the value of the obtained data, make full use of information to explain the actual needs of sports, and help athletes better improve their training.

Data Availability

The experimental data used to support the findings of this study are available from the corresponding author upon request.

Conflicts of Interest

The authors declare that they have no conflicts of interest regarding this work.

Acknowledgments

This work was sponsored in part by the Research Project of Humanities and Social Sciences of Chongqing Municipal Education Commission (20SKGH273) and the Research Project of Higher Education's Teaching Reform of Chongqing College of Humanities, Science and Technology (18CRKXJJG25).

References

- [1] K. E. A. Van de Sande, J. R. R. Uilings, T. Gevers, and A. W. M. Smeulders, "Smeulders.segmentation as selective search for object recognition," in *Proceedings of the IEEE Conference on International Conference on Computer Vision*, vol. 14, no. 8, pp. 1879–1886, Barcelona, Spain, November 2011.
- [2] K. He, X. Zhang, S. Ren, and J. Sun, "Spatial pyramid pooling in deep convolutional networks for visual recognition," *IEEE Transactions on Pattern Analysis and Machine Intelligence*, vol. 12, no. 3, pp. 1904–1916, 2015.
- [3] L. Zhang, "Research on human body movement posture based on inertial sensor," *International Journal Bioautomation*, vol. 22, no. 2, pp. 179–186, 2018.
- [4] A. D. Kuo and F. E. Zajac, "Human standing posture: multi-joint movement strategies based on biomechanical constraints," *Progress in Brain Research*, vol. 97, no. 7, pp. 297–349, 1993.

- [5] S. Wang, J. W. Dang, Y. P. Wang, and X. Du, "Research on real-time action recognition approach," *Computer Engineering and Applications*, vol. 53, no. 3, pp. 28–31, 2017.
- [6] R. Liu, J. Liu, and H. Liu, "Gesture feature extraction and recognition based on acceleration track," *Application Research of Computers*, vol. 34, no. 3, pp. 924–927, 2017.
- [7] W. Shen, K. Deng, X. Bai, T. Leyvand, B. Guo, and Z. Tu, "Exemplar-based human action pose correction," *IEEE Transactions on Cybernetics*, vol. 44, no. 7, pp. 1053–1066, 2014.
- [8] H. Wang and C. Schmid, "Action recognition with improved trajectories," in *Proceedings of the IEEE International Conference on Computer Vision*, no. 7, pp. 3551–3558, IEEE, Sydney, Australia, June 2014.
- [9] J. Zbontar and Y. Le Cun, "Stereo matching by training a convolutional neural network to compare image patches," *Journal of Machine Learning Research*, vol. 17, no. 1, pp. 2287–2318, 2015.
- [10] S. A. Haghpanah and F. Haghpanah, "Adaptive control of human posture in a specific movement[C]," in *Proceedings of the 2015 2nd international conference on knowledge-based engineering and innovation (KBEI)*, no. 23, pp. 78–91, IEEE, Tehran, Iran, November 2015.
- [11] L. I. Wen-Feng, W. U. Xiang, J. Sun et al., "Angle Algorithm of human body posture tracking based on accelerometer," *Journal of Hubei University of Technology*, no. 23, pp. 11–17, 2011.
- [12] M. A. Guoquan, J. Yang, S. Zhang et al., "Research on auxiliary judgment strategy about anti-doping based on performance profiling," *Journal of Capital University of Physical Education and Sports*, no. 27, pp. 47–58, 2014.
- [13] R. Molikova, M. Bezdickova, K. Langova et al., "The relationship between morphological indicators of human body and posture," *Biomedical papers*, vol. 150, no. 2, pp. 261–265, 2006.
- [14] S. W. Chang, N. J. Delleman, and M. Wang, "Approach strategy and working posture in manual hand tool operation," *Human Movement Science*, vol. 29, no. 2, pp. 228–242, 2010.
- [15] M. Kleiber, G. A. Horstmann, and V. Dietz, "Body sway stabilization in human posture," *Acta Oto-Laryngologica*, vol. 110, no. 3-4, pp. 168–174, 1990.
- [16] A. M. Ingram, "A study of the external forces and moments at the shoulder and elbow while performing every day tasks," *Clinical Biomechanics*, vol. 19, no. 6, pp. 586–594, 2004.
- [17] K. Willimczir, *Biomechanik Der Sportarten*, Rowohlt Taschenbuch Verlag GmbH, no. 20, Hamburg, Germany, 1989.
- [18] A. Cappozzo, T. Leo, and A. Pedotti, "A general computational method for the analysis of human locomotion," *Journal of Biomechanics*, vol. 8, pp. 307–320, 1975.
- [19] X. Ning, P. Duan, W. Li, and S. Zhang, "Real-time 3D face alignment using an encoder-decoder network with an efficient deconvolution layer," *IEEE Signal Processing Letters*, vol. 27, pp. 1944–1948, 2020.
- [20] X. Ning, K. Gong, W. Li, and L. Zhang, "JWSAA: joint weak saliency and attention aware for person re-identification," *Neurocomputing*, vol. 453, pp. 801–811, 2021.
- [21] W. Cai, D. Liu, X. Ning, C. Wang, and G. Xie, "Voxel-based three-view hybrid parallel network for 3D object classification," *Displays*, vol. 69, no. 1, 2021.
- [22] S. Han, W. Tao, X. Wu, X.-c. Tai, and T. Wang, "Fast image segmentation based on multilevel banded closed-form method," *Pattern Recognition Letters*, vol. 31, no. 3, pp. 216–225, 2010.
- [23] X. Ji and H. Liu, "Advances in view-invariant human motion analysis: a review," *Systems Man & Cybernetics Part C Applications & Reviews IEEE Transactions*, vol. 40, no. 1, pp. 13–24, 2010.
- [24] A. Mohan, C. Papageorgiou, and T. Poggio, "Example-based object detection in images by components," *IEEE Transactions on Pattern Analysis and Machine Intelligence*, vol. 23, no. 4, pp. 349–361, 2001.
- [25] R. Ronfard, C. Schmid, and B. Triggs, "Learning to parse pictures of people," *Lecture Notes in Computer Science*, vol. 2353, no. 6, pp. 700–714, 2002.
- [26] V. Ferrari, M. J. Marín-Jiménez, and A. Zisserman, "Pose search: retrieving people using their pose," in *Proceedings of the IEEE Conference on Computer Vision and Pattern Recognition*, no. 3, pp. 1–8, Miami, FL, USA, June 2009.
- [27] M. Gorlatova, J. Sarik, G. Grebla, M. Cong, I. Kymissis, and G. Zussman, "Movers and shakers: kinetic energy harvesting for the internet of things," *IEEE Journal on Selected Areas in Communications*, vol. 33, no. 8, p. 1, 2015.

Research Article

Research on Financial Risk Prediction Based on Improved Random Subspace

Yinghui Li 

Henan Finance University, Zhengzhou 450046, China

Correspondence should be addressed to Yinghui Li; liyingshui@hafu.edu.cn

Received 8 November 2021; Revised 9 December 2021; Accepted 7 January 2022; Published 4 March 2022

Academic Editor: Man Fai Leung

Copyright © 2022 Yinghui Li. This is an open access article distributed under the Creative Commons Attribution License, which permits unrestricted use, distribution, and reproduction in any medium, provided the original work is properly cited.

In order to provide timely and effective information and decision support for financial market entities, combined with random subspace and weight fused Lasso, this paper constructs a financial risk prediction model based on the improved random subspace method. Firstly, the basic principles of random subspace and SVM algorithm are introduced. Then, WFL and AI methods are introduced to improve random subspace, so as to reduce the dimension of multisource heterogeneous data and realize the adaptive fusion of features. Then, a financial risk prediction model based on weighted fusion adaptive random subspace is constructed, in which SVM is used as the basic classifier and the output strategy of result integration is introduced. Finally, based on the data of some listed companies, the improved random subspace method is compared with other methods. The results show that the improved random subspace method has a higher prediction value, which indicates that the method is reasonable and effective in financial risk prediction. In the improved random subspace method, combined feature $F1 + F2 + F3$ is better than other methods in $T-3$, $T-4$, and $T-5$, and the prediction value is more than 95%, which fully demonstrates the rationality of the improved random subspace method in financial risk prediction. The area under the ROC curve (AUC) predicted by weight fused adaptive integration-based random subspace (FAIB_RS) method is about 95% in $T-3$, 93% in $T-4$, and 95.5% in $T-5$, which is obviously higher than that of the other eight methods.

1. Introduction

With the rapid development of the financial industry and the continuous popularization of the internet financial model, the financial market is facing more severe financial risks. In order to improve the ability of financial market subjects to obtain financial risk early warning information, domestic experts and scholars have done a lot of research on financial risk and put forward a variety of financial risk prediction methods. For example, literature [1] used RBF network model to establish Jiangsu Province's financial risk early warning model and predicted the regional total risk in 2019 with the sample set in 2018, so as to obtain the prevention and treatment suggestions of Jiangsu Province's financial risk. Literature [2] constructed the regional financial risk index; evaluated and predicted the financial risk of 31 provinces, cities, and autonomous regions (excluding Hong Kong, Macao, and Taiwan) in China; and concluded that the overall financial risk of China and the 6

regions showed a synchronous trend of change and got the enlightenment of formulating preventive measures. According to the current situation of financial development, literature [3] proposed a multifactor international supply chain financial risk prediction model including external environmental risk factors, obtained the structural characteristics and formation mechanism of international supply chain financial risk system, and put forward countermeasures and suggestions. Most of the above studies are based on a single data source, and the prediction accuracy is low; the effect is not good. Therefore, combined with the financial risk prediction problem, this paper constructs a new weighted fusion adaptive stochastic subspace financial risk prediction method and verifies the rationality and effectiveness of the method. Literature [4] shows that the data of compliant financial activities are of high quality and quantity in all aspects. On the contrary, the data of informal financial activities are of low quality. Therefore, the machine learning method based on

single-source data can only detect the risks of formal financial activities, while the effect of using multisource data to detect financial risks is not good. Then, TSAIB_RS method is proposed to integrate various data adaptively. Literature [5] makes quarterly observations from 225,813 company samples. After investigation, it is found that financial system risks play a great role in predicting the failure of an enterprise when its internal financial sector fluctuates greatly; its scale is small; and its debts are large. Although the integration of classifiers in reference [6] has been applied in the financial industry, there are also some wrong factors that hinder the prediction performance, such as irrelevant features, inclined categories, and so on. In the event of such an error, the cost of the wrong classification is far greater than the cost associated with the non-default or non-insolvency (negative) category. In the future, we need to deeply study the potential relationship between classifier ensemble and positive sample type. In today's "big data" era [7], big data has been gradually integrated with finance and become the core of the financial industry. How to make good use of big data to effectively predict and prevent is of great significance to the financial industry, which is also the essence of financial management, that is, risk management and control. Combined with the advantages of big data prevention and control and prediction, this paper summarizes feasible and effective financial risk management and control countermeasures.

The reasoning method based on belief rule in reference [8] is widely used in risk assessment of research and development (R&D) projects. Because there are many risk factors in the performance evaluation of R&D projects, the BRB method will produce a rule base. Therefore, the stochastic subspace BRB model has been experimented and applied as a new RS-BRB model. It constructs several subspaces from sampling; then develops BRB subsystems according to the subspaces, thus obtaining results; and finally carries out combination mode according to different subsystem results. The traditional forecasting model can no longer meet the current forecasting needs [9], and then researchers put forward a method called RS-multiple boosting to improve the accuracy of forecasting credit risk. This method is a combination of two classical integrated ML methods: random subspace (RS) and multiple boosting. There are many methods for risk assessment and prediction in the financial market, but most of the above studies are based on a single data source, with low prediction accuracy and poor results. The random subspace method can be used for portfolio selection in different data sets, which shows that it is essentially superior to the traditional bagging-based resampling portfolio. In order to solve the problem of single information source, less data application, low prediction accuracy, and poor prediction accuracy of financial risk prediction at present. In this study, a financial risk prediction method based on the adaptive fusion of multisource heterogeneous data is constructed for the financial risk of listed companies and the default risk of individual borrowers, and its effectiveness is verified by using various types of real data sets collected from online platforms. It has a good effect on the prediction effect and accuracy and can solve the problems existing in the financial system. In view of the current

financial data with heterogeneous, redundant, and other issues, the current prediction model in the multisource heterogeneous data prediction is not very satisfactory. This paper proposes a financial risk prediction method based on the adaptive fusion of multisource heterogeneous data, which can effectively predict the multisource data of financial companies and improve the prediction accuracy. In this paper, the problems of financial risk prediction are introduced in detail; then, a financial risk prediction method WFAIB_RS based on the weighted fusion of adaptive random subspace is constructed; finally, through the experimental comparison of the data sets of listed companies, WFAIB_RS has a better prediction effect.

2. Introduction to Basic Methods

2.1. Random Subspace Brief Introduction of Algorithm. Random subspace [10, 11] (RS) is a kind of ensemble learning. Random subspace trains each classifier by using random partial features instead of all features to reduce the correlation between each classifier. Therefore, this method is very suitable for learning tasks with high feature dimensions. The RS steps are as follows:

Step1: according to the feature dimension of data samples, data samples are randomly selected to form data subsets of similar sizes. The subspace ratio parameter r is used to adjust the size of the data subset.

Step2: the sampled data subsets are input into the base classifier and trained.

Step3: finally, according to the training results, the sample results are fused.

2.2. SVM Classification Principle. Using SVM [12] as the base classifier can be solved according to the following objective function:

$$\begin{aligned} s.t. & y_i(\omega^T \varphi(x_i) + b) \geq 1 - \xi_i, \quad i = 1, 2, \dots, n, \\ & \zeta_i, \quad (1) \\ \min_{\omega, b} & = \frac{1}{2} \|\omega\|^2 + C \sum_{i=1}^n \end{aligned}$$

where C is the normal vector, C is the penalty coefficient, B is the displacement term, and C is the non-negative relaxation factor.

The above problem is transformed into a dual problem:

$$\begin{aligned} s.t. & \sum_{i=1}^n a_i y_i = 0, \quad 0 < a_i < C, \quad i = 1, 2, \dots, n, \\ & (2) \\ \max_a & \sum_{i=1}^n a_i - \frac{1}{2} \sum_{i=1}^n \sum_{j=1}^n a_i a_j y_i y_j \varphi(x_i)^T \varphi(x_j). \end{aligned}$$

In the calculation process of dual problem, through the calculation of $\varphi(x_i)^T \varphi(x_j)$, which is mainly the inner product operation after the sum of pairs. Then the inner product operation is input into the kernel function. The expression of the kernel function is as follows:

$$k(x_i, x_j) = \varphi(x_i)^T \varphi(x_j). \quad (3)$$

The final decision function is obtained:

$$y(x) = \text{sign} \left(\sum_{i=1}^n a_i y_i k(x_i, x_j) \right) + b, \quad (4)$$

where a_i and b are constant real numbers; $a_i > 0$. The kernel function $k(i, j)$ using radial basis function kernel function is defined as follows:

$$k(x_i, x_j) = \exp \left(-\gamma \|x_i - x_j\|^2 \right). \quad (5)$$

$$s_{ij} = \text{sgn}(p_{ij}) = \begin{cases} +1, & p_{ij} > 0 \\ -1, & p_{ij} < 0 \end{cases},$$

$$a_{ij} = \frac{p_{ij}}{1 - p_{ij}},$$

$$\beta^* = \arg_{\beta} \min \left\{ \frac{1}{2} \left\| y - \sum_{i=1}^p x_i \beta_i \right\|_2^2 + \lambda |\beta_i| + \frac{\lambda_2}{p} \sum_{i < j} a_{ij} (\beta_i - s_{ij} \beta_j)^2 \right\}. \quad (6)$$

Here, $\lambda_2/p \sum_{i < j} a_{ij} (\beta_i - s_{ij} \beta_j)^2$ is the penalty term added based on the Lasso model, p_{ij} is the correlation coefficient between any two features x_i and x_j , and λ_2 represents the regular penalty parameter, which mainly adjusts the penalty intensity for feature correlation.

2.3. Random Subspace Algorithm Improvement. In order to ensure the accuracy of financial risk prediction and the problem of multisource heterogeneous financial data, the random subspace algorithm needs to be improved first. Therefore, there is a need for multisource heterogeneous data fusion in financial risk prediction data. Based on the Lasso model, the weighted fusion adaptive stochastic subspace model (WFAIB_RS) is introduced for the adaptive fusion of multisource heterogeneous data features. The Lasso model takes the form of

The WFL model can effectively solve the multicollinearity problem between features and improve the stability of the model. After the Lasso model is introduced into WFL, the model form is as follows:

$$\beta^* = \arg_{\beta} \min \left\{ \frac{1}{2} \left\| y - \sum_{i=1}^p x_i \beta_i \right\|_2^2 + \lambda w_i^{(1)} |\beta_i| + \frac{\lambda_2}{p} \sum_{i < j} a_{ij} (\beta_i - s_{ij} \beta_j)^2 \right\}. \quad (7)$$

Here, $w_i^{(1)}$ represents the adaptive weight, which can be added to the WFAL model to obtain a more accurate feature subset; $1/\sqrt{n}$ denotes the smoothing item. λ with the increasing of parameters, more feature weights are 0. As the regular penalty parameter λ_2 becomes larger, more features will be regarded as related features.

The adaptive feature weights $W = (w_1, w_2, \dots, w_p)^T \in R_+^p$ based on weighted fusion are obtained by WFAL model estimation, and then the features are sampled according to the weights, and the data subsets $\{D_{\text{sub}}^1, D_{\text{sub}}^2, \dots, D_{\text{sub}}^M\}$ and $D_{\text{sub}}^i = \{(x_1^i, y_1^i), \dots, (x_j^i, y_j^i), \dots, (x_{p_i}^i, y_{p_i}^i)\}$ that can be used for base classifier training are obtained. The sampling process is mainly adjusted by subspace ratio parameters. The larger the r , the higher the feature dimension of the obtained sample subset.

3. Construction of Financial Risk Prediction Model

3.1. Financial Risk Forecasting Process. Set $D_{\text{train}} = \{(x_1, y_1), \dots, (x_i, y_i), \dots, (x_n, y_n)\}^T$ and test set

$D_{\text{test}} = \{(x_1, y_1), \dots, (x_i, y_i), \dots, (x_n, y_n)\}$. Firstly, Lasso estimation is carried out on the data to obtain the adaptive weight, specifically as follows:

$$w_i^{(1)} = \frac{1}{|\beta_{i\text{Lasso}} + 1/\sqrt{n}|}. \quad (8)$$

Secondly, the adaptive weight is used to estimate the data by WFAL to obtain the feature weight vector $W = (w_1, w_2, \dots, w_p)^T \in R_+^p$.

Thirdly, the feature weight is taken as the sampling probability, and the sampling $\{D_{\text{sub}}^1, D_{\text{sub}}^2, \dots, D_{\text{sub}}^M\}$ of data subset is carried out under the adjustment of subspace ratio r .

Fourthly, the base classifier is trained according to the sampled data subset. Fifthly, according to the rules of evidential reasoning, the prediction results of the base classifier are synthesized to get the final prediction results.

3.2. Base Classifier. Support vector machine (SVM) is selected as the base classifier [13–15]. This method is a typical

classification algorithm, and its characteristic is that it can solve high-dimensional and non-linear classification problems by using the principle of structural risk minimization and can efficiently classify data samples with few samples and high feature dimensions [16, 17]. Therefore, SVM is chosen as the base classifier of the financial risk prediction model.

3.3. Integration Strategy. In the result fusion, evidential reasoning is used as a new ensemble strategy to synthesize the results produced by different base classifiers. Evidential

reasoning is to treat the classification results of different base classifiers as evidence and the accuracy as evidence reliability and initial weight when fusing the results of base classifiers and finally fuse the results by continuous optimization [18, 19].

Firstly, all the classification results are regarded as a set of mutually exclusive identification frames, which can constitute a complete set, and are designated as Θ . The results produced by the base classifier s can then be converted into the following evidence:

$$e_s = \left\{ (y_j, p_{y_j, s}) \mid j = 1, 2, \dots, N, \sum_{j=1}^n p_{y_j, s} = 1 \right\}, \quad s = 1, 2, \dots, S, \quad (9)$$

where e_s represents the evidence of transformation from the classification results obtained from the s -th base classifier and $p_{y_j, s}$ denotes the probability that the classification result goes to y_j .

In the process of evidential reasoning, weight W and reliability R are often used to define the reliability distribution function, which is mainly to ensure that the result information of the base classifier does not conflict. The expression of the reliability distribution function is as follows:

$$m_s = \left\{ (y_j, \tilde{m}_{j, s}); (P(\Theta), \tilde{m}_{P(\Theta), s}) \right\}. \quad (10)$$

Here, $\tilde{m}_{j, s}$ represents the holding degree of evidence e_s considering reliability and weight to y_j , which is defined as follows:

$$\tilde{m}_{y_j, s} = \begin{cases} 0, & y_j = \Phi, \\ c_{r\omega, s} m_{y_j, s}, & y_j \in \Theta, y_j \neq \Phi, \\ c_{r\omega, s} (1 - r_s), & y_j \in P(\Theta), \end{cases} \quad (11)$$

where $m_{y_j, s} = \omega_s p_{y_j, s}$, $c_{r\omega, s} = 1/(1 + \omega_s - r_s)$ is the normalization factor.

Secondly, by fusing S pieces of evidence e_1, e_2, \dots, e_n provided by different base classifiers, the reliability function $p_{y_j, e(s)}$ of S pieces of evidence jointly supporting y_j is obtained, and the expression of reliability function $p_{y_j, e(s)}$ is as follows:

$$\begin{aligned} \hat{m}_{y_j, e(s)} &= \left[(1 - r_s) \hat{m}_{y_j, e(s-1)} + m_{P(\Theta), e(s-1)} m_{y_j, s} \right] \\ &+ \sum_{B \cap C = D_j} m_{B, e(s-1)} m_{C, s}, \quad \forall y_j \in \Theta, \\ P_{y_j, e(s)} &= \begin{cases} 0, & y_j = \Phi \\ \frac{\hat{m}_{y_j, e(s)}}{\sum_{y_j \in \Theta} \hat{m}_{y_j, e(s)}}, & y_j \in \Theta, y_j \neq \Phi \end{cases} \end{aligned} \quad (12)$$

After evidential reasoning, the fusion result of the base classifier is the category corresponding to the maximum $p_{y_j, e(s)}$ value of the final classification result of $\{(y_j, p_{y_j, e(s)}), j = 1, 2, \dots, N\}$ model.

Finally, this paper takes different classification results as evidence, takes accuracy as the reliability and initial weight of evidence, and then obtains the optimization weight of the base classifier through repeated optimization.

The training model is as follows:

$$\left\{ \min \varepsilon = \frac{1}{m} \sum_{i=1}^m d_E(u_i - v_i)^2, 0 \leq \omega_s \leq 1, \quad s = 1, 2, \dots, S, \right. \quad (13)$$

where m represents the amount of data in the training set; u_i represents the distribution of true classification results, and v_i represents the probability distribution of base classifier results on different categories after synthesis.

4. Experimental Verification

In this paper, the improved random subspace method is used to predict the financial risk of listed companies. The experimental flow chart is shown in Figure 1.

4.1. Experimental Data Set and Model Evaluation Indicators.

In this study, 1,726 listed companies in China were used as experimental samples, and 1,597 normal samples and 129 risk samples were obtained according to ST markers. The time panel for collecting experimental data of risk samples is divided into 3 years ahead of schedule, 4 years ahead of schedule, and 5 years ahead of schedule, which are expressed by $T-3$, $T-4$, and $T-5$, and the time span is 5 years from 2016 to 2020. The specific distribution is 14 in 2016, 27 in 2017, 22 in 2018, and 32 in 2019.

The experimental data set consists of 39 financial features, 12 emotional features, and qualitative text features, which are represented by $F1$, $F2$, and $F3$, respectively.

In the experimental process of financial risk prediction of listed companies, we mainly adopt four evaluation criteria: average accuracy (AA), type I error, type II error, and

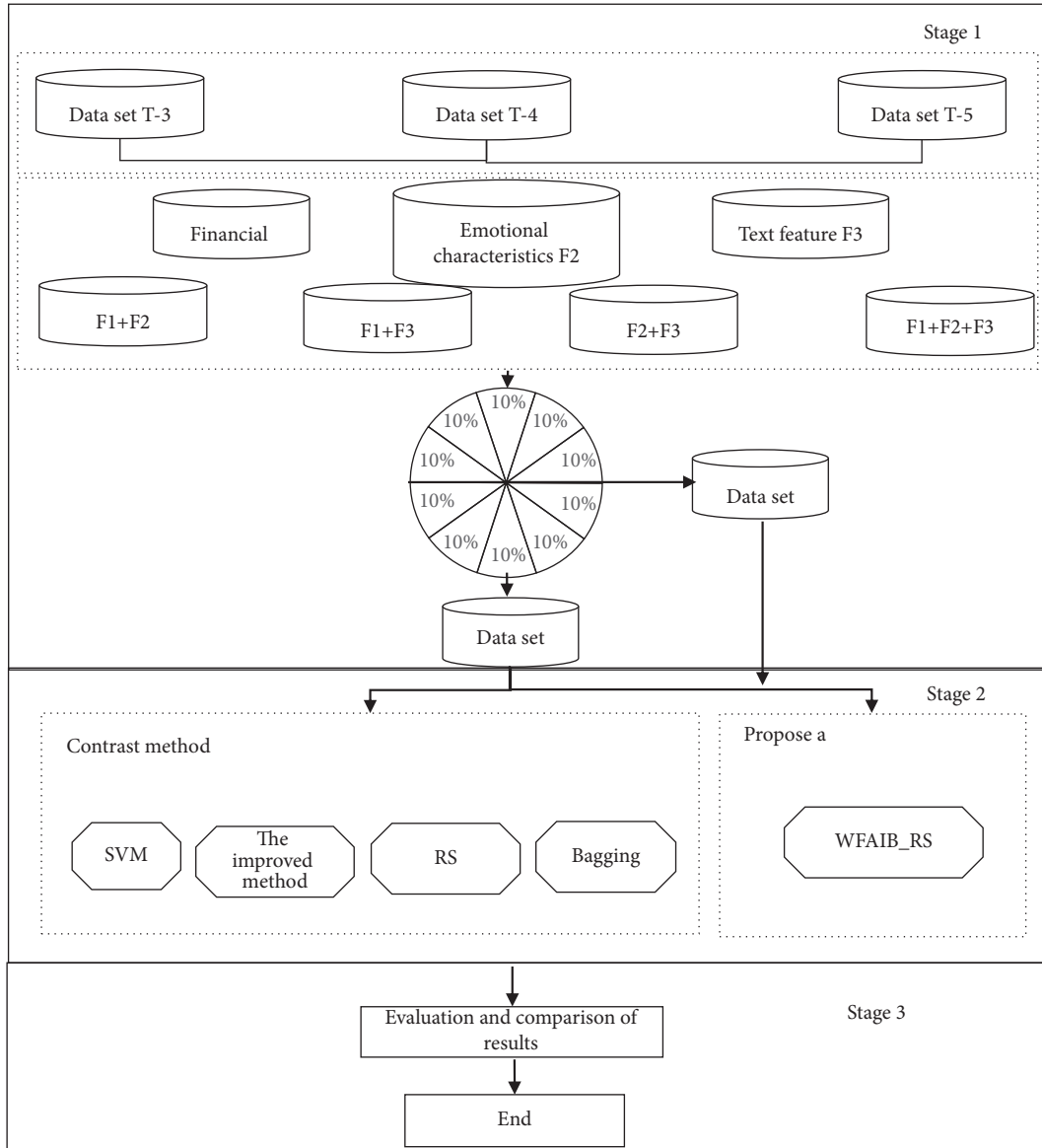


FIGURE 1: Experimental flow chart.

AUC [20, 21] (the area under the ROC curve). The main classification results are true positive (TP), true negative (TN), false positive (FP), and false negative (FN). The calculation formula of specific indicators is as follows.

$$\begin{aligned} \text{Type II Error} &= \frac{FN}{TP + FN}, \\ \text{Type I Error} &= \frac{FP}{FP + TN}, \end{aligned} \quad (14)$$

$$\text{Average Accuracy} = \frac{TP + TN}{TP + FP + FN + TN}.$$

AUC is the area below the ROC curve, which is usually between 0 and 1. ROC is a curve in two-dimensional coordinates, and its horizontal axis is false positive case rate, and its vertical axis is true case rate.

4.2. Comparison Methods. In this paper, the base classifier, three ensemble learning methods, and unbalanced classification methods are used as comparison methods. Therefore, the comparison methods in this paper include SVM, bagging, RS, and the improved random subspace method.

In this experiment, the stability of the experimental results is verified by the cross method of tenfolds and ten times.

The specific steps are as follows.

- (1) Dividing the data set into 10 data with the same size and scale on average; 1 of them is used as the test set, and the other 9 are used as the training set. In the process of training, each fold should be repeatedly trained 10 times. The average value of 100 experimental results obtained after training is calculated, and the final result is obtained.

TABLE 1: Experimental results under different characteristics, different methods, and different time panels for evaluation indexes AA and AUC.

Characteristic Method	F1		F2		F3		F1 + F2		F1 + F3		F2 + F3		E1 + F2 + F3	
	AA	AUC	AA	AUC	AA	AUC	AA	AUC	AA	AUC	AA	AUC	AA	AUC
SVM	76.33	81.40	62.60	60.12	74.50	74.62	79.55	85.18	77.64	84.27	77.15	81.67	80.80	84.83
Bagging	92.87	92.13	89.65	71.32	91.39	81.61	93.22	93.31	93.79	92.84	93.20	83.80	95.27	92.99
RS	92.71	91.83	90.69	69.17	91.43	80.78	93.76	93.85	93.13	92.90	92.86	89.39	95.10	93.02
WEAIB_RS	92.79	82.94	90.69	68.76	93.61	93.09	92.99	84.22	94.78	93.70	95.05	93.93	96.39	95.24
SVM	76.72	82.53	62.83	60.33	74.61	77.04	77.67	84.91	77.76	85.63	77.49	81.70	80.75	86.47
Bagging	92.83	87.95	89.79	76.80	91.50	82.33	92.91	91.59	93.29	92.70	94.40	85.77	95.91	93.04
RS	92.60	85.27	90.84	75.24	91.58	81.33	93.03	91.33	94.89	93.91	93.40	87.67	95.59	94.04
WFAIB_RS	92.92	83.22	90.78	74.74	94.53	84.91	92.92	85.28	95.59	94.12	94.37	88.53	96.77	94.30
SVM	75.58	8008	62.66	60.29	75.83	78.87	76.55	83.21	77.91	86.00	78.27	83.06	81.46	88.24
Bagging	92.73	87.86	89.70	74.58	92.06	82.95	93.87	92.64	95.13	94.22	94.42	87.11	96.67	94.36
RS	92.65	88.45	90.79	73.64	91.75	82.62	93.29	92.61	95.85	95.05	95.37	92.25	96.55	95.26
WFAIB_RS	92.66	83.16	90.84	75.04	95.79	93.96	93.69	86.34	96.17	95.45	96.03	94.30	97.67	95.91

During the experiment, the ratio of random subspace increased from 0.1 to 0.9 according to the increase of 0.1. The setting ratios of misdivision cost for positive and negative cases are 1,726/129 and 1,726/1,597, respectively. The regularization parameters are 0.001, 0.01, 0.1, 1 and 10, respectively. The regularization parameter λ_2 is optimized by cross-validation.

4.3. Experimental Results. It works with different characteristics, different methods, and different time panels, and the experimental results are shown in Table 1. The bold data in Table 1 is the highest value of this feature.

It can be seen from the bold data in Table 1 that the improved random subspace method has achieved excellent results compared with other methods in this experiment. In the AA index, the improved random subspace method achieves good results on higher dimensional feature sets $F3$, $F1 + F3$, $F2 + F3$, and $F1 + F2 + F3$. In $T - 3$, the values of the improved random subspace method are 93.61%, 94.78%, and 96.39%. In $T - 4$, the values of this method are 94.53%, 95.59%, and 96.77%. In $T - 5$, the values of this method are 95.79%, 96.17%, and 96.67%. The comparison analysis shows that the improved random subspace method has achieved the highest results in financial risk prediction among all methods, especially in the feature set of $F1 + F2 + F3$ under the time panel $T - 5$, which has achieved an average rate of 97.67%.

In the AUC index, the improved random subspace method also achieves good results, especially in the feature set $F1 + F2 + F3$; for example, the value of $T - 3$ is 95.24%. The value in $T - 4$ was 94.3%. The value of $T - 5$ was 95.91%, which was higher than that of other eight methods. Therefore, the improved random subspace method is very suitable for financial risk prediction.

From the bold data in Table 2, it can be seen that the improved random subspace method can balance the two types of error rates of type I error and type II error, which shows that this method can effectively deal with both high-dimensional problems and unbalanced problems in financial risk prediction. Among them, the error rate of type II error is

higher than that of type I error as a whole. The main reason is that the data distribution is uneven, and there are few samples in a few classes, which leads to insufficient training. Therefore, the data of a few samples are easy to be misclassified in prediction.

4.4. Analysis of Experimental Results

4.4.1. Analysis of Prediction Results of Different Feature Sets. According to the above experimental results, this paper will compare and analyze the prediction results of different features and different time panels. The comparison results of features under $T - 3$, $T - 4$, and $T - 5$ time panels are shown in Figure 2.

It can be seen from the figure that in a single feature, the performance of $F1$ is relatively stable, the prediction performance of $F2$ is relatively weak, and the prediction effect of $F3$ is obviously better than that of $F2$. This result shows that financial features play the strongest role in the financial risk prediction of listed companies and are in a leading position. Compared with the single features $F1$, $F2$, and $F3$ and the combination features $F1 + F2$, $F1 + F3$, $F2 + F3$, and $F1 + F2 + F3$, the combination feature $F1 + F2 + F3$ is better than the single feature. In the improved random subspace method, combined feature $F1 + F2 + F3$ is better than other methods in $T - 3$, $T - 4$, and $T - 5$, and the prediction value is more than 95%, which fully demonstrates the rationality of the improved random subspace method in financial risk prediction.

4.4.2. Analysis of Prediction Results by Different Methods. According to the prediction results of AUC by different methods, the effectiveness of the improved random subspace method in financial risk prediction is shown in Figure 3 for the prediction results of AUC of $T - 3$, $T - 4$, and $T - 5$.

As can be seen from Figure 3, among the combined features $F1 + F2 + F3$, the AUC predicted by the improved random subspace method is the highest, and the AUC predicted by FAIB_RS method is about 95% in $T - 3$, 93% in $T - 4$, and 95.5% in $T - 5$, which is obviously higher than that

TABLE 2: Experimental results of type I error and type II error under different characteristics, different methods, and different time panels.

Characteristic Method	F1		F2		F3		F1 + F2		F2 + F3		F2 + F3		F1 + F2 + F3	
	I	II	I	II	I	II	I	II	I	II	I	II	I	II
SVM	22.67	36.05	36.00	54.73	24.51	37.76	19.38	33.70	21.66	31.03	22.15	31.52	18.26	30.84
Bagging	6.64	13.20	8.13	37.83	7.25	25.69	6.03	16.06	4.17	18.22	6.37	12.12	3.72	17.23
RS	6.31	19.42	8.09	24.41	7.33	23.92	6.01	9.09	5.16	28.04	6.04	20.76	4.01	15.92
WFAIB_RS	6.28	18.72	8.09	24.41	5.21	21.00	6.16	17.53	3.84	22.30	3.73	20.05	5.17	9.06
SVM	22.71	30.34	35.81	54.01	24.28	39.13	2136	34.34	2164	29.67	21.92	29.81	18.62	27.05
Bagging	6.71	12.86	8.01	37.45	6.90	28.31	6.23	17.74	5.82	17.73	5.26	9.81	2.86	1932
RS	6.46	19.04	7.92	24.51	7.14	24.27	6.42	13.78	4.39	14.02	5.86	15.76	3.58	1469
WFAIB_RS	6.24	17.48	8.01	24.20	4.96	11.78	6.51	14.14	11.84	4.76	4.76	13.72	2.79	8.68
SVM	23.41	36.92	35.99	54.05	23.59	31.35	22.69	32.86	21.55	28.78	20.92	31.76	18.03	24.85
Bagging	6.51	16.68	8.02	38.53	6.73	22.92	5.34	15.91	3.90	16.88	5.24	9.79	2.68	11.38
RS	6.45	18.49	7.98	24.44	7.08	22.73	6.26	12.28	3.61	10.84	4.33	8.34	3.02	8.77
WFAIB_RS	6.43	18.61	7.86	25.25	3.92	7.80	5.47	16.71	3.32	10.14	3.64	8.06	1.92	7.41

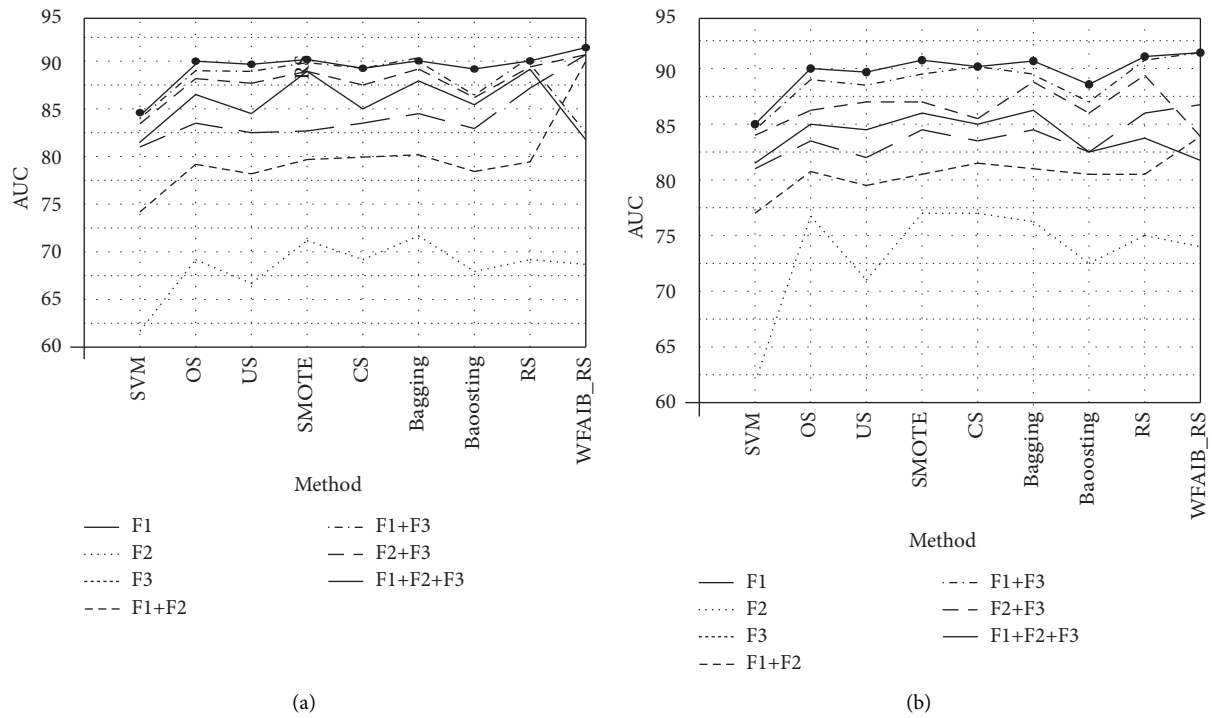
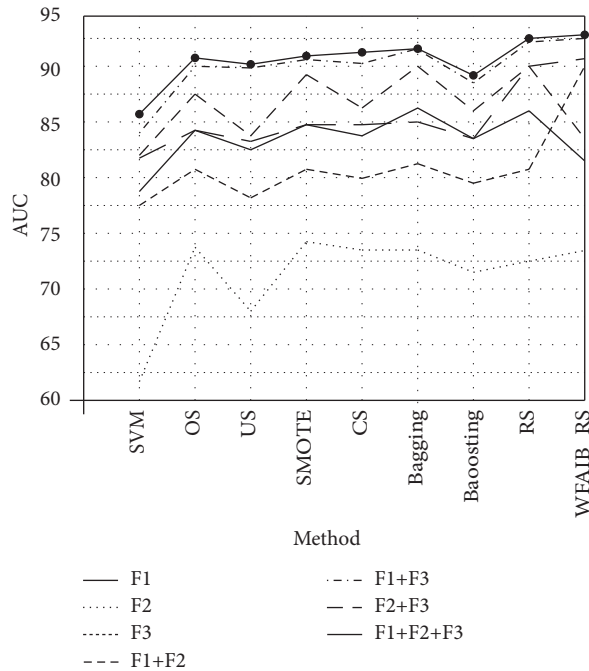
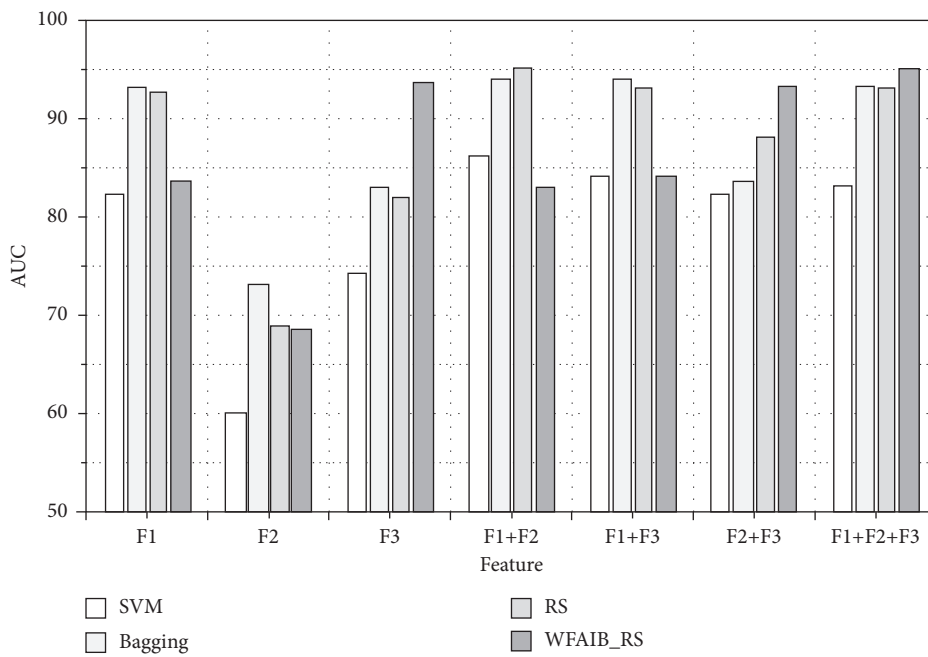


FIGURE 2: Continued.



(c)

FIGURE 2: Feature comparison results under $T-3$, $T-4$, and $T-5$ time panels: (a) $T-3$ time panels, (b) $T-4$ time panels, and (c) $T-5$ time panels.



(a)

FIGURE 3: Continued.

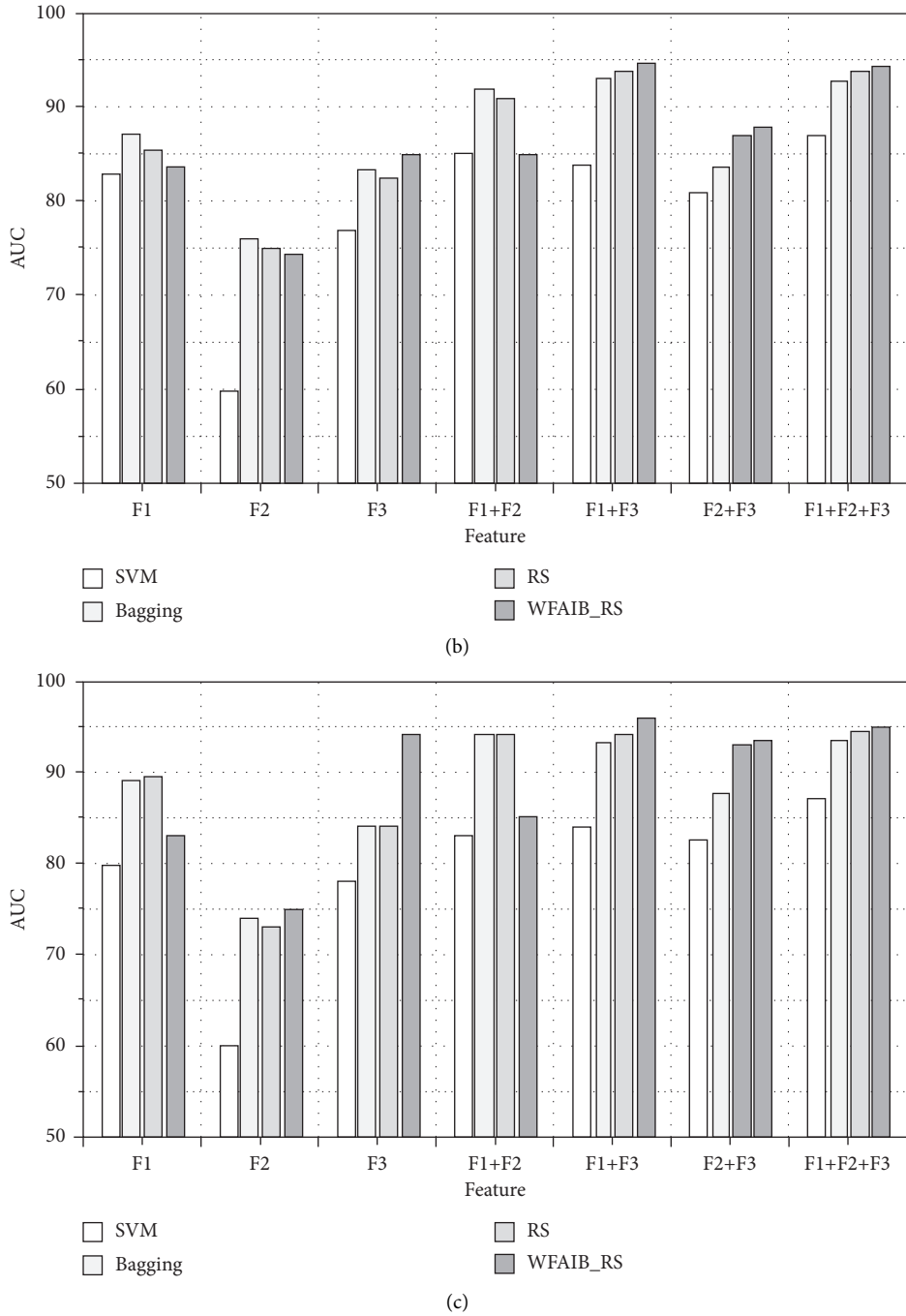


FIGURE 3: AUC prediction results of $T-3$, $T-4$, and $T-5$: (a) AUC of $T-3$, (b) AUC of $T-4$, and (c) AUC of $T-5$.

of the other eight methods. The possible reason why these methods improve the sum of $F2$ is that compared with financial features and text features, $F2$ has smaller feature dimensions and contains less prediction information, while SVM and bagging methods can effectively supplement samples, thus playing a good role in strengthening $F2$. Therefore, it shows that the improved random subspace method is effective in financial risk prediction and can predict financial risk more accurately.

5. Conclusion

In this paper, a new financial risk prediction method, the improved stochastic subspace method, is constructed. Firstly, multisource heterogeneous features are extracted based on multisource data sets, including quantitative financial features and emotional features and text features based on qualitative text information. Secondly, the advantages of the stochastic subspace method are fully

absorbed in the model construction, and it is taken as the model foundation. At the same time, a new adaptive fusion method considering the relationship between features is obtained by introducing the regularized sparse model to integrate adaptive and weighted feature fusion strategies into the stochastic subspace method.

In order to verify the effectiveness of the proposed method, an experiment is carried out on the real data set of Chinese listed companies, and different characteristics and different methods are compared in the experiment. Finally, through the analysis of the experimental results, the effectiveness and stability of the proposed method in the financial risk prediction of listed companies are fully demonstrated. The future work will focus on the reanalysis of the prediction effect of data sets under different models, such as the discussion of prediction accuracy and time.

Data Availability

The experimental data used to support the findings of this study are available from the corresponding author upon request.

Conflicts of Interest

The author declares that there are no conflicts of interest regarding this work.

References

- [1] D. Marcek and L. Falat, "Volatility forecasting in financial risk management with statistical models and ARCH-RBF neural networks," *Journal of Risk Analysis and Crisis Response*, vol. 4, no. 2, p. 77, 2014.
- [2] H. Sun and D. L. Zhi, "Estimate of capital stock of provinces in China and the typical fact from 1978 to 2008," *Journal of Financial Economics*, vol. 25, pp. 107–115, 2010.
- [3] H. Akkermans and K. E. van Oorschot, "Pilot error? Managerial decision biases as explanation for disruptions in aircraft development," *Project Management Journal*, vol. 47, no. 2, pp. 79–102, 2016.
- [4] A. Huang and F. Wu, "Two-stage adaptive integration of multi-source heterogeneous data based on an improved random subspace and prediction of default risk of micro-credit," *Neural Computing & Applications*, vol. 33, no. 4, pp. 1–11, 2020.
- [5] Z. Jia, Y. Shi, C. Yan, and M. Duygun, "Bankruptcy prediction with financial systemic risk," *The European Journal of Finance*, vol. 26, 2020.
- [6] G. Vicente, A. I. Marqués, and S. J. Salvador, "Exploring the synergetic effects of sample types on the performance of ensembles for credit risk and corporate bankruptcy prediction," *Information Fusion*, vol. 47, pp. 88–101, 2019.
- [7] Y. Li, "Research on Financial Risk Prediction and Prevention Countermeasures Based on Big Data," in *Proceedings of the 2019 11th International Conference on Measuring Technology and Mechatronics Automation (ICMTMA)* Qiqihar, China, IEEE, April, 2019.
- [8] Y. Ying, W. Jun, W. Gang, and C. Yu-Wang, "Research and development project risk assessment using a belief rule-based system with random subspaces," *Knowledge-Based Systems*, vol. 178, pp. 51–60, 2019.
- [9] Y. Zhu, L. Zhou, C. Xie, G.-J. Wang, and T. V. Nguyen, "Forecasting SMEs' credit risk in supply chain finance with an enhanced hybrid ensemble machine learning approach," *International Journal of Production Economics*, vol. 211, no. MAY, pp. 22–33, 2019.
- [10] A. Mosavi, A. Shirzadi, B. Choubin et al., "Towards an ensemble machine learning model of random subspace based functional tree classifier for snow avalanche susceptibility mapping," *IEEE Access*, vol. 8, Article ID 145968, 2020.
- [11] N. García-Pedrajas and D. Ortiz-Boyer, "Boosting random subspace method," *Neural Networks*, vol. 21, no. 9, pp. 1344–1362, 2008.
- [12] G. Chen and S. Li, "Research on location fusion of spatial geological disaster based on fuzzy SVM," *Computer Communications*, vol. 153, pp. 538–544, 2020.
- [13] U. Bhosle and J. Deshmukh, "Mammogram classification using AdaBoost with RBFSVM and Hybrid KNN-RBFSVM as base estimator by adaptively adjusting γ and C value," *International Journal on Information Technology*, vol. 11, no. 4, pp. 719–726, 2019.
- [14] G. Chen, X. Xie, and S. Li, "Research on complex classification algorithm of breast cancer chip based on SVM-RFE gene feature screening," *Complexity*, vol. 2020, pp. 1–12, 2020.
- [15] X. Ning, K. Gong, W. Li, and L. Zhang, "JWSAA: joint weak saliency and attention aware for person re-identification," *Neurocomputing*, vol. 453, pp. 801–811, 2021.
- [16] S. Qi, X. Ning, G. Yang et al., "Review of multi-view 3D object recognition methods based on deep learning," *Displays*, vol. 69, Article ID 102053, 2021.
- [17] G. Wang, W. Li, and L. Zhang, "Encoder- X,: Solving Unknown Coefficients Automatically in Polynomial Fitting by Using an Autoencoder," *IEEE Transactions on Neural Networks and Learning Systems*, 2021.
- [18] Z.-G. Liu, Q. Pan, J. Dezert, and A. Martin, "Combination of classifiers with optimal weight based on evidential reasoning," *IEEE Transactions on Fuzzy Systems*, vol. 26, no. 3, pp. 1217–1230, 2018.
- [19] Z.-f. Ma, H.-p. Tian, Z.-c. Liu, and Z.-w. Zhang, "A new incomplete pattern belief classification method with multiple estimations based on KNN," *Applied Soft Computing*, vol. 90, no. 4, Article ID 106175, 2020.
- [20] M. Kottas, O. Kuss, and A. Zapf, "A modified Wald interval for the area under the ROC curve (AUC) in diagnostic case-control studies," *BMC Medical Research Methodology*, vol. 14, no. 1, p. 26, 2014.
- [21] W. Chen, X. Yan, Z. Zhao, H. Hong, D. T. Bui, and B. Pradhan, "Spatial prediction of landslide susceptibility using data mining-based kernel logistic regression, naive Bayes and RBFNetwork models for the Long County area (China)," *Bulletin of Engineering Geology and the Environment*, vol. 78, no. 1, pp. 247–266, 2019.

Research Article

Research on Evaluation Model of Music Education Informatization System Based on Machine Learning

Daliang Wang  and Xiaowen Guo

Music Academy, Henan Polytechnic, Zhengzhou 450046, China

Correspondence should be addressed to Daliang Wang; daliangwang@hnzj.edu.cn

Received 6 November 2021; Revised 11 December 2021; Accepted 27 December 2021; Published 24 February 2022

Academic Editor: Hangjun Che

Copyright © 2022 Daliang Wang and Xiaowen Guo. This is an open access article distributed under the Creative Commons Attribution License, which permits unrestricted use, distribution, and reproduction in any medium, provided the original work is properly cited.

Music education informatization system can promote music teaching; in addition, due to the characteristics of music disciplines such as the audiovisual nature of music, the influence of informatization on music teaching is self-evident. With the rapid development of the human ability to obtain information, machine learning algorithms have been widely used in various fields of scientific research and engineering, involving chemical production statistical process control, archeology text recognition, social and criminal investigation field fingerprint and image recognition, and genomic information research in the field of biomedicine. In order to correctly evaluate the music education information system based on machine learning, through the comparison of four models, it is concluded that the construction of the GBDT model is optimal.

1. Introduction

In the information environment, new information technology has brought about the rapid development of basic education informatization, but sometimes, it also shows the lack of a good operating mechanism and the imbalance of obvious structural differences. For the development of informatization, for example, expanded audiovisual channels and forms of music discipline [1], mathematical evaluation model [2], fuzzy evaluation model of industrial park informatization [3], corporate information based on graying weight cluster analysis evaluation model for the level of integration [4], primary education information system [5], evaluation index system for preschool education in colleges and universities [6], fuzzy comprehensive method [7], evaluation model for in-service slopes of in-service roads [8], management information system [9], comprehensive performance evaluation model [10], and community information system [11].

Machine learning, located at the intersection of computer science and statistics, is one of the fastest-growing technical fields today, and it is also the core of artificial intelligence and data science. Examples of applications are as follows: predicting song types [12], the effectiveness of detecting credit card fraud [13], CASD

system for skin lesion analysis [14], predicting the two-stage protein-protein interaction, providing a set designed to enhance guidelines for future anomaly detection research [15], expert system [16], MXNet [17], CNN and DBN [18], potential pitfalls of brain imaging data [19], covariate shift algorithm [20], data-intensive-based machine learning methods [21], land cover types in agricultural environments, aquaculture robot technology research project evaluation model [22], and real-time online analysis and evaluation of CPS reliability.

2. Introduction to the Theoretical Basis

2.1. Introduction to Music Education. Music education is one of the important ways for schools to implement aesthetic education. It has the effects of cultivating aesthetics, harmonious body and mind, sound personality, and purification of the soul. It has an irreplaceable role in promoting the overall development of students.

2.2. Music Education Classification. This article divides the methods and contents of music education into four categories: traditional music education, special music education,

multicultural music education, and modern music education as shown in Figure 1.

2.2.1. Traditional Music Education. The breadth and depth of China's excellent traditional culture are created and continued after thousands of years of history. It is the root and soul of our Chinese nation, and it is also the foundation for China to stand firm in the world's culture. There are many types of traditional Chinese music. It is an indispensable part of our traditional culture.

Traditional music generally refers to local music with national characteristics that have been passed down from generation to generation. It mainly includes folk songs and instrumental music. Newly created music based on these artistic traditions belongs to the extension and development of traditional music.

2.2.2. Special Music Education. Special music education is an education that is of great significance to special people's attention, and it is also one of the important contents of music education. The development of special music education can benefit more special people and the education field.

2.2.3. Music Education in Multiculturalism. Music education under multiple cultures is a diversified and diversified music education based on different cultures, social structures, and nationalities. As a branch of multicultural education, multicultural music education advocates the richness and diversity of music education and strives to realize the equal right to be educated for the music of all nationalities in the world and achieve the diversity and coprosperity of music culture heterogeneity.

2.2.4. Modern Music Education. Modern music education is combined with technology to realize education informatization. Educational informatization refers to the integration of the improvement of information literacy into the educational goals and the cultivation of talents suitable for the information society, the effective application of information technology to teaching and scientific research, and the emphasis on the development and utilization of educational information resources. Teaching is the central task in the field of education, and teaching informatization is to make teaching methods scientific and technological, education dissemination informatization, and teaching methods modernized, through the use of modern information technology based on computers, multimedia, etc., to promote education reform, so as to adapt to the new requirements of the coming information society.

2.3. The Concept of Machine Learning. "Learning" is the most basic ability inherent in humans and all kinds of animals. It is a kind of intelligent behavior that humans have. Since the day when people try to express human intelligence on computers, "learning" has naturally become the main issue of research. In real life, people can summarize general laws

through analysis and research on actual cases and estimate events that are difficult or impossible to observe directly. From the above, the general laws obtained through analysis can not only explain the known examples reasonably but also correctly estimate and predict future events or phenomena to meet the requirements of social development. In fact, the core issue of many scientific research studies is the process of quantitatively analyzing an object or event in life and establishing a model. The model can achieve the purpose of control, prediction, etc. The above modeling process is the machine learning process.

The learning process includes two main aspects. One is knowledge acquisition: acquiring knowledge, accumulating experience, discovering laws, etc.; second, improving ability: improving performance, adapting to the environment, etc. In the learning process, the two are closely related and serve as the core and result of learning, respectively.

As shown in Figure 2, the model contains the four most basic links in the learning process. The learning link and the execution link represent two processes. The environment and the knowledge base are the collections of information in the way of knowledge expression. The learning link similar to the learning algorithm processes the information provided by the outside world to improve the content in the knowledge base. A large amount of information expressed in some form is stored in the knowledge base. The execution link uses the information in the knowledge base to achieve a certain goal, and then the execution result is fed back to the learning link. The research of machine learning is divided into two aspects. One is that the machine automatically captures useful information to make it smarter; the other is that it summarizes the laws of human thinking and the mystery of learning, which makes people's learning efficiency increase.

2.3.1. Machine Learning Meaning. The significance of machine learning is very important. It can continue learning, avoid a lot of repeated learning, and make knowledge accumulation reach a new height. At the same time, machine learning contributes to the dissemination of knowledge.

2.3.2. Application Areas of Machine Learning. Machine learning is a very important research field in computer science and artificial intelligence. In recent years, machine learning has not only played its role in many fields of computer science but has also become an important technical support for some interdisciplinary subjects. It has absorbed the research results of cognitive science, probability and statistics, artificial intelligence, and other disciplines. In particular, in the pharmaceutical industry, data mining, robotics, bioinformatics, industrial process control, and other fields have achieved certain results. At present, the research fields of machine learning are mainly based on the following three aspects:

- (1) Task-oriented research: analyze and research a set of predetermined tasks to improve their execution performance

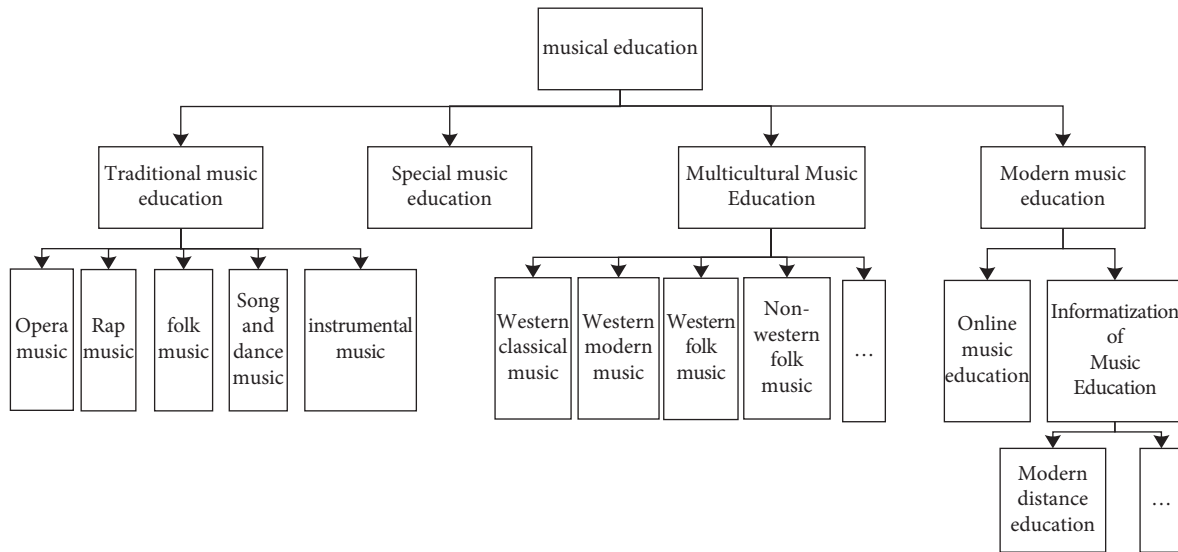


FIGURE 1: Classification of music education.

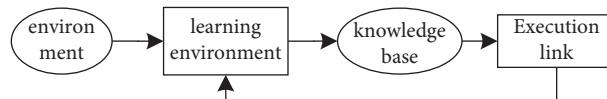


FIGURE 2: Machine learning model.

- (2) Cognitive model: study the process of human thinking and learning, and use computers to simulate
- (3) Theoretical analysis: theoretically study feasible learning methods

Machine learning is another research field of artificial intelligence after expert systems, and it is also one of the important research directions of artificial intelligence and neural computing. At present, the learning ability of artificial intelligence and computer systems is relatively poor, so they cannot meet the requirements of modern production and technology. Therefore, research and discussion on machine learning will surely lead to the rapid development of artificial intelligence and the entire science and technology.

Data mining is an important aspect of machine learning. The technology originated from the massive data caused by database technology and people’s interest in the use of these data. The data is stored in a data management system, and then machine learning methods are used to analyze and mine the potential information in the massive data, which leads to the emergence of data mining. In general, data mining is to extract unknown, human-interested, and potentially useful information from a large database.

3. Overview of Machine Learning Algorithms

3.1. Introduction to Machine Learning Algorithms. Learning certain laws or features by analyzing a large number of sample data, so as to summarize, identify, and predict unknown results or unobservable data, is called a machine learning algorithm.

Machine learning algorithms include logistic regression, random forest, support vector machine, and GBDT. Among them, the logistic regression model is widely used in classification learning because of its simple implementation, fast speed, and easy update. The random forest model that is popular in machine learning mainly uses average decision trees to reduce the risk of overfitting and make the model relatively stable. Support vector machine has become one of the most commonly used classifiers with the best effect due to its excellent generalization ability. The GBDT model is known for its high prediction accuracy and flexibility to handle various types of data.

3.1.1. What Is an Algorithm? There can be many definitions of algorithms. Here, the concept of the human brain “algorithm” is proposed, and an attempt can be made to incorporate the human brain “algorithm” into the philosophical algorithm concept. The “algorithm” of the human brain has all the attributes of the full cognition of the human brain, achieving an abstract meaning of the full cognition of the human brain.

“Algorithm” has now become a term specifically referring to the logical methods used in computer programs. From an intuitive and practical perspective, algorithms are an integral part of computer science. An algorithm is a set of domains with a partial ordering of transition mapping to determine the state and a “definable recursive body” for the mapping value to determine the result. In the past, an algorithm was an entity that satisfies the assumptions of continuous time, abstract state, and limited search. The

classic definition of “algorithm” is usually embodied in the mathematical context that formed early computer science. Common elements are deterministic rules or steps, calculations about a given input to produce an output, etc.

With the development of computers, algorithms have gradually become huge networks, and their original definition has obviously changed. An algorithm is a kind of effective, limited, abstract, compulsory command and completes a specific purpose compound control structure in accordance with regulations.

3.1.2. Algorithm Related Concepts

Algorithms and Computers. A computer is a machine that executes symbolic algorithms. However, not all carriers that execute algorithms are machines. For example, abacuses are not “machines” because they cannot calculate on their own. However, having certain attributes of a computer is not necessarily a computer in the true sense, because a computer is not only multifunctional but also universal and can execute all symbolic algorithms. In the age of computer networks, almost everything is controlled by algorithms. As a result, algorithms and computers are complementary and inseparable.

Algorithms and Artificial Intelligence. People with different research backgrounds often hold different views on the meaning of artificial intelligence. The artificial intelligence simulation method of the algorithm is used to make the intelligent behavior of the computer similar to the intelligent behavior of human beings. The higher the similarity, the more intelligent. This kind of research can achieve the purpose of explaining the human cognitive mechanism through the realization of algorithms so that people can have a deeper understanding of themselves and the nature of cognition. Although people have different opinions on the meaning of artificial intelligence, everyone still has the most basic consensus: to further understand human intelligence by constructing intelligent systems.

Algorithms and Cognitive Computing. Relying on the strong development of artificial intelligence, a unique way of thinking through computer principles to reflect on human’s own cognitive mechanism has formed. However, regardless of the interpretation of cognitive methods, the view of computationalism is based on computers and recognizes the basic premise that cognition is computable. A series of analogies under this premise achieve the purpose of trying to unravel the mystery of cognition.

3.2. Overview of Machine Learning Algorithms

3.2.1. Logistic Regression. Basic Principle. It is a two-classification model in machine learning. Because the logistic regression algorithm is simple in principle and efficient in classification, it is very widely used in practical applications. Its idea comes from linear regression in statistics. The difference from linear regression is that its dependent variable is discrete. The basic principle is as follows: the output of the

dependent variable y in the binary classification problem can only be 0 or 1, which is not a continuous value within a certain range. In order to convert the continuous output into a binary problem, the continuous value is converted into a discrete binary value through a nonlinear function.

Algorithm introduction: $X = \langle x_1, x_2, \dots, x_n \rangle$ represents the n -dimensional feature vector, n -dimensional column vector $\theta = \langle \theta_1, \theta_2, \dots, \theta_n \rangle$ represents the corresponding weight or coefficient, b represents the intercept, and the linear relationship is expressed as

$$F(\theta, X, b) = \theta^T X + b. \quad (1)$$

The value range of F is R . When dealing with the simplest binary classification problem, it is necessary to map the value of F to $(0,1)$. Commonly used S-shaped Korean (sigmoid function) to express: its expression is shown in the publicity:

$$g(z) = \frac{1}{1 + e^{-z}}. \quad (2)$$

The value of z is $(-\infty, +\infty)$, the value of g is $(0, 1)$, and the odd function image is as shown above: the logistic regression function can be obtained from Figure 3 and has the following characteristics: when $z \gg 0$, $y = 1$; when $z \ll 0$, $y = 0$. In terms of classification, the probability that y maps the result to a value between 0 and 1 represents the probability of belonging to the correct particle.

Regularization. Realize regularization by modifying the cost function formula of the algorithm, the expression of the hypothesis function, and updating the iterative method, so as to punish the training samples by the degree model to avoid overfitting of the model and improve the generalization ability of the model. During its operation, the regularization coefficient can be set to $L1$ or $L2$, where $L2$ is the default value. The cost function of the logistic regression model is

$$J(\theta) = -\frac{1}{m} \sum_{i=1}^m [y^{(i)} \log(h_{\theta}(x^{(i)})) + (1 - y^{(i)}) \log(1 - h_{\theta}(x^{(i)}))]. \quad (3)$$

Among them, m represents the number of samples for magic training, y represents the y value in the training samples of the hospital, $h_{\theta}(x)$ represents the y value predicted by the parameters θ and x , and (t) represents the t -th sample. The logistic regression minimization cost function under binary classification $L2$ regularization and the logistic regression cost function under $L1$ regularization are as follows:

$$\min \frac{1}{2} \omega^T \omega + C \sum_{i=1}^n \log(\exp(-y_i(x_i^T \omega + c)) + 1), \quad (4)$$

$$\min_{\omega_f} \omega_1 + C \sum_{i=1}^n \log(\exp(-y_i(x_i^T \omega + c)) + 1).$$

3.2.2. Random Forest. Basic Principle. The random forest can explain the effect of several independent variables X_1, X_2, \dots, X_k on dependent variable Y . Among them, the

dependent variable Y has n observations, and it will choose the bootstrap resampling method to randomly select n observations from the original data. Some observations are selected multiple times, and some are not selected. It will randomly select some variables from the k independent variables to determine the node of the classification tree. In this way, the classification tree constructed each time may be different. In general, random forests randomly generate hundreds to thousands of classification trees and then choose the tree with the highest degree of repetition as the final result.

Algorithm Introduction. From the original training data set, K new self-service sample sets are randomly selected using the bootstrap method with replacement, K classification and regression trees are constructed from this, and the samples that are not drawn each time constitute K out of the bag data; there are n features, randomly selected m_{try} features ($m_{\text{try}} \leq n$) at each node of each tree; by calculating the amount of information contained in each feature, select one of the m_{try} features with the most classification ability to split the node. Each tree grows to the utmost extent without any tailoring; the generated multiple trees are formed into a random forest, and the new data is classified with it, and the classification result is determined by the number of votes of the tree classifier.

3.2.3. SVM. Basic Principle. By solving the quadratic programming problem, a classifier based on structural risk minimization is searched for the optimal hyperplane that divides the data into two categories. It can also be simply described as follows: finding an optimal classification hyperplane that meets the classification requirements, so that it can maximize the blank area on both sides while ensuring the classification accuracy so that the support vector machine can achieve linearly separable data. *Optimal Classification.* Among them, the optimal classification plane should meet the following conditions:

$$\begin{aligned} & \max_{w,b} \frac{2}{w} \\ & s.t. y_i [(W \cdot x_i) + b] - 1 \geq 0, i = 1, 2, 3, \dots, n. \end{aligned} \quad (5)$$

Among them, $2/w$ represents the size of the classification interval of the classifier. In order to make the classification plane robust, it is necessary to find the largest classification interval to reach the optimal hyperplane. In addition, in the constraint condition, $y_i [(W \cdot x_i) + b]$ means the distance from the sample point to the classification plane, and $y_i [(W \cdot x_i) + b] \geq 1$.

Algorithm Introduction. By introducing the kernel function, the core of the support vector machine, an algorithm that is nonlinear with respect to the original space can be realized in a high-dimensional space. The kernel function of a support vector machine is the inner product of a certain high-dimensional space, which plays a vital role in a support vector machine. Choosing different kernel functions will produce different support vector machine algorithms. There are three kinds of kernel functions: the first kind is a polynomial kernel function of order q , as follows:

$$K(x_i, y_i) = (x_i \cdot x_j + 1)^q. \quad (6)$$

The second kind is the radial basis function kernel function, as follows:

$$K(x_i, y_i) = \exp \left[-\frac{|x_i - x_j|^2}{\sigma^2} \right]. \quad (7)$$

The third kind is the neural network kernel function, as follows:

$$K(x_i, y_i) = \tanh [c_1 (x_i \cdot x_j)] + c_2. \quad (8)$$

The standard support vector machine is using the structural risk principle: the loss function is the error selected in the optimization objective δ_i , where δ_i is the slack variable that allows misclassification. For classic support vector machines, the optimization problem is

$$\min J(w, \delta) = -\frac{1}{2} w \cdot w + c \sum_{i=1}^l \delta_i, \quad (9)$$

$$s.t. \quad y_i [(\Psi \cdot (x_i) \cdot w) + b] \geq 1 - \delta_i, i = 1, 2, 3, \dots, l.$$

Through the Lagrangian method, the standard support vector machine optimization problem can be transformed into the following quadratic programming:

$$\max W(a) = -\frac{1}{2} \sum_{i,j=1}^l a_i y_i y_j K(x_i, y_i) a_j + \sum_{i=1}^l a_i, \quad (10)$$

$$s.t. \quad \sum_{i=1}^l a_i y_i = 0, \quad 0 \leq a_i \leq c, i = 1, 2, 3, \dots, l.$$

3.2.4. Gradient Boosted Decision Trees. Basic Principle. An iterative decision tree algorithm is composed of multiple decision trees. There are usually hundreds of trees, and each tree is small in size. In model prediction, for an input sample instance, an initial value is first assigned, then each decision tree will be traversed, each tree will adjust and correct the predicted value, and finally, the results of each decision tree will be accumulated the final prediction result.

Algorithm Introduction. Including regression algorithm and classification algorithm, classification algorithm also includes two-classification and multiclassification models. The loss function that defines the two classifications is

$$L(y, f(x)) = \log(1 + \exp(-yf(x))). \quad (11)$$

Among them $y_i \in \{-1, +1\}$; the negative gradient error at this time is

$$\begin{aligned} r_{mi} &= -\left[\frac{\partial L(y_i, f(x_i))}{\partial f(x_i)} \right]_{f(x)=f_{m-1}(x)} \\ &= \frac{y_i}{1 + \exp(y_{i,f}(x_i))}, i = 1, 2, \dots, N. \end{aligned} \quad (12)$$

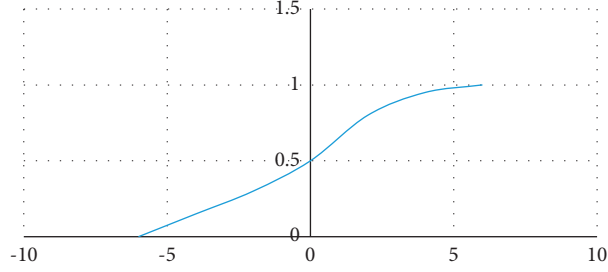


FIGURE 3: Logistic regression function image.

For the generated decision tree, the best residual fitting value of each leaf node is

$$c_{mi} = \arg \min_c \sum_{x_i \in R_{mi}} \log(1 + \exp(-y_i(f_{m-1}(x_i) + c))). \quad (13)$$

Because the above formula is difficult to optimize, we generally use approximate values instead:

$$c_{mi} = \frac{\sum_{x_i \in R_{mi}} r_{mi}}{\sum_{x_i \in R_{mi}} |r_{mi}| (1 - |r_{mi}|)}. \quad (14)$$

Regularization is mainly used to solve the overfitting phenomenon of the model. For the GBDT algorithm, the method to deal with the regularization problem can be summarized as follows.

One is to use a method similar to Adaboost to set the step size (learning rate) parameter for the regularization setting. For the first few iterations of the weak learner, there are

$$f_x(x) = f_{k-1}(x) + h_k(x). \quad (15)$$

If the regularization term is added, there are

$$f_x(x) = f_{k-1}(x) + \nu h_k(x). \quad (16)$$

The value range is $0 \leq \nu \leq 1$. When it is smaller, it means that the number of iterations is more; on the contrary, the number of iterations is less. Therefore, in the process of building a model, in order to achieve a better fitting effect, the step size and the maximum number of iterations are usually adjusted together. The second is to set the regularization by changing the subsampling ratio. In general, concerning the subsampling ratio $(0,1]$, when the value is 1, it means full sampling; that is, all samples are used; when the value is less than 1, the corresponding samples are drawn according to the ratio to fit the model to avoid overfitting. The third is to use a weak learner for regularization and pruning.

3.2.5. GP. GP (Kriging model) algorithm is a modeling technique based on the assumption that the input variables obey the joint Gaussian distribution. It can be used for both regression problems and classification problems. It can not only accurately establish complex nonlinear industrial process models but also quantify the uncertainty in predictions.

The GP algorithm based on Bayesian theory obtains its posterior distribution by studying the prior distribution of

the training set parameters. Assume a set of random variables $\{Y(x)|x \in X\}$ indexed by the input space X , where p is the number of input variables $X = (x_1, x_2, \dots, x_p)$. The Gaussian process is defined by its mean function $\mu(x) = E[Y(x)]$ and covariance function:

$$C(x, x^T) = E[(Y(x) - \mu(x))(Y(x^T) - \mu(x^T))]. \quad (17)$$

That is, once the mean function and covariance function are determined, the Gaussian model is determined. In general, the military assumes that the Gaussian process is zero-mean, ie $\mu(x) = 0$ ^[39,40].

According to the training set obeys the joint Gaussian distribution, the Gaussian distribution of the test sample can be obtained from the mean function $\hat{y}(x)$ and the covariance function $\sigma_y^2(x)$. The specific form is as follows:

$$\begin{aligned} \hat{y}(x) &= k^T K^{-1} t, \\ \sigma_y^2(x) &= C(x, x) - k^T(x) K^{-1} k(x). \end{aligned} \quad (18)$$

In the above formula, $k(x) = (C(x, x(1)), \dots, C(x, x(n)))^T$, K is the covariance function, in terms of the training set $K_{ij} = C(x(i), x(j))$, $t = (t(1), \dots, t(n))$, and n is the number of training samples.

For the application of the GP algorithm, there are a variety of covariance functions to choose from. Generally, the covariance function has a specific requirement; that is, for all sample point sets $(x(1), \dots, x(n))$, the covariance matrix generated by the covariance function must be nonnegative; for example,

$$\begin{aligned} C(x^{(i)}, x^{(j)}) &= v_0 \exp \left\{ -\frac{1}{2} \sum_{l=1}^p w_l (x_l^{(i)} - x_l^{(j)})^2 \right\} \\ &+ a_0 + a_1 \sum_{l=1}^p x_l^{(i)} x_l^{(j)} + v_1 \delta(i, j). \end{aligned} \quad (19)$$

In the above formula, $\theta = (a_0, a_1, v_0, w_1, \dots, w_p, v_1)^T$ is the hyperparameter that defines the covariance function, and T is the symbol for rank conversion. θ is obtained by finding the maximum likelihood function, and the expression is as follows:

$$L = \log p(y|\theta, X) = -\frac{1}{2} \log |C| - \frac{1}{2} y^T C^{-1} y - \frac{N}{2} \log(2\pi). \quad (20)$$

C is the covariance function.

Use gradient method to solve it; for example, conjugate gradient method. Usually, the estimation of the maximum likelihood function is a convex function solving problem, so there may be several local optimal solutions. Through multiple random selections of initial values for calculation, the shortcomings of misunderstanding of the local optimal solution as the global optimal solution are overcome.

4. Brief Introduction to the Design of Music Education Information System

4.1. Feasibility Analysis. The music education information system can collect, organize, and archive the relevant materials of the music subject. The feasibility analysis mainly analyzes the three levels of technical level, management operation level, and economic behavior.

The construction of the system framework is mainly divided into the selection of hardware equipment and the construction of the software framework, by adopting Tomcat as a service container, B/S development framework, MySQL database, and other mature technologies. In the development process, IntelliJ IDEA is used as the website development tool, Microsoft's MySQL Workbench is used as the database development tool, and Visual Studio Code is used as the front-end page development tool. We use Java technology to develop the system.

The operation level of the music education information system mainly takes into account the operability of the staff. Convenience, flexibility, and simple operation are the criteria for evaluating the operability of the system. Different classifications of operating system personnel mean that operators in different positions can perform different tasks. Operators operate through dialog boxes, buttons, etc., through the comprehensive factors of the system to ensure the practicability, functionality, and convenience of the system.

4.2. Demand Analysis of Music Education Information System Design

4.2.1. System Design Principles. The design principles of the actual music education information system are completeness, systematicness, and reliability.

Completeness means that the music education information system is fully functional and complete and can fulfill the requirements of music education information. The music education information system must have music data collection, music education information detection, data processing, query, and editing in the system. There should be display, analysis, and execution results. Make it a safe and reliable operation.

Systematicity is mainly reflected in the coordination between the exterior and the various functional modules of the system to form an organic whole.

Reliability refers to the ability to accurately perceive the status changes of the various components of the system and to make accurate judgments and predictions on module

queries through detection so that the system can operate stably and reliably.

4.2.2. System Function Requirements. This system focuses on the realization of the design of the integrated platform, the core framework of the integrated platform music education informatization, which plays a role in the data exchange and data integration of each platform. The establishment of this system can clearly understand the deficiencies of music education and realize the further development of the music education industry. The responsibilities of the system are divided into system administrators, user administrators, and data administrators.

5. Model Construction and Effect Analysis

The following uses a confusion matrix to judge the superiority of the model to show the prediction effect of each model.

5.1. Model Building

5.1.1. Logistic Regression. Logistic regression has a regularization item by default, and the value of the penalty parameter can be selected: $L1$ represents $L1$ regularization, $L2$ represents $L2$ regularization, and different regularization items can be selected according to different purposes. In the actual model construction process, if the main purpose is to solve overfitting, the penalty parameter generally selects $L2$ regularization. In special cases, the problem of overfitting may not be solved after $L2$ regularization is used; that is, $L1$ regularization is considered. In addition, $L1$ regularization can also solve the situation where there are more model features, and achieve sparse model coefficients by zeroing the unimportant feature coefficients. Based on this article, in order to be able to compare that model better, we select $L2$ and $L1$, respectively, for regularization settings and get the confusion matrix of the logistic regression as shown in Table 1.

Through the confusion matrix of each model, the correct rate, accuracy rate, recall rate, $F1$ value, and AUC calculated by each model can be obtained, so that the quality of each model can be judged. The specific calculation results are shown in Table 2 and Figure 4.

Through the intuitive presentation of tables and graphs, in the logistic regression model, the effect of logistic regression $L2$ is better than that of logistic regression $L1$.

5.1.2. Random Forest. Random forest requires additional attention: the number of trees' parameters and the number of subdata sets generated by sampling the original data set with replacement, that is, the number of decision trees. If the number of trees is too small, it is easy to underfit, and if the number of trees is too large, the model cannot be improved significantly. Therefore, the number of trees needs to be selected with a moderate value, the default value is 100; the maximum tree depth parameter is the maximum depth of the decision tree. If it is equal to none, it means that the

TABLE 1: Logistic regression model detection data set confusion matrix.

Model	Real category forecast category	Forecast excellent	Good prediction
Logistic regression <i>L2</i>	Forecast excellent	3902	1539
	Good prediction	4023	22890
Logistic regression <i>L1</i>	Forecast excellent	5291	1204
	Good prediction	3029	21378

TABLE 2: Logistic regression model test data set results.

	Correct rate	Accuracy	Recall rate	F1 value	AUG
Logistic regression <i>L2</i>	0.7900	0.7280	0.4375	0.5628	0.8728
Logistic regression <i>L1</i>	0.8427	0.8628	0.5639	0.8762	0.9827

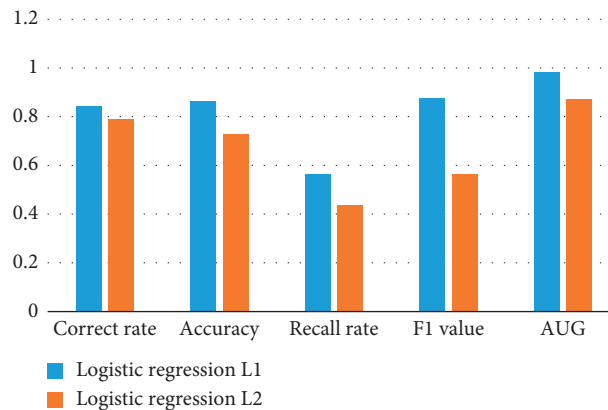


FIGURE 4: Logistic regression model test data set results.

decision tree will not limit the depth of the subtree when constructing the optimal model. If the model has a large sample size and features, it is recommended to limit the maximum depth; if the sample size is small or the features are few, the maximum depth is not limited; the minimum sample number parameter of the leaf node, that is, the minimum number of samples contained in the leaf node. If the number of leaf node samples is less than this parameter, then the leaf node and sibling leaf nodes are pruned, leaving only the parent node of the leaf node. The default is 50. Since the model fitting effect is not very sensitive to its parameters, parameter tuning is generally to adjust the number of decision trees. This paper keeps the maximum depth of the tree and the minimum sample of the leaf nodes unchanged and sets the number of trees to 90, 100, and 110, respectively, to obtain the confusion matrix of the random forest model, as shown in Table 3:

Judge the quality of each model. The specific calculation results are shown in Table 4 and Figure 5:

Through the visual presentation of tables and graphs, in the random forest model, random forest 3 is better than random forest 1 and random forest 2.

5.1.3. Support Vector Machines. This article uses support vector machines to build predictive models. C , which punishes misclassified training samples in the model, is the penalty factor, which is a manually set parameter, and its default value is 1. Generally, the larger the C , the more

accurate the model obtained through training. In this paper, the penalty factor is set to 1, 5, and 20 to obtain the confusion matrix of different models, as shown in Table 5.

Judge the quality of each model. The specific calculation results are shown in Table 6 and Figure 6.

5.1.4. GBDT. This paper selects the GBDT model that comes with the platform in the data factory to configure the parameters. The number of iterations is `n_estimators`. Generally, if the number of iterations is too small, it is easy to underfit; if the number of iterations is too large, it is easy to overfit. Generally, we choose a moderate value, and the default is 100. The learning rate (`learning_rate`) is the weight reduction coefficient ν of each weak learner, also called the step size. From the previous chapter, the iterative formula of the strong learner is $f_x(x) = f_{k-1}(x) + \nu h_k(x)$. The value range is $0 \leq \nu \leq 1$. The closer the ν value is to 0, the weaker learner needs more iterations; conversely, the closer the ν value is to 1, the weaker learner needs fewer iterations. Based on the opposite relationship between the two, when adjusting the parameters of the GBDT algorithm, the weight reduction coefficient and the number of iterations are adjusted together. The parameters can be adjusted from a smaller ν , and the default is 1. The maximum depth of the tree is `max_depth`; the default value that can be omitted is 3. In the case of a few data features or data, the value may not be adjusted. If the amount of data is large or there are many

TABLE 3: Confusion matrix of random forest model detection data set.

Model	Real or forecast category	Forecast excellent	Good prediction
Random forest 1	Forecast excellent	582	290
	Good prediction	8379	24579
Random forest 2	Forecast excellent	2763	762
	Good prediction	7638	27622
Random forest 3	Forecast excellent	3729	1204
	Good prediction	8732	21378

TABLE 4: Random forest model test data set results.

	Correct rate	Accuracy	Recall rate	F1 value	AUG
Random forest 1	0.7520	0.7280	0.04375	0.0982	0.8728
Random forest 2	0.8725	0.7023	0.1892	0.2876	0.7992
Random forest 3	0.6728	0.6782	0.2108	0.3598	0.9735

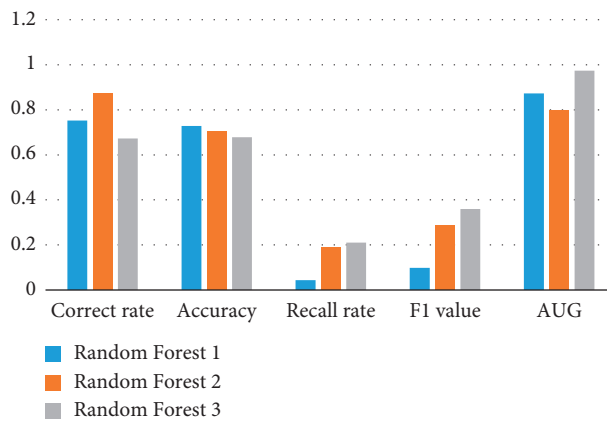


FIGURE 5: Random forest model test data set results.

TABLE 5: Confusion matrix of linear SVM model detection data set.

Model	Real or forecast category	Forecast excellent	Good prediction
SVM 1	Forecast excellent	2210	1290
	Good prediction	5289	23579
SVM 2	Forecast excellent	2763	1762
	Good prediction	6500	22622
SVM 3	Forecast excellent	4729	2204
	Good prediction	6732	18378

TABLE 6: Support vector machine model test data set results.

Model	Correct rate	Accuracy	Recall rate	F1 value	AUG
SVM 1	0.7520	0.7280	0.04375	0.0982	0.8728
SVM 2	0.8725	0.7023	0.1892	0.2876	0.7992
SVM 3	0.6728	0.6782	0.2108	0.3598	0.9738

data features, the value should be selected. The general value range is $[10, 100]$, and the specific value can be determined according to the distribution of the data. The other last parameter is the minimum number of samples of leaf nodes (min_samples_leaf), which is mainly used to limit the minimum number of samples of leaf nodes. If the number of samples is very large, we set a large parameter; if the

parameter is set to be less than the number of samples, it will be pruned together with the sibling nodes. This paper selects different parameter combinations based on the GBDT model, as shown in Table 7 and Figure 7.

Through the intuitive presentation of tables and graphs, GBDT3 is better than GBDT1, GBDT2, and GBDT4 in the GBDT model.

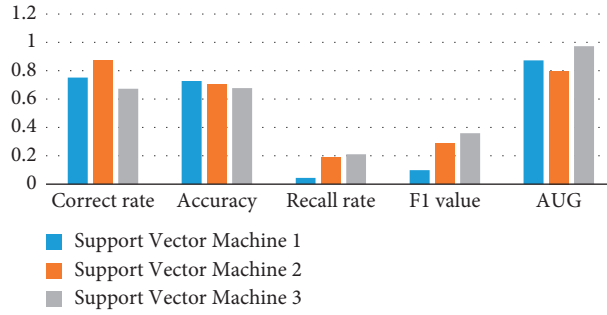


FIGURE 6: Support vector machine model test data set results.

TABLE 7: Confusion matrix of GBDT model detection data set.

Model	Real or forecast category	Forecast excellent	Good prediction
GBDT1	Forecast excellent	4472	1790
	Good prediction	4289	23479
GBDT2	Forecast excellent	6763	1362
	Good prediction	2500	22722
GBDT3	Forecast excellent	6753	1187
	Good prediction	2009	23090
GBDT4	Forecast excellent	4729	1099
	Good prediction	6732	21988

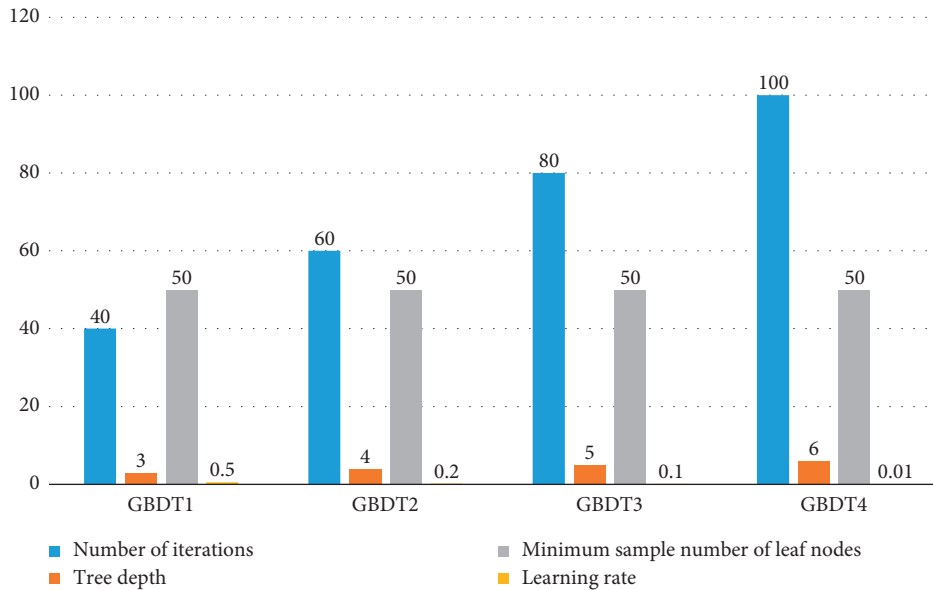


FIGURE 7: GBDT parameter settings.

Through different settings of model parameters, confusion matrices of different models are obtained, as shown in Table 7.

Judge the quality of each model. The specific calculation results are shown in Table 8 and Figure 8.

To sum up, through the independent comparison of the four models, logistic regression $L2$, random forest 3, support vector machine 2, and GBDT3 are the better models for each

test data. By comparing the four models, it can be concluded that the model effect of GBDT3 is the best.

5.2. Effectiveness Analysis. Through the comparative analysis, the effects of the above four models are shown in Figure 9.

The model effect of GBDT3 is the best.

TABLE 8: GBDT model test data set results.

	Correct rate	Accuracy	Recall rate	F1 value	AUG
GBDT1	0.8520	0.7180	0.5375	0.5982	0.8428
GBDT2	0.8910	0.8305	0.7527	0.7798	0.9460
GBDT3	0.8925	0.8423	0.7892	0.7876	0.9492
GBDT4	0.8728	0.7882	0.5108	0.5598	0.8734

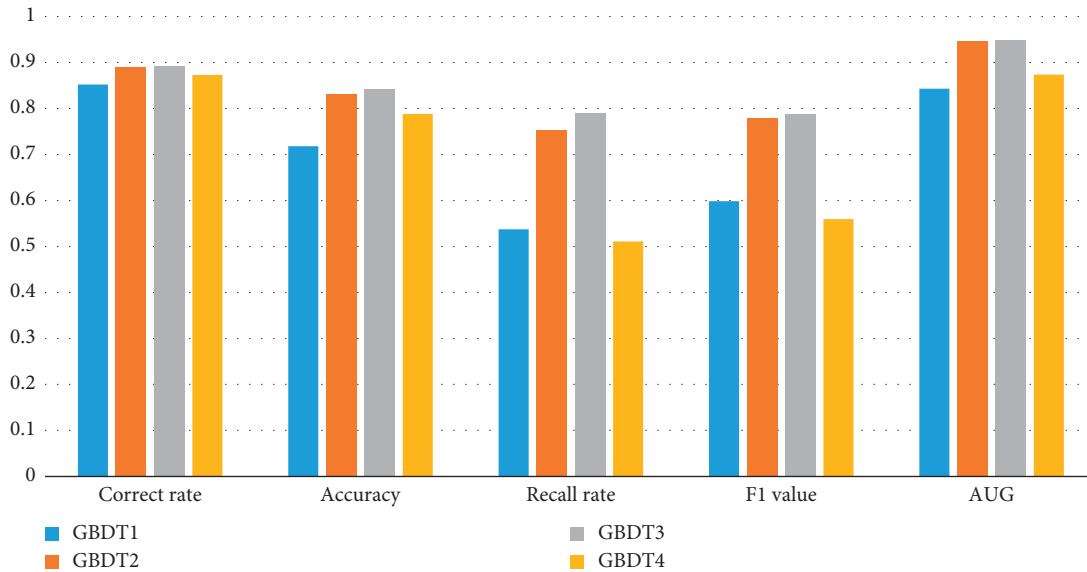


FIGURE 8: GBDT model test data set results.

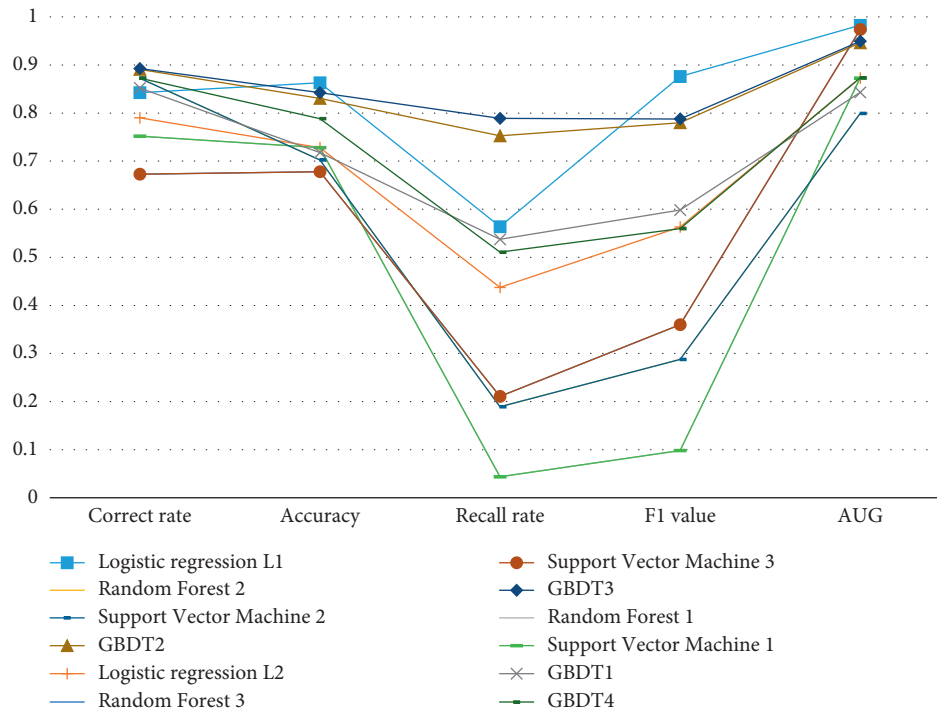


FIGURE 9: Model test data set results.

6. Conclusion

Through the introduction of related concepts of music education and machine algorithms, a logistic regression model, a random forest model, a support vector machine model, and a GBDT model were constructed for the music education information system based on machine learning. There is a systematic evaluation. Through the comparison of the four models, it is concluded that the construction of the GBDT model is optimal. The model used in this article still has limitations, and it is hoped that better algorithms can be found in the development of machine learning algorithms in the future.

Data Availability

The experimental data used to support the findings of this study are available from the corresponding author upon request.

Conflicts of Interest

The authors declare that they have no conflicts of interest regarding this work.

References

- [1] S. Lalit, "Fundamentals of machine learning for predictive data analytics: algorithms, worked examples, and case studies," *Computing Reviews*, vol. 57, no. 4, pp. 237-238, 2016.
- [2] X. Danyan and X. Guangwen, "Applications based on the principal component analysis of informatization evaluation model in university informatization evaluation," in *International Conference on Information Technology and Management Science (ICITMS 2012) Proceedings*, B. Xu, Ed., Springer, Berlin, Germany, pp. 391-398, 2013.
- [3] D. L. Yang and W. M. Chen, "An evaluation model of enterprise informatization level based on grey whitenization weight cluster analysis," *Advanced Materials Research*, vol. 189-193, pp. 823-829, 2011.
- [4] J. Du, W. Ning, and S. N. University, "Study on the construction of informatization evaluation model of elementary education from the viewpoint of ecology," *China Educational Technology*, vol. 7, 2014.
- [5] S. Hu and J. Zhang, "Cost-benefit analysis and evaluation of education informatization in colleges and universities," *Modern Distance Education Research*, vol. 188, no. 12, pp. 6278-6286, 2012.
- [6] L. Zhou, F. Shan, P. Liu, and Y. Wang, "The establishment of the enterprise informatization evaluation model based on supply chain," *Journal of Xi'an Polytechnic University*, vol. 29, no. 6, pp. 772-779, 2015.
- [7] G. Chen and S. Li, "Research on location fusion of spatial geological disaster based on fuzzy SVM," *Computer Communications*, vol. 153, pp. 538-544, 2020.
- [8] Z. Weimei, "Selection and planning of human resource management informatization system," in *Proceedings of the 2011 National Academic and Teaching Seminar on Electronic Information Specialty in Higher Vocational Education*, pp. 250-252, Wuxi, China, September 2011.
- [9] B. Huang, C. Zhu, J. Huang, and F. Li, "Performance evaluation of informatization construction on teaching administrative system in colleges from user's perspective," *China Educational Technology*, vol. 380, no. 9, pp. 69-74, 2018.
- [10] W. Wang, "Community informatization evaluation: model construction and analysis," *Information Studies: Theory and Application*, 2011.
- [11] A. Rahman and S. Tasnim, "Application of machine learning techniques in aquaculture," *International Journal of Computer Trends and Technology*, vol. 10, no. 4, 2014.
- [12] T. Guo and G. Y. Li, "Neural Data Mining for Credit Card Fraud detection," in *Proceedings of the International Conference on Machine Learning & Cybernetics*, pp. 3630-3634, IEEE, Kunming, China, July 2008.
- [13] G. Chen and S. Li, "Network on chip for enterprise information management and integration in intelligent physical systems," *Enterprise Information Systems*, vol. 15, no. 7, pp. 935-950, 2021.
- [14] J. Zubek, M. Tatjewski, A. Boniecki, M. Mnich, S. Basu, and D. Plewczynski, "Multi-level machine learning prediction of protein-protein interactions in *Saccharomyces cerevisiae*," *PeerJ*, vol. 3, no. 1, Article ID e1041, 2015.
- [15] P. M. Tag and J. E. Peak, "Machine learning of maritime fog forecast rules," *Journal of Applied Meteorology*, vol. 35, no. 5, pp. 714-724, 2010.
- [16] A. Matoga, R. Chaves, P. Tomas, and N. Roma, "A Flexible Shared Library Profiler for Early Estimation of Performance Gains in Heterogeneous systems," in *Proceedings of the International Conference on High Performance Computing and Simulation*, pp. 461-470, IEEE, Helsinki Finland, July 2013.
- [17] I. Arel, D. C. Rose, and T. P. Karnowski, "Deep machine learning—a new frontier in artificial intelligence research (research frontier)," *IEEE Computational Intelligence Magazine*, vol. 5, no. 4, pp. 13-18, 2010.
- [18] S. Lemm, B. Blankertz, T. Dickhaus, and K.-R. Müller, "Introduction to machine learning for brain imaging," *NeuroImage*, vol. 56, no. 2, pp. 387-399, 2011.
- [19] N. Adams, "Dataset shift in machine learning," *Journal of the Royal Statistical Society: Series A*, vol. 173, no. 1, p. 274, 2010.
- [20] M. I. Jordan and T. M. Mitchell, "Machine learning: trends, perspectives, and prospects," *Science*, vol. 349, no. 6245, pp. 255-260, 2015.
- [21] D. C. Duro, S. E. Franklin, M. G. Dubé, and G. Dubé, "A comparison of pixel-based and object-based image analysis with selected machine learning algorithms for the classification of agricultural landscapes using SPOT-5 HRG imagery," *Remote Sensing of Environment*, vol. 118, no. 6, pp. 259-272, 2012.
- [22] H. Wang, "Research on real-time reliability evaluation of CPS system based on machine learning," *Computer Communications*, vol. 157, no. 1, 2020.

Research Article

Implementation of Financial Audited Robot Question and Answer Technology of Feature Processing and Improved Bi-LSTM

Bingru Liu¹ and Qing Zhao² 

¹Hebei Intelligent Financial Technology Innovation Center, Hebei University of Chinese Medicine, Shijiazhuang 050000, China

²Accounting Department, Xingtai University, Xingtai 054001, China

Correspondence should be addressed to Qing Zhao; 201120399@xttc.edu.cn

Received 1 December 2021; Accepted 13 January 2022; Published 23 February 2022

Academic Editor: Hangjun Che

Copyright © 2022 Bingru Liu and Qing Zhao. This is an open access article distributed under the Creative Commons Attribution License, which permits unrestricted use, distribution, and reproduction in any medium, provided the original work is properly cited.

In order to improve the accuracy of financial robot audit question answering, we propose, on the premise of processing corpus features, combining Bi-LSTM network and CRF to identify the domain entities, so as to solve the problem of low recognition rate of financial knowledge domain entities, and introducing the mechanism based on attention and CNN network to construct the multigranularity feature question-answering matching model. Finally, the above methods are verified by experiments. The results show that the AUC, MAP, and MRR increase by 0.74%, 0.85%, and 0.81%, respectively, indicating the feasibility of the improved method.

1. Introduction

Enterprise financial audit is the focus of enterprise financial management, but the key is that auditors have a solid professional knowledge. Therefore, there is an urgent need to provide professional auditors with rapid and massive professional financial field knowledge. The traditional financial domain knowledge acquisition is through the web search method, which has a lot of redundant information and needs to be manually screened. Therefore, people began to turn their attention to the question and answer system, which achieves the answer to the question by simple natural language. And there are many kinds of key technology of question-answering system derived, such as natural language processing, naming entity extraction, intent recognition, knowledge map, deep learning, and so on. For example, QIU XiPeng summarized the current training models of natural language and expounded the value and significance brought to NLP by the emergence of training model [1]. Hu et al. apply natural language processing technology to some popular words in online communities. The results show that the overall performance of NLP algorithm is 0.77. But when concluding popular words in the

direction of smoking cessation, it is summarized as edible nicotine [2]. Patra Braja et al. applied NLP to the analysis of health determinants. The results show that NLP can tap the health determinants, and it has great potential for development [3]. Wilfredo et al. applied NLP technology to intelligent robots to make robot capture human emotions by extracting intelligent semantics. In addition to the above technologies, ANN, Bi-LSTM, and other methods are also applied to robots to better recognize semantic features [4]. For example, Man and Bai et al. used SVM and other algorithms to identify features, so as to find the English semantics well. The result shows that it provides a reference for semantic extraction [5]. Zhai used Bi-LSTM to extract emotional semantics. The results show that this method can obtain important text feature information [6]. However, the research of integrated question-answering robot mainly solves the problem of extracting semantic and then matching the problem. In this regard, combined with the above research, an improved Bi-LSTM feature extraction question-answering method is proposed, and the method is verified.

The length of natural language text used by people is not fixed in real life, so it is difficult to divide natural language sequences into uniform fixed dimensions. In this regard, a

Recurrent Neural Network (RNN) was created to divide the natural language sequence by the academic community [6–9]. The design purposes are initially achieved, but there were still some inherent disadvantages, one is only to consider the short-term dependence and that it cannot save long-distance information, and the other is to address long-series problems which may cause gradient explosion or gradient disappearance. In view of this, Hochreiter et al. created the Long Short-Term Memory (LSTM), which retained the advantages of the traditional RNN model and controlled the memory block state by using input gate, forgot gate, and output gate. The frame structure of the LSTM is shown in Figure 1.

It can be seen from Figure 1 that when the input gate is opening, the new input can change the existing information of the neural network, when the output door is open, access to historical information is allowed, and the subsequent output value can be changed. The main function of the forget gate is to clear historical information.

In order to explain the update mechanism of LSTM conveniently, x is set as the input data, h means the unit input of LSTM at time t , and C represents the value of LSTM memory unit.

- (1) Use the circular memory network formula to calculate the value \tilde{c}_t of the candidate memory unit at the current moment.

$$\tilde{c}_t = \tanh(w_{sc}x_t + w_{hc}h_{t-1} + b_c), \quad (1)$$

where w_{sc} represents the corresponding input data, and w_{hc} represents the weight of LSTM output at the last moment.

- (2) Solve the value i_t of the input gate, which is mainly affected by the current input data x_t and the previous moment h_{t-1} and C_{t-1} . The formula is as follows:

$$i_t = \sigma(W_{xi}x_t + W_{hi}h_{t-1} + W_{ci}c_{t-1} + bi). \quad (2)$$

- (3) Solve the value f_t of the forget gate, which represents the effect of historical information on the state value of the current memory unit. The formula is as follows:

$$f_t = \sigma(W_{xf}x_t + W_{hf}h_{t-1} + W_{cf}c_{t-1} + b_f). \quad (3)$$

- (4) Solve the state value c_t of the memory unit at the current moment, which is mainly affected by its own state c_{t-1} and the value \tilde{c}_t of the candidate memory unit at the current moment. The formula is as follows:

$$c_t = f_t \odot c_{t-1} + i_t \odot \tilde{c}_t. \quad (4)$$

- (5) The formula of solving the input gate o_t is

$$o_t = \sigma(W_{xo}x_t + W_{ho}h_{t-1} + W_{co}c_{t-1} + b_o). \quad (5)$$

- (6) The output formula of LSTM is

$$h_t = o_t \odot \tanh(c_t). \quad (6)$$

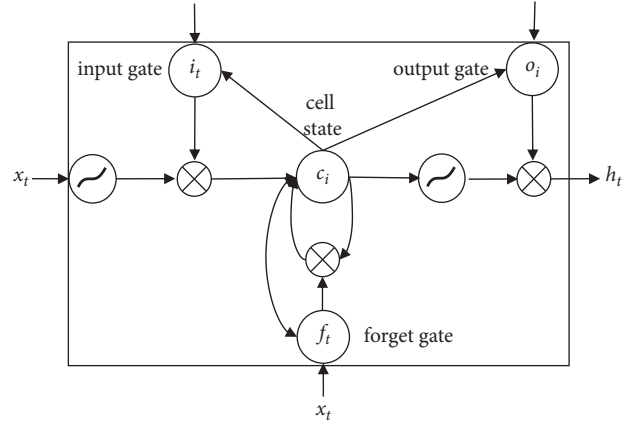


FIGURE 1: The frame structure of the LSTM.

In terms of application effect, LSTM has obvious advantages over RNN in information storage, reading, and long-term information update. Bi-LSTM is based on LSTM and adopts bidirectional feature extraction. The specific structure is shown in Figure 2.

The principle of Bi-LSTM is to take the output of CNN network pooling layer as the input of two opposite LSTM, in which the forward LSTM mainly obtains the above information of the sequence, and the backward mainly obtains the below information. Finally, the final context information is obtained by splicing calculation.

1.1. Conditional Random Field (CRF). The CRF model is usually a model that analyzes the conditional probability distribution of another random variables group under a set of random variables being given. The characteristic of this model is to assume that the output random variable can constitute MRF, and through the special conditional random field of linear chain to annotate the semantics, the specific labeling process is shown in Figure 2 [10–12].

In Figure 3, Y represents the output variable, which is mainly used to mark the sequence, and X represents the input variable, which is mainly used to represent the observation sequence that needs to be labeled. In the course of model training, the model probability is estimated mainly by maximum likelihood; the maximum output sequence Y of the model is solved under the condition of given input sequence X .

2. Domain Entity Recognition Algorithm Based on Bi-LSTM + CRF Fusion

In order to better realize entity recognition of financial domain knowledge, which combined the basic principles of Bi-LSTM model, the fusion of CRF model and domain knowledge establishes distributed semantic vector representation of the words. Bi-LSTM model performs feature extraction and encoding for input sequence, and CRF model carries out entity annotation. The overall recognition model includes three parts: input layer, Bi-LSTM layer, and CRF

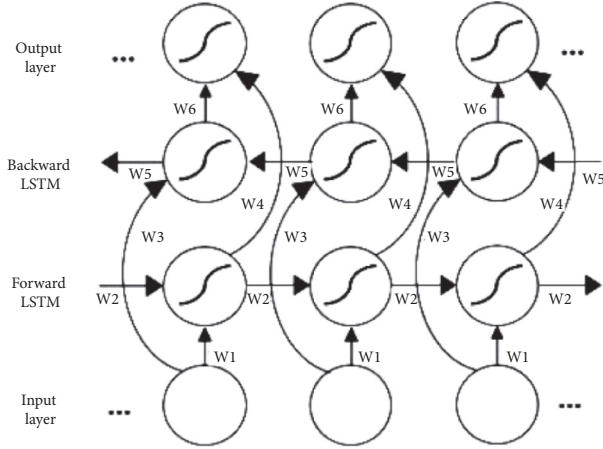


FIGURE 2: The Bi-LSTM structure.

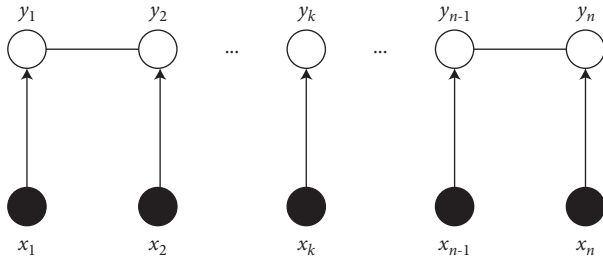


FIGURE 3: CRF model.

entity annotation layer. The model framework structure is shown in Figure 4.

2.1. Input Layer. Different from ordinary deep learning models, the input layer of this model applies the strong characteristics of lexical information and being domain-related. The expression is as follows [13]:

$$r_x = r_s^{\text{ward}} \cdot r_s^{\text{ent}} \cdot r_s^{\text{poi}}, \quad (7)$$

where r_s^{ward} , r_s^{poi} , and r_s^{ent} are word vector input, entity indicator word features, and the characteristics of entities in the field of candidate words dictionary, respectively.

2.2. Bi-LSTM Cod Layer. LSTM is driven in a left-to-right order, and capturing information bias may occur under this operating mechanism. For example, once the word “financial audit” is captured, and if you do not understand it with contacting the context information of finance, it is likely that the “audit” will be labeled independently. For domain entity identification tasks, the vocabulary in the statement is equal, and the following information is as important as the above information, so it is not safe to use the LSTM model alone. Bi-LSTM model is created to capture information, which can take into account and utilize context information. The Bi-LSTM model has built-in forward and backward layers, with the former advancing from the front of the sentence and the latter advancing from the end of the sentence. In this process,

storing and utilizing the context information of the sentence can better play the function of entity recognition. The frame structure of Bi-LSTM model is shown in Figure 5.

The Bi-LSTM encoding layer learns the context information of the word through forward and backward operations, so the word can be represented, and it can help to determine whether the word is an entity. The forward and backward calculation formulas of Bi-LSTM cod layer are shown as follows:

$$h_i = \text{Bi LSTM}(r_s^i). \quad (8)$$

In the formula, r_s^i refers to the semantic vector representation of the input words, and h_i refers to the output of the hidden layer of each word in Bi-LSTM.

2.3. Entity Labeling Layer of CRF. The CRF model is responsible for entity labeling, which is divided into labeling, computational features, model training, entity recognition, and so on. The first is to label the corpus with preset labels. For example, the corpus “What is the steps of duplicate certificate audits/audited?” is labeled, and the results are listed in Table 1 [14].

The CRF model has the ability to calculate the probability distribution of the global sequence and is used to estimate the entity label probability distribution for the entire sequence, so as to obtain the entity label distribution of the whole sequence. During model training, entity transition probability matrix is used to regulate the transition probability between entities, and the formula is as follows [15, 16]:

$$p(y_t | h, y_{t-1}) = \text{CRF}(h_t) + A_{y_{t-1}, y_t}, \quad (9)$$

where A is the entity transition probability matrix.

3. Constructing the Multigranularity Question-Answering Matching Model

On the basis of completing the knowledge entity identification of financial robots in the area of finance, to implement financial Q&A is also needed to match the problems. Both question-question matching and question-answer matching belong to the category of text matching task, and their corresponding model structure is consistent; the only difference lies in the selection of matching function. The key to text matching is to capture semantic information at different levels of text. LSA, statistics as well as learning, and LDA are the traditional text matching models matching based on the single semantic information, which is different from human text matching habits. The reason is that people will make a judgment on text matching by comprehensively analyzing global semantic information, contextual semantic information, word similarity, as well as other external knowledge, and so on. On the premise of integrating information of different granularity levels, the text matching model is established by using the input layer, presentation layer, and matching layer, and its frame structure is shown in Figure 6 [17].

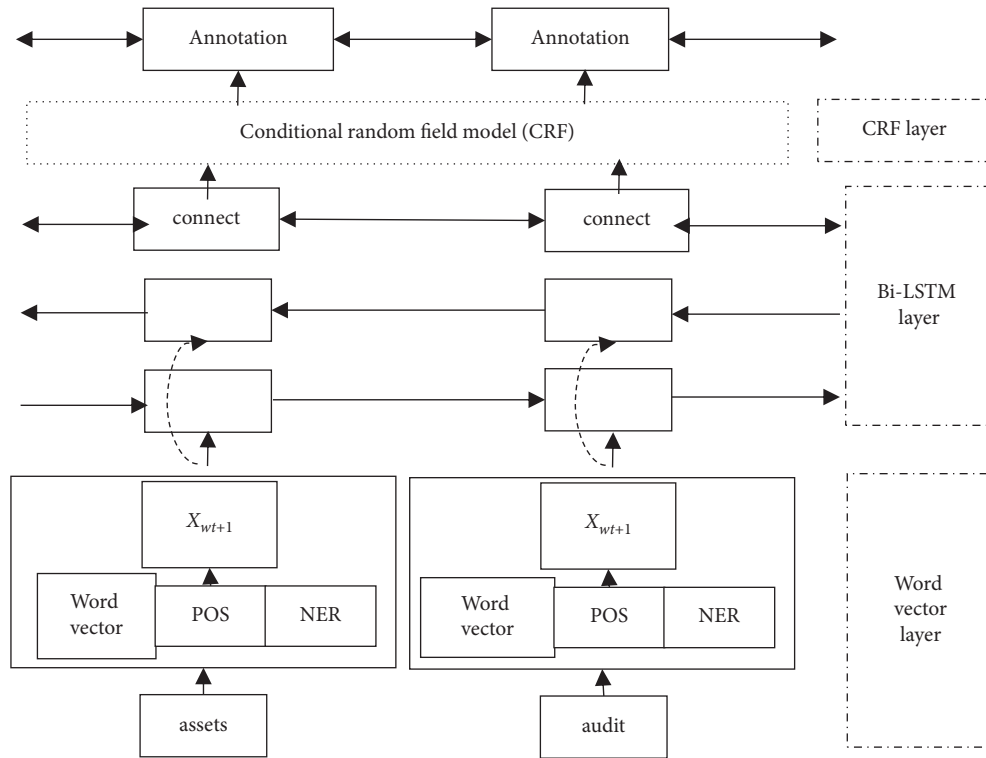


FIGURE 4: The frame diagram of entity identification model.

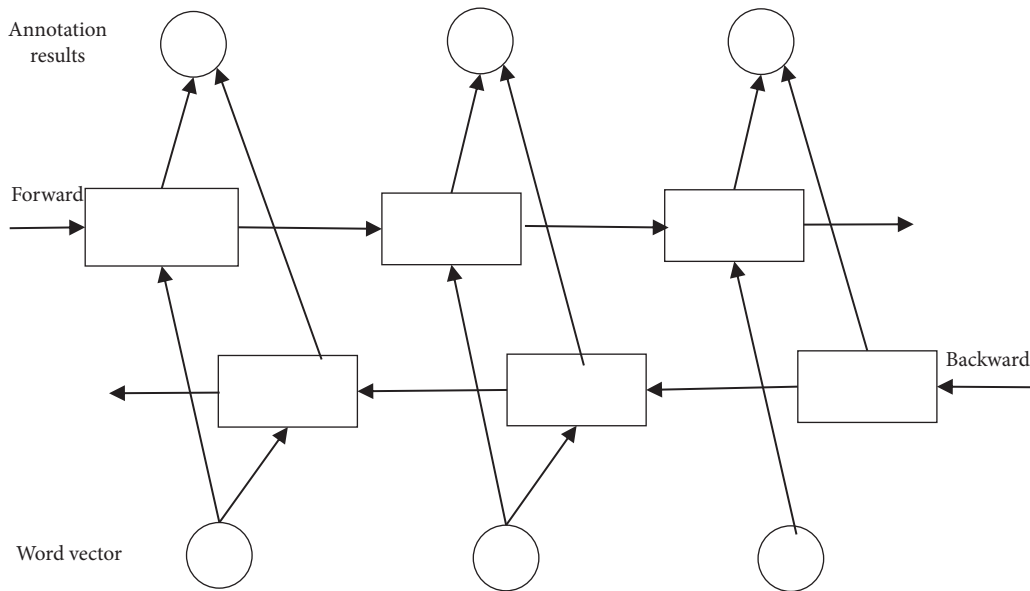


FIGURE 5: The frame structure of Bi-LSTM.

TABLE 1: The labeling example of CRF.

Voucher duplicate number	Audit	Of	Step	Yes	What
PRO	PRO	N	ATT	N	N

3.1. *Input Layer.* The input layer contains the input of the original word sequence and the input of the entity recognition result. What can be known is that the two input

sentences are $S_1 = \{w_1, w_2, \dots, w_n\}$, $s_2 = \{w'_1, w'_2, \dots, w'_n\}$, so the entity recognition result $E_1 = \{e_1, e_2\}$, $E_2 = \{e'_1\}$ can be calculated. Entity E is composed of multiple words, and word sequence input is represented by the idea that word vector matrix is mapped to word vector. The formula is as follows:

$$r^w = w^{\text{word}} \cdot v^w. \tag{10}$$

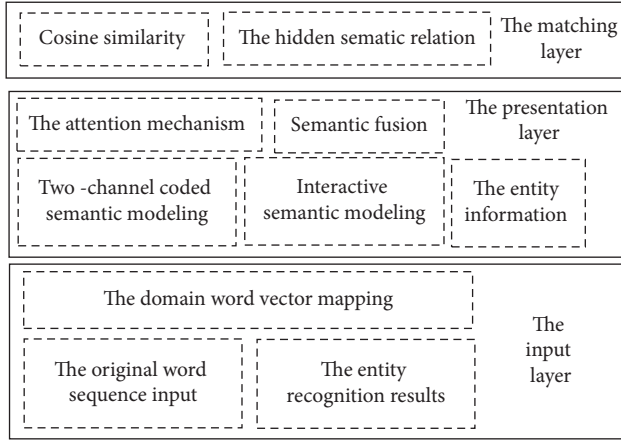


FIGURE 6: The frame structure of text matching model.

Here, r^w and v^w are word vector and one-hot vectors, respectively.

Accordingly, entity input is represented by entity vector matrix mapped to entity vector, and the formula is as follows:

$$r^e = w^{\text{entity}} \cdot v^e. \quad (11)$$

In the formula, r^e and v^e are entity vectors and one-hot vectors, respectively.

3.2. The Presentation Layer. The presentation layer encodes the input and maps it to the same semantic space as the input features of the matching layer, which is classified as follows.

3.2.1. The Two-Channel Encoded Text Relationship Modeling Based on Attention Mechanism. At present, there are two kinds of commonly used text semantic encoding models. One is the model based on RNN, which can capture global sequence information and model by analyzing context information. The second model is based on CNN, which can effectively capture local information at phrase level. Obviously, the two kinds of semantic cod models are complementary to each other. RNN model can store the captured context information of the word, but the traditional RNN model cannot store long-distance information, so the improved Bi-LSTM model is selected to deal with the long-distance dependence problem. It can model the above information of the word and store the following information, which enriches the representation of word level. Bi-LSTM model is used to map two word sequences into word vectors in the same semantic space, and the formula is as follows [18–20]:

$$\begin{aligned} h_i^{\text{forward}} &= \text{LSTM}^{\text{forward}}(s_i\{r_1^w, r_2^w, \dots, r_n^w\}), \\ h_i^{\text{backward}} &= \text{LSTM}^{\text{backward}}(s_i\{r_1^w, r_2^w, \dots, r_n^w\}), \\ h_i &= h_i^{\text{forward}} \cdot h_i^{\text{backward}}, \end{aligned} \quad (12)$$

where s_i refers to the input word vector matrix, h_i refers to the semantic representation of words, and forward and

backward refer to forward operation and backward operation.

People usually understand texts with questions, so they focus on certain words or fragments, which does not take into account the weight information of different words. Therefore, attention mechanism should be introduced to highlight the importance of some words in the process of semantic information expression. Based on the characteristics of domain and model, common attention mechanisms include the attention mechanism based on answer and that based on entity information, having the same principle but different representation.

The attentional mechanism is vested with the corresponding weights depending on the importance of different words for the sentence expression, and the formula is as follows [21]:

$$\begin{aligned} \alpha_i &= \sigma(r_q^T M_{qi} h_i), \\ h'_i &= \alpha_i \times h_i. \end{aligned} \quad (13)$$

In the formula, α_i represents the weight of words solved by the attention mechanism, r_q^T represents the context vector operated by participating weight, M represents the parameter matrix of the attention mechanism, h_i represents the hidden layer output of the Bi-LSTM model, and σ represents the nonlinear transformation function.

Local feature of the original word vector can be extracted by using the convolution and pooling operations of CNN model, which can help to obtain phrase-level local information, and the output of each hidden layer in Bi-LSTM model is taken as the input of CNN model, which can further enrich the information of word vector and integrate the global semantic information. The core formula of CNN model is as follows [22]:

$$r_i^1 = f(\text{conv}(h_i^{\text{Bi-LSTM}})) + \text{bias}. \quad (14)$$

Here, r_i^T is defined as the text semantic vector represented by the two-channel coded text relation model; f stands for nonlinear function; $h_i^{\text{Bi-LSTM}}$ refers to the output of Bi-LSTM model; bias represents the bias.

The two-channel coded model based on attention mechanism is shown in Figure 7 [23].

3.2.2. Interactive Text Relationship Modeling. Two-channel cod text relationship modeling uses the correlation model to represent the semantic vector of two texts, respectively, which are independent of each other and have the probability of losing subtle semantic information. In the interactive text relationship modeling, the interactive process of interactive text semantic representation has begun at the input layer, and the mapping of text to matrix is realized by means of dot product, 1–0, similarity operation, etc., and then feature extraction is carried out to obtain more subtle relationships.

In terms of the interactive text relationship modeling, the first step is to establish an interactive matrix to control the maximum length of the two texts. If the length is insufficient,

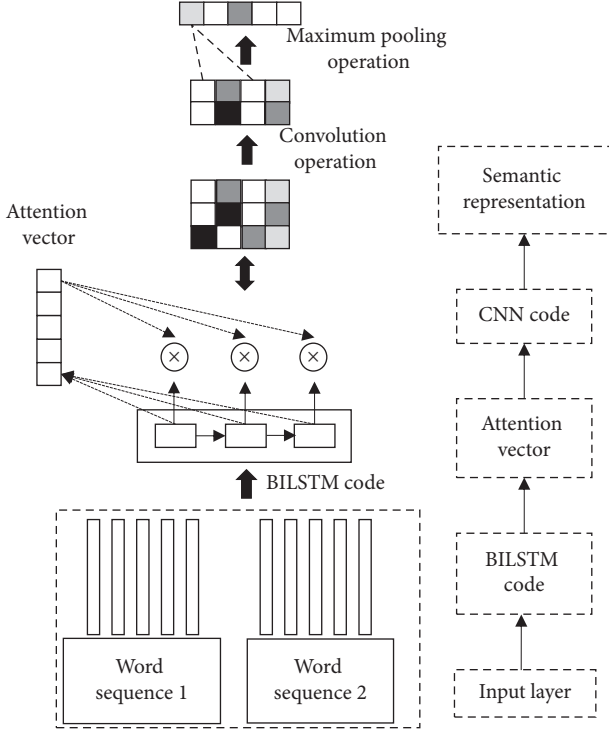


FIGURE 7: The two-channel coded model based on attention mechanism.

it should be completed. The second step is to conduct word-by-word matching operation, as shown in the following formula:

$$\text{score}_{ij} = F(w_i, w_j). \quad (15)$$

In the formula, F represents various calculation methods. Taking 0–1 calculation method as an example, if the two words w_i and w_j are consistent, 1 will be output; otherwise, 0 will be output. Taking cosine similarity calculation method as an example, text interaction matrix is firstly established, and then it is input into multilayer CNN model, and more subtle semantic information is obtained through multilayer convolution-pooling operation. Cosine similarity calculation formula is as follows:

$$r^2 = f(\text{conv}(M^{\text{score}})) + \text{bias}, \quad (16)$$

where r^2 refers to semantic vector representation, and M^{score} refers to text interaction matrix.

The framework of the interactive text relation model is shown in Figure 8 [24].

3.2.3. The Entity Information Integration. We can judge the matching problem between problems according to entity information, and inputting entity information into the model can improve its effect. The schematic diagram of entity representation is as follows as Figure 9 [25].

The recognition results of the two texts (entity information) are represented by the entity vector matrix, respectively, mapped to entity vector. Since the entity information occupies a low proportion in all word

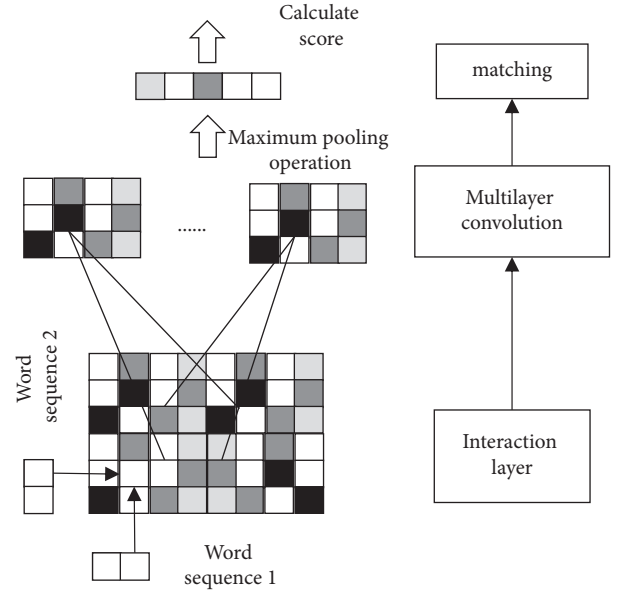


FIGURE 8: The interactive text matching model.

information, the word-average method is used to encode and represent the entity information, and it is used as the input feature of the matching layer. The formula is as follows:

$$r^3 = \frac{1}{n} \sum_i^n r_i^{\text{entity}}, \quad (17)$$

where r^3 refers to entity-related sentence semantic representation; r_j^{entity} is the entity vector.

3.3. The Matching Layer. The matching layer calculates the matching score based on the semantic representation of the presentation layer. A knowledge point consists between a question and an answer. If you just match according to the question or answer, there may be serious deviation. For example, the two questions are very similar, but the answer does not match the questions. In this regard, it is necessary to realize the fusion of Paraphrase Identification and Answer Selection to train the final model. In addition, although the model structure of the two matching modes is consistent, there are still some differences, and the appropriate matching methods need to be selected.

3.3.1. Problem-Problem Matching. In this matching mode, the user issues and the problem of knowledge base are in the same semantic space. And according to the semantic similarity, the matching of the two problems can be determined. The semantic vector can be obtained through the problem-matching pattern, and it represents the semantic vector representation of two texts and their similarity features. The expression is as follows:

$$\text{score}_{\text{cosine}} = \text{cosine}(r_1^1, r_2^1). \quad (18)$$

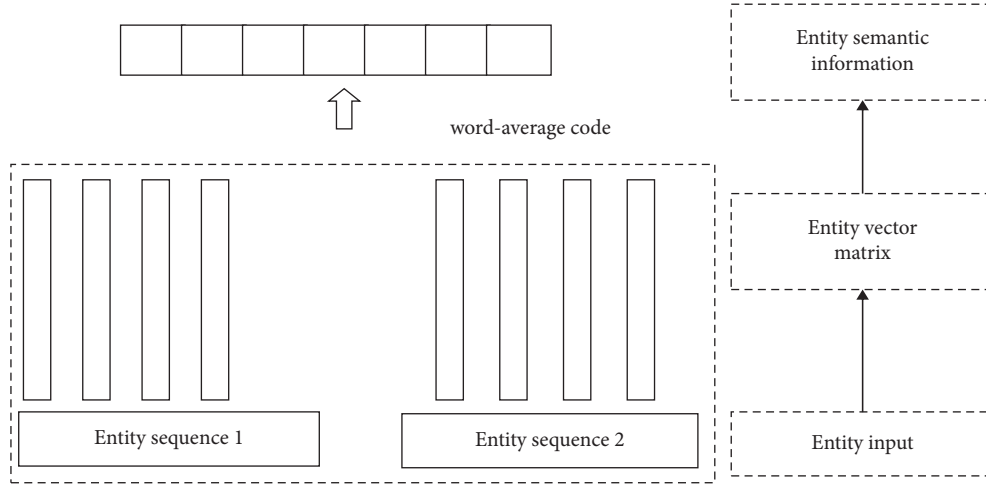


FIGURE 9: The schematic diagram of entity representation.

Here, score_{\cosine} refers to the cosine similarity between the semantic vectors r_1^1, r_2^1 .

3.3.2. Question-Answer Matching. In this matching mode, user issues and answers are in different semantic space, and their correlation or subordination is determined through the semantic matching. Since the matching of question and answer is not the similarity feature of two kinds of semantics, the similarity feature cannot be used to represent their relationship. A more abstract relationship should be established. The nonlinear function is used to ensure the semantic correlation of the two vectors, as follows:

$$\text{score}_M = r_1^1 \times M \times r_2^1, \quad (19)$$

where M represents the implicit abstract relation, which can map the two vectors into the same semantic space.

The semantic representation features that concentrate multigranularity are integrated; at the same time the two-channel cod output vectors are connected. The subtle difference of semantic representation between problems can be more fully exploited. Then, input it into the fully connected neural network model for learning, and solve the final match score; the related calculating formula is as follows:

$$\text{features}_{qq} = [r_1^1 \cdot r_2^1 \cdot \text{diff}(r_1^1, r_2^1) \cdot \text{mul}(r_1^1, r_2^1) \cdot r^2 \cdot r_1^3, r_2^3 \cdot \text{score}_{\cosine}], \quad (20)$$

$$\text{features}_{qa} = [r_1^1 \cdot r_2^1 \cdot \text{diff}(r_1^1, r_2^1) \cdot \text{mul}(r_1^1, r_2^1) \cdot r^2 \cdot r_1^3, r_2^3 \cdot \text{score}_M]. \quad (21)$$

In the formula, features_{qq} and features_{qa} are the input characteristics of question-question matching and question-answer matching, respectively; $P(y|\text{features}_{qq})$ and $P(y|\text{features}_{qa})$ are the matching probabilities between question-question and question-answer, respectively.

4. Experimental Verification

4.1. Entity Identification Experiment in the Field of Enterprise Financial Audit

4.1.1. Model Training and Parameter Tuning. TensorFlow platform is used for model development. The model related parameters include the term vectors, the implied relation parameter M , entity type vector, full-connection layer parameters, CNN and LSTM parameters, etc. According to the implied relationship matrix M in the question-answer matching, the implied relation parameter can be determined. And the other hyperparameters can be determined by using the gradient search. Thus, the optimal parameter

combination can be obtained. The specific optimal parameters are shown in Table 2.

4.1.2. Evaluation Indicators. The entity recognition method based on deep learning and integrating domain knowledge proposed in this paper is tested by experiment. The training data used for evaluation is obtained through manual annotation, and the appropriate evaluation standards are set. In this experiment, F1, precision, and recall were used to evaluate the model. The formula of each index is as follows [26]:

$$\text{precision} = \frac{TP}{TP + FP}, \quad (22)$$

$$\text{recall} = \frac{TP}{TP + FN}, \quad (23)$$

$$F1 = \frac{2 * \text{precision} * \text{recall}}{\text{precision} + \text{recall}}. \quad (24)$$

TABLE 2: The model parameters.

Parameter name	The word vector dimensions	The entity vector dimension	The hidden dimensions of LSTM	The layers of LSTM	The convolution kernel size
Value	128	128	128	1	[128, 3]
Parameter name	The matrix size	Dropout	Weight	The number of hidden nodes	The hidden layers numbers
Value	[128, 64]	0.8	0.8	128	2

4.1.3. *Experimental Results and Analysis.* Comparing the effects of referencing different features, the validity of domain knowledge characteristics referred to this paper is verified.

Based on Bi-LSTM + CRF model, the different features such as indicators, entity dictionary, and part of speech are introduced to conduct comparative experiments with the proposed model. The results are listed in Figure 10; the M_1 to M_5 represent the model without attention mechanism introduction, the model with entity attention mechanism, the model with answer attention mechanism, and the proposed model, respectively.

It can be seen from Figure 10 that, based on the Bi-LSTM + CRF model, introducing different features is beneficial to entity recognition. For example, introducing the part-of-speech features can increase F1 value by 0.35%. This is because the introduced part-of-speech features complement the word vector information, but the word vector information already contains rich semantics. Therefore, the introduction of part-of-speech features is of little benefit to entity recognition. The introduction of entity features can increase F1 value and recall rate by 1.24% and 1.47%, respectively, because the introduction of entity dictionary in the professional field of corporate financial audit has an important effect on identifying those relatively sparse entities. The introduction of indicator features can increase F1 value and accuracy by 0.87% and 0.92%, respectively, because the introduction of indicator features can correct the error-prone entities. By comparison, the entity recognition effect of the proposed model is superior to the Bi-LSTM + CRF model and the Bi-LSTM + CRF model with a single feature. It indicates that there is complementarity among several features. After integrating the multiple features, introducing the Bi-LSTM + CRF model can significantly improve the final entity recognition effect.

4.2. Question and Answer Retrieval Experiment

4.2.1. *Experimental Settings.* The setup of question and answer retrieval experiment mainly involves two aspects: the training data construction and the model evaluation standard.

(1) *Training Data Construction.* The collected basic financial data are preprocessed to obtain a total of 10,000 training data of “user question-knowledge point title-answer-label format.” Then the training data is manually annotated. Finally, they are randomly assigned to the training set, verification set, and test set with an allocation ratio of 8 : 1 : 1, which is,

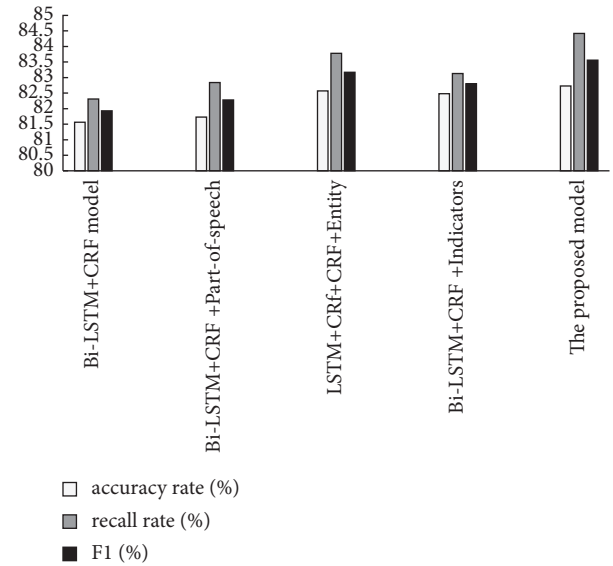


FIGURE 10: The validation experiment results of domain knowledge features.

respectively, used for model training, model parameter tuning, and model effect verification.

(2) *Model Evaluation Criteria.* The key to question and answer retrieval task is to solve the sentence similarity, and the setting of similarity threshold directly affects the evaluation indexes of each model. In this paper, two sets of evaluation criteria are proposed to evaluate the model. One is AUC, which has nothing to do with the threshold of classification criteria and is often used to evaluate dichotomy models. The second is average precision MAP and average accuracy MRR, which are associated with information retrieval ranking.

4.2.2. *Experimental Results and Analysis.* This section tests the validity of the Q&A model proposed in this paper by comparing the recognition effects of different attention mechanisms and entity features.

(1) *Comparative Experiments of Different Types of Attention Mechanisms.* The model in this paper introduces the entity attention mechanism and the answer attention mechanism. The former is based on the entity cod vector, which is used to solve the weight of each word in the problem. The latter is based on the answer cod vector, which is used to solve the weight of each word in the problem. The comparative experimental results are listed in Figure 11; the M_1 to M_4

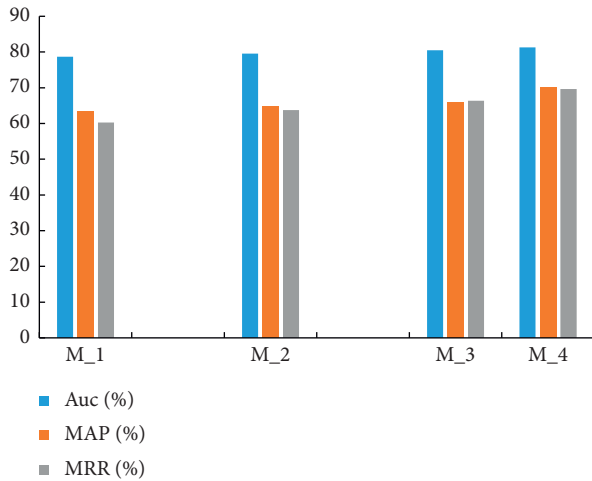


FIGURE 11: The results of comparative experiments of different types of attention mechanisms.

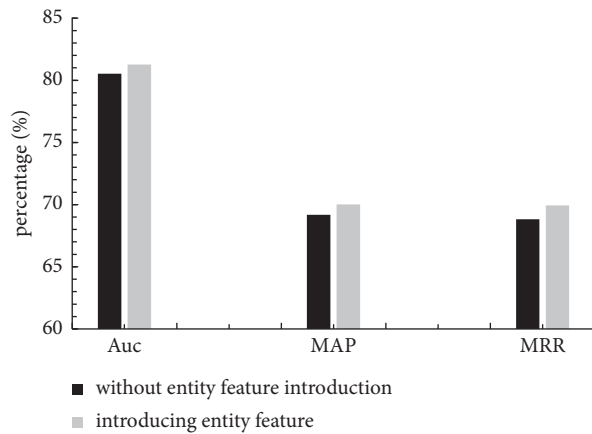


FIGURE 12: The results of comparative experiment of entity feature.

represent the model without attention mechanism introduction, the model with entity attention mechanism, the model with answer attention mechanism, and the proposed model, respectively.

As can be seen from Figure 11, compared with the model without attention mechanism, the model that introduces attention mechanism has better effect. Comparing the effect of the entity attention mechanism model with the answer attention mechanism model, the improvement effect of the entity attention mechanism is more significant, because in the model in the process of problem representation, the entity attention mechanism can restrict the model to pay more attention to the entity information, so as to identify the core semantics more accurately.

(2) *Comparative Experiment of Entity Feature.* By comparing the effect of the model without introducing entity feature information with that introducing entity feature information, the effectiveness of introducing entity feature information in improving the effect of Q&A matching model is verified. The experimental results are listed in Figure 12.

According to Figure 12, compared with the Q&A model introducing entity feature information, after entity feature information was introduced, the AUC, MAP, MRR, and other evaluation indicators of the Q&A model increased by 0.74%, 0.85%, and 0.81%, respectively. It indicates that the introduction of entity feature information was feasible and effective, because the entity feature information contains a large amount of entity feature prior knowledge. The question + answer matching model uses training data to learn automatically. So the influence mechanism of entity feature information on the final matching relationship can be clarified, which is helpful to improve the effect of entity recognition.

5. Conclusion

As can be seen from the above studies, the relevant indicators obtained by the improved entity recognition method in this paper have obvious advantages over the traditional methods. In addition, the AUC, MAP, and MRR indicators, etc. obtained by the improved entity recognition method are higher than those of other methods. Therefore, the improved method has obvious advantages. What is more, it can be seen that the accuracy of semantic recognition method is greatly improved; the fundamental reason is that, after combining the Bi-LSTM with CRF to process and extract the entity features of financial knowledge field, there is a large amount of prior knowledge in the features, so as to greatly improve the accuracy of recognition.

Data Availability

The experimental data are available from the corresponding author upon request.

Conflicts of Interest

The authors declare that they have no conflicts of interest regarding this work.

Acknowledgments

This work was sponsored in part by Hebei Intelligent Financial Technology Innovation Center.

References

- [1] T. Sun, Y. Xu, Y. Shao, N. Dai, and X. Huang, "Pre-trained models for natural language processing: a survey," *Science China Technological Sciences*, vol. 63, no. 10, pp. 1872–1897, 2020.
- [2] M. Hu, B. Ryzen, T. Chen Annie, S. H. Zhu, and M. Conway, "Determining the prevalence of cannabis, tobacco, and vaping device mentions in online communities using natural language processing," *Drug and Alcohol Dependence*, vol. 228, 2021.
- [3] B. G. Patra, M. M. Sharma, V. Vekaria et al., "Extracting social determinants of health from electronic health records using natural language processing: a systematic review," *Journal of the American Medical Informatics Association*, vol. 28, no. 12, pp. 2716–2727, 2021.

- [4] N. Wilfredo, J. D. Amado, I. Cardinale, E. Lopes-Silva, and C. S. Libarino, "Emotion detection for social robots based on NLP transformers and an emotion ontology," *Sensors*, vol. 21, no. 4, p. 1322, 2021.
- [5] L. Man and R. Bai, "Recognition of English information and semantic features based on SVM and machine learning," *Journal of Intelligent and Fuzzy Systems*, vol. 40, no. 2, pp. 2205–2215, 2021.
- [6] N. Zhai, "Research on text sentiment analysis based on attention mechanism," *International Core Journal of Engineering*, vol. 7, no. 8, pp. 211–216, 2021.
- [7] N. Bao and C. Wang, "A multi-agent knowledge integration process for enterprise management innovation from the perspective of neural network," *Information Processing & Management*, vol. 59, no. 2, Article ID 102873, 2022.
- [8] N. Atefi, N. Ali, and M. M. Ebrahimi, "Sparse deep LSTMs with convolutional attention for human action recognition," *SN Computer Science*, vol. 2, no. 3, 2021.
- [9] Y. Tian, Y. Wu, D. Zhang, and H. Li, "Relationship modeling between vehicle-induced girder vertical deflection and cable tension by BiLSTM using field monitoring data of a cable-stayed bridge," *Structural Control and Health Monitoring*, vol. 28, no. 2, 2020.
- [10] D. Jha, P. H. Smedsrud, D. Johansen et al., "A comprehensive study on colorectal polyp segmentation with ResUNet++, conditional random field and test-time augmentation," *IEEE journal of biomedical and health informatics*, vol. 25, no. 6, pp. 2029–2040, 2021.
- [11] N. Warjri, P. Pakray, S. Lyngdoh, and A. Maji, "Part-of-speech (POS) tagging using conditional random field (CRF) model for Khasi corpora," *International Journal of Speech Technology*, vol. 24, no. 4, pp. 1–12, 2021.
- [12] I. Yoshida, T. Yukihisa, and O. Yu, "Estimation of trend and random components of conditional random field using Gaussian process regression," *Computers and Geotechnics*, vol. 136, 2021.
- [13] N. Cheng, C. W. Hsu, G. J. Horng, and S. Y. Chen, "Across-camera object tracking using a conditional random field model," *The Journal of Supercomputing*, vol. 77, pp. 1–28, 2021.
- [14] X. Ning, P. Duan, W. Li, and S. Zhang, "Real-time 3D face alignment using an encoder-decoder network with an efficient deconvolution layer," *IEEE Signal Processing Letters*, vol. 27, pp. 1944–1948, 2020.
- [15] W. Cai, D. Liu, X. Ning, and G. Xie, "Voxel-based three-view hybrid parallel network for 3D object classification," *Displays*, vol. 69, no. 1, 2021.
- [16] C. A. Tovey, C. Tsuji, A. Egerton et al., "Autoinhibition of CNN binding to γ -TuRCs prevents ectopic microtubule nucleation and cell division defects," *The Journal of Cell Biology*, vol. 220, no. 8, 2021.
- [17] J. Xie, S. Chen, Y. Zhang, D. Gao, and T. Liu, "Combining generative adversarial networks and multi-output CNN for motor imagery classification," *Journal of Neural Engineering*, vol. 18, no. 4, 2021.
- [18] P. A. Marina, M. H. Doweidara, M. Doblaré, and J. A. Jiménezabc, "Predicting cell behaviour parameters from glioblastoma on a chip images," *A Deep Learning Approach. Computers in Biology and Medicine*, vol. 135, Article ID 104547, 2021.
- [19] Y. Miao, "A review on the application of blind deconvolution in machinery fault diagnosis," *Mechanical Systems and Signal Processing*, vol. 163, 2022.
- [20] Z. Qiao, Y. Lei, and N. Li, "Applications of stochastic resonance to machinery fault detection: a review and tutorial," *Mechanical Systems and Signal Processing*, vol. 122, pp. 502–536, 2019.
- [21] N. Wang, J. Cao, C. R. Bowen, and G. Litak, "Probability and output analysis of asymmetric bistable energy harvesters subjected to Gaussian white noise," *The European Physical Journal Plus*, vol. 134, no. 11, pp. 1–16, 2019.
- [22] Y. Jin, S. Xiao, and Y. Zhang, "Enhancement of tristable energy harvesting using stochastic resonance," *Journal of Statistical Mechanics: Theory and Experiment*, vol. 2018, no. 12, Article ID 123211, 2018.
- [23] B. Yan, S. Zhou, and G. Litak, "Nonlinear analysis of the tristable energy harvester with a resonant circuit for performance enhancement," *International Journal of Bifurcation and Chaos*, vol. 28, no. 7, 2018.
- [24] H. Tian, S. Deng, C. Way, and X. Ni, "A novel method for prediction of paraffin deposit in sucker rod pumping system based on CNN indicator diagram feature deep learning," *Journal of Petroleum Science and Engineering*, vol. 206, 2021.
- [25] Y. Wang, J. Wang, and H. Che, "Two-timescale neurodynamic approaches to supervised feature selection based on alternative problem formulations," *Neural Networks*, vol. 142, pp. 180–191, 2021.
- [26] H. Che, C. Li, X. He, and T. Huang, "An intelligent method of swarm neural networks for equalities-constrained nonconvex optimization," *Neurocomputing*, vol. 167, pp. 569–577, 2015.

Research Article

The Social Public Issues Analysis Model Based on Deep Learning

Yanqiong Gu  and **Jianyong Shi**

Shanghai University of Engineering Science, Shanghai 201620, China

Correspondence should be addressed to Yanqiong Gu; m030617160@sues.edu.cn

Received 19 December 2021; Revised 10 January 2022; Accepted 11 January 2022; Published 17 February 2022

Academic Editor: Man Fai Leung

Copyright © 2022 Yanqiong Gu and Jianyong Shi. This is an open access article distributed under the Creative Commons Attribution License, which permits unrestricted use, distribution, and reproduction in any medium, provided the original work is properly cited.

To improve the governance effect of public communities and protect community security, combined with the basic principles and network structure of CNN network in deep learning, a community security risk prediction model based on improved single-channel CNN network and decision tree is constructed. The experimental results show that expanding the single channel to the multichannel network greatly extends the receptive field of CNN network. Simultaneously, the accuracy of the prediction model is improved, which is as high as 87.7%. After inputting the output values of every single model into the comprehensive model, the prediction accuracy of the comprehensive model is improved by 4.8%. The feasibility and effectiveness of this method are further demonstrated.

1. Introduction

In recent years, with the rapid development of deep learning, the probability prediction of crime occurring in the field of public community has become the focus of the current research in the field of community safety protection. The role of community crime prediction is to help the police patrol, prevent crime ahead of time, and ensure people's safety of life and property. At present, some cities have designed and developed a police prediction system. However, the system still has the problem of low accuracy of risk prediction and cannot effectively protect community security. Among them, the wide application and popularization of deep learning make this artificial intelligence technology in image classification, speech recognition, and motion capture and other fields have achieved good application results. Based on this, combined with the learning characteristics and feature extraction ability of deep learning, it is applied to public community safety management and risk prediction.

For risk prediction, many scholars and experts have carried out a lot of exploration and analysis. For example, Savadkoohi and others applied neural network to motion prediction. And the corresponding neural network prediction model is constructed. Moreover, the model was compared with recursive neural network (RNN), short and

long-time memory (LSTM), and one-dimensional convolutional neural network (1D-CNN). The comparison results show that the constructed neural network model can accurately predict human motion state through time-series signals (based on FES measurement) and has certain effectiveness [1]. Shuang and Tiantian applied the prediction model to power electronic equipment. Thus, an early warning model based on FPGA and neural network with radiation function is built to accurately predict and analyze the currency risks from 2010 to 2015. The results show that combining radiation with the neural tissue model makes the error between the prediction effect and the actual effect less than 11%, which has certain predictability [2]. Rui proposed to build a risk prediction model in the field of financial risk. The neural network in deep learning is used for feature extraction and learning of financial text information, so as to realize effective risk prediction in the financial market [3]. Tu et al. applied the deep learning method to the risk prediction of lung cancer to improve the diagnostic accuracy of lung cancer [4]. Fangneng et al. applied the genetic algorithm to risk assessment, providing a reference for the application of machine learning in risk prediction [5]. Soft computing and others applied the deep learning model to the prediction of social security risk in the United States, thus opening up the application of deep learning in security risk management

[6–9]. Based on this, a community security risk prediction model based on deep learning is proposed. And the feasibility of the model is verified experimentally, which provides reference data for risk prediction in the same field.

2. Basic Methods

2.1. Convolutional Neural Network Algorithm. The concept of convolutional neural network was proposed by emulating the biological vision system. Enlightened by the receptive field mechanism, and citing relevant theories in neuro-cognitive, the Fukushima's team created the first convolutional neural network framework. It is a classical artificial neural network framework, which has advantages in processing data like network, such as image and video data. Convolutional neural network uses convolutional mathematics, namely, a mathematical operation of two real variable functions, as shown in the following formula [10–12]:

$$s(t) = (x * w)(t). \quad (1)$$

There are input layer, convolution layer, pooling layer, full connection layer, and output layer in the convolutional neural network. The architecture is shown in Figure 1.

The input layer enters data into the convolutional neural network, and the data contains different feature information.

Convolution layers use multiple feature faces to extract feature information of input data. For example, the deep convolution layers are used to extract the advanced features, while the shallow convolution layers are used to extract the low-level features. The convolution kernel is similar to the feature extractor. Where each convolution kernel is responsible for extracting the feature information of local areas. For example, the convolution core for two-dimensional data is a weight matrix of 5×5 or 3×3 . The length and width of the convolution kernel are limited. And multiplying the length by the width of the convolution layer can determine the size, while the depth of the convolution kernel is consistent with the depth of the current image. Therefore, when specifying the convolution kernel, only two parameters, length and width, are required to be set.

The pooling layer mainly has two functions. One is to use multiple feature maps to extract feature information. At the same time, it tries to reduce the low-latitude operation under the premise of fully retaining the features. The second is to reduce the number of full connections between convolution layers, thereby reducing the computational volume. There are a variety of pooling methods created to better extract global or local features, which are maximum pooling, spectrum pooling, mixed pooling, mean pooling, spatial pyramid pooling, and so on [13]. If a classifier is laid after the pooling layer, the overfitting may be induced due to the high input dimension of the classifier, which can be solved by deploying the convergence layer after the convolution layer.

The full connection layer maintains full connection with all neurons in the previous layer, which performs global integration and clustering of feature information in the

input layer or convolution layer. The full connection of the convolutional neural network is shown in Figure 2 [14–17].

For the output layer, it can be seen that the output is determined by the function of convolutional neural network. If the function is supervised learning, the output layer acts as a classifier, just like SoftMax, SVM, and so on. If the function is unsupervised learning, the output of output layer is feature reconstruction.

Convolutional neural network has local connectivity and weight sharing, and some panning, scaling, and rotation can remain unchanged. From the application effect, the convolutional neural network has the advantages of sparse interaction, parameter sharing, and so on.

2.2. CART Decision Tree. CART decision tree algorithm is a binary tree, which is a classification and regression tree algorithm. It can be used for both classification and regression. Whether it applies to regression tree or decision tree is determined by the target task. If the results to be predicted are discrete data, the CART can generate the classification decision tree. If the result to be predicted is continuous data, the CART can generate the regression decision tree. When the CART is a classification tree, the GINI value is used as the basis of node splitting. When the CART is a regression tree, the MSE (mean square error) is used as the basis of node splitting. Since this paper mainly predicts the number of community issues, which is a continuous value, the CART regression tree algorithm is selected.

CART regression tree adopts mean square error to carry out model measurement. Then, feature screening is achieved by establishing regression equation and pruning, and the specific calculation formula is as follows [18]:

$$MSE(D) = \frac{1}{M} \sum_1^M (y_m - \hat{y}_m)^2,$$

$$\min_{j,s} \left[\min_{c_1} \sum_{x_1 \in R_{2(j,s)}} (y_1 - c_2)^2 \right], \quad (2)$$

$$C_a(T_t) = C(T_t) + a|T_t|,$$

$$C_a(T) = C(T) + a,$$

$$a = \frac{C(T) - C(T_t)}{|T_t| - 1}.$$

3. Construction of Community Security Prediction Model

This paper adopts the number of community security cases as the basic feature attribute. And the other characteristic attributes, which is closely related to it, are also selected. On

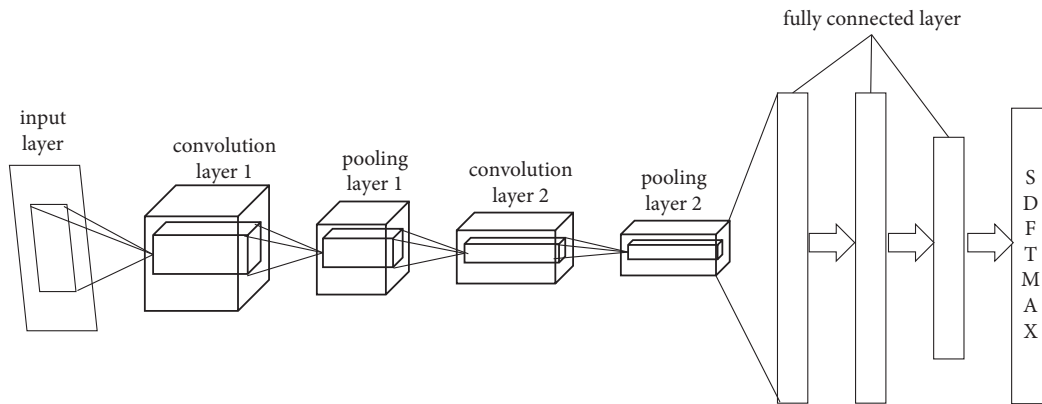


FIGURE 1: The architecture of convolutional neural network.

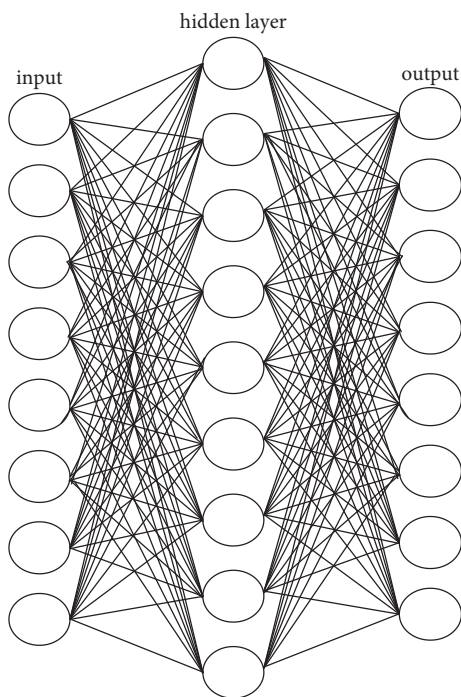


FIGURE 2: The full connection of convolutional neural network.

this basis, the prediction model of community security is constructed.

3.1. Construction Ideas of Comprehensive Prediction Model.

Using feature filter to sift out the relevant data to select the key feature factors and divide them into training sets and test sets. The community security prediction model is constructed. In order to meet the prediction requirements, this paper integrates the CART regression tree model to construct a comprehensive prediction model under the framework of convolutional neural network model. It can accurately predict the number of community security cases. The construction process of community security prediction model is shown in Figure 3.

Step 1. Read the data. The selected key feature factors are included in the Python, including the number of

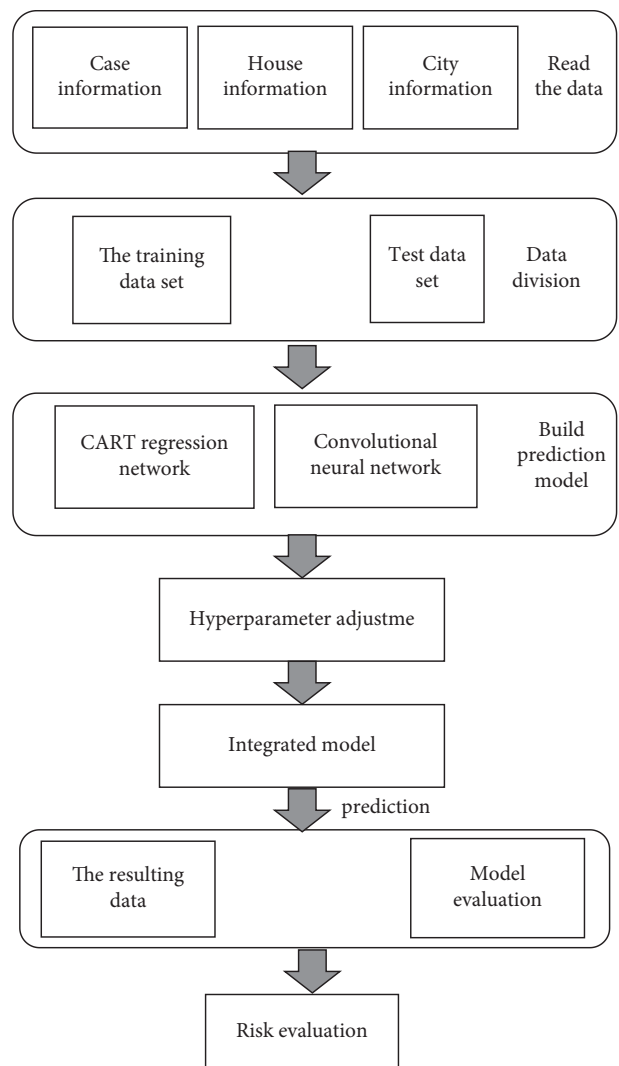


FIGURE 3: Flowchart of community security risk model construction.

community security cases, H-City climate data, community second-hand housing prices, holiday data, and so on.

Step 2. Classify the relevant data. The 80% of the data are included in the training set, and the 20% of the data are included in the test set.

Step 3. Build an intelligent prediction model. The multichannel convolution neural network prediction model and CART regression tree prediction model are established to predict the number of community security cases, respectively.

Step 4. Use the training set data to train the convolutional neural network model and the CART regression tree prediction model. And at the same time, carry out hyperparameter mediation to determine the optimal output of each model.

Step 5. Improve the applicability of the comprehensive prediction model. The comprehensive prediction model is constructed based on the framework of neural network. Use the test set to verify the comprehensive prediction model and optimize the evaluation index of the model.

Step 6. Evaluate the risk. Use the comprehensive prediction model to predict the number of community security cases in the future and evaluate the risk of community security.

3.2. Data Source Acquisition and Feature Selection. The community security data of community Z in H city from 2017 to 2019 are collected through official channels to evaluate the community risk value. When collecting community security data, it is inevitable to encounter the absence of a dataset. And the appropriate measures should be taken according to the importance of missing values and the difficulty of obtaining them. Specifically, if the missing values are not significant to the objectivity of the data information and the validity of the results, the missing values can be deleted. If the amount of missing value data is small and easy to obtain, manual filling can be adopted. If the missing value has a great impact on the research work, moving window mean value can be used to fill, and the formula is as follows [19–22]:

$$X_m = \frac{1}{6} (X_{m-3} + X_{m-2} + X_{m-1} + X_{m+1} + X_{m+2} + X_{m+3}). \quad (3)$$

There are differences for the obtained data in the unit magnitude. And the analysis results of the community security characteristics are affected. Therefore, it is necessary to normalize the collected data. And map them all to the interval [0,1], so as to eliminate the influence of unit magnitude on the analysis results. The formula for data normalization is as follows:

$$y = \frac{x - \text{Min}}{\text{Max} - \text{Min}}. \quad (4)$$

When constructing the community security case prediction model, the feature attribute data in the attribute table of the basic dataset should be selected first. The characteristic factors most closely related to the number of community

security cases can be selected. In general, the selected characteristic factors are more correlated with the number of community security cases. Therefore, the improved Pearson correlation coefficient is used for correlation analysis in this paper, and the formula is as follows [23]:

$$R = \frac{\sum_1^n (X_i - \bar{X})(Y_i - \bar{Y})}{\sqrt{\sum_1^n (Y_i - \bar{Y})^2} \sqrt{\sum_1^n (X_i - \bar{X})^2}}. \quad (5)$$

After the analysis, this paper finally selects the number of public security cases, holiday data, climate score, and community second-hand housing prices as the input characteristic attribute of the prediction model to build the number of community security cases.

3.3. Case Prediction Model Based on Convolutional Neural Network

3.3.1. Construction of Convolutional Neural Network Model. To predict the number of community security cases, first of all, it is necessary to identify the various factors associated with the risk of community policing. Then, the characteristics of data source are analyzed. Finally, the characteristic attributes that have the greatest impact on community security risk are selected, including the number of community daily security cases, climate data of H City, community second-hand housing prices, and holiday data.

The prediction accuracy of community security cases depends on whether the extraction of characteristic attributes is reasonable. The traditional convolutional neural network can only extract local feature, so it is necessary to improve it. This paper proposes an autoregressive multichannel convolutional neural network model. There are input layer, convolution layer, maximum pooling layer, flatten layer, dropout layer, and full connection layer in the model. At the same time, the DenseNet is deployed behind the full connection layer to achieve the connection of different layers and the connection of each feature maps [24–26]. It can be seen that the gradient disappearance problem can be effectively suppressed.

Using the convolution neural network for prediction, the input attribute features will directly affect the predictions. Therefore, improving the traditional neural network model from the input layer, the multichannel convolutional neural network prediction model can be obtained. And there are outstanding advantages for the improved model, the wider receptive field, and the higher prediction accuracy.

The structure of traditional convolutional neural network model and multichannel convolutional neural network model is shown in Figure 4.

The first step is to compile dataset. The input data needs to be transformed into a 7×4 matrix. Where the seven rows, respectively, represent the data of each day in the previous seven days, and the four columns, respectively, represent the extracted four feature datasets. The data input to the model can be expressed as 1,4, and 7. Here, “1” represents a sample, “7” represents the continuous data of the previous seven days, and “4” represents the variable dimension.

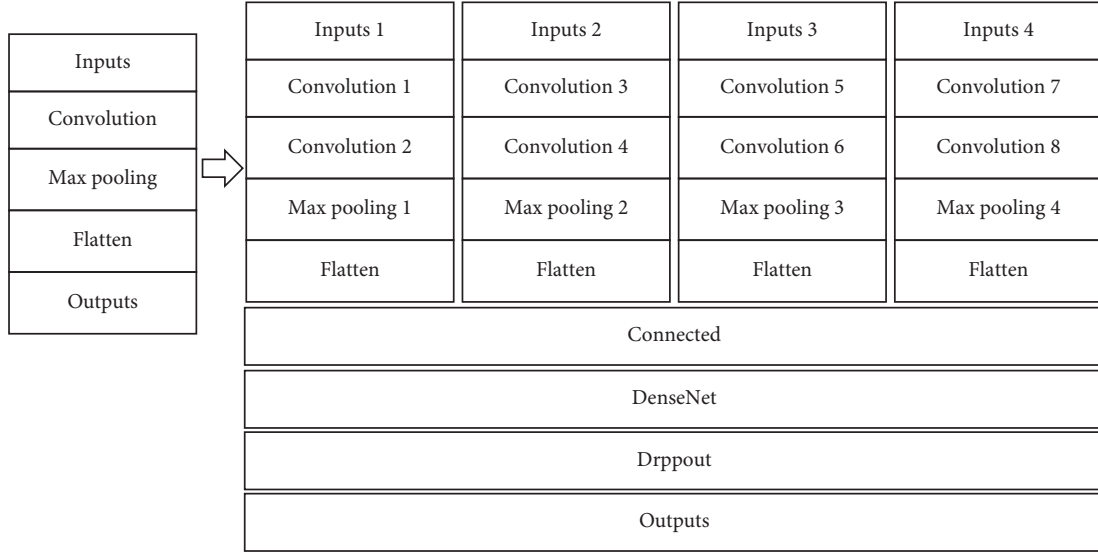


FIGURE 4: The structure of convolutional neural network.

The second step is to establish the deep convolutional neural network. First, using the one-dimensional convolution kernel to extract the feature of variable vector $V_i = [D_1, D_2, D_3, D_4, D_5, D_6, D_7]$ in input layer L_i . Then, build a one-dimensional convolution nuclear feature extractor, and there are 32 convolution kernels of size equal to 3. What is more, the activation function is ReLU function.

The convolution layer is connected to a convolution kernel with a one-dimensional size equal to 3 and then connected to a maximum pooling layer with a one-dimensional size equal to 2. After that the flatten is performed on the extracted features to obtain the flattening layer F_i .

There are two full-connect layers D1 and D2 connected after the flattening level. Both use the ReLU function. And there are 200 and 100 neurons, respectively, within the hierarchy. After the full-connection layer D2, an output layer is connected, which contains only one neuron, corresponding to the data values of the prediction day.

The third step is to train and verify the model. After the deep convolutional neural network is established, it is also necessary to train it with the training set. The closer the model value is to the observation value, the smaller the mean square error (MSE) is. After the model training is completed, the test set is predicted by the model to verify the model prediction accuracy. The ReLU function is used as the activation function, which can effectively avoid the problem of gradient disappearance in the process of model training.

After establishing the autoregressive multichannel convolutional neural network model and the completing the model training and verification, the N-dimensional vector of the next day (i.e., the eighth day) is predicted by using the community feature vector of the previous seven days. And the new feature vector is finally output by window sliding.

Considering that both the input and output data of the model are multiples of 7, it is necessary to perform data cutting. The initial and predicted datasets are represented as follows:

$$\begin{pmatrix} A_{11}A_{12}A_{13}A_{14}A_{15}A_{16}A_{17}, \\ A_{21}A_{22}A_{23}A_{24}A_{25}A_{26}A_{27}, \\ \dots\dots\dots \\ A_{n1}A_{n2}A_{n3}A_{n4}A_{n5}A_{n6}A_{n7}, \end{pmatrix} \rightarrow \begin{pmatrix} A_{18}, \\ A_{28}, \\ \dots\dots\dots \\ A_{a8}, \end{pmatrix}, \quad (6)$$

$$\begin{pmatrix} A_{12}A_{13}A_{14}A_{15}A_{16}A_{17}A_{18}, \\ A_{22}A_{23}A_{24}A_{25}A_{26}A_{27}A_{28}, \\ \dots\dots\dots \\ A_{n2}A_{n3}A_{n4}A_{n5}A_{n6}A_{n7}A_{n8}, \end{pmatrix} \rightarrow \begin{pmatrix} A_{19}, \\ A_{29}, \\ \dots\dots\dots \\ A_{a9}, \end{pmatrix},$$

where $(A_{11}A_{12}A_{13}A_{14}A_{15}A_{16}A_{17})$ represents a feature of the first seven days, n rows represent n features of a week, and the feature vector of the predicted eighth day is on the right. After the prediction results of day eight are obtained, the feature vectors of day nine can be predicted by window sliding, as shown in formula (6). Therefore, long-term prediction can be performed by window sliding.

4. Analysis of Experimental Results

4.1. Optimal Parameter Optimization. The parameter settings of convolutional neural networks are directly related to the advantages and disadvantages of the prediction results, and parameters are experimentally tuned to determine a set of optimal parameter combinations that can achieve the best prediction performance.

The correlation coefficient (R), determination coefficient (R -squared), root mean square error (RMSE), and other evaluation indicators are used to achieve quantitative evaluation. Among them, the larger the R and R^2 values are, the smaller the error between the predicted value and the actual value is, so the higher the prediction accuracy of the model is. RMSE represents the amount of deviation between the predicted value and the actual value. The smaller RMSE is, the closer the predicted value is to the observed value.

4.1.1. Parameter Optimization of Convolution Layer. The established convolutional neural network model contains two convolution layers. And it is compared with the convolutional neural network model with one convolution layer. The experimental results are listed in Table 1.

After the convolution layer changed from 2 to 1, the correlation coefficient R in the model evaluation results is decreased by 2%; the determination coefficient R -squared is decreased by 1%; and the root mean square error is increased by 0.06. This indicates that the prediction accuracy of the model containing two convolution layers is higher, so the optimal parameter of the convolution layer of the convolutional neural network model is two layers.

4.1.2. Convolution Kernel Parameter Optimization. The function of convolution kernels is to extract feature vectors, and the number of convolution kernels directly affects the network framework performance. In general, appropriately increasing the number of convolution kernels is conducive to extract the feature more fully. However, if the number of convolution kernels is too large, it may induce the overfitting problem. This experiment compares and analyzes the prediction performance of two types of convolutional neural network models with convolution kernels 32 and 16, respectively. The experimental results are shown in Table 2.

Here, the correlation coefficient R corresponding to the prediction model with 16 convolution kernels is equal to 0.9542, which is 1% lower than that of the prediction model containing 32 convolution kernels. Similarly, the determination coefficient R^2 also decreases, while the root mean square error increases by 0.02. It can be seen that the prediction performance of the convolutional neural network model with 32 convolution kernels is better than that of the convolutional neural network model with 16 convolution kernels.

4.1.3. Optimization of Activation Function. ReLU function and tanh function are common nonlinear activation functions, where the ReLU function has the advantages of high operation efficiency, effective avoidance of gradient explosion, gradient disappearance, and overfitting. The tanh function has the characteristics of fast convergence, which can map the output results to the interval $[-1, 1]$. If the input value is too large or too small, the activation function is saturated. In order to test the application effect of ReLU function, this experiment compares the performance of the tanh function, and the results are shown in Table 3.

It can be seen that the correlation coefficient R corresponding to the network model of using ReLU activation function is higher than the network model of using tanh activation function. And the determination coefficient R -squared is 4% higher, but the root mean square error is smaller, which indicates that using ReLU activation function can better improve the prediction effect of the convolutional neural network model.

4.1.4. Optimizer Optimization. At present Adam is the most widely used optimizer. It not only has the advantages of low

TABLE 1: Comparison of experimental results for different convolution layers.

The number of convolution layers	R	R -squared	RMSE
Conv. layer = 1	0.9643	0.9299	0.8799
Conv. layer = 2	0.9692	0.9391	0.8192

TABLE 2: Comparison of experimental results for different convolution kernel.

The number of convolution kernels	R	R -squared	RMSE
32	0.9692	0.9391	0.8192
16	0.9542	0.9106	0.8389

TABLE 3: Comparison of experimental results for different activation functions.

Activate function	R	R -squared	RMSE
ReLU	0.9692	0.9391	0.8192
tanh	0.9469	0.8968	1.0677

memory footprint and fast convergence but also can adapt to application scenarios such as high-dimensional space, large datasets, and so on. In addition to Adam, RMSprop is another common optimizer. By comparing and analyzing Adam and RMSprop, the optimizer optimization of prediction model is completed. The test results are listed in Table 4.

What can be seen that the correlation coefficient (R), determination coefficient (R -squared), and other indicators of the network model using Adam optimizer are higher than those using RMSprop optimizer, and the root mean square error (RMSE) is smaller, which indicates that Adam optimizer has better performance in this experiment.

4.1.5. Optimization of Pooling Layer. Pooling layer can improve the generalization ability of the model. It can avoid the problem of overfitting in the process of model prediction and maintain the stability of the feature vector. The max pooling layer is adopted to compare with average pooling layer in this experiment. The experimental results are shown in Table 5.

The results show that the correlation coefficient R and judgment coefficient R -squared corresponding to max pooling have a small difference with average pooling. However, the root mean square error corresponding to max pooling is significantly smaller than average pooling. Therefore, The convolution neural network model in this paper selects max pooling to obtain more accurate prediction results. After the parameter optimization, the hyperparameter combination scheme of multichannel convolutional neural network model is finally determined: 2 convolution layers, 32 convolution kernels, max pooling, ReLU activation function, and Adam optimizer. Dropout = 0.5. In addition, considering the training set is small, the number of training cycles epoch is equal to 20 and the number of single batch training batch size is equal to 4.

TABLE 4: Comparison of experimental results for different optimizer.

Optimizer	R	R -squared	RMSE
Adam	0.9692	0.9391	0.8192
RMSprop	0.9594	0.9206	0.8789

TABLE 5: Comparison of experimental results for different pooling layer.

Pooling layer	R	R -squared	RMSE
Max pooling	0.9692	0.9391	0.8192
Average pooling	0.9678	0.9368	0.8354

4.2. *Prediction Results of Autoregressive Multichannel Convolutional Neural Network Model.* Figure 5 shows the comparison of the prediction results with the actual observations of the autoregressive multichannel convolutional neural network model, where the blue line and the red line coincide in many positions, it shows that this model prediction accuracy is higher. In addition, the third peak of the red line means the predicted value of the model, which deviates from the actual observations by a small amount.

The LSTM prediction model and logistic regression model are compared to objectively define the prediction performance of the autoregressive multichannel convolutional neural network model established in this paper, and the results are listed in Figure 6. For the evaluation indicators, the R -squared value is 77.1% and the RMSE value is 0.857.

Here, the determined error R -squared of the proposed model is higher than that of the other two kinds of prediction models, and the root mean square error is smaller, which indicates that the overall prediction performance of the model in this paper is better.

4.3. *Comprehensive Prediction Effect.* Considering that the single prediction model can only produce the ideal performance in a specific task environment, the task characteristics are adopted to assign the corresponding weight strategy for each single prediction model, so as to establish a comprehensive prediction model that can be applied to many task environments.

4.3.1. *Construction of Comprehensive Prediction Model.* Based on the idea of ensemble learning, the training set is used to synchronically train the multichannel convolutional neural network model and CART regression tree model, and the community security risks are predicted, respectively. Then, the output values of the two single prediction models are listed as the input values of the comprehensive prediction model to obtain the final prediction results.

The comprehensive prediction model is constructed as follows.

First, use the original feature data to train the two single models

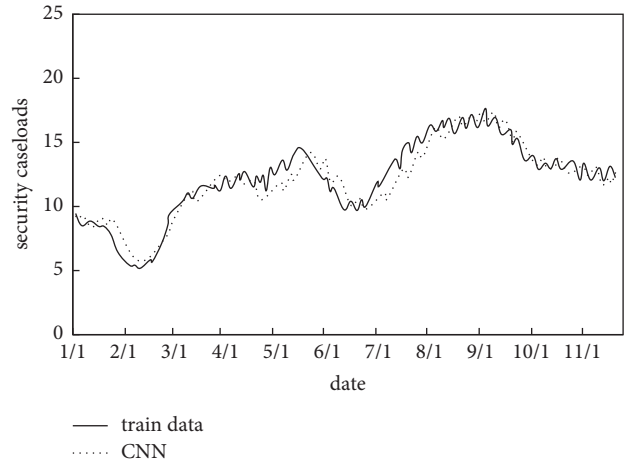


FIGURE 5: Comparison of CNN prediction model results.

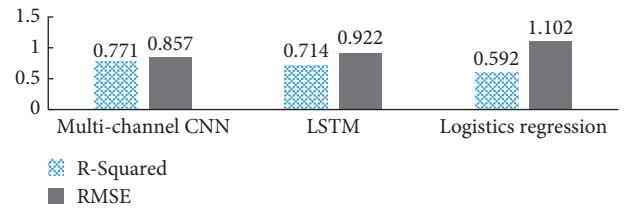


FIGURE 6: Comparison of prediction results of community security caseload.

Second, label the new features of the trained single model as Out1 and Out2, respectively

Third, integrate the original feature data and the two new feature Out1 and Out2 data, and then, output the new feature data, namely, Out3.

Fourth, input the Out3 data into the comprehensive prediction model, and the comprehensive prediction model selects suitable models according to the feature conditions to train Out3 data more fully

The neural network structure of the comprehensive prediction model is shown in Figure 7.

As shown in Figure 7, the neural network structure contains three input values, namely, feature vector, Out1 data, Out2 data, and two hidden layers. Each of the hidden layers contains two neurons and four neurons, respectively. In addition, the output layer in the neural network structure contains one neuron, and the output value is the actual label value.

Neural network model can integrate information from different sources and accurately simulate nonlinear relationship. Multiple single models are integrated under the framework of neural network, and the relationship between each single model is not complicated. In the multilayer sensor, the layers are fully connected, with the input layer at the bottom, the hidden layer in the middle, and the output layer at the end. In practical applications, the gradient descent method (SGD) is usually used for parameter optimization. Its implementation steps are as follows: first,

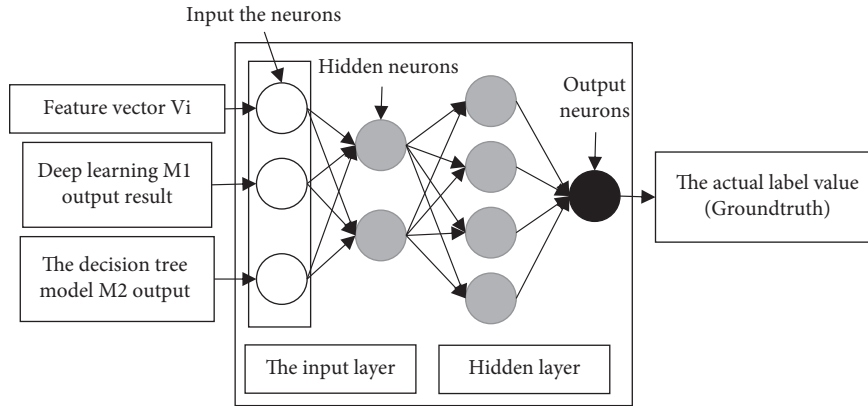


FIGURE 7: The neural network structure of the comprehensive prediction model.

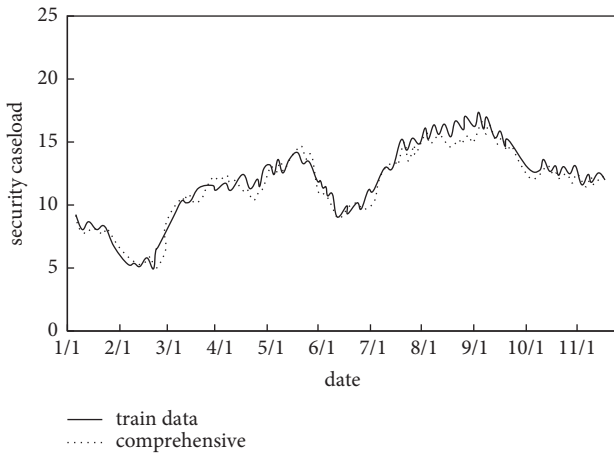


FIGURE 8: Comparison of comprehensive prediction model results.

initialize the parameters, and then perform the iterative training. At the same time, the gradient parameters are updated until the termination condition is reached.

4.3.2. Analysis of Experimental Results. The comparison between the prediction results of the comprehensive prediction model on the test set and the actual observed values is shown in Figure 8.

The ordinates in Figure 8 are the community policing caseloads, the horizontal coordinates are the date, the blue line represents the actual observations, and the black line represents the comprehensive model prediction values. It can be seen that the extension trend of the blue line and the black line is consistent, and the number of coincidence points of the blue line and the black line are more than the number of coincidence points corresponding to the two single prediction models. Therefore, it can be judged that the prediction performance of the comprehensive prediction model is better than that of the two single prediction models. In terms of model evaluation index, the R value of the comprehensive prediction model on the test set is 92.5%, R -squared value is 85.5%, and the RMSE value is 0.703. The correlation between the prediction value and the actual value

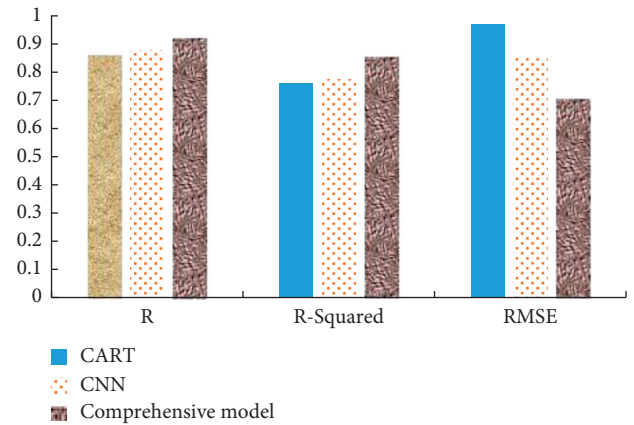


FIGURE 9: Comparison of prediction accuracy of the three prediction models.

is high, and the comprehensive prediction model can obtain the excellent prediction performance.

The prediction accuracy of the three prediction models on the same dataset is listed in Figure 9.

Figure 9 shows that the R values of the three prediction models are greater. The R values of the multichannel convolutional neural network model are higher than that of the CART regression tree model, and the mean square error is lower. Therefore, the prediction performance of the multichannel convolutional neural network model is better. In addition, the R value of the comprehensive prediction model is higher than that of the multichannel convolutional neural network model, and the mean square error is lower, so the prediction performance of the comprehensive prediction model is better.

5. Conclusion

According to the prediction results of the three models for the number of security cases of community Z, although all kinds of models can achieve ideal prediction accuracy, the prediction accuracy of the comprehensive prediction model is higher than that of the convolutional neural network model and the CART regression tree prediction model.

Furthermore, our research also provides a new information approach for the current community security governance.

Data Availability

The experimental data used to support the findings of this study are available from the corresponding author upon request.

Conflicts of Interest



The authors declare that they have no conflicts of interest regarding this work.

References

- [1] M. Savadkoobi, T. Oladunni, and L. A. Thompson, "Deep neural networks for human's fall-risk prediction using force-plate time series signal," *Expert Systems with Applications*, vol. 182, 2021.
- [2] W. Shuang and W. Tiantian, "Risk prediction of financial insurance based on FPGA and neural network," *Microprocessors and Microsystems*, vol. 2020, Article ID 103406, 2020.
- [3] W. Rui, "Prediction research and application of financial time series based on big data," *Journal of Physics: Conference Series*, vol. 1881, no. 2, 2021.
- [4] Y. Tu, Y. Wu, Y. Lu, X. Bi, and T. Chen, "Development of risk prediction models for lung cancer based on tumor markers and radiological signs," *Journal of Clinical Laboratory Analysis*, vol. 35, Article ID e23682, 2020.
- [5] H. Fangneng, Y. Mei, and J. Zhou, "Genetic algorithm-based power system information security risk assessment method," *Journal of Physics: Conference Series*, vol. 1852, no. 2, 2021.
- [6] E. Lima, T. Vieira, and E. Costa, "Evaluating deep models for absenteeism prediction of public security agents," *Applied Soft Computing*, vol. 91, 2020.
- [7] H. Tian, S. Deng, C. Wang et al., "A novel method for prediction of paraffin deposit in sucker rod pumping system based on CNN indicator diagram feature deep learning," *Journal of Petroleum Science and Engineering*, vol. 206, 2021.
- [8] G. Li, L. Runze, and J. Bin, "A data-driven long time-series electrical line trip fault prediction method using an improved stacked-informer network," *Sensors*, vol. 21, no. 13, p. 4466, 2021.
- [9] N. Farhi, E. Kohen, H. Mamane, and Y. Shavitt, "Prediction of wastewater treatment quality using LSTM neural network," *Environmental Technology & Innovation*, vol. 23, 2021.
- [10] H. Zhe, X. Yancai, and C. Jiadong, "Misalignment fault prediction of wind turbines based on improved artificial fish swarm algorithm," *Entropy*, vol. 23, no. 6, p. 692, 2021.
- [11] X. Chen, "The fruit classification algorithm based on the multi-optimization convolutional neural network," *Multi-media Tools and Applications*, vol. 80, pp. 1–18, 2021.
- [12] D. Wang, F. Tian, S. X. Yang, Z. Zhu, D. Jiang, and B. Cai, "Improved deep CNN with parameter initialization for data analysis of near-infrared spectroscopy sensors," *Sensors*, vol. 20, no. 3, p. 874, 2020.
- [13] Y. Pan, S. Wang, and X. Xu, "Classification method of IPv6 traffic based on convolutional neural network," *Journal of Physics: Conference Series*, vol. 1883, no. 1, 2021.
- [14] T. Stewart, P. Hume, and G. R. Tomkinson, "Prediction of military combat clothing size using decision trees and 3D body scan data," *Applied Ergonomics*, vol. 95, Article ID 103435, 2021.
- [15] V. M. Olga, L. Husáková, J. Patočka, S. Ghidini, and E. Zanardi, "Classification of transformed anchovy products based on the use of element patterns and decision trees to assess traceability and country of origin labelling," *Food Chemistry*, vol. 360, Article ID 129790, 2021.
- [16] L. Ruhua, L. Yalan, Y. Pan, and Z. Wenfen, "Facial expression recognition based on convolutional neural network," *Journal of Physics: Conference Series*, vol. 1757, no. 1, Article ID 012100, 2021.
- [17] A. Hakan, B. Umit, K. Deniz, and Y. Ceyhun, "WSFNet: an efficient wind speed forecasting model using channel attention-based densely connected convolutional neural network," *Energy*, vol. 233, 2021.
- [18] A. Voutilainen, C. Brester, M. Kolehmainen, and T. P. Tuomainen, "Effects of data preprocessing on results of the epidemiological analysis of coronary heart disease and behaviour-related risk factors," *Annals of Medicine*, vol. 53, no. 1, pp. 890–899, 2021.
- [19] X. Xiao, Y. Xiao, Y. Zhang, J. Qiu, J. Zhang, and T. Yildirim, "A fusion data preprocessing method and its application in complex industrial power consumption prediction," *Mechatronics*, vol. 77, 2021.
- [20] P. Shengliang, S. Shujun, and Y. YuDong, "A survey of modulation classification using deep learning: signal representation and data preprocessing," *IEEE Transactions on Neural Networks and Learning Systems*, 2021.
- [21] B. C. Mateus, M. Mendes, T. J. Farinha, and A. M. Cardoso, "Anticipating future behavior of an industrial press using LSTM networks," *Applied Sciences*, vol. 11, no. 13, p. 6101, 2021.
- [22] B. Tian, G. Wang, Z. Xu, Y. Zhang, and X. Zhao, "Communication delay compensation for string stability of CACC system using LSTM prediction," *Vehicular Communications*, vol. 29, Article ID 100333-, 2021.
- [23] J. Zhou, Q. Lu, R. Xu, L. Gui, and H. Wang, "EL_LSTM: prediction of DNA-binding residue from protein sequence by combining long short-term memory and Ensemble learning," *IEEE/ACM Transactions on Computational Biology and Bioinformatics*, vol. 17, no. 1, pp. 124–135, 2020.
- [24] X. Chen and Z. Yang, "Compression of trajectory data based on LSTM and smoothed analysis," *International Core Journal of Engineering*, vol. 7, no. 6, pp. 306–312, 2021.
- [25] M. Filipovska and H. S. Mahmassani, "Reliable trajectory-adaptive routing strategies in stochastic, time-varying networks with generalized correlations," *Transportation Research Part C*, vol. 133, 2021.
- [26] N. Yudistira, S. B. Sumitro, A. Nahas, and N. F. Riama, "Learning where to look for COVID-19 growth: multivariate analysis of COVID-19 cases over time using explainable convolution-LSTM," *Applied Soft Computing*, vol. 109, Article ID 107469-, 2021.

Research Article

Research on 3D Rendering Effect of Marine Bionic Packaging Container Based on Deep Learning and Visualization

Jie Ning , Xiaonan Ren, and Joung Hyung Cho 

Department of Marine Design Convergence Engineering, Pukyong National University, Busan 48513, Republic of Korea

Correspondence should be addressed to Joung Hyung Cho; jhcho7@pknu.ac.kr

Received 5 November 2021; Revised 13 December 2021; Accepted 22 December 2021; Published 17 February 2022

Academic Editor: Man Fai Leung

Copyright © 2022 Jie Ning et al. This is an open access article distributed under the Creative Commons Attribution License, which permits unrestricted use, distribution, and reproduction in any medium, provided the original work is properly cited.

Three-dimensional rendering includes the test of system development environment and running environment. Three-dimensional rendering influencing factors test: the number and size of parallel blocks affect the average rendering frame rate of 26.9 when the number is 9600 and the size is 10×10 , and the average rendering frame rate is 13.7 when the number is 600 and the size is 40×40 . According to relevant data, it is inferred that the average rendering frame rate is higher when the number of parallel blocks is large and the size of parallel blocks is small, and the number is inversely proportional to the size. The rendering window size also has a relative influence on the rendering frame rate. When the window size is 600×400 , only the terrain frame rate is 77.3, and when the window size is 1200×800 , the frame rate is 68.1, which shows that when only the terrain frame rate is rendered, the frame rate decreases with the increase in the window size, and its performance is not high when only CPU is used. However, when CPU is combined with GPU, the performance is greatly improved, reaching the highest of 29.3 and the lowest of 21.5, which is much higher than that when only CPU is used. According to the influence of the number of sampling points on the frame rate, the 5×5 sampling method and 2×2 sampling method proposed in this paper have better frame rate performance than the traditional template shadow method. Through the above data, we know that the number of parallel blocks, size, window size, sampling method, and other factors have a certain impact on the average rendering frame rate. Marine bionics is a marginal subject between marine biology and technical engineering science. Deep networks have had a huge impact on the field of machine learning research and application, but at the same time, they cannot clearly explain the ins and outs of deep networks. People have been working to understand the complex process more thoroughly. Since humans' cognition and experience of the world mainly come from vision, good visualization can effectively help people understand the deep network and perform effective optimization and adjustment.

1. Introduction

Through the analysis of deep learning and 3D rendering of marine bionic packaging containers under visualization, we know the deep neural network process of deep learning, visualization method, 3D rendering principle and process analysis, and marine bionic principle. By studying the deep learning function mode to improve visualization, 3D rendering principle, and process analysis accuracy, according to the factors affecting 3D rendering to improve its rendering performance, the marine bionic packaging container is manufactured through the principle of marine bionic so as to analyze its 3D rendering effect.

In literature [1], the topic of computer vision has recently had an impact on food detection and medical applications. The deep learning paradigm of computer vision object segmentation and the visual paradigm learning of online or offline intensive training are the main contents of this paper. Literature [2] reduced the growing number of malicious software by combining RNN with CNN. Learning from raw data [3], that is, deep learning, changes computer vision through end-to-end learning. Through research, we know that this method improves the decoding performance of deep convolution network, and the average decoding is improved from 82.1% to 84%. Good performance is achieved. Literature [4] explored the ability of some microorganisms to manipulate host behavior through the serial

block scanning electron microscope and visual image segmentation algorithm based on deep learning. Literature [5] solved the problem of the visualization method of driving behavior by measuring driving behavior with various types of sensors. In order to help people identify the unique driving patterns in continuous driving, we set up driving behavior visualization. In order to distinguish malware and reduce the threat of malware to the Internet [6], we use the MCSC static feature method to transform malware code into gray image for recognition. Experiments show that the MCSC method is very effective in reducing Internet malware, and it can also be combined with main block selection to improve resolution. Literature [7] was proposed to promote the absorption of trace metals, iron in stomach and manganese and zinc in intestine in seaweed decoction. Biomimetic digestion in vitro and biomimetic biofilm extraction can be realized by biomimetic technology, and the absorption of organic matter in stomach and intestine can be promoted. Literature [8] showed that the potential information revealed by VEA learning crystal structure is obtained through VAE and XRD through simulation and experimental data analysis. At the same time, this method can effectively classify XRD data and can quickly identify data outside the distribution, such as new phase and mixture, all of which reflect the value of the VEA method. The YOLO deep learning model combined with the block matching algorithm locates myocardial wall [9], obtains its flow velocity, and draws eddy current graph by nonlinear weight function. The method of YOLO vectorogram analysis and evaluation is based on the visualization analysis of cardiac fluid movement and combined with the analysis of ultrasonic images of cardiac flow field. Finally, the correctness of the proposed method is verified by experiments, which provides a new basis Literature [10] was proposed to solve the problem of limited number of labeled medical images. The lung inflammation caused by COVID-19 was effectively distinguished from other lung inflammations by implementing transfer learning pipeline, and the overall detection accuracy was 90%, 94.3%, and 96.8%. Literature [11] learnt the mapping through the minimum primitive space method of deep neural network, which is a visual learning method. The visualization ability of neural network can be improved by training additional virtual data of neural network and using new activation function of neural network. In literature [12], in order to get the best visualization effect, the shadow method combination can be used. Four methods are used to detect the quality of the surface coloring algorithm: z-buffer gradient, gray gradient, adaptive gray gradient, and two extended cubes. In contrast, except for thin objects, gray gradient has stronger ability. Literature [13] proposed 3D rendering of VR, SSD, and maximum intensity projection of computed tomography data to scan for many years. Among them, MPR is useful for identifying small cracks, VR is useful for identifying bare ankle tendons, and 3D is helpful for patients with arthritis. In literature [14], hydrocephalus can be tested by 3D rendering, and surface rendering and conventional linear CSF imaging are valuable for judgment. Compared with planar scanning, it has the advantages of improving high-quality images and more

intuitive and clear judgment of disease condition, but its diagnostic value estimation needs further investigation. Literature [15] showed that 3D rendering is especially suitable for free-view video applications. The new depth map compression strategy introduces an effective compression strategy for the shape of the segmented region and then predicts the surface shape from the segmented region and a group of samples with regular intervals, so as to effectively compress a few prediction residuals. The marine bionic packaging container is limited by the actual application scene, and the biological movement scene in the marine environment is realized by simulating the 3D technology. This article mainly highlights the practical application scenarios that this kind of 3D can achieve. In the literature research, there are many application scenarios of 3D technology, but the application scenarios considered are relatively single, and the application in more complex scenarios is not considered, especially the complex transformation of different application objects in ocean simulation scenarios. Therefore, it is of great significance to study the application of 3D technology in marine bionic packaging containers.

In this paper, 3D rendering effect, deep neural network, and visualization technology are combined to analyze the 3D rendering of deep learning and visualization of marine bionic packaging containers. By analyzing the influencing factors of 3D rendering (the size and number of parallel blocks, the size of rendering window, the amount of terrain data, and the number of sampling points), we use the LOD model to optimize 3D rendering, realize the relevant advantages of marine life simulation scene, and create a marine bionic packaging container suitable for human use.

2. Research on 3D Rendering of Deep Learning and Visualization

2.1. Deep Neural Network of Deep Learning. The input layer transmits the information to the hidden layer, and then the hidden layer transmits the data to the value output layer [16] as shown in Figures 1 and 2.

2.2. Visualization Method and Process. The data set is processed, tested, trained, and verified [17], and the specific process is shown in Figures 3 and 4.

By inputting data, the data are mapped to visualization and transformed into knowledge through user interaction in visualization [17]. Firstly, the data are mined to the model; secondly, the model is transformed into knowledge through parameter improvement; finally, the knowledge can also be recycled through feedback loop to form data again.

2.3. Three-Dimensional Rendering Analysis. The 3D application is passed to the 3D application program interface [18]. The GPU front-end program can transfer the loading of vertex data to the primitive assembly and change from point to point, line, and plane; finally, it is transferred to the cache, and the frame cache displays pixels at a time as shown in Figures 5 and 6.

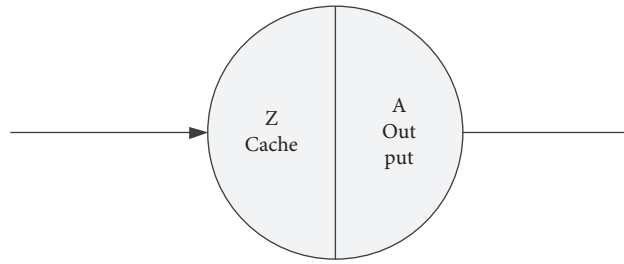


FIGURE 1: Node diagram of deep neural network for deep learning.

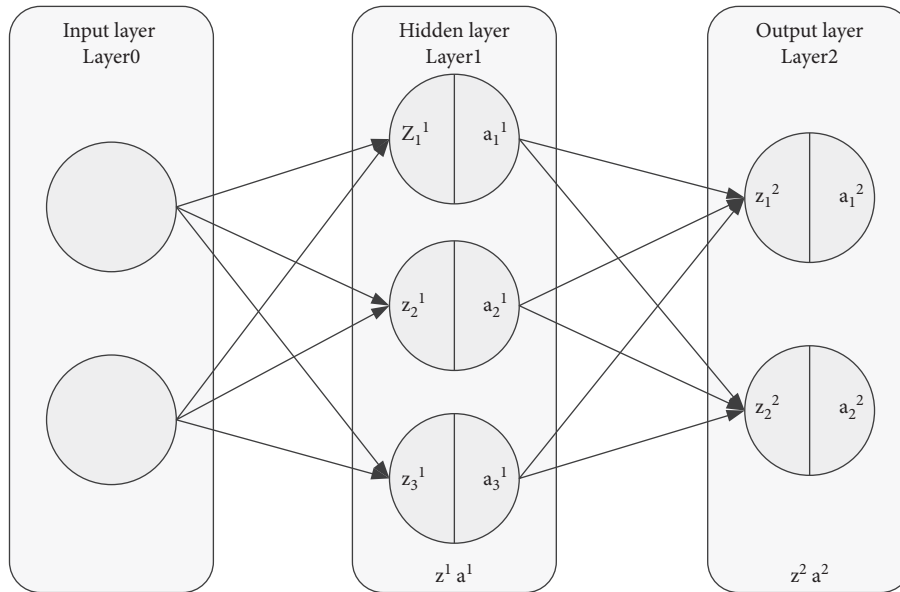


FIGURE 2: Basic structure diagram of deep neural network.

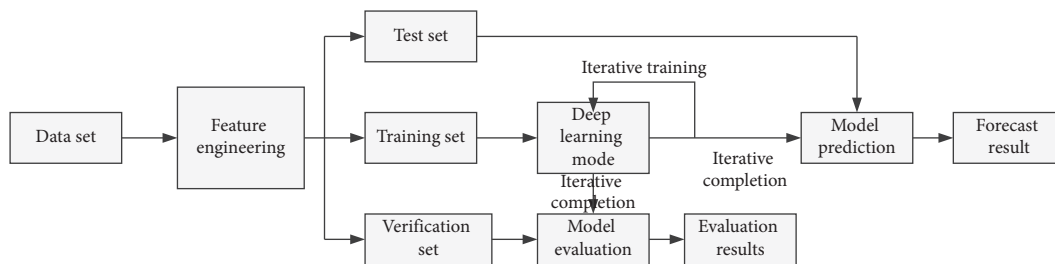


FIGURE 3: Flow chart of visual dataset.

Two-dimensional vector is transformed into the three-dimensional coordinate system by the plane coordinate system and is transformed into the observation coordinate system by using the camera [19].

2.4. Marine Bionics

2.4.1. Principle of Marine Bionic Packaging Container. The problem of man and nature has always been a major concern of our human beings. In the long process of development, mankind has been constantly changing nature, and at the same time, it has been affected by nature. From the ancient primitive society to today, human beings have created their own colorful lifestyle and living environment through

their own power, but these are all based on the use, change, and sacrifice of nature. In the long process of getting along with nature, many bionic creatures have been created through the influence of many creatures, and the average living standard of citizens has been continuously improved. Of course, these should be realized on the basis of peaceful coexistence between man and nature as shown in Figure 7.

Packaging container modeling design is a visual form that combines function with beauty and combines application with science to make packaging container a three-dimensional design. The processing technology made of paper, plastic, metallic glass, and other materials creates a three-dimensional form, so as to achieve the main purpose of holding, storing, protecting goods, and conveying information.

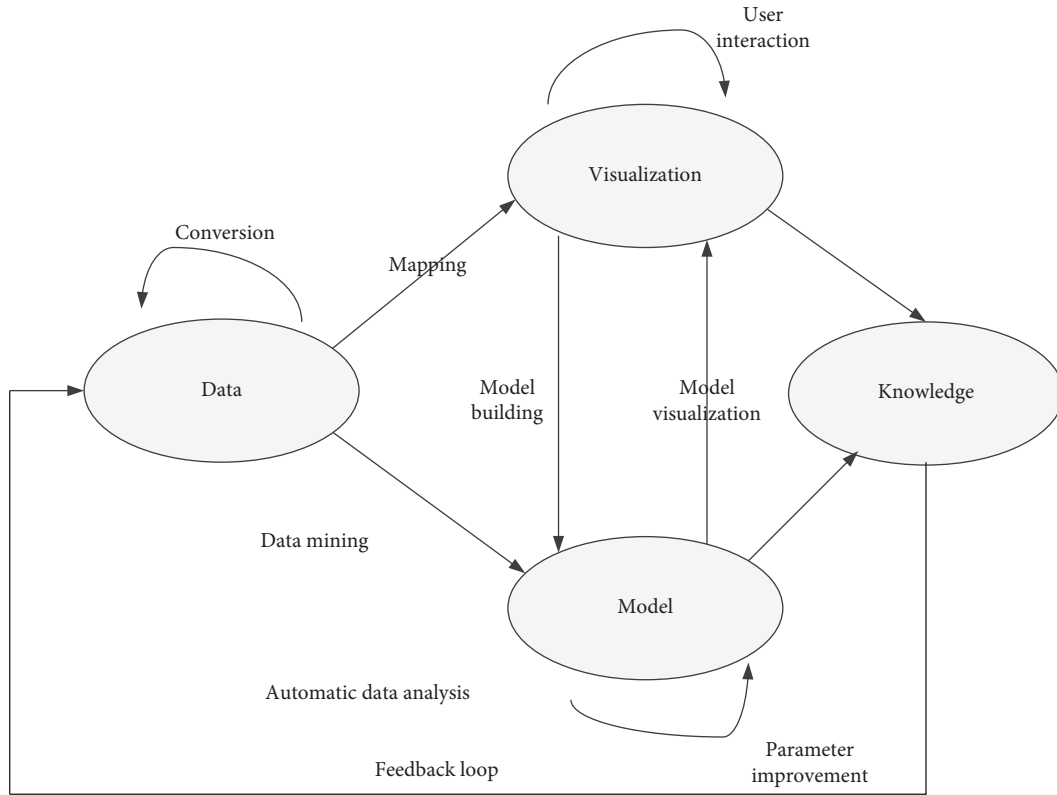


FIGURE 4: Visual data loop diagram.

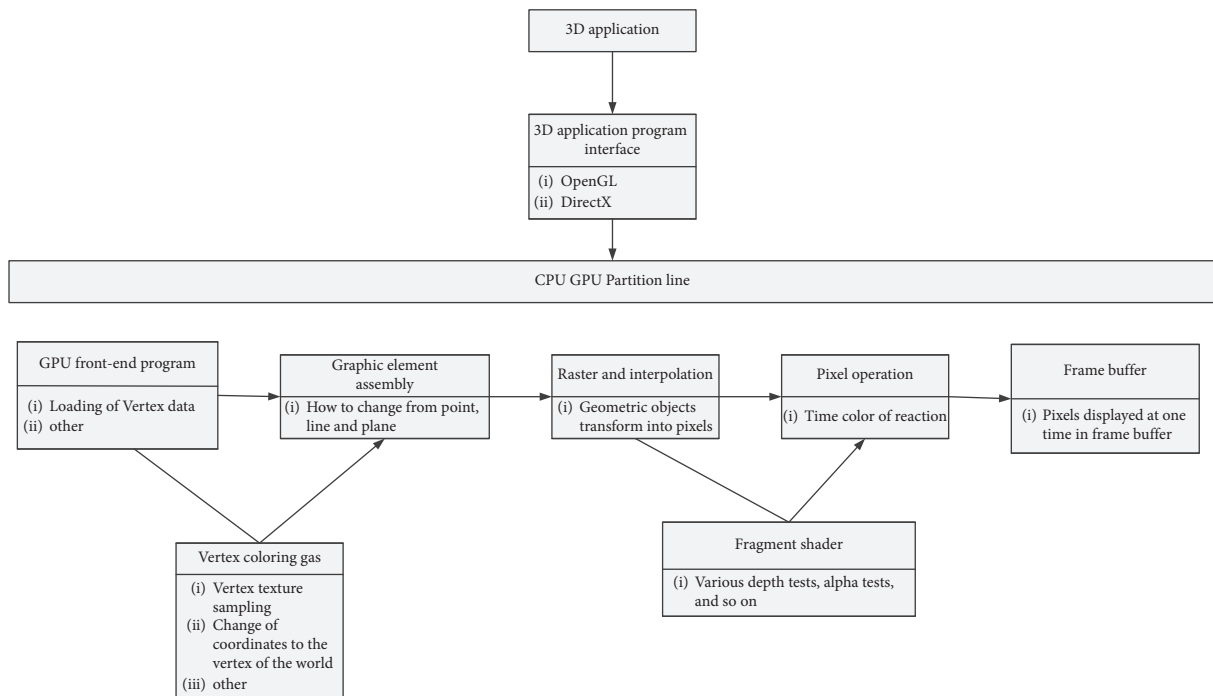


FIGURE 5: Flow chart of 3D rendering analysis.

2.4.2. *Marine Bionic Process.* First of all, we collect the experimental data of marine life movement, then scan it by using 3D scanner to get the relevant model, input the data into MATLAB to process and get the relevant movement

law, compile the UDF file, then import the data in the file into the model, establish the watershed, divide the grid, set it into FLUENT file, and calculate its hydrodynamic characteristics as shown in Figure 8.

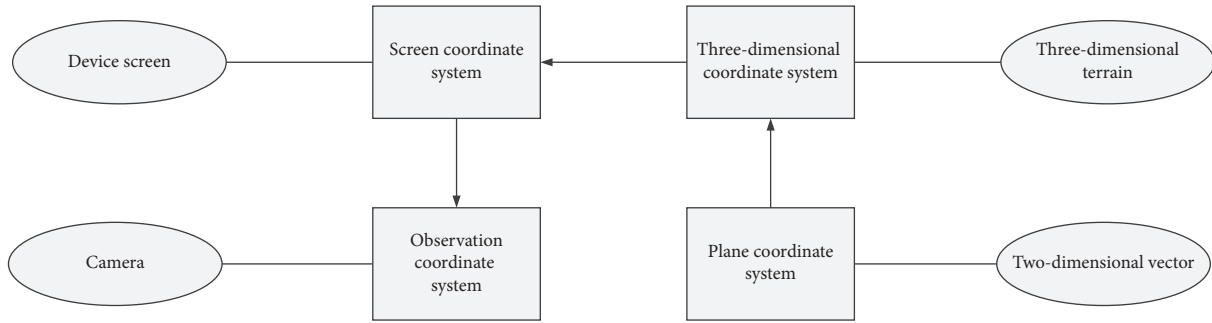


FIGURE 6: Schematic diagram of the coordinate system and its relationship.

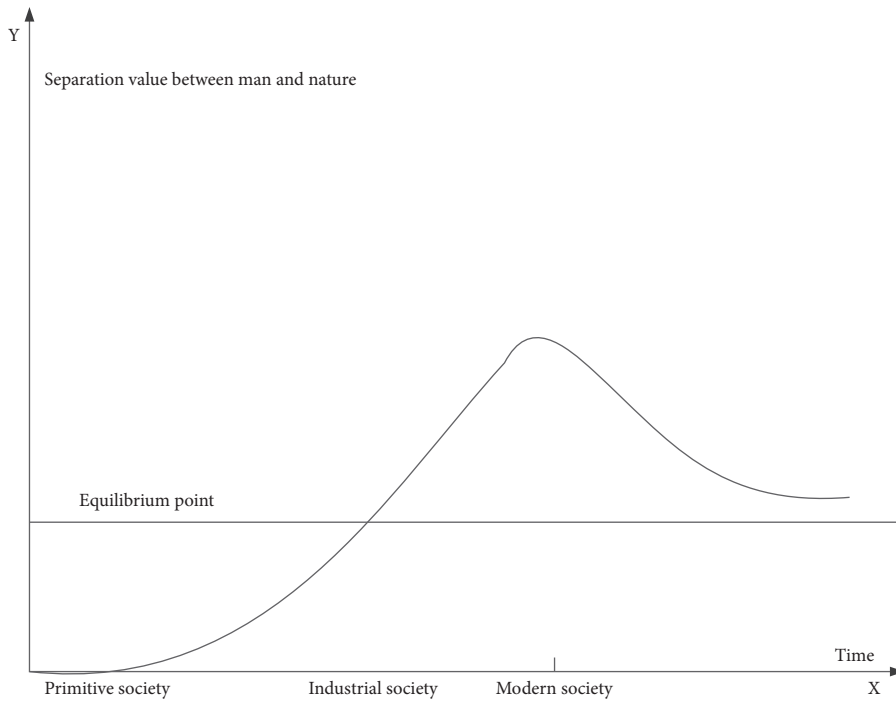


FIGURE 7: Relationship between man and nature.

3. Deep Learning and 3D Rendering Model

3.1. Three-Dimensional Rendering Formula

3.1.1. Transformation Matrix Calculation

(1) Camera transformation matrix is as follows:

$$CM = C^{-1} = (TR)^{-1} = R^{-1}T^{-1},$$

$$CM = \begin{bmatrix} U_x & U_y & U_z & -U \cdot T \\ V_x & V_y & V_z & -V \cdot T \\ N_x & N_y & N_z & -N \cdot T \\ 0 & 0 & 0 & 1 \end{bmatrix}. \quad (1)$$

(2) Perspective projection matrix formula is as follows:

$$PM = \begin{bmatrix} \frac{\cot(1/2 \text{fov})}{\text{aspect}} & 0 & 0 & 0 \\ 0 & \cot\left(\frac{1}{2} \cdot \text{fov}\right) & 0 & 0 \\ 0 & 0 & \frac{Z_f}{Z_f - Z_n} & 1 \\ 0 & 0 & \frac{Z_f \cdot Z_n}{Z_n - Z_f} & 0 \end{bmatrix}. \quad (2)$$

(3) Viewport transformation matrix formula

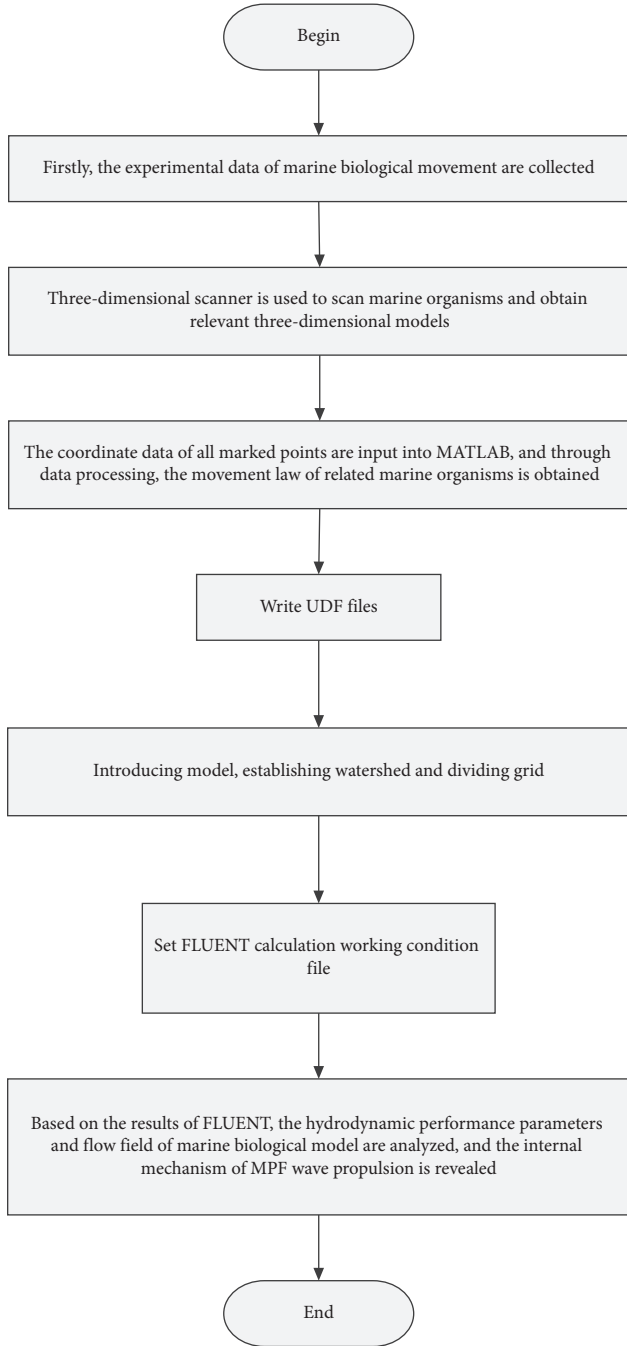


FIGURE 8: Flow chart of marine bionic packaging container.

3.2. Deep Learning Formula

3.2.1. Score Function

$$SM = \begin{bmatrix} \frac{\text{Width}}{Z} & 0 & 0 & 0 \\ 0 & \frac{\text{Height}}{2} & 0 & 0 \\ 0 & 0 & \text{MaxZ} - \text{MinZ} & 0 \\ X + \frac{\text{Width}}{2} & Y + \frac{\text{Height}}{2} & \text{MinZ} & 1 \end{bmatrix},$$

$$f(x, W) = Wx.$$

(3)

3.2.2. *Calculation of SVM Loss Function.* Loss is calculated for categories other than the marked category of the sample; that is, the marked category is not included in the loss, and other categories are calculated and accumulated as the loss of a sample.

$$L = \frac{1}{N} \sum_{i=1}^N \sum_{j \neq y_i} \max(0, f(x_i, W)_j - f(x_i, W)_{y_i} + 1). \quad (4)$$

3.2.3. *SVM Loss Function with Regularization Penalty Term [20]*

$$L = \frac{1}{N} \sum_{i=1}^N \sum_{j \neq y_i} \max(0, f(x_i, W)_j - f(x_i, W)_{y_i} + 1) + \lambda R(W). \quad (5)$$

Among them, $\lambda R(W)$ is the regularization penalty term.

3.2.4. *L2 Regularization*

$$R(W) = \sum_K \sum_L W_{K,L}^2 = \frac{1}{2} W^2. \quad (6)$$

The regularization penalty term SVM loss function is added [21].

$$L = \text{data_loss} + w_loss. \quad (7)$$

3.2.5. Cross Entropy Loss Function

$$Li = -\log\left(\frac{e^{f_{yi}}}{\sum_j e^{f_j}}\right). \quad (8)$$

Among them,

$$f_j(Z) = \frac{e^{Z_j}}{\sum_k e^{Z_k}}. \quad (9)$$

3.2.6. The Learning Rate of Deep Learning Is the Gradient Descent Step [22]

$$\frac{df(x)}{dx} = \lim_{h \rightarrow 0} \frac{f(x+h) - f(x)}{h}. \quad (10)$$

3.2.7. Single Layer Neural Network[23]

$$\begin{aligned} f &= W_2 \max(0, W_1 x), \\ f &= W_3 \max(0, W_2 \max(0, W_1 x)). \end{aligned} \quad (11)$$

3.2.8. Position Coding

$$\begin{aligned} PE_{(pos,2i)} &= \sin\left(\frac{pos}{10000^{2i/d_{model}}}\right), \\ PE_{(pos,2i+1)} &= \cos\left(\frac{pos}{10000^{2i/d_{model}}}\right), \end{aligned} \quad (12)$$

$$\begin{aligned} \frac{1}{10000^{2i/d_{model}}} &= e^{\log\{1/10000^{2i/d_{model}}\}} = e^{-\log\{10000^{2i/d_{model}}\}} \\ &= e^{-2i/d_{model} \log\{10000\}} = e^{2i * (\log\{10000\}/d_{model})}. \end{aligned}$$

3.3. Location Information Embedding Calculation

$$\begin{aligned} v_{2i} &= \sin\left(\frac{P}{f^{2i}}\right), \\ v_{2i+1} &= \cos\left(\frac{P}{f^{2i}}\right). \end{aligned} \quad (13)$$

P is position information [24]; F is the frequency parameter.

3.4. Cyclic Neural Network Calculation

$$\begin{aligned} O_t &= f(V \cdot s_t), \\ s_t &= g(U \cdot x_t + W \cdot s_{t-1}), \\ O_t &= f(V \cdot g(U \cdot X_t + W \cdot s_{t-1})). \end{aligned} \quad (14)$$

3.5. Calculation Method of Attention Mechanism

(1) Point multiplication:

$$f(Q, K_i) = Q^T K_i. \quad (15)$$

(2) Weight:

$$f(Q, K_i) = Q^T W K_i. \quad (16)$$

(3) Splicing weight:

$$f(Q, K_i) = W [Q^T; K_i], \quad (17)$$

(4) Perceptron:

$$f(Q, K_i) = V^T \tanh(WQ + UK_i). \quad (18)$$

4. Research and Test of Deep Learning and 3D Rendering

4.1. Research and Test of 3D Rendering

4.1.1. System Development Test. Through investigation, we know that the test of the 3D rendering system includes system development environment and system running environment. From these two aspects, we can know that the specific parameters of development environment and running environment are as follows.

It can be seen from the table that the system development environment includes the following four parts, such as system development platform, 3D rendering engine, GPU parallel computing toolset, and terrain data processing toolset. The required parameters are shown in Table 1.

The system operating environment parameters are shown in Table 2.

4.1.2. Factor Influence Test. Influence of Parallel Block Size and Number on 3D Rendering. By studying the influence of the size and number of parallel blocks on the average rendering frame rate, as can be seen from Table 3, when the number of parallel blocks is 600 and the size is 40×40 , the average rendering frame rate is 13.7; when the number of parallel blocks is 1600 and the size is 20×30 , the average rendering frame rate is 16.6; when the number is 2400 and the size is 20×20 , the frame rate is 19.8 and the number is 4800; when the size is 10×20 , it is 23.5, the number is 9600, and the size is 10×10 . According to the icon and data, it can be seen that with the increase in the number of parallel blocks, the size of parallel blocks decreases and the average rendering frame rate will gradually increase.

Influence of Rendering Window Size and Cooperation on Rendering Frame Rate. The table judges whether the window size affects the rendering frame rate by studying only rendering terrain frame rate, only CPU, and CPU + GPU. From the data in Table 4, it can be seen that when the window size is 600×400 , only the terrain frame rate is 77.3, and when the window size is 1200×800 , only the terrain frame rate is 68.1. With the increase in the window size, the terrain frame rate decreases and the

TABLE 1: System development environment parameters.

Project	Related data
System development platform	Three-dimensional rendering engine GPU Parallel Computing
Toolset	Terrain data processing tool set
	2012OpenSceneGraphCUDAGDAL

TABLE 2: System running environment parameters.

Name	Related data
Central processing unit	Intel®Xeon®CPU E5-2609@2.4GHz
Graphics processor	Fermi
Internal memory	16 GB
Operating system	Windows7

TABLE 3: Test chart of influence of size and quantity.

Number of parallel blocks	Parallel block size (width × height)	Average rendering frame rate (FPS)
600	40 × 40	13.7
1600	20 × 30	16.6
2400	20 × 20	19.8
4800	10 × 20	23.5
9600	10 × 10	26.9

TABLE 4: Window size image test chart.

Window size (width × length)	Render terrain frame rate	CPU (fps)	CPU + GPU (fps)
600 × 400	77.3	1.1	29.3
800 × 600	75.2	1.1	26.4
1024 × 768	70.1	1.0	23.3
1200 × 800	68.1	<1.0	21.5

CPU frame rate also decreases, but the efficiency is low, but when CPU + GPU renders, the efficiency is greatly improved.

It can be seen from Figure 9 that only CPU runtime utility is low, but the rendering frame rate efficiency is greatly improved when CPU and GPU run at the same time.

Influence of Terrain Data Quantity on Rendering Frame Rate. From the data, it can be seen that the number and level have no great influence on the average rendering in Table 5.

Influence of Sampling Point Number on Rendering Performance. The abscissa represents time, and the ordinate represents the rendering frame rate. Figures 10 and 11, respectively, represent two sets of data tests. From the trend of this graph, we can see that the method proposed in this paper is better than the traditional template shadow volume method in rendering and its performance is better. At the same time, the frame rates of MASS, 5 × 5 sampling method, and 2 × 2 sampling method are all within the acceptable range, and their performance is better. Relatively speaking, the traditional template shadow volume method has lower frame rate and lower performance. 5 × 5 sampling and 2 × 2 sampling can be selected to ensure good rendering performance as shown in Figures 10 and 11.

4.1.3. Optimization of 3D Rendering Performance of Marine Bionic Packaging Container. Using CARD Model to Optimize 3D Rendering. Three-dimensional modeling refers to

the process of building a three-dimensional model on a two-dimensional plane. After the creation of the three-dimensional model is completed, it needs to be subjected to material mapping and lighting layout, and the software is used to fit and integrate these with the model to make the three-dimensional model present as real, photo-quality images. This whole process is 3D modeling and rendering. Table 6 compares simplified and nonsimplified model 3D rendering with a minimum required time of 16.773 and a maximum required time of 18.552. The average time is 17.773; the minimum required time without simplification is 21.457, the maximum required time is 26.838, and the average required time is 24.663. In contrast, the time required for simplification is significantly lower than that required for nonsimplification. Through the LOD model to improve performance, better three-dimensional rendering of marine life, using the advantages of marine life, and combining with the current environment, the marine bionic packaging container is developed, which makes people develop continuously in the process of getting along with marine life. In order to improve performance, 3D rendering should be simplified as shown in Figure 12.

4.1.4. Three-Dimensional Rendering Memory Management Test. By comparing the cached memory management of 3D rendering with the common memory management, according to the structure, it can be known that the maximum time of cached memory management is 0.87 s and the minimum time is 1.00 s when the number of experiments and allocated memory is the same and 1000000 times. Comparing the experimental data, we can see that the time required when using cached memory management is faster than that of ordinary memory management, so using cached memory management can improve the efficiency of 3D rendering memory management. Therefore, for marine bionics, cache memory management is better than 3D rendering. Under certain conditions, cache memory management should be preferred as shown in Tables 7 and 8 and Figure 13.

4.2. Optimization Scheme of Deep Learning Model

4.2.1. Activation Function. The Sigmoid derivative function moving steeply is not easily derived by comparison and has a nonzero center point as shown in Figures 14 and 15.

Series 1 is sigmoid derivative

Series 2 is a sigmoid function

Figure 15 shows the tanh function.

Series 1 is tanh function

Series 2 is tanh derivative

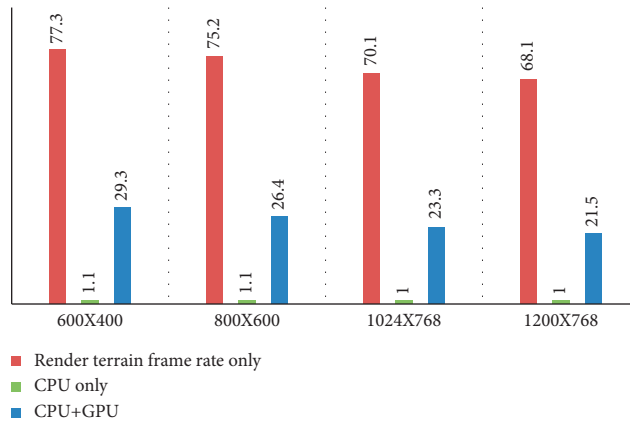


FIGURE 9: Factors affecting rendering by rendering window size.

TABLE 5: Influence factors of terrain data quantity and level on test.

Number of triangular patches of the terrain model	LOD hierarchy of terrain data	Average rendering frame rate (fps)
454	1	21.5
3023	3	21.6
1065	5	22.3
22480	9	22.1

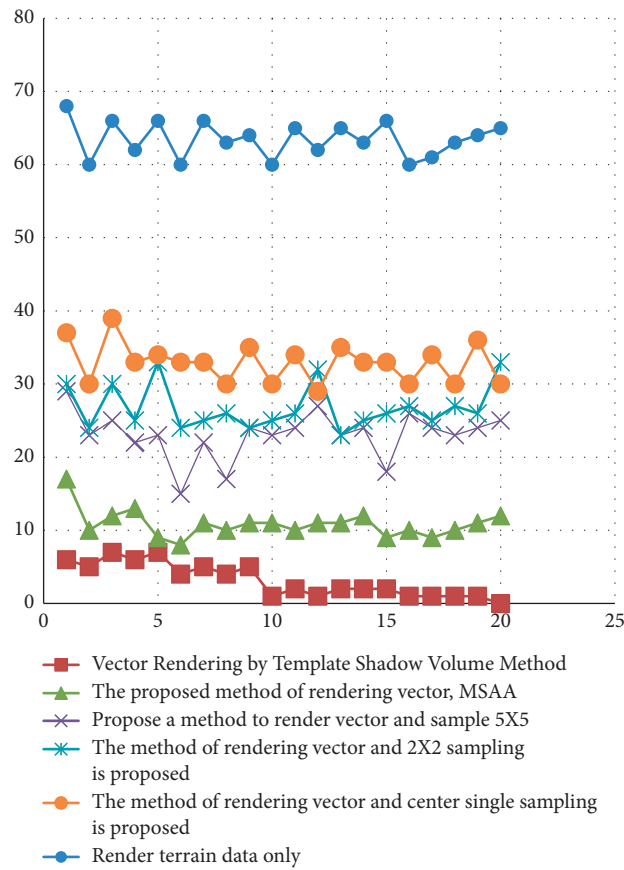


FIGURE 10: Curves of different sampling frame rates by different methods.

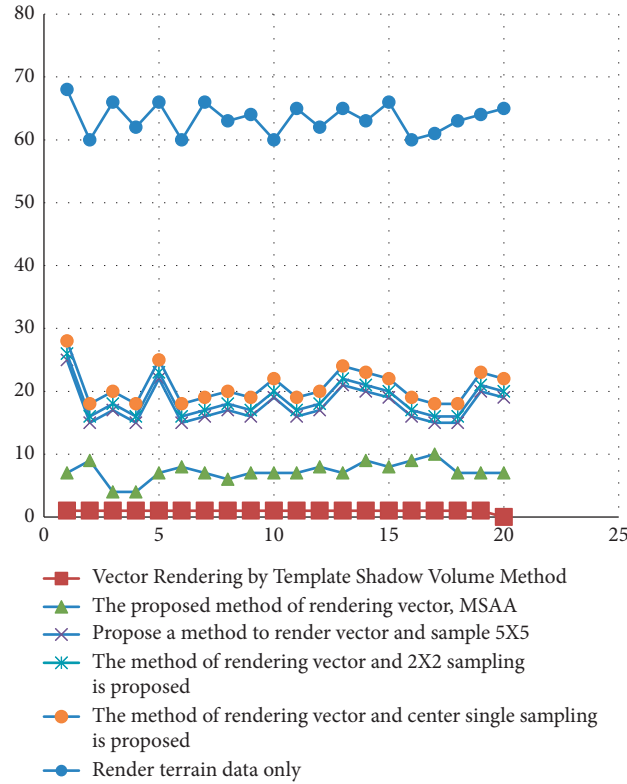


FIGURE 11: Curves of different sampling frame rates by different methods.

TABLE 6: Optimization table of 3D rendering of the LOD model.

Experimental method	1	2	3	4	5	Average
Not simplified/s	21.457	23.556	26.838	25.334	26.132	24.663
Simplify/s	16.773	18.223	16.994	18.324	18.552	17.773

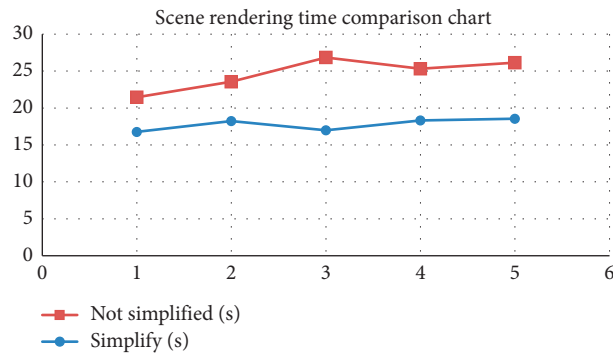


FIGURE 12: LOD model scene rendering time comparison diagram.

TABLE 7: Cached memory management.

Number of tests	Number of memory allocations/times	Time spent (s)
1	1000000	0.87
2	1000000	1.00
3	1000000	0.95
4	1000000	0.88
5	1000000	0.97

TABLE 8: Normal memory management.

Number of tests	Number of memory allocations/times	Time spent (s)
1	1000000	1.26
2	1000000	1.45
3	1000000	1.23
4	1000000	1.43
5	1000000	1.38

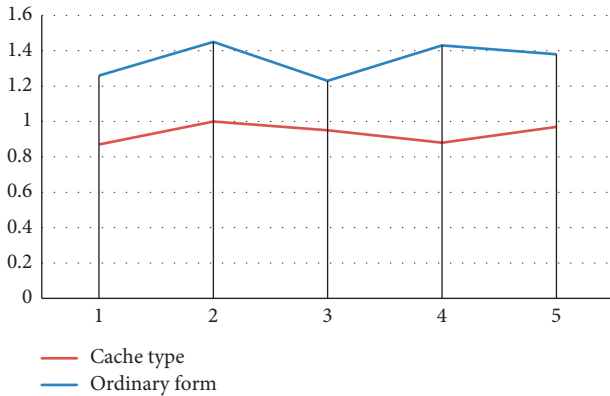


FIGURE 13: Comparison diagram of 3D rendering memory management.

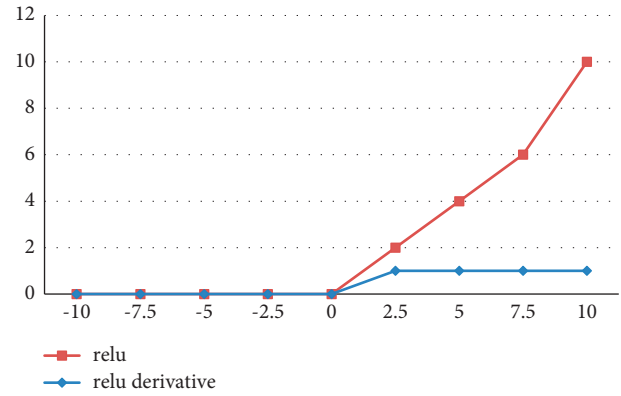


FIGURE 16: ReLU function graph.

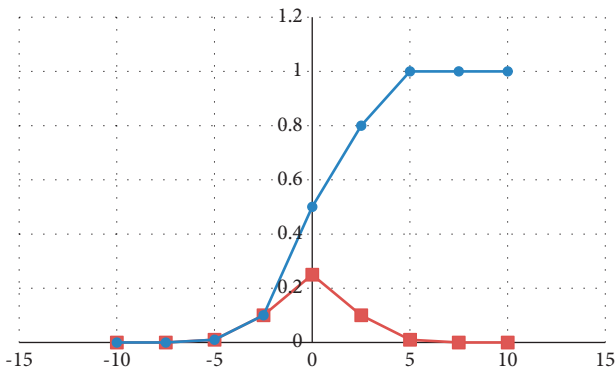


FIGURE 14: Sigmoid function graph.

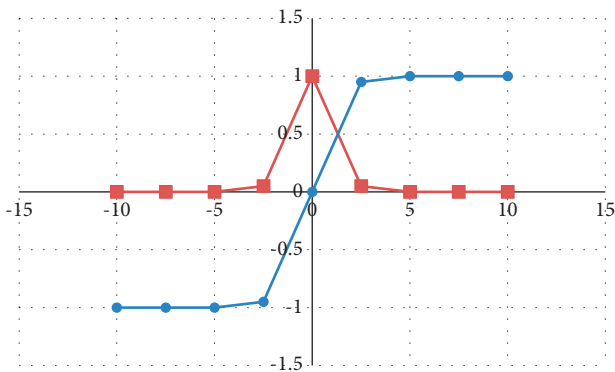


FIGURE 15: Tanh function graph.

A characteristic of that ReLU function is that the value of the function is zero before the coordinate zero. After the zero coordinate point, the trend of one line is more gentle, while the

trend of one line is steeper, but it is more accurate than the above two functional models. The optimization model of deep learning neural network is discussed by using the sigmoid derivative function, tanh derivative function, and ReLU function of deep learning neural network. The ReLU function graph is shown in Figure 16.

5. Conclusion

Through the combination of 3D rendering effects, deep neural networks, and visualization methods, the 3D rendering of deep learning and visualization of marine bionic packaging containers is analyzed. Through testing the three-dimensional rendering, the influencing factors include the size and number of parallel blocks, the size of the rendering window, the amount of terrain data, and the number of sampling points; according to the relevant influencing factors, the LOD model is used to optimize the three-dimensional rendering. Through the optimization of the deep learning model, the three activation functions are studied, and the advantages and disadvantages are analyzed. Through the research in this article, the relevant advantages of marine organisms can be used to create marine bionic packaging containers suitable for human use, which will make our lives more convenient.

Data Availability

The experimental data used to support the findings of this study are available from the corresponding author upon request.

Conflicts of Interest

The authors declare that they have no conflicts of interest regarding this work.

Acknowledgments

This work was supported by a grant from Brain Korea 21 Program for Leading Universities and Students (BK21 FOUR) MADEC Marine Designing Education Research Group.

References

- [1] T. D. Le and H. V. Pham, *Intelligent data analysis: deep learning and visualization*, Springer, Berlin, Germany, pp. 85–114, 2020.
- [2] G. Sun and Q. Qian, “Deep learning and visualization for identifying malware families,” *IEEE Transactions on Dependable and Secure Computing*, vol. 8, no. 1, pp. 283–295, 2018.
- [3] R. T. Schirrmeste, J. T. Springenberg, L. Fiedere et al., “Deep learning with convolutional neural networks for EEG decoding and visualization,” *Human Brain Mapping*, vol. 3, no. 3, pp. 21–23, 2017.
- [4] M. A. Fredericksen, Y. Zhang, M. L. Hazen et al., “Three-dimensional visualization and a deep-learning model reveal complex fungal parasite networks in behaviorally manipulated ants,” *Proceedings of the National Academy of Sciences*, vol. 114, no. 47, pp. 12590–12595, 2017.
- [5] H. L. Liu, T. Taniguchi, Y. Tanaka, K. Takenaka, and T. Bando, “Visualization of driving behavior based on hidden feature extraction by using deep learning,” *IEEE Transactions on Intelligent Transportation Systems*, vol. 18, no. 9, pp. 2477–2489, 2017.
- [6] S. Ni, Q. Qian, and R. Zhang, “Malware identification using visualization images and deep learning,” *Computers & Security*, vol. 77, no. AUG, pp. 871–885, 2018.
- [7] V. Gulshan, L. Peng, M. Coram et al., “Development and validation of a deep learning algorithm for detection of diabetic retinopathy in retinal fundus photographs,” *Jama*, vol. 65, no. 23, pp. 134–145, 2016.
- [8] L. Banko, P. M. Maffettone, D. Naujoks, D. Olds, and A. Ludwig, “Deep learning for visualization and novelty detection in large X-ray diffraction datasets,” *Npj Computational Materials*, vol. 7, no. 5, pp. 47–65, 2021.
- [9] Z. Zhuang, G. Liu, W. Ding et al., “Cardiac VFM visualization and analysis based on YOLO deep learning model and modified 2D continuity equation,” *Computerized Medical Imaging and Graphics*, vol. 82, Article ID 101732, 2020.
- [10] T. Zebin, S. Rezvy, and P. Wei, “COVID-19 detection and disease progression visualization: deep learning on chest X-rays for classification and coarse localization,” *Applied Intelligence*, vol. 51, no. 6, 2021.
- [11] W. Zhu, Z. T. Webb, K. Mao, and J. Romagnoli, “A deep learning approach for process data visualization using t-distributed stochastic neighbor embedding,” *Industrial & Engineering Chemistry Research*, vol. 58, no. 22, 2019.
- [12] U. Tiede, K. H. Hoehne, M. Bomans, A. Pommert, M. Riemer, and G. Wiebecke, “Investigation of medical 3D-rendering algorithms,” *IEEE Computer Graphics and Applications*, vol. 10, no. 2, pp. 41–53, 1990.
- [13] R. H. Choplin, K. A. Buckwalter, J. Rydberg, and J. M. Farber, “CT with 3D rendering of the tendons of the foot and ankle: technique, normal anatomy, and disease,” *RadioGraphics*, vol. 24, no. 2, pp. 343–356, 2004.
- [14] H. Henkes, G. Huber, J. Hierholzer, M. Cordes, C. Kujat, and U. Piepgras, “Radionuclide cisternography, using SPECT and 3D rendering,” *Computer Assisted Radiology/Computer-gestützte Radiologie*, vol. 32, no. 1, pp. 43–56, 1991.
- [15] P. Zanuttigh and G. M. Cortelazzo, “Compression of depth information for 3D rendering,” in *Proceedings of the 3DTV conference: the true vision - capture, transmission and display of 3D video*, vol. 21, no. 3, pp. 65–78, IEEE, Copenhagen, 2009.
- [16] G. E. Dahl, D. Yu, L. Deng, and A. Acero, “Context-dependent pre-trained deep neural networks for large-vocabulary speech recognition,” *IEEE Transactions on Audio Speech and Language Processing*, vol. 20, no. 1, pp. 30–42, 2011.
- [17] G. Dennis, B. T. Sherman, D. A. Hosack et al., “DAVID: database for annotation, visualization, and integrated discovery,” *Genome Biology*, vol. 4, no. 9, pp. 108–119, 2003.
- [18] P. Diazgutierrez, A. Bhushan, R. Pajarola, and M. Gopi, “Constrained strip generation and management for efficient interactive 3D rendering,” in *Proceedings of the Computer Graphics International 2005*, vol. 32, no. 5, pp. 66–83, IEEE, Washington, DC, USA, June 2005.
- [19] V. Verma and W. Ekta, “3D rendering - techniques and challenges,” *International Journal of Engineering & Technology*, vol. 2, no. 2, 2010.
- [20] J. P. Shanjiang and J.C.. Online, “LS-SVM for function estimation and classification,” *Journal of University of ence & Technology Bjing*, vol. 10, no. 5, pp. 73–77, 2003.
- [21] J. Schmidhuber, “Deep learning in neural networks: an overview,” *Neural Networks*, vol. 61, pp. 85–117, 2015.
- [22] S. L. Lin and Z. Liu, “Parameter selection in SVM with RBF kernel function,” *Journal of Zhejiang University of Technology*, vol. 65, no. 3, pp. 76–98, 2007.
- [23] O. Fontenla-Romero, B. Guijarro-Berdiñas, B. Pérez-Sánchez, and A. Alonso-Betanzos, “A new convex objective function for the supervised learning of single-layer neural networks,” *Pattern Recognition*, vol. 43, no. 5, pp. 1984–1992, 2010.
- [24] X. Xian Wang, X. Xianfu Lei, P. Pingzhi Fan, R. Q. Hu, and fnm Shi-Jinn Horng, “Cost analysis of movement-based location management in PCS networks: an embedded Markov chain approach,” *IEEE Transactions on Vehicular Technology*, vol. 63, no. 4, pp. 1886–1902, 2014.

Research Article

Quality Improvement of College Students' Innovation and Entrepreneurship Education Based on Big Data Analysis under the Background of Cloud Computing

Wenhui Zhang 

Qingdao Huanghai University, Qingdao, Shandong 266555, China

Correspondence should be addressed to Wenhui Zhang; zhangwh02@qdhhc.edu.cn

Received 1 December 2021; Revised 29 December 2021; Accepted 22 January 2022; Published 10 February 2022

Academic Editor: Wenming Cao

Copyright © 2022 Wenhui Zhang. This is an open access article distributed under the Creative Commons Attribution License, which permits unrestricted use, distribution, and reproduction in any medium, provided the original work is properly cited.

China is in a critical period of national rejuvenation and national prosperity. Innovation is the soul of a nation and an inexhaustible driving force for national development. Youth are the hope and future of a country. In order to enable young people to have the entrepreneurial ability and innovative spirit of the development of the new era, it has become a very important link for college students to better enter the society and realize their own value. It has become a key link in the development of individuals and China, and has attracted the attention of the whole society. With the continuous development of Internet technology and the deepening of application exploration, in the context of cloud computing, the improvement of the quality of college students' innovation and entrepreneurship education based on big data analysis has also become the focus of universities, society, and the country. The core of the system is the discrete dynamic modeling technology of complex systems. This paper will discuss ways to improve the quality of college students' innovation and entrepreneurship education based on big data under the background of cloud computing by introducing the development and principle of complex system discrete dynamic modeling technology and analyzing the deficiencies and problems of college students' innovation and entrepreneurship quality in many aspects.

1. Introduction

In the process of production practice, people often encounter some complex events. The emergence and disappearance of these events are often random, rather than following a specific mathematical or physical law. Discrete event dynamic systems [1] (DEDS) are dynamic systems driven by such asynchronous and abrupt events. With the rapid development of science and technology, production, and life, there are more and more kinds of discrete event dynamic systems, which are applied in all aspects. The common fields are production practice, aerospace [2], communication, and military. After years of development and research, discrete event dynamic system has developed into a multimodel, multilevel, and multifaceted system, which can be used to analyze and predict the development and trend of events [3].

The quality of college students' innovation and entrepreneurship education [4] also conforms to the category of discrete event dynamic system. The quality of innovation and entrepreneurship education depends on various factors, and these factors are distributed discretely. These discrete events interact according to certain laws in order to meet certain quality requirements. With the enhancement of China's national strength, the improvement of its international status, and the improvement of industrialization, the single traditional economic model originally relied on has begun to change to an innovative and diversified modern economic model [5]. With the development of science and technology, cloud computing, big data, artificial intelligence, and other concepts have entered all aspects of people's life. Today's society has moved from tradition to modernity, from workers and farmers to informatization. This requires college students in the new era to adapt to a more changeable

social environment. They also hope that college students who go out of the campus are talents with pioneering spirit, rather than traditional conservatism. Therefore, schools, society, and the state pay more and more attention to college students' innovation and entrepreneurship education. However, over the years, there have been many problems to improve and improve the quality of college students' innovation and entrepreneurship education. Therefore, in this paper, we hope to rely on cloud computing [6], analyze big data through complex system discrete dynamic modeling technology, timely predict and evaluate college students' innovation and entrepreneurship education, and design a perfect quality improvement path.

By introducing the development and principle of complex system discrete dynamic modeling technology, this paper discusses how to improve the quality of college students' innovation and entrepreneurship education based on big data under the background of cloud computing. There are many aspects of innovation and entrepreneurship quality. Innovative contributions include the following: (1) it has changed college students' concept of innovation and entrepreneurship. The school can organize a special team of teachers to provide students with professional and personalized services and improve students' interest in innovation and entrepreneurship, (2) analyze the deficiencies and problems of college students' innovation and entrepreneurship education, so that college students have the courage to innovate and practice, (3) improve the quality evaluation system of innovation and entrepreneurship and provide sufficient funds for college students' innovation and entrepreneurship practice, improve the practice guarantee of college students' innovation and entrepreneurship, and improve the project incubation rate and business transformation rate, and (4) through the big data analysis platform, realize the organic connection between the school and society, strengthen the business value of college students' innovation and entrepreneurship projects and establish a business value evaluation system. This research strengthens the learning and application ability of colleges and universities and teachers to learn cloud computing and big data, learn to use data analysis and evaluation, and use data to promote the quality of innovation and entrepreneurship education

This paper is divided into five parts. The first part expounds the research background and analyzes the deficiencies and problems of college students' innovation and entrepreneurship education. The second part makes a reference to the research of related work. The third part introduces the development, principle, and research methods of discrete dynamic modeling technology for complex systems. The research methods are further elaborated. The fourth part expounds the results and points out the problems of college students' low awareness and participation in innovation and entrepreneurship, uneven distribution of innovation and entrepreneurship education, imperfect top-level design, obvious homogenization, and generally low incubation rate of innovation and entrepreneurship. It also analyzes the reasons for the failure of

college students' innovation and entrepreneurship incubation rate. Finally, it summarizes the full text, which provides guidance for young people to have the entrepreneurial ability and innovative spirit of the development of the new era.

2. The Related Works

Discrete event dynamic system first appeared in queuing phenomenon [7] and network research. In queuing, the whole system follows a set of artificial rules rather than the so-called physical or mathematical logic or laws [8]. With the development of computer and other technologies, Weingartene et al. formally put forward the concept of discrete event dynamic system [9] around 1980. At that time, people paid more and more attention to discrete event dynamic system and hoped to develop some man-made systems to deal with discrete events in the fields of communication, production, transportation, and military with the help of intelligent technology. Therefore, this term also refers to this kind of man-made system. During this period, people's research on man-made systems and performance [10] greatly promoted the emergence and development of the theory of discrete event dynamic systems.

Discrete event dynamic system is now roughly defined as a dynamic system with asynchronous and sudden event driven state evolution [11]. The most basic problem in the research of discrete event dynamic system is modeling [12]. According to the levels of logic, time, and statistical performance, we can divide the distributed event dynamic system into logic level model, time level model, and statistical performance level model [13]. These three models have developed very well and formed their respective theoretical frameworks.

China's research on discrete event dynamic system has made great progress from the implementation of 863 high-tech computer integrated manufacturing system theme plan [14] in 1987. In the following three years [15], it has conducted extensive research and development on logical hierarchical model, time hierarchical model, and statistical performance hierarchical model and achieved very valuable achievements. For example, Liu F's research on the centralized diagnosis of discrete event dynamic system [16]. Wang Shouguang researched the attack of information physical system under the framework of discrete event system [17]. Zhang Wenggang studied DEDS designed for flow shop to solve the coordination control problem [18]. Dai et al. analyzed the flow characteristics of knowledge workers in high-tech enterprises according to nonlinear discrete dynamic system modeling [19]. Zhang studied the application of discrete event dynamic system in network simulation [20]. Wang et al. studied the modeling and repair capability analysis of military aircraft repair line [21]. In recent ten years, the research on the modeling mode and behavior characteristics of discrete event dynamic system of manufacturing system has become a very important research proposition in the world [22].

3. Research Method

Discrete event is the basic component of discrete event dynamic system [23] and the inducement leading to the change of discrete dynamic system. It has three basic characteristics: uniqueness, asynchrony, and subjectivity [24]. Compared with continuous dynamic system, discrete event dynamic system only changes in discrete time. Its changes are asynchronous, concurrent, and uncertain. It cannot be modeled in a conventional way like continuous dynamic system, but through special human rules [25]. Figure 1 is a conceptual diagram of a discrete event dynamic system.

The queuing system consists of arrival mode, service desk, and queuing rules. For the arrival mode, the arrival law was described, and the average arrival interval is t . The system is a common statistical performance hierarchical model in discrete event dynamic systems. In the queuing network, many service centers form a system through a certain structure, and each service center can include multiple service desks.

In the queuing system, the arrival model we choose is the Poisson distribution with the parameter λ , the service time obeys the exponential distribution with the parameter μ , and the stay time W of the customer in the system, in the single service center model $M/M/1$, obeys the negative exponential distribution of the parameter $\mu - \lambda$, the average stay time is $E[W]$, and the average waiting time is equal to the average stay time minus the service time.

According to normalization conditions,

$$\sum_{n=0}^{\infty} P_n = 1, \rho = \frac{\lambda}{\mu} < 1. \quad (1)$$

N is the number of customers, P_n is the steady-state probability with the number of customers n , λ is the average speed of the input customer flow, and μ is the average service rate.

It can be obtained that the steady-state probability distribution of customers is

$$P_n = P^0 (1 - \rho)^n, n \geq 1. \quad (2)$$

The steady-state average number of customers L is

$$L = \frac{\lambda}{\mu - \lambda}. \quad (3)$$

The steady-state average pair length L_q is

$$L_q = \frac{\lambda^2}{\mu(\mu - \lambda)}. \quad (4)$$

The average waiting time w_q of customers is

$$w_q = \frac{\lambda}{\mu(\mu - \lambda)}. \quad (5)$$

The steady-state average stay time w of customers is

$$w = \frac{1}{\mu - \lambda}. \quad (6)$$

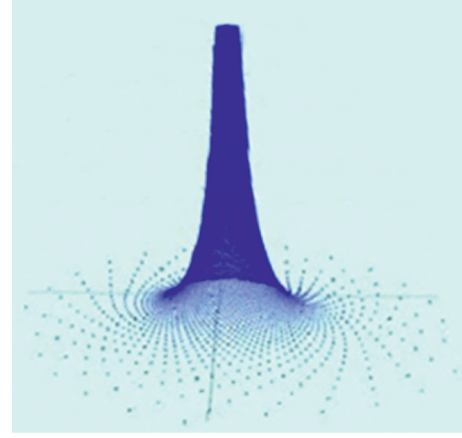


FIGURE 1: Discrete dynamic modeling of complex systems.

Little formula holds in $M/M/c$ system as follows:

$$\lambda w_q = L_q, \lambda w = L. \quad (7)$$

According to the steady-state performance analysis of $M/M/C$ and the normalization condition (1), the steady-state probability distribution of customers is

$$P_0 = \left[\sum_{n=0}^{c-1} \frac{\rho^n}{n!} + \frac{c\rho^c}{c!(c-\rho)} \right]^{-1}, \quad (8)$$

$$P_n = \begin{cases} \frac{\rho^n}{n!} P_0 & n \leq c \\ \frac{\rho^n}{c^{n-c} c!} P_0 & n > c \end{cases}, \quad \rho = \frac{\lambda}{\mu} \quad (9)$$

The steady-state average pair length is

$$L_q = \left[\frac{(\lambda/\mu)^c \lambda \mu}{(c-1)!(c\mu - \lambda)^2} \right] P_0. \quad (10)$$

The average waiting time of customers is

$$w_q = \left[\frac{(\lambda/\mu)^c \lambda \mu}{(c-1)!(c\mu - \lambda)^2} \right] P_0. \quad (11)$$

The steady-state average residence time is

$$w = \left[\frac{(\lambda/\mu)^c \mu}{(c-1)!(c\mu - \lambda)^2} \right] P_0 + \frac{1}{\mu}. \quad (12)$$

Steady-state average number of customers is as follows:

$$L = \left[\frac{(\lambda/\mu)^c \lambda \mu}{(c-1)!(c\mu - \lambda)^2} \right] P_0 + \frac{\lambda}{\mu}. \quad (13)$$

Under the condition of the existence of the solution of the steady-state probability distribution, if the accretion and extinction rates of the birth and death process $N(t)$ are bounded, that is, the supremum $\sup_n \{\lambda_{n-1}\} < \infty$, $\sup_n \{\mu_n\} < \infty$, the necessary and sufficient condition for the existence of the steady-state probability distribution of the birth and death process $N(t)$ is as follows:

$$\sum_{n=1}^{\infty} \prod_{i=1}^n \frac{\lambda_{i-1}}{\mu_i} < \infty. \quad (14)$$

When the steady-state probability distribution $\{p_n\}$ exists, the parametric expression of p_n

$$p_n = p_0 \prod_{i=1}^n \frac{\lambda_{i-1}}{\mu_i}, p_0 = \left[1 + \sum_{n=1}^{\infty} \prod_{i=1}^n \frac{\lambda_{i-1}}{\mu_i} \right]^{-1}. \quad (15)$$

For the research topic of improving the quality of college students' innovation and entrepreneurship education, in addition to the modeling of discrete event dynamic system itself, it also needs to be organically combined with other technologies such as big data to build an innovation and entrepreneurship education quality system. Figure 2 shows the application process of big data in innovation and entrepreneurship education. It can be found that, in this application system, data is very important for the presentation of results. Among them, the acquisition, integration, and screening of data will affect the analysis and prediction of the system.

Among them, the data acquisition channels can be roughly divided into eight categories, including management data, capital data, industry data, scientific and technological innovation data, policy data, market demand data, resource data, and university education model. It is hoped that through the objective understanding and mining of these eight kinds of big data, we can make a comprehensive analysis of the policies and practices of schools, society, and the state on college students' innovation and entrepreneurship. We can also analyze different data, predict later results, and put forward improvement schemes.

According to the data characteristics of college students' innovation and entrepreneurship education, we designed an education quality improvement path for complex system discrete dynamic modeling technology, as shown in Figure 3, hoping to improve the quality of college students' innovation and entrepreneurship education in China in the future. We subdivide the service desk into three layers: collection and storage layer, analysis and visualization layer, and statistical evaluation layer. Through the analysis of different discrete events in the innovation and entrepreneurship education database, we can find the relationship between them and the impact on the results. Finally, we can help us quickly analyze and predict the results, including the guidance direction of entrepreneurship programs, evaluate and analyze innovation and entrepreneurship, predict risks, and analyze and evaluate the level of teachers.

Based on big data analysis and complex system discrete dynamic modeling technology, this paper studies and compares the quality of innovation and entrepreneurship education of college students in national key universities and key universities in foreign developed countries and obtains the following results and analysis contents, hoping to help establish a platform for improving the quality of innovation and entrepreneurship education of college students.

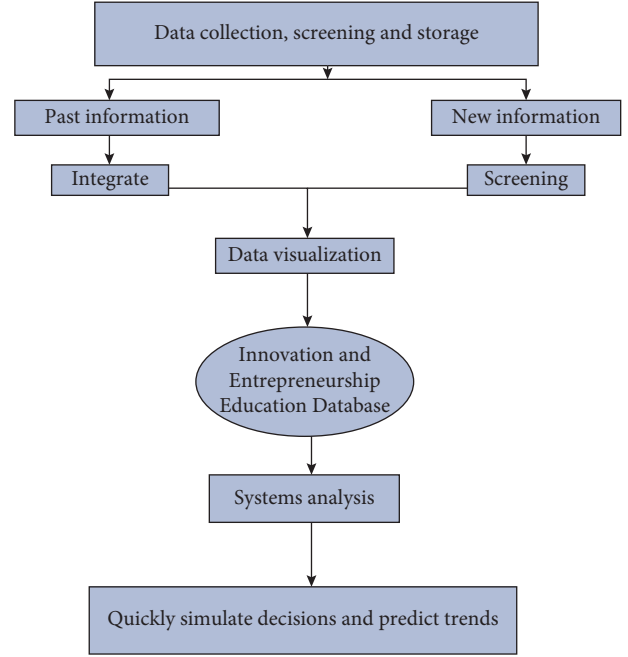


FIGURE 2: Application process of big data in innovation and entrepreneurship education.

4. Results and Analysis

4.1. College Students' Awareness and Participation in Innovation and Entrepreneurship Are Not High Enough. Research Object and Data Source. In the survey, college students from different colleges were selected as the research object, and the samples were randomly investigated in classrooms, study rooms, dormitories, and other student gathering places in their spare time. The questionnaire was distributed on-site, and the big data was obtained by recovering the effective questionnaire. The questionnaire consists of three parts: the first is the basic situation; the second is the questionnaire of entrepreneurial intention; the third is the questionnaire of innovation intention. The big data analysis on the willingness and participation of national college students in innovation and entrepreneurship education is shown in Figure 4. 12% of college students are not interested in or understand innovation and entrepreneurship education, only 4% of college students have plans to start a business after graduation, and 41% of college students have received relevant theoretical knowledge of innovation and entrepreneurship. However, only 19% of college students have really participated in practical projects of innovation and entrepreneurship. The lack of awareness and participation of college students in innovation and entrepreneurship is mainly due to the lack of guidance from the school and society, as well as the imperfect establishment of policies and security system in all aspects. The school's management mode of innovation and entrepreneurship cannot cover all students enough to arouse the interest and attention of all students, mostly relying on students' initiative and willingness or academic credit requirements. On the other hand, it is related to college students' own

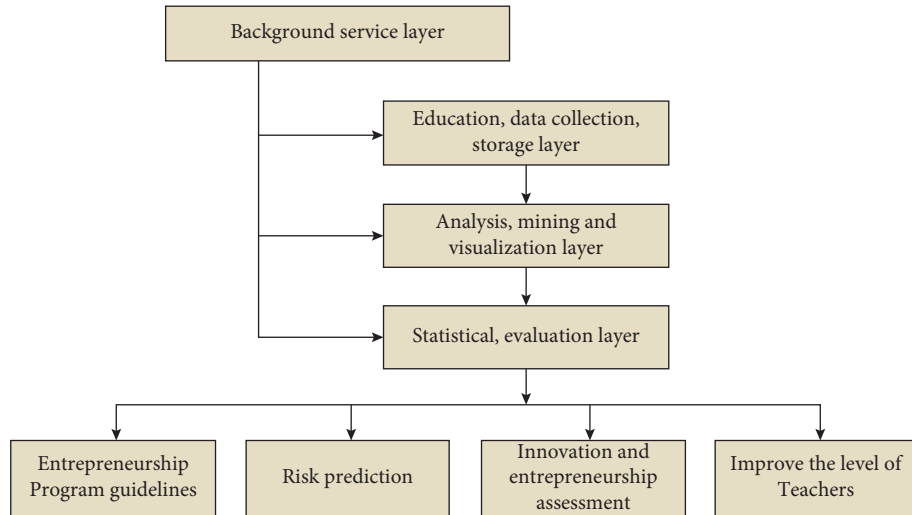


FIGURE 3: Ways to improve the quality of college students' innovation and entrepreneurship education under big data.

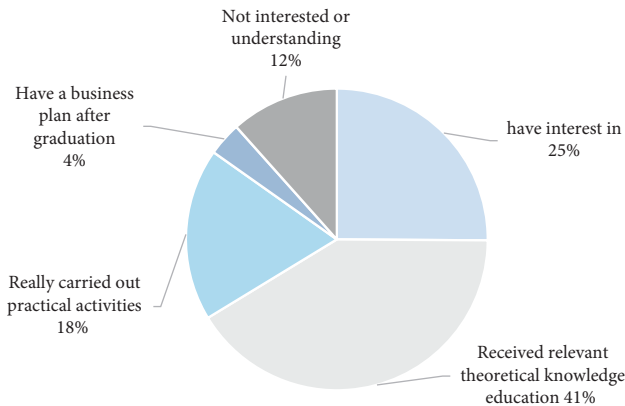


FIGURE 4: Survey on innovation and entrepreneurship awareness and participation.

personality and growth experience and generally lack the spirit of innovation and pioneering practice. In the past, under the responsive education system, college students only paid attention to and cared about the selective examination, and most college students' intention after graduation is to stabilize the traditional work, so they do not pay much attention to the practice of innovation and entrepreneurship.

4.2. *The Distribution of College Students' Innovation and Entrepreneurship Education in China Is Uneven.* Through the big data investigation and analysis of the distribution and development of national college students' innovation and entrepreneurship education, Figure 5 is obtained, which can show the general distribution of national innovation and entrepreneurship education. As can be seen from the figure, compared with the economically developed coastal and southern regions in China, such as Beijing, Jiangsu, and Guangzhou, the provinces with better development of innovation and entrepreneurship education, and the remote and economically backward provinces such as Xinjiang and

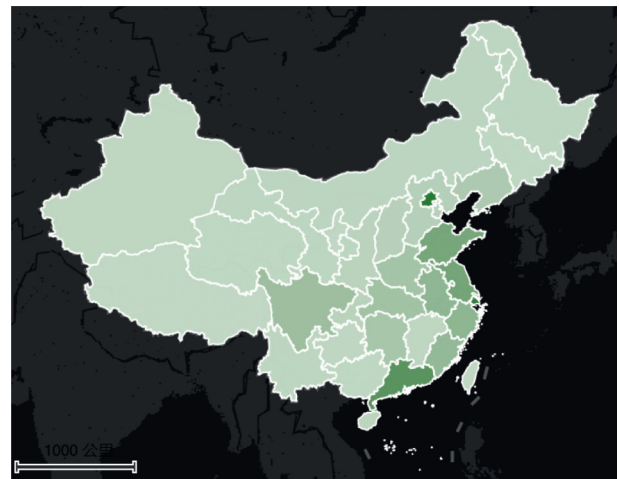


FIGURE 5: National innovation and entrepreneurship distribution map.

Gansu in the northwest and southwest, the development of innovation and entrepreneurship education for college students is still relatively weak. On the whole, the distribution of innovation and entrepreneurship education in China shows an unbalanced trend. It is preliminarily speculated that the reason for this situation is related to the financial support and policy preference of local provinces, cities, and universities for college students' innovation and entrepreneurship education. These schools have given better support and actively created a practice environment, which not only makes college students more interested and involved, but also ensures the more stable and smooth development of innovation and entrepreneurship practice activities. Then, the success rate and total number of college students' innovation and entrepreneurship practice are improved. Areas with weak innovation and entrepreneurship development can learn from excellent provinces to formulate policies and change the school management mode.

4.3. The Top-Level Design of College Students' Innovation and Entrepreneurship Education Is Not Perfect. We further analyzed and visualized the big data of the top-level design of college students' innovation and entrepreneurship education in colleges and universities across the country and drew a model diagram of the top-level design, as shown in Figure 6. We can see that colleges and universities mostly focus on courses and speeches, in which course design accounts for a large proportion, and practice is mostly carried out in the form of competition, which is relatively single. In addition, when college students carry out innovation and entrepreneurship activities, they lack the guidance and help of professional elders and encounter problems that are not easy to solve, and there is a shortage of funds, which is not enough to support the smooth development of the activities, which is easy to make the project die prematurely or uncompleted halfway. The school's policy is not very perfect, and it does not pay enough attention to innovation and entrepreneurship education. The unreasonable top-level design will make it difficult to improve the quality of college students' innovation and entrepreneurship education, and there is no substantive promotion, which cannot really mobilize college students' enthusiasm and explore students' innovation and practice ability.

4.4. The Homogenization of College Students' Innovation and Entrepreneurship Is Obvious. In the big data analysis of college students' innovation and entrepreneurship projects, we get Figure 7. When analyzing and extracting the keywords selected for innovation and entrepreneurship practice, we find that there is an obvious homogenization of college students' innovation and entrepreneurship projects, and there is an obvious phenomenon of following the crowd in content selection. They are carried out in groups and lack of innovative spirit in content. The form of the project is too single, and there is no scene of a hundred flowers blooming. At the same time, the innovation and entrepreneurship projects of college students are too conservative, which is also contrary to the original intention of innovation and entrepreneurship education. In other aspects, it is found that the practicality of college students' innovation and entrepreneurship is not strong, and most of the innovation and entrepreneurship activities are not well incubated, and the business conversion rate is very low. This homogenization phenomenon is contrary to our original intention of carrying out innovation and entrepreneurship education. We hope to see college students innovate and practice boldly, inject vitality into social development and progress, achieve a career, and transport more excellent talents in line with the development of the times.

4.5. The Incubation Rate of Innovation and Entrepreneurship of Various Projects Is Generally Not High. According to the big data analysis of the incubation rate of college students' innovation and entrepreneurship projects, as shown in Figure 8, we mainly divide the projects into six categories: high-tech field, chain franchise field, intellectual service field, store opening, technological entrepreneurship, and other

categories. The incubation rate of innovation and entrepreneurship practice in high-tech neighborhood and intellectual service neighborhood is relatively high, and the incubation rate of entity entrepreneurship is relatively low. However, on the whole, the incubation rate of all college students' innovation and entrepreneurship projects is very low, which shows that the commercial conversion rate of college students' innovation and entrepreneurship projects in school can bring very low expectations of economic benefits in the future. This is a problem worthy of thinking and analysis, which will be analyzed later.

4.6. There Is Still a Gap between College Students' Innovation and Entrepreneurship Education in China and Developed Countries. This paper also makes a horizontal big data comparative analysis of innovation and entrepreneurship education at home and abroad, as shown in Figure 9. It compares the five levels: the flexibility of the education system, the promotion of social atmosphere, the superiority of the education system, the participation of college students in innovation and entrepreneurship, and the success rate and conversion rate of college students' innovation and entrepreneurship. Through comparison, we can see that the education system of colleges and universities in developed countries is more flexible, which is conducive to the development of innovation and entrepreneurship activities and stimulate students' innovative spirit. The social atmosphere in developed countries is also more promotive, which is conducive to the effective connection between schools and society, and can improve the commercial conversion rate of innovation and entrepreneurship. Therefore, the innovation and entrepreneurship enthusiasm of college students in developed countries are also much higher than the domestic students, and the practical success rate and commercial conversion rate of innovation and entrepreneurship are many times higher than the domestic students. However, the superiority of China's education system should be obviously stronger than that of developed countries, which is our characteristic and strength. While improving and developing other aspects, maintaining and giving full play to the superiority of the education system with Chinese characteristics is our direction and goal.

4.7. Analysis on the Failure of College Students' Innovation and Entrepreneurship Incubation Rate. Finally, we analyze the reasons for the failure of college students' innovation and entrepreneurship incubation rate according to big data, as shown in Figure 10. The failure reasons are mainly divided into six factors: lack of funds, weak team professional ability, lack of policy support, problems of teachers' team level, low students' willingness, and lack of professional guidance. Based on the analysis of specific factors one by one, students' willingness is low. Most students only regard innovation and entrepreneurship practice as a means to obtain credits and a voucher for future work, rather than as a way to cultivate ability and practice of innovation and entrepreneurship. Therefore, they do not attach great importance to the incubation rate of the project and the conversion rate of

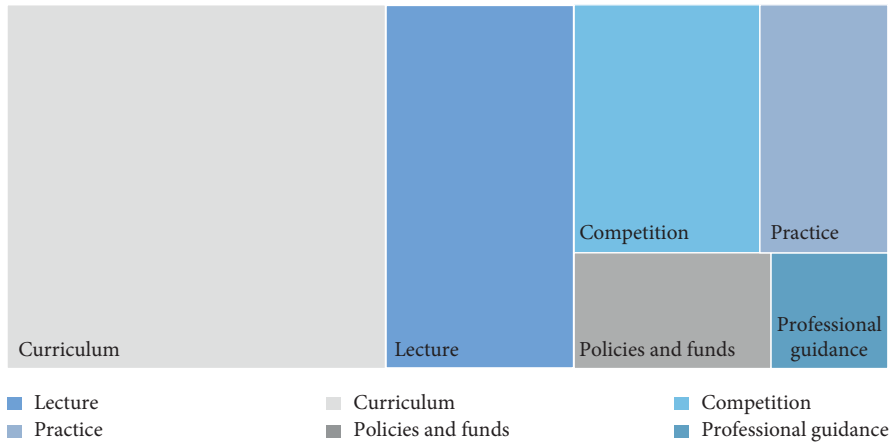


FIGURE 6: Research on top-level design of innovation and entrepreneurship in colleges and universities.

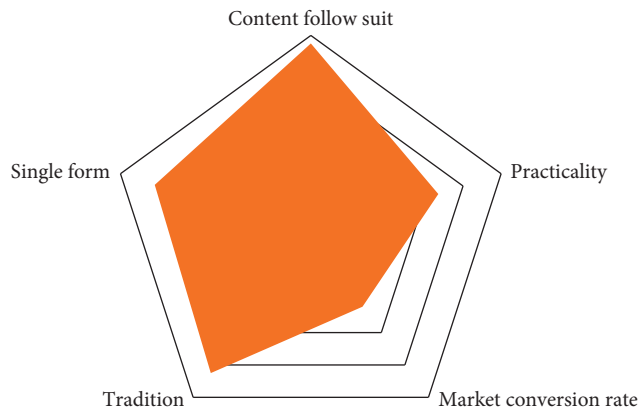


FIGURE 7: Homogeneity analysis of innovation and entrepreneurship.

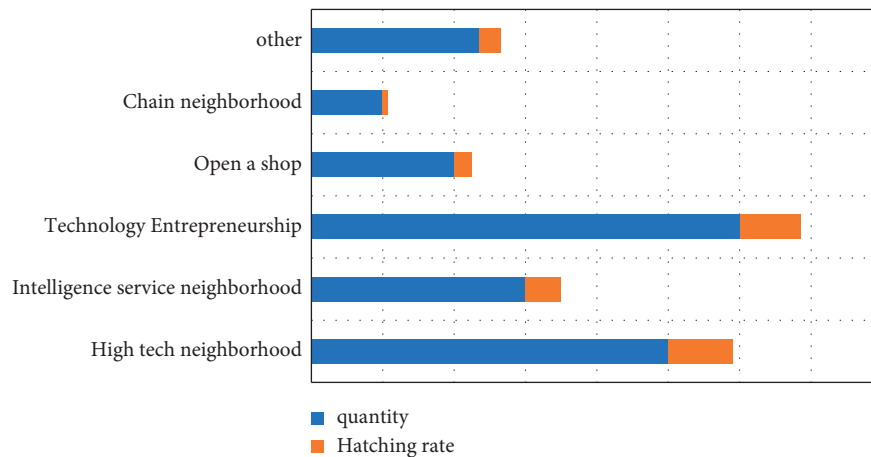


FIGURE 8: Investigation on incubation rate of innovation and entrepreneurship.

business, and it can be seen from the above. The homogeneity of college students' innovation and entrepreneurship is obvious. Students' entrepreneurship lacks innovation and is too traditional and conservative, which is not conducive to improving college students' entrepreneurial enthusiasm.

On the other hand, the low willingness of college students to innovate and start a business is partly due to the lack of funds in the process of project practice, which makes the whole entrepreneurial process difficult and frustrating. In addition, there is no special teacher for guidance, and the

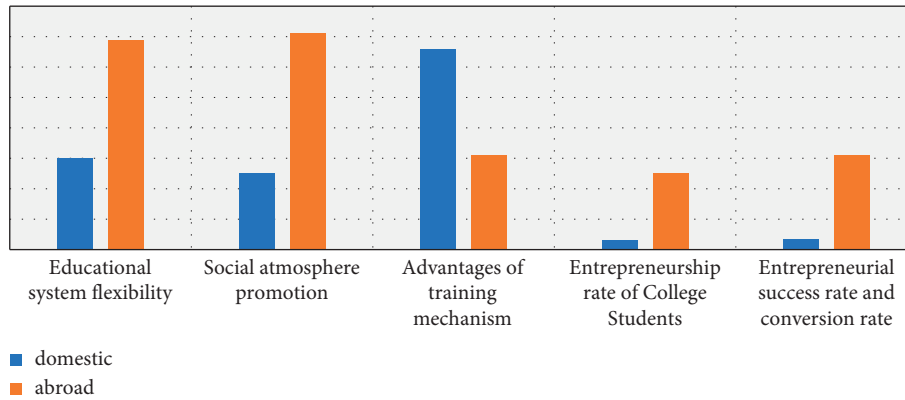


FIGURE 9: Comparison of innovation and entrepreneurship at home and abroad.

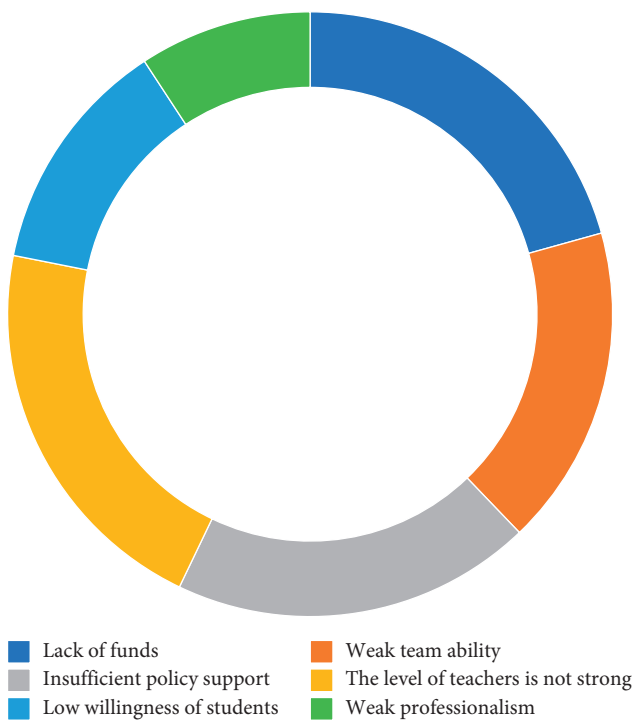


FIGURE 10: Reasons for failure of innovation and entrepreneurship incubation rate.

professional ability of the team is weak, which is not enough to support the later incubation of the project. From the previously mentioned data, it is not difficult to find that the practice way of college students' innovation and entrepreneurship is mainly through competition, and the competition is mainly to pursue novelty and novelty. Sometimes, it will cause pseudoinnovation and cannot produce commercial value, which is also one of the reasons for the low hatching rate. These reasons for failure can be guided and improved through innovation and entrepreneurship policies, but at present, the government's management of innovation and entrepreneurship education needs to be further strengthened.

5. Countermeasures to Improve the Entrepreneurship Rate of College Students

5.1. Strengthening Entrepreneurship Training for College Students. Constructing college students' entrepreneurship education system and improving college students' entrepreneurship literacy are the most important factors to improve the success rate of college students' entrepreneurship. As colleges and universities, first, we should build a curriculum system, form layered and classified curriculum modules, teach entrepreneurship basic courses in the lower grades, and gradually introduce entrepreneurship practice courses in the higher grades. Second, we should explore the reform of curriculum system and introduce flexible school system. Third, we focused on providing entrepreneurship practice training programs and encouraged college students to actively participate in entrepreneurship competitions and entrepreneurship training programs. In addition, some colleges and universities offer entrepreneurship classes for students with entrepreneurial intention, which is a more effective way. For college students themselves, they should actively learn entrepreneurial knowledge, actively carry out entrepreneurial practice, and constantly accumulate entrepreneurial experience.

5.2. Improving College Students' Entrepreneurship Policy. From the perspective of the government, we should formulate entrepreneurship policies for university and provincial groups in terms of laws and regulations, taxation, registration, and business handling and lower the policy threshold based on necessary preference. From the perspective of colleges and universities, we should introduce policies to encourage college students to start businesses.

5.3. Building a Platform for College Students' Entrepreneurship. Colleges and universities should break the barriers between colleges and markets, build a win-win entrepreneurial platform, and introduce investors and

entrepreneurs into the entrepreneurial platform. Conditional colleges and universities can even move the entrepreneurship platform off campus to truly accept the market test, so that students can be tempered in the real market.

6. Conclusion

Based on the previously mentioned analysis of the current situation of college students' innovation and entrepreneurship education quality based on big data analysis in the context of cloud computing, it is not difficult to find that at present. There are still many problems to be solved for college students' innovation and entrepreneurship in China, and there is also a large gap with developed countries. The main manifestations are that students' enthusiasm is not high enough, and their cognition and understanding of innovation and entrepreneurship are not clear enough. The policy and financial support of colleges and universities and the state for innovation and entrepreneurship are not enough to ensure the normal development and incubation of college students. The teaching staff is also very weak, and there is no special teacher to provide guidance. There are also problems in the connection between universities and society. The social environment and insufficient attention to college students' innovation and entrepreneurship are also one of the reasons for the low rate of business transformation.

Through the discrete dynamic modeling technology of complex systems and the storage, processing, and analysis technology of big data mining, we have realized the recombination and visualization of data, found the internal relationship between discrete events, clearly seen the existing problems of college students' innovation and entrepreneurship, and found the path to improve the quality of innovation and entrepreneurship education. First, in the future, it is suggested to change the concept of college students' innovation and entrepreneurship. The school can organize a special team of teachers, provide students with professional and personalized services, and improve students' interest in innovation and entrepreneurship. Second, let college students be bold in innovation and practice. Third, improve the quality evaluation system of innovation and entrepreneurship and provide sufficient funds for college students' innovation and entrepreneurship practice, so as to improve the guarantee for college students' innovation and entrepreneurship practice and improve the incubation rate and business conversion rate of the project; Fourth, through the big data analysis platform, we can realize the organic connection between schools and society, strengthen the business value of college students' innovation and entrepreneurship projects, and establish a business value evaluation system. Fifth, universities and teachers should strengthen the learning and application ability of cloud computing and big data, learn to use data analysis and evaluation, and use data to drive the quality of innovation and entrepreneurship education. However, this paper does not have an in-depth discussion on the specific conditions that college students should have for innovation and entrepreneurship, which needs to be investigated in the future research. We hope this paper can help improve the quality of

college students' innovation and entrepreneurship education and contribute to national development and talent training.

Data Availability

The data used to support the findings of this study are available from the corresponding author upon request.

Conflicts of Interest

The author declares that there are no conflicts of interest.

Acknowledgments

This work was supported by the Qingdao Huanghai University.

References

- [1] Y. Feng, "Route queuing model of railway 12306 call center," *Railway Computer Application*, vol. 27, no. 9, pp. 17–20, 2018.
- [2] R. Hu and Y. H. Tang, "The transient queue length distribution of M/G/1 queueing system with delayed vacation and min (N,V)-policy," *Journal of Mathematics in Practice and Theory*, vol. 49, no. 13, pp. 145–155, 2019.
- [3] J. X. Li, T. Dai, and C. M. Ye, "Service design of distributed contact centers in cloud computing," *Journal of University of Shanghai for Science and Technology*, vol. 36, no. 4, pp. 338–344, 2014.
- [4] X. Eryong and J. Li, "What is the ultimate education task in China? Exploring "strengthen moral education for cultivating people" ("Li De Shu Ren")," *Educational Philosophy and Theory*, vol. 53, no. 2, pp. 128–139, 2021.
- [5] X. Xu and Y. Ye, *Curriculum Design and Effectiveness Evaluation of Entrepreneurship Education -- Taking the MOOC Course of Fundamentals of Entrepreneurship Education of Zhejiang University as a Sample*. (1), Journal of East China Normal University, Shanghai of China, 2018.
- [6] G. Gao and L. Li, *Research on the Evaluation and Promotion Strategy of the Effectiveness of Entrepreneurship Education in Colleges and Universities*. (2), Journal of East China Normal University, Shanghai of China, 2016.
- [7] D. Zheng and Q. C. Zhao, *Discrete Event Dynamic System*, pp. 1–10, Tsinghua University Press, Beijing, 2001.
- [8] A. Choudhury and P. Medhi, "Balking and reneging in multiserver Markovian queueing system," *International Journal of Mathematics in Operational Research*, vol. 3, no. 4, pp. 377–394, 2011.
- [9] E. Weingarten, S. Bhatia, and B. Mellers, "Multiple Goals as reference points: one failure makes everything else feel worse," *Management Science*, vol. 65, no. 7, pp. 3337–3352, 2018.
- [10] X. W. Hu, R. C. Wang, and X. L. Wang, "Model and algorithm for the shift scheduling and rostering problem of call centers with shift-type constraints," *Industrial Engineering & Management*, vol. 25, no. 2, pp. 51–58, 2020.
- [11] I. Bychkov, A. Kazakov, A. Lempert, and M. Zharkov, "Modeling of railway stations based on queueing networks," *Applied Sciences*, vol. 11, no. 5, p. 2425, 2021.
- [12] J. X. Li and X. N. Wang, "Shift scheduling based on fatigue and routing capacity limitation in contact centers," *Journal of Applied Sciences*, vol. 36, no. 6, pp. 122–135, 2018.

- [13] V. Mehrotra, K. Ross, G. Ryder, and Y.-P. Zhou, "Routing to manage resolution and waiting time in call centers with heterogeneous servers," *Manufacturing & Service Operations Management*, vol. 14, no. 1, pp. 66–81, 2012.
- [14] S. Mattia, F. Rossi, M. Servilio, and S. Smriglio, "Staffing and scheduling flexible call centers by two-stage robust optimization," *Omega*, vol. 72, pp. 25–37, 2017.
- [15] Z. Y. Hu and J. Nasiry, "Are markets with loss-Averse Consumers more sensitive to losses," *Management Science*, vol. 64, no. 3, pp. 1384–1395, 2017.
- [16] F. Liu, "Safe diagnosability of fuzzy discrete-event systems and a polynomial-time verification," *IEEE Transactions on Fuzzy Systems*, vol. 23, no. 5, pp. 1534–1544, 2015.
- [17] S. Wang, Y. Zhao, D. you, and R. Ning, "A review of research on Information Physics system attack under the framework of discrete event system," *Control and Decision Making*, 2021.
- [18] W. Zhang and C. Li, "On coordination control of A class of DEDS," *Journal of Yangtze University(Natural Science Edition)*, vol. 16, no. 6, p. 120~124, 2019.
- [19] D. Dai, Z. Cai, and B. Zhang, "Discrete dynamic system modeling and resilient control of knowledge workers in high-technology enterprises," *Journal of China University of Metrology*, vol. 32, no. 1, 2021.
- [20] G. Sathishkumar, "Bivariate regression adaptive wald's boost energy aware routing for Wsn with IoT," *Turkish Journal of Computer and Mathematics Education (TURCOMAT)*, vol. 12, no. 7, pp. 2224–2241, 2021.
- [21] P. Wang, Y. Chen, Z. Cai, and L. chao, "Modeling and repair capability analysis of military overhaul line," *Systems Engineering and Electronics*, vol. 40, no. 6, 2018.
- [22] M. K. Girish and J.-Q. Hu, "Higher order approximations for the single server queue with splitting, merging and feedback," *European Journal of Operational Research*, vol. 124, no. 3, pp. 447–467, 2000.
- [23] B. Kim and J. Kim, "The waiting time distribution for a correlated queue with exponential interarrival and service times," *Operations Research Letters*, vol. 46, no. 2, pp. 268–271, 2018.
- [24] S. K. Iyer and D. Manjunath, "Queues with dependency between interarrival and service times using mixtures of bivariate," *Stochastic Models*, vol. 22, no. 1, pp. 3–20, 2006.
- [25] G. Panda, A. D. Banik, and M. L. Chaudhry, "Stationary distributions of the R[X]/R/1 cross-correlated queue," *Communications in Statistics-Theory and Methods*, vol. 46, no. 17, pp. 8666–8689, 2017.

Research Article

Research on High-Quality Development of Auto Parts Manufacturing Industry Based on Machine Learning Model

Xuchang Yang, Qian Zheng, Yueying Hu, Ronghui Chen , Xuepeng Wang, and Yanan Liu

College of Management, Anhui Science and Technology University, Bengbu 233030, China

Correspondence should be addressed to Ronghui Chen; chenrh@ahstu.edu.cn

Received 29 December 2021; Accepted 17 January 2022; Published 10 February 2022

Academic Editor: Man Fai Leung

Copyright © 2022 Xuchang Yang et al. This is an open access article distributed under the Creative Commons Attribution License, which permits unrestricted use, distribution, and reproduction in any medium, provided the original work is properly cited.

At present, in China's automobile manufacturing industry, the main problem is the manufacturing of parts and on-board equipment. Most domestic industries still adopt the step-by-step production of parts, and each manufacturer customizes the required parts according to the scale and production needs of its own enterprise. This situation is easy to cause unstable quality of parts and serious unqualified quality inspection problems. Based on the above situation, we study the high-quality development, parts quality optimization, and remanufacturing of auto parts manufacturing industry with the support of machine learning model. Firstly, based on the analysis of auto parts procurement and production mode, this paper briefly describes the basic problems in the manufacturing process of auto parts in China. Machine learning technology is used to count the changes of quality data in manufacturing, and the quality standard is reflected in the learning model. The machine learning algorithm is used to diagnose and analyze the faults of auto parts and equipment, so as to turn high-quality production to high-quality production. The projection feature extraction algorithm is used to quantitatively analyze the low quality state of automobile parts. Finally, 3D printing technology is used to solve the quality manufacturing problem of parts with high-precision requirements, and the later materials are processed again to achieve the purpose of remanufacturing planning. The results show that the transformation of auto parts manufacturing to high quality can improve the economic development of the auto industry and meet the needs of modern society. The data analysis of parts controlled by machine learning model can help the precision manufacturing of automobile parts.

1. Introduction

With the rapid development of China's economic strength, the parts manufacturing industry in the automotive industry has also started a wide range of production and processing (Chen Min et al.) [1]. The advantages of auto parts development can promote the transformation and innovation of the auto industry. The parts manufacturing industry needs to focus on high-tech quality transformation and strictly control the quality of its products to meet the needs of modern cities. In different regions of China, the development of auto parts manufacturing industry is different, and most cities with high-tech technology are relatively smooth (Chen et al.) [2]. Auto parts manufacturing needs to be supported by the urban economy and obtain new transformation opportunities from the development of

high-tech technology. Solving the problem of auto parts manufacturing can improve the economic benefits of the whole city, which plays an important role and helps in urban innovation and development (Wu et al.) [3]. At present, the economic benefits that China's auto parts manufacturing industry can create are limited by many reasons. Enterprises can not control the overall quality of parts in normal operation. The sales scope and export channels of auto parts are relatively few, and cross international exchanges and transactions cannot be realized globally (Lu Yanqing et al. 2021) [4]. The above factors are unfavorable to the development of China's automobile industry, especially the quality problems caused by auto parts, which has always been the primary link to be solved (Jin Hongji et al. 2021) [5]. Our government has promulgated many new policies according to the development

status of the automobile industry, and there are new standards and restrictions in quality control and enterprise management. With the advent of the Internet and big data environment, new technology development can help optimize and reform the quality of auto parts manufacturing industry (Kong Ningning et al.) [6].

The main factors affecting the quality change of China's auto parts manufacturing industry also include production cost. Each enterprise has its own cost range, and the reduction of profits leads to many problems in enterprise production (Hu Chun et al. 2021) [7]. The investment growth of foreign investors in the industry is low, and this bad cycle leads to the failure of new technologies in time. The traditional processing method of auto parts is relatively single, and the product renewal and creativity have not been optimized and improved (Qiu Shaohu et al. 2021) [8]. Obviously, the processing efficiency can not meet the production demand of the current automobile industry. At present, the following problems are easy to appear in the process of auto parts manufacturing: first, the production line in many manufacturing industries is too long, which makes it easy to slow down the progress and efficiency of engineering manufacturing in complex environment. The enterprise does not control and allocate the production management, and the complexity of the production line has brought many work difficulties to most employees (Jinxi et al. 2021) [9]. The problems in the production process can not be found immediately. In order to improve the quality of parts, it needs to be analyzed from the production process. Finally, the development of China's automobile industry is relatively diversified and there are many kinds of automobiles. This diversity leads to the need to consider processing parts from many aspects. Therefore, in the development of parts manufacturing industry, it is necessary to increase the types and characteristics of products, improve their own quality, and stand out from various industry competitions (Wang Chuan et al. 2021) [10].

This paper puts forward new measures and ideas for the reuse of parts in China. Its innovative contributions are as follows: 1. Starting from the market economy of automobile products, this paper discusses the influence of cost price and material selection on automobile performance. Starting with the quality control management of parts, the core structure in the manufacturing process is improved. 2. Introduce machine learning model to statistically analyze material data. The training samples are used to obtain the optimal results of quality data, which are added to the manufacturing process of auto parts. 3. Based on the actual situation of China's automobile industry, the fault data are extracted from the part processing process, and the quality parameters are optimized by using the simulation environment. In order to improve the manufacturing quality of parts, machine learning model is used to train the fault analysis performance in sample making.

This paper is mainly divided into three parts. The first part mainly describes the background of automobile industry and automobile parts manufacturing industry and analyzes the current situation of the application of machine learning algorithm in various industries from the perspective

of parts manufacturing process. The second part first analyzes the quality control problems in the process of auto parts manufacturing and transforms the trend of parts manufacturing into high-quality development. Starting with the control of raw materials, the influencing factors of material selection on quality are analyzed by using big data and machine learning algorithm. After data acquisition, the monitoring effect of machine learning model on part manufacturing is analyzed. 3D printing technology is adopted to increase material selectivity and optimize and improve individual parts with high-precision requirements. Finally, it analyzes the industry discovery trend and optimizes the quality problems from the concept of parts remanufacturing in the automotive industry. The third part analyzes the results of high-quality transformation of auto parts manufacturing industry based on machine learning model, as well as the research on parts remanufacturing and quality optimization.

2. Related Work

In the process of automobile manufacturing, it is necessary to analyze and investigate the quality and process of parts. The selection of raw material quality of parts and components has a great impact on the results of the whole manufacturing (Zhang Shibin et al.) [11]. Therefore, it is necessary to collect and analyze the data before the use of raw materials. The statistical results of data analysis are constructed by using machine learning model. Machine learning model can be widely used in computer field, natural language field, and intelligent recognition field (Liu Qixu et al. 2021) [12]. It provides accurate data support and algorithm support for the above industries. Most machine learning models can show good results in sample data detection and prediction. However, the training data of the model needs to select the appropriate range and input method. In order to improve the quality development in automobile parts manufacturing, we need to build a relatively safe and reliable machine learning model. The risk analysis and data prediction of learning model are used to ensure the quality standard of parts. In the training of machine learning model, it is also necessary to ensure the integrity of data and detect the location and specific factors of automobile component faults according to the above data (Wang et al. 2021) [13].

Water conservancy projects in Japan have always been the main industry with risks and accidents. In order to enhance the accuracy of water conservancy work management and risk assessment, they added machine learning algorithm to Engineering Research (Liu Haipeng et al. 2021) [14]. Using machine learning model to construct data association structure, risk assessment and data prediction are carried out for the operation links of water conservancy projects. Under the influence of human beings, the mining effect in the data framework of hydraulic engineering can analyze the key influencing factors and establish corresponding emergency treatment and guarantee measures. With the support of computer technology, many intelligent robots are also widely used in people's life. It is easy for

intelligent robot to face the danger of obstacles in the process of moving. In order to improve the robot's ability to avoid obstacles in real time, it is necessary to use machine learning algorithm to transform the robot system (Yu Hong et al. 2021) [15]. Machine learning algorithm is used to judge the distance of obstacles in real time, and the travel direction is planned. The results show that the robot optimized by the algorithm can form a reliable and stable path in motion. The development of China's automotive machinery field is a hot industry in the near future. Automotive machinery and equipment are prone to many problems in operation. In order to solve the fault problem and improve the diagnosis accuracy, we use machine learning algorithm to ensure the normal operation of automobile mechanical equipment. With its own advantages, machine learning algorithm can change the structure of data calculation and realize fault diagnosis and real-time monitoring of mechanical equipment. Based on the application status of machine learning algorithm in various fields, this paper studies the high-quality transformation and quality optimization measures of auto parts manufacturing industry.

3. Methodology

3.1. Research on High-Quality Transformation of Auto Parts Manufacturing Based on Machine Learning Model. With the continuous improvement of China's economic development, people's use frequency and ownership penetration rate of cars are increasing exponentially. With the growth of automobile sales, the development of the industry is also facing a new turn. The demand for the quality of auto parts and equipment in the auto market is higher and higher. When choosing an automobile brand, we first need to consider its quality and durability. The quality standard of auto parts also provides a data reference for selecting auto brands. Steadily promoting the development of China's automobile industry can play a positive role in national economic growth. At present, although China's automobile has basically reached the state of popularization, people's demand for high quality is becoming closer and closer. The shift of auto parts from quantitative development to high-quality development has become the main factor affecting the process of the industry. From the analysis of automobile sales market, we try to reduce the gap with partners in terms of quality requirements and shorten the distance from manufacturing process and core technology, control automotive equipment and related parts, and constantly innovate and optimize to achieve the purpose of stable industrial development.

Most manufacturers in China's automobile manufacturing industry contract to the corresponding units for parts manufacturing, which is unfavorable to the control of parts quality. It is easy to cause unqualified parts, which can directly affect the overall quality of automotive products. The production process is mainly composed of several processes, as shown in Figure 1.

As can be seen from Figure 1, firstly, it is divided in part manufacturing for different automobile types. Product quality control is divided into inspection stage, statistical

data stage, data detection stage, and overall quality management stage. According to the characteristics of auto parts and the operation process, select the appropriate detection method. Manually control the composition of parts in quality inspection. According to the above process, the supervision of parts and automobile quality can be realized. Although the quality problems can be mastered in their own production links, there are also prominent defects. For example, the order of parts in production will bring some difficulties to quality monitoring, which not only reduces the production efficiency, but also expands the actual cost. In order to improve the overall quality of parts, the industry can only transform active intervention into passive intervention and control. At this stage, parts production is still the focus of research. Many data will be used in the process of component quality accounting, and the work content of this large amount of data calculation is more complex. The use of raw material parameters and the accuracy of calculation data will bring some difficulties to quality accounting. In order to solve the problem of data accounting, this paper uses machine learning algorithm to construct data analysis model.

Machine learning algorithm can select targeted detection methods according to the detection requirements in automobile parts manufacturing. Carry out data detection and tracking from raw material distribution and manufacturing process. The test data in the process of parts manufacturing is divided into two parts. One is the data information inside the part, and the other is the detection information of external equipment. In order to better realize tracking and analysis in component production, we need machine learning algorithm as technical support. A mathematical model is established for the internal and external inspection data of parts, and the position of inspection nodes is defined by data analysis technology. Firstly, the parts manufacturing of an automobile product is randomly selected as the prototype. The internal inspection data needs to correct the position of the inspection node. We define the gap between the front and rear positions of the main target as follows:

$$\arg \min L[g(H), Z]. \quad (1)$$

In the formula, H is the actual position of the detection node and Z is the corresponding position of the specific data. The capture function in machine learning algorithm is used to define the relationship of data quality inspection gap. The input and output variable formula of the model is

$$\begin{aligned} X_{n \times m} &= \begin{pmatrix} x_1 x_2 \dots x_m \\ x_2 x_2 \dots x_n \\ x_n x_n \dots x_{nm} \end{pmatrix}, \\ Y_n &= \begin{pmatrix} y_1 \\ y_2 \\ \dots \\ y_n \end{pmatrix}. \end{aligned} \quad (2)$$

In the formula, n variable is the number of samples and m is the number of eigenvalues of the input data. The mapping relationship between data nodes in machine

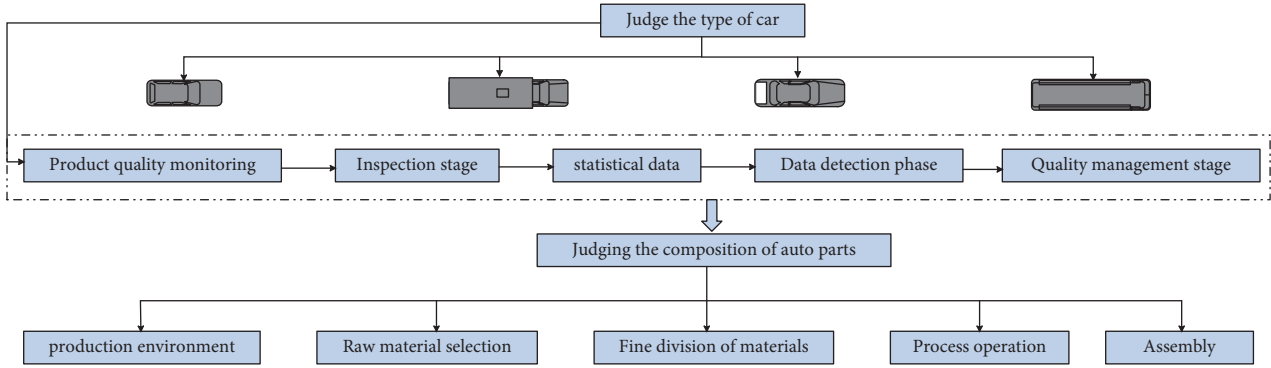


FIGURE 1: Production process.

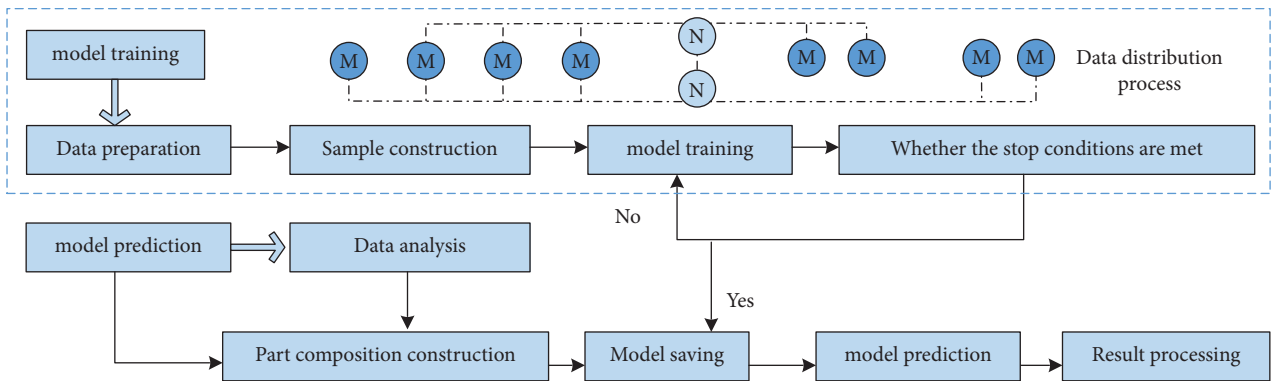


FIGURE 2: Quality data enhancement process constructed by machine learning algorithm.

learning model is reflected by linear regression analysis. It can also quickly judge the correlation between data input and output in feature screening. The calculation formula is

$$f(X) = W_T X + B. \tag{3}$$

A large amount of data needs to be added to the machine learning model for training. Select the data with stable iteration times to obtain accurate data results. The ratio between the predicted value of error measurement and the actual data is used to optimize the parameter model. The error coefficient can be obtained according to the following formula:

$$E_d = \frac{1}{n} \sum_{t=1}^n (\hat{y}_t - y_t). \tag{4}$$

y_t and \hat{y}_t represent the actual value and the predicted value, respectively. In the data mining in Figure 2, it is necessary to judge the location relationship of data nodes. The relationship between internal and external positions of parts is predicted and analyzed, and the purpose of data enhancement is constructed through linear regression. The quality data enhancement process constructed by machine learning algorithm is shown in Figure 2.

As can be seen from Figure 2, the data generated in the manufacturing of parts are obtained. Build corresponding models for different vehicle samples, preprocess the mapping data, and generate sample cases. In the training model, an appropriate algorithm is used to optimize the quality

parameters. Save the optimal parameter model for result processing. Test the influence range of different data on the quality of parts. Due to the technical differences between different manufacturers, dynamic data changes will occur in each component manufacturing engineering. The best quality data we calculated can only provide a certain range of reference efficacy. Next, we need to further study the quality optimization and specific measures of auto parts.

3.2. *Research on Remanufacturing and Quality Optimization of Auto Parts Based on Machine Learning Model.* The manufacturing quality of automobile parts plays an important role and influence on the overall performance and sales of automobile. Parts manufacturing cost and core technology have a great relationship with quality optimization. In quality control, the selection and processing of raw materials can directly affect the change of quality coefficient in production. Raw materials and customer quality cost are internal quality problems of parts. In order to improve the overall performance of automobile, we also need to explore the factors affecting quality from actual production and manufacturing. Step errors or operation failures in the manufacturing process will affect the quality parameters of parts. We also need to detect and judge all aspects of parts in automobile quality inspection. In order to improve the accuracy and effectiveness of fault detection, a component model based on machine learning algorithm needs to be added to the manufacturing process. Control the production

process through the characteristic changes in the manufacturing process of parts. Judge whether there is a manufacturing fault according to the characteristic data. If there is a fault, it can be handled and located in time. Firstly, the projection algorithm is used to extract the fault features in the manufacturing process of auto parts. The model is represented by spatial matrix coefficients:

$$\min \sum \|L\|, +\lambda E_{2,1}, s, 1, X = XL. \quad (5)$$

In the formula, the variable $\lambda E_{2,1}$ represents the fault characteristic data. We judge whether there are similar variables from the matrix data and simulate the information of the same sample:

$$\begin{aligned} x_{ij} &= X^w i_j + E_{ij} \\ &= \sum_{i=1}^c X w_i^s j) + e_{ij}, \end{aligned} \quad (6)$$

where X represents the noise data generated by the fault. The approximate position change of fault is simulated by sample similarity vector. If the training sample does not change, then

$$y = P^T. \quad (7)$$

The calculation variation of the above formula is

$$\begin{aligned} y_{ij} &= p(X w_{ij} + e) \\ &= \sum_{x=1}^c p^T X w_{ij} + p^T e_{ij}, \\ &P^T X_i w_{ij}^i + \sum_{x=1}^c P^T X w_s^{ij} + p^t e_{ij}. \end{aligned} \quad (8)$$

In order to improve the accuracy of the analysis data in the calculation, we need to control the measurement within the minimum distance. The minimum distance is defined as

$$\|y_{ij} - p^T X w_{ij}^s\|^2. \quad (9)$$

Therefore, in the manufacturing process, the specific problem can be analyzed through the fault space. The transformation calculation formula is

$$\sum_n^{ij} \sum_m^{ij} \|y_{ij} - p^T X w_{ij}^s\|^2 = \text{tr}(p^T S_b^L p). \quad (10)$$

In the formula, in order to achieve reasonable data distribution and keep the accuracy above the standard coefficient, the minimum norm needs to be planned:

$$\begin{aligned} \sum_{ij} \|P_{eij}^T\| &= \sum_{ij} \|p^t(x_{ij} - x_s w_{ij}^s)\|^2, \\ \sum_{ij} \|P_{eij}^T\| &= \text{tr}(p_s^T S_e^L p). \end{aligned} \quad (11)$$

In order to make the calculation process simpler, we can also use the identity matrix to express it. The mean value of the above results is the highest, and the vector of the

projection matrix can be represented by the generalized eigenvalue. Finally, in the data analysis level, the part of identifying fault characteristics needs to be judged by data units. The machine learning model is highly adaptable in automatic learning. We use clustering conditions to plan the automatic learning efficiency of machine learning:

$$\eta(t+q) = \eta_0 \left(\frac{a_1}{\eta_0} \right)^s. \quad (12)$$

According to the above formula and machine learning model, the quality changes of parts can be monitored in real time in the manufacturing process, and the steps beyond the stable range can be rearranged and combined. In order to further reflect the effect of parts quality optimization, we can also start from parts remanufacturing. Conduct secondary processing and treatment for unqualified parts and improve the quality coefficient to the standard range and flow into the market again. We investigated the sales of remanufactured products of automobiles and parts, as shown in Figure 3.

It can be seen from Figure 3 that, with the increase of years, the transaction amount in China's automobile market has exceeded the upper limit over the years. Parts remanufacturing accounts for a large proportion in the market. It shows that good sales results can be achieved after secondary processing and improving quality standards. In the quality optimization measures, machine learning model is used to monitor the manufacturing process, which brings core technical support to the secondary manufacturing of auto parts.

4. Result Analysis and Discussion

4.1. Analysis of Research Results of High-Quality Transformation of Automobile Parts Manufacturing Based on Machine Learning Model. In the above research, we found that controlling the quality coefficient of automobile parts can improve the overall performance of automobile. Quality inspection of selected materials should be carried out in the manufacturing process of auto parts. After data acquisition, simulation comparison is carried out to analyze the influence range of material parameters on parts. In order to save costs and increase competitive advantage, many manufacturers will choose to reduce raw material indicators, which affects the purpose of the transformation of the auto parts industry to high quality to a certain extent. This paper establishes a machine learning model to study the high-quality transformation of parts. Firstly, a certain automobile product is randomly selected to establish a virtual model for the distribution of parts and components, as shown in Figure 4.

It can be seen from Figure 4 that the distribution of parts in the automobile structure is complex, and there are many factors affecting the overall quality. We need to fit the overall data and conduct unified calculation in the manufacturing and inspection of parts. In the detection, the change of actual quality data is significantly greater than that of predicted data, so it needs to be subdivided by manual intervention. Estimate the key positions in parts manufacturing from

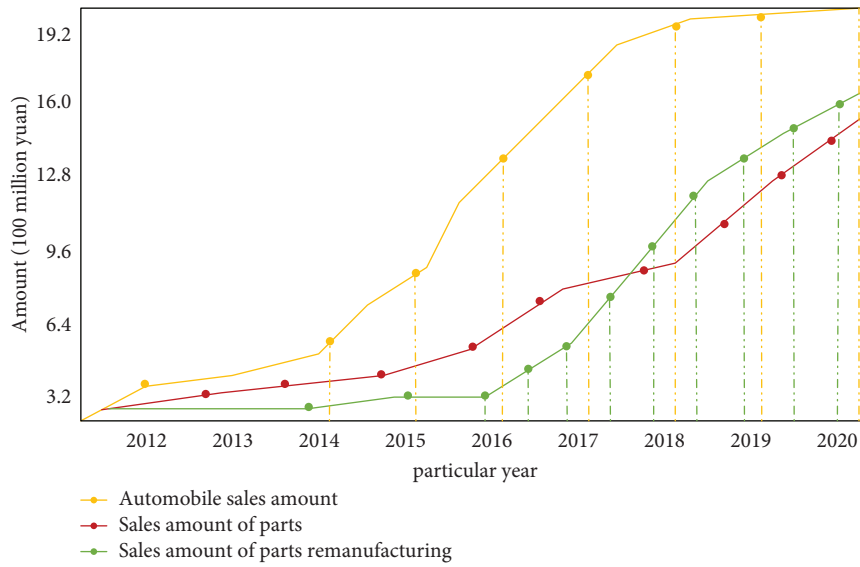


FIGURE 3: Sales of remanufactured products of automobiles and parts.

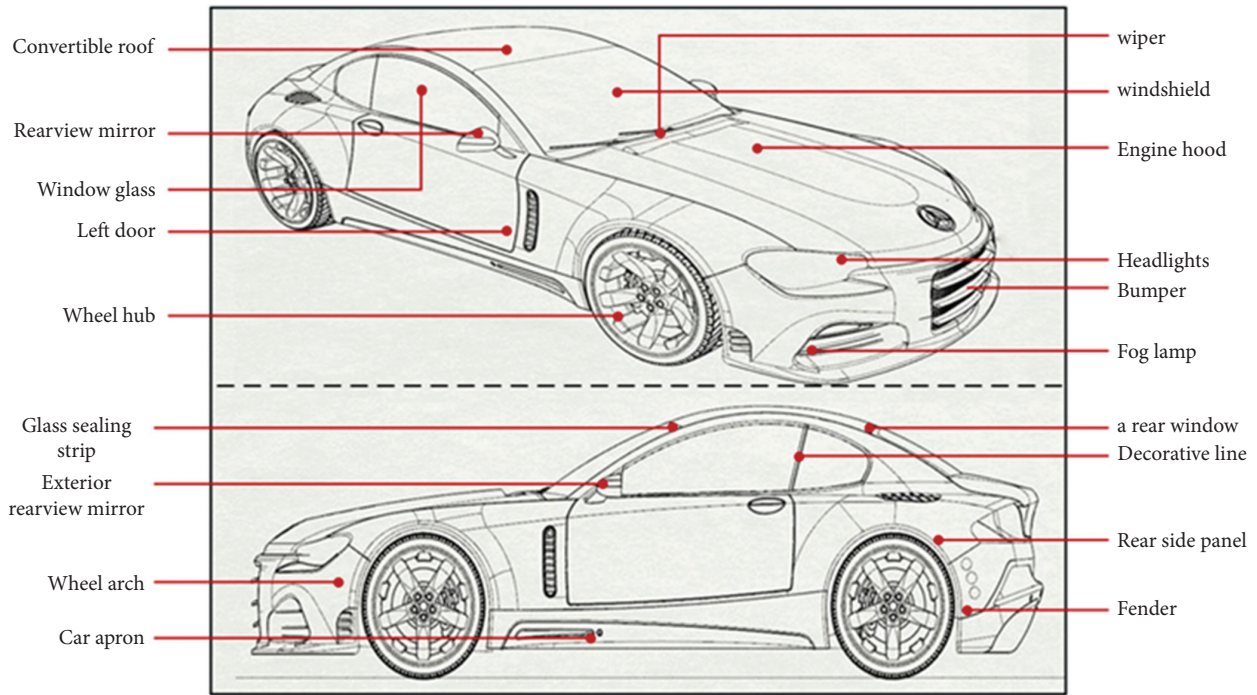


FIGURE 4: Virtual model of automobile parts distribution.

different angles, and record the position changes and material selection. We compare the quality parameters of parts processed with different raw materials, as shown in Figure 5.

As can be seen from Figure 5, with the gradual increase of the stiffness of raw materials, the quality parameters of corresponding products also increase. The material data predicted by machine learning model can highly meet the product demand. Therefore, this algorithm has obvious advantages in practical application. Finally, we can also use 3D printing to solve the problem of high-precision design parts.

The higher the precision, the higher the quality of the finished product delivered by printing. Therefore, for high-precision 3D printing, the primary technical difficulty is the printing precision, that is, the optical resolution: the size of a single pixel of the projection light. Printing speed is also one of the technical difficulties to be broken through in high-precision 3D printing. The formation process of $P\mu$ SL 3D printing technology is as follows: firstly, the three-dimensional structure model is constructed by modeling software; then, the slicing software is used to slice the three-dimensional model with a certain layer thickness to obtain a series of two-dimensional

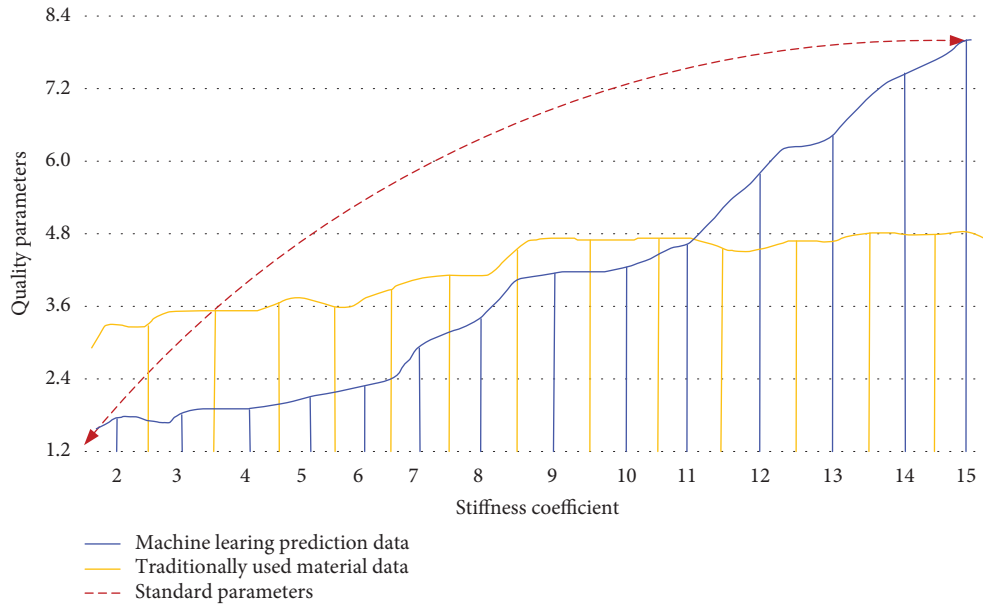


FIGURE 5: Comparison of quality parameters of parts processed with different raw materials.

pictures with specific patterns; then use P μ SL 3D printing system performs full face projection exposure on each layer of pattern after slicing. Repeat the previous step repeatedly and stack layers to finally form the required three-dimensional structure. In addition, the printing system can also splice and print large-size samples through the movement of the printing platform, so as to realize high-precision, large format, and cross-scale processing.

The corresponding shapes and structures are generated directly from the virtual platform. Using 3D printing technology can also reduce the cost of parts and improve the precision of products. Among them, this technology can be used in shape design, interior decoration matching, plug-ins, and other links.

4.2. Analysis of Research Results of Automobile Parts Remanufacturing and Quality Optimization Based on Machine Learning Model. Improving the quality problems in automobile parts manufacturing needs to be considered from many aspects. Firstly, to improve the quality management of parts, it is necessary to establish the corresponding management model and standard rules. This paper analyzes the characteristics of China’s automobile industry and carries out targeted transformation from the domestic environment. Introduce reasonable control measures into quality control and management and establish corresponding departments. Take quality optimization as the core part of manufacturing process. Secondly, in the process of manufacturing, it is also necessary to ensure the transparency of parts production and ensure that each link can be monitored in real time. Record the problems encountered in the production process and achieve accurate positioning. The automatic training model is established according to the recorded information of fault location, and the automatic learning model is transformed and

upgraded by machine learning algorithm. That is, in the face of the next quality problem, the fault node can be located in time to achieve targeted solution. Firstly, we analyze the problem of low quality caused by incorrect operation in automobile parts manufacturing, select a certain position of automobile parts to establish a fault analysis model, and use 3D printing technology to compare the internal structure of normal parts and faulty parts, as shown in Figure 6.

We extract the feature points of the model from the automobile parts structure in Figure 6 and verify the accuracy of the data through comparative experiments. At the same time, it is added to the machine learning training model to synchronize multiple fault factors for common analysis. The change trend of component quality parameters after training with machine learning model is shown in Figure 7.

It can be seen from Figure 7 that, with the enhancement of model training time, the quality parameters of parts change obviously. The quality trend of machine learning training is better; the quality parameters of parts in traditional manufacturing process fluctuate greatly and decrease slowly with the time of feature recognition. In the test data, we randomly select 50 normal data and 50 abnormal data of an automobile product and compare the quality optimization in the model after training, respectively. We find that the efficiency of machine learning model diagnosis is relatively fast and can effectively solve the low efficiency problem caused by repetitive operation. Quality certification and optimization are the main channels to improve the economic changes of automobile market. In order to improve the market sales status, we also need to start from the manufacturing and reuse of parts. For some products that fail to meet the quality inspection standards, the reuse transformation can improve the utility rate of the products

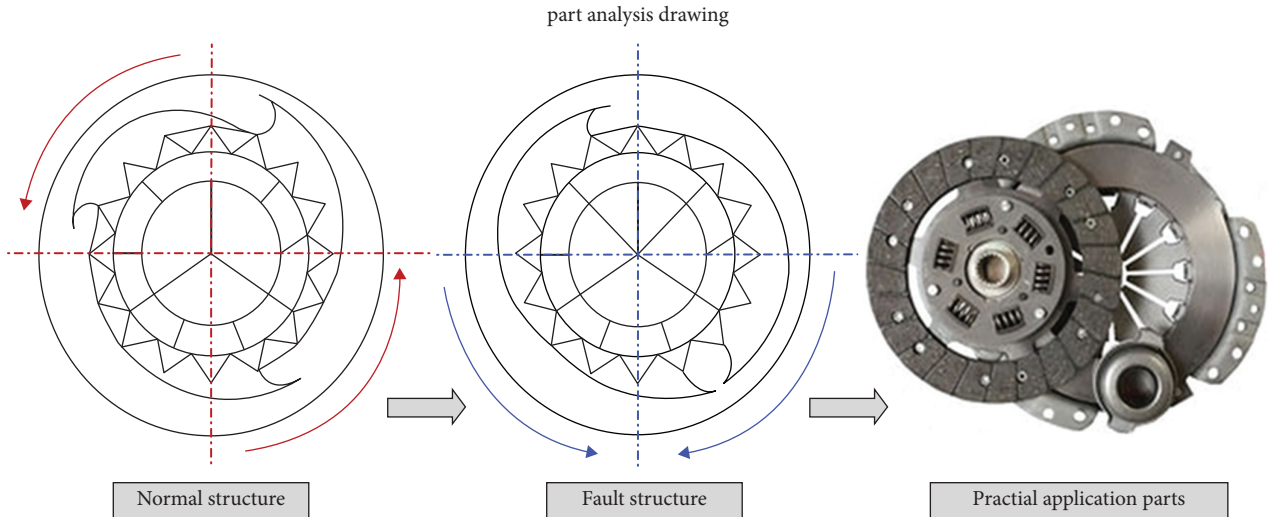


FIGURE 6: Actual application drawing after internal structure comparison of parts.

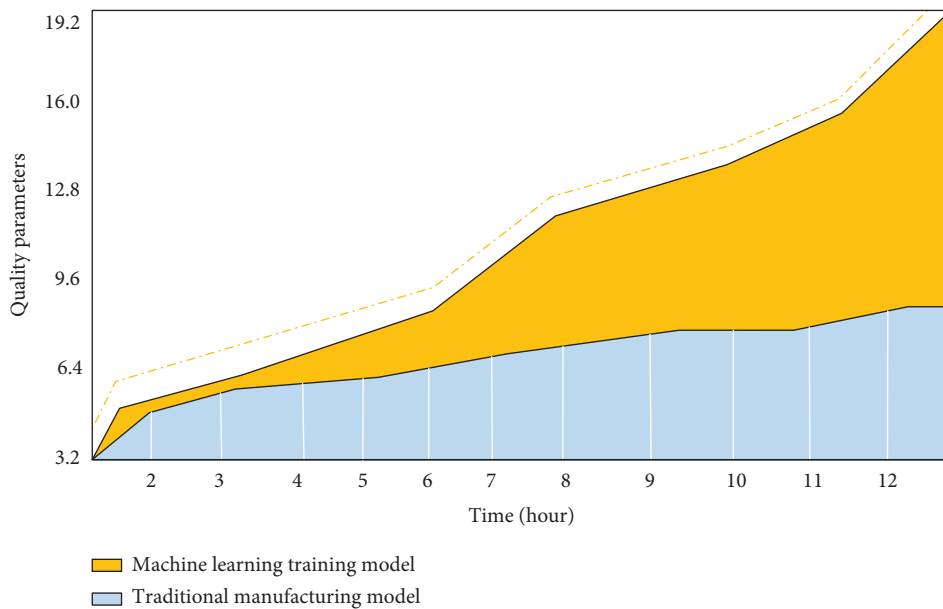


FIGURE 7: Changes of parts quality parameters before and after machine learning model training.

and reduce the average cost of the automobile industry to a certain extent. At the same time, in view of the uneven product quality level in the auto parts market, it is also necessary to start with the quality standard certification and use the quality certification mark to shift the manufacturing of parts from quantity to quality.

5. Conclusion

With the rise of national economic strength, the automobile industry is developing more and more rapidly. The increase of automobile types has brought new challenges to the manufacturing of parts and components. In the process of parts manufacturing, the selection of materials, process flow, processing, and testing technology are the main factors affecting product quality. This demand for higher quality

puts forward requirements for the parts industry from the aspects of structural design, manufacturing mode, and quality inspection. In order to unify product quality standards and transform parts manufacturing from high quantity to high quality, we study the automobile parts manufacturing industry under the machine learning model. Firstly, starting from the market economy of automobile products, this paper explores the impact of cost price and material selection on automobile performance. It is found that the selection of raw materials has an obvious influence on the composition and quality of parts. Starting from the quality control management of parts, improve the core structure in the manufacturing process. The machine learning model is introduced to statistically analyze the material data. Using training samples to obtain the optimal results of quality data, it is added to the manufacturing

process of auto parts. Finally, starting from the actual situation of China's automobile industry, the fault data are extracted from the parts process, and the simulation environment is used to optimize the quality parameters. In order to improve the manufacturing quality of parts, the fault analysis performance in sample making is trained by machine learning model. 3D printing technology is used to solve the problem of parts with high-precision requirements. This paper puts forward new measures and ideas for the reuse of parts and components in China. The results show that the auto parts manufacturing industry needs to change from paying attention to product quantity to paying attention to high-quality development. The product quality optimization based on machine learning model can improve the nonstandard operation in the manufacturing process of parts industry and provide new help for China's automobile industry in the market competition.

Data Availability

The datasets used during the current study are available from the corresponding author on reasonable request.

Conflicts of Interest

The authors declare that they have no conflicts of interest.

Acknowledgments

This work was sponsored in part by the "2021 Anhui University Humanities and Social Science Research Project (Grant no. SK2021A0479)" and "The sixth 2021 of Applied Social Science Research in Chuzhou (Grant no. A2021014)."

References

- [1] m. Chen, "Research on quality control measures of automobile parts manufacturing," *Metallurgy and materials*, vol. 41, no. 5, pp. 17-18, 2021.
- [2] K. Chen, "Promote enterprise quality management system certification and standardize the development of China's auto parts remanufacturing industry," *Automobile and accessories*, no. 19, pp. 52-53, 2021.
- [3] D. Wu, "Nondestructive testing technology and its application in automobile parts manufacturing process," *Modern manufacturing technology and equipment*, vol. 57, no. 9, pp. 149-150, 2021.
- [4] Y. Lu, "Suggestions on optimization of internal control system of auto parts manufacturing enterprises," *China foreign capital*, no. 16, pp. 68-70, 2021.
- [5] H. Jin and Y. Jiang, "Discussion on key technologies of remanufacturing internal combustion engine and its parts," *Internal combustion engines and accessories*, no. 21, pp. 192-193, 2021.
- [6] N. Kong and P. Cui, "On the casting process of new die casting parts of automobile," *Internal combustion engines and accessories*, no. 13, pp. 105-106, 2021.
- [7] C. Hu and Y. Wang, "Analysis of quality control and optimization measures for automobile and parts manufacturing," *Times automobile*, no. 13, pp. 153-154, 2021.
- [8] S. Qiu, H. Zhao, and K. Fang, "Application of 3D printing and CNC processing in different stages of automobile and parts manufacturing," *Automotive technologist*, no. 6, pp. 33-37, 2021.
- [9] J. Ge, P. Guo, and Q. Li, "Research on the development trend of automobile parts manufacturing technology," *Auto parts*, vol. 1, no. 5, pp. 107-109, 2021.
- [10] C. Wang, "Analysis on key technologies of remanufacturing internal combustion engine and its parts," *Internal combustion engines and accessories*, vol. 5, no. 18, pp. 132-133, 2021.
- [11] S. Zhang, X. Huang, Y. Chang, L. Yan, and W. Cheng, "Research progress and development trend of quantum machine learning in big data environment," *Journal of University of Electronic Science and technology*, vol. 50, no. 6, pp. 802-819, 2021.
- [12] Q. Liu, j. Wang, J. Yin, Y. Chen, and J. Liu, "Application of anti machine learning in network intrusion detection," *Journal of communications*, vol. 42, no. 11, pp. 1-12, 2021.
- [13] Z. Wang and L. Ge, "Credit risk quantification and decision analysis based on machine learning," *Software engineering*, vol. 24, no. 12, pp. 40-44, 2021.
- [14] H. Liu, S. Gu, Q. Liu et al., "Alignment method of pipeline internal and external inspection data based on machine learning algorithm," *Oil and gas storage and transportation*, vol. 40, no. 11, pp. 1236-1241, 2021.
- [15] H. Yu, W. Cheng, Z. Dai, J. Wang, and y. Xu, "Design of emergency material demand forecasting model based on machine learning," *Electronic design engineering*, vol. 29, no. 22, pp. 19-23, 2021.

Research Article

Research on Children's Education App Network Transmission Based on 5G Mobile Computing Technology

Mou Tangjuan ^{1,2} and Kim Il-Tae¹

¹Art and Sports, Chosun University, Gwangju Metropolitan 61448, Republic of Korea

²School of Digital Arts and Media, Shandong University of Art and Design, Jinan, Shandong 250001, China

Correspondence should be addressed to Mou Tangjuan; mtj@sdada.edu.cn

Received 30 December 2021; Accepted 18 January 2022; Published 8 February 2022

Academic Editor: Man Fai Leung

Copyright © 2022 Mou Tangjuan and Kim Il-Tae. This is an open access article distributed under the Creative Commons Attribution License, which permits unrestricted use, distribution, and reproduction in any medium, provided the original work is properly cited.

With the continuous improvement of China's scientific and technological level, the popularity of mobile network technology is becoming more and more widespread. Many big data technologies and wireless sensor technologies have brought new changes to people's lives. At present, the functions of communication technology and network transmission have moved from perfection to new innovation and development. 5G mobile network technology has played an important role in various fields. When China's economy and science and technology develop better and better, people pay more and more attention to children's education. The research on children's education has become a hot topic. From the above background, this paper studies the network transmission function and network transmission path of children's education app in 5G era mobile computing technology. First, starting from the development trend and main functions of 5G, this paper briefly describes the functional requirements of children's education app. The efficient data transmission in the 5G mobile wireless sensor network is applied to children's education app. Starting from the distance of network transmission nodes, the data transmission optimization algorithm is adopted, and the network transmission module is composed of the best transmission path of nodes. Combined with the energy-saving effect of mobile computing technology, the problem of excessive consumption of network transmission resources is optimized. Finally, the data transmission path is studied in the 5G mobile network. The results show that 5G mobile computing technology can optimize the network transmission performance, improve the operation efficiency of the server, and has a good effect in solving the problems of delay and low coverage. In the process of children's education app network transmission under 5G mobile computing technology, it can ensure the user's personal information and improve the security of system feedback.

1. Introduction

The existing 4G network has been widely used in the Internet of things and is constantly developing to meet the application needs of the Internet of things in the future. New applications and business models of the future Internet of things need new performance standards, such as large-scale connection, security, reliability, wireless communication coverage, ultralow delay, high throughput, etc. In order to meet these needs, 5g technology is expected to provide new interfaces for future Internet of things applications. 5g will not only provide 1000 times of Internet traffic growth in the next decade but also provide various industries with basic

technologies to support the development of the Internet of things. (1) The Internet of things can promote classroom teaching, realize the interaction between students and students and students and machines through sensor technology, provide an intelligent environment for teaching, improve the traditional learning environment and learning methods, and adjust the teaching structure at any time. (2) The Internet of things can be used for extracurricular learning. It supports extracurricular research, mobile learning, and ubiquitous learning to enrich extracurricular learning methods and promote the development of students' ability. (3) The Internet of things can also be used for school management such as attendance management, school

library management, teaching instruments, and equipment management and school education safety management, so as to innovate school management means and improve management efficiency and quality.

With the rising level of science and technology in China, the coverage effect and popularity of mobile network are gradually expanding. People's daily life has been inseparable from the support of Internet and mobile technology [1]. Although the traditional 4G network can meet our daily use, it has obvious defects in the use of intelligent devices and intelligent terminals [2, 3]. Therefore, the advent of 5G mobile network has brought new opportunities and changes to network transmission in all walks of life [4]. At present, this technology is in the preliminary development stage and has a good application prospect. In practical applications, many communication industries and electronic information industries have predicted it. With the research upsurge of 5G technology in various countries, many scholars found that compared with 4G network technology, this technology has obvious efficiency in the use of intelligent devices [5]. In the process of using 5G mobile network and related technologies, it is necessary to make a reasonable selection of network environment and equipment [6]. We need to integrate more advanced technology and imported equipment to build it. With the advent of 5G era, our country has also significantly improved in the process of base station construction, and the number and scale are showing a positive upward trend [7]. In the network transmission, we also need to consider the urban area coverage effect and establish a large-scale network structure for the whole area. Therefore, the regional network using 5G mobile network and communication technology can be faster and more stable and has good performance in coverage [8].

At present, children's education app has become the main application in the field of education in China [9]. With the rapid development of mobile network technology, all walks of life have formed their own professional app applications [10]. With the rapid improvement of people's living standards, people pay more and more attention to children's education industry. Children's education, with children as the main body and education as the main purpose, has become the focus of every family [11, 12]. When children's education combines intelligent devices and mobile networks to form the current form of app, it has been widely used in the field of education [13]. This educational app can use mobile phones or computers as the carrier of interactive devices to realize the interactive process between children and teachers. Use the network equipment as the medium to connect the data transmission function [14]. Therefore, children's education app has high research value and important significance. As educational software has become the focus of research, the network transmission performance and process in actual operation have also become the main research content [15].

Starting from the development trend and main functions of 5g, this paper briefly describes the functional requirements of children's education app. Research and innovation contributions include the following: (1) using the data transmission optimization algorithm, the network

transmission module is composed of the best transmission path of the node. Combined with the energy-saving effect of mobile computing technology, the problem of excessive consumption of network transmission resources is optimized. (2) The data transmission path in the 5g mobile network is studied. The results show that 5g mobile computing technology can optimize the transmission performance of the network, improve the operation efficiency of the server, and have a good effect in solving the problems of delay and low coverage. (3) In the process of children's education app network transmission under 5g mobile computing technology, it can ensure the user's personal information and improve the system feedback security.

This paper is mainly divided into three parts. The first part analyzes the development of 5G mobile computing network and the research status of children's education app in various countries. The second part first combines wireless communication technology with 5G mobile computing to analyze the transmission process of educational app network. Aiming at the optimization and improvement of data processing in network transmission, the tree structure is used to simulate the transmission algorithm in big data environment. The optimal transmission process is calculated according to the distance between network transmission nodes. The energy-saving link of 5G network and mobile computing in network transmission is studied. Finally, the factors affecting the efficiency of network transmission are analyzed, and the optimal transmission path of children's education app network under 5G mobile computing technology is explored. The third part first analyzes the results of the research on the network transmission of children's education app under the mobile network technology and the network transmission path.

2. The Related Works

In the construction of 5G mobile computing network, a variety of schemes and requirements need to be met. The construction of network transmission needs to include whether there is a source, and the cost requirements of the two options for network transmission are also different [16]. In the overall application process, it is necessary to consider whether the efficiency of information resource transmission will increase the actual cost after accessing the 5G network. In the application of reducing network transmission cost, it is also necessary to ensure network security performance [17]. In order to improve the network construction and transmission quality, we need to start from the broadband configuration and network structure and choose a flexible design that can ensure the needs of educational app [18]. Research and development shall be carried out in strict accordance with the network transmission protocol and the functional requirements of children's education app. Due to the complexity of the network structure, different requirements and performance have very different requirements for the level. In the specific implementation process, it is necessary to not only pay attention to the existing network structure but also use wireless communication technologies such as big data to support the 5G network environment

[19]. At present, China's network transmission structure has many forms. With the continuous development of mobile technology, in order to promote transmission efficiency and applicability, we need to consider it in 5G environment [20]. Select the environment with strong coverage in the application scenario, maximize the popularity of children's education app network by using 5G transmission performance, and ensure that the network application can realize the function of cross regional and cross domain transmission. Bring better experience and services for users and children [21].

The development of mobile technology and Internet in the United States is relatively advanced, and people are familiar with the integration of Internet into daily life and work [22]. The idea of mobile learning is also widely recognized in American universities. This kind of learning behavior has had a good effect in children's education schools. They use mobile applications to build a children's learning platform and system, so that mobile learning has achieved good results in the field of children's education [23]. It can not only help children learn knowledge better, but also be free from the constraints of time and place, and realize the real-time interaction with teachers.

The development of online education resources and mobile network devices in Japan is also relatively rapid [24]. With the popularization of intelligent equipment, online library and other applications have enriched people's daily life. Many colleges and universities have realized online teaching and after-school learning services. Educational app software improves students' learning efficiency in their daily life and shows information-based and intelligent learning resources to students in need. In the field of children's education, they first chose platforms such as online counseling as the basis. Subsequently, with the rapid development of mobile technology, online counseling was gradually transformed into the form of mobile application software, which brought a lot of help to children's learning and cognitive society [25].

The scale of Internet users in China has become the top form in the world, including hundreds of millions of mobile phone users. Using mobile phone to surf the Internet has become a common living habit. With the advent of the 5G network era, it is more convenient for everyone to obtain information by using mobile phones and mobile terminals. In the field of education, network counseling, distance teaching, and other modes have become widely used. People also put forward the idea of intelligent app in the development of children's education software. Many educational institutions have specially developed educational apps to help students expand their knowledge structure according to children's habits and learning frequency. Many children's education apps can also be combined with virtual devices to form a 3D live learning atmosphere. Based on the development status of children's education app in various countries, this paper studies the network transmission performance and path of education app by using mobile computing technology and wireless network technology in 5G environment.

3. Research on Children's Education App Network Transmission and Optimal Path Based on 5G Mobile Computing Technology

3.1. Research on Transmission Optimization Algorithm of Children's Education App Network Based on 5G Mobile Computing Technology and Wireless Sensor Network. To research on network transmission optimization algorithm of children's education app based on 5G mobile computing technology and wireless sensor network in order to realize the effective application of 5G mobile network in children's education app, we need to analyze from the actual network application environment. On the basis of coverage, ensure users' excellent sense of experience and efficient information services to meet the needs of most people and children. In order to better realize the network operation, we need to choose a high-capacity environment to provide technical support for traffic transmission and information transmission. In the direction of improving the use effect and popularity of children's education app, it is necessary to choose the operation mode that consumes less resources. Select the technology with less data content and low consumption, and combine it with the education app network transportation module. We study the 5G network coverage in various regions of the country, as shown in Figure 1.

As can be seen from Figure 1, the national network coverage basically reaches above the standard range. Among them, 5G in the eastern region develops rapidly and has obvious advantages in coverage. When the 5G network is selected as the technical support of application software, it is necessary to scientifically analyze the system function. First of all, the user experience should meet the provision of children's learning resources. And resource allocation is carried out for students of different ages. From the interactive experience, we should set some options convenient for children to meet the personalized needs of students. Distinguish the children's operation process from their parents, and set the corresponding parent mode and learning mode. In data management, we should focus on data management and personal information management. Finally, the background mode needs to be established to facilitate the administrator to modify and improve the platform. The specific functional framework is shown in Figure 2.

After analyzing the system functional requirements, we also need to analyze the application status of children's education apps, starting with the acceptance of parents and students. Using the questionnaire and evaluation form, analyze the evaluation coefficients of parents and children on the use experience of children's education app software, as shown in Figure 3.

As can be seen from Figure 3, with the increase of the number of people, we can clearly see that parents generally have a high degree of recognition of children's education app, and students are also satisfied with the actual application process. In the process of network transmission, the transmission of software application generally adopts the digital system. Although this method is relatively stable, it can not guarantee the quality of information and data

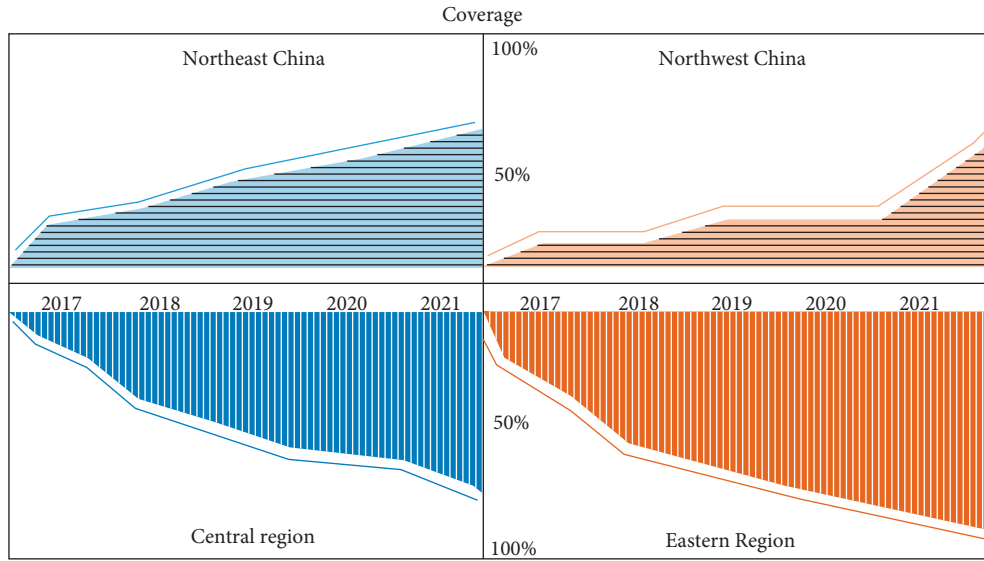


FIGURE 1: 5G network coverage in all regions of the country.

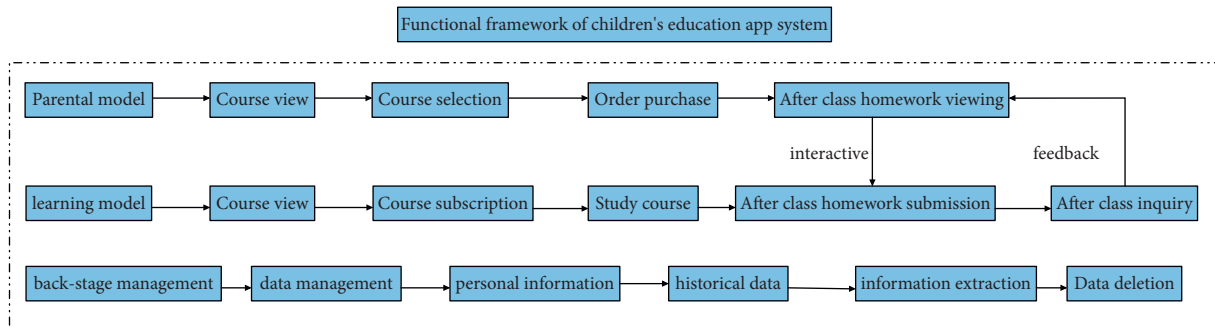


FIGURE 2: Specific functional framework.

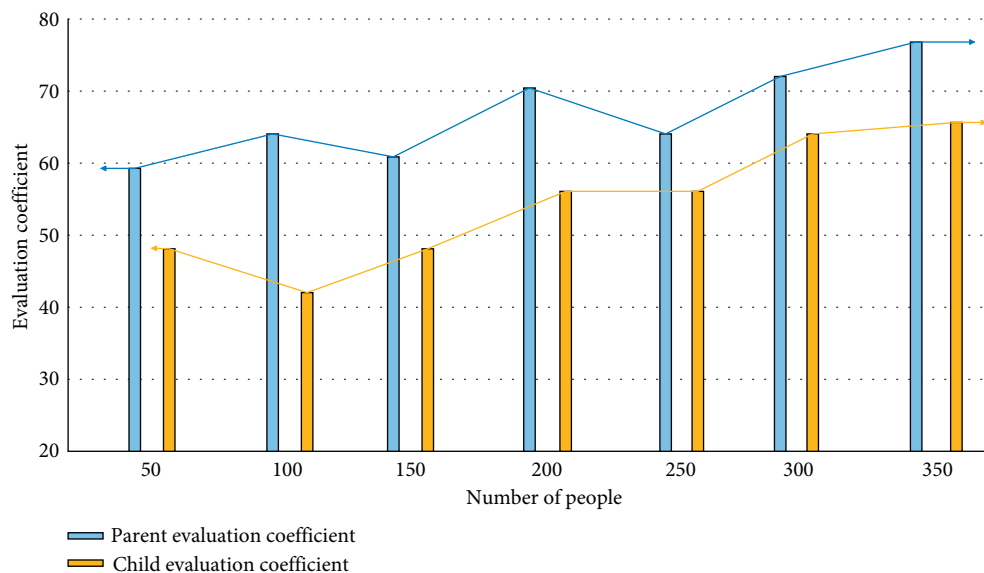


FIGURE 3: Comparison of APP use experience between parents and children.

transmission in the big data environment. With the rapid development of wireless sensor technology and mobile network, many mobile computing technologies in 5G environment have also been widely used. Based on the mobile computing network, this paper analyzes the transmission process and the factors affecting the performance. First, different data nodes are used for distribution in the network model. It is assumed that the data flow consumed by each node is as follows:

$$\begin{aligned} E_{tr} &= l * E_{elec} + l * \varepsilon_{fs} * d^2, & d \leq d_0, \\ E_{tr} &= l * E_{elec} + C * \varepsilon_{mp} * d^3, & d > d_0. \end{aligned} \quad (1)$$

The specific formula after calculation is simplified as follows:

$$d_0 = \sqrt{\frac{\varepsilon_{fs}}{\varepsilon_{mp}}}. \quad (2)$$

The energy consumption of a network node receiving a signal is as follows:

$$E_{rx} = l * E_{elec}. \quad (3)$$

The variable ε_{fs} represents the maximum distance between nodes, and ε_{mp} represents the specific energy consumed in the transmission process of each data. According to the mobile computing algorithm, we select the network node in a certain area as the test location in advance. Under comprehensive conditions, select places with too much data storage, and calculate the data change value according to the above factors. The energy consumption of each node is represented by the data set:

$$CH_{candldata-l} = a * \left(\frac{E_{Remain-1}}{E_{Initial}} \right) + \beta * \left(\frac{Deg_{max}}{Deg_1} \right). \quad (4)$$

The parameters a and β represent data greater than 0 and less than 0, respectively. Set the optimal data transmission route to the number and specific location of nodes to form the communication radius:

$$T_{(n)} = \frac{P}{1 - p * (r * \text{mod})} n \in G, \quad (5)$$

$$\text{rand}(v_i) < T(v_i).$$

After the data transmitted through the network is classified, the optimal transmission path is established according to the maximum coverage level and minimum consumption of the link. In order to reduce the communication complexity of mobile computing technology in educational app, we also need to implement multipath concurrency in network transmission. Finally, the contact terminal is improved and 5G network transmission technology is implemented in the application of children's education app. We draw and analyze the real-time network transmission structure of 5G mobile computing technology, as shown in Figure 4.

As can be seen from Figure 4, in addition to connecting the mobile terminal, the coverage of the core network and

the base station also need to be considered and finally ensure the effective operation of each link in the network transmission.

3.2. Research on Path Optimization of Children's Education App Network Based on 5G Mobile Computing Technology. With the coming popularity of 5G in China, it can drive most of the global networks to realize the connection and transmission function. Intelligent devices and intelligent terminals can appear in many forms. 5G mobile computing network programs are becoming more and more advanced and complex. Although the 5G network system can quickly handle server identification and information transmission, it can not handle the path node optimization in network transmission to a better state. We optimize the design and research of children's education app network path. Select the distributed network server in network path design. This server can connect the virtual environment with the mobile base station to realize the rapid processing and transmission of data. The network coverage is also stronger than the original structure, and the strength of receiving data is above the standard range. In order to meet the real-time interaction performance of APP users, we need to adopt this network structure with high coverage as the choice of the optimal path. Compare the high coverage mobile network with the ordinary mobile network in real-time interactive response, as shown in Figure 5.

As can be seen from Figure 5, the greater the response coefficient, the higher the efficiency of the network in the interaction process. 5G networks with high coverage are obviously more interactive than ordinary mobile networks. Subsequently, in order to ensure the stability of data information in network transmission, it is necessary to establish relevant models for transmission nodes. During the request process of each data unit, an independent set shall be configured to realize effective division. In the stable transmission demand, the independent data of the transmission request are controlled within the following range, and the expression is as follows:

$$M_i(c) = \frac{i * q}{(c + 1) * G_i(c)}. \quad (6)$$

In the formula, the variable q represents the number of budget steps in the transmission process. Effective selection by allocation method in network data set is as follows:

$$w_y = \sum^n M_i(c) * q. \quad (7)$$

Assuming that the data node in the formula does not schedule the minimum distance, the equilibrium expression of the transmission coefficient is as follows:

$$C_{ain} = \sum_{i=1}^N [g(\Delta w_i) - l(\Delta w_i)] * w. \quad (8)$$

$l(\Delta w_i)$ represents the priority of the assigned path and can represent the stability change of the network transmission data set. The task is scheduled for each data set

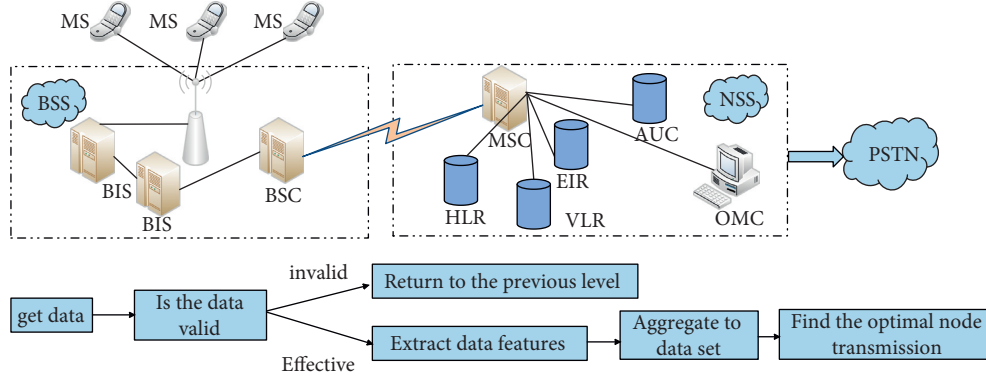


FIGURE 4: Network transmission structure diagram.

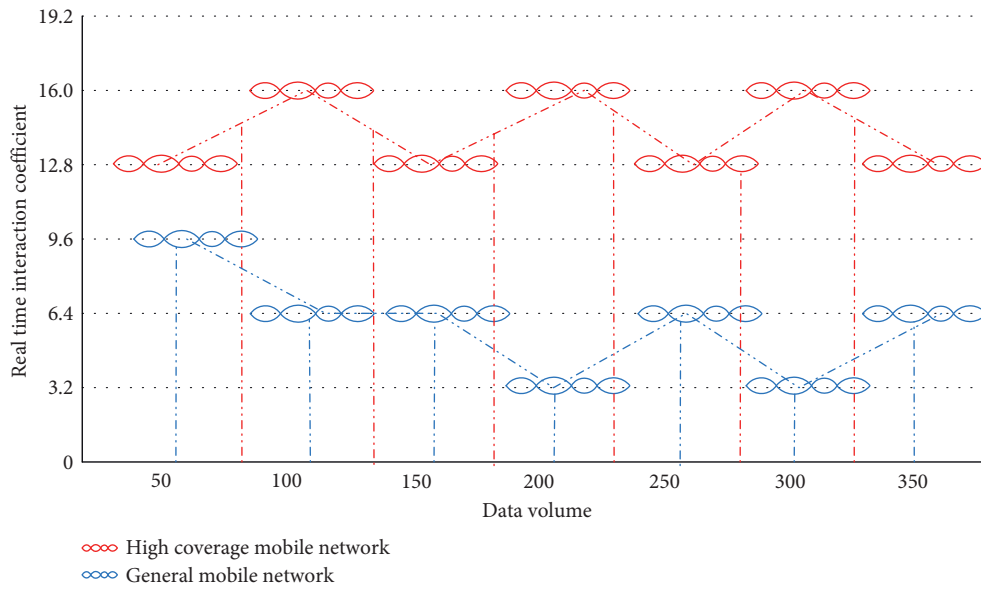


FIGURE 5: Comparison of real-time interactive response between high coverage mobile network and ordinary mobile network.

through sorting calculation, and the minimum coefficient of time is selected as the allocation point. The specific operation model expression is as follows:

$$C = \frac{(D, W^n, Q, Z)}{(V, W, E, C)}. \quad (9)$$

Among them, the relationship described by the set represented by the data is the change of stability coefficient. It is assumed that the data operation in the model is related to the storage performance:

$$L_p = G \cdot \begin{Bmatrix} l_{p-1} * p \\ 1 \end{Bmatrix}, \quad (10)$$

$$p_i = \bar{T}_i \cdot l_p,$$

where p_i is the data size coefficient and \bar{T} represents the number of network transmission nodes. The path of the transmission task is represented according to the order of the above values:

$$W_i = \sum_{ni} \frac{w_{i,j}}{P_i}. \quad (11)$$

According to the above expression, the processing expression under different states of path in network transmission can be clearly obtained:

$$\text{rank}(n_i) = \frac{1}{|k|} * \sum_{j=1}^k w_i(n_i, p_j). \quad (12)$$

In the path optimization of mobile network nodes, in addition to considering the location and communication range of data nodes, it is also necessary to set nodes as marker points. When the access location in data transmission is outside the coverage, we do not need to consider the location of this node, which is called edge node. Compare the position changes of data nodes before and after network transmission path optimization, as shown in Figure 6.

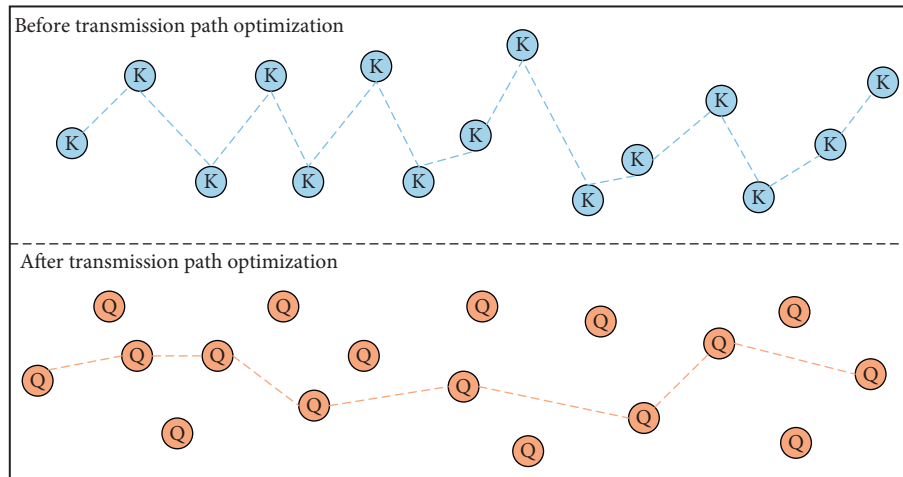


FIGURE 6: Changes of data node position before and after network transmission path optimization.

As can be seen from Figure 6, the node position change after the network transmission path optimization can find the optimal line from multiple location nodes to realize the shortest distance task transmission. Therefore, selecting the optimal network transmission path can effectively improve the operation of the whole platform. Finally, we also need to analyze the transportation consumption of 5G mobile network. In the process of data flow and information transmission in the service center, there will be different degrees of consumption. According to the system platform load and evaluation data, it can be seen that data transmission consumes the most resources. We should analyze the way in which children's education app consumes the least energy. In addition to the necessary core program operation and peripheral equipment operation, it is also necessary to calculate the access nodes and received data. The energy consumption distribution of children's education app network is shown in Figure 7.

As can be seen from Figure 7, the network consumption is divided into two parts, one is the normal energy consumption in the process of data exchange and the energy consumption in information transmission. The other includes the energy consumption of core programs and terminal devices. In the process of using the children's education app, the long-time standby service will not completely cut off the energy consumption but reduce the network energy consumption and reduce the average consumption. We also need to take the transmission consumption into account in designing the optimal network transmission path.

4. Analysis of Research Results of Children's Education App Network Transmission and Optimal Path Based on 5G Mobile Computing Technology

4.1. Analysis of Research Results of Children's Education App Network Transmission Optimization Algorithm Based on 5G Mobile Computing Technology and Wireless Sensor Network.

As a device to realize dynamic interaction and information transmission in software applications, children's education app needs to meet the performance of fast data transmission, smooth data interaction, safe storage location, and so on. With the rapid development of 5G technology, the network transmission process is facing new update and optimization. The transmission process needs to send information and data to users within the network coverage through mobile network lines. In order to meet the people's demand for software signals, the transmission lines and external equipment are also different. When information is sent from the interactive platform, there is an underlying physical channel formed by data flow between the receiver and the sending node. This form can judge the speed that affects the network data transmission. The subsequent wireless network transmission changes this physical channel mode and takes speed and clarity as the core content in information transmission. The transmission speed of children's education app network optimized by mobile computing technology under the 5G network is compared with that of traditional mobile network, as shown in Figure 8.

As can be seen from Figure 8, APP software using 5G mobile network computing technology has obvious advantages in transmission speed within the same data flow range. The transmission efficiency of traditional mobile networks is not high in the big data environment.

As an important direction of the evolution and upgrading of the new generation of information and communication technology, 5g is the key information infrastructure to realize the interconnection of all things and an important driving force for the digital transformation of economy and society. However, while 5g technology benefits society and people, it also raises new network security risks. Because mobile providers must support GPRS Tunneling Protocol on their 5g network for traditional reasons, users will still be vulnerable to attacks even if the 5g protocol itself contains security functions to prevent similar attacks. If it includes user information disclosure (including location data for user tracking), spoofing can be used for fraud and simulated attacks. Denial of service (DOS) attacks on

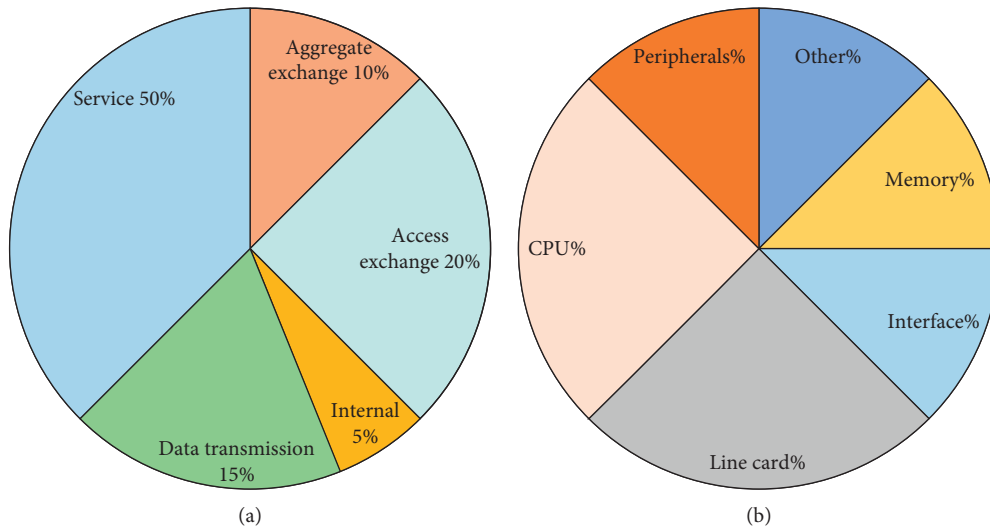


FIGURE 7: Energy consumption distribution of children's education app network. (a) Data management. (b) Terminal services.

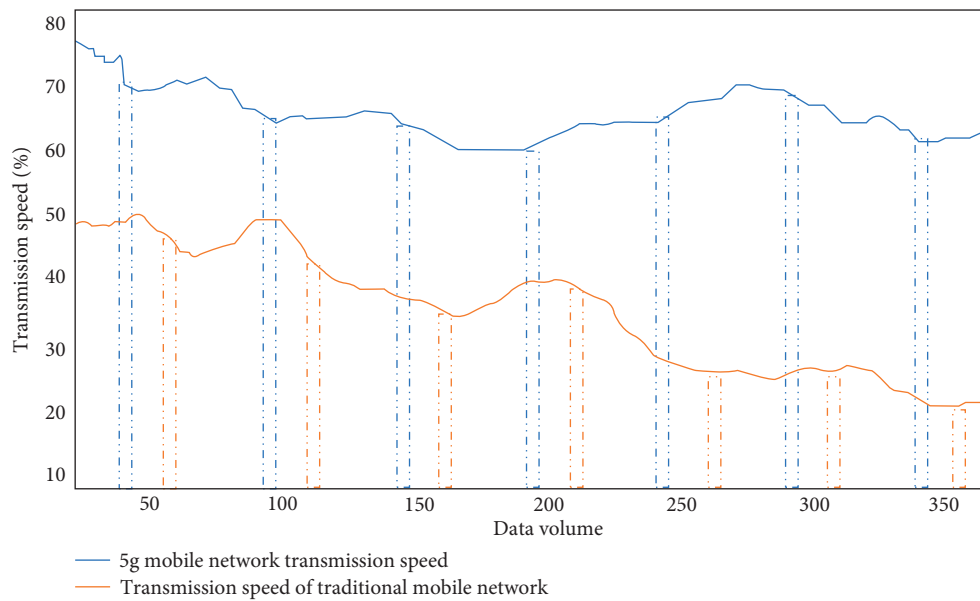


FIGURE 8: Comparison of transmission speed between 5G network and ordinary network.

network devices lead to large-scale interruption of mobile communication.

5G adopts the following technical countermeasures: first, strengthen the system security, track and audit the management control operation, and improve the anti attack ability. Secondly, provide end-to-end, multilevel resource security isolation measures to encrypt and backup key data. Third, strengthen the security management of open source third-party software.

With the increasing popularity of the Internet in China, the amount of data in daily contact is also increasing. In order to meet the normal use needs of educational app, we need to consider the efficiency of network transportation and select appropriate network technology for

improvement. Personal information and data security need to be considered in data transmission over the mobile network, and programs with strong encryption performance should be selected in database establishment to protect private information. The 5G mobile network generates a large amount of data and information, and a data security mechanism is added to the network transmission process. We compare the data security of traditional mobile networks, as shown in Figure 9.

As can be seen from Figure 9, the security coefficient of traditional mobile networks gradually stabilizes with the increase of the amount of data. This security mechanism can not meet the needs in the big data environment. When using the children's education app software, we need to focus on

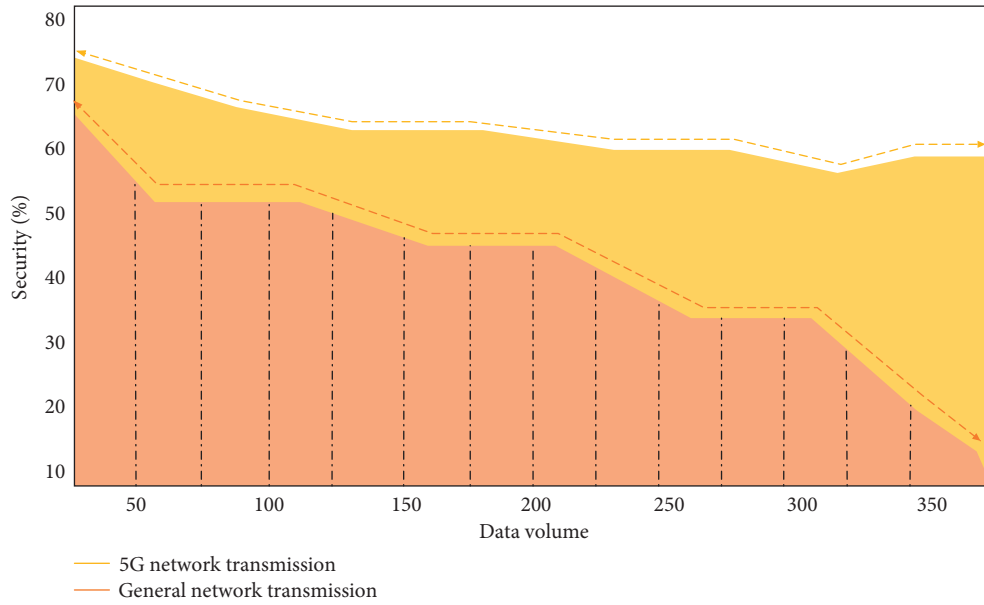


FIGURE 9: Comparison of data security between 5G network and traditional mobile network.

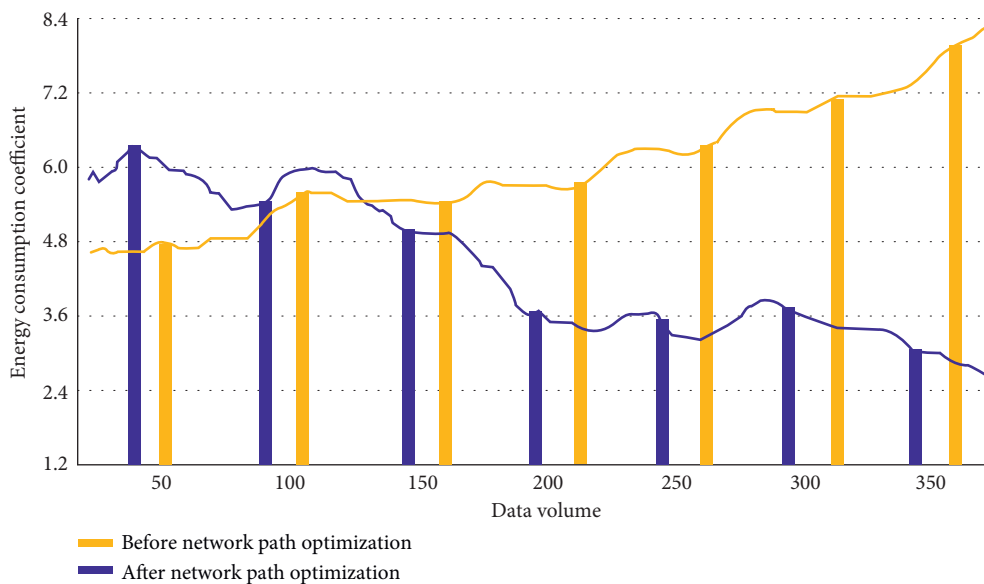


FIGURE 10: Changes in energy consumption of children’s education app system before and after network path optimization.

the user’s personal information. Therefore, the network transmission performance of 5G mobile computing technology has an obvious effect on the security mechanism.

4.2. Analysis of Research Results on Path Optimization of Children’s Education App Network Based on 5G Mobile Computing Technology. We study the node location and path optimization of children’s education app network under 5G mobile computing technology. First, we need to consider whether it can support the operation of 5G network in the selection of mobile terminals. In the process of user mobile node change, select the appropriate center position for signal diffusion. During this period, users within each

network transmission path can receive the information released by the software. Network nodes and transmission paths form a regional network structure. When the amount of data is small, we find that the path area coverage has a negative impact. In order to study the impact of environment on path optimization, we need to monitor applications and network nodes from a variety of performance. In the subsequent research, it is found that the optimal network transmission path will change the energy consumption. The resources consumed by network transmission nodes need to be less than those consumed by data transportation. This paper selects the way of data collection in network path optimization to reduce the energy consumption in the transmission process. In the face of the data preprocessing

behavior of transmission nodes, effective energy consumption optimization is realized while ensuring the amount of data and transmission times. Compare the energy consumption changes of children's education app system before and after network path optimization, as shown in Figure 10.

It can be seen from Figure 10 that before the network path optimization, the energy consumption of each function has exceeded the average coefficient. When we use data set to remove complex useless information, we can reduce unnecessary consumption links and improve the performance of the system. This data set structure can supplement the applications under different network coverage, improve the utilization efficiency of network frequency, and play a positive role in the network performance in 5G environment.

5. Conclusion

With the popularization of Internet and mobile communication technology, the traditional mobile network can not meet the needs of intelligent devices. With the gradual improvement of people's daily living standards, the masses pay more and more attention to the field of education. Children's education has always been the main content of attention. When modern technology is combined with children's education, many distance teaching platforms and application software emerge one after another. We study the network transmission design and network path optimization of children's education app under 5G mobile computing technology. First, the application environment and advantages of 5G mobile network are analyzed, and the functional requirements of children's education app are briefly described. From the perspective of students and parents, different application functions are designed, respectively, and the network transmission model is established in each function module. Using the real-time nature of data transmission to change the transmission delay rate, the hierarchical data transmission algorithm is used to obtain the optimal transmission path from the distance of network nodes. Continue to analyze the network transmission from the average efficiency, node coverage, and feedback efficiency. Finally, the security mechanism in data transmission is analyzed, and the transmission standard with protecting personal privacy as the core is selected as the support. The optimal transmission path is found by network node allocation, and the change of energy consumption in the transmission process is analyzed. The results show that in the process of children's education app network transmission under 5G mobile computing technology, the user's personal information can be guaranteed and the system feedback efficiency and operation performance can be improved. It has obvious advantages in the change of delay rate and realizes the purpose of reducing the overall energy consumption of the system.

Data Availability

The data used to support the findings of this study are available from the corresponding author upon request.

Conflicts of Interest

The authors declare that they have no conflicts of interest.

References

- [1] Y. Yang, "Analysis of network transmission technology based on 5G ultra real time," *Network security technology and application*, vol. 2021, no. 11, pp. 72-73, 2021.
- [2] J. Li, "Innovative design and practice of detainee mobile supervision system supported by 5G network," *Police technology*, vol. 2021, no. 6, pp. 30-33, 2021.
- [3] L Li, "Application of 5G technology in civil aviation air traffic control service transmission network," *China Aviation weekly*, vol. 18, no. 42, pp. 60-61, 2021.
- [4] B. Qin, "Research on multi robot cooperation technology based on 5G," *Modern navigation*, vol. 12, no. 5, pp. 363-366, 2021.
- [5] X. Liu, "Research on the construction strategy of 5G communication network for operators," *China new communication*, vol. 23, no. 19, pp. 5-6, 2021.
- [6] P. Wang, "UAV communication control system based on 5G network," *Modern industrial economy and informatization*, vol. 11, no. 9, pp. 147-148, 2021.
- [7] X. Xu, Y. Ni, and M. Sun, "5G signal transmission train set network scheme based on network slice," *Radio and television network*, vol. 28, no. 9, pp. 28-30, 2021.
- [8] J. Wang, "Exploration of cable TV transmission under the background of 5G era," *News communication*, no. 18, pp. 115-116, 2021.
- [9] Z. Zhou, "Distributed UHD video processing system for 5G network," *Television technology*, vol. 45, no. 9, pp. 1-4, 2021.
- [10] C. Lei and S. Li, "Research on application mechanism of immersive 3D video transmission to public security under the background of 5G network," *Chinese market*, vol. 22, no. 26, pp. 118-119, 2021.
- [11] C. Zhou, "Research on 5G mobile communication transmission network construction," *Science and technology and innovation*, vol. 6, no. 17, pp. 76-77, 2021.
- [12] S. Q. Qian, "Technical analysis of 5G communication transmission bearer network framework," *Digital communication world*, vol. 2021, no. 9, pp. 133-134, 2021.
- [13] J. Gao, "Analysis of optical fiber communication network transmission technology," *Information and computer (theoretical Edition)*, vol. 33, no. 16, pp. 176-178, 2021.
- [14] N. Xiao, "Discussion on ensuring data transmission reliability in 5G Communication," *China new communication*, vol. 23, no. 16, pp. 15-16, 2021.
- [15] Y. Liang, "5G technology practice and research," *Metallurgical automation*, vol. 45, no. S1, pp. 258-261, 2021.
- [16] R. Wang, "Analysis of network information security strategy in 5G era," *Software*, vol. 42, no. 8, pp. 116-118, 2021.
- [17] B. Wu, Y. Yang, and X. Zhang, "Design of highly reliable data transmission terminal based on 5G technology," *Information technology and network security*, vol. 40, no. 8, pp. 78-83, 2021.
- [18] W. Tao, "Scheme research and field test of 5G communication network carrying CBTC system service," *Urban rail transit research*, vol. 24, no. 8, pp. 150-155, 2021.
- [19] X. Chen, J. she, A. Wang, and H. Tang, "Research on automatic control system of railway crossing in mining area based on 5G technology," *Computer knowledge and technology*, vol. 17, no. 21, pp. 143-145, 2021.

- [20] J. Xi, "Research and Exploration on 5G network information security threat and protection technology," *Digital technology and application*, vol. 39, no. 7, pp. 178–180, 2021.
- [21] S. Huang, "On the application and thinking of "learning power" app in children's education," *Southeast communication*, no. 8, pp. 110-111, 2021.
- [22] Z. Yu, R. Liu, and L. Xiang, "Design and implementation of children's Pinyin card based on AR technology," *Computer programming skills and maintenance*, vol. 5, no. 7, pp. 139–141, 2021.
- [23] H. Q. Kun, "Research on app for preschool children's enlightenment education based on emotional design," *Public standardization*, no. 14, pp. 140-141, 2020.
- [24] R. Zhou and Z. He, "Research on Interactive Narrative in language education app based on children's characteristics," *Journal of Qiqihar University (PHILOSOPHY AND SOCIAL SCIENCES EDITION)*, vol. 24, no. 4, pp. 180–184, 2021.
- [25] C. Duan, X. Zhao, Y. Liu, and F. Wang, "App Design of forest museum guide system for children," *Design*, vol. 33, no. 5, pp. 44–46, 2020.

Research Article

Design and Analysis of Chinese-Korean Translation System Based on Deep Transfer Learning

Jun Xu 

The Department of Korean Studies, Dalian University of Foreign Languages, Dalian 116044, China

Correspondence should be addressed to Jun Xu; xujun@dlufl.edu.cn

Received 13 December 2021; Revised 6 January 2022; Accepted 13 January 2022; Published 7 February 2022

Academic Editor: Hangjun Che

Copyright © 2022 Jun Xu. This is an open access article distributed under the Creative Commons Attribution License, which permits unrestricted use, distribution, and reproduction in any medium, provided the original work is properly cited.

In order to better establish the Chinese-Korean translation system model, the deep transfer learning and the model system are tested and analyzed, and the following analysis results are obtained. By discussing the different adjustment mechanisms of deep transfer learning under MMD metric and Wasserstein metric, we can see that, in the MMD metric model, through analyzing datasets 1 and 2, the highest accuracy rate is 83.1% under multisource weight adjustment mechanism under MMD metric and the lower accuracy rate is 62.7% under no weight adjustment mechanism, and the accuracy rates of datasets 1 and 2 are higher than the average. Under Wasserstein metric, the accuracy of dataset 1 is 82.5% under multisource weight and 68.5% under no source weight, both of which are higher than the average. Three EEGNet models, EEGNet_0, EEGNet_1, and EEGNet_2, were established for comparative testing; according to the test results, it can be seen that EEGNet_1 has high accuracy and can be preferred for system establishment. By comparing the Chinese-Korean translation model with the blockchain model and the traditional translation model, it can be seen that when the translation sentences are 100 sentences, the average response time and peak traffic response time of the Chinese-Korean translation model are lower than those of the traditional translation model and the test conclusion is passed. When the test sentences are 1000 sentences, the average response time and peak traffic corresponding time of the Chinese-Korean translation model are still lower than those of the traditional method. Therefore, it can be seen that the efficiency and winning rate of the Chinese-Korean translation model are higher than those of the traditional translation system and meet the needs. According to the analysis of the performance test results of the translation system, it can be seen that the average response time and success rate of the Chinese and Korean translation system under different data are higher than those of the traditional translation system. When the test data are 500, the average response time of the translation system is 13 ms and the accuracy rate is 100%. When the test data are 3000, the average response time is 99 ms and the success rate is 99.6%. Therefore, the success rate of the translation system is basically above 99.6%, which is higher than that of the traditional translation system. In contrast, the Chinese-Korean translation system can improve the translation efficiency and accuracy and can be preferred.

1. Introduction

Through the model building and comparison of deep transfer learning, we choose the best transfer learning method to support the Chinese-Korean translation system to achieve higher accuracy and efficiency. By establishing the Chinese-Korean translation model systematically, comparing the system with the blockchain system and traditional translation system, it is known that the translation system has higher accuracy and efficiency.

Literature [1] combines nonlinear photons, traditional black box deep learning, and deep learning integral equation

through a new method, i.e., deep learning method. It can be used to prove whether artificial intelligence can learn nonlinearly. Experiments show that deep learning network can simulate training to judge the abnormal position of moving objects. Literature [2] trains deep learning network through a large amount of training and data to promote CNN's progress in related fields. Literature [3] realizes NF scale-out and load balancing by flexibly migrating related traffic. In this way, the challenges related to minimizing service resources are solved. Through GNN and DRL to further improve QOS and reduce the delay of deep migration, compared with its most advanced technology, the

required time is increased by 71.6%. In order to solve the problem of extracting biological information from a large amount of weather radar data, literature [4] studies the deep learning method. Two methods, rendering and mapping, are used to segment the convolution network image and reveal the intensity and depth of the migration pattern. Literature [5] studies the recognition of vehicle-related information by studying deep migration and studies ImageNet data under VGG-19 in the same space. The research shows that its accuracy is as high as 97.73%, which solves a series of problems caused by insufficient samples, and it has high efficiency. Literature [6] seismic imaging is an active research field recently, and this method is used to solve the problem of map imaging. At present, the least square method is the most advanced method for seismic structure acquisition. The depth migration convolution method, which combines Hessian with least square migration method, can provide higher quality images than traditional methods. Literature [7] proposes the Faster R-CNN algorithm in order to improve the high similarity of colors in complex background and reduce the efficiency reduction caused by occlusion. Through relevant experiments, it is proved that transplanting the training model into the system can accurately improve the detection accuracy. It lays a foundation for the research of automatic picking device. Literature [8] uses the Faster R-CNN method to improve the efficiency of collecting and recognizing the characteristic part of TCM tooth pattern tongue. Combining Faster-CNN with the fine-tune model, the experimental results show that the model is not affected by the location of pathological changes in images, has strong adaptability, and can well complete the task of local feature recognition and improve the recognition efficiency. Literature [9] aims to alleviate the problem that the depth learning DL model can effectively record and reconstruct underground velocity images, but the knowledge of adjoint operators will be discarded, resulting in poor reconstruction quality. This paper introduces the development of a DLFWI method, which improves the reconstruction speed and high resolution method, and at the same time, its antinoise ability is greatly enhanced. Literature [10] solves the problem of difficult recognition of fruit image, color, size, and other features in the process of automatic picking by developing a deep migration fruit image recognition method. The research shows that, by introducing this deep transfer learning method, the recognition accuracy is greatly improved and the accuracy is increased to 99%. Translation needs to be in multiple dimensions [11], and a common problem needs to be transformed into a different form. Through the OntoMorph method, the syntax is transformed. OntoMorph has become the core of communication translation. Literature [12] translates multiple languages through the NMT single neural machine translation model. According to its research results, it can translate the multilingual model of up to 12 languages and improve the translation quality. At the same time, it shows us some interesting cases in mixed language translation. The EBMT translation model [13] has been proved to be successful in translation function by experimental research. Through EBMT, the “low-density” language is reduced to

ensure its translation quality. The translation database is accurately matched, so that its translation is unlimited, and the amount of text required for translation and the time required for translation are reduced. Literature [14] develops cell-free protein synthesis technology to meet the increasing demand of *in vitro* expression system and optimizes its transcription and translation system, so as to increase the yield of protein and provide a new way for its metabolism. There are still controversial arguments about translation strategies in transfer methods and interlingual methods [15].

2. Deep Transfer Learning and the Process of Chinese-Korean Translation System

2.1. Transfer Learning Diagram. As shown in Figure 1, transfer learning is divided into two parts: source domain and target domain. The process of transforming learning tasks into knowledge by source domain and knowledge into learning tasks by target domain is transfer learning [16]. Transfer learning also refers to the influence of one kind of learning on another kind of learning.

2.2. Detailed Explanation of Deep Transfer Learning

2.2.1. Deep Transfer Learning Classification. Deep transfer learning can be divided into four methods: transfer learning in case of instance, transfer learning in network fine-tuning, and deep transfer learning in confrontational and non-confrontational domain adaptation. In use, the required deep transfer learning method can be selected according to the fine-tuning of examples and networks [17] and non-confrontational and confrontational classification in Figure 2.

2.2.2. Schema of Deep Transfer Learning under Fine Adjustment. As shown in Figure 3, deep migration learning is divided into two parts: source domain and target domain, and the targets of source domain and target domain are fine-tuned [18]. The corresponding research cost is increased. However, after fine-tuning, the goal has more efficient and accurate results [19].

An important concept of deep learning is fine-tuning. This method is mainly to use the network that has been trained in the source domain, as shown in Figure 3, by freezing, and fine-tuning some network layers, adjusting for the target domain tasks, and obtaining the optimal network fine-tuning strategy, so as to achieve the target domain requirements.

2.3. Establishment and Analysis of Translation System Model. Language analysis is carried out through the user interaction interface, such as inputting the required translation, selecting the types of sentences, and finally displaying them at the front end [20]. The model interface includes multilingual decoding of multilingual encoder, generation of batch decoded data, and selection of language representation layer by labeling languages, so as to achieve the optimization result of simulation level. At the same time, the data

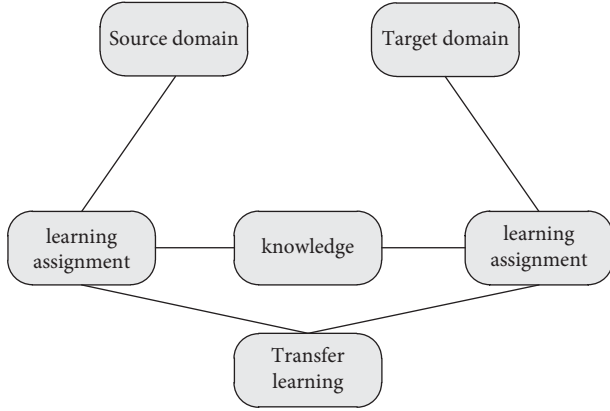


FIGURE 1: Transfer learning diagram.

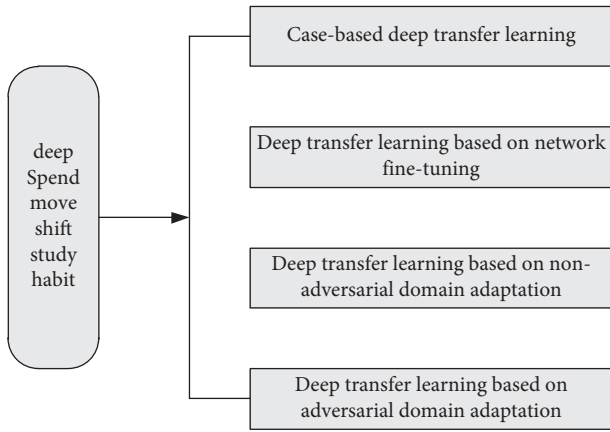


FIGURE 2: Deep transfer learning classification.

processing steps in this model include data cleaning, word segmentation regularization, and word segmentation. Data cleaning [21], word segmentation regularization, and word segmentation also achieve the functions of multilingual optimization in Figure 4.

2.4. Translation Process between China and Korea. The process of Chinese-Korean translation system is to input the Korean data to be translated first, then count the word frequency of the data, reduce the word frequency after the statistics are completed, and then reorganize the operation and train the relevant Korean data by using the BPE method. Finally, the related subwords are segmented to help more accurate translation [22], and the translation-related results are output in Figure 5.

2.5. Comparison of Chinese and Korean Translation

- (1) It is a comparison of non-subject-predicate zero sentences in Chinese and Korean, which express interjection such as call, response, and question and answer in Table 1

- (2) Interjection non-subject-predicate zero sentences expressing anger, dissatisfaction, and criticism in Table 2

- (3) Interjection non-subject-predicate zero sentences expressing joy and happiness in Table 3

- (4) Interjection non-subject-predicate zero sentences expressing surprise, sigh, and lament in Table 4

Through the comparison of non-subject-predicate zero sentences expressing anger, amazement, surprise, and joy in spoken Chinese and Korean, we can realize the differences in translation between Chinese and Korean.

3. Deep Migration and Translation System

3.1. Deep Learning Model

3.1.1. Definition of Deep Network Loss.

$$l = l_c(D_s, y_s) + \lambda l_A(D_s, D_t), \quad (1)$$

where ℓ represents target loss, ℓ_c represents classification loss, and λ is a balance parameter.

3.1.2. Deep Network Loss Composition.

$$L = L_c(D_s, y_s) + \lambda L_D(D_s, D_T), \quad (2)$$

where L_c represents classified loss and L_D represents domain judgment loss [23].

3.1.3. MMD Metrics and Application Networks. MMD is the maximum mean difference. In formula (3), H represents the regenerative Hilbert space with a feature core, p, q represents two probability distributions, and $\phi(\cdot)$ represents the nonlinear feature Yingshe function. Formula (4) represents the minimum batch source data and target domain data sampled from S and T , respectively, and K_1 represents the core selected for layer l of the deep neural network.

$$MMD_H(p, q) \triangleq \left\| E_p[\phi(x_i^s)] - E_q[\phi(x_i^t)] \right\|_H^2, \quad (3)$$

$$\begin{aligned} MMD_1 &= \frac{1}{n_s^2} \sum_{i=1}^{n_s} \sum_{j=1}^{n_s} K_1(\phi_1(X_i^s), \phi_1(X_j^s)) \\ &\quad + \frac{1}{n_t^2} \sum_{i=1}^{n_t} \sum_{j=1}^{n_t} K_1(\phi_1(X_i^t), \phi_1(X_j^t)) \\ &\quad - \frac{2}{n_s n_t} \sum_{i=1}^{n_s} \sum_{j=1}^{n_t} K_1(\phi_1(X_i^s), \phi_1(X_j^t)). \end{aligned} \quad (4)$$

3.1.4. DDC Method

$$l = l_c(D_s, y_s) + \lambda MMD^2(D_s, D_t). \quad (5)$$

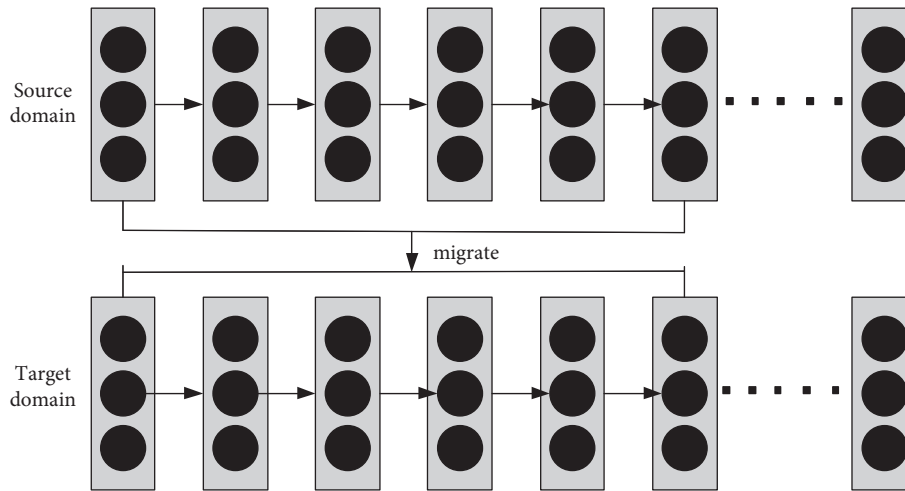


FIGURE 3: Diagram of deep transfer learning under fine-tuning.

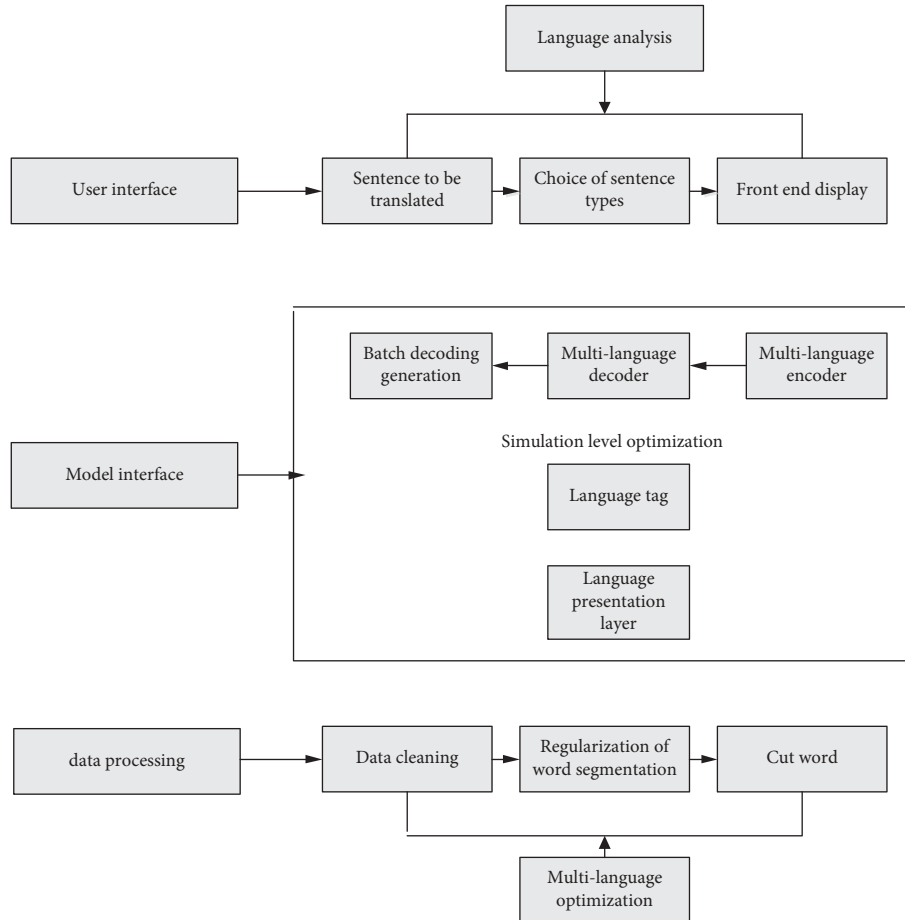


FIGURE 4: Establishment of the translation system model.

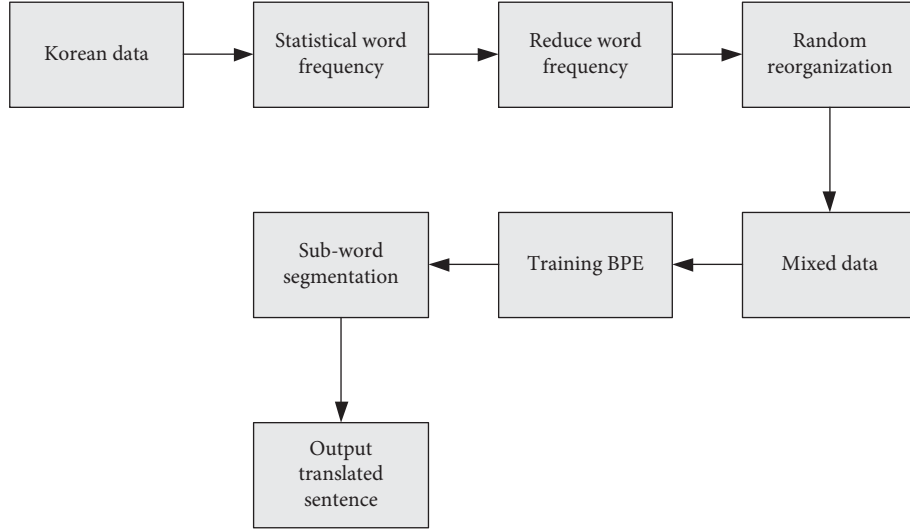


FIGURE 5: Chinese and Korean language translation process.

3.1.5. Wasserstein Metric.

$$W_p(f, g) \stackrel{\text{def}}{=} \left[\inf_{\gamma \in \Pi(f, g)} \int_{R^d \times R^d} \|x - y\|^p d\gamma(x, y) \right]^{(1/p)},$$

$$W_1(f, g) = \sup_{\|f\|_{L^1} \leq 1} E_{x \sim f}[f(x)] - E_{y \sim g}[f(y)],$$

$$L_{wdD}(D_j) = E_{x_i^{s_j} \sim p_{s_j}} D_j(F(x_i^{s_j})) - E_{x_i^t \sim p_t} D_j(F(x_i^t)),$$

$$\text{optimization formula : } L_{wdD}(D) = \sum_{j=1}^N L_{wdD}(D_j), \quad (6)$$

$$\text{gradient penalty expression : } L_{\text{grad}}(D_j) = \left(\left\| \nabla_x \hat{D}_j(x) \right\|_2 - 1 \right)^2,$$

$$\text{maximum optimization training : } \max_{D_j} \sum_{j=1}^N L_{wdD}(D_j) - \beta L_{\text{grad}}(D_j).$$

WDGRL deep transfer learning loss function [24]:

$$\min_{\theta_g, \theta_c} \left\{ \ell_c + \lambda \max_{\theta_w} [\ell_{wd} + \gamma \ell_{\text{grad}}] \right\}. \quad (7)$$

3.1.6. Domain Distribution Similarity.

$$\text{Objective function : } \min_{G, c} \sum_{i=1}^N L_{D_i} + \lambda \min_G MD^2(D_s, D_T),$$

$$MD^2(D_s, D_T) = \sum_{K=1}^2 \left(\frac{1}{N} \sum_{i=1}^N \|E(X_i^k) - E(X_T^k)\|_2 + \binom{N}{2}^{-1} \sum_{i=1}^{N-1} \sum_{j=i+1}^N \|E(X_i^k) - E(X_j^k)\|_2 \right). \quad (8)$$

Single molecule heparin loss:

$$L_{\text{total}} = L_{\text{cls}} + \lambda L_{\text{mmd}} + \gamma L_{\text{disc}}. \quad (9)$$

TABLE 1: The comparison of Chinese and Korean statements such as response.

	Enjoy the non-subject-predicate zero sentence of part of speech
<i>Chinese</i>	1. Express a call 2. Hey! Hi! Hey! Hey! 3. Indicate a response 4. Zhe! Mmm! Mmm! Mmm! 5. Express a question and answer Huh?
<i>Korean</i>	1. Indicate a response 2. 응.(Hmm) 그래(equivalent to “um” in Chinese)

TABLE 2: Comparison of Chinese and Korean sentences such as anger.

	Enjoy the non-subject-predicate zero sentence of part of speech
<i>Chinese</i>	1. Express anger, etc. 2. Yo! Hum! Bah! 3. Show contempt Yo!
<i>Korean</i>	1. Express anger, etc. 2. 음, 응 ! (Mm-hmm!) 아, 그래(Hey) 3. Express criticism 글썄 ! (Uh!)

TABLE 3: Comparison of Chinese and Korean sentences such as joy.

	Enjoy the non-subject-predicate zero sentence of part of speech
<i>Chinese</i>	1. Express happiness, happiness ha ha ha!
<i>Korean</i>	1. Express happiness, happiness 하하하 ! (Ha ha ha!) 헤헤헤 ! (Hey hey hey!) 2. Express a sigh 오!(Oh!) 야!(Yah!)

TABLE 4: Comparison of Chinese and Korean sentences such as exclamation.

	Enjoy the non-subject-predicate zero sentence of part of speech
<i>Chinese</i>	1. Express surprise Ouch! Ah! Oh, my God! 2. Express lamentation Ouch!
<i>Korean</i>	1. Express surprise 아!(Ah!) 아이참!(Cough!) 오!(Oh!) 어머니나!(Oh, my God!) 아야!(Ouch!) 2. Express comprehension 맞다!(That’s right!)

3.2. EEGNet Model

3.2.1. Convolution Calculation.

$$y = \sum_{i=1}^{k_1} \sum_{j=1}^{k_2} \sum_{l=1}^d w_{ijl} x_{ijl} + b, \quad (10)$$

where W_{ijl} is the weight and y and b are the offsets [25].

3.2.2. Depth Separable Convolution.

$$\frac{D_k \times D_k \times M + M \times N}{D_k \times D_k \times M \times N} = \frac{1}{N} + \frac{1}{D_k \times D_k},$$

$$\frac{D_k \times D_k \times M \times D_F \times D_F + M \times N \times D_F \times D_F}{D_k \times D_k \times M \times N \times D_F \times D_F} = \frac{1}{N} + \frac{1}{D_k \times D_k}. \quad (11)$$

3.2.3. Softmax Model

$$P(i) = \frac{\exp(\theta_i^T x)}{\sum_{k=1}^k \exp(\theta_k^T x)}. \quad (12)$$

3.3. Machine Translation Model.

$$h_n = f(U \cdot x_n + W \cdot h_{n-1} + b),$$

$$c = q(\{h_1, \dots, h_n\}). \quad (13)$$

The probability p of the resulting translation y is

$$P(y) = \prod_{t=1}^T p(y_t | \{y_1, \dots, y_{t-1}\}, c),$$

$$p(y_t | \{y_1, \dots, y_{t-1}\}, c) = g(y_{t-1}, s_t, c),$$

$$c_t = \sum_{j=1}^n \alpha_{t,j} h_j, \quad (14)$$

$$\alpha_{t,j} = \frac{e^{e_{t,j}}}{\sum_{k=1}^n e^{e_{t,k}}}, e_{t,j} = a(s_{t-1}, h_t).$$

4. Deep Transfer Learning and the Design and Analysis of Chinese-Korean Translation System

4.1. Deep Transfer Learning Model

4.1.1. Accuracy Analysis of Different Adjustment Mechanisms Based on Different MMD Measures. As shown in Table 5, the dataset is divided into three parts: dataset 1, dataset 2, and average, and the accuracy of datasets 1 and 2 under different adjustment mechanisms under MMD measurement is investigated. Among them, the accuracy of dataset 1 is 62.7% without weight adjustment mechanism, 68.9% under single source weight, and 67.1% under multiple weights. Under the weightlessness mechanism, the average value is 59.0%, the

single source weight is 64.6%, and the multisource weight is 75.1%. Through three sets of data, we can see that the accuracy under MMD measurement is lower under no weight adjustment mechanism and higher under multisource weight and the overall accuracy is on the rise. Among them, the correct rate of dataset 1 under different adjustment mechanisms is above the average correct rate.

In order to make the accuracy trend more intuitive, the following chart is drawn. As shown in Figure 6, the accuracy rate of datasets 1 and 2 is the highest under the multisource weight adjustment mechanism, while the accuracy rate of datasets 1 and 2 is lower under the nonweight adjustment mechanism. The accuracy of dataset 1 in different adjustment mechanisms under MMD measurement is generally higher than the average.

4.1.2. Accuracy Analysis of Different Adjustment Mechanisms Based on Different Wasserstein Measures. Through the data values 1 and 2 and the average value, the accuracy of data under different adjustment mechanisms under Wasserstein metric is discussed. The accuracy of dataset 1 is 68.5% under no weighting mechanism, 72.8% under single source weighting mechanism, and 82.5% under multisource weighting mechanism. The accuracy rate of dataset 2 is 55.4% under no weight adjustment mechanism, 59.8% under single source weight, and 66.8% under multisource weight. The average accuracy rate is 61.2% under no weight, 66.7% under single source weight, and 73.2% under multisource weight. Among them, the accuracy of dataset 1 is higher under different adjustment mechanisms in Table 6.

It can be seen from Figure 7 that the correct rate of datasets 1 and 2 and the average value is on the rise under the adjustment mechanism of weightlessness, single source weight, and multisource weight, while the correct rate of weightlessness mechanism is lower and the correct rate of multisource weight is higher. Also, the accuracy rate of dataset 1 is higher than that of dataset 2 and the average value. Combined with the chart under MMD metric, we can see that the accuracy rate under multisource weight is higher than that under no weight and the accuracy rate of multisource weight in dataset 1 under Wasserstein metric is 82.5% which is lower than that under MMD metric (83.1%).

4.1.3. Comparative Analysis. Comparing the Wasserstein model with the MMD without weight, the average accuracy of MMD without weight was 59%, the average accuracy under multisource weight was 61.2%, the average accuracy under single source weight was 64.6% and 66.7%, and the average accuracy under multisource weight was 75.1% and 73.2%, respectively. Through data analysis, it is learned that the accuracy rate of Wasserstein model is higher than MMD under no weight and single source weight and should be preferred, but the correct rate of MMD model is higher under multisource weight.

4.2. Nonlinear Activation Function of Deep Transfer Learning. Based on the analysis of inactive function under deep transfer learning, ReLU function has countless values after

TABLE 5: Accuracy analysis of MMD regulation mechanism.

Dataset	No weight (%)	Single source weight (%)	Multisource weight (%)
Dataset 1	62.7	68.9	83.1
Dataset 2	55.3	60.2	67.1
Average	59.0	64.6	75.1

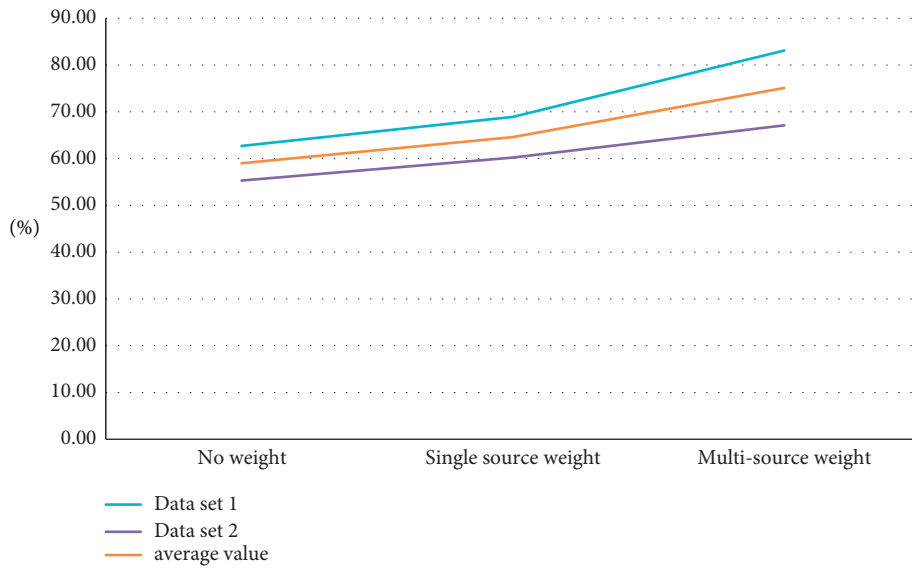


FIGURE 6: Accuracy of different mechanisms under MMD measurement.

TABLE 6: Accuracy analysis of Wasserstein regulation mechanism.

Dataset	No weight (%)	Single source weight (%)	Multisource weight (%)
Dataset 1	68.5	72.8	82.5
Dataset 2	55.4	59.8	66.8
Average	61.2	66.7	73.2

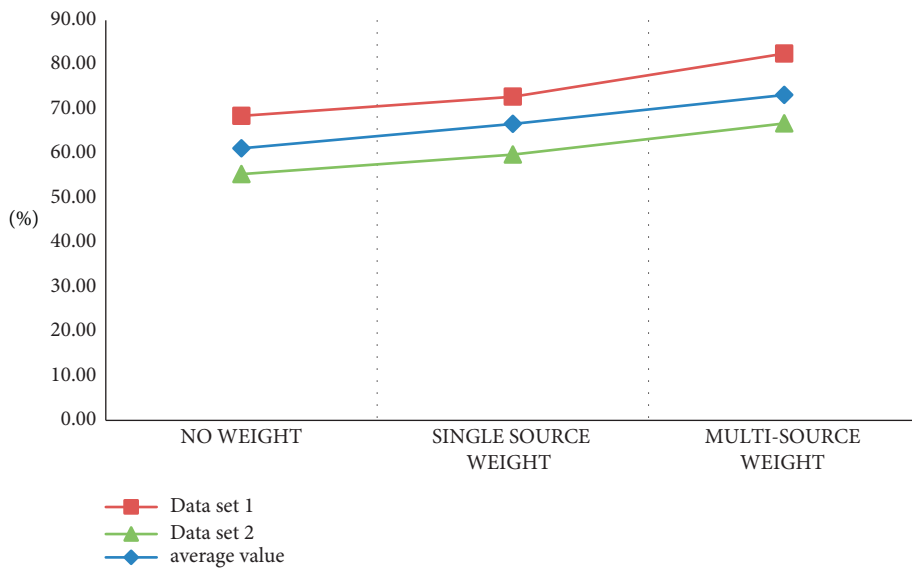


FIGURE 7: Accuracy of different mechanisms under Wasserstein metric.

zero and shows an upward trend after zero. The sigmoid function image shows a slow upward trend after zero point and approaches the value 1 when x is about 5, and the value infinitely approaches 1 when x is about 10. Tanh's function is -1 before zero, rises slowly after zero, and finally approaches the value of 1 infinitely in Figure 8.

ReLU Function. Pros: fast convergence speed, avoid gradient disappearance, and simple calculation. Cons: no boundaries.

Sigmoid Function. Pros: from the image point of view: is a continuous function and easy to guide; mathematically: there is a good spatial mapping effect; functional point of view: a number into a popular sense of grasp representation. Cons: the gradient disappears when it is propagated in reverse.

Tanh Function. Pros: has all the advantages of sigmoid function. Cons: gradients disappear and $\exp()$ calculations are expensive.

4.3. Comparison of EEGNet Method Models. It can be seen from Figure 9 that the correct rate of EEGNet_0 model is about 59%, the correct rate of EEGNet_1 model is 66.5%, and the correct rate of EEGNet_2 model is about 62.3%. Through data analysis, we can see that the correct rate of EEGNet_1 model is higher than that in EEGNet_0 and EEGNet_2. Its overall average law is also higher than 50%. The effect of EEGNet_1 was higher than that of EEGNet_0 and EEGNet_2.

4.4. Analysis of Chinese and Korean Translation System Model. According to the comparison of N-grams and EL-grams translation models, the correct rate of N-grams translation into Korean is 75.1% and the correct rate of EL-grams translation into Chinese is 89.43%. The perplexity of translating into Korean is 126.39%, while the perplexity of translating into Chinese is 34.54%. In the EL-grams model, the correct rate of translation into Korean is 80.34% and the correct rate of translation into Chinese is 93.21%. The perplexity of translating into Korean is 105.33% and that of Chinese is 18.88%. By comparison, we can see that the accuracy of N-grams model is higher than that of EL-grams model in Chinese and Korean translation models and the confusion of N-grams model is lower than that of EL-grams model. Therefore, the performance of N-grams model is better than that of EL-grams system (Table 7).

It can be seen from Figure 10 that the accuracy of N-grams Chinese-Korean translation system model is higher than that of EL-grams model, but its confusion is lower than that of EL-grams translation model system. Therefore, the performance of EL-grams translation model is lower than that of N-grams translation model. In order to ensure the accuracy of translation, the N-grams Chinese-Korean translation system model should be given priority when choosing translation system.

4.5. Investigation on the Difficulty of Korean Translation. According to the survey, most people think that the translation between China and South Korea is difficult,

accounting for 48%, and only 3% think it is very easy. It shows that there are some difficulties in Chinese-Korean translation. Through this Chinese-Korean translation system, the translation difficulty is reduced and the translation efficiency is improved (Figure 11).

Through data and graph analysis, we know that the vast majority of the people surveyed think that Chinese and Korean translation is more difficult, but now, trade, travel, etc. are inseparable from Chinese and Korean translation, so it is necessary to design a high-efficiency, high-performance Chinese-Korean translation system.

4.6. System Test

4.6.1. Performance Test of Three Methods. The related system tests are carried out. Based on Table 8, it can be seen that, in the Chinese-Korean translation system based on blockchain, when the translation sentences are 100 sentences, the average response time is 1.230 ms and the peak traffic response time is 1.556 ms; when 500 sentences are translated, the average response time is 1.556 ms and the peak traffic response time is 1.890 ms. When 1000 sentences are translated, the average response time is 2.098 ms and the peak traffic response time is 2.121 ms. According to the performance tests of 100 sentences, 500 sentences, and 1000 sentences, the performance tests are all passed, which proves that this method is feasible.

Based on the performance test of the Chinese-Korean translation system proposed in this paper, the average response time and peak traffic response time are 1.980 ms and 2.021 ms, respectively, when the translation sentences are 100 sentences. When 500 sentences are translated, the average response time and peak traffic response time are 2.99 ms and 3.005 ms, respectively. When 1000 sentences are translated, the average response time and peak traffic response time are 4.236 ms and 4.653 ms, respectively. The performance test results are all passed, and the method proposed in this paper is feasible (Table 9).

According to the analysis of traditional Chinese and Korean translation system methods, the average response time of translated sentences with 100, 500, and 1000 sentences is higher than that of the method proposed in this paper and the peak traffic response time is also higher than that of the translation system proposed in this paper and the blockchain translation system. However, the performance test of its translation system has passed (Table 10).

From Figure 12, it can be seen that the performance test results of the Chinese-Korean translation system proposed in this paper are higher than those of the traditional Chinese-Korean translation system, and the data of the Chinese-Korean translation system in blockchain are close, indicating that the Chinese-Korean translation system proposed in this paper can meet the daily Chinese-Korean translation needs and its performance is excellent. The Chinese-Korean translation system is feasible.

The Chinese-Korean translation system used in this paper passes the system test, and the test results are shorter and more efficient than the traditional Chinese-Korean

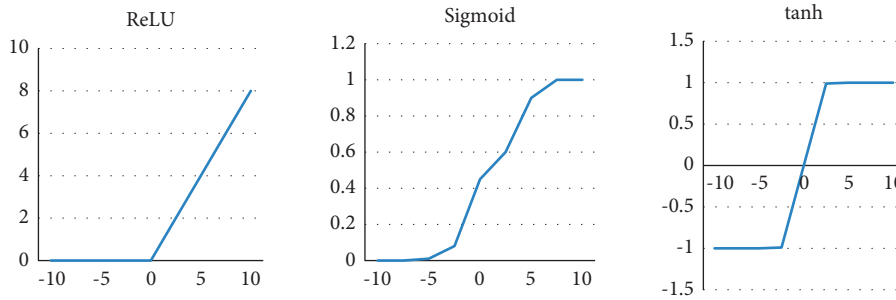


FIGURE 8: Deep transfer learning inactive function.

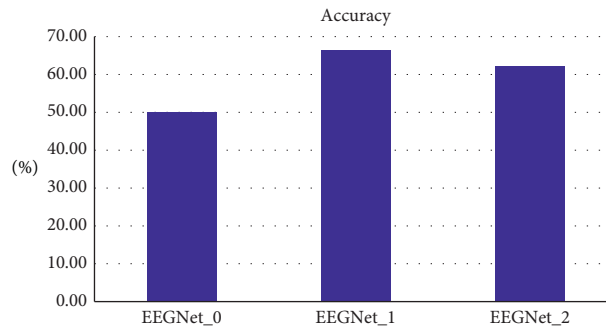


FIGURE 9: Comparison of EEGNet models.

TABLE 7: Comparative analysis of different translation models.

Model	PPL_{Korean} ; $accuracy_{\text{Korean}}$	PPL_{Chinese} ; $accuracy_{\text{Chinese}}$
N-grams	126.39; 75.18	34.54; 89.43
EL-grams	105.33; 80.34	18.88; 93.21

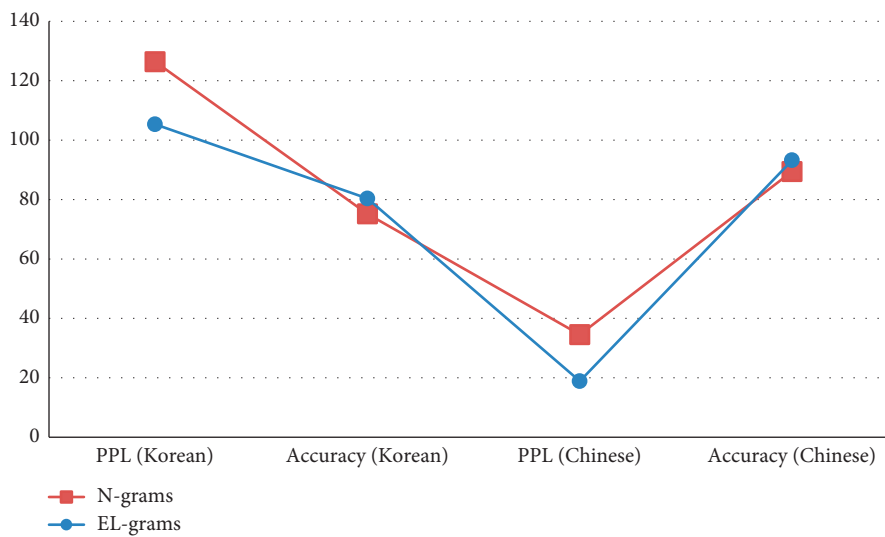


FIGURE 10: N-grams and EL-grams model testing.

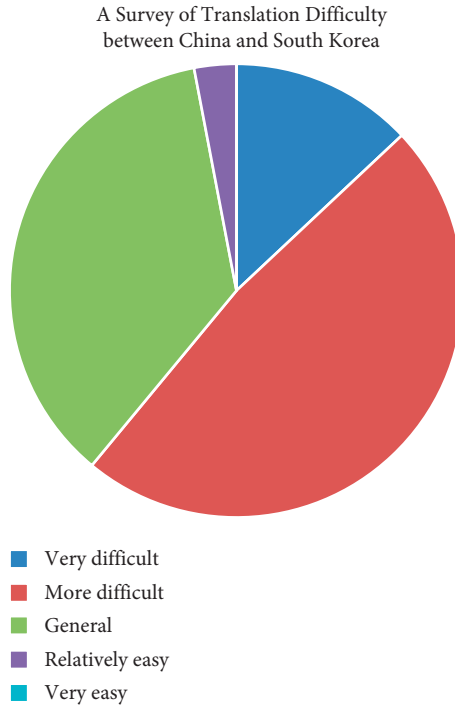


FIGURE 11: Survey of translation difficulty between Chinese and Korean.

TABLE 8: Performance test of Chinese and Korean translation system based on blockchain.

Translated sentence	Average response time (ms)	Peak flow response time	Test conclusion
100	1.230	1.556	Pass
500	1.556	1.890	Pass
1000	2.098	2.121	Pass

TABLE 9: Performance test of Chinese and Korean translation system based on this method.

Translated sentence	Average response time (ms)	Peak flow response time	Test conclusion
100	1.980	2.021	Pass
500	2.997	3.005	Pass
1000	4.236	4.653	Pass

TABLE 10: Performance test of Chinese-Korean translation system based on traditional methods.

Translated sentence	Average response time (ms)	Peak flow response time	Test conclusion
100	1.988	3.210	Pass
500	3.497	6.334	Pass
1000	4.936	7.203	Pass

translation system. When the translation statement is 1000, the average response time of the Chinese-Korean translation system proposed in this paper is 4.236 ms, while that of the traditional translation system is 4.936 ms. In contrast, the Chinese and Korean translation systems perform better.

4.6.2. *Performance Test Analysis.* It is divided into the following groups of data: 500, 1000, 1500, 2000, 2500, and 3000.

There are seven sets of data, and the specific analysis is shown in the following table. According to the comparison of blockchain system method, Chinese and Korean translation system, and traditional translation system, the average time of blockchain method and this translation method is close, both within 13 ms, and the success rate is 100%, while the average time of traditional translation method exceeds 20 ms. The success rate of blockchain method is 100%, the highest success rate of this translation system is 100%, and

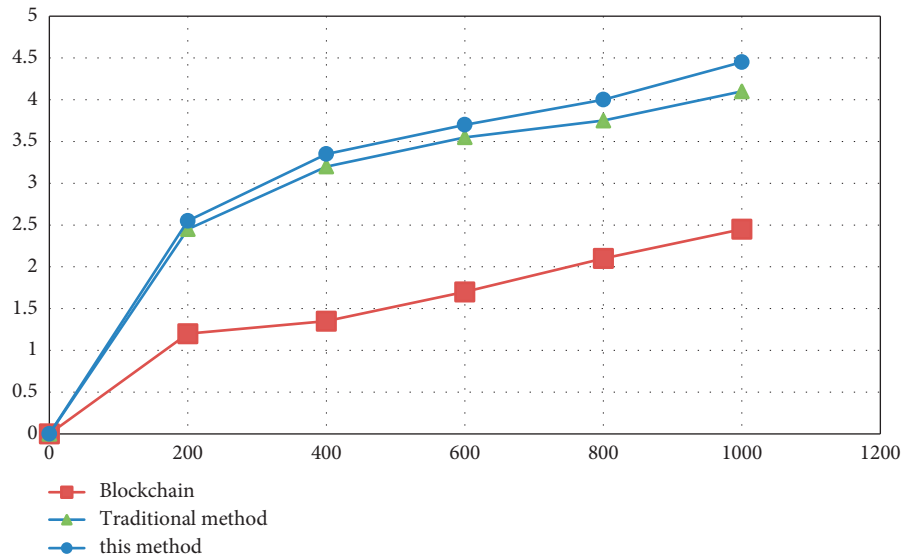


FIGURE 12: Comparative analysis of average response time.

TABLE 11: System test structure.

System	Number of query requests	500	1000	1500	2000	2500	3000
<i>Blockchain method</i>	Mean response time (MS)	10	23	33	58	73	97
	Success rate (%)	100	100	100	100	100	100
<i>The Chinese-Korean translation system</i>	Mean response time (MS)	13	24	38	59	75	99
	Success rate (%)	100	99.8	99.7	99.64	99.75	99.6
<i>Traditional translation system</i>	Mean response time (MS)	21	42	59	83	101	134
	Success rate (%)	100	99.3	98.3	97.8	99.3	99

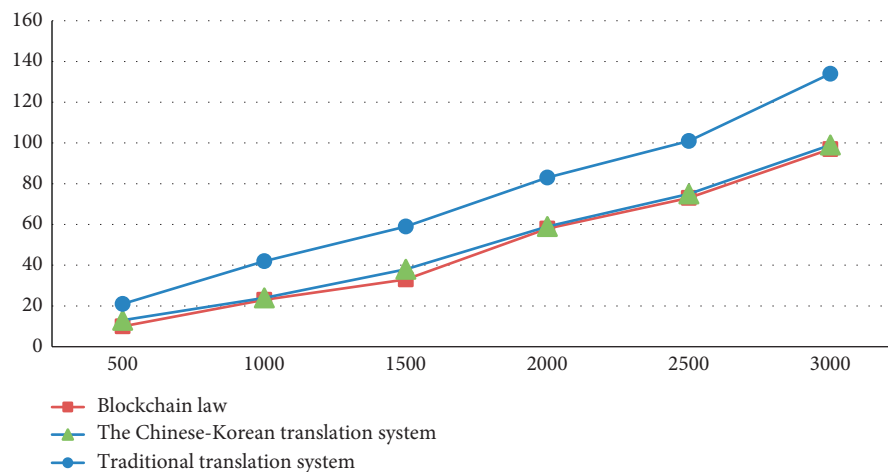


FIGURE 13: Time performance test analysis of translation system.

the lowest success rate is 99.6% when the data are 3000. The highest accuracy rate of traditional translation method is 100%, and the lowest accuracy rate is 99% when the data are 3000. According to the data, the accuracy of this translation method is higher than that of the traditional translation system and the average response time is slightly lower than that of the traditional translation system (Table 11).

It can be seen from Figure 13 that the average response time of the proposed Chinese-Korean translation system is lower than that of the traditional translation system, which saves translation time and improves translation efficiency. This system can meet the needs of normal translation.

From Figure 14, we can see that the correct rate of Chinese and Korean translation system is higher than that of

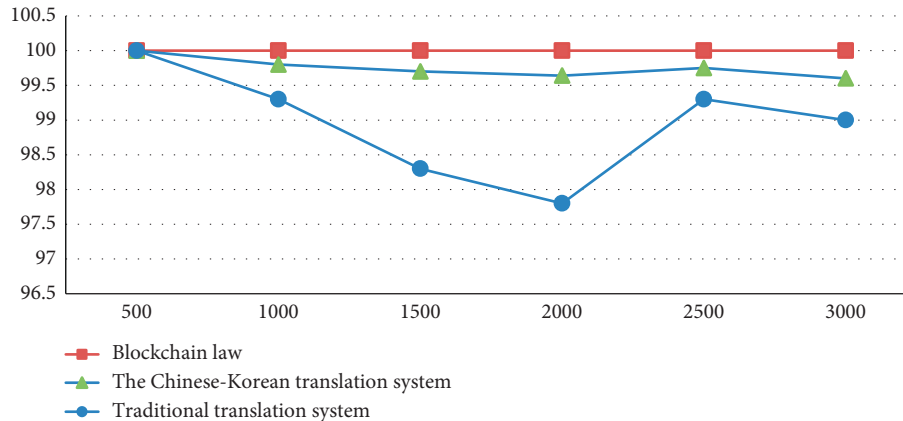


FIGURE 14: Performance test analysis of translation system accuracy rate.

traditional translation system, which is close to 100%. Also, the accuracy rate fluctuates little when the data increase.

5. Conclusion

Through the analysis of the loss composition of deep migration and the accuracy under different adjustment mechanisms under MMD and Wasserstein metrics, this paper discusses and analyzes the requirements of maximizing the efficiency and accuracy of the Chinese-Korean translation system. By systematically testing the Chinese-Korean translation system model, blockchain model, and traditional translation system, it can be seen that the Chinese-Korean translation model meets the daily translation requirements. All the tests are passed, and the accuracy and efficiency are higher than those of the traditional translation system, thus improving the accuracy and efficiency of the Chinese-Korean translation system. In real life, it is inevitable to communicate with different people, so in order to solve the language problem, the Chinese-Korean translation system reflects its value. In the process of future research, it should be optimized with a variety of translation models to improve the accuracy and efficiency of translation system.

Data Availability

The experimental data used to support the findings of this study are available from the corresponding author upon request.

Disclosure

This is the current achievement of “Parallel Corpus-Based Hybrid Translation Teaching Reform and Practice,” a teaching reform project in 2019 by The Education Department of Liaoning Province.

Conflicts of Interest

The authors declare that they have no conflicts of interest regarding this work.

References

- [1] J. Yoo, S. Sabir, and D. Heo, “Deep learning can reverse photon migration for diffuse optical tomography,” *IEEE Transactions on Medical Imaging*, vol. 23, no. 5, pp. 23–45, 2017.
- [2] C. Sun, Y. Yang, C. Wen, K. Xie, and F. Wen, “Voiceprint identification for limited dataset using the deep migration Hybrid model based on transfer learning,” *Sensors*, vol. 18, no. 7, Article ID 2399, 2018.
- [3] P. Sun, J. Lan, J. Li, Z. Guo, Y. Hu, and T. Hu, “Efficient flow migration for NFV with Graph-aware deep reinforcement learning,” *Computer Networks*, vol. 183, no. 4, Article ID 107575, 2020.
- [4] K. Cui, C. Hu, R. Wang, Y. Su, H. Mao, and H. Li, “Deep-learning-based extraction of the animal migration patterns from weather radar images,” *Science China. Information Sciences*, vol. 63, no. 4, Article ID 140304, 2020.
- [5] Q. Tong, L. I. Taijun, and X. Liu, “Vehicle information recognition method based on deep migration learning,” *Video Engineering*, vol. 55, no. 8, pp. 54–75, 2019.
- [6] M. Avila, L. N. Osorio, J. Fernandes et al., “Migration deconvolution via deep learning,” *Pure and Applied Geophysics*, vol. 178, no. 2, 2021.
- [7] J. Sun, X. He, X. Ge, X. Wu, J. Shen, and Y. Song, “Detection of key organs in tomato based on deep migration learning in a complex background,” *Agriculture*, vol. 8, no. 12, 2018.
- [8] M. Liu, X. Wang, and L. Zhou, “Study on extraction and recognition of traditional Chinese medicine tongue manifestation: Based on deep learning and migration learning,” *Journal of Traditional Chinese Medicine*, vol. 34, no. 7, pp. 67–89, 2019.
- [9] W. Zhang and J. Gao, “Deep-learning full-waveform inversion using seismic migration images,” *IEEE Transactions on Geoscience and Remote Sensing*, vol. 60, no. 99, pp. 1–18, 2021.
- [10] P. Xiao, G. Zhou, and M. He, “Apple image recognition based on deep and migration learning,” *International Agricultural Engineering Journal*, vol. 27, no. 3, pp. 371–379, 2018.
- [11] H. Chalupsky, “OntoMorph: a translation system for symbolic knowledge,” *Principles of Knowledge Representation & Reasoning*, vol. 45, no. 12, pp. 66–87, 2000.
- [12] M. Johnson, M. Schuster, Q. V. Le et al., “Google’s multi-lingual neural machine translation system: Enabling zero-shot translation,” *Transactions of the Association for Computational Linguistics*, vol. 5, no. 2, pp. 109–112, 2016.

- [13] R. D. Brown, "Adding linguistic knowledge to a lexical example-based translation system," *Tmi*, vol. 7, no. 3, pp. 55–76, 1999.
- [14] F. Caschera and V. Noireaux, "Synthesis of 2.3mg/ml of protein with an all *Escherichia coli* cell-free transcription-translation system," *Biochimie*, vol. 99, pp. 162–168, 2014.
- [15] M. Kay and J. M. Gawron, "Verbmobih a translation system for face-to-face dialog," *Csli Lecture Notes*, vol. 87, no. 23, pp. 134–156, 1994.
- [16] M. Duggan, J. Duggan, E. Howley, and E. Barrett, "A reinforcement learning approach for the scheduling of live migration from under utilised hosts," *Memetic Computing*, vol. 65, no. 23, pp. 178–196, 2017.
- [17] L. Morrice, "The learning migration nexus: Towards a conceptual understanding," *European Journal for Research on the Education and Learning of Adults*, vol. 5, no. 2, pp. 149–159, 2014.
- [18] K. Monkman, "Transnational migration and learning processes of Mexican adults constructing lives in California," *International Journal of Educational Development*, vol. 19, no. 4-5, pp. 367–382, 1999.
- [19] K. Caskey and B. Subirana, "Supporting SME e-commerce migration through blended e-learning," *Journal of Small Business and Enterprise Development*, vol. 14, no. 4, pp. 670–688, 2007.
- [20] M. Arif, A. Kiani, and J. Qadir, "Machine learning based optimized live virtual machine migration over WAN links," *Telecommunication Systems: Modeling, Analysis, Design and Management*, vol. 34, no. 21, pp. 56–78, 2017.
- [21] V. A. Kolb, E. V. Makeyev, and A. S. Spirin, "Co-translational folding of an eukaryotic multidomain protein in a prokaryotic translation system." *Journal of Biological Chemistry*, vol. 275, no. 22, pp. 16597–16601, 2000.
- [22] S. Nakamura, K. Markov, H. Nakaiwa et al., "The ATR multilingual speech-to-speech translation system," *IEEE Transactions on Audio Speech and Language Processing*, vol. 14, no. 2, pp. 365–376, 2006.
- [23] Y. Chadani, K. Ono, S. I. Ozawa, and Y. Takahashi, "Ribosome rescue by *Escherichia coli* ArfA (YhdL) in the absence of trans-translation system." *Molecular Microbiology*, vol. 78, no. 4, pp. 796–808, 2010.
- [24] B. S. Negrutskii, R. Stapulionis, and M. P. Deutscher, "Supramolecular organization of the mammalian translation system," *Proceedings of the National Academy of Sciences*, vol. 91, no. 3, pp. 964–968, 1994.
- [25] J. M. . Betton, "Rapid translation system (RTS): A promising alternative for recombinant protein production," *Current Protein & Peptide Science*, vol. 4, no. 1, pp. 73–80, 2003.

Research Article

Design and Analysis of Nanchong Sports Public Service Information Platform Based on Multiobjective Optimization

Dujuan Li 

Department of Physical Education, North Sichuan Medical College, Nanchong, Sichuan 637000, China

Correspondence should be addressed to Dujuan Li; yangyang0809@nsmc.edu.cn

Received 5 November 2021; Revised 10 December 2021; Accepted 3 January 2022; Published 7 February 2022

Academic Editor: Hangjun Che

Copyright © 2022 Dujuan Li. This is an open access article distributed under the Creative Commons Attribution License, which permits unrestricted use, distribution, and reproduction in any medium, provided the original work is properly cited.

Through the design and analysis of the Nanchong sports public service information platform, we can see that in order to improve the city's sports public service, we should improve the sports public service according to the factors such as the amount of activities, funds, and promotion. In view of the multiobjective optimization of sports public service in Nanchong City, the century establishment and analysis of the information platform were carried out. Its information platform includes intelligent venues, information platforms, sports safety, and other topics so as to achieve the purpose of healthy sports and relaxed sports, improve Nanchong people's sports interest and experience as a whole, and enhance satisfaction. In order to alleviate the financial difficulties, relevant departments can carry out public welfare activities to sponsor sports public services in Nanchong City. According to the investigation, 29.4% of the randomly asked citizens have high satisfaction, 32.3% have no experience, and 16.5% are dissatisfied, which shows once again that Nanchong people have low awareness of the sports public service platform. In order to realize the good development of sports public service in this city, we should comprehensively promote the development of sports public service and improve citizens' awareness, experience, and satisfaction.

1. Introduction

Through the design and analysis of the sports public service platform under multiobjective optimization in Nanchong City, it is known that the related platform can improve Nanchong citizens' awareness and participation in sports public service. At the same time, through the analysis of data, it is known that there are still many imperfect developments in sports public services in Nanchong City, which should be continuously improved and popularized in a large area through relevant influencing factors so as to improve people's awareness and solve related problems such as scarce funds, venues, and activities. By analyzing the problems in the public sports services in Nanchong City and analyzing and explaining the related factors of the problems, we can improve the public sports services in Nanchong City.

Literature [1] proposes a multiobjective evolutionary algorithm with nondominant ranking because of its non-elitist computational complexity and specified shared parameters. In order to solve the difficulties while speeding up

the nondominant sorting method, a selection operator is proposed to establish a mating pool by selecting N best solutions with the combined parent-child population. Literature [2] makes the combination of multiple objectives form scalar objective function temporarily by the linear combination of multiple objectives and transforming the objectives into constraints. It shows the ability of maintaining diversification in the open problem of a water conservancy system. Literature [3] proves the effectiveness of the multiobjective algorithm in dealing with more than two objective problems by constructing the optimal frontier with simplicity, an arbitrary number of decision variables, and positions. Literature [4] uses advanced algorithms to solve two or more conflicting objective function problems, which is the related ability of "evolutionary multiobjective optimization." Therefore, we research and develop the most representative algorithms and applications through the relevant historical framework. The advantages, fields, and future trends of related algorithms are discussed. Literature [5] uses a supply chain network (SCN) to design the optimal

solution of the problem efficiently and effectively in order to solve the multiobjective conflicts such as cost and resource utilization. In this paper, the actual data of Turkish Plastics Company are studied in two stages and solved by SCN. In literature [6], the development of sports public service is based on its main basic characteristics and basic structure. Literature [7] combines sports public service with economics and practice, understands the imbalance and incompleteness of sports public service development, and enhances the sustainability of sports public service development. In literature [8], the sports public service usually represents the comprehensive strength of sports and enhances the transformation of sports public service. In literature [9], at present, fairness, public welfare, diversity, convenience, and high efficiency are the characteristics of sports public service in the development stage. To build people-oriented sports public service value is the goal and mission of developing sports public service. Literature [10] simplifies the data of sports public service through VER (Building Sports Public Service) model and understands the influence of the sports public service field. The design and analysis method of the information platform in literature [11] is one of the main development directions of digital campus. Literature [12] aims at the shortcomings of urban and rural sports public services, including the differences in facilities, to promote the development of rural sports public services so as to achieve balanced development. Literature [13] improves the accuracy of parts by considering different objectives. By collecting the objective function to assign the weight of part precision, the part precision can be better grasped to achieve the specified precision. High quality of parts and high efficiency of construction are ensured. Literature [14] studies public services through literature and related laws, including establishing legal status, reward and punishment system, and evaluation system. In literature [15], the information platform of cloud computing is a new method of sharing facilities at present. The second part of the article puts forward corresponding solutions to the current multiobjective problems; the third part puts forward the theoretical basis of the multiobjective model. The fourth part designs and analyzes the methods proposed in this paper.

2. Multiobjective Problem Solving

2.1. Content of Multiobjective Solution Problem. Figure 1 shows a multiobjective feasible solution. The feasible solution includes the infeasible solution and the Pareto optimal solution, and the optimal solution includes the satisfactory solution. To solve a multiobjective problem, multiple objectives are usually transformed into one objective, among which there are many solutions, such as the ideal point method, linear weighting method, maximum-minimum method, goal programming method, and fuzzy digital solution [16], as shown in Figure 1.

2.1.1. Pareto Sorting and Genetic Algorithm Solving Steps. Pareto chart is a chart used to arrange quality problems and quality improvement items in order of importance. It is

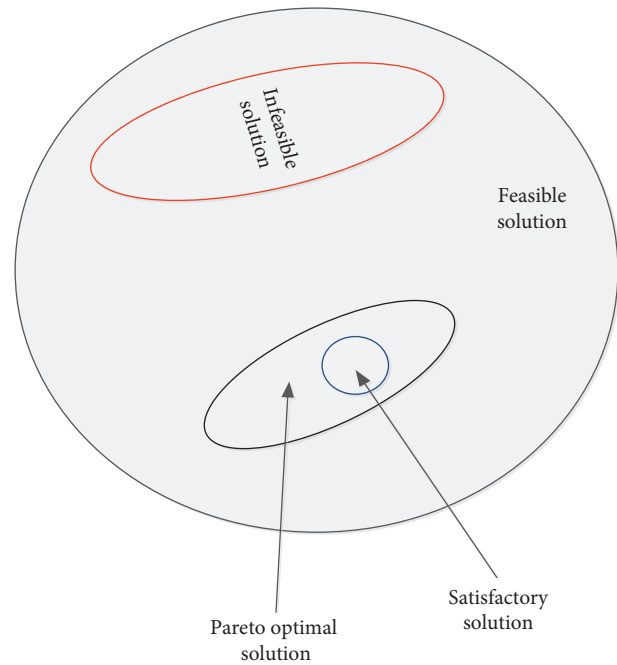


FIGURE 1: Schematic diagram of multiobjective solution.

named after the Italian economist V. Pareto. A Pareto chart, also called permutation chart and primary and secondary chart, is a histogram drawn in order of frequency of occurrence, indicating how many results are caused by confirmed types or categories. The steps are as follows: inputting initial parameters and carrying out initial inference, carrying out various target calculations and discussions, carrying out genetic suboperation to generate degrees of freedom after completion, and then judging by $g = G$, if the output is the Pareto optimal solution, calculating the corresponding target value, and finally outputting it in graphic mode; otherwise, the loop is repeated according to the prompt, as shown in Figure 2.

2.1.2. NSGA-II Algorithm Steps. The NSGA-II algorithm was proposed by Srinivas and Deb on the basis of NSGA in 2000. It is superior to the NSGA algorithm; it uses a fast nondominated sorting algorithm, and the computational complexity is greatly reduced than that of NSGA. Its use creates congestion and crowding. The degree comparison operator replaces the shared radius shareQ that needs to be specified and is used as the winning criterion in the same-level comparison after quick sorting so that the individuals in the quasi-Pareto domain can be extended to the entire Pareto domain and distributed evenly, maintaining the population's diversity; the introduction of the elite strategy expands the sampling space, prevents the loss of the best individuals, and improves the calculation speed and robustness of the algorithm. At first, a value is assigned, the order is changed into a set, the value is reassigned, the number is judged whether it is equal to the maximum algebra, it is output if it is equal and rejudged if it is not equal, as shown in Figure 3.

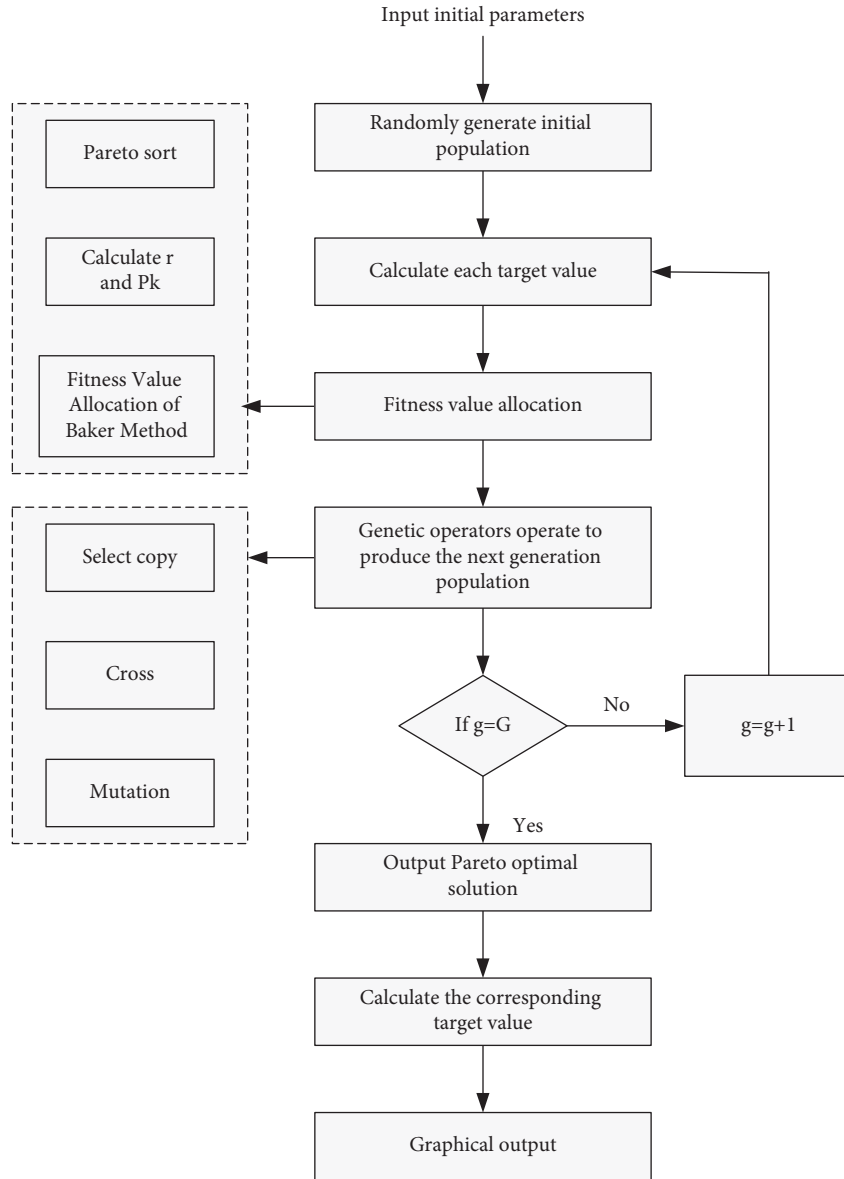


FIGURE 2: Solution step diagram.

2.2. Design of Sports Public Service Platform

2.2.1. *Sports Public Service Content.* In order to facilitate Nanchong citizens' sports awareness and improve sports duration and frequency, better planning is carried out through platform design and analysis.

2.2.2. *Platform Design.* As shown in Figure 4, the sports public service platform is designed through payment methods, understanding methods, participation methods, security, and other aspects. The establishment of smart venues can facilitate the use of Nanchong citizens, and the specific contents of sports activities can be understood through web pages and small programs and ensure the safety of citizens' sports by means of video surveillance.

3. Multiobjective Optimization Model

3.1. Multiobjective Optimization

3.1.1. Multiobjective Mathematical Description.

$$\text{Min (&Max)} y = f(x) = [f_1(x), f_2(x), \dots, f_n(x)] \quad (1)$$

$$(n = 1, 2, \dots, N),$$

$$\text{s.t.} \begin{cases} g(x) = [g_1(x), g_2(x), \dots, g_k(x)] \leq 0, \\ h(x) = [h_1(x), h_2(x), \dots, h_m(x)] = 0, \\ x = [x_1, x_2, \dots, x_d, \dots, x_d], \\ x_{d_min} \leq x_d \leq x_{d_max} (d = 1, 2, \dots, D). \end{cases} \quad (2)$$

In formula (1), $f(x)$ is the maximum or minimum value

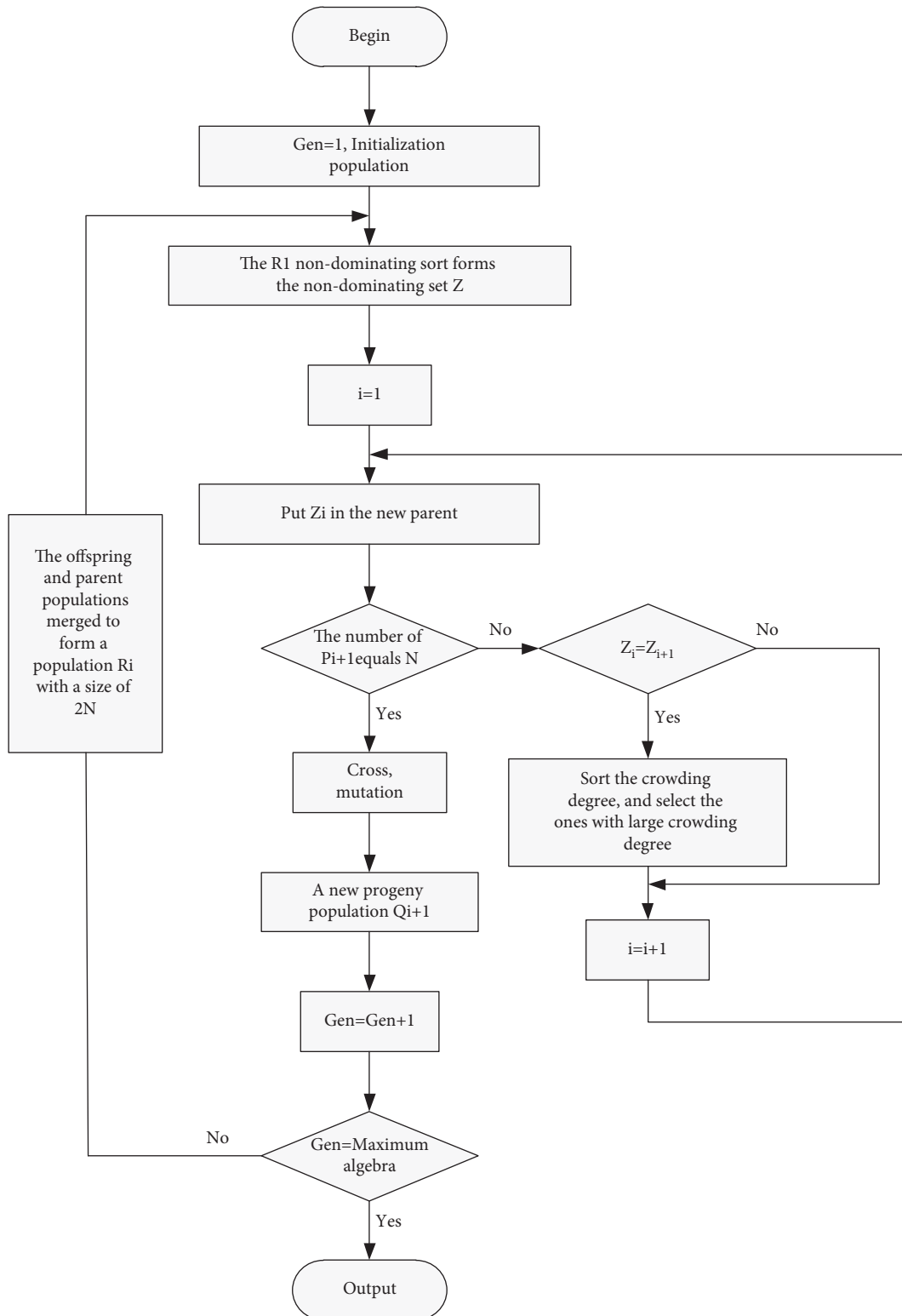


FIGURE 3: NSGA-II algorithm step diagram.

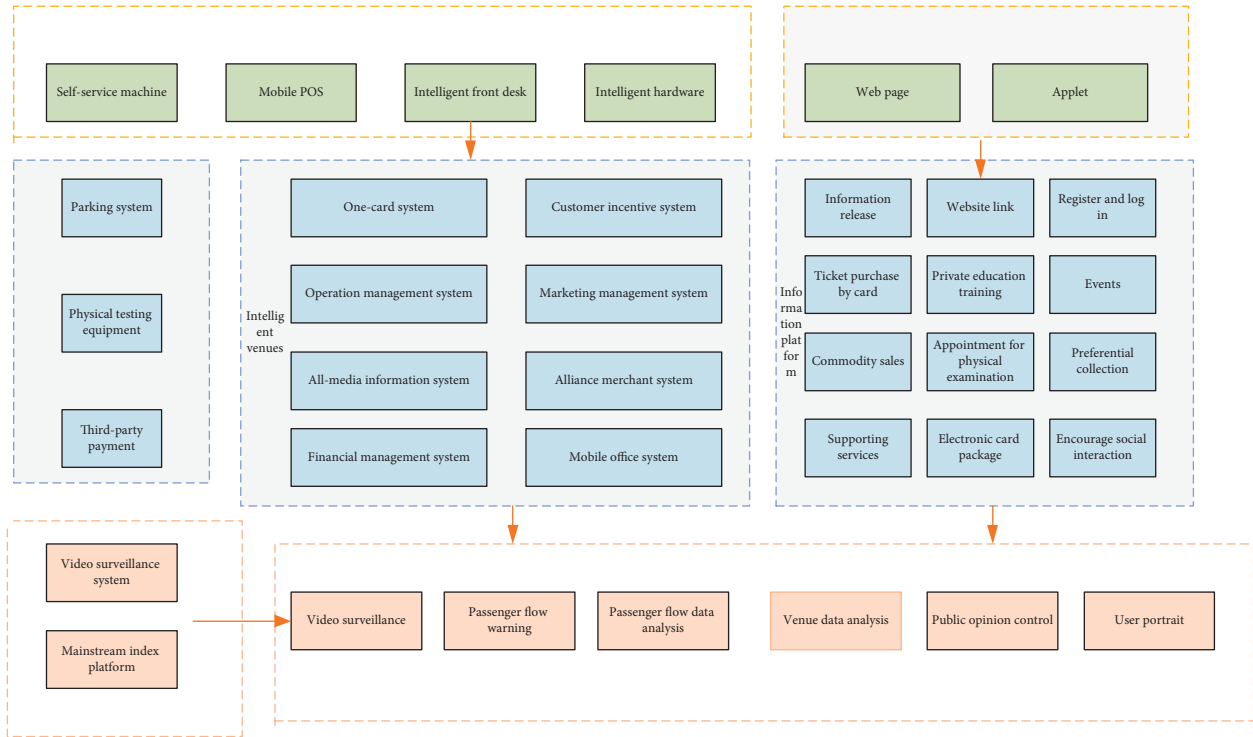


FIGURE 4: Design drawing of sports public service platform.

of the objective function, and formula (2) is the corresponding conditional constraint to formula (1).

3.1.2. Fast Nondominated Sorting. Quick nondominated sorting stratifies the individuals in the population, the best individual is in the first layer, and then in addition to the first layer, nondominated individuals are found from the rest of the individuals, and so on. Sp refers to an individual dominated by p , that is, an individual with no outstanding individual. Fast nondominant sorting sorts the population according to the dominant relationship among individuals [17]. Each individual corresponds to two parameters, n_i and s_i . The individual with n_i being 0 is stored in the set $F1$, and if n_i is subtracted by 1, the result is 0, which is stored in the set $F2$., where m is the number of objective functions, and n is the population size in Algorithm 1.

3.1.3. Crowding Degree. The calculation of the congestion coefficient needs to sort the population according to the ascending order of the value of each objective function (that is, if the first-level nondominated layer is obtained, it is sorted according to the size of the objective function, and then the congestion degree is calculated). The perimeter of the largest rectangle formed in Figure 5 is the desired result.

The smaller nondominant level is dominant [13]; when the nondominant levels are the same, the individuals with greater congestion are dominant in Algorithm 2.

3.1.4. NGA-II Process. The process is first initialized, and then the data are judged according to the process [18], as shown in Figure 6.

3.2. Multiobjective Optimization Problem Model. Taking the minimization problem as an example, the equation is as follows:

$$\begin{aligned} \min F(x) &= (f_1(x), f_2(x), \dots, f_m(x))^T, \\ \text{subject to } x &\in \Omega \subseteq R^n, \end{aligned} \quad (3)$$

where M is the scale of the objective function, Ω is the decision variable, and $fi(x)$ is the objective function [19], as shown in Figure 7.

(1) Pareto dominates:

$$\begin{cases} \forall i \in \{1, 2, \dots, m\}, f_i(x) \leq f_i(y), \\ \exists j \in \{1, 2, \dots, m\}, f_j(x) < f_j(y). \end{cases} \quad (4)$$

(2) Pareto nondominated solution: there is no corresponding solution set.

(3) Pareto optimal solution set:

$$PS = \{x \in \Omega | y \in \Omega, y < x\}. \quad (5)$$

(4) Pareto's best frontier:

$$PF = \{F(x) | x \in PS\}. \quad (6)$$

```

for each  $p \in P$ 
if ( $p > q$ ) then // If  $P$  dominates  $Q$ 
 $S_p = S_p \cup \{q\}$  // Add  $q$  to  $S_p$ 
else if ( $q > p$ ) then // If  $P$  is dominated by  $Q$ 
 $n_p = n_p + 1$  //  $N_p$  plus 1
If  $n_p = 0$  then // If  $P$  is not dominated
 $F_1 = F_1 \cup \{p\}$  //  $P$  is a member of the first frontier
 $i = 1$ 
While  $F_i \neq \phi$ 
 $H = \phi$ 
for each  $p \in F_i$  // For every  $p$  in  $F_i$ 
for each  $q \in S_p$  // For each  $q$  in  $S_p$ 
 $n_q = n_q - 1$  //  $N_q$  minus 1
if  $n_q = 0$ 
then  $H = H \cup \{q\}$ 
 $i = i + 1$ 
 $F_i = H$  // Current frontier

```

ALGORITHM 1: Fast nondominated sorting.

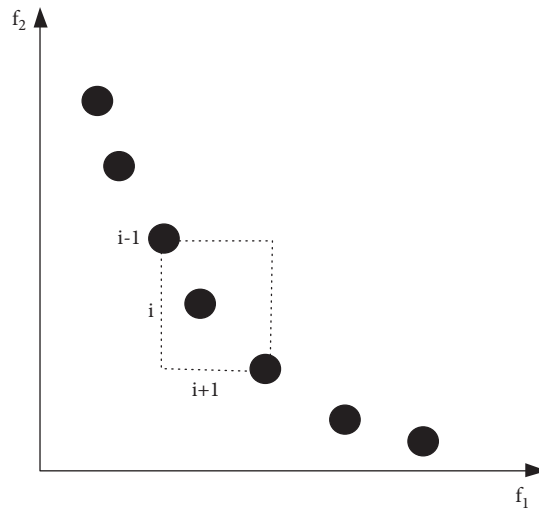


FIGURE 5: Schematic diagram of crowding degree.

```

 $j = |L|$ 
for each  $L$ , set  $L[i].\text{distance} = 0$  // Initialization distance
for each objective  $m$ 
 $L = \text{sort}(L, m)$  // Sort by each target value
 $L[1].\text{distance} = L[j].\text{distance} = \infty$  // Always keep boundary points
for  $i \leftarrow 2$  to  $j - 1$ 
 $L[i].\text{distance} = L[i].\text{distance} + (L[i + 1].m - L[i - 1].m)$ 

```

ALGORITHM 2: Congestion distance algorithm.

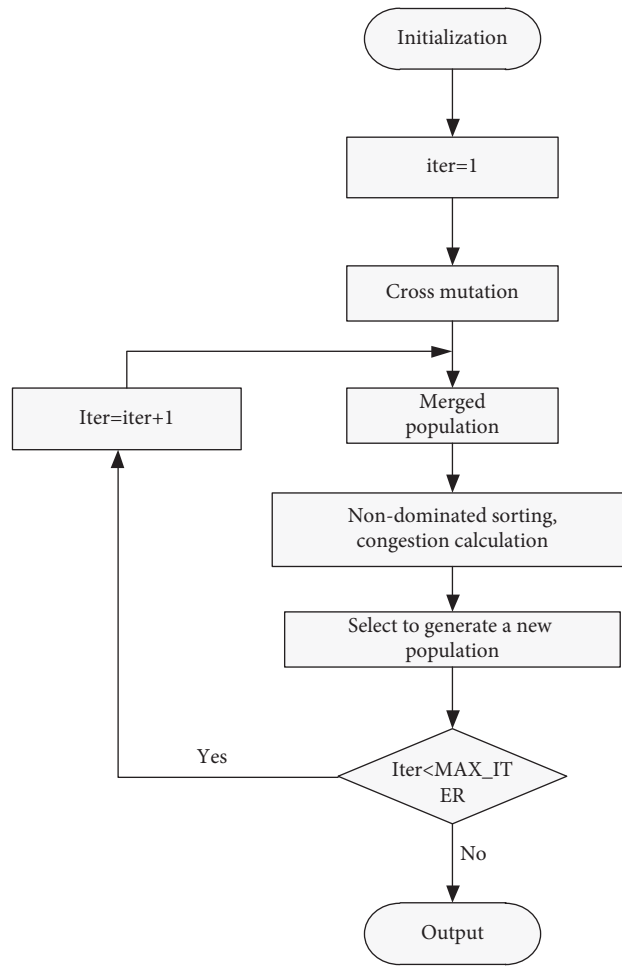


FIGURE 6: NSGA-II flowchart.

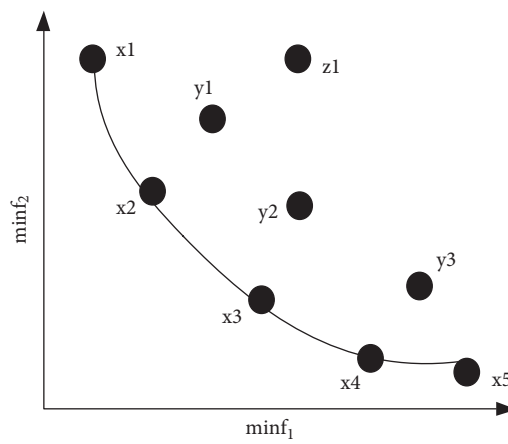


FIGURE 7: Pareto model diagram.

- (5) Convergence: it refers to the proximity of the optimal frontier of Pareto's optimal solution [20].
- (6) Diversity: Pareto optimal solution and dispersion of real frontier [21].

3.3. Basic Theory of Multiobjective Optimization.

$$\min F(x) = [F_1(x), F_2(x), \dots, F_n(x)]^T, \quad (7)$$

$$\text{s.t. } \begin{cases} X = \{X | g_i(X) \geq 0, i = 1, 2, \dots, p, h_j(X) = 0, j = 1, 2, \dots, q\}, \\ X = [x_1, x_2, \dots, x_m]^T. \end{cases} \quad (8)$$

Among them, $X = [x_1, x_2, \dots, x_m]^T$, M is the decision variable. Equation (7) is the minimum value of the objective function, and equation (8) is the objective function constraint.

3.4. Basic Concepts of MOEA. The general form of MOEA and MOP is as follows [22]:

$$\begin{aligned} \min f(x) &= [f_1(x), f_2(x), \dots, f_M(x)]^T, \\ g_j(x) &\geq 0, j = 1, 2, \dots, p, \\ h_k(x) &= 0, k = 1, 2, \dots, q, \\ x_i^l &\leq x_i \leq x_i^u, i = 1, 2, \dots, n. \end{aligned} \quad (9)$$

(1) Pareto domination

$$\forall m \in \{1, \dots, M\} f_m(\mu) \leq f_m(v), \exists m \in \{1, 2, \dots, M\} \text{ Satisfy } f_m(\mu) < f_m(v) \text{ then } \mu < v. \quad (10)$$

(2) Pareto optimal solution

$$P^* = \{x \in \Omega | \exists x' \in \Omega, f(x') < f(x)\}. \quad (11)$$

(3) Pareto optimal frontier

$$\text{PF}^* = \{f(x), x \in P^*\}. \quad (12)$$

DM: width of all solution sets as follows:

$$\Delta = \frac{d_f + d_i + \sum_{i=1}^{N-1} |d_i - \bar{d}|}{d_f + d_i + (N-1)\bar{d}}. \quad (16)$$

HV: nondominated front surface and reference point forming area hypervolume [24] are as follows:

$$\text{HV} = \delta \left(\bigcup_{i=1}^{|s|} v_i \right). \quad (17)$$

3.4.1. Function Performance Evaluation. GD: average minimum distance from each point in P to P^* .

$$\text{GD}(P, P^*) = \frac{\sqrt{\sum_{y \in P} \min_{x \in P^*} \text{dis}(x, y)^2}}{|P|}. \quad (13)$$

IGD: reference point to nearest individual mean.

$$\text{IGD}(P, P^*) = \frac{\sum_{x \in P} \min_{y \in P^*} \text{dis}(x, y)}{|P^*|}. \quad (14)$$

Spacing: standard deviation to minimum distance [23].

$$\text{Spacing}(P) = \sqrt{\frac{1}{|P|-1} \sum_{i=1}^{|P|} (\bar{d} - d_i)^2}. \quad (15)$$

3.5. Static Multiobjective Optimization Algorithm. MOEA/D

(1) Weighted method:

$$\begin{aligned} \text{Minimize } g^{\text{ws}}(x|\lambda) &= \sum_{i=1}^m \lambda_i f_i(x), \\ \text{s.t. } x &\in \Omega. \end{aligned} \quad (18)$$

(2) Chebyshev method:

$$\begin{aligned} \text{Minimize } g^{\text{tc}}(x|\lambda, z^*) &= \max_{1 \leq i \leq m} \{\lambda_i |f_i(x) - z_i^*|\}, \\ \text{s.t. } x &\in \Omega. \end{aligned} \quad (19)$$

(3) Boundary intersection method:

$$\text{Minimize } g^{\text{bip}}(x|\lambda, z^*) = d_1 + \theta d_2, \quad (20)$$

subject to $x \in \Omega$

$$d_1 = \frac{\|(z^* - F(X))^T \lambda\|}{\|\lambda\|}, \quad (21)$$

$$d_2 = \|F(x) - (z^* - d_1 \lambda)\|.$$

4. Design and Analysis of Sports Public Service Platform in Nanchong City

4.1. Analysis on the Present Situation of Sports Public Service

4.1.1. List of Sports Public Service Efficiency in Different Regions. Through Table 1 and Figure 8, we know that Chengdu ranks first in the efficiency of sports public service among Chengdu, Nanchong, Yibin, and Zigong. Nanchong City followed closely in the second place. In contrast, the efficiency of sports public service in Zigong is low. Since 2013–2017, the average efficiency of sports public services in the four cities surveyed is about 0.751, which is a good situation. The maximum value is 1.000, and the minimum value is 0.643, which has a big gap. Therefore, it is analyzed that the efficiency of public service is seriously differentiated. We should know that the factors affecting the efficiency through investigation improve the efficiency of sports public service in Nanchong from many aspects. Combined with Figure 8, it can be seen that the development efficiency of sports public services in the four cities investigated in recent years is gentle and has not changed much, so we should investigate from many aspects to further improve the efficiency of sports public services. The related efficiency of sports public services in the surveyed cities can be clearly seen through the list of sports public service efficiency. Regarding the source of funds for public sports services in Nanchong City, it can be seen that organizing sports competitions accounts for the largest proportion. Through the investigation and analysis of public sports services in Nanchong City, it is found that the lack of professional guidance accounts for the largest proportion of the reasons for the lack of development. In order to improve this factor, a large number of professional instructors should be trained in many places.

4.1.2. Investigation of Sports Public Service Supply in Nanchong City. It can be seen from Figure 9 that the management contents of the Nanchong sports public service platform include financial support, sports venue management, sports activity organization management, sports competition organization, and publicity of beneficial knowledge of physical exercise. Among them, organizing sports competitions accounts for 30.20% of the public service platform, while the financial support is only 7.88%, so sports public services are also facing problems such as insufficient financial management.

TABLE 1: List of sports public service efficiency.

	2013	2014	2015	2016	2017	Ranking
Chengdu	0.830	0.833	0.960	1.000	0.994	1
Nanchong	0.634	0.798	0.823	0.790	0.770	2
Yibin	0.669	0.721	0.660	0.587	0.664	3
Zigong	0.654	0.590	0.660	0.700	0.690	4
Average	0.699	0.736	0.776	0.770	0.780	5
Minimum	0.643	0.590	0.660	0.587	0.664	
Maximum	0.830	0.833	0.960	1.000	0.994	

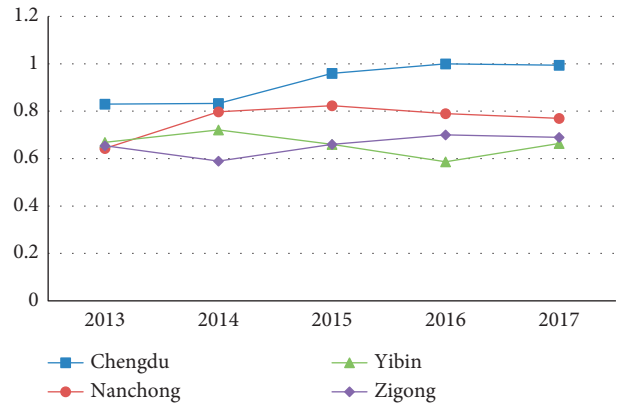


FIGURE 8: Efficiency comparison chart of four cities.

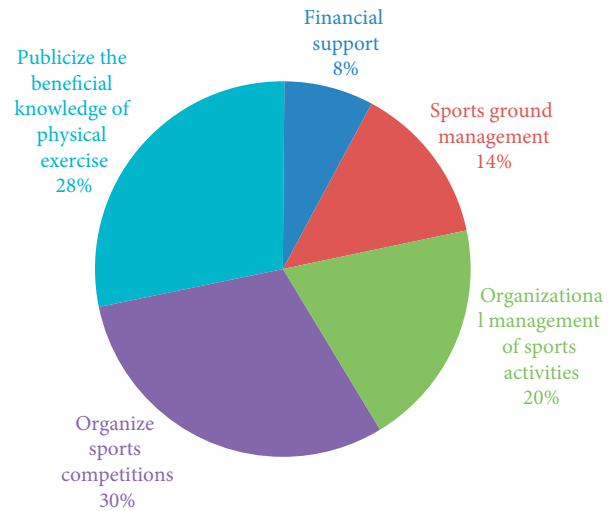


FIGURE 9: Sports public service supply map.

4.1.3. People's Cognition of Sports Public Service in Nanchong City

(1) Understanding Degree of Nanchong People. Through the investigation of 215 people's cognition of sports public service in Nanchong City, it is known that 83 of the 215 people know about the sports public service platform, accounting for 38.6%; 78 people did not understand it, accounting for 36.2%. The masses who know and do not know account for a large proportion, and the polarization is serious. We should popularize the knowledge of the sports public service platform for Nanchong people through various channels, such as community propaganda, government

information push, and lectures. The understanding degree of Nanchong people is presented in Table 2.

(2) *Statistics of Public Sports Activities in Nanchong City.* Through the investigation on the frequency of sports activities of 215 people randomly selected in Nanchong City, it can be seen that 38 people have a lot of activities, accounting for 17.7%; there are 34 people with few activities, accounting for 15.8%; there were 44 people without related activities, accounting for 20.5%. According to the data, the proportion of sports activities is 20.5%, which shows that sports public services have not been fully promoted, and there are still no related sports activities in most areas. The statistics of public sports activities in Nanchong City is presented in Table 3.

4.2. *Present Situation of Sports Public Service Construction in Nanchong City*

4.2.1. *Venue Provided.* According to Figure 10, it is known that there are five departments, including shopping malls, communities, neighborhood committees, sports departments, and subdistrict offices, which provide venues for sports activities in Nanchong City, among which sports departments provide venues accounting for 37%, providing advantages for sports public services of Nanchong citizens.

4.2.2. *Expenditure of Sports Public Service in Nanchong City*

(1) *Funding Input.* It can be intuitively known from Figure 11 that the sports public service funds provided by government departments account for 55.57% at most, and social welfare organizations account for the least investment. In order to alleviate the financial difficulties of sports public services in Nanchong City, donations can be made for social welfare activities, such as organizing charity sales and performances, so as to provide activity funds for sports activities in Nanchong City, thus having the ability to organize activities, making Nanchong citizens more convenient for sports, and improving the efficiency and satisfaction of sports public services.

(2) *Use of Funds.* It can be seen from Figure 12 that the cost of paying the venue accounts for 26%. In order to alleviate the financial difficulties, the cost of paying the venue can be slightly adjusted through multiparty coordination, and the maximum proportion of organizing activities is 30%.

4.2.3. *Insufficient Development Status.* According to the analysis of the development of sports public service in Nanchong City, we know that there are some shortcomings as follows: scarcity of venues, insufficient funds, shortage of activists, and scarcity of professional guidance personnel, weak sports awareness, large labor costs, and others. Among them, the scarcity of professionals is the most serious. In order to alleviate the related problems, sports safety guidance majors can be opened in some universities so as to train professional sports guidance personnel to prevent the harm caused by wrong sports actions. Among them, aiming at the

TABLE 2: Understanding degree of Nanchong city.

Degree of understanding	Number of people	Proportion (%)
Understand	83	38.6
General	54	25.1
Do not understand	78	36.2
Summation	215	100

TABLE 3: Number of public sports activities in Nanchong city.

Number of activities	Number of people	Proportion (%)
A lot	38	17.7
More	20	9.3
General	47	21.9
Less	32	14.9
Very few	34	15.8
No	44	20.5
Total	215	100

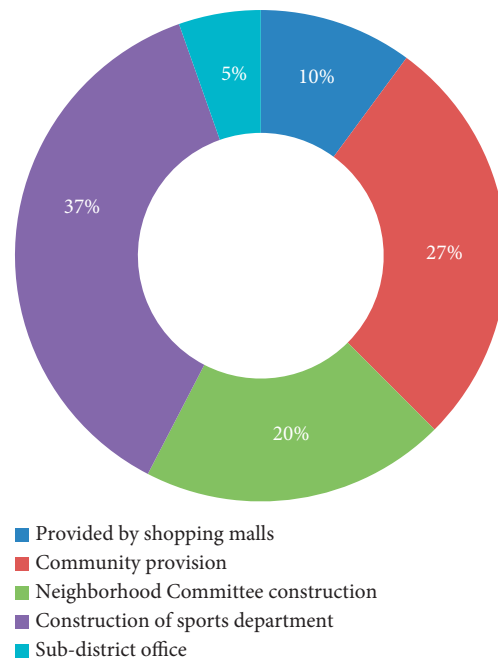


FIGURE 10: Proportion of site provision.

problems of weak sports awareness and shortage of activists, the sports public service platform can be developed in Nanchong City in an all-round way so that Nanchong citizens can have a deeper understanding of the sports public service platform, as shown in Figure 13.

4.2.4. *Number of Professional Sports Instructors in Various Places from 2015 to 2019.* According to the six regions selected in Table 4, since 2015–2019, the number of registered sports professional instructors in Chengdu, Nanchong, Yibin, Zigong, Guangyuan, Aba, and other places has increased year by year, which is embodied in the increase of citizens’ awareness of sports and their participation in sports activities. Among them, the major of the registered sports in Nanchong has developed well. Combined with Figure 14, it can be seen that the related aspects in Chengdu are

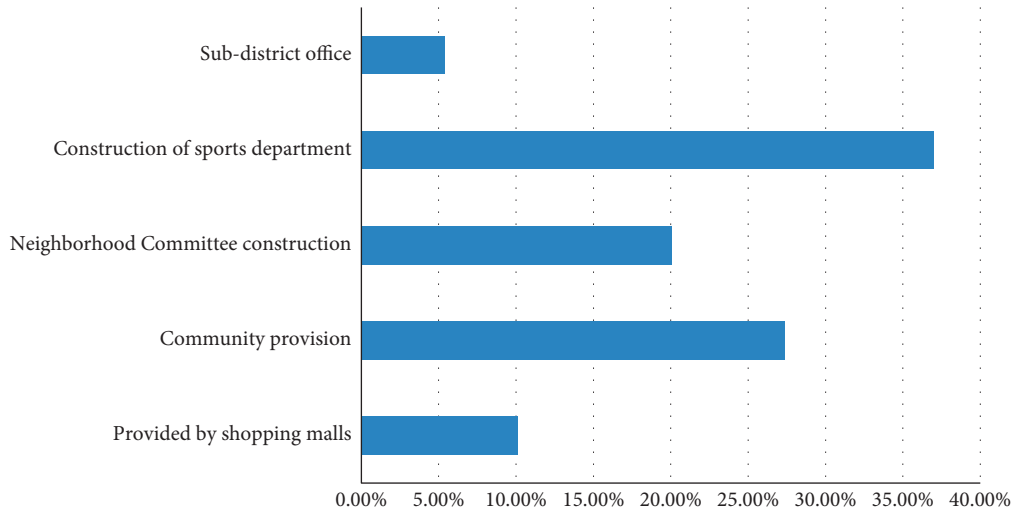


FIGURE 11: Proportion of fund input.

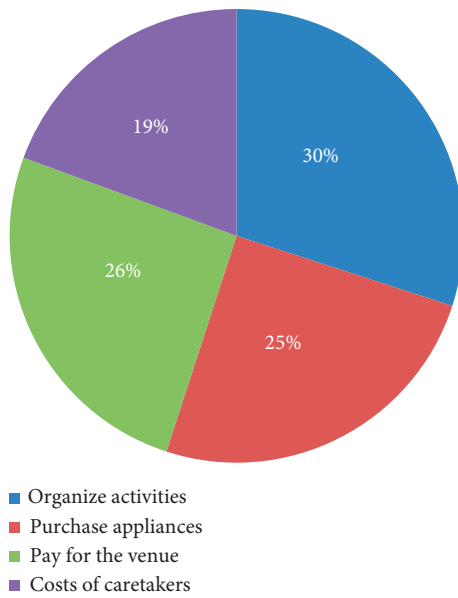


FIGURE 12: Proportion of funds used.

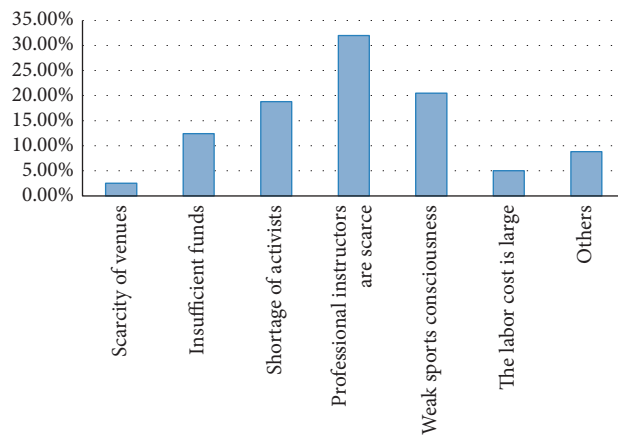


FIGURE 13: Underdevelopment factor chart.

TABLE 4: Statistical table of registered sports professional guidance.

Region	Number of people in 2015	Number of people in 2016	Number of people in 2017	Number of people in 2018	Number of people in 2019
Chengdu	5	10	17	20	24
Nanchong	6	9	14	16	21
Yibin	4	6	10	14	19
Zigong	4	8	13	10	16
Guangyuan	5	7	12	11	19
Aba prefecture	2	4	9	9	16

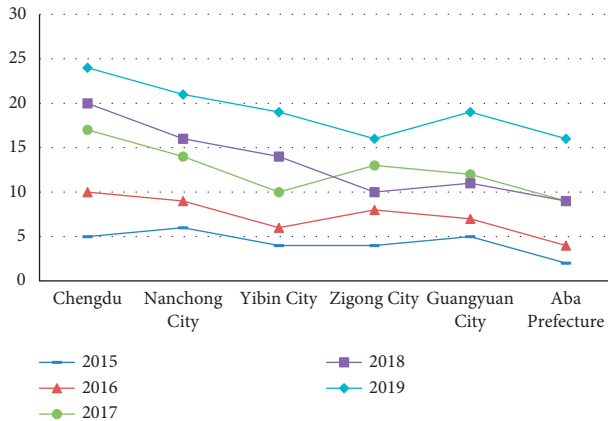


FIGURE 14: Comparison of registered sports professionals in six cities.

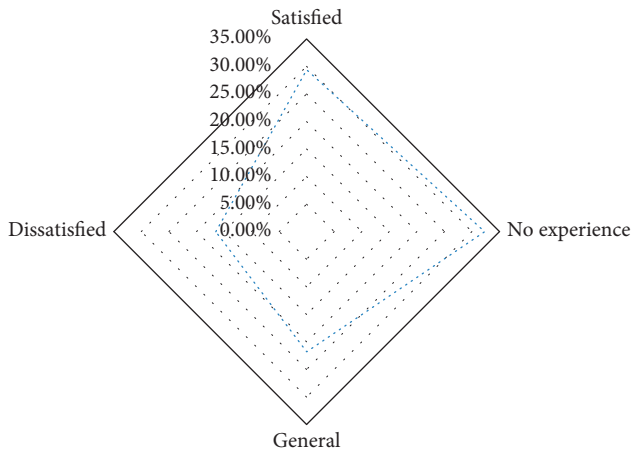


FIGURE 15: Investigation on the satisfaction of citizens in Nanchong city.

developing rapidly, and the development speed of related aspects in Nanchong is closely followed. It can be seen that the sports public service platform is widely promoted in Chengdu and Nanchong, and its awareness is higher than that of other urban areas surveyed.

4.2.5. *Nanchong Citizens Satisfied with the Sports Public Service Platform.* By inquiring 170 citizens randomly interviewed in Nanchong City, the largest proportion of people without experience was 32.3%, which was 29.4% higher than that with satisfaction. Most of the surveyed

TABLE 5: Satisfaction questionnaire.

Options	Number of people	Proportion (%)
Satisfied	50	29.4
No experience	55	32.3
General	37	21.8
Dissatisfied	28	16.5

people have not experienced the services brought by the sports public service platform, which shows that the sports public service has not been widely promoted in Nanchong City, and the benefits of the masses are not high. Combined with Figure 15 and Table 5, it can be seen that the platform and services are satisfactory among most people, and the platform should be upgraded and improved according to the limitations of the platform to provide better services for Nanchong citizens. Through related simulations, it can be seen that the current problems in Nanchong’s public sports services include insufficient public awareness of sports public services, insufficient sports activities, insufficient sports facilities, and insufficient funding and high costs.

5. Conclusion

In view of the multiobjective optimization of sports public service in Nanchong City, the establishment and analysis of the information platform were carried out. The main content includes intelligent venues, information platform, sports safety, and other topics for research and application. In the platform construction, the service efficiency is constantly rising, and citizens need to constantly improve their civic awareness. Urban construction needs citizens to improve their service awareness and improve the utilization rate of urban sports services. In the future, further works will focus on the study of the use efficiency of service facilities and continuously improve the utilization rate of resources. The article improves the efficiency and public service of the sports public platform by establishing and analyzing the information platform of the sports public service in Nanchong. In response to the number of activities and funding issues raised in this article, the lack of professional sports coaches and other issues need to be improved in order to promote the good development of the city’s public services and promote public sports.

Data Availability

The experimental data used to support the findings of this study are available from the corresponding author upon request.

Conflicts of Interest

The authors declare that they have no conflicts of interest regarding this work.

Acknowledgments


This work was sponsored in part by Nanchong City Philosophy and Social Science Research Planning Project (NC2019B181).

References

- [1] K. Deb, S. Agrawal, A. Pratap, and T. Meyarivan, "A fast elitist non-dominated sorting genetic algorithm for multi-objective optimization: NSGA-II," in *Proceedings of the International Conference on Parallel Problem Solving from Nature*, vol. 20, no. 03, pp. 37–41, Paris, France, September 2000.
- [2] J. Horn, N. Nafpliotis, and D. E. Goldberg, "A niched Pareto genetic algorithm for multi-objective optimization[C]// evolutionary computation," in *Proceedings of the 1994. Proceedings of the First IEEE Conference on IEEE World Congress on Computational Intelligence*, vol. 32, no. 09, pp. 11–15, IEEE, Orlando, FL, USA, July 1994.
- [3] K. Deb, L. Thiele, M. Laumanns, and E. Zitzler, "Scalable test problems for evolutionary multiobjective optimization," in *Evolutionary Multiobjective Optimization. Advanced Information and Knowledge Processing*, A. Abraham, L. Jain, and R. Goldberg, Eds., Springer, London, pp. 105–145, 2005.
- [4] C. A. Coello Coello, "Evolutionary multi-objective optimization: a historical view of the field," *IEEE Computational Intelligence Magazine*, vol. 1, no. 1, pp. 28–36, 2006.
- [5] F. Altıparmak, M. Gen, L. Lin, and T. Paksoy, "A genetic algorithm approach for multi-objective optimization of supply chain networks," *Computers & Industrial Engineering*, vol. 51, no. 1, pp. 196–215, 2006.
- [6] J. Cai-Xing, "Establishing a perfect sports public service system," *Sport Science Research*, vol. 28, no. 02, pp. 1–13, 2008.
- [7] G. Y. Feng, "Equalization of sports public service and choice of relevant fiscal policy," *Journal of Shanghai University of Sport*, vol. 31, no. 06, pp. 26–31, 2007.
- [8] L. I. Jian-Guo, "Basis of a sports power-construction of sports public service system," *Sport Science Research*, vol. 30, no. 04, pp. 15–18, 2009.
- [9] L. I. Jing, "Study on sports public service system," *Journal of Nanjing Institute of Physical Education*, vol. 23, no. 01, pp. 62–65, 2009.
- [10] J. Yao and X. Ding, "VEC-Model-Based sports public service analysis," *International Journal of Digital Content Technology and its Applications*, vol. 6, no. 17, pp. 226–234, 2012.
- [11] L. I. Pei-Feng and Q. M. Zhu, "Design and implementation of campus information platform based on web services," *Computer Engineering and Design*, vol. 27, no. 19, pp. 3564–3567, 2006.
- [12] Y. U. Li-Ping, "Equality of sports public service in China," *Journal of Wuhan Institute of Physical Education*, vol. 45, no. 07, pp. 31–35, 2011.
- [13] W. Cheng, J. Y. H. Fuh, A. Y. C. Nee, Y. S. Wong, H. T. Loh, and T. Miyazawa, "Multi-objective optimization of part-building orientation in stereolithography," *Rapid Prototyping Journal*, vol. 1, no. 4, pp. 12–23, 1995.
- [14] W. T. Jia, J. L. Hao, H. F. Liu, and H. O. N. G. liang, "Research to equalization of sports public service under the law," *Journal of Nanjing Institute of Physical Education*, vol. 23, no. 03, pp. 78–81, 2009.
- [15] J. Liu, H. Yong, and X. Zhou, "Cloud computing science and technology information service system platform design," *Bulletin of Science and Technology*, vol. 28, no. 10, pp. 19–21, 2012.
- [16] X. Tao and H. W. Chen, "Evolutionary algorithms for multi-objective optimization and decision-making problems," *Engineering and Science*, vol. 4, no. 2, pp. 59–68, 2002.
- [17] M. Gong, L. Jiao, D. Yang, and W. Ma, "Research on evolutionary multi-objective optimization algorithms," *Journal of Software*, vol. 20, no. 2, pp. 112–134, 2009.
- [18] L. I. Li, "Sports public service: the demand of sports business development on public finance," *China Sport Science*, vol. 30, no. 06, pp. 53–58+80, 2010.
- [19] E. L. Zhang, "The research review on Chinese sports public service and sports public policy," *Journal of Hebei Institute of Physical Education*, vol. 26, no. 01, pp. 8–11, 2012.
- [20] X. P. Qin, J. Wang, and L. U. Chang-Fen, "A study on the way of sports public service equalization based on comparative analysis," *Journal of Beijing Sport University*, vol. 33, no. 02, pp. 15–18, 2010.
- [21] J. H. Shen, "Demand for shanghai sports public service," *Sport Science Research*, vol. 02, pp. 37–41, 2008.
- [22] C. X. Wang, "Comparison and revelation of sports public service," *Sport Science Research*, vol. 02, pp. 27–31, 2008.
- [23] L. Q. Wang, G. U. Jian-Wei, Y. J. Cao, Y. U. Li, C. X. Guo, and B. Liu, "Design and implementation of power real-time information platform based on CIM/CIS," *Proceedings of the Chinese Society of Universities for Electric Power System and its Automation*, vol. 20, no. 01, pp. 46–51, 2008.
- [24] R. J. Kauffman and L. Lally, "A value platform analysis perspective on customer access information technology[J]," *Decision Sciences*, vol. 25, no. 5-6, pp. 767–794, 2010.

Research Article

Automatic Scoring of Spoken Language Based on Basic Deep Learning

Zhong Cheng^{1,2} and Zonghua Wang¹ 

¹*School of Foreign Languages, Anhui University of Science and Technology, Huainan 232001, China*

²*School of English Studies, Shanghai International Studies University, Shanghai 201620, China*

Correspondence should be addressed to Zonghua Wang; 2011046@aust.edu.cn

Received 26 November 2021; Revised 13 December 2021; Accepted 3 January 2022; Published 25 January 2022

Academic Editor: Hangjun Che

Copyright © 2022 Zhong Cheng and Zonghua Wang. This is an open access article distributed under the Creative Commons Attribution License, which permits unrestricted use, distribution, and reproduction in any medium, provided the original work is properly cited.

The oral English test in domestic universities requires teachers to modify a large number of candidates' oral recordings. This is the work of using time repeatedly. Using the CALL system to realize the automation of conversation recording can reduce the burden of teachers' work. Therefore, it is of great practical significance to develop an automatic and accurate scoring system for oral English. With the development of artificial intelligence, deep learning technology has been gradually applied in various fields. Similarly, in the application of oral scoring, deep learning technology makes the implementation of such a system possible. Based on the deep learning technology, this paper proposes an automatic scoring algorithm for spoken language and implements a detailed design and evaluation system. The system consists of two modules. The pronunciation standard of spoken pronunciation and the content of spoken pronunciation are scored, and the sum of these two scores is the final score. Finally, this paper uses 650 oral English recordings from a college English test to train the artificial neural network. Experimental results show that if the training data set is small, the BP network model can obtain better comprehensive evaluation performance.

1. Introduction

In recent years, information technology has been widely used in the field of education. In language education, the popularity of English education in China is getting higher and higher, and the traditional language education methods are difficult to meet people's needs [1]. In this context, Computer Assisted Language Learning (CALL) has become a research hotspot [2]. CALL system not only is used in online education, but also includes English education platforms such as text, image, audio, and video, which also play an important role on the Internet. Instead of teachers automatically revising students' test questions and homework between classes, teachers are freed from taking time to revise. The automatic correction system like now has almost reached the completely correct level in the correction task facing objective problems. As for composition questions and oral questions, automatic revision is still the research focus that should be broken through. Oral problems can be

divided into two types [3]. One is retelling, reading aloud, and reciting what is known. Another point is that candidates are free to play games around specific problems and topics. We are often called "open spoken English." With the development of speech recognition technology, the first question can be well evaluated by comparing and analyzing the examinee's pronunciation with the standard pronunciation [4], such as using the classical Goodness of Pronunciation (GOP) algorithm. In addition, it is necessary to comprehensively evaluate candidates' answers from multiple dimensions, for example, fluency, rhythm, intonation, richness of vocabulary, and meaning. For a long time, the research on open oral scoring technology has not made great breakthrough. With the development of machine learning technology, some scholars have studied how to apply it to automatic oral evaluation. Thus, the famous automatic scoring system of speed competition appeared [5].

In universities, the English skills training service system of universities is used for examination in the teaching of

situational English. At least mid-term and final evaluations are conducted every semester. In two exams, each teacher is usually responsible for the educational tasks of multiple classes. Because of the complicated manual grading method, teachers' burden is aggravated, and their educational energy is insufficient. If we study the intelligent correction system needed in the oral test of senior high schools in China [6], we can greatly reduce the pressure on teachers, and teachers can put more strength into practical teaching activities to improve their teaching ability.

There are extremely few ways to score speakers with speech disorders. We study an automatic speech score, which is a kind of assessment for speakers with language disorders [7]. With the development of society and the integration of global economy, people's demand for English learning is increasing day by day, so the research on automatic assessment of oral proficiency is particularly important. In the previous automatic evaluation system, recording conditions are a challenge for learners' pronunciation, noisy sounds, etc. In addition, it is necessary to deal with nonfluent, nongrammatical, and spontaneous sounds with unknown potential text. To solve these series of problems, we propose a method of combining speech recognition system based on deep learning with Gaussian process (GP) scorer, which is a measure to evaluate the performance of rejection scheme [8].

2. Related Technology Research

2.1. Research on Natural Language Processing Related Technologies

2.1.1. Latent Semantic Analysis. Latent Semantic Analysis, also known as Latent Meaning Index, is a document modeling method for natural language processing [9]. Like the previous vector space model, LSA method also uses vectors to represent words and documents and judges the relationship between words and documents according to the relationship between vectors, which leads to two shortcomings: (1) vector space model uses correct sentence matching. (2) You cannot ignore the meaning of a word and provide semantic search. LSA solves the above problems by statistically analyzing a large number of text libraries and mapping documents from sparse n -dimensional space to low-dimensional space. Vector space is called inclusion space. The document modeling process using LSA method is as follows, shown in Figure 1:

- (1) Analyze the document set and create a word-document matrix
- (2) Singular value decomposition of word-document matrix
- (3) Dimension reduction of the matrix after singular value decomposition

The TF-IDF is calculated by the following formula:

$$A_{i,j} = \frac{N_{i,j}}{N_j} \log\left(\frac{D}{D_i}\right). \quad (1)$$

		Terms				
		T1	T2	T3	...	Tn
Documents	D1	0.2	0.1	0.5	...	0.1
	D2	0.1	0.3	0.4	...	0.3
	D3	0.3	0.1	0.1	...	0.5

	Dm	0.2	0.1	0.2	...	0.1

FIGURE 1: Word-document matrix.

Matrix S is an $m \times m$ dimensional diagonal matrix, and each value on the diagonal represents the importance of various topics, and this value is also called a singular value. Then, in Step 3, the matrix after SVD decomposition only stores the largest K topics of U , and a dimension descent process is performed, in which only K topic vectors corresponding to S and V are maintained. As shown in Figure 2, the resulting Matrix A can be expressed by the following formula:

$$A_{m \times n} = U_{m \times k} S_{k \times k} V_{k \times n}^T. \quad (2)$$

If you use query text to calculate the similarity of all the text in the document set, you need to map the query text to the meaning space:

$$q_{1 \times k} = q_{1 \times n} V_{n \times k} S_{k \times k}^{-1}. \quad (3)$$

2.1.2. Word Embedding. To score the spoken language, considering the learning model, it is necessary to use the neural network model to score the spoken content of the examinee [10, 11]. The existing model scoring has the following main problems: (1) there is only one word in the number vector; so if there are N words in the text, it needs to use the N -dimensional vector for coding. Therefore, if the number of nonrepeated words in the text is large, the dimension of the vector becomes large. In addition, as the number of neurons increases, the computation becomes more complex. (2) Simple hot coding scheme cannot describe the meaning relationship between words. Words can be represented by low-dimensional vectors. For words with similar meanings, the vector displays are also close, as shown in Figure 3. More abundant information can be embedded into low-dimensional vectors, which are represented by single hot coding and term embedding, respectively.

When using neural network to solve text problems, the network architecture shown in Figure 4 is usually used. The first layer of the network is the word embedding layer, which transforms the words in the input text into word vector representation. For example, the length of the word embedding vector is set to 50 for the text containing 20 words, and it becomes 20 through the word embedding layer. Two-dimensional matrix of $\times 50$. The word embedding layer is interpreted as a dictionary model, and the word index and its corresponding word vector graph are stored in the dictionary. This model can be obtained through data training or

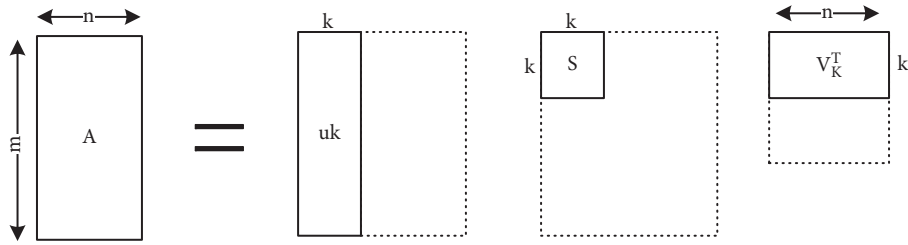


FIGURE 2: Svd matrix.

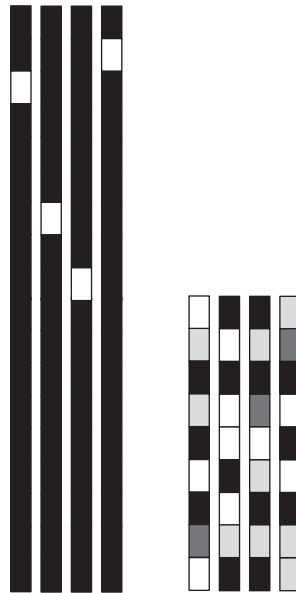


FIGURE 3: Word vectors represented by one-hot encoding and word embedding.

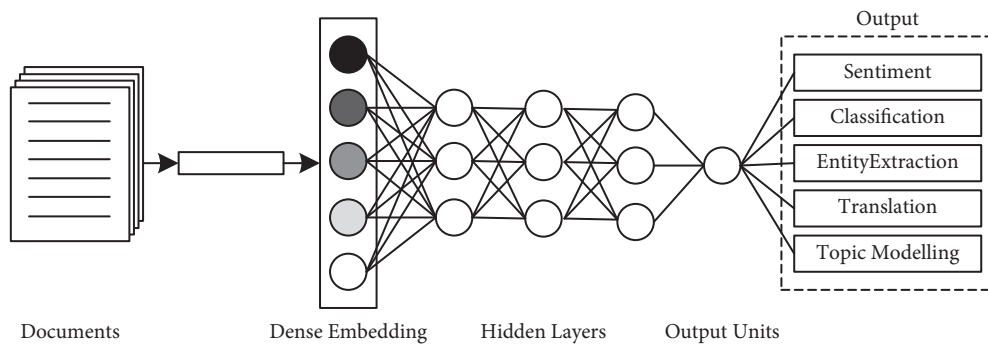


FIGURE 4: Neural network model architecture with word embedding layer.

loaded with trained models. Word 2 vector and GloVe are the commonly used models of preparation training language [12]. Based on the latter, this paper constructs a scoring model of oral content.

2.2. Research on Related Technologies of Scoring Model

2.2.1. Basic Concepts of Artificial Neural Networks.

When an artificial neuron is stimulated, if the stimulus exceeds a certain threshold, the neuron will be activated and convey

information to other neurons. The process of information transmission between neurons can be explained by Figure 5. Artificial neurons receive m input signals from other neurons. These input signals have a weight w during transmission. The weighted value can be abstractly understood as signal strength. After weighted addition, these input signals are processed by an “activation function” to generate an output signal Y .

The learning ability of neural network is strong because of its great activation function. If the activation function is not used, the network can only perform simple linear

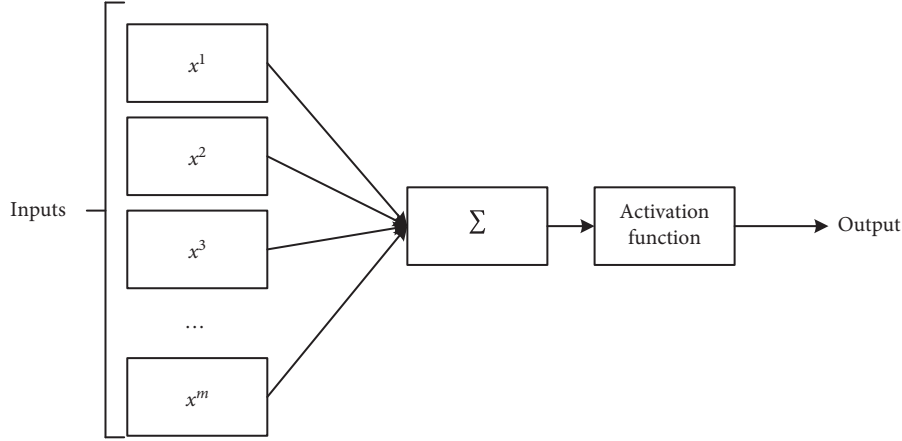


FIGURE 5: Mechanism of information transmission between neurons.

transformation, so the performance of this network is limited. On the other hand, the activation function introduces nonlinear elements into the network, which makes the neural network approximate to various nonlinear curves arbitrarily and makes the network have strong representation ability. The general active functions are Sigmoid, Hyperbolic Tangent, and Lireer, as shown in Figure 6, and there are function graphs of these three active functions.

The information transfer relationship between nodes is explained in the following formula:

$$y_j = \text{activation} \left(b_j + \sum_i x_i w_{ij} \right), \quad (4)$$

where x_i represents the output value of the i -th node of the previous layer (or the input value of the current node j), w_{ij} represents the weight value between the i -th node of the previous layer and the j -th node of the current layer, b_j represents the paranoid value of the j -th node of the current layer (the paranoid value is introduced to make the model converge better), and y_j represents the output value of the j -th node of the current layer.

2.2.2. Basic Concepts of Deep Learning. The differences between deep learning and traditional machine learning are as follows. Feature items are fully automated, so people do not have to go all out to find a more suitable initial input feature. Data becomes higher-level and more abstract display form through the network. This process is the core step in traditional machine learning. In Figure 7, the process can be described simply (or as close as possible to the expected result).

Briefly introduce some core terms contained in the above figure.

- (1) Loss function: it is used to calculate the difference between the predicted data and the actual data of neural network.
- (2) Optimizer: determine the algorithm to update the network weight by using the loss value, among which

the commonly used optimization algorithms are Adam, SGD, and RMSProp.

- (3) Backpropagation error: reverse transmission loss values are sent from the output layer to the input layer (the loss values obtained at each node are allocated by a weighted contribution ratio), and the weight values and polarization values in the network are updated using a gradient descent algorithm during transmission.

In the current field of deep learning, various deep learning models have been developed. In this paper, we pay attention to convolution neural network and cyclic neural network.

2.2.3. BP Neural Network. BP neural network has strong nonlinear mapping ability and can approximate any discontinuous function with high precision [13]. It is an extremely effective model to solve problems such as regression and classification. The training process of BP neural network is mainly divided into two stages [14]. The first stage is the forward propagation of signals, from the input layer to the hidden layer and finally to the output layer. In the second stage, backpropagation algorithm is used to backpropagate the error from the output layer to the hidden layer, and finally the weight and bias voltage are adjusted to the input layer in turn. When a network is trained using a large amount of data including a plurality of samples, the mean square error is exemplified as a loss function, and the mean square value of the error after forward propagation of the training data is as follows:

$$E = \frac{1}{N} \sum_{k=1}^N (y_k(i) - t_k(i))^2, \quad (5)$$

where $y_k(i)$ represents the true output value of the i -th data sample, and $t_k(i)$ represents the predicted value obtained after the i -th data sample passes through the neural network. The BP neural network uses learning rate and gradient descent algorithm to update the connection weights and

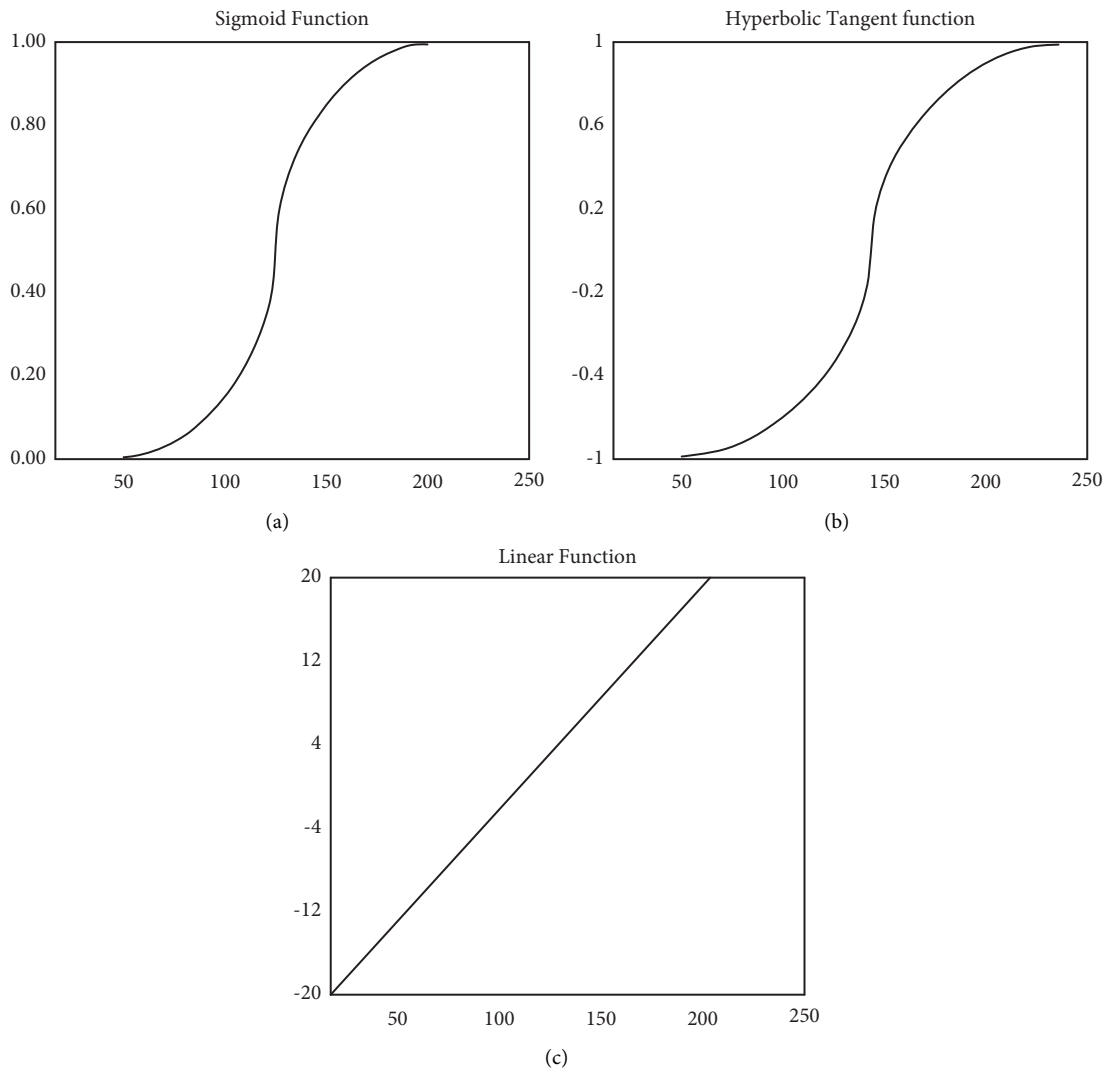


FIGURE 6: Activation function graph. (a) Sigmoid function image. (b) Image of hyperbolic tangent function. (c) Pure linear function image.

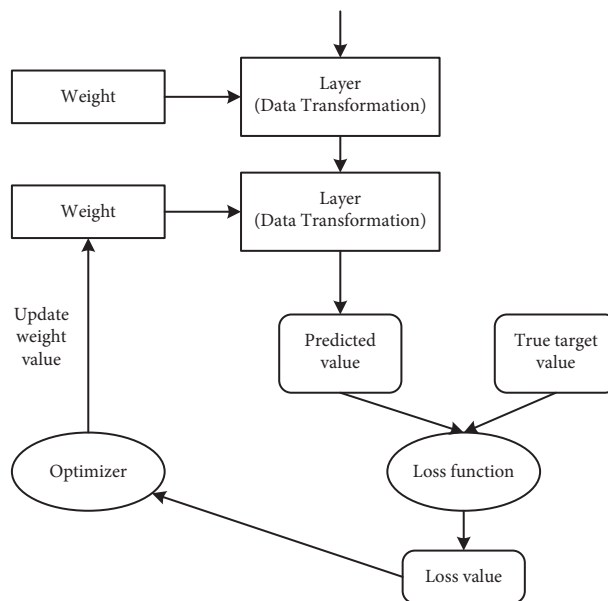


FIGURE 7: Working principle of neural network.

polarization values of each layer. The whole backpropagation process can be explained by the following formula:

$$E^{(n)} = (w_c)^T \cdot E^{(n+1)}, \quad (6)$$

$$w_{ji}^{(n-1)} = w_{ji}^{(n-1)} + \text{learn}_{\text{rate}} * \frac{\partial E_i^{(n)}}{\partial w_{ji}^{(n-1)}}, \quad (7)$$

$$b_j^{(n)} = b_j^{(n)} + \text{learn}_{\text{rate}} * \frac{\partial E_i^{(n)}}{\partial b_j^{(n-1)}}. \quad (8)$$

2.2.4. Convolution Neural Network. One-dimensional convolution neural network is well applied to sequence data, such as audio signals and text data, and in some cases, the performance of this network can match that of cyclic neural network [15, 16]. The computational cost is usually quite small, and the model can achieve better performance. As shown in Figure 8, as the operation principle of one-dimensional convolution network, feature is the data length of each feature. The network output data format after convolution operation is samples. The new step is the length of the feature sequence after the convolution operation, and filters are the number of convolution kernels.

2.2.5. Cyclic Neural Network. Cyclic neural networks (RNN) can circulate information in the network, but unlike networks such as CNN, their output only considers the influence of the previous input and does not consider the influence of other time inputs. In RNN, the output of each moment is not only related to the input of the current moment, but also related to the input of the previous moment. The network has the function of "storage." Therefore, RNN is extremely suitable for processing sequence data, especially text data. h_t in terms of o_t can be calculated by the following formulas:

$$h_t = \text{activation}(U h_{t-1} + W x_t + b), \quad (9)$$

$$o_t = V h_t. \quad (10)$$

Conventional RNN model is only applied to the processing of short sequence data. In order to solve the problem of insufficient "long-term storage" capacity in traditional RNN networks, some researchers improve the model, which is called Short Term Storage Network (LSTM). LSTM model selectively adds new information and selectively forgets previously accumulated information by introducing grid control mechanism. A new state c_t is introduced in LSTM network for circulating information transmission.

The states of the hidden layer and the memory cell are represented by the following equations:

$$c_t^* = \tanh(W_c x_t + U_c h_{t-1} + b_c), \quad (11)$$

$$c_t = f_t \tanh \odot \tanh(c_t^*). \quad (12)$$

The states of the three gate controllers can be calculated from the following equations:

$$f_t = \sigma(W_f x_t + U_f h_{t-1} + V_f c_{t-1} + b_f), \quad (13)$$

$$i_t = \sigma(W_i x_t + U_i h_{t-1} + V_i c_{t-1} + b_i), \quad (14)$$

$$o_t = \sigma(W_o x_t + U_o h_{t-1} + V_o c_{t-1} + b_o). \quad (15)$$

3. Design of Oral Scoring System

3.1. Overall System Design. Combining deep learning technology and object-oriented design idea, the oral scoring system designed in this paper includes six modules as shown in Figure 9.

- (1) Oral scoring module: call the scoring mode module, load the training scoring mode, automatically correct the oral data, and save the scoring results in Excel file form.
- (2) Sound noise reduction module: in order to make the results of speech recognition and feature extraction more accurate, the examinee's spoken language is noise reduced.
- (3) Speech recognition module: convert the examinee's dialogue recording into the corresponding text content through the speech recognition engine.
- (4) Data processing module: this module mainly extracts spoken speech recording and speech recognition text. The score of CNN + LSTM is converted into digital display form for spoken language recognition text.
- (5) Systematic evaluation module: analyze the evaluation results of main evaluation and evaluation models.
- (6) Scoring Model Module: define the scoring model based on BP + CNN + LSTM, respectively, and save the training model for loading directly.

Intelligent spoken language evaluation refers to the dynamic process from audio to total point output and can be described as the scoring system in Figure 10 [17]. The speech recognition engine first performs noise reduction processing through the sound noise reduction module and then transfers the beautiful recording to the corresponding text content. The general scoring system fits the characteristic value according to the scoring model. Two scoring models are used here. Speech Scoring Model and Text Scoring Model are designed to improve the accuracy of the scoring system. In addition, in the actual correcting environment, the teacher also evaluates the examinee's conversation from the level of sound and content. This design is consistent with the manual scoring method. The design of the core module of the system is described in detail.

3.2. Design of Speech Noise Reduction Module. Because of the problem of the recording device, the recording of spoken language is often mixed with current sound and noise. This

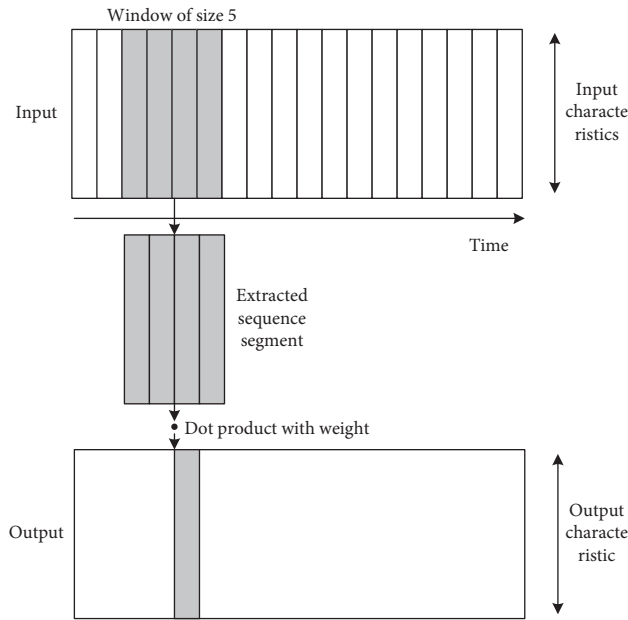


FIGURE 8: Working principle of one-dimensional convolution network.

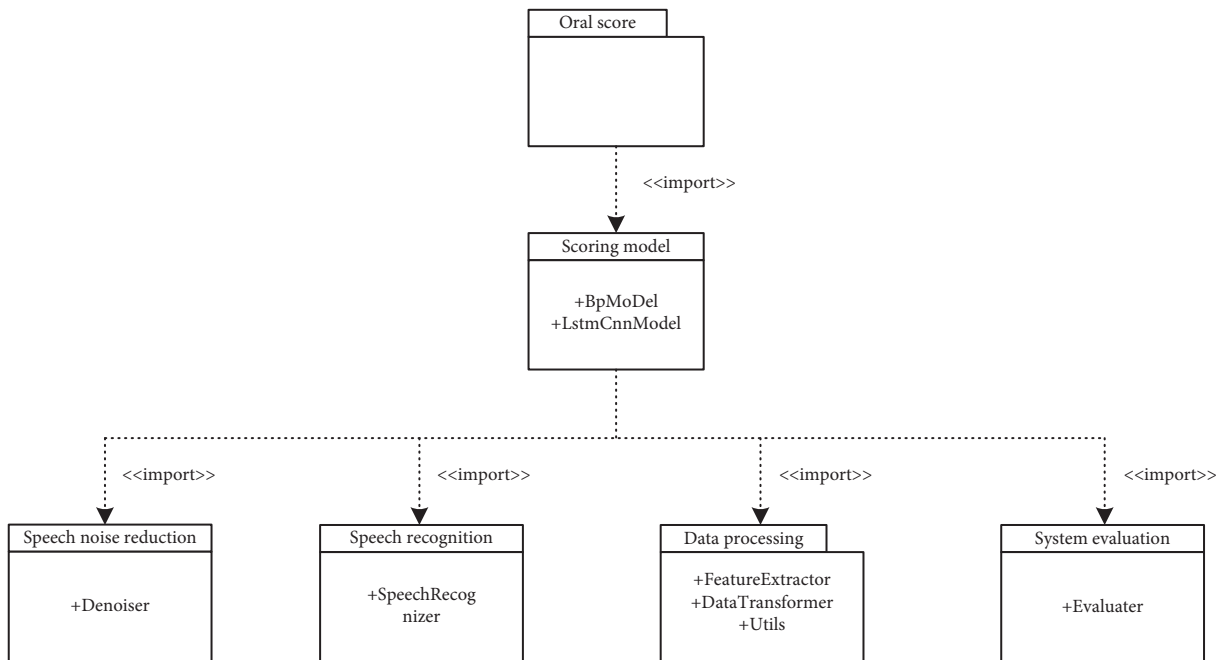


FIGURE 9: System module design.

affects the correctness of subsequent feature extraction and speech recognition. Traditional noise reduction methods use spectrum subtraction or adaptive filtering. In recent years, due to the successful application of learning in the field of sound processing, the use of deep learning technology in reducing sound noise has been improved and is popular. In this paper, RnNoise, an open source noise suppression library, is used to realize the header noise reduction module, in which RNNOIS uses grid control loop unit to realize noise reduction neural network, and GRU is a variant of LSTM. By

introducing grid control mechanism, GRU network can store information for a long time. RnNoise uses beautiful sound data (English conversation recordings) and noise data (computer fan sounds, office noises, street people noises, etc.) to train the model. Therefore, a wider range of signal-to-noise ratio is obtained, and the noise reduction effect becomes more remarkable. In addition, RnNoise is made in C language. In the speech noise reduction module, the RnNoise wrapper is made by using Python language, and RnNoise is integrated into the system.

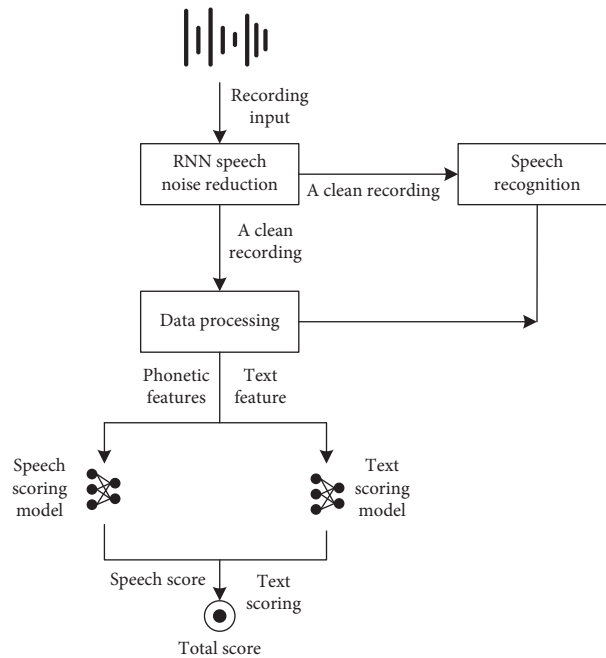


FIGURE 10: System scoring process.

3.3. *Design of Speech Recognition Module.* On the basis of evaluating the accuracy of speech recognition engine, a

unified standard of Word Error Rate (WER) is reached. WER can be calculated using the following formula:

$$\text{WER} = \frac{\text{Number of words replaced} + \text{Number of words deleted} + \text{Number of words inserted}}{\text{The total number of words in the correct recognition sequence}}. \quad (16)$$

Microsoft uses a local recognition engine. The recognition speed is the fastest, but the ambiguity is extremely high.

3.4. Design of Data Processing Module

3.4.1. *Data Cleaning.* Because of the oral fluency of the examinee and the recognition error of the speech recognition engine itself, there are often recognition results that affect the accuracy of the text scoring model in the speech recognition text. For example, this video is about the Chinese and China great wall, um; the great wall is built by the king in dynasty. These features include the number of syntax errors and the depth of syntax tree. In addition, there are also onomatopoeia words like uh and um. In addition to these onomatopoeia words, you can be more specific about the grammar of the text without affecting the entire text content. To build the topic model of LSA, “stop words” such as “the,” “is,” and “at” must be removed [18]. These stop words have little substantive meaning for the topic model. In addition, the generated model can be more efficient.

3.4.2. *Feature Extraction.* Feature extraction is an extremely important step before machine learning, which determines the reliability and accuracy of the evaluation model. In this

paper, in feature screening, the importance of each feature can be measured by calculating the Pearson correlation coefficient with manual scoring, and the feature with correlation coefficient below 0.2 should not be selected [19]. In this paper, there is generally no fixed reference answer for open oral scoring, so when choosing features, besides the features of similarity in meaning, we mainly choose the features of common type. As shown in Table 1, each feature finally selected and used here will be briefly described.

In this paper, the characteristics of four scales are extracted to evaluate the oral scoring model. The characteristic of speed is often called Rate of Speech (ROS), which is mainly used to explain the fluency of spoken language and calculated by the following formula:

$$\text{ROS} = \frac{N_{\text{words}}}{t - t_s}, \quad (17)$$

where N_{words} represents the total number of words contained in the examinee’s spoken language, t represents the total duration of oral recording, and t_s represents the mute duration of recording.

Besides the characteristics of sound speed, the number of quiet sounds during recording can also reflect the fluency of oral English of the tester to a certain extent. In the evaluation of pronunciation quality, the probability characteristic after

TABLE 1: Summary of features.

Feature category	Feature name	Brief description of characteristics
Phonetic class	articulationRate	Speed of speech
	numSilence	Number of voice pauses
	posteriorScore	Number of pronunciation pauses
	speakingRatio	Posterior probability score of pronunciation
Text class	eassyLength	Total number of words in text
	uniqueWords	Number of nonrepeating words in the text
	parseTreeDepth	Sum of all syntactic tree depths in text
	semanticSimilarity	Semantic similarity between text and theme
	goodGrammerRatio	Correct rate of text grammar

pronunciation is adopted by many oral scoring systems. This paper uses this characteristic to explain the correctness of the examinee’s pronunciation. In addition, when extracting effective spoken language, the proportion of long-term recording can also reflect a certain degree of rich spoken content. In the oral evaluation of traditional reading problems, the standard oral sequence corresponding to the benchmark text is usually displayed, the test speech is forced to be configured, and the postprobability average of each phoneme is calculated by the classical GOP algorithm. However, there is no reference text in the open oral score, so it is necessary to combine the speech recognition engine with the speech model of standard English pronunciation training and calculate the average postprobability as the feature of pronunciation quality.

Chapter structure and other features are not suitable for text scoring model of text design. For such short text, sentence structure is a very good alternative, and the depth of grammar tree is used to describe the structural features of sentences. Candidates who are not used to dialogue will have a lower depth of grammar tree than usual. There are algorithms to calculate the similarity of the meanings of commonly used articles. Vector Space Model (VSM) [20], Latent Meaning Analysis (LSA), and Latent Directory Distribution (LDA) are three methods that are based on the word back model, but the degree of meaning varies depending on the method. As a result of the actual test, it is found that the topic model of LSA is more effective in the data set used here. As shown in Figure 11, it is the process of building the topic model of LSA.

Some common part-of-speech tags are shown in Table 2.

There are no grammatical errors in famous English original novels. This paper refers to the method in EASE, an open source composition scoring system. After the part-of-speech tags of Sherlock Holmes’ novel collections are displayed, the combination of 3 Yuan tags and 4 Yuan tags is taken out, and the extracted results are saved as a retrieval library of local tag combinations. If you cannot find it, the grammar is wrong. We use the following formula to calculate the correct rate of text syntax:

$$\text{correct}_{\text{ratio}} = \frac{N_g}{N_s}. \quad (18)$$

3.4.3. Data Conversion. Deep learning can automatically extract features, so feature engineering is not needed. As shown in Figure 12, the quantization flow of the entire text

removes onomatopoeia words by first performing data cleansing on the speech recognition text and eliminates duplicate words in the text due to recognition errors.

Mel Frequency Cepstrum Coefficients (MFCC) are extracted from spoken recording data as input to the sound scoring model. MFCC contains integrated voice information. Figure 13 is a schematic flowchart showing converting spoken speech recording data into MFCC feature vectors:

3.5. Scoring Model Module Design. Using Keras deep learning framework, all neural networks in this study are constructed. Keras is a highly neural network framework made by *Python* and can run on TensorFlow, CNTK, or Thano.

3.5.1. Scoring Model Based on BP Neural Network. Through repeated experiments, the number of hidden layers and the number of neurons are determined. When the training results do not converge, the number of hidden layers or layer nodes is increased. After the results converge, reduce the number of nodes appropriately and observe whether better results will be obtained. Taking the text scoring model as an example, the sound scoring model with the number of input segments other than 4 has the same structure.

3.5.2. Scoring Model. If the manually extracted features are always invalid, and the correlation between manually extracted features and manually evaluated features is low, it is difficult for the trained model to fit the data accurately. Deep learning technology can automatically mine features, and the learning data can be displayed deeper, which can break through the boundaries of artificial design features. Combine these two networks to construct speech scoring mode and text scoring mode. The computational cost of cyclic neural network is very high when dealing with very long sequence data, so one-dimensional convolution neural network is used as preprocessor step before LSTM network, and shortening sequence can take out higher-level feature display to deal with LSTM layer. As shown in Figure 14, the design of the speech scoring model includes two consecutive convolution blocks. Finally, all connection layers pseudo-combine the one-dimensional vectors to output corresponding speech evaluation results.



FIGURE 11: LSA topic model building process.

TABLE 2: Part-of-speech standard effect.

Part-of-speech tags	Describe
NN	Noun (singular)
NNS	Noun (plural)
VB	Verb (prototype)
VBD	Verb (past tense)
VBNJJ	Verb (past participle)
RB	Adjectives
IN	Adverb
CC	Subordinate conjunctions
PRP	Conjunctions Personal pronoun

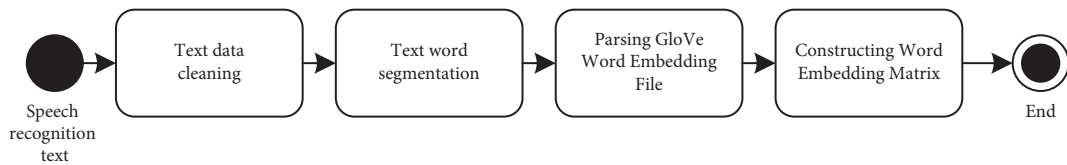


FIGURE 12: Text vectorization process.

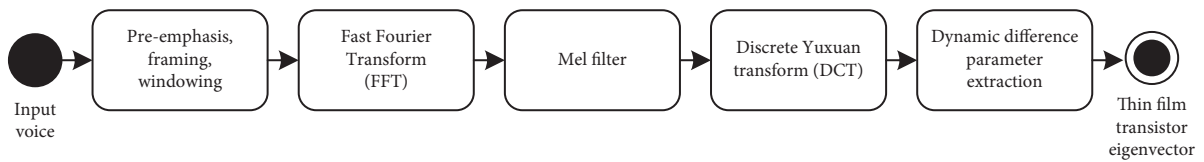


FIGURE 13: MFCC feature extraction flow.

The design of the text scoring model is shown in Figure 15, and the neural network model shares five layers of networks. The first layer is the word embedding layer, which is defined by GloVe model. The second layer is a one-dimensional flip layer for reducing the length of the network input sequence and extracting more effective features. The third layer network is the LSTM layer, and the LSTM network can select “stored” and “forgotten” information. And it is a one-dimensional vector after pseudooutput MeanOverTime processing and outputs the evaluation result of spoken content.

4. Experimental Results and Analysis

4.1. Means for Evaluating System Performance. In this paper, Pearson correlation coefficient is used to evaluate the performance index of oral evaluation, which is used to evaluate the correlation of different vectors. Its mathematical expression is as follows:

$$\rho_{X,Y} = \frac{\text{cov}(X,Y)}{\sigma_X \sigma_Y} . \quad (19)$$

The second evaluation index is the difference of man-machine scoring, which is mainly used to describe the

difference between manual and machine scoring. Its calculation formula is as follows:

$$d = E|S_{\text{Machine}} - S_{\text{Human}}| . \quad (20)$$

The third evaluation index is accuracy. This paper establishes the maximum value of man-machine evaluation error to determine whether the evaluation result is correct or not.

4.2. Analysis and Evaluation of Scoring Model

4.2.1. Effectiveness Analysis of Feature Extraction. There are Pearson correlation coefficients for different features in the speaking score, and the results are shown in Table 3 and Table 4. As can be seen from the following two tables, the characteristics of speech types are numbSilence and speakingRatio. This shows that when grading oral English, teachers are most concerned about the fluency of oral English and the long effective time of oral English. In particular, fluency is characterized by recording the more stops, and the lower it is, the lower the score is. This shows that, for oral content, teachers are more interested in candidates’ vocabulary grasp and rich conversation content. ParsetreedDepth and goodGrammerRatio features are affected by the recognition accuracy of the speech recognition engine.

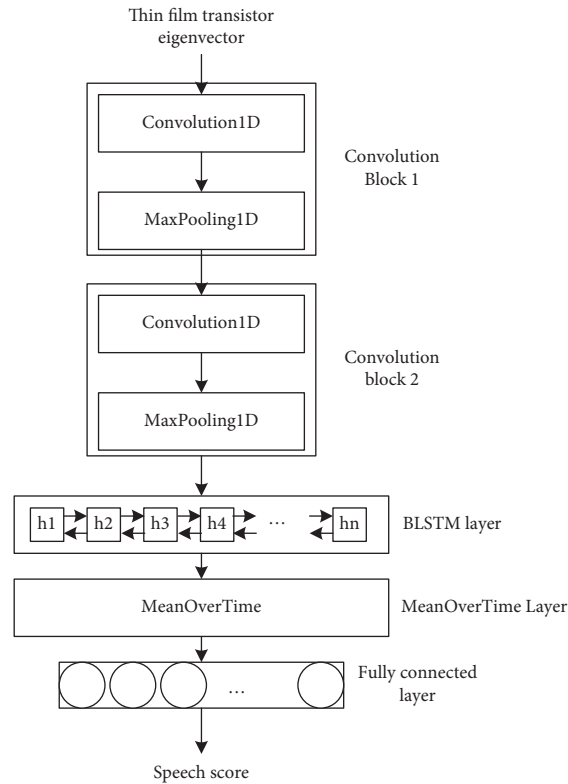


FIGURE 14: Speech scoring model.

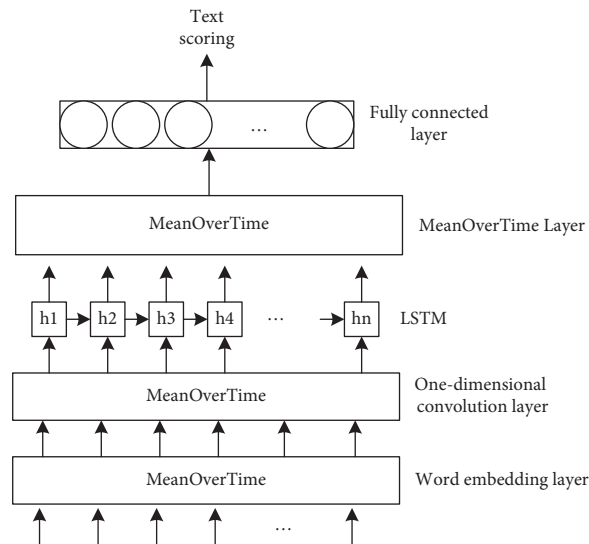


FIGURE 15: Text scoring model.

On the other hand, teachers also make great efforts to analyze the grammatical errors and sentence structures of candidates' dialogues when scoring manually, and the relationship between these two characteristics and manual scoring is low.

4.2.2. Analysis of Model Scoring Results. We use 150 pieces of test data to test two different neural network scoring models and calculate three evaluation indexes introduced in

the first section of this paper to comprehensively evaluate the performance of the two scoring models.

Figures 16 and 17 are the prediction results of oral comprehensive evaluation of BP scoring model and CNN + LSTM scoring model, respectively. It is found from the figure that BP model shows better fitting effect than CNN + LSTM model. In addition, from the lowest students' scores, BP neural network shows better adaptability in the face of extreme values (minimal and maximal). As shown in

TABLE 3: Correlation between phonetic features and manual scores.

Phonetic features	Pearson correlation coefficient
articulationRate	0.38
numSilence	0.45
posteriorScore	0.32
speakingRatio	0.43

TABLE 4: Correlation between text class features and manual scoring.

Text class feature	Pearson correlation coefficient
contentLength	0.58
uniqueWords	0.60
parseTreeDepth	0.28
semanticSimilarity	0.34
goodGrammerRatio	0.25

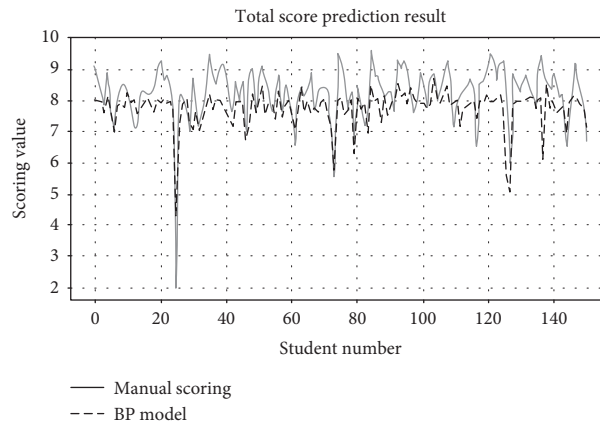


FIGURE 16: Scoring results of BP model.

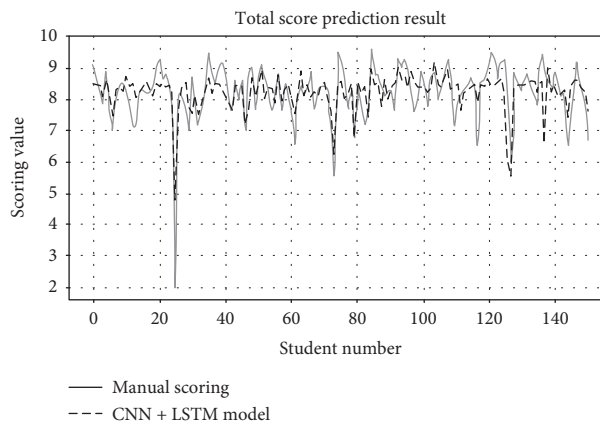


FIGURE 17: Scoring results.

TABLE 5: Performance evaluation of scoring model.

	Pearson correlation	Average difference	Accuracy
Between manual scoring	0.764	0.485	—
BP model	0.695	0.645	82.6%
CNN + LSTM model	0.545	0.602	80.1%

Table 5, the performance of Pearson correlation coefficient and accuracy of BP model is better than that of CNN + LSTM model, and the evaluation of the two machines is highly correlated. In the average difference index, CNN + LSTM is slightly better than BP model.

5. Conclusion

Firstly, this paper introduces the overall design and scoring process of the scoring system. After that, the detailed designs of voice noise reduction module, speech recognition module, data processing module, and scoring model module are explained, respectively.

Then, we analyze the experimental results of the oral scoring system and evaluate the performance of the scoring model. This paper introduces three evaluation indexes to evaluate the performance of the model. There are Pearson correlation coefficient, average score difference of man-machine evaluation, correctness of scoring model, and so on. After using these evaluation indexes to analyze the training and evaluation results of the evaluation model, it is found that the comprehensive evaluation performance of BP model is higher than that of CNN + LSTM scoring model when the data set is small. The spoken language scoring model is based on deep learning or other algorithm models, and there are different scoring effects under different algorithms, which lead to different scoring differences. Therefore, the later work to solve this problem needs to combine the advantages of different algorithms for fusion research.

Data Availability

The experimental data used to support the findings of this study are available from the corresponding author upon request.

Conflicts of Interest

The authors declare that they have no conflicts of interest regarding this work.

Acknowledgments

This work was sponsored in part by the Anhui University of Science and Technology School of Foreign Languages Curriculum Ideological and Political Project and Anhui University of Science and Technology University Student Innovation and Entrepreneurship Project.

References

- [1] A. Bartolomeo, S. Shukla, H. A. Westra, N. S. Ghashghaei, and A. Olson, "Rolling with resistance: a client language analysis of deliberate practice in continuing education for psychotherapists," *Counselling and Psychotherapy Research*, vol. 21, no. 2, pp. 1–9, 2020.

- [2] J. Buendgens-Kosten, "The monolingual problem of computer-Assisted Language learning," *ReCALL*, vol. 32, no. 3, pp. 307–322, 2020.
- [3] T. Yamaguchi, W. Endo, and Y. Shinoda, "Interrogation system with automatic recognition and delay correction functions of fiber bragg gratings by pulse modulation with wavelength-swept laser," *IEEE Sensors Journal*, vol. 19, no. 22, Article ID 10519, 2019.
- [4] J. Joseph, Z. E. H. Moore, D. Patton, T. O'Connor, and L. E. Nugent, "The impact of implementing speech recognition technology on the accuracy and efficiency (time to complete) clinical documentation by nurses: a systematic review," *Journal of Clinical Nursing*, vol. 29, no. 13-14, pp. 2125–2137, 2020.
- [5] M. D. Kiselev and O. E. Pudovikov, "Optimization of parameters of automatic speed control system of a freight train with distributed traction," *Russian Electrical Engineering*, vol. 91, no. 9, pp. 568–576, 2020.
- [6] T. Lin and X. Liu, "An intelligent recognition system for insulator string defects based on dimension correction and optimized faster R-CNN," *Electrical Engineering*, vol. 103, no. 6, pp. 1–9, 2021.
- [7] A. Loukina and H. Buzick, "Use of automated scoring in spoken language assessments for test takers with speech impairments," *ETS Research Report Series*, vol. 2017, no. 1, pp. 1–10, 2017.
- [8] Y. Wang, M. J. F. Gales, K. M. Knill et al., "Towards automatic assessment of spontaneous spoken English," *Speech Communication*, vol. 104, pp. 47–56, 2018.
- [9] J. Zhang, D. Fang, W. Zhao et al., "An Improved Biomedical Event Trigger Identification Framework via Modeling Document with Hierarchical Attention," in *Proceedings of the 2019 IEEE International Conference on Bioinformatics and Biomedicine (BIBM)*, pp. 583–589, IEEE, San Diego, CA, USA, November 2019.
- [10] H. Mohammadzadeh Jamalian, M. Tamjidi Eskandar, A. Chamanara, R. Karimzadeh, and R. Yousefian, "An artificial neural network model for multi-pass tool pin varying FSW of AA5086-H34 plates reinforced with Al 2 O 3 nanoparticles and optimization for tool design insight," *CIRP Journal of Manufacturing Science and Technology*, vol. 35, pp. 69–79, 2021.
- [11] M. Shirmohammadi, S. J. Goushchi, and P. M. Keshtiban, "Optimization of 3D printing process parameters to minimize surface roughness with hybrid artificial neural network model and particle swarm algorithm," *Progress in Additive Manufacturing*, vol. 6, pp. 1–17, 2021.
- [12] S. Bairoliya, A. Goel, W. Zhang, and B. Cao, "Laboratory preparation of monochloramine for environmental research: a comparison of four commonly used protocols," *Environmental Research*, vol. 197, no. 7, Article ID 111009, 2021.
- [13] B. Shao, C. Ni, J. Wang, and Y. Wang, "Research on venture capital based on information entropy, BP neural network and

- CVaR model of digital currency in Yangtze River Delta,” *Procedia Computer Science*, vol. 187, pp. 278–283, 2021.
- [14] N. Yang, H. Tang, J. Yue, X. Yang, and Z. Xu, “Accelerating the training process of convolutional neural networks for image classification by dropping training samples out,” *IEEE Access*, vol. 8, Article ID 142393, 2020.
- [15] G. Li, H. Tang, Y. Sun, J. Kong et al., “Hand gesture recognition based on convolution neural network,” *Cluster Computing*, vol. 22, no. 2, pp. 2719–2729, 2019.
- [16] J. Feng, S. Cai, and X. Ma, “Enhanced sentiment labeling and implicit aspect identification by integration of deep convolution neural network and sequential algorithm,” *Cluster Computing*, vol. 22, no. 6, pp. 1–19, 2019.
- [17] H. S. Das and P. Roy, “A deep dive into deep learning techniques for solving spoken language identification problems,” *Intelligent Speech Signal Processing*, vol. 2019, pp. 81–100, 2019.
- [18] G. Jorge-Botana, R. Olmos, and J. M. Luzón, “Bridging the theoretical gap between semantic representation models without the pressure of a ranking: some lessons learnt from LSA,” *Cognitive Processing*, vol. 21, no. 1, pp. 1–21, 2020.
- [19] D. Wu, R. Yang, and C. Shen, “Sentiment word co-occurrence and knowledge pair feature extraction based LDA short text clustering algorithm,” *Journal of Intelligent Information Systems*, vol. 56, no. 20, pp. 1–23, 2020.
- [20] C. Ke, Z. Jiang, H. Zhang, Y. Wang, and S. Zhu, “An intelligent design for remanufacturing method based on vector space model and case-based reasoning,” *Journal of Cleaner Production*, vol. 277, Article ID 123269, 2020.

Research Article

Analysis of Key Indicators in English Teaching Evaluation Based on Big Data Model

Weili Hou 

School of Foreign Languages, Yulin University, Yulin 719000, China

Correspondence should be addressed to Weili Hou; houweili@yulinu.edu.cn

Received 23 November 2021; Accepted 27 December 2021; Published 18 January 2022

Academic Editor: Man Fai Leung

Copyright © 2022 Weili Hou. This is an open access article distributed under the Creative Commons Attribution License, which permits unrestricted use, distribution, and reproduction in any medium, provided the original work is properly cited.

With the advent of the era of big data, the traditional English teaching methods in the past can no longer accurately assess the comprehensive level of English teachers and classrooms because of various factors. In order to reexamine and plan English teaching content, based on the big data model, we will carefully analyze the key indicators in English teaching evaluation using computer technologies such as particle swarm optimization and support vector machine, hoping to dig out the characteristics of English education in a deeper way, so as to make a series of index adjustments to English classroom and improve English teaching level. The results of this study show the following: (1) The average accuracy of the evaluation index of the model designed in this study is as high as 96.56%; after 20 tests, the test time of this model method is the least, and the test time can be as low as 13.32 ms. (2) For eight first-class indexes of A, B, C, D, E, F, G, and H and 29 second-class indexes, the expert scores are all greater than 3.66, and the standard deviation is all less than 1, which accords with the standard of reaching common opinions. The key index test system is reasonable. (3) We find that the weights of A2, D1, H1, and H2 are all higher than 0.5, the weights of A1, B3, C5, E5, F4, and G4 are all higher than 0.3, and the weights of other indexes are all less than 0.3. This shows that each index has a different weight and emphasis on English teaching evaluation. (4) Taking a certain teacher as an example to assess English proficiency can effectively analyze the key indicators of English teachers and enable the teacher to make corresponding improvements and formulate strategies. On the whole, the teacher has strong writing ability and listening ability; the ability of speaking and translating is slightly weak, both of which are about 0.8; for listening analysis, idiom and sentence ability are generally to be enhanced, about 0.8. (5) The comprehensive scoring of English teaching is carried out, large difference in scoring values is avoided, and fairer test results are given. It is found that after big data analysis, the key indicators of English are analyzed accurately, the classroom teaching is diversified, and the students' final classroom evaluation reflects well, so this method has obvious advantages.

1. Introduction

With the increasing affluence of people's lives, both material and spiritual conditions have been greatly increased, and the demand for education and related standards has also been improved. How to use the key indicators of teaching to evaluate the quality of higher education is very important, which can help educators understand the needs of students and teachers and make a series of adjustments. Taking English teaching evaluation as an example, English teaching evaluation represents English teachers' ability and teaching quality, which can evaluate whether students' education meets the standards from various key indicators and accurately reflect the characteristics of English as a subject and

students' educational needs. With the wide application of big data boom at home and abroad, it is an inevitable trend to use big data model to mine demand characteristics when evaluating teaching analysis indicators. To better measure and evaluate English teaching content, this study makes a comprehensive analysis and comparison of English teaching characteristics based on big data model, assisted by support vector machine, particle swarm optimization, and other contents, from teaching theory to actual teaching feedback. This study provides a lot of theoretical support according to the achievements and documents made by predecessors. Literature [1] analyzes the best teaching mode in big data environment and applies it to college English teaching. Literature [2] analyzes the current situation and hot spots of

college English textbook compilation with the help of big data and CiteSpace software. Literature [3] analyzes the influence of big data on college English education. Literature [4] examines “general chemical effects” and analyzes the class size and teaching evaluation. Literature [5] evaluates the overall teaching effect of higher education institutions. Literature [6] constructs a teaching quality data monitoring platform to improve the supervision level of teaching data literacy. Literature [7] integrates big data information fusion and K-finger clustering algorithm to realize clustering and integration of English teaching ability index parameters. Literature [8] analyzes the characteristics of English teachers’ educational ability in a massive open online course (MOOC) environment with a fuzzy C method algorithm. Based on big data analysis, literature [9] discusses the selection and acquisition of teaching resources, the trajectory analysis of teaching and learning behaviors, teaching monitoring and evaluation, etc. Literature [10] establishes an “online + offline” hybrid learning model based on a large amount of data and analyzes the feasibility of combining online and offline English classes in colleges and universities. Literature [11] realizes feature clustering and multiple regression analysis and realizes quantitative evaluation of the correlation between college English teaching mode reform and performance. Literature [12] uses big data analysis to study the evaluation methods of students’ English classroom performance. Literature [13] uses big data analysis technology to construct a college English TQA model and obtains high-precision English teaching quality evaluation results. Literature [14] combines subjectivity and objectivity and applies data mining technology to the evaluation of English teaching quality. Literature [15] reconstructs the monitoring mode of autonomous English learning under the background of big data and establishes an effective comprehensive evaluation system. The method proposed in the above literature discusses English teaching in combination with other issues in depth and gains advantages in the process of English teaching through evaluation. However, the accuracy and efficiency of the evaluation are low in the research process of the above methods. This study proposes a literature review on big data model and English teaching evaluation and refers to the experience of predecessors in many aspects, such as integrating big data information fusion and establishing blended learning model based on large amounts of data, to help us select research methods and applications appropriate to this topic from practice. The method proposed in this study uses big data to analyze and make decisions, and the analysis results are studied and analyzed. The model can effectively extract the characteristics and needs of English teaching. It can help to improve the efficiency of modeling and reduce the workload of researchers. The hybrid model includes particle swarm optimization and support vector machine, which effectively improves the accuracy and efficiency of teaching index evaluation and can give fairer test results based on data.

2. Theoretical Basis

2.1. Big Data Model. Big data first appeared in the information technology (IT) industry. With the in-depth study of it by researchers, the world is quietly setting off a wave of big data. After deep mining of data information, big data interpret the elegant demeanour of the world from a new angle. People are surprised to find that what lurks under ordinary data information is not an iceberg, but a whole brand-new world. Various optimized application technologies based on big data are constantly emerging. It is common to make analysis decisions and research and analysis with big data, which further illustrates versatility and availability.

Big data application [16] describes business requirements and patterns, uses big data to build models [17], mines data features from huge data [18], and proposes problem solutions. These workflows can be carried out using professional data modeling tools: PowerDesigner, Sparx Enterprise Architect, CA Erwin, ER/Studio, etc. Making good use of the above tools can help improve modeling efficiency and reduce the workload of modelers. Figure 1 shows several common big data analysis models.

In the fields of big data, artificial intelligence, biomedicine, etc., the Bayesian formula, a very important mathematical formula given by Laplace [19], is used. A denotes event A , B denotes event B , and P denotes probability [20]:

$$P\left(\frac{A}{B}\right) = P\left(\frac{B}{A}\right) * \frac{P(A)}{P(B)}. \quad (1)$$

2.2. English Teaching. English is a common language in the world. Since the 1990s, the teaching methods and means of English in colleges and universities have gradually become rich and varied, and teachers are no longer instilling the content of this language as before. The quality of English teaching in colleges and universities is improved, the fairness and rationality of English teaching indicators are ensured, and an excellent English teaching system is established [21]; these are the enduring hot topics and key tasks of the education department.

Traditional English teaching mainly depends on the teaching methods and contents of teachers, which has strong and distinct personal characteristics and styles of teachers. The teaching quality is uneven, and the teaching evaluation is difficult to evaluate. The key teaching indicators are mainly teachers’ methods, contents, effects, etc., which have great autonomy and are difficult to judge accurately. Teaching results often vary from person to person, which leads to the uncertainty of students’ English literacy and level. To cultivate students’ English ability and use language tools flexibly, we need the help of science and technology. Big data mining technology is used to mine the indicators that are easily overlooked in English teaching, and the evaluation indicators that were originally roughly divided from all aspects and angles are refined comprehensively; only by

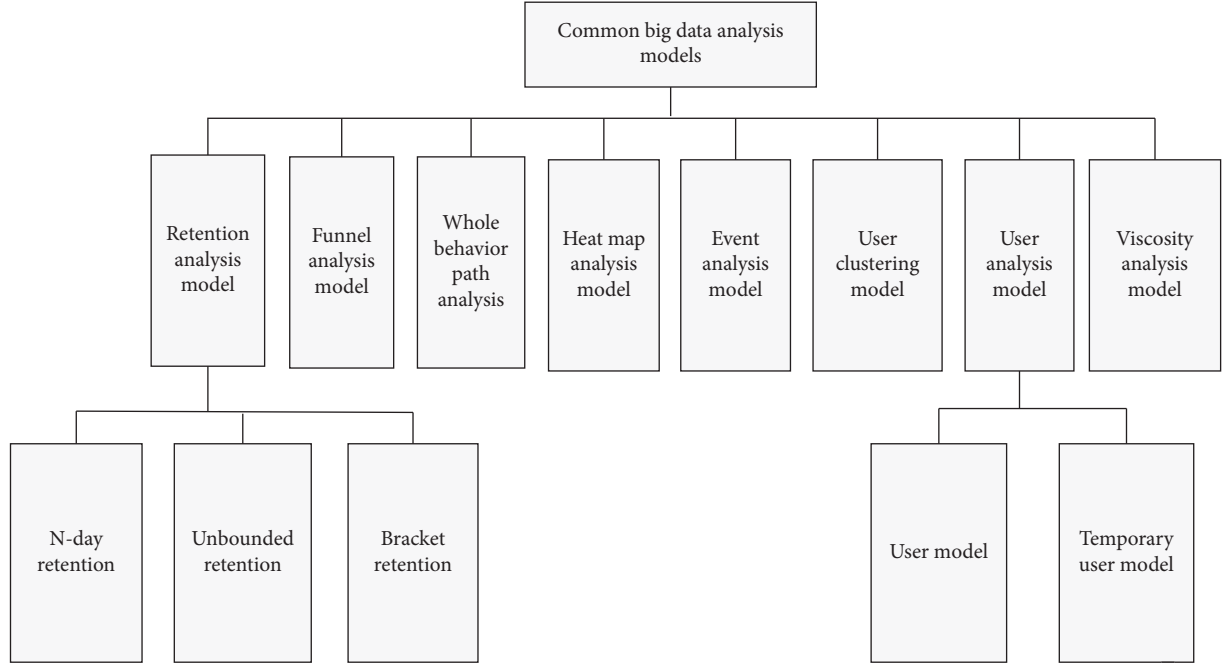


FIGURE 1: Big data analysis model.

adding objective evaluation factors as much as possible can educators design a scientific evaluation system for English teaching and teachers to find and solve practical problems in students' learning process.

2.3. *Support Vector Machines.* Support vector machine (SVM) is a binary classification model, which belongs to one of the machine learning algorithms, and is mainly used for classification and regression analysis. Least-squares support vector machines [22] are used. w represents the weight vector, b represents the deviation, and the linear regression function is as follows:

$$y = w^T x + b. \quad (2)$$

In high-dimensional eigenspace, $\varphi(x)$ is a nonlinear mapping:

$$f(x) = w^T \varphi(x) + b. \quad (3)$$

The optimization objective function and constraints are as follows:

$$\min = \frac{1}{2} \|w\|^2 + \frac{1}{2} c \sum_{i=1}^l e_i^2, \quad (4)$$

$$\text{s.t. } w^T \varphi(x_i) + b + e_i = y_i, \quad i = 1, 2, \dots, l.$$

The Lagrange multiplier (denoted by λ) [23] is introduced to solve unconstrained optimization problems:

$$\min J = \frac{1}{2} \|w\|^2 + \frac{1}{2} c \sum_{i=1}^l e_i^2 - \sum_{i=1}^l \lambda_i (w^T \varphi(x_i) + b + e_i - y_i). \quad (5)$$

According to the Karush–Kuhn–Tucker (KKT) optimization conditions:

$$\frac{\partial L}{\partial w} = 0 \Rightarrow w = \sum_{l=1}^L a_l \varphi(x_l),$$

$$\frac{\partial L}{\partial b} = 0 \Rightarrow \sum_{l=1}^L a_l = 0, \quad (6)$$

$$\frac{\partial L}{\partial e_i} = 0 \Rightarrow a_i = \gamma e_i,$$

$$\frac{\partial L}{\partial a_i} = 0 \Rightarrow \gamma_i - w^T \varphi(x_i) - b - e_i = 0.$$

The Gaussian kernel function is chosen:

$$K(x_i, x_j) = \exp\left(-\frac{\|x_i - x_j\|^2}{2\sigma^2}\right). \quad (7)$$

Regression estimation is as follows:

$$h(x_*) = \sum_{l=1}^L a_l K(x_*, x_l) + b. \quad (8)$$

The Gaussian kernel function chosen in this study is the most widely used one. In most cases, if you do not know what kernel function to use, the Gaussian kernel function is preferred. Both large and small samples have better performance. In addition, it has fewer parameters than the polynomial kernel function, so it is more convenient to use.

2.4. Particle Swarm Optimization. Particle swarm optimization (PSO) is a kind of swarm intelligence optimization algorithm. The core formula of particle swarm optimization algorithm is as follows:

$$\begin{aligned} v_i^d &= wv_i^{d-1} + c_1r_1(p \text{ best}_i^d - x_i^d) + c_2r_2(g \text{ best}^d - x_i^d), \\ x_i^{d+1} &= x_i^d + v_i^d. \end{aligned} \quad (9)$$

The calculation process is as follows:

$$f = \sum_{i=1}^N |y_i - y'_i|. \quad (10)$$

2.5. Decision Tree Algorithm. The decision tree algorithm [24] uses branch nodes to represent classification problems, predicts each path from root node to leaf node of decision tree corresponding to categories, and classifies information through a series of rules [25]; with the help of decision tree algorithm, we can find out the important factors behind teaching achievements.

Decision tree is a prediction model. The common decision tree algorithms include ID3 algorithm, C4.5 algorithm, CART algorithm, and random forest algorithm. The C4.5 algorithm is chosen, which is easy to understand classification rules and has high accuracy:

(1) Information entropy

$$H(D) = - \sum_{k=1}^K \frac{|c_k|}{|D|} \log_2 \frac{|c_k|}{|D|}. \quad (11)$$

(2) Conditional entropy

$$H(D|A) = - \sum_{k=1}^n \frac{|D_i|}{|D|} \left(\sum_{k=1}^K \frac{|D_{ik}|}{|D_i|} \log_2 \frac{|D_{ik}|}{|D_i|} \right). \quad (12)$$

(3) Information gain

$$\text{Gain}(D, A) = H(D) - H(D|A). \quad (13)$$

(4) Calculated gain ratio

$$\begin{aligned} \text{Gain}_{\text{ratio}}(D, A) &= \frac{\text{Gain}(D, A)}{H_A(D)}, \\ H_A(D) &= - \sum_{k=1}^n \frac{|D_i|}{|D|} \log_2 \frac{|D_i|}{|D|}. \end{aligned} \quad (14)$$

(5) Predicting random forest

$$H(x) = \arg \max_{t=1}^T (h_t(x) = y) \cdot (x \notin D_t). \quad (15)$$

(6) No pruning needs to meet conditions

$$\begin{aligned} &E(\text{Misjudgment times of subtree}) \\ &+ \text{std}(\text{Misjudgment times of subtree}) \quad (16) \\ &< E(\text{Misjudgment times of leaf nodes}). \end{aligned}$$

(7) Pruning condition

$$\begin{aligned} &E(\text{Misjudgment times of subtree}) \\ &+ \text{std}(\text{Misjudgment times of subtree}) \quad (17) \\ &\geq E(\text{Misjudgment times of leaf nodes}). \end{aligned}$$

3. Model Design and Method

3.1. Research, Analysis, and Design. Using scientific tools to analyze the key indicators of English teaching is focused, and the improved method with the original one after feedback is compared. By referring to various related literature studies at home and abroad, using theoretical basis and analysis of the current situation of English teaching, this study constructs a complete system for analyzing English teaching evaluation indicators, as shown in Figure 2.

In order to ensure sufficient theoretical support for the study, this study uses a variety of research methods, such as literature review, questionnaire survey, Delphi method, and data analysis, and invites relevant English education experts to give their opinions and guidance. After determining the research content and theme, the rational use of contemporary scientific and technological strength, a big data analysis model, and a hybrid model of support vector machine and particle swarm optimization, which can assist the big data model to process data samples, are preliminarily constructed. Let the two models as the carrier of the analysis work improve the test index system to establish a new test index system for English teaching. Finally, according to the experimental data, the advantages and disadvantages of this method are summarized and analyzed.

3.2. Big Data Analysis Model. Huge data information needs to be mined, managed, and traced. We build an analysis data model of big data, choose the core idea of Ralph Kimball's dimension model to model, and refer to the implementation method of OneData model. As shown in Figure 3, we introduce the core functions of OneData tools.

As shown in Figure 3, the OneData tool has three core functions: specification definition, detailed model design, and summary model design. Under these three core functions, there are different specific functions.

The model follows the principles of consistency, clarity and efficiency, high cohesion, and low coupling. Data research: the business system is understood and the needs are analyzed; the business process or dimension is abstractly collected, the data domain is divided, the bus rectangle is constructed, and the statistical index is defined; code development: ETL tasks for deployment and operation and

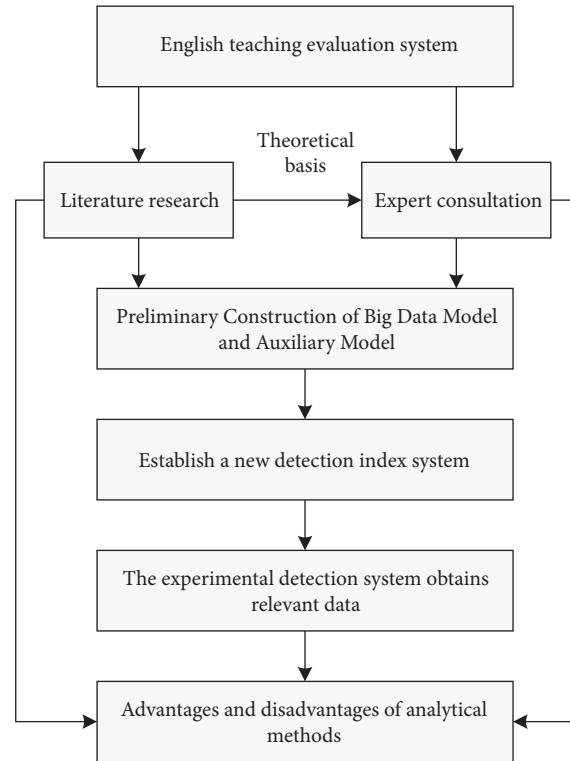


FIGURE 2: English teaching evaluation system.

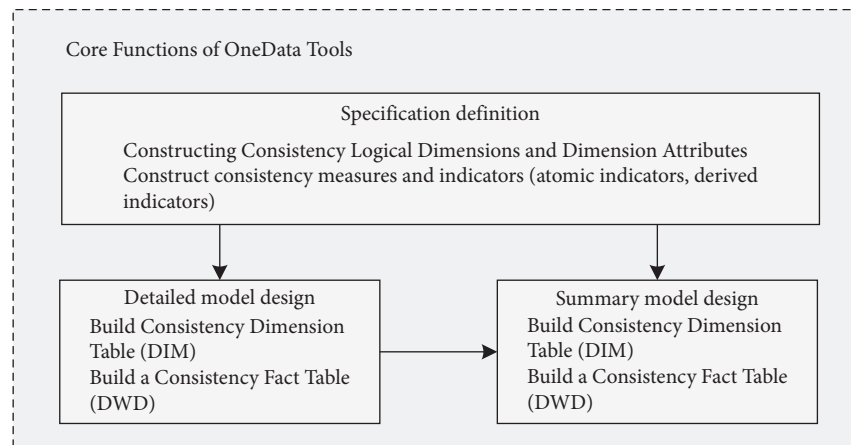


FIGURE 3: Core functionality of the OneData tool.

maintenance are generated. Figure 4 shows the architecture of the model.

As shown in Figure 4, the data import layer (ODS) is mainly responsible for importing basic data into Max-Compute and recording the historical changes in basic data. The common data layer (CDM) mainly completes data processing and integration, establishes consistent dimensions, constructs reusable detailed fact tables for analysis and statistics, and summarizes indicators of common granularity. After ODS and CDM processing, it is processed by personalized analysis, data retrieval, and data application layer.

3.3. Hybrid Model of Support Vector Machine and Particle Swarm Optimization. The purpose of this model is to assist the big data analysis model to analyze English teaching evaluation indicators. To improve the accuracy and efficiency of teaching index evaluation, the particle swarm optimization algorithm searches the parameters of least-squares support vector machine, and the particle swarm optimization algorithm solves the optimal solution of the parameters of least-squares support vector machine, optimizing the evaluation process and making a mixed model. Figure 5 illustrates a flow chart of processing data samples by particle swarm optimization algorithm and support vector machine.

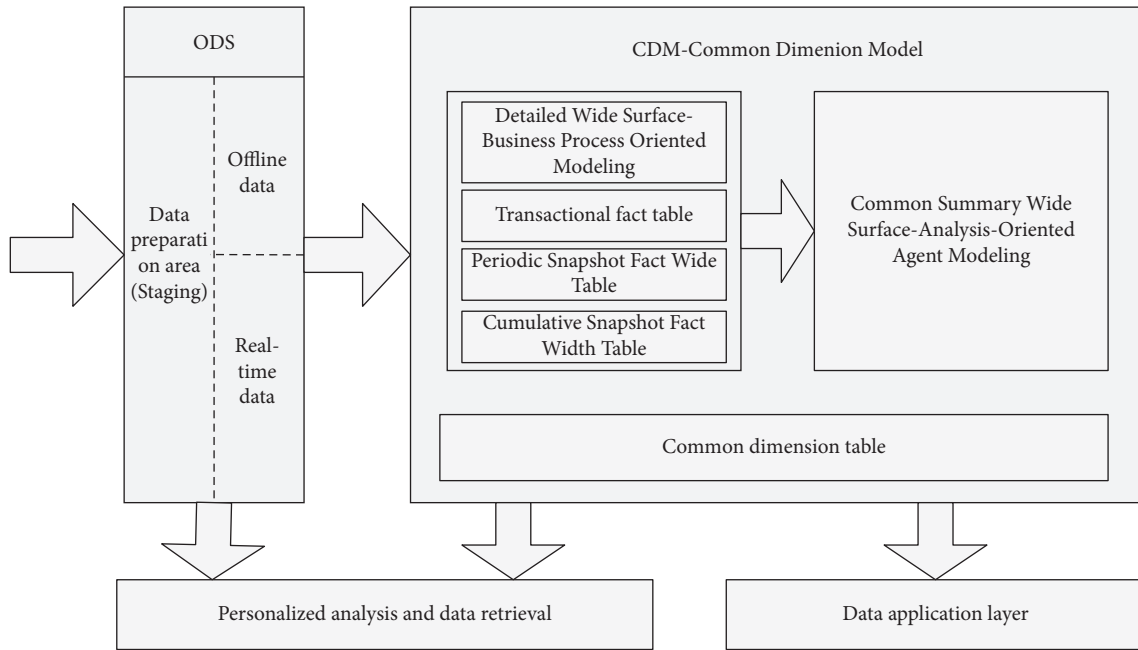


FIGURE 4: Big data model architecture.

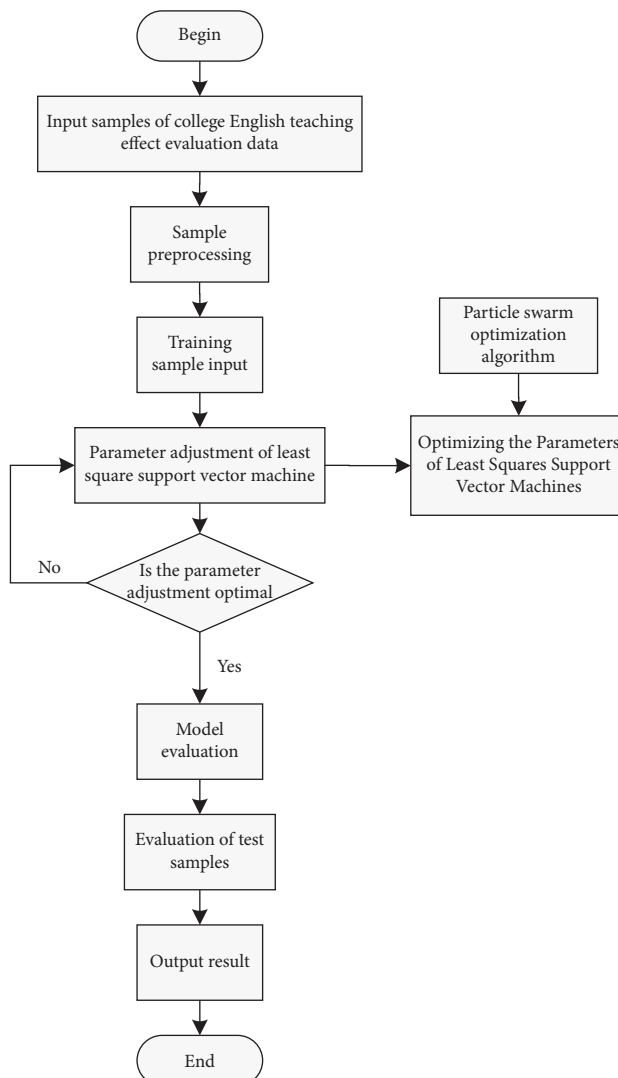


FIGURE 5: Flow chart of data sample processing by particle swarm optimization algorithm and support vector machine.

3.4. Index System Analysis. The evaluation index follows the principles of scientificity, universality, comparability, systematicness, and conciseness. The content of the original index system is simple, the evaluation of human factors is large, and there is no specific standard. To improve the evaluation index system of English teaching, we consulted 10 well-known college English education experts from different levels, and the specific proportion is shown in Figure 6.

We are generally divided into two parts—the student part and the teacher part. Compared with before, we add more feedback evaluation indicators from the student part, to evaluate the teacher’s English teaching more comprehensively from the perspective and experience of students. We set up three first-level indicators in the student part and five first-level indicators in the teacher part and design two-level indicators with different numbers under each first-level indicator. As shown in Table 1, the evaluation index system of college English teaching is listed, which lists all the evaluation criteria of secondary indexes.

In particular, it is stated here:

- (1) Determining the weight of each index reflects the importance level of an index, X represents the ranking corresponding score, Y represents the weight coefficient, n represents the total number of experts, and N represents the ranking number. The calculation formula of index weight coefficient is as follows:

$$Y = \frac{\sum X \cdot n}{N \cdot \sum X} \quad (18)$$

- (2) The evaluation part of students’ English ability can include five parts: listening, speaking, reading, writing, and translation, which are represented, respectively. The calculation formula of their overall scores can be expressed as follows:

$$\begin{aligned} \text{Score}_{\text{English}} &= \text{Score}_{\text{Listening}} \times W_L + \text{Score}_{\text{Oral}} \times W_O \\ &+ \text{Score}_{\text{Reading}} \times W_R + \text{Score}_{\text{Writing}} \times W_W \\ &+ \text{Score}_{\text{Translation}} \times W_T. \end{aligned} \quad (19)$$

4. Experimental Analysis

4.1. Model Testing. This part mainly tests the model constructed in this study and selects the English classroom teaching evaluation of the same major in a certain university as the test sample (a total of 200 data samples), which is divided into 10 groups with 20 data samples in each group. To see the test results of this model method more intuitively, the traditional evaluation model, the optimized BP neural network model, and the category weighted grey target decision model are selected for comparative analysis, as shown in Figure 7.

From Figure 7, we can find that the accuracy of English teaching evaluation index of this model method is the highest, and the average evaluation accuracy is as high as

96.56%; compared with the other three methods, this method is 7% higher than the optimized BP neural network method, 18.68% higher than the class-weighted grey target decision method, and 29.49% higher than the traditional method. Therefore, this method has the highest accuracy and the best effect, and its superiority can be seen.

Using these four model methods to test 20 times, respectively, comparing their test time, we can find that the test time of this model method is the least, and the test time can be as low as 13.32 ms. The specific data comparison is shown in Figure 8.

4.2. Index Scoring Results. Although the evaluation index system of English teaching created by us has been agreed upon, it still needs to be evaluated by experts in the field of English education for each first-level index and second-level index. It is necessary to ensure the rationality of each index, define the score with 1 to 5 points, and collect the average value, mode, and standard deviation of the score; according to Osborn, if more than two-thirds of the experts’ score is above 4 (i.e., the average score of experts is above 3.66), it can be considered that all ten experts have reached a common opinion on this index. Excel is used to count the data of experts on the first-level index and the second-level index, as shown in Figures 9 and 10.

As shown in Figure 9, we can find that the expert scores of eight first-class indicators of A, B, C, D, E, F, G, and H are all greater than 3.66, and the standard deviation is all less than 1. Moreover, only one expert gives 4 points, and the other indicators are all 5 points, which meets the standard of reaching common opinions. Therefore, we can judge that ten experts have reached a consensus on the first-class index. When we observe the data shown in Figure 10, we can find that the average scores of 29 secondary indicators are all greater than 3.66 points, which meets our evaluation criteria, and the standard deviation is all less than 1. All 29 secondary indicators have reached the standard. According to the evaluation results of all indicators, the test system of key indicators in English teaching evaluation in this study is reasonable and meets the requirements of this study.

4.3. Comparison of Indicator Weights. After scoring the key test indicators of English teaching in this study reasonably, it is necessary to determine the weight of each indicator, as shown in Figures 11 and 12.

According to Figure 11, we can find that the weight of C index is the least, the weight of D index is as high as 0.205, and the weight of each first-level index is different, which means that each index has a different weight and emphasis for English teaching evaluation, and some indexes are the most important, while others are relatively less important, just a simple reference factor. According to Figure 12, we find that the four secondary indexes of A2, D1, H1, and H2 are all higher than 0.5, the six secondary indexes of A1, B3, C5, E5, F4, and G4 are all higher than 0.3, and the rest indexes are all less than 0.3.

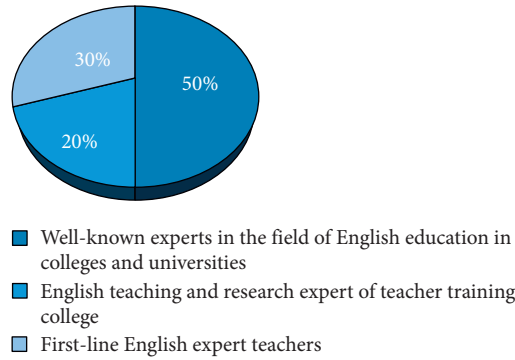


FIGURE 6: Proportion of expert types.

TABLE 1: Evaluation index system of college English teaching.

Classification	First-class index	Secondary index
Students	A English proficiency	A1 Listen, speak, read, write, and translate A2 Words, sentences, text, logical relations, idioms
	B Teacher evaluation	B1 Teachers' sense of responsibility B2 Teacher's seriousness in correcting homework B3 Teacher's attitude B4 Teachers' approval of ability
	C Teaching evaluation	Reasonable degree of C1 course content The quality of C2 classroom atmosphere Does C3 course have practical significance? The organization and hierarchy of C4 lectures C5 Vividness of teaching skills
Teachers	D Teaching Plan	D1 formulates a comprehensive curriculum ideological and political teaching plan and selects teaching contents rich in ideological and political elements D2 adjusts the teaching plan in time to ensure that it is completed on time E1 is full of teaching content and large amount of information E2 teaching content can reflect or connect with the development frontier of the subject
	E Teaching methods	E3 organizes diversified ideological and political teaching forms, which can effectively use multimedia teaching E4 open classes or elective courses E5 participates in the construction of online teaching resources E6 undertakes teaching reform projects or publishes teaching-related papers and monographs, etc.
	F Teaching process	F1 teaching content conforms to the syllabus, and the amount of lecture information is reasonable and rich F2 English phonetic standard, language flow 1 smooth; explains the problem with clear thinking and clear rules Chu; can highlight key points, disperse difficulties, and grasp key points
	G Teaching attitude	F3 caring for students, teaching and educating people, enhancing the sense of contrast between China and the West, enhancing the ability of value speculation, improving cultural self-confidence, enhancing cultural comparison ability, and cultivating philosophical consciousness F4 class is full of energy, infectious, and can attract students' attention G1 is serious about teaching work and strictly manages classroom discipline G2 answers students' questions seriously, and both teaching and learning learn from each other
	H Teaching effect	G3 attaches importance to homework information feedback, makes timely comments, and completes performance registration G4 class time arrangement is reasonable, not late, not delayed The H1 course has a high degree of ideological and political participation, and the effectiveness of educating people is in line with the society

4.4. *Teacher Ability Assessment.* The evaluation system of key indicators of English teaching based on big data model established in this study can be formally tested after evaluation. This test is mainly aimed at English proficiency, and

the evaluation criteria for English proficiency data analysis are shown in Table 2.

The decimals in Table 2 represent the weight ratio of the index for the English proficiency level. For example, the

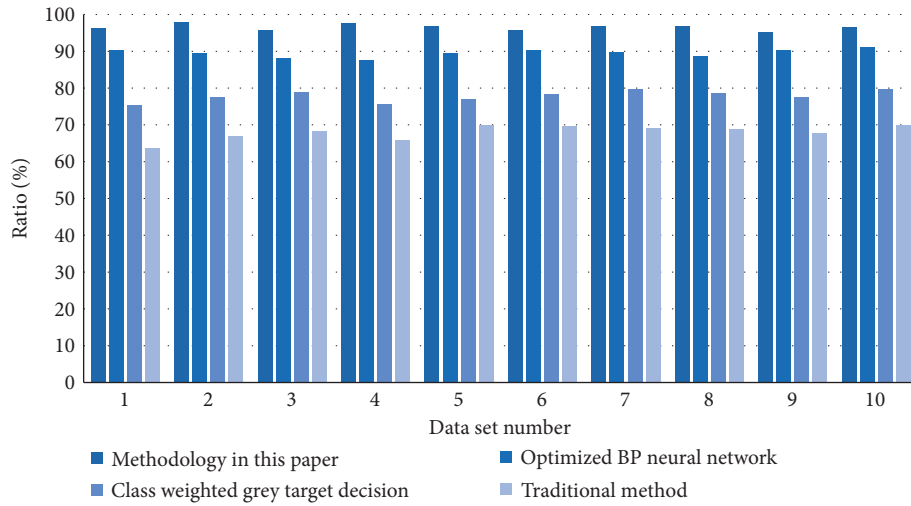


FIGURE 7: Comparison results of evaluation accuracy.

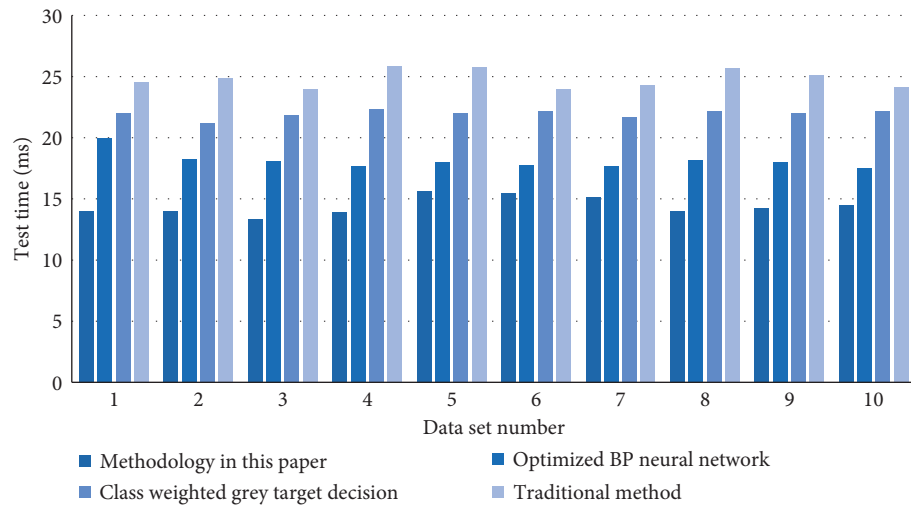


FIGURE 8: Comparison of test time data.

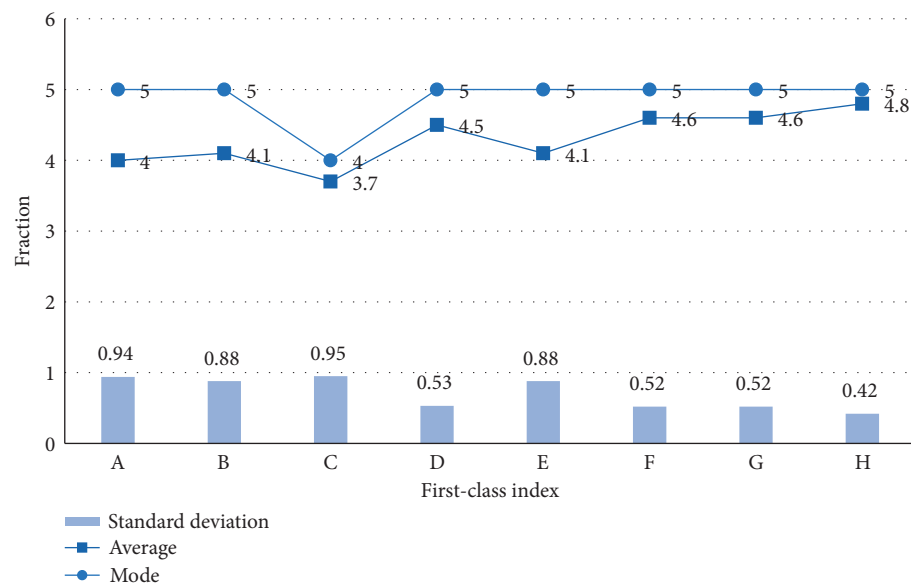


FIGURE 9: Scoring statistics of first-class indicators.

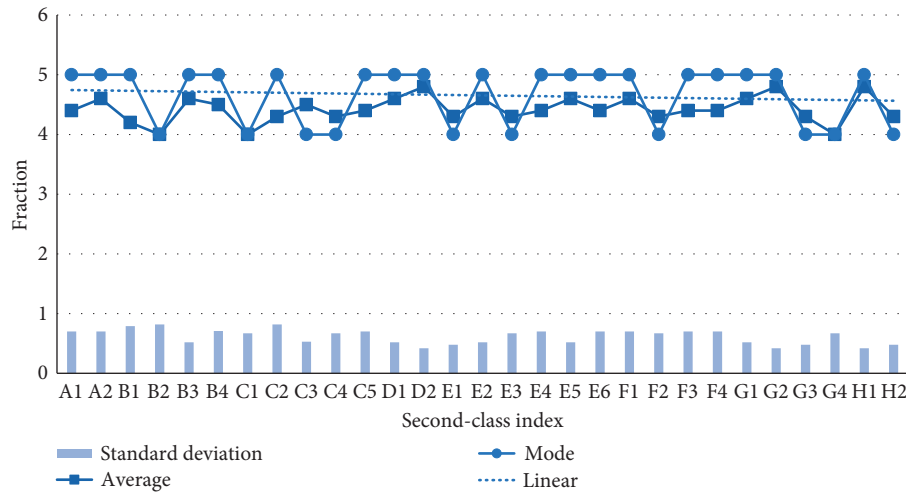


FIGURE 10: Scoring statistics of secondary indicators.

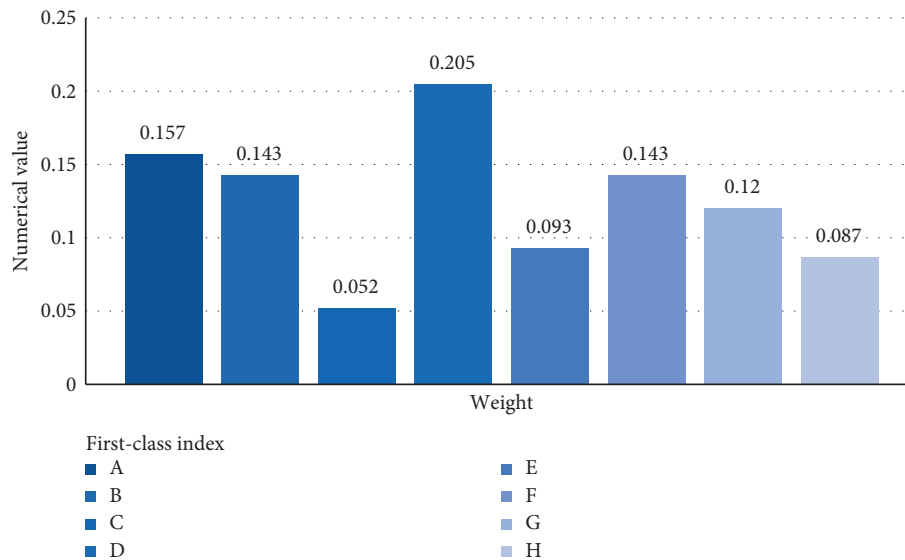


FIGURE 11: Weight of first-level indicators.

weights of the five subordinate indicators of listening are 0.2 for words, 0.2 for sentences, 0.2 for texts, 0.3 for logical relations, and 0.1 for idioms. The weights of the five indicators add up to exactly 1. The remaining indicators are the same.

As shown in Figure 13, we first invited a teacher to test and analyze his English proficiency. The scores measured by this model and index system are compared with those obtained by the original evaluation system, and we can find that there is little difference in the evaluation of his listening, speaking, and translation abilities, while the results of reading and writing abilities are relatively deviated due to different evaluation standards due to subjective factors. The method in this study can effectively correct the errors and make an accurate judgment of the teacher’s ability. On the whole, the teacher’s writing ability is extremely strong and his listening ability is strong; however, the ability of speaking and translating is about 0.8, which needs further training and strengthening.

As shown in Figure 14, we further take the teacher’s listening ability as an analysis case for detailed test, and we can find that the evaluation and correction effect of text and logic relationship are the greatest, and both abilities are closest to the perfect score standard. However, the ability of idioms and sentences is relatively average, about 0.8, so the teacher needs to analyze and formulate strategies to improve his level according to these two points. Thus, the model test in this study can effectively analyze the key indicators of English teachers, and then, teachers can improve their abilities and correct their mistakes according to the relevant data.

Finally, we select 10 teachers of the same major to score English teaching comprehensively, of which students account for 0.5 and teachers account for 0.5. We can find that when there is a big difference between students’ scores and teachers’ scores, we can effectively integrate the two and give a fairer test result, as shown in Figure 15.

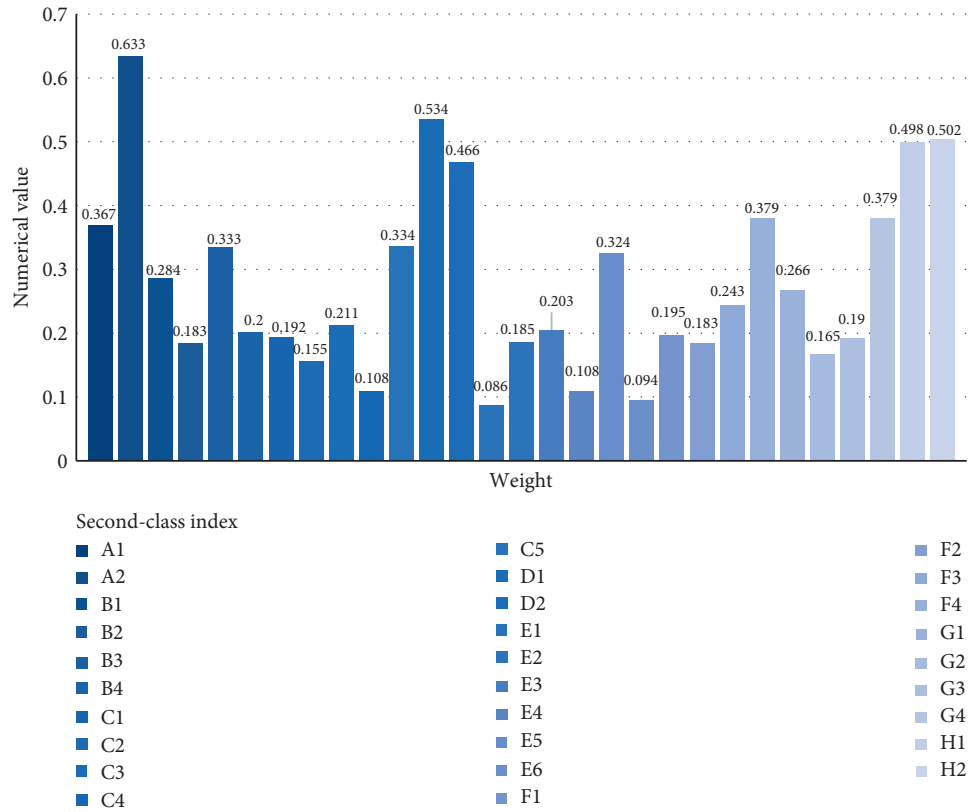


FIGURE 12: Weight of secondary indicators.

TABLE 2: Evaluation of English proficiency.

Name	Specific classification				
Listen	Word 0.2	Sentence 0.2	Text 0.2	Logical relation 0.3	Idiom 0.1
Say	Pronunciation 0.5	Broken sentence 0.3	Tone and intonation 0.2	—	—
Read	Vocabulary 0.3	Sentence pattern 0.3	Syntax 0.4	—	—
Write	Vocabulary 0.5	Format 0.2	Organizational structure 0.3	—	—
Translated	Interpretation 0.4	Translation 0.4	Shorthand 0.2	—	—

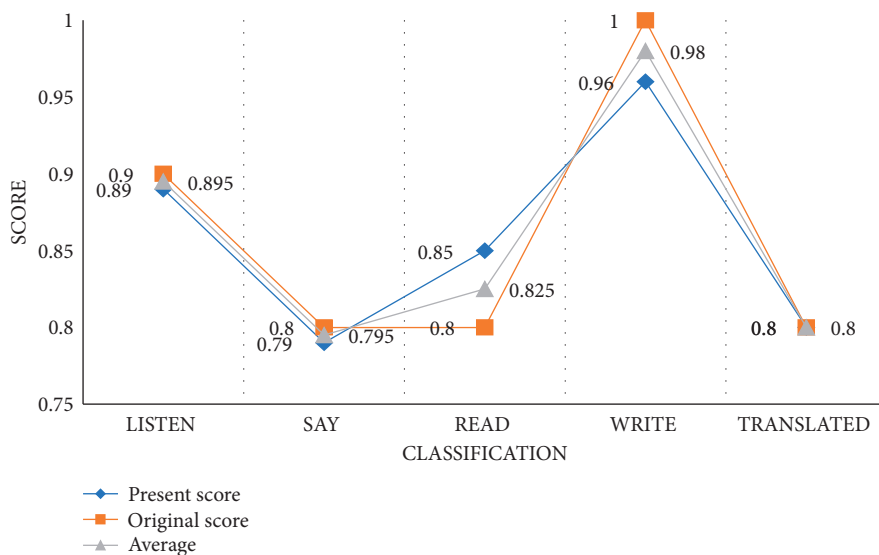


FIGURE 13: A teacher's English level.

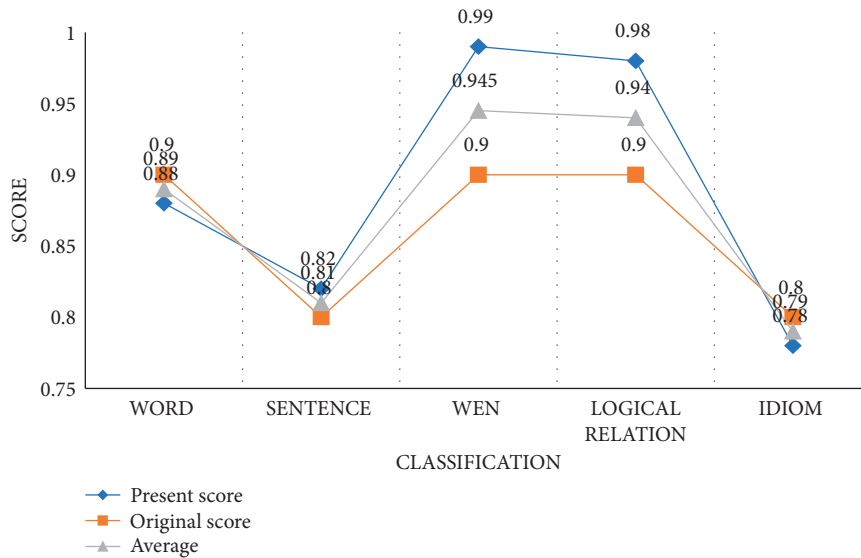


FIGURE 14: Analysis of a teacher's listening ability.

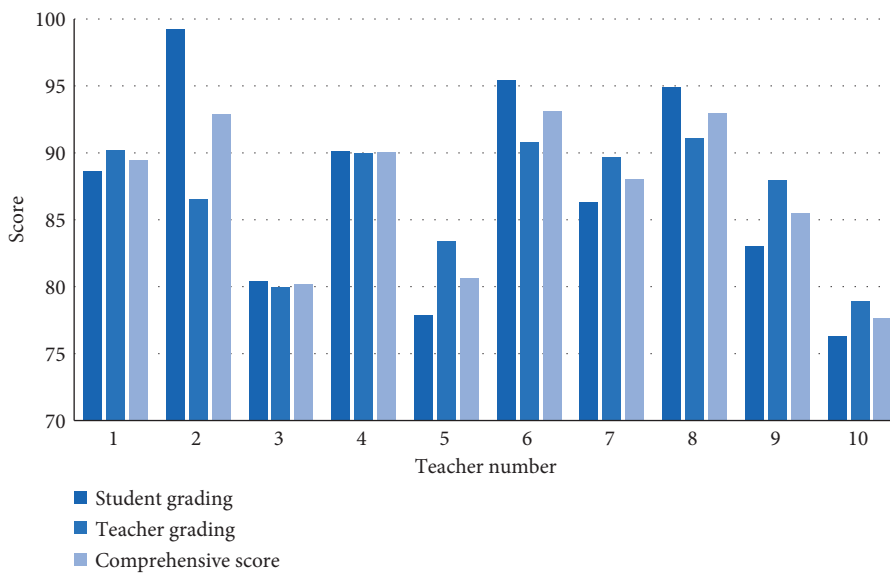


FIGURE 15: Comprehensive score.

The sample size of the evaluation was corrected by referring to the method of similar evaluation and repeating the experiment, so as to minimize random errors. The number of students participating in the scoring was determined to be 30 students of different majors, with a ratio of 3:1 to the number of teachers. Comprehensive scoring is to score each evaluation index according to the evaluation criteria of different indicators, and then, weighted addition is used to obtain the total score.

5. Conclusion

In the new era, teachers are given heavier responsibilities and obligations. How to be closer to the needs of society and students and how to accurately evaluate the overall level of

teaching quality, so as to better teach students to learn English content, are urgent tasks. The method proposed in this study to analyze English teaching evaluation indicators using big data model has the advantages of short evaluation time, high operation efficiency, clear key indicators, and best effect. It effectively extracts the characteristics of English teaching and students' needs, helps English teachers to improve the evaluation system of teaching effect and improve the comprehensive quality of classroom education, and has extremely important practical research significance.

The research results of this study show the following:

- (1) The average evaluation accuracy of the model designed in this study is as high as 96.56%; after 20 tests, the test time of this model method is the least, and the test time can be as low as 13.32 ms.

- (2) For eight first-class indexes of A, B, C, D, E, F, G, and H and 29 second-class indexes, the expert scores are all greater than 3.66, and the standard deviation is all less than 1, which accords with the standard of reaching common opinions. The key index test system is reasonable.
- (3) We find that the weights of A2, D1, H1, and H2 are all higher than 0.5, the weights of A1, B3, C5, E5, F4, and G4 are all higher than 0.3, and the weights of other indexes are all less than 0.3. This shows that each index has a different weight and emphasis on English teaching evaluation.
- (4) Taking a certain teacher as an example to assess English proficiency can effectively analyze the key indicators of English teachers and enable the teacher to make corresponding improvements and formulate strategies. On the whole, the teacher has strong writing ability and listening ability; the ability of speaking and translating is slightly weak, both of which are about 0.8; for listening analysis, idiom and sentence ability are generally to be enhanced, about 0.8.
- (5) The comprehensive scoring of English teaching is carried out, large difference in scoring values is avoided, and fairer test results are given.

Although the results of this method have obvious advantages, however, the test samples of this study only focus on the evaluation of English teaching-related indicators. The sample size is low and the test scope is not large, so the research conclusion of this study still has certain limitations and inaccuracy, which needs further research to verify its universality, make the whole English teaching evaluation system more complete and scientific, and strive to make big data-related technologies create more practical value.

Data Availability

The experimental data used to support the findings of this study are available from the corresponding author upon request.

Conflicts of Interest

The authors declare that they have no conflicts of interest regarding this work.

References

- [1] B. Peng, "Construction and application of the BEST teaching mode of college English in big data," *International Journal of Emerging Technologies in Learning*, vol. 12, no. 9, p. 41, 2017.
- [2] F. Mao, Q. Li, and W. U. Biyu, "A review on the compilation of college English textbooks in China based on big data," *English Teaching in China and America: English Edition*, vol. 18, no. 3, p. 6, 2021.
- [3] S. Zheng and S. Zhu, "Integration of big data and college English education," *Journal of Physics: Conference Series*, vol. 1646, Article ID 012059, 2020.
- [4] S. Toby, "Class size and teaching evaluation: or, the "general chemistry effect" revisited," *Journal of Chemical Education*, vol. 70, no. 6, pp. 465-466, 1993.
- [5] T. L.-P. Tang, "Teaching evaluation at a public institution of higher education: factors related to the overall teaching effectiveness," *Public Personnel Management*, vol. 26, no. 3, pp. 379-389, 1997.
- [6] C. Yu and J. Wang, "Analysis on the teaching evaluation of ideology and political Courses in universities in the era of big data," *Journal of Hebei Normal University for Nationalities*, vol. 39, no. 1, pp. 92-98, 2019.
- [7] Z. Chen, "Using big data fuzzy K-means clustering and information fusion algorithm in English teaching ability evaluation," *Complexity*, vol. 2021, no. 5, 9 pages, Article ID 5554444, 2021.
- [8] W. U. Junmin, "Empirical analysis of evaluation of English teachers' educational ability under MOOC environment," in *Proceedings of the 2018 International Conference on Intelligent Transportation, Big Data and Smart City (ICITBS)*, pp. 86-88, IEEE, Xiamen, China, January 2018.
- [9] S. Yang, "Analysis of practical path of college English teaching reform based on big data," in *Proceedings of the 2019 Asia-Pacific Conference on Advance in Education, Learning and Teaching (ACAELT 2019)*, Guangzhou, China, November 2019.
- [10] X. Yang, "Feasibility analysis of online and offline combination in college English classroom based on big data," in *Proceedings of the 2019 International Conference on Reform, Technology, Psychology in Education (ICRTPE 2019)*, pp. 26-30, New Delhi, India, October 2019.
- [11] Q. Wang and X. Q. Jiang, "Empirical study on reform model of college English teaching model based on computer and big data," in *Proceedings of the International Conference on Measuring Technology and Mechatronics Automation*, pp. 412-415, IEEE Computer Society, Changsha, China, February 2018.
- [12] W. Ma, "Study on the evaluation method of students' English classroom performance based on big data analysis," *International Journal of Continuing Engineering Education and Life Long Learning*, vol. 31, no. 1, p. 1, 2021.
- [13] J. Guo and S. Yu, "Evaluation model of college English teaching quality based on big data analysis," *IOP Conference Series: Materials Science and Engineering*, vol. 750, no. 1, p. 7, Article ID 012077, 2020.
- [14] J. Huizhen, "Construction of teaching evaluation system for integrated data mining," *IPPTA: Quarterly Journal of Indian Pulp and Paper Technical-A*, vol. 30, no. 7, pp. 891-897, 2018.
- [15] X. Sun, "Research on the construction of English autonomous learning monitoring mode under the background of big data," *Journal of Contemporary Educational Research*, vol. 5, no. 1, 2021.
- [16] A. McAfee and E. Brynjolfsson, "Big data: the management revolution," *Harvard Business Review*, vol. 68, no. 10, pp. 60-66, 2012.
- [17] C. Lynch, "How do your data grow?" *Nature*, vol. 455, no. 7209, pp. 28-29, 2008.
- [18] Y. Wen, J. Liu, W. Dou, X. Xu, B. Cao, and J. Chen, "Scheduling workflows with privacy protection constraints for big data applications on cloud," *Future Generation Computer Systems*, vol. 108, pp. 1084-1091, 2020.
- [19] M. Xiaofeng, "Big data management: concepts, techniques and challenges," *Journal of Computer Research and Development*, vol. 50, no. 1, pp. 146-169, 2013.

- [20] P. Davies and E. Pearse, "Success in English teaching," *ELT Journal*, vol. 56, no. 4, pp. 424-425, 2002.
- [21] Z. Li-biao, Z. Chun-guang, M. A. Ming, X. H. Liu, Z. Q. Ma, and Y. C. Liang, "Solving multi-objective optimization problems based on particle swarm optimization," *Computer Research and Development*, vol. 4, no. 7, pp. 1286-1291, 2004.
- [22] H. Wang, N. Wang, and D. Wang, "A Memetic particle swarm optimization algorithm for dynamic multimodal optimization problems," *Information Science*, vol. 197, pp. 1577-1586, 2013.
- [23] S. Zhang, Y. Yang, and A. Forces, "Analysis of Weibo user influence based on multi-learning factor particle swarm optimization," vol. 31, no. 10, pp. 140-144, 2017.
- [24] X. Peng, "TSVR: an efficient twin support vector machine for regression," *Neural Networks*, vol. 23, no. 3, pp. 365-372, 2010.
- [25] C.-L. Huang and C.-J. Wang, "A GA-based feature selection and parameters optimization for support vector machines," *Expert Systems with Applications*, vol. 31, no. 2, pp. 231-240, 2006.

Research Article

Research and Implementation of English Grammar Check and Error Correction Based on Deep Learning

Xiuhua Wang¹ and Weixuan Zhong² 

¹Science and Technology College of Gannan Normal University, Ganzhou 341000, China

²School of Foreign Language, Hechi University, Yizhou 546300, China

Correspondence should be addressed to Weixuan Zhong; 03016@hcnu.edu.cn

Received 24 November 2021; Revised 22 December 2021; Accepted 28 December 2021; Published 18 January 2022

Academic Editor: Man Fai Leung

Copyright © 2022 Xiuhua Wang and Weixuan Zhong. This is an open access article distributed under the Creative Commons Attribution License, which permits unrestricted use, distribution, and reproduction in any medium, provided the original work is properly cited.

English as a universal language in the world will get more and more attention, but English is not our mother tongue, and there exist differences in culture and thinking. English grammar is the most difficult problem to solve. There are many English learners, and the number of English teachers is limited, and it is inevitable to use Internet technology to solve the problem of lack of resources. The article uses deep learning technology to propose an ASS grammar detection model, which can quickly and efficiently detect grammatical errors. The research results show the following. (1) This study selects data from the GEC evaluation task and analyzes the four modules of article, noun, verb, and preposition through algorithms under different models. The results indicate the accuracy of the four modules. The recall rate has been improved to a certain extent, the accuracy rate of nouns is the highest, which can reach 63.99%, the accuracy rate of prepositions is improved to a lesser extent, and the inspection accuracy rate after improvement is 12.79%. (2) In the experiment to verify the effectiveness of the ASS grammar detection model, compared with the detection effect of the ordinary model, the accuracy of the ASS comprehensive inspection has been greatly improved. The comprehensive accuracy of the ordinary detection model is 28.01%, and the ASS model's comprehensive accuracy rate of the inspection was 82.82%, and the accuracy rate was increased by 54.81%. The result shows that the performance of the ASS inspection model has been improved by leaps and bounds compared with the traditional model. (3) After transforming and upgrading the ASS model, the three models and other models obtained were run on the test set and the mixed test set, respectively. The results show that the accuracy, precision, recall, and F1 score of ASS model are the highest in the test set, which are 98.71%, 98.83%, 98.64%, and 98.73%, respectively, the Bayesian network check model has the lowest accuracy rate of 51.74%, and the ROC curve value and AUC value of the ASS model are both the largest. The accuracy of the ASS model on the mixed test set is also the highest, reaching 98.01%. The JaSt model on the mixed test set has a significant downward trend, with the accuracy rate dropping from 92.16% to 56.68%. It can be concluded that the ASS model can accurately and efficiently monitor grammatical errors.

1. Introduction

With the increasing update of computers and the Internet, tens of thousands of users tend to write and communicate in English in their daily work. For users whose native language is not English, writing in English is a major obstacle for them. Grammar checking technology originated from the application of natural language understanding. Clément et al. [1] proposed an open grammar checking system under

the deep learning model to analyze and train the grammar in depth. The standard of grammar directly affects the fluency of sentences. The grammar checking system introduced in this article can efficiently check out grammatical errors in sentences and automatically generate correct sentences to replace the wrong ones. Xu [2] improved the algorithm and accuracy of grammar checking and designed and developed a grammar checking system. Sankaravelayuthan [3] proposed an MS-Word tool to check spelling errors in text.

Because a word is composed of many English letters, after we enter the English word, there will inevitably be input errors. The tools proposed in the article will help us solve these problems and will automatically check the spelling errors in the article. Jacobs and Rodgers [4] discussed the use of French computer grammar checker as a learning and teaching resource. They conducted an experiment in which students use a screen checker or other methods to check for grammatical errors in English articles. Lüthy et al. [5] studied the method of segmenting offline cursive handwritten text lines into individual words. Prins [6] found some of the most common mistakes made by Taiwanese students in writing and provided some strategies that teachers use in ESL classrooms. Keong [7] wrote an expert system for English grammar teaching for personal computer users. The system uses a parser to implement a grammatical checking tool, and the system can check for grammatical errors in the text. You can also create files to store grammatical errors and corresponding information from the text. Kann [8] realized the writing method of long text in computer and determined the writing process through the relevant model. Xie [9] implemented the rules of grammar checking according to the principles of practicality and validity. The article simplifies the analysis of the algorithm and expands the coverage of errors. Grammar error checking is a very important task in correcting the text. For people with poor English, writing in English is a relatively difficult task. If English is not good, you cannot use the grammar in English correctly, thus increasing the demand for grammar checking software. The purpose of the literature [10] is to examine the existing literature, highlight current issues, and propose potential directions for future research. The article observes and analyzes the error analysis program, summarizes the error experience, and finds the correct program. The development of computer technology helps enrich the content of English education and provides more convenience for English learning. Pan and Zhou [11] realized personalized inspection and diagnosis of college students' English grammar. Amrhein [12] discussed the importance of correct use of conjunctions and semicolons in the preparation of policy tables to avoid misunderstanding of the intended meaning. Shephard [13] introduced a method of self-study English grammar, through which you can formulate grammar rules for yourself. Using this learning method can help us learn and understand grammar without the guidance of a teacher. The system will list students' common grammatical errors, and students can conduct intensive training based on the grammatical errors listed by the system. Mondal and Mondal [14] introduced a proprietary software application. The program can provide many services, including helping us detect grammatical errors in English articles and automatically generate correct sentences. Richards et al. [15] introduced a two-level general English course for Italian middle school students. The course mainly emphasizes the communication methods of accuracy and fluency. The course includes three parts: communication check, grammar check, and study check. The above research methods are based on artificial intelligence or modern technology applied to English grammar detection

TABLE 1: Classification of grammatical errors [17].

Type	Content
Vt	Verb tense
Vm	Verb modality
V0	Missing verb
V form	Verb form
SVA	Subject-verb agreement
Art or Det	Article
Nn	Noun (singular and plural)
Npos	Word possessive
Pform	Pronoun form
Pref	Pronoun reference

and verification. However, the detection efficiency of grammar is low, the error rate is high, and the prediction efficiency is not ideal. In this paper, an ASS grammar detection model is proposed by using deep learning technology, which can detect grammar errors quickly and efficiently.

2. Research and Realization of English Grammar Check

2.1. The Significance of Grammar Checking Research. Due to the great flexibility and uncertainty of natural language itself, English is a typical representative of many vocabulary, complex grammar, and extensive usage scenarios, which increases the difficulty of computer automatic error detection and correction. Another important reason that affects the development of grammatical error correction is the lack of relevant corpus. It is very difficult to construct a corpus marked with grammatical errors. The current mainstream research methods of grammatical error correction are all based on statistical machine learning, which requires a large amount of corpus for model training and testing [16]. However, with the attention of universities and research institutions on this issue, the problem of lack of corpus has been greatly improved, laying a solid foundation for further research. Therefore, this article will study deep learning technology and use it to solve the problem of English grammar error correction. Based on the proposed error correction algorithm, the algorithm model experiment and verification are carried out, and considering the application of the algorithm, a grammatical error correction system similar to Google translation is constructed, providing a simple and convenient way for English learners to use. The combination of theory and practice has a certain promotion effect on solving the problem of English grammar error correction and improving the grammar level of English learners. The classification of common grammatical errors is shown in Table 1.

2.2. The Overall Framework Design of English Grammar Check. According to the results of the functional analysis of business requirements, the architecture of the grammar error correction system model [18] is shown in Figure 1.

The core module of grammar error correction mainly includes three functional modules: data processing, model

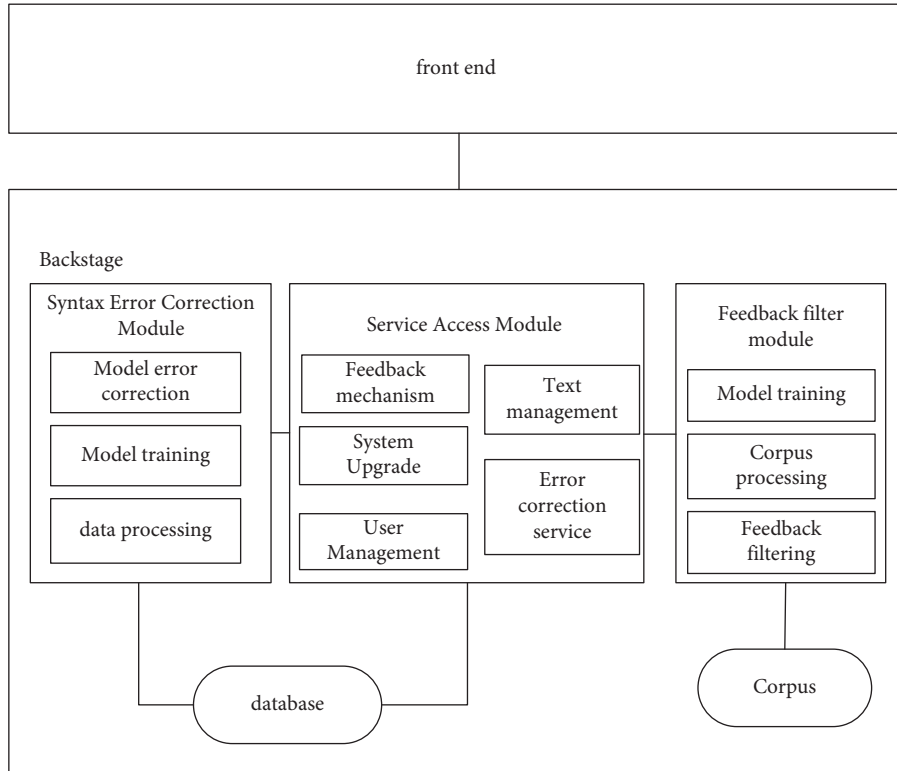


FIGURE 1: Framework diagram of grammatical error correction model.

training, and model error correction, and model error correction is the core function of the whole algorithm [19]. The main function of data processing is to preprocess the original corpus data, to store the processed corpus data in a structured way, and to learn the module and get the standard dataset. Model training is to train the data in the corpus, save the trained features in the database, and apply them in the later test and matching [20]. Model error correction is to use the error correction model stored in the training library to match the input sentence grammar and output the correct sentence. The error correction service model can accept the error correction request from the user in real time, analyze it through the error correction model of the corpus, and return the correct content to the user.

2.3. Implementation of Syntax Error Correction. Firstly, learning is carried out according to the characteristics of grammar error correction, and an English error correction application submitted by a user is received. First determine whether the submitted parameters are valid and then enter the next step to split the sentence. Then, the error correction model trained before is used for grammar error correction. When the error correction of the last sentence is completed, the error correction sentences returned to the segmentation are merged. If the sentence is simple, the error correction model can be used directly without sentence segmentation. Feedback suggestion means that when the user is not satisfied with the grammatical error correction given by the system or there is a better way to modify it, the modification suggestion is fed back to the

system. As mentioned above, we will filter the modification suggestions submitted by users, so the previous feedback suggestion filtering model will be used in the feedback suggestion function. Similar to grammatical error correction, we also carry out the design of feedback suggestions from two aspects. One is the feedback filtering interface itself, and its work flowchart is given; the other is the call flow between modules, which is explained using sequence diagrams. First, we introduce the feedback filtering interface. According to the syntax error correction process, first determine whether the request parameters are legal; if not, directly end [21]. The probabilities of the error correction statement and the original system modification statement are calculated, respectively, for the error correction model.

3. Error Correction Model

3.1. Deep Learning Technology. The seq2seq model is composed of an encoder and is a cyclic neural network; in the encoding stage, a semantic vector is generated according to the input sequence (x_1, x_2, \dots) and conversion rule f [22], and the calculation formula is

$$h_t = f(h_{t-1}, x_t). \quad (1)$$

Summarize the semantic vector:

$$C = q(h_1, h_2, h_3, \dots, h_t). \quad (2)$$

Decoding:

$$y_t = \arg \max P(y_t) = \prod_{i=1}^T p(y_i | \{y_1, y_2, \dots, y_{t-1}\}, C). \quad (3)$$

The calculation formula of the hiding algorithm:

$$h'_t = f(h'_{t-1}, y_{t-1}, C). \quad (4)$$

3.2. Evaluation Criteria for English Grammar Error Correction. The most commonly used evaluation algorithm for grammatical error correction is MaxMatch (M^2). The principle of the algorithm MaxMatch is introduced below [23]; correction rate P :

$$P = \frac{\sum_{i=1}^n |g_i \cap e_i|}{\sum_{i=1}^n |e_i|}. \quad (5)$$

Correction rate R :

$$R = \frac{\sum_{i=1}^n |g_i \cap e_i|}{\sum_{i=1}^n |e_i|}. \quad (6)$$

The key evaluation index in Max Match is $F_{0.5}$, and the formula is defined as follows:

$$F_{0.5} = \frac{(1 + 0.5^2) * R * P}{R + 0.5^2 * P}. \quad (7)$$

3.2.1. Syntax Error Correction Model. In the Soft Attention Mechanism, the weight a_{ij} is determined by the $(i-1)$ th hidden state s_{i-1} and each hidden state variable in the input [24]. The calculation formula is as follows:

$$a_{ij} = \frac{\exp(e_{ij})}{\sum_{k=1}^{T_x} \exp(e_{ik})}, \quad (8)$$

$$e_{ij} = a(s_{i-1}, h_j).$$

LN is calculated by inputting the entire layer of neurons in RNN [25]:

$$\mu = \frac{1}{H} \sum_{i=1}^H x_i, \quad (9)$$

$$\sigma = \sqrt{\frac{1}{H} \sum_{i=1}^H (x_i - \mu)^2}.$$

Anti-filtering algorithm:

$$p(\omega_i | \omega_1, \dots, \omega_{i-1}) = p(\omega_i | \omega_{i-n-1}, \dots, \omega_{i-1}). \quad (10)$$

When $n=2$, bigram is

$$p(\omega_i | \omega_1, \dots, \omega_m) = \prod_{i=1}^m p(\omega_i | \omega_{i-1}). \quad (11)$$

When $n=3$, bigram is

$$p(\omega_i | \omega_1, \dots, \omega_m) = \prod_{i=1}^m p(\omega_{i-2} \omega_{i-1}). \quad (12)$$

Estimate the value of $p(\omega_i | \omega_{i-2} \omega_{i-1})$, and the formula is

$$p(\omega_i | \omega_{i-2} \omega_{i-1}) = \frac{c(\omega_{i-2} \omega_{i-1} \omega_i)}{c(\omega_{i-2} \omega_{i-1})}. \quad (13)$$

According to the N-gram grammar model introduced above, we can get

$$P(S) = P(\omega_1, \omega_2, \dots, \omega_m). \quad (14)$$

Confusion:

$$PP(S) = P(\omega_1, \omega_2, \dots, \omega_m)^{1/m}$$

$$= \sqrt[m]{\frac{1}{P(\omega_1, \omega_2, \dots, \omega_m)}}. \quad (15)$$

According to the chain method, it can be written as

$$PP(S) = \sqrt[m]{\prod_{i=1}^m p(\omega_i | \omega_{i-n-1}, \dots, \omega_{i-1})}. \quad (16)$$

3.2.2. ASS Model Design. The objective function of a single-layer neural network is

$$\text{vec}(p) \approx \tanh \left(\sum_{i=1}^n \frac{\Omega(p)}{\Omega(c_i)} W_{\text{code},i} \cdot \text{vec}(c_i) + b \right), \quad (17)$$

$$W_{\text{code},i} = \eta_l W_{\text{code}}^l + \eta_r W_{\text{code}}^r.$$

The coefficients η_l and η_r are

$$\eta_l = \frac{\Omega(p) - i}{\Omega(p) - 1}, \quad (18)$$

$$\eta_r = \frac{i - 1}{\Omega(p) - 1}.$$

The matrix parameters of the only child node are

$$W_{\text{code},i} = \frac{1}{2} W_{\text{code}}^l + \frac{1}{2} W_{\text{code}}^r. \quad (19)$$

Square of Euclidean distance:

$$d = \left\| \text{vec}(p) - \tanh \left(\sum_{i=1}^n l_i W_{\text{code},i} \cdot \text{vec}(c_i) + b \right) \right\|_2^2. \quad (20)$$

The error function of training sample $x^{(i)}$ and its corresponding negative example $x_c^{(i)}$ is

$$J(d^{(i)}, d_c^{(i)}) = \max(0, \Delta + d^{(i)} - d_c^{(i)}). \quad (21)$$

The final training objective function is

TABLE 2: Data statistics of evaluation tasks.

Type of error	Training set number	Training set percentage	Test set number	Test set percentage
Article	665	14.8	690	19.9
Preposition	240	5.3	312	9.0
Noun	377	8.4	396	11.4
Subject-verb agreement	145	3.2	122	3.5
Verb form	152	3.4	124	3.6
Five types	582	35.1	1644	47.4
All types	651	100	3470	100.0

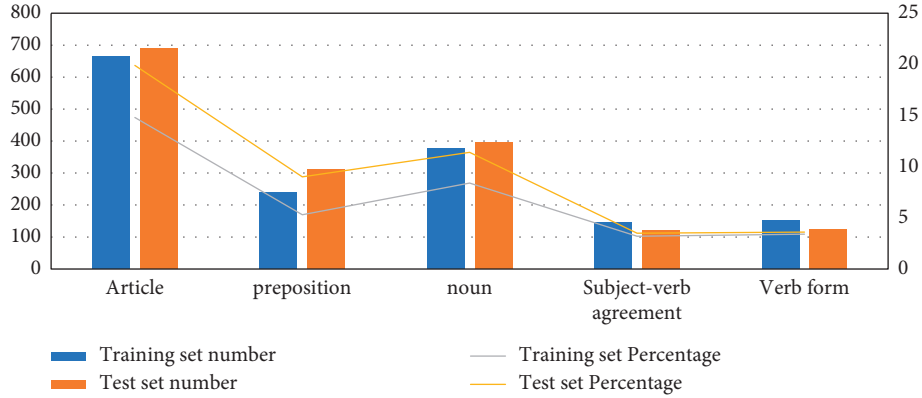


FIGURE 2: Statistical graph of experimental results.

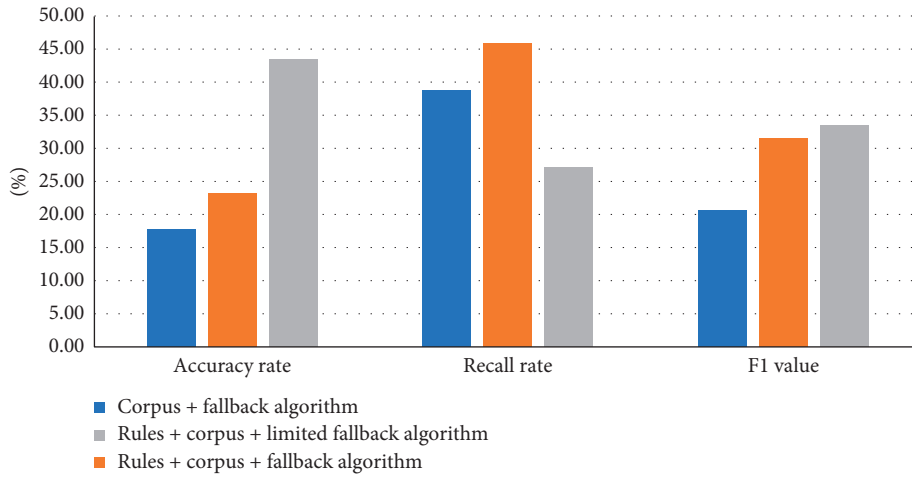


FIGURE 3: Statistics of article inspection results.

$$\min_{W^l} \frac{1}{2N} \sum_{i=1}^N J(d^{(i)}, d_c^{(i)}) + \frac{\lambda}{2M} \left(\|W_{\text{code}}^l\|_F^2 + \|W_{\text{code}}^r\|_F^2 \right). \quad (22)$$

4. Simulation Experiment

4.1. Data Analysis. In order to effectively analyze the data, we select the data in the GEC evaluation task and analyze the algorithms of the four modules of article, noun, verb, and preposition under different models. The experiment compares the results by setting whether to use the law library, and in order to enhance for the persuasiveness of the

experiment, we have added a comparative experiment with the common algorithm. The statistical results of various error types in the training data and test data are shown in Table 2 and Figure 2.

The five types include errors in articles, errors in prepositions, errors in names, grammatical errors in subject-verb agreement, and errors in verb forms, while the all types include errors in verb tenses, missing verbs, verb forms, subject-verb agreement, articles, singular and plural nouns, possessive words, and pronoun forms. Table 2 shows an experimental analysis of five common types of grammatical errors.

TABLE 3: Comparison of article check module results.

Model	Accuracy rate (%)	Recall rate (%)	F1 value (%)
Corpus + fallback algorithm	17.79	38.70	20.71
Rules + corpus + fallback algorithm	23.25	45.88	31.44
Rules + corpus + limited fallback algorithm	43.49	27.12	33.45

TABLE 4: Comparison of noun check module results.

Model	Accuracy rate (%)	Recall rate (%)	F1 value (%)
Corpus + fallback algorithm	63.99	30.05	40.90
Corpus + limited fallback algorithm	4.06	51.26	45.3

TABLE 5: Comparison of verb check module results.

Model	Accuracy rate (%)	Recall rate (%)	F1 value (%)
Corpus + fallback algorithm	12.79	22.36	16.27
Corpus + limited fallback algorithm	19.37	22.36	20.27

TABLE 6: Comparison of results of preposition checking module.

Model	Accuracy rate (%)	Recall rate (%)	F1 value (%)
Corpus + fallback algorithm	8.01	25.32	12.17
Corpus + limited fallback algorithm	13.46	18.83	15.70

4.1.1. Article Inspection Module. The accuracy and recall rate of adding the rule library to the article check module have been significantly improved, indicating that the automatic extraction of the rule library is effective for the entire inspection and correction process as shown in Figure 3 and Table 3. At the same time, the fallback algorithm is improved. After the limited back-off algorithm, the accuracy rate has also been greatly improved, and the correction process is more accurate, thereby increasing the final F1 value.

4.1.2. Noun Check Module. In the noun checking module of Table 4, after using the model algorithm, the accuracy and recall rate have been greatly improved, and the accuracy rate is up to 63.99% because nouns account for the highest proportion of sentences. When using the grammar check module, you can correct more noun errors, thereby increasing the F1 value of the noun check module.

4.1.3. Verb Check Module. *4.1.4. Preposition Checking Module.* As shown in the data in Tables 5 and 6, in the grammar detection module, the accuracy and recall rate of verbs and prepositions have been improved, but the accuracy of prepositions has been improved to a lesser extent. The improved inspection accuracy rate is 12.79%. After using the fallback algorithm, the model's judgment on grammar detection is stricter. The accuracy measure is the ratio of the number of correct samples to the number of all samples in the test set. The larger the index value is, the more accurate the recommendation result is. The F1 measurement index can effectively balance the precision and recall by biasing the objects with small values. The larger the index

value is, the more accurate the recommendation result is. The improved recall of the verb and preposition checking modules of Table 5 and Table 6 illustrates that the results of the verb and preposition checking modules are more precise.

4.2. Comparison of Test Results. We compared the inspection effect of the ASS model with the inspection effect of the ordinary model; the inspection effect of the grammar inspection module under the ordinary algorithm is shown in Table 7, and the comprehensive grammar inspection result of the ASS model is shown in Table 8.

From the data in Figures 4 and 5, we can conclude that the accuracy of the ASS comprehensive inspection has been greatly improved compared with the inspection effect of the ordinary model. The comprehensive accuracy of the ordinary inspection model is 28.01%, and the ASS model inspection is better. The overall accuracy rate is 82.82%, the accuracy rate is increased by 54.81%, and the overall recall rate of the ASS model is also increasing, indicating that the performance of the ASS inspection model has been improved by leaps and bounds, and the efficiency of grammar detection and the correctness of grammar detection have been improved.

4.3. Model Performance Testing. We run each model on the test set and the mixed test set and record the experimental data. In the process of using the ASS model to detect grammar, the grammar needs to be converted into a mathematical representation that the model can handle, as shown in Figure 6.

According to the data in Table 9 and Figure 7, we can conclude that the accuracy of the ASS model is the highest among several models, reaching 99.71%, indicating that the

TABLE 7: Common model detection effect.

	Accuracy rate (%)	Recall rate (%)	F1 value (%)
Verb error detection	21.67	21.21	30.41
Subject-verb consistency error detection	29.39	33.84	31.46
Noun singular and plural error detection	31.32	30.61	30.96
Article error detection	27.12	18.26	21.83
Preposition error detection	27.62	36.58	31.47
Overall error detection	28.01	37.19	31.96

TABLE 8: ASS comprehensive inspection results.

	Accuracy rate (%)	Recall rate (%)	F1 value
Verb error detection	30.12	20.12	34.21%
Subject-verb consistency error detection	40.00	21.33	31.71%
Noun singular and plural error detection	45.51	28.77	35.50%
Article error detection	67.39	42.84	52.38
Preposition error detection	72.13	37.87	49.66%
Overall error detection	82.82	25.57	39.07%

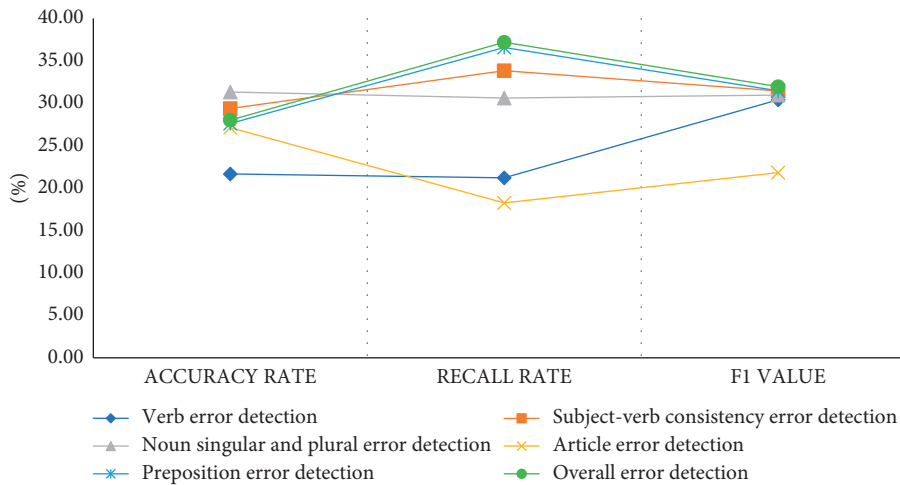


FIGURE 4: Statistics of general inspection results.

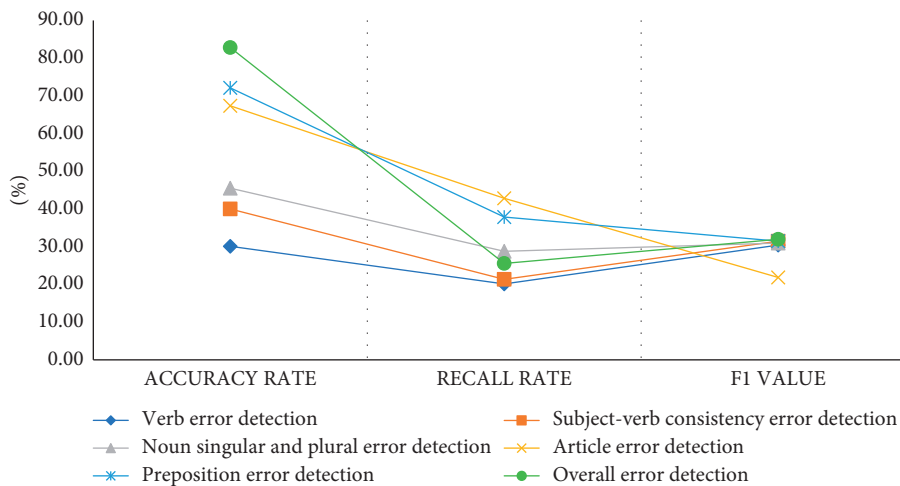


FIGURE 5: Statistics of ASS inspection results.

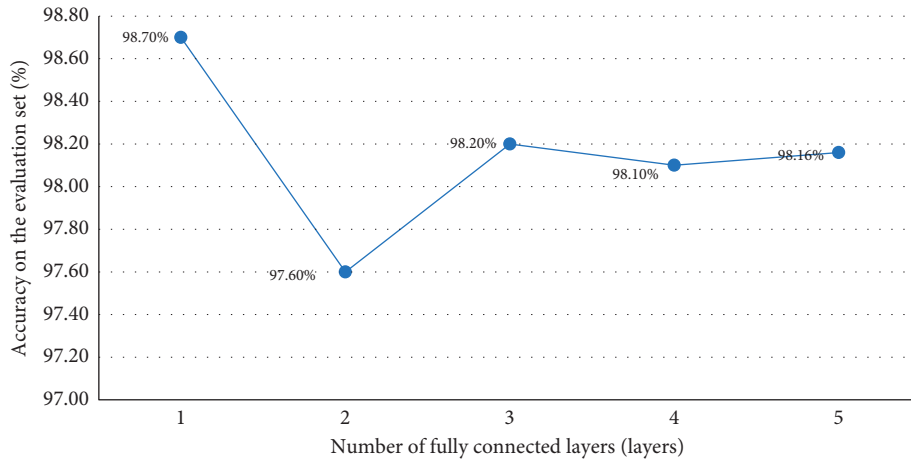


FIGURE 6: The influence of the number of fully connected layers on the model.

TABLE 9: Performance of each model on the test set.

Model	Accuracy rate (%)	Precision rate (%)	Recall rate (%)	F1 score (%)
RBF core support vector machine	85.00	93.06	76.13	83.75
Bayesian network	51.74	51.29	97.83	67.30
Decision tree	89.12	88.83	89.87	89.35
JaSt	92.16	96.71	92.53	94.57
ASS-T	97.97	98.10	97.89	98.00
ASS-G	96.52	98.26	94.83	96.52
ASS-TG	99.71	98.83	97.74	98.82

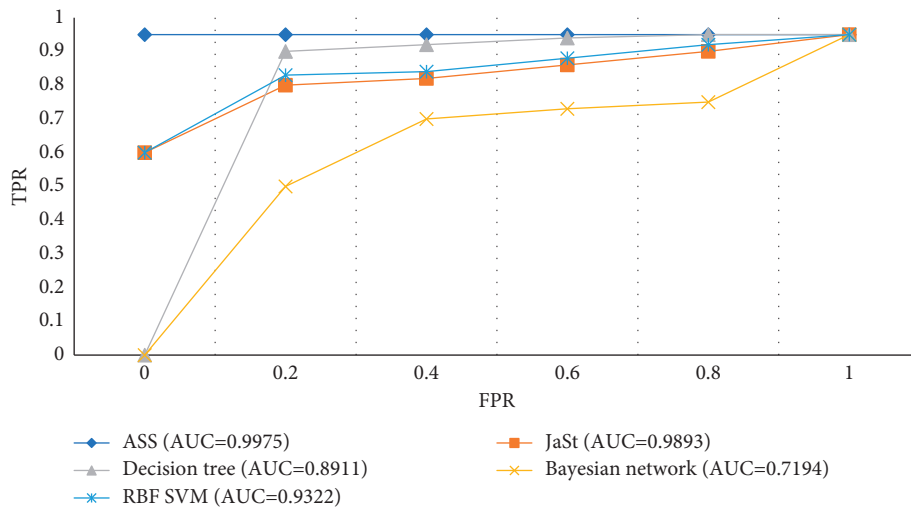


FIGURE 7: ROC curve on the test set.

performance of ASS detection is the highest, and the accuracy of the Bayesian network is the lowest, which is 51.74%, indicating that the detection efficiency of the Bayesian network model is not good enough.

ASS-T is a test of the data model and the overall syntax, starting with the creation of a new window or table. For each participating object, list the different domains and syntaxes. With the help of field definitions and basic techniques, ASS-G analyzes test data, overall syntax tests, partitions, and boundary values. The ASS-TG data model is the detailed

syntax test. For the strictly syntactically controlled parts, you need to perform more detailed tests.

According to the data in Table 10 and Figure 8, it is concluded that the accuracy rate of the ASS-G model is as high as 98.01%. The JaSt model's various indicators on the mixed test set have a significant downward trend, and the accuracy rate has dropped from 92.16% to 56.68%, because that syntax information in the test set is obfuscated, and the excellence of the ASS model is also reflected in the ROC curve.

TABLE 10: Performance of each model on the mixed test set.

Model	Accuracy rate (%)	Precision rate (%)	Recall rate (%)	F1 score (%)
RBF core support vector machine	47.51	80.77	7.45	13.63
Bayesian network	57.70	56.37	90.75	69.55
Decision tree	54.49	61.25	49.63	54.83
JaSt	56.68	71.49	24.75	36.77
ASS-T	92.71	95.03	91.70	93.33
ASS-G	98.01	98.67	97.73	98.20
ASS-TG	96.72	98.54	95.53	97.01

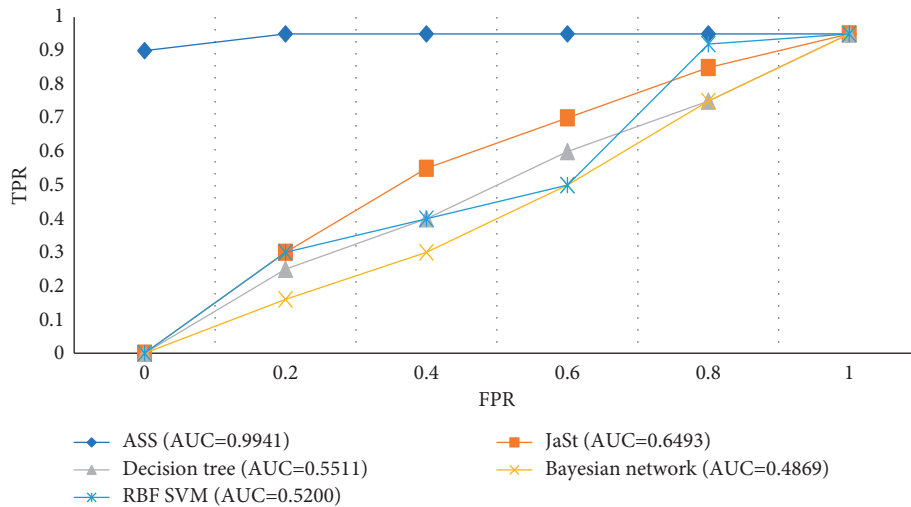


FIGURE 8: ROC curve on the mixed test set.

5. Conclusion

At present, there are more and more English learners, and the English grammar module is also a very important part of the English learning process. However, due to the particularity of English teaching, the auxiliary teaching of English grammar detection is particularly important, although the current grammar-assisted teaching has been combined with computers. Technology and network technology have greatly reduced the error rate, but there are still some problems with poor user experience. There is still a lot of room for improvement in English assisted teaching. Therefore, it should combine the current problems to improve constantly and propose a more intelligent and accurate grammar detection model to make English teaching easier and more efficient.

Data Availability

The experimental data used to support the findings of this study are available from the corresponding author upon request.

Conflicts of Interest

The authors declare that they have no conflicts of interest.

References

- [1] L. Clément, K. Gerdes, and R. Marlet, "A grammar correction algorithm – deep parsing and minimal corrections for a grammar checker," in *Proceedings of the 14th international conference on Formal grammar*, vol. 12, no. 6, pp. 11–17, Springer, Berlin, Germany, July 2009.
- [2] X. Xu, "Exploration of English composition diagnosis system based on rule matching," *International Journal of Emerging Technologies in Learning*, vol. 13, no. 7, pp. 161–172, 2018.
- [3] R. Sankaravelayuthan, "Spell and grammar checker for Tamil," *Developing computing tools for Tamil*, vol. 05, no. 23, pp. 52–64, 2015.
- [4] G. Jacobs and C. Rodgers, "Traacherous allies: foreign language grammar checkers," *CALICO Journal*, vol. 16, no. 4, pp. 87–95, 1999.
- [5] F. Lüthy, T. Varga, and H. Bunke, "Using hidden markov models as a tool for handwritten text line segmentation," in *Proceedings of the international conference on document analysis & recognition*, vol. 12, no. 8, pp. 117–123, IEEE, Curitiba, Brazil, September 2007.
- [6] H. Prins, "Conquering Chinese English in the ESL classroom," *Internet Tesl Journal*, vol. 03, no. 11, pp. 25–36, 2006.
- [7] C. C. Keong, "An expert system for the teaching of English grammar," in *Proceedings of the IEEE Region 10 Conference on Computer & Communication Systems, IEEE Tencon*, vol. 08, no. 12, pp. 52–57, IEEE, Hong Kong, China, September 1990.

- [8] V. Kann, "CrossCheck – a grammar checker for second language writers of Swedish," *KTH Nada*, vol. 23, no. 12, pp. 78–82, 2008.
- [9] K. W. Xie, "An grammar check research based on instance," *Journal of Hubei University for Nationalities Natural Science Edition*, vol. 23, no. 12, pp. 22–31, 2009.
- [10] M. Soni and J. S. Thakur, "A systematic review of automated grammar checking in English language," *Computation and Language*, vol. 07, no. 12, pp. 112–121, 2018.
- [11] D. Pan and H. Zhou, "English learning system design for college students personalized English grammar check and diagnosis," *International Journal of Emerging Technologies in Learning*, vol. 13, no. 4, pp. 51–59, 2018.
- [12] C. Amrhein, "Grammar check," *Property & Casualty*, vol. 07, no. 12, pp. 141–152, 2016.
- [13] J. Shepherd, "Teach yourself English grammar as a foreign language," *Academic Leadership Journal in Student Research*, vol. 23, no. 6, pp. 12–18, 2003.
- [14] H. Mondal and S. Mondal, "Free grammar check for your manuscript," *Indian Journal of Vascular and Endovascular Surgery*, vol. 11, no. 3, pp. 21–27, 2020.
- [15] J. C. Richards, J. Hull, S. Proctor, and D. Haines, *Changes 1 workbook Italian edition: English for International Communication*, Cambridge University Press, Cambridge, England, 2010.
- [16] P. Ratanaworabhan, B. Livshits, and B. Zorn, "Nozzle: a defense against heap-spraying code injection attacks," in *Proceedings of the SSYM'09 18th conference on USENIX security symposium*, pp. 169–186, Berkeley, CA, August 2009.
- [17] T. N. Hwee, S. M. Wu, T. Briscoe, C. Hadiwinoto, and C. Bryant, "The CoNLL-2014 shared task on grammatical error correction," in *Proceedings of the Eighteenth Conference on Computational Natural Language Learning*, pp. 1–14, Shared Task, Baltimore, MA, USA, January 2014.
- [18] H. G. Kim, D. J. Kim, S. J. Cho, and M. j. Park, "Efficient detection of malicious web pages using high-interaction client honeypots," *Journal of Information Science and Engineering*, vol. 28, no. 5, pp. 911–924, 2012.
- [19] K. A. Moore, C. Rutherford, and K. A. Crawford, "Supporting postsecondary English language learners' writing proficiency using technological tools," *Journal of International Students*, vol. 6, no. 4, pp. 857–872, 2016.
- [20] Y. Guo and G. H. Beckett, "The hegemony of English as a global language: reclaiming local knowledge and culture in China," *Convergence*, vol. 40, pp. 117–132, 2006.
- [21] E. S. Atwell and S. Elliot, "Dealing with ill-formed English text the computational analysis of English," *A Corpus-Based Approach*, vol. 12, pp. 120–138, 1987.
- [22] R. Dale and A. Kilgarriff, "Helping our own: the HO0 2011 pilot shared task," in *Proceedings of the 13th European Workshop on Natural Language Generation*, vol. 05, no. 14, pp. 242–249, Association for Computational Linguistics, Nancy, France, September 2011.
- [23] P. Bhaskar, A. Ghosh, S. Pal, and S. Bandyopadhyay, "May I check the English of your paper," in *Proceedings of the 13th European workshop on natural language generation*, vol. 03, no. 12, pp. 250–253, Association for Computational Linguistics, Nancy, France, September 2011.
- [24] E. Ivanova, D. Bernhard, and C. Grouin, "Handling outlandish occurrences: using rules and lexicons for correcting NLP articles," in *Proceedings of the 13th European Workshop on Natural Language Generation*, vol. 12, no. 1, pp. 254–256, Association for Computational Linguistics, Nancy, France, September 2011.
- [25] K. Kukich, "Techniques for automatically correcting words in text," *ACM Computing Surveys*, vol. 24, no. 4, pp. 377–439, 1992.

Research Article

Research on Village Planning and Rural Architectural Design Based on Discrete Dynamic Modeling Technology

Junhang Lin ^{1,2}

¹Faculty of Architecture and Urban-Rural Planning, Zhuhai College of Science and Technology, Zhuhai 519041, Guangdong, China

²Faculty of Innovation and Design, City University of Macau, Macau 999078, China

Correspondence should be addressed to Junhang Lin; linjunhang@zcst.edu.cn

Received 14 December 2021; Accepted 29 December 2021; Published 17 January 2022

Academic Editor: Man Fai Leung

Copyright © 2022 Junhang Lin. This is an open access article distributed under the Creative Commons Attribution License, which permits unrestricted use, distribution, and reproduction in any medium, provided the original work is properly cited.

With the advent of the era of big data, the combination of science and technology and urban and rural planning has become the focus of many countries. The improvement of village planning and the redesign of rural buildings can promote the rapid development of villages and strengthen rural cohesion. Based on the above situation, this paper proposes a dynamic programming algorithm combined with discrete dynamic modeling technology to improve rural planning. Firstly, the dynamic programming algorithm is used to reconstruct the village layout and optimize the original village model. The dynamic monitoring technology is used to update the dynamic data in real time to provide specific information for the follow-up rural architectural design. Secondly, the dynamic modeling technology is used to build the building model, which can calculate the building location and building angle of the village. In order to further improve village development, we also put forward the concept of green building design. The performance of traditional modeling technology and discrete dynamic modeling technology in the green building design model is compared. The results show that the discrete dynamic modeling technology can improve the overall performance of rural buildings and improve the operation efficiency of the system in the batch design of green buildings. The village layout improved by dynamic planning reduces the specific travel distance of villagers and provides effective help for rural construction and economic development. Compared with traditional modeling technology, dynamic modeling technology has a shorter workflow and less time. Discrete dynamic modeling technology can realize dynamic batch architecture design and has higher applicability than traditional algorithms.

1. Introduction

In response to the call of rural revitalization strategy, many researchers have put forward the concept of village construction based on a dynamic programming algorithm [1]. Facing the ownership of village residents, the corresponding planning should follow the villagers' own wishes for improvement [2]. The completion of village planning is the basis and guarantee for the construction and management of rural areas and is conducive to promoting the construction of a new socialist countryside [3]. At present, there is a lack of overall supervision on village construction and land use in China. With the continuous acceleration of urbanization, many village construction lands have been transformed into other functions [4]. This situation leads to less and less land needed by villagers, reducing land use and improving

quality, which is obviously not suitable for the current environment. Our planning for rural construction is still in the urban perspective, so we need to change our thinking and replan the layout from the specific situation of the countryside [5]. In the process of rural construction, we should also focus on the use of buildings. How to improve the whole life cycle of the building model and reduce pollution is the content that every building designer needs to consider. Therefore, when designing residential buildings or commercial buildings, it is necessary to consider the impact of environmental, economic, and natural factors [6, 7]. Green performance and minimum cost of architectural design have to be ensured.

Dynamic programming algorithm is an important way for the research of village planning and rural architectural design [8]. In order not to destroy the ecological

environment, we need to improve the layout of the whole village in combination with science and technology. Because there are great differences in terrain, land composition, and natural factors in each region, we cannot layout according to population flow in rural design [9, 10]. Targeted design models are needed. With different personnel densities, the change of population flow belongs to dynamic data change, and the traditional modeling technology cannot meet the needs of dynamic change [11]. When building the model, with the continuous production of historical data, it is easy to cause the problem of increasing the error coefficient. Therefore, this paper mainly uses discrete dynamic modeling technology in a big data environment to analyze personnel flow and architectural design data [12]. The advantage of discrete dynamic modeling is that it can obtain accurate data from dynamic information, eliminate data redundancy caused by repeated information, and improve the overall performance of the model [13].

The innovative contributions of this paper include: (1) dynamic modeling technology has a shorter workflow and shorter time than general models; (2) discrete dynamic modeling technology can realize dynamic batch architecture design, which has higher applicability than traditional algorithms; (3) different from the traditional modeling technology, it can process the dynamic building data and calculate the interval distance of the building model according to the change of sunshine data; and (4) the improved village layout through dynamic planning reduces the specific travel distance of villagers and provides effective help for rural construction and economic development.

This paper is mainly divided into three parts. The first part briefly describes the application of dynamic programming algorithms and big data discrete dynamic modeling technology in village planning and architectural design. The development status of dynamic modeling technology in various countries is analyzed. The second part first studies the application of dynamic programming algorithm in village layout and adds dynamic monitoring technology to dynamic data acquisition. The discrete dynamic modeling technology is used to study the batch design of rural buildings. Compare the advantages and disadvantages between traditional modeling technology and dynamic modeling technology. Finally, the discrete dynamic modeling technology is used to design the green building model and optimize the service cycle of the building model. The third part analyzes the results of dynamic programming algorithms in village planning and compares the results of traditional and discrete dynamic modeling algorithms. Finally, the research results of discrete dynamic modeling technology in green building design are analyzed.

2. Related Works

With the rapid development of urbanization, the research on village planning and rural architectural design has become the focus of attention [14, 15]. In order to keep economic development in a balanced state, rural construction and planning have become one of the main

tasks. In rural improvement, village planning is undoubtedly a very important part. Village planning should clarify the architecture of architectural design and implement hierarchical management according to the requirements of space management and control [16]. And all levels cooperate with each other to clarify goals and Directions [17]. In order to ensure the rationality of village planning, relevant governments need to implement rural architectural design research based on sustainable theory [18]. Dynamic programming arithmetic and dynamic modeling technology have been widely used in the medical field, military field, and economic field. They also respond to the concept of rural planning and construction in the new era. The dynamic programming algorithm is used to design the village layout, and the use of dynamic modeling technology is conducive to the design of the house model and the analysis of the respective properties of building materials [19].

The idea of deep learning dynamic modeling technology was formed relatively early [20]. With the continuous development and use of the human brain and the continuous upgrading and application of computer technology, it has made a great contribution to the dynamic modeling technology of artificial neural networks. A variety of design models with research value can be created through discrete dynamic models. It plays an important role in model recognition, signal connection, automatic processing, diagnosis network, and so on [21].

The development of discrete dynamic modeling technology is still in the transformation of virtual reality products [22]. With the continuous development and innovation of science and technology, virtual reality (VR) has gradually entered people's vision and been accepted by people. Scientists conduct dynamic modeling of virtual reality products through dynamic modeling technology, study the performance evaluation of virtual sensor models, and establish relevant evaluation systems.

Scientists put forward the effective application of dynamic modeling technology in the VR industry according to dynamic modeling technology and cases [23]. In the application of virtual reality products, discrete models can be used to create a 3D dynamic virtual environment. At the same time, managers can correct the problems in the system in time and solve them by accurate and rapid means.

The development of dynamic modeling technology is also among the best in the world [24]. Many scientists are committed to studying the relationship between dynamic modeling technology and power system. With the continuous innovation and strengthening of the power system, the power system also tends to be complex and personalized. Important technical means in system function improvement, safety, and stability reflect the applicability and effectiveness of dynamic discrete modeling technology [25]. Based on the above situation, this paper proposes a dynamic programming algorithm combined with discrete dynamic modeling technology to study village planning and rural architectural design.

3. Research on Village Planning and Discrete Dynamic Modeling Design of Rural Buildings Based on Dynamic Programming Algorithm

3.1. *Research on Discrete Dynamic Modeling Technology and Batch Design of Village Layout and Rural Buildings Based on Dynamic Programming Algorithm.* With the continuous development of urbanization, more and more people turn their focus to the development of rural planning and rural architectural design. In the planning of the village construction path and overall residential layout, we use a dynamic programming algorithm to study it. Dynamic programming is the best mathematical algorithm to find the solution strategy, which can optimize the minimum path problem. At present, it is widely used in the fields of economic management, production and processing, mechanical design, and so on. The main contents of the solution also include finding the optimal path, equipment detection, resource allocation, and so on. Assuming that the overall layout of the village is relatively scattered, we need to consider the distance of each household out of the village and into the village. There will be multiple roads from one area to another, but each line takes a different time. Using a dynamic programming algorithm can increase the utilization rate of some land and provide a good environment for subsequent rural architectural design. The principle equation of dynamic programming is as follows:

$$\begin{aligned} f_i(S_K) &= \text{opt}\{R_i(S_{K-1} \rightarrow S_K) + f_{i-1}(S_{K-1})\}, \\ f_i(S_{K-1}) &= \text{opt}\{R_i(S_K \rightarrow S_{K-1}) + f_{i-1}(S_K)\}. \end{aligned} \quad (1)$$

The above formulas are the forward and reverse calculation results of the planned path, respectively. According to the dynamic equation, the following variable functions can be obtained as follows:

$$f_2(J_1) = \text{opt} \left\{ \begin{array}{l} R_2(I_1J) + f_1(I_1), \\ R_2(I_2J) + f_1(I_2), \\ R_2(I_3J) + f_1(I_3). \end{array} \right\}. \quad (2)$$

In the process of forward calculation, the operation path schemes from one variable function to another variable function are as follows:

$$f_2(C_1) = \min \left\{ \begin{array}{l} R_2(B_1C_1) + f_1(B_1), \\ R_2(B_2C_1) + f_1(B_2). \end{array} \right\}. \quad (3)$$

From the second stage, there will be reverse possible results, so we choose reverse calculation. The formula is

$$f_4(D_1) = \min \left\{ \begin{array}{l} R_4(E_1D_1) + f_5(E_1), \\ R_4(E_2D_1) + f_5(E_2), \\ R_4(E_3D_1) + f_2(E_3). \end{array} \right\}. \quad (4)$$

After calculating the best path of village layout, we replan the distribution map of actual rural households, as shown in Figure 1.

It can be seen from Figure 1 that in the distribution of original villages, many architectural designs cannot be

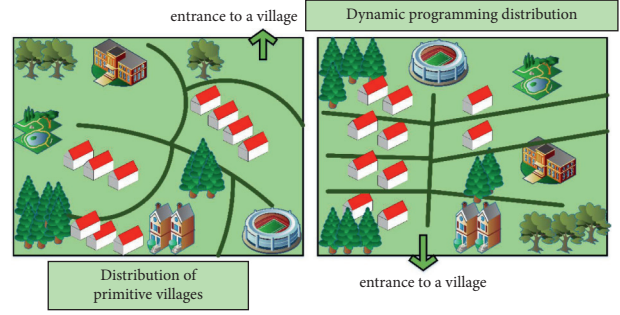


FIGURE 1: Replanning of rural household distribution.

successfully used due to the unreasonable design of the village entrance. The distribution map calculated according to the dynamic programming algorithm can meet the basic requirements of rural architectural design. In order to better monitor the selection of rural architectural design sites, we use the method of dynamic monitoring to collect and classify the data. Due to different geographical environments and equipment resolutions, we need to reduce the terrain scale. Monitoring technology uses satellite remote sensing technology to extract changes in rural images. The whole process of dynamic monitoring is shown in Figure 2.

It can be seen from Figure 2 that the basic data of layout is collected in the early stage, and the planning mathematical model is obtained according to remote sensing data processing. The ownership information of the place of use is obtained by drawing speckle extraction. Therefore, dynamic planning path and dynamic monitoring technology can accurately analyze land use and rural construction layout. It provides a model framework for subsequent architectural design. Before the big data environment, rural architectural design mainly used traditional modeling technology. However, the traditional modeling technology can only create rural buildings through logic and imagination. Such buildings may not be able to withstand the test of the social and natural environment. The traditional modeling technology is only helpful for some specific building models and will produce similarities. The discrete dynamic modeling technology used in this paper can quickly complete the modeling work and can also be modified uniformly in the aspect of model modification, which greatly saves time and energy. The comparison of time spent in the establishment of the same model between traditional modeling technology and dynamic modeling technology is shown in Figure 3.

As can be seen from Figure 3, when the data details exceed 100, the time spent on the project by dynamic modeling technology is much shorter than that by traditional modeling technology. The first mock exam is more complex, and the time taken to build the same model is longer. Compared with traditional modeling technology, dynamic modeling technology has a shorter workflow and less time, as shown in Figure 4.

As can be seen from Figure 4, the workflow comparison between the two is very obvious. Dynamic modeling technology improves the work efficiency of the model by simplifying the steps of data analysis. Due to the dynamic nature

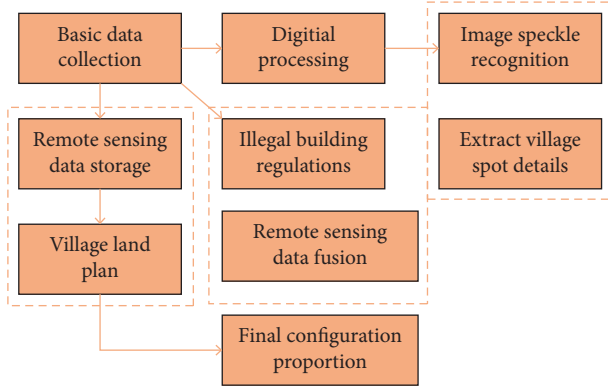


FIGURE 2: Flowchart of dynamic monitoring.

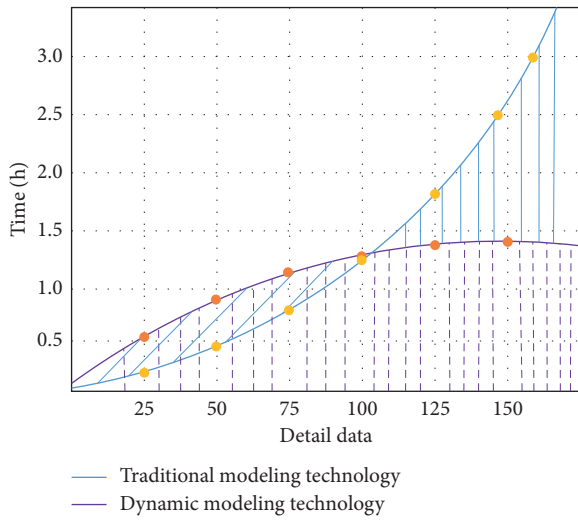


FIGURE 3: Comparison of time spent by traditional modeling technology and dynamic modeling technology.

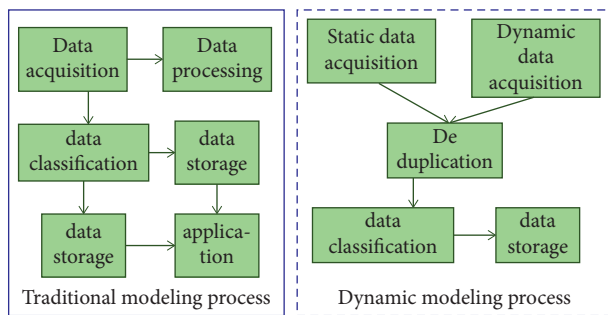


FIGURE 4: Comparison of workflow between dynamic modeling technology and traditional modeling technology.

of data information, traditional modeling technology cannot simplify this part. Therefore, dynamic modeling technology can quickly describe the rural building model. The discrete dynamic model can calculate the model orientation, bottom shape, model shape, model height, coordinate position, rotation size, model size, and so on. Designers can simply use dynamic modeling technology to create and modify models.

In the discrete dynamic modeling technology, the content of batch buildings is extremely rich, and the distribution is relatively uniform, with a certain level. In many aspects, it can balance distribution and achieve excellent results. For example, in the application of folding beam, when the beam forms a fixed angle with the ground as the maximum value, there is

$$\sin \beta \leq \frac{H-h}{l_{10}}, \quad l_{10} > 0. \quad (5)$$

In order to obtain the fixed included angle of each wood strip relative to the ground on a straight line, the formed straight line is expressed as a vector as follows:

$$e_i = \frac{P_i Q_i}{\|P_i Q_i\|}. \quad (6)$$

We express the vector obtained by the above formula in geometric relation as follows:

$$\cos \beta_i = e_i \cdot e_y. \quad (7)$$

Finally, it can be seen that the angular relationship between the beam and the ground is as follows:

$$\beta_i = \arccos\left(\frac{P_i Q_i}{\|P_i Q_i\|} \cdot e_y\right). \quad (8)$$

The dynamic process of building details can be known through the angle β_i between the wood strip and the ground. In the discrete dynamic modeling of rural architectural design, we map the angle between each building and the ground for dynamic distribution. Finally, the purpose of a batch design can be achieved.

3.2. Research on Simulation Design of Green Rural Buildings Based on Discrete Dynamic Modeling Technology. Due to the national regulation of the space system, village construction land and housing construction have ushered in a new development situation. However, land resources are limited. How to correctly use village resources and construction land is the key content to ensure the development of rural construction. The construction purpose of saving needs to be reflected to achieve the integration of ecology, beauty, and applicability. In the design and planning of rural buildings, it is necessary to determine the rationality of specific land use and eliminate differential allocation. According to the infrastructure, geographical environment, and population development of the village, the architectural design distribution is carried out from many aspects. We should not only pay attention to the current rural development but also evaluate the future potential. As the change of villages will be affected by nature and the economy, we need to establish green rural buildings to protect the natural environment while developing villages. The core content of green building is low-carbon environmental protection. It is necessary to optimize the building model and concept in architectural design to realize environmental protection design. Under the theme of green environmental protection in rural

architectural design, this paper uses discrete dynamic modeling technology to form the evaluation model of green building materials. The characteristic analysis of energy, carbon emission, and other indicators is carried out.

In the green building design model, we analyze the stability of the parameters according to each performance index. The influencing factors include light, temperature, and so on. The weight values of these independent variables are as follows:

$$K = [K_1^T K_2^T K_3^T K_4^T K_5^T]^T I = [I_1^L I_2^L I_3^L I_4^L I_5^L]^L. \quad (9)$$

The above two variables form an evaluation quantitative matrix to realize the grade evaluation of green rural buildings, which needs to meet the following conditions:

$$r_{x,y}(n) = \begin{cases} \hat{r}_{x,y}(n+L) - (M-1) \leq n \leq -1, \\ \hat{r}_{x,y}(n) 0 \leq n \leq N-1, \end{cases} \quad (10)$$

$$\hat{f}_t(n) = \begin{cases} f(n) n = 0, 1, 2, \dots, M-1, \\ 0, n = N, N+1, \dots, L-1, \end{cases}$$

where $r_{x,y}(n)$ represents the edge factor of the building structure, $\hat{f}_t(n)$ represents the absorption rate of carbon change, and the following formula is obtained:

$$\begin{aligned} Q_{CO_2} &= W_{CO_2} \cdot ILAI, \\ Q_{O_2} &= W_{O_2} \cdot ILAI. \end{aligned} \quad (11)$$

where Q is the carbon emission after the optimal design of green buildings and Q_{CO_2} is the carbon emission in the design of rural buildings. Finally, we need to evaluate the environmental protection of the architectural design model, use the light intensity and fuzzy function to express the overall purification amount, and use the assimilated calculation formula for hierarchical fusion. The final set of evaluation formulas for rural green buildings is as follows:

$$\begin{aligned} \psi_{11} &= PA + A^T P + Q_1 + R_1 + R_2 + K_1 + K_1^T, \\ \psi_{12} &= W_1 - K_1 + M_1 + K_2^T. \end{aligned} \quad (12)$$

In the process of designing rural green buildings, how to improve the service cycle of buildings, change the utilization rate of models, and reduce resource consumption is an urgent problem to be solved. Generally speaking, we should not only reduce the timber but also improve the building service life, and improving the service life mainly depends on the design, development, and packaging in the early and later stages and more investment. Therefore, in the daily work of design projects, the control of quick setting cost and management cost is the key to the precision and benefit of design work. The key to cost control is the utilization rate of high investment construction resources, which needs to go through the whole process of project implementation. Improving the utilization rate of construction resources, high work efficiency, and management level are areas that need continuous reform and innovation. We analyze the changes of traditional building and green building models from two aspects: sunlight oxidation and rainwater erosion, as shown in Figure 5.

It can be seen from Figure 5 that the service life of the traditional building structure model is gradually shortened with the increase of oxidation rate. At the initial stage of oxidation, the adaptability of green buildings to oxidation is less than that of traditional buildings. With the gradual increase of oxidation degree, the oxidation tolerance of traditional buildings has been gradually worse than that of green buildings. This shows that the green environment has the ability to fully adapt to the natural environment, which can also be called sustainable development building. The building model with a green design can ensure that the overall cycle is above the standard range. In rural architectural design, we need discrete dynamic modeling and analysis of pavement permeability. In order to ensure the beauty and stability of the building, this paper uses a permeable ground design to improve the building ground. The traditional modeling technology intelligently analyzes the factors that the water permeability will affect the growth of ground plants. Discrete dynamic modeling technology can detect the change speed and durability of water permeability. Due to the need for a green environment, we can also combine a sunken green design on the original road surface. The optimized building ground design is shown in Figure 6.

It can be seen from Figure 6 that the optimized green building ground can ensure the normal growth of vegetation and solve the problem of soil loss in rain. Therefore, this technology can be applied to the transformation and matching of gardens in rural architectural design. Finally, we analyze the accuracy of the green environmental protection evaluation coefficient in building model construction by traditional modeling technology and discrete dynamic modeling technology, as shown in Figure 7.

It can be seen from Figure 7 that discrete dynamic modeling technology can automatically analyze dynamic data changes in model construction and has a high grasp of model accuracy. Compared with traditional modeling technology, it has greater advantages and can provide more accurate data in green rural architectural design.

4. Analysis of Research Results of Village Planning and Discrete Dynamic Modeling Design of Rural Buildings Based on Dynamic Programming Algorithm

4.1. Analysis of Results of Batch Design of Rural Buildings Based on Discrete Dynamic Modeling Technology. Due to the dynamic change of rural planning according to the actual geographical location and facing the dynamic data, this paper uses discrete dynamic modeling for building batch design and data collection. According to the improvement of layout simulation and miscellaneous data, a new target batch construction model is created, and the final building model is generated. The update and optimization of the whole system can continuously innovate and improve efficiency with the increase of dynamic data. Since the illumination distribution changes dynamically with time, we need to consider whether the illumination rate of each house meets the requirements in architectural design. Therefore, we need

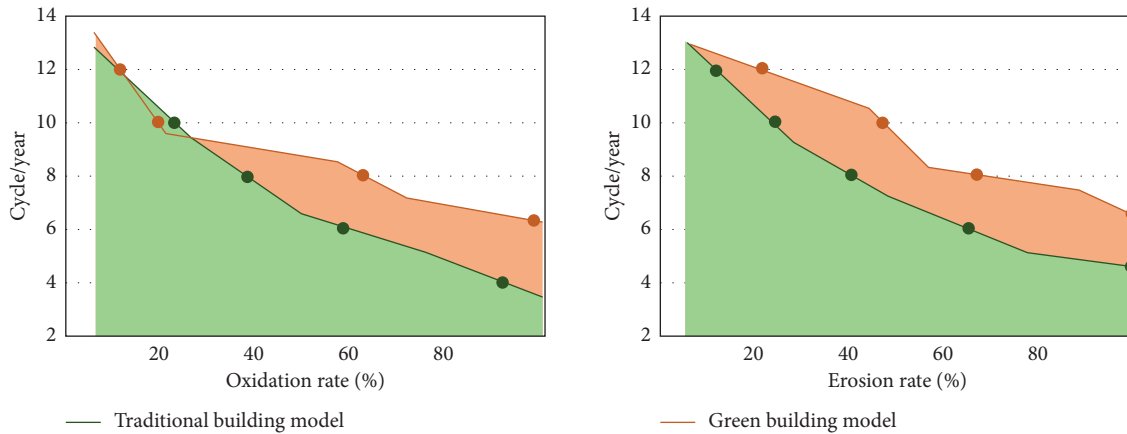


FIGURE 5: Changes of traditional building and green building models in oxidation rate and erosion rate.

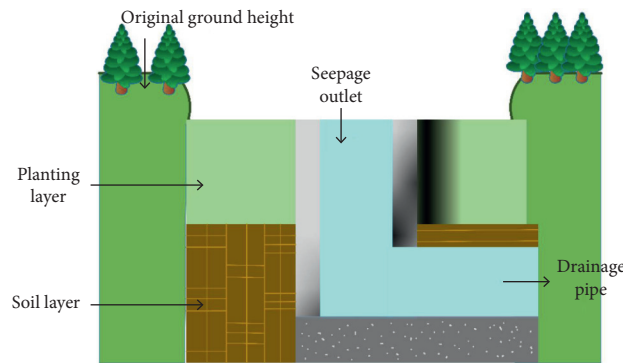


FIGURE 6: Optimized building ground design drawing.

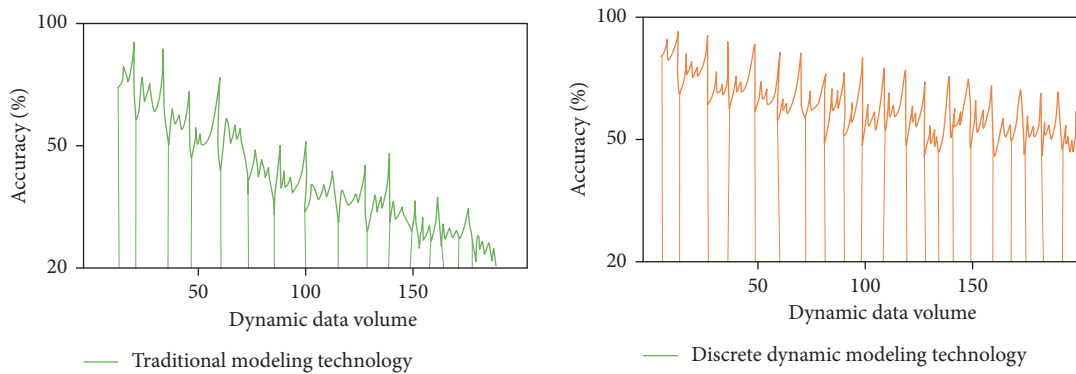


FIGURE 7: Comparison results of accuracy between the two in green environmental protection evaluation coefficient.

to use dynamic modeling technology to simulate and analyze the illumination threshold. As time changes, the illumination threshold range also changes, as shown in Figure 8.

As can be seen from Figure 8, compared with traditional modeling buildings, discrete dynamic modeling house design can raise the illumination range to the maximum threshold, so it is effective for the environmental optimization of the whole household. Finally, we analyze the efficiency of traditional dynamic modeling technology and dynamic modeling technology in building design batch model construction, as shown in Figure 9.

As can be seen from Figure 9, compared with traditional modeling technology, dynamic modeling technology has higher efficiency with the continuous increase of modeling data. Under the constraints of any model structure data, dynamic modeling technology can complete the task of batch architectural design models. It can be seen that the design system using dynamic programming and discrete dynamic modeling can ensure that the number of architectural design is in an advantageous state. According to the dynamic building model, users can choose the house they need under clear lighting conditions. Users only need to

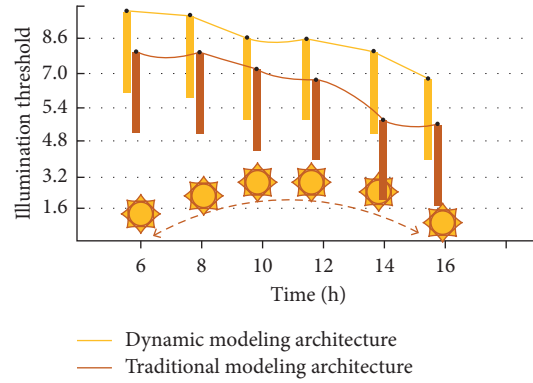


FIGURE 8: Change diagram of illumination threshold data.

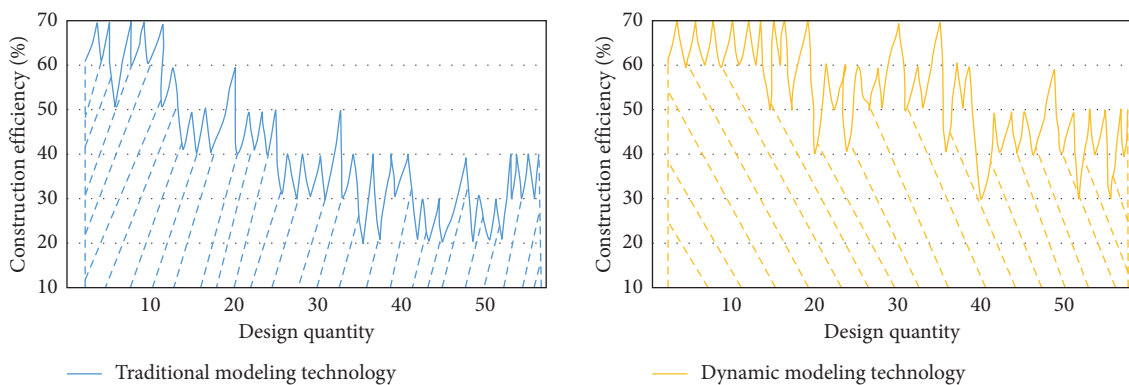


FIGURE 9: Efficiency comparison between traditional dynamic modeling technology and dynamic modeling technology in batch model construction of the architectural design.

enter the house keywords they are looking for in the model search interface, and they can obtain the specific data information that meets the personalized needs. For village planning, the use of this model can also meet the preferences and needs of villagers to the greatest extent and make choices under reasonable conditions. It not only meets the government’s task of rural construction but also meets the personal needs of the local people.

4.2. Analysis of Research Results of Green Rural Building Simulation Design Based on Discrete Dynamic Modeling Technology. In rural planning and architectural design, in order to improve the overall living environment of villagers, we need to provide residents with comfortable living spaces and a green living environment. It is conducive to people’s physical and mental health and the rise of living standards. In order to achieve this goal, the ultimate goal is to ensure that the village planning has a good field of vision, a quiet living environment, and an appropriate sunshine duration. When designing green building materials, this paper uses discrete dynamic modeling technology to build the model. It mainly analyzes the overall service cycle of the building structure and the utilization degree of resources. In order to reduce unnecessary construction waste, we also need to consider the actual needs of villagers. Therefore, this paper studies permeable asphalt ground buildings and

sunken green vegetation buildings. It can optimize the landscape effect in architectural design and use green vegetation to improve the quality of life. In the dynamic modeling, the residential model needs to consider the problems of lighting and shading. Especially in seasonal and weather changes, indoor space needs enough light. In discrete modeling, the overall layout needs to be considered, and the distance between each building will affect the change of illuminance.

In the use of energy-saving and environmental protection substances, we compare the substance detection results of traditional modeling technology and discrete dynamic modeling technology, as shown in Figure 10.

As can be seen from Figure 10, with the increase of the number of materials, the traditional modeling technology cannot accurately analyze the pollution coefficient of each building material. The discrete dynamic modeling technology used in this paper can form a tracking curve according to the material dynamic pollution data. Therefore, in green building design, the discrete dynamic model not only can reduce environmental pollution but also can analyze the performance of building materials. The application of green building design concepts in different environments will continue to rise. With the progress of people’s thinking, innovative schemes using green design will continue to increase in village planning and rural construction.

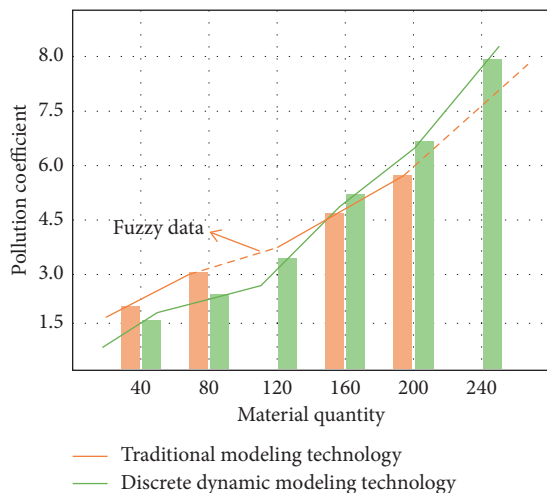


FIGURE 10: Pollution coefficient results of traditional modeling technology and discrete dynamic modeling technology for material detection.

5. Conclusion

With the continuous development of science and technology, in urban and rural construction, more and more people begin to pay attention to the research of rural planning and rural architectural design. In architectural design, the concept of green design is also expanding. In addition to the land planning for environmental protection, the range of pollution coefficient shall be strictly controlled in the use of materials. Based on the above situation, this paper proposes to use a dynamic programming algorithm to optimize the village layout and use discrete dynamic modeling technology to optimize the architectural design model under the background of big data so as to improve the overall performance of the model. Using the dynamic programming algorithm, combined with the actual situation of the village, the distribution of land use rate is analyzed to form an intelligent village layout optimization structure. This structure improves the daily travel of villagers and plays an important role in economic development. Dynamic monitoring technology is used to obtain village change and sunshine data so as to provide dynamic data for the establishment of subsequent rural construction models. Different from the traditional modeling technology, it can process the dynamic building data and calculate the interval distance of the building model according to the change of sunshine data. It is ensured that users in each village can get comfortable living conditions. This paper analyzes the concept of green building design, analyzes the main factors of environmental pollution, and reduces the incorrect use of building materials. The results show that the dynamic programming algorithm can improve the living environment of villagers and provide convenient conditions for economic development. Discrete dynamic modeling technology can realize dynamic batch architecture design and has higher applicability than traditional algorithms. However, there is still the problem of simulation data simulation in this paper, which makes the complex conditions in the

actual situation not considered in the architectural design. Further discussion is needed in future research.

Data Availability

The data used to support the findings of this study are included within the article.

Conflicts of Interest

The author declares that there are no conflicts of interest.

References

- [1] M. Chen, Y. Zhou, X. Huang, and C. Ye, "The integration of new-type urbanization and rural revitalization strategies in China: origin, reality and future trends," *Land*, vol. 10, no. 2, p. 207, 2021.
- [2] W. Li, Y. Zhou, and Z. Zhang, "Strategies of landscape planning in peri-urban rural tourism: a comparison between two villages in China," *Land*, vol. 10, no. 3, p. 277, 2021.
- [3] L. Ye, "Exploration of rural tourism planning under the background of land and space planning," *Shanxi architecture*, vol. 47, no. 16, pp. 21–23, 2021.
- [4] T. Wang, "Analysis of practical village planning based on land spatial planning," *Low carbon world*, vol. 11, no. 7, pp. 118–119, 2021.
- [5] W. Zheng, "Research on village planning based on industrial upgrading," *Urban architecture*, vol. 18, no. 21, pp. 55–57, 2021.
- [6] W. Li, Z. Zhang, and Y. Zhou, "Policy strategies to revive rural land in peri-metropolitan towns: resource identification, capitalization, and financialization," *Land*, vol. 10, no. 2, p. 132, 2021.
- [7] C. Liu, F. Wang, X. Gao, and H. Smith, "Exploring solutions to improve the evaluation of development of rural villages: a case study of the application of the evaluation for the construction of beautiful villages (ECBV) in a village in South China," *Sustainability*, vol. 13, no. 2, p. 685, 2021.
- [8] J. Chen, "Discussion on practical village planning based on land spatial planning," *Low carbon world*, vol. 11, no. 6, pp. 178–179, 2021.
- [9] L. Zhang and W. Li, "Research on landscape design under the mode of pastoral complex," *Agriculture and technology*, vol. 41, no. 17, pp. 138–140, 2021.
- [10] A. Cheshmehzangi, "Low carbon transition at the township level: Feasibility study of environmental pollutants and sustainable energy planning," *International Journal of Sustainable Energy*, vol. 40, no. 7, pp. 670–696, 2021.
- [11] S. Xu, "Research on rural landscape design methods and strategies under beautiful rural construction," *Residential buildings*, no. 21, pp. 104–105, 2021.
- [12] S. Sabri, S. Suhatman, and N. Nasfi, "N. Nagari or village government communication strategies in improving rural economic development," *International Journal of Social and Management Studies*, vol. 2, no. 2, pp. 56–65, 2021.
- [13] R. Lu, "Research on spatial model of rural architecture in wusheng County assisted by design," *Housing industry*, no. 7, pp. 27–28, 2021.
- [14] L. Yan, S. Yu, and Y. Shang, "Discussion on rural building reconstruction design based on adaptability," *Engineering construction*, vol. 53, no. 7, pp. 44–50, 2021.
- [15] B. Liu, J. Yang, L. Gao, and N. Asefi, "Bio-inspired heuristic dynamic programming for high-precision real-time flow

- control in a multi-tributary river system,” *Knowledge-Based Systems*, vol. 230, 2021.
- [16] L. Ma, “Study on power generation optimal operation model of Zipingpu Reservoir Based on dynamic programming,” *Sichuan Hydropower*, vol. 40, no. 4, pp. 133–136, 2021.
- [17] Q. Wu, Y. Zhang, K. Guo, and X. Wang, “Reinforcement learning dynamic environment path planning algorithm combined with LSTM,” *Small microcomputer system*, vol. 42, no. 2, pp. 334–339, 2021.
- [18] Y. Qian and Z. Zhu, “Research on UAV search path planning based on improved dynamic programming,” *Computer simulation*, vol. 38, no. 1, pp. 32–36, 2021.
- [19] M. Mbahand and A. Franz, “Revitalization and branding of rural communities in Cameroon using a circular approach for sustainable development—a proposal for the Batibo Municipality,” *Sustainability*, vol. 13, no. 12, Article ID 6908, 2021.
- [20] X. Li, “Ship scheduling optimization of bulk cargo port based on dynamic programming algorithm,” *Computer simulation*, vol. 37, no. 11, pp. 393–397, 2020.
- [21] Q. Chen, Y. Zheng, H. Jiang, and C. Yan, “Dynamic path planning based on improved particle swarm optimization algorithm based on neural network,” *Journal of Huazhong University of Science and Technology (Nature Science Edition)*, vol. 49, no. 2, pp. 51–55, 2021.
- [22] Z. Ding, W. Chen, T. Hu, and X. Xu, “Evolutionary double attention-based long short-term memory model for building energy prediction: case study of a green building,” *Applied Energy*, vol. 288, Article ID 116660, 2021.
- [23] J. M. Davila Delgado, L. Oyedele, T. Beach, and P. Demian, “Augmented and virtual reality in construction: drivers and limitations for industry adoption,” *Journal of Construction Engineering and Management*, vol. 146, no. 7, Article ID 04020079, 2020.
- [24] W. Ma, X. Wang, J. Wang, X. Xiang, and J. Sun, “Generative design in building information modelling (BIM): approaches and requirements,” *Sensors*, vol. 21, no. 16, p. 5439, 2021.
- [25] A. Zhou, J. Zhang, and J. Zhang, “Application of cultural heritage health check in the immovable cultural heritage conservation practice in Beijing,” *ISPRS Annals of the Photogrammetry, Remote Sensing and Spatial Information Sciences*, vol. VIII-M-1-2021, pp. 215–221, 2021.